

---

This is a reproduction of a library book that was digitized by Google as part of an ongoing effort to preserve the information in books and make it universally accessible.

Google<sup>TM</sup> books

<https://books.google.com>







## NBS SPECIAL PUBLICATION 570

U.S. DEPARTMENT OF COMMERCE/National Bureau of Standards

# Structure Shielding Against Fallout Gamma Rays From Nuclear Detonations









BOOKSTACKS-  
DOCUMENTS



NI







# Structure Shielding Against Fallout Gamma Rays From Nuclear Detonations

---

6.9.16  
2/25/2016

L. V. Spencer

Center for Radiation Research  
National Measurement Laboratory  
National Bureau of Standards  
Washington, D.C. 20234

A. B. Chilton

University of Illinois  
Urbana, IL 61801

C. M. Eisenhauer

Center for Radiation Research  
National Measurement Laboratory  
National Bureau of Standards  
Washington, D.C. 20234



---

U.S. DEPARTMENT OF COMMERCE, Philip M. Klutznick, Secretary

Luther H. Hodges, Jr., Deputy Secretary

Jordan J. Baruch, Assistant Secretary for Productivity, Technology and Innovation

NATIONAL BUREAU OF STANDARDS, Ernest Ambler, Director

Issued September 1980



**Library of Congress Catalog Card Number: 80-600120**

**National Bureau of Standards Special Publication 570**

**Nat. Bur. Stand. (U.S.), Spec. Publ. 570, 984 pages (Sept. 1980)**

**CODEN: XNBSAV**

**U.S. GOVERNMENT PRINTING OFFICE**

**WASHINGTON: 1980**

---

**For sale by the Superintendent of Documents, U.S. Government Printing Office  
Washington, D.C. 20402 - Price \$20.00**

## PREFACE

This book summarizes the research and development progress towards evaluating protection provided by existing and planned structures against gamma radiation from radioactive fallout. Measurements and procedures are described for complex as well as elementary structures; and we have included a fairly complete summary of the concepts of gamma ray transport, as well as additional background information on the relevant gamma ray sources and on dosimetry. Comparisons indicate that some procedures are highly accurate and others rather questionable, with the combination yielding an accuracy probably limited as much by data obtainable on actual structures as by deficiencies in the procedures.

Attempts to develop satisfactory methods for estimating the shielding properties of ordinary buildings against gamma rays from radioactive fallout began in the early 1950's. Intensive research of many kinds was carried out during the decade from about 1956 to 1966; but in the past decade, there has been a steady decline of new research on these problems. There are many reasons for this, one of which is not, however, the achievement of a fully satisfactory state of the technology. An updating and improvement of the material presented here is overdue, but is not easily effected.

We intend this publication to serve 1) as a reference for engineering students, 2) as a reference and source of ideas for engineers engaged in research and development on radiation shielding problems, 3) as a basic reference by architects and engineers concerned with the design of buildings with protective features, and 4) a reference for officials responsible for civil protection in nuclear emergencies. These multiple uses are expected partly because this is the first attempt to bring together and summarize much of the material presented.

Because this monograph is designed to serve as a reference for readers with varying technical backgrounds, highly technical discussions are sometimes juxtaposed with sections requiring little technical background. Hence we point out some features of the presentation in order to make things easier for the reader:

Chapters I and II give general background information on historical developments (chapter I) and fallout gamma ray sources (chapter II). Much of chapter II should be understandable by the general reader. It is not required reading for everyone concerned with the main applications of this book. But is important for general orientation and reference purposes.

Chapters III and IV discuss general concepts of radiation transport, with relevant theorems and derivations. While a reader with little technical background may wish to avoid these chapters, most of chapter III and sections A and B of chapter IV should be readable by a varied audience.

Sections A and B of chapter V give essential definitions of terms to be used in the remainder of the monograph. The remainder of chapter V gives descriptions and theoretical data for functions mainly useful for simple configurations. Similarly, chapter VI discusses and presents experimental data for the main reference configuration, which is the free-field case.



Chapters VII and VIII give engineering concepts and procedures (chapter VII) and experimental studies (chapter VIII) relating to elementary structural configurations.

Chapters IX and X likewise give engineering concepts and procedures (chapter IX) and experimental studies (chapter X) relating to complex structural configurations.

Finally, chapters XI and XII contain supplementary discussions on special problem areas (chapter XI) and certain aspects of the accuracy problem.

Thus, in a general way, the historical, physical, and mathematical background is contained in chapters I-V, and the engineering aspects are in chapters VI-XI. Readers interested only in design or analysis procedures may wish to limit their study mainly to chapters VII, IX, and perhaps XI, with reference use of chapter V.

# STRUCTURE SHIELDING AGAINST FALLOUT GAMMA RAYS FROM NUCLEAR DETONATIONS

L. V. Spencer, A. B. Chilton, and C. M. Eisenhauer

Conversion Table . . . . .	xiii
Acknowledgments . . . . .	xv
I. HISTORICAL INTRODUCTION . . . . .	1
A. Elementary Aspects of the Radiation Source, Detectors, and Attenuation . . . . .	1
1. Radioactive Fallout: Background and Early History . . . . .	1
2. Measurement of Gamma Rays . . . . .	9
a. Early Developments . . . . .	9
b. Other Types of Detectors . . . . .	12
3. Early Gamma-Ray Penetration Studies . . . . .	14
B. Development of Fallout Radiation Shielding Methods and Programs . . . . .	17
1. Early Technical Work . . . . .	17
2. Early Policy on Fallout Shelters (1951-1961) . . . . .	22
3. Experiments on Buildings (1951-1961) . . . . .	27
4. Later Experiments (1962-1973) . . . . .	34
5. Continued Development of Engineering Procedures (1958-1961) . . . . .	35
6. The Federal Surveys of Existing Fallout Shelter . . . . .	37
7. More Recent Trends . . . . .	42
II. PHYSICAL AND SOME BIOLOGICAL ASPECTS OF THE FALLOUT PHENOMENON . . . . .	49
A. Radioactive Debris Formation by Nuclear Bursts . . . . .	49
1. Introductory Description of Fission-Generated Nuclear Processes . . . . .	49
2. Nuclear Bursts and Fallout Formation . . . . .	54
3. Some Fallout Particle Characteristics . . . . .	58
a. Component Particle Types and Origins . . . . .	58
b. Particle Activity - Fractionation . . . . .	62
B. Intensity of Fission Product Nuclear Activity . . . . .	65
1. Theoretical Procedures for Investigating Activity of Fission Products . . . . .	65
2. Gamma Rays from Fission Products . . . . .	70
3. Gamma Ray Intensities . . . . .	73
4. Gamma Ray Spectra from Fission Products . . . . .	85
C. Some Properties of Residual Radiation . . . . .	96
1. Effects of Fractionation on Fallout Gamma Ray Properties . . . . .	96
a. The Portion of Activity Deposited in Local Fallout . . . . .	96
b. Variation of Activity with Particle Size and Position . . . . .	100
c. Effect of Fractionation on the Spectrum . . . . .	105
2. Neutron-Capture Gamma Rays . . . . .	107
3. Penetration of Fallout Gamma Rays . . . . .	117
4. Beta-Ray Spectra and Penetration from Fallout . . . . .	120



D.	Debris Transport and Deposition . . . . .	125
1.	Computation of Fallout Surface Distributions . . . . .	125
a.	The WSEG Model . . . . .	129
b.	The Miller Model . . . . .	129
c.	The DELFIC Model . . . . .	131
d.	SEER Models . . . . .	133
2.	Continuing Problems of Fallout Phenomena . . . . .	133
a.	Effects of Small Changes in Burst Height or Depth . . .	134
b.	Problems of Fallout Formation . . . . .	134
c.	Problems of Fallout Transport . . . . .	135
d.	Problems of the Radiation Field . . . . .	135
e.	Long Term Fallout Problems . . . . .	136
E.	Biological Hazards from Fallout Radiations . . . . .	136
1.	The Direct External Threat . . . . .	137
2.	Direct Internal Hazards . . . . .	141
3.	Food Chain and Other Indirect Hazards . . . . .	144
4.	Ecological Problems . . . . .	146
5.	Late Problems . . . . .	147
III.	ELEMENTARY CONCEPTS OF PHOTON TRANSPORT . . . . .	163
A.	Interaction Probability Functions . . . . .	163
1.	Basic Gamma-Ray Interactions . . . . .	163
2.	Cross Sections . . . . .	166
3.	Exponential Attenuation . . . . .	169
4.	Gamma Ray Scattering . . . . .	177
B.	Flux Density, Current Density and Energy Deposition . . . . .	182
1.	Flux Definitions and Current Density Definitions . . . . .	182
2.	Energy Deposition in the Medium . . . . .	189
3.	Source Descriptions and Superposition . . . . .	193
C.	Energy Balance Concepts . . . . .	198
1.	The Energy Degradation Problem . . . . .	198
2.	Energy-Loss Calculations . . . . .	201
3.	The Transport Equation . . . . .	207
4.	Fano's Theorem . . . . .	210
D.	Dosimetry and Related Biophysical Matters . . . . .	212
1.	Basic Concepts of Gamma-Ray Dosimetry . . . . .	212
2.	Some Aspects of Radiation Biophysics . . . . .	216
E.	The Stochastic Approach to Radiation Transport . . . . .	219
1.	Schematized Photon Trajectories . . . . .	219
2.	A Monte Carlo Model . . . . .	223
a.	The Case History Loop . . . . .	226
b.	The Scattering Loop . . . . .	230
c.	Evaluation of the Albedo Probability Distribution . . .	232
3.	Other Stochastic Procedures and Problems . . . . .	234
F.	Radiation Quantities and Units . . . . .	236

IV.	TRANSPORT PROBLEMS AND SHIELDING CONCEPTS . . . . .	244
A.	Unscattered Photons from Simple Source Types . . . . .	244
1.	Introductory Comments . . . . .	244
2.	Point Isotropic Source . . . . .	246
3.	Plane Oblique Source . . . . .	249
4.	Plane Isotropic Source . . . . .	252
5.	Circular Disk and Ring Sources . . . . .	254
B.	Density Scaling Theorems, and Detectors Near an Interface . . . . .	255
1.	Introductory Comments . . . . .	255
2.	The Theorem on Plane Density Variations . . . . .	256
3.	Density Scaling Theorem . . . . .	261
4.	Elementary Detectors Near an Interface . . . . .	265
C.	Aspects of the Photon Field in Infinite Homogeneous Media . . . . .	270
1.	Once-Scattered Photons from Simple Source Types . . . . .	270
a.	Plane Oblique Source . . . . .	270
b.	Plane Isotropic Source . . . . .	276
c.	Point Isotropic Source . . . . .	278
2.	Trends for Small Penetrations . . . . .	284
a.	Plane Oblique Source . . . . .	284
b.	Point Isotropic Source . . . . .	289
c.	Plane Isotropic Source . . . . .	290
3.	Trends for Deep Penetrations . . . . .	291
D.	Moments Method of Calculation . . . . .	293
1.	Derivation of Moment Equations . . . . .	295
2.	Calculation of Solutions to the Moment Equations . . . . .	299
3.	Construction of Penetration Trends . . . . .	302
a.	Point Isotropic Source . . . . .	303
b.	Plane Isotropic Source . . . . .	304
c.	Plane Oblique Source . . . . .	305
4.	Construction of Angular Distributions . . . . .	307
a.	Direct Approach . . . . .	307
b.	Early Fission Source Calculations . . . . .	308
c.	$^{60}\text{Co}$ and $^{137}\text{Cs}$ Source Calculations . . . . .	309
d.	More Recent Procedures for the Plane Isotropic Source . . . . .	310
5.	Remarks on Accuracy . . . . .	310
E.	Adjoint Calculations . . . . .	312
1.	The Adjoint Equation . . . . .	312
2.	Remarks on the Adjoint Approach . . . . .	315
V.	PENETRATION DATA FOR SHIELDING APPLICATIONS . . . . .	320
A.	Introduction . . . . .	320
B.	Definitions of Shielding Variables . . . . .	320
1.	Protection Factors (PF) and Reduction Factors (RF) . . . . .	320
2.	Effective Mass Thickness . . . . .	323
3.	Solid Angle Fraction ( $\omega$ ) . . . . .	329
4.	Types of Shielding Factor . . . . .	333
C.	Types of Differential Penetration Distribution . . . . .	340
1.	Plane Isotropic Source ( $\ell$ ) . . . . .	340
2.	Point Isotropic Source ( $\underline{p}$ ) . . . . .	342
3.	Plane Oblique Source ( $s$ ) . . . . .	345
4.	Albedo Data ( $\alpha$ ) . . . . .	349

D.	Integral Shielding Data: Standard Fission Product Source . . .	350
1.	Reduction Factors for Plane Isotropic Sources ( <u>L</u> ) . . .	350
a.	Barrier Factors . . .	353
b.	Geometry Factors . . .	356
2.	Reduction Factors for Point Isotropic Sources ( <u>P</u> ) . . .	357
a.	Barrier Factors . . .	357
b.	Geometry Factors . . .	362
3.	Vertical Wall/Window Reduction Factors ( <u>W</u> ) . . .	368
a.	Barrier Factors . . .	368
b.	Geometry Factors . . .	374
4.	Skyshine and Foxhole Reduction Factors ( <u>S,E</u> ) . . .	376
a.	Barrier and Attenuation Factors . . .	376
b.	Geometry Factors . . .	382
c.	Special Data for Foxhole Lip Contributions . . .	382
VI.	FREE FIELD EXPERIMENTS . . .	388
A.	Introduction . . .	388
B.	Use of Artificially-Radioactive Sources . . .	389
C.	Free Field . . .	390
1.	Experiments with Point Sources . . .	390
2.	Determination of Exposure at the Standard Unprotected Location . . .	395
3.	Plane Isotropic Source in an Infinite Medium . . .	401
a.	Exposure from Uncollided Radiation . . .	401
b.	Total Exposure . . .	403
c.	Exposure from Skyshine Radiation . . .	406
d.	Angular Distributions . . .	408
e.	Energy Distributions . . .	411
f.	Energy-Angular Distributions . . .	411
4.	Effects of Ground-Air Interface . . .	413
a.	Air/Condensed Air . . .	413
b.	Ground-Air Interface . . .	420
5.	Limited Field Effects . . .	421
a.	Total Exposure . . .	421
b.	Skyshine Exposure . . .	422
D.	The Foxhole . . .	428
1.	Skyshine . . .	428
2.	Lip Effects . . .	438
E.	Ground Irregularities . . .	443
1.	Ground Roughness . . .	443
a.	Standard Unprotected Location . . .	443
b.	Spatial Trends . . .	445
c.	Effect on Angular Distribution . . .	451
d.	Effect on Energy Distribution . . .	453
2.	Macroscopic Variations . . .	453



VII.	SHIELDING ANALYSIS FOR SIMPLE STRUCTURES IN AN IDEALIZED FIELD . . .	465
A.	Introduction . . . . .	465
B.	Elementary Blockhouses . . . . .	467
1.	Standard Method . . . . .	467
2.	Other Methods of Blockhouse Analysis . . . . .	493
a.	Spencer's Method . . . . .	493
b.	Point Kernel Method . . . . .	495
c.	Monte Carlo Method . . . . .	498
C.	Blockhouses with Floor Level not on Grade . . . . .	499
1.	Detector Above Grade . . . . .	499
2.	Detector Below Grade . . . . .	499
D.	Blockhouse with Variable Thickness Roofs and Walls . . . . .	503
1.	Preliminary . . . . .	503
2.	Roofs . . . . .	504
3.	Walls . . . . .	514
4.	Apertures . . . . .	531
5.	Ceiling-Shine . . . . .	533
6.	Ribbed Structural Elements . . . . .	536
E.	Off-Center Detector Positions . . . . .	538
F.	Summary . . . . .	539
VIII.	Experimental Data on Simple Blockhouses . . . . .	543
A.	Introduction . . . . .	543
B.	Horizontal Barrier . . . . .	543
1.	Barrier Factor; Experiment . . . . .	543
2.	Geometry Effects; Inverted Roof Experiment . . . . .	548
C.	Vertical Barrier . . . . .	553
1.	Barrier Factor, Infinite Source . . . . .	553
a.	Experiments . . . . .	553
b.	Calculations . . . . .	559
c.	Skyshine through Vertical Barrier . . . . .	562
2.	Barrier Factor, Finite Sources . . . . .	565
D.	Simple Blockhouse . . . . .	573
1.	NDL Experiments . . . . .	573
a.	Roof Source . . . . .	573
b.	Ground Source . . . . .	576
2.	RTF Experiments . . . . .	577
a.	Roof Source . . . . .	577
b.	Ground Source . . . . .	584
3.	Kansas State University Blockhouse . . . . .	587
4.	Blockhouse Models . . . . .	590
5.	Calculations for Cylindrical Blockhouse . . . . .	594
6.	Apertures . . . . .	594
E.	Blockhouse Shape Effects . . . . .	598
1.	Discussion of Method for Evaluating Shape Effects . . . . .	598
2.	Experiments to Determine Shape Effects . . . . .	600
a.	Tech/Ops Experiments . . . . .	600
b.	NDL Experiments . . . . .	603

F.	Ceiling Shine . . . . .	606
G.	Ribbed Structural Elements . . . . .	614
1.	RTF Experiments . . . . .	614
2.	Experiments at University of Illinois . . . . .	619
3.	Calculations at University of Illinois . . . . .	619
IX.	SHIELDING ANALYSIS FOR COMPLEX SITUATIONS . . . . .	623
A.	Introduction . . . . .	623
B.	Complications in Source . . . . .	624
1.	Limited Fields of Ground Contamination . . . . .	624
a.	Direct Ground Contribution (Zero-Thickness Wall) . . . . .	625
(1)	Blockhouse with Symmetric Courtyard . . . . .	625
(2)	Other Cases -- General Comments . . . . .	625
(3)	Parallel Outer Boundary on One Side . . . . .	627
(4)	Perpendicular Outer Boundary on One Side . . . . .	630
(5)	Oblique Outer Boundary on One Side . . . . .	631
(6)	Sector-Independent Approaches . . . . .	632
b.	Skyshine and Ceiling-Shine Contributions . . . . .	633
c.	Wall-Scattered Contribution . . . . .	635
(1)	Square Blockhouse/Square Courtyard . . . . .	639
(2)	Rectangular Blockhouse/Geometrically Similar Courtyard Boundary . . . . .	641
(3)	Parallel Outer Boundary on One Side (Unlimited) . . . . .	643
(4)	Limited Parallel Outer Boundary on One Side . . . . .	645
(5)	Non-Parallel Outer Boundaries on One Side . . . . .	648
(6)	Estimation of Limited Field Length . . . . .	648
(7)	Final Comment on Incremental Wall Area Approach . . . . .	656
d.	Additional Comments on Limited Fields . . . . .	656
2.	Slightly Buried Sources (Ground Roughness) . . . . .	658
3.	Elevated Ground Sources . . . . .	660
4.	Sloping Source Planes . . . . .	669
a.	Standard Approach . . . . .	670
b.	Alternate Approach . . . . .	674
C.	Complications in Structure . . . . .	675
1.	Internal Compartmentation . . . . .	675
a.	Introduction . . . . .	675
b.	Roof Source, Interior Floor Barriers . . . . .	678
c.	Roof Source, Interior Wall Barriers . . . . .	681
d.	Ground Source, Interior Floor Barrier ("In-and-Down") . . . . .	683
e.	Ground Source, Interior Barriers Parallel to Outer Wall . . . . .	686
f.	Ground Source, Interior Wall Barrier Perpendicular to Outer Wall . . . . .	692
g.	Ground Source, Combination of Parallel and Perpendicular Interior Wall Barriers . . . . .	692
h.	Combination of Floor Barriers with One or More Interior Wall Partitions . . . . .	693
2.	Roof Complexities . . . . .	693
a.	Non-Horizontal Overhead Roofs . . . . .	693
b.	Non-Horizontal Roofs of Adjacent Buildings . . . . .	697
c.	Roof Overhang . . . . .	697
d.	Set-Back Roofs . . . . .	699

3.	Non-Rectangular Wall Plan . . . . .	701
a.	Non-Reentrant Structures . . . . .	701
b.	Reentrant Structures . . . . .	703
c.	Round and Quasi-Round Structure Plans . . . . .	703
4.	Ducts, Passageways, Shafts, and Tunnels . . . . .	705
a.	Introduction . . . . .	705
b.	Penetration from a Ground Source . . . . .	706
(1)	Horizontal Passageways . . . . .	706
(2)	Vertical Shafts . . . . .	708
(3)	Multilegged Ducts . . . . .	710
(4)	Shielded Openings . . . . .	710
X.	EXPERIMENTAL DATA ON COMPLEX STRUCTURES . . . . .	713
A.	Introduction . . . . .	713
B.	Limited Fields . . . . .	714
1.	Background of Problem . . . . .	714
2.	Experiments at the Radiation Test Facility . . . . .	714
3.	Steel Model Study by Technical Operations Inc. . . . .	720
C.	Compartmented Blockhouse . . . . .	723
1.	Roof Sources and Horizontal Barriers . . . . .	723
2.	Ground Sources and Vertical Barriers . . . . .	727
3.	Ground Sources and Horizontal Barriers . . . . .	732
4.	Peripheral Roof Contribution . . . . .	736
5.	Apertures and Interior Partitions . . . . .	743
6.	Core Structure Below Grade . . . . .	746
D.	"In-and-Down" . . . . .	754
1.	Background . . . . .	754
2.	Skyshine Attenuation . . . . .	757
3.	"In-and-Down" Attenuation . . . . .	764
4.	Calculations of "In-and-Down" Attenuation . . . . .	768
E.	Residential and Commercial Structures . . . . .	773
1.	Residential Structures at Nevada Test Site . . . . .	774
2.	Boston Harbor Building . . . . .	778
3.	General Structures at Nevada Test Site . . . . .	779
4.	Other Structures at Nevada Test Site . . . . .	782
a.	CP-40 Building, Communications Building . . . . .	782
b.	CP-45 Building, Light Laboratory . . . . .	783
c.	CP-1, Main Control Building . . . . .	794
d.	CP-2, Rad-Safe Building . . . . .	794
5.	AEC Headquarters Building, Germantown, Maryland . . . . .	800
a.	Roof Sources . . . . .	800
b.	Ground Sources . . . . .	803
6.	Brookhaven National Laboratory Medical Research Center . . . . .	806
7.	Los Angeles Buildings . . . . .	809
a.	UCLA Laboratory of Nuclear Medicine . . . . .	812
b.	Home Fallout Shelter . . . . .	814
c.	Los Angeles Police Department Building . . . . .	814
d.	Classroom Building at North Hollywood High School . . . . .	814
F.	Summary . . . . .	816

XI.	PROBLEMS IN THE APPLICATION OF THE FALLOUT SHIELDING METHODOLOGY . .	821
A.	Introduction . . . . .	821
B.	Factors Relating to the Source . . . . .	822
1.	Non-Uniform Deposition of Source . . . . .	822
2.	Hold-Up in Trees and Shrubs . . . . .	823
3.	Fallout Deposition on Window Sills and Other Wall Projections . . . . .	824
4.	Fallout Ingress Through Windows . . . . .	826
5.	Ground Contour Variations . . . . .	826
6.	Irregular or Curved Limits to Finite Fields . . . . .	827
C.	Factors Relating to the Structure . . . . .	827
1.	Simplification of Very Complex Structures . . . . .	827
2.	Handling of Curved Structural Elements . . . . .	829
3.	Unusual Shapes of Wall Panels, Roof Panels, and Apertures . . . . .	829
4.	Small, Irregularly Placed Masses . . . . .	830
5.	Approach Based on Small Azimuthal Sectors of Arbitrary Size . . . . .	830
6.	Alternative Approaches . . . . .	832
7.	Accurate Input Data . . . . .	834
D.	The Question of Accuracy . . . . .	835
1.	Types of Investigation . . . . .	835
2.	Studies Oriented Primarily Toward Accuracy Questions . . . . .	838
3.	Further Comments . . . . .	843
XII.	SHELTER PROGRAMS AND SYSTEMS . . . . .	848
A.	Sensitivity Studies of Shelter PF Criteria . . . . .	848
1.	Hypothetical Effectiveness of PF in Large Nuclear Disasters . . . . .	848
2.	Overall Impact of Errors in Shielding Estimates . . . . .	850
B.	Fallout and Other Burst Phenomena . . . . .	853
C.	Fallout Shelters and Strategic Evacuation . . . . .	860
APPENDIX A.	PROPERTIES OF IMPORTANT SPECIAL FUNCTIONS, AND CONSTRUCTION METHODS . . . . .	864
1.	Spherical Functions . . . . .	864
a.	Description . . . . .	864
b.	Some Other Important Properties . . . . .	865
c.	Application to the Point-to-Plane Source Conversion . . . . .	867
2.	U-Functions . . . . .	868
a.	Description . . . . .	868
b.	Recursion Formulae for Coefficients . . . . .	872
3.	Function Fitting Representations . . . . .	873
4.	Plural Series Representations . . . . .	875
APPENDIX B.	$^{60}\text{Co}$ AND $^{137}\text{Cs}$ DIFFERENTIAL AND INTEGRAL PENETRATION DISTRIBUTIONS . . . . .	878
APPENDIX C.	CHARTS FROM OCD STANDARD METHOD FOR FALLOUT GAMMA RADIATION SHIELDING ANALYSIS . . . . .	925
GLOSSARY . . . . .		942
INDEX OF AUTHORS . . . . .		948
INDEX . . . . .		952

# CONVERSION TABLE

Quantity	Old special unit and symbol	New named unit and symbol	Conversion factor	Remarks
cross section	barn (b)	$\text{cm}^2$	$10^{-24} \text{ cm}^2/\text{b}$	
disintegration rate	Curie (Ci)	$\text{s}^{-1}$	$3.7 \times 10^{10} \text{ s}^{-1}/\text{Ci}$	
energy	MeV	J	$1.6 \times 10^{-13} \text{ J/MeV}$	
length	$\left\{ \begin{array}{l} \text{inch (in)} \\ \text{foot (ft)} \\ \text{mile (mi)} \\ \text{micron} \end{array} \right\}$	centimeter (cm)	2.54 cm/in	$\left\{ \begin{array}{l} \text{In some equations in this} \\ \text{book the unit of feet is} \\ \text{indicated by '}; \text{ e.g., } 3'. \end{array} \right\}$
		centimeter (cm)	30.48 cm/ft	
		kilometer (km)	1.609 km/mile	
		centimeter (cm)	$10^{-4} \text{ cm/micron}$	
mass	$\left\{ \begin{array}{l} \text{pound (lb)} \\ \text{megaton (mt)} \end{array} \right\}$	kilogram (kg)	0.454 kg/pound	$\left\{ \begin{array}{l} \text{This unit is used to} \\ \text{describe the amount of} \\ \text{energy equivalent to} \\ \text{that liberated by} \\ \text{megatons of TNT.} \end{array} \right\}$
		kilogram (kg)	$9.08 \times 10^8 \text{ kg/megaton}$	
mass thickness	pounds per square foot	$\text{g cm}^{-2}$	$0.489 \text{ g cm}^{-2}/\text{psf}$	
temperature	Fahrenheit (F)	Celsius (C)	$T(C) = \frac{5}{9} [T(F) - 32]$	



# Recently Revised Radiation Units

Quantity	Old special unit and symbol	New named unit and symbol	In other SI units	Conversion factor	Remarks
absorbed dose	rad (rad)	gray (Gy)	$\text{J kg}^{-1}$	1 Gy/100 rad	
activity	curie (Ci)	becquerel (Bq)	$\text{s}^{-1}$	1 Bq/2.7 x 10 <sup>-11</sup> Ci	
dose equivalent	rem (rem)	sievert (Sv)	$\text{J kg}^{-1}$	1 Sv/100 rem	
exposure	Roentgen (R)	-	$\text{C kg}^{-1}$	1 C kg <sup>-1</sup> /3876 R	C refers to coulombs of released charge of one sign

## ACKNOWLEDGMENTS

The authors would like to acknowledge the financial support of the Defense Civil Preparedness Agency (Now the Federal Emergency Management Agency) and the Defense Atomic Support Agency (now the Defense Nuclear Agency) in the preparation of this book. We would also like to thank J. Velletri, R. Ponzini, D. Steele, Z. Burson, A. Kaplan, E. Bramlett, R. Tompkins and C. Miller for reviewing portions of the draft of this work.

The contributions of the many scientists and engineers who have worked in the field of fallout shielding are mentioned in the body of this book. We should, however, note the administrators of the DCPA whose interest and encouragement led to the achievements in this field, in particular P. Gallagher, J. Buchanan, J. Greene, D. Benson, and J. Roembke.

The authors would like to acknowledge the special contribution made by N. FitzSimons to the development of fallout shielding technology. His drive, intelligence, and enthusiasm stimulated much of the early developments in what is now called the Standard Method and the simplified methods springing from it, as well as much of the related experimentation. E. Clarke of Technical Operations, Inc., was also a constant supporter of technical and administrative aspects of the research effort.

The preparation of this book required a great deal of devoted assistance from a number of people. Margaret Jones provided typing and secretarial support; and M. Weinart, K. Crosson, H. Beck, L. Phillips, N. Wilson, and M. Ahalt provided editorial assistance. Finally, we would like to thank Gloria Wiersma for the many hours she spent on typing, reviewing, and editing this work, and for her patience and competence in handling the task.

STRUCTURE SHIELDING AGAINST FALLOUT GAMMA RAYS  
FROM NUCLEAR DETONATIONS

L. V. Spencer  
National Bureau of Standards  
Washington, D.C. 20234

A. B. Chilton  
University of Illinois  
Urbana, Illinois 61801

C. M. Eisenhauer  
National Bureau of Standards  
Washington, D. C. 20234

ABSTRACT

This book summarizes the extensive effort during the twenty years following 1956 to understand the protective capability of structures against fallout gamma radiation from nuclear weapons. It describes both experimental and theoretical efforts that were sponsored for the most part by the U.S. Defense Civil Preparedness Agency, now part of the Federal Emergency Management Agency.

The first two chapters of the book give a historical review of methods and programs associated with fallout radiation shielding, and a description of the physical and biological aspects of fallout radiation. The production, transport and deposition of fallout are described and biological hazards are reviewed.

The next three chapters describe a series of calculations which formed the data base for a set of procedures to evaluate shielding from fallout radiation. Basic concepts such as cross sections, flux density and energy deposition are discussed. Examples of photon transport in simple configurations are given. A detailed discussion is given on the moment method of photon transport. Curves are given for calculating photon transport in configurations applicable to structures.

The next six chapters describe the procedures for calculating protection from fallout radiation and the extensive series of experiments which were carried out to test these procedures. Discussion begins with the simple configuration of a point detector located above a plane isotropic source and proceeds to increasingly complex structural configurations. Comparisons of experimental and calculated results are given for many of these configurations.

The final chapter discusses sources of error and sensitivity studies. The problem of accuracy, in general, and sensitivity of protection factors to uncertainties in the calculations are discussed.

Key Words;      Cesium-137; civil defense; cobalt-60; dose; fallout; gamma rays;  
nuclear weapons; photons; radiation transport; shielding;  
structures.

## I. HISTORICAL INTRODUCTION<sup>\*</sup>

### A. ELEMENTARY ASPECTS OF THE RADIATION SOURCE, DETECTORS, AND ATTENUATION

#### 1. Radioactive Fallout: Background and Early History

The natural environment has always contained radiation from two types of sources, a) decay of unstable radioactive nuclides, and b) high energy particles penetrating the atmosphere from outer space. Radioactive decay of uranium was discovered by Becquerel in 1895, while cosmic rays were discovered in 1912 by V. F. Hess.

The most common type of uranium nucleus decays by emitting an alpha particle. The resulting nuclei are unstable as well, and further nuclear transitions occur. In such a chain of reactions, beta rays are emitted and also gamma rays. The fact that uranium exists and is fairly abundant is due to a very long half-life ( $4.51 \times 10^9$  yr) which is comparable with estimations of the age of the earth ( $\sim 4.6 \times 10^9$  yr) and also comparable with available information about galactic lifetimes in general.

That nuclear transitions could result from collisions between high energy radiations and nuclei was first demonstrated in Rutherford's experiments in 1919, in which alpha particles were incident on aluminum nuclei. But although cosmic rays do generate nuclear transitions as they penetrate the atmosphere and the ground, the radioactivity of the nuclei resulting from such transitions is of much lower intensity<sup>2</sup> than that of the cosmic radiation.

---

<sup>\*</sup>We are indebted to Dr. C. M. Huddleston for the use of some material from an unpublished manuscript of his on this subject [1]<sup>1</sup>.

<sup>1</sup>Figures in brackets indicate the literature references at the end of each chapter in this publication.

<sup>2</sup>We use intensity as a general term for "amount" despite the narrower and more specific connotations that have been given this term.

It is not possible to induce nuclear transitions with low-energy heavy charged particles, due to the electrostatic force exerted by nuclei. And it is likewise not possible to induce transitions with low-energy x rays, because the energy separations of the two lowest nuclear states tend to be of the order of 1 MeV, and this gives a lower bound for nuclear interactions with photons. Neutrons are not affected by the Coulomb barrier; and since they change the nucleus to a new species, the energy gap between the two lowest states of the same nuclide is not relevant to the transition probabilities relating to neutron capture by nuclei. Hence the discovery of the neutron in 1932 by Chadwick really opened up the field of nuclear studies.

Following Chadwick's discovery, neutron-induced transitions became the object of intensive studies, during which the different elements of the periodic system were subjected to neutron bombardment, with attempts to understand the resulting transitions. The bombardment of uranium by E. Fermi in 1934 produced puzzling results, which were first interpreted as transmutations to heavier elements. In 1939, O. Hahn and F. Strassmann demonstrated the presence of barium in the products, and are as a result usually credited with the discovery of nuclear fission. Frisch and Meitner, also in 1939, postulated that the uranium nuclei were reacting to neutron absorption by splitting into two very large fragments. This suggestion initiated rapid and very intensive study in many laboratories, which developed details of the fission process. As a result of these studies it became clear that slow-neutron fission was not occurring in the main isotope of uranium ( $^{238}\text{U}$ ) but in  $^{235}\text{U}$ , which constitutes less than 1 percent of natural uranium. It turned out also that a few other nuclides can undergo slow neutron fission, among which are plutonium ( $^{239}\text{Pu}$ ), whose half-life is  $2.44 \times 10^4$  yr, and  $^{233}\text{U}$ , whose half-life is  $1.62 \times 10^5$  yr. Both of these materials can be manufactured.



It was quickly realized after discovery of fission that these interactions offered a possibility for new energy sources. The mass difference between the uranium nucleus and the fission fragments indicates a large energy release ( $\sim 200$  MeV/fission). Equally important was the strong likelihood that neutrons are released as a result of fission, due to the high neutron-to-proton ratio in the heavy elements relative to the fragment elements in their stable state.

It was also quickly realized that fission fragments are highly radioactive, to the point of being a rich and varied source of nuclear transitions for experimental investigation.

Work followed on chain reactions which led both to power reactors and to nuclear weapons. The research was directed largely toward a) isolation of large quantities of  $^{235}\text{U}$ , b) production and study of the properties of  $^{239}\text{Pu}$ , c) experiments to determine the average number of neutrons emitted as a result of fission, d) construction of a prototype reactor, thus demonstrating a chain reaction, e) experiments to determine critical masses for  $^{235}\text{U}$  and  $^{239}\text{Pu}$  in bulk, and f) design work to ensure utilization of a substantial fraction of the fissile material in nuclear explosions. The weapon aspect of this work culminated in the "Trinity" experimental detonation in New Mexico in 1945 of a  $^{239}\text{Pu}$ -powered prototype weapon.

The potential hazard of radioactive fallout was recognized by scientists even before the Trinity shot at Alamogordo, New Mexico, July 16, 1945 [2]. In fact, elaborate precautions were taken to minimize the hazard. The device was detonated on a 100-ft tower to avoid having a large amount of the gravelly desert surface sucked up into the fireball. Soldiers as far away as Albuquerque, more than 100 mi distant from the burst point, were stationed to evacuate the civilian population in the event of radiological danger. Meteorological data were carefully analyzed, and the time and place of the shot were constrained

by the necessity for favorable weather conditions, so that radioactive debris would not be blown over nearby populated areas, and so that there was little likelihood of having a rain shower wash radioactivity out of the air.

After the Trinity shot, mobile monitors, in radio contact with chief radiologist, Stafford Warren, toured the New Mexico countryside seeking signs of fallout. Half an hour after detonation, it became necessary for observers to flee from the observation post 10,000 ft north of ground zero.

About three weeks after the Trinity shot, radioactivity due to fallout was discovered at a mill in Vincennes, Indiana, producing raw materials for photographic film manufactured by Eastman-Kodak.

It soon became clear, however, that the fallout hazard was not very great. Some cattle were grazing about 10 to 20 mi downwind from ground zero. The two bulls and approximately 40 cows suffered superficial burns from the radioactive ashes. The Atomic Energy Commission (AEC) rounded up the herd of Hereford cattle and had them sent to Oak Ridge National Laboratory (ORNL) for observation. The effect of the fallout was mainly on the hair and skin. The skin lesions healed and the hair grew back, but grey or white where it had been red. The cattle were subsequently bred, and the offspring were normal. The cows lived for some 15 years after receiving the fallout injury, which was mainly the result of beta-ray burns.

The two bombs detonated in Japan at Hiroshima and Nagasaki (August 1945) made the existence of nuclear weapons known to the world and had a profound and permanent effect on world attitudes. These were air bursts and did not generate significant local fallout.

AEC study of radioactive fallout continued during the latter 1940's and early 1950's, although fallout was not regarded as a major menace to civilian populations. The 1950 edition of the Effects of Atomic Weapons discusses

radioactive contamination (see ref. [3], sec. VIII), and includes discussions of high air bursts, low air bursts including a surface burst, underground bursts, and underwater bursts. In the case of a low air burst, the conclusion is that fallout would be more an inconvenience than a hazard, while for a surface burst, expectation of a serious hazard was recorded [3].

In a general way, these early discussions distinguished between "local" fallout contamination and the widespread contamination due to radioactivity carried by very small particles<sup>3</sup> traveling great distances. We refer to the latter as "world-wide" fallout. Local fallout, which is the main concern of this book, results from descent of relatively large particles, and is defined as that occurring during a time period of 24 hours following detonation. Distances traveled by the fallout during this period are largely determined by the wind velocities operative during the fall of the particles.

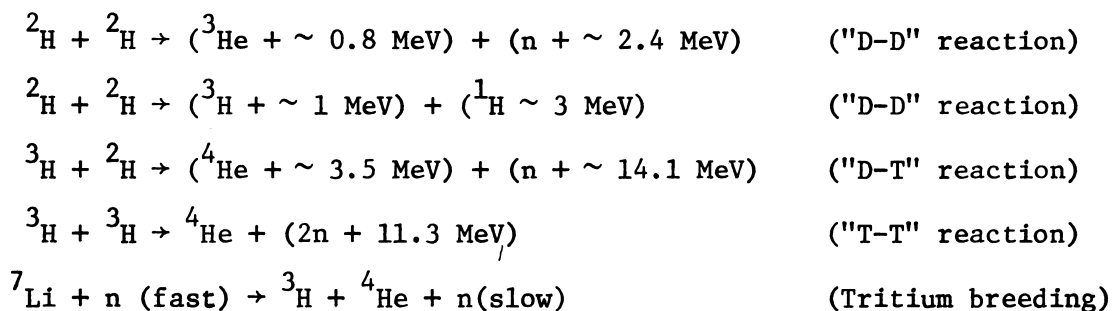
In addition, it was early appreciated that the main contributors to fallout radioactivity were a) the radioactive fission products, b) materials in the weapon which are rendered radioactive by neutron capture, c) materials in the ground similarly affected by neutron capture and drawn up into the cloud, and d) unreacted fuel.

In the late 1940's, interest developed in the feasibility of nuclear explosions in which detonation of fissionable material would produce the extremely high temperatures and densities for efficient energy production by thermonuclear reactions. The raw materials for this secondary process included deuterium ( $^2\text{H}$ ), tritium ( $^3\text{H}$ ), and perhaps lithium. The relatively

---

<sup>3</sup>See chapter II for more information on particle sizes. Large particles correspond to grains of fine sand, while small particles are more like dust particles.

short lifetime of tritium, 12 yr, makes necessary the manufacture of this isotope. The nuclear reactions considered most important are as follows:



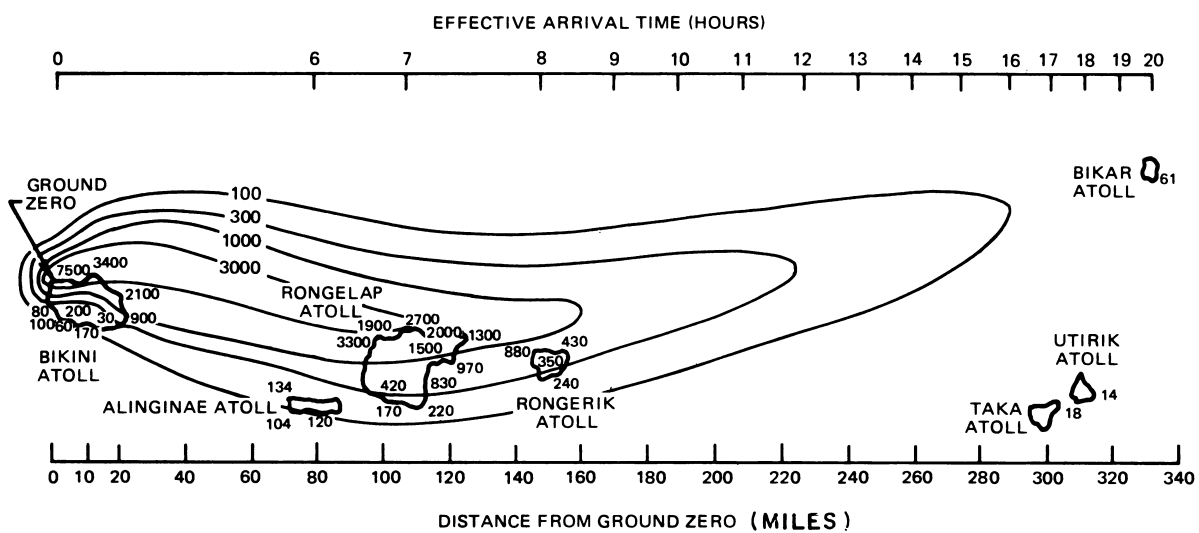
The result of intensive but highly classified (secret) research<sup>4</sup> on this subject was a successful thermonuclear explosion in 1952.

In the early 1950's there was work on explosions in which high-energy neutrons from the above "fusion" reactions were used to produce fission in ordinary <sup>238</sup>U, which occurs with neutrons above  $\sim 1$  MeV rather than with slow neutrons. Thermonuclear detonations produce relatively small amounts of fission products.

On March 1, 1954, an American task force detonated such a device on the surface at Bikini Atoll in the Pacific Ocean. This detonation, called "Castle Bravo," was almost 1000 times more powerful than that of the Hiroshima bomb. Two hours after the explosion, a fine ash began to fall on the fishing sampan Fukuryu Maru (Blessed Dragon) anchored 80 mi east of Bikini [4]. This ash continued to fall for several hours. Figure I.1 gives fallout radiation contours for this explosion. Unaware of the danger, the crew of the fishing boat took no precautions to wash the fallout particles from themselves or to protect their 40-ton cargo of fish. Two weeks later the Fukuryu Maru returned to Japan. Upon arrival, crewmen's hair was loose enough to be pulled out by

---

<sup>4</sup>The term "classified" in this context refers to a security classification of confidential or secret.



I.1 Estimated dose contours in roentgens, cumulative to 96 hours after the Castle Bravo test explosion [3].



the handful. They were also suffering from itch and skin blisters, and a few weeks later there was bleeding from the intestines, nose and gums. Seven months after exposure, one of the crew members, Aikichi Koboyama, died from causes either resulting from, or exacerbated by, his exposure to the radiation. After 10 months, the other crew members were alive, but they had still not fully recovered.

An unexpected wind change also caused appreciable fallout to be deposited on four inhabited Marshall islands east of Bikini: Ailinginae, Rongelap, Rongerik, and Utirik [5]. Greatest contamination was on Rongelap, 105 nautical miles east of ground zero.

Altogether, 239 natives of these islands received significant exposures to fallout radiation, together with 28 American servicemen on Rongerik. The Americans and the Marshallese were quickly evacuated and given proper decontamination and medical treatment at Kwajalein, about 150 mi south of Rongelap. Utirik islanders quickly returned to their homes. But it was necessary for the Rongelap islanders to be moved to temporary quarters on Majuro Atoll.

These events made it clear that in the case of large nuclear weapons, local fallout had to be considered as a potentially serious hazard. Major research programs were instituted or augmented by the AEC, various branches of the Department of Defense (DOD), other government agencies such as the National Bureau of Standards (NBS) and the U.S. Weather Bureau, and many university laboratories. Topics of intensive study included the formation and nature of fallout materials, effects of weather on their transport, anticipated and actual radiation fields, and biological effects on man, animals, and plants. These researches were largely conducted in conjunction with the test programs of the AEC, which utilized a substantial proportion of the available scientific research manpower in related areas.

Perhaps the best summary of the progress of these investigations is still that of the Congressional Hearings of the Joint Committee on Atomic Energy, June 22-26, 1959 [6].

## 2. Measurement of Gamma Rays

### a. Early Developments

In addition to gamma rays, the fission products and other constituents of fallout emit alpha and beta rays, and x-rays. The alpha and beta rays do not generate structure shielding problems because they are totally absorbed in, say, a pane of glass. X-rays contribute only in a minor way to shielding problems, and are usually included in computations of fallout gamma ray source spectra. Hence in what follows, reference is made only to gamma ray shielding aspects.

At the same time, we must note that serious problems do arise in connection with beta ray production by fallout components. These include ingestion hazards and biological damage occurring when fallout is in contact with, or in close proximity to the exposed skin. Ingestion hazards also involve alpha rays.

At the time of the first nuclear explosions, the capability for assessing gamma-ray hazards was already comparatively well developed. Because we will refer frequently in this book to gamma-ray "exposure," "spectra," "detector response," and other terms well established through long usage in the history of radiation measurements, we sketch here the development of the main types of measuring instruments.

The human eye unaided is not a useful detector for gamma rays and other penetrating radiations. Nevertheless, suitable detectors do exist, and have been used in the large effort, extending over this century, to explore both physical and biological properties of gamma rays. Photographic emulsions are affected, and this was, in fact, what called Roentgen's attention to x rays in 1896. It was determined shortly thereafter, a) that air is ionized in the presence of x rays, b) that x rays can burn the skin, and c) that certain

crystals scintillate when exposed to radiation. There were measurement techniques devised over the next 2 decades which used these effects, and there exist families of detectors today based on photographic film, air ionization, and crystal scintillation, as well as other known chemical and solid state effects [7]. Even skin-reddening (erythema) played an early role in dose measurement to humans.

Through the years, ionization of air has played the dominant role in measurement of radiation and in the definition of the units of measurement. Unlike photographic effects, air ionization follows rather simple laws, and its measurement with precision and reproducibility is not difficult. Despite this advantage, however, early attempts to gauge biological damage were based on the phenomenon of skin reddening because of the feeling that other biological effects must be in some relation to the one which was readily detectable. Accordingly the radiation biology literature of the 1920's frequently makes references to an "erythematous dose," which is that dose required to "redden the skin." Unfortunately, "reddening" could not easily be made quantitative, and there were substantial differences in the amounts of radiation assigned to the erythematous dose by different investigators [8].

Such arbitrariness in dose measurement and specification disappeared in the 1930's, due largely to the 1928 action of the International Commission on Radiological Units and Measurements (ICRU), which recommended use of the Roentgen as "the international unit of x-radiation."<sup>5</sup> At the same time, the ICRU recommended development of the free air ionization chamber as a primary standard of reference, with associated use of cavity ionization chambers which were calibrated in terms of the primary standard.<sup>6</sup> Within the energy

---

<sup>5</sup>For further discussion and definitions, see section III.F. The roentgen is a measure of the ions which can be produced in air.

<sup>6</sup>In cavity chambers, e.g., the familiar pocket dosimeter, electrons produced by gamma-ray interactions in the cavity wall are the agent giving rise to most of the ions measured. The principles are elaborated in section III.D. Free-air chambers are designed to measure all ions resulting from interactions in a known volume of air exposed to x rays or gamma rays [7].

range of x-ray sources in common use during the 1930's, the free air chamber has the capability of measurement of air ionization in terms of roentgens with an uncertainty of  $\sim 0.1$  percent. Development of cavity chambers as absolute, rather than calibrated, instruments took place during the 1930's and early 1940's [9], and was largely due to L. H. Gray. These instruments can likewise make measurements interpretable in terms of roentgens. And although in practice their uncertainty is perhaps 1 percent under ideal conditions, rather than 0.1 percent, they are more versatile and can be used for gamma-ray energies which are included in the fallout spectrum.

Thus, by the 1940's, when nuclear reactors and explosives were developed, some of the leading problems of practical radiation measurement were problems of instrumental design to a wide range of types of specifications. Rate-meters, and pocket chambers to measure accumulated exposure, represent a part of the product of this design effort.

More recent developments in dosimetry include the introduction by the ICRU in 1953 of the "rad," 100 erg/g, as the basic unit of energy absorption in a given medium. This unit did not displace the roentgen, since the latter air ionization unit was retained as a measure of the strength of the radiation field. A radiation field whose ionization in air would correspond to 1 roentgen would dissipate 0.87 rads in air, so the two units turn out to be comparable in many applications [10].

At the Fifteenth General Conference on Weights and Measures, held in June, 1975, at Paris, France, a new international (SI) unit for absorbed dose was proposed: the gray (Gy), corresponding to an energy deposition of one joule per kilogram:

$$100 \text{ rad} = 1 \text{ Gy} = 1 \text{ J/kg} \quad .$$

The term "dose" refers to energy absorption per unit mass of irradiated material, a quantity not easily measured directly. "Dosimeters" usually measure a related quantity and hence their measurements require suitable conversion.

#### b. Other Types of Detectors

For some purposes, photographic film has advantages that outweigh its main problem, which is the difficulty of interpreting and standardizing measurements based on the photographic effect. By standardizing film production and processing, as well as exposure techniques, it has been possible to make routine usage of films as dosimeters. This standardization effort occurred during the late 1950's and early 1960's, and was largely due to G. Ehrlich and K. Becker [7].

Geiger-Müller (GM) gas-filled counting tubes have been in use since 1908; but although they are very sensitive to the presence of radiation they have not played a strong role in gamma-ray dosimetry. The reason for this is largely that their response is quite different from that of ionization chambers; and it is not proportional to dose nor easily related to biological effects. Nevertheless, in addition to their ability to signal the presence of a radiation field, they also provide an estimate of the strength of a radiation field.

The principal difference between GM counters and ionization chambers is not the physical event which triggers the response, since GM counters are a type of ionization chamber. But in the case of GM counters a high voltage across the chamber results in a cascade amplification of the ionization due to strong collecting fields near a central wire which serves as the anode. The pulses which result are all equal in size if the voltage is high enough. But counters can be operated at lower voltages at which the pulse size is proportional to the size of the triggering event. Such "proportional" counters

combine the sensitivity of the GM counter with a type of measurement which can be interpreted similarly to that of the cavity ionization chambers [7].

Many specialized types of radiation detectors have been developed in recent years. Perhaps the most versatile, however, are the solid state detectors, represented by the use of the thermoluminescence effect. Thermoluminescent detectors (TLD's) must be calibrated, but they combine the reproducibility of the ionization chamber with the small-size advantages of the photographic film.

Few of the instruments thus far mentioned can be used to measure the photon energy distribution (spectrum) which characterizes a radiation field, although spectral information can be inferred from proportional counters. Spectral measurements have become routine with the development of multichannel pulse-height analyzers.<sup>7</sup> In addition, large single crystals which emit pulses of scintillation light of strength approximately in proportion to energy dissipation by individual photons, have been combined with photomultiplier tubes and multichannel pulse-height analyzers to provide spectral measurements.<sup>7</sup> In either case, conversion from pulse-height distributions to spectra requires a further mathematical analysis ordinarily called "unfolding." This is because a given pulse size can result from any of a band of photon energies, i.e. monoenergetic photons give rise to a pulse-height "distribution".

Most of the preceding discussion relates to measurement of beam intensities and characteristics. Another fundamental aspect of "dosimetry" is the determination of effects on biological systems, and their sensitivity to different components of radiation. Radiation biology studies over many decades have resulted in many generally accepted concepts of the action of radiation on cells. Section III.D introduces some aspects of this subject.

---

<sup>7</sup>In these instruments, photomultiplier tubes magnify the pulse size to produce effects measureable with ordinary electronic equipment; multichannel analyzers sort the pulses into "channels" according to size, thus producing "pulse-height" distributions.



### 3. Early Gamma-Ray Penetration Studies

The most basic law of gamma-ray penetration is the following: When slabs of material are interposed between a single-photon-energy source and a detector, addition of layers of equal composition and thickness will, under most conditions, reduce the detector response by roughly equal fractions. This "exponential" law of attenuation is discussed in detail in section III.A; and it has been known since 1896. More precisely, if monoenergetic radiation emitted by a source is confined to a narrow channel by collimation, as shown in figure I.2.a, then the detector response  $D$  is the following function of the thickness  $x$  of material between source and detector:

$$D = ke^{-\mu x}, \quad (\text{I.1})$$

here  $k$  is a proportionality constant, and  $\mu$  is called the linear attenuation coefficient and has units of reciprocal distance.

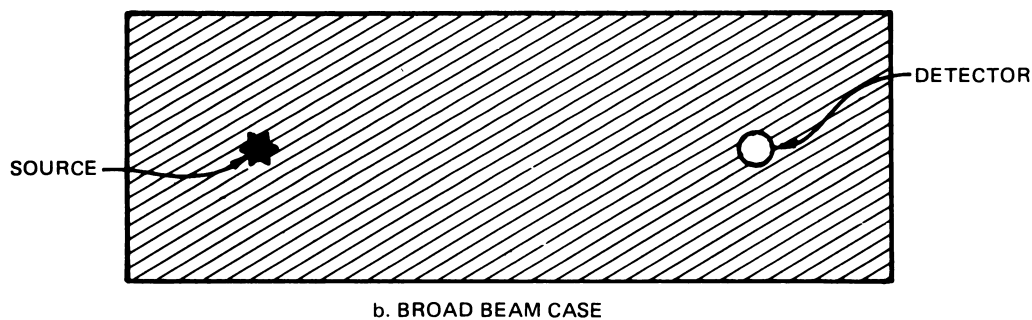
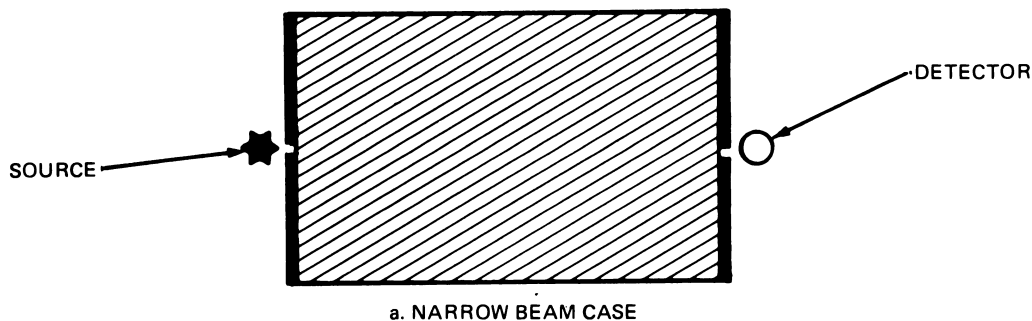
Much of the experimental work on gamma-ray penetration over the years has focused on determination of  $\mu(Z,E)$  for all atomic numbers  $Z$ , or at least those of practical use in radiation fields, and for a wide range of photon energies  $E$ .<sup>8</sup> Such data have been available with steadily increasing accuracy and completeness throughout this century.

Beginning about 1950, G. White at NBS and C. M. Davisson at MIT combined the available experimental data on attenuation coefficients with the available data from theoretical studies of gamma-ray interactions. The resulting tables, published in 1952, represented a major advance both in accuracy and in completeness [11-13]. These tables have since been revised and extended [14,15].

---

<sup>8</sup>The parameter  $\mu/\rho$ , where  $\rho$  is the density, traditionally is designated the mass attenuation coefficient, in units  $(\text{g}/\text{cm}^2)^{-1}$  or  $(\text{lbs}/\text{ft}^2)^{-1}$ . Correspondingly, the product  $x\rho$  measures the barrier thickness in mass/area units  $(\text{g}/\text{cm}^2)$  or  $(\text{lbs}/\text{ft}^2)$ . A variation of this product called the "effective mass thickness" will be later defined (sec. V.B).

The simple rule of eq (I.1) applies only to the "narrow-beam" case. If the collimators are not present, one has "broad-beam" attenuation (see fig. I.2). While the trend of eq (I.1) still describes in a rough way the attenuation of the detector response by interposition of layers of different thickness, quantitative work ordinarily requires better data than are thus provided. But there never has been a systematic experimental effort to provide fundamental broad-beam attenuation data for monoenergetic sources. Instead, most broad-beam experiments have been performed in nonideal configurations, and for radiation sources in which the spectrum has not been monoenergetic but has



I.2 A "narrow-beam" configuration (case a) excludes radiation not proceeding directly along the line from source to detector. Here the heavy barrier at the ends is to be considered impenetrable except at the pinholes, which must be much longer than their width, and "aimed" at each other. A "broad-beam" configuration (case b) detects also the scattered radiation from all directions.

contained a wide distribution of photon energies. Such broad-beam data are specific to the source spectrum and geometry used. These data have been useful for medical purposes, in connection with x-ray machines of standardized construction and therefore reasonably standardized source spectra [16,17].

Most broad-beam penetration data useful for shielding purposes have been calculated by numerical solution of integro-differential (transport) equations, with the use of tabulated data on the attenuation coefficient. This approach was made possible by the derivation, in 1929, of the law of scattering of photons by free electrons, by O. Klein and Y. Nishina [18].

Electronic computers became widely available only after 1950, and hence the extensive computations required to obtain accurate broad-beam attenuation data were not very feasible until about 1952. Nevertheless, remarkably successful approximations were developed by Hirschfelder as early as 1948 [19], by Faust in 1949 [20], and by Peebles and Plesset in 1951 [21]. The analytic theory of penetration trends for neutrons rather than gamma rays through very thick barriers was published in 1949 by G. C. Wick [22], and was applied shortly thereafter to gamma rays by U. Fano [23].

The "moments" method for solving transport equations, which is the procedure used to provide most of the fallout gamma-ray shielding data and which is described in detail in section IV.D, was developed by L. V. Spencer and U. Fano in 1951 [24], and was one of the first computational problems to which the early NBS computer, SEAC, was applied in 1952. Systematic tabulations of broad-beam data for monoenergetic sources, calculated jointly by H. Goldstein and J. E. Wilkins of Nuclear Development Associates and L. V. Spencer of NBS, were published in 1954 [25,26].

Statistical (Monte Carlo) methods for solving the transport equation were suggested by J. Von Neumann in the late 1940's, but their practicality only

began with the availability of large, high speed computers in the early 1950's. Many of the concepts used since that time were first suggested by either J. Von Neumann or by H. Kahn [27]. They are discussed in section III.E.

Other methods which likewise depend on computer capabilities have since been developed, but have not made much contribution as yet to fallout shielding problems.<sup>9</sup>

From the preceding short summary, it is clear that while capabilities for measuring gamma-ray dose with accuracy have been available since the 1930's, corresponding capabilities for performing accurate calculations date from the early 1950's. Thus at the time (1954) that the magnitude of the fallout hazard was first realized, both experimental and theoretical procedures for developing a shielding technology existed; but a directed effort was necessary to provide useful tools for general use in problems of locating or developing a shielded area, and in monitoring of fallout gamma-ray fields.

## B. DEVELOPMENT OF FALLOUT RADIATION SHIELDING METHODS AND PROGRAMS

### 1. Early Technical Work

The first serious attempt in this country to estimate the shielding properties of structures against fallout radiation seems to have been that initiated in 1952 at the Naval Radiological Defense Laboratory. The chief investigator was E. Shapiro, and the report issued in 1955 was classified "Confidential" until 1957 [28]. Navy interest in these matters apparently began with the problem of decontamination of the ships exposed to the underwater nuclear detonation at Bikini Atoll in 1946. A natural followup to the studies

---

<sup>9</sup> These include ( $S_n$ ) iterative methods which replace continuous direction and space distributions by a finite set of regions in space, and finite sets of directions. Also included are (multigroup) methods which replace continuous distributions by a finite set of energies.

contamination problems was the problem of fixed coastal installations which might be similarly contaminated, hence the initiation of this project before there was a general realization of the potential magnitude of the fallout hazard.

In Shapiro's study, as in all but one of the approaches to the structure shielding problem later developed, the fundamental data were obtained by computations rather than experiments. Shapiro used simple assumptions about the attenuation of fallout gamma rays. Because he did not have data on the spectrum emitted by fallout particles, he performed calculations for both 0.5 MeV and 1.25 MeV, with the thought that these would provide upper and lower bounds to the attenuation of the actual spectrum. For penetration data, he used a combination of exponential attenuation, inverse square law, and an assumed linear buildup factor to take account of single and multiple scatterings.<sup>10</sup> Attenuation data for a point monoenergetic source could be approximated from these factors; and by adding contributions from point sources located in different positions, he simulated the detector response due to fallout fields of infinite extent as well as fallout fields of simple shape and finite extent. The difference between fallout fields of finite and infinite extent gave data for fallout fields beginning beyond "cleared areas."

From these data Shapiro calculated detector response due to fallout on the roof of a structure, and due to fallout on the ground beyond a point such that a straight trajectory to the detector would not pass through both floor

---

<sup>10</sup> See sections III.A, IV.A, and IV.B, for more discussion of all these factors. The buildup factor is the ratio of the total detector response to that produced only by unscattered photons. Use of point source data to simulate different parts of a distributed source is commonly called the "point kernel" method. Shapiro's application was a simple example of what was later made much more elaborate [29]. (See also sec. VII.B.2.6)

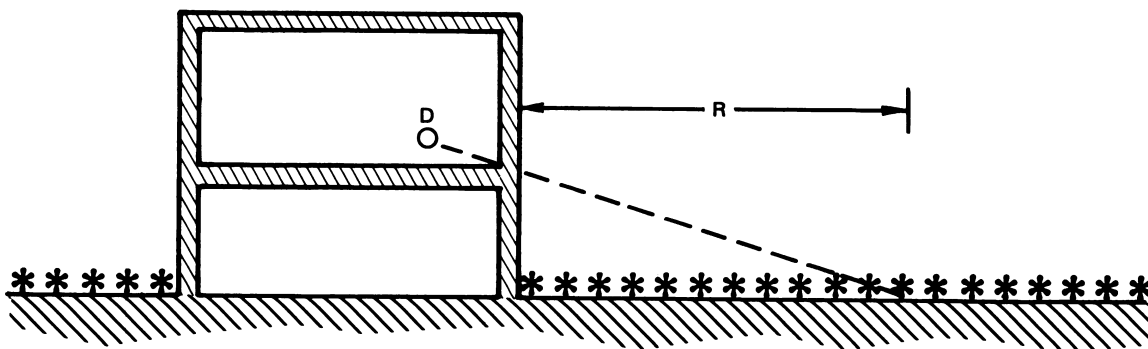
and exterior wall (see fig. I.3). The justification for that criterion depended on the heavy floors in the buildings Shapiro was concerned with.

There was no attempt (by Shapiro) to make calculations for basements which would take account of sources anywhere but on the roof; and there was no attempt to determine or make use of angular distributions of the radiation.

In addition to Shapiro's general study, there were also reports in this period of time on protection against initial radiations, which later turned out to be relevant to fallout shielding problems [30].

When news of the enormous hydrogen bomb explosions was released early in 1955, new efforts to determine the shielding properties of structures were stimulated. A second Navy project was established at the Naval Research Laboratory. The chief investigators were C. W. Malich and L. A. Beach.

The Federal Civil Defense Administration (FCDA), itself less than 5 years old, started two projects late in 1955, one at the NBS under L. S. Taylor [31], and the other, a part of Project Civil, at the Berkeley campus of the University of California, and including R. R. Putz and A. Broido as investigators. In



I.3 The radius  $R$  within which E. Shapiro assumed that fallout sources would not contribute to the response  $D$  of the detector, because of attenuation by the heavy floor [28].

addition, the work of Shapiro was modified and extended to civilian structures with support from the Office of Defense Mobilization (ODM), which had an interest in the shielding provided by relocation centers for a municipal population under an evacuation policy.

A concurrent effort in England was likewise initiated following the hydrogen bomb test of 1954. Unlike the studies in the United States, this development depended on experiments performed on existing British structures with  $^{60}\text{Co}$  sources. Experiments with  $^{60}\text{Co}$  were performed in England in 1955. Development of engineering procedures followed, and made use of these data [32].

Nearly all of these projects progressed to the point of at least preliminary reports in 1957. The Malich and Beach report, which was in part directed to the analysis of a standard barracks building for enlisted men, was issued in March of that year [33]. The ODM report became available in the middle of the year [34]. Putz and Broido's report, which described in general terms what has been called the "point kernel" method,<sup>10</sup> was published in December [35]. The British report, also published in 1957, gave a detailed procedure applicable to structures in general, which became known as the "points" method due to the assignment of percentage "points" to different parts of the structure in obtaining an overall measure of protection [36].

The project at NBS developed more slowly, partly because it was initially focused on obtaining and using a wide variety of data types, including radiation angular distributions. Angular information used in the other studies was limited by the approximation that photon trajectories be confined to a straight line from source point to detector point. It also was the intention at NBS to use realistic source spectra for the fallout; and these were not really available prior to 1958 [37]. "Mean" or "representative" energies were used

in the other studies for lack of more realistic spectra. For these reasons, usable data became available at NBS only late in 1957, and a full report was only begun at that time and was not published until 1962 [38].

Although there was not a great deal of collaboration among the different projects, many ideas that were in one study were either identical with, or very similar to those of another; they had been a part of the technical discussion of these questions for some years and are to be found in earlier and more fragmentary studies of the general shielding problem [30]. These include a) the assumption of a uniform fallout density, b) use of a reference dose at a height 3 ft or 1 m, with corresponding use of a ratio as an index of protection, c) simulation of earth by compressed air of equivalent density, and d) distinction between geometric and barrier types of radiation attenuation. The terminology of the 1957 ODM report, for example, is very similar to that in recent literature [34].

Some of the deficiencies in 1957 should also be mentioned. There was little available experimental information about spectra, and almost no experimental information about the penetration of fallout gamma rays. There were no unclassified experimental reports in this country on the shielding properties of buildings, and almost no classified information of this type. Finally, although procedures for making estimations of structure shielding were being developed, there was little or no experience with these procedures, and knowledge about them was limited to the very small number of people directly engaged in their development.

The problem of source spectra is discussed in detail in the next chapter. This type of information was eventually obtained both by experimental and by theoretical studies; but the former required development of a satisfactory technology of scintillation spectrometers and the latter required the accumulation



of an adequate data bank of nuclear transitions and their product radiations. All of these developments were actively being pursued during the middle and latter 1950's, hence the rather late date for good-quality spectral information.

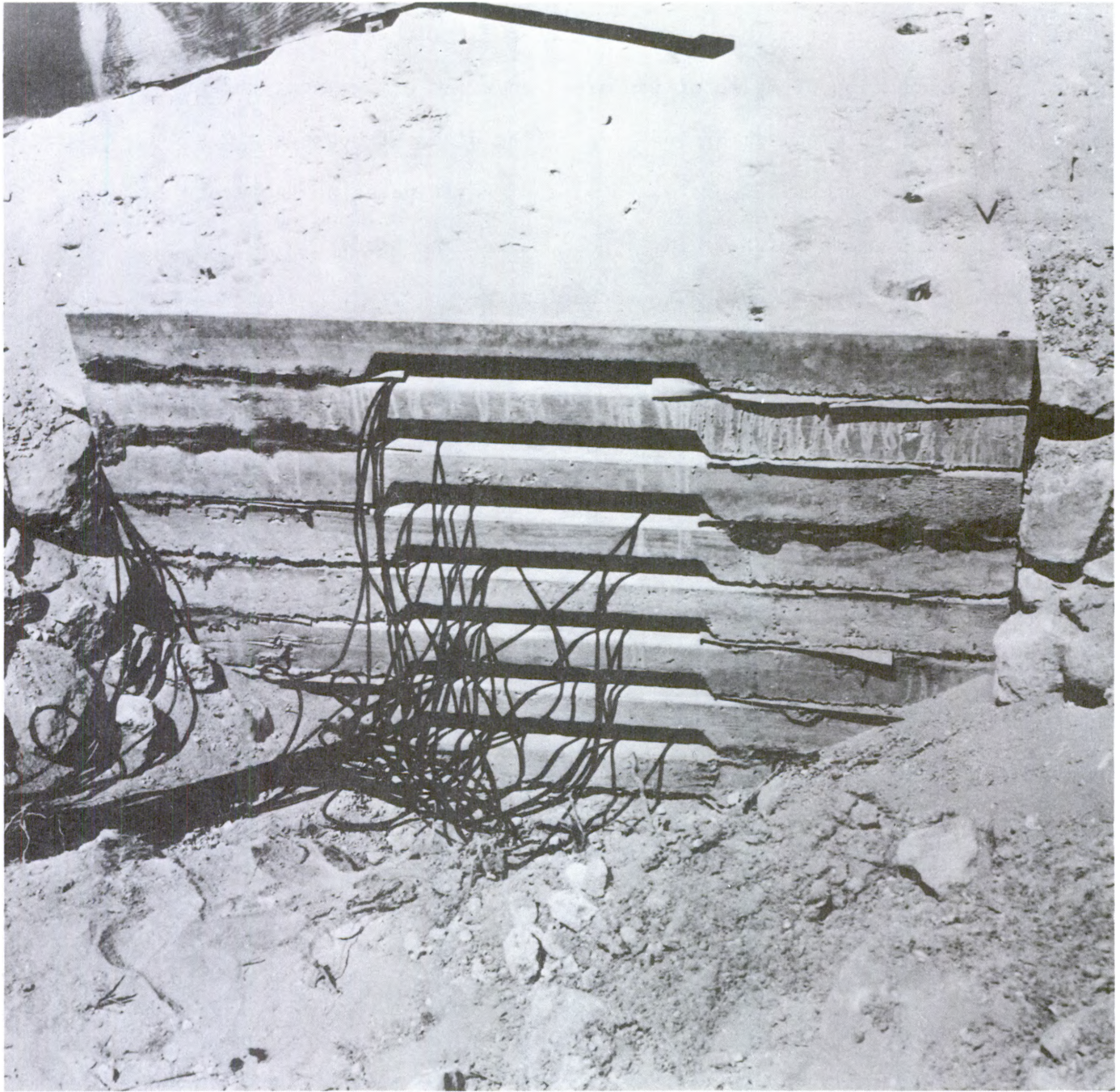
One might have expected the nuclear tests to include experiments in which buildings were exposed to fallout. But even though rather detailed wind data were available as input to a variety of fallout prediction methods, the time of detonation was usually fixed so far in advance that the likelihood of fallout occurring on a structure built for the purpose at the test site was rather small. Hence only the simplest of constructions was attempted. Perhaps the most productive shielding experiment was performed by F. Titus, who built a multilayer concrete sandwich which was twice exposed to fallout from detonations in Operation Plumbbob, in mid-1957 [39]. The data from this experiment were important in confirming general attenuation characteristics of the radiation; but the configuration was too idealized to be used to predict shielding by ordinary buildings (see fig. I.4).

## 2. Early Policy on Fallout Shelters (1951-1961)<sup>11</sup>

In May 1958 the Federal civil defense policy was changed in such a way as to focus attention on the design of fallout shelters. Prior to this, the Federal policy had stressed other things: After formation of the Federal Civil Defense Agency (FCDA) in 1951, there was a brief period in which the policy of the agency stressed the design of blast-resistant shelters. This was followed by a policy aimed at location and upgrading of existent blast-resistant shelters. In both cases the agency was reacting to the threat of the time, the Hiroshima-type weapon delivered by airplane.

---

<sup>11</sup>For a more detailed discussion, see references [46] and [94].



I.4 The multi-slab concrete sandwich for the experiments on penetration of fallout gamma rays, carried out by F. Titus as part of the Plumbob test series [39].

With the change of FCDA administrators in 1953, and the refusal of Congress to fund a program to support earlier policy, there was a shift of emphasis to evacuation of metropolitan areas in times of imminent threat. This was based on an assumed warning time of the order of hours and was recognized at the time as temporary, in view of anticipated developments in weapon delivery systems which would reduce the warning time.

Following the development of thermonuclear weapons, with accompanying regional and even country-wide fallout threats, as well as the development of missile delivery systems with much shorter warning times, there was a policy review by the Eisenhower administration. The policy declared in the spring of 1958 placed primary civil defense emphasis on the fallout threat, and essentially ignored the prompt effects. The policy specified that there was to be a) Federal encouragement of personally financed home fallout shelters, b) subsidy of shelter construction in new Federal buildings, c) pilot construction of prototype fallout shelters of various types and sizes, and d) public information on the hazard and on protective measures.

Attempts to implement the various parts of this policy began immediately, though the technology was not quite ready to support major programs of these types; and there resulted both a high degree of research and development activity and some important misapplications. Both are illustrated in the problem of defining a "fallout shelter."

*bull*  
The first criterion for a fallout shelter traces to an AEC news release early in 1955 stating that a cyclone cellar with an earth covering 3 ft thick would reduce the radiation level by a factor of about 5000, which would be completely safe, even in the most heavily contaminated areas [40,41]. Following this suggestion, the FCDA literature effectively defined a fallout shelter as having a "protection factor" (PF) requirement of 5000 or greater,

although the term protection factor<sup>12</sup> was not employed at the time [42]. This was still the official position in 1958 when the fallout policy was declared; and it is interesting to speculate about the influence of such a large PF on the formation of the policy. Certainly the design emphasis which resulted from the new policy featured heavy construction. Requirements for incorporation of fallout shelters in future Federal buildings stated that all exposed walls surrounding the shelter would have to be windowless and not less than 26 inches (~ 66 cm) of concrete. Overhead wall thickness had to total 20 inches (~ 51 cm) of concrete. These figures appear in the guidelines prepared later in 1958 for use by the Budget Bureau (now the Office of Management and Budget, or OMB) in making cost estimates for design of fallout shelters in new government buildings [43,44]. The resulting estimated costs were high, of course, and little construction of this kind was financed despite the policy statement, although other factors may have influenced the situation as well.

There was a feeling from the first that a PF of 5000 was too high; hence, despite the AEC pronouncement already referred to, and in view of the lack of other sources of guidance, the PF criterion of FCDA was lowered to 1000 later in 1958 [45]. But the research of the times was not particularly inhibited by the value of this criterion. Both shelter surveys of a pilot nature and design research of 1959 and 1960 covered levels of protection in which the official criterion represented almost an upper, rather than a lower, limit.

Eventually, studies were made, using hypothetical nuclear disasters, of the sensitivity of shelter effectiveness, estimated statistically for the

---

<sup>12</sup>A precise definition of "protection factor" is given in section V.A. For many practical purposes, this factor can be considered the ratio of dosimeter response in a "standard unprotected location" to dosimeter response in a "protected" location.



nation as a whole, to the shelter criterion [46]. As a result of these studies, the PF criterion was lowered late in 1960 to 100 [47]. But the public information policy, which had been vigorously pursued during the previous 2 1/2 years, had instilled the concept of great shielding thickness, requiring largely single-purpose construction. And this continued to be a predominant concept for the public for some years after it was recognized as inappropriate by the Office of Civil Defense (OCD).<sup>13</sup>

There was a later reduction of the PF criterion to 40 in 1961 or 1962, with the justification that the increase in the number of available shelters would more than compensate for the structures of this type which might be exposed to radiation fields so intense as to render the shelter inadequate [48]. New shelter construction was not being emphasized by this time.

The prototype shelter construction which was authorized and funded as a result of item c) of the Eisenhower policy statement on construction of prototype shelters, produced little of lasting value. This was due in part to the fact that many designs were outmoded when the PF criterion was lowered by a factor of 10 in 1960. On the other hand, the survey activity in support of the Eisenhower policy produced results of more lasting consequence. Between 1958 and 1961 a total of five pilot surveys were conducted in medium-sized metropolitan areas in different parts of the country to identify potential shelters and the type of equipment which they might need to function in this way. The first such survey was in Tulsa, Oklahoma, and it was underway before the end of 1958 [49].

The surveys required analysis procedures; and hence a simple set of calculations designated a "Guide for Fallout Shelter Surveys" was prepared

---

<sup>13</sup>The sequence of acronyms for the Federal Civil Defense Agency goes FCDA → OCDM → OCD → DCPA → FEMA.

for this purpose [50]. It was based on data and ideas available at that time from the NBS calculations. As already stated, shelter categories covered the complete range from thin-walled structures giving virtually no protection, to heavy structures giving protection factors effectively infinite. These surveys not only provided information on the distribution of shelter PF values existing in different parts of the country; they also represented a fund of experience on which the later and much more ambitious Federal surveys could be based.

### 3. Experiments on Buildings (1951-1961)

When we turn to experimental studies of structure shielding, we see that some of the earliest work was performed in England, in 1954. A. G. MacDonald reported studies in which a gamma-ray source was placed at many points in succession distributed over the area around, and on top of, a structure [51]. Similar experiments were performed by Stewart, Chisholm, Crooks, and Gale [52].  $^{60}\text{Co}$  gamma rays were used for the source in all cases.

Soon after the work just mentioned, experiments on buildings were performed in Canada by Cunningham, Wilson, Bury, and Flexman [53]. Figure I.5 shows how the radioactive source was deployed: In the foreground can be seen a pulley, similar to a movable clothesline. By moving the source of radiation at a constant speed along the pulley line and measuring the dose at points of interest, the experimenters could determine the response due to a line source. By summing the contributions from many such line sources, it is possible to simulate an area source.

Data provided by the British experiments were used in the development of the "points" method for estimating shielding by structures, and this method was then used in a survey directed by D. T. Jones of about 100,000 private homes. Results of this survey were published in November 1958, and provided a great deal of information about the shielding properties of British





I.5 An early experiment using a pulley-controlled source for measurements of the protection afforded by a (Canadian) house [53].



structures [54]. The whole effort was based on the assumption, later verified rather impressively, that <sup>60</sup>Co gamma rays were suitably representative of the fallout spectrum in their penetration and scattering properties.

When the 1958 Federal policy on fallout protection for the U.S. was announced, there were no published experimental data on the protective properties of U.S. buildings, light or heavy. The first attempt in this country to make measurements on buildings occurred in May 1958, at the AEC test site in Nevada, on structures which had been built there for other purposes [55]. This experiment was financed by AEC, and resulted from the personal interest in these matters on the part of AEC Commissioner W. Libby [56]. The project was carried out jointly by personnel from the Office of Civil and Defense Mobilization (OCDM),<sup>13</sup> Oak Ridge National Laboratory (ORNL), NBS, and other personnel on AEC contract. The technical program was under the general direction of J. Auxier of ORNL.

These "May" experiments<sup>14</sup> were the equivalent of the earlier British experiments. They were conducted primarily with point <sup>60</sup>Co sources on light structures. Because the development of analysis procedures was already in progress, some features were included in this series of experiments that were suggested by engineering problems already encountered. For example, in addition to the buildings, measurements were also carried out on a "phantom" structure with no walls or floors, as a comparison case. To speed up the collection of data, the point sources were embedded in pieces of plastic tubing, which were positioned to simulate line sources [55].

Although the "May" experiments represent the first attempt to measure the shielding properties of U.S. structures, there were similar but more general "blockhouse" studies already in progress at the Edgewood Arsenal in Maryland.

---

<sup>14</sup>We refer elsewhere to these experiments with this same designation, which was adopted by participants.



These experiments were supervised by R. E. Rexroad and M. A. Schmoke, at what was then the Nuclear Defense Laboratory (NDL) and is now a part of the Ballistics Research Laboratory (BRL). The different parts of the blockhouse were erected in turn, with measurements using  $^{60}\text{Co}$  and  $^{137}\text{Cs}$  sources being made at each stage [57]. This work was initiated in 1957, with the intention of providing data on "elementary structures" to serve as a check on the calculations, under circumstances that would permit close comparison between theory and measurement. Point sources were used in these experiments until the "tube" source became available.

A great advance in experimental technique occurred late in 1958 with the development by J. Batter and E. Clarke, of Technical Operations, Inc. (T/O), of the tube source. Instead of using many small radioactive sources tied together, or a single large source positioned many times, the Batter-Clarke tube source uses a single large source encapsulated so that it can be driven through a length of plastic tubing by water pressure. In this manner the tubing can be carefully positioned before the source is exposed. Then the source can be pumped out of its lead "pig," through the tubing, and back into the pig by remote control. The source usually moves at constant velocity, but the possibility of stopping, or changing velocity exists [58].

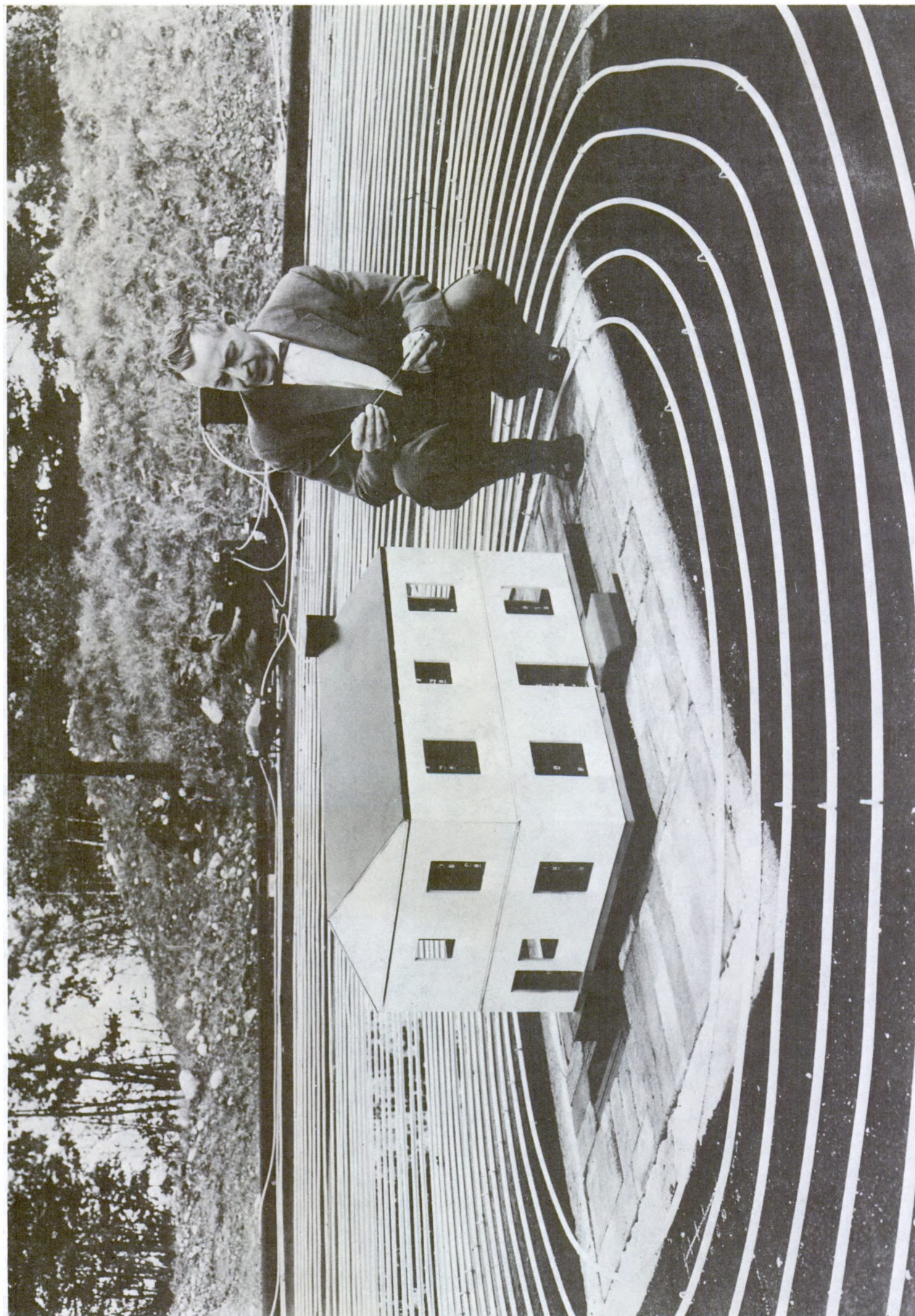
With this device, simulation of an area source requires only the positioning of the tubing along lines closely spaced relative to substantial variations of the detector response with the tube position. In an early experiment with steel scale models, which was designed to check the validity of the scaling concept, the tube was positioned in concentric rings about the model; but other configurations were used in other experiments (see figs. I.6 and I.7).

The tube source rendered measurements on large buildings really feasible for the first time, because of the tremendous simplification of procedure and



I.6 An early experiment using a circulating source in a plastic tube.





I.7 A circulating source arranged for measurements of penetration into a steel model.



the corresponding decrease in the time required for the measurements. Over the next few years, in addition to work with steel models, Batter and others at T/O carried out a series of measurements on large buildings which were in suitably isolated locations. One such building was a large, former army barracks on an island in Boston Harbor [58]. A second was the newly built AEC headquarters building in Germantown, Maryland [59].

A second series of experiments on large buildings, using the tube source, was carried out in 1961 by Z. Burson and others of Edgerton, Germeshausen, and Grier (EGG). These buildings were located in the Los Angeles area, and included various types of modern construction [60]. Another series of experiments on residential structures, using the tube source, was carried out in Oak Ridge, Tennessee, by T. D. Strickler and J. Auxier in 1959 [61].

Thus, by 1961, a fairly wide variety of experiments on both light and heavy structures existed, which included some experiments for such elementary configurations as a vertical wall, an overhead barrier, and a blockhouse [62].

To these data can be added the results of a program of experimentation on steel models, carried out by Batter and co-workers at T/O [63]. The scaling principle on which model studies are based is derived in section IV.B: by replacing concrete with steel, and by increasing the ratio of wall thickness to room width, one can get usable shielding data from experiments on models a few feet in extension, which can represent large and complex buildings. Problems of interpretation of such data exist and are discussed in detail in section VIII.D. One of the most serious of these problems is how to allow for radiation which penetrates through edges of apertures. Such "lip effects" do not scale in the way designated by the scaling theory. Another problem has been the required scaling of air density.

#### 4. Later Experiments (1962-1973)

Beginning in the early 1960's, the emphasis in experimentation shifted from attempts to make measurements on whole buildings, to measurements on components of buildings, in more refined tests of different analysis procedures.

In this direction, perhaps most important were early experiments by Schmoke and Rexroad at NDL (now BRL) on the shielding by vertical walls against radiation due to fallout on the ground [64]. These experiments were well underway by 1960; and in later experiments which made use of the tube source they performed related studies which included investigations of the "in-and-down" problem, in which radiation which has passed through such vertical walls encounters additional shielding by floors as it penetrates downward to the basement or lower floors [65].

Other studies of building components were carried out at a special facility designed for this purpose, the Radiation Test Facility at Ft. Belvoir, Virginia [66]. This was a three-story concrete structure, 26 ft by 38 ft (i.e., 7.9 m by 11.6 m), on a large concrete and gravel pad. The structure was designed so that floors and interior partitions of varying thicknesses could be inserted temporarily for purposes of studying interior shielding effects.

More elementary studies, such as measurement of effects due to an interface between regions of different density (e.g. earth and air) were also performed by C. E. Clifford of the Defense Research Board of Canada [67]. Clifford's many studies gave information on a) effects due to fallout fields of finite, rather than infinite extent [68]; b) effects due to foliar retention of fallout [69]; c) shielding effects due to the roughness of the ground [70,71], and other important phenomena (see chapter XI).

Studies of full-scale, complex structures were also further extended. At Kansas State University, measurements were made on a specially constructed blockhouse with basement [72]; and a lightweight building was also constructed whose floor could be raised or lowered, and which provided data on effects due to floor height relative to ground level [73].

#### 5. Continued Development of Engineering Procedures (1958-1961)

From the preceding sketch, it is clear that after establishment of the Federal policy in May 1958, many agencies besides the federal agency for civil defense participated in the development of analysis procedures for structure shielding. These included AEC, ORNL, NBS, the Department of Defense (DOD) laboratories, and private contractors working for OCDM and the Defense Atomic Support Agency, now the Defense Nuclear Agency (DNA).<sup>15</sup>

Beginning about mid-1958, the analysis procedures began showing a greater degree of sophistication. In July 1958, F. C. Brooks and others issued a report prepared for FCDA, giving general guidance on radiological defense planning [32]. An appendix to this report, "Shielding Factors and Shelter Protection from Fallout," presented general analysis procedures based on  $^{60}\text{Co}$  data and point kernel concepts. Procedures for estimating protection factors in basements were included, and these for the first time attempted to calculate the "in-and-down" contribution, due to radiation from the surrounding area which is scattered downward by vertical walls [74].<sup>16</sup>

---

<sup>15</sup>Correlation of much of the research work then and later was facilitated by the Advisory Committee on Civil Defense of the National Academy of Sciences. Formation of a Radiation Shielding subcommittee occurred at the request of OCDM in the fall of 1957, at a time when the pressure for technical backup to the Federal policy was particularly acute.

<sup>16</sup>The British "Points" method interpolated linearly between the value at the first floor level as calculated, and an assumed value of zero at the basement floor.

In 1959 Putz and others developed a computer program based on the point kernel technique described in their earlier report [35]. With this they analyzed the data from the "May" experiment [75]. They were able to reproduce data for above-ground locations fairly well, but had no procedure for estimating protection in basements.

Reasonable fallout gamma-ray spectra became available early in 1958, as will be discussed in chapter II. With these data, the program at NBS was very soon producing results of several types which could be used for purposes of shielding analysis. These included computer programs to generate penetration data for point and plane sources of various types, including angular distributions of the gamma rays. One particularly important type of data calculated was for penetration through a vertical wall, by gamma radiation originating on a horizontal plane, e.g., the ground.

The next step toward use of the data for applications was the development of procedures for analyzing many elementary types of structure. These procedures together with data and general definitions were described in a monograph by L. V. Spencer which was in circulation in draft form by late 1959 and finally published in 1962 [38].

A very early application required survey procedures, for which it was adequate to apply methods for elementary components in a rather simple way to the study of the complex structures existing. The first draft of such procedures for surveys was prepared by N. FitzSimons of OCDM late in 1958 [50], as previously mentioned. Shielding estimates obtained using these procedures were compared with data from the "May" experiment.

A full set of engineering procedures which could be used in design application was next developed by C. Eisenhauer and N. FitzSimons, using both computational data and available experimental data. The resulting manuscript

became the foundation for what is referred to in this text as the "Standard Method" [76].<sup>17</sup> The first drafts were circulated in 1960, but official publication was delayed until 1965 [77].

During this same period, but on a more basic level, the theory of gamma-ray penetration, as distinct from the many applications, was summarized in a monograph published in 1959 in the Handbuch der Physik, by U. Fano, L. V. Spencer, and M. J. Berger [78].

The data and concepts contained in the four manuscripts just mentioned are the basis for the bulk of the material in this book.

The question of validity of the procedures of the Standard Method has stimulated many more recent research projects whose results are also discussed in appropriate sections of this text. Concepts originally employed in the Project Civil method, the T/O method, Shapiro's methods, the British "Points" method, Malich and Beach's method, and others are used here without a detailed attempt in each case to trace the history of the idea. Numerical data from these reports have largely been superceded. Hence there is no attempt to make intercomparisons of calculations performed according to the different publications embodying these methods. Some procedures, such as the point kernel approach, have been used in more recent calculations [29] and will be explained later (see sec VII.B.2.b).

## 6. The Federal Surveys of Existing Fallout Shelter

While drafts of early versions of the Standard Method were still circulating, President Kennedy announced, on July 25, 1961, a civil defense program that strongly implemented the Eisenhower fallout-shelter policy, except that it shifted emphasis from individually financed shelters in homes, to shelters in existing public buildings. The heart of the program was a

---

<sup>17</sup>The Standard Method is described and explained in chapter VII, et seq., of this text.



nationwide survey to locate the shelter areas, with a followup program to mark and stock these shelter areas. Concurrently with this announcement, the Presidential Executive Order No. 10952 delegated authority for civil defense programs to the Secretary of Defense. An agency for this purpose was promptly established in the Department of Defense (DOD), and was entitled the "Office of Civil Defense" (OCD) [79].

To support the new program, a special congressional appropriation of \$200 million was obtained, and responsibility for organizing to accomplish this task was assigned to Steuart L. Pittman, a Washington, D.C., lawyer who was appointed Assistant Secretary of Defense. Assisting Secretary Pittman, and in actual direction of the task, was Paul S. Visher [80].

It was quickly decided that the task of analyzing a substantial fraction of the large buildings in the country required use of computer methods not only in the performance of shielding calculations but also in handling of data on the buildings. Accordingly, a computer program was prepared in the fall of 1961 by Spencer and Eisenhower to perform the shielding calculations [88]. This program, subsequently changed in several ways, was itself a modified version of the Guide for Architects and Engineers [81]. The data required for the calculations were arranged on FOSDIC<sup>18</sup> forms by a group working at NBS under D. Mittlemen, for processing by the Bureau of the Census. A large educational program was instituted by DOD to prepare representatives of engineering and architectural firms to select the buildings and gather data [80]. The total number of buildings examined in the surveys was about 350,000, distributed throughout the country. The survey was completed within a year at a cost of about \$60 million [82], most of which was paid to architectural and engineering firms for inspection of buildings and data procurement.

---

<sup>18</sup>Film Optical Scanning Device for Input to Computers.

This National Fallout Shelter Survey (NFSS) did not represent the first project to computerize shielding calculations. Earlier work in this direction had been done in Canada [83]. But the NFSS program gave greater stimulus to computerization of the analysis data and procedures as a natural engineering procedure. Further, the NFSS effort was followed by a continuing program to encourage incorporation of fallout shelter into the design of large buildings at minimal cost. This is known as "slanting" the construction. Slanted designs require specialized shielding calculations and an understanding of shielding principles by those members of architectural and engineering firms who perform the design work.

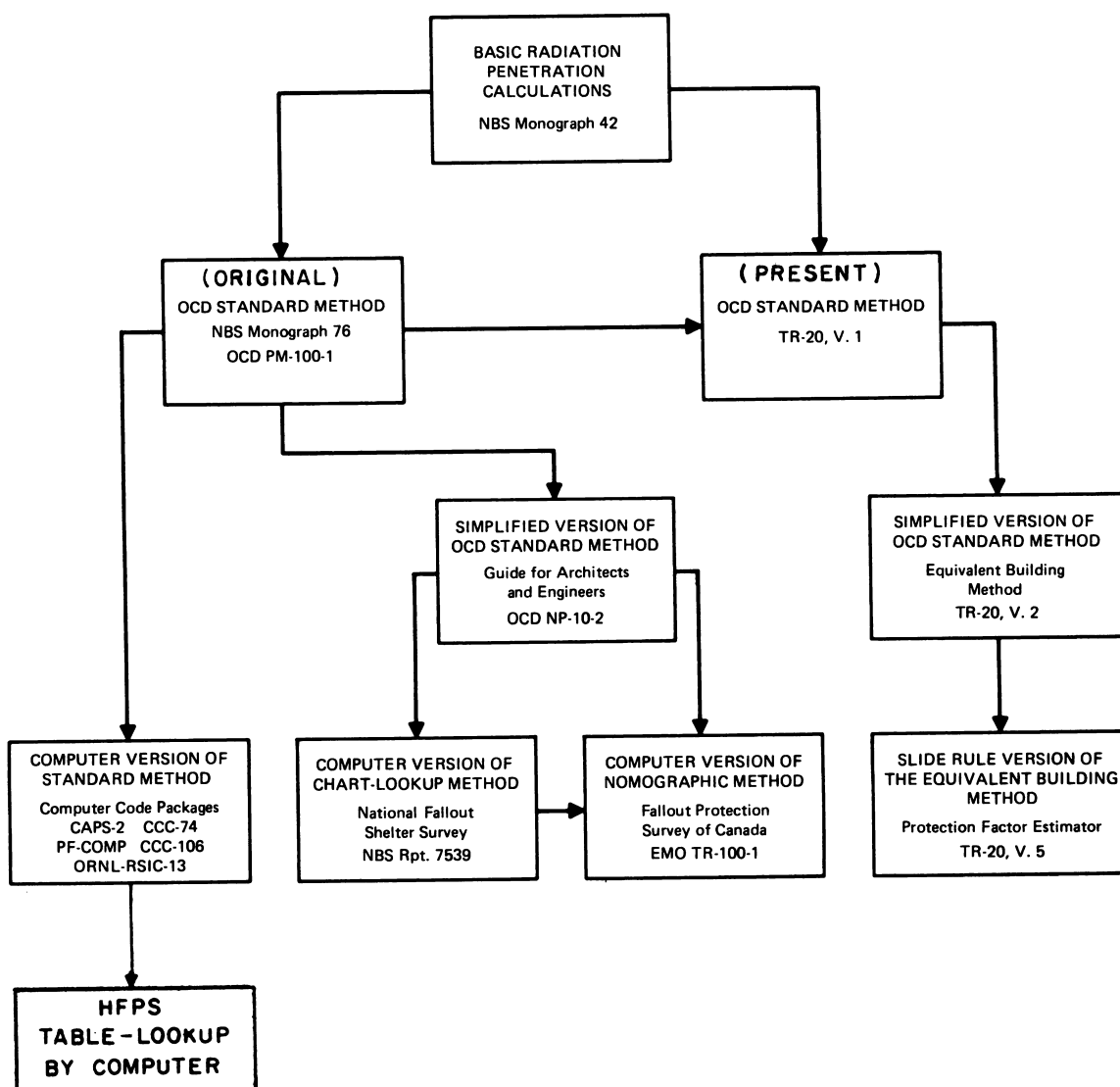
In 1962, J. C. LeDoux devised a method for analyzing buildings which was simpler than the Standard Method, and which he felt to be better than the existing Guide for Architects and Engineers [84]. With this beginning, simplified or modified methods were developed in some profusion. Also, the method used in the NFSS program did not correspond in all details to that in the Guide. But all simplified methods developed after 1958 were based on the Standard Method. Figure I.8 is a sketch relating the different techniques for making an analysis of structure shielding (see also the review by K. G. Farrell [89]):

a) NBS Monograph 42 contains data and procedures for analyzing elementary structures of 8 to 10 different types. In general, complex structures are viewed as an agglomeration of elementary structures, so that both data and methods of NBS Monograph 42 are basic to the Standard Method.

b) Two different documents presenting the Standard Method exist, of which PM-100-1 [77,85] represents the culmination of the original development, and TR-20, V. 1 [86] is largely a text further developing the method and presenting the materials in a style more suited to teaching. A version of this

text has been prepared by E. Bramlitt [87]. PM-100-1 has not been updated and now has mainly historical interest.

c) The version shown below PM-100-1 represents a basic simplification of the analysis which is designed for use in surveys, and which is considered to be satisfactory but not as accurate as the OCD Standard Method [77,86,87]. Computerization of the Standard Method itself has also been accomplished and will be discussed in chapter XII. The main code packages are listed in the box in the lower left corner of figure I.8.



I.8 Relationships between different sets of analysis procedures which have been used to estimate structure shielding against fallout gamma rays.

d) The Equivalent Building Method [84,90] and its slide rule version are shown as derived from TR-20 because of their pedagogic value, and also because they were part of the same effort toward suiting the procedures to design purposes of structural engineers and architects. But the Equivalent Building Method is also a valuable tool in making rapid, on-the-spot estimates of structural shielding.

The search for additional fallout shelter following the NFSS program led to a search for inexpensive ways to locate fallout protection in existing private homes. A requirement for such an effort is an analysis procedure which uses data provided by homeowners. Beginning in the fall of 1962, studies were directed to maximum simplification of the shielding calculations consistent with retention of a defensible degree of accuracy. It was found that an acceptable estimate could be made for home basements if six types of data were recorded, namely, presence of basement, amount of basement exposure, number of stories, type of wall constructions, type of roof, and the shielding provided by adjacent structures [91,92] (see chapter XII).

Simple questions covering these factors were developed for printing on a data processing card questionnaire, and a computer program was written which assigned the protection factor by a "table look-up" procedure (see fig I.8). With the help of the Bureau of the Census, a Home Fallout Protection Survey (HFPS) was carried out, beginning in 1965 with preliminary feasibility test surveys.

By the end of 1968, some 28 states, including the District of Columbia, had completed their surveys. About 10 million home basements had been analyzed, with PF-40 shelter spaces identified in about 500 thousand homes [93].

Since completion of the main HFPS effort, there has been study of the availability of protection below PF 40, in areas where little PF 40 or above construction exists, with the philosophy that information about the best available shelter in each locality should be available to local civil defense authorities.

#### 7. More Recent Trends

Federal funding of civil defense programs has been generally on the decline since the mid-1960's. As a result, the attention of DCPA turned to the least costly of the significant policies, i.e., emergency movement of a threatened civilian populace to safer locations. Such a policy carried with it many new requirements. Among those was a firmly established and usable information base about locations that were "safer" in regards to radiation protection as well as protection against other detonation hazards. Another concern was for shelter designs which could be improvised by a threatened and possibly displaced population. Interest also to some extent focussed on shelters resistant to blast and initial radiations, largely from the point of view of protection of maintenance personnel who would not be displaced even during a general evacuation.

One can infer from these developments that design and analysis of structures which protect against fallout radiations is a technology which can be expected to fluctuate strongly with federal policies, which are themselves a reflection of the sense of awareness of the public to the existence and possible threat of nuclear hazards.

A recent reorganization combined DCPA with other disaster-oriented federal organizations into a Federal Emergency Management Agency (FEMA). It is possible that this will lead to emphasis on a broader concept of shelter against radiation hazards, as other sources of large-scale radiation threats are given increased attention.

## References

- [1] Huddleston, C. M., A History of the Development of Fallout Shielding Technology, 95 pages, unpublished.
- [2] Smyth, H. D., Method of Assembly, 12.19, Atomic Energy for Military Purposes, p. 212 (Princeton University Press, 1948).
- [3] Glasstone, S., Ed., The Effects of Atomic Weapons, 456 pages (Atomic Energy Commission, Los Alamos Scientific Laboratory, Sept. 1950).
- [4] Nasaizumi, M., and Tsuzwki, M., Ed., Medical Science, Part 8, Research in the Effects and Influences of the Nuclear Bomb Test Explosions, Vol. 2, 1281-1284 (Japan Society for the Promotion of Science, 1956).
- [5] Conrad, R. A., Meyer, L. M., Sutow, W. W., et al., Medical Survey of the People of Rongelap and Utirik Islands Nine and Ten Years After Exposure Radiation, Brookhaven National Laboratory Report BNL 908 (T-371), 174 pages (May 1965).
- [6] Biological and environmental effects of nuclear war, Hearing Before the Special Subcommittee on Radiation, Joint Committee on Atomic Energy, 86th Congress, June 22-26, 1959, 966 pages (1959).
- [7] Attix, F. and Roesch, W., Instrumentation, Radiation Dosimetry, Vol. 2, 2d edition, 462 pages (Academic Press, 1966).
- [8] Weatherwax, J. L., Physics of Radiology, 204 pages (Paul B. Hoeber, Inc., 1931).
- [9] Attix, F. and Roesch, W., Fundamentals, Radiation Dosimetry, Vol. 1, 405 pages (Academic Press, 1968).
- [10] Physical Aspects of Irradiation, Recommendations of the International Commission on Radiological Units and Measurements, Nat. Bur. Stand. (U.S.), Handbook 85, Report 10b, 106 pages (March 1964).
- [11] White, G., X-Ray Attenuation Coefficients from 10 keV to 100 MeV, NBS Report 1003, 93 pages (1952).
- [12] Grodstein, G. (White), X-Ray Attenuation from 10 keV to 100 MeV, NBS Circular 583, 54 pages (1957).
- [13] Davisson, C. M. and Evans, R., Gamma ray absorption coefficients, Rev. Mod. Phys. 24, 79-107 (1952).
- [14] Davisson, C. M., Interaction of  $\gamma$ -radiation with matter, Ch. 2, 24-51, Gamma-ray absorption coefficients, Appendix 1, 857-874, Beta- and Gamma-Ray Spectroscopy, Siegbahn, K., Ed. (North-Holland Publishing Company, Amsterdam, 1955).
- [15] Hubbell, J., Photon Cross-Sections Attenuation Coefficients, and Energy Absorption Coefficients from 10 keV to 100 GeV, Nat. Stand. Ref. Data Ser., Nat. Bur. Stand. (U.S.), 29, 85 pages (Aug. 1969).

- [16] Kirn, F. S., Kennedy, R. J., and Wyckoff, H. O., The attenuation of gamma rays at oblique incidence, *Radiology* 63, 94 (1954).
- [17] Medical x-ray and gamma-ray protection for energies up to 10 MeV, Structural Shielding Design and Evaluation Handbook, NCRP Report No. 34, 117 pages (Mar. 2, 1970).
- [18] Klein, O., and Nishina, Y., Über die Streuung von Strahlung durch Freie Elektronen nach der relativistischen Quantendynamik von Dirac, *Zeitschrift f. Physik* 52, 853-868 (1929).
- [19] Hirschfelder, J. O., Magee, J. L., and Hall, M. H., The penetration of gamma radiation through thick layers. I. Plane geometry Klein-Nishina scattering, *Phys. Rev.* 73, 853-856 (1948).
- [20] Faust, W. R., Multiple Compton scattering, *Phys. Rev.* 77, 227 (1950).  
Faust, W. R., and Johnson, M. H., Multiple Compton scattering, *Phys. Rev.*, 75, 467-472 (1949).
- [21] Peebles, G. H., and Plesset, M. S., Transmission of gamma rays through large thickness of heavy materials, *Phys. Rev.* 81, 430-439 (1951).
- [22] Wick, G. C., On the space distribution of slow neutrons, *Phys. Rev.* 75, 738-756 (1949).
- [23] Fano, U., Penetration and diffusion of x-rays through thick barriers. II. The asymptotic behavior when pair production is important, *Phys. Rev.* 76, 739-742 (1949).
- [24] Spencer, L. V., and Fano, U., Penetration and diffusion of x-rays. Calculation of spatial distributions by polynomial expansion, *J. Res. Nat. Bur. Stand. (U.S.)*, 46A (Phys. and Chem), 446-456 (1951).
- [25] Goldstein, H., Wilkins, J. E., and Spencer, L. V., Systematic Calculations of gamma-ray penetration, *Phys. Rev.* 89, 1150 (1953).
- [26] Goldstein, H., and Wilkins, J. E., Calculation of the Penetration of Gamma-Rays, USAEC Report NYO-3075, 196 pages (1954).
- [27] Kahn, H., Random sampling (Monte Carlo) technique in neutron attenuation problems, *Nucleonics* 6, No. 5, 27-33, and No. 6, 60-65 (1950).
- [28] Shapiro, E., A Technique for Predicating Radiation Fields in Military Structures, Research and Development Technical Report USNRDL-TR-63, 120 pages (Sept. 26, 1955).
- [29] Degelman, L., Foderaro, A., and Kowal, G., Evaluation of the Shielding Characteristics of Structures for Simulated Residual Radiation, Report NUC-E 15, 62 pages (Penn. State U., Nov. 1963).
- [30] Berger, M. J., The Dose Received by Partially Shielded Gamma Ray Detectors, NBS Report No. 2902, 30 pages (Oct. 8, 1954).

- [31] Astin, A. V., Director, NBS, Letter to the Administrator, FCDA (Dec. 23, 1965).
- [32] Brooks, F. C., Callahan, E. C., Clarke, E. T., Batter, J. F., and Kaplan, A. L., Radiological Defense Planning Guide, Technical Operations Report No. TOI 58-26, 330 pages (July 31, 1958).
- [33] Malich, C. W., and Beach, L. A., Radiation Protection Afforded by Barracks and Underground Shelters, NRL Report 5017, 45 pages (Sept. 18, 1957).
- [34] Dhein, E., and Shapiro, E., A Method for Evaluating the Protection Afforded by Buildings Against Fallout Radiation, 49 pages (Office of Defense Mobilization, Sept. 1957).
- [35] Putz, R., and Broido, A., A Computation Method for Gamma-Radiation Intensity in the Presence of General Shielding and Source Configurations, 34 pages (Inst. of Eng. Res., Univ. of Calif., Richmond, Calif., Dec. 18, 1957).
- [36] Assessment of the Protection Afforded by Buildings Against Gamma Radiation From Fallout, 18 pages (Home Office, Scottish Home Dept., 1957).
- [37] Berger, M. J., and Lamkin, J. C., Sample Calculation of Gamma-Ray Penetration Into Shelters: Contribution of Sky-Shine and Roof Contamination, NBS Report 5297, 34 pages (May 16, 1957).
- [38] Spencer, L. V., Structure Shielding Against Fallout Radiation From Nuclear Weapons, Nat. Bur. Stand. (U.S.), Monogr. 42, 134 pages (June 1, 1962).
- [39] Titus, F., Penetration in Concrete of Gamma Radiation from Fallout, USAEC Report ITR-1477, 32 pages (Aug. 22, 1958).
- [40] Strauss, L. L., Fallout Pattern of 1954 Test in the Pacific, USAEC Statement, 6 pages (Feb. 15, 1955).
- [41] Shelter from Radioactive Fallout, Federal Civil Defense Administration (FCDA) Tech. Bulletin 5-2, 8 pages (Jan. 1957).
- [42] Fallout Shelter Criteria, FCDA Memorandum, 2 pages (May 12, 1958).
- [43] General Requirements for Incorporation of Fallout Shelter in Future Federal Buildings, Guide for Arch. and Eng., 6 pages (Dept. of Defense, Office of Civil Defense, Dec. 1961).
- [44] Incorporation of Fallout Shelters in Future Federal Buildings OCDM Memorandum, 2 pages (Sept. 29, 1958).
- [45] Inclusion of Fallout Shelters in Buildings, OCDM Advisory Bulletin No. 243, 7 pages (Aug. 24, 1959).
- [46] The Shelter Program in Civil Defense 1945-1969, 24 pages (Office of Civil Defense, 1969).
- [47] Inclusion of Fallout Shelters in Buildings, OCDM Advisory Bulletin No. 243 6 pages (rev. Oct. 10, 1960).



- [48] Basis of Policy for a Minimum Protection Factor of 40, OCD Tech. Memorandum 67-2, 7 pages (Sept. 1, 1967).
- [49] Annual Report of the Office of Civil and Defense Mobilization, Fiscal Year 1959, 63 pages (1960).
- [50] Guide for Fallout Shelter Surveys, OCDM Interim Edition, 73 pages (Dec. 1958).
- [51] McDonald, A. G., The Penetration of Gamma Radiation From a Uniform Contamination Into Houses: A First Report on Some Field Trials, Office Report CD/SA 69, 12 pages (Home Office, Scottish Home Dept., Jan. 1956).
- [52] Stewart, N. G., Chisholm, J. M., Crooks, R. N., and Gale, H. J., The Shielding Provided by a Brick House Against Gamma Radiation From a Uniformly Deposited Source. Experiments with Cobalt-60, Report FWE-104, 29 pages (Atomic Energy Research Establishment, Oct. 1955).
- [53] Cunningham, J. R., Wilson, R., Bury, F. A., and Flexman, J. K. M., Protection Factors for Houses Using Radioactive Sources, DRCL Report No. 260 (Nov. 1957).
- [54] Jones, D. T., Survey of the Protection Afforded in Private Homes Against Radiation from Fallout, Home Office Report CD/SA 89, 25 pages (Home Office, Scottish Home Dept., Nov. 1958).
- [55] Auxier, J. A., Buchanan, J. O., Eisenhower, C., and Menker, H. E., Experimental Evaluation of the Radiation Protection Afforded by Residential Structures Against Distributed Sources, Report CEX-58.1, 133 pages (Civil Effects Test Organization, Jan. 19, 1959).
- [56] Gallagher, G. R., Evaluation of Improvised Radiation Protection, private communication, 4 pages (Dec. 27, 1957).
- [57] Gordon, M. G., private communication, 5 pages (Nov. 5, 1956).
- [58] Clarke, E., Batter, J., and Kaplan, A., Measurement for Attenuation in Existing Structures of Radiation from Simulated Fallout, OCDM Report TO-B 59-4, 101 pages (Apr. 27, 1959).
- [59] Batter, J., Kaplan, A., and Clarke, E., An Experimental Evaluation of the Radiation Protection Afforded by a Large Modern Concrete Office Building, CEX-59.1, 69 pages (Civil Effects Test Organization, Jan. 22, 1960).
- [60] Burson, Z., Experimental Evaluation of the Fallout-Radiation Protection Provided by Selected Structures in the Los Angeles Area, CEX-61.4, 106 pages (Civil Effects Test Organization, Feb. 26, 1963).
- [61] Strickler, T., and Auxier, J., Experimental Evaluation of the Radiation Protection Afforded by Typical Oak Ridge Homes Against Distributed Sources, CEX-59.13, 51 pages (Civil Effects Test Organization, Apr. 14, 1960).
- [62] Status Report of the AD HOC Subcommittee on Radiation Shielding, Draft, 26 pages (National Academy of Sciences, National Research Council, Apr. 21, 1960).

- [63] Kaplan, A. L., and Koepp-Baker, N. B., The Use of Scale Models in Structure Shielding Experiments, Final Report, Technical Operations Report No. TO-B67-25, 116 pages (Apr. 21, 1967).
- [64] Schmoke, M. A., and Rexroad, R. E., Attenuation of Fallout Radiation as a Function of Concrete Blockhouse Wall Thickness, NDL-TR-43, 103 pages (Nuclear Defense Lab., Oct. 1963).
- [65] Schmoke, M. A., In-and-Down Scattered Radiation in a Simple Concrete Structure, Ballistic Research Laboratory Report No. 1665, 161 pages (Sept. 1973).
- [66] McDonnell, C., Velletri, J., Starbird, A. W., and Batter, J. F., Description, Experimental Calibration, and Analysis of the Radiation Test Facility at the Protective Structures Development Center, Report No. P.S.D.C.-TR-14, 86 pages (Conesco, Division of Flow Corp., Watertown, Mass., Sept. 1, 1964).
- [67] Clifford, C. E., Effects of interfaces on gamma shielding, Trans. Am. Nucl. Soc. 6, No. 1, 197 (1963).
- [68] Clifford, C. E., Dependence of Total Dose Rate and Skyshine Dose Rate on the Area of Contamination, Technical Memo. No. 104, 3 pages (Defense Research Chemical Labs., Ottawa, Canada, Mar. 1970).
- [69] Clifford, C. E., and Wait, G. D., Limitations on the Assessment of Hazard in a Fallout Field, Technical Note 66-3, 11 pages (Defense Chemical, Biological and Radiation Labs., Ottawa, Canada, Mar. 1970).
- [70] Clifford, C. E., Effects of the ground on the gamma dose from distributed cesium-137 sources, Can. J. Phys. 42, 2373-2383 (1964).
- [71] Clifford, C. E., Effects of Ground Roughness on the Gamma Dose From Cs-137 Contamination, Report No. 401, 16 pages (Defense Chemical Research Lab., Ottawa, Canada, Mar. 1963).
- [72] Kimel, W. R., ed., Radiation Shielding, Analysis and Design Principles as Applied to Nuclear Defense Planning, TR-40, 883 pages (Office of Civil Defense and Kansas State University, Nov. 1966).
- [73] Reynolds, R. S., Faw, R. E., and Robinson, M. J., A University Design Study of Reduction Factors in Typical American Houses With Fallout Shelters, Kansas State University Bulletin No. KEES-SR-92, 61 pages (Feb. 15, 1971).
- [74] The Calculation of Protective Factors of Buildings Against Gamma Radiation From Fallout, Preliminary Working Draft, 18 pages (Home Office, Scottish Home Dept., July 1959).
- [75] Putz, R., and Kuykendall, E. L., A Comparison of Computed and Experimentally Observed Intensity Levels for Various Gamma Radiation Source Distributions and Shielding Conditions in Residential Structures, Series 2, Issue 16, Contract No. CD-SR-58-40, 51 pages (Inst. of Eng. Res., Univ. of Calif., Berkeley, Calif., Feb. 12, 1959).
- [76] Design and Review of Structures for Protection From Fallout Gamma Radiation, OCDM Engineering Manual, Part A, 52 pages (Dec. 1, 1960).

- [77] Design and Review of Structures for Protection From Fallout Gamma Radiation, OCDM Report PM-100-1, Interim Edition, 121 pages (Office of Civil Defense, Feb. 1965).
- [78] Fano, U., Spencer, L., and Berger, M., Penetration and diffusion of x-rays, Handbuch der Physik, Encyclopedia of Physics, S. Flugge, Ed., Vol. 382, 660-817 (Springer-Verlag, Berlin, 1959).
- [79] Civil Defense-1961, Hearing Before a Subcommittee on Government Operations, House of Representatives, Eighty-Seventh Congress, Aug. 1-9, 1961, 554 pages (1961).
- [80] National fallout shelter program, 16th Report by the Committee on Government Operations, Union Calendar No. 738, House Report No. 1754, 97 pages (May 31, 1962).
- [81] Guide for Architects and Engineers, Fallout Shelter Surveys, 52 pages (Office of Civil Defense, Dec. 1961).
- [82] Civil Defense 1965, OCD MP-30, 114 pages (Apr. 1965).
- [83] Curry, R. B., An Engineer Looks at Fallout Shelters, 145 pages (Emergency Measures Organization, Ottawa, Canada, 1961).
- [84] Shelter Design and Analysis-Equivalent Building Method, Vol. 2, 57 pages (Office of Civil Defense, Feb. 1963).
- [85] Eisenhower, C. M., An Engineering Method for Calculating Protection Afforded by Structures Against Fallout Radiation, Nat. Bur. Stand. (U.S.), Monogr. 76, 20 pages (July 1964).
- [86] Shelter Design and Analysis-Fallout Radiation Shielding, TR-20, Vol. 1, 424 pages (Dept. of Defense, Office of Civil Defense, June 1968).
- [87] Bramlitt, E., Private communication (Oct. 1973).
- [88] Spencer, L. V., and Eisenhower, C., Calculation of Protection Factors for the National Fallout Shelter Survey, NBS Report 7539, 38 pages (July 3, 1962).
- [89] Farrell, K. G., Fallout Protection Survey of Canada-Computer Calculation Routines for the Pilot Survey of Fallout Protection in the Province of Alberta, EMO-TR-1, 31 pages (Emergency Measures Organization, Ottawa, Canada, 1964).
- [90] Shelter Design and Analysis-Equivalent Building Method, TR-20, Vol. 2, 67 pages (Dept. of Defense, Office of Civil Defense, Oct. 1964).
- [91] A Summary of the Methodology and Engineering Techniques Utilized in the HFPS System, Technical Report TR-45, 59 pages (Office of Civil Defense, June 1967).
- [92] Evaluation of Fallout Protection in Homes Program, EFPM, Status Report, 26 pages (Dec. 1965).
- [93] Annual Report of the Office of Civil Defense, Fiscal Year 1968, 140 pages (1969).

## II. PHYSICAL AND SOME BIOLOGICAL ASPECTS OF THE FALLOUT PHENOMENON\*

Studies of fallout gamma ray shielding are based on the spectrum emitted by fission fragments about 1 hour after the fission event. Many physical phenomena can modify the actual fallout gamma ray spectrum, so that it is in reality a function of position, time, and detonation parameters. While these complexities cannot be taken into account when one rates structures for their protective properties, an understanding of many aspects of this subject is desirable. For this reason the presentation in this chapter gives a much more extensive introduction than is required only to document the radiation source actually assumed.

We begin in section II.A.1 with a description of the fission process, because this serves as necessary background for the main body of information immediately following in sections II.A.2 and II.A.3, as well as useful background for much of the rest of the chapter.

### A. RADIOACTIVE DEBRIS FORMATION BY NUCLEAR BURSTS

#### 1. Introductory Description of Fission-Generated Nuclear Processes

After absorption of a neutron by a  $^{235}\text{U}$  or  $^{239}\text{Pu}$  nucleus, fission occurs extremely rapidly, so quickly as to be effectively instantaneous [1]. The nucleus normally breaks into two massive but unequally sized pieces. Because the original nucleus is relatively rich in neutrons, both fragments have too many neutrons to be stable; and there would usually be produced from one to several unattached neutrons as well, called fission neutrons.

The two fission fragments maintain their mass unchanged at later times;<sup>1</sup> hence the "fission yield curve," i.e., probability for formation of different

---

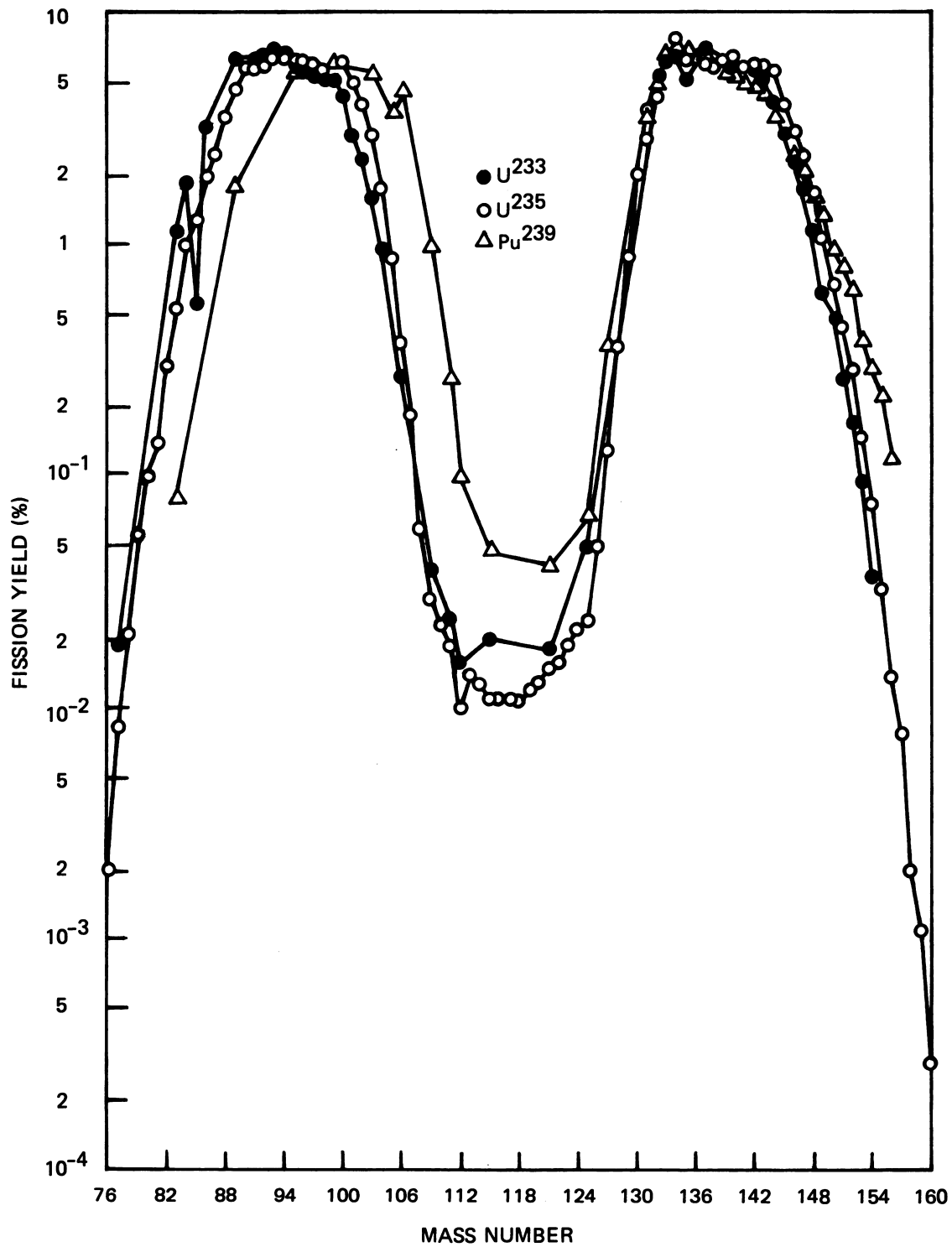
\*The physical properties of fallout, and the processes involved in its formation, have been described and analyzed in detail in the following useful summary report by Carl F. Miller, whose research has contributed extensively to this field: Biological and Radiological Effects of Fallout from Nuclear Explosions, Chapters 1 and 2, Stanford Research Institute, Project No. IMU-4536, March 1964.

<sup>1</sup>Delayed neutron emission does occur, but only for a few of the 800+ fission product nuclear states.

fragment masses expressed as yield ( $y^A$ ) divided by number of fissions, can be investigated with high accuracy. Figure II.1 shows the type of distribution revealed by these experiments (expressed in percent of fissions). Note that twice the midpoint atomic mass number ( $A$  about 116 or 117) is a little less than the mass number of the original nucleus ( $A = 233, 235$  or  $239$ ). For each heavy fragment one expects a corresponding light one; and, since they occur together, one expects a high degree of symmetry about a central value. The symmetry is not complete, because the number of neutrons emitted during fission can vary; for any fissioning isotope the "midline" varies according to the number of emitted neutrons, so that each curve shown can be viewed as the combination of several slightly different cases with different midlines.

In addition to differences shown with different isotopes, there are also changes in these curves due to changes in the energy of the captured neutron. These changes are likewise rather small except at high neutron energy; and they are in the direction of filling the central depression, as seen in figure II.1. Fission yield data have accumulated and improved over the years since discovery of the fission process. Recent summary papers include refs. [2-4].

The characteristic double-humps shown are found when a heavy nucleus with  $Z$  near 92 breaks into two pieces [5]. There have been many attempts to understand it: Early theory by Bohr and Wheeler considered nuclear stability to be determined by the interplay of nuclear charge and a kind of "surface tension" resulting from unbalanced nuclear forces at the surface [6]. But these simple "liquid drop" concepts have not led to a firm understanding of the asymmetry of the "mass yield" curves shown in figure II.1. This is now thought to be a consequence of the nuclear stability of the nascent fission fragments [7,8].



II.1 Yield data for several cases of nuclear fission [2].

For each atomic mass number ( $A$ ) in figure II.1, many nuclear charge values ( $Z$ ) are possible. Characteristic distributions of charge must result from the fission process; and these will differ according to the mass of the fission fragment. Much less is known about these fission-yield charge distributions than about the mass distributions, because the nuclear charges do not retain their value and cannot be readily measured during the short time interval before significant changes occur.

The changes in nuclear charge are the result of emission of beta rays. Each such process increases the nuclear charge of one of the fission fragments by unity and reduces the neutron excess. And the nucleus which results from beta decay would ordinarily be in an excited state and would rapidly drop to states of lower energy through emission of gamma rays.

Table II.1 is from a recent paper [60], and shows the evolution of fission product materials, with mass fixed and charges increasing with successive beta decays [9]. Each value of the mass characterizes a "chain" or a "family" of radioactive species; and each transition "arrow" is accompanied by emission of a beta ray followed by one or more gamma rays necessary to minimize energy of the product nucleus. Where there is a branching, as in the case of  $^{90}\text{Kr}$ , two different nuclear states are involved; and it is possible for a transition to occur between these two states. Several nuclides shown can produce delayed neutrons.

The mass number 95 is near the lower peak of the fission yield curve and 137 is near the upper peak [9]. The average yields for these mass numbers are over 600 per 10,000 fissions of  $^{235}\text{U}$ , induced by thermal neutrons.

The charges  $Z_i$  in a given mass chain represent different atomic species, with differing chemical properties. For example, krypton is a noble gas which does not easily enter into chemical combinations. But its daughter element, rubidium, is an alkali metal and extremely active chemically. Thus the





sequence of beta decays is accompanied by a series of changes in chemical properties. This vastly complicates the study of properties of fallout at different times following a nuclear detonation.

The beta-ray and gamma-ray emissions which accompany transitions between different nuclides constitute most of the radiation from fallout particles. The main additional component results from neutrons released in fission or fusion processes and later absorbed by nearby materials in the casing of the device, in the ground, or in objects near the explosion. These "neutron capture" interactions also produce unstable nuclei; and such nuclei achieve stability by interactions much like those of fission product nuclides, but usually with emission of excitation energy in the form of gamma rays or possibly a single beta-ray transition.

The fusion process does not itself produce long-lived radioactivity; but it does produce neutrons which can, through capture and fission processes, generate long-lived radioactive nuclei.

## 2. Nuclear Bursts and Fallout Formation<sup>2</sup>

The energy release in a nuclear detonation occurs during a time interval of the order of a tenth of a microsecond. In this extremely short interval, most fissions constituting the first stage of the explosion take place, with resulting formation of fission products, neutrons, and gamma rays. Within a somewhat longer interval the thermonuclear reactions take place, with accompanying release of fast neutrons which may then produce additional fission interactions. All this occurs before the material in the weapon has time to expand very much. As a result the prompt gamma rays which are emitted at the occurrence of fission can be largely absorbed in the weapon material if there is a heavy, non-reactive outer casing. Further, the

---

<sup>2</sup>See references [10-12] for additional information on this topic.

neutrons which are emitted by both fission and fusion processes are in part captured by the weapon material to form radioactive species which add to the radioactivity represented by the fission products.

Those neutrons which escape to the exterior air are mostly slowed down and captured within a distance of a few hundred meters, and in a time interval of less than a second. Capture of the neutrons by nitrogen nuclei in air molecules is immediately followed by emission of penetrating gamma rays with energies as high as 10.8 MeV, which represent an important pulse of radiation over approximately the same short time interval as that of the neutron transport.

If the explosion occurs on or near the surface of the earth, some of the fast neutrons are captured in the local constituent materials of the earth and form radioactive product materials, some of which have long lifetimes and which must likewise be added as a part of the total radioactivity produced by the explosion.

Thus, before the blast effects take place, fission products, neutron-induced radioactivity in the weapon materials, and neutron induced radioactivity within the air, earth, or other neighboring materials have been generated. Also, the prompt neutron and accompanying prompt gamma ray penetration within a distance of 1-3 miles has occurred. The material of the weapon, and any other nearby materials, have been vaporized.

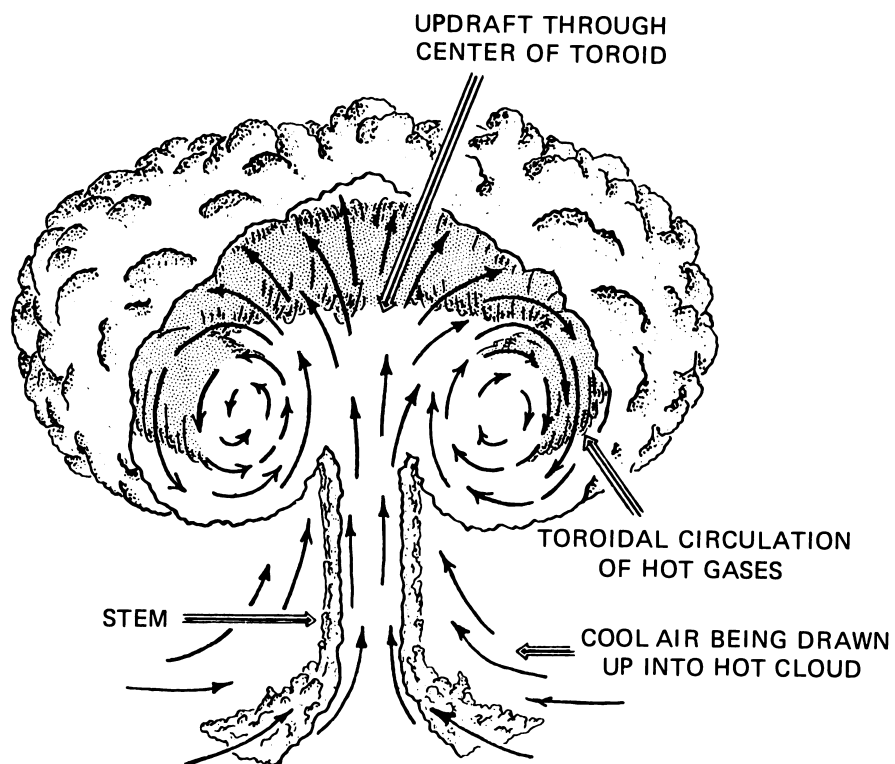
Following this very early stage, the fireball continues to expand and the shock front continues to move outward. If the detonation is near the surface of the earth, some material from the earth is vaporized, some is liquified, and some is fragmented; both vaporized material and melted or fragmented material would be "entrained" in the fireball and resulting cloud. The dynamics of this process are not known in detail, nor is it known what fractions of the entrained material are vaporized, melted, or fragmented.

The upward movement of material from below the burst point participates in the formation of toroidal circulation of a large vortex (see fig. II.2). Because the fireball material is very hot, there is a rapid movement upwards of this vortex, at the rate of several hundred miles per hour. During this upward development of the cloud, the fission fragments from the initial reactions are strongly radiating gamma rays, and constitute an intense, upward-moving source of fission-product gamma rays during the ten to twenty seconds which it takes the hot bubble to reach an altitude sufficient for complete shielding by air layers beneath. This fission-product radiation from the fireball penetrates outward to 1-3 miles, and should be considered as made up of one component which arrives before the pressure wave and a second component of comparable size which arrives after the pressure wave, and therefore after any associated destruction of buildings or building walls.

While this upward movement occurs, the material in the fireball is cooling. At the point of condensation, the vaporized material will, in the absence of unvaporized particles, condense into extremely small but very radioactive particles. In the presence of solid or liquid matter, the vaporized material will partly diffuse into the surfaces of the particles.

One sees therefore, that for explosions at high altitude which do not entrain unvaporized solid materials, only very tiny particles are produced; and there results little or no local fallout. But if large quantities of material from the surface of the earth are entrained in the fireball, there result a variety of much larger sizes comprising the particle "mass spectrum". The smallest components of this particle spectrum tend to remain airborne for long periods of time, but the larger components make up the local fallout and may leave the cloud before its toroidal motion ceases.

When vortices encounter an interface they spread outward: This effect occurs with the nuclear explosion at the tropopause, at which there occurs a



II.2 Cutaway showing artist's conception of toroidal circulation within the radioactive cloud from a nuclear explosion [12].

very rapid lateral growth of the "mushroom" part of the cloud. The form of the developing cloud includes a vertical "stem" as shown in figures II.2 and II.3, which consists of debris-laden air rushing in to fill the space left behind by the hot cloud.

Following stabilization of the cloud, the materials are subjected to gravitational fall and translation with the winds. The heavier particles tend to fall to earth relatively close to ground zero, depending on the maximum altitude to which the explosion carries them. These particles include unvaporized materials with a surface coating of radioactive materials, and glassy particles with radiative components uniformly distributed throughout.

The lighter particles are carried to greater distances and tend to have a more uniform distribution of radioactivity, resulting from a rather different history of formation. As already noted, the very lightest particles remain airborne, perhaps until "scavenged" by rainfall thousands of miles away.

### 3. Some Fallout Particle Characteristics<sup>3</sup>

#### a. Component Particle Types and Origins

In the case of detonations at sufficient altitude to prevent contact of the fireball with solid materials, commonly called air-bursts, the resulting condensation of vaporized materials of the device yields particles which are small and spherical, a few microns or less in diameter, and are composed of metal oxides; and the radioactive atoms which they contain are distributed throughout their volume [13].

In the case of surface bursts, however, most of the material results from fragmentation, liquifaction, or vaporization of the surroundings of the device at detonation. There is evidence for two rather distinct components to the radioactive particle population [13-16]:

---

<sup>3</sup>For a fairly recent discussion of many of these topics, see ref. [14].



II.3 Explosion of a nuclear weapon showing the toroidal structure of the fireball shortly after its formation. The fireball did not touch the ground, but the detonation was sufficiently low that dust dislodged from the surface by the blast wave is being sucked into the fireball [12].

1) crystalline particles which entered the radioactive cloud late enough to avoid the intense early heat. Such particles have radioactivity primarily distributed over their surface: and

2) glassy particles which have been subjected to heat at least sufficient for partial melting. Some of these particles have only been partially melted, and have accumulated radioactivity primarily on their surface. Others, tending to be spherical and very highly radioactive, apparently represent a coalescence of small and melted particles with vaporized material; these are thought to exhibit a volume distribution of radioactivity. They can be attached to unmelted particles.<sup>4</sup>

The crystalline particles are distributed about a peak at smaller particle diameter than the peak of the size distribution of the glassy particles. The largest particles appear to be agglomerates of small glassy particles [13,14].

While one expects the overall size distribution of fallout particles to reflect the natural distribution of the soil near the detonation, the effects of agglomeration, melting, and condensation modify this basic distribution. There is evidence that larger weapons produce smaller mean particle sizes than do smaller weapons [15-17], but data for large detonations pertain to coral rather than silicate soils.

Overall particle size distributions are difficult to measure and difficult to interpret. Among other problems is the evidence that different classes of component particles have different size distributions, as already mentioned [14,15]. Systematic studies of surface bursts over both silicate and coral soils show that particle frequency apparently varies approximately inversely

---

<sup>4</sup>Formation of these particles appears to be enhanced (a) by siliceous materials as compared with calcareous materials in the fireball, and (b) by larger energy/mass ratios for the fireball. (See [125], Report DC-FR-1219.)

with particle mass, for diameters from perhaps 1 micron to 70 or more microns [16]. Particles with diameters  $\gtrsim 40$  microns are particularly important for local fallout [15].

The particle size distribution, even for land surface bursts, is thus peaked at the small particle end; and small particles tend to remain suspended for long time periods. These small particles do not represent a large fraction of the total mass of local fallout except in the case of airbursts. But below 2-3 microns, the "specific abundance" (called "specific activity" in older literature), which is radioactivity in terms of an equivalent number of fissions required to produce the radioactivity, per gram of particle mass, increases sharply with decreasing particle size [13,18]. Hence the fraction of the total detonation radioactivity in these small particles tends to be much larger than the fraction of the total fallout mass. It is commonly assumed that only about 20% of the radioactivity remains suspended for long periods of time, while 80% of it descends with the local fallout in the first day. But the fraction of the radioactivity which remains suspended more than 24 hours has been estimated to be as large as 50%, and there is no consensus on most probable values [19].

A rule which has been found true in first approximation for land surface bursts is that the total amount of mass comprising radioactive particles is proportional to the total yield of the detonation, rather than to that part of the yield produced by fission [19]. On the other hand, the total amount of radioactivity in the debris of the explosion must be nearly proportional to the fission yield, because the fission fragments produce a much larger part of the residual radioactivity than do other components. Due to the problems of restricted information, one can only guess the magnitude of fission/fusion ratios in modern weapons. But the assumption of 100% fission can be used to provide a conservative estimate of the total amount of fallout radioactivity.



## b. Particle Activity - Fractionation

Studies of fallout particles have shown that radionuclide composition is not constant from sample to sample. That is to say, two nuclides produced by the fission process will be found in different ratios from one particle sample to another. This non-uniformity is referred to as fractionation.<sup>5</sup> That such a phenomenon is the expected result of nuclear explosions can be seen from a qualitative description of the physical chemistry of particle formation: At early times in the fireball, all materials of the weapon are in vapor form, as well as materials originally positioned near the burst point. Still other material may be entrained into the fireball and partially vaporized.

As the fireball cools, however, the vaporized material will begin to attach itself to particles not completely vaporized but perhaps melted, and it will also begin to condense into particles made up entirely from the vaporized matter. Those atoms which become attached to liquified particles may diffuse to the interior of the particles. One expects important features of these processes to be governed by the temperatures at which different elements condense, and at which attachment is preferred to a scattering collision with the surface of a particle. This differs from one atomic species to another, with noble gas elements preferring always to remain gaseous, alkali metals condensing at relatively low temperatures, and most other metals condensing at high temperatures. Elements with high condensation temperatures are referred to as refractory, while elements with low condensation temperatures are referred to as volatile.

In a general way, one expects refractory elements to become attached to fallout particles early in the history of the fireball, while volatile

---

<sup>5</sup>Note that fractionation occurs when the specific abundance of any product nuclide or chain differs from the value characteristic of the burst. Hence comparison of two nuclides is not an essential requirement for fractionation although it is common practice, as one notes in this discussion.

elements should become attached late. But this simple concept does not take account of the rapid changes of fission fragments from one element to another, which are caused by beta ray transitions. This brings about a far more complex time dependence in the attachment process of any given nuclide among the fission products, although it does not particularly affect attachment of nuclides which become radioactive through neutron capture.

A careful empirical study of fractionation was carried out by E. C. Freiling and reported in 1961 [20]. His procedure made use of a representative fission product chain composed mainly of refractory elements and a second representative fission product chain composed mainly of volatile elements. These two chains, which have mass numbers 95 and 89, respectively, are shown in table II.1. During the first 60 seconds, chain 89 is dominated by the volatile element krypton, while chain 95 consists of a sequence of refractory elements. In addition, both chains terminate in a long-lived isotope which can be readily studied.

Freiling's method was based on evaluation, through radiochemical studies, of the number of atoms  $a_i$  belonging to the  $i$ 'th mass chain, per gram of debris. Division of this number by the fission yield for the chain,  $Y_i$ , would give an estimate of the number of fissioning atoms required to produce the fragments terminating in the fallout mass chain under study, per gram of fallout material, i.e., the quantity termed specific abundance. In absence of fractionation the specific abundance should be the same for all mass chains.<sup>5</sup> Accordingly, the ratio of specific abundances for two different mass chains,

$$r_{i,j} = \frac{a_i/Y_i}{a_j/Y_j} , \quad (II.1)$$

measures degree of fractionation, expressed by difference from unity. In particular, one expects fractionation effects to appear prominently in  $r_{95,89}$ ,

which compares refractory with volatile chains. Values of  $r_{95,89}$  have indeed been found to vary by as much as factors of 50-100 from sample to sample.

The main result of Freiling's study was a demonstration that other radioactive mass chains could be characterized with a high degree of confidence by the empirical expression<sup>6</sup>

$$r_{i,89}^j = A_i (r_{95,89}^j)^{B_i}, \quad (\text{II.2})$$

where the superscript  $j$ , which is usually omitted, refers to the  $j$ -th sample of fallout, and where  $A_i$  and  $B_i$  are constants characteristic of the  $i$ 'th chain. For many chains which are comparatively refractory,  $B_i$  has a value near unity and  $A_i$  is of order of magnitude unity. This means a basically linear behavior which was noted earlier by Stevenson [20]. There is comparatively little fractionation in the case of these similar chains. Hence fractionation can be viewed as largely due to the special characteristic of a more limited number of volatile chains.

These results give a rather simple way of describing most of the data on fractionation; but  $r_{95,89}$  varies from sample to sample and from shot to shot, and these variations must also be understood. Further, possible differences between coral and silicate soils must be kept in mind.

A theory of fractionation was first attempted by C. Miller in 1960 [21]. He assumed that fallout particles were molten above 1400°, and that a volume distribution resulted from ideal dilute solutions of fission products acquired above that temperature, while only surface deposition could occur below 1400° C. Miller made use of the populations of chain member elements as a function of time in estimating distributions of nuclides in molten and gaseous phases as a function of time. Radioactive materials remaining in vapor state below the

---

<sup>6</sup>See also an alternate expression later proposed by Heft [13] and given in eq (II.14).

freezing point of the particles were assumed to condense rapidly on surfaces as a mixture not subject to further differentiation except that decay chain daughters of rare gases would continue indefinitely to condense at the rate formed.

A model due to Korts and Norman [22], emphasized condensed state diffusion inward from fallout particle surfaces by fission products, during the cooling process. Much work to support these models was also performed by Norman and co-workers [23,24] and by Adams, Quan and Balkwell [25], by improving the data base for the temperature-dependent systematics of condensation on surfaces followed by diffusion inward according to surface conditions.

While these concepts and data open the possibility of basic quantitative studies of the formation of radioactive fallout particles, the subject is complex and our understanding remains in a rudimentary state.

Section II.C.1 contains further discussion of fractionation.

#### B. INTENSITY OF FISSION PRODUCT NUCLEAR ACTIVITY

##### 1. Theoretical Procedures for Investigating Activity of Fission Products

Gamma rays and beta rays emitted by fission fragments can be studied both experimentally and theoretically. Experimental studies involve pulsed or short time-interval exposure of uranium or plutonium to neutrons to generate the fission fragments. Detectors of known efficiency then measure the radiations emitted in other short time intervals as the fission products age. These detectors may count events, or they may measure the energy of the emitted radiation.

In the 1940's and early 1950's, experimental results constituted the primary source of information on the total activity of fission products; and this is still the case for times following the fission process up to perhaps a minute. But for long times after fission, the theoretical studies have long since developed to the point that experiments have assumed the role of

benchmark tests for the calculations. Hence our concern for times following fission of the order of hours or greater leads to a greater preoccupation with the calculations.

Theoretical studies require a large data base on the fission process: The beta ray transitions, and the nuclear level systematics of several hundred isotopes. A table published in 1959 by R. Björnerstedt (table II.2) shows how the data base broadened during the 1950's from 24 nuclides to over 100 [26]. Data on fission yields and on gamma rays emitted has likewise improved.

Requirements for three basic types of information are clearly exhibited in a formal statement of the equations to be solved and the integrals which must be evaluated: Let  $N_n^A(t)$  be the number of atoms of charge  $Z_n$  and atomic mass number  $A$  at time  $t$  after fission, where  $n = 1, 2, \dots$ , and  $Z_1$  is the lowest value of  $Z$  having significant yield. Also, let  $\lambda_n$  be the corresponding decay constants, which are reciprocals of mean lifetime (i.e., the half life divided by  $\ln 2$ ). Finally, let  $Y_n^A$  be the fission yield of the nuclide. Then the following Bateman equations [27] must be solved for each mass value and simultaneously for all  $Z$  values of the chain  $A$  to determine  $N_n^A(t)$  for each  $Z$ :

$$\frac{dN_n^A}{dt} = -\lambda_n N_n^A(t) + \lambda_{n-1} N_{n-1}^A(t) + Y_n^A \delta(t) \quad , \quad (\text{II.3})$$

where the Dirac function  $\delta(t)$  is of unit strength, concentrated at  $t = 0$ . The first term on the right side of the equation expresses losses through decay of the species  $N_n^A$ , while the second (positive) term expresses gains through decay of the parent nuclide  $N_{n-1}^A$ . The last term gives the direct production of the nuclide  $N_n^A$  at the time ( $t = 0$ ) of the fission event.

These conservation equations have an elementary solution in closed form:

Table II.2 Publications as of 1959 giving activity and yield data for simultaneous fission of a mass of fissionable material [26]. Reference numbers are those of [26].

Reference	Published	Fission	S or C	1 or 2	Time	Yields	Decay data	Comments
Hunter, Ballou [4]	1949	$U^{235}, n_{th}$	S	1	1 s-100 y	1948	1948	Only total decay. No $\gamma$ -spectra.
Howlett, Josephs, Rennie, Story [5]	1950	$U^{235}, n_{th}$	S, C	1, 2	1 d-1000 d	1950	1950	Only total $\beta$ - and $\gamma$ -energies are given. No $\gamma$ -spectra. ( $U^{235}, n_f$ ) is briefly considered.
Faller, Chapman, West [6]	1952	$U^{235}, n_{th}$		1				Reference not available.
Heiman [7]	1952	$U^{235}, n_{th}$	S	2		1948		Reference classified. Based on (4).
Thornton, Houghton [8]	1953	$U^{235}, n_{th}$	S, C	1	0-100 y	1946	1946	Only the total decay rate is given.
Moteff [9]	1953	$U^{235}, n_{th}$	C	1, 2	3 h-10 d	1951	1952	Seven gamma energy groups. 24 nuclides considered.
Clark [10]	1954	$U^{235}, n_{th}$	C	1, 2	3 h-3 y	1954	1954	Seven gamma energy groups. Extension of (9).
Heiman [11]	1954	$U^{235}, n_{th}$	S	2		1948		Reference classified. Based on (4).
Björnerstedt, Löw, Ulvönäs [12]	1955	$U^{235}, n_{th}$ $Pu^{239}, n_{th}$	S	1, 2	1 h-3 y	1951	1954	30 gamma energy groups. 45 nuclides considered.
Frederick [13]	1955	$U^{235}, n_{th}$	C	1	14 d-420 d	1954	1954	No $\gamma$ -spectra.
Bolles, Ballou [14]	1956	$U^{235}, n_{th}$	S	1	0 s-550 y	1951	1953	Extension of (4).
Miller [15]	1957	$U^{235}, n_{th}$	S	2	45 m-300 y	1951	1953	Based on (14). No $\gamma$ -spectra.
Dillon, Burris [3]	1957	$U^{235}, n_f$ $Pu^{239}, n_f$	C	1, 2	200 d-10 y	1955	1955	Only total $\gamma$ -decay is given.
Löw, Björnerstedt (I)	1957	$U^{235}, n_{th}$	S	1	1 h-100 y	1957	1956	Extension of (12). No $\gamma$ -spectra.
Blomeke, Todd [16]	1957-1958	$U^{235}, n_{th}$	C	1, 2	25 d-30 y	1955	1955	4 gamma energy groups. 112 nuclides considered.
Prawitz, Rydberg [17]	1958	$U^{235}, n_{th}$	C	1	20 d-15 y	1957	1957	No $\gamma$ -spectra.
Perkins, King [18]	1958	$U^{235}, n_{th}$	S, C	1, 2	100 s-3 y	1957	1957	7 gamma energy groups. 110 nuclides considered.
Scoles [19]	1958	$U^{235}, n_{th}$	C	1, 2	1 d-400 d	1957	1957	Extension of (10).
Miller, Loeb [20]	1958	$U^{235}, n_{th}$	S	2				6 gamma energy groups.
Prawitz, Löw, Björnerstedt [III]	1958	$U^{235}, n_{th}$	C	2	20 d-15 y	1958	1958	Reference not available.
Knabe, Putnam [21]	1958	$U^{235}, n_{th}$	S, C	2	1 s-3 y	1957	1957	15 gamma energy groups. 73 nuclides considered.
Leipunskii [22]	1959	$U^{235}, n_{th}$ $Pu^{239}, n_{th}$	S	1, 2	1 h-100 y	1956	1956	Based on (17).
Nelms, Cooper [23]	1959	$U^{235}, n_{th}$	S	2	30 m-120 y	1951	1957	12 gamma energy groups. Extension of (18).
Present work (Björnerstedt)	1959	$U^{235}, n_{th}$ $U^{235}, n_f$ $Pu^{239}, n_f$ $U^{238}, n_f$ $U^{238}, n_{14}$ $U^{235}, n_{14}$	S	2	1 h-100 y	1959	1959	3 gamma energy groups.
								22 gamma energy groups. 128 nuclides considered. Based on (14).
								50 gamma energy groups. 118 nuclides considered. Based on I. Extension of III.

$$N_n^A(t) = \sum_{k=1}^n \eta_{nk} e^{-\lambda_k t} \quad (\text{II.4})$$

where

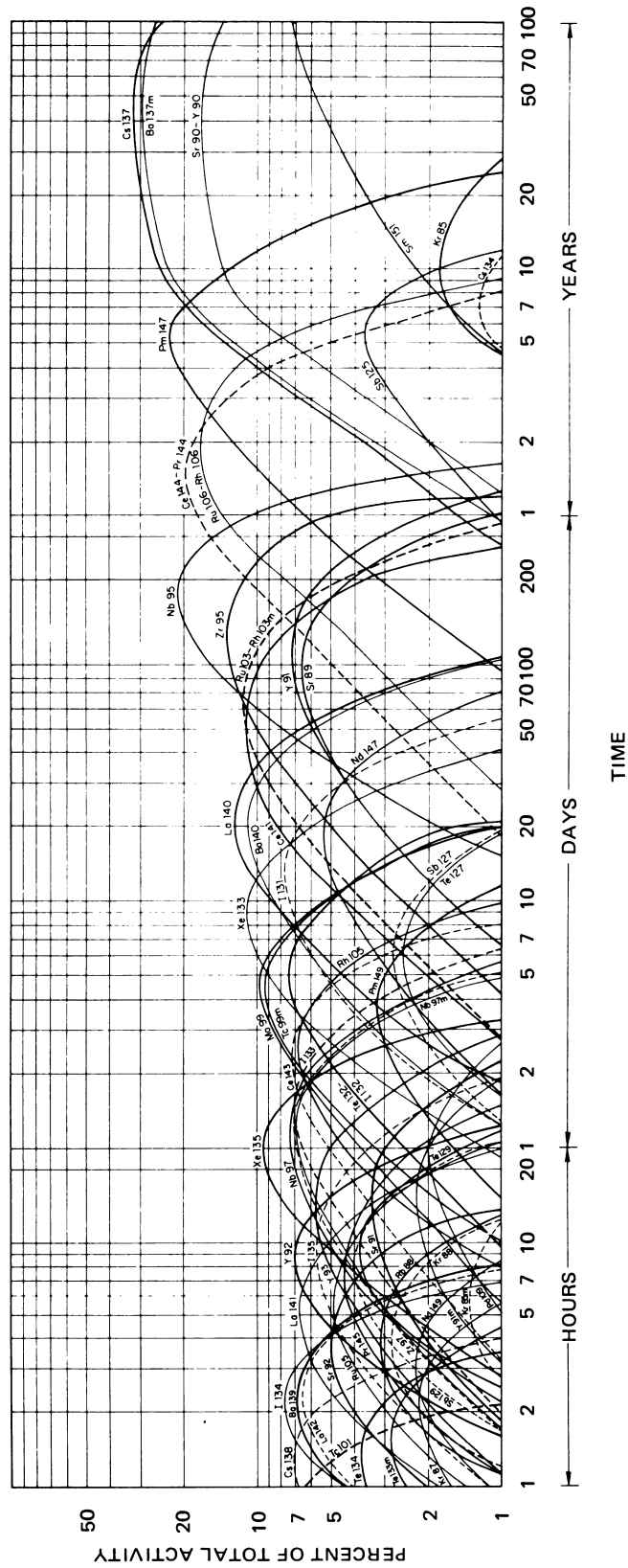
$$\eta_{nk} = \sum_{i=1}^n y_i^A \left( \prod_{j=1}^{n-1} \lambda_j \right) / \prod_{\substack{j=1 \\ j \neq k}}^n (\lambda_j - \lambda_k) \quad .$$

Because of the large number of chains, and the very large number of nuclides, evaluation by computer is a necessity.

Typical results of such calculations are shown in figure II.4, taken from a report by G. R. Crocker and T. Turner [28]. The build-up and decay of different nuclides is clearly shown as well as the tendency for each to be most prominent at a characteristic time after fission which is determined by the longest of the lifetimes prior to, and including, that of the given nuclide. Note particularly the case of 9.5 hr (half life) strontium-91, which gives rise eventually to 58 day yttrium-91; also note the 28 year strontium-90, which decays into 64 hour yttrium-90. In the latter case, the term  $e^{-\lambda_n t}$  rapidly becomes negligible in eq (II.4) and the terms  $N_{n-1}^A$  and  $N_n^A$  take the form

$$\begin{aligned} N_{n-1}^A(t) &\rightarrow e^{-\lambda_{n-1} t} \sum_{i=1}^{n-1} y_i^A \quad , \\ N_n^A(t) &\rightarrow e^{-\lambda_{n-1} t} \left( \frac{\lambda_{n-1}}{\lambda_n} \right) \sum_{i=1}^{n-1} y_i^A \quad . \end{aligned} \quad (\text{II.5})$$

The total beta-ray and gamma ray activities ( $\beta(t)$  and  $\gamma(t)$ ) of the fission products can be stated formally by the sums



II.4 Principle contributions to the activity of unfractionated fission products from thermonuclear neutron fission of  $^{238}\text{U}$  [28].



$$\beta(t) = \sum_{n,A} \lambda_n N_n^A(t) \quad , \quad (II.6)$$

and

$$\gamma(t) = \sum_{n,A} v_n \lambda_n N_n^A(t) \quad , \quad (II.7)$$

where  $v_n$  is the average number of gamma rays produced at the decay of the species  $(Z_n, A)$ .<sup>7</sup>

While the sum in eq (II.7) can be directly evaluated, it has been common to determine the gamma ray activity indirectly from an energy integration over the spectrum, which involves a rather different computation, in which  $v_n$  is replaced by a yield factor for each of a set of gamma ray energy groups produced.

## 2. Gamma Rays from Fission Products

Gamma rays are emitted when a nuclide, produced in an excited state as a result of a beta ray transition, drops to the ground state, either directly or by way of states of intermediate energy. It is possible for long-lived states of excitation to exist (isomeric states), and consequently for long lifetimes to occur in the emission of gamma rays; but this is unusual.

There is another type of transition (K-shell conversion) in which an inner atomic electron receives excitation energy from the nucleus and is ejected from the atom. Usually the electron is from the K shell, hence the name. In this type of transition, a vacancy is created in the K shell, which is rapidly filled by an electron from the L shell, or possibly one of the more loosely bound electrons. There is then a high probability that an x-ray

---

<sup>7</sup>Note that this average may be evaluated for photons above an arbitrary cut-off energy which is not always the same from one research worker to another, and that  $\gamma(t)$  is sensitive to this cut-off, thus complicating comparisons.

photon will be emitted having energy a little less than the K-shell binding energy. Such fluorescence photons have energies less than 100 keV.

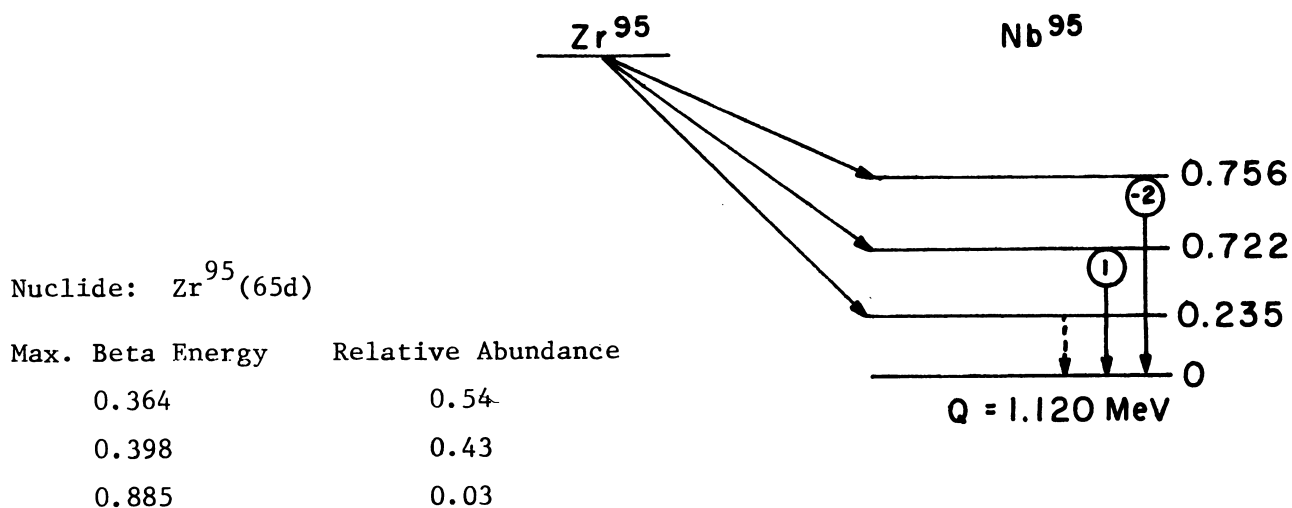
Table II.3 presents typical information on the gamma-ray and x-ray photons resulting from these post-fission nuclear transitions. These data are reproduced from an early paper by C. Miller [29] and are suitably illustrative even though not fully current. At the top of the table a beta ray transition is indicated from zirconium-95 to one of three different excited states of niobium-95. While the excitation energy may be given to an atomic electron, this K-conversion process is shown to be of negligible probability, hence the assumption here that no x-rays would be emitted.

Only two of the three niobium excited states have any significant probability for producing gamma rays, hence only two gamma ray energies are listed: one interprets the state at .235 MeV to be a long-lived isomeric state which does not contribute significantly. Note that only 97 gamma rays are produced per 100 disintegrations by the top two states. The fractions 43/100 and 54/100 act as weights (gamma rays per disintegration) determining the probabilities for emission of the two gamma ray photon types resulting from such a transition.

To combine these gamma ray data with calculated results such as are shown in figure (II.4), we would assume that disintegration of  $^{95}\text{Zr}$  according to its characteristic half life ( $0.693/\lambda = 65$  days) produces 0.722 MeV and 0.756 MeV gamma rays at the rates  $0.43\dot{N}_{\text{Zr}}^{95}$  and  $0.54\dot{N}_{\text{Zr}}^{95}$ , respectively, where  $\dot{N}_{\text{Zr}}^{95}$  is the disintegration rate for  $^{95}\text{Zr}$ .

Because each nuclide contributes in this fashion to the spectrum, the result of hundreds taken together is seen to be a very complex "line" spectrum in which the components shift in strength with time as different nuclides wax and wane in number among the fission products. For presentation and computational convenience, the thousands of spectral lines are grouped into energy

Table II.3 Data on the disintegration of  $^{95}\text{Zr}$  and subsequent de-excitation of  $^{95}\text{Nb}$ .  $N_g$ ,  $E_g$ ,  $N_k$ , and  $E_k$  give numbers and energies of gamma and k-conversion x-rays.  $N_p$  and  $n_p$ , respectively, give average numbers of photons emitted by the nucleus, and leaving the atom.  $\alpha$  is the total k conversion coefficient. Half lives are given in parentheses.  $Q$  is the sum of maximum beta-ray energy plus the subsequent gamma ray energy. (Data are reproduced from reference [29], and although old, are not misleading.)



Photon Abundance per 100 disintegrations

No.	$E_g$	$N_g$	$\alpha$	$N$	$N_k$	$\frac{N E_g}{100}$ (MeV/dis)
1	0.722	43	< 0.001	43	--	0.3106
2	0.756	54	"	54	--	0.4084
Sum	--	97	"	97	--	0.7190

$$E_k = 0.0190; \quad N_k E_k = 0; \quad N_p = 0.97; \quad n_p = 0.97$$

$$E = 0.719 \text{ MeV/dis}$$

$$E = 0.741 \text{ MeV/photon}$$

intervals, thus producing a histogram approximation. Calculations of gamma ray attenuation by such radiation may be further simplified by use of a set of a few monoenergetic components which represent the combined total of all photons within the energy group of the representative component.

### 3. Gamma Ray Intensities

While fractionation and neutron capture components make fallout spectra differ from fission product spectra, and introduce corresponding changes in intensity, the resulting spectrum is dominated by the fission product component. We therefore next review some of the major experimental and theoretical developments on this subject.

From 1943 to 1945, as part of the Manhattan Project, studies were made of the time dependence of the activity (disintegrations per second) of fission products [30], largely through experiments in which the number of beta rays emitted per second were counted. Other (calorimetric) studies were made of the total energy emitted as a function of time after fission. These early studies consistently showed that the activity and gamma ray intensity decreases with time according to a power law which was a little stronger than  $t^{-1}$ , except that for time after fission shorter than a few seconds a much slower variation occurs.

A talk in 1946 by K. Way and E. Wigner, followed by a paper in 1948, presented arguments that such a time variation for  $\beta$ -ray disintegrations could follow from known nuclear properties, and that one should expect a  $t^{-1.2}$  trend to be dominant [31]. The arguments by Way and Wigner made use of several approximations based on simplifying features of the phenomenon, of which the following are particularly important:

a) The complicated time dependence of the daughter products along the chains was simplified to elementary exponentials on the grounds that lifetimes

systematically increase, so that all daughter products have ancestors with so much shorter lifetimes that ancestor lifetimes could always be equated to zero. This approximation corresponds to the first of the two expressions of eq (II.5).

b) Lifetimes and beta ray disintegration energies  $E$  for different nuclides are so related that the quantity  $\log(\lambda/E^5)$ , which does not vary widely among beta-decaying nuclides, is equally likely to occur anywhere between specified upper and lower limits which are characteristic of the beta ray process.

Also in 1948, H. F. Hunter and N. E. Ballou made an extensive and systematic calculation of fission-product activities as a function of time, on the basis of decay constants and yield data [32]. These rather preliminary results confirmed the  $t^{-1.2}$  law for the longer time-intervals.<sup>8</sup>

Between 1955 and 1959 a series of calculations were performed to obtain fission product beta and gamma ray activities and spectra, as listed in Table II.2. The Hunter-Ballou data were revised and up-dated by R. C. Bolles and N. E. Ballou [34]. They performed two sets of calculations, based on two different types of charge distribution for fission fragments with the same nuclear mass [35,36]. The study [35] by Glendenin, Coryell, and Edwards, for example, postulates a most probable charge,  $Z_p$ , which is displaced from stability by about the same amount for both light and heavy fragments from a fission event,<sup>9</sup> together with an estimated probability distribution, which we designate  $p(Z)$  for the actual charges of fission fragments, which falls off rapidly with  $|Z-Z_p|$  in a manner somewhat resembling  $P(Z)$ :

---

<sup>8</sup>Note that some samples of fractionated fallout have been observed to decay more nearly in proportion to  $t^{-1.26}$  [33]. See also figure II.7.

<sup>9</sup>This is often called "Glendenin's rule."

$$p(Z) \approx P(Z) = (c\pi)^{-1/2} \exp\left[-(Z-Z_p)^2/c\right], \quad (\text{II.8})$$

with  $c \approx 1$ . In the empirical use of a Gaussian representation, suitable account must be taken of the discrete nature of  $Z$  (but not  $Z_p$ ); and while the Gaussian form is not accurate for large  $|Z-Z_p|$ ,  $|Z-Z_p| > 2$  is very unlikely.

R. D. Present applied a general nuclear model to estimate the division of charge between the fragments of the fissioning nucleus [36]. His results agree with Glendenin's rule for the most probable fission product chains, but give shorter chain lengths to the light fragment for the more asymmetric (and less probable) chains.

The Bolles-Ballou data on basic activities, which were limited to the case of thermal neutron fission of  $^{235}\text{U}$ , were the basis for at least three calculations of gamma ray activities and spectra: those of C. F. Miller and P. Loeb [37], A. Nelms and J. Cooper [38], and P. J. Dolan [39]. Miller computed total detector response above a contaminated plane.<sup>10</sup> Dolan calculated fission product spectra in fine energy increments (170 intervals between 0 and 5 MeV). He made comparisons with some existing experimental data for short time-intervals following fission; and he performed similar calculations [40] of gamma ray spectra for the case of 14 MeV-neutron fission of  $^{238}\text{U}$ , on the basis of activities determined by a calculation similar to that of Bolles and Ballou.

---

<sup>10</sup>Two years later, Miller published improved data which had been extended to fast neutron as well as to thermal neutron fission spectra and to  $^{238}\text{U}$  and  $^{239}\text{Pu}$  [21]. A theory of fallout formation made possible estimates of fractionation effects in this remarkable paper (see p. 64).

Nelms and Cooper calculated spectra which were intended for use in related transport calculations. Energy intervals were selected of approximately equal size in  $\log(E)$  rather than  $E$ , to keep these to a minimum number.

About the time of publication of the Bolles-Ballou report, A. C. Pappas undertook a re-evaluation of both Glendenin's rule and Present's theory to take account both of more data on fission yields and of new knowledge of nuclear shell structure [41]. This resulted mainly in a modified Glendenin's rule for determining  $Z_p$ , together with reduction of differences of experimental values from this modified Glendenin's rule derived by the (modified) theory of Present. In 1958, calculations by J. F. Perkins and R. W. King [42] utilized the results of Pappas. Gamma ray energy was determined in seven energy groups; and time integrals were performed to give a presentation tailored to nuclear reactor applications.

Also in 1958, A. J. Wahl re-examined the charge distribution problem from the point of view that the postulated probability distribution  $p(Z)$  of ref [35] could be taken seriously enough to help refine the  $Z_p$  values [43]. With this approach, plus some additional data, new charge probability data were deduced. These were used in 1959 in a general calculation of activities and fission product spectra for many isotopes, by R. Björnerstedt [26].

As indicated in table II.2, the calculations generally used differing compilations of data on nuclear mass yields, beta ray transition parameters, nuclear energy levels and gamma ray transition probabilities, though Miller's compilation was used by Dolan and by Nelms and Cooper also. Later reports used more complete data, as a rule.

The years 1955-1959, which encompassed such a high level of activity in the computation of fission product spectra and activity, did not have a correspondingly intense experimental effort to determine these same quantities. But a productive experimental program at ORNL to determine early fission product gamma rays was conducted by F. A. Maienschein, R. W. Peelle, W. Zobel, and T. A. Love [44]. In their experiments, thermal neutrons generated in a reactor thermal column produced fissions in a "fission chamber". The number of fissions thus produced could be readily determined by counting the large pulses of ionization due to the fission fragments. Gamma rays were detected in a multiple-crystal spectrometer which gave a fairly accurate measure of photon energy. Intensity limitations restricted the time-interval duration after fission to less than an hour.

In 1958, Knabe and Putnam combined the calculated data of Perkins and King with the ORNL experimental data, and extended the number of energy groups to twelve [45]. A further revision by Zigman and Mackin [46] incorporated experimental data from NRDL.

In 1959, measurements of fission product gamma rays by Y. I. Petrov were reported [47]. No attempt was made to determine spectra; total gamma ray energy emitted per fission per second was determined for periods up to about 10 hours after fission. Petrov's procedure included making attenuation measurements of the gamma rays, with integration over the penetration curve to determine energy absorption by the attenuator.

On the whole, experiments and calculations at this point (1960) had produced information which was difficult to cross-check for consistency in detail. The experimental data were best and most complete for times less than 1 hour after fission; while the calculations were most reliable for times greater than 1 hour after fission. For example, there was no overlap between

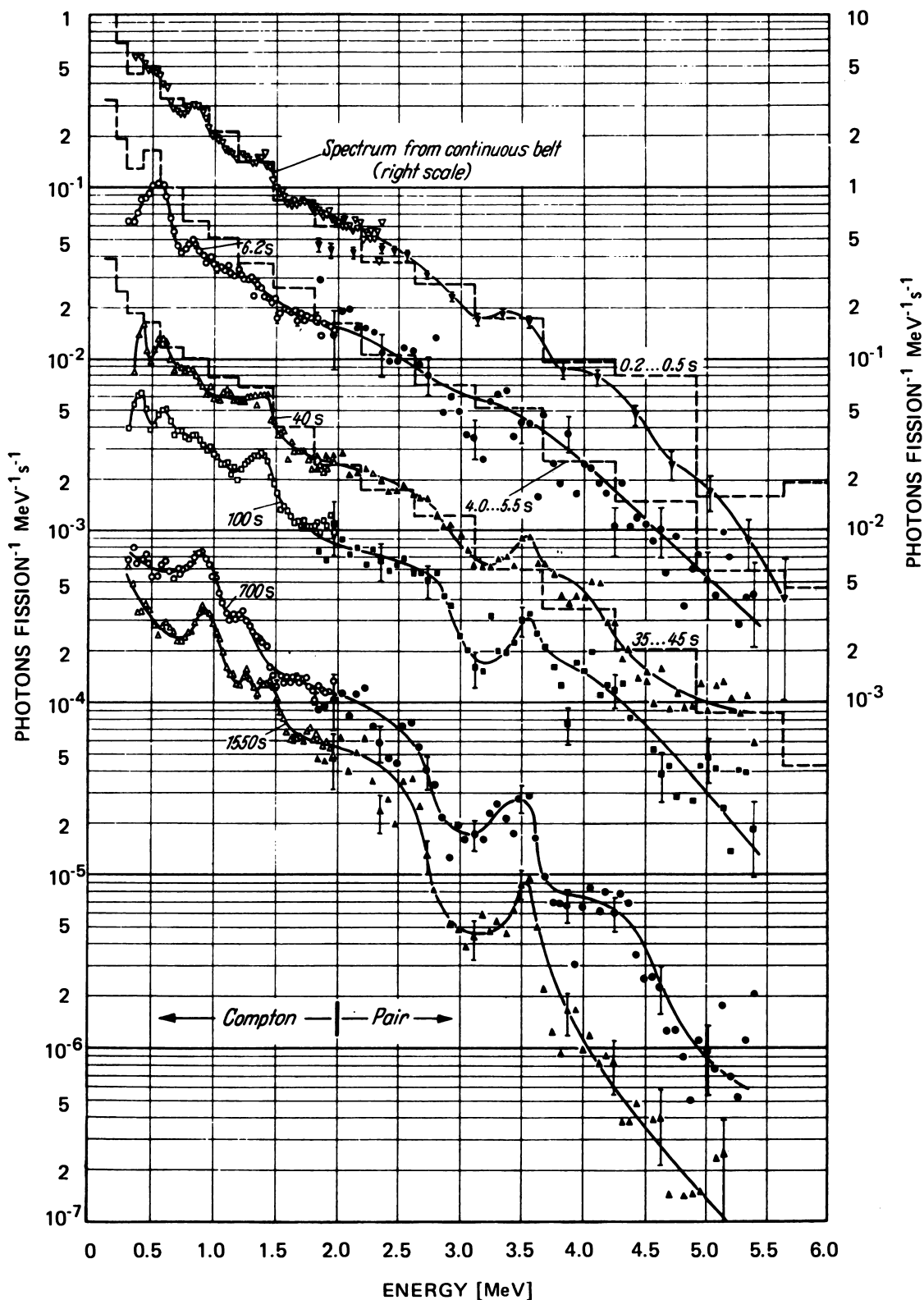


the excellent calculation by Björnerstedt and the careful and systematic experiments performed at ORNL.

Later research efforts have tended to provide some, but not enough of this cross-checking. In a paper published in 1964, J. Griffin performed a calculation for short times in which properties of an "average" decay chain representative of the whole fission fragment population were deduced [48,49]. Solution of the time-dependent chain equations then provided activities for times less than about 10 seconds following fission. Concurrently, an extensive experimental study was conducted by P. G. Fisher and L. B. Engle along the lines of the earlier ORNL project but with fast neutrons from a fission source, and using as many as five different heavy isotopes which undergo fission [50]. Their detector was a large NaI single-crystal spectrometer. Reduction of the pulse-height distribution to a spectrum was more of a problem for Fisher and Engle than for the ORNL experiments because the detector response function was much broader; This "unfolding" was accomplished by use of a technique in which a rather coarse energy grid, corresponding to the rather broad response peak, rendered the spectral results somewhat insensitive to inaccuracies in the data and the response function.

The Fisher and Engle spectra for short times after fission covered about the same time range as the ORNL experimental spectra, and have been shown to be in agreement with Zigman and Mackin's summary data in both shape and intensity [51]. More direct comparisons with ORNL spectra were included in the later review article by F. C. Maienschein, and are shown in figure II.5 [52].

Attempts by Löw and Edvarson [53] and by L. R. Bunney and D. Sam [54,55] were later made to extend the experimental data of both Maienschein, et al., and Fisher and Engle to much longer times. Bunney and Sam used a variety of



II.5 Gamma-ray spectra for different time intervals after fission of <sup>235</sup>U. The points and solid lines are from ORNL studies of thermal fission using Compton and pair types of multiple-crystal scintillation spectrometers which covered energy regions as indicated in the figure [44]. The histograms are from LASL studies of fission induced by neutrons from a bare critical assembly, using a single crystal scintillation spectrometer with correction for the spectrometer response [50].

neutron sources, and several fissioning isotopes in experiments extending to 3 days after fission. They likewise used a sodium iodide single crystal spectrometer, thallium activated. Some of their pulse height distributions are shown in figure II.6. Their (unfolding) process for determining spectra from pulse-height distributions was somewhat similar to that of Fisher and Engle, but based on a fine energy grid.

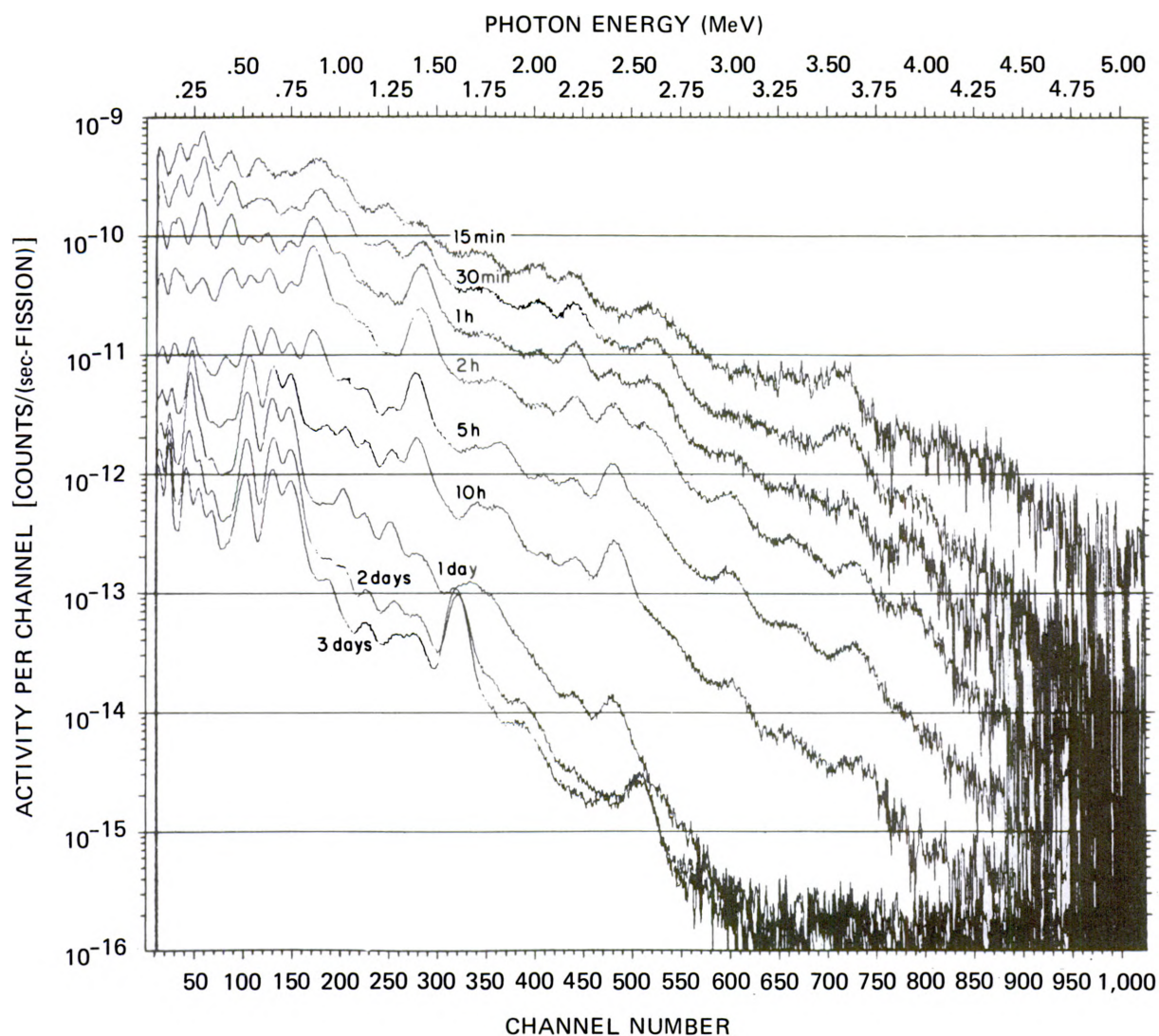
The computations of spectra and gamma ray activities were redone in 1965 by G. R. Crocker and T. Turner [28]. Crocker and Turner used a 1961 re-evaluation of the charge distributions due to C. D. Coryell, M. Kaplan, and R. D. Fink, which took account of preceding work by Wahl, Pappas, Present, Glendenin, and many others [56]. Crocker and Turner also used more recent compilations of fission yield data, beta ray transition data, and nuclear systematics. Results for times equal to and greater than 1 hour are presented; and these are similar to, and can be considered an updating of, the Björnerstedt report.

There has been a large effort in the ten years from 1966 to 1976 to improve both experimental and theoretical data on the properties of radiation from fission products. Much of this effort has been stimulated by the requirements of reactor technology, and has emphasized the power output of beta and gamma rays, both separately and added together (see, e.g., refs. [57-59]).

Beginning in 1973, several projects were organized to expand ENDF/B<sup>11</sup> fission-product data files and develop computer programs for computation of integral data and gamma and beta ray spectra [60-62]. These powerful new tools have been applied to intensity as measured by radiation power, and to spectra mainly of radiation from reactor fuel elements. Comparisons of data for emitted gamma ray power and decay heat with new measurements shows agreement to within  $\sim 10\%$  for times from about 1 minute to 6-12 hours after fission [63,64].

---

<sup>11</sup>Evaluated Nuclear Data File.



II.6 Pulse-height distributions of gamma rays from fission products of thermal-neutron fission of  $^{235}\text{U}$  at selected times after fission [55].

Figure II.7 shows recent data for the gamma ray activity,  $G(t)$ , multiplied by  $t$ . For comparison, functions  $.6 t^{-.2}$  and  $.6t^{-.25}$ ,  $t$  in hours, have been drawn. Likewise in table II.4 gamma ray activity data are given for several types of fission sources, from several experiments, and from calculations performed with progressively more complete and sophisticated data banks. We have found it convenient to divide  $t G(t)$  by the simple power function used for comparison purposes in figure II.7,

$$f(t) = .6 t^{-.2} \text{ photons/fission.} \quad (\text{II.9})$$

This embodies the Way-Wigner rule; and the constant  $.6$  is chosen for convenience.

From figure II.7 and table II.4 we note a number of things:

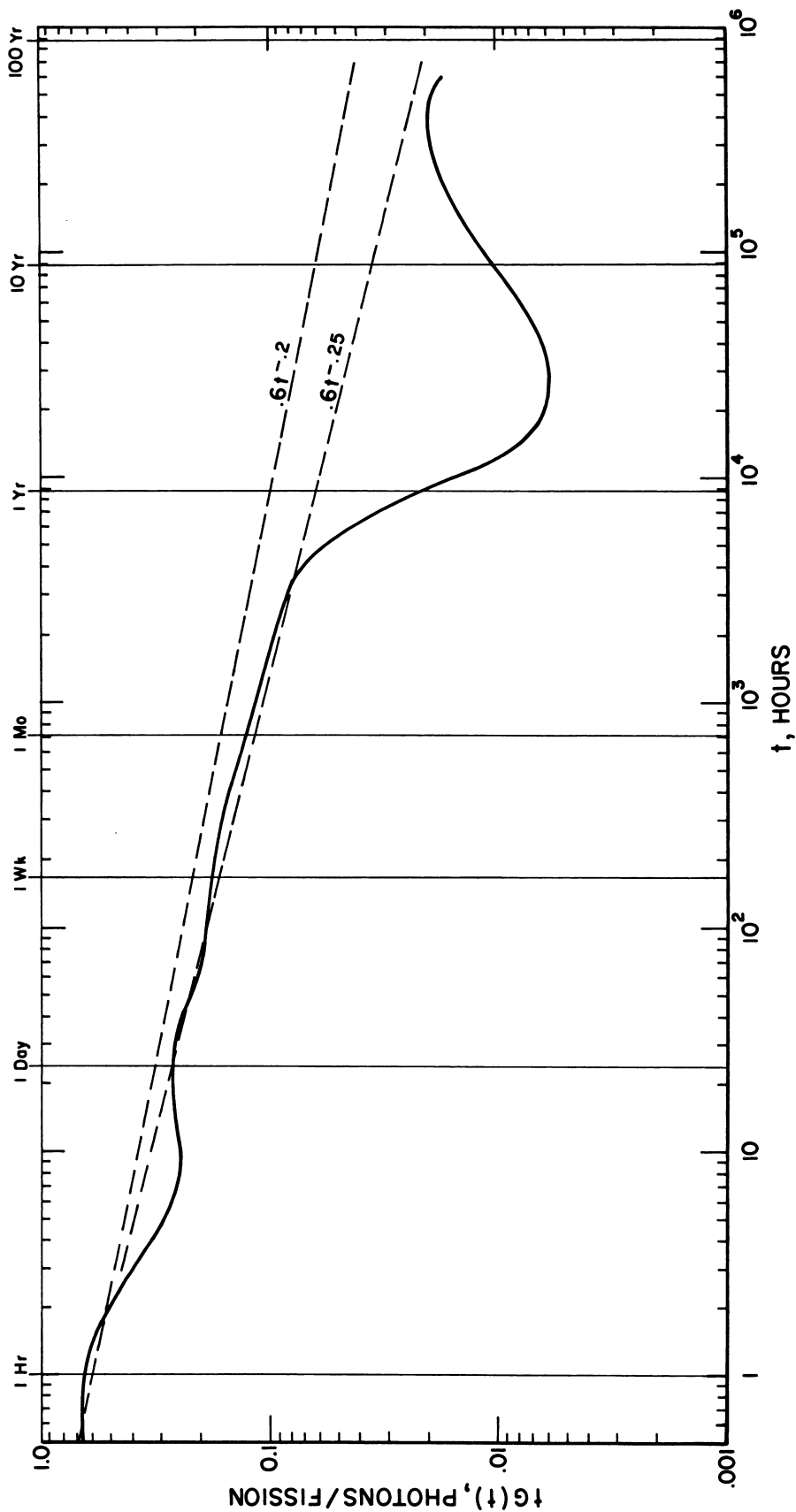
a) The calculations show that the  $t^{-1.2}$  law is impressively realistic for several months and can be used for order-of-magnitude estimates for up to 100 years. Experiments validate this for the first few days. (For practical purposes  $t^{-1.25}$  may be even better.)

b) Experiments validating the calculations at long times are lacking. This is still true, although few isotopes are involved.

c) Activities calculated in 1957 have been altered by less than a factor of two. (Miller's earlier data on  $\gamma$ -ray "pulses" have been used to obtain this comparison. Later data in [21] are not shown here).

d) Activities determined for different fission isotopes or neutron energy spectra are shown by the calculations to be so little different that they may be ignored for many applications. There seem to be somewhat larger differences between different experiments, but the conclusion that such differences are probably ignorable is not altered.

e) Earlier experiments and calculations are shown to agree to within about 30%; the current level of agreement is  $\sim 10\%$  for times of one-half to 3 hours. Even recent experiments still hardly agree better with one another than with calculations.



II.7 Gamma-ray yield  $G(t)$ , weighted by the time  $t$  following fission, for the case of  $^{235}\text{U}$  fission by fission-spectrum neutrons [65]. The dashed lines give elementary comparison functions.

Table II.4 Gamma rays per fission,  $tG(t)$ , for time intervals  $t$  after fission, relative to a normalizing function  $.6t^{-.2}$  evaluated for  $t$  measured in hours. Superscripts designate the mass number of the fissioning isotope; subscripts refer to fission by thermal, fission, and fusion spectrum neutrons. Data to the right of the double line give gamma ray activity for other cases relative to thermal neutron fission of  $^{235}\text{U}$ .

$t \text{ } G_{\text{Th}}^{235}(t)/(.6t^{-.2})$										
Time	Miller [37]	Björner- stedt [26]	Crocker, Turner [28]	Finn, Simmons [65]	Bunny, Sam (EXPT) [55]	ORNL (EXPT) [66]	$G_{\text{Fi}}^{235}/G_{\text{Th}}^{235}$		$G_{\text{Fu}}^{238}/G_{\text{Th}}^{235}$	
							EXPT [54]	Theory [28]	EXPT [54]	Theory [28]
Hours										
.5				.97	1.12	.85	1.12			
1	.73	.79	.83	1.06	1.19	~ .91	.98	.98	.94	.96
2	.75	.84	.84	.97	1.09		.85	.94	.87	.95
5		.68	.77	.73	.82		1.21	.99	.96	1.01
12	.88	-	.89	.75	-		-	1.03	-	1.05
Days										
1	.88	.77	1.04	.86	.98		1.25	1.00	1.02	.97
3	.78	-	1.19	.75	.96		1.28	1.01	1.16	.93
30	1.17	.69	1.06	.77				.97		.94
Years										
1		.21	.25	.28				1.05		1.16
10		.17	.17	.15				1.13		1.08
30		.37	.39	.35				1.04		.89

There is one other observation which should be made, but which is not evident in the table. Nelms and Cooper, as well as Dolan, attempted in a crude fashion to take some account of fractionation in part of their output data. Nelms and Cooper simply dropped components due to rare gases and some other well-known volatiles, without taking account of the effect of a volatile on the presence or absence of daughter isotopes. On the other hand, Dolan took account of fractionation by removing products with a strongly volatile ancestor (I, Kr, Xe). The resulting activity in photons/fission/second at 1 hour was reduced by nearly 40%. Presumably, neutron-induced activities would partially compensate for such reductions; but this indicates that the data of figure II.6 are not accurate to better than 40% when one uses them to represent fallout source intensities.

#### 4. Gamma Ray Spectra from Fission Products

Gamma ray spectra at early times after fission are important for their application to protection against prompt effects, rather than to the delayed hazards of fallout. Thus we present figure II.5 mainly for completeness. One sees here good agreement in shape and in absolute value between the ORNL experiments of Maienschein, et al. [44], and the LASL experiments of Fisher and Engle [50].

All experimental results involve "unfolding" a pulse-height distribution  $P(E_p)$ , such as that shown in figure II.6 to obtain a spectrum  $N(E)$ :

$$P(E_p) = \int_0^{\infty} dE N(E) R(E_p, E) \quad , \quad (II.10)$$

where  $R(E_p, E)$  is the detector response function, e.g., the pulse height distribution for photon energy  $E$ . For single crystal spectrometers, particularly if their response function is relatively broad, the solution of eq (II.10), i.e., the "unfolding", introduces errors whose size can only be

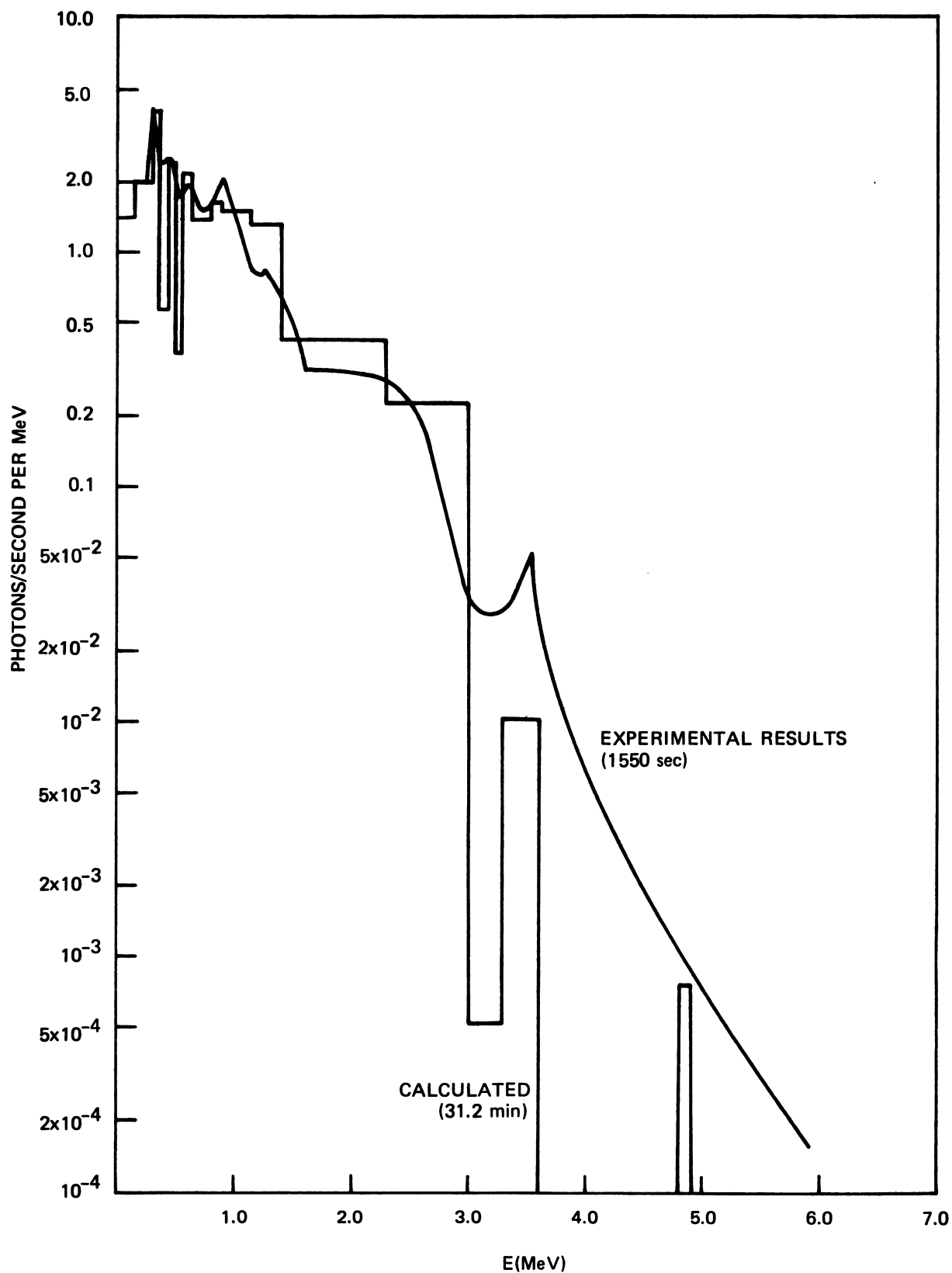


guessed with the aid of analysis of mockup "trial" spectra which are known exactly. With decreasing intensity of the gamma rays at longer times, statistical fluctuations become more serious, and the experiments become much more difficult; hence the extension to only 3 days. One interprets figure II.6 as confirming the known, regular softening of the spectrum during this period: High energy pulses become relatively less frequent at longer time.

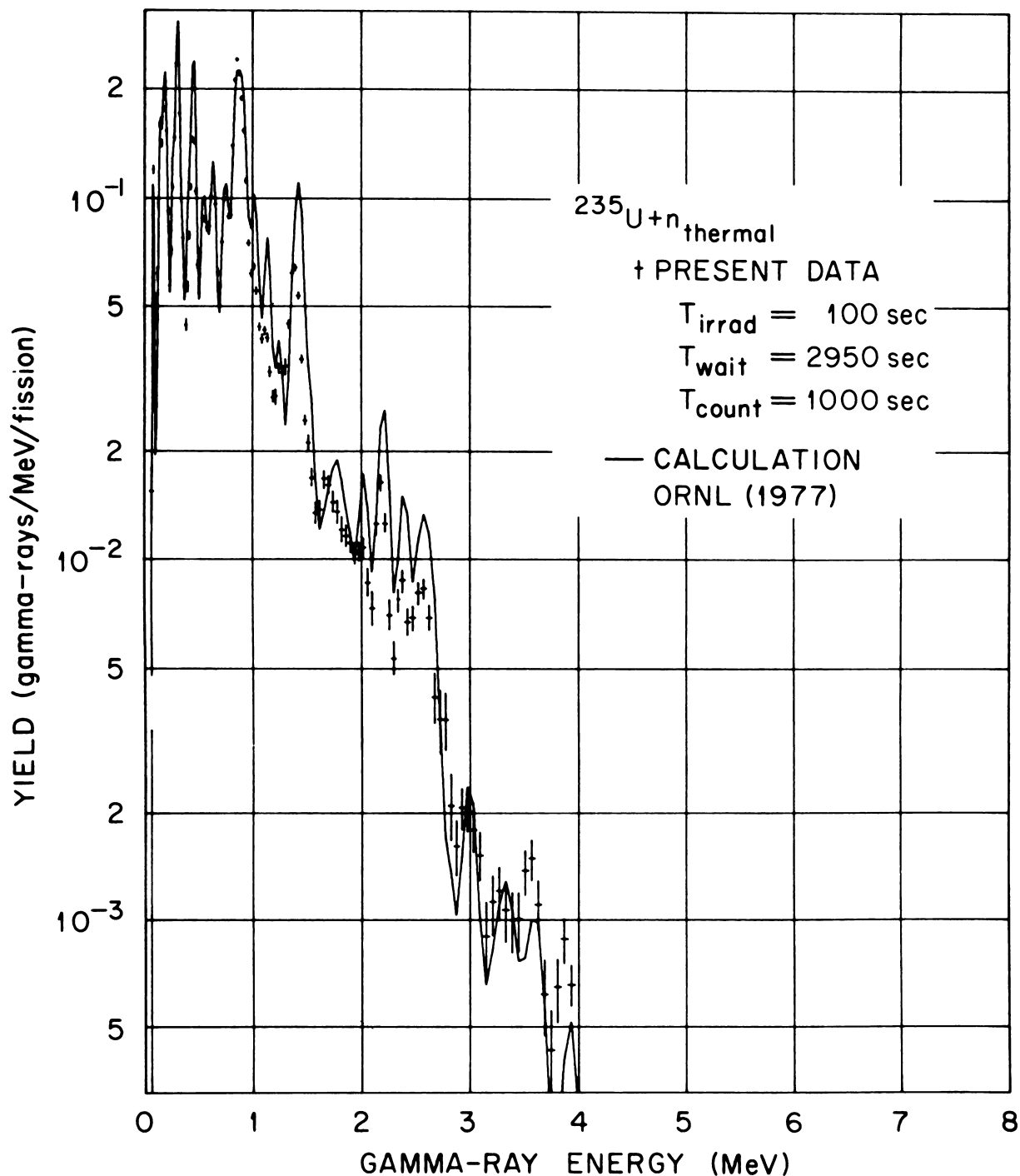
Figure II.8 shows an early comparison between theory by Dolan [39] and experiment by Peelle, Zobel and Love [67]. Comparison is rather satisfactory in most regards up to 3 MeV, and the experimental results are higher at greater energies. Note that steep drops appear in both sets of data at about 3 MeV. By and large such correlations are difficult to make because the experimental unfolding does not resolve the line structure. The times do not exactly correspond; but this is the greatest time duration for the ORNL experiments, and about the shortest time duration at which the calculations of Dolan can be taken seriously.

Progress in recent years on the data base, as well as on both experimental and theoretical procedures, has greatly improved the situation in regards to comparisons between experiments and calculations. Figure II.9 shows a recent comparison of this type due to J. K. Dickens, et al, [68] for fission products from thermal neutron fission of  $^{235}\text{U}$ , after almost 1 hour. Further comparisons with ORNL and other experimental data have been reported by T. R. England and M. G. Stamatelatos [63].

This problem of making comparisons of spectra is difficult, even between two calculations. When the computational energy groups differ, differently grouped line intensities can give rise to apparent but spurious fluctuations in the histogram. Largely for this reason, little effort has been previously



II.8 Fission product spectrum at an intermediate time after fission: an early comparison between experiment [67] and calculation [40] for thermal neutron fission of  $^{235}\text{U}$ , for 104 fissions.



II.9 Recent comparison of theory and experiment for spectra due to thermal neutron fission of  $^{235}\text{U}$  [68]. Data correspond to a time interval centered at 57.5 minutes after fission. An estimated 1.6% of the gamma rays are omitted due to escape of fission product gases. The sample was irradiated for 100 sec; and 2950 sec later a 1000 sec counting period began.

made to compare the many different computations in any regular manner, although Crocker and Turner [28] did include comparisons with Björnerstedt [26], made possible by the use of very similar energy grids.

To get around this problem in a general way, rather drastic measures appear to be necessary. One way is to calculate a single integral parameter such as the average energy of the spectrum, and make comparisons of values for this parameter. Unfortunately, one cannot equate agreement or disagreement in this parameter with agreement or disagreement between two spectra.

We adopt a different procedure here, in which one sums all photons above a specified energy. Comparison of spectral "quality" by use of integral data over the photon spectrum from fission products,

$$I(E) = \int_E^{\infty} dE' N(E') \quad , \quad (II.11)$$

$$= \int_E^{\infty} d(\log E') E' N(E') \quad , \quad (II.12)$$

can be made by proper normalization; we use unity for the total integrated number. These comparisons avoid many questions of histogram structure, and yet they permit general and meaningful conclusions to be drawn.

Figure II.10 gives comparisons of two of the later calculations, viz. Björnerstedt, and Crocker and Turner, with two experimental series. In addition, we have added a very simple analytic expression which gives an approximate fit to the 1 hour data. Each group of curves is normalized to unity at  $E = 0$ . We observe the following from these data:

a) At 1/2 hour the agreement between theory and experiment is extremely good as to shape. One perhaps expects this from the agreement already evident in figure II.7.

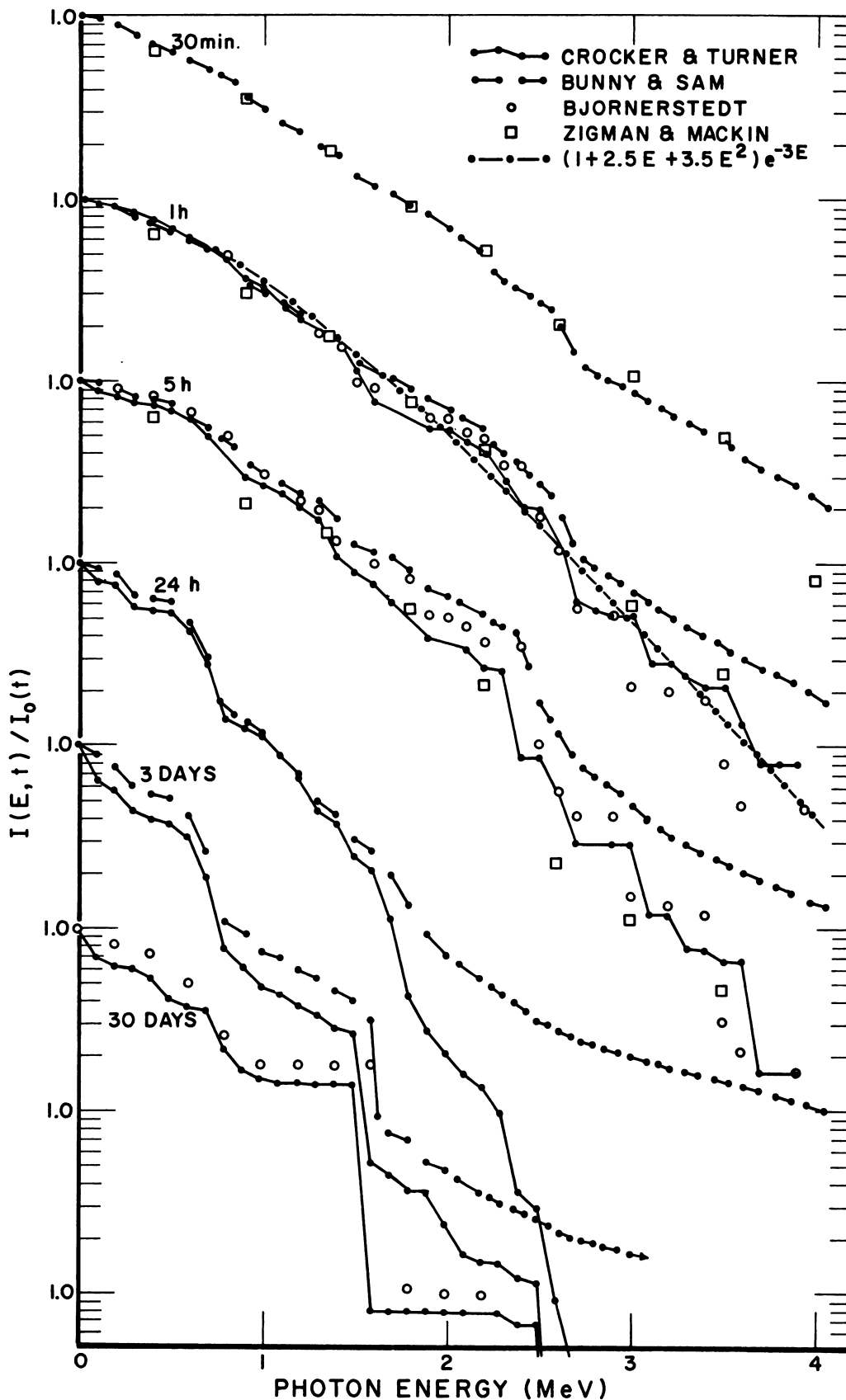
b) The general trends shown in the Bunney-Sam experiments [54] closely resemble the calculations out to energies covering 99% of the photons. Differences stay within about 30%, with experiments being uniformly high at the greater photon energies. Beyond this, the experiments give a probably spurious trend which remains much higher than the calculations. A more reasonable high energy shape would reduce the 30% discrepancies just noted at lower energies. The Zigman-Mackin data [46] show quite a different behavior at high energies and are in much more satisfactory agreement with, say, the Crocker-Turner data.

c) Björnerstedt agrees very well with Crocker-Turner at 1 hour, but tends to be a little higher at the later times.

d) Differences between different sets of data of magnitude  $\sim 20\text{-}30\%$  over a wide energy region affect exponentially attenuated results by no more than  $\sim 20\text{-}30\%$ , according to eq (II.12). Hence the smooth curve in figure II.10 representing the 1 hour spectrum should give results within perhaps 10% of those given by Crocker and Turner spectrum in all transport calculations except those with great attenuations.

e) Note again a very substantial softening of the spectrum evident between times of 1-2 hours and times 1 day or greater. This appears in all experimental and theoretical studies.

To expand the study of 1 hour spectra, we give additional comparisons in figures II.11 and II.12. These indicate the following:



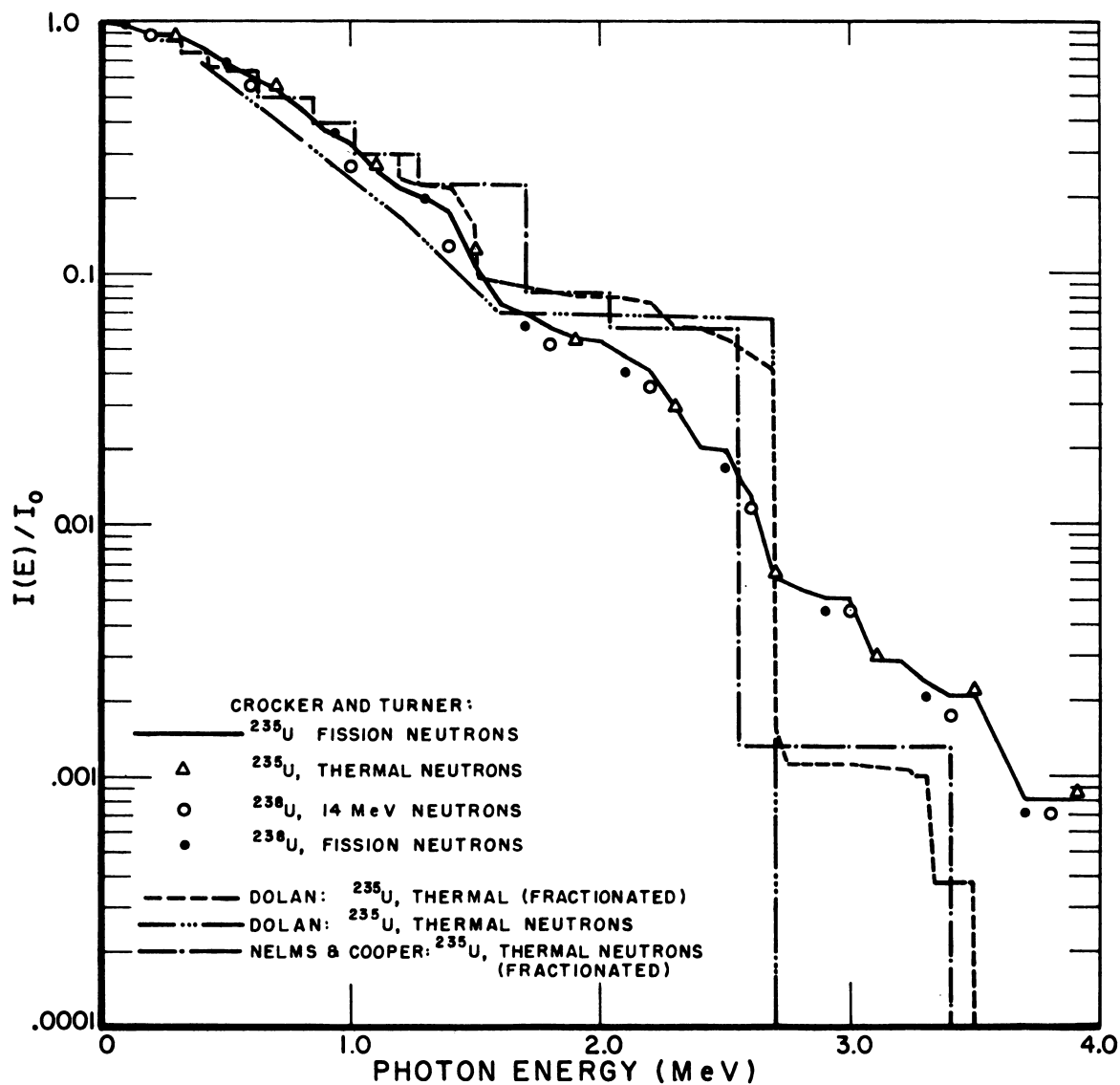
II.10 Comparisons between cumulative, unfractionated fission product spectra at different times after fission, normalized to unity at low energies, for thermal neutron fission of  $^{235}\text{U}$ . Data due to Crocker and Turner [28] and Björnerstedt [26] are theoretical. Data due to Bunney and Sam [55] and Zigman and Mackin [46] are experimental. A formula approximating the 1 hour spectrum has been added.

a) Gamma spectra for different neutron source spectra and different fissioning isotopes are so closely similar that the differences can surely be ignored.

b) The dash-dot curves, giving Nelms and Cooper data with their modification to take some account of fractionation, agree remarkably well with Dolan's unfractionated data. One would expect this because only a few radiating isotopes were involved in the modification. Even the Dolan fractionation modifications make a surprisingly small change in shape. The Nelms-Cooper (fractionated) spectrum, which is given in table II.5, has been used in most of the fallout shielding calculations performed to date. It is higher than the spectrum of Crocker-Turner out to about 2.5 MeV, and lower at greater energies. Accordingly, one expects the Nelms-Cooper spectrum to give conservative results except at great penetrations. From figure II.12 one sees that the expected crossover must be at greater penetrations than those of interest to fallout gamma ray shielding.

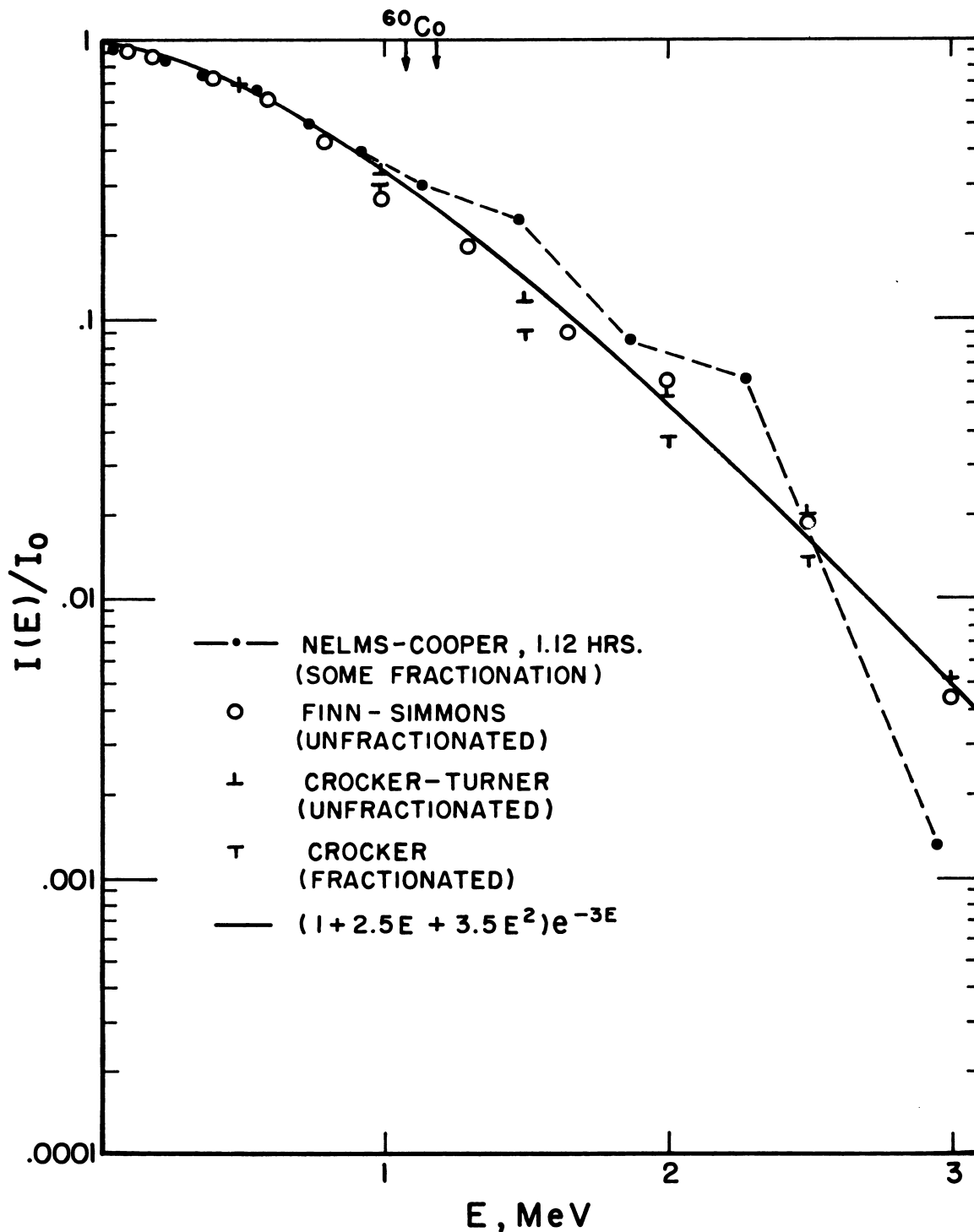
c) The changes introduced in the attempt by Dolan to take account of fractionation are not very realistic, and one can see that resulting fractionation effects do not appear to make actual fallout spectra different from fission product spectra in important ways. But the far more realistic calculations of fractionated spectra by Crocker [28,70], as shown in figure II.12, make it evident that the degree of fractionation can have significance for shielding applications.

d) Future calculations should presumably use a more up-to-date spectrum or some suitable representation. Changeover from Nelms-Cooper to Finn-Simmons



II.11 Comparison of integral spectra from different investigators [28,38-40], for gamma rays from 1 hour old fission products. All data are theoretical. The histogram data of Dolan and Nelms-Cooper were concentrated at midpoints of intervals, hence the rectangular structure.





II.12 Comparison of cumulative spectra for fission products at 1 hour. All spectra correspond to  $^{235}\text{U}$  fission; Nelms-Cooper [38] data are for fission due to thermal neutrons while spectra due to Finn-Simmons [65], Crocker-Turner [28], and Crocker [70] are for fast (fission spectrum) neutrons. The  $^{60}\text{Co}$  spectral lines are indicated at the top.

Table II.5 Delayed gamma ray spectra from  $^{235}\text{U}$  fission products. The Nelms-Cooper data [38] correspond to fission by thermal neutrons ( $n_{\text{Th}}$ ) and have been modified for fractionation by removal of some volatiles. The Finn-Simmons data [65] are for fission by fission-spectrum neutrons.

<u>Energy Limits</u> (MEV)	Nelms-Cooper ( $n_{\text{Th}}$ ) 1.12 Hours (Photons)	<u>Energy Limits</u> (MeV)	Finn-Simmons ( $n_{\text{Fi}}$ , Unfractionated)		
			<u>1 Hour</u> (Photons)	<u>1 Week</u> (Photons)	<u>3 Months</u> (Photons)
0.0		0.0			
	.0492		.0271	.0463	.1200
.0381		.05			
	.0201		.0137	.0818	.0050
.0492		.10			
	.0005		.0737	.1351	.1049
.0644		.20			
	.0001		.0476	.0999	.0016
.0864		.30			
	.0064		.0929	.0798	.0074
.1142		.40			
	.0309		.1373	.1227	.1284
.1475		.60			
	.0146		.1717	.2528	.5923
.1904		.80			
	.0267		.1627	.0614	.0097
.2332		1.00			
	.0054		.0889	.0105	.0009
.2856		1.33			
	.0915		.0957	.1016	.0279
.3687		1.66			
	.0922		.0299	.0015	.00002
.4664		2.0			
	.0194		.0397	.0035	.0010
.5712		2.5			
	.1500		.0148	.0031	.0009
.7374		3.0			
	.0996		.0042	.00002	
.9328		4.0			
	.0923		.0001		
1.1424		5.0			
	.0747				
1.4738					
	.1418				
1.8655					
	.0225				
2.2848					
	.0601				
2.9496					
	.0013				
3.7310					

[65], for example, would significantly increase most calculated protection factors, because the Nelms-Cooper spectrum is harder in the important 1 - 2.5 MeV region.

A recommendation has been made that a 1 hour spectrum be used with fractionation appropriate to close-in fallout, when and if an up-dating of the standard spectrum occurs [69]. In figure II.13 a "moderately fractionated" spectrum ( $r_{89,95} = .5$ ) for close-in fallout at 1 hour after fission has been included, corresponding to reduction of total radiation intensity by a factor .73 [70]. Attenuation properties would be sensitive to fractionation mainly for rather large attenuations (moderately large to large PF values), where PF values would be thereby increased, as already noted.

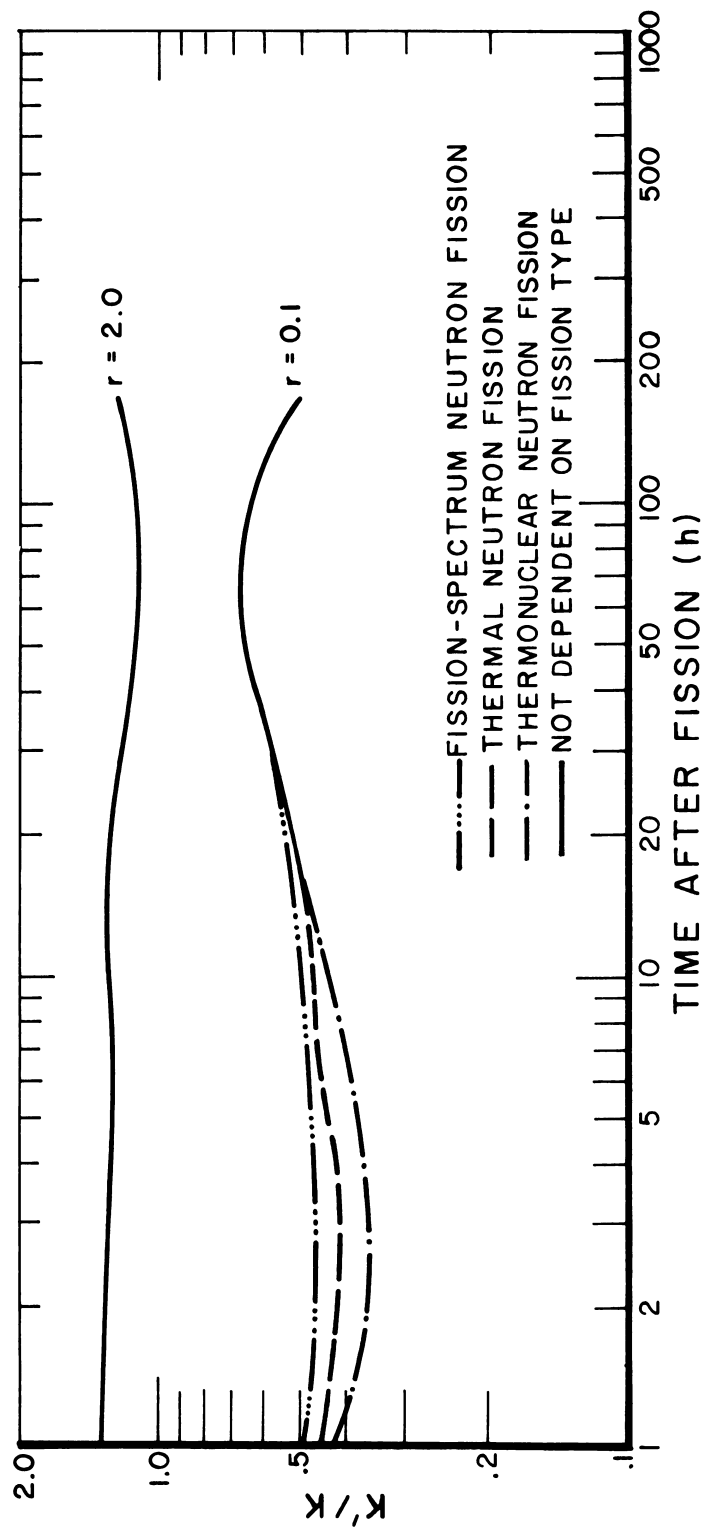
Table II.5 gives values for the standard Nelms-Cooper spectrum and several unfractionated spectra recently calculated by S. P. Finn and G. L. Simmons. The latter are conservative, but not unreasonably so, if used for PF estimates.

### C. SOME PROPERTIES OF RESIDUAL RADIATION

#### 1. Effects of Fractionation on Fallout Gamma Ray Properties

##### a. The Portion of Activity Deposited in Local Fallout

A central problem in the study of fallout gamma rays is the amount of the radioactivity from a detonation which is deposited "locally." Because this is associated with the larger fallout particles, it is affected by fractionation. The usual discussion depends on the concept of "K-factor," which has always been given in units  $(\text{Roentgens/hour})/(\text{kiloton/mile}^2)$ , and is a gamma ray exposure rate per unit contamination density defined at a height of 3 ft above the plane of fallout contamination. Note that weapon yield is specified in kilotons (KT) of TNT giving equivalent explosive energy.



II.13 The  $K$ -factor due to fractionated fission products ( $K'$ ) divided by that for unfractionated fission products ( $K$ ). Values for  $r = r_{89,95}$  correspond to volatiles largely removed ( $r = 0.1$ ) or augmented ( $r = 2.0$ ) [70].

The K-factor averaged over the "local" fallout field and at 1 hour after detonation is determined empirically from an intensity integral over the area [71]:

$$K_1 = \frac{1}{W_f R_{gr}} \int_0^{A_m} I \, dA, \quad (\text{II.13})$$

where  $W_f$  is the fission yield in kilotons,  $I$  is the exposure in Roentgens/hour corrected back to 1 hour postdetonation and also corrected for detector self-shielding. The factor  $R_{gr}$  is an intensity reduction factor representing ground roughness and other shielding effects, which for level ground would typically have a value of  $\sim .75$  (see section VI.D.1). The integral is taken over curves of constant  $I$  out to a curve of smallest intensity accurately measurable enclosing area  $A_m$ .<sup>12</sup> It thus depends on  $A_m$ , as well as on parameters of the detonation.

Estimated upper limits ( $K_0$ ) to the K-factor, based on an ideally smooth plane, unfractionated fission products with complete local deposition, and inclusion of scattered radiation, vary from about 2700 (R/hr)/(KT/mi<sup>2</sup>) at one hour to about 3400 depending on the nuclide undergoing fission, and the energy of the neutrons causing fission. A typical value, corresponding to thermonuclear fission of <sup>238</sup>U, would be  $K_0 \approx 2900$  [73]. Values for  $K_1$  obtained by numerical integration of eq (II.13) for many different tests, scatter about a mean, corrected for ground roughness, of  $K_1 \approx 1930$ , which has been recommended for general use [71].<sup>13</sup>

---

<sup>12</sup>  $A_m$  differs from one experiment to another, making comparisons more difficult. Typically it would be the area enclosed by the 1 r/hr contour, or possibly the .5 r/hr contour.

<sup>13</sup> Note that these values are not much different from 1960 estimates [21]. Some values based on experimental spectra appear to be greater than these theoretical estimates by  $\sim 40\%$  [72]. One should also note the difficulty of accurately "extrapolating to 1 hour" exposure measurements.

The ratio  $K_1/K_0 \approx (1930/2900) \approx 2/3$ , measures the fraction of activity deposited "locally," with the remaining 1/3 remaining aloft, much of it to be later deposited as intermediate or long range fallout. This ratio, like  $K_0$ , is affected only to a minor extent by neutron-induced radioactivity.

Attempts have been made by L. R. Bunney and D. S. Sam [74] and by G. R. Crocker [70,75] to determine the overall effect of fractionation on the K-factor. In the experimental studies of Bunney and Sam, a separation was made between solid and gaseous fission products, at various times after thermal neutron fission of  $^{235}\text{U}$ . Pulse height distributions were measured for the solid component and also for the "gross fission products" (solid and gas products combined). These pulse height distributions were unfolded to give spectra; and the spectra were applied to the plane isotropic source configuration to obtain spectral intensities at the 3 ft height. Exposure was then obtained from a suitably weighted integral over this spectrum.<sup>14</sup>

Bunney and Sam found a) that the solid fission products give a K-factor about 70% that of the gross fission products at 1 hour, and b) that this fraction rises steadily with time for the first two days after fission.

The calculations by Crocker utilized fission product gamma ray spectra obtained from calculations like those of section II.B [75]. The effect of fractionation was evaluated using Freiling's approach, for the values for  $r_{89/95}$  of .1, .5 and 2 covering much of the observed range. Some results are shown in figure II.13. At 1 hour post-fission, the reduction in the K-factor due to fractionation is seen to be by about a factor 2.5. This is more nearly a practical lower limit than an estimate, and as such it is reasonably consistent with an average reduction by about a factor 1.5, which would apparently correspond to  $r_{89,95} \sim 0.5$ .

---

<sup>14</sup>See sections III.D.1 and III.F. In this monograph we use the term "dose" generically. Hence it can be interchangeable with "exposure" and "air kerma." These are featured both by calculations and by common use of air ionization chambers.

While there is an apparent consistency to the studies of average or overall fractionation effect, the studies just mentioned are not really comparable in detail; and the conclusion that we know the approximate value of  $K_1$  is not warranted. The available information is too slight to provide more than an initial estimate. Further, one would expect variations with differences of surface at ground zero, such as soil type. But the data only suggest such variations, while not really exhibiting the differences clearly enough to say either that they exist, or that they are qualitatively in any given direction [76].

b. Variation of Activity with Particle Size and Position.

General effects of fractionation on the K-factor can be discussed with careful use of studies of the K-factor as a function of particle size, noting that the average particle size decreases as the distance from the detonation increases. Figure II.14 gives data on the reduction of detector response due to fractionation, as a function of the mean particle size in different size groups obtained by sieving after the shot Small Boy [77]. This is equivalent to the reduction in K-factor if the fallout at different locations were as homogeneous in size as the sieved samples. One immediately notes two features: 1) the larger particles, corresponding to close-in fallout, are reduced by fractionation to about 1/4 the unfractionated intensity, and 2) the smaller particles show much less reduction, and even the possibility of a fractionation enhancement. This last is in agreement with the top curve of figure II.13 and appears to be a real effect. Because of the discrepancy between values as small as .25 (even smaller values have been observed) and  $K_1/K_0 \approx 2/3$ , one expects the average value  $K_1$  to reflect the influence of many small particles, some possibly with fractionation enhancement. But one might note that values of  $K_1$  estimated for Small Boy were only a little over half the overall average value  $K_1 \approx 1930$  for many shots [71].





Despite the progress evident in the discussion of section II.A.3, the problem of predicting fractionation in real fallout fields from basic principles and data cannot at this time be fully solved. Attempts to predict fractionation have therefore resorted to rather drastic simplifying assumptions. Freiling [78] has proposed a method in which refractory mass chains are always assumed to be uniformly distributed through the volume of all fallout particles, whereas volatile chains are assumed to be uniformly distributed over the surface of all fallout particles. Because the amount of the former is then proportional to the 3rd power of the particle radius, whereas the amount of the latter is proportional to the 2nd power of the particle radius, the degree of fractionation is strictly a function of particle size. Fractionation predictions then require only an assumed basic particle size distribution and a consistent way of treating chains which are of mixed nature, i.e., neither completely refractory nor completely volatile. Freiling's method of treating mixed chains involves specification of the constants in eq (II.2) for each chain or group of similar chains. From these constants he infers an effective power of the particle radius for use in describing fractionation of the aforesaid chains. By further assuming a standard log-normal analytic form for the particle size distribution,<sup>15</sup> Freiling has only to refer to available fractionation data from various nuclear tests to infer activity and gamma ray spectrum as a function of particle size.

A similar but contrasting empirical analysis of particles from different types of detonations is due to Heft [14]. In the case of surface bursts over

---

<sup>15</sup> The lognormal distribution function is

$$P(x)d(\log x) = (\sigma\sqrt{2\pi})^{-1} \exp[-\log^2(x/\bar{x})/2\sigma^2]d(\log x) \quad ,$$

where  $\sigma$  and  $\bar{x}$  are constant. This type of frequency distribution has experimental support, as well as useful analytic properties when Freiling's assumptions are made.

coral, Heft makes use of Freiling's concepts regarding specific abundance except that his volatile chain is selected to be atomic mass number 137 (cesium) and his refractory chain is 155 (europium). Further, instead of eq (II.2), he used the linear relationship

$$r_{i,155} = A_i + B_i(r_{137,155}) \quad . \quad (II.14)$$

As previously mentioned, Heft identifies two components in the size distribution, one corresponding to early presence in the fireball and one to late injection. He finds that the data permit the assumption that both particle groups have a surface distribution of radioactivity; and he calculates the specific abundance of  $^{155}\text{Eu}$  and  $^{137}\text{Cs}$  which should be assigned to each group as determined by studies of large and small particle size ranges in which the two components are more or less separated. He then fits each particle group with a log-normal distribution of sizes, and weights the two particle groups so that the total amounts of  $^{137}\text{Cs}$  and  $^{155}\text{Eu}$  atoms are in the observed ratio. His result is an estimate of the specific abundance of  $^{137}\text{Cs}$  and  $^{155}\text{Eu}$ , as functions of the particle size. From these, with  $A_i$  and  $B_i$  values for the  $i$ 'th mass chain inserted into eq (II.14), one can in principle determine the spectrum as a function of particle size. By carrying this to its final conclusion by means of models which distribute the fallout spatially according to particle size and wind patterns, one can estimate spectrum as a function of position and time. Unfortunately, however, this program has not been carried out.

Freiling's model and that of Heft both feature a combination of two particle populations in which the smaller particle population is enriched in volatile constituents and the larger particle population is correspondingly

depleted in volatile constituents. Freiling appeals to a contrast between surface and volume attachment, while Heft uses populations resulting from early and late injection. But the results are qualitatively similar.

There remains an apparent conflict between power-law mass frequency curves observed, e.g., by Nathans, Thews, and Russell [16] and the two-component superposition of log-normal distributions such as used by Heft. This conflict is not considered serious, because such superpositions can resemble power-law distributions (see, e.g., ref. [13]). A strong case for the use of log-normal distributions has been made by Nathans, Thews, Holland, and Benson who showed that distributions which are self-preserving in the coagulation process resemble log-normal functions [79].

Freiling's model has been programmed for application to bursts by S. H. Cassidy [80], by methods in which different particle size groups are described by different log-normal distributions.<sup>16</sup> Following Freiling's studies [81], the constants  $B_i$  determining  $r_{i,95}$  are obtained from estimates of  $(F_R)_i$ , the fraction of the atoms of mass chain  $i$  which are refractory at the time of solidification of the carrier material (coral, silicon, etc.). A sensitivity study of this type by S. H. Cassidy and G. R. Crocker [82] and a later study by R. C. Tompkins [33] show that fractionation is little influenced by type of fissioning isotope, yield, or neutron energy; but the condensation temperature of the carrier material strongly affects the particle size distribution and related fractionation effects. Thus soils dominated by silicon should differ in these effects from soils dominated by calcium. Coral fallout of the latter type appears to retain more of the volatile components.

---

<sup>16</sup>This modified version of Freiling's model has been used in recent fallout models [33,83].

### c. Effect of Fractionation on the Spectrum

While fractionation effects on the spectrum were taken for granted in section II.B.4, some of the occasional studies of this phenomenon are worth describing, even though they tend to support the overall conclusion that these effects are of minor significance.

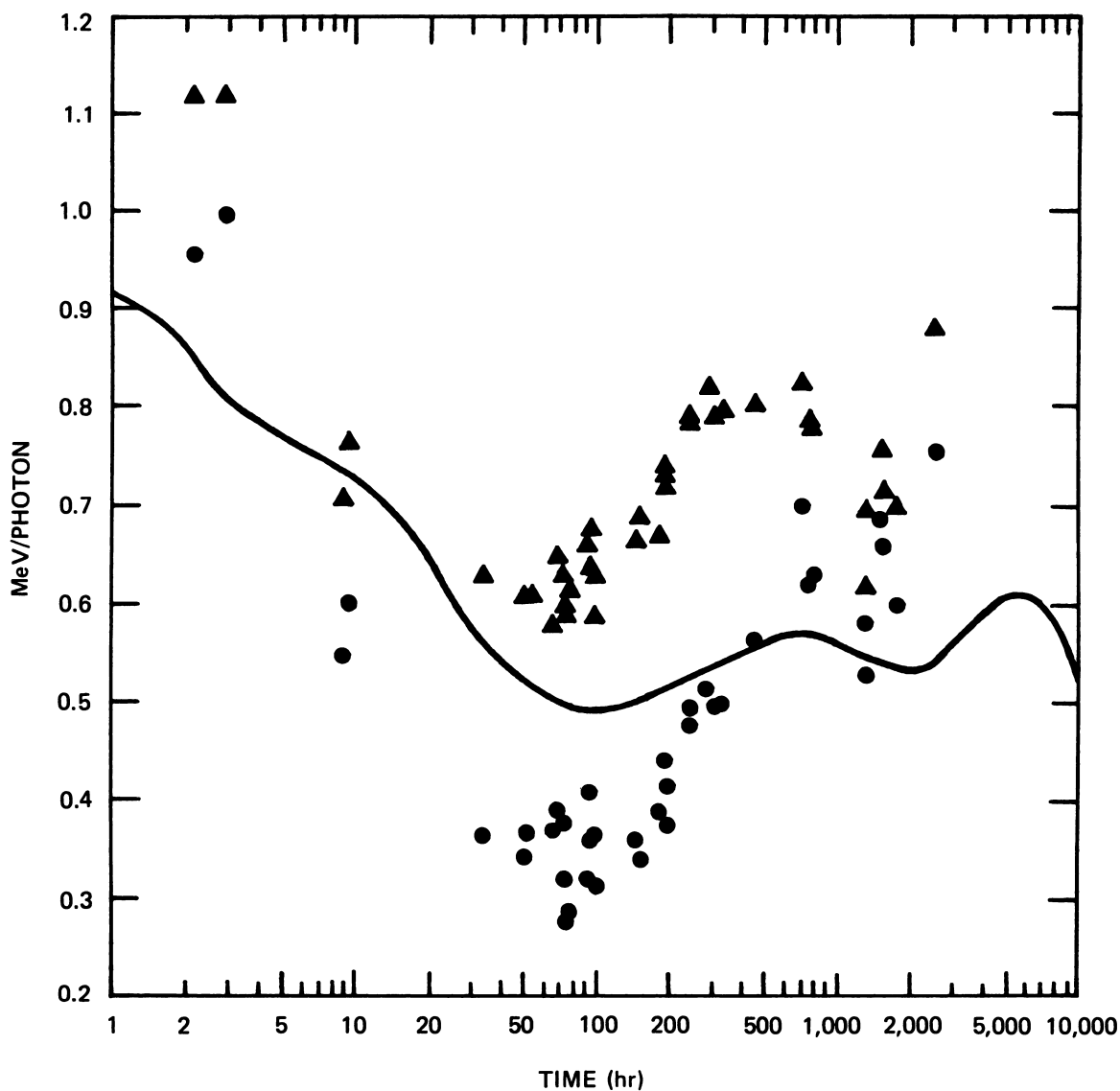
In 1959 Cook made comparisons between spectral measurements on actual fallout samples and the various available spectra, both fractionated and unfractionated [84]. There was so much scatter in his results that it was difficult to draw conclusions beyond some general similarities; but he concluded that the treatments of fractionation by Nelms and Cooper [38] and by Dolan [39] were inadequate. Figure II.15 reproduces data on the mean spectral energy which he calculated for many of his experimental samples, and compared with an early calculation by Miller [85].<sup>17</sup> Both the scatter and the general similarities are evident in this comparison of integrals over the spectrum. In general, the curve should lie below the triangles because it takes account of components below .29 MeV; likewise large  $^{239}\text{Np}$  contributions could put the points well below the curve.

In his 1968 report, Crocker studied fractionation effects on the spectrum as well as on the intensity. He calculated mean spectral energies which were essentially in agreement with Miller's curve as given in figure II.13; but Crocker also found that the mean energy changed by no more than about 10% as a result of fractionation.

Figure II.12 shows that fractionation softens the spectrum primarily in the region from 1 to 2.5 MeV. In table II.6 we give Crocker's differential

---

<sup>17</sup>One should be aware that different mean value determinations can have different low or high energy effective cut-offs, modifying the results significantly.



II.15 Mean energy per photon as a function of time after detonation. The solid line is a calculation by Miller [37] for fission product gamma radiation. Triangles are from experimentally determined spectra for radiations above 0.286 MeV, from individual fallout samples. Circles are likewise from experimentally determined fallout spectra, but take account of radiations below 0.286 MeV, including large  $^{239}\text{Np}$  components. Data and figure are due to C. S. Cook [84].

spectra for  $^{238}\text{U}$  fission by a thermonuclear spectrum of neutrons, cumulated over intervals of width 0.5 MeV at one hour and at one week after detonation, for various values of  $r_{89,95}$ . Although the overall effect on intensity (bottom line) shows factors almost as large as 2, the (normalized) spectra are less affected by the degree of fractionation. The one-week-old fission products show a much softer spectrum, but otherwise the same type and magnitude of fractionation effects.

The fractionation effect on spectrum is more time-dependent than would appear from table II.6. Crocker has noted that fractionation effects should be minimal during the period from 150 to 250 days after fission as a result of the dominance of  $^{95}\text{Zr} - ^{95}\text{Nb}$ . And beginning several years after fission, the depletion of cesium in fractionated fallout will sharply decrease the gamma ray activity relative to the unfractionated case [73].

In their studies of gamma ray properties above real fallout fields, Mather, Johnson and Tomnovec measured the spectrum of the radiation source from ground contaminated by 9-day-old fallout [86]. But we know of no comparisons of these data with theoretical spectra incorporating fractionation effects.

## 2. Neutron-Capture Gamma Rays

Neutrons from a nuclear burst are captured a) in the materials which constitute the device; b) in the air; or in other nearby materials, notably c) the soil, for explosions on or near the ground; and d) sea water, for explosions at or below the surface of the ocean.

In all cases the design of the weapon affects the number and location of neutron captures, as does the location of the burst. Hence there is great variability in the resulting induced gamma ray source strengths and spectra. Also, precise information has sufficient connection with weapon design to ensure that most of the data has a security classification. Despite this

Table II.6 (Normalized) spectra due to Crocker, for different degrees of fractionation as indicated by  $r = r_{89,95}$ , at 1 hour and 1 week after fission. Total activities are given below, relative to unfractionated fission products [70].

	$r = .1$	$r = .5$	$r = 1.$	$r = 2.$	$r = .1$	$r = .5$	$r = 1.$	$r = 2.$
	$\frac{1}{\text{hr}}$	$\frac{1}{\text{hr}}$	$\frac{1}{\text{hr}}$	$\frac{1}{\text{hr}}$	$\frac{1}{\text{wk}}$	$\frac{1}{\text{wk}}$	$\frac{1}{\text{wk}}$	$\frac{1}{\text{wk}}$
0 - .5 MeV	.396	.354	.350	.304	.695	.662	.678	.637
.5 - 1.	.385	.379	.363	.357	.262	.270	.245	.265
1. - 1.5	.1605	.1863	.1914	.232	.01339	.01358	.01218	.01273
1.5 - 2.	.0327	.0466	.0558	.0596	.0287	.0519	.0591	.0790
2. - 2.5	.01628	.0203	.0279	.0290	.001114	.001313	.001268	.001445
2.5 - 3.	.00429	.00717	.01192	.01305	.001372	.00253	.00291	.00388
3. - 3.5	.00340	.00301	.00267	.00273	.0000260	.0000490	.0000564	.0000760
> 3.5	.001425	.001187	.001705	.00214	0	0	0	0
Total								
Relative Act.	.547	.756	1.	1.25	.563	.768	1.	1.12

situation, there is enough available information to give a general picture both of the nature and importance of gamma ray components generated in this way.

Neutrons from the fission process are comparable in number with fission product atoms. Hence the neutron-induced components in fallout from pure fission weapons, which act like fission product components with short-lived predecessors, have intensities which can be estimated using the ratio of the likelihood of the capture process to the likelihood of generating a specific product mass number. Thus these components can be prominent in the spectrum, but they contribute only a small fraction of the total exposure.<sup>14,18</sup> Moreover, their relative importance varies as the ratio  $(e^{-\lambda t}/t^{-1.2})$ , increasing as the mean lifetime  $(= 1/\lambda)$  increases (see section II.B.3 and reference [87]).

In the case of air, it turns out that neutron capture in nitrogen generates penetrating gamma rays; but the half-life is only a few seconds. Thus these gamma rays are important constituents in the prompt radiations but do not contribute to the residual radiation. On the other hand, argon, which has much the largest cross section for capturing neutrons of any of the constituents in air, and which also has half-lives long enough for consideration as a residual component, is only present in air in small quantities. Finally, carbon, a low-energy beta emitter which is likewise present in small quantities, has a very long half-life, thus ensuring importance only as a result of buildup over many centuries.

We thus find residual radioactivity in the air is mainly due to argon isotopes and is of minor importance relative to other residual radiation sources.

---

<sup>18</sup> In a detonation with fusion energy comparable to the fission energy, the neutron capture components can be an order of magnitude more intense relative to the fission product components.



In the case of sea water, the most important residual activity is due to the dissolved salt, because of the high energy of the gamma rays and the 15 hour half-life of  $^{24}\text{Na}$ , together with the 37.3 minute half-life of  $^{38}\text{Cl}$ , which also emits energetic gamma rays. While there are many other elements present in sea water, they do not present the same combination of abundance, capture cross section, and half-life which is neither very short nor very long.

In regards to the soil, constituents vary with location. But nearly everywhere one would expect to find sodium, aluminum, manganese, calcium, silicon and iron. For times up to the first few days, one knows that fallout from a surface burst should emit significant numbers of photons from  $^{24}\text{Na}$ ,  $^{28}\text{Al}$  (2.3 minutes), and  $^{56}\text{Mn}$  (2.6 hours). This was demonstrated by R. L. Mather [88]. Since the  $^{45}\text{Ca}$  half-life is 163 days and the  $^{55}\text{Fe}$  half-life is 2.4 years, these activities may be significant constituents of fallout at long times after a surface burst.

All three cases mentioned above are summarized in table II.7, together with some of the other significant activities occurring when neutrons are captured in the soil [89]. Corresponding gamma ray spectra are given in table II.8 [90,91].

The case of neutrons captured in weapon materials has been summarized in a rough way by H. A. Knapp [92]. The most important activity due to neutron capture is that of  $^{239}\text{Np}$ , as can be seen from table II.9. The neptunium is produced by neutron capture in  $^{238}\text{U}$ . Fortunately, the gamma rays emitted are low in energy.<sup>19</sup> Note that the other activities due to uranium isotopes likewise have low photon energy and short half-lives.

---

<sup>19</sup>This discussion is limited to gamma rays. One must not forget that  $^{239}\text{Np}$  decays to  $^{239}\text{Pu}$ . Plutonium is discussed in section II.D.

Table II.7 Radioactivity induced in air, sea water, and Nevada Test Site soil by capture of  $10^{26}$  neutrons per megaton [89]. (Half-life values are as of about 1969).

<u>Nuclide</u>	<u>Half-life</u>	<u>0</u>	<u>1 hr</u>	<u>1 day</u>	<u>1 month</u>	<u>1 year</u>
<u>Air</u>						
$^{37}\text{A}$	35.1 y	75.5	75.5	74.7	40.8	.035
$^{41}\text{A}$	1.83 h	7,760	5,350	0.75	-	-
<u>Sea Water</u>						
$^{24}\text{Na}$	15.0 h	480	456	159	-	-
$^{38}\text{Cl}$	37.3 m	3,320	1,102	-	-	-
<u>Soil</u>						
$^{24}\text{Na}$	15.0 h	282,500	249,000	94,250	$5 \times 10^{-6}$	-
$^{28}\text{Al}$	2.3 m	$1.33 \times 10^8$	253,000	-	-	-
$^{31}\text{Si}$	2.62 h	157,000	122,500	282	-	-
$^{32}\text{P}$	14.3 d	192	192	182	43.8	-
$^{42}\text{K}$	12.4 h	32,400	30,800	7,950	-	-
$^{45}\text{Ca}$	163 d	47.4	47.4	47.4	41.5	8.95
$^{49}\text{Ca}$	8.8 m	174,300	21,400	-	-	-
$^{56}\text{Mn}$	2.6 h	336,000	262,00	606	-	-
$^{55}\text{Fe}$	2.4 y	17.4	17.4	17.4	17.15	13.8

Table II.8 Gamma-ray spectra from thermal-neutron capture, photons/100 captures [90].

Energy (MeV)	Silicon	Calcium	Potassium	Sodium	Chlorine	Manganese*	Iron	Aluminum
1-1.5	15.3	20.9	35.0	14.8	45.2	8.8	5.0	18.6
1.5-2	0	79.6	25.6	11.9	45.4	6.8	15.0	10.4 <sup>a</sup>
2-2.5	23.0	41.5	37.2	26.9	14.3	8.8	3.9	13.1
2.5-3	4.6	14.3	23.5	47.6	19.3	5.5	6.0	20.5
3-3.5	5.4	7.9	16.7	14.2	12.3	4.1	9.2	15.9
3.5-4	76.6	13.5	23.2	34.0	9.1	3.1	3.5	14.3
4-4.5	0.8	19.4	20.2	6.4	6.5	2.4	7.2	16.1
4.5-5	70.3	6.6	7.7	2.65	9.0	8.4	3.3	17.6
5-5.5	6.4	2.5	16.2	2.2	3.4	15.3	1.0	6.8
5.5-6	0.2	12.1	17.3	5.9	11.7	8.5	9.9	2.8
6-6.5	12.2	40.0	0.95	21.5	26.2	2.4	10.0	6.0
6.5-7	0.8	0	2.15	0	18.3	5.2	0.5	2.2
7-7.5	9.7	0	0.45	0	12.4	26.9	5.5	0.7
7.5-8	0	0	5.65	0	10.0	0	50.6	32.4
8-8.5	2.2	0	0	0	0	0	0.3	0
8.5-9	0	0	0	0	3.2	0	0.5	0
9-9.5	0	0	0	0	0	0	3.3	0

<sup>#</sup> Does not include small contribution below 1 MeV to binding energy previously determined by others.

<sup>a</sup> Does not include the 100% 1.78-MeV gamma rays of <sup>28</sup>Si following  $\beta$ -decay of <sup>28</sup>Al.

\* From Groshev et al [91].

Table II.9 Approximate contributions of induced activities and fission products to fallout dose, integrated to infinite time after fission [92].  
(Half life values are as of about 1969)

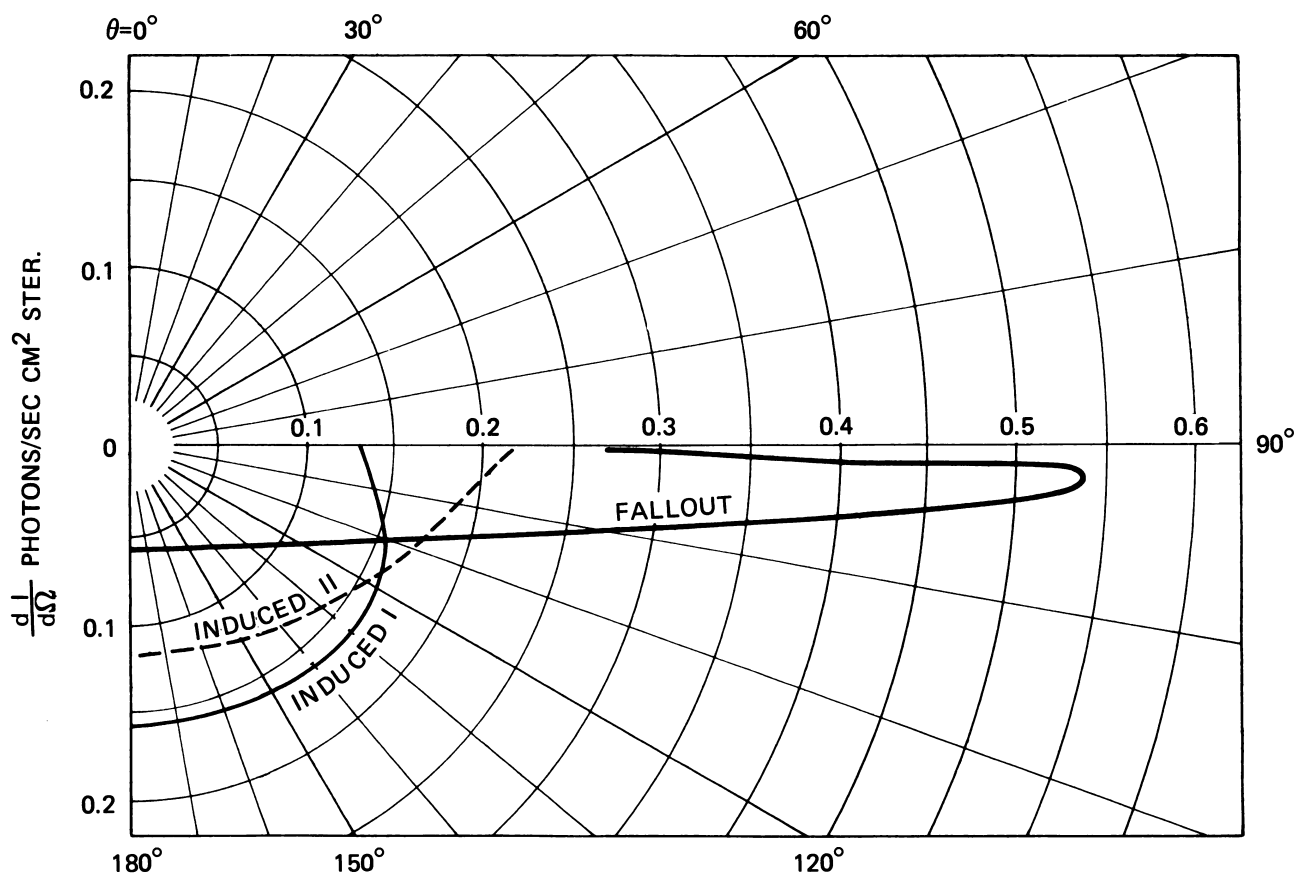
Activity	Half-Life	Average Mev/ Disintegration	Infinity Dose in Roentgens					
			Surfaceburst			Airburst		
			Low	Typical	High	Low	Typical	High
<sup>240</sup> U	14.1 hours	0.34	10	60	300	10	60	300
<sup>24</sup> Na	15 hours	4.10	50	250	600	1	5	10
<sup>239</sup> Np	2.35 days	0.27	40	250	900	40	250	900
<sup>237</sup> U	6.75 days	0.16	35	150	350	35	150	350
<sup>59</sup> Fe	45 days	1.10	0	1	2	0	1	2
<sup>58</sup> Co	71 days	0.97	1	2	20	1	2	20
<sup>57</sup> Co	272 days	0.13	0	1	10	0	1	10
<sup>54</sup> Mn	312 days	0.84	1	3	30	1	3	30
<sup>60</sup> Co	5.24 years	2.50	3	20	30	3	10	30
<sup>56</sup> Mn	2.58 hours	1.80	15	100	600	0	0	0
Total Induced				837			482	
Fission Products				6000			6000	

Note: Estimates based on 50 percent fission yield. Fission products assumed unfractionated.

Infinity dose = dose from 1 hour to  $\infty$ .

The early studies by R. L. Mather emphasize that residual radioactivity near "ground zero", i.e., the point at the surface below the burst, is not only due to fallout, but also to induced activities in soil remaining in place [88]. This would be true particularly for small detonations, and for that part of the surface near the crater. (Presumably the neutrons captured in the missing material of the crater produced activities which are part of the fallout.) But the angular distribution of gamma rays above the ground from a fallout source is quite different from the angular distribution of gamma rays due to materials made radioactive below the surface of the earth by penetrating neutrons. Figure II.16 due to R. L. Mather [88] shows the effect clearly. A consequence of this, together with the high energy of the  $^{24}\text{Na}$  component, is a surprisingly large contribution by induced activities to the gamma ray intensity at altitudes of a few hundred feet. Depth distributions of activation have been measured [93]. This effect is confined to the vicinity of the crater, as has already been mentioned.

The variability of the neutron-induced components, together with the limited amount of unclassified data on intensities, explains their not being included in standard fallout spectra. The neptunium component of the fallout spectrum softens the spectrum even as it augments the intensity; hence adoption of a fission spectrum as standard for shielding calculations is conservative in this connection. This additional component is presumably present in experimental determinations of fallout radiation intensities.



II.16 Calculated angular radiation intensity distribution giving an integrated radiation field of one photon per second [86]. Assumed photon energy = 0.82 MeV. The fallout curve is for a surface activity of 0.746 gamma-ray photon per second per  $\text{cm}^2$  and  $\alpha = 0.04$ , where  $\alpha$  is an effective mean free path for overlying material. The "induced I" curve (solid line) uses a surface-specific soil activity of  $0.1145 \text{ photons/sec}^{-1} \text{ gm}^{-1}$ , with  $\alpha = 0$  and activation  $\propto [10 \exp(-.0787x) - 10 \exp(-.1181x) + \exp(-.3937x)]$ ,  $x$  in centimeters. The "induced II" curve (dotted line) uses a surface specific soil activity of  $0.1905 \text{ photons/sec}^{-1} \text{ gm}^{-1}$ , with  $\alpha = 0$  and activation  $\propto \exp(-.0787x)$ ,  $x$  in centimeters.

One possibility which has been the subject of public controversy is the "salting" of nuclear weapons by introducing materials such as cobalt or sodium into the device. The induced "cobalt" gamma ray intensity has been compared with fission product gamma ray intensities by J. R. Dunning [94], in connection both with local fallout and with worldwide fallout. In the former case, Dunning concludes that for time periods of a few days the fission product gamma rays are from one to two orders of magnitude more intense. While there is a cross-over time beyond which the intensity of the induced component is greater, it occurs relatively late and in such a manner as to add to, but not to change the character of, decontamination problems.

Regarding fallout distributed on a worldwide scale in connection with air bursts, Dunning calculates that a 1 MT fission airburst might create a local gamma ray exposure of around .19 roentgens between  $30^{\circ}$  and  $60^{\circ}$  north latitude, with the accumulation occurring over 35 years. This does not take weathering, structure shielding, or other types of naturally occurring protection into account, however; and Dunning estimates that this value could be up to a factor of 10 too high due to these effects.

Even so, this means a far higher dose per megaton than the internal dose estimated more recently for the longlived fission products  $^{137}\text{Cs}$  and  $^{90}\text{Sr}$  by R. S. Russell, B. O. Bartlett, and R. S. Bruce [95]. These investigators estimate that after fission of 5000 megatons there would be a cumulation of  $\lesssim 2$  rads to the bone marrow and  $\lesssim 1$  rad to the whole body from these long-lived isotopes, in the hemisphere where the detonations occur.<sup>20</sup> This estimate is based on measurements of internal dose due to test detonations and is from 2 to 3 orders of magnitude smaller than the  $^{60}\text{Co}$  external dose estimated by Dunning.

---

<sup>20</sup>This estimate roughly agrees with that of the recent NRC study of long-term, world-wide effects of a hypothetical nuclear holocaust [96].

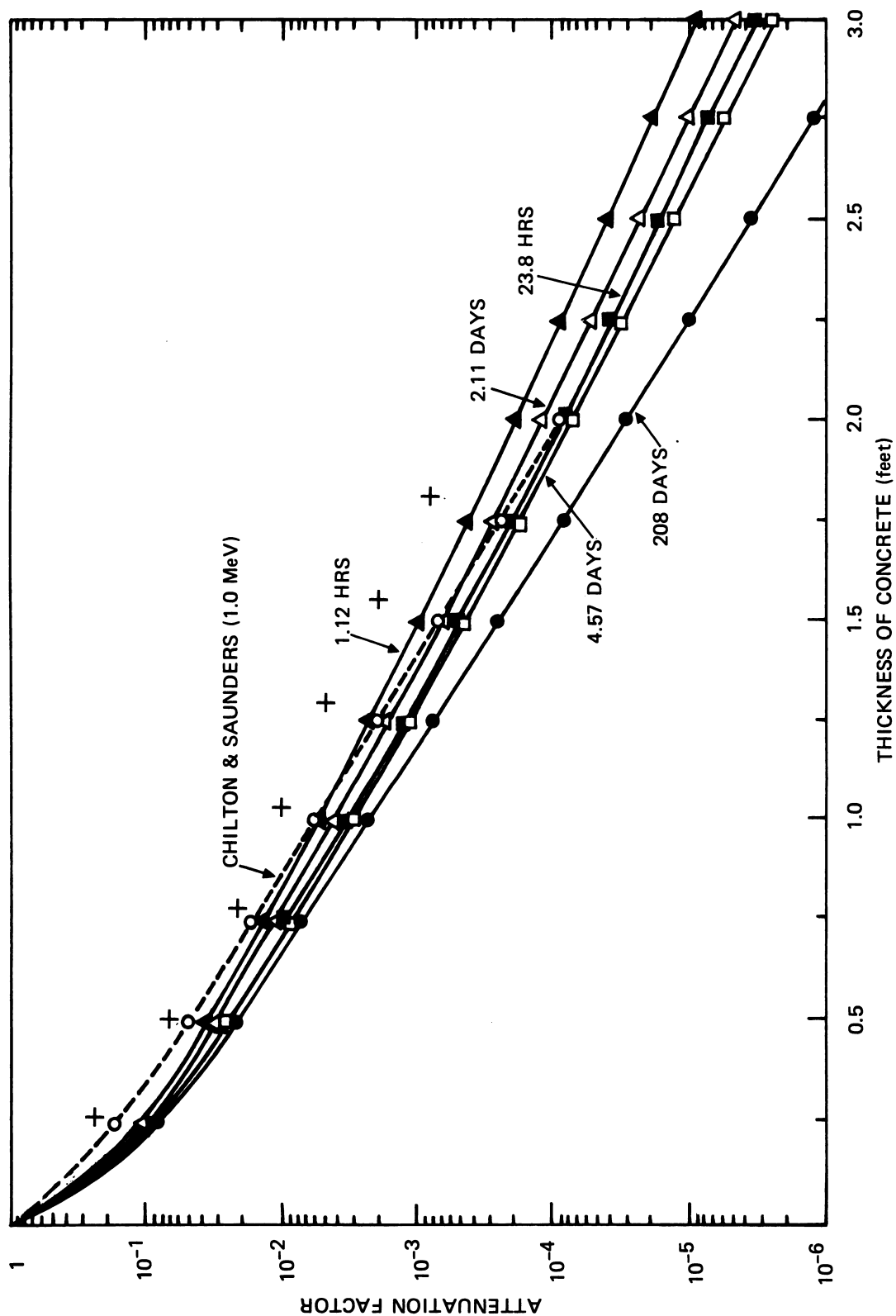
### 3. Penetration of Fallout Gamma Rays

Most of our information about the penetration of gamma rays from radioactive fallout derives from calculations; and this monograph contains much detail on the subject in later chapters. It is somewhat surprising, therefore, to learn how little was included in the nuclear test plans of the 1950's to yield usable data from actual measurements. This is the more true because at the time of the tests, the computational effort was still fragmentary and almost no information existed on which realistic shielding estimates could be based. One reason for this was the difficulty of predicting the location of significant amounts of fallout. The experiment had to be pre-positioned as near the test as feasible; and the actual fallout area depended critically of the wind pattern at the time of the detonation perhaps many days later.

Despite these difficulties, the series of experiments mentioned in section I.B.1 was successfully conducted by F. Titus [97] in the summer of 1957, in which fallout from two shots was measured in concrete at 3.15 inch intervals, as shown in figure I.4. Attenuation data as a function of time was obtained at each level, plus free-field data at the heights of 3 ft and 9 ft above ground. Figure II.17 gives ratios (the bold-face plus signs) for one of the shots, of the detector response of the detectors in concrete to the detector at the 3 ft height. The other curves in figure II.17 were calculated by L. K. Donovan and A. B. Chilton [98] on the basis of (unfractionated) spectra due to A. Nelms and J. Cooper [38]. The 1.12 hour curve of Donovan and Chilton agrees to within 20% or better with the data based on a Nelms and Cooper fractionated spectrum [99].

There are several observations to be made from this figure: First, note that the experimental points lie parallel to, but about a factor of 2 above the 1.12 hour curve. Part of this difference is due to reduction by ground roughness of the dose measured by the detector at height 3 ft, which





II.17 Curves give attenuation factor versus concrete thickness for a smooth isotropic plane source emitting various fission spectra [93]. The heavy plus signs lying above the curves give experimental data due to Titus (shot B, 2 hours after detonation) [97].

normalizes the other dose measurements. Part also can be due to non-linearity of the detectors below about 90 keV. Unfortunately, a detailed investigation of these points was not made; but a factor of 2 is not unreasonable as a result of the combination of effects.

The Titus data for later times show much more scatter; but a tendency for the spectrum to become less penetrating over the first day after detonation is clearly discernable; and this effect agrees in general magnitude and direction with Donovan and Chilton results.

The Titus data should be restudied more carefully, and in connection with attenuation data based, e.g., on Crocker's fractionated spectra [70]. Corrections should be made to the aboveground detector response for both ground roughness reduction and detector response reduction. But the general agreement in attenuation trends shown would no doubt be verified.

The other set of comparatively simple attenuation experiments was carried out by C. M. Cialella and others as Project 2.15 of Shot Small Boy [100,101]. A set of cubic and spherical enclosure shields were exposed to fallout. These shields consisted of concentric iron shells, with the space between alternately filled with water, which was emptied 5 hours after detonation to magnify the detector response and permit continuation of the measurements to far longer times.

The enclosure shields were positioned with their centers 50.5 inches above ground, 16000 ft from ground zero. Unshielded detectors were also positioned at the same height to measure the free-field dose.

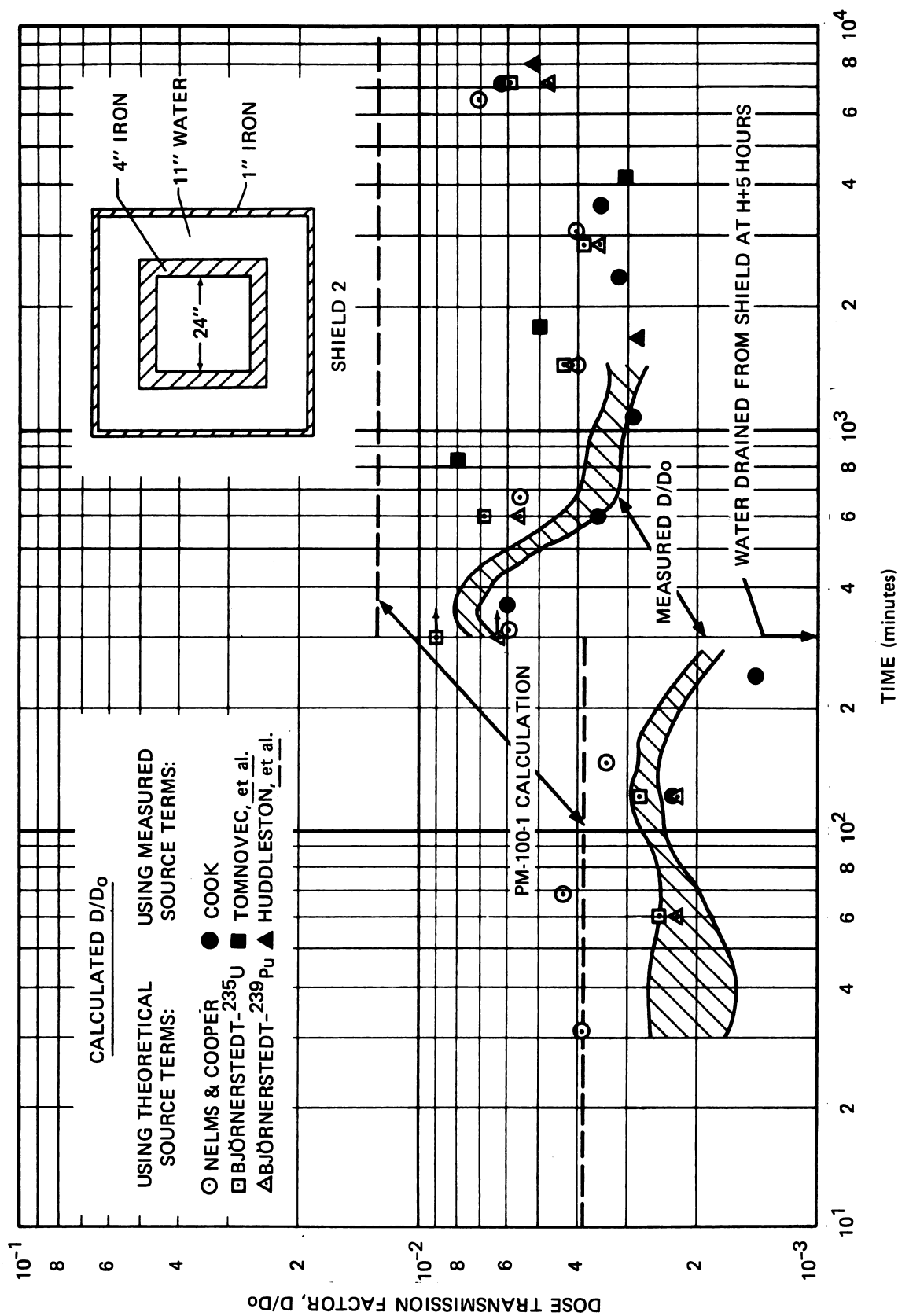
Subsequent to the basic field experiments, analyses were undertaken by Cialella and N. D. King, with the aid of additional laboratory experiments using  $^{60}\text{Co}$  and  $^{137}\text{Cs}$  [102]; and further analysis was undertaken by R. L. French, J. H. Price, and K. W. Tompkins, mainly with Monte Carlo computer programs [101],

but also using attenuation data from reference [99]. Figure II.18 shows one set of comparisons between the inside-outside experimental ratios and calculations based on various theoretical and experimental fallout spectra. Note that the filled points correspond to spectra inferred from pulse-height distribution measurements on actual fallout gamma rays; but the filled squares and triangles, which are based on spectral data from Small Boy [103,104], the detonation on which the enclosure measurements were also made, show scatter similar to that of the data based on computed fission product spectra (open circles, squares, and triangles).

In general, time variations appear to be more or less reproduced by the collection of theoretical points; but the calculations tend to lie higher than the enclosure measurements. Principal sources of error given by French, Price, and Tompkins are 1) deficiency of low energy gamma rays in the source spectra, which contribute to the free-field but not to the internal dose; 2) omission of consideration of structural details (such as supports) in the calculations; and 3) effects of ground roughness. The effect of ground roughness in this case would be to decrease the unscattered relative to the (softer) scattered gamma ray component incident on both the enclosure shields and the unshielded detectors. In addition, the PM-100-1 calculation is based on a 1.12 hour Nelms-Cooper spectrum, which is comparatively hard, as has already been demonstrated. The enclosure shield was approximated for calculation purposes by vertical walls extending upward from the ground indefinitely, with the detector at 3 ft rather than 50.5 inches above ground.

#### 4. $\beta$ -Ray Spectra and Penetration from Fallout

For completeness, we record here some of the characteristics of the  $\beta$ -radiation emitted by radioactive fallout. While this monograph is concerned with gamma ray shielding, any sketch of the full problem of protection against the hazards of radioactive fallout requires some reference to the  $\beta$ -ray aspects.



II.18 Calculated and measured dose transmission factors for the cubical enclosure shield shown. Calculations are based on spectra from references [26,38]. The points shown were calculated from experimental spectra due to references [84,103,104]. Dashed lines are from data of reference [99].

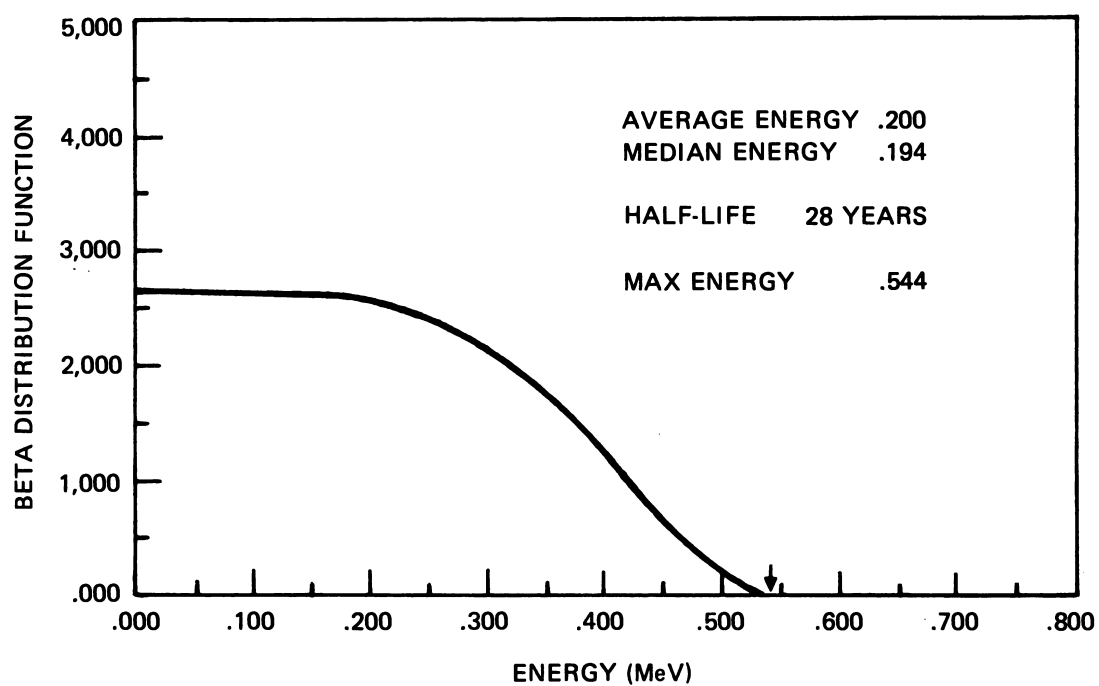
On the other hand, because  $\beta$ -spectra are distributed smoothly in energy rather than as monoenergetic spikes, predicted spectra for gross fission products can be expected to include those features most important to penetration properties even more surely than is the case for the gamma rays. Figure II.19 gives a spectrum calculated for  $^{90}\text{Sr}$  which is typical enough to illustrate this point. Other nuclides have spectra extending to higher energies, or spectra including peaks and/or different trends at low or near-maximum energies [105]. But these component spectra all cover the whole energy range from zero to maximum energy in a comparatively smooth manner.

One of the earliest series of calculations of  $\beta$ -ray spectra was due to A. T. Nelms and J. W. Cooper [106]. Many other calculations have been made more recently [107,108], and the computations of spectra have been written into computer subroutines [109,110].

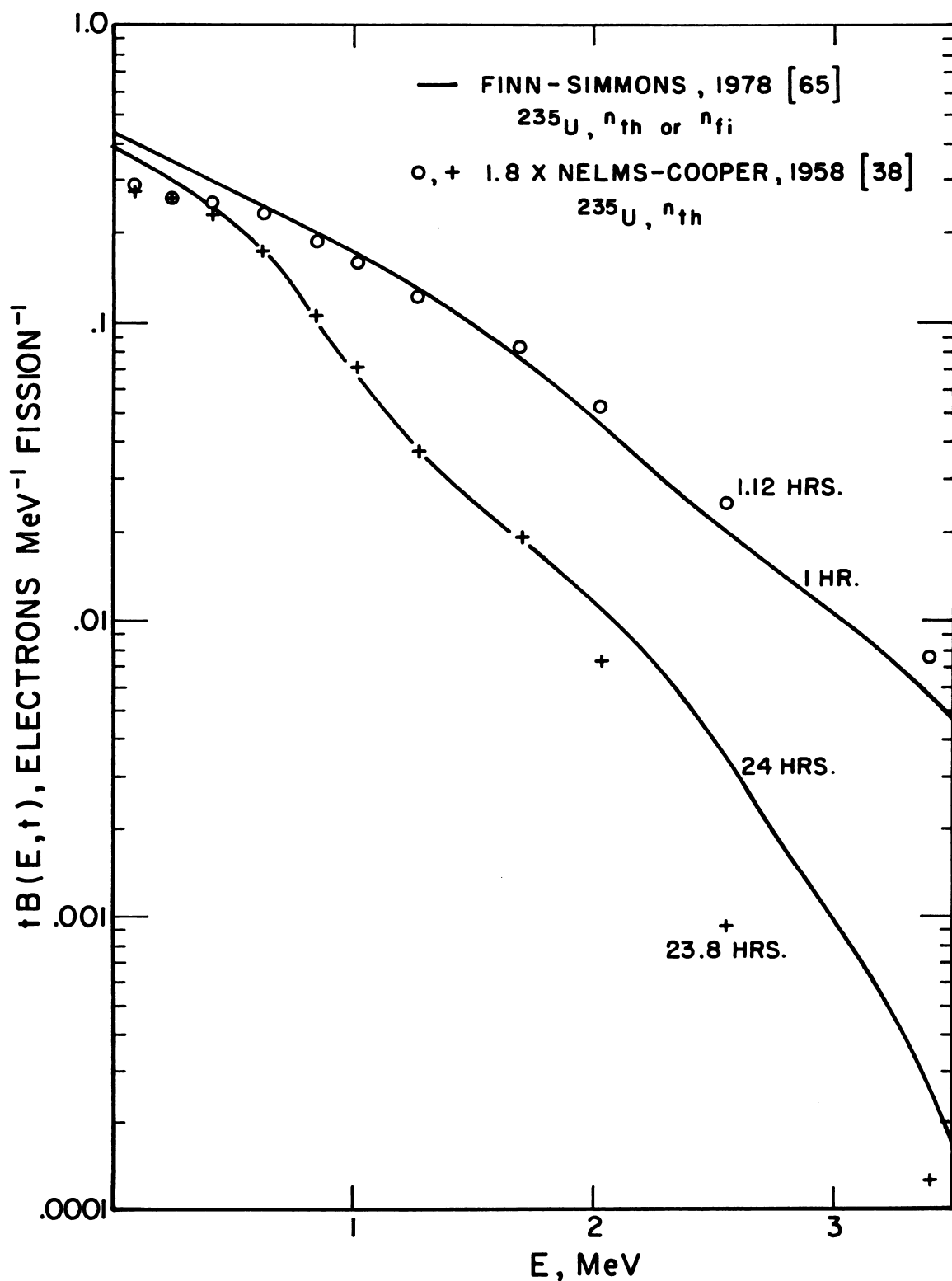
A series of experiments in 1966 by J. W. Kutcher and M. E. Wyman [111] show good agreement above 1 MeV in both shape and magnitude with calculations by R. B. Heller [107]. In figure II.20 we present recent spectra for  $^{235}\text{U}$  fission due to S. P. Finn and G. L. Simmons [60,62,63]. These are compared with some of the oldest available data which is reasonably comparable [38]. The older data differ in that fission is due to thermal neutrons, while for the recent calculation neutrons with a fission-neutron spectrum were used. While the absolute intensities do not agree closely -- the Nelms-Cooper data is about a factor 1.8 lower -- the shapes and shape change compare rather well.

Recent measurements of beta ray spectra are in remarkably close agreement with recent theoretical spectra for times varying from a few seconds to a few hours [63,68].

Removal of volatiles apparently hardens the spectrum of  $\beta$ -rays, so that fallout  $\beta$ -rays should be somewhat more penetrating than calculations based on unfractionated data. This type of effect does not appear to have been studied, however.



II.19 Beta-ray spectrum for  $^{90}\text{Sr}$ , normalized to an integrated total of one emitted particle [105].



II.20 Comparison of recently calculated  $\beta$ -ray spectra from unfractionated fission products, with early computations of these spectra. By  $n_{Th}$  and  $n_{Fi}$  we refer to fission due to thermal or fission spectrum neutrons.

In 1960, A. E. Boyd and E. E. Morris published  $\beta$ -ray penetration data for two fission product spectra in air (Nelms-Cooper, some volatiles removed); these results are reproduced in figure II.21 [106]. They apply roughly to flesh and to cellulose also, because of range and scattering cross section similarities of these materials. The range of electrons in air is about 13% greater (in  $\text{g/cm}^2$ ) than the range of electrons in muscle; hence, to apply to muscle the abscissa values of figure II.21 should be reduced by about .87. But since flesh has a density of about 0.9, the lower abscissa of figure II.21 can be fairly accurately relabeled "centimeters of flesh."

Substantially all the beta ray energy is absorbed within about 25 ft of air, or rather less than a centimeter thickness of flesh.

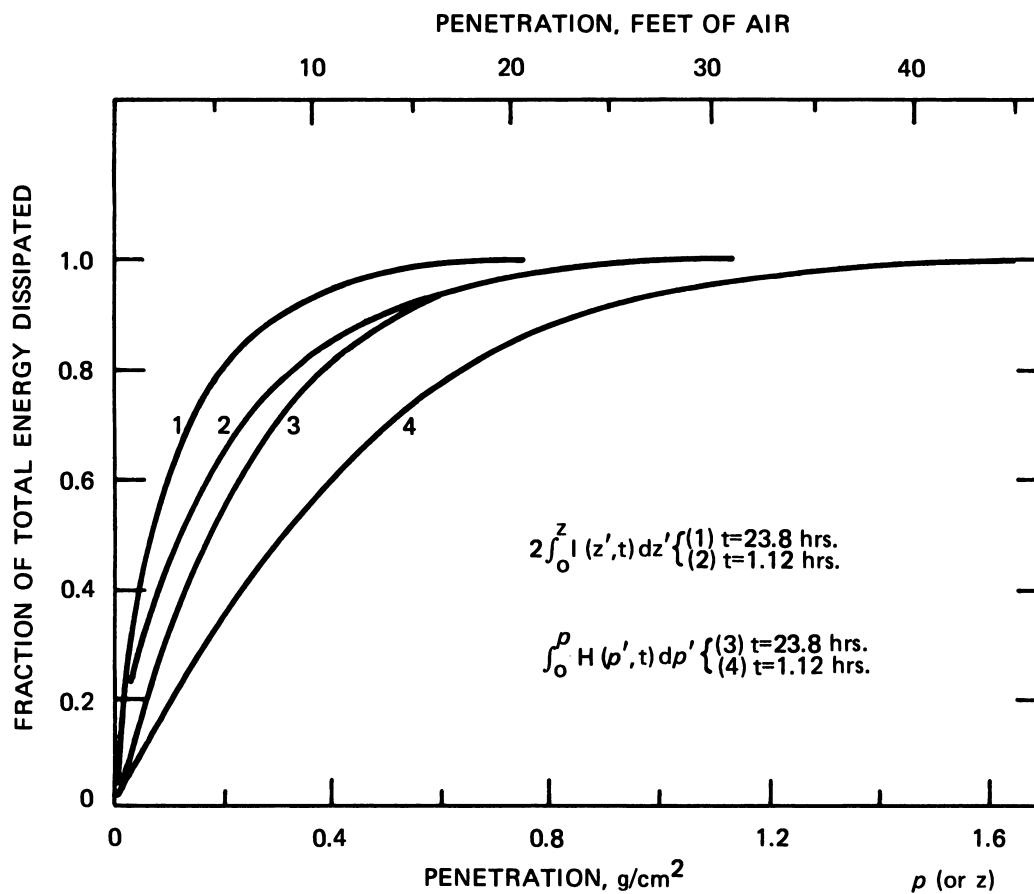
A more recent and more systematic study of beta ray dose to the skin has been made by S. Z. Mikhail [112]. He calculates tissue dose in rads as a function of fallout deposition density and retention time.

#### D. DEBRIS TRANSPORT AND DEPOSITION

##### 1. Computation of Fallout Surface Distributions

In the 1950's, following the discovery of the importance of fallout in the first large thermonuclear tests, many agencies participated in a concerted effort to develop mathematical procedures capable of reproducing the measured fallout position and time distributions for ground bursts. Two rather different lines of approach to the problem of predicting fallout surface distributions were pursued from very early investigations to the present day. The scaling approach is based on the idea that features observed in a few carefully documented detonations can, with proper scaling, be applied to other detonations differing in size, meteorological conditions, ground composition, and possibly detonation height. The other approach, by "wafers", assumes or determines a cloud geometry, and activity and particle size distribution which can vary





II.21 The fraction of total energy dissipated out to a given sphere radius or layer thickness [106]. Integrals over  $I$  correspond to plane isotropic sources, while those over  $H$  correspond to point isotropic sources.

throughout the cloud. The cloud is subdivided into segments, and each segment is repeatedly assigned a specified particle size and called a wafer. These are transported according to wind patterns and estimated fall rates.

The prototype of the scaling studies was due to C. F. Ksanda and coworkers in 1953 [113] at the Naval Radiological Defense Laboratory (NRDL), whose study was based on fallout patterns from Operation Jangle (1951) which were described by R. K. Laurino and I. B. Poppoff [114]. Results of early scaling studies were incorporated in the 1957 edition of Effects of Nuclear Weapons [12]; but W. W. Kellogg, in his 1957 testimony to Congress, documented the discouragingly poor agreement among different fallout prediction systems at that time [115]. A fallout symposium held in March 1957 concluded that "without a more thorough understanding of the mechanics of the fallout process, from the early stages of the fireball until a major fraction is deposited on the ground, we cannot expect to construct a fallout model that will yield reasonably accurate predictions" [116].

Much early work on fallout models was incompletely published, partially classified, or suited only to some highly specialized application. The 1957 Congressional Hearings are a good source for early results and general approaches, particularly Kellogg's presentation [115], and Schuert's discussion [117]. Unclassified and reasonably complete presentations of particular methods a few years later include A. D. Anderson's paper in 1961 [116] and the 1960 report by Callahan and coworkers [118].

Widespread work on fallout prediction systems in the late 1950's led to a second symposium in September, 1962, at which intercomparisons of many models were discussed on the basis of hypothetical burst conditions previously circulated to interested groups. This conference was fortunately followed up by extensive analysis of 18 of the models, even though many models were still not well documented [119,120]. Comparisons again showed that predictions of different models were very diverse.

A third symposium was held in April, 1966, and was far better focussed on the basic physics problems fundamental to the important processes [121]. By this time it was clear that only a few models would receive extensive additional development and use. In fact, much of the symposium consisted of reports about work on subunits of the DELFIC prediction system, a wafer system intended to satisfy requirements by all the different branches of the Department of Defense, thus superceding a large fraction of the existing models.

In the remaining paragraphs of this section we sketch four systems for calculating fallout intensities and spectra which remain relevant to current applications. These are the WSEG model, a Miller model, the DELFIC model, and a SEER model.

One should be aware throughout this discussion that the intercomparisons of reference [120] have not been fully extended to the more recent models or versions of older models.<sup>21</sup> Further, no systematic study seems to have been made of any model in comparison with data from most of the tests which have been conducted. This is largely because of the state of information about the test detonations, which is fragmentary except for a few cases. But there is also a difficulty of interpretation of differences because of the large number of variables involved.

This problem of pinning prediction systems to adequate, incontrovertible data leads to the opinion that these systems have their main application in hypothetical attack studies, and that they would not be dependable as a sole basis for fallout intensity estimates after a nuclear attack or for operational decisions on which the lives of people near a detonation might depend.

---

<sup>21</sup>A step in this direction was taken by C. J. Seery [122], in a paper describing a "TINCAN" model suggested by I. Russell. Sensitivity studies were included, with data on cloud radius, cloud height, particle fall rate, refractory mass fraction, and particle frequency distribution. Comparisons of TINCAN with the other models described here were made.

#### a. The WSEG Model<sup>22</sup>

Of the scaling models, that of G. E. Pugh and R. J. Galiano is the currently most important because it is used nearly universally in the hypothetical attack studies which attempt to assess damage to this country [119]. In this model the cloud activity is described by a Gaussian distribution whose height and lateral spread are functions of the yield. Neither particle size distribution nor fall rates are explicitly used in this model; and the cloud is not divided into wafers. Instead, there is a carefully specified function of the time after detonation which determines the rate of activity deposition on the ground. A scaling rule changes "time" in this function to downwind distance, by use of an effective wind speed. A crosswind shear dependent on cloud thickness must also be specified.

Dose rate on the ground is specified by the product of separate functions of the downwind and crosswind distances: The crosswind function is a Gaussian, and the downwind function is the product of a falling exponential function of downwind distance with a cumulative normal function.

This model is implemented by a very fast code, clearly suitable to studies which must cumulate the effect of many bursts, when details tend to be unimportant because of effects of superposition.

#### b. The Miller Model

A scaling approach was developed by Miller in the period 1962-64 based on data from the test shots Jangle 5 and Castle Bravo, and has been described in a 1969 paper [124]. More complex and physical than the WSEG model, it has been used in some damage assessment studies.<sup>23</sup>

---

<sup>22</sup>For Weapons System Evaluation Group [123].

<sup>23</sup>A later model (see ref. [125] by C. F. Miller is more empirical and comparable with DELFIC. While Miller's most recent model reflects the state of the art, we prefer to describe here Miller's earlier, more conceptual approach.

The Miller model distinguishes between the stem and the cloud of the mushroom due to a ground burst. The stem generates a high intensity "ridge" downwind, with intensity decreasing laterally. Superimposed on this is the broader cloud fallout pattern carried by the wind to greater distances because of its initially greater altitude. For both stem and cloud, intensities and distances are specified along the pattern centerline as functions of the yield and the wind velocity, and along a line of maximum lateral extent by use also of wind correction and shear factors. Both stem and cloud patterns are then described by contours in the shape of half-ellipses smoothly joined together and in agreement with the centerline and width values. The two components are summed to get the total "intensity", which is identified as a specific detector measurement 3 ft above an extended open area. The result in a simple wind pattern is to reproduce the fallout as a sort of shadow of the mushroom cloud, a characteristic observed with atmospheric nuclear tests.

Particle fall from the stem is assumed to be unaffected by lateral wind shear, but shear is taken into account in a simple way in the description of fallout from the cloud. Wind velocity is assumed to have an average magnitude at all altitudes. Particle concentrations are assumed to be uniform in the original mushroom cloud; but larger particles are assumed to fall from lower altitudes in the stem, and particle concentrations in the stem are assumed to decrease gradually with height. Contributions to exposure are functions of particle size expressed through fall speed; and at any location, the fallout varies between minimum and maximum fall speeds characteristic of the position. This leads to definite times of arrival and cessation of the fallout, and to exposure rate as a function of time and position, taking account of fractionation.

c. The DELFIC Model<sup>24</sup>

Beginning about 1965, an effort was instituted by the Defense Atomic Support Agency (now the Defense Nuclear Agency) to develop a single model for all applications. It was intended that this model, called DELFIC, would combine the best features available. But the model would have to be a compromise in many respects and in this regard one more among many systems.

DELFIC consists of five principal modules: Initial Conditions, Cloud Rise, Transport, Particle-activity, and Output-processor.

The "Initial Conditions" module requires yield and height data, together with data on the type<sup>25</sup> and natural particle-size distribution of the soil. It identifies an effective starting time for cloud rise and specifies for that time the average temperature of the nuclear cloud, the total amount of entrained soil material together with the fractions in vapor and condensed phases, and the size-frequency distribution of the soil particles. In constructing the code, it was eventually concluded that the natural size distribution of soil particles could be used except possibly for large-yield detonations. Most other output data are determined by scaling relationships based on test measurements and on estimates of energy partition among different processes.

The "Cloud Rise" module is based on a modified version of a model developed by I. O. Huebsch [128-130]. There are two stages of the calculation. In the first, the cloud is treated as a whole, with uniform density and temperature, water and water vapor conditions, and turbulent kinetic energy density. Mass of the cloud can change due to entrainment and particle fallout and these affect the dynamic behavior. Vertical wind shear is accounted to increase entrainment

---

<sup>24</sup>Department of DEfense Land and Fallout Interpretive Code. The Monterey Symposium Report [126] has been superceded by [127] and should be used with caution.

<sup>25</sup>In general, soil types can be classified as either siliceous (melting temperature near 1673 K) or calcareous (melting temperature near 2887 K).

through changes in shape which are not otherwise considered. Cloud volume and mass are related through assumption of an expanding oblate spheroidal shape.

In the second part of the Cloud Rise module, particle wafers are identified at the initial time by subdividing the cloud into horizontal disk segments and assigning to each segment a set of wafers, each with characteristic particle size interval. The wafers are then subdivided into horizontal segments to permit horizontal distortion; the upper and lower wafer boundaries are followed separately to take account of vertical stretching. The full set is then followed in space through the rise processes, as position and shape are modified by the forces effective. The resulting output is a set of distorted wafers distributed vertically and suitable for the transport process. Wafers with different particle size intervals will be at different heights after cloud rise.

The "Atmospheric Transport" module utilizes an atmosphere divided into sub-volumes, each with properties uniform throughout. Large cells are used to take account of region of macro-meteorological phenomena, while small cells can be used to take account of local circulation systems such as those affected by topographical features such as a mountain. With this approach, wind-patterns characteristic of certain regions and having considerably complexity, including vertical components, can be utilized. Standard settling rates are used based on formulae for spheres of different sizes. Wind effects and fallout during cloud rise are taken into account.

The "Particle Activity" module distributes activity with particle size according to a modified version of Freiling's radial-distribution model; that is to say, volatile chains are assumed to condense on surfaces while refractory chains are distributed through particle volumes, as previously discussed. Fractionation is thus taken into account and predictions for specific types of

nuclides can be made as well as for total activity. Induced activities are also included. Dose rates 3 ft above a smooth plane are determined according to the local spectrum.

The "Output Processor" module sets up the format for the various selections of output data of greatest interest [131].

#### d. SEER Models<sup>26</sup>

While DELFIC was developed to be as realistic as the state-of-the-art permitted, this same requirement implies long and comparatively expensive runs. Other requirements for fast and cheap computations led to attempts to develop simplified versions of DELFIC, in competition with the WSEG Model but hopefully giving results more nearly equivalent to those of DELFIC for the intended applications. The SEER Models (Simplified Estimation of Exposure to Radiation) are of this type, with running times for a single case 1/50 to 1/100 that of DELFIC, and with rather good agreement for sample cases.

To achieve short running times assumptions such as the following are used: Starting point at stabilized cloud, with parameters from DELFIC-generated library, wind profiles constant in time and space, a log-normal particle size distribution, precalculation of falling times for deposition of cloud wafers, uniform cloud, and use of standard function types to represent lateral distributions relative to the "hot-line" for a cloud layer.

## 2. Continuing Problems of Fallout Phenomena

Research into different aspects of fallout phenomena has been at a low level for many years. This is due in part to the lack of new data; but much research has been cut back despite the possibility of significant progress. Hence we sketch here briefly the status of some representative problem areas. As our model we use a similar discussion in ref. [133], which was divided into the four categories which we use below. See also [13], Appendix VII.

---

<sup>26</sup>See reference [132].



a. Effects of Small Changes in Burst Height or Depth

The K factor depends on the amount of material near the detonation which is available for entrainment and contamination. This depends sensitively on burst height or depth, and on the amount of material projecting above the ground.

In regards to burst height, a summary of data from test detonations is given in ref. [71], together with a "best current answer" in the form of tentative rules to use in calculations for low altitude bursts, with and without nearby buildings and other projecting structures. The data show large fluctuations; and no dependable theory exists. The analogous problem of radioactivity as affected by detonation burial has been the subject of several studies [14,134-136] and is described in Effects of Nuclear Weapons (ENW) [12]. DELFIC includes options for buried detonations. But no unifying study of the problem in its various aspects exists as yet.

b. Problems of Fallout Formation

Soil type is important for two reasons: Different soil types have different natural particle size distributions; and soil types with different dominant constituents have different temperatures of melting and vaporization.<sup>25</sup> Thus attachment of refractory chains relative to attachment by volatile chains is in principle affected, as is the fraction of radioactivity which is deposited with local fallout.

Examination of available test data, which include tests over soil, hard rock, wet coral, and water, show differences which are suggestive but not conclusive. While such effects are assumed to exist, theory tends to remain unproven.

There is evidence of at least two components of fallout with different histories of formation, as indicated in section II.A.4. But there is no fully satisfactory theory of related processes in the fireball. As already seen, for example, work on high energy processes of diffusion and condensation does

not extend to problems of agglomeration and particle scavenging. Further, while particle studies conclude that the natural particle distribution of the soil is significantly modified in the fireball [18], DELFIC ignores such effects.

The related problem of the extent to which the shock of the detonation changes the particle size-frequency distribution is not settled.

In principle, the distribution of fallout particles in the original cloud can be studied by calculations in which two-dimensional hydrodynamics is applied to a multi-cell decomposition of the cloud. This "microscopic" approach is far more feasible today than was earlier the case; and it constitutes an important alternative to the studies on which DELFIC is based.

#### c. Problems of Fallout Transport

The assumption that the fallout remains physically unchanged during transport ignores effects whose importance has never been established. The observed dispersion of particle sizes is larger than that indicated by terminal velocity considerations. This could be due to further agglomeration, fracture of the more fragile agglomerates, or the fall of heavy particles could entrain small particles in a turbulent wake. In addition, air heavily weighted with particles could undergo mass subsidence.

The scavenging of particles by precipitation includes an important set of interrelated problems on which information is incomplete (see ref. [137]). While local fallout occurs so rapidly that concurrent precipitation is comparatively unlikely, rain-scavenging is a dominant mechanism for long distance fallout of very small particles; and it should also be important for so-called "intermediate" fallout.

#### d. Problems of the Radiation Field

The effects of non-uniform fallout distribution on or near a structure comprise a family of little-studied but potentially important problems.

Fallout can drift and pile up like snow with the wind, can stick to the sides of buildings when wet, and can collect at the edge of smooth surfaces. Such changes of source configuration affect the radiation field. Investigation of these effects has been at best exploratory.

#### e. Long Term Fallout Problems

A useful interpretive summary document has been published by a committee of the National Research Council [96] on the problems of fallout disseminated in patterns of global extent. The basic quantity utilized by this study is as follows: "A mix of high- and low-yield bursts of  $10^4$  MT would probably produce an average cumulative fallout of  $^{90}\text{Sr}$  of approximately  $1 \text{ Ci/km}^2$  in the middle latitudes of the northern hemisphere. ... A fission-fusion fraction of about 0.4 has been assumed. ... About two thirds of the total fallout in the northern hemisphere would be received during the first year."

One sees immediately that the long term problems due to local fallout are more severe by orders of magnitude. But in event of a nuclear conflict far removed from the continental United States, the resulting radioactive hazards can raise questions of possible remedial actions. To date, this class of problems has received limited attention only.

#### E. BIOLOGICAL HAZARDS FROM FALLOUT RADIATIONS

Because radiation intensities are highest at early times after detonation, our general emphasis is on externally incident gamma rays from not-very-old fission products. But in this section we describe other ways in which radioactive fallout can be a source of injury. Some aspects of this subject have been discussed in two important symposium reports [138,139].

These other hazards require countermeasures rather different from shielding. Perhaps the main alternative countermeasure is decontamination. While the effort to devise and evaluate decontamination procedures has been

much less than the effort directed towards shelter studies, enough literature exists on the subject to justify a review monograph. Introductions to relevant subtopics are given in references [140,141]. Unfortunately, we cannot do justice to the subject here.

Several processes provide natural decontamination beyond the obvious process of radioactive decay [142,143]: Radioactive particles can be removed by surface water runoff, or they can migrate deeper into the earth. Soluble materials may be removed by surface water, or they can penetrate to greater (and less harmful) depths. Volatile components can be removed by the winds and disseminated in the atmosphere. These processes operate to reduce radiation hazards where they are relatively intense.

By contrast, the various categories of hazard which we next discuss often call for procedures specific to the problem identified.

#### 1. The Direct External Threat

There is evidence that heavy fallout observed during atmospheric nuclear tests has been visible as individual particles falling and striking objects, or as deposits accumulating on the surfaces of various objects ([71] p. 19ff, and [144]). Similar particulate fallout from volcanoes in similar quantities has been visible [145]. Further, a K-Factor of  $2000 \text{ (R/hr)/(KT/mi}^2\text{)}$  is equivalent to about  $4 \times 10^{-13} \text{ (R/hr)/(fissions/ft}^2\text{)}$ . Typical specific abundances of fallout particles are  $5 \times 10^{14}$  fissions/gram (see, e.g., [13,18]). Thus, for each R/hour at 1 hour occurring, 5 milligrams of particles would be deposited per square foot of area. In terms of spherical, 100 micron diameter particles, and assuming a density of 2, this would correspond to  $\sim 5$  particles per  $\text{cm}^2$ . This amount of fallout would be clearly visible on a clean surface; and if this much should fall in a few minutes, it should be evident by sight, sound, or touch.

From such an argument and from experience with nuclear tests, the supposition is strong that in daylight, with no competitive precipitation such as rain or snow, dangerous levels of fallout would be observable without special instrumentation. But in bad weather, or at night, other indicators of hazard must be available.

There are several types of natural "shielding" against fallout gamma rays. Ground roughness including grass coverage, which will be described in greater detail in section VI.D, is often considered to reduce by about 30% the dose over level ground at a height of 3 ft [146,147,71]. Foliage retention can either increase or decrease the dose, depending on whether the fallout particles are kept farther away or brought closer than the detector height. In the case of grass, particles would be held slightly closer to the detector and the dose would increase; high shrubbery could increase the dose considerably; and trees could decrease the dose significantly, although foliage retention also has the effect of eliminating the ground roughness effect for the elevated particles. Ground contours would usually operate to shield against part of the direct radiation and reduce the dose: The smaller the visible source area the smaller the dose.

H. A. Knapp noted that film badge readings on people living in the vicinity of the Nevada Test Site were reported as averaging  $2/3$  the average readings on badges placed at fixed locations out-of-doors [148]. This means that normal homes and routines reduced the dose by about a factor  $2/3$ , no doubt largely as a result of residential structure shielding. If one combines this factor with ground roughness, one obtains a natural dose reduction by about  $1/2$  from an established standard value 3 ft above a smooth plane. For greater dose reductions, special measures must be taken.

# II.10 Summary of relationships between brief radiation exposure and acute injury [148].

Type of Exposure	Type of Injury	Probable Condition of Majority during Emergency		Probable Mortality Rate during Emergency <sup>a</sup>	Comments
		Medical Care Required	Able to Work		
A. Brief, wholebody, gamma rays <sup>b</sup>					
12-50 R	Asymptomatic	No	Yes	0	
50-200 R	Acute radiation sickness, Level I	No	Yes	Less than 5%	Deaths will occur in 60, or more, days.
200-450 R	Acute radiation sickness, Level II	Yes	No <sup>c</sup>	Less than 50%	Deaths will occur within 30 to 60 days.
450-600 R	Acute radiation sickness, Level III	Yes	No <sup>c</sup>	More than 50%	Deaths will occur within about one month.
More than 600 R	Accute radiation sickness, Levels IV and V	Yes	No	100%	Deaths will occur in two weeks or less.
B. Internal Deposit	Acute radiation sickness, with severity proportional to internal dose and its location.	Varies	Varies	Low Probability	No reliable data on relation between internal dose and whole-body brief external dose. Effects may be combined.
C. Beta irradiation of skin					
Less than 1,000 rads	Radiation dermatitis Type I	No	Yes	0	Associated with whole-body external radiation dose of variable size. Effects may be combined.
1,000-5,000 rads	Radiation dermatitis Types II and III	Yes	No	Uncertain	Mortality possible with extensive skin area involved or with added external whole-body exposure.
More than 5,000	Radiation dermatitis Type IV	Yes	No	Uncertain	Mortality possible with extensive skin area involved or with added external whole-body exposure.

<sup>a</sup>This refers to acute mortality: death during first 60 days after onset of exposure.

<sup>b</sup>For electromagnetic radiation (such as gamma radiation) the exposure units (R for roentgen) can be converted approximately to absorbed dose units (rad), at the midline of the body, by multiplying the number of R units by 2/3.

<sup>c</sup>Except during illness-free latent period.

Table II.11 Beta-ray dose rate as a function of penetration below the skin surface and due to contamination by fission products, vs the gamma ray exposure rate 3 ft above the ground [149].

Case 1			Case 2		
$2.1 \times 10^{17}$ fissions			$2.1 \times 10^{19}$ fissions		
$1.95 \times 10^{12}$ fissions/sq ft			$1.95 \times 10^{14}$ fissions/sq ft		
$\gamma$ Exposure Rate			$\gamma$ Exposure Rate		
1.48	r/hr @ 1 hr		$1.48 \times 10^2$	r/hr @ 1 hr	
0.434	r/hr @ $10^4$ sec		2.74	r/hr @ $10^5$ sec	
<u>z (<math>\mu</math>m)</u>	(10 <sup>4</sup> seconds)		(10 <sup>5</sup> seconds)		
	<u><math>\beta</math> Dose Rate</u>	<u><math>\beta/\gamma</math> Ratio</u>	<u><math>\beta</math> Dose Rate</u>	<u><math>\beta/\gamma</math> Ratio</u>	
30	18.33 rad/hr	42.	141.1 rad/hr	51.	
100	12.12	28.	83.9	31.	
300	7.71	18.	48.4	18.	
1,000	3.75	8.6	17.7	6.5	
3,000	1.21	2.8	3.4	1.2	
10,000	0.06	0.1	0.0	0.0	

This monograph is not directed to the pathological consequences of radiation exposure. Information on this subject has been published by NCRP [149], from which table II.10 is reproduced. This table summarizes some of the more operationally significant facts.

Another aspect of the direct threat is the dose delivered by fallout particles in contact with the tissues of the body. This would be mainly due to beta rays, because their energy is deposited in a volume of radius  $\sim 100$  times smaller than is the case for gamma rays. Note that a 40 micron particle may emit as much as  $10^6$  ergs of beta ray energy, and that the volume of tissue encompassing most beta ray energy deposition is rather less than a gram in mass. This would mean  $10^4$  rads within the irradiated region. Table II.11 gives results of some calculations by S. L. Brown [150,151], for ratios of  $\beta$ -ray absorbed dose at different tissue depths to the  $\gamma$ -ray exposure at 3 ft above the ground. Both cases are for 100 micron particles; and case 1 corresponds to  $10^4$  seconds after detonation, while case 2 is a larger contamination at the later time of  $10^5$  seconds after detonation. Since exposure roughly equals absorbed dose, one sees that the two doses are comparable at a depth of  $\lesssim 1$  centimeter.

Body parts most susceptible to beta burns are exposed areas, or areas accessible to dust and grime, and which, once contaminated, require washing or other positive measures to remove the foreign substance [152].

## 2. Direct Internal Hazards<sup>27</sup>

Eating, drinking, and breathing each can introduce radioactive materials into the body. We first limit the discussion to mechanisms which do not involve food chains, and extend the discussion in the following subsection.

---

<sup>27</sup>See references [71,139,143,153-156].



Fallout particles can themselves be ingested into the lungs; but this does not turn out to be the major concern for several reasons: Only very small particles would be carried by the breath into nostrils or mouth; filtration in the nasal passage is effective against all except very small particles. In the case of drinking water, exposed reservoirs can collect fallout particles. But the heavier particles would rapidly settle; and the lighter particles would tend to remain on the surface and settle at a later time. The amount remaining in suspension and therefore pumped to users would be a rather small fraction of the total. Preparation of solid foods should remove fallout particles, with careful washing of uncooked fruits and vegetables.

More subtle hazards arise because some of the fission products are gaseous, and some are quite soluble. In particular, three elements combine the important properties of intermediate lifetime, solubility, and quantity produced by nuclear detonations. These are iodine, strontium, and cesium. To these we should add  $^{239}\text{Pu}$ , which results from neutron capture in  $^{238}\text{U}$  and is not gaseous nor particularly soluble, because of its special properties. Lesser hazards include iron, barium, and lanthanum. Properties of these important nuclides are listed in table II.12.

$^{131}\text{I}$  stands out as a major concern at early times after detonation. It has a fairly short lifetime. It can be a dissolved contaminant in drinking water and can be ingested into the lungs. A concentration of the radioactivity occurs as the iodine collects in the thyroid gland. Marshallese children exposed to fallout in a nuclear test conducted in the South Pacific had external exposures estimated at perhaps 175 roentgens; and about 60% of these children developed (benign) thyroid tumors.

Table II.12 Data for some of the more important residual and radioactive nuclides.

<u>Nuclide</u>	<u>Half Life</u>	<u>Important Decay Mode</u>	<u>Source</u>	<u>Maximum Energy Emitted</u>	<u>Body Organ Irradiated</u>
$^{89}\text{Sr}$	52.0 days	$\beta(100\%)$	Fission Prod.	1.49 MeV	Bone
$^{90}\text{Sr}$	28.1 years	$\beta(100\%)$	Fission Prod.	0.55 MeV	Bone
$^{131}\text{I}$	8.04 days	$\gamma(99\%)$	Fission Prod.	0.72 MeV	Thyroid
$^{137}\text{Cs}$	30.1 years	$\gamma(95\%)$	Fission Prod.	0.66 MeV	Whole Body
$^{239}\text{Pu}$	24,360 years	$\alpha(100\%)$	Induced in $^{238}\text{U}$	5.15 MeV	Bone, Lung, Lymph Nodes

This highlights the question of the major route of ingestion of  $^{131}\text{I}$  in the case of the Marshallese. To answer this question, studies have been made of the inhalation of  $^{131}\text{I}$  [157]. Iodine arises from a rather volatile nuclear chain, and hence presumably collects on the surface of fallout particles, where it is available either for volatilization or for solvation. It can be volatilized either from solution with evaporating water, or with the passage of warm moist air over the fallout. But for maximum inhalation hazard, the contaminated air must remain near the ground (due to atmospheric conditions) or inside a building. The conclusion of the studies is that inhalation of  $^{131}\text{I}$  is probably less important than ingestion with liquids and solids.

Contaminated drinking water results from the concentration of soluble materials such as  $^{131}\text{I}$  and Sr in reservoirs which utilize surface, rather than ground sources of water. But standard water treatment methods provide a substantial degree of decontamination; and while the resulting dose can be very significant, it should not reach lethal levels, but rather add to the overall dose accumulation.

### 3. Food Chain and Other Indirect Hazards<sup>28</sup>

Several early indirect radiation hazards should be noted. Exposed farm animals may be killed; and food crops may be either killed or reduced in yield. As a result, the food supply would be reduced.

In the case of farm animals, there are known differences in their susceptibility to radiation. But the similarities to each other and to man are strong enough that one expects both lethality and countermeasures to be generally similar to those for man. Animals under cover would receive lower direct radiation doses than animals in the open; and there exist natural ravine-type ground configurations in which animals would be less exposed than

---

<sup>28</sup>See references [139,143,153,158-161]. For contamination studies based on volcanic ash, see reference [145].

in an open field. In addition, animals fed stored silage would avoid the large internal radiation dose expected for animals grazing on open pastures.

Studies of crop reduction indicate that the main dose causing this is due to beta rays; and it is postulated that the terminal meristems of growing plants are the most radiosensitive regions. These are the rapidly growing tips; and they are particularly vulnerable at certain times, such as the seedling stage. These plants would be exposed to both beta rays and gamma rays from all nearby contaminated surfaces; and they would also retain some particles in particularly lethal positions on their own foliage.

Significant crop reductions can result, particularly at times of the year (such as June) when major crops are at vulnerable stages of growth.

The threat of  $^{131}\text{I}$  in the milk consumed by children is singled out as unusually important. Cattle would ingest fallout as they eat pastureland grass; they would drink surface water containing this and other soluble contaminants; and they would inhale volatilized  $^{131}\text{I}$ . Cow's milk contains substantial amounts of this material; but radiation from ingested  $^{131}\text{I}$  is largely confined to the thyroid, as already noted.

Fortunately, this threat is limited to a few weeks after detonation; and a number of countermeasures exist. In addition to precautions regarding food and water for the cattle, there is the possibility of special processing for the milk; and there remains an additional possibility of medicines which either temporarily block the uptake of this chemical or else speed its elimination from the body [162-164].

$^{131}\text{I}$  is typical of mechanisms along a food chain which can result in unusual concentrations of some radioactive element. Many such cases are known; and some general rules for predicting the effect have been worked out [139].

#### 4. Ecological Problems<sup>29</sup>

Ecological problems first came to public attention in the form of concern about explosive growth of insect populations if unchecked by death of the more radiosensitive birds. But the problem is far more complex, as can be seen from the simple observation that sterilization of insects occurs at a few thousand rads, whereas lethality for birds occurs at about 1000 rads. But conversely, many types of insects would tend to remain at all times in extremely close proximity to any particular fallout material, with correspondingly large doses.

Ecological systems apparently recover from nuclear disaster along a pattern very similar to that observed in other massive disasters such as fires, droughts, etc. Devastated areas are reinvested with a time sequence of plant and animal life from small and comparatively short-lived at earlier times to large and longer-lived at later times. Radiation from nuclear detonations is unique mainly in covering an exceptionally large fraction of the available ground area.

There has been special attention to insect populations, partly as pests which destroy the crops, and partly as pollinators necessary for plant fertilization. Note that pollinating insects include crawling insects which have special vulnerability. Sterilization reduces insect populations and, because of differential radiosensitivity between species, some species are more vulnerable than others. Widespread radioactive fallout has thus been likened to insecticide use. Insect species whose natural enemy populations are reduced undergo explosive multiplication, which saturates and reverses as other species multiply in turn. The result is a type of oscillation about equilibrium populations.

---

<sup>29</sup>See references [139,143,159,160,165-167].

Destruction of entire species of plant or animal life is unlikely, partly because of great fluctuations of radiation field intensity, and partly because of the relative insensitivity to radiation of seeds.

#### 5. Late Problems<sup>30</sup>

Long-term internal hazards are apt to involve food chains; and these begin with the uptake of radioactive materials through plant root systems, rather than from fallout retained on foliage. Different plant species exhibit great differences in chemical uptake through root systems, just as there are great difference in the proclivity for foliage retention.

Of the isotopes constituting major late hazards because of long half-lives,  $^{137}\text{Cs}$  is a gamma ray emitter which behaves chemically like potassium;  $^{89}\text{Sr}$  and  $^{90}\text{Sr}$  are beta emitters which behave in the body like calcium; and  $^{239}\text{Pu}$  is an alpha emitter, and also tends to collect in the bone or at bone interfaces.

The internal hazard due to  $^{137}\text{Cs}$  is much less than that due to  $^{90}\text{Sr}$  even though the lifetimes of both are about 30 years. There are several reasons for this: Cesium tends to remain bound more tightly in the soil, so that its uptake by root systems is less. Turnover rate of cesium in the body is much shorter than is the case for strontium, with the result that residual concentrations are smaller. Also, gamma rays from  $^{137}\text{Cs}$  give a generalized irradiation to the body, partly because of the penetrability of the gamma rays and partly because of the more general distribution of cesium internally. Beta emission by radioactive strontium tends to result in dosage to the bone.

Studies show that there is some promise of drugs which can reduce the concentration of both contaminants in the body.

---

<sup>30</sup>See references [139,143,168-170].

$^{239}\text{Pu}$  presents a rather different series of problem potentialities than radioactive strontium. Its lifetime is more than 1000 times longer, with a corresponding reduction in relative dose rate for equal concentrations. Also, it tends to be rather tightly bound in the soil. But this comparison does not take account of two factors: Buildup of plutonium contamination must be evaluated over time periods of many centuries; and the energy emitted in the form of an alpha particle is concentrated in a very small volume located in one of the most radiosensitive regions of the body -- the bone interface.

We should note again that major attempts have been made in various studies to assess the long-term effects of these nuclides [97,171].

Finally, the problems of delayed biological effects of whole body gamma ray exposure, including formation of cataracts, cancers, leukemias, and genetic problems should be noted. Much attention has been directed to these problems due to their involvement in low-dose exposures of many types.

## References<sup>\*</sup>

- [1] Weinberg, A. M., and Wigner, E. P., The Physical Theory of Neutron Chain Reactors, 115 (U. of Chicago Press, Chicago, Ill. 1958).
- [2] Crouch, E. A. C., Fission-Product Yields from Neutron-Induced Fission, At. Data and Nucl. Data Tables 19, 417-532 (1977).
- [3] Rajagopalan, M., Pruys, H. S., Grütter, A., von Gunten, H. R., Hermes, E. A., Richmond, R., Rössler, E., Schmid, A., and Wydler, P., Mass Yields in the Fission of Uranium-235 and Plutonium-239 in the Neutron Spectrum of a Gas-Cooled Fast Reactor, Nucl. Sci. Eng. 58, 414-419 (1975).
- [4] Lisman, F. L., Abernathey, R. M., Maeck, W. J., and Rein, J. E., Fission Yields of Over 40 Stable and Long-Lived Fission Products for Thermal Neutron Fissioned  $^{233}\text{U}$ ,  $^{235}\text{U}$ ,  $^{239}\text{Pu}$ , and  $^{241}\text{Pu}$  and Fast Reactor Fissioned  $^{235}\text{U}$  and  $^{239}\text{Pu}$ , Nucl. Sci. Eng. 42, 191-214 (1970).
- [5] Evans, R. D., The Atomic Nucleus, 392-394 (McGraw-Hill, 1955).
- [6] Fraser, J. S., and Milton, J. C. D., Nuclear Fission, Annual Review of Nuclear Science 16, 379-444 (Annual Reviews, Inc., Palo Alto, Calif., 1966).
- [7] Mustafa, M. G., Mosel, U., and Schmitt, H. W., Asymmetry in Nuclear Fission, Phys. Rev. 7, 1519-1532 (April 1973).
- [8] Specht, H. J., Nuclear Fission, Rev. Mod. Phys. 46, 773-787 (October 1974).
- [9] Kochendorfer, D. B., Calculated Activities of U-235 Fission Products for Very Short Nuclear Reactor Operation, Vol. 1, Report No. USNRDL-TR-757, 49 pages (June 18, 1964).
- [10] Norman, J., and Winchell, P., Cloud Chemistry of Fallout Formation, Fallout Phenomena Symposium, April 12-14, 1966, Monterey, Calif., 12-54 (Office of Civil Defense or Defense Atomic Support Agency, Washington, D.C., 1966).
- [11] Brode, H. L., Review of Nuclear Weapons Effects, Annual Review of Nuclear Science 18, 153-202 (Annual Reviews, Inc., Palo Alto, Calif., 1968).
- [12] Glasstone, S., and Dolan, P. J., ed., The Effects of Nuclear Weapons, Third Edition, 644 pages (U.S. Dept. of Defense and Dept. of Energy., Washington, D.C. 1977). Earlier editions: 1957, 1962 (also 1950, The Effects of Atomic Weapons).
- [13] Heft, R. E., The Characterization of Radioactive Particles from Nuclear Weapons Tests, Advan. Chem. Ser. 93, 254-281 (1970).
- [14] Tompkins, R. C., Radiochemical Interpretations of Small Boy Fallout, BRL Report No. 1623, 45 pages (Ballistic Research Laboratories, Aberdeen Proving Ground, Md., Nov. 1972), AD 908895.

---

<sup>\*</sup> Reports labeled NRDL, or USNRDL, were published by the Naval Radiological Defense Laboratory, which no longer exists.



- [15] Russell, I. J., Size Distribution and Specific Activity Characteristics of Radioactive Debris as Related to Mode of Production, unpublished notes, 30 pages (Oct. 4, 1968).
- [16] Nathans, M. W., Thews, R., and Russell, I. J., The Particle Size Distribution of Nuclear Cloud Samples, *Advan. Chem. Ser.* 93, 360-380 (1970).
- [17] Björnerstedt, R. and Edvarson, K., Physics, Chemistry, and Meteorology of Fallout, *Annual Review of Nuclear Science* 13, 505-534 (Annual Reviews, Inc., Palo Alto, Calif., 1963).
- [18] Tompkins, R. C., Russell, I. J. and Nathans, M. W., A Comparison between Cloud Samples and Close-In Ground Fallout Samples from Nuclear Ground Bursts, *Advan. Chem. Ser.* 93, 381-400 (1970).
- [19] A Critique of Some Technical Aspects of Civil Defense, Report for the Director, Office of Civil Defense, 164 pages (Advisory Committee on Civil Defense, National Academy of Sciences, Washington, D.C., 1969). See Appendix VII.
- [20] Freiling, E. C., Radionuclide Fraction in Bomb Debris, *Science* 133, 1991-1998 (June 1961). Also Stevenson, P.S., Hicks, H.G., Nervik, W.E., and Levy, W.B., Correlation of Fractionation Phenomena in the TEWA Event of Operation Redwing: Suggestions for the Control of Fractionation, Report No. UCRL-2057 (Classified), (Lawrence Radiation Laboratory, Livermore, Calif., 1957).
- [21] Miller, C. F., A Theory of Formation of Fallout from Land-Surface Nuclear Detonations and Decay of the Fission Products, R&D Tech. Report No. USNRDL-TR-425, 123 pages (May 27, 1960).
- [22] Korts, R. F., and Norman, J. H., A Calculational Model for Condensed State Diffusion Controlled Fission Product Absorption During Fallout Formation, Report No. GA-7598, 91 pages (General Atomic Div. of General Dynamics, Jan. 10, 1967).
- [23] Norman, J. H., and Winchell, P., Cloud Chemistry of Fallout Formation, Report No. GA-9945, 57 pages (Feb. 15, 1970); and Norman, J. H., Winchell, P., and Staley, H. G., Report No. GA-9180, 53 pages (Gulf General Atomic, Inc., San Diego, Calif. 92113, Jan. 31, 1969). See also reference [10].
- [24] Norman, J. H., and Winchell, P., Physical, Chemical, and Radiological Properties of Fallout, AEC Symp. Series 24, 9-30 (U.S. Atomic Energy Commission, Dec. 1971); and Norman, J. H., Henry's Law Constants for Dissolution of Fission Products in a Silicate Fallout Particle Matrix, Report GA-7058, 38 pages (General Atomic Div. of General Dynamics, San Diego, Calif. 92112, Dec. 29, 1966).
- [25] Adams, C. E., Quan, J. T., and Balkwell, W. R., High Temperature Measurements of the Rate of Uptake of Molybdenum Oxide, Tellurium Oxide, and Rubidium Oxide Vapors by Selected Oxide Substrates, *Advan. Chem. Ser.* 93, 35-62 (1970).

- [26] Björnerstedt, R., Health Hazards from Fission Products and Fallout. II. Gamma Radiation from Nuclear Weapons Fallout, Arkiv för Fysik 16, 293-313 (1959).
- [27] Bateman, H., The Solution of a System of Differential Equations Occurring in the Theory of Radio-active Transformations, Proc. Cambridge Phil. Soc. 15, 423-427 (Cambridge University Press, London, 1910).
- [28] Crocker, G. R., and Turner, T., Calculated Activities, Exposure Rates, and Gamma Spectra for Unfractionated Fission Products, Report No. USNRDL-TR-1009, 180 pages (Dec. 28, 1965).
- [29] Miller, C. F., Proposed Decay Schemes for Fission-Product and Other Radionuclides, Report No. USNRDL-TR-160, 101 pages (May 1957).
- [30] Coryell, C. D., and Sugarman, N., editors, Radiochemical Studies: The Fission Products, Book 1, Part IV, pages 341-435 (McGraw-Hill Book Company, Inc., 1951).
- [31] Way, K., and Wigner, E. P., The Rate of Decay of Fission Products, Phys. Rev. 73, 1318-1330 (1948).
- [32] Hunter, H. F., and Ballou, N. E., Fission-Product Decay Rates, Nucleonics 9, c2-c7 (1951).
- [33] Tompkins R. C., Sensitivity Analysis of the Delfic Particle Activity Module, BRL Report No. 1523, 132 pages (Ballistic Research Laboratories, Aberdeen Proving Ground, Md., January 1971), AD 880619.
- [34] Bolles, R. C., and Ballou, N. E., Calculated Activities and Abundances of  $U^{235}$  Fission Products, Report No. USNRDL-456, 257 pages (Aug. 30, 1956).
- [35] Glendenin, L. E., Coryell, C. D., and Edwards, R. R., Distribution of Nuclear Charge in Fission, Radiochemical Studies: The Fission Products. C. D. Coryell and N. Sugarman, eds., 489-516 (McGraw-Hill Book Co., Inc. New York, 1951).
- [36] Present, R. D., On the Division of Nuclear Charge in Fission, Phys. Rev. 72, 7-15 (1947).
- [37] Miller, C. F., and Loeb, P., Ionization Rate and Photon Pulse Decay of Fission Products from the Slow-Neutron Fission of  $U^{235}$ , Report No. USNRDL-TR-247, 91 pages (Aug. 4, 1958).
- [38] Nelms, A. T., and Cooper, J. W.,  $U^{235}$  Fission Product Decay Spectra at Various Times after Fission, Health Physics 1, 427-441 (1959).
- [39] Dolan, P. J., Gamma Spectra of Uranium-235 Fission Products at Various Times after Fission, Report No. AFSWP-524, 77 pages (Armed Forces Special Weapons Project, Washington, D.C., March 5, 1959).

- [40] Dolan, P. J., Gamma Spectra of Uranium-238 Fission Products at Various Times after Fission, Report No. DASA 526, 52 pages (Defense Atomic Support Agency, Washington, D.C., May 7, 1959). See also Dolan, P. J., Calculated Abundances and Activities of the Products of High Energy Neutron Fission of Uranium-238, Report No. DASA 525 (Defense Atomic Support Agency, Washington, D.C., May 7, 1959).
- [41] Pappas, A. C., The Distribution of Nuclear Charge in Low Energy Fission, P/881, Proc. Int. Conf. on Peaceful Uses of Atomic Energy, Aug. 8-20, 1955, Geneva, Switzerland, Session 8B.1, 7, 19-26 (United Nations, New York, 1956).
- [42] Perkins, J. F., and King, R. W., Energy Release from the Decay of Fission Products, Nucl. Sci. Eng. 3, 726-746 (1958).
- [43] Wahl, A. C., Nuclear-Charge Distribution in Fission: Cumulative Yields of Short-Lived Krypton and Xenon Isotopes from Thermal-Neutron Fission of  $^{235}\text{U}$ , J. Inorg. Nucl. Chem. 6, 263-277 (1958).
- [44] Maienschein, F. C., Peelle, R. W., Zobel, W., and Love, T. A., Gamma Rays Associated with Fission, P/670, Proc. 2nd Int. Conf. on the Peaceful Uses of Atomic Energy, September 1-13, 1958, Geneva, Switzerland, Session A-22, 15, 366-372 (United Nations, New York, 1958).
- [45] Knabe, W. E., and Putnam, G. E., The Activity of the Fission Products of  $\text{U}^{235}$ , APEX-448 (Atomic Energy Commission, Tech. Info. Service, Oak Ridge, Tenn., October 1958).
- [46] Zigman, P., and Mackin, J., Early Time Decay of Fission Product Mixtures-II  $\gamma$ -Energy Release and Ionization Rates Following Thermal Neutron Fission of  $\text{U}^{235}$ , Health Physics 5, 79-84 (1961).
- [47] Petrov, V. I., Gamma-Radiation of the Fission Fragments of  $\text{U}^{235}$  and  $\text{P}^{239}$ , At. Energ. [Sov. J. At. Energy] 7, 168-171 (Aug. 1959).
- [48] Griffin, J., Beta Decays and Delayed Gammas from Fission Fragments, Report No. LA-2811, 48 pages (Los Alamos Scient. Lab., Los Alamos, N.M., Feb. 18, 1963).
- [49] Griffin, J., Beta Decays and Delayed Gammas from Fission Fragments, Phys. Rev. 134, B817-B823 (1964).
- [50] Fisher, P. C., and Engle, L. B., Delayed Gammas from Fast-Neutron Fission of  $\text{Th}^{232}$ ,  $\text{U}^{233}$ ,  $\text{U}^{235}$ ,  $\text{U}^{238}$ , and  $\text{Pu}^{239}$ , Phys. Rev. 134, B796-B816 (1964).
- [51] Watson, J. E., Jr., An Analysis of Calculated and Measured Fission Product Activities, BRL Report No. 1239, 53 pages (Ballistic Research Labs., Aberdeen Proving Grounds, Maryland, Feb. 1964).
- [52] Maienschein, F. C., Fission Product Gamma Rays, Engineering Compendium on Radiation Shielding, Vol. 1, Shielding Fundamentals and Methods, 77-85 (Springer-Verlag, Inc., New York, 1968).

- [53] Löw, K., and Edvarson, K., Gamma Spectra from Mixed Fission Products of Ages Between 2 Hours and 7 Days, Arkiv för Fysik 29, 359-365 (1965).
- [54] Bunney, L. R., and Sam, D., Gamma-Ray Spectra of the Products of Fast-Neutron Fission of  $^{235}\text{U}$  and  $^{238}\text{U}$  at Selected Times after Fission, Nucl. Sci. Eng. 29, 432-443 (1967).
- [55] Bunney, L. R., and Sam, D., Gamma-Ray Spectra of the Products of Thermal-Neutron Fission of  $^{235}\text{U}$  at Selected Times after Fission, Nucl. Sci. Eng. 39, 81-91 (1970).
- [56] Coryell, C. D., Kaplan, M., and Fink, R. D., Search for Correlations of Most Probable Nuclear Charge  $Z_p$  of Primary Fission Fragments with Composition and Excitation Energy, Can. J. Chem. 39, 646-663 (1961).
- [57] Holden, N. E., Mendelson, M. R., and Dudley, T. E., Total Gamma Energy Release Due to Thermal-Neutron Fission in  $^{235}\text{U}$ , Nucl. Sci. Eng. 30, 461-463 (1967).
- [58] Tasaka, K., and Sasamoto, N., Calculation of the Decay Power of Fission Products, Nucl. Sci. Eng. 54, 177-189 (1974).
- [59] Schenter, R. E., and Schmittroth, F., Radioactive Decay Heat Analyses, Proc. Conf. on Nuclear Cross Sections and Technology, March 3-7, Washington, D.C., NBS Spec. Publ. 425, Vol. I, 21-28; Devillers, C., Nimal, B., Fiche, C., Noël, J. P., Blachott, J., and de Tourreil, R., Sensitivity of the Afterheat from  $^{235}\text{U}$  and  $^{239}\text{Pu}$  Thermal Fission to Errors in Fission Product Nuclear Data, *ibid.*, 29-38, (National Bureau of Standards, Washington, D.C. 20234, October 1975).
- [60] England, T. R., and Schenter, R. E., ENDF/B-IV Fission-Product Files: Summary of Major Nuclide Data, Report No. LA-6116-MS, 39 pages (Los Alamos Scientific Lab., Los Alamos, N.M. 87545, Oct. 1975).
- [61] Stamatelatos, M. G., and England, T. R., FPDCYS and FPSPEC: Computer Programs for Calculating Fission-Product Beta and Gamma Multigroup Spectra from ENDF/B-IV Data, Report No. LA-NUREG-6818-MS, 82 pages (Los Alamos Scientific Lab., Los Alamos, N.M. 87545, May 1977).
- [62] England, T. R., and Stamatelatos, M. G., Multigroup Beta and Gamma Spectra of Individual ENDF/B-IV Fission-Product Nuclides, Report No. LA-NUREG-6622-MS, 186 pages (Los Alamos Scientific Lab., Los Alamos, N.M. 87545, Dec. 1976).
- [63] England, T. R., and Stamatelatos, M. G., Comparisons of Calculated and Experimental Delayed Fission-Product Beta and Gamma Spectra from  $^{235}\text{U}$  Thermal Fission, Report No. LA-NUREG-6896-MS, 61 pages (Los Alamos Scientific Lab., Los Alamos, N.M. 87545, July 1977).
- [64] England, T. R., Schenter, R. E., and Schmittroth, F., Integral Decay-Heat Measurements and Comparisons to ENDF/B-IV and V, Report No. LA-7422-MS, 41 pages (Los Alamos Scientific Lab., Los Alamos, N.M. 87545, Aug. 1978).

- [65] Finn, S. P., and Simmons, G. L., Calculation of Fission Product Gamma Ray and Beta Spectra at Selected Times after Fast Fission of  $U^{238}$  and  $U^{235}$  and Thermal Fission of  $U^{235}$ , Report No. SAI-78-782-LJ, 41 pages (Science Applications, La Jolla, Calif. 92037, July 15, 1978).
- [66] Dickens, J. K., Emery, J. F., Love, T. A., McConnell, J. W., Northcutt, K. J., Peelle, R. W., Weaver, H., Fission-Product Energy Release for Times Following Thermal-Neutron Fission of  $^{235}U$  Between 2 and 14000 Seconds, Report No. ORNL/NUREG-14, 228 pages (Oak Ridge Natl. Lab., Oak Ridge, Tenn. 37830, Oct. 1977).
- [67] Peelle, R.W., Zobel, W., and Love, T. A., Applied Nuclear Physics Div. Annual Report, 93 pages (Oak Ridge Natl. Lab., Oak Ridge Tenn. 37830, Sep. 10, 1956).
- [68] Dickens, J.K., Love, T.A., McConnell, J.W., Emery, J.F., Northcutt, K.J., Peelle, R.W., and Weaver, H., Delayed Beta- and Gamma-Ray Production Due to Thermal-Neutron Fission of  $^{235}U$ , Spectral Distributions for Times After Fission Between 2 and 14000 sec: Tabular and Graphical Data, Report No. ORNL/NUREG-39, 148 pages (Oak Ridge Natl. Lab., Oak Ridge, Tenn. 37830, Aug. 1978).
- [69] Fallout Phenomena Symposium, Proceedings/Part 1, April 12-14, 1966, Monterey, Calif., 468 (Office of Civil Defense or Defense Atomic Support Agency, Washington, D.C., 1966).
- [70] Crocker, G. R., Radiation Properties of Fractionated Fallout; Predictions of Activities, Exposure Rates and Gamma Spectra for Selected Situations, Report No. NRDL-TR-68-134, 287 pages (June 27, 1968).
- [71] Response to DCPA Questions on Fallout, DCPA Research Report No. 20, 44 pages (Subcommittee on Fallout, Advisory Committee on Civil Defense, National Academy of Sciences, Washington, D.C., Nov. 1973).
- [72] Sam, D., and Bunney, L. R., Exposure Rates from the Products of Thermal-Neutron Fission of  $^{235}U$  at Selected Times After Fission, Health Physics, 21, 585-589 (Oct. 1971).
- [73] Crocker, G. R., Predictions of Some Radiation Properties of Unfractionated and Fractionated Fallout Fields, Proc. Fallout Phenomena Symposium, April 12-14, 1966, Monterey, Calif., 302-317 (Office of Civil Defense or Defense Atomic Support Agency, Washington, D.C., 1966).
- [74] Bunney, L. R., and Sam, D., Exposure Rates from Experimentally Fractionated Fission Products, Report No. NOLTR 71-154, 10 pages (Naval Ordnance Lab., Silver Springs, Md., Sept. 2, 1971).
- [75] Crocker, G. R., The Effect of Radionuclide Fractionation on the Normalization Factor for Fallout Fields, Report No. USNRDL-TR-892, 41 pages, (Aug. 4, 1965).
- [76] Response to DCPA Questions on Fallout, DCPA Research Report No. 20, 12 (Subcommittee on Fallout Advisory Committee on Civil Defense, National Academy of Sciences, Washington, D.C., Nov. 1973).

- [77] LaRiviere, P. D., Yu, S., and Miller, C. F., Intensity--Activity Relations for Shot Small-Boy, Proc. Fallout Phenomena Symposium, April 12-14, 1966, Monterey, Calif., 403-437 (Office of Civil Defense or Defense Atomic Support Agency, Washington, D.C., 1966).
- [78] Freiling, E. C., Fractionation III. Estimation of Degree of Fractionation and Radionuclide Partition for Nuclear Debris, Report No. USNRDL-TR-680, 35 pages (September 12, 1963).
- [79] Nathans, M. W., Thews, R., Holland, W. D., and Benson, P. A., Particle Size Distribution in Clouds from Nuclear Airbursts, J. Geophysical Research 75, 7559-7572 (1970). Note also Freiling, E. C., A Comparison of the Fallout Mass-Size Distributions Calculated by Lognormal and Power-Law Models, Report No. USNRDL-TR-1105, (1967).
- [80] Cassidy, S. H., FORTRAN Statement of the Generalized Land Fallout Model Computer Program (GLFMCP), Report No. USNRDL-LR-176 (1966); and The Computer Program (TSABND) which Produces the Tables of Mass Chain Refractory and Fission Product Radioactivity Content for the Particle Activity Module of the DOD Fallout Model, Report No. USNRDL-LR-173 (1966).
- [81] Freiling, E. C., Kay, M. A., and Sanderson, J. V., Fractionation IV. Illustrative Calculations of the Effect of Radionuclide Fractionation on Exposure Dose Rate from Local Fallout, Report No. USNRDL-TR-715, 38 pages (Jan 6, 1964).
- [82] Cassidy, S. H., and Crocker, G. R., Sensitivity Analysis of the Radial Distribution Model. Sensitivity to Carrier Material, Yield, and Type of Fission, Report No. USNRDL-TR-67-70, 68 pages (May 22, 1967).
- [83] Tompkins, R. C., Department of Defense Land Fallout Prediction System, Vol. V--Particle Activity, Report No. NDL-TR-102, 264 pages (US Army Nuclear Defense Lab., Edgewood Arsenal, Md., Feb. 1968).
- [84] Cook, C. S., Energy Spectrum of Gamma Radiation from Fallout, Health Physics 4, 42-51 (1960).
- [85] Miller, C. F., Gamma Decay of Fission Products from the Slow Neutron Fission of  $^{235}\text{U}$ , Report No. USNRDL-TR-187 (July 11, 1957).
- [86] Mather, R. L., Johnson, R. F., and Tomnovec, F. M.,  $\gamma$ -Radiation Field Above Fallout-Contaminated Ground, Health Physics 8, 245-260 (1962).
- [87] LaRiviere, P. D., Estimating the Importance of Individual Radionuclides in Fission and Induced Product Mixtures, Report, SRI Project No. MU-5779, 10 pages (Stanford Research Institute, Menlo Park, Calif., June 1966).
- [88] Mather, R. L., Residual Gamma Radiation Fields From Induced Soil Activities, Report No. USNRDL-TR-240, 27 pages (April 9, 1958).
- [89] Klement, A. W., Jr., A Review of Potential Radionuclides Produced in Weapons Detonations, AEC Report WASH-1024, 102 pages (July 30, 1959).

- [90] Maerker, R. E., and Muckenthaler, F. J., Gamma-Ray Spectra Arising from Thermal-Neutron Capture in Elements Found in Soils, Concretes, and Structural Materials, Report No. ORNL-4382, 264 pages (Oak Ridge Natl. Lab., Oak Ridge, Tenn. 37830, August, 1969).
- [91] Groshev, L. V., Demidov, A. M., Lutsenko, V. N., and Pelekhov, V. I., Atlas of  $\gamma$ -Ray Spectra from Radiative Capture of Thermal Neutrons, 198 pages, translated from the Russian by J. B. Sykes, (Pergamon Press, 1959).
- [92] Knapp, H. A., Magnitude and Distribution of Weapon Effects for the Design of Shelters for Protection against Fallout, Research Paper P-194, 124 pages (Inst. for Defense Analyses, Weapons System Evaluation Division, Arlington, Va., July 1965); and USAEC External Gamma Doses and Dose Rates from the Fallout from Nuclear Explosions, Hearings on Civil Defense before a Subcommittee of the Committee on Government Operations, 86th Congress, p. 527 (May 16, 1960).
- [93] Tomnovec, F. M., and Ferguson, J. M., Neutron-Field and Induced-Activity Measurements -- Operation BREN, Report No. CEX-62.50, 42 pages (U.S. Atomic Energy Commission, Sept. 1965).
- [94] Dunning, G. M., Cobalt-60 Bombs, Health Physics 4, 52-54 (1960).
- [95] Russell, R. S., Bartlett, B. O., and Bruce, R. S., The Significance of Long-Lived Nuclides After a Nuclear War, AEC Symp. Series 24, 548-565 (U.S. Atomic Energy Commission, Dec. 1971).
- [96] Long-Term Worldwide Effects of Multiple Nuclear-Weapons Detonations, NAS-NRC Report, 213 pages (Natl. Acad. of Sciences, Washington, D.C., 1975).
- [97] Titus, F., Penetration in Concrete of Gamma Radiation from Fallout, NBS Report No. 6143, 38 pages (Natl. Bureau of Standards, Washington, D.C., Sept. 4, 1958).
- [98] Donovan, L. K., and Chilton, A. B., Dose Attenuation Factors for Concrete Slab Shields Covered with Fallout as a Function of Time after Fission, Tech. Report No. R-137, 31 pages (U.S. Naval Civil Eng. Lab., Port Hueneme, Calif., June 1, 1961).
- [99] Spencer, L. V., Structure Shielding Against Fallout Radiation from Nuclear Weapons, NBS Monograph 42, 92 pages (Natl. Bureau of Standards, Washington, D.C., June 1, 1962).
- [100] Cialella, C. M., et al., Shielding Effectiveness of Enclosure Shields in a Fallout Field, POR-2221 (1963). (Confidential)
- [101] French, R. L., Price, J. H., and Tompkins, K. W., An Analysis of the Performance of Enclosure Shields in a Real Fallout Field, Report No. RRA-T55, 110 pages (Radiation Research Associates, Inc., Ft. Worth, Texas, Dec. 31, 1965).
- [102] Cialella, C. M., and King, N. D., The Shielding Properties of Simple Enclosure Shields, Report No. BRL MR 1663 (Ballistic Research Laboratories, Aberdeen Proving Ground, Md., 1965).

- [103] Tomnovec, F. M., Ferguson, J. M., and Weldon, D. M., The Effect of a Changing Gamma-Ray Fallout Spectrum on the Ground Roughness Factor, Report No. USNRDL-TR-915, 30 pages (Sept. 22, 1965).
- [104] Huddleston, C. M., Klingler, Q. G., Burson, Z. G., and Kinkaid, R. M., Ground Roughness Effects on the Energy and Angular Distribution of Gamma Radiation from Fallout, Health Physics 11, 537-548 (1965).
- [105] Hogan, O. H., Zigman, P. E., and Mackin, J. L., Beta Spectra II. Spectra of Individual Negatron Emitters, Report No. USNRDL-TR-802, 212 pages (Dec. 16, 1964).
- [106] Boyd, A. E., and Morris, E. E., Spatial Distribution of Energy Dissipated by Fallout  $\beta$ -Rays, Health Physics 2, 321-325 (1960).
- [107] Heller, R. B., Energy and Time Beta Ray Spectra of Fission Products of  $U^{235}$  by Fission Neutrons and  $U^{238}$  by 14 MeV Neutrons, WSEG Research Memo. No. 19, 56 pages (Weapons System Evaluation Group, Feb. 16, 1961).
- [108] Hogan, O. L., Beta Spectra. III. Spectra of  $U^{235}$  Fission Products at Selected Times After Fission, Report No. USNRDL-TR-1093, 50 pages (Oct. 3, 1966).
- [109] Curtis, B. G., and Petty, J. S., A Program to Compute Beta Radiation Dosage, Vol. 1 - Program Description, Report No. ARC 67-48/TRC-67-20, 123 pages, (American Research Corp., Fullerton, Calif., Aug. 1, 1967).
- [110] Mackin, J. L., Brown, S. L., and Lane, W. B., Beta Radiation Dosimetry for Fallout Exposure Estimates: Comparison of Theory and Experiment, Report No. TRC-69-26, 64 pages (Stanford Research Institute, Menlo Park, Calif., June 1969).
- [111] Kutcher, J. W., and Wyman, M. E., An Experimental Study of the Time Dependence of the Beta Energy Spectrum from  $^{235}\text{U}$  Fission Fragments, Nucl. Sci. Eng. 26, 435-446 (1966).
- [112] Mikhail, S. Z., Beta-Radiation Doses from Fallout Particles Deposited on the Skin, Report No. ESA-TR-71-01, 91 pages (Environmental Science Associates, Burlingame, Calif. 94010, Jan. 1971).
- [113] Ksanda, D. V., Minvielle, L., and Moskin, A., Scaling of Contamination Patterns, Surface and Underground Detonations, Report No. USNRDL-TR-1 (Classified Report) (1953).
- [114] Laurino, R. K., and Poppoff, I. G., Contamination Patterns at Operation JANGLE, Report No. USNRDL-399 (Classified Report) (1953).
- [115] Kellogg, W. W., The Nature of Radioactive Fallout and its Effect on Man, Hearings before the Special Subcommittee on Radiation of the Joint Committee on Atomic Energy, May 27-29 and June 3, 1957, Part 1, 85'th Congress, 104-141 (U.S. Govt. Printing Office, Washington, D.C., 1957).
- [116] Anderson, A. D., A Theory for Close-In Fallout From Land-Surface Nuclear Bursts, J. Meteorology 18, 431 (August 1961).



- [117] Schuert, E. A., The Nature of Radioactive Fallout and its Effect on Man, Hearings before the Special Subcommittee on Radiation of the Joint Committee on Atomic Energy, May 27-29 and June 3, 1957, Part 1, 85'th Congress, 267-307 (U.S. Govt. Printing Office, Washington, D.C., 1957).
- [118] Callahan, E., Rosenblum, L., Kaplan, J., and Batten, D., The Probable Fallout Threat over the Continental United States, Report No. TO-B 60-13, 198 pages (1960); see also Brooks, F. C., Callahan, E. D., Clark, E. T., Batter, J. F., and Kaplan, A. L., Radiological Defense Planning Guide, Report No. TOI 58-26, 327 pages (Technical Operations, Inc., Burlington, Mass. July 31, 1958).
- [119] Polan, M., An Analysis of the Fallout Prediction Models. Vol. 1: Analysis, Comparison, and Classification of Models, Report No. USNRDL-TRC-68, 145 pages (Sept. 8, 1966).
- [120] Seery, C. J., and Polan, M., An Analysis of the Fallout Prediction Models, Vol. II: Analysis, Comparison, and Evaluation of Model Predictions, Report No. NRDL-TRC-68-59, 74 pages (Aug. 28, 1968).
- [121] Fallout Phenomena Symposium, Proceedings, Part 1, April 12-14, 1966, Monterey, Calif., 486 pages (Office of Civil Defense or Defense Atomic Support Agency, Washington, D.C., 1966).
- [122] Seery, C. J., Fallout Model Analysis, Report No. TRC-68-46, 166 pages (Office of Civil Defense, Washington, D.C., Nov. 1968).
- [123] Pugh, G. E., and Galiano, R. J., An Analytical Model of Close-In Deposition of Fallout for Use in Operational-Type Studies, Research Memo. No. 10 (Weapons System Evaluation Group, 1959).
- [124] Miller, C. F., Biological and Radiological Effects of Fallout from Nuclear Explosions. Chapter 3. Distribution of Local Fallout, Report No. URS 702-1/TRC-68-61, 97 pages (URS Research Co., Burlingame, Calif. 94010, May 1969).
- [125] Miller, C. F. The Analysis and Correlation of Fallout Pattern Data. Part Two: Derivation of a Statistical Fallout Pattern Computational System, Dikewood Corp. Report No. DC-FR-1216-II, 100 pages, May 1973; Part Three: Computer Program User's Instructions, Dikewood Corp. Report No. DC-FR-1216-III, March 1974. Also, see Fallout Modifications Due to Unusual Burst Conditions, Dikewood Corp. Report No. DC-FR-1219, 66 pages, Dec. 1974; and Constraints of Prior Dose on Postattack Operational Planning for Areas Affected by Radioactive Fallout, Center for Planning and Research, Inc. Report, Aug. 31, 1975.
- [126] Tompkins, R. C., The DOD Land Fallout Prediction System, Fallout Phenomena Symposium, Proc., Part I, April 12-14, 1966, Monterey, Calif., 291-300 (Office of Civil Defense or Defense Atomic Support Agency, Washington, D.C., 1966).

- [127] Department of Defense Land Fallout Prediction System, Report No. DASA-1800, Vol. I, System Description, 24 pages (June 1966); Vol. II, Initial Conditions, 64 pages (Sept. 1966); Vol. III, Cloud Rise, 210 pages (Sept. 1970); Vol. IV, Atmospheric Transport, 306 pages (Feb. 1967); Vol. V, Particle Activity, 264 pages (Feb. 1968); Vol. VI, Output Processor, 112 pages (Feb. 1967); and Vol. VII, Operator's Manual 434 pages (Defense Atomic Support Agency, Washinton, D.C., April 1968).
- [128] Huebsch, I. O., Development of a Land Surface Burst Cloud Rise Model, Report No. USNRDL-LR-145 (November 1965).
- [129] Huebsch, I. O., The Energy Cycle and the Energy Cascade of the Atomic Cloud, Fallout Phenomena Symposium, Proc., Part I, April 12-14, 1966, Monterey, Calif., 129-180 (Office of Civil Defense or Defense Atomic Support Agency, Washington, D.C., 1966).
- [130] Huebsch, I. O., Wind Shear, Turbulence, and Interface Criteria for Nuclear-Explosion Cloud, Debris and Fallout Models, Report No. NRDL-TR-69-72 (July 10, 1969).
- [131] Schwenke, T. W., Transport and Output Processor Modules for the DOD Fallout Prediction System, Fallout Phenomena Symposium, Proceedings, Part 1, April 12-14, 1966, Monterey, Calif., 215-235 (Office of Civil Defense or Defense Atomic Support Agency, Washington, D.C., 1966).
- [132] Lee, H., Wong, P. W., and Brown, S. L., Seer II: A New Damage Assessment Fallout Model, Report No. DNA 3008F, 137 pages (Defense Nuclear Agency, Washington D.C. 20305, May, 1972). AD 754144.
- [133] Fallout Phenomena Symposium, Proceedings, Part I, April 12-14, 1966, Monterey, Calif., Summaries and Recommendations of the Working Groups: Radiation Fields, 467-474 (Office of Civil Defense or Defense Atomic Support Agency, Washington, D.C., 1966).
- [134] Heft, R. E., Phillips, W., and Steele, W., Radionuclide Distribution in the Particle Population Produced by the Schooner Cratering Detonation, Nucl. Tech. 11, 413-443 (July 1971).
- [135] Tompkins, R. C., Effect of Depth of Burial on Fallout from Atomic Demolition Munitions, Report No. BRL MR 2317 (Ballistic Research Lab., Aberdeen Proving Ground, Md., August 1973).
- [136] Knox, J. B., Prediction of Fallout from Subsurface Nuclear Detonations, AEC Symp. Series 5, 331-353 (U.S. Atomic Energy Commission, Nov. 1965).
- [137] A Precipitation Scavenging Model for Studies of Tactical Nuclear Operations, Vol. I, Theory and Preliminary Results, Report No. DNA 3661F-1, 61 pages (Mt. Auburn Research Associates, Inc. June 18, 1965). Note also observational data in the papers by Huff, F. A.; Saucier, W. J., et al; Hall, S. J., Gatz, D. F., and Dingle, A. N.; Kruger, P., et al; Kuroda, P. K., et al; and Volchok, H. L.; AEC Symp. Series 5, 507-628 (U.S. Atomic Energy Commission, November 1965).

- [138] Survival of Food Crops and Livestock in Event of Nuclear War, AEC Symp. Series 24, 718 pages (Brookhaven National Lab., Dec. 1971).
- [139] Radioecological Concentration Processes, Proc. International Symp., April 25-29, 1966, Stockholm, Sweden, 1040 pages (Pergamon Press, 1966).
- [140] Cowan, F. P., and Meinhold, C. B., Decontamination, Chapter 10, Survival and the Bomb, Methods of Civil Defense, 307 pages (Indiana U. Press, Bloomington, Indiana, 1969).
- [141] Straub, C. P., Decontamination of Food and Water Following Nuclear Attack, Proc. Symp. on Postattack Recovery from Nuclear War, Nov. 6-9, 1967, Ft. Monroe, Va., 171-180 (Office of Civil Defense or Natl. Acad. of Sciences, Washington, D.C., April 1968).
- [142] Tamura, T., Movement of Cesium-137 by Runoff, Erosion, and Infiltration from a Soil Under Different Cover Conditions, Proc. Symp. on Postattack Recovery from Nuclear War, Nov. 6-9, 1967, Ft. Monroe, Va., 149-168 (Office of Civil Defense or Natl. Acad. of Sciences, Washington, D.C., April 1968).
- [143] Mackin, J. L., and Mikhail, S. K., A Discussion of the State of the Art in Fallout Research, Reviews and Lectures No. 157, 73 pages (U.S. Naval Radiological Defense Lab., San Francisco, Calif., Dec. 7, 1965).
- [144] Nishiwaki, Y., Kawai, H., Hyono, A., Kondo, M., Goshi, N., Nishiwaki, J., Yamatera, H., Kudo, I., Mori, M., Azuma, T., Tsumori, K., and Nagayama, O., Studies on the Radioactivity of Bikini Ash, Research in the Effects and Influences of the Nuclear Bomb Test Explosions, page 461 (Japan Society for the Promotion of Science, Ueno, Tokyo, 1956).
- [145] Miller, C. F., Operation Ceniza-Arena: The Retention of Fallout Particles from Volcan Irazu (Costa Rica) by Plants and People, Part 2 247 pages; Part 2 Appendices, 281 pages (Dec. 1966); and Part 3, 255 pages, SRI Report No. TRC-68-17 (Dec. 1967); (Stanford Research Institute, Menlo Park, Calif.)
- [146] Evans, E. C., and Young, C. A., Differences in Transport and Deposition of Close-in and Intermediate Fallout, Fallout Phenomena Symposium, Proc., Part I, April 12-14, 1966, Monterey, Calif., 236-290 (Office of Civil Defense or Defense Atomic Support Agency, Washington, D.C., 1966).
- [147] Soule, R. R., Gamma Ray Fields Above Rough Contaminated Surfaces, Fallout Phenomena Symposium, Proc., Part I, April 12-14, 1966, Monterey, Calif., 319-336 (Office of Civil Defense or Defense Atomic Support Agency, Washington, D.C., 1966).
- [148] Knapp, H. A., Gamma Ray Exposure Dose from the Surface Deposition of Nuclear Test Fallout, 40 pages (U.S. Atomic Energy Commission, Div. of Biology and Medicine, Washington, D.C., July 21, 1962).
- [149] Radiological Factors Affecting Decision-Making in a Nuclear Attack, NCRP Report No. 42, 66 pages (National Council on Radiation Protection Measurements, Nov. 15, 1974).

- [150] Brown, S. L., Disintegration Rate Multipliers in Beta Emitter Dose Calculations, Fallout Phenomena Symposium, Proc., Part I, April 12-14, 1966, Monterey, Calif., 337-356 (Office of Civil Defense or Defense Atomic Support Agency, Washington, D.C., 1966).
- [151] Brown, S. L., and Yu, O. S., Computational Techniques in Beta Dose Problems, Report No. TRC-68-13 (Stanford Research Inst., Menlo Park, Calif., Jan. 1968).
- [152] Dunham, C. L., The Long-Range Biological Effects on Man, Proc. Symp. on Postattack Recovery from Nuclear War, Nov. 6-9, 1967, Ft. Monroe, Va., 181-190 (Office of Civil Defense or Natl. Acad. of Sciences, Washington, D.C., April, 1968).
- [153] Brown, S., Lee, H., and Yu, O., Postattack Food Production and Water Contamination, SRI Report to OCD, 115 pages (Stanford Research Institute, Menlo Park, Calif., June 1968).
- [154] Radioactive Fallout from Nuclear Weapons Tests, AEC Symp. Series 5, 953 pages, (U.S. Atomic Energy Commission, Nov. 1965).
- [155] The Nature of Radioactive Fallout and its Effects on Man, Hearings before the Special Subcommittee on Radiation of the Joint Committee on Atomic Energy, May 27-29 and June 3, 1957, Parts 1 & 2, 85'th Congress, 2065 pages (U.S. Govt. Printing Office, Washington, D.C., 1957).
- [156] Biological and Environmental Effects of Nuclear War, Hearings before the Special Subcommittee on Radiation of the Joint Committee on Atomic Energy, June 22-26, 1959, Part 1, 87'th Congress, 966 pages (U.S. Govt. Printing Office, Washington, D.C., 1959).
- [157] Cole, R., Assessment of the Hazards of Fallout Radioiodines, Report for DCPA (Environmental Science Associates, Burlingame, Calif., Aug. 1972).
- [158] Damage to Livestock from Radioactive Fallout in the Event of Nuclear War, NAS-NRC Publication 1078, 93 pages (National Academy of Sciences, National Research Council, Washington, D.C., 1963).
- [159] Shinn, A. F., Food Crops and Postattack Recovery, Proc. Symp. on Post-attack Recovery from Nuclear War, Nov. 6-9, 1967, Ft. Monroe, Va., 23-42 (Office of Civil Defense or Natl. Acad. of Sciences, Washington, D.C., April 1968).
- [160] Osburn, W. S., Forecasting Long-Range Recovery from Nuclear Attack, Proc. Symp. on Postattack Recovery from Nuclear War, Nov. 6-9, 1967, Ft. Monroe, Va., 107-136 (Office of Civil Defense or Natl. Acad. of Sciences, Washington, D.C., April 1968).
- [161] Brown, S., and Pilz, U., U.S. Agriculture: Potential Vulnerabilities, Report for DCPA, 83 pages (Stanford Research Institute, Menlo Park, Calif., Jan. 1969).

- [162] Comar, C. L., Wentworth, R. A., and Lengeman, F. W., Incorporation and Control of Fission Products Ingested by Livestock, Report for OCD, 36 pages (Dept. of Physical Biology, N.Y. State Veterinary College, Cornell U., Ithaca, N.Y., Oct. 1970).
- [163] Comar, C. L., Wentworth, R. A., and Lengemann, F. W., Incorporation and Control of Strontium, Cesium, and Iodine Secretion in Milk, Report for OCD, 64 pages (Dept. of Physical Biology, N.Y. State Veterinary College, Cornell U., Ithaca, N.Y., July 1969).
- [164] Protection of the Thyroid Gland in the Event of Releases of Radioiodine, NCRP Report No. 55, 60 pages (Natl. Council on Radiation Protection and Measurements, Washington, D.C. 20014, August 1, 1977).
- [165] Effects of Fallout on Agricultural Ecosystems in California, Report for OCD, 90 pages (U. of Calif., Riverside, Calif., May 1972).
- [166] Insect Pests of Major Food Crops, Their Reinvasion Potential and the Effects of Radiation on Arthropods, Report No. TRC-68-70, 199 pages (U. of Calif., Riverside, Calif., June 1969).
- [167] Auerback, S. I., Postattack Insect Problems, Proc. Symp. on Postattack Recovery from Nuclear War, Nov. 6-9, 1967, Ft. Monroe, Va., 137-142 (Office of Civil Defense or Natl. Acad. of Sciences, Washington, D.C., April, 1968).
- [168] Reitemeier, R. F., Soil-Plant Relationships of Radioactive Nuclides in Fallout, Proc. Symp. on Postattack Recovery from Nuclear War, Nov. 6-9, 1967, Ft. Monroe, Va., 143-148 (Office of Civil Defense or Natl. Acad. of Sciences, Washington, D.C., April, 1968).
- [169] Tompkins, P. C., Rise and Fall of Important Fission Products in the United States Food Supply, Proc. Symp. on Postattack Recovery from Nuclear War, Nov. 6-9, 1967, Ft. Monroe, Va., 169-170 (Office of Civil Defense or Natl. Acad. of Sciences, Washington, D.C., April 1968).
- [170] Blincoe, C., and Bohman, V. R., Decrease of Bovine Cesium-137 Concentrations Following the Cessations of Atmospheric Nuclear Weapons Testing, Advances in Chemistry Series 93, 427-435 (American Chemical Society, Washington, D.C. 1970).
- [171] Russell, R. S., Bartlett, B. O., and Bruce, R. S., The Significance of Long-Lived Nuclides after a Nuclear War, AEC Symposium Series 24, 548-565 (December 1971).

### III. Elementary Concepts of Photon Transport

#### A. INTERACTION PROBABILITY FUNCTIONS<sup>1</sup>

##### 1. Basic Gamma Ray Interactions

As radiation moves through a material, interactions occur which determine the nature of the penetration process. We wish to discuss these interactions. It will be advantageous to refer both to the photon energy,  $E$ , and to the photon wavelength, designated  $\lambda$ , and given by

$$\lambda = .511/E, \quad (\text{III.1})$$

where  $E$  is in MeV, and .511 MeV is the rest mass energy of an electron. When this definition is made, the photon wavelength is said to be "in Compton units." (One Compton unit =  $3.85 \times 10^{-11}$  cm).

Photons can interact with atomic electrons or atomic nuclei. Two types of interactions with atomic electrons are dominant. In the first, called photoelectric absorption, the photon disappears, its total energy being transferred to an atom or to an atomic electron. In the second, called scattering, the photon remains after the interaction, but has a new direction and usually a decreased energy. The most important type of interaction with atomic nuclei is called pair production in the field of the nucleus. Strictly speaking it is not a "nuclear" interaction because electromagnetic rather than nuclear forces are involved; the photon disappears and a pair of electrons, one positive and one negative, takes its place.

Interactions which terminate the photon trajectory are called "absorption" interactions, in contrast to "scattering" interactions, from which a "scattered"

---

<sup>1</sup>See references [1,2,3].

photon emerges to continue the trajectory. Assignment of specific types of interaction to one or the other of these classes is not always unique, however. In the following paragraphs we note some interaction types and aspects to be ignored as well as remarking further on the three types referred to in the preceding paragraph.

Because the rest-mass energy of two electrons,  $2 \times .511 = 1.022$  MeV, must be supplied for an electron pair, the pair production interactions occur only for photon energies above this threshold. The presence of a nucleus is required to conserve momentum. It is also possible for pair production to occur in the field of an atomic electron; but the probability for pair production interactions in general is proportional to  $Z^2$ , where  $Z$  is the atomic charge. Since  $Z^2 = 1$  for each of  $Z$  electrons in the atom, pair production in the field of an electron is only about  $Z(1/Z^2) = 1/Z$  as likely as in the field of a nucleus of charge  $Z$ ; and it is lumped with the latter in penetration studies by replacing the factor  $Z^2$  with  $(Z^2 + Z)$ , although the two types of cross section differ somewhat.

In photoelectric absorption, the total photon energy is given to atomic electrons, one of which is usually then removed from the atom, leaving it in a highly excited state. In the sequence of events by which the atom rids itself of excess energy, fluorescence x-rays or "Auger" electrons will be emitted. The fluorescence x-rays are of comparatively low energy, and are usually, though not always, disregarded in penetration studies, as they will be here.

Scattering by atomic electrons can occur either with the electrons acting as separate entities or with the atomic field -- nuclear plus electron -- acting as the scattering field. The former is referred to as "incoherent" or "inelastic" scattering, and the latter as "coherent" or "elastic" scattering. In both cases a direction change of the photon occurs; but in the case of

coherent scattering, the whole atom takes up momentum with the result that only a negligible energy loss by the photon results and the direction change is usually very small.<sup>2</sup>

Atomic electrons are in bound states, but binding effects on the inelastic scattering cross section usually have little consequence for penetration. Further, coherent scattering is of importance mainly at low energies or small deflection angles. Hence a description of scattering interactions for use in penetration studies can be provided to a satisfactory degree of accuracy by using a very simple rule: All atomic electrons are treated as if they were "free", that is, not bound to atoms. Thus all electrons are considered alike for calculations of the scattering process, and coherent scattering is ignored. The interaction of photons with free electrons is known as Compton scattering.

Neither pair production in the field of the nucleus nor coherent scattering leaves the atom in an excited state. Incoherent scattering may remove either inner or outer shell electrons from the atom, and by the former can induce ionizing fluorescence radiation or Auger electrons. The positrons produced in pair production ultimately annihilate with atomic electrons, usually producing two photons of energy 0.511 MeV each, and traveling in opposite directions. These annihilation photons are sufficiently high in energy that they are often treated as part of the penetrating radiation. But for most fallout shielding problems, low-Z materials for which pair production is comparatively unimportant are used; and penetration by the annihilation photons has been neglected in many studies, particularly the older ones.

Another phenomenon, which is always neglected in studies for practical shielding applications though not always in penetration studies, is polarization.

---

<sup>2</sup>At very low photon energies, below those of major concern here, large direction changes become probable as a result of coherent scattering.



Scattering interactions leave the gamma radiation partially polarized relative to the "scattering" plane, which is parallel to photon directions before and after scatter. As a result, subsequent scatterings show preference for this plane so that any given photon has a trajectory in which the sequence of straight segments tends to be more nearly coplanar than would be the case if successive directions had randomly distributed azimuths. The effect of this on penetration has been investigated and shown to be slight [4,5].

## 2. Cross Sections

The different types of interaction are each described by an appropriate "cross section," designated  $\sigma$ . The term originates with the concept of a "target" having a probability of being "hit" proportional to the cross-sectional area. Hence the units of  $\sigma$  are those of an area.

The cross section  $\sigma_{ph}$  for photoelectric interactions is the total for all atomic electrons. The largest contribution at high photon energies is made by K-shell electrons, which are the most tightly bound. Approximate evaluation of the cross section  $\sigma_K$  for each of the 2 electrons in the K shell gives the result

$$\sigma_K \approx \sigma_{Th} 4\sqrt{2} \lambda^{7/2} Z^5 / 137^4, \quad (III.2)$$

for  $\lambda > .511/E_K$ , where  $E_K$  is the K electron binding energy. The constant  $\sigma_{Th}$  is given by

$$\sigma_{Th} = \frac{8}{3} \pi (e^2/mc^2)^2 = .6653 \times 10^{-24} \text{ cm}^2, \quad (III.3)$$

and is called the Thomson cross section. Cross sections for outer shell electrons tend to have somewhat similar trends with photon wavelength and

atomic number  $Z$ , but are much smaller. They are important at low photon energies, however, because for each type of electron, the photoelectric cross section vanishes for photon energies below that required to raise the energy of the electron to an unfilled higher state, Thus for photon energies below  $E_K - E$ , where  $E$  is the binding energy of the  $K$  electron in the lowest possible excited state, the photoelectric cross section is due to higher shell electrons only. So also for the  $L$  and still higher shells.

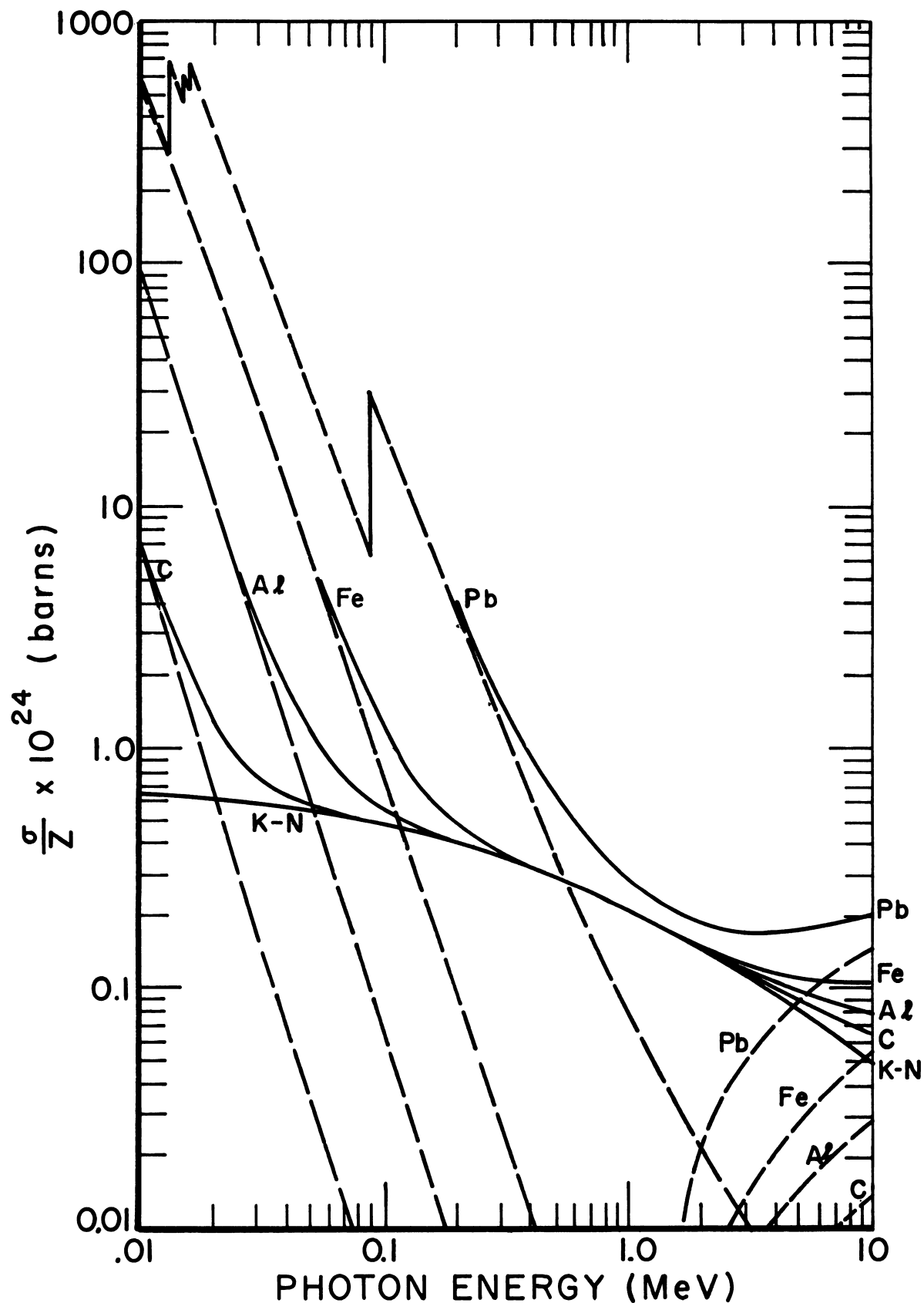
Figure III.1 gives the photoelectric cross section per atom using the scaling factor  $(\sigma_{Th}/Z) \times 10^{24}$ , for several types of atoms, according to a report by Hubbell [6]. The discontinuities at low energy are at thresholds for different shells, and exhibit the effects of the inner atomic structure very clearly. The electrons outside the  $K$ -shell increase the photoelectric cross section by about a factor 1.3 over that for  $K$ -shell electrons only, for energies greater than the  $K$ -shell binding energy. The more accurate calculations and experiments on which figure III.1 is based give data a little different from that of eq (III.2), which has value mainly in the indication of trends and general magnitudes.

As shown in figure III.1, the pair production cross section per atom rises for energies above the 1.022 MeV threshold; and it becomes essentially flat at high energies. Because it is roughly proportional to  $Z^2$ , it is much more important for high- $Z$  materials than for low- $Z$  materials.

The cross section for Compton scattering is known as the Klein-Nishina cross section [7]. The cross section integrated over all deflection angles will be designated  $\sigma_{KN}^3$ . For each electron it has the form

---

<sup>3</sup>The subscript  $KN$  should not be confused with the subscript  $K$ , referring to  $K$ -shell electrons. The total scattering cross section "per atom" has an additional factor  $Z$  to account for the full set of  $Z$  electrons in the atom.



III.1 Total cross sections (solid curves) in barns per atom per unit of nuclear charge. The dashed lines to the left represent photoelectric cross sections, while those rising to the right represent pair production cross sections. bottom solid curve is the Klein-Nishina cross section.

$$\sigma_{KN} = \sigma_{Th} \frac{3}{8} \lambda [(1-2\lambda-2\lambda^2)\log(1+2/\lambda) + 2(1+9\lambda+8\lambda^2+9\lambda^3)/(\lambda+2)^2] \quad (\text{III.4})$$

Figure III.1 shows that the Klein-Nishina cross section decreases with increasing energy, but that it tends to be much less strongly energy-dependent than the photoelectric absorption cross section. The total scattering cross section per atom is less strongly  $Z$  dependent than either photoelectric absorption or pair production cross sections; and it tends to dominate for low- $Z$  materials over a very wide range of energies. This energy region of scattering dominance narrows as  $Z$  increases, until it almost disappears for lead and uranium.

### 3. Exponential Attenuation

Interactions are chance events. When a gamma ray photon moves through a material, there will be probabilities  $p_1, p_2, \dots$ , that interactions of different types 1, 2,  $\dots$ , may occur, per unit path length traveled. These probabilities are not correlated, and therefore they may be added to obtain the total probability per unit path length that an interaction of some type occurs. The total probability per unit path length for occurrence of some kind of interaction can be designated by  $\mu$ , and is identical with the linear attenuation coefficient. It depends on the material through which the photons travel and on the energy of the photons. We indicate this by writing  $\mu(E, Z)$ , where  $Z$  here is used in a general sense to indicate any type of material, including compounds and mixtures.

There is a well-known relationship between interaction probability per unit path length, and interaction cross section. For a given element of mean atomic mass  $A$ ,<sup>4</sup>

---

<sup>4</sup>Not the atomic mass number, which this symbol commonly designates in nuclear physics.  $A$  is in atomic mass units, which are of such a size that  $A$  for  $^{12}\text{C}$  is exactly equal to 12.

$$\mu = (N_A/A)\rho\sigma \text{ cm}^{-1}, \mu_{\text{KN}} = (N_A/A)\rho(Z\sigma_{\text{KN}}) \quad , \text{ etc.}, \quad (\text{III.5})$$

where  $N_A$  is Avogadro's number,  $\rho$  is the density, say in  $\text{g/cm}^3$ ,  $\sigma$  is the total cross section per atom, say in  $\text{cm}^2$ , and  $\sigma_{\text{KN}}$  is the Klein-Nishina cross section per atom, say in  $\text{cm}^2$ . Since the combination  $N_A/A$  has units atoms per gram,  $\mu$  is then clearly in  $\text{cm}^{-1}$ . It is also convenient to remember that the product of universal constants,  $N_A \cdot \sigma_{\text{Th}}$ , which appears implicitly if not explicitly in most expressions for  $\mu$ , is almost exactly given by

$$N_A \sigma_{\text{Th}} = 0.4 \text{ cm}^2/\text{mole} \quad . \quad (\text{III.6})$$

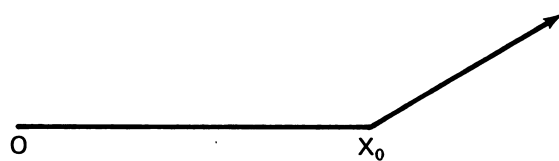
To obtain the value of  $\mu$  for a compound or mixture, it is only necessary to form a suitable linear combination, and if in a molecule there are  $n_i$  atoms of the  $i$ 'th type, we assume that these atoms can be treated independently and write

$$\mu = \left( \sum_i n_i A_i \right)^{-1} N_A \rho \sum_i n_i \sigma_i \quad , \quad (\text{III.7})$$

where  $\sigma_i$  is the cross section per atom of the  $i$ 'th type.

Gamma rays effectively travel in straight lines between interactions. Figure III.2 is a sketch representing a gamma photon originating at 0 and undergoing an interaction after traveling a distance  $x_0$ .

Let  $p(x)$  be the probability that a gamma ray will have no interaction for a distance  $x$  along its trajectory. We divide this distance into two segments,  $x = x_1 + x_2$ , and note that  $p(x)$  must be of the form



III.2 A scattering interaction after a straight trajectory of path length  $x_0$ .

$$p(x) = p(x_1) p(x_2) ,$$

since no interaction for a distance  $x$ , means no interaction for  $x_1$ , followed by no interaction for  $x_2$ . The probabilities  $p(x_1)$  and  $p(x_2)$  are uncorrelated and must have the same functional form as  $p(x)$ .

This simple product relationship implies that  $p(x)$  can be written in the form

$$p(x) = e^{-Bx} ,$$

because the exponential is the functional form possessing this property.<sup>5</sup>

To determine  $B$ , we examine the case of a very small path length  $\Delta x$ . Since  $1 - p(x)$  represents the probability for an interaction in distance  $x$ , and

$$1 - p(\Delta x) = 1 - e^{-B\Delta x} \approx B\Delta x ,$$

we find that  $B$  is the probability per unit path length for occurrence of an interaction. We identify  $B$  with  $\mu$  and write

$$p(x) = e^{-\mu x} . \tag{III.8}$$

The related quantity, probability that an interaction occurs between  $x$  and  $x + \Delta x$ , is clearly

---

<sup>5</sup> Another simple derivation utilizes  $x + dx$ ,  $x$ , and  $dx$  for  $x$ ,  $x_1$ ,  $x_2$ , respectively, with the constant  $\mu$  given by  $\lim_{\Delta x \rightarrow 0} (1 - p(\Delta x)) / \Delta x$ . The resulting differential equation is readily solved to give eq (III.8).

$$p(x) [1 - p(\Delta x)] = \mu \Delta x e^{-\mu x} . \quad (\text{III.9})$$

We now consider a source which produces a large number  $N_0$  of photons of identical energy. The number  $N$  avoiding interaction for a path length at least as long as  $x$  should be

$$N = N_0 p(x) = N_0 e^{-\mu x} . \quad (\text{III.10})$$

If these photons form a narrow beam traveling away from the source, any interaction will in principle remove a photon from the beam. We thus expect exponential attenuation of such narrow beams.

The coefficient  $\mu$  is referred to as an "attenuation coefficient."<sup>6</sup> Its reciprocal, the average distance traveled before an interaction, is the familiar "mean free path," which will here be occasionally abbreviated by MFP. In table III.1, values of the mean free path for 1 MeV photons are listed, this energy being typical for gamma rays from fission fragments.

There are several interesting things which can be said on the basis of this table [8]. The most important, from the point of view of fallout gamma ray protection, concerns room and building dimensions. Typical dimensions for rooms might range from 15 ft to 50 ft; while buildings or major segments of buildings can be larger, usually by factors  $\lesssim 2$ . The mean free path in air is larger than this by about an order of magnitude. On the other hand, the mean free path in concrete and wood is at least an order of magnitude smaller than room dimensions. Because of these facts, two approximations become very attractive and useful. If air has such a large mean free path, what will

---

<sup>6</sup>See footnote 8 of chapter I.



Table III.1 A few mean free path values for common materials; data are for 1 MeV photons. See references [5,6].

<u>Material</u>	<u>MFP (ft)</u>
Concrete	0.22
Wood	0.89
Air	430.0
Lead	0.04

happen inside buildings? The gamma rays emerging from one wall will go unimpeded across to another wall, in nearly all cases. We can therefore perform realistic calculations for structures which omit any effects of air. While the presence of air can be very important, this will not usually be so inside structures.

On the other hand, concrete and wood have mean free paths that are so short -- less than a foot -- that it is possible to do realistic calculations of the penetration through walls by assuming that gamma rays do not move laterally inside the walls. They can be considered to re-emerge either at the point of entry or at the opposite point on the other side of the wall. This also means that we need not be much concerned about corner and edge effects, which will involve only that small fraction of all the entering gamma rays which penetrate within a few inches of the edge or corner.

Table III.2 presents selected mass attenuation coefficients, defined as the linear attenuation coefficient divided by the density, as a function of photon energy in English units of  $\text{ft}^2/\text{lb}$  [6]. The metric units of  $\text{cm}^2/\text{g}$  would result if we multiply all values by 2.0482, and hence shift all data up by the same factor, without changing relationships.

When the density of the material has been divided out of the expression for  $\mu$ , as has been done in table III.2, values of the mass attenuation coefficient for different materials turn out to be closely comparable, particularly in that energy region .5 - 2 MeV where the most important components of fission spectra are located. The values depend on the ratio of atomic mass (expressed by the average value for  $A$  for each element) to the number of atomic electrons (expressed by  $Z$ ). The somewhat different values for  $\text{H}_2\text{O}$ , as compared with concrete and air, are due to hydrogen, which has the unusually small value  $A/Z \approx 1$ . The value of this ratio averaged over the

Table III.2 Attenuation coefficients for some common materials ( $\text{ft}^2/\text{lb}$ ). Data are from reference [5]. Note that  $(\text{cm}^2/\text{g})/(\text{ft}^2/\text{lb}) = 2.0482$ .

<u>E(MeV)</u>	<u>H<sub>2</sub>O</u>	<u>Air</u>	<u>Muscle</u>	<u>Concrete</u>	<u>Fe</u>	<u>Pb</u>
.01	2.44	2.35	2.49	12.9	84.0	
.015	.723	.708	.747	3.91	27.2	L edges
.02	.347	.337	.357	1.68	12.3	40.7
.03	.165	.155	.167	.547	3.85	13.9
.04	.121	.112	.122	.272	1.69	6.40
.05	.104	.0957	.104	.176	.898	3.53
.06	.0962	.0874	.0962	.133	.552	2.16
.08	.0874	.0791	.0869	.0976	.269	1.01
(.088)	Pb	K edge				{ .791 3.53
.1	.0820	.0737	.0810	.0830	.167	2.55
.15	.0727	.0654	.0723	.0684	.0898	.923
.2	.0664	.0601	.0659	.0610	.0679	.461
.3	.0576	.0518	.0571	.0522	.0522	.187
.4	.0518	.0465	.0513	.0468	.0450	.107
.5	.0472	.0425	.0468	.0426	.0405	.0752
.6	.0437	.0393	.0433	.0394	.0372	.0586
.8	.0384	.0345	.0380	.0346	.0325	.0418
1.	.0342	.0311	.0342	.0311	.0291	.0337
1.5	.0281	.0253	.0278	.0253	.0238	.0249
2.	.0241	.0217	.0239	.0219	.0208	.0220
3.	.0194	.0175	.0192	.0178	.0177	.0203
4.	.0166	.0150	.0165	.0156	.0162	.0202
5.	.0148	.0134	.0146	.0142	.0153	.0207
6.	.0135	.0123	.0134	.0132	.0149	.0212
8.	.0119	.0109	.0117	.0120	.0145	.0224
10.	0.108	.00996	.0107	.0113	.0145	.0236

constituent elements of wood is about 10% smaller than for concrete or air because of its hydrogen content. The fact that lead has nearly the same value as the other materials in the .5 to 2 MeV range is due to a combination of effects: The  $A/Z$  ratio is substantially larger for lead than for concrete, and this would tend to increase the mean free path. Counteracting this is a substantial probability per unit path length in lead for photoelectric interactions, an additional contribution that is lacking for the materials with lower  $Z$ . This lowers the value relative to the other materials. The two effects nearly compensate one another.

The fact that lead is so expensive, while being so nearly comparable in shielding effectiveness to more common materials on a mass basis, rules out the possibility of using lead as a standard construction material for shelters. Note, however, that lead has a strong differential effect against low energy gamma rays, and may be particularly useful under special circumstances as a shield against gamma rays which have lost much of their original photon energy of, say, 1 MeV or greater.

#### 4. Gamma Ray Scattering

Due to the presence of scattering interactions, the penetration process is far more complicated than the simple analysis of the preceding section, which gives an exponential law of attenuation, might lead one to believe. Photons scattered once, twice, or many times, contribute to the intensity, with larger "orders" of scattering having increasing importance at greater penetration distances. In addition, photons can change direction and thus generate hazards "around corners", as it were. Thus both analytical and shielding difficulties are so much increased by scattering that it is not extreme to say that gamma ray shielding research and engineering analysis is largely the detailed study of consequences of Compton scattering interactions in the materials through which gamma rays pass.

Figure III.3 shows the geometry of a Compton scattering interaction. A gamma ray with wavelength  $\lambda'$  before the interaction, is deflected through an angle  $\Theta$ . The wavelength after the interaction,  $\lambda$ , corresponds to a lower energy, and is related to  $\lambda'$  and  $\Theta$  by the Compton formula,

$$\lambda - \lambda' = \frac{h}{m_0 c} (1 - \cos\Theta) . \quad (\text{III.11})$$

The differential cross section per electron for this interaction,  $d\sigma_{\text{KN}}$ , is that calculated by Klein and Nishina [7]; it can be written

$$d\sigma_{\text{KN}} = \left( \frac{d\sigma}{d\lambda} \right)_{\text{KN}} \frac{1}{2\pi} \delta(\cos\Theta - 1 + \lambda - \lambda') d\lambda d\Omega , \quad (\text{III.12})$$

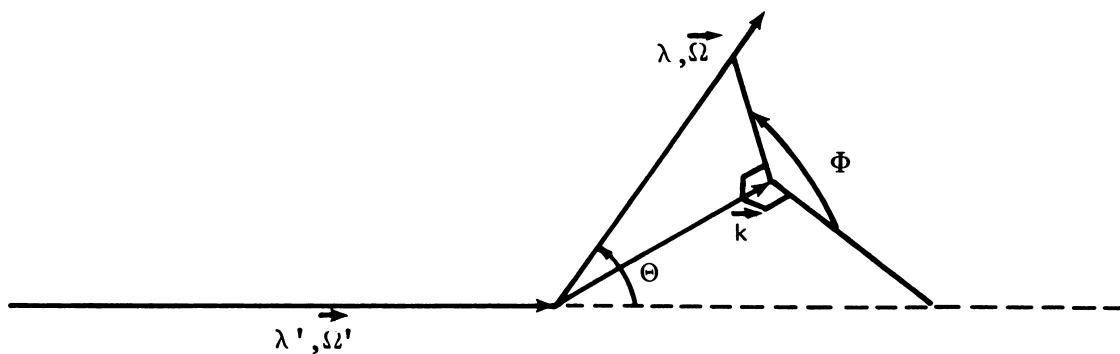
where

$$\left( \frac{d\sigma}{d\lambda} \right)_{\text{KN}} = \frac{3}{8} \sigma_{\text{Th}} (\lambda'/\lambda)^2 \left[ \lambda/\lambda' + \lambda'/\lambda - 2(\lambda - \lambda') + (\lambda - \lambda')^2 \right] , \quad (\text{III.12}')$$

and where the differential solid angle,  $d\Omega$ , includes the new direction  $\vec{\Omega}$ , and the wavelength interval  $d\lambda$  contains  $\lambda$ . The Dirac delta function expresses the requirement that the Compton formula be satisfied; and its use allows one to treat  $\lambda$  and  $\Theta$  formally as independent variables.

Integration of eq (III.12) over all deflection angles reduces it to a function of photon wavelength only; and if we then multiply by the factor  $\rho N_A Z/A$  we obtain a function which we designate  $k(\lambda', \lambda)$ ,

$$k(\lambda', \lambda) d\lambda = \rho N_A (Z/A) \left( \frac{d\sigma}{d\lambda} \right)_{\text{KN}} d\lambda . \quad (\text{III.13})$$



III.3 The spherical trigonometry of a Compton scattering. The reference axis passes through the interaction point and is designated  $\vec{k}$ . The vectors  $\vec{\Omega}'$  and  $\vec{\Omega}$  are parallel to the photon directions before and after scattering, respectively. The plane of the scattering passes through the interaction point and parallels both photon direction vectors, i.e., it is here the plane of the paper. The azimuthal angle  $\Phi$  is between half-planes which join along the reference axis.

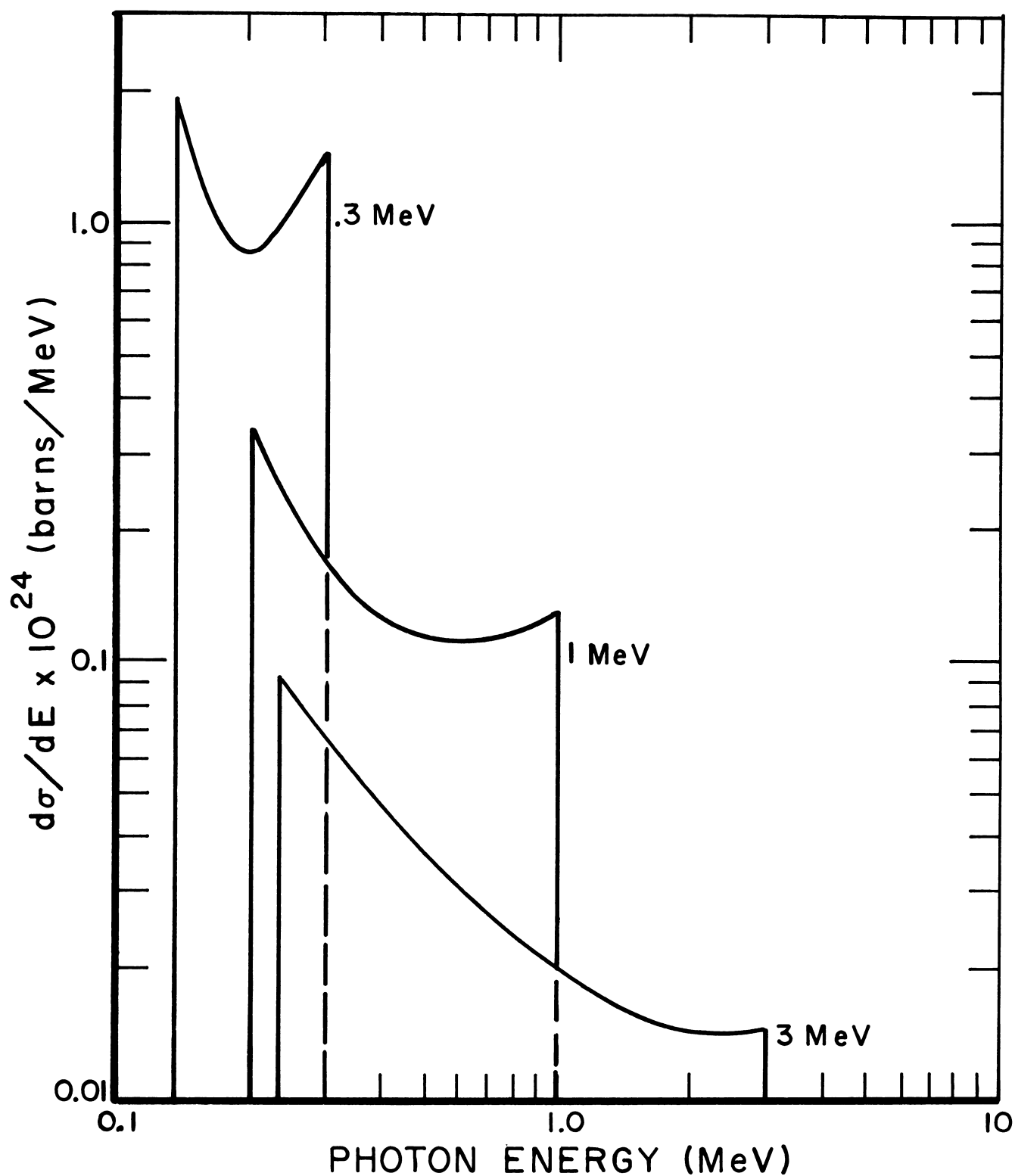
This function is analogous to the linear attenuation coefficient,  $\mu$ , as developed in the preceding section III.A.3. It is the probability per unit path length for photons of wavelength  $\lambda'$  to undergo a scattering interaction which changes the wavelength to a value between  $\lambda$  and  $\lambda + d\lambda$ .

Integration of  $k(\lambda', \lambda)$  over all final wavelengths  $\lambda$  produces values proportional to those shown by the curve designated K-N in figure III.1. Figure III.4 gives curves of  $(d\sigma/dE)_{KN} = (d\sigma/d\lambda)_{KN} |d\lambda/dE|$ , where  $|d\lambda/dE| = \lambda^2/511$  [9]. An important feature of the distributions illustrated in figure III.4 is the tendency, as the initial (highest) energy increases (and the corresponding wavelength decreases), for the scattering probabilities to be concentrated at small deflections and diminished for large deflections. The validity of this statement can be inferred from the curves in figure III.4 if one notes for example (from eq (III.11)) that scattered energies  $E$  (in MeV) above  $E_0/(E_0+1)$  correspond to deflections below  $\sim 60^\circ$ .

A simple, but indicative, ratio of integrals over the differential scattering cross section is the following:

$$\frac{\int_{\lambda' + 1}^{\lambda' + 2} \int_{4\pi} d\lambda d\Omega d\sigma_{KN} \lambda^{-1}}{\int_{\lambda'}^{\lambda' + 2} \int_{4\pi} d\lambda d\Omega d\sigma_{KN} \lambda^{-1}} \quad (III.14)$$

According to the integration limits, the numerator is proportional to the average energy of gamma rays scattered through an angle larger than  $90^\circ$ , while the denominator is proportional (by the same proportionality constant) to the average energy of gamma rays scattered through any angle, in a single



III.4 The Klein-Nishina scattering cross section per electron per MeV, i.e.,  $(-\lambda^2/.511)(d\sigma/d\lambda)_{KN}$ , where  $(d\sigma/d\lambda)_{KN}$  is given by eq (III.12).



interaction. The ratio is a rough measure of the size of the "energy albedo," the fraction of energy which backscatters from a thick wall.<sup>7</sup> For 1 MeV photons, the ratio is approximately 0.2.

This simple calculation indicates that the reflected energy is expected to be small, about an order of magnitude less than the incident energy. This, in turn, means that in buildings, the radiation penetrating through a wall directly to the detector, without backscattering from other walls, provides the largest contribution to the dose, much larger than contributions back-scattered from one or more walls. It should thus prove reasonably accurate to perform calculations that treat the backscattering as a small correction to the contribution coming directly through each wall. Moreover, one can proceed with some confidence to perform independent wall-by-wall analyses of the shielding properties of structures.

## B. FLUX DENSITY, CURRENT DENSITY AND ENERGY DEPOSITION<sup>8</sup>

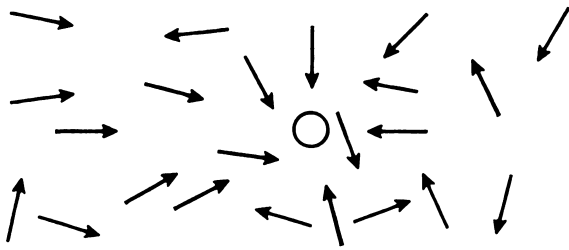
### 1. Flux Definitions and Current Density Definitions

One basic problem of radiation physics is to provide an adequate and useful description of a radiation field. We might conceive of a radiation field more or less as in figure III.5(a), in which the arrows represent gamma ray photons traveling in all directions through different regions of space. As indicated by the small circle, a probe is introduced to sample the field. This probe is small so that the characteristics of the radiation are uniform over the region of space which the probe is to occupy, and also so that the

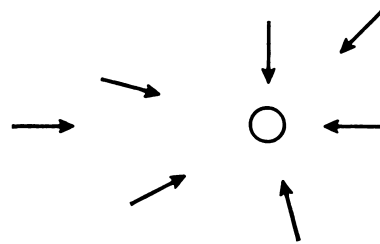
---

<sup>7</sup>We refer to the fraction backscattered for energy, photon number, or (loosely) dose, as various albedos: energy albedo, number albedo, or dose albedo. Note that expression (III.14) is not the energy albedo, but simply a number expected to be the same order of magnitude.

<sup>8</sup>See references [2,3,10].



a



b

III.5 The sketch a depicts a spherical detector in a radiation field. In b, the subset of photons shown in a which would strike some part of the detector is shown.

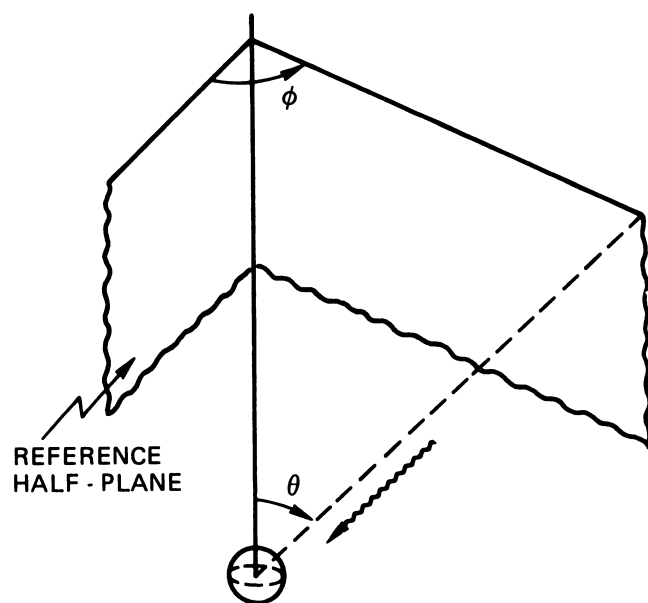
presence of the probe doesn't modify the radiation field appreciably.<sup>9</sup> In shape, the probe is spherical, so that it presents the same shape and apparent size regardless of the direction from which it is approached. Ideally the probe is capable of registering the characteristics of each photon which passes through it. Photons not passing through the probe are not recorded. Thus, from the total set of photons, a subset is selected which passes through the probe, and which we indicate by the sketch of figure III.5(b). Note that each photon in the sketch is traveling on a collision course with some part of the probe--its center or its edge.

The photons which strike the probe are characterized by energy, direction, and the time they strike. The probe itself is characterized by its cross section area, which we call  $a$ , and the location of its central point, which we designate by a set of Cartesian coordinates,  $x$ ,  $y$ ,  $z$ . To classify photons by direction, we choose an arbitrary polar axis extending out from the center of the probe, and an arbitrary azimuthal reference half-plane as in figure III.6. Radial lines from the center of the probe can be identified by an obliquity angle  $\theta$  relative to the reference axis, and azimuthal angle  $\phi$  between reference half-plane and the half-plane from the polar axis which contains the radial line.

Each photon trajectory passing through some part of the probe is then identified by the angles  $\theta, \phi$  of the radial line starting at the center of the probe and lying parallel to the photon trajectory. To render  $\theta$  and  $\phi$  unique, we must specify that we will either choose consistently the radial line directed back along the path of approach, or directed with the direction of motion of the photon. Both are used; in figure III.6 the first possibility is indicated.

---

<sup>9</sup> On the other hand it is not so small that statistical variability in the photon field is significant.



III.6 A photon striking near the edge of a spherical detector is shown, together with its directional coordinates  $\theta, \phi$  relative to a reference axis and half-plane.

With a classification system for direction, and some mechanism for identifying photon energy, we can in principle determine the number of photons passing through the detector with energies between  $E$  and  $E + dE$ , with directions in a differential solid angle  $d\Omega$  in which the direction  $\theta, \phi$  lies, in the time interval between  $t$  and  $t + dt$ . This number will be proportional to  $dE$ ,  $d\Omega$ , and  $dt$ , and will be indicated by

$$\mathcal{N}(E; \theta, \phi; x, y, z; t) dE d\Omega dt,$$

where  $\mathcal{N}$  may also be written  $\mathcal{N}(E; \vec{\Omega}; \vec{r}; t)$ .

Finally, we note that the number of photons passing through the probe will increase or decrease as the size of the probe is increased or decreased. For small probes there will be a proportionality between  $\mathcal{N}$  and the size of "target" presented by the probe, as measured by its cross sectional area  $a$ . The fundamental quantity which we call the doubly differential flux density and designate by  $N$ , is the ratio

$$N(E; \theta, \phi; x, y, z; t) = \frac{1}{a} \mathcal{N}.$$

It clearly has the units

$$\frac{\text{Number of Photons}}{\text{Energy-Steradian-Area-Time interval}}.$$

If one integrates  $N$  over energy and direction, the result is commonly called "flux density."<sup>10</sup> To avoid some resulting confusion, the integral of  $N$  over

---

<sup>10</sup>There are many designations for this quantity. References [2] and [3] use "flux" rather than "flux density." We choose the latter to be more consistent with recent glossaries, such as references [11] and [12].

energy or direction, but not both, can be referred to as the flux density angular distribution and spectrum, respectively.

The time integral of flux density is referred to as the "fluence." Concepts of differential fluence will be used similar to differential flux density, though the term "fluence spectrum" will usually be used instead of the "differential energy fluence." In this book, the problem of time variations does not often come up, not because of integrations performed over time, but because time dependence cancels out when we calculate the ratios which we call "protection factors." The term "fluence" is therefore used, and we include it in the list of formal definitions given in the glossary.

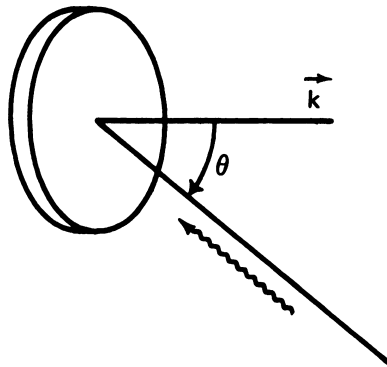
To prepare the way for future discussions, we consider also the case of a probe which is not spherical, but shaped like a small flat plate of area  $\underline{a}$ , oriented so that the plane of the detector is perpendicular to a unit vector  $\vec{k}$ , as in figure III.7. In this case the target presented by the probe clearly depends on the direction of approach. Further, it is advantageous to choose  $\vec{k}$  as the reference polar axis in classifying photon directions. The number of photons passing through this detector will be indicated by

$$\mathcal{N}'(E; \theta, \phi; x, y, z; t) dE d\Omega dt \quad .$$

Since the target size is proportional to  $|\cos\theta|$ , we find that

$$\frac{1}{a} \mathcal{N}' = |\cos\theta| \frac{1}{a} \mathcal{N} = |\cos\theta| N(E; \vec{\Omega}; \vec{r}; t) \quad .$$

The quantity  $|\cos\theta| \cdot N$  is often referred to as the current density, as distinguished from the flux density,  $N$ .



III.7 A flat probe detector, with (normal) reference polar axis  $\vec{k}$  and obliquity angle  $\theta$  for the incident photon shown.

The current density depends on the direction of  $\vec{k}$ . Normally one speaks about current density in connection with some flat surface, and with the detector plane oriented parallel to the surface. The direction of  $\vec{k}$  is then normal to the surface. One may also distinguish between the current density into, and the current density out from, the surface, each referring only to those values of  $\theta$  which correspond to photons going "into", or "out from," the surface.

## 2. Energy Deposition in the Medium

In the first section of this chapter, it was mentioned that each of the basic interaction types transfers energy to the medium by some sequence of events. One of the fundamental problems of dosimetry is the determination of energy deposition at specified positions in an irradiated medium. If the flux or fluence spectrum is known, this information can be obtained by a straightforward calculation using information about cross sections. Thus, let  $N(E)dE$  be the fluence spectrum (number per  $\text{cm}^2$ ) of photons having energy between  $E$  and  $E + dE$  at some position. Then, if  $\mu(E)/\rho$  is the mass attenuation coefficient ( $\text{cm}^2/\text{g}$ ), the number of interactions occurring in the energy interval, per gram of a small amount of material, is  $(\mu/\rho)NdE$ . To obtain the energy deposition the number of interactions must be weighted by the average energy which is transferred from the photons to the atoms. If we write this average energy as a fraction  $f(E)$  of the photon energy  $E$ , and integrate over all photon energies, we obtain the simple expression

$$D = \int_0^{\infty} dE E N(E) [\mu(E) f(E)]/\rho, \quad (\text{III.15})$$

where  $D$  is the energy "absorbed" in the medium ( $\text{MeV/g}$ ).



For the three major types of interaction identified in the section III.A, evaluation of the fraction  $f$  appears at first glance to be an elementary problem. We proceed first to outline this calculation and then to discuss why the problem is by no means resolved so easily.

Let us write  $\mu_a$  in place of  $\mu f$ :<sup>11</sup>

$$\mu_a(E) = \mu(E)f(E) \quad . \quad (\text{III.16})$$

Contributions to  $\mu_a$  must occur from each of the major types of interactions. If we write  $\mu$  in terms of component cross sections, it is clear that each type of interaction has its own fraction, so that we must identify  $f_{ph}$ ,  $f_{sc}$ , and  $f_{pp}$  for photoelectric, scattering, and pair production interactions, respectively, with

$$\mu_a(E) = (N_A/A)\rho[\sigma_{ph}(E) f_{ph}(E) + \sigma_{sc}(E) f_{sc}(E) + \sigma_{pp}(E) f_{pp}(E)] \quad . \quad (\text{III.17})$$

For photoelectric and pair production interactions, the photon disappears entirely, its energy being transferred to an atom or to a pair of charged particles, hence we provisionally assign the values  $f_{ph} = f_{pp} = 1$ . The value for  $f_{sc}$  can be readily obtained from an average in which the probability distribution for different scattered photon energies is weighted by the energy loss of the photons:

$$f_{sc}(E') = \frac{.511}{E' \sigma_{KN}(E')} \int_{\lambda'}^{\lambda'+2} d\lambda \left( \frac{d\sigma}{d\lambda} \right)_{KN} (\lambda'^{-1} - \lambda^{-1}) \quad ,$$

---

<sup>11</sup>The subscript "a" here is used to agree with notation in [6].

where  $\sigma_{KN}$  is given by eq (III.4),  $\left(\frac{d\sigma}{d\lambda}\right)_{KN}$  is given by eq (III.12') and  $(.511/E') = \lambda'$  is the relationship of eq (III.1).<sup>12</sup>

While  $\mu_a$  suffices for our purposes, alternative approaches to the problem of energy deposition exist. The ambiguity arises from the processes by which energy is further degraded after transfer to charged particles or to atomic systems. We have already noted that in the case of pair production, the positron subsequently annihilates and produces two photons of energy .511 MeV. Either of two self-consistent points of view towards these secondary photons can be taken: One can either assume that the region within which these photons give up their energy is of negligible dimensions, so that this energy is assumed to be deposited locally at the site of the primary photon interaction, or one can assume that these photons rejoin the primary irradiating flux and require more exact calculation as to the sites of later interactions. In the latter case this annihilation energy must not be counted in the determination of  $f_{pp}$ , and this quantity is reduced accordingly.

The general rule being applied here is that conservation of energy requires that one consistently assign the energy resulting from any interaction to the photon flux or to the medium, but not to both.

Similarly, photoelectric interactions and incoherent scattering interactions will generate fast electrons from local atoms. De-excitation of these atoms then produces fluorescence photons. One must decide to include these photons in the irradiating flux and reduce the  $f_{sc}$  and  $f_{ph}$  accordingly, or else one makes the assumption that these radiations are locally absorbed -- at the place of the original interaction, so to speak.

---

<sup>12</sup>This type of integral can also be written in terms of energy variables,

using  $\frac{d\sigma}{dE}_{KN} = \frac{d\sigma}{d\lambda}_{KN} |d\lambda/dE|$ , where  $|d\lambda/dE| = \lambda^2/.511$ .

We should mention also that the fast secondary electrons produced by all three processes can generate bremsstrahlung photons. The energy represented by such photons must likewise be assigned either to energy deposition or to the radiation field.

Various kinds of "energy deposition coefficients" have been defined and used. In the standard tabulations of  $\mu_{\text{en}}$  in [6], the energy represented by all the above-mentioned secondary photons is assumed to be carried by the photon flux rather than becoming a part of the energy locally deposited. Another tabulation in reference [6] is of a function  $\mu_{\text{K}}$ , which can be used as the deposition coefficient under the assumption that secondary bremsstrahlung photon energy is deposited at the site of the primary interaction, but Compton and annihilation photons are part of the irradiating flux.

The coefficients  $\mu_{\text{en}}$  and  $\mu_{\text{tr}}$  ( $\mu_{\text{K}}$  of [6]) are given formal definitions in reference [11], the recent report of the International Commission on Radiation Units and Measurements (ICRU). Physically, the secondary photons are part of the irradiating flux, but in mathematical studies these cascade products may or may not be included in the photon transport calculation. Hence the fact that some types of deposition coefficients are used in conjunction with experimental studies by no means implies that they are appropriate to a calculation; different types of calculations usually require different definitions of energy deposition coefficient for consistency.

Because the 1-2 MeV region of the fission spectrum is most important for shielding studies, and low-Z materials are predominant,  $\mu_{\text{tr}}$ ,  $\mu_{\text{a}}$ , and  $\mu_{\text{en}}$  can be used interchangeably without significant error in fallout shielding calculations. The data of chapter V were calculated using  $\mu_{\text{a}}$ . In future studies, it would be preferable to use  $\mu_{\text{tr}}$ , since techniques exist for including annihilation radiation in the calculated photon fluence.

Table III.3 gives a listing of values for the mean fraction  $\mu_{tr}/\mu$  of the photon energy deposited in the medium for interactions occurring at different photon energies [13]. One should note the close similarity between air and water values. Likewise, values for muscle are about the same.

### 3. Source Descriptions and Superposition

To complete the description of the "ingredients" of radiation transport physics, we turn to the radiation source and its various aspects.

The gamma ray sources of greatest relevance are 1) radioactive nuclei undergoing transitions, and to a lesser extent, 2) electrons radiating in the electric fields of nuclei (bremsstrahlung), and 3) excited atoms undergoing electronic rearrangements.

One is always concerned not only with the overall intensity of a source, but also with its spectrum and angular distribution as a function of position. Hence one describes sources mathematically as follows: Let

$$S(E; \theta, \phi; x, y, z; t) dE d\Omega = S(E; \vec{\Omega}; \vec{r}; t) dE d\Omega$$

be the number of photons generated per unit volume at position  $\vec{r}$ , per second, in the energy interval  $dE$  at  $E$ , and in the solid angle element  $d\Omega$  containing the direction  $\vec{\Omega}(\theta, \phi)$ .

Sources may also have the shape of thin layers, lines, points, etc. Accordingly, the layer and line sources are appropriately described by, respectively, numbers of photons per unit area, and per unit length. In the case of the point source the source strength is simply the number of photons produced per second.

Table III.3 The average fraction of the photon energy transferred in some common materials. Data were prepared by Hubbell and reported in reference [6].

<u>E</u>	<u>Air</u>	<u>H<sub>2</sub>O</u>	<u>Muscle</u>	<u>Concrete</u>
.01	.956	.960	.957	.962
.015	.876	.865	.863	.956
.02	.740	.720	.730	.936
.03	.465	.442	.450	.836
.04	.292	.273	.282	.703
.05	.207	.195	.201	.565
.06	.170	.162	.167	.454
.08	.150	.146	.148	.311
.1	.155	.152	.153	.248
.15		.186		.207
.2		.218		.232
.3		.268		.276
.4		.309		.311
.5		.342		.344
.6		.368		.368
.8		.409		.410
1		.441		.441
1.5		.494		.493
2		.531		.530
3		.578		.581
4		.615		.621
5		.644		.648
6		.668		.678
8		.702		.718
10		.732		.753

Because gamma ray trajectories and interactions are not affected by the presence of other gamma rays, any two sources produce a total fluence which is the sum of the fluences for the two sources separately considered. This basic "superposition" property greatly simplifies the mathematics of gamma ray transport. It means that the equations describing the radiation transport are linear; and because there is a large literature on linear equations, there are available many mathematical methods and concepts for use in gamma ray transport studies.

It is common to combine elementary source types to obtain representations of more complex sources; and the appropriate superposition sum or integral may involve position, energy, direction, or even time. There are many examples: One may describe monoenergetic sources with the Dirac delta function  $\delta(E - E_o)$  multiplied by a strength,  $S(E_o)$ . Polychromatic sources,  $S(E)$ , can then be represented by integration,

$$S(E) = \int_0^{\infty} dE_o S(E_o) \delta(E - E_o) , \quad (\text{III.19})$$

and the resulting fluence spectrum due to polychromatic sources is accordingly given by

$$N(E) = \int_0^{\infty} dE_o S(E_o) N(E_o, E) , \quad (\text{III.20})$$

where  $N(E_o, E)$  is the fluence spectrum due to a monoenergetic source of unit strength at  $E_o$ .

In very similar fashion, a point source can be described by the factor

$$\delta(x - x_o) \delta(y - y_o) \delta(z - z_o)$$

multiplied by the strength  $S(x_o, y_o, z_o)$ . To obtain a plane source, we integrate over point sources at all points on the plane. If the source is confined to the plane  $z = 0$ , say, and  $S(x_o, y_o, 0)$  is independent of  $x_o, y_o$ , and is thus abbreviated to  $S_o$ , then the plane source can be written as

$$S(z) = \int_{-\infty}^{\infty} dx_o \int_{-\infty}^{\infty} dy_o S_o \delta(x-x_o) \delta(y-y_o) \delta(z) = S_o \delta(z) \quad . \quad (\text{III.21})$$

By the principle of superposition, the fluence from a plane source must then be given by

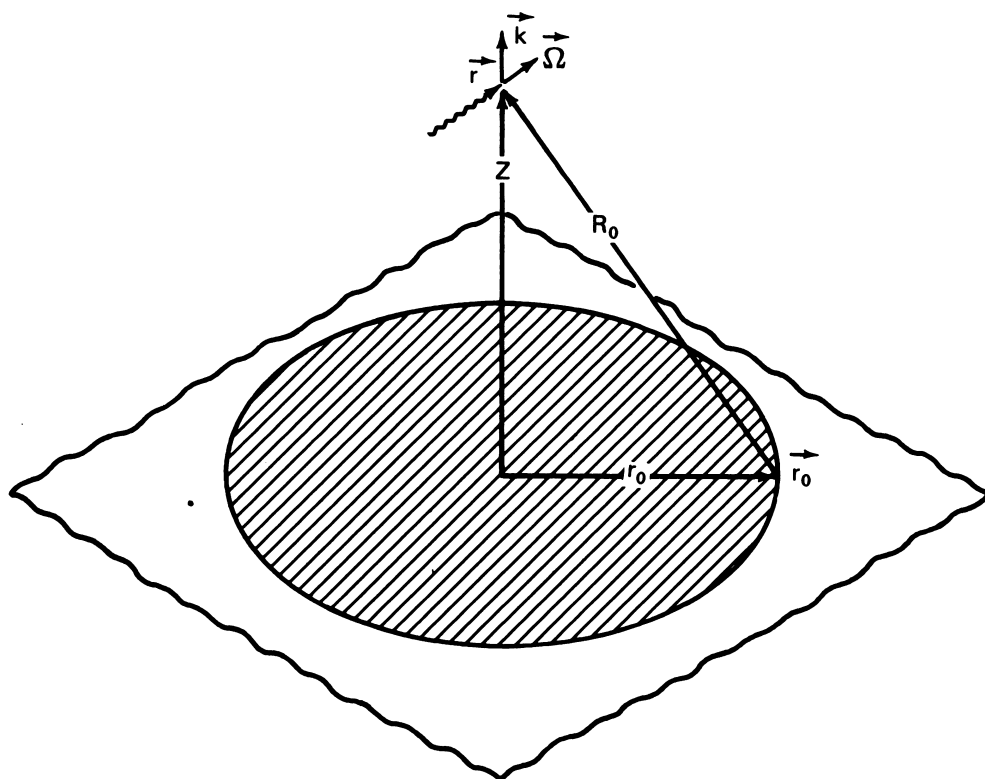
$$N_{PL}(z) = \int_{-\infty}^{\infty} dx_o \int_{-\infty}^{\infty} dy_o S_o N_{PT}(\vec{r}-\vec{r}_o) \quad , \quad (\text{III.22})$$

where  $N_{PT}$  is the fluence due to a point source of unit strength at  $\vec{r}_o$ . We can carry this a stage further, and obtain some useful results for later reference. In some important cases,  $N_{PT}$  is a function only of the distance  $R = |\vec{r}-\vec{r}_o| = \sqrt{\rho_o^2 + z^2}$  and so depends on  $x_o$  and  $y_o$  only through  $\rho_o = (x_o^2 + y_o^2)^{1/2}$  (see fig. III.8). Then, since a change to cylindrical coordinates gives

$$dx_o dy_o = \rho_o d\rho_o d\phi_o = d\phi_o \frac{1}{2} d|\vec{r}-\vec{r}_o|^2 = d\phi_o \frac{1}{2} d(R^2)$$

we can reduce eq (III.22) to the simple result

$$N_{PL}(z) = 2\pi \int_{R_s}^{\infty} R dR S_o N_{PT}(R) \quad , \quad (\text{III.23})$$



III.8 A point  $\vec{r}$  is indicated which is distant  $z$  from a source plane.  $R_0$  is the distance to a point  $\vec{r}_0$  on a circle in the source plane which is centered below  $\vec{r}$ . The unit vector  $\vec{k}$  is perpendicular to the plane, while  $\vec{\Omega}$  is a unit vector in the direction of photon propagation at  $\vec{r}$ .



where  $R_s$  is the rectilinear distance from the point  $\vec{r}$  to the nearest source point on the plane. This nearest point would be the point of the plane directly below  $\vec{r}$ , with  $R_s = z$ , if the source completely covers the plane or otherwise covers the region directly below the detector (see fig. III.8). But  $R_s$  may also measure the distance to the edge of an inner circular bound to the radiation source, the center of which is directly below the point  $\vec{r}$ . In either case,  $S_0$  is often assigned a constant strength per unit area for  $R > R_s$ , in which case it may be taken outside the integral.

Numerous other examples of superposition occur. In chapter IV, for example, the plane "isotropic" source is obtained by combination of plane sources radiating at specific obliquity angles relative to the perpendicular to the source plane (the so-called "plane oblique" sources.)

### C. ENERGY BALANCE CONCEPTS<sup>13</sup>

#### 1. The Energy Degradation Problem

Many radiation transport phenomena can be studied by making very simple geometric assumptions; and the results can be of use even when a configuration is very complicated. The most elementary case of this kind is the photon energy loss or photon energy degradation problem. To set up this problem, we assume that a medium exists which is infinite in extent in all directions, homogeneous, and of uniform density; and because such a medium will be referred to again, let us abbreviate and refer to it as an IHU medium. Here, homogeneous refers to the constituent materials; and while boundaries and variations of density or constituent materials can be overlapping concepts, we use separate terms to avoid ambiguity. Both infinite, non-uniform-density media, and finite media of uniform density can be considered homogeneous.

---

<sup>13</sup>See references [2,3,10].

One senses intuitively that if a radiation source is distributed through an IHU medium in such a way that no changes of source strength or source spectrum occur anywhere in the medium, the radiation flux will be everywhere the same, not dependent on position.

Let us assume that such a medium and source exist, with the source emitting  $S_o^*$  photons, all of the same energy  $E_o$ , per second, per  $\text{cm}^3$ . The density  $D_p$  of photons of this energy in the medium then depends on the rapidity with which interactions take place. Since photons travel with the velocity of light  $c$ , the rate at which interactions occur per photon is given by

$$\mu(E_o)c .$$

The reciprocal of this quantity is the mean lifetime for the photons prior to interaction, and the photon density  $D_p$  is the mean lifetime times the source strength  $S_o^*$ , per second per unit volume, i.e.,

$$D_p = \frac{S_o^*}{c\mu(E_o)} . \quad (\text{III.24})$$

This simple argument can be applied more generally to write expressions for the scattered photon components. Thus, let the density of photons with energy between  $E$  and  $E + dE$  be  $D_p(E)dE$ ,

$$D_p(E)dE = \frac{S(E)dE}{c\mu(E)} , \quad (\text{III.25})$$

where  $S(E)$  is the source strength,  $\text{cm}^{-3}\text{sec}^{-1}\text{MeV}^{-1}$  say, of such photons. Now,  $S(E)dE$  are the result of scattering interactions at higher energies. Since the source must basically have the structure

(photon density)x(velocity)x(interaction probability per cm) ,

we write

$$S(E)dE = \int_{E' > E} [D_p(E')dE'] c [k(E',E)dE] \quad , \quad (III.26)$$

where  $k(E',E) = k(\lambda',\lambda) |d\lambda/dE|$ ,<sup>12</sup> and  $k(\lambda',\lambda)$  is the function defined by eq (III.13). Inserting this into eq (III.25) we have

$$D_p(E)dE = \frac{1}{c\mu(E)} \int_{E' > E} D_p(E') c k(E',E)dE \quad . \quad (III.27)$$

To the density of scattered photons we add the density  $D_p^0$  of unscattered photons; but we must write the latter in analogous form, taking into account the spectral dependence, which has a sharp peak at  $E = E_0$ :

$$D_p^0(E)dE = S_0^* \delta(E-E_0)dE / [\mu(E)c] \quad . \quad (III.28)$$

Finally, to put the equation in the form in which it usually appears, we drop the differential  $dE$  from all terms, introduce the fluence spectrum  $N(E)$ , which must be density times velocity integrated over time,

$$N(E) = \int D_p(E)cdt, \quad S_0 = \int S_0^*dt \quad ,$$

so that the sum of terms in eq (III.27) and (III.28) yields the "energy-loss" equation,

$$\mu(E)N(E) = \int_{E' > E} dE' N(E')k(E',E) + S_0 \delta(E-E_0) \quad . \quad (III.29)$$

We can note also that a still simpler form occurs if we write this equation in terms of the variable  $(N/S_0)$ , a quantity which can be interpreted as an average "path-length" per photon traveled by photons of energy  $E$ . In analogous charged particle problems this quantity is referred to as "track-length".

In the next section (III.C.2) we discuss this equation and approaches to its solution. But one feature should be mentioned immediately, to make the connection with some of the preceding discussion: The interactions which govern the fluence spectrum also dissipate energy in the medium, through production of excited atoms and the kinetic energy of fast electrons. When these interactions take place, the energy not remaining in the spectrum must be considered as deposited in the medium; and conservation of energy demands that the total energy generated by the source at  $E_0$  precisely equal the total energy deposited in the medium. Referring back to eqs. (III.15) and (III.16), and noting that the total energy/cm<sup>3</sup> must be  $S_0 E_0$ , we write

$$\int_0^{\infty} dE N(E) E \mu_a(E) = S_0 E_0 \quad . \quad (III.30)$$

This expression, which is exact, can be derived by integration over eq (III.29) multiplied by  $E$ . Similar expressions using  $\mu_{tr}$  or  $\mu_{en}$  require additional source terms in eq (III.29).

## 2. Energy-Loss Calculations

The "energy loss" equation can be partially solved and studied by determining successive "orders of scattering." To this end we write the fluence spectrum as the sum of the components which have been scattered  $i$  times,  $i = 0, 1, 2, \dots$ ,

$$N(E) = \sum_{i=0}^{\infty} N^{(i)}(E) \quad . \quad (III.31)$$

We insert this expression into eq (III.29). The resulting formal solution is obtained by making the following sequence of definitions, in which  $i$  is the number of times the scattering operator is applied:

$$N^{(i)}(E) = \frac{1}{\mu(E)} \int_{E' > E} dE' N^{(i-1)}(E') k(E', E), \quad i = 1, 2, \dots, \quad (\text{III.32})$$

and

$$N^{(0)}(E) = \frac{1}{\mu(E_0)} S_0 \delta(E_0 - E) \quad . \quad (\text{III.33})$$

Insertion of the right hand side of eq (III.33) into the integral of eq (III.32) gives an expression for the once-scattered component,

$$N^{(1)}(E) = \frac{1}{\mu(E)} \frac{S_0}{\mu(E_0)} k(E_0, E) \quad . \quad (\text{III.34})$$

This component has a discontinuity at the energy  $(E_0^{-1} + 2/.511)^{-1}$  MeV, where the fluence spectrum falls abruptly to zero for all lower energies, as shown in figure III.4.<sup>14</sup>

Insertion of the right hand side of eq (III.34) into the integral of eq (III.32) gives an expression for the twice-scattered flux component, which is occasionally calculated. There is a smallest energy  $E_{\min}^{(2)}$  for this component at  $E_{\min}^{(2)} = (E_0^{-1} + 4/.511)^{-1}$  MeV. The corresponding wavelength is

---

<sup>14</sup>Note that  $\lambda(E_0) + 2 = 2 + .511/E_0 = .511/E_{\min}$ , where  $E_{\min}$  is the cutoff energy for the first scattering. This, and similar features for  $i > 1$ , determine the effective lower limit of the integral in eq (III.32). Note that  $E' > E$  implies only that the scattering process cannot increase the energy of a photon. Further,  $E' \leq E_0$ , and due to the Compton condition, one also has  $E' < (E_0^{-1} - 2/.511)^{-1}$ .

$\lambda_{\max}^{(2)} = \lambda(E_0) + 4$ . The fluence spectrum is not discontinuous at this wavelength, but has a discontinuity of slope. One can generalize to still higher orders of scattering, say the  $n$ 'th, for which the largest wavelength is  $\lambda_0 + 2n$ . At this maximum wavelength the fluence spectrum has a discontinuity in the  $(n-1)$ st derivative.

Solution of eq (III.29) by no means requires the calculation of all scattered components separately; but it is usually convenient to rewrite the equation so that the source term corresponds to the once-scattered component. The unscattered component would then require a separate calculation. To do this we may write eq (III.31) in the form

$$N(E) = N^{(o)} + N^{(s)} \quad , \quad (\text{III.35})$$

where the superscript  $\underline{s}$  stands for "scattered." Insertion into eq (III.29) and cancellation of  $N^{(o)}$  as given by eq (III.33) from both sides produces the equation

$$\mu(E)N^{(s)}(E) = \int_{E' > E} dE' k(E', E) N^{(s)}(E') + \frac{S_0}{\mu(E_0)} k(E_0, E) \quad . \quad (\text{III.36})$$

This equation belongs to a well-known class of integral equations, called Volterra equations of the second kind, which can be evaluated by ordinary numerical integration procedures. To this end we replace the integral by a sum,

$$\int_{E' > E} dE' k(E', E) N^{(s)}(E') \approx \sum_{j=0}^n w_{jn} k(E_j, E_n) N^{(s)}(E_j) \quad , \quad (\text{III.37})$$

where the  $w_{jn}$  represent integration weights for the integral from  $E_n$  to  $E_0$ . Such integration weights may be obtained using the trapezoidal rule, Simpson's rule, or other standard formulae.

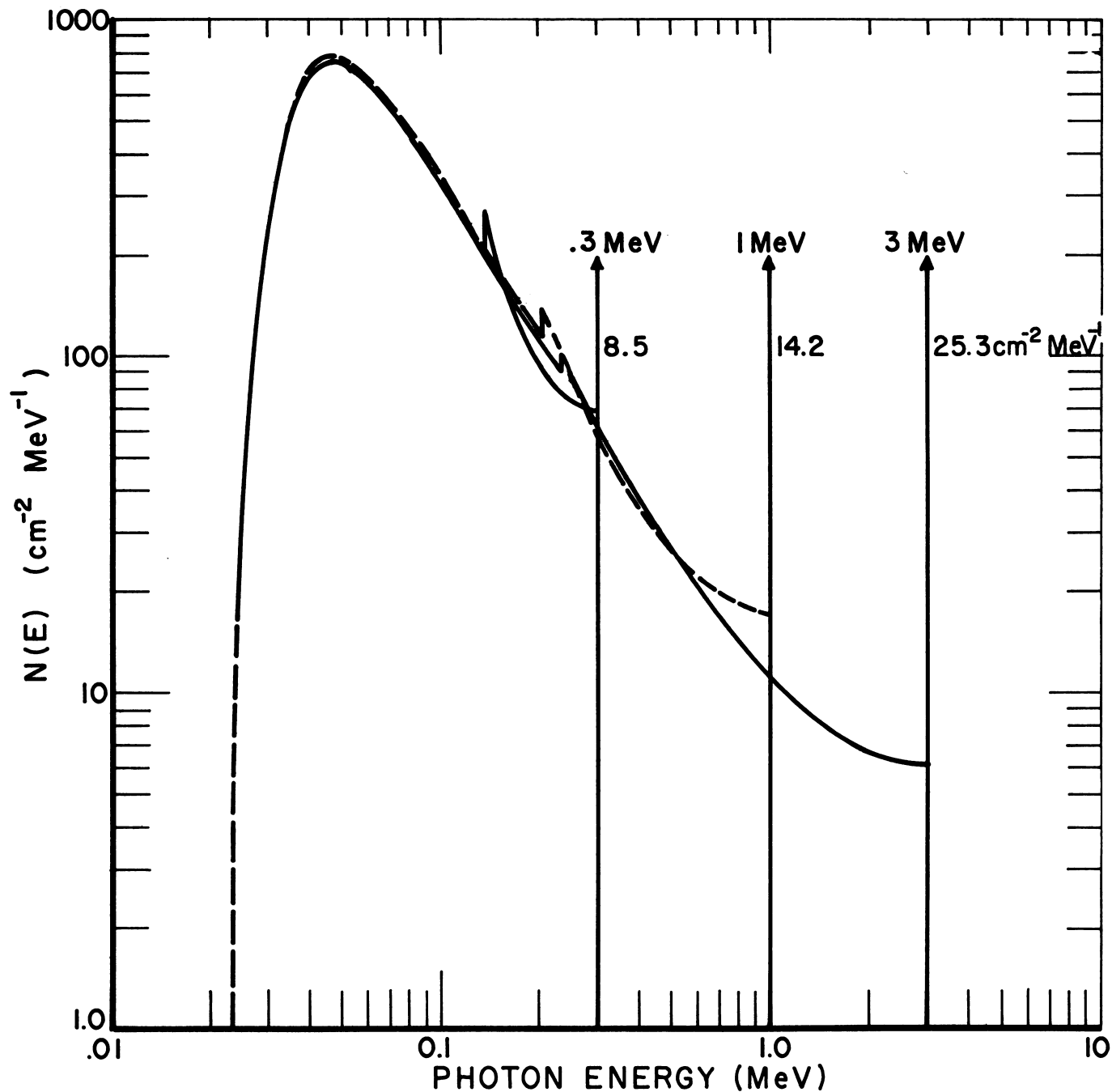
One proceeds by solving eq (III.36) for  $N^{(s)}(E_n)$ , making use of the sum given in eq (III.37) to obtain

$$N^{(s)}(E_n) = \frac{1}{\mu(E_n) - w_{nn}k(E_n, E_n)} \sum_{j=0}^{n-1} w_{jn} k(E_j, E_n) N^{(s)}(E_j) \quad . \quad (\text{III.38})$$

Chainwise evaluation can then proceed, since  $N^{(s)}(E_0)$  is known to equal  $N^{(1)}(E_0)$ . One precaution which should usually be taken is the avoidance of an integration over the discontinuity in the once-scattered component at  $\lambda_0 + 2$ . This requires two separate regions of integration, above and below  $\lambda_0 + 2$ ; but the practical effect of such a modification is only a different set of  $w_{jn}$  values, in which the two fluence spectrum values at  $\lambda_0 + 2$  are separately weighted.

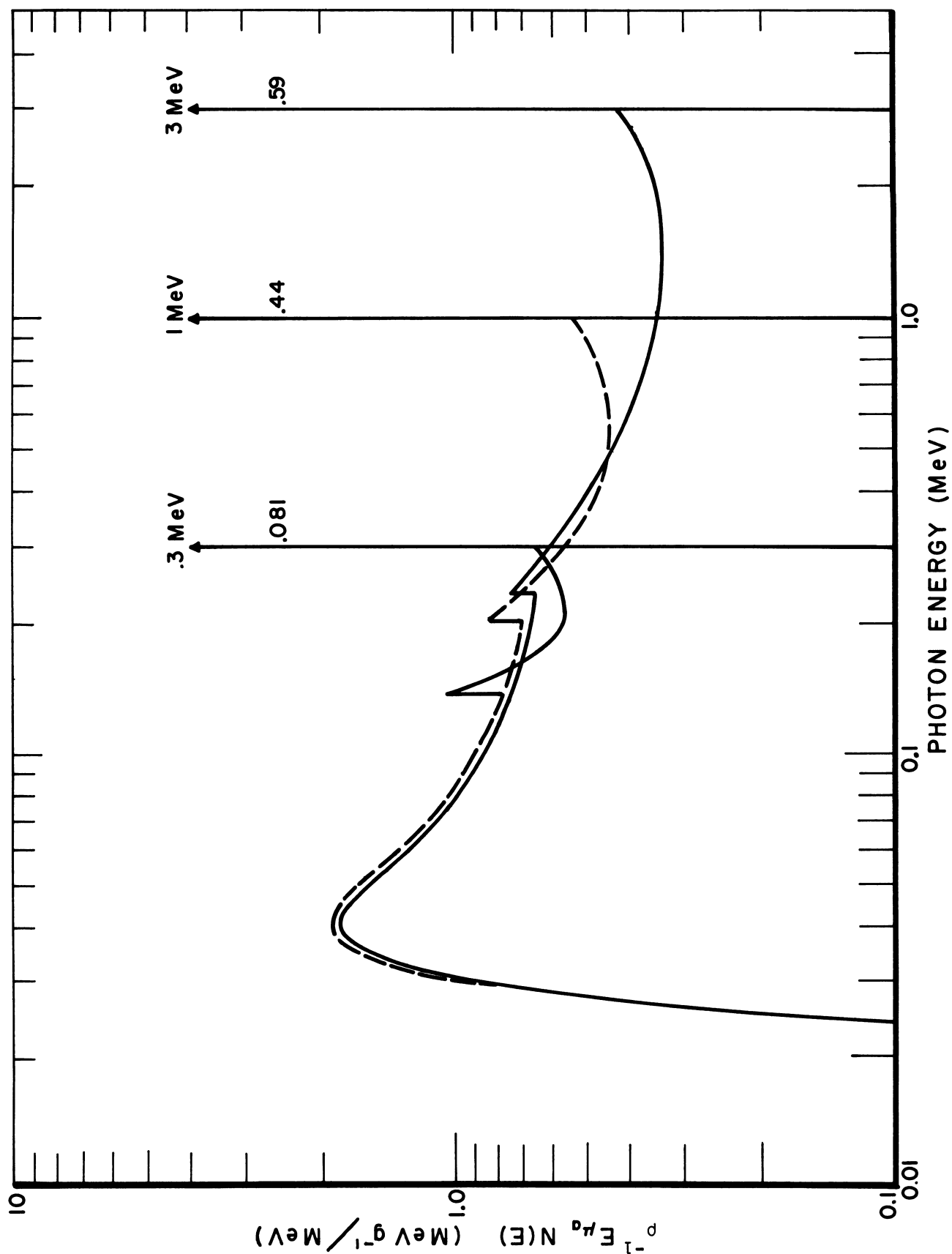
Figure III.9 gives the scattered photon spectral distributions for different photon source energies in water. All distributions show a peak at about 50 keV, where photoelectric absorption, which is very small at higher energies, begins to remove photons from the flux. Figure III.10 shows the same distributions weighted by  $E\mu_a/\rho$  to show the spectral distribution of energy deposition to the medium.

Perhaps the main feature of these results is the tendency for the curves for different source energies in the same material to become parallel and often virtually identical at the lower energies. A type of equilibrium shape, characteristic of the medium and independent of source energy, occurs in most radiation penetration problems at low energies. This simplifies both the theoretical studies of the penetration process and the problems of radiation dosimetry.



III.9 Fluence spectra for three monoenergetic sources in water, as a function of photon energy. The arrows represent the unscattered component, whose strength is in each case indicated to the right. The .3 MeV source data and the 1 MeV data nearly coincide below the discontinuity in the former.





III.10 The spectrum of energy deposition in water, for the three spectra shown in figure III.9. The numbers to the right of the arrows give the fraction of the total energy deposition due to unscattered photons. The .3 MeV source data and the 1 MeV data nearly coincide below the discontinuity in the former.

### 3. The Transport Equation

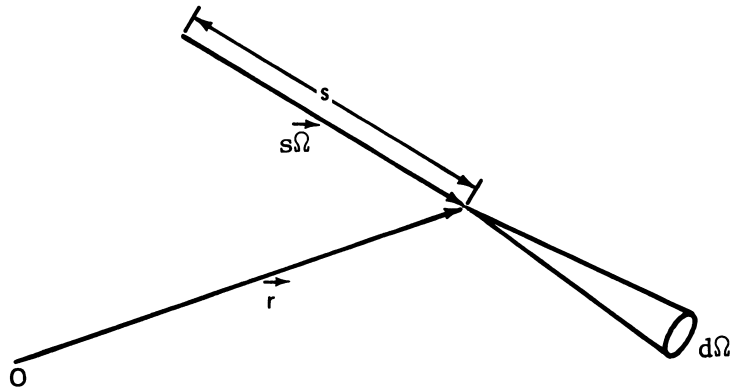
In figure III.11 a beam of gamma rays is shown traveling through a material. Let the photon wavelength be  $\lambda$  and the direction of travel be  $\vec{\Omega}$ . The fluence within a wavelength increment  $d\lambda$  at  $\lambda$  and a differential solid angle  $d\Omega$  at  $\vec{\Omega}$  will be designated  $aNd\Omega d\lambda$ , where  $a$  is the cross sectional area of the beam and is of a very small size. If one measures distance parallel to the photon direction by a variable designated  $s$ , one can determine the change of fluence between two nearby positions  $s$  and  $s + ds$ . Since the probability of an interaction during traverse of  $ds$  is  $\mu ds$ , the reduction in the beam strength is  $-\mu ds aNd\Omega d\lambda$ . On the other hand, there will be sources of photons which add to the beam; and we designate the total source strength  $\mathcal{S}d\Omega d\lambda$  photons per unit volume per second. The contribution of such a source is  $ads(\mathcal{S}d\Omega d\lambda)$ ; and our resulting equation is

$$[N(s+ds) - N(s)] d\Omega dE = -\mu ds N d\Omega dE + ds \mathcal{S} d\Omega dE ,$$

or

$$\frac{dN}{ds} = -\mu N + \mathcal{S} . \quad (\text{III.39})$$

Now, let us observe that this equation holds at all positions in the medium, and it holds for all directions. Therefore, if one can write the derivative and the source term in very general forms, one has an equation of wide applicability. In the case of the derivative, the desired quantity is the directional derivative along the direction of travel, that is  $\vec{\Omega} \cdot \nabla N$ . The source term can be considered as the sum of two terms, 1) the production of photons by scattering of higher energy photons and 2) the production of photons by other mechanisms. If we designate the latter by  $S$ , we may write



III.11 Coordinates describing a photon beam parallel to  $\hat{\Omega}$ , at position vector  $\mathbf{r}$  measured from the reference point  $O$ . The path length  $s$  is measured from an arbitrary fixed point along the trajectory. The differential solid angle  $d\Omega$  encompasses a small set of directions about  $\hat{\Omega}$ .

$$\mathcal{S} \, d\Omega dE = S \, d\Omega dE$$

$$+ \int_{E' > E} \int_{4\pi} [N \, d\Omega' dE'] [k(E', \vec{\Omega}'; E, \vec{\Omega}; \vec{r}) \, d\Omega dE] \quad (\text{III.40})$$

where the final quantity in square brackets is the probability per unit path length for scattering of a photon with the primed energy and direction into the unprimed differential energy and solid angle intervals;  $N = N(E', \vec{\Omega}', \vec{r})$ , and the integration is over the primed variables. With this interpretation of  $\mathcal{S}$  eq (III.39) becomes

$$\vec{\Omega} \cdot \nabla N = -\mu N + S + \int_{E' > E} dE' \int_{4\pi} d\Omega' N(E', \vec{\Omega}', \vec{r}) k(E', \vec{\Omega}'; E, \vec{\Omega}; \vec{r}) \quad , \quad (\text{III.41})$$

where  $N$ ,  $S$ ,  $\mu$ , and  $k$  are all dependent on position variables in principle. These position variables may be the usual Cartesian, cylindrical, or polar quantities, or they may be indicated more generally by use of a position vector,  $\vec{r}$ , say, depending on the requirements of the discussion.

For shielding calculations, the function  $k$  can be obtained from eq (III.12) and (III.13) by writing  $k(E', E) = k(\lambda', \lambda) |d\lambda/dE|$  ,

$$k(E', \vec{\Omega}'; E, \vec{\Omega}) = k(E', E) \frac{1}{2\pi} \delta(\vec{\Omega}' \cdot \vec{\Omega} - 1 + \lambda - \lambda') \quad , \quad (\text{III.42})$$

where  $\lambda = .511/E$  and  $\lambda' = .511/E'$ , and  $E, E'$  are both expressed in MeV.

An integral form for the transport equation which is useful for discussion purposes can be derived by solving the elementary differential equation (III.29)

and writing the position vector  $\vec{r}'$  of the previous interaction in terms of the unit photon direction vector  $\vec{\Omega}$  and the pathlength  $s - s'$  measured to  $\vec{r}$  along the photon trajectory,

$$\vec{r} - \vec{r}' = (s - s')\vec{\Omega}$$

We write eq (III.39) in differential form,  $d[e^{\mu s'} N] = e^{\mu s'} \mathcal{J} ds'$  for the special case of position-independent  $\mu$ , integrate over  $s'$  from  $-\infty$  to  $s$ , and write  $t = s - s'$ . Then, in the general case in which the cross sections depend on position, we replace  $\mu t$  by  $\int_0^t dt' \mu(E, \vec{r} - t'\vec{\Omega})$  and obtain

$$N(E, \vec{\Omega}, \vec{r}) = \int_0^\infty dt \mathcal{J}(E, \vec{\Omega}, \vec{r} - t\vec{\Omega}) \times \exp\left[-\int_0^t dt' \mu(E, \vec{r} - t'\vec{\Omega})\right], \quad (\text{III.43})$$

where  $\mathcal{J}(E, \vec{\Omega}, \vec{r})$  is given by eq (III.40) in terms of the flux  $N(E, \vec{\Omega}, \vec{r})$  and the source function  $S(E, \vec{\Omega}, \vec{r})$ . In eq (III.43), we recognize that the attenuation coefficient  $\mu$  may or may not depend on position.

#### 4. Fano's Theorem

Partly to gain additional familiarity with the transport equation, let us demonstrate that a general form of the energy-loss equation (III.29) applies to a wide class of source and medium configurations. To this end, let us assume that there exists a medium of uniform atomic properties and infinite in extent, but subject to density variations. Thus both functions  $\mu$  and  $k$  which characterize eq (III.41) are proportional to the density. That is to say, if  $\rho(\vec{r})$  is the position-dependent density function, then the ratios  $\mu/\rho$  and  $k/\rho$  do not depend on position.

Let us further assume that a photon source  $S$  exists in the medium with the same property: the ratio  $S/\rho$  does not depend on position, although both numerator and denominator are position dependent.

Then we may divide all terms in the transport eq (III.41) by the density, to obtain

$$\frac{1}{\rho} \vec{\Omega} \cdot \nabla N = - \left( \frac{\mu}{\rho} \right) N + \left( \frac{S}{\rho} \right) + \int_{E' > E} dE' \int_{4\pi} d\Omega' N \left[ \frac{1}{\rho} k(E', \vec{\Omega}'; E, \vec{\Omega}; \vec{r}) \right] \quad (\text{III.44})$$

Let us now consider the closely related equation,

$$0 = - \left( \frac{\mu}{\rho} \right) \bar{N} + \left( \frac{S}{\rho} \right) + \int_{E' > E} dE' \int_{4\pi} d\Omega' \bar{N} \left[ \frac{1}{\rho} k(E', \vec{\Omega}'; E, \vec{\Omega}; \vec{r}) \right] , \quad (\text{III.45})$$

which we regard as simply a mathematical integral equation with solution  $\bar{N}$ . All three known functions which appear in this equation, namely  $\mu/\rho$ ,  $S/\rho$ , and  $k/\rho$ , are independent of position. Therefore the solution  $\bar{N}$  to this equation does not depend on position.

If we insert  $\bar{N}$  into the more general equation, eq (III.44), as a trial solution, we find that because of eq (III.45) the three terms on the right combine to give zero. But because  $\bar{N}$  is not dependent on position, the derivative term on the left vanishes also. Hence,  $N = \bar{N}$  is a solution to eq (III.44); and because eq (III.45) is thought to have generally a unique solution, this is regarded as the only solution to eq (III.44).

We conclude that for infinite homogeneous media with density variations, if the source is everywhere proportional to the local density, the doubly differential radiation flux density is everywhere the same in all details.

This theorem, first stated by Sir William Bragg [14] and proven in slightly more general form by U. Fano [15], not only illustrates the information which can be derived from the transport equation but it has wide applications in dosimetry as indicated in the discussion of section III.D.<sup>15</sup> Extension of the argument to electron transport is possible, and has the consequence that except for so-called "density effects", in which electron cross sections depend on density through electromagnetic polarization of the medium, the electron energy-loss spectra generated by gamma ray interactions are also independent of local density [16,17]. Hence energy absorption per gram by the medium is everywhere the same when the conditions of Fano's theorem are satisfied for photons, except that for photon energies generally above those of interest in this treatise, electron density effects begin to break down this simple result.

#### D. DOSIMETRY AND RELATED BIOPHYSICAL MATTERS<sup>16</sup>

##### 1. Basic Concepts of Gamma Ray Dosimetry

Radiation detectors are often generically referred to as "dosimeters," and their study is part of the field called dosimetry. This term implies that the function of the instrument is "measurement of a dose." (In addition to its biological application, the term dose has often designated the energy deposited per unit mass at a selected point in a medium which may or may not be a biological entity. This quantity is called "absorbed dose." See sec III.F.)

---

<sup>15</sup>An alternative statement of the proof making use of the integral equation of eq (III.43) has recently be developed [18].

<sup>16</sup>See references [10,17,19,20,21].

More generally, we consider that the function of detectors, or dosimeters, is either a) that of providing interpretable data on characteristics of a radiation field, or b) that of providing interpretable estimates of the nature and magnitude of some radiation effect in the medium. The "effect" might be energy deposited in some volume or mass element, or it might be something else, such as the number of ion pairs or the number of chemical reactions of a given type resulting from irradiation in such an increment.

One requirement of a good detector is that it disturb the radiation field in only negligible amounts, or else in amounts which can be precisely calculated. Hence good radiation detectors are preferably small relative to distances in the surrounding medium over which there are significant changes in the radiation field. But even with this requirement satisfied, it is not often a simple matter to gain a satisfactory understanding of the response of a given type of instrument.

When the surrounding medium is air under usual atmospheric conditions, substantial changes in the radiation field may not occur over distances much less than a meter, and detectors can be relatively large, i.e. at least a few centimeters in diameter. Many types of detector have proven useful, including those which measure ionization in a cavity, light output by a scintillator, darkening of photographic films, electric pulses in a Geiger counter, current in a proportional counter, or thermoluminescence in a crystal.

Typically, the sensitive volume of a detector is surrounded by an outer layer of material which a) is of a thickness greater than the secondary electron ranges, and b) is of a material similar to that comprising the sensitive volume. As a result of property a), the sensitive volume is encompassed by an effectively infinite wall of material, so far as electron transport is concerned. In addition, the detector is constructed to be of



small thickness relative to the mean free path of the gamma ray spectral components in the detector material. Under these circumstances, all parts of the detector are exposed to approximately the same gamma ray flux density, which generates fast electrons everywhere in proportion to the local density of material.

In this simple case, Fano's theorem applies to the secondary electron flux density and the electron energy generated per unit mass in the sensitive volume will equal that dissipated in the sensitive volume, and will be proportional to detector response, whatever form that may take. Hence the problem of measurement of either the strength of the radiation field or the energy absorbed at the position of the detector is reduced to determination of proportionality constants, and these are either characteristic of the detector, or of the medium. They are not dependent on the details of the joint detector-medium configuration.

The requirement for surrounding the sensitive volume of the detector by an outer shell is usually stated as a requirement for obtaining "electron equilibrium." Here, the reference is to changes in the detector response which occur as this outer shell is increased up to an optimal value which corresponds approximately to maximum electron ranges. Further increase in the outer shell brings only slow change which can be interpreted as due to attenuation of the incident gamma rays.

The organs of the human body which are most sensitive to radiation are interior and therefore shielded from incident radiation by outer layers of flesh. This illustrates that the response of a small detector in the absence of body shielding will not necessarily be proportional to bodily damage caused by gamma radiation. A small detector records what is sometimes called a "single-collision" dose because the gamma rays would seldom interact more than

once in a small detector. On the other hand, the response of the human body considered as a large detector is typical of what has been termed a "multi-collision" dose.<sup>17</sup> There has been movement towards use of multi-collision dose concepts in connection with gamma ray shielding problems [22,23];<sup>17</sup> but presently small detectors and single-collision dose concepts are used in the definition of protection factors, and in experimental investigations related to this subject. The basis for doing so is explained as follows.

Multi-collision dose has usually been defined in terms of the maximum dose level interior to a slab, cylinder, or sphere irradiated perpendicularly with a monoenergetic beam of radiation [24]. This concept affords a rather satisfactory means of taking account of the complexities of neutron-produced energy deposition in, say, prompt radiation dose from nuclear detonation. But the point of maximum energy deposition from an external beam of gamma rays does not necessarily coincide with the point of maximum energy deposition from an external source of neutrons, hence it is hardly more consistent to add gamma ray multi-collision dose to neutron multi-collision dose, than to add gamma ray single-collision dose to neutron multi-collision dose. Consistency in superpositions does not dictate a preferred choice. More importantly, because the differences between gamma ray multi-collision and single-collision dose values are of the order of 10% [23], there has been no strong reason to shift away from single-collision dose concepts for fallout gamma rays.

In the special case of a small air equivalent detector (e.g., a cavity chamber) constructed as just described, the detector response  $D$  is called "exposure" or air "kerma" (which are essentially the same within the degree of

---

<sup>17</sup>Reference [11] introduces a "dose index" concept closely related to the multi-collision dose concept.

approximation acceptable here; see sec. III.F); and it is ideally expressed formally by the following integral over the gamma ray spectrum  $N(E)$ :

$$D = \int_0^{\infty} dE E (\mu_a^{\text{air}}/\rho) N(E) \quad , \quad (\text{III.46})$$

where  $\mu_a$ , though inserted here, may be less appropriate than  $\mu_{\text{en}}$  or  $\mu_{\text{tr}}$  depending on the type of approximation involved in calculating  $N(E)$ .

## 2. Some Aspects of Radiation Biophysics<sup>18</sup>

Gamma rays which penetrate into a living organism will produce fast electrons, as already noted. These electrons travel distances which are short in comparison with the gamma-ray mean free paths, but long in comparison with average cell dimensions. Table III.4 gives electron ranges in microns, as a function of kinetic energy [25]: cells are typically about 1 micron in diameter. The cell nucleus is perhaps an order of magnitude smaller.

Two classes of mechanisms for radiation damage are generally recognized: those in which chemicals produced as a consequence of the energy deposition may be transported inside the cell and act as poisons; and those in which chromosome damage is directly brought about by energy deposition inside the cell nucleus. The latter has received more study, though not exclusive attention.

The fast electrons give rise to excitations, ionizations, and very low energy electrons, and also to  $\delta$ -rays (energetic knock-on secondary electrons.) The secondaries, when produced, are apt to transport kinetic energy away from the primary electron track. Hence one of the fundamental questions of radiation biology relates to the amount of energy deposited "locally,"

---

<sup>18</sup>See, e.g., references [11,26,27].

Table III.4 Electron ranges in muscle, assuming unity density. This gives a practical limit to the distance over which energy deposition occurs. Data are from reference [24].

<u>E (MeV)</u>	<u>Range (Microns)</u>
.01	2.467
.03	17.33
.1	141.7
.3	835.9
1.	4350.

i.e., along and near the path, or track, of the fast electron. If this local energy deposition dominates over energy deposition far from the track, the radiation damage can be simply related to the average number of fast primary electrons which penetrate cell nuclei.

The statistical theory of local energy deposition is an active research area at present, and we cannot discuss these questions further here. But along this same line, it should be noted that for some years different radiations have been described in terms of their capacity to deposit energy near the particle track, a property designated Linear Energy Transfer (LET). This is essentially a mean energy loss per path length traveled by fast charged particles due to a class of energy losses which are of such a type that the energy would be expected to remain near the track. When uncharged particles such as neutrons are considered, the designation of LET really means the average LET of the fast secondary charged particles which they generate through interactions with nuclei.

The cells most sensitive to radiation damage tend to be those which divide rapidly to provide for constant renewal of certain types of tissues. These include the bone marrow cells which generate the blood corpuscles, and the cells which renew the intestinal lining. Radiation damage to the skin to the extent observed is likewise related to the comparatively rapid renewal of the skin tissues.

A frequent consequence of irreversable damage to the chromosomes is that of destroying the capacity of the cell to reproduce. When too many of the seed cells<sup>19</sup> of one of the critical body organs are thus altered, the organism cannot survive. In addition there is the possibility that alteration of cell

---

<sup>19</sup>These are the rapidly dividing cells which regenerate the tissues of the skin, bone marrow, intestinal lining, etc.

chromosomes may produce descendant cells whose presence is inimical to the normal function of the surrounding tissues to an extent which may likewise cause death to the organism, as exemplified by various types of cancer.

At least part of the radiation damage to tissues is known to be reversible. For example, surviving seed cells of the bone marrow or the intestinal lining will multiply to replace those killed by radiation. Thus radiation damage and radiation recovery tend to run parallel courses during extended periods of exposure, and criteria for likely survival are complicated. Additional complications involve the extent to which the radiation exposure may be localized to certain parts of the body only. When these complicating circumstances are absent, as in the case of a massive, short-term exposure to radiation over the whole body, a simple parameter such as the Median Lethal Dose (MLD) is useful in analyzing the consequences. This is the dose, usually taken to be 450 rads<sup>20</sup> for humans exposed to gamma rays, which would result in long-term survival of only 50% of those people or organisms. But even when the conditions of exposure are conceptually simple, the conditions of care and treatment are highly variable, hence this criterion can be misleading.

#### E. THE STOCHASTIC APPROACH TO RADIATION TRANSPORT<sup>21</sup>

##### 1. Schematized Photon Trajectories

The transport equation governs the average value of the fluence of photons; and most of the preceding discussion in this chapter is concerned only tangentially with the statistical aspect of the photon transport process. To conclude the chapter, we focus more directly on the stochastic (i.e. random) side of the process by making a limited development of procedures

---

<sup>20</sup>1 rad equals 100 ergs/g in the material irradiated. See section III.F.

<sup>21</sup>See references [2,28,29].

whereby the photon behavior is duplicated mathematically as closely as our knowledge of cross sections permits. This will serve as an introduction and an elementary reference for discussions of contributions to shielding literature on "Monte Carlo" methods like those described in the next section (III.E.2).

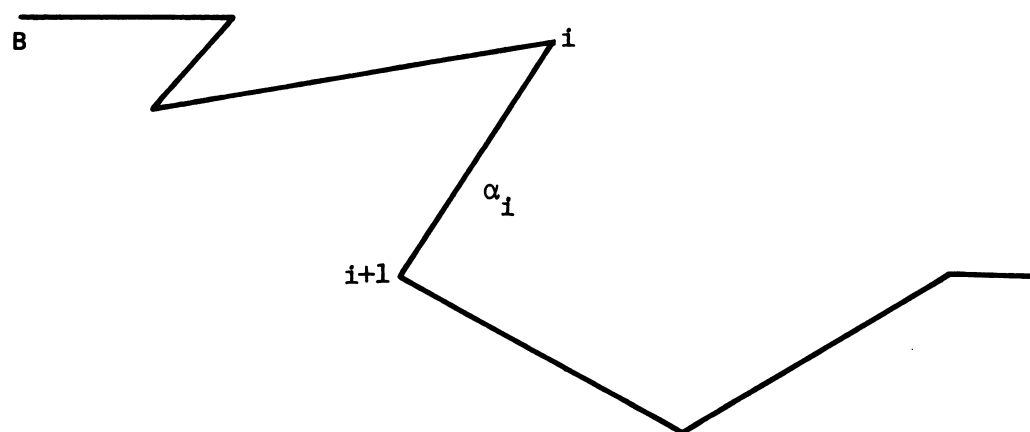
Consider the path of a photon as it penetrates through some medium. Because many scatterings will occur, such a path is expected to zig-zag more or less as in figure III.12. In this sketch the photon starts at B, where it is emitted with a given energy and a given direction. It has a free flight until there is an interaction. While the interaction can be either a scattering or an absorption, we assume that it is a scattering. The photon accordingly loses some energy and changes direction. This loss of energy with change of direction is a random process; that is, there is a probability distribution for different energy losses and changes of direction. After this first scattering the particle has another free flight and makes another interaction, and so on.

Let us consider how to describe the state of the photon at any point along its path. One needs coordinates  $x, y, z$  to describe the position, coordinates  $\theta, \phi$  to describe the direction of motion, and an energy variable  $E$ . The state of the particle, which we shall refer to as  $\alpha$ , might accordingly be written<sup>22</sup>

$$\alpha = (x, y, z, E, \theta, \phi) ,$$

---

<sup>22</sup>We omit the time variable, which could be included, as well as polarization variables.



III.12 A photon trajectory which begins at point B. Between the  $i$ 'th and the  $(i + 1)$ 'st interactions, the photon state is indicated by  $\alpha_i$ .



so that it depends on a total of six variables. An alternative representation of the photon direction utilizes a unit vector  $\vec{\Omega}$ ,

$$\vec{\Omega} = \vec{\Omega}(\sin\theta\cos\phi, \sin\theta\sin\phi, \cos\theta),$$

whose components are direction cosines.

A photon "trajectory" can be described by a sequence of states,  $\alpha_0, \alpha_1, \alpha_2$ , etc., up to some  $\alpha_n$ , where  $\alpha_0$  is the initial state at emission by the source,  $\alpha_1$  is the state immediately after the first interaction, and so on to  $\alpha_n$ , the final state before absorption or disappearance from the space or energy region of interest.

As already indicated,  $\alpha_i$  is a statistical quantity whose distribution depends only on the immediately preceding state,  $\alpha_{i-1}$ . That is, there exists a probability distribution of  $\alpha_i$  conditional on  $\alpha_{i-1}$  alone:

$$\psi(\alpha_i | \alpha_{i-1})$$

This probability distribution,  $\psi$ , is given by the local cross sections for the particular radiation considered. To generate a chain of states which would correspond to a trajectory like that of figure III.13, one would first pick an  $\alpha_0$  corresponding to initial conditions. Then one would pick an  $\alpha_1$  from the distribution  $\psi(\alpha_1 | \alpha_0)$ , then  $\alpha_2$  from  $\psi(\alpha_2 | \alpha_1)$ , and so on, each choice being made by random sampling except possibly the choice of  $\alpha_0$ . The "case-history" of a photon can be expressed by the following array:

$$\begin{array}{ccccccc}
x_0 & x_1 & \cdot & \cdot & \cdot & \cdot & x_n \\
y_0 & y_1 & \cdot & \cdot & \cdot & \cdot & y_n \\
z_0 & z_1 & \cdot & \cdot & \cdot & \cdot & z_n \\
E_0 & E_1 & \cdot & \cdot & \cdot & \cdot & E_n \\
\theta_0 & \theta_1 & \cdot & \cdot & \cdot & \cdot & \theta_n \\
\phi_0 & \phi_1 & \cdot & \cdot & \cdot & \cdot & \phi_n \quad .
\end{array}$$

We obtain such an array one column at a time.

Note that a new state is generated in two stages: 1) The path length of the next flight is determined, and from this the position of the next interaction; and 2) the nature of the interaction is determined, as well as the energy loss and associated deflection, which then determine the new direction and energy, or possibly the termination of the case history. These two stages, the displacement and the scattering, correspond to two integral operators of the transport equation, as given in eq (III.43). And the kernels of the two integral expressions are the probability distributions describing the two processes.

## 2. A Monte Carlo Model

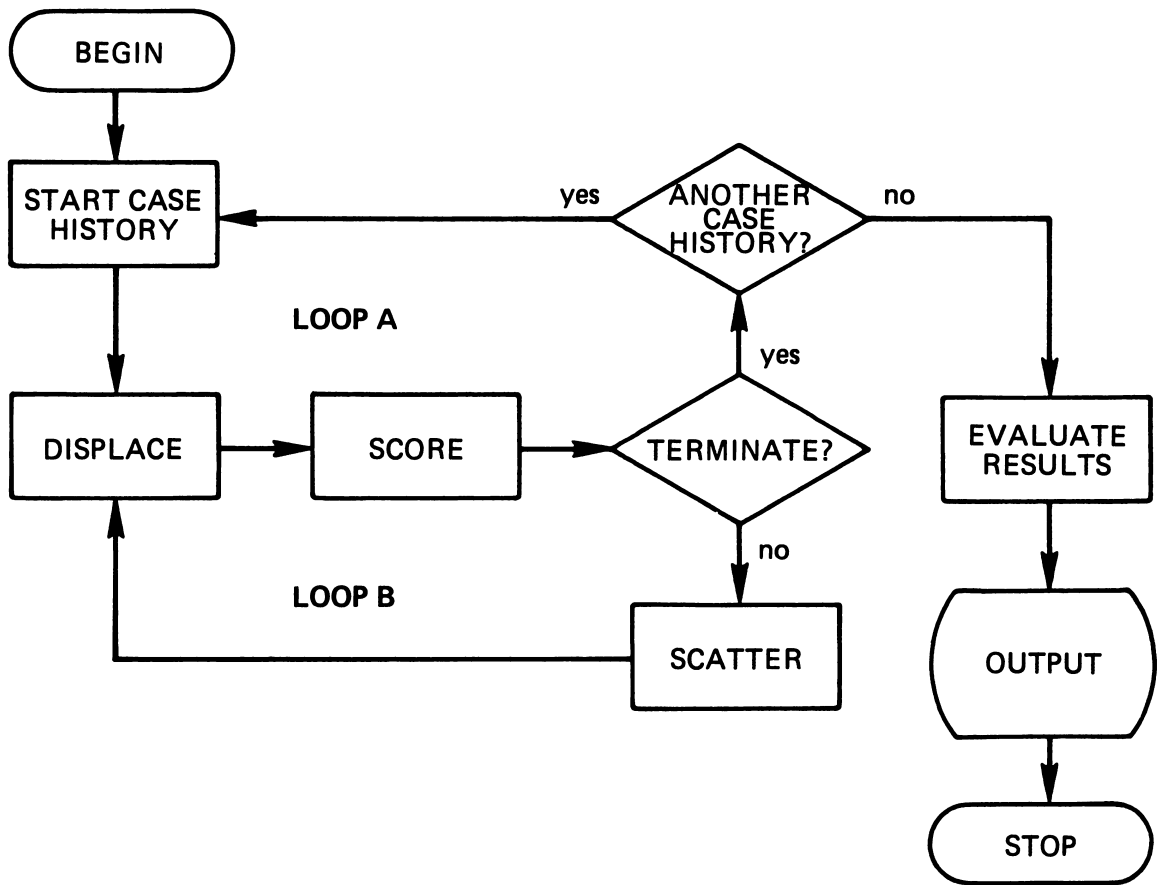
"Monte Carlo" calculations make use of schematized photon trajectories in an idealized analog to a given physical configuration. From these trajectories, or "case histories," one can infer answers to problems of interest, to a degree of accuracy which depends on the number of case histories employed. In this section, we illustrate the method with a simple but typical example, namely an "albedo" problem: The problem of determining the number of photons backscattered from a semi-infinite medium, when an isotropic fluence of gamma photons is incident.

Figure III.13 gives a simple "flow" diagram of the calculation. The arrows form a loop on the top which is designated LOOP A, and there is also a LOOP B on the bottom. The rectangular boxes in LOOP B refer to the operations which generate the  $(n+1)$ 'st state from the  $n$ 'th. Thus LOOP B will be cycled as many times in a case history as there are segments in the photon trajectory. LOOP A, on the other hand, initiates trajectories, and will be cycled as many times as there are case histories in the calculation.

In starting a case history, displacement, termination, and scatter are all accomplished using "random sampling," which is the selection of a value for some variable quantity using a random number and a probability distribution. What we refer to as a "random" number is more precisely called a "pseudo-random" number because it is calculated by a definite formula and thus cannot be considered random in the strict sense. By far the most popular formula for generating pseudo-random numbers  $y_1, y_2, \dots$  evaluates  $y_{n+1}$ , the  $(n+1)$ 'st, from  $y_n$ , by

$$y_{n+1} = (\eta y_n + \psi) \bmod p, \quad (\text{III.47})$$

where  $\eta$ ,  $\psi$ , and  $p$  are integers which are held constant. The meaning of this is as follows:  $(\eta y_n + \psi)$  is calculated and then divided by  $p$ . The remainder after division is taken to be  $y_{n+1}$ . This recursion yields a chain of numbers  $y_1, y_2, \dots$ , for each  $y_0$ . Because there can be no more than  $p$  such numbers, at most, while each uniquely generates the following, the succession eventually repeats and forms a cycle which may or may not be as "long" as  $p$ . But it turns out that by judicious choice of the constants, this type of sequence can be made to have a very long cycle. Further, when the numbers are divided by  $p$ , they all lie between zero and unity; and



III.13 Flow diagram of a simple Monte Carlo program.

constants  $\eta$ ,  $\psi$ , and  $p$  can be chosen so that on the basis of empirical tests, significant types of correlations are not important. Table III.5 gives a few numbers calculated using  $\eta = 5^5$ ,  $\psi = 0$ ,  $p = 2^{11}$ , and  $y_0 = 3$ . Note that the  $y_n$  are all odd in this case, so that the cycle length is  $\leq 1024$ . (To be exact, the cycle length for this example is 512.)

Tests of such number chains to determine degree of randomness are of several types: a) Estimates of cycle length, b) correlation calculations between successive numbers or, say, each with the second or third preceding, and c) tests to determine whether all parts of the segment from zero to unity are equally represented. Equation (III.47) turns out to be generally usable, with some simple rules such as choice of large enough (and odd) values for  $p$  and  $\lambda$ . But some care must be exercised in fixing on a pseudo-random number sequence [30]. Quite satisfactory pseudo-random sequences can be obtained with  $\psi = 0$ .

#### a. The Case History Loop

Starting a case history requires assigning numbers to the six variables which identify the initial state  $\alpha_0$ . Thus, for an albedo problem we take  $z = 0$  as the interface on which the radiation impinges, and we specify the position as  $x = y = z = 0$  initially.

We assume that the azimuthal direction variable  $\phi_0$  is measured relative to the  $x$ - $z$  plane, and that  $\phi_0$  is equally likely for all values between zero and  $2\pi$ . Hence we may specify the initial azimuth,  $\phi_0$ , by use of a random number  $R_\phi$  as follows:

$$\phi_0 = 2\pi R_\phi \quad (\text{III.48})$$

Table III.5 A few pseudo-random numbers calculated using  $\lambda = 3125$ ,  $\mu = 0$ ,  $p = 2048$ , and  $y_0 = 3$ . There is at least a temporary excess of very small numbers.

<u>n</u>	<u>y<sub>n</sub></u>	<u>R<sub>n</sub> = y<sub>n</sub>/p</u>
1	1183	.57764
2	235	.11475
3	1191	.58154
4	659	.32178
5	1135	.55420
6	1787	.87256
7	1527	.74561
8	35	.01709
9	831	.40576
10	11	.00054
11	1607	.78467
12	179	.08740

Choice of the initial obliquity,  $\theta_o$ , relative to the positive  $z$  axis, is almost as simple. The incident current density corresponding to isotropic fluence is proportional to  $(\cos\theta)$ . Thus the probability  $dP$  for  $\theta$  to occur within a differential angle  $d\theta$  is given by

$$dP = d \left\{ \frac{\int_0^\theta d\theta' \cos\theta'}{\int_0^{\pi/2} d\theta' \cos\theta'} \right\} = d(\sin\theta) \quad . \quad (\text{III.49})$$

Accordingly, a random number  $R_\theta$  fixes  $\theta_o$  by means of

$$\theta_o = \sin^{-1} R_\theta \quad . \quad (\text{III.50})$$

Notice that eq (III.50) equates the random number to a value for the cumulative probability distribution. This is a fully general approach. To specify an initial photon energy, one can tabulate a cumulative (normalized) spectral distribution. Interpolation on this table at a value equal to a random number  $R_E$  would then fix the initial energy  $E_o$ .

The preceding operations complete the initial photon state. The next problem is to determine the geometry of the first track segment, i.e. photon "displacement" at the first interaction. The magnitude of the segment to the first interaction is fixed using the probability distribution

$$dP = \mu e^{-\mu\ell} d\ell = d[1 - e^{-\mu\ell}] \quad , \quad (\text{III.51})$$

according to eq (III.9). Hence, as before, we equate the bracketed quantity in eq (III.51) with a new random number  $R_\ell$ , to obtain

$$\ell_o = -\mu^{-1} \log (1 - R_\ell) ,$$

or, since  $(1 - R_\ell)$  is distributed like  $R_\ell$ ,

$$\ell_o = -\mu^{-1} \log R_\ell . \quad (\text{III.52})$$

Given this segment length and the unit photon direction vector  $\vec{\Omega}(\theta_o, \phi_o)$ , the first interaction is at  $\vec{r} = \ell_o \vec{\Omega}$ , which has coordinates  $x_1 = \ell_o \Omega_x$ ,  $y_1 = \ell_o \Omega_y$ ,  $z_1 = \ell_o \Omega_z$ .

Returning to our simple albedo problem, a score corresponds to emergence from the medium (to negative  $z$  values). Hence we can now apply this very simple scoring test; there can be no score for the initial segment, however, because uncollided photons must interact at  $z > 0$ .

Termination of the case history occurs either upon emergence (i.e. a score) or upon disappearance of the photon due to some absorbing reaction. The latter case can occur with probability  $P$  equal to the ratio between the absorption cross section and the total interaction cross section,

$$P(E_o) = (\sigma_K + \sigma_{pp}) / (\sigma_K + \sigma_{pp} + \sigma_{KN}) . \quad (\text{III.53})$$

Hence, we terminate if the photon scores, otherwise we choose a new random number  $R_t$  and terminate if  $R_t < P(E_o)$ . (Note that  $\mu$  or  $\mu/\rho$  values can be used instead of  $\sigma$  values in eq (III.53).)

Following termination we check to see that the number of the case history just concluded does not exceed a preset number  $N$  of case histories desired. This being so, we start LOOP A again to initiate the next case history.



## b. The Scattering Loop

Failure to terminate means that we proceed through the scattering loop. This loop (LOOP B) begins with evaluation of the photon energy after scatter. The differential Klein-Nishina formula, eq (III.13), must be transformed into a probability function by dividing by its integral, which is proportional to  $\sigma_{KN}$  (see eq (III.14)); and the resulting probability distribution must be sampled.

While this can be done using cumulative integrals of the probability distribution, as already seen, we instead make use here of "rejection sampling." To this end we regard the function  $\frac{dP}{d\lambda} = k(\lambda_n, \lambda) / \mu_{KN}(\lambda_n)$ , sketched in figure III.14, as dividing the rectangle shown into two parts:

- 1) The part below the curve, which has unit area, with differential elements  $dP$  as shown, and 2) the part above the curve, which we consider meaningless.

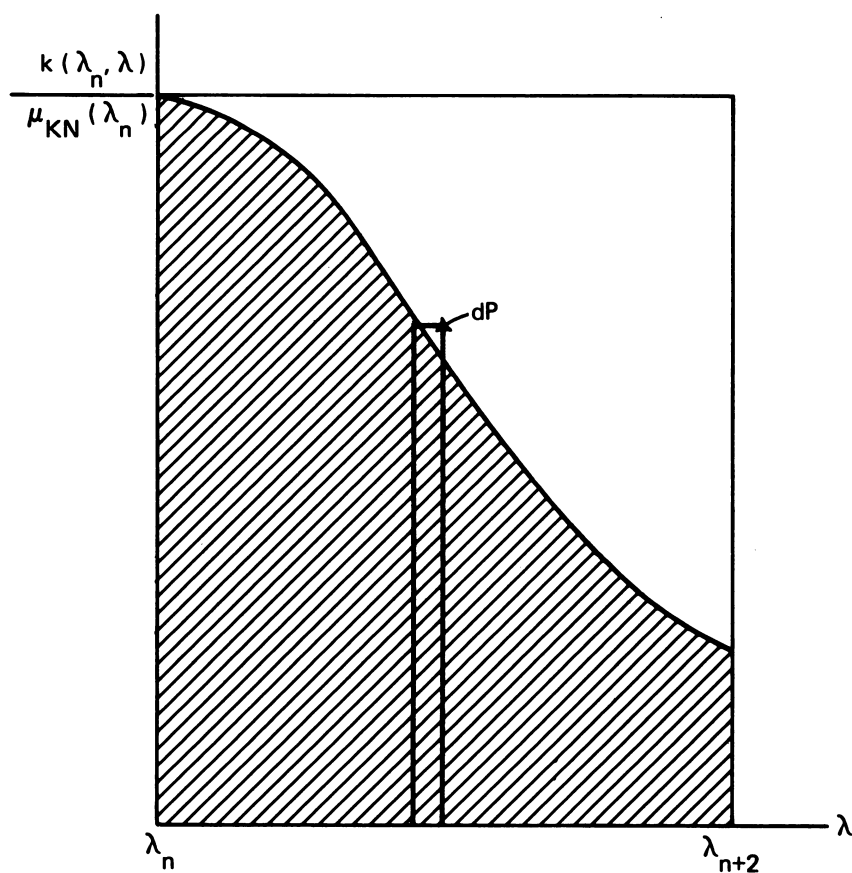
If we sample points on the whole rectangle uniformly, any points above the curve should be discarded (or "rejected").<sup>23</sup> The remaining points clearly have the correct probability distribution, and can be used to determine  $\lambda_{n+1}$ . Our procedure is to select two new random numbers,  $R_\lambda$  and  $R_{test}$ . Defining  $\lambda_{n+1}$  by

$$\lambda_{n+1} = \lambda_n + 2R_\lambda, \quad (III.54)$$

we evaluate  $R_{test} - k(\lambda_n, \lambda_{n+1}) / \mu_{KN}(\lambda_n)$ . A positive sign for this difference leads to rejection of the random number doublet; a negative sign leads to

---

<sup>23</sup>Use of a rectangle here is not essential. The top curve must only lie above the probability curve everywhere, as well as extending to the right of all random abscissa points selected. But the test as stated in this paragraph is based on the rectangle.



III.14 A sketch indicating the differential probability distribution for Klein-Nishina scattering. Thus normalized, the shaded area is unity.

the choice of the  $\lambda_{n+1}$  given by eq (III.54). If the random number pair is rejected, a new pair must be selected and tested.

The deflection angle for the photon wavelength  $\lambda_{n+1}$  immediately follows from the Compton formula

$$\cos\Theta_{n+1} = 1 - \lambda_{n+1} + \lambda_n, \quad (\text{III.55})$$

and the deflection azimuthal angle is assumed to be random and is obtained with a new random number  $R_\phi$  by  $\phi_{n+1} = 2\pi R_\phi$ .

Finally, one must calculate new direction coordinates,  $\theta_{n+1}$ ,  $\phi_{n+1}$ , determined from  $\theta_n$ ,  $\phi_n$ , and from the deflection coordinates  $\Theta_{n+1}$  and  $\Phi_{n+1}$ . This requires standard formulas of spherical trigonometry.

The remainder of LOOP B involves displacement, scoring, and a test of termination, all of which have been described in connection with LOOP A.

#### c. Evaluation of the Albedo Probability Distribution

Because all photon trajectories either emerge or do not emerge, each of the  $N$  case histories is weighted 1 if a score was registered before termination by an absorption process; otherwise the weighting is 0.

The sample of  $N$  numbers 1 or 0 constitutes a measure of the true albedo probability distribution, which must have the simple form

$$p(u) = (1-A) \delta(u) + A \delta(1-u), \quad 0 \leq u \leq 1, \quad (\text{III.56})$$

where  $A$  is the albedo to be determined. For  $N$  trajectories this gives a simple binomial distribution whose properties are well known [29,31]. The means  $\bar{u}$  and  $\bar{u}^2$  and variance  $V_u$  of such a probability distribution are readily calculated to be

$$\bar{u} = u = \int_0^1 du u p(u) = (1-A) \cdot 0 + A \cdot 1 = A, \quad (\text{III.57})$$

$$\overline{u^2} = \int_0^1 du u^2 p(u) = A, \quad (\text{III.57}')$$

$$V_u = \langle (u - \bar{u})^2 \rangle = \overline{u^2} - \bar{u}^2 = A - A^2. \quad (\text{III.58})$$

We really must solve two problems: 1) The problem of estimating a value of  $A$  using our sample and 2) the problem of estimating the error, i.e., the difference between the true value for  $A$  and our estimate. The first part of this problem is easily resolved, because the "expected value" of the simple average is  $A$ :

$$\left\langle N^{-1} \sum_{i=1}^N u_i \right\rangle = n^{-1} \sum_{i=1}^N \langle u_i \rangle = A. \quad (\text{III.59})$$

Our estimate is therefore the number of scores divided by  $N$ .

The expected value for the error,  $\left\langle N^{-1} \sum_{i=1}^N (u_i - u) \right\rangle$ , vanishes; and we therefore use the expected value for the "squared error,"<sup>24</sup>

$$\left\langle \left[ N^{-1} \sum_{i=1}^N (u_i - \bar{u}) \right]^2 \right\rangle = N^{-2} \sum_{i=1}^N \sum_{j=1}^N u_i u_j - \bar{u}^2 = N^{-1} V_u. \quad (\text{III.60})$$

---

<sup>24</sup>The simple result that follows is readily derived because  $u_i$  and  $u_j$  are uncorrelated; this means that they can be averaged separately.

We choose here to measure the fractional error  $\delta A$  of  $A$  with the square root of the expected value of the squared error, divided by the mean:

$$\frac{\delta A}{A} = \frac{1}{\bar{u}} \sqrt{N^{-1} V_u} = N^{-\frac{1}{2}} \sqrt{(1-A)/A} . \quad (\text{III.61})$$

Since  $A$  is not known precisely, one can estimate  $\delta A/A$  by using the value of  $A$  obtained by averaging the sample, although this involves an error which requires study [32].

Equation (III.61) illustrates a general property of Monte Carlo calculations: The error in any Monte Carlo estimation of a quantity decreases in proportion  $N^{-\frac{1}{2}}$ , where  $N$  is the size of the sample.

This elementary example does not do justice to the subject of the statistics of scoring, particularly when the procedure and the quantity to be determined are complex. For more information on this subject see references such as [29,33,34,35].

### 3. Other Stochastic Procedures and Problems

More detailed treatments of Monte Carlo methods give many alternative approaches with special advantages. Mostly these are aimed at reducing the computation time. For example, the arcsine calculation of eq (III.50) is fairly long. There are ways of using the trigonometric properties of double angles to speed up evaluation of random direction parameters [16]. Similarly, the calculation of the logarithm in eq (III.5) may be bypassed by interpolation on a pre-calculated list of logarithms if high accuracy is not paramount.

One device commonly used is cumulation of absorption probability factors into an overall factor which is used to "weight" the case history. If this is done, another rationale is necessary for termination; and a low energy cutoff, or a cutoff at some large value for the cumulated absorption probability, can be used.

For many problems with basic geometric symmetry, some variables may be irrelevant: One need keep track of only the depth of penetration,  $z_n$ , and the cumulative obliquity angle  $\theta_n$  for the simple albedo problem given. This gives a substantial reduction in necessary computations.

On the other hand, the data required may be more complex than the simple number albedo. One may wish to have an albedo weighted by energy, or perhaps by a detector response spectrum. A suitably calculated mean value suffices for the estimate; but estimates of the error become more complex even though the simple  $N^{-1/2}$  factor persists.<sup>25</sup>

Still more complicated problems involve determinations of spectra and/or directional distributions. Each part of a distribution is described by fewer case histories than its integral. Hence, spectral and angular distributions are determined with greatly reduced statistical accuracy.

A commonly used approach to reduce the variance is a transformation on the fluence which makes the basic probability functions more tractable in a favorable way. Perhaps the best known example of this is the so-called "exponential transformation," whereby the fluence is increased by a rising exponential function of the penetration distance. In compensation, the total interaction probability  $\mu$  is correspondingly decreased [3,36].

Still another way to reduce the variance is by selective (or biased) sampling: In our simple albedo problem, photons incident near grazing angles are more likely to score, although there are fewer of them. If there were

---

<sup>25</sup>For example, if the basic probability distribution is the probability of emergence,  $p(u)$ , times the probability  $\epsilon(E)$  say, that if emergent a photon has spectral energy  $E$ . If  $\overline{E^n} = \int dE E^n \epsilon(E)$ , then  $\overline{uE} = \overline{EA}$ ,  $V_{uE} = \overline{AE^2} - A^2 \overline{E^2}$ , and eq (III.61) takes the more complicated but similar form  $(\overline{uE})^{-1} \sqrt{V_{uE}/N} = N^{-1/2} [(1-A)/A + (\overline{E^2}/\overline{E}^2 - 1)/A]^{1/2}$ .

reason to believe that the grazing incidence contribution to the albedo is disproportionately large, one could gain by taking a disproportionate number of such case histories, while reducing the scoring weight of each in compensation.

Simple albedo problems are particularly suited to what is termed the "collision density method." In this approach, all interactions are recorded and a theoretically possible score for each is calculated. Each interaction then contributes to the final average, and the variance is correspondingly reduced because of the large number of contributions to the score.

As a last example, we mention correlated sampling. This method is particularly suited to the study of two problems which differ only slightly. Here, one evaluates the difference (or ratio) directly, by use of identical random number sequences in parallel case histories for the two problems being compared. The statistical error of the resulting difference or ratio can be expected to be much less than that obtained by separate calculation of the quantities so compared.

While a Monte Carlo estimate of many quantities can be readily obtained, the quality of this estimate cannot be firmly established without a full study, which is not easy and which is not always attempted. It sometimes even turns out that the variance (and/or its estimated value) is not a good measure of the true accuracy of a mean value [3], as for example when the true variance is not a finite number. Results can then be misleading [37].

#### F. RADIATION QUANTITIES AND UNITS

We conclude this chapter with the listing of definitions of some of the most important radiation quantities and units, as presented in reference [11].

1. "The stochastic quantity energy imparted,  $\epsilon$ , by ionizing radiation to the matter in a volume is:

$$\epsilon = \epsilon_{in} + \epsilon_{ex} + Q ,$$

where

$\epsilon_{in}$  = the sum of the energies (excluding rest energies) of all those directly and indirectly ionizing particles which have entered the volume.

$\epsilon_{ex}$  = the sum of the energies (excluding rest energies) of all those directly and indirectly ionizing particles which have left the volume, and

$Q$  = the sum of all the energies released, minus the sum of all the energies expended, in any transformations of nuclei and elementary particles which have occurred within the volume."

"The mean energy imparted,  $\epsilon$ , is the expectation value of the energy imparted. NOTE:  $\epsilon$  has sometimes been called the "integral dose in the volume."

2. "The absorbed dose  $D$  is the quotient of  $d\bar{\epsilon}$  by  $dm$ , where  $d\bar{\epsilon}$  is the mean energy imparted by ionizing radiation to the matter in a volume element and  $dm$  is the mass of the matter in that volume element.

$$D = \frac{d\bar{\epsilon}}{dm} .$$

The special unit of absorbed dose is the rad:

$$1 \text{ rad} = 10^{-2} \text{ J/kg.}"$$



One should note here that "indirectly ionizing particles" includes neutrons and gamma ray photons, and that the integral dose specifically excludes nuclear and elementary particle transitions except as represented by fragments which enter or leave the volume. The exemption of rest energies means that an excess of positrons entering the volume, say, would carry annihilation energy in, which would then exit if the volume were small. The result would be an artificial decrease in  $\bar{\epsilon}$  due to recording the one form but not the other. This aspect of the definition would not be a problem for delayed fission gamma rays in low Z materials, but the definition could be unsatisfactory for nitrogen capture gamma rays, which have up to 10.9 Mev and generate electron-positron pairs with significant frequency.

3. "The fluence ( $\Phi$ ) of particles is the quotient of  $dN$  by  $da$ , where  $dN$  is the number of particles which enter a sphere of cross sectional area  $da$ ,

$$\Phi = \frac{dN}{da} ."$$

4. "The flux density or fluence rate, of particles is the quotient of  $d\Phi$  by  $dt$  where  $d\Phi$  is the increment of particle fluence in the time interval  $dt$ ."

5. "The kerma ( $K$ ) is the quotient of  $dE_{tr}$  by  $dm$ , where  $dE_{tr}$  is the sum of the initial kinetic energies of all the charged particles liberated by indirectly ionizing particles in a volume element of the specified material and  $dm$  is the mass of the matter in that volume element,

$$K = \frac{dE_{tr}}{dm} ."$$

6. "The kerma rate,  $\dot{K}$ , is the quotient of  $dK$  by  $dt$ , where  $dK$  is the increment of kerma in the time  $\Delta t$ ."

7. "The exposure,  $X$ , is the quotient of  $dQ$  by  $dm$  where  $dQ$  is the absolute value of the total charge of the ions of one sign produced in air when all the electrons (negatrons and positrons) liberated by photons in a volume element of air, having mass  $dm$  are completely stopped in air,

$$X = \frac{dQ}{dm}."$$

The special unit of exposure is the roentgen (R).

$$1 \text{ R} = 2.58 \times 10^4 \text{ coulomb/kg}^1 \text{ (exactly)}$$

8. "The exposure rate,  $\dot{X}$ , is the quotient of  $dX$  by  $dt$  where  $\Delta X$  is the increment in exposure in time  $\Delta t$ ."

There is a close relationship between exposure and kerma. One might say that exposure is essentially "kerma in air," since one gets kerma from exposure by multiplying the latter by the energy per ion pair,  $(W)$ , which is essentially constant. But there is one additional distinction--kerma includes all the energy which would go into bremsstrahlung production on the part of the fast electrons produced by gamma rays, while exposure does not. This difference is only rarely significant for problems of shielding against gamma rays from nuclear weapons.

Lastly, let us record definitions of stopping power and linear energy transfer:

9. "The total mass stopping power,  $S/\rho$ , of a material for charged particles is the quotient of  $dE$  by  $\rho d\ell$ , where  $dE$  is the energy lost

by a charged particle of specified energy in traversing a distance  $d\ell$ , and  $\rho$  is the density of the medium,

$$\frac{S}{\rho} = \frac{1}{\rho} \frac{dE}{d\ell} ."$$

10. "The linear energy transfer .....  $L_{\Delta}$  of charged particles in a medium is the quotient of  $dE$  by  $d\ell$ , where  $d\ell$  is the distance traversed by the particle and  $dE$  is the energy loss due to collisions with energy transfers less than some specified  $\Delta$ ,

$$L_{\Delta} = \left( \frac{dE}{d\ell} \right)_{\Delta} ."$$

It is clear that the difference between stopping power and LET comes at the point of restricting the set of interactions which contribute. The type of restriction written into the definition is that of an energy cut-off. It should be noted, however, that in most practical problems the energy cut-off  $\Delta$  has been set at infinity, and the two quantities have thus been identical for electrons.

## References

- [1] Heitler, W., The Quantum Theory of Radiation, 2nd edition, 430 pages (Oxford University Press, 1947).
- [2] Goldstein, H., Fundamental Aspects of Reactor Shielding, 416 pages (Addison-Wesley, Reading, Mass., 1971).
- [3] Fano, U., Spencer, L. V., and Berger, M., Penetration and diffusion of x-rays, Handbuch der Physik, Encyclopedia of Physics, ed. S. Flugge, Vol. 38/2, 660-817 (Springer-Verlag, Berlin, 1959).
- [4] Spencer, L. V. and Wolff, C., Penetration and diffusion of hard x-rays: Polarization effects, Phys. Rev. 90, No. 4, 510-514 (May 15, 1953).
- [5] Vesely, W. E., Jr., A Study of the Effects of Polarization, Electron Binding, and Rayleigh Scattering in Monte Carlo Gamma Ray Transport Calculations, Vol. VI, VII, VIII, 328 pages (Ph.D. Thesis), University of Illinois, Urbana (1968).
- [6] Hubbell, J., Photon Cross Sections, Attenuation Coefficients, and Energy Absorption Coefficients from 10 keV to 100 GeV, Nat. Stand. Ref. Data Ser., NBS-29, 85 pages (August 1969).
- [7] Klein, O., and Nishina, Y., Uber die Streuung von Strahlung durch Freie Elektronen nach der relativistischen Quantendynamik von Dirac, Zeitschrift f. Physik 52, 853-868 (1929).
- [8] Spencer, L. V., Structure Shielding Against Fallout Radiation from Nuclear Weapons, NBS Monograph 42, 134 pages (June 1, 1962).
- [9] Nelms, A. T., Graphs of the Compton Energy-Angle Relationship and the Klein-Nishina Formula from 10 keV to 500 MeV, NBS Circular 542, 90 pages (Aug. 28, 1953).
- [10] Radiation Protection Instrumentation and Its Application, ICRU Report 20, 60 pages (International Commission of Radiation Units and Measurements, Washington, D.C., Oct. 1, 1971).
- [11] Radiation Quantities and Units, ICRU Report 19, 21 pages (International Commission on Radiation Units and Measurements, Washington, D.C., July 1, 1971).
- [12] USA Standard Glossary of Terms in Nuclear Science and Technology, 111 pages, (United States of America Standards Institute, New York, N.Y., Oct. 1967).
- [13] Evans, Robley D., X-ray and  $\gamma$ -ray Interactions, Radiation Dosimetry, 1, 94-153 (Academic Press, New York, 1968).
- [14] Bragg, W. H., Studies in Radioactivity, 91-99, 161-169 (MacMillan and Co., London, 1912).

- [15] Fano, U., Note on the Bragg-Gray cavity principle for measuring energy dissipation, Rad. Res. 1, No. 3, 237-240 (June 1954).
- [16] Kimel, W. R., ed., Radiation Shielding, Analysis and Design Principles as Applied to Nuclear Defense Planning, TR-40, 883 pages (Office of Civil Defense and Kansas State University, Nov. 1966).
- [17] Physical Aspects of Irradiation: Recommendations of the International Commission on Radiological Units and Measurements, NBS Handbook 85, Report 10b, 106 pages (March 1964).
- [18] Spencer, L. V., Some comments on Fano's Theorem, Rad. Res. 63, 191-199 (1975).
- [19] Attix, F. and Roesch, W., Fundamentals, Radiation Dosimetry, Vol. 1, 405 pages (Academic Press, 1968).
- [20] Attix, F. and Roesch, W., Instrumentation, Radiation Dosimetry, Vol. 2, 2nd Ed., 462 pages (Academic Press, 1966).
- [21] Holm, N. W. and Berry, R. J., Eds., Manual on Radiation Dosimetry, 450 pages (Marcel Dekker, Inc., New York, 1970).
- [22] Schaeffer, N. M., Reactor Shielding for Nuclear Engineers, 801 pages (National Technical Information Service, Springfield, Va., 1973).
- [23] Claiborne, H. C. and Trubey, D. K., Dose rates in a slab phantom from monoenergetic gamma rays, Nucl. Appl. Tech. 8, No. 5, 450-455 (1970).
- [24] Auxier, J. A., Snyder, W. S., and Jones, T. D., Neutron interactions and penetration in tissue, Chapter 6, Fundamentals, Radiation Dosimetry, Vol. 1, eds. F. Attix and W. Roesch, 275-315 (Academic Press, New York, 1968).
- [25] Berger, M. J., and Seltzer, S. M., Additional Stopping Power and Range Tables for Protons, Mesons, and Electrons, NASA SP-3036, 40 pages (1966).
- [26] Ebert, M., and Howard, A., eds., Radiation Effects in Physics, Chemistry and Biology, Proc. of the 2nd International Congress of Radiation Research, Harrogate, Gt. Britain, Aug. 5-11, 1962 pages (Year Book Medical Publishers, Inc., Chicago, 1963).
- [27] Casarett, A. P., Radiation Biology, 368 pages (Prentice-Hall, Englewood Cliffs, N. J., 1968).
- [28] Spanier, J. and Gelbard, E. M., Monte Carlo Principles and Neutron Transport Problems, 234 pages (Addison-Wesley, Reading, Mass., 1969).
- [29] Kendall, M. G., The Advanced Theory of Statistics, Vol. 1, 3rd edition, 458 pages (Charles Griffin & Co., Ltd., London, (1947)).
- [30] Coveyou, R. R. and MacPherson, R. D., Fourier analysis of uniform random number generators, Jour. of the Assoc. for Computing Machinery 14, No. 1, 100-119 (Jan. 1967).

- [31] Aitken, A. C., Statistical Mathematics, 8th edition, 153 pages (Oliver and Boyd, Edinburgh and London, 1962).
- [32] Amster, H. J., Prediction of Statistical Error in Monte Carlo Transport Calculations, Nucl. Science and Eng., 60, 131-142 (1976).
- [33] Biro, G. G., Application of the Monte Carlo method to shielding, Chapter 3.1. Engineering Compendium on Radiation Shielding, Vol. 1, Shielding Fundamentals and Methods, ed. R. G. Jaeger, 101-124 (Springer-Verlag, New York, 1968).
- [34] Hammersley, J. M. and Handscomb, D. C., Monte Carlo Methods, 178 pages (Wiley, 1964).
- [35] Meyer, H. A., ed., Symp. on Monte Carlo Methods, University of Florida, March 16-17, 1954, 382 pages (1956); see in particular Bulter, J. W., Machine sampling from given probability distributions, Symp. on Monte Carlo Methods, University of Florida, March 16-17, 1954, 249-264 (1956).
- [36] Chilton, A. B., A new variant to the exponential transformation technique in Monte Carlo shielding calculations, Nucl. Sci. and Eng. 24, 200-208 (1966).
- [37] Kahn, H., Random sampling (Monte Carlo) technique in neutron attenuation problems, Nucleonics 6, No. 5, 27-33, and No. 6, 60-65 (1950).

#### IV. TRANSPORT PROBLEMS AND SHIELDING CONCEPTS

##### A. UNSCATTERED PHOTONS FROM SIMPLE SOURCE TYPES

###### 1. Introductory Comments

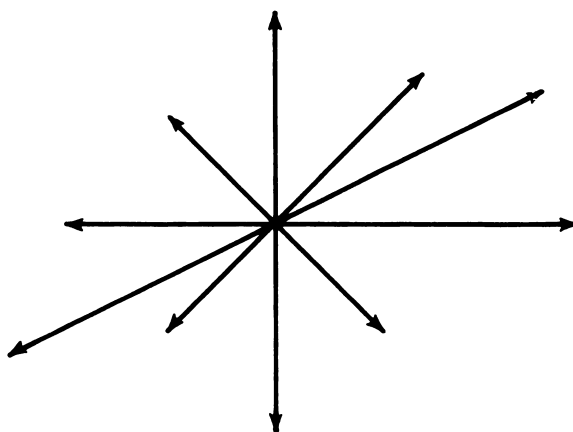
The study of radiation penetration has always leaned heavily on information about elementary problems. These not only give instruction about the solutions to more realistic but more difficult problems; they also give usable approximations to solutions for other problems.

The elementary source of fallout gamma radiation is a tiny particle of material containing fission fragments, or atoms which have absorbed neutrons from the explosion. The gamma rays which are emitted from such a tiny particle show no preference of direction. We therefore call the particle an "isotropic" source, meaning that gamma rays emerge with equal strength in all directions; and we idealize by considering them "point" sources rather than sources with small but finite dimensions.

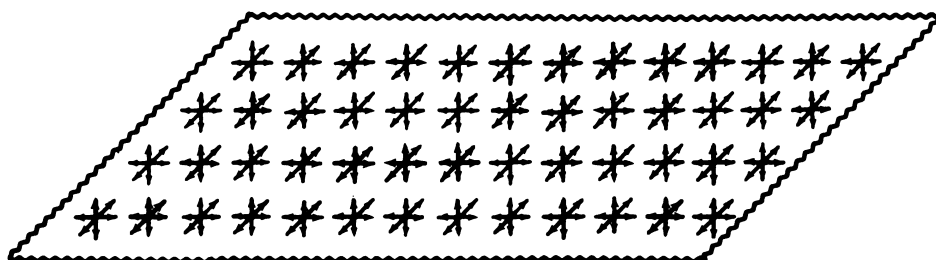
A second important elementary source type cannot be related so directly to the fallout problem. It consists of gamma ray sources uniformly distributed on a plane and emitting photons only at an obliquity angle  $\theta_0$  to one of the two directions perpendicular to the plane, as shown in the sketch of figure IV.1. For brevity, we refer to this as a "plane oblique" or PLO source, while the "point isotropic" source first described will be referred to as the PTI source.

Still a third source type is that corresponding to uniform distribution of point isotropic sources on a plane. This plane isotropic (PLI) source is an idealized analog to the fallout on smooth ground, hence it is more important to the fallout shielding applications than the other two types, though they also

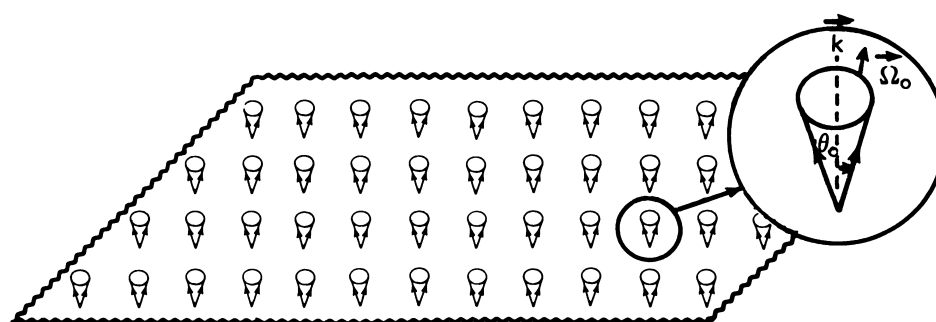
POINT  
ISOTROPIC  
(PTI)



PLANE  
ISOTROPIC  
(PLI)



PLANE  
OBLIQUE  
(PLO)



#### IV.1 Three elementary source types.



have applications. Mathematical expressions for this source are most easily derived from those for PTI or PLO sources; hence we consider it last of the three in this section.

In section IV.A we wish to develop expressions for the unscattered photons from all three source types; in a later section (sec. IV.C) we discuss some features of other components of the radiation field. We limit our attention in both sections to penetration in media without boundaries or irregularities, the case for which exact expressions can be most readily obtained.

## 2. Point Isotropic Source

Let  $S_0$  photons be emitted from a point source, equally in all directions. As they travel outwards, the photons can be considered to pass through successive spheres of increasing radii  $r$  about the source point. The points of intersection of the photon trajectories with these spheres will be spread more thinly as the sphere radius increases; in fact the number per  $\text{cm}^2$  of these intersection points on any of the spheres is

$$\frac{S_0}{4\pi r^2} \text{ photons/cm}^2, \quad (\text{IV.1})$$

and this must also be the fluence, because it would be the number intersecting a small detector at the distance  $r$ , per  $\text{cm}^2$  of the cross sectional area perpendicular to the photon direction.

This expression does not take account of interactions. Any interaction with intervening atoms would remove a photon from the uncollided components, and the exponential reduction factor discussed in section III.A would operate. For simplicity, let us consider only a single energy  $E_0$  of emitted photons,

and characterize the medium as having a total attenuation coefficient  $\mu_0$  for gamma rays of this energy. The fluence of uncollided photons must then be

$$N^0 = \frac{S_0 e^{-\mu_0 r}}{4\pi r^2} \text{ photons/cm}^2. \quad (\text{IV.1'})$$

But eq (IV.1') gives no information about either spectrum or directional distribution. To indicate that the photons have only the single energy  $E_0$  one attaches as a factor a Dirac delta function,  $\delta(E - E_0)$ .<sup>1</sup> The simplest description of the directional distribution is that all photons travel parallel to the unit radial vector

$$\vec{u} = \vec{r}/r.$$

which points from source to photon position. Representing this formally requires use of another Dirac delta function, and care that integration of this factor over all directional solid angle elements gives unity. These requirements are met by  $(2\pi)^{-1} \delta(\vec{\Omega} \cdot \vec{u} - 1)$ , where the vector  $\vec{\Omega}$  is defined to have magnitude unity and direction parallel to that of the photon trajectory.<sup>1</sup>

Combination of these two factors with eq (IV.1') gives the following expression for photons in the energy interval  $dE$  containing  $E$ , and the element of solid angle  $d\Omega$  containing the direction  $\vec{\Omega}$ :

$$N^0(E, \vec{r}, \vec{\Omega}) dE d\Omega = \frac{S_0}{2\pi} \delta(\vec{\Omega} \cdot \vec{u} - 1) \delta(E_0 - E) \frac{e^{-\mu(E)r}}{4\pi r^2} dE d\Omega. \quad (\text{IV.2})$$

---

<sup>1</sup>The Dirac delta function formalism permits us to treat  $N^0$  as a density function with respect to energy and direction and to use continuum mathematics in the analysis. For a brief discussion of its properties see [1].

The subscript has been removed from the attenuation coefficient  $\mu(E)$ , because it is now unnecessary: the factor  $\delta(E - E_0)$  singles out the effective coefficient  $\mu(E_0) = \mu_0$ .

The fallout case is typical of sources which generate polychromatic spectra. For such sources the different component energies must be weighted according to their emission strength, which we can represent by  $S_0 = S(E_0)dE_0$  in the interval  $dE_0$ , where  $E_0$  is regarded now as an emission energy variable. Addition of all source components is accomplished by integration over  $E_0$ , and since

$$\int_0^\infty dE_0 S(E_0) \delta(E - E_0) = S(E) \quad ,$$

we have a fluence spectrum represented by

$$N^0(E, \vec{r}, \vec{\Omega}) dE d\Omega = \frac{S(E)}{2\pi} \frac{e^{-\mu(E)r}}{4\pi r^2} \delta(\vec{\Omega} \cdot \vec{u} - 1) dE d\Omega \quad , \quad (\text{IV.2'})$$

as discussed in section II.B.3.

While detectors may assign differing weights both to differing spectral components and to different directions, we limit ourselves throughout to the case of ideal isotropic detectors. Hence with no angular dependence the detector response to unit fluence can be denoted by  $R(E)$ , and upon integration of eq (IV.2') weighted by this function over both photon energy and direction variables, we obtain an expression for the detector response to uncollided photons:

$$D^0(r) = \int_0^\infty dE R(E) S(E) \frac{e^{-\mu(E)r}}{4\pi r^2} \quad . \quad (\text{IV.3})$$

### 3. Plane Oblique Source

Let  $S_0$  photons be generated per  $\text{cm}^2$  from an idealized plane oblique source, and assume that these photons start their trajectory with energy  $E_0$ , obliquity angle  $\theta_0$  relative to the normal to the plane, and uniformly distributed in  $\phi_0$ , as shown in figure IV.1. Any given source direction  $\vec{\Omega}_0(\theta_0, \phi_0)$  identifies a set of uncollided photons traveling parallel to this direction, and therefore having trajectories which intersect planes parallel to the source at points which always maintain the same relative spacing. Hence a uniform source generates a uniform radiation field at any plane parallel to the source plane and distance  $z$  from it.

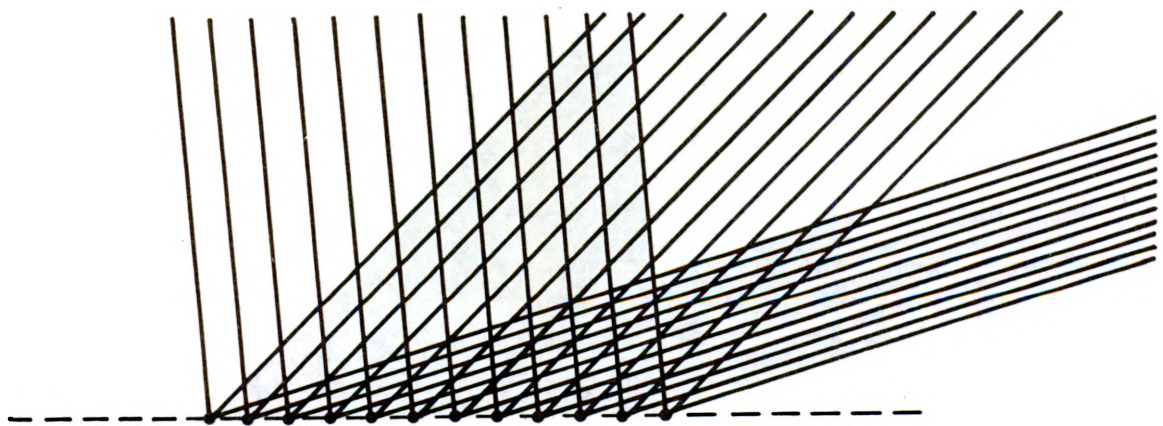
Since interactions remove photons from the uncollided component, an exponential reduction in this component occurs, and the corresponding fluence at the detector position  $\vec{r}$ , where  $z = \vec{r} \cdot \vec{k}$ , and  $\vec{k}$  is a unit vector perpendicular to the source plane, is

$$N^0 = S_0 \frac{e^{-\mu_0 z / \cos \theta_0}}{\cos \theta_0}, \quad (\text{IV.4})$$

with  $\mu_0 = \mu(E_0)$  as in eq (IV.1) and  $\cos \theta_0 = \vec{\Omega}_0 \cdot \vec{k}$ . The factor  $(\cos \theta_0)^{-1}$  which increases this result with increasing obliquity angle is due to the crowding together of trajectories shown in figure IV.2. Note that all the photons with parallel directions from any given source area pass through the projection of the source area on planes perpendicular to the photon trajectories; and this projected area is smaller by a factor  $\cos \theta_0$ .

To take account of spectrum and directional distribution, Dirac delta functions can be used very much as in eq (IV.2):

$$N^0(E, z, \Omega) = \frac{S_0}{2\pi} \delta(\cos \theta - \cos \theta_0) \delta(E - E_0) \frac{e^{-\mu(E) z / \cos \theta}}{\cos \theta}, \quad (\text{IV.5})$$



IV.2 Crowding of unscattered trajectories from a plane oblique source as the initial obliquity increases, with the number emitted held constant.

where  $\cos\theta = \vec{\Omega} \cdot \vec{k}$ .

Extension to a polychromatic spectrum  $S(E_0)$  and to an isotropic detector with response function  $R(E)$  produces expressions analogous to eqs (IV.2') and (IV.3),

$$N^0(E, z, \Omega) = \frac{S(E)}{2\pi} \delta(\cos\theta - \cos\theta_0) \frac{e^{-\mu(E)z/\cos\theta}}{\cos\theta}, \quad (\text{IV.5'})$$

$$N^0(E, z) = S(E) \frac{e^{-\mu(E)z/\cos\theta_0}}{\cos\theta_0}, \quad (\text{IV.6})$$

and

$$D^0(z) = \frac{1}{\cos\theta_0} \int_0^\infty dE R(E) S(E) e^{-\mu(E)z/\cos\theta_0}. \quad (\text{IV.7})$$

It is instructive to show that  $N^0$ , as given by eq (IV.5'), satisfies the transport equation (eq (III.41)). For plane sources, which generate distributions constant with respect to lateral coordinates,  $\vec{\Omega} \cdot \nabla = \cos\theta \frac{\partial}{\partial z}$ ; and it is clear that for  $z \neq 0$ ,  $(\cos\theta \frac{\partial}{\partial z} + \mu) N^0 = 0$ . At  $z = 0$ ,  $\exp(-\mu z/\cos\theta)$  undergoes a discontinuous change of unity, whose spatial "derivative" is  $\delta(z)$ . Hence, we obtain

$$\left( \cos\theta \frac{\partial}{\partial z} + \mu \right) N^0(E, r, \Omega) = \frac{S(E)}{2\pi} \delta(\cos\theta - \cos\theta_0) \delta(z); \quad (\text{IV.8})$$

and the expression on the right is the correct source term.

While this type of calculation can also be applied to the PTI source, the suitable form for  $\vec{\Omega} \cdot \nabla$ , and the resulting argument, are much more complicated.

#### 4. Plane Isotropic Sources

Either the PTI or the PLO source expression can be used to derive expressions for the plane isotropic source. Our interest is confined here to unscattered photons, for which such a derivation is simple from both PTI and PLO cases, by superposition. But for the once-scattered component it is distinctly easier to use the PLO source for such derivations; hence we use this also for the unscattered component.

A PLI source can be considered a superposition of PLO sources in which different source obliquity angles contribute equally to the current density emerging from the source plane. Since  $(\cos\theta_o)N^o \rightarrow S_o$  as  $z \rightarrow 0$  in eq (IV.4) for all obliquity angles, we weight the different  $\theta_o$  components  $N^o$  by unity in our superposition. The fluence at a distance  $z$  from a plane isotropic source is then given by the following elementary integral over the expression given in eq (IV.6),<sup>2</sup>

$$N_{PLI}^o = \int_{4\pi} d\Omega_o \frac{1}{4\pi} N_{PLO}^o = \frac{1}{2} \int_0^1 d(\cos\theta_o) S_o \frac{e^{-\mu_o z / \cos\theta_o}}{\cos\theta_o}$$

$$= \frac{1}{2} S_o E_1(\mu_o z) \quad , \quad (IV.9)$$

where

$$E_1(\mu_o z) = \int_{\mu_o z}^{\infty} \frac{ds}{s} e^{-s} \quad (IV.10)$$

---

<sup>2</sup>Note that the PLI source term corresponding to that of eq (IV.8) is  $1/4\pi S(E) \delta(z)$ ; and the factor  $(4\pi)^{-1}$  in eq (IV.9) is required to obtain this by superposition of sources of the type in eq (IV.8). The extra factor  $1/2$  expresses the fact that half the photons of a PLI source start towards negative  $z$  values and hence make no contribution at positive  $z$ .

is the exponential integral, which for small values of  $\mu_0 z$  is approximately given by  $E_1(\mu_0 z) \approx -\log(e^\gamma \mu_0 z)$ ,  $e^\gamma = 1.78\dots$ . Since the logarithm, and therefore the exponential integral, diverges weakly as  $z \rightarrow 0$ , so also does the PLI fluence diverge as the source plane is approached. This divergence can be attributed to the bunching together of trajectories as illustrated in figure IV.2, or it can be viewed as a consequence of the inverse square law when elements of the source are approached.

Extension to a more complex spectrum proceeds just as in the other two source types; and the directional distribution must at each obliquity correspond to the PLO case. Thus, writing  $\cos\theta = \vec{\Omega} \cdot \vec{k}$ , we have expressions for the doubly differential fluence, the fluence spectrum, and the dose:

$$N^O(E, z, \vec{\Omega}) = \frac{S_0}{4\pi} \delta(E - E_0) \frac{e^{-\mu(E)z/\cos\theta}}{\cos\theta}, \quad \text{(Mono-energetic source)} \quad (\text{IV.11})$$

$$N^O(E, z, \vec{\Omega}) = \frac{S(E)}{4\pi} \frac{e^{-\mu(E)z/\cos\theta}}{\cos\theta}, \quad \text{(general source spectrum)} \quad (\text{IV.12})$$

$$N^O(E, z) = \frac{1}{2} S(E) E_1[\mu(E)z], \quad (\text{IV.12'})$$

$$D^O(z) = \int_0^\infty dE R(E) S(E) \frac{1}{2} E_1[\mu(E)z]. \quad (\text{IV.13})$$

Since the logarithmic divergence for  $z \rightarrow 0$  applies to each source component, it must also apply to  $D^O(z)$ .



Equations (IV.11) and (IV.12) give the angular distribution of the fluence of uncollided radiation. The combination of the exponential function and the cosine factor produce a peak in the angular distribution at  $\cos\theta = \mu_0 z$  for penetration distances less than  $\mu_0 z = 1$ . This peak is very sharp for  $\mu_0 z \ll 1$  and grows progressively broader as  $\mu_0 z$  increases.

### 5. Circular Disk and Ring Sources

Expressions for limited sources, such as circular disk and ring shapes, can be obtained by superposition of PTI sources, as discussed in section III.B.3. If  $S(\vec{r}_0)$  is the (PTI) source strength per unit area at  $\vec{r}_0$  on the plane, then  $\int_A dA' S(\vec{r}_0)$  is the required superposition, where  $A$  is either a circle or ring area. From this, together with the fact that all source components equidistant (distance  $R'$ ) from the detector contribute equally to the dose so that we can take  $dA' = 2\pi\rho'd\rho' = 2\pi R'dR'$ , we obtain for the circular disc source,

$$\begin{aligned} D^0(z, R) &= \int_0^\infty dE R(E) \int_z^R 2\pi R' dR' \frac{S(E) e^{-\mu(E)R'}}{4\pi(R')^2} \\ &= \int_0^\infty dE R(E) S(E) \frac{1}{2} [E_1(\mu z) - E_1(\mu R)] \quad , \quad (IV.14) \end{aligned}$$

where  $R$  is the distance from detector to the outer rim of the source circle,  $z$  is the height of the detector above the center of the circle; and the variables  $R', R$  in this instance should not be confused with the response function  $R(E)$ .

The expression for a ring source, whose inner and outer edges are distances  $R_1$ ,  $R_2$ , respectively, from the detector, is then obtained as the difference of two such expressions,

$$D^0(R_1, R_2) = \int_0^{\infty} dE R(E) S(E) \frac{1}{2} [E_1(\mu R_1) - E_1(\mu R_2)] \quad . \quad (\text{IV.15})$$

The circular disk source has been discussed by Rockwell [2]. For essentially similar treatments see also references [3] and [4].

## B. DENSITY SCALING THEOREMS, AND DETECTORS NEAR AN INTERFACE<sup>3</sup>

### 1. Introductory Comments

The first theorem proven in this section, on plane density variations, has its most prominent application in the practical approximation of the earth-air interface configuration by an infinite homogeneous configuration. It is true that earth and air differ in their properties; but the effect of this difference on the detector response in air is very small -- in the few percent range -- and it is largely confined to spectral differences below 50 keV photon energy [6,7]. The theorem is also important in the design of experiments conducted in plane geometry, even when the conditions of the theorem are not fulfilled precisely.

The second theorem, on density scaling, is the basis for all the experiments which utilize scale modeling. Its conditions are seldom if ever fulfilled exactly; and the effects of the departure from the exact fulfillment have been the subject of additional studies.

Although one might think that these two theorems were in some sense equivalent, in fact they are not. One cannot generalize the plane density

---

<sup>3</sup>Much of the material of this section is from reference [5].

theorem even to one-dimensional cases of cylindrical or spherical symmetry; and the general scaling theorem applies a single parameter to the whole configuration which may not be of the type having multiple density variations and covered by the plane density theorem.

The final section gives an elementary discussion of detectors in a manner which clarifies the difference between "flux" and "current" density descriptions while demonstrating the equivalence of these points of view. (In radiation physics there is no more common source of confusion than these two related concepts.)

## 2. The Theorem on Plane Density Variations

Let us consider those configurations in which the medium has density variations but with the density constant on parallel planes. The most relevant situation of this type is the ground-air interface, with the ground considered to be equivalent to compressed air of the same density. Other configurations of this type have importance also.

The restriction to density variations would allow us to apply Fano's theorem if the radiation source were everywhere proportional to the local density. (See sec. III.C.4). We do not make this assumption, but instead assume only that the radiation source is likewise constant on planes parallel to the planes of constant density. The theorem is as follows:

Theorem. In an infinite medium in which the material is everywhere the same except for plane density variations ( $\rho = \rho(z)$ ), if there is a source of radiation, which may be distributed arbitrarily except that it is likewise constant along planes of constant density, the doubly differential flux density is exactly the same as in a corresponding configuration with constant density ( $\bar{\rho}$ ) everywhere. In two such equivalent cases the strength of the radiation source and its spectrum and angular distribution, per unit mass of material, must be the same at corresponding distances  $z$  and  $\bar{z}$  from

corresponding reference planes, where the relation between these distances is given by

$$\int_0^z \rho(z') dz' = \bar{\rho} \bar{z} ; \quad (\text{IV.16})$$

the comparison between flux densities must be made at distances also corresponding in this way; and boundary conditions must be the same.

We are contrasting two cases, one in which the density has everywhere the value  $\bar{\rho}$ , and the other with a variable density function  $\rho(z)$ . The argument resembles that used in the proof given in chapter III of Fano's theorem. The parts of the gradient term of eq (III.41) involving derivatives with respect to  $x$  and  $y$  are zero, and the transport equations for the two cases may be written

$$\begin{aligned} \frac{1}{\rho(z)} \cos\theta \frac{\partial N}{\partial z} + \frac{1}{\rho} \mu N(E; \theta, \phi; z) &= \int_E^\infty dE' \int_{4\pi} d\Omega' \frac{1}{\rho} k(E', E, \cos\Theta, z) N(E'; \theta', \phi'; z) \\ &+ \frac{1}{\rho} S(E; \theta, \phi; z) , \end{aligned} \quad (\text{IV.17})$$

$$\begin{aligned} \frac{1}{\bar{\rho}} \cos\theta \frac{\partial \bar{N}}{\partial \bar{z}} + \frac{1}{\bar{\rho}} \bar{\mu} \bar{N}(E; \theta, \phi; \bar{z}) &= \int_E^\infty dE' \int_{4\pi} d\Omega' \frac{1}{\bar{\rho}} \bar{k}(E', E, \cos\Theta) \bar{N}(E'; \theta', \phi'; \bar{z}) \\ &+ \frac{1}{\bar{\rho}} \bar{S}(E; \theta, \phi; \bar{z}) , \end{aligned} \quad (\text{IV.17}')$$

where  $\theta$  is the photon obliquity relative to the  $z$ -axis and  $\Theta$  is the scattering angle. In eqs (IV.17) and (IV.17') we have divided all terms in both equations by the density, because we expect to use the position independence of the functions  $\frac{1}{\rho(z)} \mu(E, z)$  and  $\frac{1}{\rho(z)} k(E', E, \cos\theta; z)$ .

Next we define new variables  $\tau(z)$  and  $\bar{\tau}(\bar{z})$ , as suggested by eq (IV.16),

$$\tau(z) = \int_0^z dz' \rho(z') \quad , \quad (IV.18)$$

$$\bar{\tau}(\bar{z}) = \int_0^{\bar{z}} d\bar{z}' \bar{\rho} = \bar{\rho} \bar{z} \quad . \quad (IV.18')$$

In terms of these variables which measure "mass" thickness, the two transport equations may be re-written as follows:

$$\begin{aligned} \cos\theta \frac{\partial N}{\partial \tau} + \frac{\mu}{\rho} N(E; \theta, \phi; \tau) &= \int_E^\infty dE' \int_{4\pi} d\Omega' \frac{1}{\rho} k(E', E, \cos\Theta, \tau) N(E; \theta', \phi'; Z) \\ &+ \frac{1}{\rho} S(E; \theta, \phi; \tau) \quad . \end{aligned} \quad (IV.19)$$

$$\begin{aligned} \cos\theta \frac{\partial \bar{N}}{\partial \bar{\tau}} + \frac{\bar{\mu}}{\bar{\rho}} \bar{N}(E; \theta, \phi; \bar{\tau}) &= \int_E^\infty dE' \int_{4\pi} d\Omega' \frac{1}{\bar{\rho}} \bar{k}(E', E, \cos\Theta) \bar{N}(E'; \theta', \phi'; \bar{\tau}) \\ &+ \frac{1}{\bar{\rho}} \bar{S}(E; \theta, \phi; \bar{\tau}) \quad , \end{aligned} \quad (IV.19')$$

where the change to  $\tau$  and  $\bar{\tau}$  as space variables does not change the basic form of the first three terms of eqs (IV.19) and (IV.19').

It is clear that the two equations are precisely the same, except possibly for the source term, since  $\frac{\mu}{\rho}$  and  $\frac{k}{\rho}$  in the first equation are not only independent of position, but numerically equal to  $\frac{\bar{\mu}}{\bar{\rho}}$  and  $\frac{\bar{k}}{\bar{\rho}}$ , respectively. If, therefore, the source terms are such that

$$\frac{S(E; \theta, \phi; \tau)}{\rho} = \frac{\bar{S}(E; \theta, \phi; \bar{\tau})}{\bar{\rho}} \quad , \quad (IV.20)$$

the two equations will be identical in all respects, except that  $\tau$  appears in one equation where  $\bar{\tau}$  appears on the other. Further, if, say,

$$\lim_{|z| \rightarrow \infty} |\tau| = \infty, \quad (\text{IV.21})$$

the boundary conditions will be the same in the two cases.<sup>4</sup> It is then clear that

$$N(E; \theta, \phi; \tau) = N(E; \theta, \phi; \bar{\tau}) \quad . \quad (\text{IV.22})$$

To illustrate this theorem, we compare two situations in each of which the source is confined to a plane and is uniform over the plane, with the same strength in both cases. In one situation the material density,  $\rho(z)$ , varies; in the other, the density  $\bar{\rho}$  is constant. The source is located at  $z = 0$  in the first problem and at  $\bar{z} = 0$  in the second. We define  $\tau(z)$  and  $\bar{\tau}(z)$  by eqs (IV.18) and (IV.18').

Using the Dirac delta function to represent a concentrated source, we write expressions for the (equal strength) sources:

$$S(E; \theta, \phi; \tau) = S(E; \theta, \phi) \delta[z(\tau)] \quad , \quad (\text{IV.23})$$

$$\bar{S}(E; \theta, \phi; \bar{\tau}) = S(E; \theta, \phi) \delta[\bar{z}(\bar{\tau})] \quad . \quad (\text{IV.23}')$$

---

<sup>4</sup>Equivalent boundary conditions are readily arranged for the constant density comparison case even for exponentially decreasing  $\rho(z)$ .

We then note that

$$\delta(z) = \delta(\tau(z)) \frac{d\tau}{dz} = \delta(\tau)\rho \quad , \quad (\text{IV.24})$$

$$\delta(\bar{z}) = \delta(\bar{\tau}) \frac{d\bar{\tau}}{d\bar{z}} = \delta(\bar{\tau})\bar{\rho} \quad , \quad (\text{IV.24}')$$

so that

$$S(E; \theta, \phi; \tau) = S(E, \theta, \phi) \rho \delta(\tau) \quad , \quad (\text{IV.25})$$

$$\bar{S}(E; \theta, \phi; \bar{\tau}) = S(E; \theta, \phi) \bar{\rho} \delta(\bar{\tau}) \quad , \quad (\text{IV.25}')$$

and the condition of eq (IV.20) is obviously satisfied.

It follows from the arguments used here that it is also possible to construct equivalent configurations in which plane layers of different materials occur. The conditions necessary for such an equivalence are 1) eq (IV.20), 2) the requirement that for  $z$  and  $\bar{z}$  such that

$$\tau(z) = \bar{\tau}(\bar{z}) \quad ,$$

and 3) the same type of material must occur at corresponding places in the configurations being compared. If these conditions are satisfied, not only the density functions  $\rho(z)$ ,  $\bar{\rho}(\bar{z})$  but also the type of material can be arbitrary, and in different materials  $\bar{\tau}$  may have different constant values.

It might appear that this argument can be extended to two or three dimensions or to one-dimensional curvilinear cases; but apparently this is not so. Equation (IV.16) is a functional requirement which is unsuited to the

other terms which occur when a more general expression is used for the gradient term.

### 3. Density Scaling Theorem

This theorem is well-known, and almost intuitively obvious. In it we compare two configurations, call them "A" and "B", exemplified in figure IV.3. Each has its own origin of coordinates.

When two points, one in A and the other in B, are related in that the coordinates of the point in B can be specified as those of the point in A multiplied by a basic scaling parameter  $\xi$ , we say that the points are "corresponding points". The two configurations are then said to be "similar" if the following requirements are met:

a) All interfaces in A occur also in B at corresponding points.

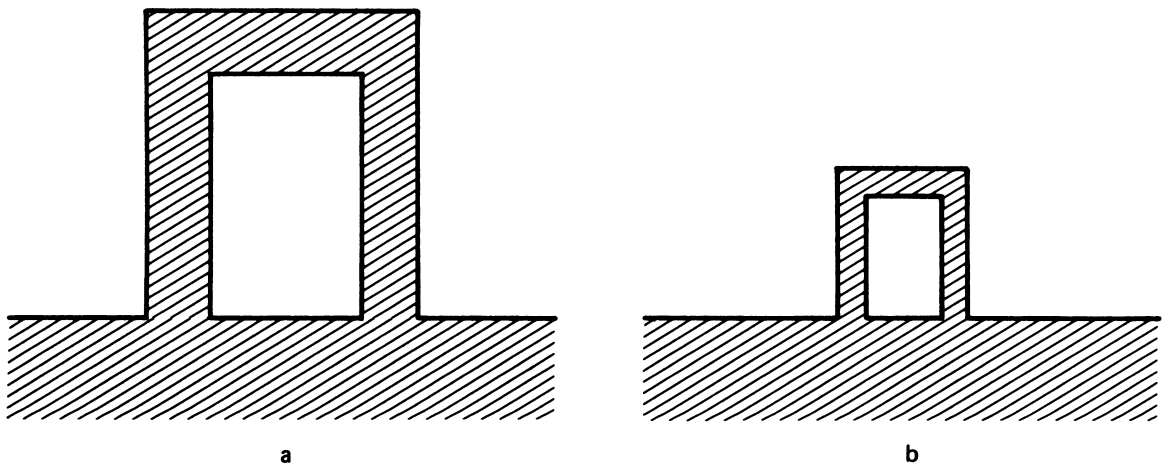
b) The material at corresponding points in A and B is always the same except that the density of the material at a point in B is  $\xi^{-1}$  times the density of the material at the corresponding point in A.

c) The radiation sources in the two problems are identical in spectrum, angular distribution, and spatial distribution, but the source strength for B is  $\xi^2$  times that for A in corresponding volume elements. If A and B have these relationships, we will refer to them (here) as "similar" configurations. The scaling theorem can then be stated as follows:

Theorem. The doubly differential radiation flux density is identically the same at corresponding points in two or more similar configurations.

The proof can be developed by comparing transport equations, as in the preceding theorem. The following relations have been stated or implied as holding at corresponding points:





IV.3 Two configurations which are similar if the density of a is less than that of b by a factor equal to the scale reduction from a to b.

$$x_B = \xi x_A; y_B = \xi y_A; z_B = \xi z_A;$$

$$\mu_B = \xi^{-1} \mu_A; k_B = \xi^{-1} k_A$$

$$S_B dx_B dy_B dz_B = \xi^2 S_A dx_A dy_A dz_A \quad . \quad (IV.26)$$

Hence  $S_B = S_A/\xi$ . It is also clear that

$$\begin{aligned} \nabla_B &= \vec{i} \frac{\partial}{\partial x_B} + \vec{j} \frac{\partial}{\partial y_B} + \vec{k} \frac{\partial}{\partial z_B} = \frac{1}{\xi} \left[ \vec{i} \frac{\partial}{\partial x_A} + \vec{j} \frac{\partial}{\partial y_A} + \vec{k} \frac{\partial}{\partial z_A} \right] \\ &= \xi^{-1} \nabla_A \quad . \end{aligned} \quad (IV.27)$$

Transport equations for the two configurations are as follows:<sup>5</sup>

$$\begin{aligned} \vec{\Omega} \cdot \nabla_A N_A + \mu_A N_A &= \int_0^\infty dE' \int_{4\pi} d\Omega k_A(E', E; \cos\Theta; \vec{r}_A) N_A(E', \vec{\Omega}', \vec{r}_A) \\ &+ S_A(E; \vec{\Omega}; \vec{r}_A) \quad , \end{aligned} \quad (IV.28)$$

$$\begin{aligned} \vec{\Omega} \cdot \nabla_B N_B + \mu_B N_B &= \int_0^\infty dE' \int_{4\pi} d\Omega' k_B(E', E; \cos\Theta; \vec{r}_B) N_B(E', \vec{\Omega}', \vec{r}_B) \\ &+ S_B(E; \vec{\Omega}; \vec{r}_B) \quad . \end{aligned} \quad (IV.28')$$

But the second equation can be written in the form

---

<sup>5</sup>In the following expressions the lower limit of the integral over  $E'$  is taken to be 0, thus including the case, not needed here, in which the radiation can gain energy through interactions.

$$\xi^{-1} \vec{\Omega} \cdot \nabla_A N_B + \xi^{-1} \mu_A N_B = \int_0^\infty dE' \int_{4\pi} d\Omega' \xi^{-1} k_A(E', E; \cos\Theta; \vec{r}_A) N_B(E', \vec{\Omega}', \vec{r}_B) + \xi^{-1} S_a(E; \vec{\Omega}; \vec{r}_A) \quad . \quad (\text{IV.29})$$

The boundary conditions at corresponding points must be the same, and it is therefore clear that

$$N_B(E; \theta, \phi; x_B, y_B, z_B) = N_A(E; \theta, \phi; x_A, y_A, z_A) \quad . \quad (\text{IV.30})$$

This is the basis for experimental work with scale models, which has been informative and useful.

Two special cases are worth mentioning. Consider duct or compartment systems with lateral dimensions sufficiently large that one can assume that gamma rays backscattered from a wall emerge at the point where they entered the wall. This is essentially equivalent to the assumption that  $\rho = \infty$ . Then any two configurations which are geometrically the same except for a scale factor satisfy the conditions of the theorem. A detailed proof similar to that for the general theorem is given in reference [8].

The main application of the general theorem to scale models involves a source on roofs and ground, i.e., a plane source. For this case the sources of interest are  $(S_A dz_A)$  and  $(S_B dz_B)$ , i.e., source strength per unit area. Since  $dx_B dy_B = \xi^2 dx_A dy_A$ , we find that plane source strengths should be equal per unit area to produce equal fluences at corresponding points in similar configurations. A similar argument leads to the conclusion that line source strengths in B should be  $\xi$  times than in A, per cm length, say.

A major problem with use of scale models is the inability to scale air density [9]. This can in principle be partially compensated for by two devices which are readily inferred from the Plane Density Theorem:

1) The layer of air directly between source and structure (up to detector height) can be approximated by a thin layer of dense material over the (plane) source; and

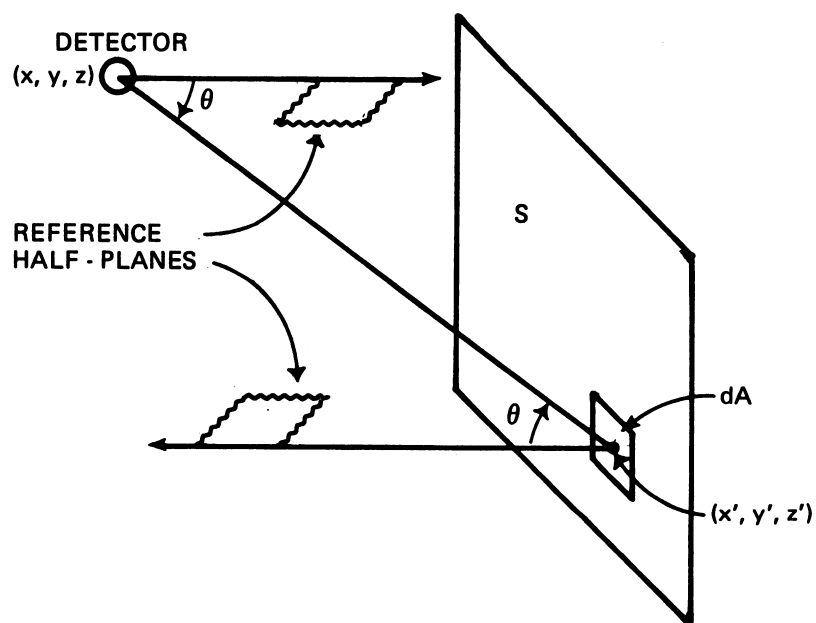
2) a dense ceiling over the scale model produces approximately the same fluence at the model as would air of suitably scaled density. Both approximations have greater accuracy when the source extends far enough from the scale model to approximate the case of infinite lateral extension.

#### 4. Elementary Detectors Near an Interface

As an introduction both to the concept of "geometry factors" and to much of the data to be presented, we now discuss the mathematical description of the radiation dose measured by a detector near an interface of finite lateral extent. As shown in figure IV.4, we visualize a flat wall or wall section, and a nearby detector measuring radiation which emerges from the wall and passes through the detector. Our purpose is to express the detector response in terms of radiation fluence at the wall surface and also radiation current density through the wall surface.

In figure IV.4, the detector position is specified as  $(x, y, z)$  in coordinate system. A small element of the wall surface  $S$  is located at  $(x', y', z')$ , and its size is  $dA$ . In our sketch, this surface element is drawn with exaggerated size; it is to be thought of as very small. The (spherical) detector is also small and has cross sectional area  $a$ .

Two reference systems are appropriate to this configuration: A natural polar axis for classification of photon directions at the detector points towards, and perpendicular to, the wall; and photon directions are measured by



IV.4 Coordinates for a detector near a radiating surface. The reference half-planes are parallel, but extend in opposite directions.

radial lines opposite the direction of photon movement and therefore pointing from detector to wall. On the other hand, at the surface, a natural polar reference axis points perpendicular to, and away from, the wall, and photon directions are measured by lines drawn from  $dA$  in the direction of photon movement.

At the detector, an azimuthal reference half-plane is selected; and at the surface  $S$ , the azimuthal reference half-plane is chosen parallel to, and extending in the opposite direction from, the one for the detector. All this is displayed in figure IV.4.

Let us refer to the doubly differential fluence at the surface element by use of  $N(E; \theta', \phi'; z', y', z')$ . As indicated it is a function of photon energy, direction, and the position of  $dA$ . We first write down an expression for the number of photons passing through  $dA$ , with energies  $E$  lying in  $dE$ , and directions  $\theta', \phi'$  lying in a solid angle element  $d\Omega'$ . Since  $dA$  behaves like a flat detector, the quantity we wish is given by

$$|\cos \theta'| N(E; \theta', \phi'; x' y' z') dE d\Omega' dA \quad . \quad (IV.31)$$

Next we determine the number of photons passing through both  $dA$  and the detector. This must be the following integral over directions intercepting some part of the detector:

$$\int_{\Omega_{\text{detector}}} d\Omega' |\cos \theta'| N(E; \theta', \phi'; x', y', z') dE dA \quad . \quad (IV.32)$$

While this is the number passing through the detector, it is not a fluence passing through the detector. We must divide by the cross sectional area a of the detector to obtain fluence:

$$dN = a^{-1} \int_{\Omega_{\text{detector}}} d\Omega' N(E; \theta', \phi'; x', y', z') dE dA \quad . \quad (\text{IV.33})$$

This fluence is called  $dN$  because it is differential and proportional to  $dE$  and  $dA$ . If we divide by the factor  $dE$ , and integrate over the complete wall surface  $S$ , we obtain the fluence per unit energy,  $N_S$ , at the detector position from all parts of  $S$ ,

$$N_S = a^{-1} \int_S dA \int_{\Omega_{\text{detector}}} d\Omega' |\cos\theta'| N(E; \theta', \phi'; x', y', z') \quad . \quad (\text{IV.34})$$

If  $\Omega_{\text{detector}}$  is very small, the integrand of eq (IV.34) is essentially a constant for a given  $dA$  during the integration over directions, since  $\theta', \phi'$  can then change only slightly. Noting that

$$\Omega_{\text{detector}} = \frac{a}{R^2} \quad , \quad (\text{IV.35})$$

where  $R = |\vec{r} - \vec{r}'|$ , and that

$$(\theta', \phi')_{\text{surface reference system}} \Rightarrow (\theta, \phi)_{\text{detector reference system}} \quad (\text{IV.36})$$

we write

$$\begin{aligned} N_S(E; x, y, z) &= a^{-1} \int_S dA |\cos\theta'| N(E; \theta', \phi'; x', y', z') \Omega_{\text{detector}} \\ &= \int_S \frac{dA |\cos\theta'|}{R'^2} N(E; \theta, \phi; x', y', z') \quad . \end{aligned} \quad (\text{IV.37})$$

Finally, observing that the solid angle subtended by  $dA$  at the detector is

$$d\Omega = \frac{dA |\cos\theta'|}{R'^2}, \quad (\text{IV.38})$$

we write

$$N_S(E; x, y, z) = \int_{\Omega_S} d\Omega N[E; \theta, \phi; x'(\theta, \phi), y'(\theta, \phi), z'(\theta, \phi)] \quad , \quad (\text{IV.39})$$

where  $\Omega_S$  is the solid angle subtended by  $S$  at  $(x, y, z)$ . In performing this integration,  $d\Omega$  is written in the appropriate  $(\theta, \phi)$  variables, with limits appropriate to  $S$ .

In this final expression, the angular distribution may or may not vary from point to point on  $S$ . If the fluence at the surface  $S$  is independent of position, the detector fluence is given by an integral over only the emergent angular distribution. But if the fluence at  $S$  depends on position, the integrand must be evaluated at the point  $(x', y', z')$  intercepted by the  $(\theta, \phi)$  radial line from the detector. Shielding calculations thus far have used the assumption that emergent angular distributions are position independent, or that this assumption is of sufficient accuracy.

Comparison of eq (IV.37) with eq (IV.39) makes it clear that we could adopt a point of view which looks from the surface  $S$  outwards, utilizing a polar axis pointing away from the surface and identifying photon directions with photon movement. It would then be natural to identify the fluence at the detector with a surface integral over emergent current density. The alternate point of view looks from the detector towards the surface, utilizing a polar axis pointed towards the surface and identifying  $(\theta, \phi)$  with the reverse of the direction of photon movement. It is then natural to describe the fluence at the detector in terms of an integral over emergent fluence at  $S$ .



The two points of view are completely equivalent. Discussions of structure shielding ordinarily utilize the detector point of view.

### C. ASPECTS OF THE PHOTON FIELD IN INFINITE HOMOGENEOUS MEDIA<sup>6</sup>

#### 1. Once-Scattered Photons from Simple Source Types

Once-scattered photons begin their trajectories at scattering points which terminate the trajectories of unscattered photons; hence the unscattered component determines the source for the once-scattered component, much as discussed in section III.C.3. But calculations for the once-scattered component are more complicated than those of section IV.A. In fact, an expression for the once-scattered flux for a PLI source requires a final integration which must be performed numerically.

Despite these difficulties, the once-scattered component can be generally evaluated for infinite homogeneous media, and can be studied through the use of expressions like those to be derived in this section. It forms an important and determining part of the scattered radiation, and must be discussed in almost every shielding problem. We therefore carry some derivations through and then in section IV.C.4 we discuss typical calculations for both unscattered and once-scattered components for all three source types.

##### a. Plane Oblique Source

We use eqs (III.40) and (III.43), which relate any two successive orders of scattering. These expressions require the spectrum and angular distribution of the unscattered fluence. Our calculation is for a monoenergetic source.

According to eq (III.40), we can write the source for the once-scattered component as the integral

---

<sup>6</sup>For another reference containing much of the material in this section, see [10].

$$\mathcal{S} = \int_E^{E_0} dE' \int_{4\pi} d\Omega' k(E', E) \frac{1}{2\pi} \delta(\vec{\Omega}' \cdot \vec{\Omega} - \cos\theta_{E'}) \\ \times \frac{S_0}{2\pi \cos\theta'} \delta(E' - E_0) \delta(\cos\theta' - \cos\theta_0) e^{-\mu(E')z/\cos\theta'} \quad , \quad (\text{IV.40})$$

where  $\cos\theta' = \vec{\Omega}' \cdot \vec{k}$ ,  $\cos\theta_{E'} = 1 - .511/E + .511/E'$  (energies in MeV), and the scattering cross section is in the form given by eq (III.42). Since there are three Dirac delta functions, no problem arises in evaluating all integrals to obtain an analytic expression. If we choose  $\vec{\Omega}$  as the reference axis for the  $d\Omega'$  integrations, we can make an immediate reduction of the expression to

$$\mathcal{S} = \frac{S_0}{2\pi} k(E_0, E) \int_0^{2\pi} d\eta \frac{1}{2\pi} \delta(\cos\theta' - \cos\theta_0) \frac{1}{\cos\theta'} e^{-\mu_0 z/\cos\theta'} \quad , \quad (\text{IV.41})$$

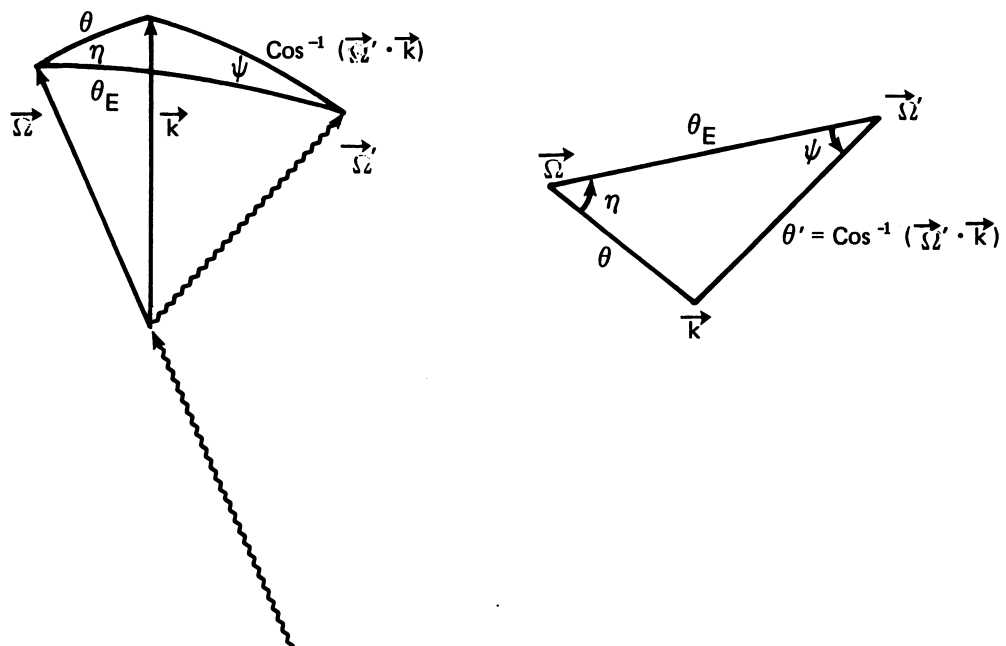
where  $\cos\theta' = \cos\theta \cos\theta_E + \sin\theta \sin\theta_E \cos\eta$ , and  $\cos\theta_E = (1 - .511/E + .511/E_0)$ . In figure IV.5 a 3-dimensional sketch of the spherical triangle is given, together with a 2-dimensional sketch which is a qualitatively correct analogue in which the unit direction vectors are represented by points.<sup>7</sup>

Up to this point,  $z$  is the coordinate of the scattering point. In what follows, however,  $z$  relates to the point of detection.

Taking  $\cos\theta_0$  to be positive, three cases arise. These are: 1)  $z > 0$  and  $\cos\theta > 0$ ; 2)  $z > 0$  and  $\cos\theta < 0$ ; and 3)  $z < 0$  and  $\cos\theta < 0$ . For these cases, which are sketched in figure IV.6, we now wish to apply eq (III.43)

---

<sup>7</sup>Note that when three direction vectors are nearly parallel, they intersect the unit sphere at points which form just such a triangle, very little distorted by the curvature of the spherical "cap". Such a triangle exhibits correct relationships qualitatively, even when the polar cap approximation does not apply; but spherical rather than plane trigonometric expressions must be used in any calculation.



IV.5 The spherical triangle formed by scattered and unscattered photon directions, with the reference direction  $\vec{k}$ . The plane triangle on the right has vertices, sides, and angles corresponding, respectively, to directions, polar angles, and azimuthal angles.

to calculate the fluence. To this end we note the following limits to the path length  $\underline{t}$ : For case 1),  $0 \leq s \leq z/\cos\theta$ ; for case 2),  $0 < t < \infty$ ; and for case 3),  $|z/\cos\theta| \leq t < \infty$ .

Evaluation of the integrals of eq (III.43) offers no difficulty in any of the cases; and the results are

$$N_{\text{PLO}}^1(E, \vec{\Omega}, \vec{r}) = \frac{S_0}{2\pi} k(E_0, E) \int_0^{2\pi} d\eta \frac{1}{2\pi} \delta(\cos\theta' - \cos\theta_0) F(z, \cos\theta', \cos\theta) \quad , \quad (\text{IV.42})$$

which is equivalent to<sup>8</sup>

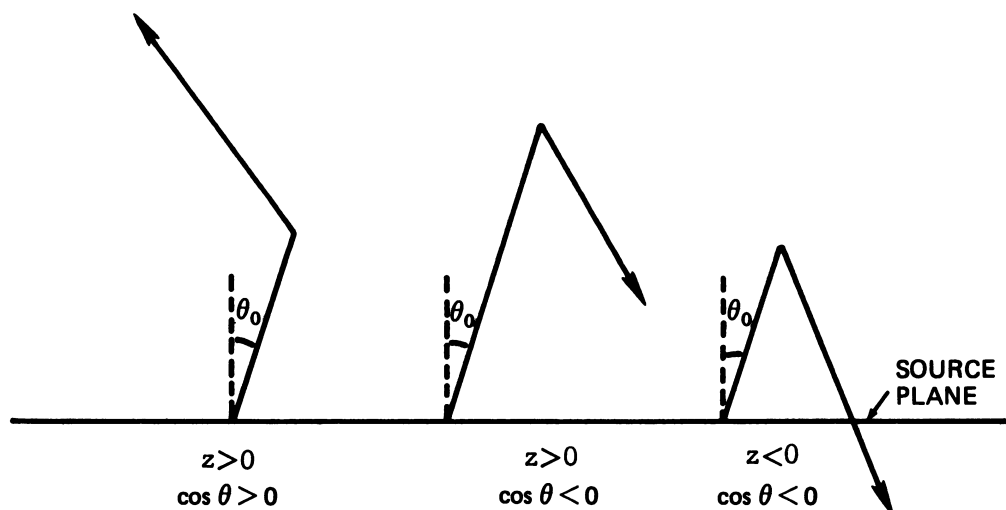
$$N_{\text{PLO}}^1(E, \vec{\Omega}, \vec{r}) = \frac{1}{2\pi} S_0 k(E_0, E) \int_0^{2\pi} d\psi \frac{1}{2\pi} \delta(\vec{\Omega} \cdot \vec{k} - \cos\theta) F(z, \cos\theta_0, \vec{\Omega} \cdot \vec{k}) \quad , \quad (\text{IV.42}')$$

where  $\vec{\Omega} \cdot \vec{k} = \cos\theta_0 \cos\theta_E + \sin\theta_0 \sin\theta_E \cos\psi$ , and

$$\begin{aligned} F(z, \cos\theta_0, \cos\theta) &= \frac{e^{-\mu_0 z / \cos\theta_0} - e^{-\mu(E) z / \cos\theta}}{\mu(E) \cos\theta_0 - \mu_0 \cos\theta} \quad , \quad z \geq 0, \quad \cos\theta \geq 0, \\ &= \frac{e^{-\mu_0 z / \cos\theta_0}}{\mu(E) \cos\theta_0 - \mu_0 \cos\theta} \quad , \quad z \geq 0, \quad \cos\theta < 0, \\ &= \frac{e^{-\mu(E) z / \cos\theta}}{\mu(E) \cos\theta_0 - \mu_0 \cos\theta} \quad , \quad z < 0, \quad \cos\theta \leq 0. \quad (\text{IV.43}) \end{aligned}$$

---

<sup>8</sup>This can be seen from figure IV.5 if  $\vec{\Omega}'$  is redesignated  $\vec{\Omega}_0$ , the direction before scatter being the uncollided direction, so that  $\cos\theta'$  can be replaced by  $\cos\theta_0$ . Note that  $d\eta = d(\cos\theta') / (\sin\theta_E \sin\theta \sin\eta)$  and that  $d\psi = d(-\vec{\Omega} \cdot \vec{k}) / (\sin\theta_E \sin\theta_0 \sin\psi)$ . The law of sines guarantees that  $\sin\theta \sin\eta = \sin\theta_0 \sin\psi$ .



IV.6 The three distinct cases of single scattering for a plane oblique source of photons.

We may now evaluate the remaining integral of eq (IV.42). To accomplish this we note that

$$d\eta = \frac{d(-\vec{\Omega}' \cdot \vec{k})}{\sin\theta \sin\theta_E \sin\eta} ,$$

so that if we take account of the fact that there are two values of  $\eta$  for which the argument of the delta function vanishes, we obtain

$$N_{\text{PLO}}^1(E, \vec{\Omega}, \vec{r}) = \frac{S_o}{2\pi^2} \frac{k(E_o, E)}{\sin\theta_E \sin\theta \sin\eta} F(z, \cos\theta_o, \cos\theta) , \quad (\text{IV.44})$$

where  $\cos\eta = (\cos\theta_o - \cos\theta\cos\theta_E)/\sin\theta\sin\theta_E$ . By the law of sines and/or eq (IV.42'), this result also can be written using  $\cos\psi = (\cos\theta - \cos\theta_o\cos\theta_E)/\sin\theta_o\sin\theta_E$ :

$$N_{\text{PLO}}^1(E, \vec{\Omega}, \vec{r}) = \frac{S_o}{2\pi^2} \frac{k(E_o, E)}{\sin\theta_E \sin\theta_o \sin\psi} F(z, \cos\theta_o, \cos\theta) . \quad (\text{IV.44}')$$

Both of eqs (IV.44) and (IV.44') exhibit the property of being independent of azimuthal angle relative to the reference system fixed in space with  $\vec{k}$  as axis. (Note that the factors  $\sin\eta$  and  $\sin\psi$  are functions only of obliquity angles  $\theta_o$ ,  $\theta$ , and  $\theta_E$ .)

To integrate over all  $\vec{\Omega}$ , we refer back to eq (IV.42'), and note the requirement that  $\cos\theta = \vec{\Omega} \cdot \vec{k}$ , and the lack of dependence on the azimuthal variable. By interchanging integrations, we obtain the following result

$$N_{\text{PLO}}^1(E, \vec{r}) = \frac{S_o}{2\pi} k(E_o, E) \int_0^{2\pi} d\psi F(z, \cos\theta_o, \vec{\Omega} \cdot \vec{k}) . \quad (\text{IV.45})$$

Expressions for dose angular distribution and total dose, in the more general case of polychromatic spectra, immediately follow from eqs (IV.44') and (IV.45')

$$D_{\text{PLO}}^1(\vec{r}, \vec{\Omega}) = \int_0^\infty dE_o S_o(E_o) \int_0^{E_o} dE R(E) k(E_o, E) \frac{1}{2\pi^2} \frac{F(z, \cos\theta_o, \cos\theta)}{\sin\theta_o \sin\theta_E \sin\psi} \quad (\text{IV.46})$$

and

$$D_{\text{PLO}}^1(r) = \int_0^\infty dE_o S(E_o) \int_0^{E_o} dE R(E) k(E_o, E) \frac{1}{2\pi} \int_0^{2\pi} d\psi F(z, \cos\theta_o, \vec{\Omega} \cdot \vec{k}) \quad (\text{IV.47})$$

Figure IV.7 compares the unscattered with the once-scattered component, for  $^{137}\text{Cs}$  gamma rays in air, for various source obliquities.

#### b. Plane Isotropic Source<sup>9</sup>

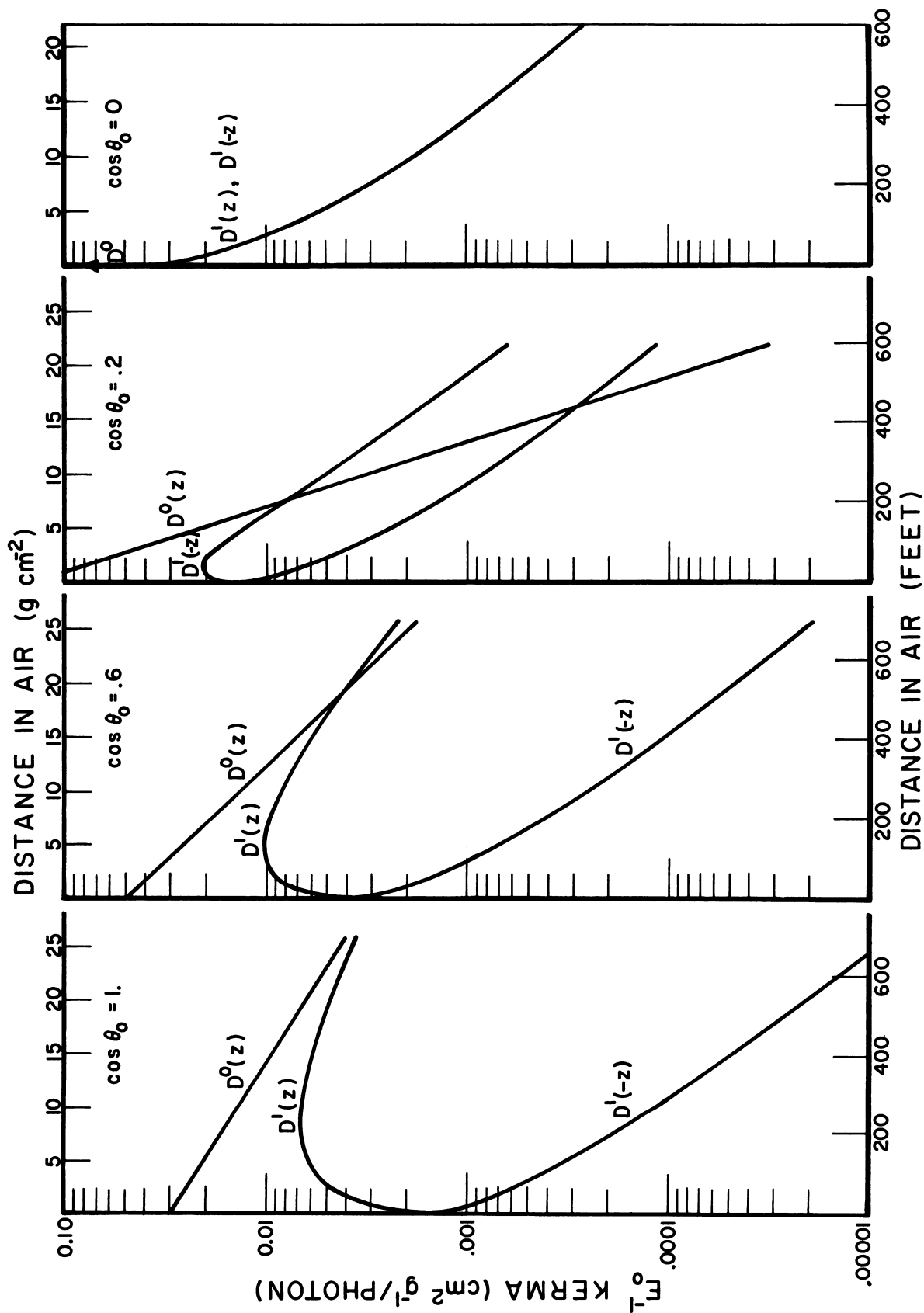
A representation for the once-scattered component of a PLI source can readily be obtained from the calculation just performed. One simply integrates eq (IV.42) over initial obliquity angles to obtain (after including a factor 1/2 to account for the fact that only half the photons travel in the positive  $z$  direction initially):

$$N_{\text{PLI}}^1(E, \vec{\Omega}, \vec{r}) = \frac{S_o}{4\pi} k(E_o, E) \frac{1}{2\pi} \int_0^{2\pi} d\eta F(z, \vec{\Omega}' \cdot \vec{k}, \cos\theta) \quad (\text{IV.48})$$

The dose distribution as a function of obliquity angle  $\theta$  immediately follows, with incorporation of a factor  $2\pi$  for integration over azimuths about the polar axis  $\vec{k}$ :

---

<sup>9</sup>See references [11], [12] for published discussions of the once-scattered component for this source type.



IV.7 Unscattered and singly scattered components for a plane oblique source of  $^{137}\text{Cs}$  photons, for several angles of emission. The lowest curve corresponds to backscattering, but has been transposed to positive abscissa values. For emission in the source plane (farthest case to the right), the unscattered component is represented by the arrow at zero.



$$D_{\text{PLI}}^1(z, \cos\theta) = \int_0^\infty dE_o S(E_o) \int_0^{E_o} dE R(E) k(E_o, E) \frac{1}{4\pi} \int_0^{2\pi} d\eta F(z, \vec{\Omega}' \cdot \vec{k}, \cos\theta) \quad . \quad (\text{IV.49})$$

The integral of eq (IV.48) over final directions requires only the differential  $2\pi d(\cos\theta)$ ,

$$N_{\text{PLI}}^1(E, z) = \frac{S_o}{4\pi} k(E_o, E) \int_{-1}^1 d(\cos\theta) \int_0^{2\pi} d\eta F(z, \vec{\Omega}' \cdot \vec{k}, \cos\theta) \quad , \quad (\text{IV.50})$$

and the expression for total dose is thus

$$D_{\text{PLI}}^1(z) = \int_0^\infty dE_o S(E_o) \int_0^E dE R(E) k(E_o, E) \\ \times \frac{1}{4\pi} \int_{-1}^1 d(\cos\theta) \int_0^{2\pi} d\eta F(z, \vec{\Omega}' \cdot \vec{k}, \cos\theta) \quad . \quad (\text{IV.51})$$

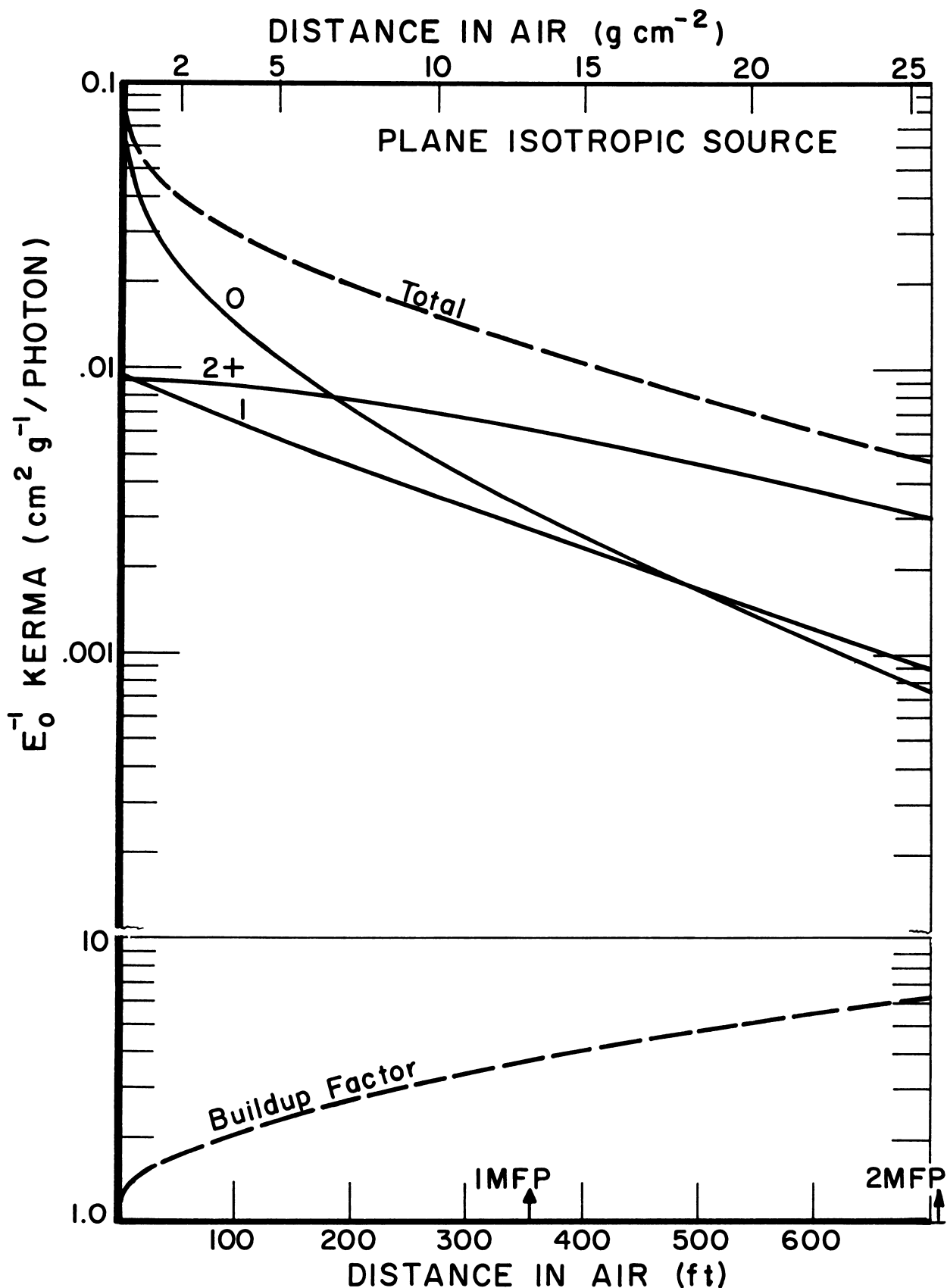
These expressions can be put in other forms which can provide advantages of interpretation or ease of computation.

Figure IV.8 gives unscattered, once-scattered, and multiply-scattered dose in air, for  $^{137}\text{Cs}$ , as a function of height above the source plane.

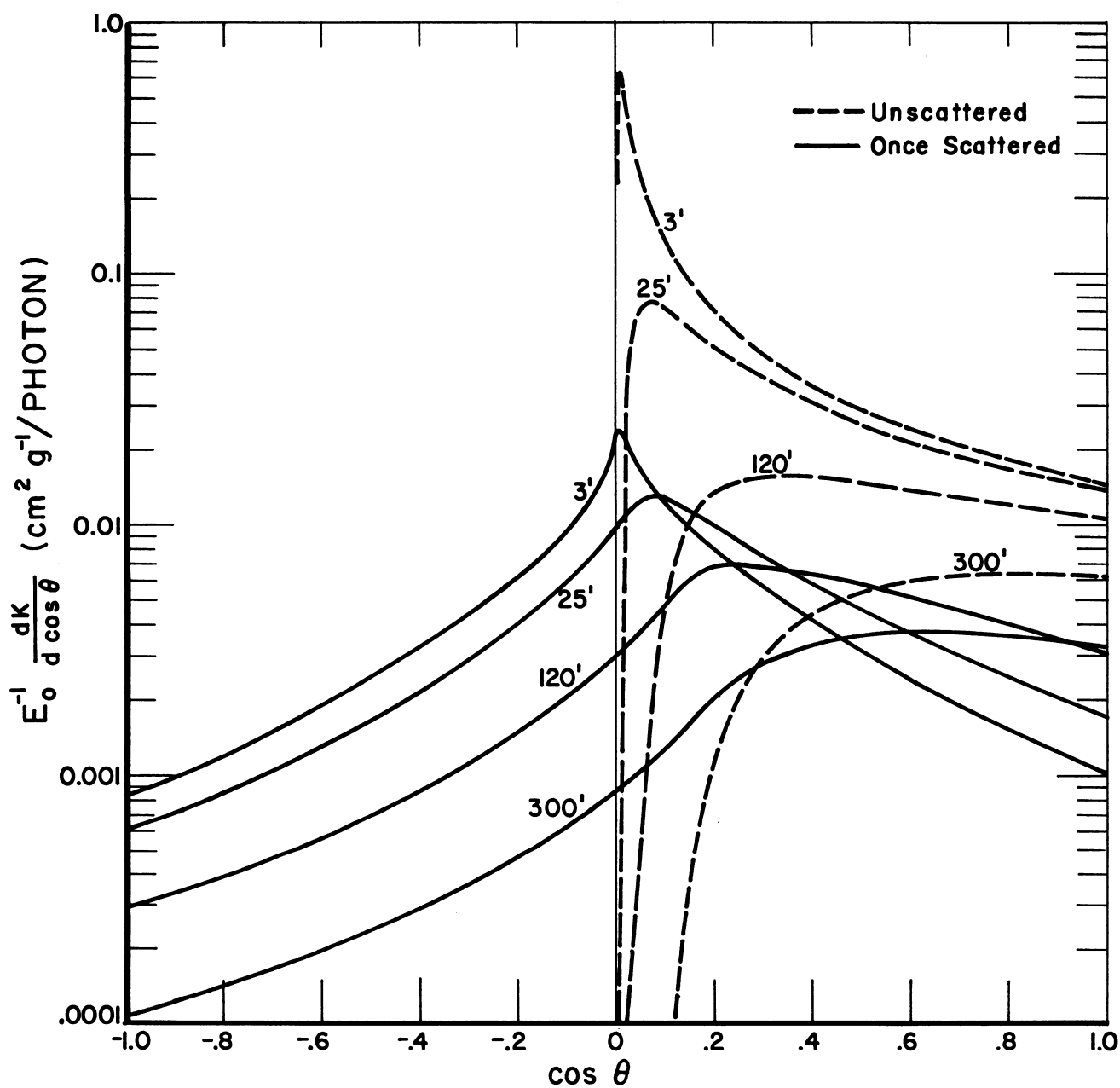
Figure IV.9 gives unscattered and once-scattered components for this source, as functions of obliquity angle for several distances.

### c. Point Isotropic Source

Unlike the PLI source, the PTI source geometry permits calculation of an analytic expression for the once-scattered component [10]. One method by which this calculation can be performed is similar to the derivation for the PLO source, with trajectories typified by that of figure IV.10. Here,  $\vec{u}$  is



IV.8 Unscattered (0), singly-scattered (1), and multiply-scattered (2+) components for a plane isotropic  $^{137}\text{Cs}$  source in air. The agreement of the two scattered components near the source is fortuitous. The curve designated "buildup factor" is the ratio of "total" to unscattered.



IV.9 Unscattered and singly-scattered angular distributions for a plane isotropic  $^{137}\text{Cs}$  source in air, for several distances from the source plane. The singly-scattered component is nearly symmetric in  $\underline{z}$  near the source plane.

a unit radial direction vector. The scattering trigonometry is indicated in figure IV.10.

The source for the once-scattered component, as given generally in eqs (III.40) and (III.42), can be written down with the aid of the unscattered component given in eq (IV.2). This turns out to be

$$\begin{aligned} \mathcal{S} &= \int_E^\infty dE' \int_{4\pi} d\Omega' \left\{ S_0 \frac{e^{-\mu(E')r}}{4\pi r^2} \delta(E' - E_0) \frac{1}{2\pi} \delta(\vec{\Omega}' \cdot \vec{u}_0 - 1) k(E', E) \frac{1}{2\pi} \delta(\vec{\Omega}' \cdot \vec{\Omega} - \cos\theta_E) \right\} \\ &= S_0 \frac{e^{-\mu_0 r}}{4\pi r^2} k(E_0, E) 2\pi^{-1} \delta(\vec{\Omega} \cdot \vec{u}_0 - \cos\theta_E) . \end{aligned} \quad (IV.52)$$

Evaluation of the integrals over  $d\Omega'$  to obtain eq (IV.52) is best done utilizing  $\vec{u}_0$  as polar axis, with a resulting explicit non-dependence of the integrand on the azimuthal variable, which then yields the factor  $2\pi$ .

Specification of the quantities in the integrand of eq (III.43) requires only recognition that  $\mu$  is position independent, so that

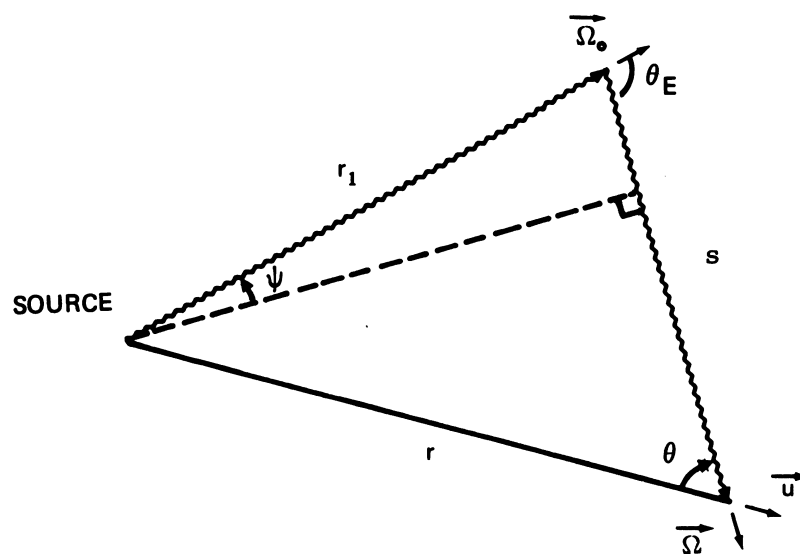
$$\exp \left\{ - \int_0^s ds' \mu(\lambda, \vec{r} - s' \vec{\Omega}) \right\} = e^{-\mu(\lambda)s} ;$$

and that  $\vec{r} = r \cdot \vec{u}$ , so that  $r$  in eq (IV.52) must be replaced by a variable  $r_1$ ,

$$r_1 = |\vec{r} - t\vec{\Omega}| .$$

We then have

$$N_{PTI}^1(E, \vec{\Omega}, \vec{r}) = \frac{S_0}{2\pi} k(E_0, E) \int_0^\infty dt \frac{e^{-\mu_0 r_1 - \mu(\lambda)t}}{4\pi r_1^2} \delta(\cos\Theta - \cos\theta_E) , \quad (IV.53)$$



IV.10 Coordinates and geometry for calculating the singly-scattered component of a point isotropic source.  $\vec{\Omega}_0$  and  $\vec{\Omega}$  are, respectively, directions before and after the scatter, which occurs a radial distance  $r_1$  from the source. The parameter  $s$  is the pathlength after scatter.

where  $\cos\Theta = \vec{\Omega} \cdot \vec{u}_0$ .

This expression can be evaluated by changing the variable of integration to make use of the properties of the angle  $\psi$  shown in figure IV.10.<sup>10</sup> We note that  $\cos\Theta = -\sin\psi$ , and that

$$t = r \cos\theta + r \sin\theta \tan\psi.$$

Hence

$$\frac{dt}{r_1^2} = \frac{r \sin\theta \sec^2\psi d\psi}{(r \sin\theta \sec\psi)^2} = \frac{d(\sin\psi)}{r \sin\theta \cos\psi} = \frac{-d(\cos\Theta)}{r \sin\theta \sin\Theta},$$

and the following expression immediately results by integration over the delta function:

$$N_{PTI}^1(E, \vec{\Omega}, r) = \frac{S_0}{2\pi} \frac{k(E_0, E)}{4\pi r \sin\theta \sin\theta_E} \exp \left\{ -\mu_0 r \frac{\sin\theta}{\sin\theta_E} - \mu(E) r \frac{\sin(\theta_E - \theta)}{\sin\theta_E} \right\}. \quad (IV.54)$$

In this expression, it is understood that  $\theta \leq \theta_E$ , i.e., that for  $\theta > \theta_E$ ,  $N_{PTI}^1 = 0$ .

Integration over scattered directions cannot be performed analytically.

It gives the following integral expression:

$$N_{PTI}^1(E, r) = \frac{S_0}{4\pi r} \frac{k(E_0, E)}{\sin\theta_E} \int_0^{\theta_E} d\theta \exp \left\{ -\mu_0 r \frac{\sin\theta}{\sin\theta_E} - \mu(E) r \frac{\sin(\theta_E - \theta)}{\sin\theta_E} \right\}. \quad (IV.55)$$

---

<sup>10</sup>Note that  $r \sin\theta = r_1 \cos\psi$  and that  $\Theta = \psi + \pi/2$ .

The total dose for the case of polyenergetic sources is

$$D_{PTI}^1(r) = \int_0^\infty dE_0 S(E_0) \int_0^{E_0} dE R(E) \frac{k(E_0, E)}{\sin\theta_E} \frac{1}{4\pi r} \\ \times \int_0^{\theta_E} d\theta \exp \left\{ -\mu_0 r \frac{\sin\theta}{\sin\theta_E} - \mu(E)r \frac{\sin(\theta_E - \theta)}{\sin\theta_E} \right\} . \quad (IV.55')$$

Since such integrations must be performed numerically, it is convenient to have in mind the possibility of using  $\theta_E$  as integration variable, noting that  $\frac{dE}{\sin\theta_E} = (E^2/.511)d\theta_E$ . The lower limit to the inner integration (over  $dE$ ) is actually  $.511(2 + .511/E_0)^{-1}$ , since the integrand must be zero below this energy.

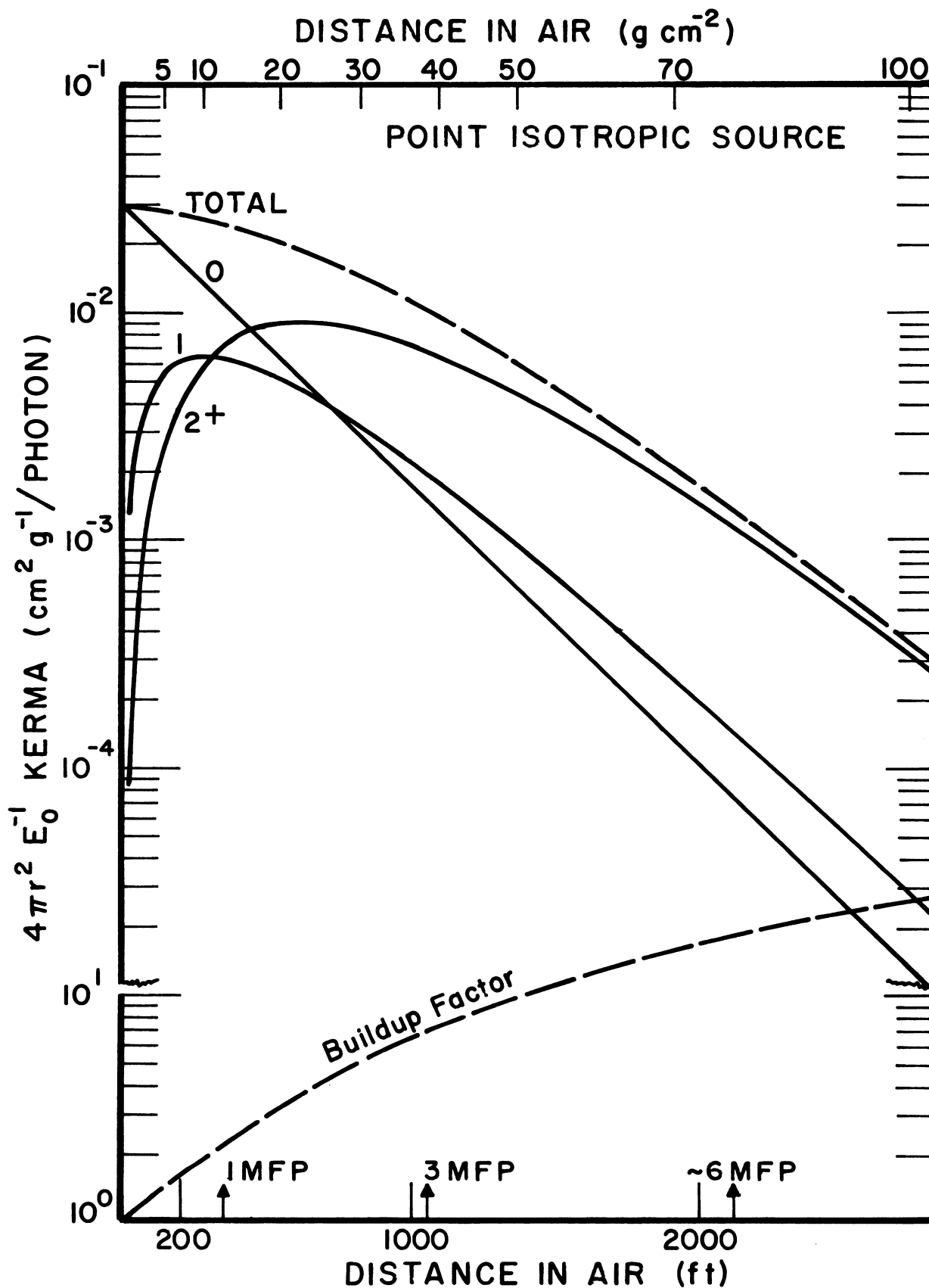
Figure IV.11 gives unscattered, once-scattered, and multiply-scattered components of the dose, for  $^{137}\text{Cs}$  in air. Figure IV.12 gives the angular distribution of the once-scattered component, for several distances in air from this source: Note that the abscissa in this figure is  $\theta$  rather than  $\cos\theta$ , so that the area under the curve is the total dose.

## 2. Trends for Small Penetrations

The expressions derived in the preceding section are useful for ascertaining trends of the fluence and its components at extreme distances, both small and large, from the source.

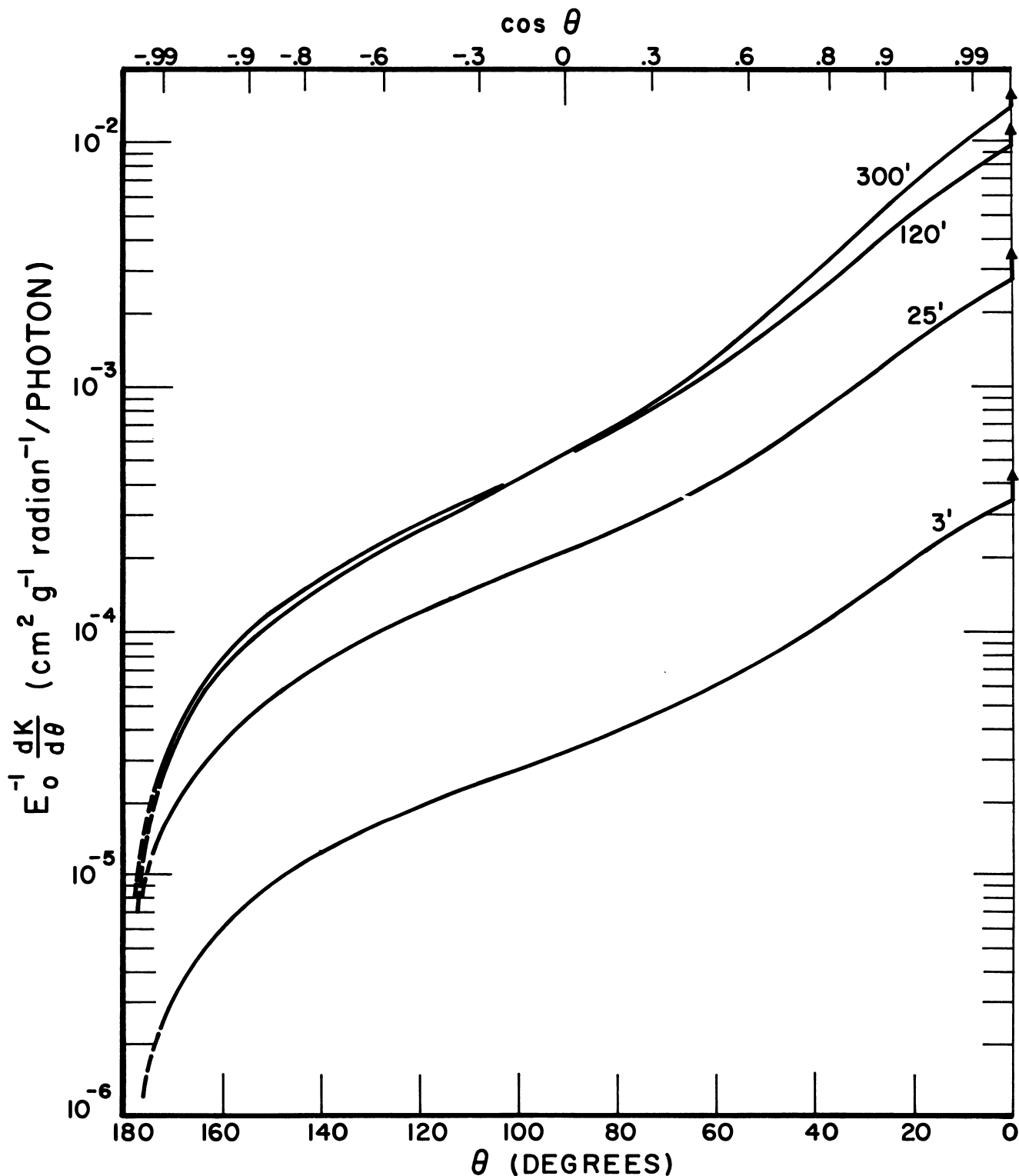
### a. Plane Oblique Source

For small values of  $z$ , the trend of the dose for a plane oblique source (see eq (IV.51)) can be determined in part by expanding  $F(z, \cos\theta_0, \cos\theta)$ , as given in eq (IV.43), in powers of  $z$ :



IV.11 Unscattered (0), singly-scattered (1), and multiply-scattered (2+) components for a point isotropic  $^{137}\text{Cs}$  source in air. The dashed curve at the bottom gives the ratio of "Total" to unscattered.





IV.12 Singly-scattered angular distributions for a point isotropic  $^{137}\text{Cs}$  source in air. The arrow at the right edge indicates the unscattered component. Note that the integration of the curves is against angle measured in radians. In this type of plot the  $(\sin\theta)^{-1}$  singularity at  $\theta = 0$  doesn't appear.

$$\begin{aligned}
F(z, \cos\theta_o, \cos\theta) &\rightarrow \frac{z}{\cos\theta_o \cos\theta} + O(z^2), \quad \text{for } z > 0, \quad \cos\theta > 0, \\
&\rightarrow \frac{1 - \mu_o z / \cos\theta_o}{[\mu \cos\theta_o - \mu_o \cos\theta]} + O(z^2), \quad \text{for } z > 0, \quad \cos\theta \leq 0, \\
&\frac{1 - \mu z / \cos\theta}{[\mu \cos\theta_o - \mu_o \cos\theta]} + O(z^2), \quad z < 0, \quad (IV.56)
\end{aligned}$$

where  $O(z^2)$  stands for terms on the order of  $z^2$  (or higher).

The case of directions nearly parallel to the source plane, i.e., very small values of  $\cos\theta$ , needs special treatment because the above expansion fails in this limit. From the differential identity

$$d\psi = d(\cos\theta) \left[ -\cos(\theta_o + \theta_E) \cos(\theta_o - \theta_E) + 2\cos\theta_o \cos\theta_E \cos\theta - \cos^2\theta \right]^{-1/2},$$

which follows from  $\cos\theta = \cos\theta_o \cos\theta_E + \sin\theta_o \sin\theta_E \cos\psi$ , we infer that for  $\cos\theta \approx 0$ , for  $|\theta_o - \theta_E| < \pi/2$ , and for  $\theta_o + \theta_E > \pi/2$ ,

$$d\psi \approx -d(\cos\theta) / \sqrt{-\cos(\theta_o + \theta_E) \cos(\theta_o - \theta_E)}. \quad (IV.57)$$

On the other hand, for  $\theta_o \pm \theta_E = \pm \pi/2$ , one finds that for small  $\cos\theta$ ,

$$d\psi \approx -d(\cos\theta) / \sqrt{2\cos\theta_o \cos\theta_E \cos\theta}. \quad (IV.57')$$

We can apply these differential expressions to estimate<sup>11</sup> the integral

---

<sup>11</sup>The other factors in the integrand of (IV.47), such as  $[\mu \cos\theta_o - \mu_o \cos\theta]^{-1}$ , tend to vary slowly in comparison with the exponential and can be expanded in powers of  $\cos\theta$ ; such terms yield rising powers  $z$ ,  $z^2$ , etc., in conjunction with eq (IV.57), or  $z^{1/2}$ ,  $z^{3/2}$ , etc., in conjunction with eq (IV.57').

$$d\psi \exp(-\mu z / \cos\theta)$$

for a small range  $0 \leq \cos\theta \leq c$ , where  $c$  is an arbitrary upper limit not dependent on  $z$ . The results are

$$\frac{c e^{-\mu z/c} - \mu z E_1(\mu z/c)}{\sqrt{-\cos(\theta_o + \theta_E) \cos(\theta_o - \theta_E)}} , \text{ for eq (IV.57) } ,$$

and

$$\frac{2\sqrt{c} e^{-\mu z/c} - 2\sqrt{\pi\mu z} \operatorname{erfc}(\sqrt{\mu z/c})}{\sqrt{2\cos\theta_o \cos\theta_E}} , \text{ for eq (IV.57')} ,$$

Because  $E_1(\mu z/c) \rightarrow -\log(e^\gamma \mu z/c)$ ,  $e^\gamma = 1.78\dots$ , as  $z \rightarrow 0$ , the first of these has the small- $z$  limiting form  $(a_o + a_1 z + a_2 z \log z)$ , while the second has the limiting form  $(a'_o + a'_1 \sqrt{z} + a_2 z)$ .

If we add together results for different regions of  $\cos\theta$  which contribute to the full  $2\pi$  range of  $\psi$  variation, we find that  $D_{PLO}^1$  has the general small  $z$  form

$$a + b_1 \sqrt{z} + c_1 z + d_1 z \log(z). \quad (\text{IV.58})$$

But because the  $\sqrt{z}$  component results only from special  $\theta_E$  values, one expects  $b_1$  to be negligible in integrals over energy. Also, one should remember that the  $z \log(z)$  terms do not appear when  $\theta_o + \theta_E < \pi/2$ .

One should note that the special case  $\cos\theta_o = 1$  does not have the complications of the above arguments; for this special case the integrand is independent of  $\Psi$ . Evaluation of this integral is thus immediate and introduces a  $2\pi$  factor, and  $\theta = \theta_E$ . But the integral over  $\theta_E$  (or,  $E$ ) nevertheless introduces both  $\sqrt{z}$  and  $z \log z$  terms to give the trend shown in eq (IV.58).

#### b. Point Isotropic Source

To obtain the dose trend for small  $\underline{r}$ , for the PTI sources, one must examine the two inner integrals in eq (IV.55'). Clearly the integrand, multiplied by  $4\pi r^2$ , is proportional to  $\underline{r}$ , for small  $\underline{r}$ , except when  $\sin\theta_E$  vanishes. This occurs both for  $\theta_E \rightarrow 0$  and for  $\theta_E \rightarrow \pi$ . We assume that the factor  $[R(E) k(E_o E)]$  is sensibly constant over these two regions and therefore study the integrals

$$\int_0^\beta d\theta_E \int_0^{\theta_E} d\theta r \exp \left[ -\mu_o r \frac{\sin\theta}{\sin\theta_E} - \mu r \frac{\sin(\theta_E - \theta)}{\sin\theta_E} \right] \quad (\text{IV.59})$$

where  $\beta$  is a small constant, and, for  $\theta_E \rightarrow \pi$ , we write  $(\pi - \theta_E)$  and  $(\pi - \theta)$  in place of  $\theta$  and  $\theta_E$ :

$$\int_{\pi-\beta}^\pi d\theta \int_{\pi-\theta}^\pi d\theta_E r \exp \left[ -\mu_o r \frac{\sin(\pi-\theta)}{\sin(\pi-\theta_E)} - \mu r \frac{\sin[(\pi-\theta) - (\pi-\theta_E)]}{\sin(\pi-\theta_E)} \right] . \quad (\text{IV.59}')$$

The small angle approximation can be used, in which we replace the sines by their arguments. Both inner integrals can then be evaluated. We also assume that  $\mu$  is sensibly constant over the range  $0 \leq \theta_E \leq \beta$ . Then

$$\int_0^\beta d\theta_E \int_0^{\theta_E} d\theta r \exp \left[ -\mu_o r \frac{\theta}{\theta_E} - \mu r \left( 1 - \frac{\theta}{\theta_E} \right) \right] = \left( \frac{\beta^2}{2} \right) \frac{e^{-\mu_o r} - e^{-\mu r}}{\mu - \mu_o} \quad . \quad (\text{IV.60})$$

For the backscattering limit, we write  $\bar{\theta} = \pi - \theta$  and  $\bar{\theta}_E = \pi - \theta_E$ ; and we assume  $\mu$  to be sensibly constant over the range  $\pi \leq \theta_E \leq \beta$ . Then,

$$\begin{aligned} & \int_0^\beta d\bar{\theta} \int_0^{\bar{\theta}} d\bar{\theta}_E r \exp \left[ -\mu_o r \frac{\bar{\theta}}{\bar{\theta}_E} - \mu r \left( \frac{\bar{\theta}}{\bar{\theta}_E} - 1 \right) \right] \\ &= \left( \frac{\beta^2}{2} \right) r e^{-\mu_o r} \left\{ 1 - (\mu_o + \mu) r e^{(\mu_o + \mu)r} E_1[(\mu_o + \mu)r] \right\} \quad . \quad (\text{IV.60}') \end{aligned}$$

Inspection of these formulae shows that the small  $r$  trend of both combined is of the type  $a_o r + a_1 r^2 \ln(br)$ , where  $a_o, a_1, b$  are constants. This modifies the inverse square factor  $(4\pi r^2)^{-1}$ , which has been omitted above.<sup>12</sup>

The second scattering has been examined also, in this case, and found to have an  $r^2 \ln(b'r)$  trend, where  $b'$  is constant [14]. This likewise is in addition to the factor  $(4\pi r^2)^{-1}$ .

### c. Plane Isotropic Source

It is clear from the fact that the plane isotropic source is a superposition of plane oblique sources that the dose due to the first scattered component has the trend  $a_o + a_1 z + a_2 z \ln z$  for small  $z$ . This same result also follows by considering the plane isotropic source as a superposition of point isotropic sources.

---

<sup>12</sup>It is also worth mentioning that a useful small penetration approximation has been studied by C. Eisenhauer [13] in which the exponential factor is set equal to unity. This approximation is poor only for the component which is scattered through an angle of nearly  $180^\circ$ , thus bringing it near the source a second time. At this cost, and the corresponding removal of the  $a_1$  term above, a substantial simplification in the analytic complexity is gained.

### 3. Trends for Deep Penetrations

For deep penetrations, several effects operate concurrently, the relative importance of which depends on type of medium, source configuration, and spectrum. Thus in filtration, components with larger attenuation coefficients, i.e., those that are "softer," tend to decrease relative to "harder" photons, i.e., with smaller attenuation coefficients. In opposition to this effect is scattering, which generates lower energy (softer) photons from higher energies.

Similar but less pronounced effects occur in connection with the photon angular distribution: Photons with directions strongly divergent from the main direction of penetration tend to be removed selectively relative to those oriented more nearly parallel the direction of penetration. This results in a type of collimation effect. But counterbalancing this is a de-collimation which results from scattering, which acts to transfer photons out of any beam, no matter how the beam may have been generated.

One can readily identify cases in which collimation and filtration will tend to dominate: Early stages of penetration from the plane isotropic source will involve removal of those photons traveling nearly parallel to the source plane while early stages of penetration by a photon source whose spectrum is heavily weighted with "soft" photons will be characterized by their being progressively filtered out. Likewise, any configuration in which photon absorption is highly favored over photon scattering will exhibit strong filtration and collimation of a penetrating flux of photons.

Conversely, scattering and resulting energy loss, and de-collimation, must dominate for initially monoenergetic and collimated photon beams.

This line of argument makes it clear that the deep penetration of photons is characterized, for any source configuration, by tendencies which seek an equilibrium, both in spectrum and in angular distribution. From a more

practical point of view, the greatest rates of change in spectrum and angular distribution occur early; and it is often possible to use the spectrum and angular distribution at a selected point of considerable depth to describe the radiation field at greater depths because changes after that are gradual and of a minor nature.

The mathematical study of deep penetration trends, particularly the approach to equilibrium, is based on the use of monoenergetic sources and simple assumptions about the functional behavior of  $E$  near the most penetrating energy ( $E_m$ ) and direction [15]. One applies 1) a Fourier transform in the space variable, 2) use of the "small angle" approximation which applies a linear approximation to functions of the direction and deflection obliquities, 3) Taylor series representation of  $\mu(E)$  for  $E$  near  $E_m$  and 4) perhaps a Laplace transformation in the wavelength variable  $(\lambda - \lambda_m)$ . The transport equation can thus be progressively reduced to a partial differential equation of known properties and solutions, which still is descriptive of photon components which penetrate more deeply than most. Deep penetration spatial trends are determined by eigenvalues of the (homogeneous) transport equation and are exhibited most clearly when this equation is transformed as just indicated. Spectra and angular distributions are determined by eigenfunctions of the transformed, homogeneous transport equation. The mathematical problem as a whole is strongly analogous to quantum mechanical studies of one- and two-dimensional oscillators. For general treatments, see references [8,11,12].

Three fundamentally different cases occur, according to whether the most penetrating photons possible for a given material are at, above, or below the source energy. Of these, we are mostly interested in the second case, in which scattering increases  $\mu(E)$ . For this case the limiting trend for deep penetrations  $\underline{r}$ , has the general form  $\text{const} \cdot r^K \cdot \exp(-\mu_0 r)$ , where the exponent

$\kappa$  has been evaluated and tabulated by eigenvalue methods [10]. Figure IV.13 illustrates the deep penetration phenomena as exhibited in recent calculations of point and plane  $^{137}\text{Cs}$  sources in air [16]<sup>13</sup>.

The functional form just given is not often useful in practical problems, because the factor  $r^\kappa$  is obscured in sources that are not monoenergetic. In the case of the fission product source, scattered photons from one source energy compete with unscattered photons from higher source energies of reduced strength; and the exponential factor tends to dominate over any such power factor.

Similarly, in the case of photons which start obliquely to the direction of penetration, deep penetration involves a favored succession of scatterings which reduce the photon energy in small steps. As a consequence, the penetration process is again dominated by exponential trends which change ever more slowly towards a limiting trend corresponding to the normal, rather than an oblique, direction of penetration.

The mathematical problem of obtaining accurate data for penetration trends fortunately can proceed on the basis of little more information than the ubiquity of exponential dominance, regardless of source spectrum or configuration. But even so, mathematical treatment of complex cases is not simple, and has involved development of new types of functional representation.

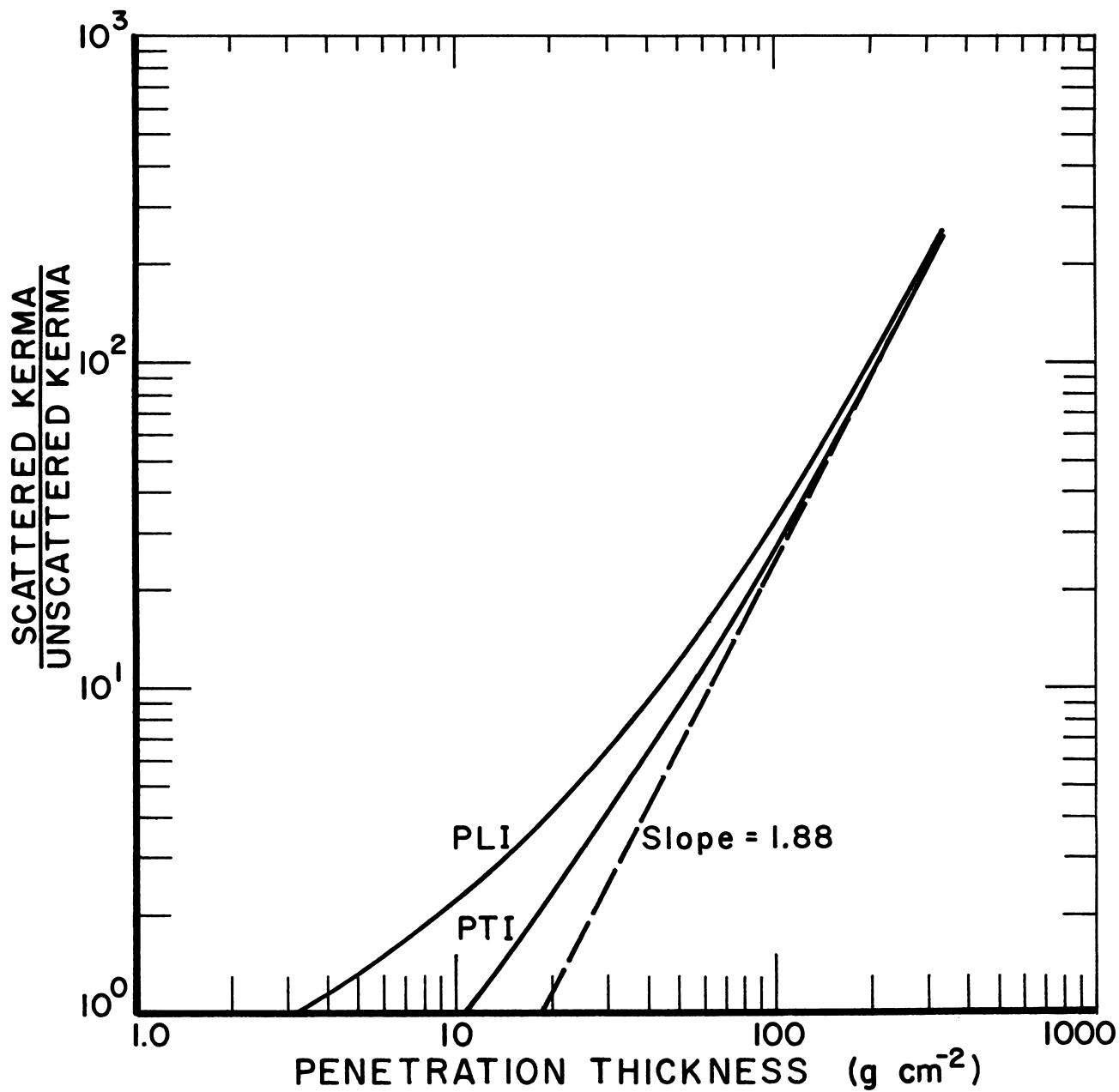
#### D. MOMENTS METHOD OF CALCULATION

The method of moments was employed to obtain most of the basic reduction factors used in the Standard Method, hence its presentation in considerable detail in this section. Chapter III contains a general description of Monte Carlo procedures. Other methods which have seen little application to these

---

<sup>13</sup>See also references [17] and [18] for more extensive calculations. For an interesting recent approach by polynomials to the limiting trend see reference [19].





IV.13 Deep penetration trends of the scattered radiation, for the case of  $^{137}\text{Cs}$  sources in air. The slope of the dashed straight line was obtained by an eigenvalue calculation.

problems include the method of invariant imbedding, and the discrete ordinates approach [20,21]. The former is based on the study of slab transmission and reflection functions; the latter utilizes an analog in which space and direction have been rendered discrete.

Assuming that the cross sections are accurately specified, moment calculations for infinite homogeneous media have great potential accuracy. Detailed comparisons with experiment have been made; a summary discussion is given in reference [10], and later developments are discussed in chapter VI. A brief discussion of the accuracy problem is given in section IV.D.5.

The material in the remainder of chapter IV is largely specific to the problem of computing important distributions by moment methods. This is true even of the brief introduction to the adjoint transport equation. Readers not interested in such computations can bypass the rest of this chapter.

#### 1. Derivation of Moment Equations

The three elementary configurations discussed in section IV.A each involve only a single space variable. Further, two of the three have uniformity on lateral planes and the third (point isotropic source) is derivable from the plane isotropic source case (see sec. III.B.2). Hence it is sufficient to study gamma ray transport in configurations with laterally uniform plane sources. In fact, it has been shown that any source configuration in an infinite, homogeneous medium is derivable by superposition of solutions to problems with laterally uniform (i.e., plane) sources [10].

The transport equation for problems with plane sources has already been written down, for example in eq (IV.17). We assume here that the medium is infinite and homogeneous, and hence that the cross sections do not depend on position.

The transformation which yields spatial moments involves multiplication of each term of the transport equation by a power of  $z$ , say  $z^\nu$ ,  $\nu \geq 0$ , followed by integration over all  $z$ ,  $-\infty < z < \infty$ . For later reference we incorporate an arbitrary scale factor,  $\alpha$ , in this operation:

$$\int_{-\infty}^{\infty} dz (\alpha z)^\nu \cos \theta \frac{\partial N}{\partial z} + \mu N_\nu(E, \theta) = \int_E^\infty dE' \int_{4\pi} d\Omega' k(E', E; \theta) N_\nu(E', \theta') \quad (\text{IV.61})$$

where  $N_\nu$  and  $S_\nu$  are defined by

$$N_\nu = \frac{1}{\nu!} \int_{-\infty}^{\infty} dz (\alpha z)^\nu N(E, \theta, z) ,$$

$$S_\nu = \frac{1}{\nu!} \int_{-\infty}^{\infty} dz (\alpha z)^\nu S(E, \theta, z) , \quad (\text{IV.62})$$

i.e., we assume that moments of the source have finite values. Evaluation of the first term in eq (IV.61) requires only integration by parts, with the condition that  $z^\nu N \rightarrow 0$  for  $z \rightarrow \infty$  and  $z \rightarrow -\infty$ , which is implied by the convergence of the integrals  $S_\nu$ .

The resulting chain of moment equations,

$$\begin{aligned} \mu N_\nu(E, \theta) - \int_E^\infty dE' \int_{4\pi} d\Omega' k(E', E; \theta) N_\nu(E', \theta') \\ = (1 - \delta_{\nu 0}) \alpha \cos \theta N_{\nu-1}(E, \theta) + S_\nu(E, \theta) , \end{aligned} \quad (\text{IV.63})$$

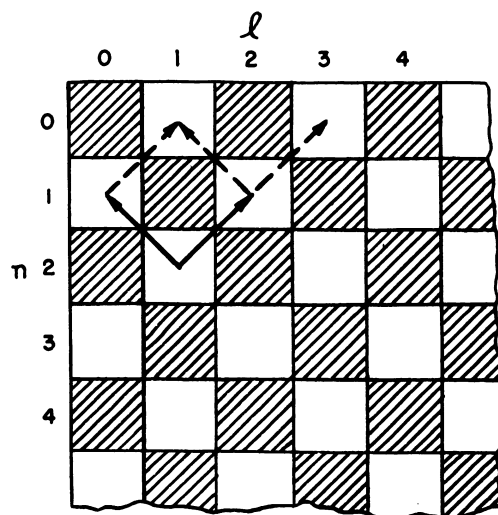
constitutes a solvable recursion system: the case  $\nu = 0$  is soluble, and the cases  $\nu = 1, 2, 3, \dots$ , are then solvable in sequence because the right side of eq (IV.13), is in principle always known.

Before proceeding to reduce the equations further, let us observe that if the cross sections were space dependent, or if the fluence were finite at a boundary, the moment transformation would not yield the simple result of eq (IV.63), except in the simple case of plane density scaling discussed in section IV.B.1. Position-dependent cross sections generally lead to folding integrals, while boundaries generally lead to additional terms involving fluence values at the boundary. The resulting equations are much more difficult to work with.

A second stage now utilizes a transformation from direction variables to Legendre coefficients. To accomplish this we multiply all terms of eq (IV.63) by  $\bar{Y}_\ell^m(\theta, \phi)$ , and integrate over all solid angles (see Appendix A, sec. A.1). The first terms on left and right side of eq (IV.63) then give integrals which we designate  $N_{\ell v}^m(E)$  and  $S_{\ell v}^m(E)$ , respectively. The second term on the left can be reduced by use of the folding rule, eq (A.9) of Appendix A. The second term on the right simplifies if one uses the recursion property given in eq (A.10). Our result is

$$\begin{aligned} \mu N_{\ell v}^m(E) - \int_E^\infty dE' k_\ell(E', E) N_{\ell v}^m(E') = S_{\ell v}^m(E) \\ + (1 - \delta_{v0}) \alpha \left\{ \left[ \frac{\sqrt{(\ell+1)^2 - m^2}}{2\ell+1} \right] N_{\ell+1, v-1}^m + \left[ \frac{\sqrt{\ell^2 - m^2}}{2\ell+1} \right] N_{\ell-1, v-1}^m \right\} \end{aligned} \quad (\text{IV.64})$$

Equation (IV.64) has three indices, but our interest is mainly in fixed values of  $\underline{m}$ , usually  $\underline{m} = 0$ . The resulting recursion system has the structure shown in figure IV.14 [22]. Solution of the first  $L$  equations with  $\underline{v} = 0$  makes possible the solution of the first  $(L-1)$  equations with  $\underline{v} = 1$ , then the first  $(L-2)$  equations with  $\underline{v} = 2$ , and so forth.



IV.14 The pattern of Legendre coefficients for the different moments. The arrows identify terms necessary for calculation of three representative cases. The linkages are such that for  $L$  known terms with  $n = 0$ , one can calculate  $L - 1$  for  $n = 1$ ,  $L - 2$  for  $n = 2$ , etc.

The cases of plane isotropic and plane oblique sources, which are mono-energetic and localized at  $\underline{z} = 0$ , are of particular interest and we complete this section by writing down the appropriate expressions for the source coefficients. For the plane isotropic case,

$$S_{\ell\nu}^o = \frac{1}{\nu!} \int_{-\infty}^{\infty} dz (\alpha z)^\nu \int_{4\pi} d\Omega \left[ \frac{4\pi}{2\ell+1} \right]^{\frac{1}{2}} \bar{Y}_\ell^o(\theta, \phi) [\delta(z) \delta(E_o - E) / 4\pi] ,$$

$$= \delta_{\nu 0} \delta_{\ell 0} \delta(E_o - E) , \quad (\text{IV.65})$$

and for the plane oblique case,

$$S_{\ell\nu}^o = \frac{1}{\nu!} \int_{-\infty}^{\infty} dz (\alpha z)^\nu \int_{4\pi} d\Omega \left[ \frac{4\pi}{2\ell+1} \right]^{\frac{1}{2}} \bar{Y}_\ell^o(\theta, \phi) \delta(z) \delta(E_o - E) \delta(\cos\theta - \cos\theta_o) / 2\pi$$

$$= \delta_{\nu 0} \delta(E_o - E) P_\ell(\cos\theta_o) . \quad (\text{IV.66})$$

We do not explicitly discuss the point isotropic case because of our assumption that data for the plane isotropic case can be used to derive the point isotropic case results. Formulae for accomplishing this are given in the following section.

## 2. Calculation of Solutions to the Moment Equations

Solution of eqs (IV.64) requires a straightforward application of the numerical procedure described in section III.C.2. One must evaluate the equations for fixed  $m$  in the order  $[\nu = 0: \ell - |m| = 0, \dots, \ell_{\max} - |m|]$ ,  $[\nu = 1: \ell - |m| = 0, \dots, \ell_{\max} - |m|]$ , ...,  $[\nu = \ell_{\max} - |m|, \ell - |m| = 0]$ . Solutions  $N_{\ell\nu}^m$  will be zero if  $S_{\ell\nu}^m$  vanishes for all equations in any interlinked set whose solution contributes to terms in the equation for  $N_{\ell\nu}^m$ .

The special cases in which we are most interested have no azimuthal variation ( $m = 0$ ) and require us to take account of the  $\delta(E_0 - E)$  spike properly. As in section III.C.2 this is possible by separate calculation of the unscattered component, together with replacement of eqs (IV.65) and (IV.66) with expressions for the corresponding once-scattered terms  $S_{\ell\nu}^{(1)}$ .

We drop the irrelevant superscript  $m$  here and in the following discussion the order of scattering takes its place as superscript.

The unscattered component is given by eqs (IV.5) and (IV.11), with  $S_0 = 1$ . The  $S_{\ell\nu}$  for the scattered component can be readily obtained by inserting  $N_{\ell\nu}$  expressions for the unscattered component into the scattering integral. For the unscattered component ( $N_{\ell\nu}^{(0)}$ ) we have (plane oblique case)

$$\begin{aligned} N_{\ell\nu}^{(0)}(E) &= \frac{1}{\nu!} \int_{-\infty}^{\infty} dz (\alpha z)^{\nu} \left[ \frac{4\pi}{2\ell+1} \right]^{\frac{1}{2}} \int_{4\pi} d\Omega \bar{Y}_{\ell}^0(\theta) \delta(\cos\theta - \cos\theta_0) \delta(E - E_0) \exp(-\mu z / \cos\theta_0) / \cos\theta_0 \\ &= \frac{1}{\mu(E)} \delta(E - E_0) P_{\ell}(\cos\theta_0) [\alpha \cos\theta_0 / \mu(E)]^{\nu}, \end{aligned} \quad (\text{IV.67})$$

and, for the plane isotropic source,

$$\begin{aligned} N_{\ell\nu}^{(0)}(E) &= \int_{-\infty}^{\infty} dz (\alpha z)^{\nu} \left[ \frac{4\pi}{2\ell+1} \right]^{\frac{1}{2}} \int_{4\pi} d\Omega \bar{Y}_{\ell}^0(\theta) \delta(E - E_0) \exp[-\mu z / \cos\theta] / \cos\theta \\ &= \frac{1}{\mu} \delta(E - E_0) (\alpha/\mu)^{\nu} C_{\ell\nu}, \end{aligned} \quad (\text{IV.68})$$

where  $C_{\ell\nu} = \frac{1}{2} \int_{-1}^1 dx P_{\ell}(x) x^{\nu}$ ,  $\ell \leq \nu$ , and  $C_{\ell\nu} = 0$ ,  $\ell > \nu$ , are numbers shown in Table IV.1. They can be evaluated using the simple recursion,  $C_{\ell\nu} = (2\ell + 1)^{-1} [(\ell + 1)C_{\ell+1, \nu-1} + \ell C_{\ell-1, \nu-1}]$ , with  $C_{\ell 0} = \delta_{\ell 0}$ . Note that the  $C_{\ell\nu}$  definition just given applies to all  $\ell, \nu$ , in contrast with that of, say, reference [5].)

Table IV.1 A few values for  $C_{\ell\nu}$ .

<u><math>\nu</math></u>	<u><math>\ell = 0</math></u>	<u><math>1</math></u>	<u><math>2</math></u>	<u><math>3</math></u>	<u><math>4</math></u>
0	1	0	0	0	0
1	0	1/3	0	0	0
2	1/3	0	2/15	0	0
3	0	1/5	0	2/35	0
4	1/5	0	4/35	0	8/315
5	0	1/7	0	4/63	
6	1/7	0	2/21		
7	0	1/9			
8	1/9				



We now obtain sources  $S_{\ell\nu}^{(1)}$  for the scattered component, by integrating the scattering integral of eq (IV.64) over the delta function (PLO case),

$$S_{\ell\nu}^{(1)} = \frac{k(E_o, E)}{\mu_o} P_\ell(\cos\theta_o) P_\ell(\cos\theta_E) (\alpha \cos\theta_o / \mu_o)^\nu, \quad (\text{IV.69})$$

and for the PLI case,

$$S_{\ell\nu}^{(1)} = \frac{k(E_o, E)}{\mu_o} P_\ell(\cos\theta_E) (\alpha / \mu_o)^\nu C_{\ell\nu}. \quad (\text{IV.70})$$

There is a residual discontinuity at  $\cos\theta_E = -1$  due to  $k(E_o, E)$ : for still lower energies  $S_{\ell\nu}^{(1)}$  vanishes. This occurs in equations for all moment-coefficients  $N_{\ell\nu}^{(S)}(E)$  of the scattered component, and complicates somewhat the numerical procedure; it is discussed in section III.C.2. Otherwise, the calculation of an arbitrarily large set of  $N_{\ell\nu}(E)$  spectra has only the problem of an integration mesh fine enough to guarantee good integration over products of the type  $P_\ell(1 - .511/E' + .511/E_o) P_\ell(1 - .511/E + .511/E')$ , where the first factor roughly describes the trend of  $N_{\ell\nu}^{(S)}(E')$ .

Moments of the dose are obtained by evaluation of integrals

$$D_{\ell\nu} = \int_0^{E_o} dE N_{\ell\nu}(E) E \mu_a(E), \quad (\text{IV.71})$$

and for the polyenergetic spectra we sum or integrate over suitably weighted  $D_{\ell\nu}$  data for different  $E_o$  values.

### 3. Construction of Penetration Trends

The first stage of the computer calculations terminates with the evaluation of  $D_{\ell\nu}$  data for monoenergetic sources. Specifically, calculations of reference [8] were originally made for

$\lambda_o = (E_o/.511)^{-1} = .05, .075, .1, .125, .15, .2, .25, .3, .4, .5, .6, .8, 1.0,$   
 $1.2, 1.6, 2.0, 2.6, 3.0, 4.0, 5.0, 7.0, 9.0, 12.0, 15.0,$

as well as the  $^{60}\text{Co}$  and  $^{137}\text{Cs}$  wavelengths  $\lambda_o = .384, .434, \text{ and } .77$ . The above list will be seen to correspond to representative energies for the different Nelms and Cooper components shown in figure II.10. Superposition of data for these source energies, weighted according to the Nelms and Cooper [23] 1.12 hour bin-heights given in table II.5, gave results for the fission source.

There remains to be described the problem of constructing penetration distributions for monoenergetic sources. This has been accomplished differently for different source types.

#### a. Point Isotropic Source

Point monoenergetic source distributions  $D_{\ell}^{\text{PTI}}(r)$  were constructed for reference [8] using the representation

$$4\pi r^2 D_{\ell}^{\text{PTI}}(r) = \sum_{i=0}^{i_{\max}} A_i (\mu_o r)^i e^{-\mu_o r} \quad (\text{IV.72})$$

where  $\mu_o = \mu(E_o)$  and  $i_{\max} = 10$ . The lead coefficient,  $A_o$ , was assigned the known value for unscattered photons. The remaining  $A_i$ ,  $i > 0$ , values were determined by inverting the matrix of the linear system obtained by integration over eq (IV.72), and use of  $\alpha = \mu_o$ :

$$D_{\ell n}^{\text{PTI}} - A_o/\mu_o = \frac{1}{\mu_o} \sum_{i=0}^{i_{\max}} A_i \frac{(n+i)!}{n!}, \quad n = \ell, \ell + 2, \dots \quad (\text{IV.73})$$

Fortunately, the inverse matrix is readily obtained inductively for arbitrary  $\ell$  and  $i_{\max}$  by use of the polynomial coefficients  $u_{ni}^k$  given by eq (A.19) of Appendix A.

The representation (IV.72) is precisely equivalent to the representation

$$4\pi r^2 D_\ell^{\text{PTI}} = \sum_{i=0}^{\ell-1} a_i(\mu_o r) U_i^{\ell+1}(\mu_o r) e^{-\mu_o r} + A_o e^{-\mu_o r} \quad (\text{IV.74})$$

which is based on the functions described in section A.2 of Appendix A. This is because the  $U_i^{\ell+1}$  are merely linear combinations of powers. By making use of this equivalence, convergence can be proven and limits to the truncation error inherent in eq (IV.74) can be estimated [16].

Applications of this method in which truncation error estimates are made are given in references [24,25].

#### b. Plane Isotropic Source

From  $D_\ell^{\text{PTI}}$  as given by eq (IV.72), we can obtain Legendre coefficients for plane isotropic sources,  $D_\ell^{\text{PLI}}$ , by integration, using eq (A.12) of Appendix A (see ref [5], p. I-95). We have

$$D_\ell^{\text{PLI}}(z) = \frac{1}{2} \int_{|z|}^{|R|} dr r^{-1} D_\ell^{\text{PTI}}(r) P_\ell(z/r) \quad (\text{IV.75})$$

$$= \frac{1}{2} \sum_{i=0}^{\ell-1} A_i \int_{|\mu_o z|}^{|\mu_o R|} ds s^{i-1} P_\ell(\mu_o z/s) e^{-s} \quad (\text{IV.76})$$

Note that if the upper limit in these expressions is finite, they apply to a plane isotropic, circular disk source, whose center and rim are distances z and R from the detector. If R is assigned the value  $\infty$ , we have the case of the infinite plane isotropic source most commonly considered.

The coefficients

$$Q_{i\ell}(z, R) = \int_{|\mu_o z|}^{|\mu_o R|} dr \, r^{i-1} P_{\ell}(\mu_o z/r) e^{-r} \quad (\text{IV.77})$$

are readily evaluated by recursion for increasing  $i$  and  $\ell$  values: A general formula can be derived using the recursion formula (A.9) of Appendix A (see ref. [5]). A special formula for  $\ell = 0$  is also derivable using integration by parts. These two recursion formulae are

$$Q_{i0} = (i-1)Q_{i-1,0} + |\mu_o z|^{i-1} e^{-|\mu_o z|} - |\mu_o R|^{i-1} e^{-|\mu_o R|}, \quad (\text{IV.78})$$

and

$$(2\ell + 1)|\mu_o z|Q_{i\ell} = (\ell + 1)Q_{i+1,\ell+1} + \ell Q_{i+1,\ell-1}. \quad (\text{IV.78}')$$

Numerical evaluation of the functions  $Q_{00}$  and  $Q_{10}$  suffices to start the recursion process.

Note that  $D_o^{\text{PLI}}$  and  $D_o^{\text{PTI}}$  express the total dose, while the higher  $\ell$  coefficients are necessary for determination of angular distributions. We return to problems of constructing the angular distributions in section IV.D.4.

### c. Plane Oblique Source

The polynomial method is not well suited for use in constructing penetration curves for plane slant sources, although it can be used if the emission obliquity is nearly normal to the source plane. For larger obliquity angles the exponential trend changes with depth, and the small- $z$  penetration features are less smooth and more sharply varying. Hence other methods have been preferred.

The procedure used for all early work on oblique or general slant sources was "function fitting," as described in section A.3 of Appendix A [10,26]. The form of this procedure applied here is based on a representation in terms of sums of exponentials, and is described in references [5,10,17]. "Even" and "odd" component distributions, here indicated by superscripts  $e$  and  $o$  can be separately evaluated. The functional form for the dose is

$$D_o^{PLS}(E_o, \cos\theta_o, z) = \frac{1}{2} \left[ \sum_{j=1}^{j_{\max}^e} \frac{A_j^e}{\beta_j^e} e^{-|\mu_o z|/\beta_j^e} + \sum_{j=1}^{j_{\max}^o} \frac{A_j^o}{\beta_j^o} e^{-|\mu_o z|/\beta_j^o} \right] \quad (IV.79)$$

where the plus sign is used for  $z \geq 0$  and the minus sign is for  $z \leq 0$ . Values for  $\beta_1^e$  and  $\beta_1^o$  are assigned the value  $\sec\theta_o$  to describe the unscattered component. Values for  $\beta_2^e$  and  $\beta_2^o$  are fixed arbitrarily to give optional distributions from the standpoint of smoothness. Evaluation of the even distribution,  $D_o^{PLS}(z) + D_o^{PLS}(-z)$ , requires solution of the moment equations obtained from eq (IV.79) by integration to determine the remaining constants  $\beta_i^e$ ,  $A_j^e$

$$D_{on}^{PLS} = \frac{1}{\mu_o} \sum_{j=1}^{j_{\max}^e} A_j^e (\beta_j^e)^n, \quad n = 0, 2, \dots, 10. \quad (IV.80)$$

while evaluation of the odd distribution,  $D_o^{PLS}(z) - D_o^{PLS}(-z)$ , requires solution of the moment equations

$$D_{on}^{PLS} = \frac{1}{\mu_o} \sum_{j=1}^{j_{\max}^o} A_j^o (\beta_j^o)^n, \quad n = 1, 3, \dots, 9. \quad (IV.80')$$

The value 4 was assigned both to  $j_{\max}^e$  and to  $j_{\max}^o$ . It was noted that the odd component, in the limit  $z \rightarrow 0$ , must equal the known strength of the unscattered component. This assigns a known value to the sum  $\sum_{j=1}^{j_{\max}^o} A_j / \beta_j^o$ , and the resulting equation completes the set (IV.80').

In practice it has turned out that trial-and-error search of values for  $\beta_1^e$  and  $\beta_1^o$  is sometimes required for an acceptable distribution. But resulting data have been of high quality except for large backward penetrations.

This trial-and-error aspect of function-fitting calculations makes alternative methods desirable. With the more recently developed "plural-series" methods [27] (see Appendix A, section A.3), direct calculations can be made; and estimates of error bounds can be made as well. But while some exploratory calculations for PLO sources have been made using the plural-series approach [28], its use to generate data for fallout shielding applications has not yet occurred.

#### 4. Construction of Angular Distributions

##### a. Direct Approach

The basic data from which geometry factors can be derived are angular distributions of the dose. A central problem therefore is the construction of these angular distributions from known values for  $D_{\ell}^{\text{PLI}}(z)$  and  $D_{\ell}^{\text{PTI}}(r)$  together with expressions for the unscattered component. The most direct method for this utilizes Legendre polynomial representations as in eq (IV.99),  $m = 0$  case:

$$D^{\text{PLI}}(z, \theta) \approx \sum_{\ell=0}^{\ell_{\max}} (\ell + \frac{1}{2}) D_{\ell}^{\text{PLI}}(z) P_{\ell}(\cos \theta) \quad (\text{IV.81})$$

where  $\cos \theta = \vec{\Omega} \cdot \vec{k}$ , with  $\vec{k}$  normal to the source plane; and

$$D^{\text{PTI}}(r, \theta_r) \approx \sum_{\ell=0}^{\ell_{\max}} (\ell + \frac{1}{2}) D_{\ell}^{\text{PTI}}(r) P_{\ell}(\cos \theta_r) \quad (\text{IV.82})$$

where  $\cos \theta_r = \vec{\Omega} \cdot \vec{r}/r$ . In both cases  $\ell_{\max} = 7$  for the data given in reference [8] and chapter V.

Unfortunately, both types of angular distributions vary too sharply to permit rapid convergence of the sums. Hence eqs (IV.81) and (IV.82) are not very satisfactory.

#### b. Early Fission Source Calculations

The fission source calculations reported in reference [29] were carried out in 1957 using a simple smoothing procedure: Analytic functions similar to the expected distributions were chosen, and sums of terms with  $\ell > \ell_{\max}$  taken from the Legendre series representations of these functions, were added to the truncated series given by eqs (IV.81) and (IV.82):

$$D^{\text{PLI}}(z, \theta) \approx \sum_{\ell=0}^{\ell_{\max}} (\ell + \frac{1}{2}) D_{\ell}^{\text{PLI}}(z) P_{\ell}(\cos \theta) + \left\{ a \sec \theta e^{-bz/\cos \theta} - \sum_{\ell=0}^{\ell_{\max}} (\ell + \frac{1}{2}) c_{\ell} P_{\ell}(\cos \theta) \right\} \quad (\text{IV.83})$$

and

$$D^{\text{PTI}} \approx \sum_{\ell=0}^{\ell_{\max}} (\ell + \frac{1}{2}) D_{\ell}^{\text{PTI}}(r) P_{\ell}(\cos \theta_r) + \left\{ a' (\cosh b' - \cos \theta_r)^{-3/2} - \sum_{\ell=0}^{\ell_{\max}} (\ell + \frac{1}{2}) c'_{\ell} P_{\ell}(\cos \theta_r) \right\} \quad (\text{IV.84})$$

Here  $c_\ell$ ,  $c'_\ell$  values are readily obtained from known series expressions for  $[a \sec\theta \exp(-bz/\cos\theta)]$  and  $a'(\cosh b' - \cos\theta_r)^{-3/2}$ , after the arbitrary  $a$ ,  $b$  and  $a'$ ,  $b'$  values have been assigned.

The selection of  $a$ ,  $b$  and  $a'$ ,  $b'$  values was accomplished by hand, again using trial-and-error search for smooth distributions. While the computation was tedious, the results were gratifying (see figs. V.6 and V.7).

#### c. $^{60}\text{Co}$ and $^{137}\text{Cs}$ Source Calculations

Later work on  $^{60}\text{Co}$  and  $^{137}\text{Cs}$  angular distributions for plane isotropic sources was carried out using a simpler but less satisfactory procedure which could be more easily computerized: The unscattered component was calculated by superposition of the monoenergetic source values, which could be calculated from eq (IV.9). This was combined with the scattered component, given by the Legendre sum, eq (IV.8). Results can be seen in figures B.6 and B.6' of Appendix B.

The angular distributions for point isotropic sources were calculated somewhat more successfully, using the expression

$$D_{\text{PTI}}^{\text{PTI}}(r, \cos\theta_r) = a(\cosh b - \cos\theta_r)^{-3/2} + \sum_{\ell=0}^{\ell_{\text{max}}} (\ell + \frac{1}{2}) \left[ D_{\ell}^{\text{PTI}}(r) - c_{\ell}(r) \right] P_{\ell}(\cos\theta_r) \quad (\text{IV.85})$$

where the  $c_{\ell}(r)$  are Legendre coefficients of  $a(\cosh b - \cos\theta_r)^{-3/2}$ , and  $a$ ,  $b$  are fixed by requiring that

$$c_{\ell}(r) = D_{\ell}^{\text{PTI}}(r) \quad (\text{IV.85}')$$



for  $\ell = \ell_{\max} - 2$  and  $\ell = \ell_{\max} - 4$ . This procedure works rather well due to the empirical fact that  $D_{\ell}^{\text{PTI}}$  is roughly exponential in its  $\ell$  dependence. The procedure is readily computerized; and resulting data are given in figures B.7 and B.7' of Appendix B.

#### d. More Recent Procedures for the Plane Isotropic Source

More recent methods for calculating angular distributions have been very satisfactory, but have not yet been used to improve the geometry factors. These include exact calculation of the once-scattered component for the plane isotropic source, which greatly reduces the importance of the remaining Legendre sum by evaluating the main remaining strongly peaked component [11].

Another procedure explored in reference [30] would evaluate 45 or more Legendre coefficients for the point isotropic source on the basis of the approximate representation of eq (IV.72), and then use these in the corresponding expression (IV.76) for the plane isotropic source. This is made possible by use of the recursion system of eqs (IV.78) and (IV.78') to evaluate the large number of  $Q_{i\ell}$  functions required. Reference [12] performs a similar extrapolation on even and odd Legendre coefficients separately, for the PLI case, extending as far as 61 coefficients.

#### 5. Remarks on Accuracy

By and large, accuracy measures the closeness of agreement between a computation and a corresponding idealized experiment. Since experiments are never ideal, a full analysis requires estimates of error both in experiment and in the calculation, and is better discussed with reference to particular experiments and calculations. Even so, it is useful at least to categorize sources of error in computed data, with general indications of relative magnitude. Some study of this has been initiated [31].

In moment methods there are three readily distinguished sources of error [16]: 1) truncation errors, resulting from use of only a finite number of moments or spherical harmonics; 2) errors associated with use of imperfect cross section data in the computations; and 3) errors due to numerical procedures by which data are obtained from the transport equation. A fourth type of error lies in the failure of the schematizations by which elementary data types are combined to give estimates for complex configurations; this last error will be referred to many times in the chapters which follow.

In the moment method, errors due to numerical integrations can be studied by use of different sizes of integration mesh [12,32]. They are of concern mainly at the point of decision on mesh size and integration formula; and they tend to be the smallest and most easily controlled of the three sources for moment methods.

Cross section problems occur both in specification of  $\mu$  values and in specification of differential cross sections, which may neglect effects such as electron binding, polarization, and higher order interactions. The main source of inaccuracy, however, relates to errors in values used for  $\mu$ . For the shielding materials and source photon energies of main concern to the fallout case,  $\mu$  is known to  $\lesssim 1\%$ . This means that errors due to this cause are  $\lesssim 10\%$  for attenuations to  $10^{-3}$ .

In the case of truncation errors, evaluation of the total dose is much more accurate than our evaluations of angular distribution. In a general way, data for the simple PLI, PTI, or PLO sources tend to have smaller error at large penetrations due to truncation of series expressions than due to inaccuracy of  $\mu$ . At small penetrations, error tends to be small because the dominant unscattered component is accurately included. A recent study of gamma ray penetration in water using 10 moments exhibited truncation errors less than 1-2% [13].

This excellent situation does not apply to angular distributions, however. Careful studies of the accuracy of angular distributions have never been carried out. Instead, violation of smoothness properties of angular distributions has been used to obtain a rough measure of computational error. On this basis, the various point isotropic angular distributions are generally felt to be more accurate than, say, the  $^{60}\text{Co}$  and  $^{137}\text{Cs}$  plane isotropic angular distributions given in Appendix B, though not substantially more accurate than the corresponding plane isotropic angular distribution for fallout. A rough guess has been made that the computed point isotropic angular distributions are generally within 20%, while there are errors more than twice greater in the  $^{60}\text{Co}$  and  $^{137}\text{Cs}$  plane isotropic curves given. In addition, differential cross section inaccuracies would produce significant errors in these angular distributions, which have never been estimated; but these are probably smaller than the truncation errors at present.

The questionable quality of some of the angular distribution data is rendered somewhat less significant by the integration process which generates geometry factors, and which reduces extremes except for the limiting case of very small range of integration over angles.

## E. ADJOINT CALCULATIONS<sup>14</sup>

### 1. The Adjoint Equation

The "dose"  $D$ , however defined, is always given by an integral, which in its general form is of the type

$$D = \int_V d\tau \int_0^\infty dE \int_{4\pi} d\Omega N(E, \vec{\omega}, \vec{r}) R(E, \vec{\omega}, \vec{r}) \quad , \quad (\text{IV.86})$$

---

<sup>14</sup>General references on this subject include [33] and [34], the latter in the context of differential operators only.

where  $d\tau$  is a differential volume element containing the point  $\vec{r}$ ,  $R$  is a detector response function, and the fluence  $N$  is the solution of the transport equation (e.g., eq (III.41)),

$$TN = [\vec{\Omega} \cdot \nabla + \mu - \int_E^\infty dE' \int_{4\pi} d\Omega' k(E', E; \vec{\Omega}' \cdot \vec{\Omega}; \vec{r})] N = S(E, \vec{\Omega}, \vec{r}) , \quad (\text{IV.87})$$

where we use  $T$  to designate the transport operator, and  $S$  as the source function.

The integral, eq (IV.86), is a simple example of what is referred to as a "linear functional", whose value  $D$  is a "function" of the choice of  $N$  and  $R$ ; a shorthand designation often used for such a linear functional is

$$D = (R, N). \quad \text{IV.86'}$$

Now,  $N$  is determined by the source function  $S$ ; and we attempt to find another function, which we designate  $\hat{N}$ , from which  $D$  can similarly be calculated and which is determined by  $R$ :

$$D = \int_V d\tau \int dE \int_{4\pi} d\Omega \hat{N}(E, \vec{\Omega}, \vec{r}) S(E, \vec{\Omega}, \vec{r}) = (\hat{N}, S) . \quad (\text{IV.87'})$$

To find out more about  $\hat{N}$ , we note that eq (IV.87) enables us to rewrite eq (IV.87') in the form

$$D = \int_V d\tau \int_0^\infty dE \int_{4\pi} d\Omega \hat{N}(TN) = (\hat{N}, TN) . \quad (\text{IV.88})$$

The operator  $T$  is made up of derivatives and integrals. By use of integration by parts, assuming for the moment that  $V$  includes all space, and by interchange of the order of integrations, the components of  $T$  can be applied to  $\hat{N}$  rather than  $N$ , though in modified form comprising a closely related operator which we designate  $\hat{T}$ :

$$D = \int_V d\tau \int_0^\infty dE \int_{4\pi} d\Omega (\hat{\hat{T}}N) = (\hat{\hat{T}}N, N) \quad . \quad (\text{IV.88'})$$

Two operators  $T, \hat{T}$ , related by an expression of the type

$$(\hat{N}, TN) = (\hat{\hat{T}}N, N) \quad , \quad (\text{IV.89})$$

are said to be adjoint with respect to each other, and we call  $\hat{T}$  the adjoint transport operator. Further, comparison of eq (IV.88') with eq (IV.86) leads to the "adjoint equation" whose solution gives us the "adjoint function"  $\hat{N}$ , namely

$$\hat{\hat{T}}N = R \quad . \quad (\text{IV.90})$$

To write out this equation explicitly, still taking for the volume  $V$  all space, we insert into eq (IV.88) the identity

$$\hat{N}(\vec{\Omega} \cdot \nabla N) = -N(\vec{\Omega} \cdot \nabla \hat{N}) + \nabla \cdot (\vec{\Omega} \hat{N}N) \quad , \quad (\text{IV.91})$$

and change the order of integrations in the scattering term of the operator  $T$  as follows:

$$\int_0^\infty dE \int_E^\infty dE' \rightarrow \int_0^\infty dE' \int_0^{E'} dE . \quad (\text{IV.92})$$

The remainder generated by the last term of eq (IV.91) vanishes if  $N$  or  $\hat{N}$  vanishes at the surface bounding the volume  $V$ , as would usually be expected if  $V$  includes all space:

$$\int d\tau \nabla \cdot (\vec{\Omega} \hat{N}) = \oint_{S_V} d\vec{\sigma} \cdot (\vec{\Omega} \hat{N}) = 0 . \quad (\text{IV.93})$$

Interchanging the names of  $E$  and  $E'$  then leads to

$$\hat{TN} = [-\vec{\Omega} \cdot \nabla + \mu - \int_0^E dE' \int_{4\pi} d\Omega' k(E, E'; \vec{\Omega} \cdot \vec{\Omega}'; \vec{r})] \hat{N} , \quad (\text{IV.94})$$

and the adjoint equation assumes a form similar to the "forward" transport equation,

$$-\vec{\Omega} \cdot \nabla \hat{N} + \mu \hat{N}(E, \vec{\Omega}, \vec{r}) = \int_0^E dE' \int_{4\pi} d\Omega' k(E, E'; \vec{\Omega} \cdot \vec{\Omega}'; \vec{r}) \hat{N}(E', \vec{\Omega}', \vec{r}) , \quad (\text{IV.95})$$

with evaluation in energy proceeding to larger  $E$  values.

## 2. Remarks on the Adjoint Approach

Equation (IV.95) is a linear equation of the same type as the "forward" transport equation, eq (III.41). The superposition principle applies with regards to energy, direction, and space variables of the function  $R$  which is usually the detector response function of a given dose integral, as in eq (IV.86). Thus, for given boundary conditions such as the vanishing of  $N$  or  $\hat{N}$  on  $S_V$ , it is possible to solve the adjoint equation for monoenergetic, monodirectional point detectors, say, and obtain  $\hat{N}$  for a given detector by superposition of these solutions.

While the source function  $S$  has units of energy generated per steradian per unit volume of the source say, the detector function  $R$  has units of energy deposited, per steradian, per unit volume of the detector. Thus both  $S$  and  $R$  have the same basic units. This means that the adjoint function  $\hat{N}$  has the same dimensions as  $N$  but the sense of the photon movement is reversed when  $R$  is considered as a "source" function for the adjoint equation.

The adjoint function  $\hat{N}$  has commonly been called the "importance function", because it measures the importance of different sources giving rise to a specified dose. Unfortunately, this terminology, like most, doesn't avoid ambiguity, because the ordinary fluence similarly measures the importance of various components of the detector response.

The various theorems and methods which have been described or referred to in Chapters III and IV can be equally well applied to the adjoint equation. We will not pursue this because little use of the adjoint approach has been made as yet in calculations of fallout gamma ray shielding.

One further aspect should be mentioned: Use of both forward and adjoint transport equations does make possible certain methods not otherwise applicable. The best known of these is the "variational" approach, whereby approximate solutions of elementary form can be optimized and their accuracy estimated [35-37]. However this type of approach has not been much utilized yet in gamma ray transport problems.

Somewhat more accessible to numerical development is an approach whereby part of the transport is evaluated by each method, with an appropriate junction at some selected surface. For example, adjoint calculations for a given detector location in a building can be connected with the free field fluence at some surface on, or outside the building. Calculations of this type have been performed [38].

## References

- [1] Morse, P. M., Feshbach, H., *Methods of Theoretical Physics, Part I*, 997 pages (McGraw-Hill, New York, 1953).
- [2] Rockwell, T., III, ed., *Reactor Shielding Design Manual*, Chapter 9, 347-425 AEC-TID-7004 (March 1956).
- [3] Blizard, E. P., Ed., *Analytical Methods of Shield Design*, Chapter 11, *Reactor Handbook*, 2nd Edition, Vol. III, Part B., Shielding, E. P. Blizard Ed. (Interscience Publishers, New York, 1962).
- [4] Blizard, E. P., Foderoro, A., Goussev, N. G., Kovalev, E. E., *Extended Radiation Sources*, Chapter 6, *Engineering Compendium on Radiation Shielding*, Vol. I, 363-416 (Springer-Verlag, New York, 1968).
- [5] Spencer, L. V., *Gamma Ray Shielding Theory*, TR-40, Vol. I, Radiation Shielding, 325 pages (Office of Civil Defense and Kansas State Univ. 1966).
- [6] Beck, H., and Bennett, B., Polynomial Solutions of the Gamma Ray Transport Equation in Infinite-Homogeneous and Two-Medium Plane Geometry, *Trans. Am. Nucl. Soc.* 10, No. 1, 400-401 (June 1967).
- [7] Morris, E. E., *Radiation Field Three Feet Above Infinite Air/Air and Air/Ground Interfaces as Plane Isotropic Sources of 1.25-MeV Gamma Radiation*, Report 15, (University of Illinois Nuclear Radiation Shielding Studies 1973).
- [8] Diaz, J., and Chilton, A. B., Modeling Relationships for Radiation Transport Within Ducts and Other Cavities in Shields, *Nucl. Sci. Eng.*, 35, No. 2, 283-285 (Feb. 1969).
- [9] Verser, F. A., and Donnert, H. J., Validity of Scale-Modeling for Gamma-Ray Attenuation, DCPA Report No. KEES-SR-113, (Sept. 1973).
- [10] Fano, U., Spencer, L. V., and Berger, M. J., Penetration and Diffusion of X-Rays, *Handbuch der Physik, Encyclopedia of Physics*, Ed. S. Flugge, Vol. 38/2, 660-817 (Springer-Verlag, Berlin, 1959).
- [11] Morris, E. E., Single Scattering of Gamma Radiation from Monoenergetic, Plane Isotropic Sources in Infinite and Semi-Infinite Media, *Nucl. Eng. and Design*, 9, 357-362 (North-Holland Publ. Co., Amsterdam, 1969).
- [12] Rubin, R. M., *Disk Source Energy and Angular Distribution*, Ph.D. dissertation, 127 pages, Dept. of Nuclear Engineering, Kansas State University, Manhattan, Kansas (1970).
- [13] Eisenhauer, C., A Study of the Angular and Energy Distributions of Radiation at Small Distances from a Point Source of Gamma Rays or Neutrons, *Nucl. Sci. Eng.*, 27, 240-251 (1967).
- [14] Morris, E. E., and Spencer, L. V., The Small-Angle Limit for Twice-Scattered Gamma Rays from a Point-Isotropic Source, *Nucl. Sci. Eng.* 27, 464-488 (Feb. 1967).



- [15] Fano, U., and Berger, M. J., Deep Penetration of Radiation, Proc. Symp. Applied Math., Vol. XI, Nuclear Reactor Theory, 43-57 (1961).
- [16] Spencer, L. V., Bounds to Truncation Errors in Biorthogonal Polynomial Approximations, with Illustrative Applications to Gamma Ray Transport Distributions, NBS J. Research, 75B, Nos. 1 and 2, 1-16 (June 1971).
- [17] Spencer, L. V., and Simmons, G. L., Improved Moment Method Calculations of Gamma-Ray Transport: Application to Point Isotropic Sources in Water, Nucl. Sci. Eng., 50, 20-31 (Jan. 1973).
- [18] Morris, E. E., Moments Method Calculation of Buildup Factors for Point Isotropic Monoenergetic Gamma-Ray Sources at Depths Greater than 20 Mean-Free-Paths, Nucl. Sci. Eng. 50, 32-37 (Jan. 1973).
- [19] Nikolaishvili, Sh. S., Gabrashvili, A. I., Dzhgarkava, N. N., and Iordanishvili, E. A., Calculation of Buildup Factors at Deep Penetrations, Atomnaya Energiya, 32, No. 6, 504-505 (Translated by Consultants Bureau, Plenum Publishing Corp, New York, 1972).
- [20] Shimizu, A., and Aoki, K., Application of Invariant Embedding to Reactor Physics, 184 pages (Academic Press, New York, 1972).
- [21] Mynott, F. R., Weapons Radiation Shielding Handbook, Section 3.3.4, The Discrete Ordinates Method (Su), Eds. L. S. Abbott, H. C. Claiborne, and C. E. Clifford, DASA-1892-3, 6 pages (Defense Atomic Support Agency, 1968).
- [22] Spencer, L. V., and Fano, U., Penetration and Diffusion of X-Rays. Calculation of Spatial Distributions by Polynomial Expansion, J. Res., NBS, 46, No. 6, (June 1951).
- [23] Nelms, A. T., and Cooper, J. W., U-235 Fission Produce Decay Spectra at Various Times after Fission, Health Physics 1, 427-441 (1959).
- [24] Spencer, L. V., and Simmons, G. L., Improved Moment Method Calculations of Gamma-Ray Transport: Application to Point Isotropic Sources in Water, Nucl. Sci. Eng. 50, 20-31 (1973)
- [25] Morris, E. E., Chilton, A. B., and Vetter, A. F., Tabulation and Empirical Representation of Infinite-Medium Gamma-Ray Buildup Factors for Mono-energetic, Point Isotropic Sources in Water, Aluminum, and Concrete, Nucl. Sci. Eng. 56, 171-178 (1975).
- [26] Spencer, L. V., Penetration and Diffusion of X-Rays: Calculation of Spatial Distributions by Semi-Asymptotic Methods, Phys. Rev., 88, No. 4, 793-803 (Nov. 1952).
- [27] Spencer, L. V., "Plural-Series" Approximations of Functions, NBS J. Research, 76B, Nos. 3 and 4, 91-108 (Dec. 1972).
- [28] Simmons, G. L., and Eisenhauer, C., Moments Method Calculations of Neutron Distributions in Concrete, Nucl. Sci. Eng., 53, 197-219 (1974).

- [29] Spencer, L. V., Structure Shielding Against Fallout Radiation from Nuclear Weapons, NBS Monograph 42, 134 pages (1962).
- [30] O'Dell, A. A., Moments Method Calculation of the Scattered Angular Energy Flux for Point Isotropic Gamma Sources in an Infinite Homogeneous Air Medium, EGG 1183-2275, 214 pages (1971).
- [31] Subcommittee on Radiation Shielding, The Accuracy of Radiation Shielding Calculations, 12 pages (Office of Civil Defense, Sept. 1965).
- [32] Stewart, J. J., Solutions of the Gamma-Ray Transport Equation using Tschebyscheff Polynomial Expansions and the Moments Method, Ph.D. dissertation, 136 pages, Dept. Nuclear Engineering, North Carolina State College, Raleigh, N.C. (1963).
- [33] Morse, P. M., and Feshbach, H., Methods of Theoretical Physics, Part I, 998 pages (McGraw-Hill, New York, 1953).
- [34] Lanczos, C., Linear Differential Operators, 554 pages (D. Van Nostrand, Princeton, N.J., 1961).
- [35] Morse, P. M., and Feshbach, H., Methods of Theoretical Physics, Part II, 980 pages (McGraw-Hill, New York, 1953).
- [36] O'Reilly, B. D., A Variation Synthesis Method for Calculating Structure Shielding Data, NRDL TRC-68-50, (Naval Radiological Defense Laboratory, June 1968).
- [37] Pomraning, G. C., A Derivation of Variational Principles for Inhomogeneous Equations, Nucl. Sci. Eng. 29, 220-236 (1967).
- [38] Beer, M., Cohen M. O., Initial Gamma Radiation Dose in Five Concrete Blockhouse Configurations, DCPA Report No. MR-7037, (Defense Civil Preparedness Agency, Oct. 1973).

## V. PENETRATION DATA FOR SHIELDING APPLICATIONS

### A. INTRODUCTION

This chapter is to serve as a general reference for the discussions of engineering methods and the experimental investigations which follow. It contains basic data for several kinds of application for fallout gamma rays; similar data for  $^{60}\text{Co}$  and  $^{137}\text{Cs}$  are given in Appendix B. Most of these data were obtained by theoretical methods discussed in chapter IV, and hence serve also as illustrations of transport studies and calculations given primarily in chapter IV, but also to a lesser extent in chapter III. Some discussion relates to prominent features and trends exhibited by various data types. Most of the material in this section is from reference [1], with additions and modifications from reference [2].

We have organized the data presentation by separating differential from integral distributions, presenting the former first. The integral distributions then follow, organized mainly by source type. Appendix B data are similarly arranged for  $^{60}\text{Co}$  and  $^{137}\text{Cs}$ , but without detailed commentary.

Section V.B, which follows, gives definitions and explanations of the main variables, thus collecting these basic matters together for ready reference.

### B. DEFINITIONS OF SHIELDING VARIABLES

#### 1. Protection Factors (PF) and Reduction Factors (RF)

We proceed to define and discuss the quantitative measures of protection to be used in analyzing the shielding by structures of all types. For this purpose we resort to the careful definition of an "unprotected" location, whose exposure is to be used as a standard of comparison. To this end, we make idealizations which simplify computational problems, so long as they do not render the standard dose unrealistic.

Our first idealization is that of specifying a spectrum characteristic of fallout 1 hour (or 1.12 hr) after the detonation.<sup>1</sup> It is clear that changes with time in the spectrum result in changes both in a standard "unprotected" dose and in the dose at any given "protected" location. If the spectrum becomes softer, absorption by shielding materials will be greater, but scattering will also be enhanced. As a result, penetration through barriers will be reduced, while scattering around barriers will be enhanced; and one expects changes in the overall protection to result. One sees from figure II.16 that such changes amount to factors of the order of 1.5 in the ratio ("protected exposure"/"unprotected exposure") if one is interested in a total reduction of  $\sim .025$ , i.e.  $(40)^{-1}$ . Figure II.16 represents a case in which the reduction is due to penetration of a barrier; but one expects comparable effects for cases in which radiation must scatter in favored directions to reach the detector.

Our second idealization is that of assuming that fallout uniformly covers all surfaces according to their horizontal projection. One knows that even in large open spaces there are significant variations with position, as a result of large scale variations in fallout patterns as well as micro-meteorological phenomena [3,4]. But the detectors integrate over large enough source areas to compensate to some degree for the latter, while linear changes due to large scale variations of the fallout field are averaged out completely.

One weakness of this idealization is that it embodies an assumption of low wind speed at the time of fallout deposition. The consequences of wind-speed and precipitation on fallout deposition are still poorly known.

---

<sup>1</sup>We believe that changeover to an updated (and less conservative) standard 1 hr source spectrum is desirable. But the rather considerable effort involved gives rise only to changes of the order of 10-20%, as suggested by figures II.11 and II.12, and unpublished numerical studies.

A third idealization is that of ignoring the inherent roughness of the ground surface, in selection of a "standard unprotected location". We assume the ground surface to be an ideally flat plane. Note that ground roughness reduces the unprotected exposure more than the protected exposure (see sec VI.D), hence the assumption of no ground roughness can be considered inherently non-conservative, by factors of perhaps 1.3. On the other hand, ground roughness can be incorporated as a separate factor which is viewed as part of the protection provided by the configuration as a whole, so that this step is fully justifiable. In any case, this idealization renders precise computations of the standard exposure feasible.

The last idealization is that of replacing ground by compressed air. Due to the Theorem on Plane Density Variations (sec IV.B.2), the density aspect of the ground-air interface can be regarded as inconsequential. Small changes, of the order of a few percent, are to be expected because the composition of the ground resembles, say, aluminum ( $Z = 13$ ) rather than nitrogen ( $Z = 7$ ). At this cost, one gains the possibility of using methods of great potential precision, appropriate only to infinite homogeneous media, to evaluate the standard exposure. For a given spectrum, the "unprotected dose" can then be calculated to perhaps 1-2 percent accuracy.

To complete the description of the "standard unprotected location", it is necessary to fix the detector position. We assume that the detector is 3 ft (or 1 meter) above the interface,<sup>2</sup> in dry air at 76 cm Hg pressure and a temperature of 20° centigrade. Note that the air characteristics above ground must be given, because they affect the mass of the air between detector and source. On the other hand, the precise density and temperature of compressed air which simulates the ground are irrelevant.

---

<sup>2</sup>The difference between a detector height 3 ft and a height of 1 meter above a plane isotropic source gives rise to a difference in dose of  $\sim 1\%$ . Hence for practical purposes the two are interchangeable.

We now designate  $D_0$  to be the detector response at the Standard Unprotected Location (sometimes called the "SUL" dose), and use  $D$  to designate the detector response at protected locations. The ratio  $D/D_0$  is referred to as a "Reduction Factor" (RF), while its reciprocal,  $D_0/D$  is called the "Protection Factor" (PF).

For sensitivity studies, one may wish to modify any of the idealizations listed above. For example, the variation of PF with spectrum can be explored with calculations not restricted to a standard spectrum. Likewise, the variation with ground roughness or ground constitution can be studied by replacing the idealization with other configurations.

## 2. Effective Mass Thickness

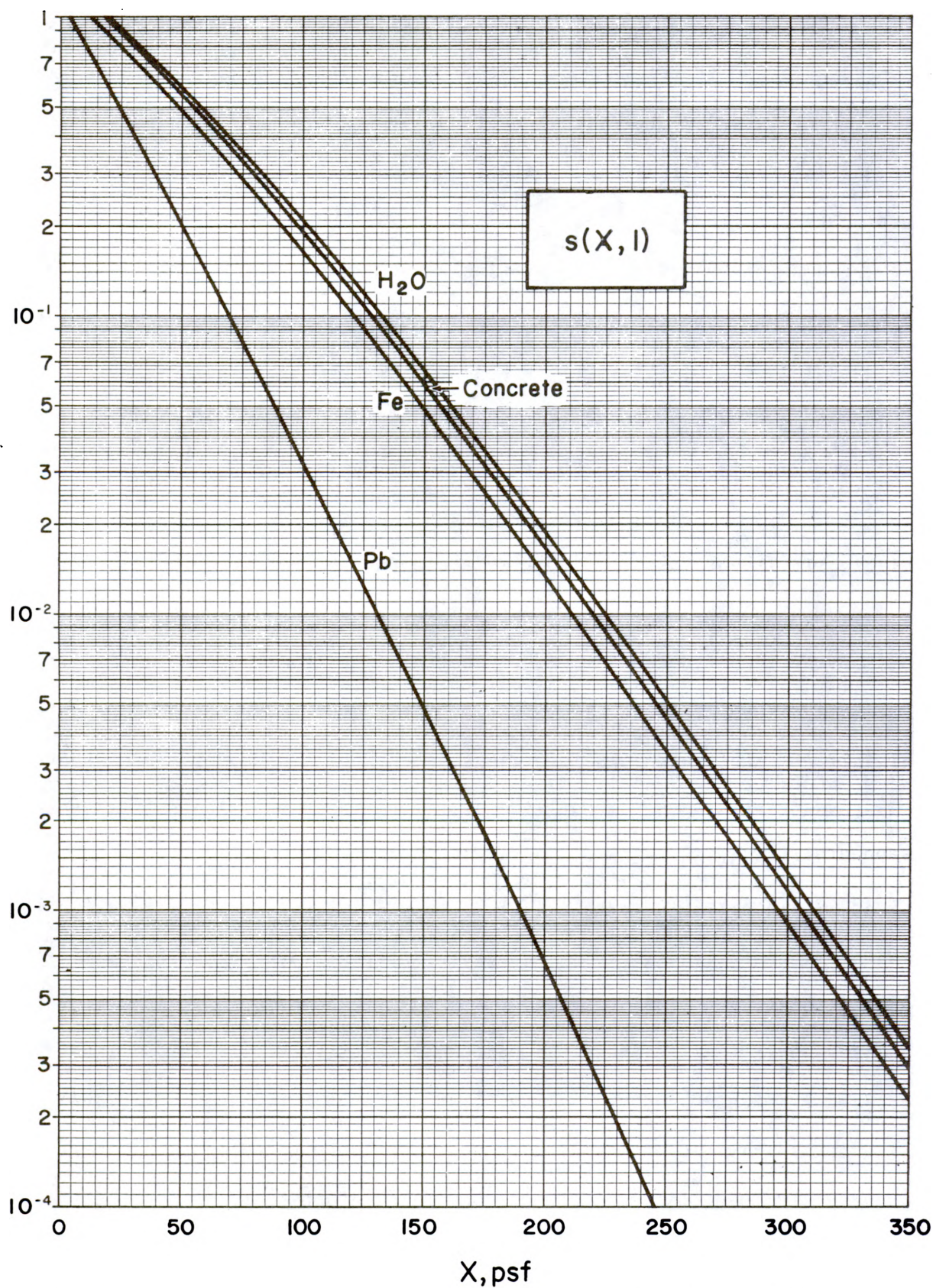
Figure III.1 shows that from 0.4 MeV to about 1.5 MeV, low-Z materials (up to Fe, with  $Z = 26$ ) are all essentially Compton scatterers, with cross sections proportional to the number of electrons per atom.

But from figure II.10 it is clear that  $1/2$  or more of the photons in typical fallout spectra fall in this range, with the 1 - 1.5 MeV region not only important to the spectrum but also sufficiently penetrating to influence strongly the attenuation properties of fallout spectra.

Also, as discussed in section IV.B.2, when the total cross section scales with electron density, attenuation data for different materials differ mainly by a proportionality factor, provided that the thickness variable is likewise measured in a unit proportional to electrons per unit area. Figure V.1 demonstrates that this proportionality holds except for small effects, and these are attributable to spectral differences below 0.4 MeV.

Construction materials are almost completely constituted of low-Z elements; and it is thus advantageous on the one hand to use a commonly understood term such as psf ( $\text{lbs/ft}^2$ ) to measure the thickness of a protective shield, while adjusting the resulting values with a dimensionless factor which renders wood,





V.1 Attenuation of 1 MeV gamma rays in different materials (plane source, initial direction of propagation normal to the source plane. Fe, concrete, and  $\text{H}_2\text{O}$  are separated by small, nearly constant factors.

water, air, iron, and concrete nearly equivalent. The parameter which we select is designated  $X$ , the "effective mass thickness", and is given by

$$X = 2 \left\langle \frac{Z}{A} \right\rangle \rho t \quad , \quad (V.1)$$

Here  $\rho$  is the density and  $t$  is the thickness of the material, and  $\langle Z/A \rangle$  refers to the average ratio of atomic charge number to atomic mass for the constituent elements,

$$\left\langle \frac{Z}{A} \right\rangle = \sum_i f_i (Z_i/A_i) \quad , \quad (V.2)$$

where  $f_i$  is the fraction of the mass due to the  $i$ 'th constituent element. The factor of 2 is introduced because  $\langle Z/A \rangle$  is very nearly 0.5 for such important construction materials as brick and concrete, so that  $2 \cdot \langle Z/A \rangle = 1$  for those materials. If this factor is considered dimensionless,  $X$  has units  $\text{lbs/ft}^2$  (psf). For many applications, then, the distinction between "effective mass thickness" and the commonly understood term "mass thickness" disappears.

Table V.1 gives the factor  $2 \cdot \langle Z/A \rangle$  for many common materials, together with the density. Table V.2 lists mass thickness values for many building components [5].

A quantity referred to as "equivalent thickness of concrete", has often been used because it is readily understood by most people. It is simply  $\rho t / \rho_{\text{concrete}}$ , where  $t$  is thickness. Because the proportionality constants illustrated by figure V.1 are so nearly unity for most construction materials, they have been almost universally ignored in the calculation of protection factors. For all except some special purpose structures,  $X$  and  $\rho t$  can both be obtained by adding contributions due to different layers of shield



Table V.1 Values of  $2\langle Z/A \rangle$ , and the density of  $\rho$ .

Material	$2\langle Z/A \rangle$	$\rho$ , Density in pcf
water	1.11	62.4
wood	1.06	34.0 (average)
air	1.0	0.076
brick	1.0	115
concrete	1.0	144
soil (depending on water content)	1.00-1.02	100 (average)
steel	0.931	480
lead <sup>a</sup>	0.791	710

<sup>a</sup>Lead is included strictly for comparison.

## V.2a Mass Thickness of Common Building Materials Used in Various Building Components

## INDIVIDUAL BUILDING MATERIALS

Item	Thickness	Weight Psf	Component
Adobe	12	116	Wall
Asbestos Board	3/16	1.7	"
Asbestos, corrugated	-	4	Roof, wall
Asbestos shingles	5/32	1.8	" "
Asphalt roofing, 3-ply ready	-	1	Roof
Asphalt roofing, 4-ply & gravel	-	5.5	"
Asphalt roofing, 5-ply & gravel	-	6.2	"
Asphalt shingles	-	2.3	"
Brick	4	39 + 1	Wall
"	8	79 + 10	"
"	12½	115 + 15	"
"	17	154 + 20	"
Clay tile shingles	-	15 + 5	Roof
Clay tile, structural	4	18	Wall
Concrete block, hollow	4	30 + 4	"
" " "	8	55 + 5	"
" " "	12	85 + 10	"
Concrete, reinforced	1	12½	
" "	12	144	
Fiber board	1/2	0.8	Wall
Fiber sheathing	1/2	0.9	"
Gypsum block	2	0.5 + 1.5	"
" "	4	12.5 + 2.5	"
Gypsum board	1/2	2.1	Wall, ceiling
Gypsum, sheathing	1/2	2.0	Wall
Marbel facing	2	25	"
Plaster, directly applied	3/4	5	Wall, ceiling
Plaster on fiber lath	1/2	5.0	" "
Plaster on gypsum lath	1/2	6.0	" "
Plaster on metal lath	3/4	6.0	" "
Plaster on wood lath	3/4	5.0	" "
Plaster, solid	2	20	Wall
" "	4	30	"
Plywood, finish	5/16	1.0	"
" "	1/2	1.5	Ceiling
Plywood, sheathing	3/8	1.1	Wall, roof
Slate	3/16	7.3	Roof
Steel, corrugated, 20 ga.	-	2	Roof, wall
Steel panel, 18 ga.	-	3.26	Wall, roof
Stone	12	130	Wall
Stone, cast, facing	2	24	"
Stucco, metal lath	3/4	9.0	"
Stucco, wood lath	3/4	8.0	"
Terra cotta facing	1	5.4	"
Wood block, flooring	3	10	Floor
Wood finish flooring	25/32	2.5	"
Wood sheathing	3/4	2.5	Floor, roof
Wood shingles	-	2.5	Roof
Wood shingles 6½ in. to weather	-	1.1	Wall
Wood siding, 8 in. bevel	-	1.5	"
Wood siding, 6 in. drop	-	2.5	"

V.2b Mass Thickness of Common Building Materials Used in Various Building Components

COMPOSITE MATERIALS

Item	Thickness Inches	Weight Psf	Component
Brick	4	-	Wall
Brick and structural clay tile	4	60	"
Ceramic tile	5/16	-	"
Ceramic tile on motar bed	3/4	11	"
" " " " "	5/16	-	Floor
" " " " "	2	-	"
Concrete, reinforced ribbed slabs (see section on components)	-	-	"
Marble or terrazzo on concrete fill	4	50	"
Plaster, hollow wall with steel studs	4	22	"
Plaster on suspended metal lath	-	10	Ceiling
Wood finish floor	3/4	-	Floor
Wood finish floor on wood sleepers	4	-	"
Lightweight concrete fill	4	23	"

V.2c Mass Thickness of Common Building Materials Used in Various Building Components

DOORS AND GLASS

Door, wood exterior, standard 3 ft-0 in X 6 ft-8 in solid core flush panel	1 3/4	4.5	Small buildings
Door, wood interior, standard 2 ft-6 in X 6 ft-8 in hollow core	1 3/8	1.9	" "
Door, wood interior, standard 2 ft-6 in X 6 ft-8 in solid core	1 3/8	4.0	" "
Door, glass, exterior, aluminum edge, standard 3 ft-0 in X 7 ft-0 in	1/4	5.1	Large buildings
Door, glass, exterior standard 3 ft-0 in X 7 ft-0 in	3/4	11.0	" "
Glass, double strength	1/8	1.6	Small buildings
Glass, plate	1/4	3.5	Large buildings

material, and are numerically almost the same except for the unusual case of large thicknesses of wood or water.

The height in air (d) is readily related to effective mass thickness (X): The effective mass thickness of 3 ft of air, at 20°C and 76 cm of Hg, is

$$X = .2257 \text{ psf} , \quad (V.3)$$

and the conversion factor is therefore

$$\frac{d}{X} = \left( \frac{3}{.2257} \right) = 13.29 \text{ ft/psf} . \quad (V.4)$$

### 3. Solid Angle Fraction ( $\omega$ )

In structure shielding problems, detectors measure radiation from barrier surfaces, and we usually assume that the spectrum and angular distribution emerging from some wall surface is independent of position of emergence. As shown in section IV.B.4, the detector response is then represented by the integral over the emergent dose angular distribution,

$$\int_{\Omega_B} d\Omega D(\vec{\omega}) , \quad (V.5)$$

where  $\Omega_B$  is the solid angle subtended at the detector by the barrier surface.

The maximum value for  $\Omega_B$  is  $2\pi$ ; hence when discussing the apparent size of walls, use of solid angle leads to the awkward maximum value of 6.283. For greater ease of interpretation we shift to use of the ratio

$$\omega = \frac{\Omega}{2\pi} , \quad (V.6)$$

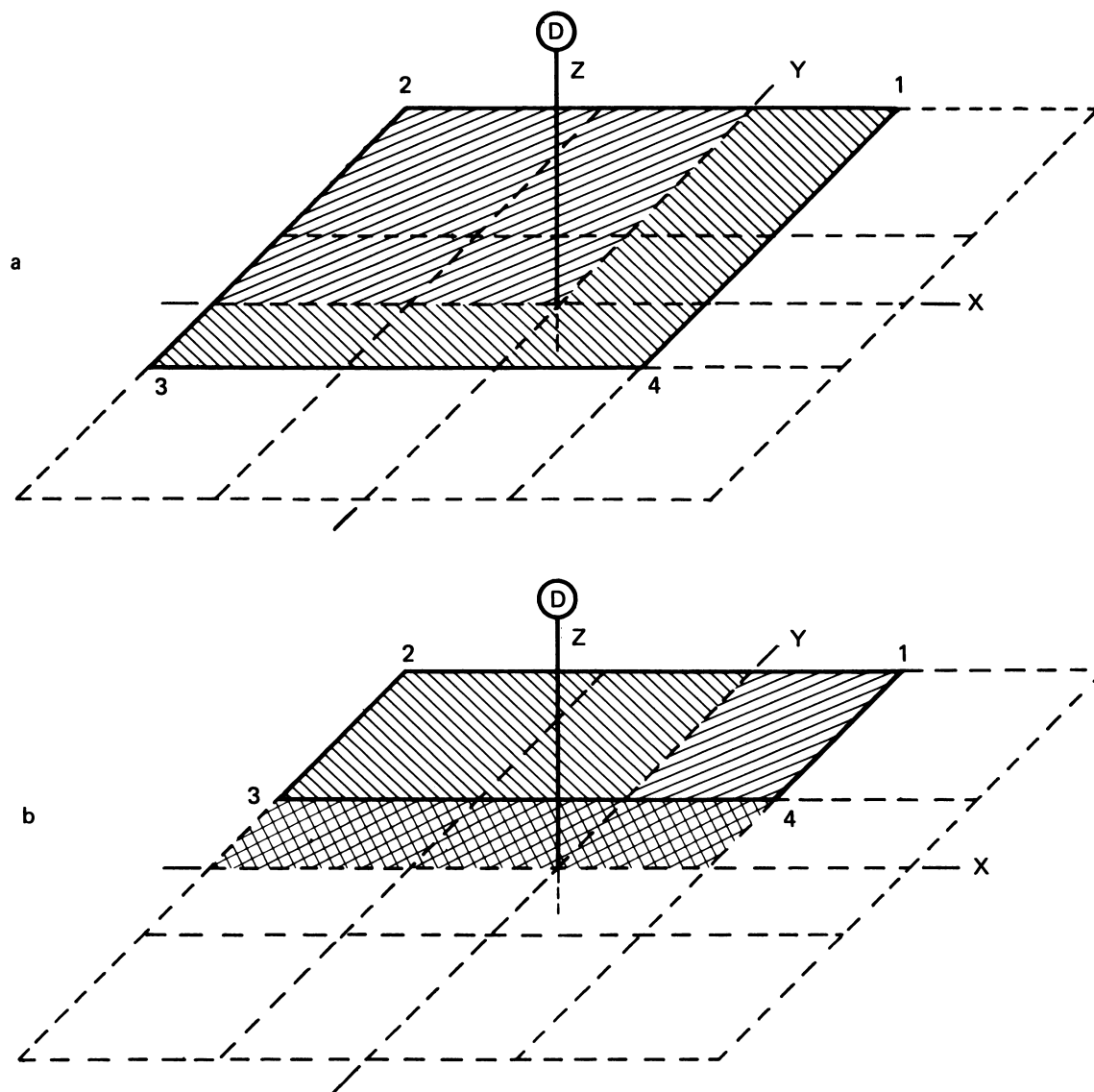
which for convenience we call the "solid angle fraction." Numerical values then usually fall between 0 and 1.

Most wall surfaces are either rectangular or representable by combinations of rectangles. Hence the solid angle fraction subtended by a rectangle is frequently required. In figure V.2 we sketch two rectangular areas and nearby detectors, with the detector position not on the perpendicular through the center of the area, but "off-center". It is clear that each corner of one of the two rectangles gives rise to a "component" rectangle whose diagonally opposite corner is at the point directly opposite the detector. From this figure it is evident that solid angle fractions for rectangular areas can be evaluated for "off-center" detector position as superpositions of data for the four component rectangles, each with the detector opposite one corner. But we find it convenient here to use data for the four rectangles which are similar to the component rectangles but 4 times larger, with the detector opposite the center, as illustrated, for example, by the dotted line extensions in figure V.2. Using such "centered-detector" data, the solid angle fraction for an off-center case is given by

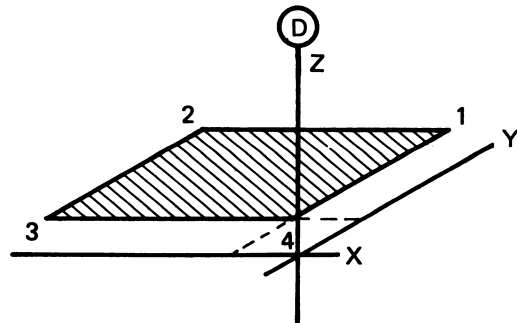
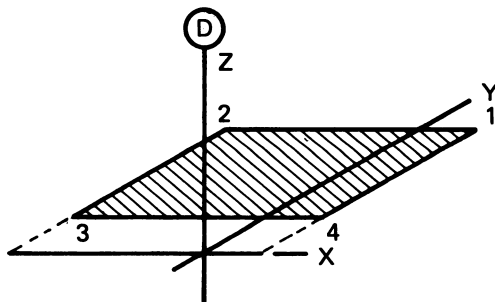
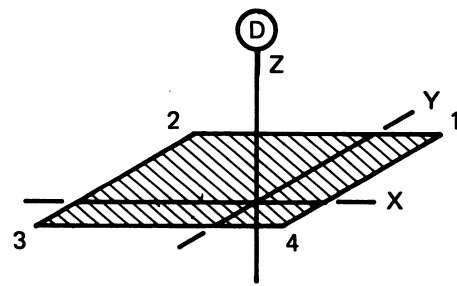
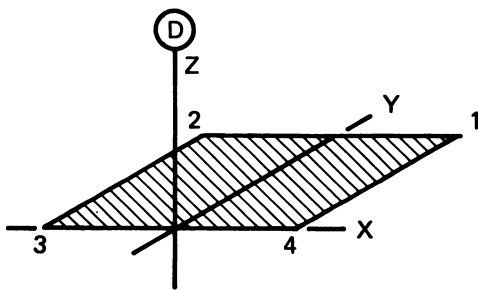
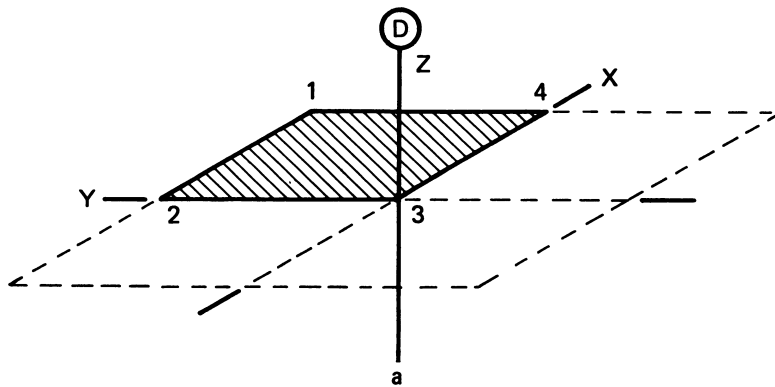
$$\Omega = \frac{1}{4} \sum_{i=1}^4 \mu_i \Omega_i, \quad (\text{V.7})$$

where  $\Omega_i$  values are "centered-detector" data, and the  $\mu_i$  values are  $\pm 1$ . Cases a-d in figure V.3 correspond to

- a)  $\mu_i = 1$ , all  $i$  values;  $\Omega_2, \Omega_3, \Omega_4 = 0$ .
- b)  $\mu_i = 1$ , all  $i$  values;  $\Omega_3, \Omega_4 = 0$ .
- c)  $\mu_i = 1$ , all  $i$  values
- d)  $\mu_1, \mu_2 = +1$ ;  $\mu_3, \mu_4 = -1$
- e)  $\mu_2, \mu_4 = +1$ ;  $\mu_1, \mu_3 = -1$ .



V.2 Source rectangles with the reference point (or detector) a) opposite an internal point, and b) opposite an external point. Corners are numbered counterclockwise, each identifying a component rectangle (dashed lines) centered below the detector and subtending four times the solid angle of a corresponding component of the rectangle under examination. In a, the components all add, while in b, components 3 and 4 subtract in order to cancel contributions from the cross-hatched area.



V.3 Rectangles with various reference point (or detector) locations:  
a) opposite a corner, b) opposite the midpoint of a side,  
c) opposite an internal point, d) opposite an external point near a side, and e) opposite an external point beyond a corner.

Data for rectangles with centered detector positions are readily obtained because the solid angle integral can be evaluated analytically for these cases. Figures V.2 and V.3 show the relevant geometry; note that  $x$  and  $y$  are half-width and half-length. If  $e = y/x$  is the eccentricity of the rectangle and  $n = z/x$  measures the scaled detector distance, then the solid angle fraction  $\omega$  is given by the function  $\tau(e,n)$ ,

$$\omega = \tau(e,n) = \frac{2}{\pi} \tan^{-1} \left( \frac{e}{n \sqrt{e^2 + n^2 + 1}} \right) . \quad (V.8)$$

Figures V.4a-d show curves of constant solid angle fraction as a function of  $e$  and  $n$ .

#### 4. Types of Shielding Factor

We distinguish between at least three types of intensity reduction ratios: Most shielding involves the interposition of a barrier between source and detector. The detector response at the position adjacent to the barrier, and on the protected side ( $B$ , in figure V.5), divided by  $D_o$ , is what we refer to as a "barrier factor."

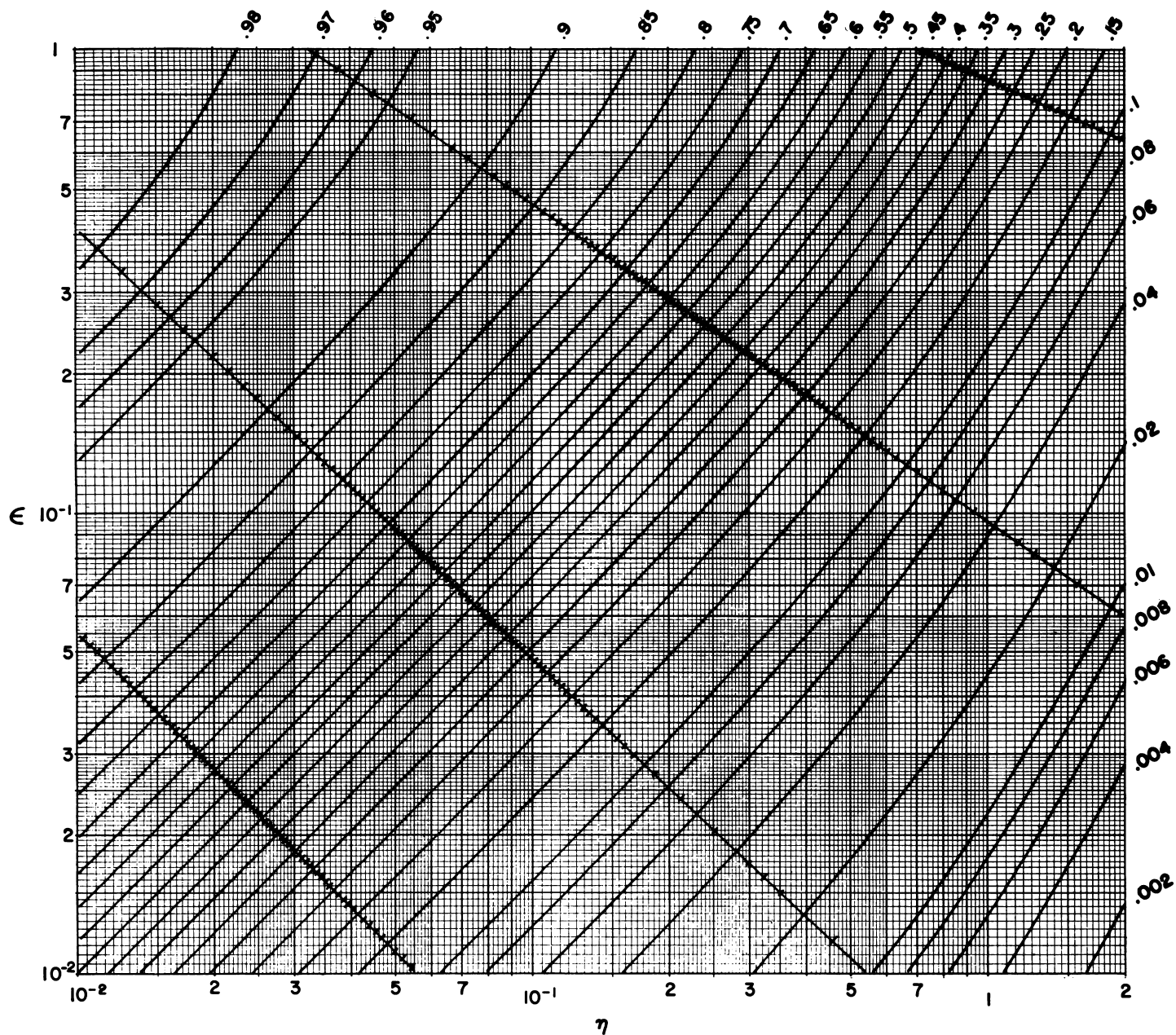
If the detector is moved to a position some distance from the barrier ( $C$ , in figure V.5), the detector response is reduced below that at  $B$ ; and the ratio of the detector response at the displaced position ( $C$ ) to that at the adjacent position ( $B$ ), exemplifies what we refer to as a "geometry factor."

Finally, there may be an internal partition, inserted, say, between  $C$  and  $B$ . Then the ratio between the detector response at  $C$  with the partition, to that without the partition would constitute an "attenuation factor."

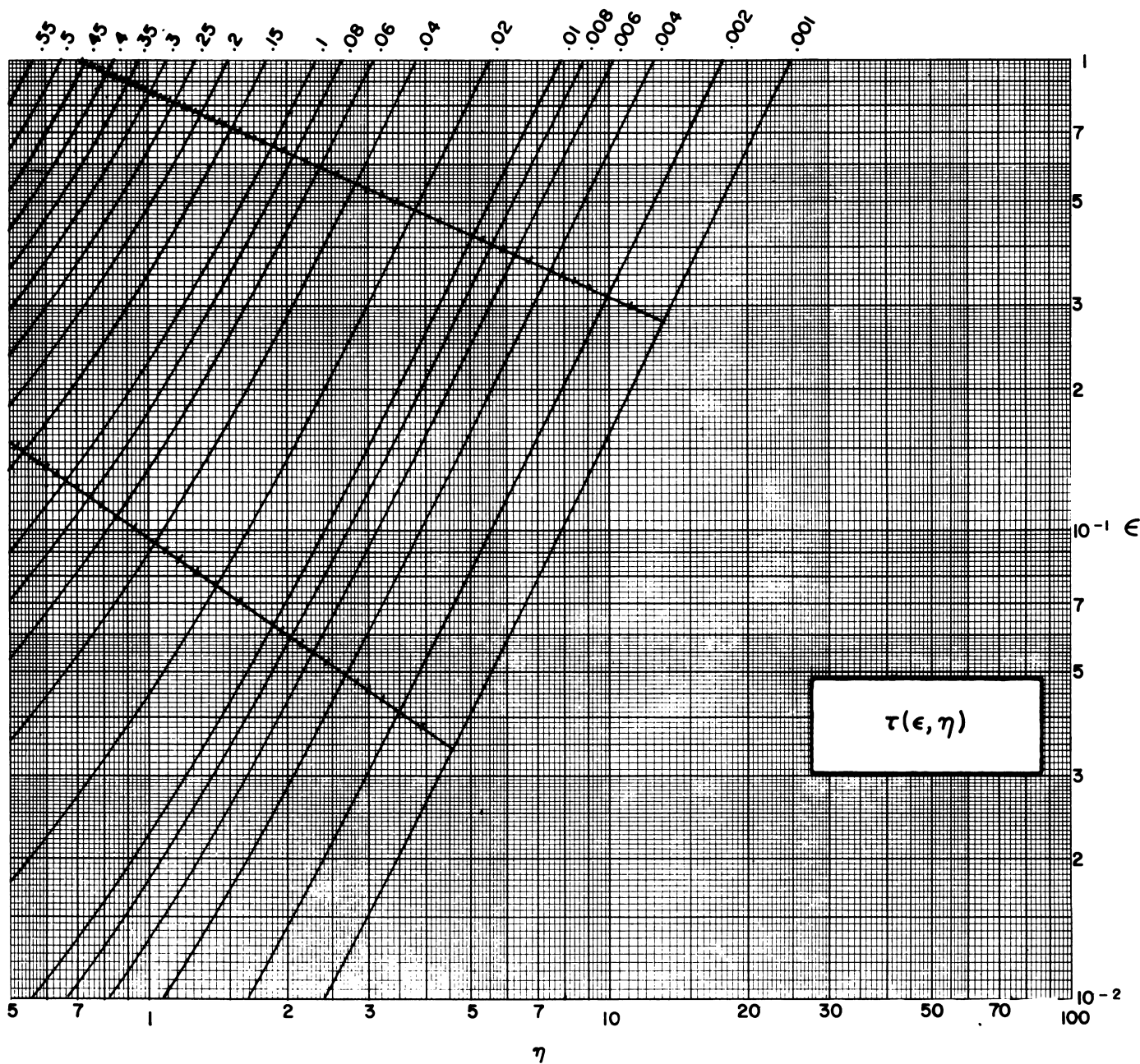
Thus the total detector response resulting from main barrier, displacement from the barrier, and perhaps an additional partition, is represented as a product

$$\text{Det. Reponse} = (\text{Att. Factor}) \cdot (\text{Geom. Factor}) \cdot (\text{Barrier Factor}) \cdot D_o \quad (V.9)$$

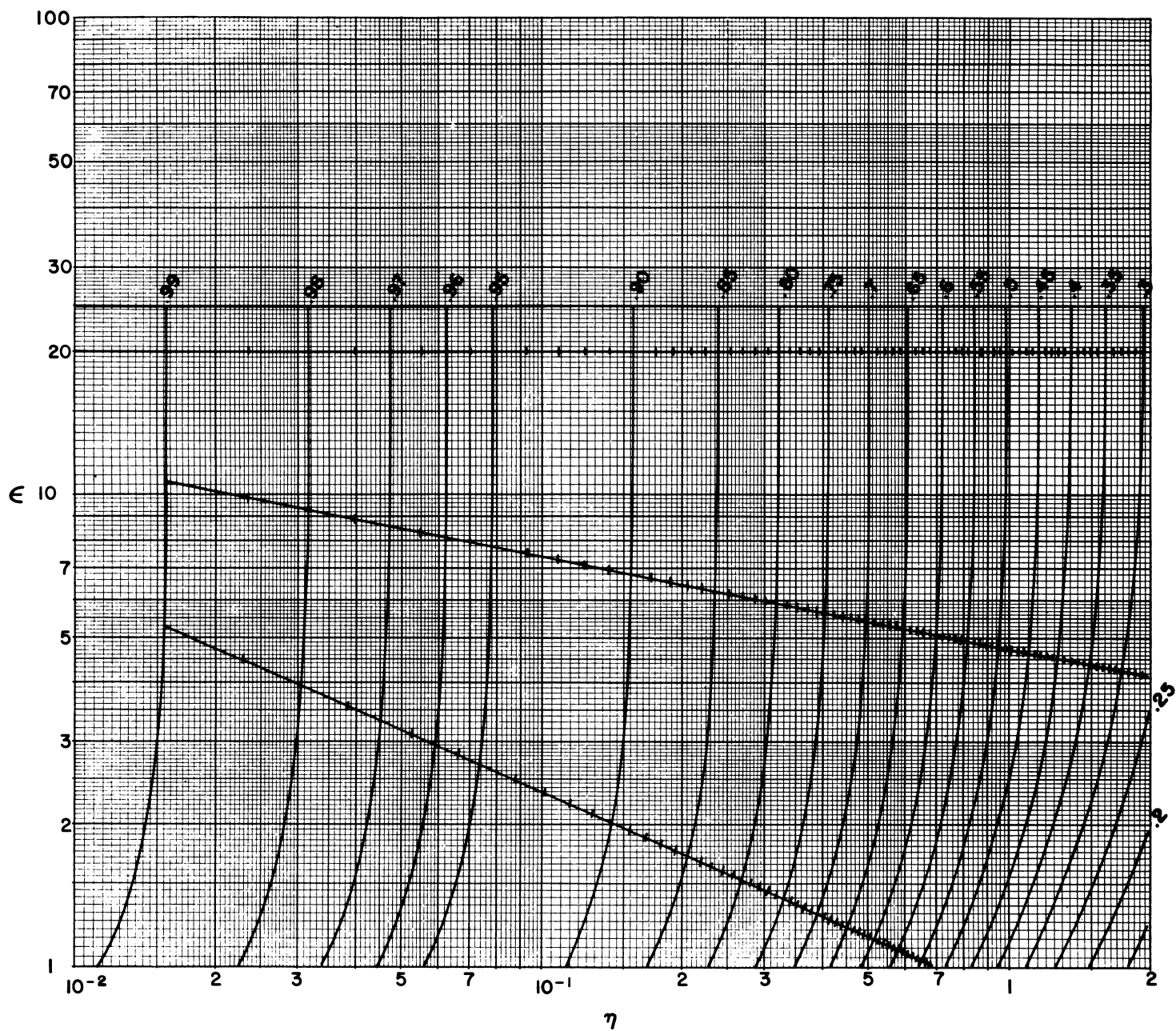




V.4.a Contours on constant  $\tau(\epsilon, \eta)$ ,  $\epsilon \leq 1$ . This function is the solid angle fraction subtended by "centered rectangles," with the longer side parallel to the  $x$  axis.

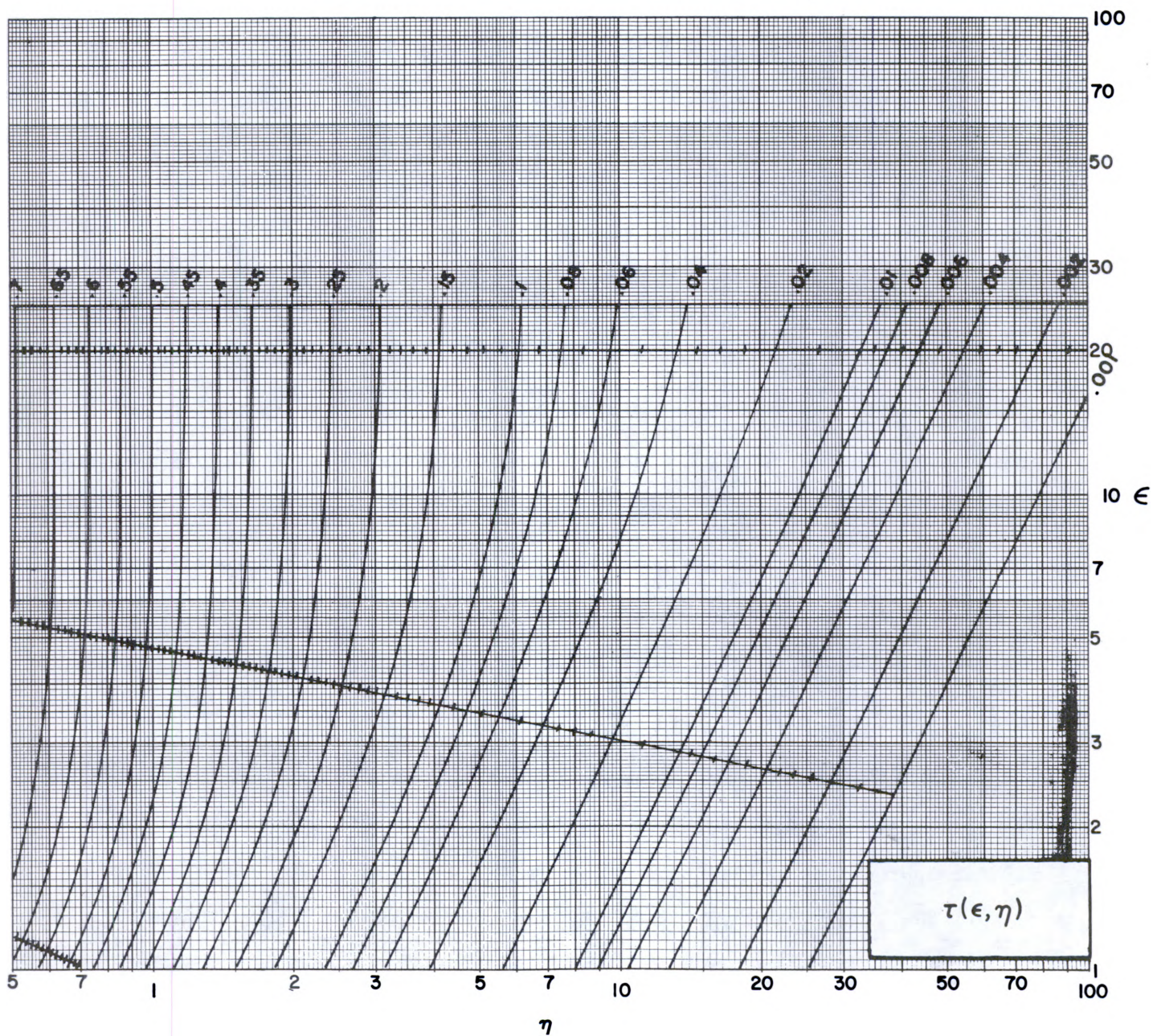


V.4.b Contours on constant  $\tau(\epsilon, \eta)$ ,  $\epsilon \leq 1$ . This function is the solid angle fraction subtended by "centered rectangles," with the longer side parallel to the  $x$  axis.



V.4.c Contours of constant  $\tau(\epsilon, \eta)$ ,  $\epsilon \geq 1$ . This function is the solid angle fraction subtended by "centered rectangles," with the longer side parallel to the  $y$  axis.





V.4.d Contours of constant  $\tau(\epsilon, \eta)$ ,  $\epsilon \geq 1$ . This function is the solid angle fraction subtended by "centered rectangles," with the longer side parallel to the  $y$  axis.

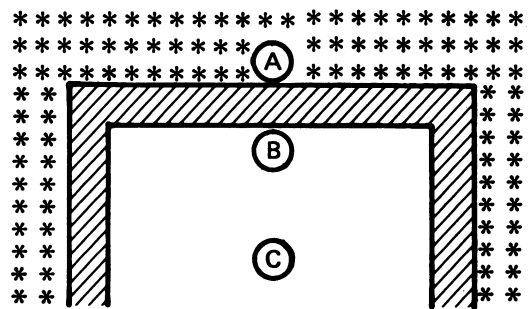
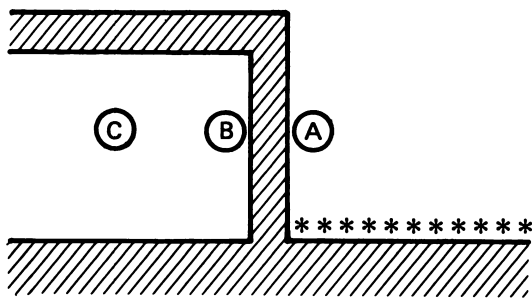
The distinguishable parts of the total detector response are the contributions due to different source components which penetrate different wall sections of the shielding structure. Hence the detector response is a sum of products like that of eq (V.9), each for a distinguishable source component and section of shielding wall.

There is an interesting contrast between geometry factors on the one hand, and barrier and attenuation factors on the other hand. The latter are basically exponential functions of the independent variable (which is usually  $X$ , the effective mass thickness). On the other hand, geometry factors are basically power law functions of distance. Commonly geometry factors are presented as functions of  $\omega$ , the solid angle fraction subtended by the wall; and their dominant trend is a power function of  $\omega$ , frequently direct proportionality. One should note that for small  $\omega$ , direct proportionality corresponds to the inverse square of the distance.

We also denote as geometry factors other intensity reduction factors whose primary variable is  $\omega$ . This will include cases in which the solid angle fraction subtended by the source at a fixed detector position is the main variable. In a sense, this geometry factor arises naturally from the adjoint approach described in section IV.E.

In addition to the main functional dependence on  $\omega$ , geometry factors usually reflect a weaker dependence on the barrier thickness,  $X$ . If we denote this explicitly with  $G(X, \omega)$ ; and if we here refer to attenuation and barrier factors as  $A(X')$  and  $B(X)$ , eq (V.9) has the following appearance:

$$D = \text{Det. Response} = A(X') \cdot G(X, \omega) \cdot B(X) \cdot D_0 \quad . \quad (V.10)$$



V.5 Detector positions A, B, and C, adjacent to vertical and horizontal walls. The sketch on the right is seen from above; the asterisks denote radioactive contamination.



### C. TYPES OF DIFFERENTIAL PENETRATION DISTRIBUTION

All distributions which follow in sections V.C.1, V.C.2, and V.C.3 are functions of a penetration variable (effective mass thickness,  $X$ , or height in air,  $d$ , and also of an angular variable (cosine of the obliquity angle at the detector,  $\cos\theta$ , or at the source,  $\cos\theta_o$ ). However, the albedo angular distribution of section V.C.4 depends only on the single variable  $\theta_o$ , which measures incident obliquity. None of these differential distributions has yet proven to be important for direct use in shielding estimates; as will be seen in section V.D which follows, geometry factor data are obtained by integrals over these distributions. The integrals which give the barrier factor data have mostly been obtained by special calculations which have yielded them directly rather than by numerical integration. (See sec. IV.D.2)

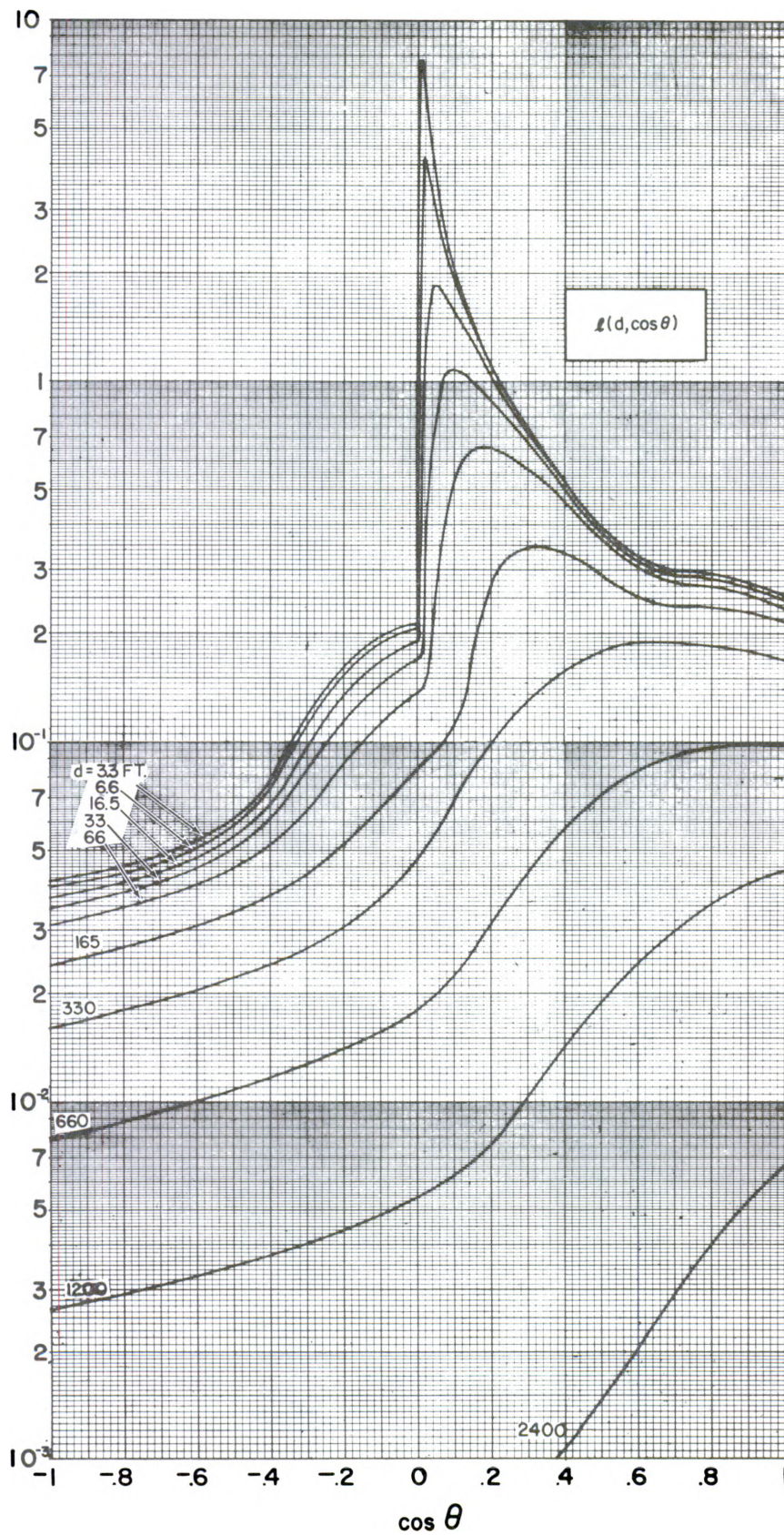
#### 1. Plane Isotropic Source ( $\ell$ )

Figure V.6 presents data for the exposure angular distribution  $\ell(d, \cos\theta)$  in air at various heights ( $d$ ) in feet above an idealized uniform plane source of fallout gamma rays, at an air/compressed-air interface (see section V.B.1). Figures B.1a and B.1b of appendix B present the same type of data for concrete and plane sources of  $^{60}\text{Co}$  and  $^{137}\text{Cs}$ , but referred to penetrations ( $X$ ) measured in pounds per square foot (psf). Calculation of these data is described in sections IV.D.3 and IV.D.4.

The normalization of the data in figure V.6 is such that

$$\int_{-1}^1 d(\cos\theta) \ell(3', \cos\theta) = 1 \quad . \quad (V.11)$$

The normalization of the data in figures B.1a, B.1b of appendix B likewise gives unity for the integral over all obliquity angles.



V.6 Dose angular distributions  $l(d, \cos \theta)$  for an idealized plane fallout source, at different heights  $d$  in air above the source plane.



The outstanding feature of these figures is the sharp peak for small barrier thickness, and for small and positive values of  $\cos\theta$ . This is due to the unscattered component, as discussed in section IV.A.4, and has mainly a  $\sec\theta \exp(-b \sec\theta)$  trend. Correspondingly, the peak approached by small negative values of  $\cos\theta$  is largely caused by the once-scattered component, which is nearly symmetric about  $\cos\theta = 0$ , for small barrier thicknesses (see sec. IV.D.2.c).

The unscattered peak is rapidly reduced with increasing penetration, with the angular distribution becoming very insensitive to height above 500 ft.

Angular distributions given in figures B.1a, B.1b of appendix B are much cruder, due to the use of a simpler and less accurate method of calculation: The oscillations for negative  $\cos\theta$ , at small penetrations, are artifacts due to the use of too few Legendre harmonics in the representation, as discussed in section IV.D.4. But revised and improved calculations for  $^{60}\text{Co}$  for  $X = .2256$  show that these oscillations do not result in more than  $\sim 20\%$  errors for negative  $\cos\theta$ , and  $\sim 5\%$  errors for positive  $\cos\theta$  (see ref. [6] and the discussion in section VI.B.3.d). Integrations to obtain geometry factors further reduce this type of error.

## 2. Point Isotropic Source ( $p$ )

We designate the dose angular distribution at a distance  $\underline{r}$  from a small source by  $p(r, \cos\theta_r)$ , where  $\theta_r$  is measured relative to the axis from detector to source.

It has proved useful to normalize  $p(r, \cos\theta_r)$  in such a manner that a uniform plane distribution of the point sources which give rise to  $p(r, \cos\theta_r)$ , generates the (plane) source strength which gives  $\ell(d, \cos\theta)$ . To translate this into an equation, we take a small differential segment  $dA$  of the source plane, which is a distance  $\underline{r}$  along a unit vector  $\vec{u}$  from a detector at

height  $\underline{d}$  above the plane. Let  $\vec{k}$  be a unit vector normal to the plane and let  $\vec{\Omega}$  be a unit vector along the photon trajectory. Then  $\cos\theta = \vec{\Omega} \cdot \vec{k}$ , and  $\cos\theta_r = \vec{\Omega} \cdot \vec{u}$ . The relationship which we require is (see eq(III.22))

$$\int \frac{dA}{4\pi r^2} p(r, \cos\theta_r) = \ell(d, \cos\theta) \quad , \quad (V.12)$$

where the integration is over the whole infinite plane. This can be further specialized by assigning  $d = 3$  ft, integrating both sides of eq (V.12) over all photon directions, and using  $dA = 2\pi\rho d\rho = 2\pi r dr$ . As a result of eq (V.11), we obtain

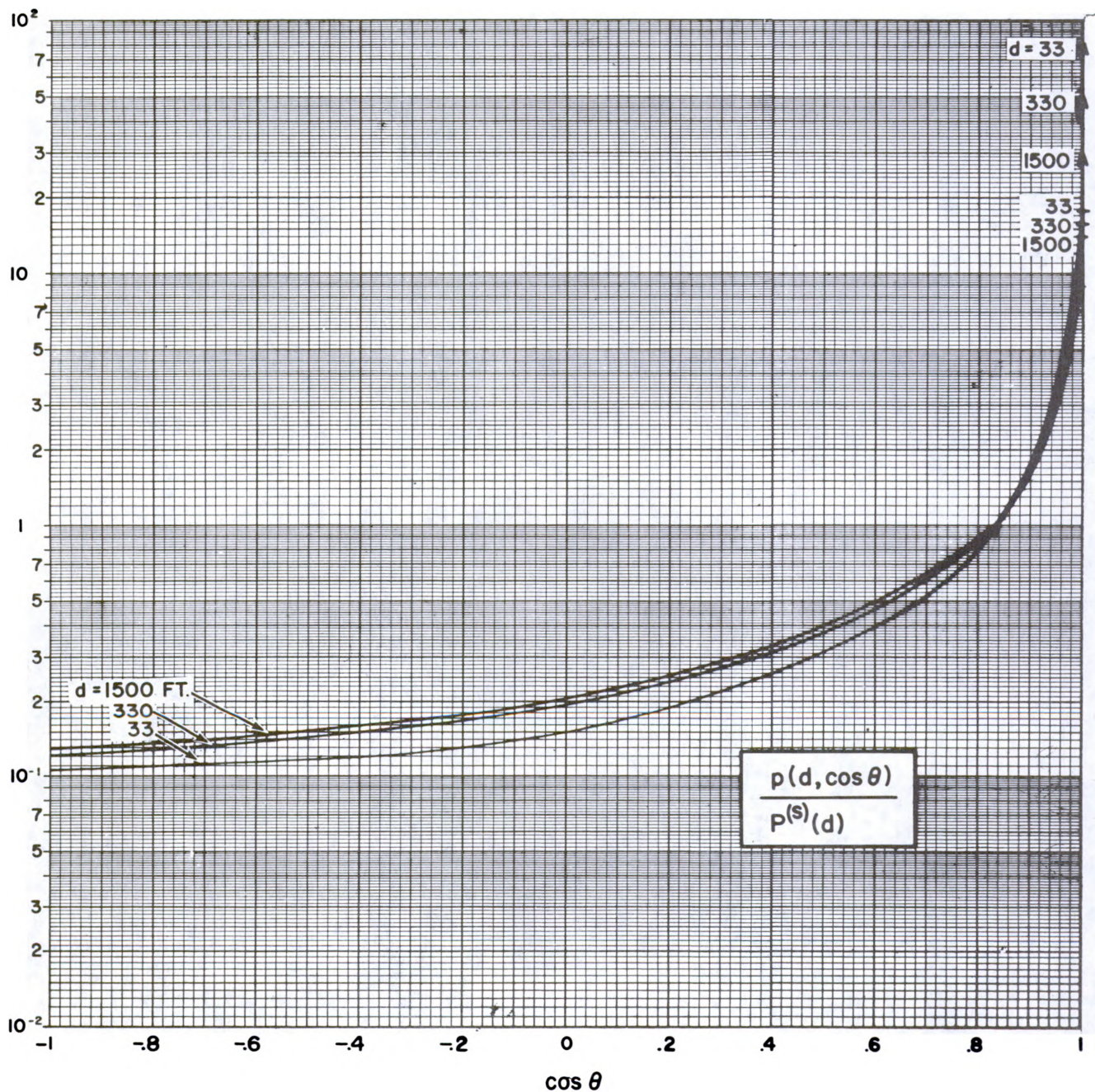
$$\frac{1}{2} \int_3^\infty \frac{dr}{r} P(r) = 1 \quad , \quad (V.13)$$

where

$$P(r) = \int_{-1}^1 d(\cos\theta_r) p(r, \cos\theta_r) \quad . \quad (V.14)$$

Figure V.7 presents curves for  $p(r, \cos\theta_r)$  as calculated for the 1.12 hr fallout spectrum. Figures B.2a and B.2b of appendix B give corresponding results for  $^{60}\text{Co}$  and  $^{137}\text{Cs}$ , respectively. In all three figures the vertical arrows represent the unscattered component, which is confined to directions radially outward from the source (i.e.,  $\cos\theta_r = 1$ ). The length of the arrows is not proportional to the dose; one can make this correlation by means of data on total dose, as given in figure V.20.

All the curves are remarkably similar, with a strong peak about the radial direction, and a comparatively low, flat tail in the radially backward direction. These features reflect both the greater probability of forward scatter, and the relatively greater energy retained by forward-scattered photons.



V.7 Dose angular distributions  $p(r, \cos \theta)$  at different distances  $r$  from a point fallout source. The arrows at  $\cos \theta = 1$  indicate the unscattered component. Their length has no quantitative significance; its strength can be obtained from figure V.20.

Two artifacts of the calculation are as follows: Oscillations in the backward direction, particularly the drop for  $\cos\theta_r \approx -1$ , are due to inadequate extrapolation of the sequence of harmonic coefficients (see the discussion in section IV.D.4).<sup>3</sup> Likewise, the angular distribution for  $\cos\theta \approx 1$  actually has a trend proportional to  $\csc\theta_r$ , as shown by eq (IV.54). The method of calculation used did not preserve this structure, but rather gave the (spurious) finite limit indicated.

### 3. Plane Oblique Source (s)

Some applications can utilize data for a plane source which emits gamma rays only at a fixed obliquity angle  $\theta_o$  relative to the normal to the source plane. The detector response at different barrier thicknesses  $X$  from such a source will be designated  $s(X, \cos\theta_o)$ ; and we should note that in addition to "forward" emission ( $\cos\theta_o > 0$ ), there can also be "backward" emission, with  $\cos\theta_o < 0$ , and "grazing" emission, with  $\cos\theta_o = 0$ .

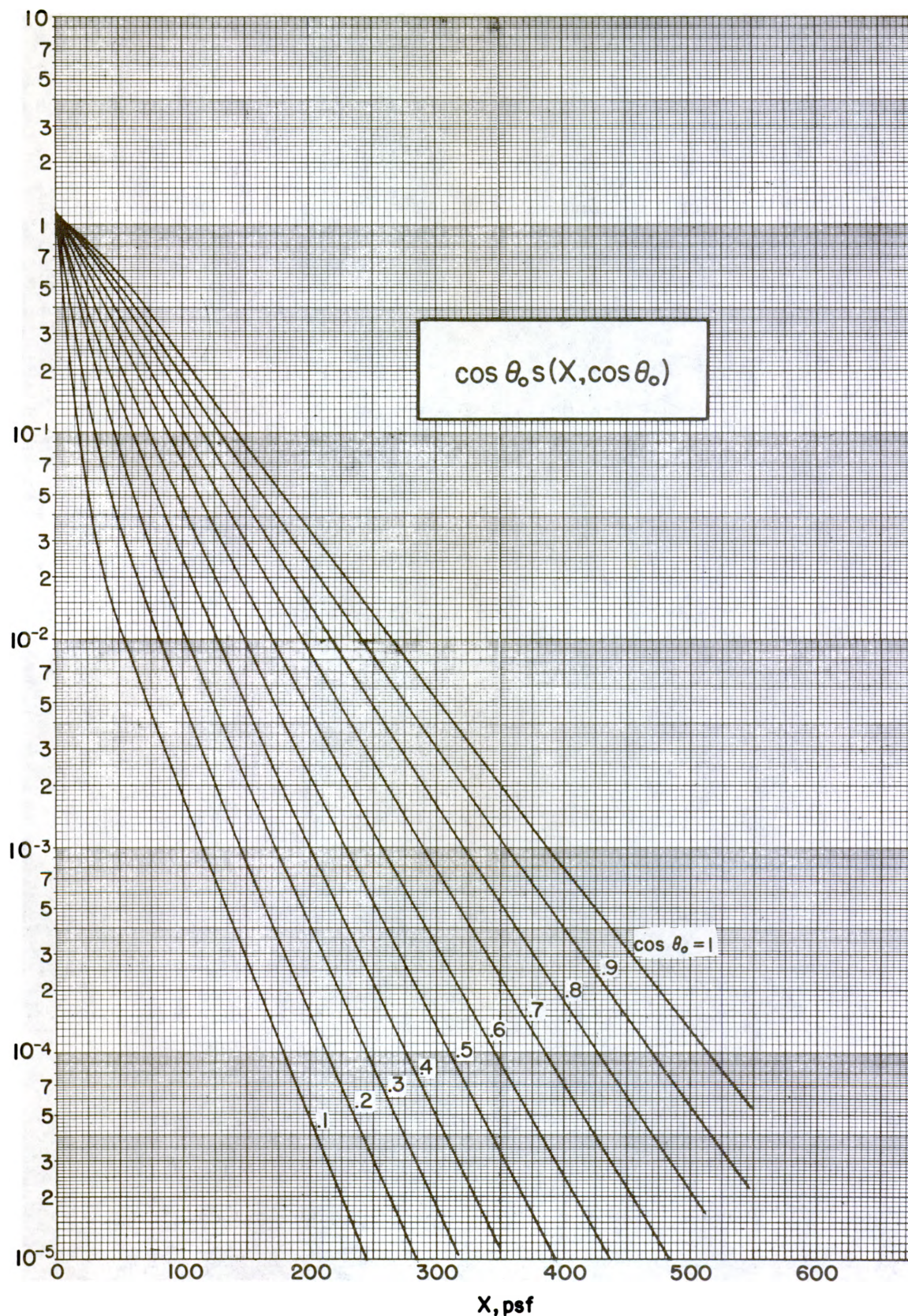
One can readily normalize this type of data relative to  $\ell(d, \cos\theta)$ , because the latter can be obtained by superposition of the  $s$  source angular results. But perhaps the main application of  $s(X, \cos\theta_o)$  is for estimation of attenuation, rather than geometry, factors. Hence we choose instead to present data normalized so that the exposure due to the source component, at the source plane, is given by  $(\cos\theta_o)^{-1}$ . This fixes the current injected into the medium by the source at unity for all  $\theta_o$ .

Figure V.8 gives the product  $\cos\theta_o s(X, \cos\theta)$  for forward emission, for the 1.12 hr fission spectrum. Figure V.9 gives the backward and grazing emission cases, but without the  $\cos\theta_o$  factor. Corresponding results for  $^{60}\text{Co}$  are presented in appendix B in figures B.3a and B.4a and those for  $^{137}\text{Cs}$  are given in figures B.3b and B.4b.

---

<sup>3</sup>These have been smoothed in drafting in figure V.7, but are evident in figures B.2a and B.2b.





V.8 Attenuation of oblique plane sources. The initial direction of propagation has angle  $\theta_0$  with respect to the normal to the source plane, with  $\cos \theta_0 > 0$ . The curves are normalized so that the unscattered component,  $s_0$ , gives  $\cos \theta_0 \cdot s_0(X, \cos \theta_0) = 1$ .



Data for all three source types are very similar qualitatively, while showing expected differences of penetrability due to the relative photon energy of the different sources. The three different source types give data which differ considerably in the amount of back-penetrating radiation, but which show similar trends because backscattering reduces the differences of both residual photon energy and attenuation coefficient.

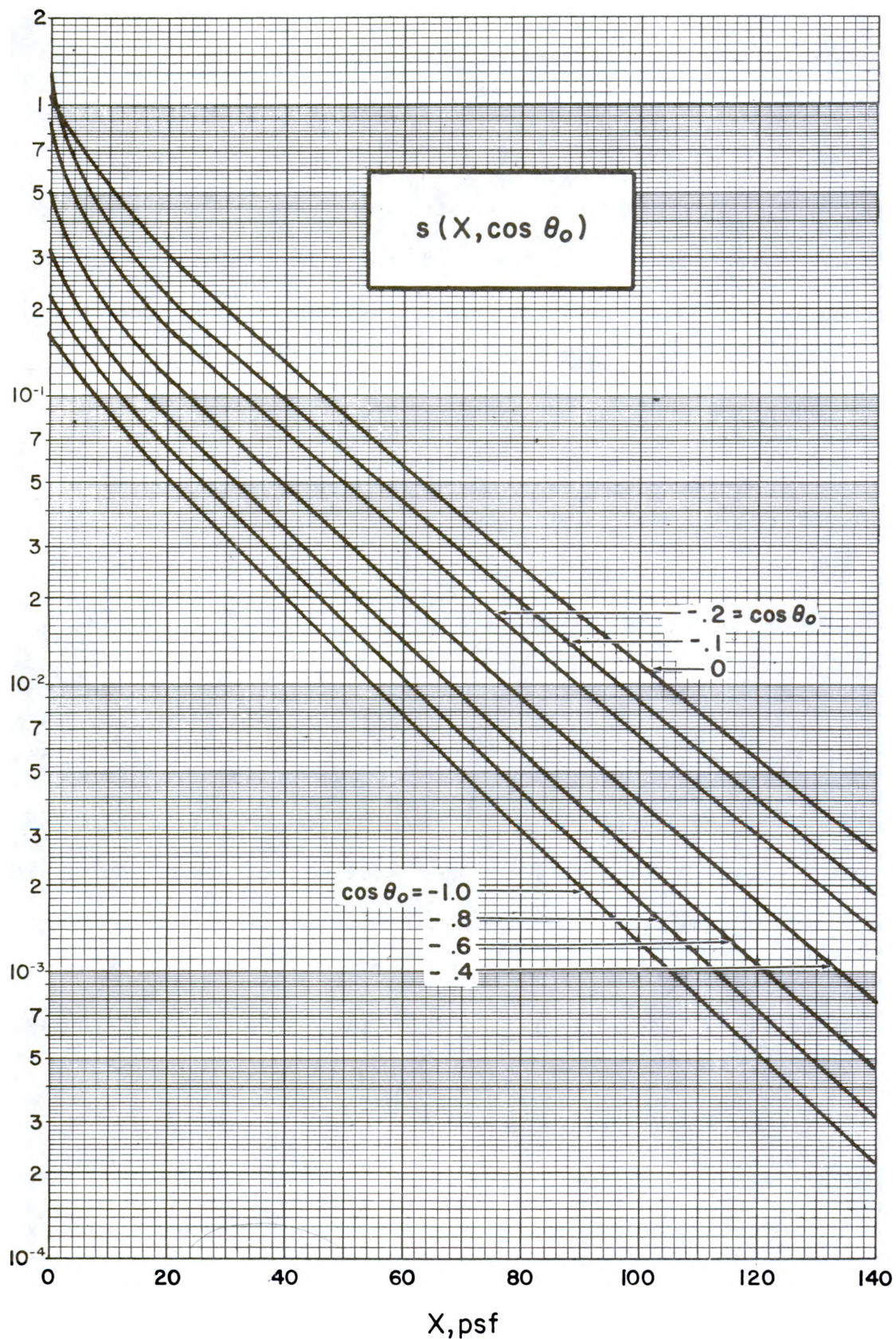
The curves for forward emission rise slightly above unity, and this effect is largest for intermediate values of  $\cos\theta_0$ . It expresses a contribution by backscattered photons at the source plane.

The major effect resulting from decreasing  $\cos\theta_0$  is a steady penetrability reduction. One should keep in mind that the integral

$$\int_0^{\infty} dX[s(X, \cos\theta_0) + s(X, -\cos\theta_0)] \quad (V.15)$$

is the same for all values of  $\cos\theta_0$ . Figures V.9 and B.4a and B.4b of appendix B do not show the unscattered component for  $\cos\theta_0 = 0$ , which is confined to the source plane,  $X = 0$ . This component must be included to apply the above integral to the grazing incidence case; but it has little relevance to shielding calculations.

All three source types show an increasing penetrability for obliquely incident photons as the thickness increases, due partly to photons which scatter to directions more nearly perpendicular to the source plane. In figure V.8 perpendicularly incident photons show a much weaker but similar effect; but because scattered photons do not then exceed the penetrability of unscattered photons, this must be due to the filtering out of all but the hardest components.



V.9 Attenuation of oblique plane sources having initial directions of propagation in the backward direction, i.e., with  $\cos \theta_0 \leq 1$ .

It is useful to establish a normalizing factor connecting  $s(X, \cos\theta_0)$  with  $\ell(X, \cos\theta)$  and  $p(X, \cos\theta)$ . We first note eq (V.13), relating the angular integral over  $\ell(X, \cos\theta)$  (designated  $L(X)$ ), with the angular integral over  $p(X, \cos\theta)$  (designated  $P(X)$ ). To simplify the required argument let us assume a monoenergetic source: For small  $X$ ,  $P(X) \rightarrow P(0)e^{-\mu_0 X}$  because the unscattered component is dominant, and for the same reason  $s(X, \cos\theta_0) \rightarrow \sec\theta_0 e^{-\mu_0 X \sec\theta_0} u(\cos\theta_0)$ , where  $u(\cos\theta_0)$  is the unit function.<sup>4</sup> By superposition,

$$L(X) = \text{const.} \int_{-1}^1 d(\cos\theta_0) s(X, \cos\theta_0) = \frac{1}{2} \int_X^\infty \frac{dX'}{X'} P(X') \quad , \quad (\text{V.16})$$

which, for  $X \rightarrow 0$ , translates to

$$\text{Const. } E_1(\mu_0 X) = \frac{1}{2} P(0) E_1(\mu_0 X) \quad .$$

Hence we conclude that

$$L(X) = \frac{1}{2} P(0) \int_{-1}^1 d(\cos\theta) s(X, \cos\theta) \quad . \quad (\text{V.17})$$

This relationship can be used to interpret some of the integral quantities derived from  $s(X, \cos\theta)$ .

#### 4. Albedo Data ( $\alpha$ )

The gamma ray albedo has already been discussed in section III. If a source is incident on a thick barrier, backscattered gamma rays will produce a dose angular distribution directed away from the slab. Hence if the dose obliquity distribution at the interface is represented by  $D(\cos\theta)$ , we define the "dose albedo", which we represent by  $\alpha$ , by means of

---

<sup>4</sup> The unit function is given by  $u(x) = \begin{matrix} 0, x < 1. \\ 1, x \geq 1. \end{matrix}$



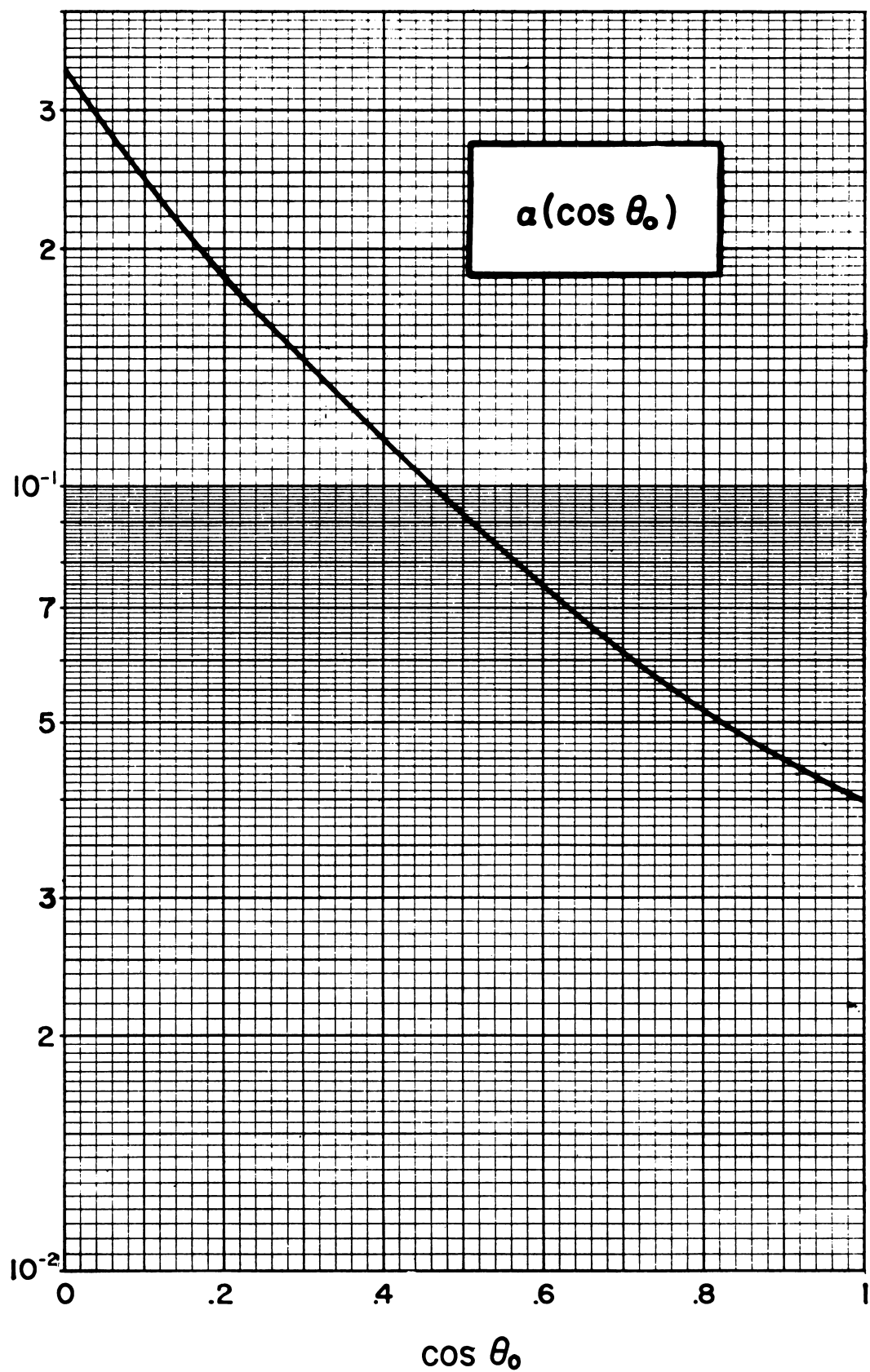
$$\alpha = \frac{\int_{-1}^0 d(\cos\theta) |\cos\theta| D(\cos\theta)}{\int_0^1 d(\cos\theta) |\cos\theta| D(\cos\theta)} \quad . \quad (V.18)$$

Figure V.10, and also B.5a and B.5b of appendix B give albedo data developed from reference [7] for sources incident at specific obliquity angles  $\theta_0$  relative to the inward normal direction. One sees clearly from these figures that the albedo increases as the source energy decreases, and that the albedo sharply increases as the source obliquity angle increases. One can relate these data to the function  $s(0, \cos\theta_0)$  previously given: note that due to multiple crossing of the source plane,  $s(0, \cos\theta_0)$  is 3 to 4 times larger than  $\alpha$  for all incident angles, but the trend with incident angle is similar.

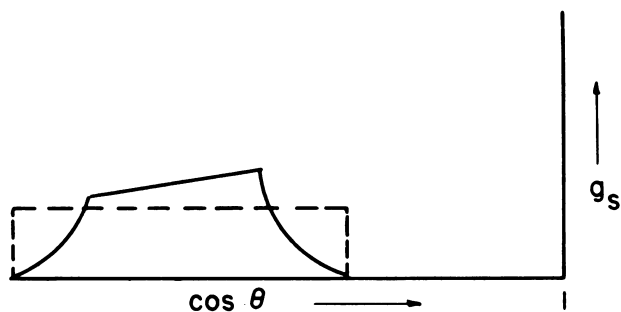
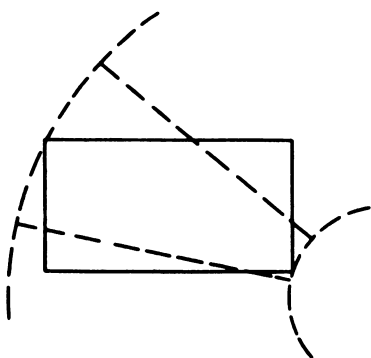
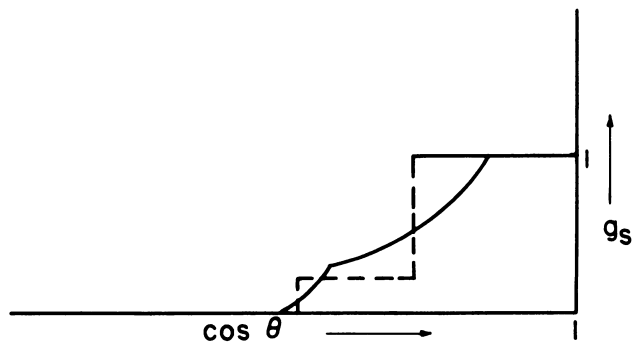
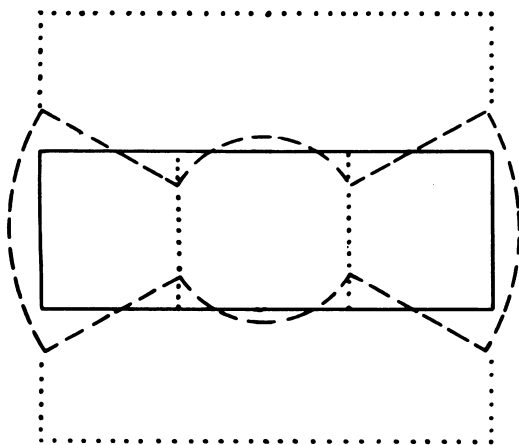
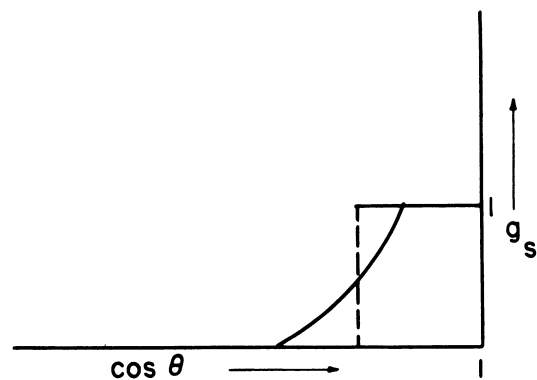
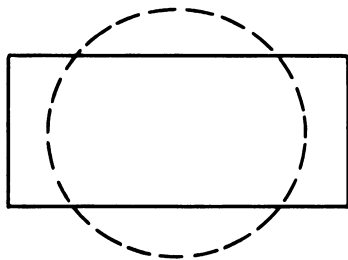
#### D. INTEGRAL SHIELDING DATA: STANDARD FISSION PRODUCT SOURCE

##### 1. Reduction Factors for Plane Isotropic Sources (L)

The geometry factor data which follow correspond to circular barriers, with no dependence on the  $e$  and  $n$  parameters used in section V.A.3 to describe rectangles. It is possible quite generally to approximate rectangles and other complex surface shapes with circular sector data. Figure V.11 demonstrates how this is done: In all three examples the solid angle of the dashed figure is intended to equal that of the rectangle. In a), a single circle is used to approximate a fairly elongated (but centered) rectangle. In b), two circular sections are used to approximate a still more elongated (but centered) rectangle. In c), part of a circular ring is used to approximate an off-center rectangle. One should note that arbitrarily accurate approximations are possible providing one uses an arbitrarily large number of circular sectors; no basic accuracy limitation exists beyond that imposed by round-off errors in the calculation of a difference quantity.



V.10 Dose albedo for gamma rays obliquely incident on concrete, as functions of the angle  $\theta_0$  between angle of incidence and inward normal for the barrier.



- V.11 Approximation of a "centered rectangle" by circles and annular sectors:  
 a) neglecting elongation, b) taking elongation into account in a simple two-term approximation, and c) using an annular sector to represent an off-center case. The graphs on the right show qualitatively how the fraction of total (i.e.,  $2\pi$ ) azimuth within the rectangle (solid curves) compares with that within the approximation (dashed curves.)

Cylinders have often been used to approximate square or rectangular structures. This approach tends to make direct use of the type of data recorded here, as will be evident in later chapters.

A better estimate for small parts of complex or elongated surfaces can be obtained by the product of solid angle fraction times a midpoint value from the  $\ell(x, \cos\theta)$  curves, or one of the other differential dose distributions, though such small contributions may not be very important.

#### a. Barrier Factors

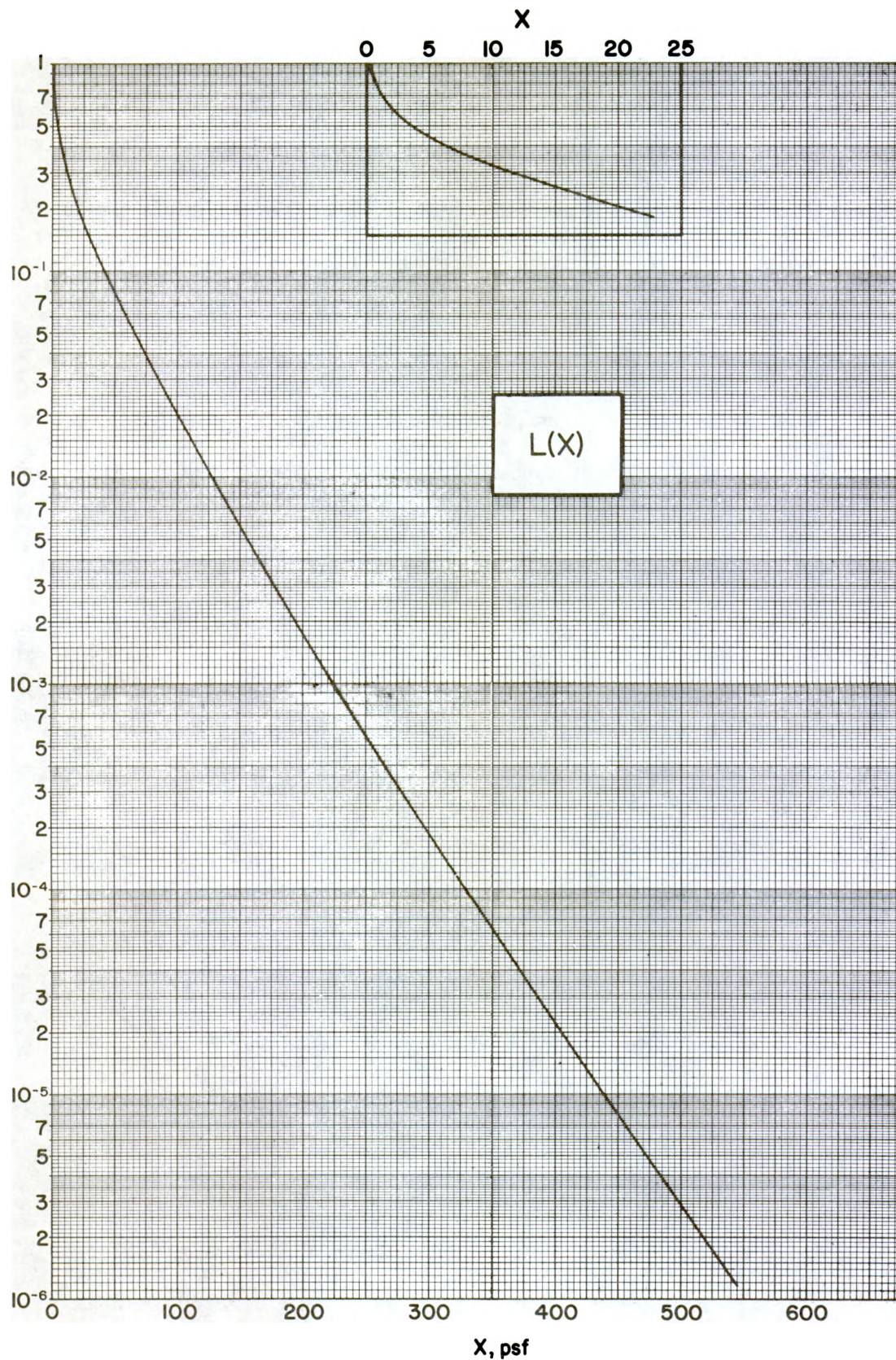
The first basic barrier factor for this type of source,  $L(X)$ , given by

$$L(X) = \int_{-1}^1 d(\cos\theta) \ell(X, \cos\theta) \quad , \quad (V.19)$$

denotes the total dose relative to the dose  $D_0$  at the Standard Unprotected Location.  $L(d)$  is similarly defined. Figure V.12 reproduces  $L(X)$  data from [1].  $L(d)$  data, for different heights in air above a contaminated interface, is also useful and is given in figure V.13. (See also figures B.6a,b and B.7a,b in appendix B.)

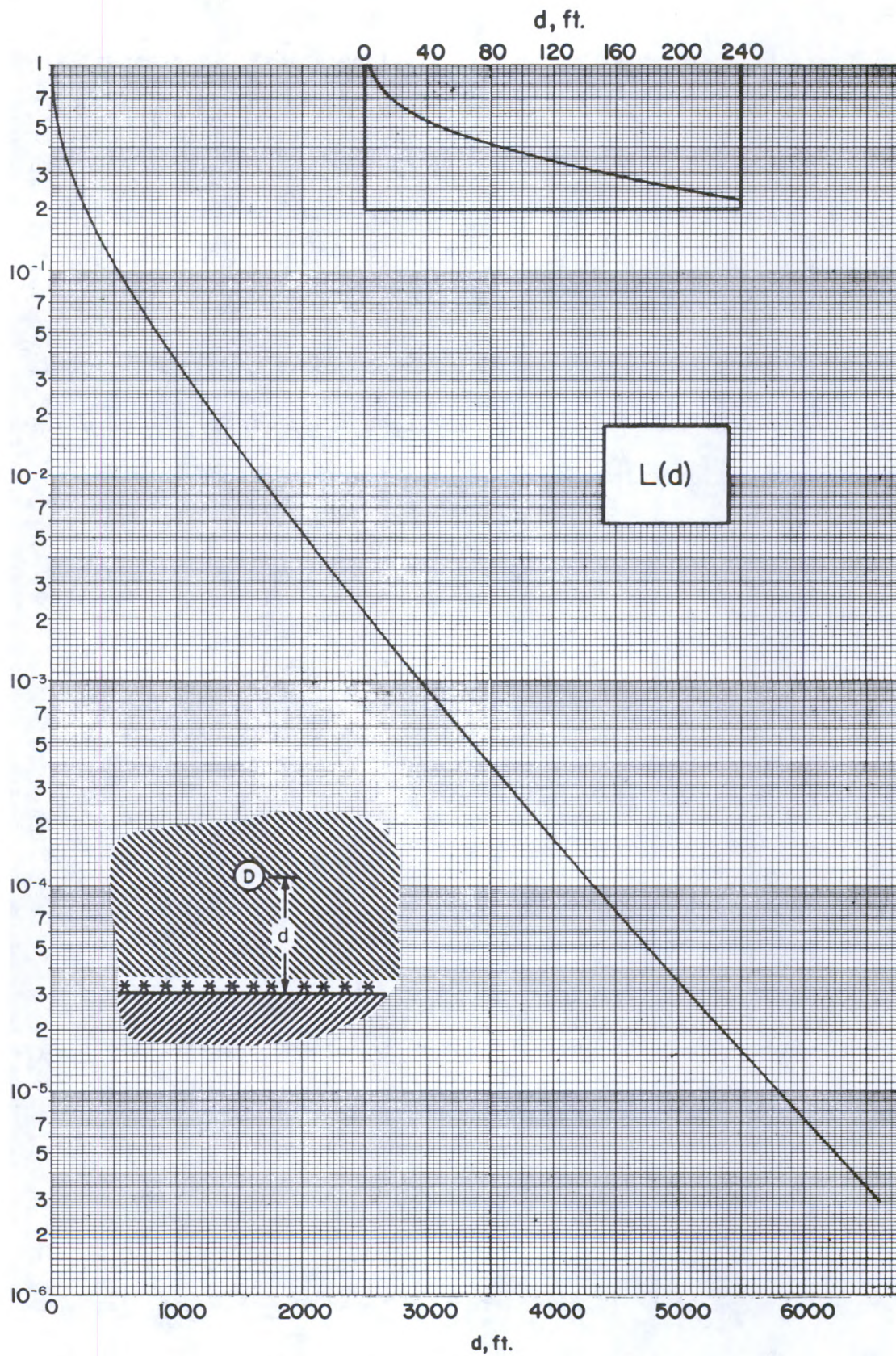
One might recall that despite the preceding definition of  $L(X)$ , the data presented in figures V.12 and V.13 were not obtained by such an integration, but were constructed directly from the moments as described in section IV.D.3. Examination of these curves shows that they exhibit the general characteristics of the exponential integral (see section IV.A.4) -- i.e., a rapid decrease with increasing depth close to the source and an exponential asymptomatic trend at great depths. The curves shown are known to diverge in proportion to  $-\log(X)$  as  $X \rightarrow 0$ . But even small irregularities in real surfaces are sufficient to interfere with this divergence, as is discussed in section VI.D. Hence the divergence has no real existence, although the sharp rise is important.





V.12 Attenuation of a plane source of fallout radiation by a barrier of effective mass thickness to attenuation in  $\text{H}_2\text{O}$ . (See also figs B.6a,b.)





V.13 Attenuation of a plane source of fallout radiation by a layer of air of thickness  $d$  ft. The data are the same as for figure V.12, but rescaled. (See also figs B.7a,b.)

It is of practical interest that the radiation intensity decreases as rapidly with height as is shown. Ground roughness has the consequence that one never really sees this sharp a trend near the ground, but it is clear that air has a very significant shielding capability for radiation incident on upper stories of buildings due to distant sources.

#### b. Geometry Factors

Three types of geometry factors have been derived from the  $\ell$  data for plane isotropic sources. The first (designated  $L_a$ ) is simply the cumulative integral of the angular distribution given as a fraction of the total dose:

$$L_a(X, \omega) = \frac{1}{L(X)} \int_{1-\omega}^1 d(\cos\theta) \ell(X, \cos\theta) \quad . \quad (V.20)$$

The second type of geometry factor (designated  $L_b$ ) is a cumulative integral over the source angular distribution, given as a fraction of the total dose. Referring to eq (V.17) we write

$$L_b(X, \omega) = \frac{P(0)}{2L(X)} \int_{1-\omega}^1 d(\cos\theta_o) s(X, \cos\theta_o) \quad . \quad (V.21)$$

A third type of geometry factor (designated  $L_c$ ) corresponds to circular sources which subtend the solid angle fraction  $\omega$  at the detector location on the centerline of the circle:

$$L_c(X, \omega) = \frac{1}{L(X)} \left\{ L(X) - L\left(\frac{X}{1-\omega}\right) \right\} \quad . \quad (V.22)$$

The two terms in braces in eq (V.22) correspond to source-free circular areas subtending solid angle fractions 0 and  $\omega$ , respectively. Note that the arguments  $X$  and  $\left(\frac{X}{1-\omega}\right)$  give the barrier thickness between the detector, and



the center and periphery, respectively, of the circle in question. The difference between terms thus refers to exposure due to a circular source region.

Figures V.14, V.15, and V.16 give these three geometry factors, which have striking similarities. The limiting value for  $\omega = 1$  in the case of  $L_a$  is less than unity because the backscattered component is given by  $1 < \omega < 2$ , which is not shown. Likewise,  $L_b \rightarrow 1$  only as  $\omega \rightarrow 2$ , because of source components initially directed away from the detector.

Uncertainty of the  $L_a$ ,  $L_b$ , and  $L_c$  data shown have been estimated [6] at  $\sim 5\%$  for  $\omega \approx 1$ , and  $\sim 5\%$  for  $L_b$ ,  $L_c$  for  $\omega \rightarrow 0$ . For  $\omega \rightarrow 0$ ,  $L_a$  is not as accurate ( $\sim 15\%$  uncertainty.)

All three geometry factors tend to become proportional to  $\omega$  as  $\omega \rightarrow 0$ ; this is a general rule holding for other source spectra and simply expressing the equivalence of different elements comprising small sources.

Figure V.17 presents data for the product  $L(X) \cdot L_a(X, \omega)$ , corresponding to the full reduction due to a wall barrier, and hence useful for reference purposes. Similar figures for  $L \cdot L_b$  and  $L \cdot L_c$  are given in reference [1].

Figures B.8a,b to B.11a,b give corresponding geometry factors for  $^{60}\text{Co}$  and  $^{137}\text{Cs}$ .

## 2. Reduction Factors for Point Isotropic Sources (P)

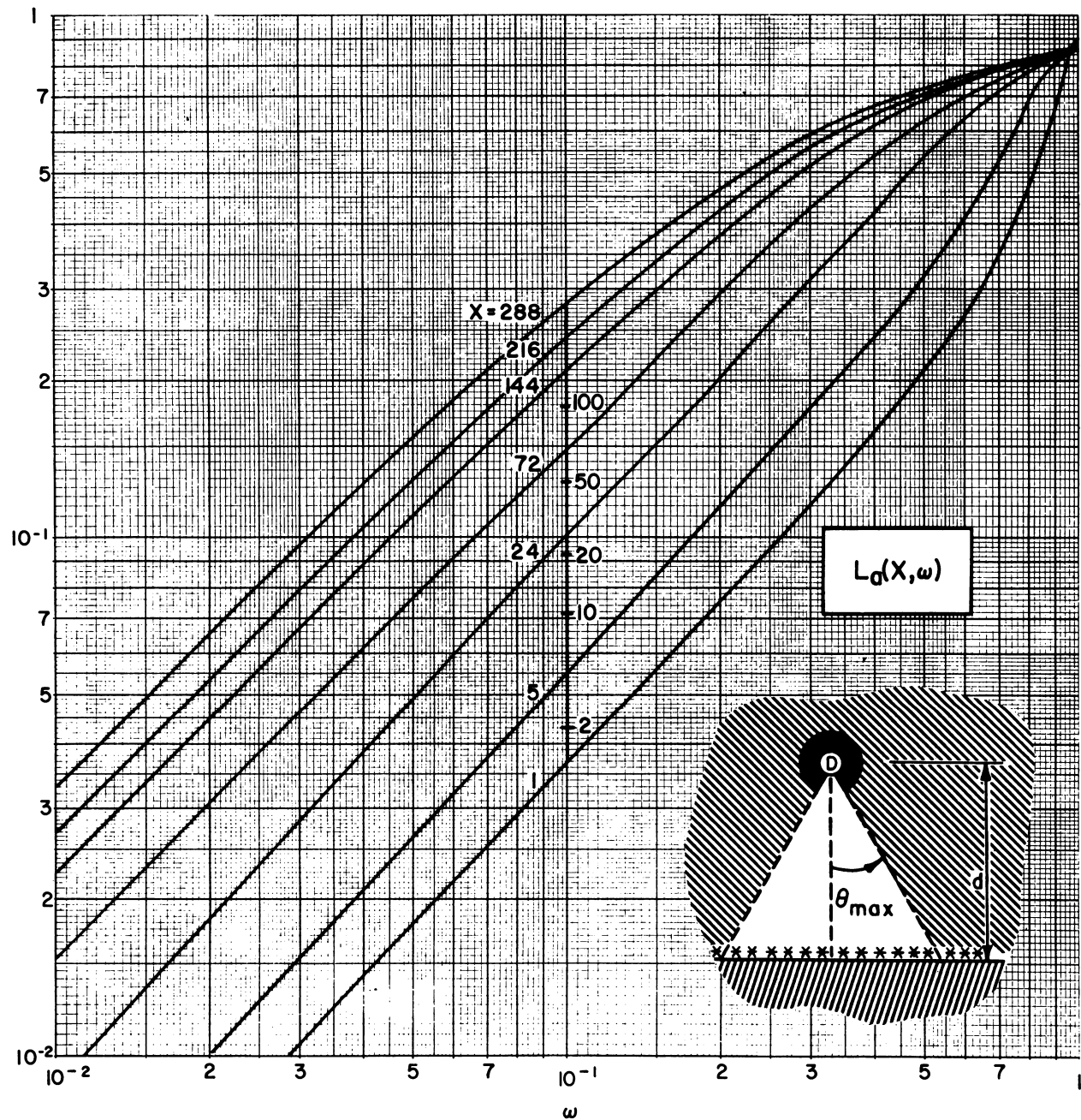
### a. Barrier Factors

This type of barrier factor has been designated  $P(d)$  in eq (V.14); equivalently,

$$P(X) = \int_{-1}^1 d(\cos\theta_r) p(X, \cos\theta_r) \quad . \quad (V.23)$$

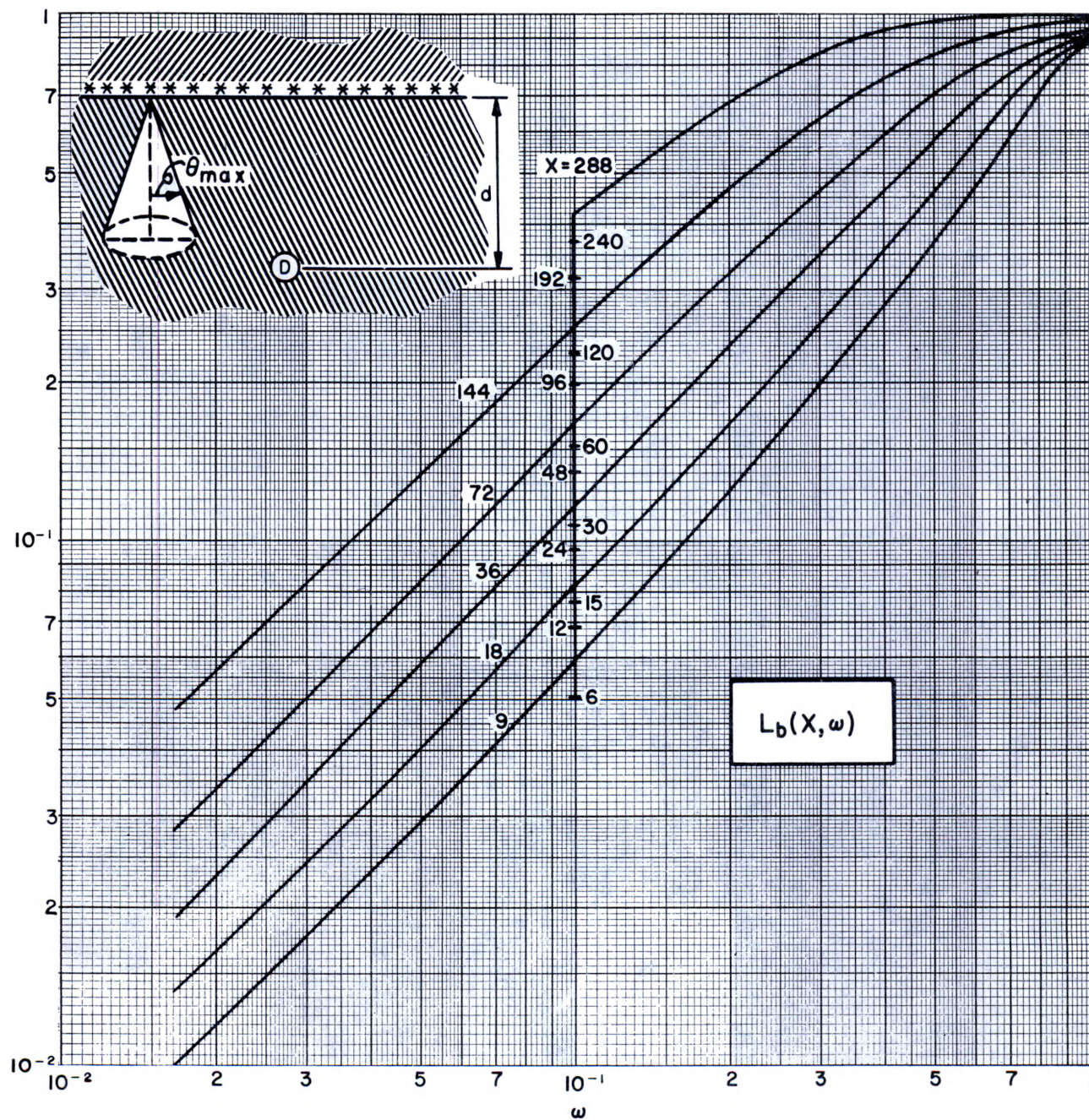
It turns out to be useful also to record unscattered and scattered components,  $P^{(o)}(X)$  and  $P^{(s)}(X)$  respectively. Figure V.18 gives data for  $P(d)$ ,





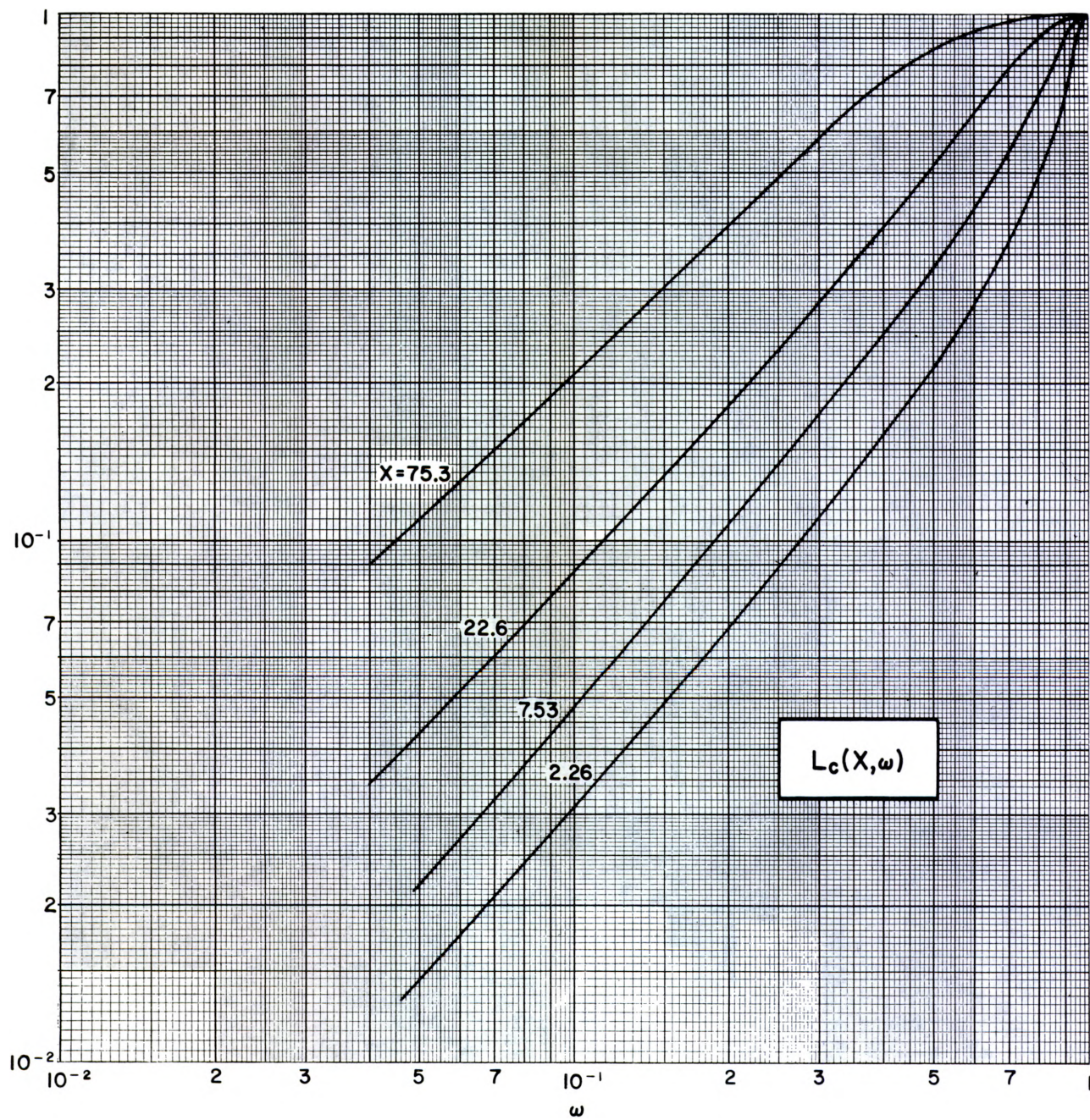
V.14 Geometry factor for detector response to radiation striking the detector from a limited cone of directions, and resulting from a plane isotropic source of fallout gamma rays. (See also figs B.8a,b.)





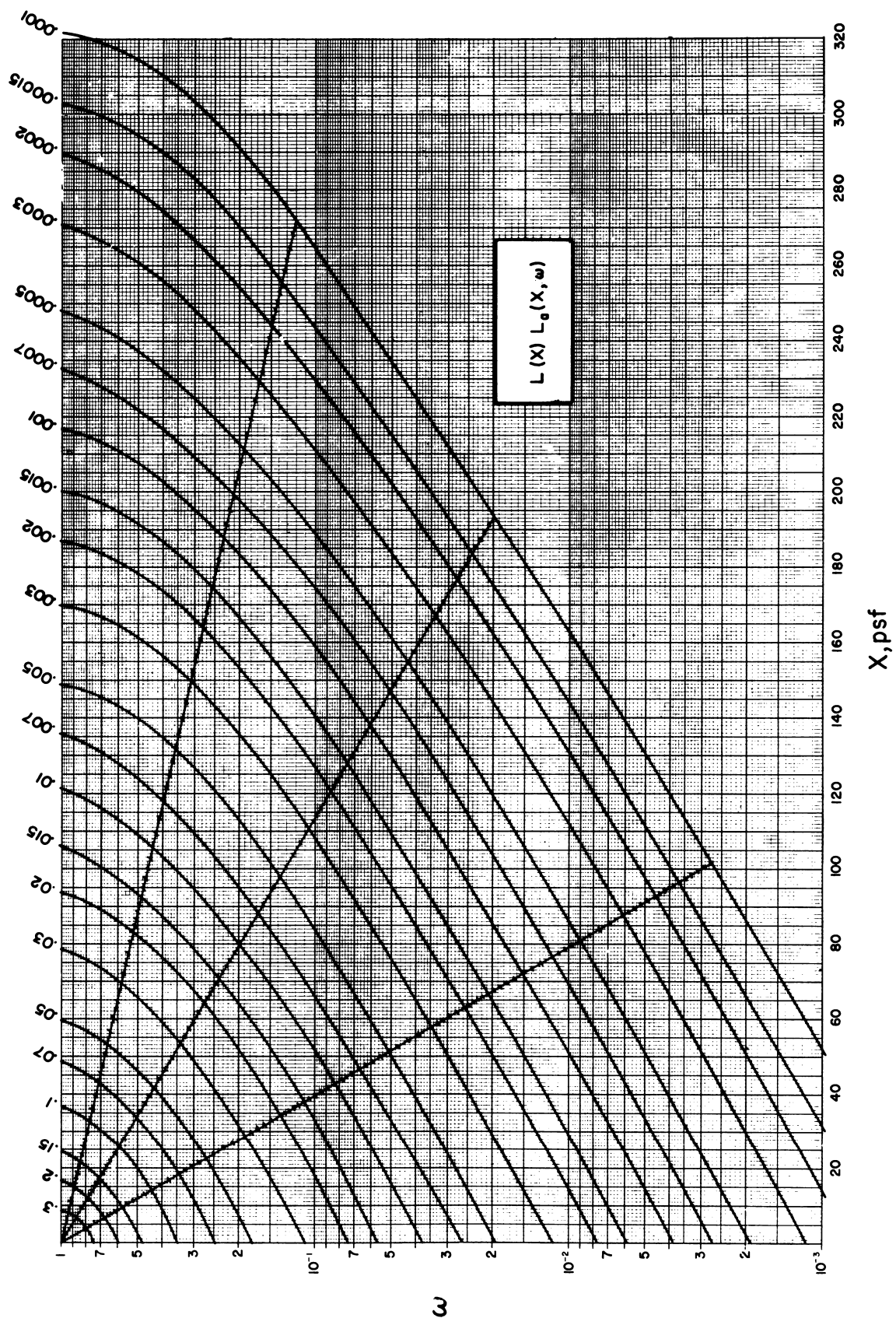
V.15 Geometry factor for response of an isotropic detector near a plane source emitting fallout gamma radiation in a limited cone of directions. (See also figs B.9a,b.)





V.16 Geometry factor describing detector response due to circular plane isotropic sources of fallout gamma radiation. (See also figs B.10a,b.)





V.17 Contours of constant  $L(X)L_a(X, \omega)$ , fallout gamma radiation in  $H_2O$ .  
(See also figs B.11a,b.)

while figures V.19 and V.20 give corresponding data for  $P(X)$  and its two components.

Data for  $^{60}\text{Co}$  and  $^{137}\text{Cs}$  are given in figures B.12a,b to B.14a,b.

#### b. Geometry Factors

Two types of related geometry factors have been defined. The first,  $P_a^{(s)}$ , is defined by

$$P_a^{(s)} = \frac{1}{P^{(s)}(d)} \int_{1-\omega}^1 d(\cos\theta_r) P^{(s)}(d, \cos\theta_r) \quad , \quad (\text{V.24})$$

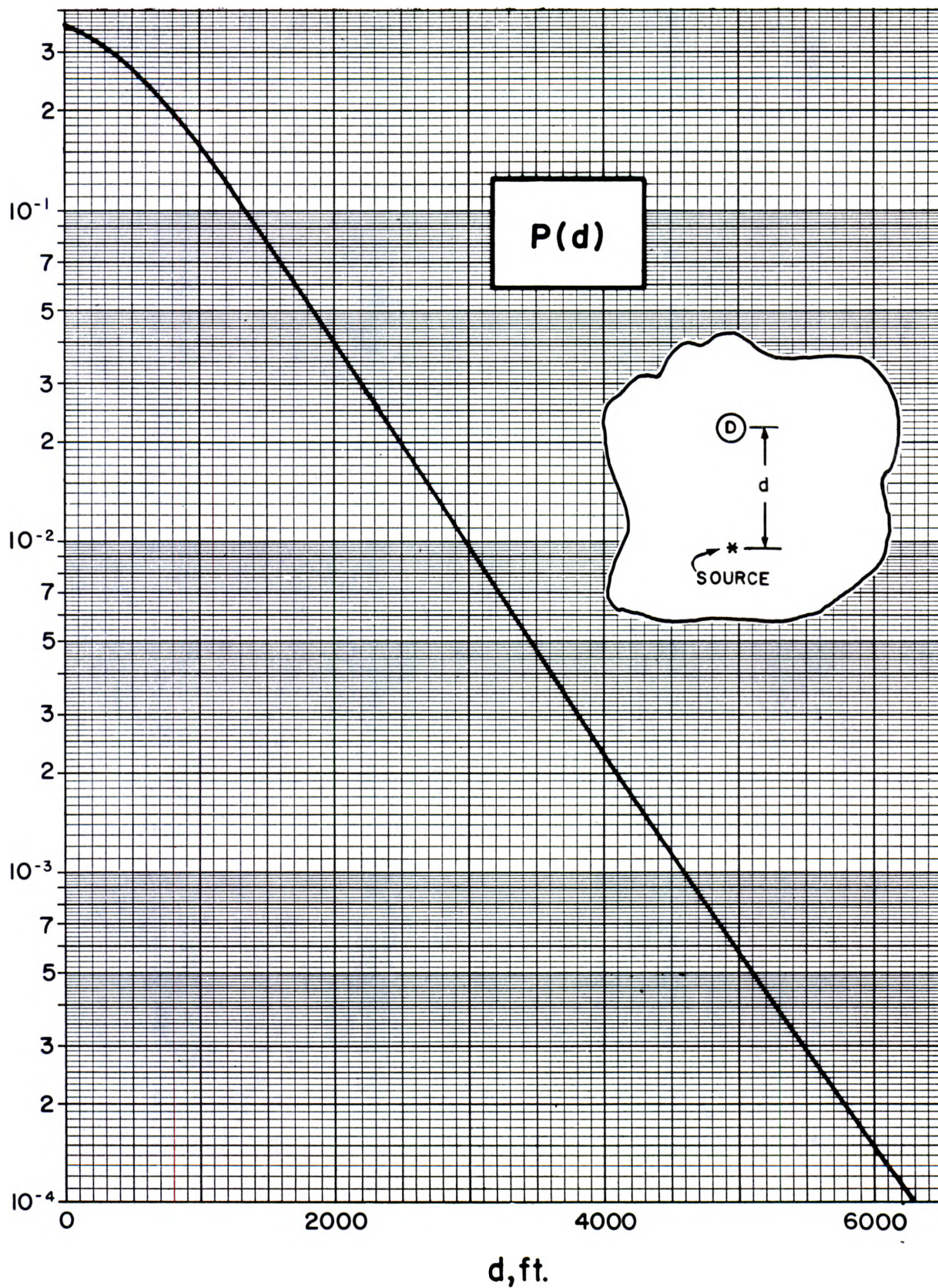
and is shown in figure V.21. It gives the fractional cumulation of dose with angle, beginning at the radial direction. Note that the unscattered component, which is not included in  $P_a^{(s)}$ , contributes with full intensity for all solid angle fractions, and need not be given beyond the data of figure V.20. These geometry factors approach unity for  $\omega \rightarrow 2$ . They stay relatively high and unaffected by penetration because the directional distribution exhibits the strong peak for  $\theta_r \approx 0$ , with little dependence on penetration, as exhibited in figure V.18 and V.19.

The second type of geometry factor,  $P_b^{(s)}(d)$  is defined by

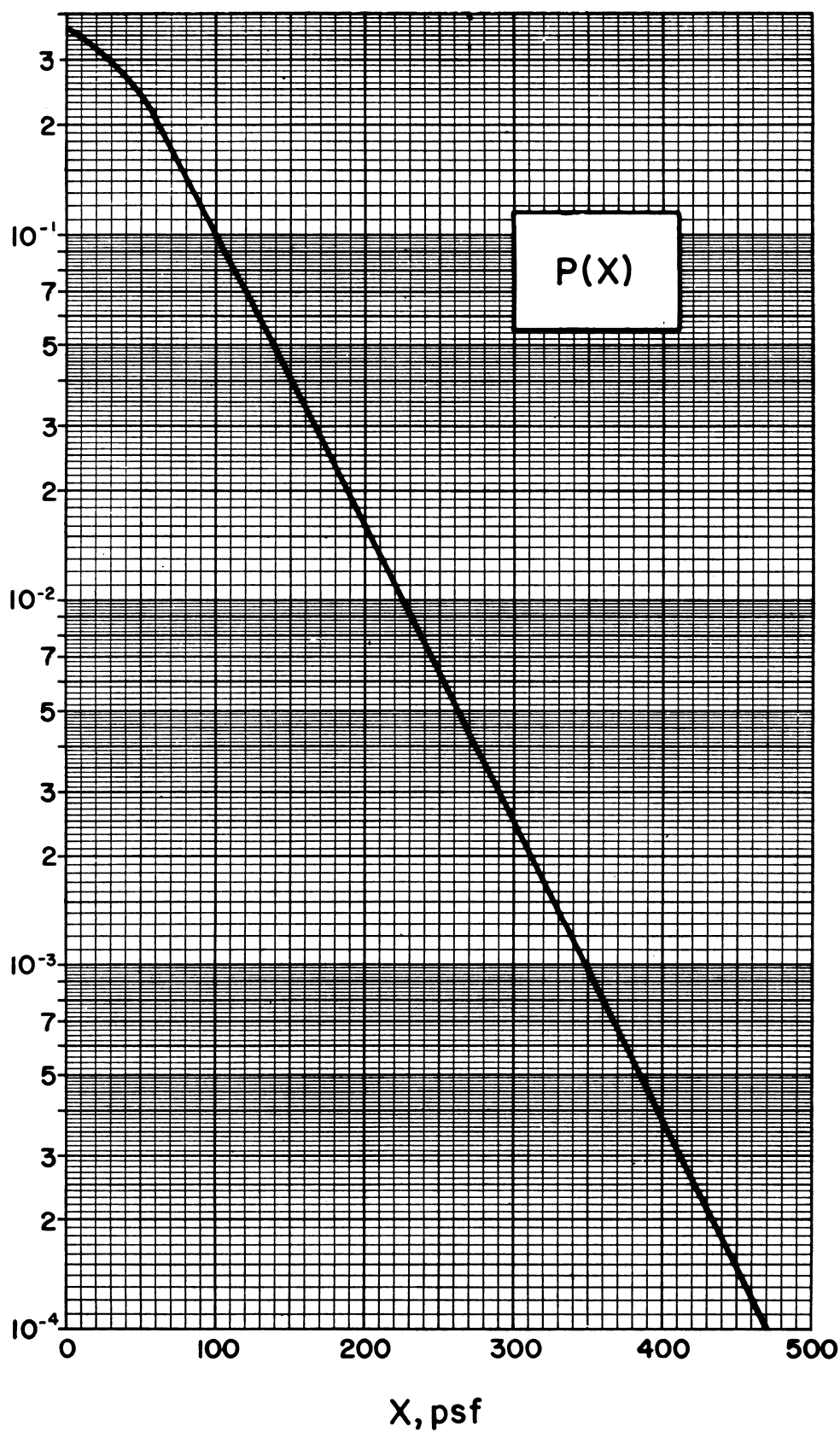
$$P_b^{(s)} = \frac{2}{P^{(s)}(d)} \int_{1-\omega}^1 d(\cos\theta_r) \frac{1}{2\pi} \int_0^{2\pi} d\phi P(d, \sin\theta_r \cos\phi) \quad , \quad (\text{V.25})$$

and is shown in figure V.22. This is the fractional cumulation of dose with angle, about an axis oriented at  $90^\circ$  from the radial, i.e.,  $\theta_r = \pi/2$ . In  $P_b^{(s)}$ , the unscattered component can contribute only for  $\omega = 1$ ; and only one side of the radiation field contributes, with half of the unscattered component. Thus a factor of two has been included in the expression to normalize the data to unity at  $\omega = 1$ . The precipitous drop of these curves



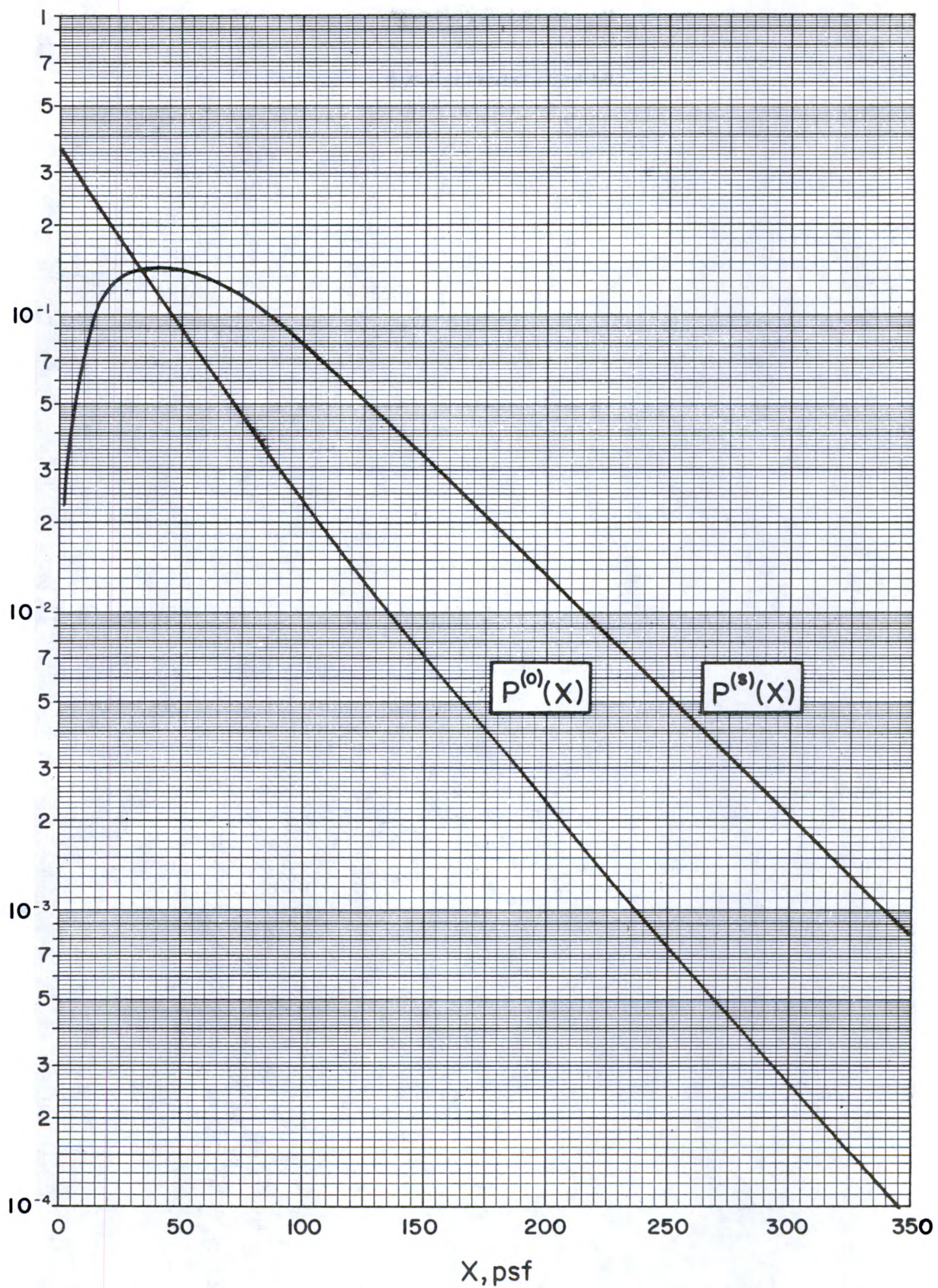


V.18 Attenuation of fallout gamma radiation from a point source, as a function of distance  $d$  in  $H_2O$  from the source. (See also figs B.12a,b.)



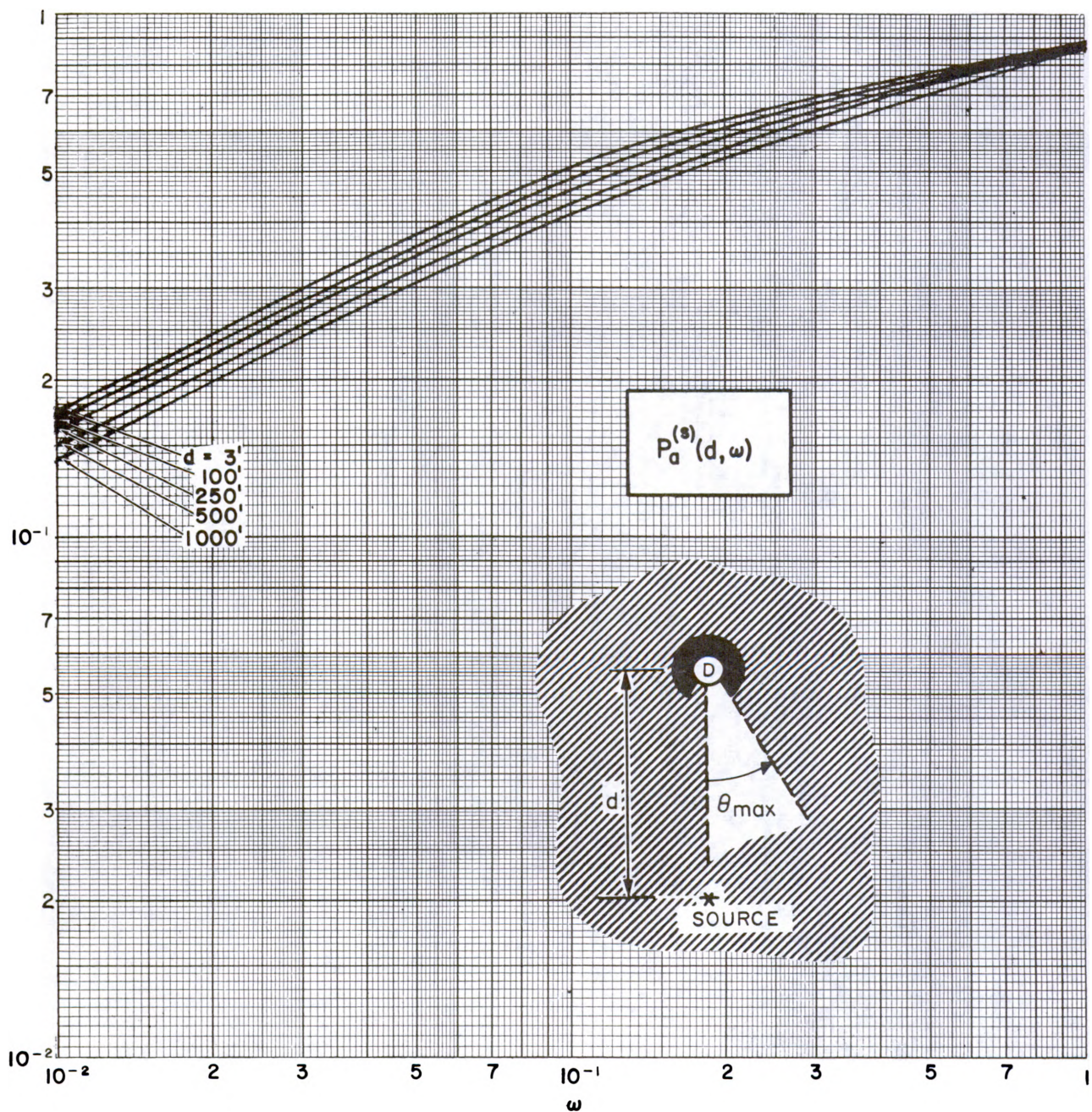
V.19 Attenuation of fallout gamma radiation from a point source, as a function of effective mass thickness  $\underline{X}$  in  $H_2O$  separating detector and source. (See also figs B.13a,b.)





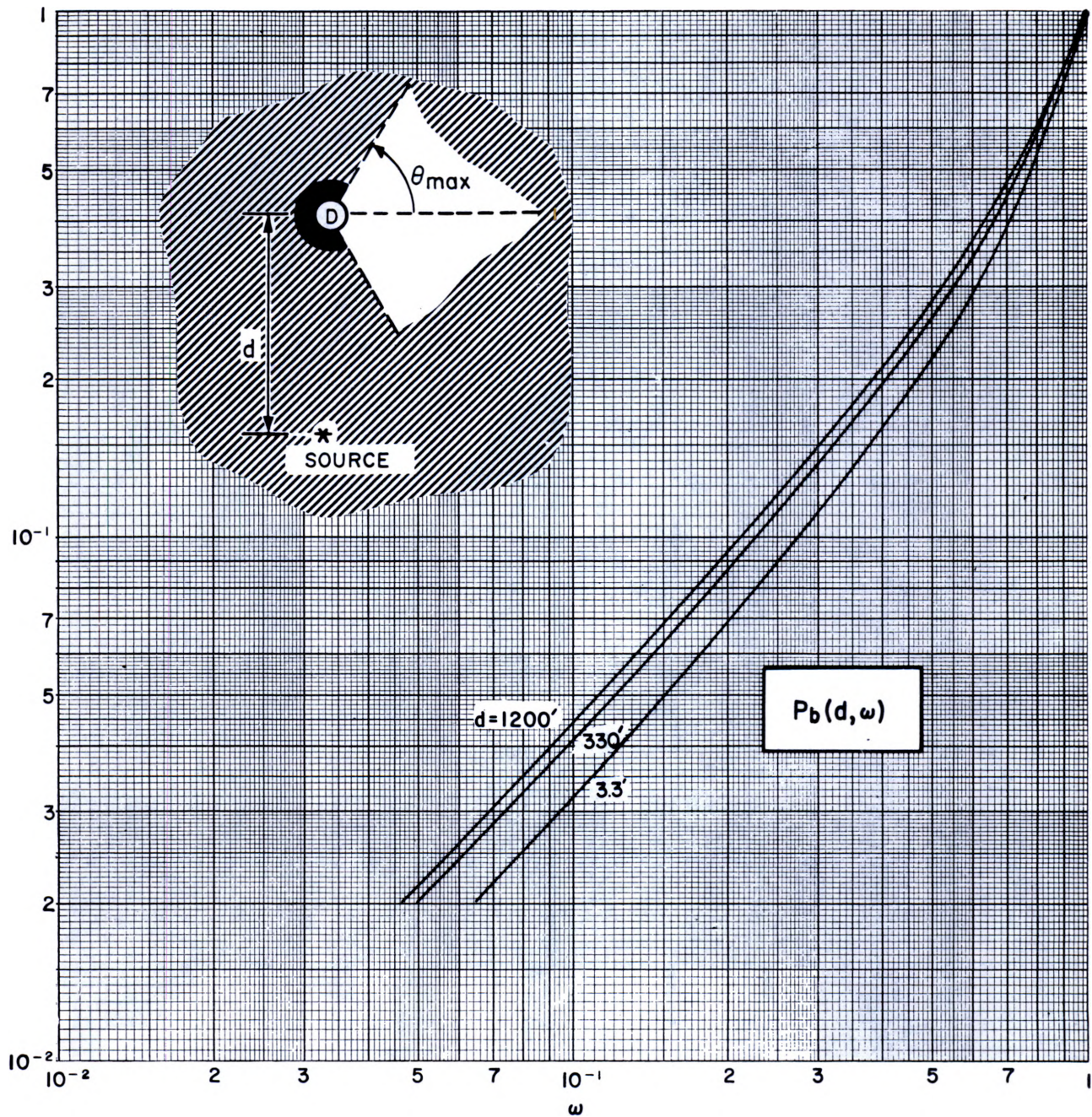
V.20 Unscattered and scattered components of  $P(X)$ . (See also figs B.14a,b.)





V.21 Geometry factor describing detector response to scattered fallout gamma rays from a point source. The radiation strikes the detector in a limited cone of directions about the line from source to detector. (See also figs B.15a,b.)





V.22 Geometry factor describing detector response to scattered fallout gamma rays from a point source. The radiation strikes the detector in a cone of directions about an axis perpendicular to the line from source to detector. (See also figs B.16a,b.)

results from the progressive removal of the sharp radial-directed peak of the angular distribution. Note also that the weak dependence of the angular distributions on penetration distance is reflected here also in the similarity of the curves. Data for  $^{60}\text{Co}$  and  $^{137}\text{Cs}$  corresponding to figures V.21 and V.22 are given in appendix B, figures B.15a,b and B.16a,b.

Errors in the  $P_a^{(s)}$  and  $P_b^{(s)}$  data have been estimated at  $\sim 5\%$  for  $\omega \rightarrow 1$ , and  $\sim 15\%$ ,  $\sim 25\%$ , respectively, for  $\omega \rightarrow 0$ .

### 3. Vertical Wall/Window Reduction Factors (W)

#### a. Barrier Factors

Data which can be used to estimate barrier factors for vertical walls require more complex calculations than for plane and point isotropic sources. Two rather similar types of calculations have been made, according to whether the data pertained to an infinite plane source of gamma rays or a limited (semicircular) field centered at a point adjacent to the vertical wall below the detector.

In the infinite field case, several approximations are made: 1) We first assume that the angular distribution incident on the wall is given by  $\ell(d, \cos\theta)$ , where  $\cos\theta$  is measured relative to a vertical axis. 2) Secondly, we assume that the spectrum of photons is the same in all directions, and is the basic (fallout) source spectrum. With these approximations it is reasonable to make an additional approximation and use data for  $s(X, \cos\theta_0)$  to estimate attenuation through the wall. As a result, the wall attenuation data  $W(X, d)$  is expressed by

$$W(X, d) = \int_0^1 d(\cos\theta) \cos\theta s(X, \cos\theta) \frac{1}{2\pi} \int_0^{2\pi} d\phi \ell(d, \sin\theta \cos\phi), \quad (\text{V.26})$$

and is given in figure V.23 (and figs B.17a,b).



In figure V.23 one sees a family of curves which are roughly parallel, and which reflect the changing angular distribution with height but not the softening of the spectrum with increasing amounts of air-scattered radiation. One therefore expects the deep penetration trends to be realistic, because they reflect the hardest spectral component, which is also least affected by the air-scattered component. On the other hand, one expects the curves for deep penetrations to lie above the true values due to neglect of the stronger filtration of air-scattered gamma rays. This is discussed in section VIII.C.1.a, where experimental confirmation is given. (See ref. [3] of chapter VIII, and data for  $^{60}\text{Co}$  and  $^{137}\text{Cs}$  given in figures B.17a,b of appendix B.)

The normalization of eq (V.26) corresponds to radiation incident from one side only, hence the close approach of  $W(0,3.3')$  to 0.5. The  $\sim 10\%$  excess is due to the use of data for  $s(X, \cos\theta_0)$ , which unrealistically incorporates a backscattered component from outside the vertical wall.

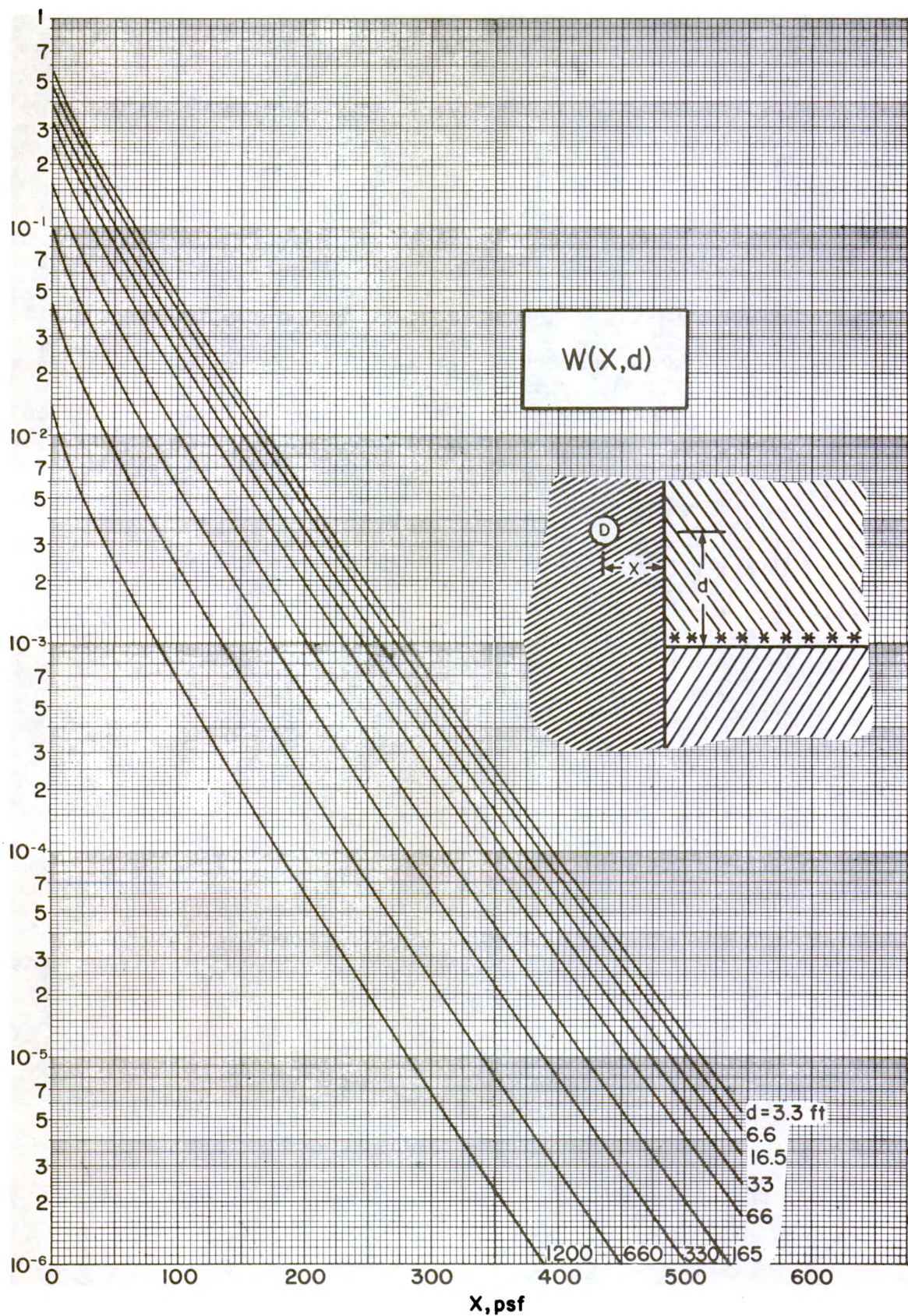
The fan source is a surprisingly realistic limiting case in which the angular distribution is incident from all those directions  $\vec{\Omega}$  which are strictly horizontal. This condition means that  $\vec{\Omega} \cdot \vec{k} = \sin\theta\cos\phi = 0$ , where the unit vector  $\vec{k}$  points vertically upward. We note that the unscattered component from a plane isotropic source satisfies this condition in the limit  $d \rightarrow 0$ :

$$\lim_{d \rightarrow 0} \ell^{(0)}(d, \sin\theta\cos\phi) \propto \delta(\sin\theta\cos\phi) \quad . \quad (\text{V.27})$$

With this delta function replacing  $\ell(d, \sin\theta\cos\phi)$  in eq (V.26), we can carry out the integral over  $\phi$  as follows:

$$\begin{aligned} F(X) &= \int_0^1 d(\cos\theta) \cos\theta s(X, \cos\theta) \frac{1}{\pi \sin\theta} \int_{\sin\phi=-1}^{\sin\phi=1} d(\sin\theta\cos\phi) \delta(\sin\theta\cos\phi) / \sin\phi \\ &= \frac{2}{\pi} \int_0^{\pi/2} d\theta \cos\theta s(X, \cos\theta) \quad . \end{aligned} \quad (\text{V.28})$$





V.23 Detector response to fallout gamma radiation from a plane isotropic source through a barrier of effective mass thickness  $X$  oriented perpendicular to the source plane. Detector response falls off with distance  $d$  from source plane to detector, but the barrier attenuation is not very sensitive to  $d$ . (See also figs B.17a,b.)



Because the unscattered photons dominate for  $d \rightarrow 0$ , the fan source closely resembles  $\ell(d, \sin\theta \cos\phi)$  in the limiting case of small  $d$ . Further, in addition to this application to the infinite source plane case, the integrand of eq (V.28) can be interpreted as due to radiation from a half-ring of sources centered on the detector point and lying in the plane  $d = 0$ ; and it even can be shown to correspond to radiation from an infinite line source lying in the  $d = 0$  plane and parallel to the slab. Evaluation of the integral in eq (V.28) results in a function of  $X$  which is very close to the function  $W(X, 3.3')$ . It therefore confirms the shape of the wall barrier function in a very satisfying manner. Equation (V.28) can also be compared with the expression for the roof barrier factor, which can be expressed, according to eq (V.17), as

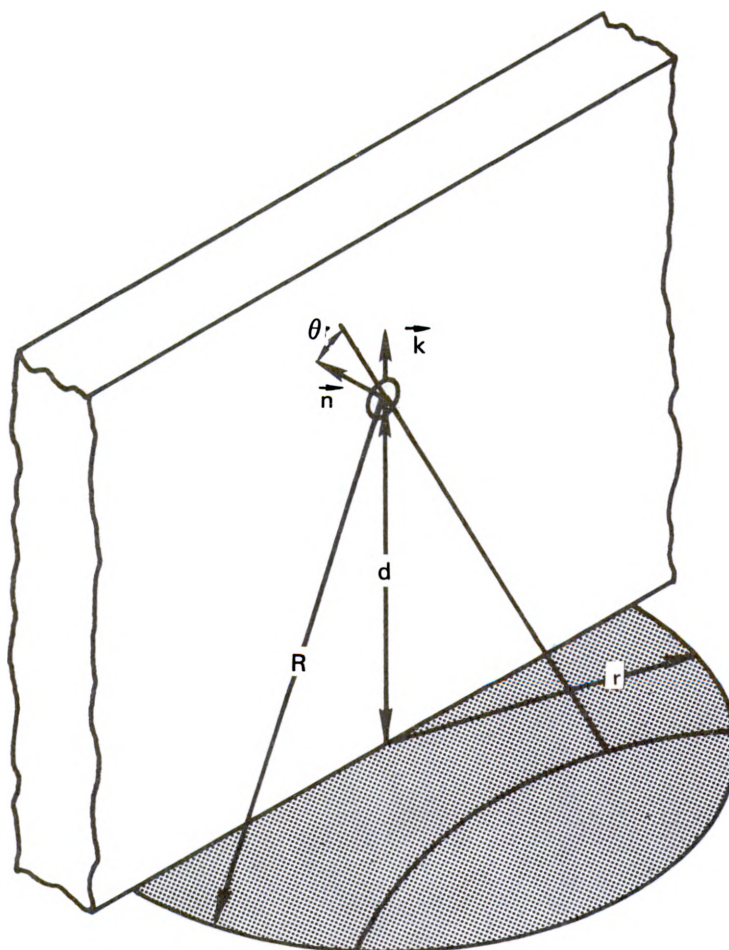
$$L(X) \propto \int_{-1}^1 d(\cos\theta) s(X, \cos\theta) . \quad (V.29)$$

But eq (V.28) can be rewritten

$$F(X) = \frac{2}{\pi} \int_0^1 d(\cos\theta) \cot(\theta) s(X, \cos\theta) . \quad (V.30)$$

In this form it can be seen that the two barrier functions differ primarily by a  $\cot\theta$  factor which preferentially weights radiation which is incident perpendicularly.

The finite source field has been approached by use of two rather different approximations [2]. In the first approximation one evaluates the angular distribution,  $\ell_\rho(d, \vec{\Omega} \cdot \vec{k})$ , at height  $d$  centered above a circular source area of radius  $\rho$  with the unit vector  $\vec{k}$  directed vertically up as sketched in figure V.24. This has been performed as described in sections IV.D.3 and IV.D.4, with application, e.g., of eq (IV.75) in the form suitable to a



- V.24 Sketch describing a plane, semicircular source of radius  $\rho$  adjacent to a vertical wall. The detector is at distance  $d$  from the source plane, behind the center of the small circle.

circular disk of finite radius. Penetration of the vertical barrier is then estimated using an expression corresponding to eq (V.26),

$$W(X,d,\rho/d) = \int_0^1 d(\cos\theta) \cos\theta s(X,\cos\theta) \frac{1}{2\pi} \int_0^{2\pi} d\phi \ell_\rho(d, \sin\theta \cos\phi) \quad . \quad (V.31)$$

Because the calculated data for angular distributions  $\ell_\rho$  deteriorate in practice when the radius of the source semi-circle becomes small, data from these computations are best applied to fields of rather large radius.

In the second approximation, the source incident on the vertical wall is taken to be the unscattered component from the semi-circular area; this is clearly accurate when the radius of the source semi-circle becomes small, or rather when the distances are small enough that the scattered component can be neglected. From eq (V.17) and eq (IV.6), we infer that for the unscattered component,

$$\ell_\rho(d, \sin\theta \cos\phi) \approx \frac{1}{2} P(0) \cdot \frac{1}{\sin\theta \cos\phi} u(d/\sqrt{d^2+\rho^2} - \sin\theta \cos\phi) \quad (V.32)$$

where  $u(X)$  is the unit function<sup>3</sup>. We insert this expression into eq (V.26). The integral over the azimuthal variable can be evaluated analytically, so that the resulting expression is

$$W(X,d,\rho/d) \approx \int_0^1 d(\cos\theta) \cot\theta s(X,\cos\theta) \frac{P(0)}{2\pi} \log(v + \sqrt{v^2-1}) \quad (V.33)$$

where  $v = \sin\theta \sqrt{d^2+\rho^2} / d$ .

Two aspects of eq (V.33) need further comment: First, we see immediately that the fan source is obtained merely by replacing the logarithm with a constant, hence its capacity for representing the wall attenuation. Further, although it is not readily apparent from eq (V.33), the  $X = 0$  case corresponds to



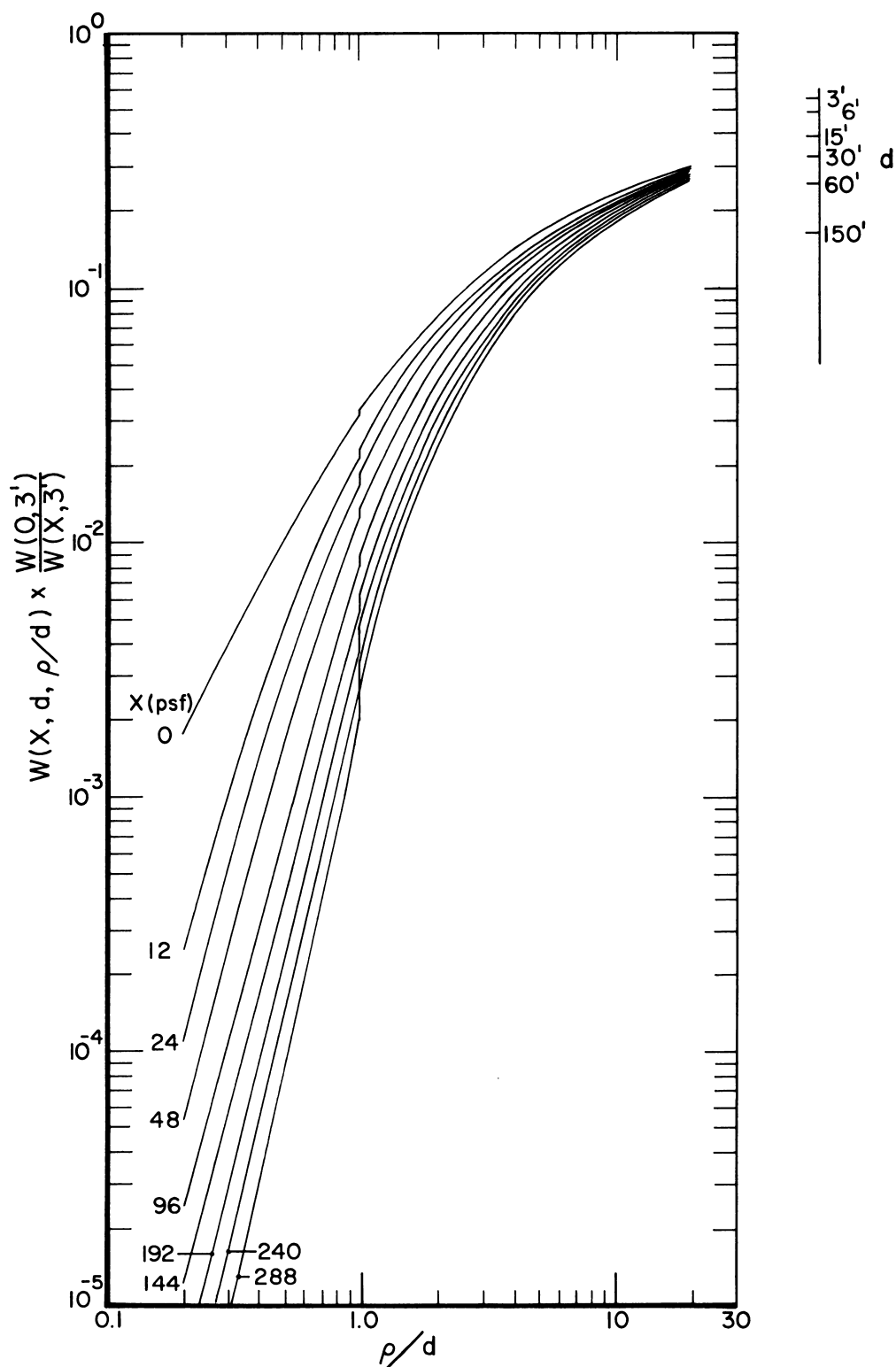
omission of the factor  $\cos\theta s(X, \cos\theta)$ , which only differs from unity for  $X = 0$  as a result of backscattering due to the use of the infinite medium approximation. The final integration then gives the simple result

$$W(0, d, \rho/d) \approx \frac{1}{4} P(0) \log \sqrt{\rho^2 + d^2} / d \quad . \quad (V.33')$$

As discussed in reference [2], un-normalized data from both approximations have been calculated for the 1.12 hour old fission product gamma ray source. We have normalized the data due to the first approximation to the value  $W(0, 3.3')$ , and we have normalized the data calculated by the second approximation by means of eq (V.33'). In figure V.25, the data from the first method has been plotted to the right of  $\rho/d = 1$ , while the data from the 2nd approximation have been plotted to the left of  $\rho/d = 1$ . It is clear that the junction at  $\rho/d = 1$  is not smooth, owing mainly to the breakdown of values for small  $\rho/d$  as calculated using the first method. This discontinuity is not serious enough to prevent use of a single smooth curve for each value of  $X$ . We should note, however, that C. Eisenhower [2] used a different approach to the problem of joining and normalizing the two data types (see section VIII.C.2).

#### b. Geometry Factors

The two types of geometry factors which we designate  $W_a$  and  $W_b$  correspond, respectively, to gamma rays incident over the full lateral cone as



V.25 Detector response to finite, plane, semicircular sources of fallout gamma rays, as a function of the ratio  $\rho/d$  and the barrier thickness  $X$ . Two types of data are used on either size of  $\rho/d = 1$ ; the data sets do not join smoothly but are in reasonable agreement.

shown in the sketch of figure V.26, and gamma rays incident only from the skyshine component, as shown in the sketch of figure V.27. They correspond to evaluation of the expressions

$$W_a(d, \omega) = \frac{1}{W(0, d)} \int_{1-\omega}^1 d(\cos\theta) \frac{1}{2\pi} \int_0^{2\pi} d\phi \ell(d, \sin\theta \cos\phi) \quad , \quad (V.34)$$

and

$$W_b(d, \omega) = \frac{2}{S(d)} \int_{1-\omega}^1 d(\cos\theta) \frac{1}{2\pi} \int_{\pi/2}^{3\pi/2} d\phi \ell(d, \sin\theta \cos\phi) \quad . \quad (V.35)$$

In the case of the skyshine radiation, only a single curve is given because the skyshine angular distribution is substantially independent of distance above the source plane for realistic building heights.

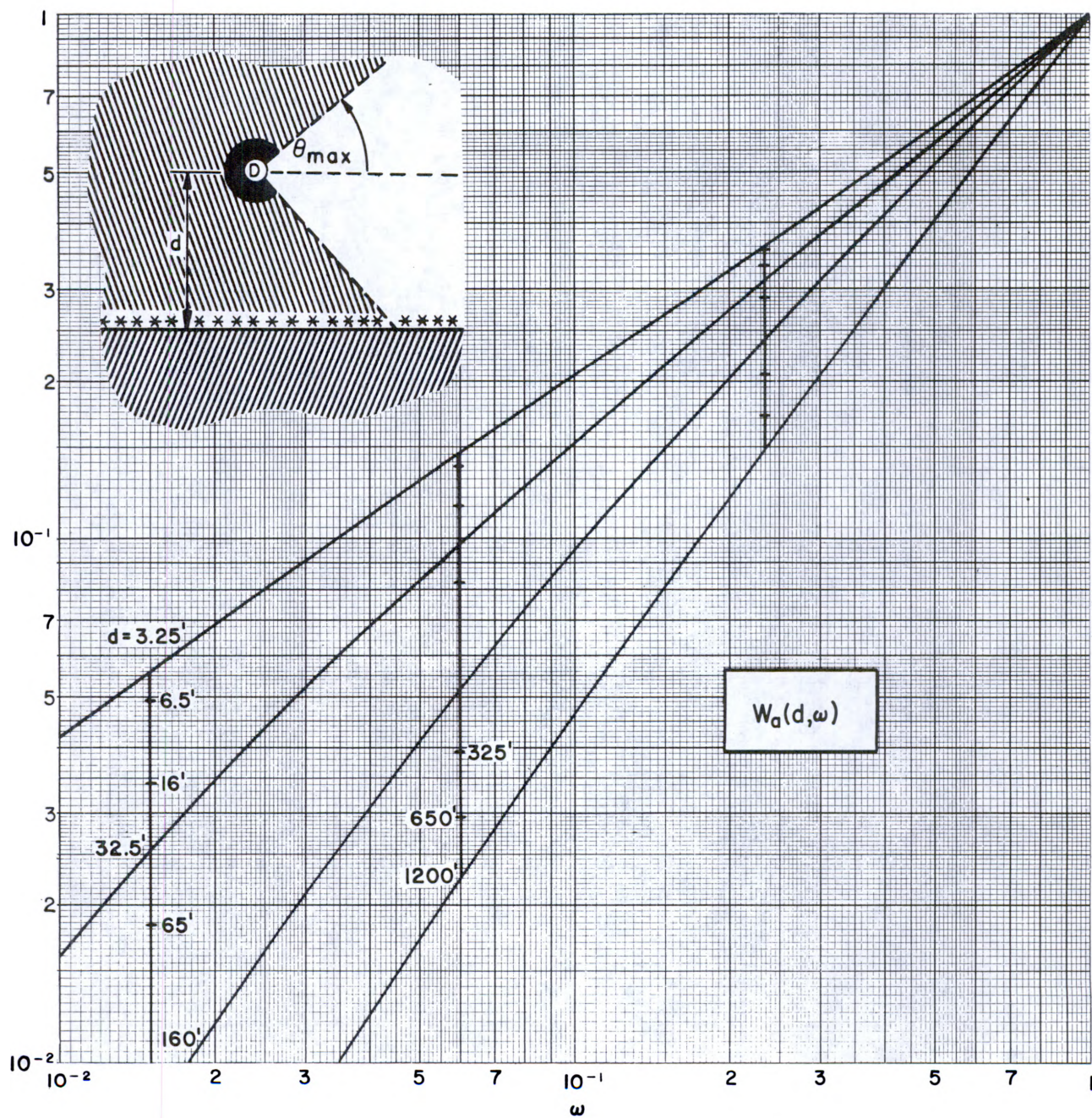
These types of basic data for geometry factors correspond to a wall of zero thickness, i.e. a window, which is reasonable because thicknesses of window panes are usually small compared to gamma ray mean free paths.

But these geometry factors have proven less useful than originally intended because the engineering procedures have mostly utilized solid angle fractions which are defined relative to a vertical axis. Such an approach more readily incorporates the  $S_a(d, \omega)$  and  $L(d, \omega)$  geometry factor data of sections V.D.4.b and V.D.1.b, suitably reduced to correspond to window and wall configurations. This is discussed in much more detail in chapter VII. Data for  $^{60}\text{Co}$  and  $^{137}\text{Cs}$  are given in figures B.18a,b and B.19a,b, respectively for  $W_a$  and  $W_b$ .

#### 4. Skyshine and Foxhole Reduction Factors ( $\underline{S}, \underline{E}$ )

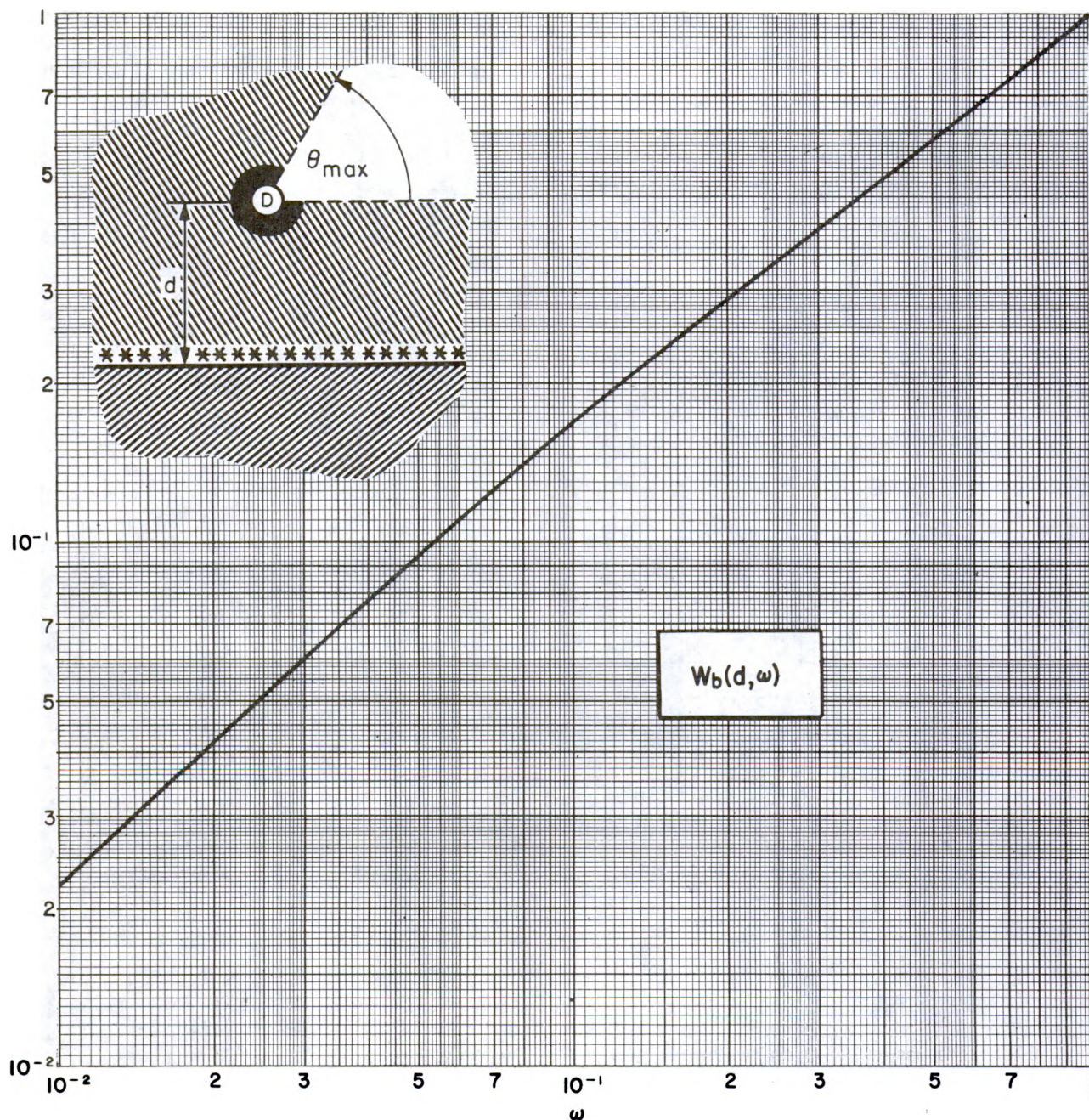
##### a. Barrier and Attenuation Factors

The first of two skyshine reduction factors for which we calculate data corresponds to the total exposure due to photons which have scattered to directions which would return them to the source. These consist only of



V.26 Geometry factor data describing detector response to fallout gamma radiation incident in a limited cone of directions about an axis parallel to the source plane, for several distances  $d$  from the source plane. (See figs V.18a,b.)





V.27 Geometry factor data describing detector response to skyshine radiation from a plane source of fallout gamma rays. The radiation is incident on the detector in a limited cone of directions about an axis parallel to the source plane; and the results apply to all distances  $d$  from the plane less than about 200 ft. (See figs V.19a,b.)

air scattered photons, and their intensity decreases with height  $\underline{d}$  above the source plane, as shown in figure V.28. The function  $S(d)$  which we evaluate to represent the skyshine component is defined by

$$S(d) = \int_{-1}^0 d(\cos\theta) \ell(d, \cos\theta) \quad . \quad (V.36)$$

Note that for  $\cos\theta < 0$ , the intense unscattered components of  $\ell(d, \cos\theta)$  nearly parallel to the plane are absent; although scattered components also peak at grazing angles. The decrease with distance is thus somewhat slower than the  $L(d)$  data. Further, at the height of 3 ft, the skyshine exposure is a little less than 10% of the total  $L(d)$  exposure.

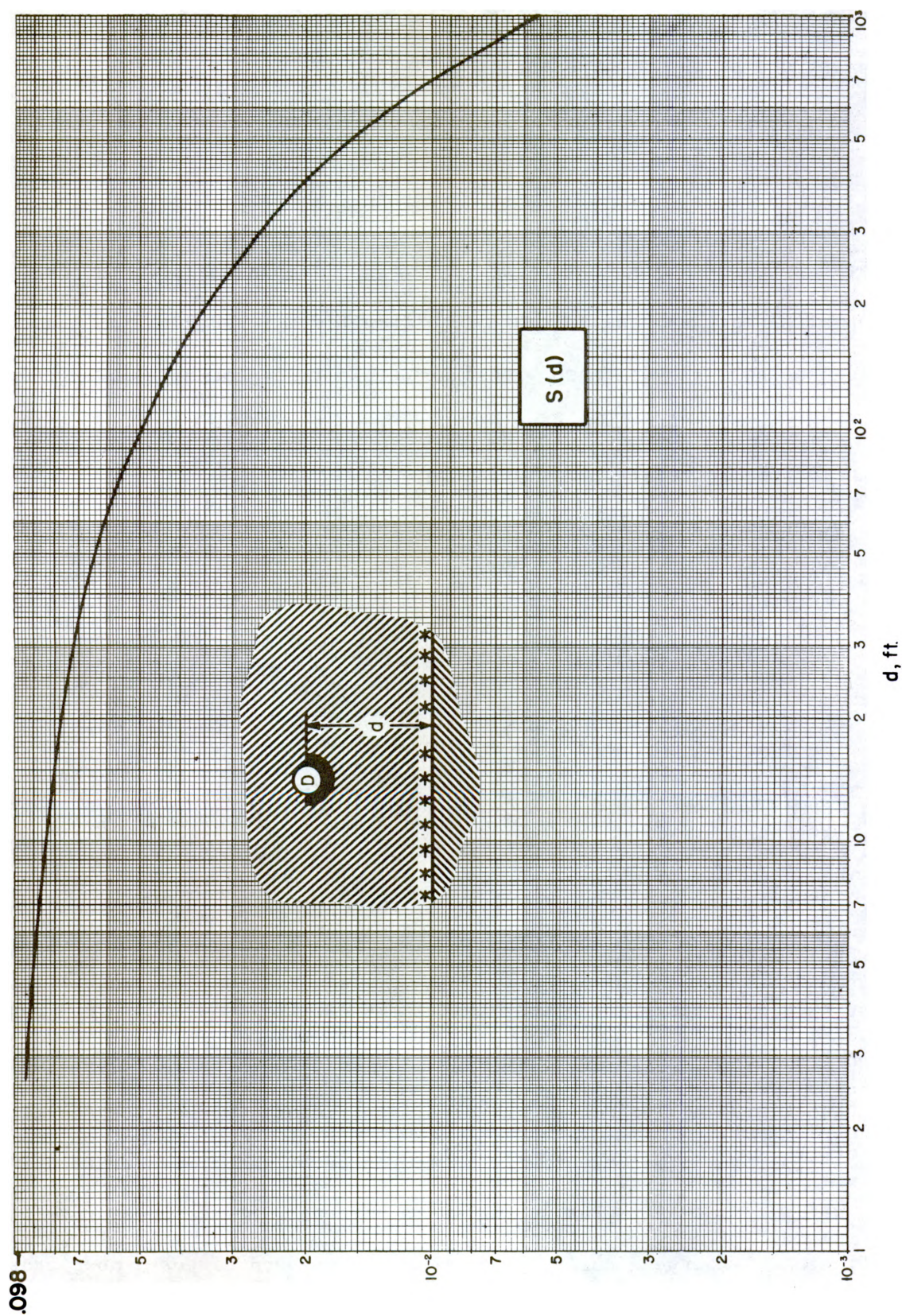
The second skyshine factor corresponds to the attenuation of skyshine gamma rays through barriers, i.e., as into the ground below the source plane. This attenuation factor, which we designate  $S'(X)$  is defined by

$$S'(X) = \frac{\int_{-1}^0 d(\cos\theta_o) s(X, \cos\theta_o)}{\int_{-1}^0 d(\cos\theta_o) s(0, \cos\theta_o)} \quad . \quad (V.37)$$

Data for  $S'(X)$ , together with a sketch of the configuration, are shown in figure V.29. Strictly speaking the attenuation here depends on the height  $\underline{d}$  also; but this dependence is so weak that it is omitted. Note the very rapid reduction for small penetrations, which is indicative both of a scattered component near grazing incidence, and of a significant low-energy spectral component. The trend must eventually be dominated by gamma rays emitted by the source upward, but at near-grazing angles, and then scattered once or twice into a direction nearly perpendicular to the source plane and directed downwards.

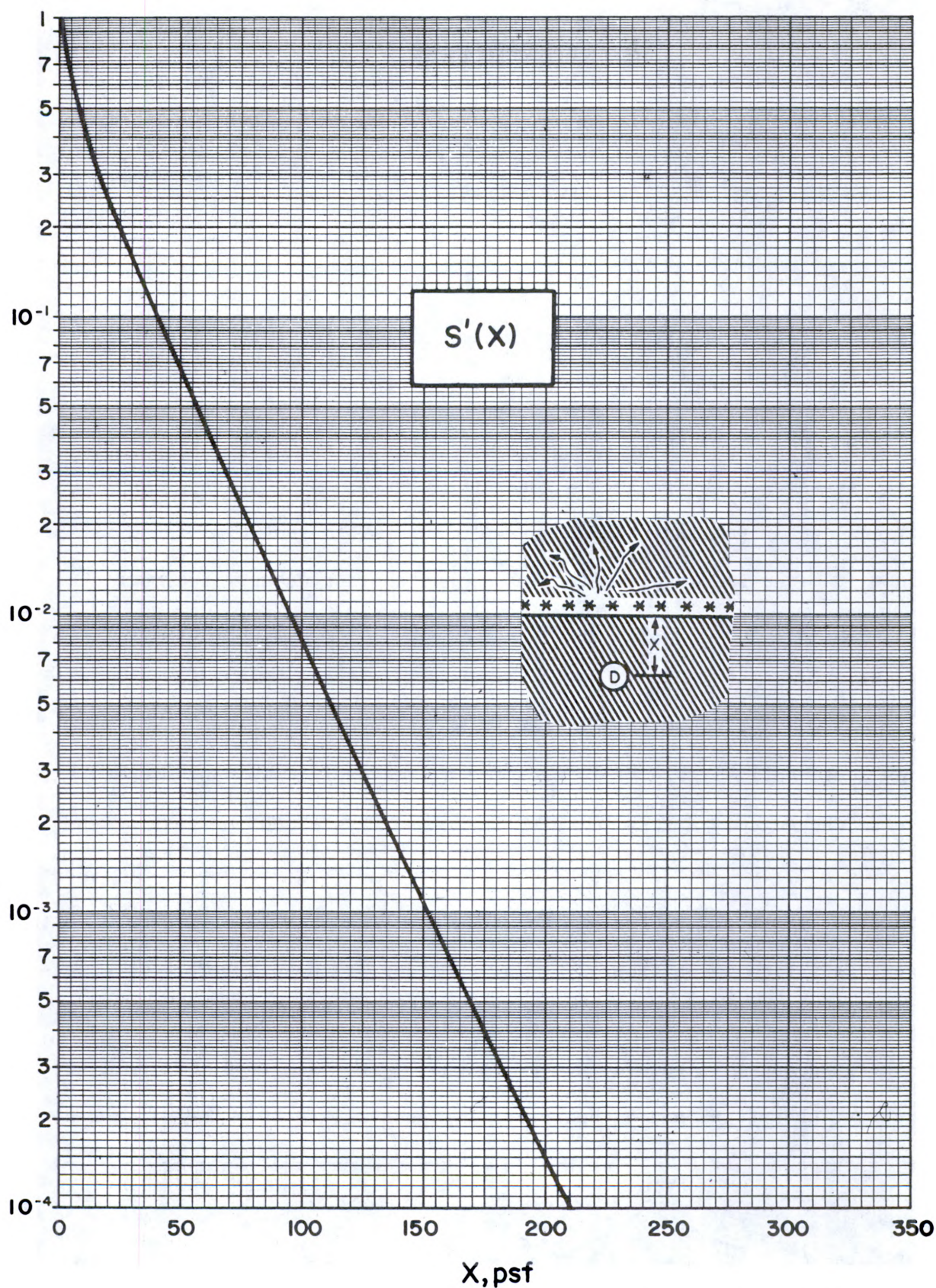
Data for  $^{60}\text{Co}$  and  $^{137}\text{Cs}$  are given in figures B.20a,b and B.21a,b, respectively for  $S(d)$  and  $S'(X)$ .





V.28 Detector response ratio  $D/D_0$  due to skyshine gamma rays, as a function of distance  $d$  from a plane source of fallout radiation. (See figs V.20a,b.)





V.29 Attenuation curve for radiation backscattered from a plane fallout source which is isotropic over the hemisphere of directions pointed away from the detector, and zero over the hemisphere of directions pointed towards the detector. An effective mass thickness  $X$  of  $H_2O$  separates source from detector. (See figs V.21a,b.)



## b. Geometry Factors

The geometry factor for backscattered (or skyshine) radiation is defined by

$$S_a(d, \omega) = \frac{1}{S(d)} \int_{-1}^{-1+\omega} d(\cos\theta) \ell(d, \cos\theta) \quad , \quad (V.38)$$

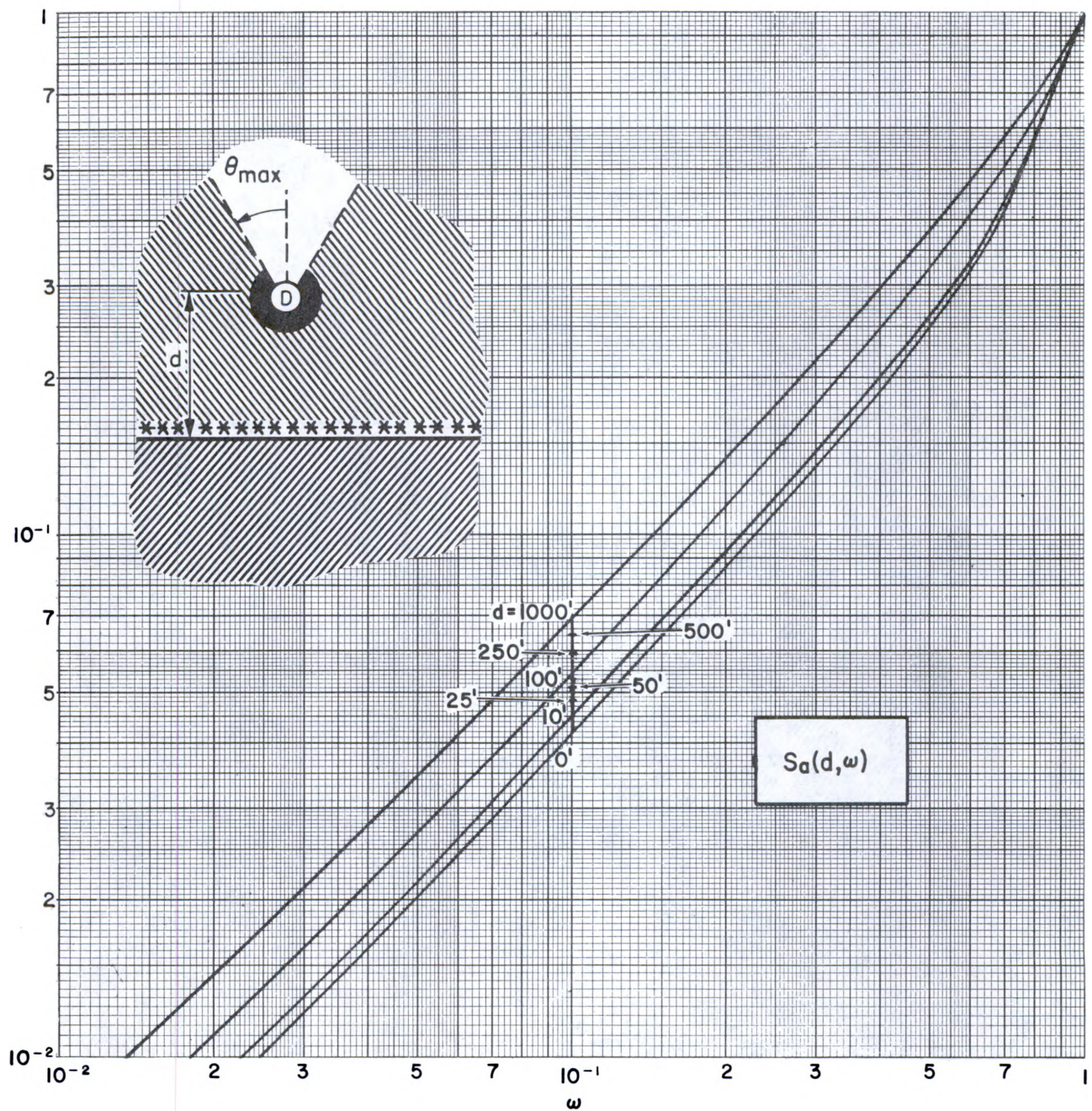
and is given for the fallout source in figure V.30 (and for  $^{60}\text{Co}$  and  $^{137}\text{Cs}$  in figures B.22a,b of appendix B). The fact that these curves are concave upward and undergo rapid reduction near  $\omega = 1$  results from the tendency for the angular distribution to exhibit a peak for (mostly once-scattered) photon directions nearly parallel to the source plane. This peak diminishes as the distance from the source plane increases, and the curves approach more closely to a straight line of  $45^\circ$  slope, which would correspond to an isotropic angular distribution.

## c. Special Data for Foxhole Lip Contributions

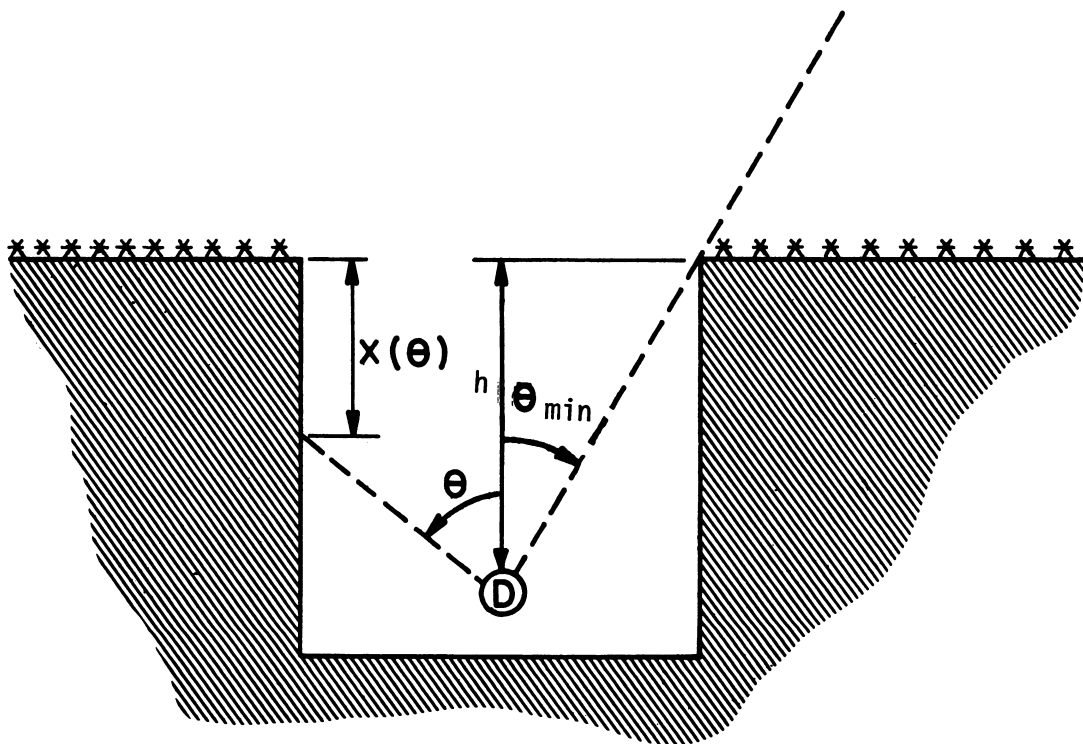
As sketched in figure V.31, when the ground surface is contaminated with a source to the edge of a vertical pit, the gamma rays which emerge from the side, within the pit, should have approximately the angular distribution  $\ell(X, \cos\theta)$  of the plane isotropic source at the ground interface. That is, we assume that emergent radiation is unaffected by the presence of the pit. This is essentially a "narrow hole" limit; but since most of the exposure is due to radiation only emerging once, it should give a reasonable approximation. In full generality, therefore, and allowing for the possibility that the pit has a cover of thickness  $X(\theta_{\min})$ , we are interested in integral data of the type

$$D/D_o = \int_{-1}^{\cos\theta_{\min}} d(\cos\theta) \ell[X(\theta), \cos\theta] \quad . \quad (V.39)$$

If the distance from the detector to the edge of the hole is large compared with the mean free path of fallout radiation in earth ( $\sim 5$  inches), the integral



V.30 Geometry factor describing detector response to skyshine radiation incident on the detector in a limited cone of directions about an axis perpendicular to the source plane and pointing towards the plane. The detector is at distance  $d$  in air from the (fallout) source plane. (See figs V.22a,b.)



V.31 Variables for the case of a detector on the centerline of a cylindrical foxhole.

can be approximated by writing  $d(\cos\theta) = \frac{d(\cos\theta)}{dX} dX$ , and assigning  $\frac{d(\cos\theta)}{dX}$  a constant value corresponding to the edge of the lip. This leads to the following expression:

$$D/D_0 = \frac{\omega(1-\omega)(2-\omega)}{\rho d} \int_X^\infty dX' \ell(X', 1-\omega) \quad , \quad (V.40)$$

which (see fig. V.31)

$\rho$  is the density of the ground,

$d$  is the depth below the ground surface, and

$\omega = 1 - \cos\theta_{\min}$  is the solid angle fraction subtended by the opening of the hole.

We therefore require data of the type

$$\int_X^\infty dX' \ell(X', \cos\theta) \quad ,$$

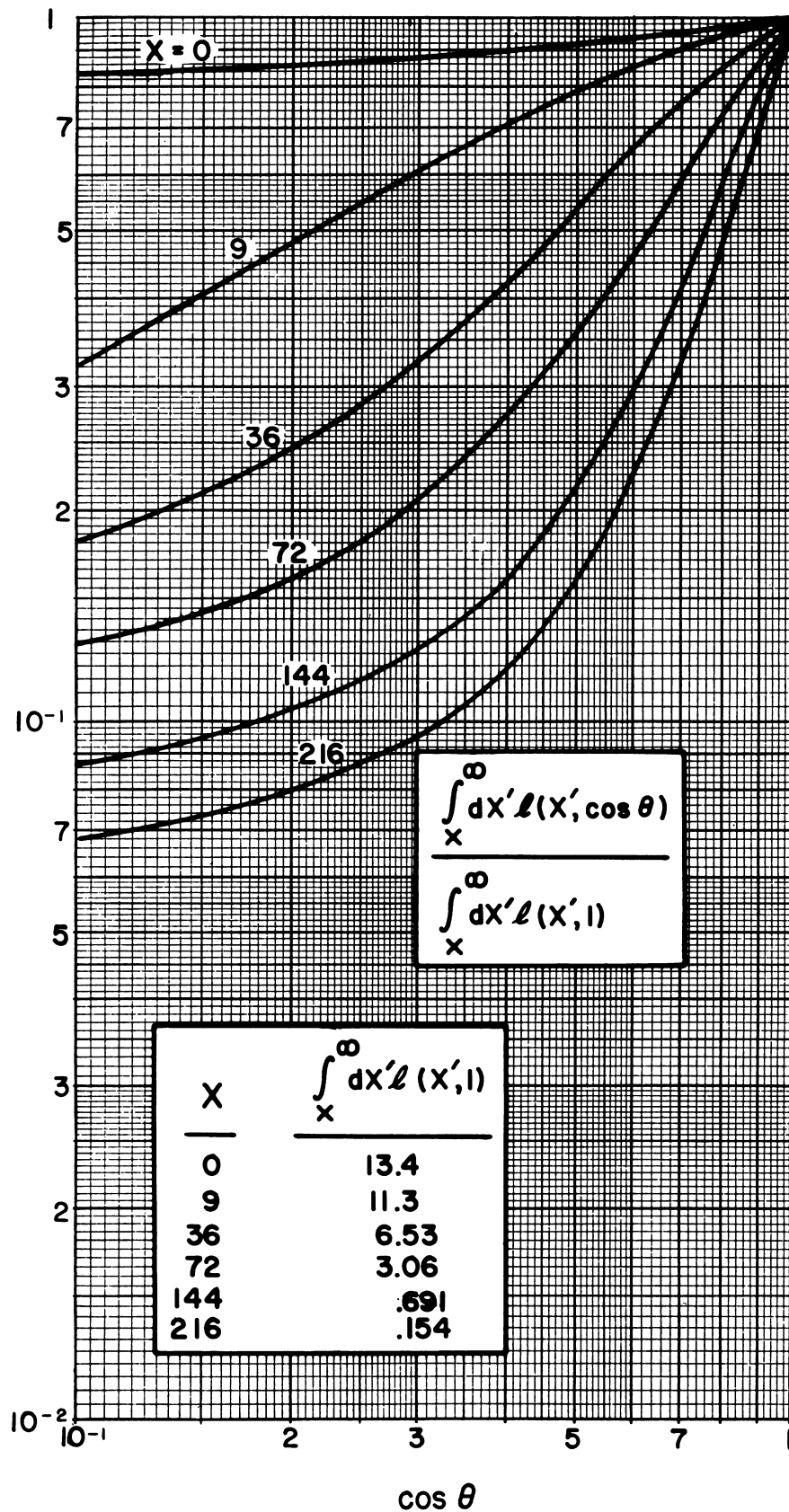
which we express in a suitably normalized form by an edge function  $E(x, \cos\theta)^5$ , for the different angles of emergence  $\theta$ , relative to a vertical (downward) axis,

$$E(X, \cos\theta) = \frac{\int_X^\infty dX' \ell(X', \cos\theta)}{\int_X^\infty dX' \ell(X', 1)} \quad . \quad (V.41)$$

The lower limit  $X$  of integration corresponds to the mass thickness of a cover between the hole and the source, so that for uncovered foxholes one assigns the value  $X = 0$ . Data for  $E(X, \cos\theta)$ , and for  $\int_X^\infty dX' \ell(X', 1)$ , are presented in figure V.32. Corresponding data for  $^{60}\text{Co}$  and  $^{137}\text{Cs}$  are given in figures B.23a,b, of appendix B.

<sup>5</sup>Not to be confused with shape factor  $E$  (see Chapter VII).





V.32 "Edge" geometry factor data  $E(X, \cos \theta)$  for calculating "lip penetration" in foxholes and the wall contribution in barrier shelters. A short table of data for the associated barrier factor is given below. (see figs V.23a,b.)

## References

- [1] Spencer, L. V., Structure Shielding Against Fallout Radiation from Nuclear Weapons, NBS Monograph 42. 134 pages (June 1, 1962).
- [2] Bramlitt, E. T., and Eisenhauer, C. M., A discussion and Tabulation of the Data Used to Construct the Charts in the OCD Standard Method for Fallout Gamma Radiation Shielding Analysis, TR-70, 63 pages (Office of Civil Defense, Dec. 1971).
- [3] Glasstone, S., ed., The Effects of Nuclear Weapons, Revised Edition, 458-460 (U.S. Atomic Energy Commission, Washington, D.C., April 1962).
- [4] Larson, Neal, Hawthorne, et al., Distribution, Characteristics and Biotic Availability of Fallout, Operation Plumbbob, Projects 37.1, 37.2, 37.2a, 37.3 and 37.6, WT-1488, 276 pages (Civil Effects Test Group, July 26, 1966).
- [5] Cannon, E. W., Building Materials as Commonly Used in Existing Urban Buildings in the United States, Project Civil Report (Inst. of Eng. Res., Univ. of Calif., Richmond, Calif., Jan. 1958).
- [6] The Accuracy of Radiation Shielding Calculations (unpublished), 12 pages (ad hoc Subcommittee on Radiation Shielding, National Academy of Sciences Advisory Committee on Civil Defense, Sept. 30, 1965).
- [7] Berger, M. J., and Raso, D. J., Monte Carlo calculations of gamma-ray backscattering, Rad. Res. 12, No. 1, 20-37 (Jan. 1960).

## VI. FREE FIELD EXPERIMENTS

### A. INTRODUCTION

The data described in chapter V can be divided into two types: (1) those which describe the radiation environment in a free field, with no structures and (2) those which estimate protection behind barriers. Curves such as figures V.6, V.13 and V.28, which predict the spatial and angular distribution of radiation in a free field are of the first type. Since this configuration determines the radiation environment of a structure, it must be thoroughly understood and evaluated before the protective capability of a structure can be predicted accurately. In this chapter we discuss experiments designed to measure spatial and angular distributions in a free field. Use of curves of the second type in the development of engineering procedures for estimating protection, and the testing of these procedures by experiment are discussed in later chapters.

In this chapter we first discuss the types of radioactive sources that have been used in experiments. We then consider the point isotropic (PTI) source in an infinite medium. This is important because early experimental results for this configuration confirmed the accuracy of transport calculations in general, and the validity of calculations by the moments method in particular. It is also important because in many experiments the intensity of the source was determined by means of a series of measurements in which it was assumed that the source and detector were small enough to be considered as points.

The plane isotropic (PLI) source in an infinite medium is then examined in detail. The specific gamma ray constant  $\Gamma$  which gives the exposure rate at unit distance from a source of unit intensity is discussed, along with relationship to the K-factor for fallout radiation. Experimental data on the spatial distribution of exposure are compared with calculations.

The foxhole also will be discussed as an example of an elementary configuration which is not part of a simple structure. The main motivation for studying the foxhole has been to obtain an understanding of skyshine radiation.

The effects of the ground-air interface on the exposure from a plane isotropic source will then be explored. The effect of the discontinuity in density at a smooth plane interface will be discussed. The effect of ground roughness of desert terrain, for example, vs paved ground, and the effect of larger ground irregularities such as rolling hills will be treated. Discussion of variations in exposure due to the presence of man-made irregularities such as nearby buildings will be deferred to section X.B.

#### B. USE OF ARTIFICIALLY-RADIOACTIVE SOURCES

Artificially-radioactive sources which reproduce the energy spectrum of fallout have not been readily available. Therefore experimenters have resorted to the use of sources that are more easily obtainable. As mentioned in section I.F, the early British [1,2] and Canadian experiments [3] used artificially-radioactive source of  $^{60}\text{Co}$  (average energy 1.25 MeV) and  $^{137}\text{Cs}$  (energy 0.66 MeV) gamma radiation. Early experiments in the United States at the Army Chemical Center [4] and the Nevada Test Site [5,6] also used  $^{60}\text{Co}$  and  $^{137}\text{Cs}$  sources. At the time, it was generally believed that a  $^{137}\text{Cs}$  source might simulate fallout radiation better than a  $^{60}\text{Co}$  source because it is closer to the average energy of fallout radiation, which is about 0.7 MeV. However, later calculations showed that the penetrability of  $^{60}\text{Co}$  radiation is closer to that of fallout radiation. Comparison of figure V.19 with figures B.13a and B.13b shows that this is indeed the case.

Because of the common use of these two sources in experiments, the penetration data described in chapter V were calculated for  $^{60}\text{Co}$  and  $^{137}\text{Cs}$  sources, as well as for fallout radiation sources. This permitted comparison



between experiment and calculations for the same source energy spectrum. Since the calculations for all three sources were made by the same method, it was assumed that good agreement between calculations and experiments with  $^{60}\text{Co}$  or  $^{137}\text{Cs}$  sources would validate the calculated results for the fallout source spectrum. This assumption is an important one which has formed the justification for the many experimental programs to be described here and in later chapters.

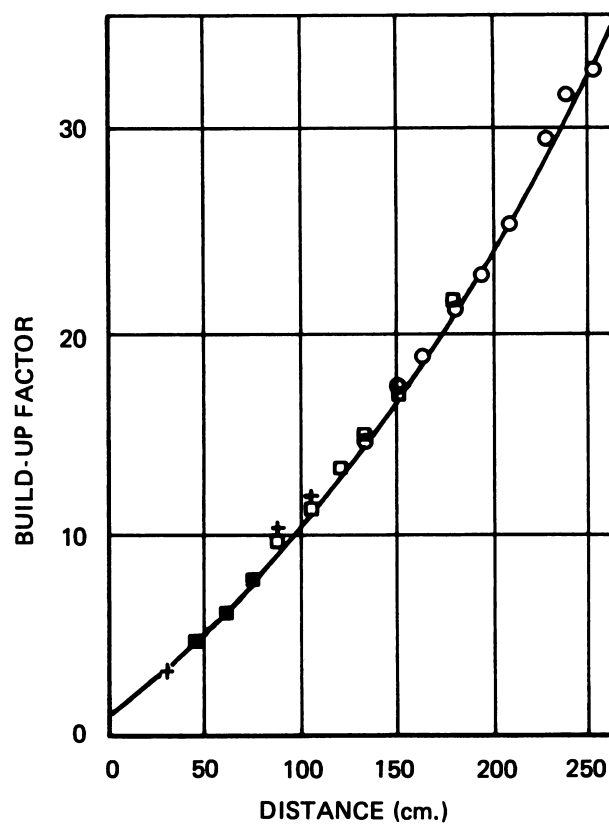
The most common detector response function used in experiments with these sources is one which measures the amount of ionization created in a small volume of air as a result of gamma (or x-ray) photons interacting with the air and (primarily) with the air-like wall surrounding that small volume. This is called exposure. (See sec. III.F.7). Since practically all of the experiments to be described in this book measured exposure, further discussion will be limited to this type of detector response.

### C. FREE FIELD

#### 1. Experiments with Point Sources

Calculations of the penetration of radiation from a point isotropic source have had many applications in radiation shielding. This is because radiation from a distributed source can often be calculated by superposition of results for point isotropic sources. Results of calculations for point isotropic and monoenergetic gamma-ray sources are often tabulated in terms of a buildup factor  $B(\mu_0 r, E_0)$ , which is defined as the ratio of the response to radiation of all energies to that for the uncollided radiation of energy  $E_0$ , at a source-detector distance of  $\mu_0 r$  in an infinite medium. The value of the buildup factor will vary with the type of response function. For our purposes the greatest interest is directed to the exposure buildup factor.

The penetration from a point isotropic source was the earliest calculation by the moments method [7] which was verified by experiment. White [8] performed the experiment in simple spherical geometry with a point source of  $^{60}\text{Co}$  gamma rays in a large tank of water. Figure VI.1, which has been reproduced



VI.1 Exposure Buildup Factors for Point Isotropic  $^{60}\text{Co}$  Source in Water;  
 □ , +, ionization data; ○ Geiger counter data; White [8]

from reference 8, shows the experimental and calculated results for the exposure buildup factor as a function of depth in water. The measurements extended out to a depth of 250 cm, and were made with an ionization chamber and a Geiger counter. This experiment, as well as others that had been made before 1956, have been discussed by Goldstein and Wilkins [9].

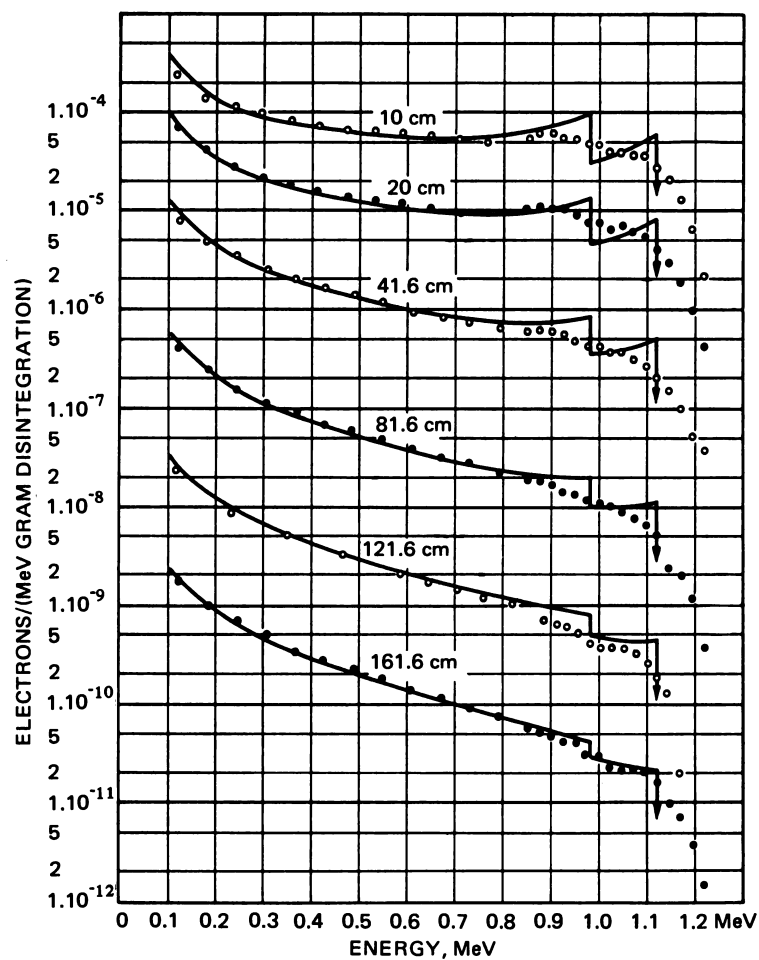
Measurements of the energy spectrum of radiation from a point isotropic source are more difficult than measurements of exposure, primarily because of difficulties in inferring a photon spectrum from a pulse-height distribution measured with a scintillation crystal spectrometer. In an early experiment by Hayward [10] the spectra of electrons produced by a point isotropic  $^{60}\text{Co}$  source in water were measured. A comparison [11] of her results with calculations by the moments method is shown in figure VI.2. For this comparison the moments results for the photon spectrum were weighted by the probability that a photon of energy  $E$  will produce an electron of energy  $T$ . From this figure it can be seen that the agreement of the calculated and measured electron spectra is very good. This confirms the accuracy of the calculated photon spectra.

More recently, evaluation of the gamma ray spectrum from a point source of  $^{137}\text{Cs}$  in water has been identified as a "benchmark"<sup>1</sup> problem [12]. Figure VI.3, from reference 12, contains a comparison of experimental values of the energy spectrum measured at 3 mean free paths<sup>2</sup> by M. Alberg and her co-workers [13] with results calculated by the moments method. It can be seen again that the agreement between the two sets of points is good. Furthermore, the calculations by the moments method agree even better with independent calculations by multi-group transport techniques.

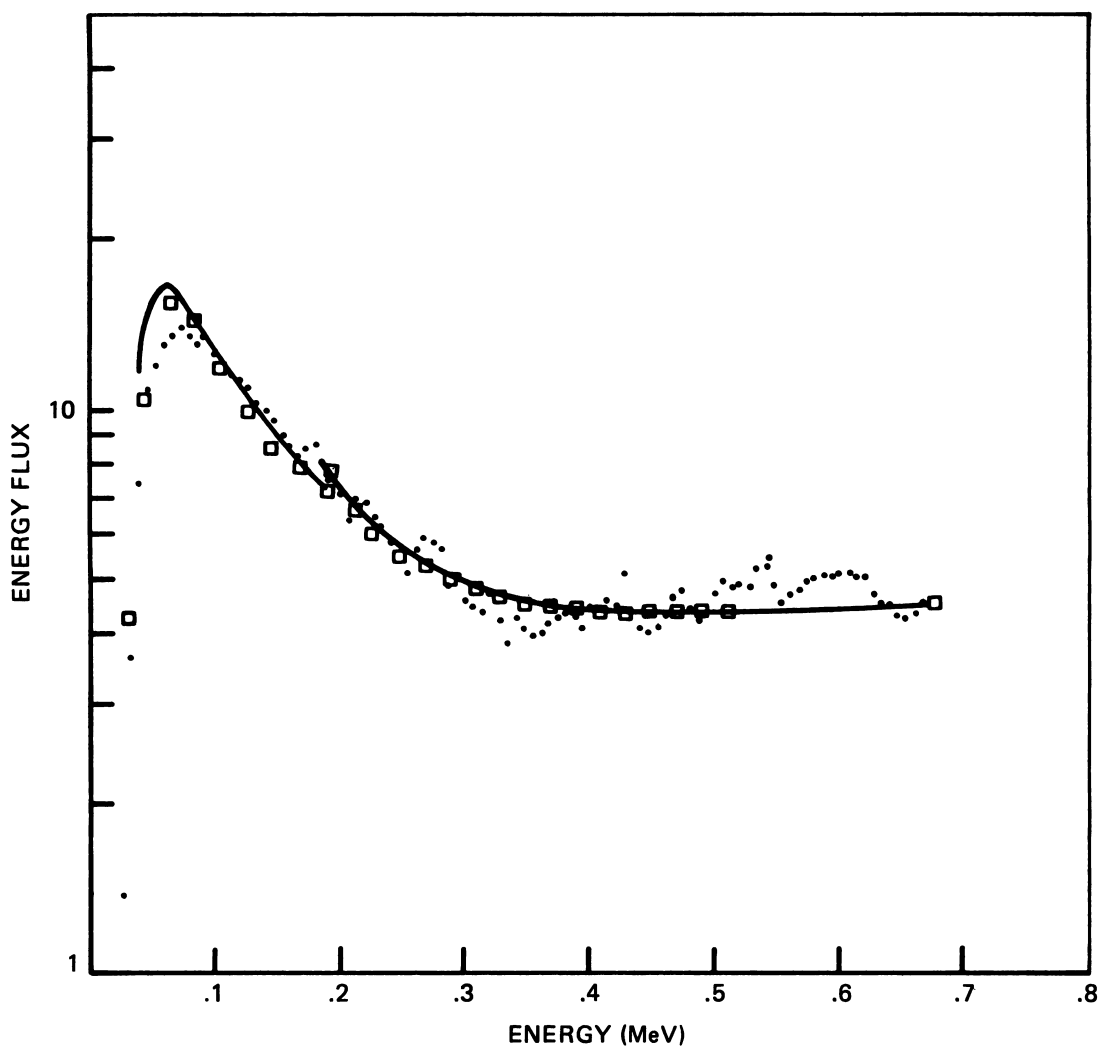
---

<sup>1</sup>Benchmark problems involve relatively simple source-detector configurations which can be used to compare results from different experiments and calculations.

<sup>2</sup>See section III.A.3 for discussion. Here the mean free path is numerically equal to  $\mu^{-1}$ , where  $\mu$  is the total attenuation coefficient of  $^{137}\text{Cs}$  gamma rays.



VI.2 Energy Spectra of Electrons Produced in an Anthracene Crystal by Photons from a Point Isotropic  $^{60}\text{Co}$  Source in Water. The points are from an experiment by Hayward [10]. The curves are calculated by the moments method [7]



VI.3 Differential Gamma-Ray Energy Spectra at 3 Mean-Free Paths in Water from a Point Isotropic  $^{137}\text{Cs}$  Source ●●● Experiment, Alberg, [13]; □□□ Moments method [9];—multi group transport calculations [12]

In summary, the results of calculations of the fluence and energy spectrum from a PTI source by the moments method are in good agreement with experimental results. Thus the accuracy of the other data discussed in Chapter V was generally accepted prior to the availability of data from structure shielding experiments.

## 2. Determination of Exposure at the Standard Unprotected Location

Many of the series of experiments on structures were preceded by preliminary experiments with sources distributed on the ground in the form of either point sources or line sources. These experiments generally involved the use of a small detector at a height of 3 ft, and a series of point sources or line sources placed at varying distances from the detector. Results for plane sources were inferred from these measurements. These preliminary experiments allowed comparison with calculations for a configuration which was well understood and for which there was a high degree of confidence in the accuracy of the calculations. In this way a large amount of experimental data were accumulated for the simple configuration of a point detector above a plane isotropic source.

In section V.A.1, the reduction factor  $R_f$  at any location was defined as the ratio of the detector response  $D$  at that location to the detector response  $D_o$  at the Standard Unprotected Location. The Standard Unprotected Location, which is discussed in more detail in that section is 3 ft above a smooth infinite plane of fallout radiation.

The reduction factor is independent of the magnitude of the source intensity because it is a ratio of responses for the same source intensity, and all responses are proportional to source intensity. However,  $D_o$  measures the magnitude of the threat from radiation and  $D_o$  does depend on the source strength. For fallout radiation the exposure  $D_o$  is expressed by

$$D_o = K_1 S_F,$$

where  $S_F$  is the contamination density - often expressed in terms of the gamma-ray activity from the energy yield of a weapon in kilotons of conventional explosives.  $K_1$  is the K-factor averaged over the "local" fallout at one hour after detonation, as discussed in section II.C.1. A value  $K_1 \cong 1930 \text{ (R/hr) / (Kt/mi}^2\text{)}$  has been recommended for general use.

In experiments designed to check approximate procedures, it would be sufficient to express all experimental results in terms of a reduction factor. Then one would have to know only that the effective source per unit area, whatever its magnitude, is the same in all experiments. However, most experimenters have carefully calibrated the strength of their sources to understand their measurements better and to facilitate comparison with other experiments. Thus many of the experiments to be described, began with a source calibration procedure.

The source calibration procedure described by McDonnell et al. [14] is typical. Three sources of  $^{60}\text{Co}$  of nominal strengths of 6, 60, and 600 Curies were calibrated by determining the exposure measured with two standard ionization chambers at various separation distances. The chambers had been calibrated earlier by comparison with standard chambers at the National Bureau of Standards. Calibration measurements were made with the source on a concrete pad and the detector elevated above the pad, and for both source and detector at the same height. The source strength for the latter arrangement was determined from the expression

$$D = S_o \Gamma_B A(\mu d) B_G(h, d) e^{-\mu d} / d^2 \quad (\text{VI.1})$$

where  $D$  is the measured exposure rate (R/hr)

$S_o$  is the source strength (Ci)

$\Gamma$  is the specific gamma ray constant (R/hr)/(Ci/ft<sup>2</sup>)

$\mu$  is the linear attenuation coefficient for <sup>60</sup>Co gamma radiation (1/448 ft for the average photon energy)

$h$  is the height of the source and detector (ft)

$d$  is the horizontal distance between source and detector

$B_A(\mu d)$  is the calculated buildup factor for air and

$B_G(h, d)$  is the enhancement due to scatter from the ground.

Source strengths inferred from this arrangement were consistent to within 1.3% with those inferred from the other geometric arrangement. In all subsequent experiments the source strengths had to be corrected for radioactive decay, using a value of 5.27 years for the half-life of <sup>60</sup>Co.

The specific gamma ray constant  $\Gamma$  requires some further comment. It is the exposure at unit distance from a source of unit strength. A recent tabulation [15] gives  $\Gamma = 13.07$  (R/hr)/(mCi/cm<sup>2</sup>) for <sup>60</sup>Co gamma rays and  $\Gamma = 3.226$  (R/hr)/(mCi/cm<sup>2</sup>) for <sup>137</sup>Cs gamma rays. When length is measured in feet, the equivalent values are, respectively, 14.1 (R/hr)/(Ci/ft<sup>2</sup>) and 3.49 (R/hr)/(Ci/ft<sup>2</sup>). Estimates of the value of these constant have varied, however, because they depend on the mass energy-absorption coefficient  $\mu_{en}/\rho$  and the average energy  $W$  required to produce an ion pair, neither of which has been known with high precision over the past twenty years. For example, Rexroad and Schmoke [4] assumed  $\Gamma = 14.3$  (R/hr)/(Ci/ft<sup>2</sup>) for <sup>60</sup>Co gamma rays. However, their measured exposure value at 3 feet may be as much as 5% high due to a questionable correction for ground scattering which was applied in the determination of the strength of the <sup>60</sup>Co source. McDonnell et al. [14] assumed a value of



14.0 (R/hr)/(Ci/ft<sup>2</sup>). From eq (VI.1) it can be seen that the source strength inferred by an experimenter is inversely proportional to the value assumed for  $\Gamma$ .

The experiments to be discussed generally required calibration of detectors as well as sources. In most cases only one or two detectors were calibrated against standard detectors such as those at the National Bureau of Standards. These were then used as secondary standards for the experiment. Again, the procedures followed by McDonnell et al. [14] are typical of those followed by other experimenters. Groups of 35 to 75 dosimeters were mounted in a circle around a source of known strength. During each exposure period the dosimeters calibrated at NBS were positioned with the other dosimeters and used to check the uniformity of exposure. On the basis of these experiments, detectors were grouped so that in any one group, the response was within  $\pm 3\%$  of the mean value. For each group of detectors further runs were made with source and detector 8 feet above the ground and for source-detector distances of four to fifty feet. For each group of dosimeters, the reading in micro amperes on a Charger-Reader was plotted against the exposure calculated from eq (VI.1). In this way calibration curves were developed for each group of dosimeters.

Table VI.1 shows the exposure per unit source strength  $D/S_0$  at the Standard Unprotected location due to a <sup>60</sup>Co source quoted for three experiments, together with the value of  $\Gamma$  assumed for their source calibration. Since the source strength  $S_0$  inferred for each experiment is inversely proportional to the value of  $\Gamma$ , the effect of uncertainties in this parameter can be eliminated by considering the dimensionless quantity  $(D/S_0\Gamma)$ . This quantity should be a better indicator of consistency among different experiments.

Table VI.1

Measured Exposure per Unit Source Strength at the Standard Unprotected

Location for a Plane Isotropic Source of  $^{60}\text{Co}$  Gamma Rays

	$D_o/S_o \left( \frac{R/\text{hr}}{\text{Ci}/\text{ft}^2} \right)$	$r \left( \frac{R/\text{hr}}{\text{Ci}/\text{ft}^2} \right)$	$D_o / (\Gamma S_o)$
Rexroad and Schmoke [4]	497	14.3	34.8
McDonnell et al. [14]	464	14.0	33.1
Schumchyk et al. [16]	468	14.3	32.7

The third experiment was performed at the same laboratory as the first, but at a later date. This table shows that the later experiment is more nearly consistent with the second, which was performed at the Protective Structures Development Center.

The value of  $D/S_o$  can also be calculated from the constant  $\Gamma$  for a point source and the buildup factor  $B_{PLI}^3$  for a plane source:

$$D/S_o = 2\pi\Gamma B_{PLI} E_1(.0063),$$

where  $E_1(x)$  is the exponential integral function given in eq (IV.7') and extensively tabulated, for example, in the NBS Handbook of Mathematical Functions [17]. The argument of .0063 is based on an assumed attenuation coefficient of .057 cm<sup>2</sup>/g and an air density of 1.205 g/l. Assuming a  $\Gamma$  value of 14.1 (R/hr)/ (Ci/ft<sup>2</sup>), and a buildup factor of 1.21 [18], the calculated value of the exposure rate per unit source strength is 482 (R/hr)/Ci/ft<sup>2</sup>). The corresponding value of  $D/(S_o\Gamma)$  is 34.2, in somewhat better agreement with the first of the experimental values shown in table VI.1.

---

<sup>3</sup>Although  $B_{PLI}$  is sometimes used to express the exposure at 3 ft above a plane source, this way of expressing the spatial distribution in general is uncommon, for reasons to be given in section VI.C.3.b.

### 3. Plane Isotropic Source in an Infinite Medium

#### a. Exposure from Uncollided Radiation

In section IV.A.4 it was noted that the expression for the fluence from a plane isotropic source can be derived from expressions for either point isotropic (PTI) or plane oblique (PLO) sources. From an experimental view it is more natural to consider the plane isotropic source as a collection of point isotropic sources uniformly distributed over a flat plane. The expression for the exposure due to uncollided photons from a point isotropic source is a modification of eq (IV.1'),

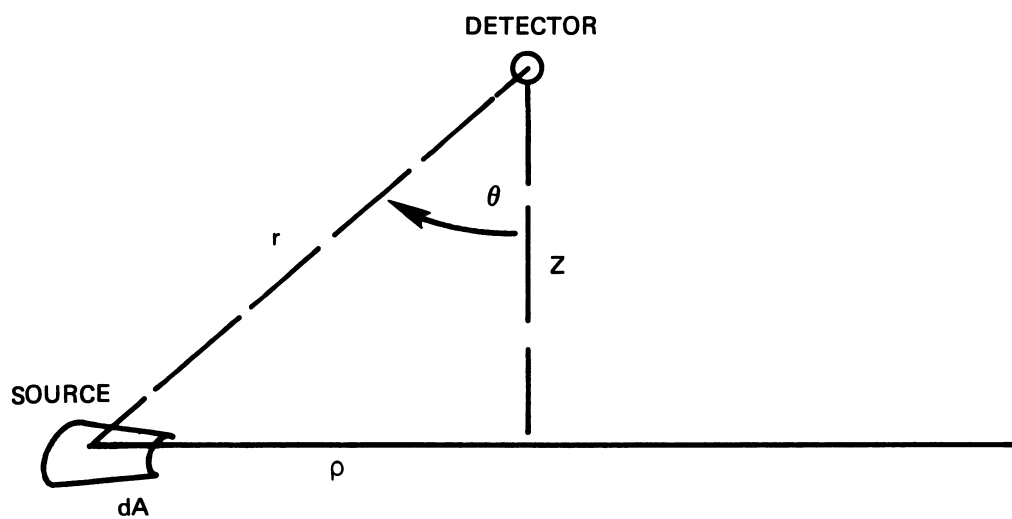
$$D_{PTI}^{(o)}(r) = \frac{S_o}{4\pi r^2} R(E) e^{-\mu_o r} \quad (VI.2)$$

where  $\mu_o$  is the attenuation coefficient at the source energy  $E$  and  $R(E)$  is the fluence-to-exposure conversion factor for photons of energy  $E$ .

The expression for the exposure from a monoenergetic plane source, analogous to eq (IV.9) is

$$D_{PLI}^{(o)}(Z) = \frac{1}{2} S_A R(E) \int_Z^{\infty} \frac{dr}{r} e^{-\mu_o r} = \frac{1}{2} S_A R(E) E_1(\mu_o Z) \quad (VI.3)$$

where  $Z$  is the height of the detector above the plane source and  $r$  is the slant radius from the differential source area to the detector. (See fig. VI.4).  $S_A$  is the source strength in photons per unit area. If the source is not monoenergetic an additional integral must be performed over the source spectrum (see eq (IV.13)).



#### VI.4 Geometrical Parameters for the Configuration of a Differential Source Area and Point Detector

## b. Total Exposure

Although knowledge of the behavior of the uncollided radiation from a plane isotropic source is useful in calculations, measurements of exposure do not distinguish between uncollided and scattered radiation. However, scattered radiation accounts for only about 20% of the total exposure from  $^{60}\text{Co}$  radiation, for example, at heights of a few feet above the ground. Therefore the total radiation at such heights behaves much like the uncollided radiation. The sky-shine portion of the scattered radiation will be discussed in the next section.

The development of the moments method by Spencer and Fano [7] led to calculations of the scattered as well as unscattered radiation from a plane isotropic source. Some early applications of the moments method to PLI source distributions were discussed by Berger and Doggett [19] and Gates and Eisenhower [20]. The first systematic tabulation of the spatial distribution of radiation from a PLI source was given by Preiser et al. [21] and later quoted by Goldstein [22].

The buildup factor is generally a useful parameter when the expression for the response  $D^0$  from uncollided radiation has a simple analytic form and when the responses to uncollided and scattered radiation are related by simple powers of the source-detector separation  $Z$ . The latter restriction breaks down as the detector approaches a PLI source because the fluence of scattered radiation remains almost constant whereas the fluence of uncollided radiation diverges, as explained in section IV.A.4. Also, for sources such as fallout, that are not monoenergetic, the exposure from uncollided radiation can no longer be represented by a single exponential function. Therefore, no attempt has been made to present the data in Chapter V in terms of buildup factors. Total exposure data for infinite PLI sources of  $^{60}\text{Co}$  ( $E_0 = 1.17$  and  $1.33$  MeV),  $^{137}\text{Cs}$  ( $E_0 = 0.66$  MeV), and the gamma spectrum from 1.12 hour fission products are reproduced in figures B.7a, B.7b, and V.13, respectively.

One of the earliest experiments with an effectively infinite PLI source was reported by Faust [23] in 1950. He measured the photon number fluence from a plane isotropic source of  $^{60}\text{Co}$  photons in a large tank of water, using a Geiger counter. He obtained fluences whose strength varied over three orders of magnitude and showed an exponential trend at deep penetration. The measured asymptotic relaxation length of  $.063 \text{ g/cm}^2$  at deep penetration is quite close to the value of  $.0615 \text{ g/cm}^2$ , which can be inferred from figure B.7a.

Early experiments by Rexroad and Schmoke [4] were restricted to detector heights of a few feet in air above a plane source on the ground. By the plane density theorem proved in section IV.B.2, the effect of the air ground interface can be ignored except for small effects due to the different elements present in the two materials. These effects are discussed in section VI.C.4.b.

The plane source was simulated by many measurements with point sources at varying distances from the detector. The measured exposure was presented as a function of the radius of a plane disk source. For disk sources of radius greater than about forty feet, the experiments agreed with calculations by Berger [24] to within about 5%. For disk sources of smaller radius, the discrepancies were as much as 20% -- due primarily to uncertainties in the contribution from ground-scattered radiation. Although Berger's calculations included the effect of the interface, they were admittedly inaccurate at these short distances.

In this and later experiments corrections were generally made to the experimental data to obtain the exposure for an infinite plane source. In this experiment measurements were made for source distance up to 800 feet, and the so-called "far field contribution" from sources beyond that distance amounted to only 3% of the estimated exposure.

Since the exposure due to uncollided radiation from a plane isotropic source can be calculated from the exponential integral function, and since the uncollided radiation accounts for about 80% of the exposure at these heights, the experiments did not provide a severe test of the calculated contribution of scattered radiation. The value of these experiments lay in the accumulation of experience in experimental procedures with radioactive sources and an assessment of the effect of the interface on the exposure due to point sources at an interface. (See section B.3 for discussion of interface effects.)

Comprehensive measurements were made at the OCD Radiation Test Facility (RTF) at Fort Belvoir, Virginia, for heights up to 33 ft above a plane source. They used a point-source circulation system [14], in which a radioactive  $^{60}\text{Co}$  source was propelled through plastic tubing at a constant rate. These measurements agreed to within a few percent with calculations shown in Fig. B.7a, except at heights below 3 ft. At these low heights the slightly rolling nature of the ground at the RTF shielded the detectors from the source during part of its trajectory through the tubing, thereby producing exposures which were lower than predicted values.

In 1965 Schumchyk and his collaborators [25] reported on measurements which extended to a height of 1200 feet above a simulated fallout field of  $^{60}\text{Co}$  radiation. These were made possible by using the 1500 ft BREN tower which had been erected earlier at the Nevada Test Site. A cable over the top of the tower was used to raise a vertical line of dosimeters. The line was maintained in a vertical position at 100 feet from the tower by three other cable and winch systems. Eleven source positions were used, out to a distance of 1200 ft from the foot of the detector line. Experimental exposures  $D(\rho)$  were measured for each source, and plane-source results were inferred for each detector by graphical integration of  $2\pi\rho D(\rho)$  plotted against the source radius  $\rho$ . A plot of the



experimental data vs height normalized to unity at 3 ft is shown in figure VI.5. The experimental results apply to a circular source of radius 1200 ft. The curve also shows the calculated result for a source radius of 1200 ft, obtained by multiplying  $L(X)$  from figure B.6a by the function  $L_c(X, \omega)$  from figure B.10a. The depth  $X$  was converted to height  $H$  in air assuming an air density of 1.1 g/l at the Nevada Test Site. The experimental results are seen to be in agreement with the calculations, with discrepancies less than about 10%.

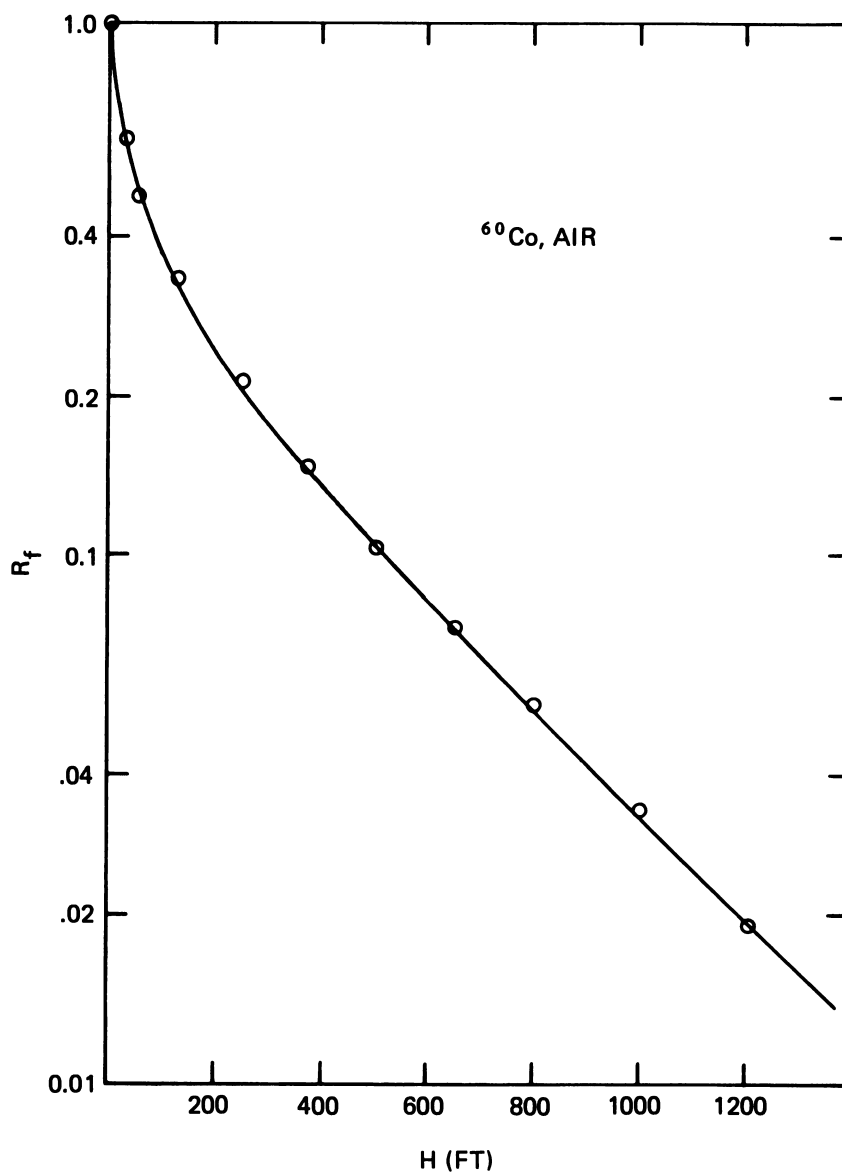
#### c. Exposure from Skyshine Radiation

In many problems one considers only that component of the radiation which reaches the detector from directions in the hemisphere away from the source. Reduction factors for this component were discussed in section V.C.4.a. For sources distributed on the ground and a detector above ground, such photons arrive from the upper hemisphere -- hence the name "skyshine."

In order to measure the exposure due to a skyshine as a function of height above the source one would need a " $2\pi$ " detector which measured radiation incident only from directions in the upper hemisphere. Furthermore, measurements would be required at heights of several hundred feet in order to detect large variations in intensity relative to that at ground level. Such measurements would require a field many hundreds of feet in diameter. Although measurements of the total exposure at great heights have been attempted [25], no definitive measurements of skyshine variation with height have been made.

The ratio of exposure integrated over the upward hemisphere to exposure integrated over all directions is a measure of the relative importance of skyshine at a particular height above the plane. This ratio, which we call  $\beta$ , is given by

$$\beta(H) = S(H)/L(H), \quad (\text{VI.4})$$



VI.5 Experimental and Calculated Values of the Exposure from a Plane Isotropic Source as a Function of Height in air. ○ Experimental, Schumchyk [25]; — Calculation,  $L(H)L_c(H,\omega)$  (Figures B.7a and B.10a)

and is shown in figure VI.6, as calculated from the data of figures V.28 and V.13. Since  $S(H)$  remains nearly constant near  $H = 0$ , while  $L(H)$  diverges, the value of  $\beta(H)$  decreases to zero as  $H$  approaches zero. For  $3 < Z < 1000$  ft of air,

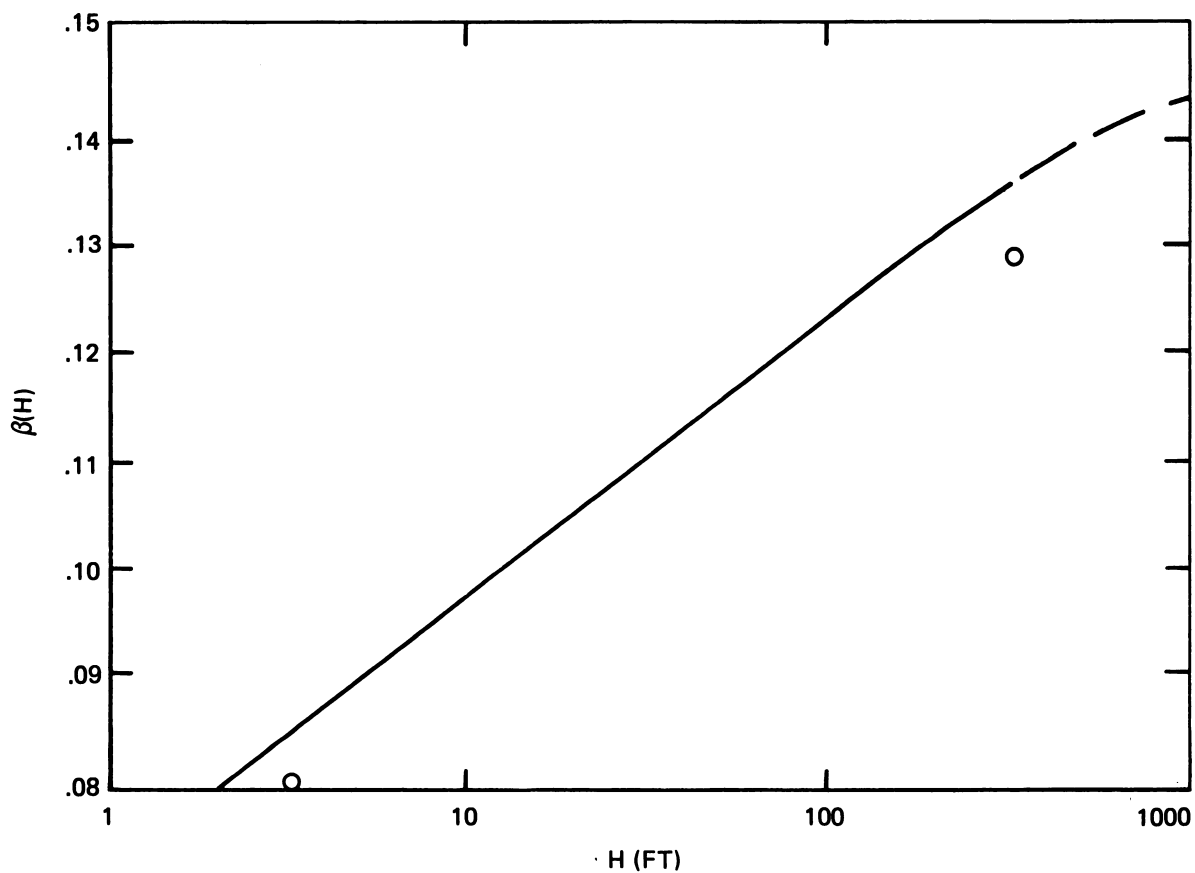
$$\beta(H) \approx .075 + .023 \log_{10} H, \quad 3 < H < 1000 \text{ ft of air.} \quad (\text{VI.5})$$

Thus the ratio increases slowly with height in this range. Despite the trend indicated by this expression,  $\beta$  must eventually level off to some asymptotic value. Since at deep penetrations the fluence from a plane isotropic source approaches that from a point isotropic source [26],  $\beta$  should approach the back-scatter ratio at large distances from a point isotropic source. This ratio can be obtained by referring to figure V.21 and noting that the value of the geometry curve  $P_a^{(s)}(d, \omega)$  for  $\omega = 1$  and large  $d$ , is about .85. The fraction back scattered is therefore about 0.15, and  $\beta(H)$  should thus approach 0.15 for very large  $H$ .

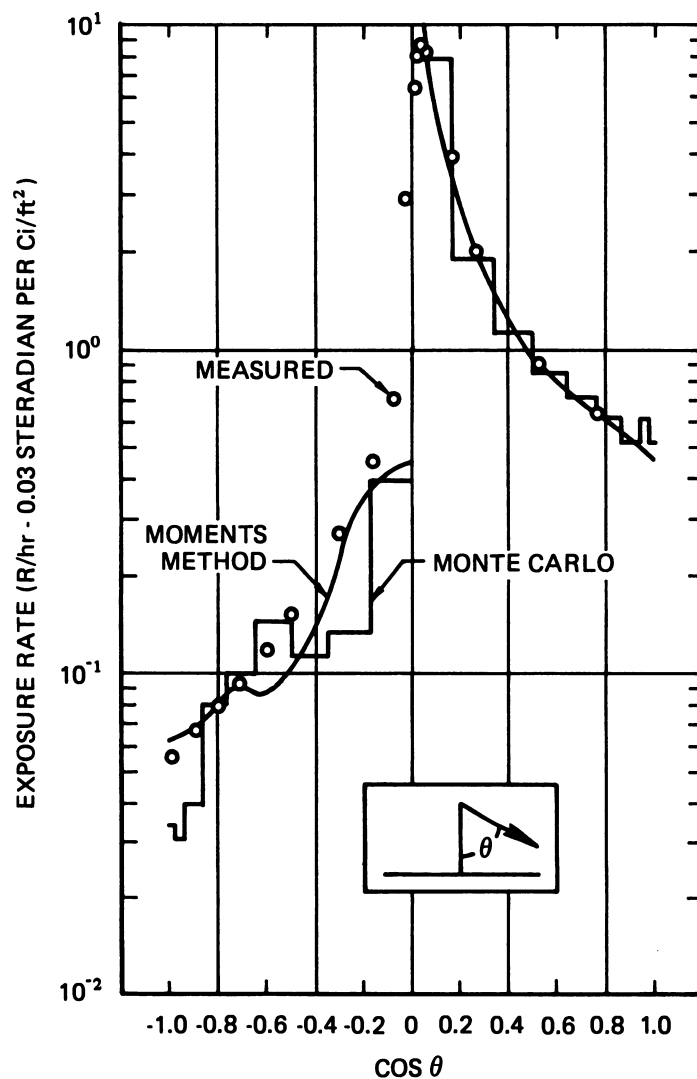
The two points shown in figure VI.6 give results of independent calculations by Beck and de Planque [27]. These calculations used an expansion in orthogonal polynomials to solve the transport problem. Their calculation took account of the change in density and composition at the ground-air interface. Although their results are about 5% lower than calculations by the moments method, they show the same general trend with height above the source.

#### d. Angular Distributions

Burson and French [28] reported on measurements of the angular distribution of exposure at a detector height of three feet, for  $^{60}\text{Co}$  ring sources of radii up to 1000 feet. From these they inferred the angular distribution data shown in figure VI.7, which are in rather good agreement with  $\ell(H, \cos\theta)$  data from figure B.1a. The experimental values in the region  $-0.2 \leq \cos\theta \leq 0$  are probably



VI.6 Calculated values of the Ratio of Skyshine Exposure to Total Exposure as a Function of Height above an Infinite Plane Isotropic Source of  $^{60}\text{Co}$  radiation.  $\circ$  Calculation, Beck and de Planque [27]; — Calculation  $S(H)/L(H)$  (Figures B.20a and Figures B.7a)



VI.7 Comparison of Measured and Calculated Angular Distribution 3 ft above an Infinite Plane  $^{60}\text{Co}$  Source.  $\circ$  Experimental, Burson and French;  $\text{—}$  Monte Carlo calculation [28];  $\text{—}$  Calculation (Fig. B.1a)

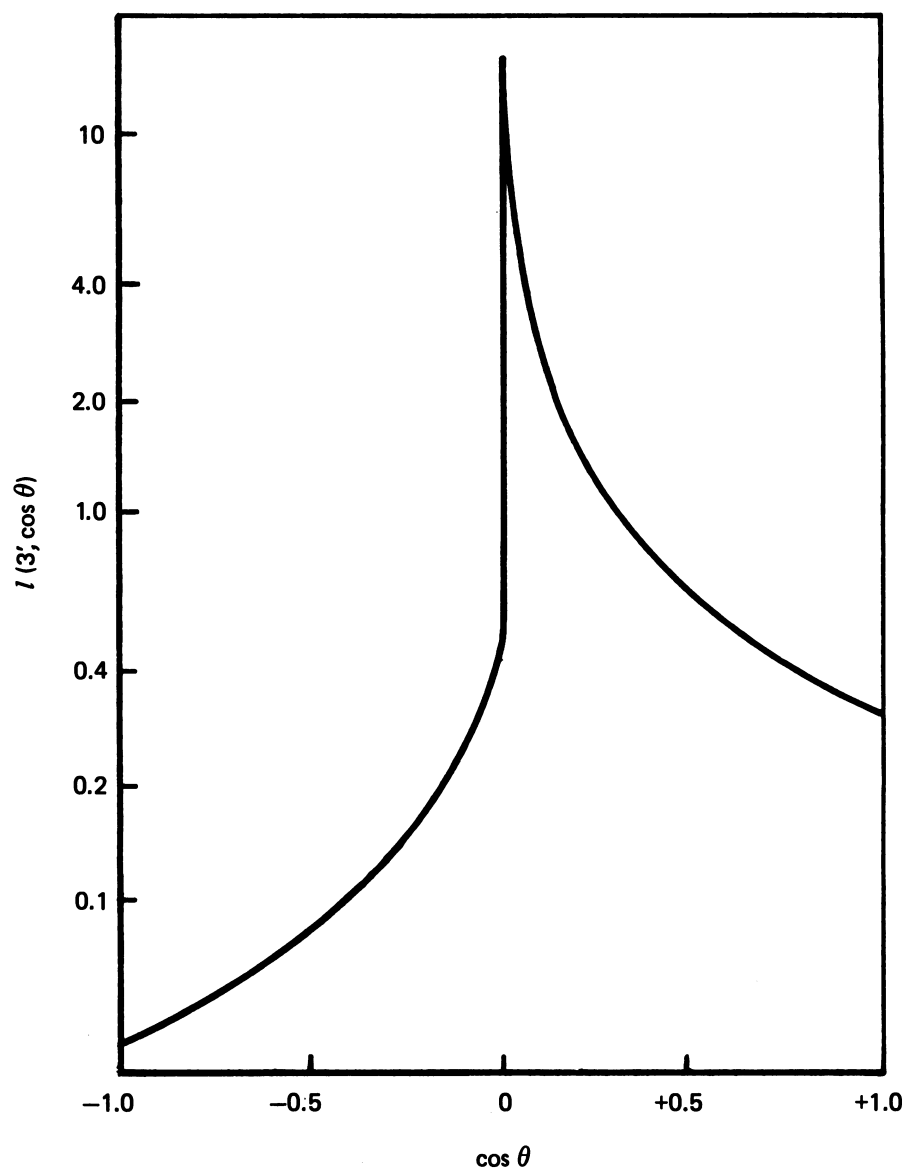
spuriously high due to radiation from just below the horizon ( $0 \leq \cos\theta \leq 0.1$ ) which was scattered in the collimator. The minimum and maximum near  $\cos\theta = -.7$  in the calculated curve (see also fig. B.1a) is an artifact which is due to the insufficient number of harmonics included. Thus the shape of the experimental curve should be more realistic. This is confirmed by figure VI.8, showing data from an accurate Monte Carlo calculation by E. Morris [29], which does not exhibit the oscillations shown in figures VI.7, B.1a, and B.1b. Other Monte Carlo data due to Collins and Wells [30] are given by the histogram in figure VI.7.

#### e. Energy Distributions

Early calculations of spectra, using NBS-NDA moments generated jointly by Goldstein, Wilkins and Spencer [7,9], were reported by Berger and Dogget [19] and by Gates and Eisenhauer [20]. But this type of data has little application to fallout gamma ray shielding, which uses only integrals over the spectrum, weighted by detector response.

#### f. Energy-Angular Distributions

Experiments designed to assess the joint angular-energy distribution of radiation are extremely difficult. Experiments must cope with the two-fold problem of spurious effects from collimators and difficulties due to unfolding pulse height data to obtain spectra. For example, Schumchyk et al. [25] reported their spectrometer data in terms of pulse-height channels, rather than attempting to infer an energy spectrum. However, Frank and Taylor [31] were able to convert their measurements of the fallout radiation at the



VI.8 Angular distribution of exposure at 3 ft above a plane isotropic source of  $^{60}\text{Co}$  radiation, calculated by combined semi-analytic and Monte Carlo methods.

Nevada Test Site into angular-energy distributions. A comparison of their measured spectrum of photons from the ground, nine days after fission, showed qualitative agreement with calculations by Björnerstedt [32] and Nelms and Cooper [33]. Also, their spectra were similar to those measured by Huddleston, et al [34] at different places and times in the same fallout field.

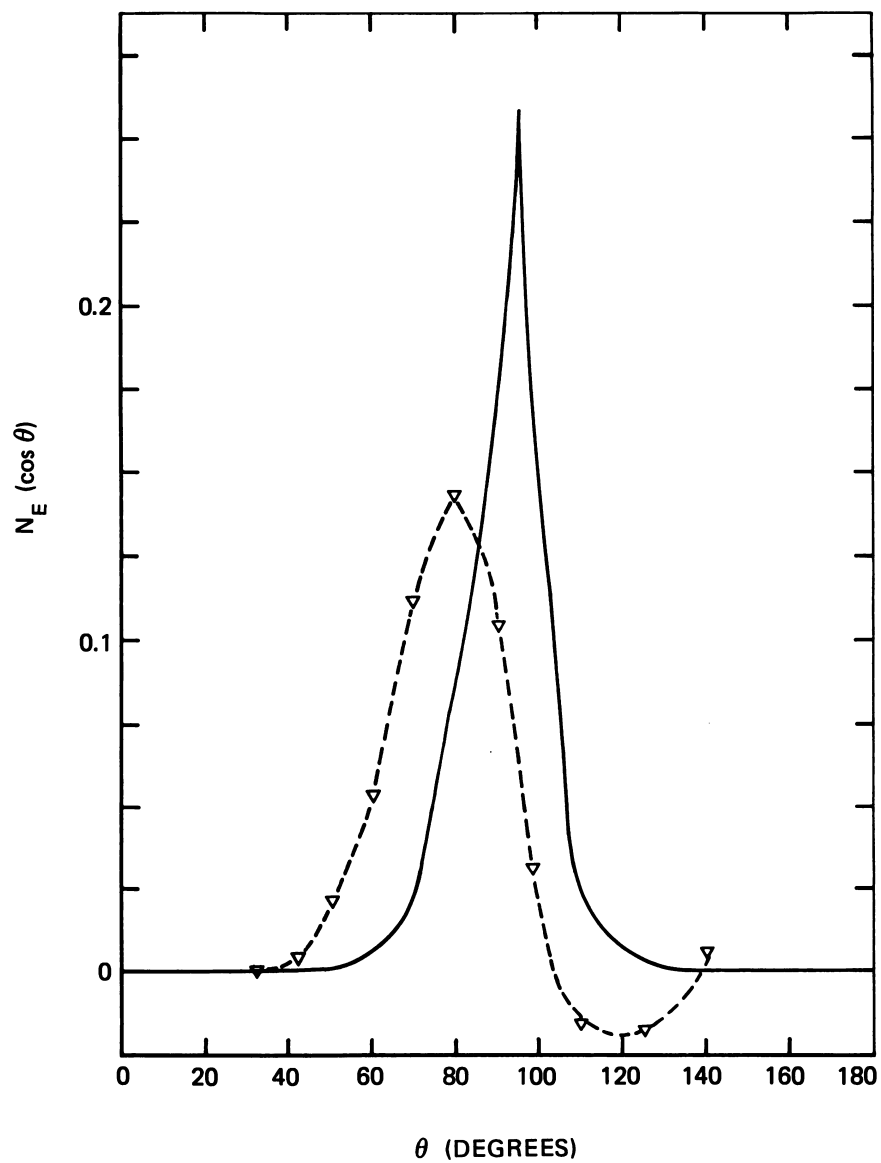
Calculations have been made by Michael and Lamonds [35] of the angular energy distribution up to 1000 feet in air above monoenergetic gamma-ray sources ranging from 0.1 to 1.33 MeV. They used the moments method with a reconstruction technique suggested by M. J. Berger [36]. Their results give a good estimate of the general nature of these distributions. However, in regions where angular distributions are rapidly varying, the lack of accuracy is illustrated by anomalous effects such as negative fluence. Early calculation of these distributions by the Monte Carlo method [37], showed large statistical fluctuations. However, Morris [29] later made Monte Carlo calculations, together with a semi-analytic calculation of the singly-scattered component, resulting in standard deviations which were generally less than 10%. An indication of the difference between the two types of calculations is shown in figure VI.9, which was taken from Morris' report. From this comparison it can be seen that the more careful treatment of single scatter by Morris affects not only the shape of the peak in the angular distribution, but also the position of the maximum.

#### 4. Effects of Ground-Air Interface

##### a. Air/Condensed Air

In experimental configurations, the source is distributed on a plane interface between media of two different densities and effective atomic numbers: air and ground. Some simplification results from considering the effects of density and atomic number separately. The effect of the density alone can be





VI.9 Comparison of Calculated Joint Energy and Angular Distributions for  $E \approx 1$  MeV at Three Feet above a Plane Isotropic Source in an Infinite Medium of Air. — Calculation, Morris [29]; — ▼ — Calculation Michael and Lamonds [35]

discussed by considering first an isotropic source distributed on a plane interface between air at normal density, and air compressed to a density equal to that of earth.

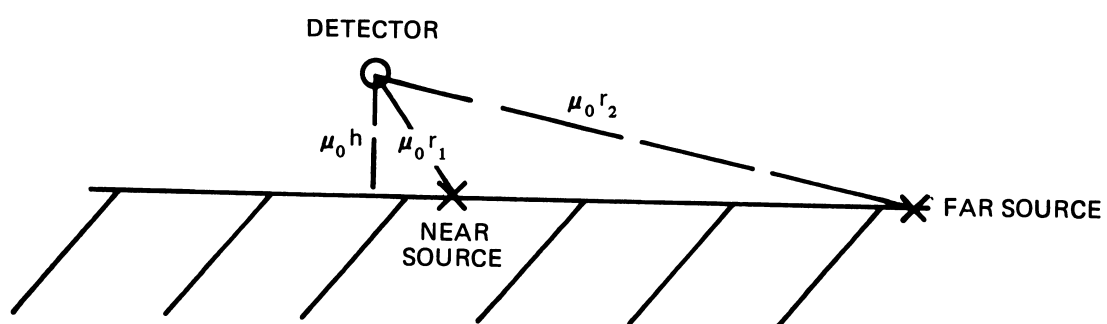
These two configurations are related by the plane density theorem proved in section IV.B.2 (see earlier discussions by Fano [38] and Spencer [39]). Thus we observe that the angular and energy distribution of fluence at a distance  $\tau$  from a plane isotropic source is not affected by a density change of the air on the other side of the source provided that the density varies only with distance from the source plane.

Although the fluence does not depend on variations in air density, the relative contribution which each differential source area makes to the scattered fluence at a given position is affected by the density distribution. For example, at a height of a few feet in air (of normal density), a given source element far from the detector will contribute relatively less to the scattered fluence in the case of compressed-air backing than in the case of an infinite homogeneous air medium, since most of the photons are re-emitted near the source and must travel a long distance before reaching the detector. The compressed medium thus contributes fewer of these photons to the detector. But the integral over all sources is the same regardless of compression (theorem of plane density variations). Therefore the nearest sources--those immediately beneath the detector--must contribute relatively more. The compressed medium thus acts as a reflector for photons from these sources.

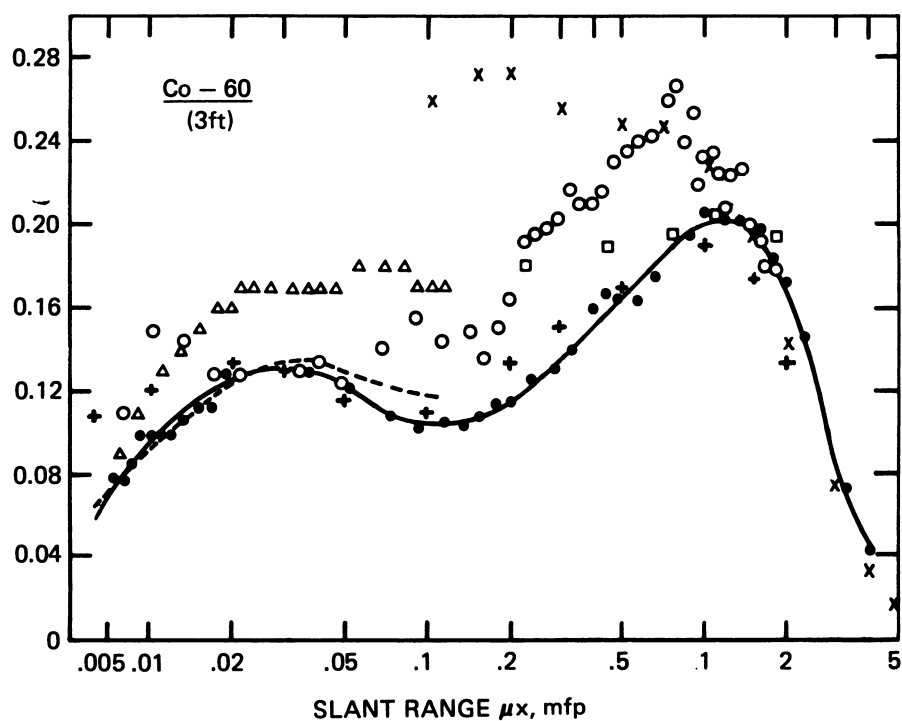
An early calculation of the effect of the density interface was made by Berger [24]. He concentrated on the range of source-detector separations between one and five mean free paths in normal air and did not consider his data valid for small fractions of a mean free path.

A quantitative though approximate estimate of this effect was given by Eisenhauer [40] who analyzed the radiation reflected from the interface in terms of an "image source". He discussed the effect of the interface in terms of the ratio of the exposure from scattered fluence to that from uncollided fluence. For a detector height  $\mu_0 h \ll 1$  and a  $^{60}\text{Co}$  radiation source, the ratio of exposures due to a source at a distance  $r_1$ , and nearly under the detector is about 0.1 for condensed air and  $0.74\mu_0 r_1$  for ordinary air. This configuration is shown in figure VI.10. Thus, for sources near the detector the compression of air below the interface to a density equivalent to that of earth is predicted to enhance the contribution from scattered radiation by a factor of 13 if  $\mu_0 r_1 = .01$ . Even so, the enhanced contribution from scattered radiation is still only 10% of the contribution from uncollided radiation. For a source whose distance  $r_2$  is at least five times the detector height  $h$ , the ratio of scattered to uncollided exposure is predicted to be about  $[0.5 h/r_2 + 0.37 \mu_0 r_2]$  for condensed air and  $0.74 \mu_0 r_2$  for ordinary air. The first term in the square brackets accounts for photons from the condensed air while the second term gives the contribution from the region of ordinary air containing the detector. This expression for far sources predicts that the compressed air reduces the contribution from scattered radiation for slant distances  $r_2$  such that  $r_2^2 > h/(.74 \mu_0)$ .

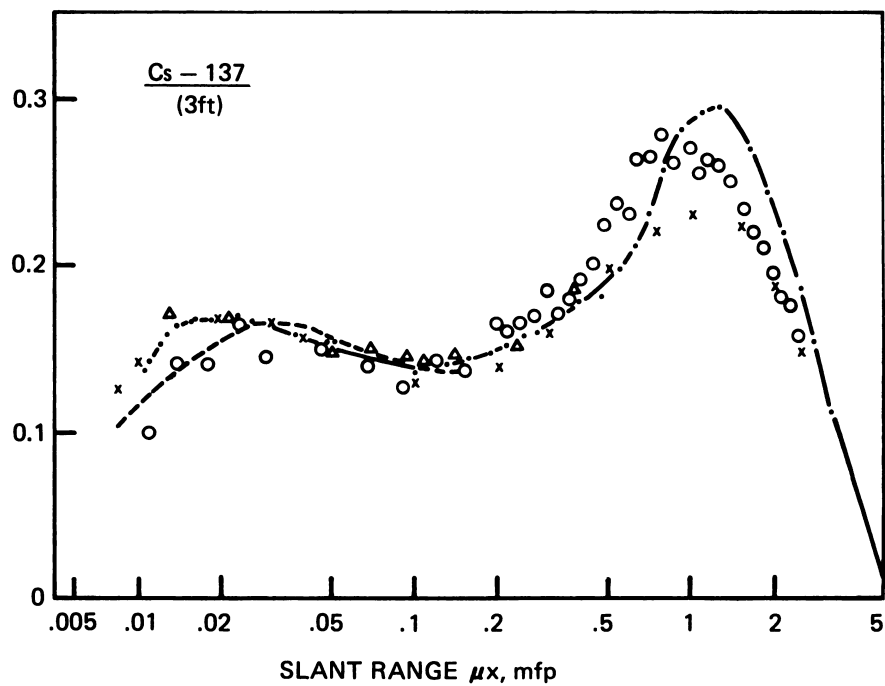
The most recent review of this effect was given by Clarke [41]. Clarke's summary of numerous experimental [4,42,43] and calculated [24, 37, 40, 44, 45] results is shown in figure VI.11. Because the direct and ground-scattered radiation from nearby sources contribute heavily to the total exposure, he plots the scattered exposure as a function of the log of the slant distance from source to detector to emphasize the close-in region. The curve then represents the "scattered radiation generated by ring sources whose widths are a constant percentage of their (slant) radius [41]." This type of plot has



VI.10 Geometric Parameters for the Configuration of Two Point Sources at the Ground-Air-Interface, Near and Far from a Point Detector. Distances are indicated in mean free paths.



VI.11a Exposure from Scattered Radiation due to a Point Source at the Ground-Air Interface <sup>60</sup>Co. Experimental,  $\bigcirc$  Rexroad and Schmoke [4],  $\Delta$  Batter [42]; Calculations  $\square$  French and Garrett [37],  $+$  Eisenhauer [40],  $x$  Berger [24],  $-\bullet-$  Marcum [44],  $- - -$  Chilton and Fu [45].



VI.11b Exposure from Scattered Radiation due to a Point Source at the Ground-Air Interface  $^{137}\text{Cs}$ . Experimental,  $\circ$  Rexroad and Schmoke [4],  $\Delta$  Clifford [43]; Calculations  $\square$  French and Garrett [37],  $+$  Eisenbauer [40],  $\times$  Berger [24],  $-\bullet-$  Marcum [44],  $- - -$  Chilton and Fu [45].

the advantage that the relative area under the curve between any two radii is a measure of the relative contribution from the sources lying between the two radii. From figure VI.11 it can be seen that roughly half of the exposure from scattered radiation comes from distances less than about 0.2 mean free paths. This contribution is due primarily to photons reflected from the ground. The remaining contribution from distances greater than 0.2 mean free paths arises primarily from photons scattered in the air.

Experimental results for the  $^{60}\text{Co}$  source in figure VI.11 are seen to be generally higher than calculated results. The reason for this is not known. The comparison for a  $^{137}\text{Cs}$  source shows much better agreement between calculations and experiment.

#### b. Ground-Air Interface

We consider next the effect of replacing the compressed air by earth or some other medium whose absorption properties differ from those of air. The effective atomic number of earth is higher than that of air and photoelectric absorption will tend to reduce the number of low energy photons which are reflected from the medium. The substitution of earth for air has been calculated by Beck and Bennett [46] to produce about a 7% reduction in scattered exposure at one meter above the interface due to a source of energy 0.662 MeV ( $^{137}\text{Cs}$ ). For source photons of 1.25 MeV (average energy for  $^{60}\text{Co}$ ) Morris [29] has calculated a reduction of 3.3% in the scattered exposure. The corresponding effect on the total exposure for photons with a source energy of the order of 1 MeV is about 1%. The uncertainty in experimental measurements of total exposure, however, usually exceeds 1%. Thus, infinite medium calculations for plane isotropic sources should be accurate to about 1% for predicting experimental results near the ground-air interface.

The energy-angular distribution of photons from a  $^{60}\text{Co}$  source near the ground-air interface was studied by Frank [47]. He compared his experimental results with Monte Carlo calculations by French with the L05 [48] and COHORT [30] computer codes. In the experiments the detector was at a height of 3 ft and the source was elevated 8 in above the ground. The elevated source enabled the collimated detector to measure the ground scatter without looking directly at the source. Comparison between experiments and calculations are not exact because the Monte Carlo calculations were made for source at ground level. Although the measured energy-angular distribution of the exposure for  $^{137}\text{Cs}$  shows somewhat greater exposure from the upward hemisphere than do the Monte Carlo calculations, the experimental exposure for  $^{60}\text{Co}$  shows factors of two to five greater exposure from most directions of the upward hemisphere. When integrated over all angles and expressed as a buildup factor, the experimental results for  $^{60}\text{Co}$  lie higher than all other experimental and calculated data. Frank was unable to explain this difference between his measurements and the Monte Carlo calculations. It is possible that this difference is related to the difference between experimental and calculated value for  $^{60}\text{Co}$  evident in figure VI.11.a.

## 5. Limited Field Effects

### a. Total Exposure

In all experiments the infinite plane isotropic source can only be approximated because practical considerations such as low radiation intensities limit experimental measurements to some maximum distances between source and detector. A correction is usually made to experimental data to account for the contribution from sources beyond the experimental cut-off distance. To make this correction and to be sure that it is small, the experimenter must know the relative contribution of sources as a function of their distance  $r$



from the detector. For uncollided radiation at a height  $h$  from a circular disk source of slant radius  $r$  this can be determined from the integrand of eq. (VI.3) as  $[1 - E_1(\mu r)/E_1(\mu h)]$ . Table VI.2 gives values for this ratio for a detector height of 3 ft and a  $^{60}\text{Co}$  source. For example, one-half of the exposure from uncollided radiation comes from sources within a distance of 30 feet. Sources beyond about 500 feet contribute less than 5% to the exposure from uncollided radiation from an infinite plane source. When the scattered radiation is included, however, the contribution from distant sources becomes more important, as we shall see.

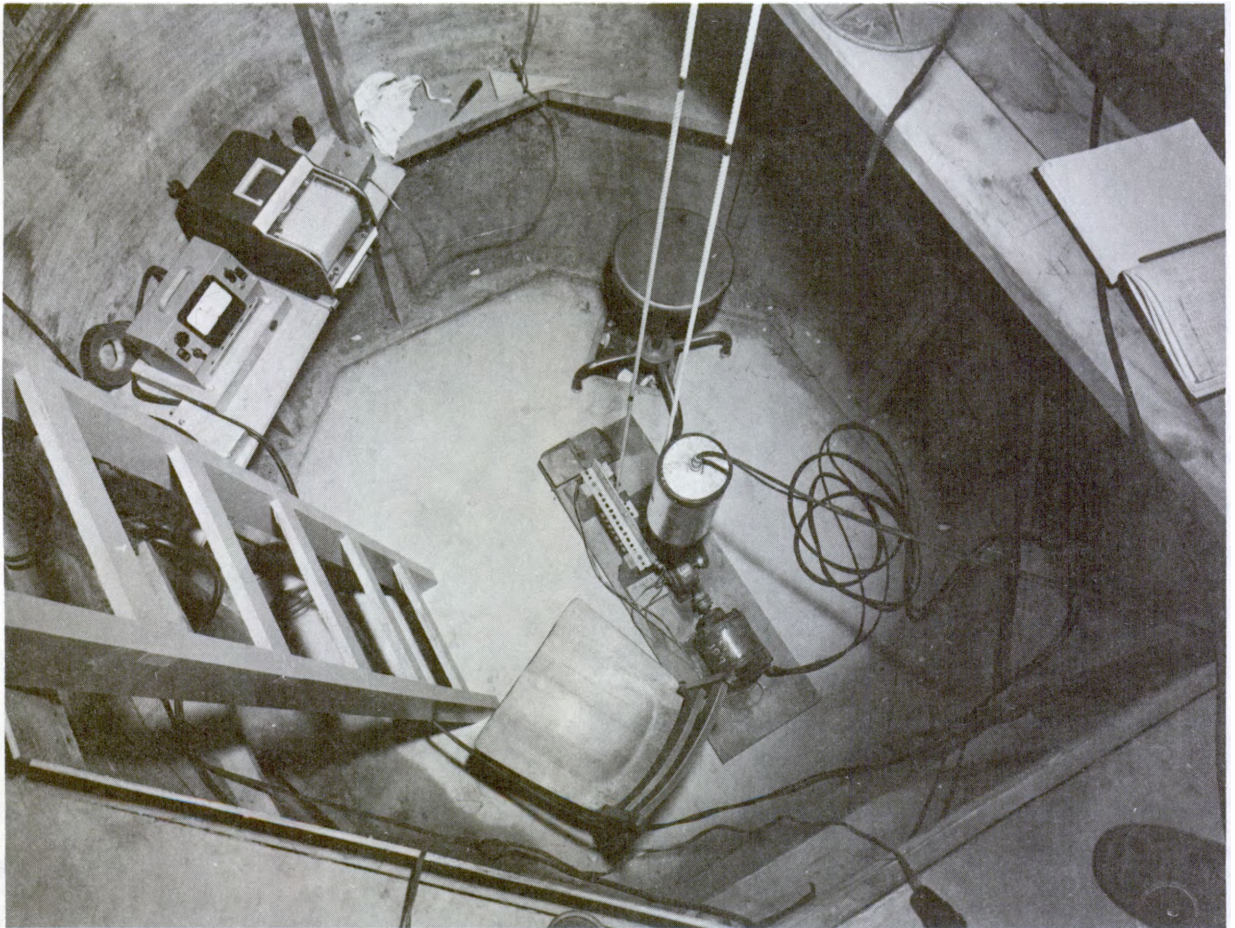
#### b. Skyshine Exposure

In subsection IV.C.2b, it was pointed out that the trend of the exposure from singly-scattered radiation at a distance  $r$  near a point source is proportional to  $r/4\pi r^2$ , whereas the uncollided radiation is proportional to  $1/4\pi r^2$ . Therefore the exposure from scattered radiation from a plane isotropic source can be estimated by multiplying the integrand in eq. (VI.3) by a factor proportional to  $r$ . The relative importance of ring sources, then, at a distance  $r$  in contributing to the scattered exposure is given approximately by  $e^{-\mu_0 r}$ . Therefore, a significant fraction (about  $1/e$ ), of the exposure due to skyshine comes from ring sources beyond one mean free path (about 450 ft in air for a source energy of 1.25 MeV) from the detector. The above statement is limited to detector positions within a few feet from the source plane, where single scatter predominates over multiple scatter.

Measurements of the skyshine exposure at the center of a circular clearing in an infinite plane source have been made. Clifford's measurements [49] of exposure at various depths in a cylindrical foxhole of 1 meter radius with  $^{137}\text{Cs}$  sources were an early source of such data. The experimental arrangement is shown in figure VI.12. A large-volume recording ionization chamber is shown attached to a motor-driven pulley for dose rate measurements on the axis of the 2-meter

Table VI.2 Tabulation of the Function  
 $[1 - E_1(\mu r)/E_1(\mu h)]$  for a  $^{60}\text{Co}$  source ( $\mu = .057\text{cm}^2/\text{g}$ )  
 And a Detector Height of Three Feet.

r(FT)	$\mu r$	$E_1(\mu r)$	$[1 - E_1(\mu r)/E_1(.0063)]$
3	.0063	4.50	0.0
10	.021	3.31	.264
20	.042	2.63	.416
30	.063	2.25	.500
40	.084	1.98	.560
50	.105	1.779	.605
100	.21	1.183	.737
150	.31	.882	.804
200	.42	.670	.851
300	.63	.428	.905
400	.84	.289	.936
500	1.05	.202	.955



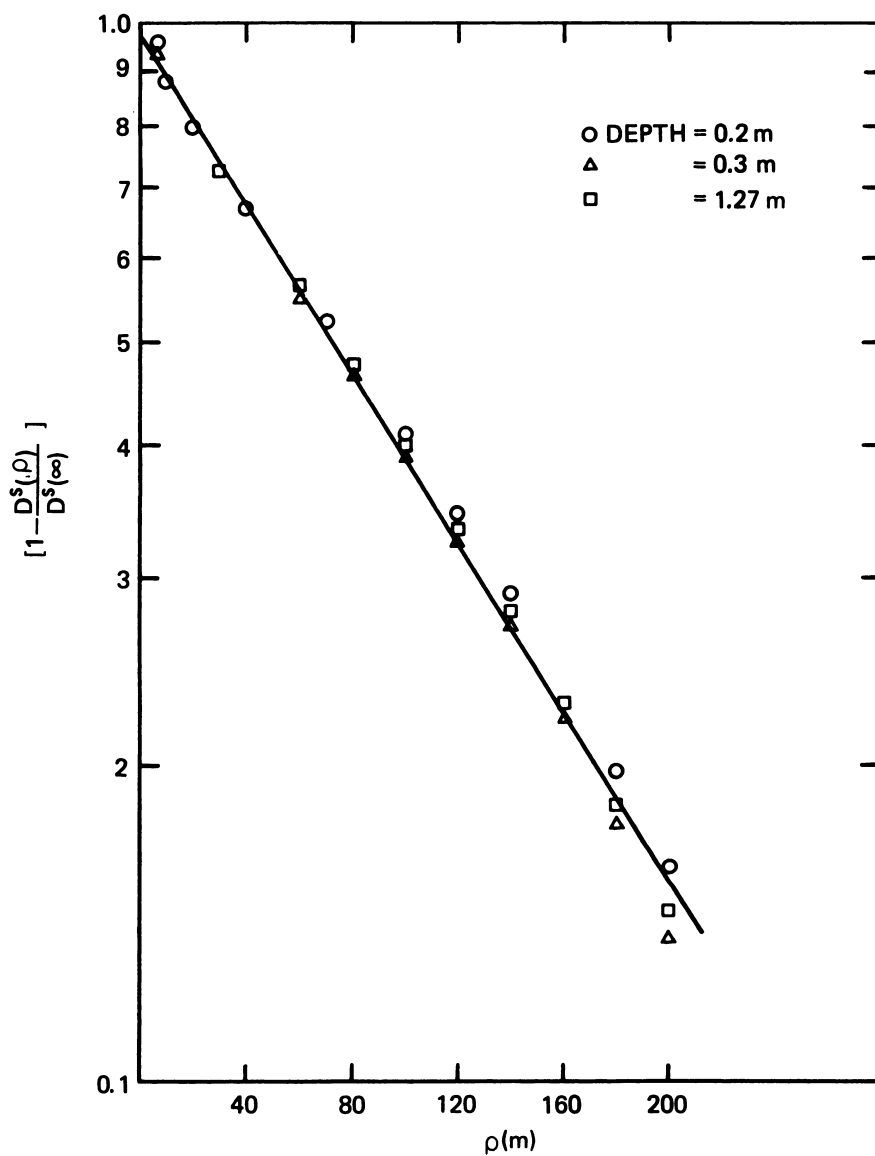
VI.12    Photograph Looking Down Into Foxhole of 2 Meter Diameter used in Clifford's Experiments [49]

diameter by 2-meter deep hole. A plot of his data as a function of the radius  $\rho$  of the clearing is shown in figure VI.13. The quantity which is plotted is unity minus the ratio of the exposure  $D^S(r)$  from a disk source of radius  $r$  to the exposure  $D^S(\infty)$  from an infinite plane. It can be seen from this figure that the value of the exposure from scattered radiation does not vary significantly with detector depth and shows a behavior which is very close to

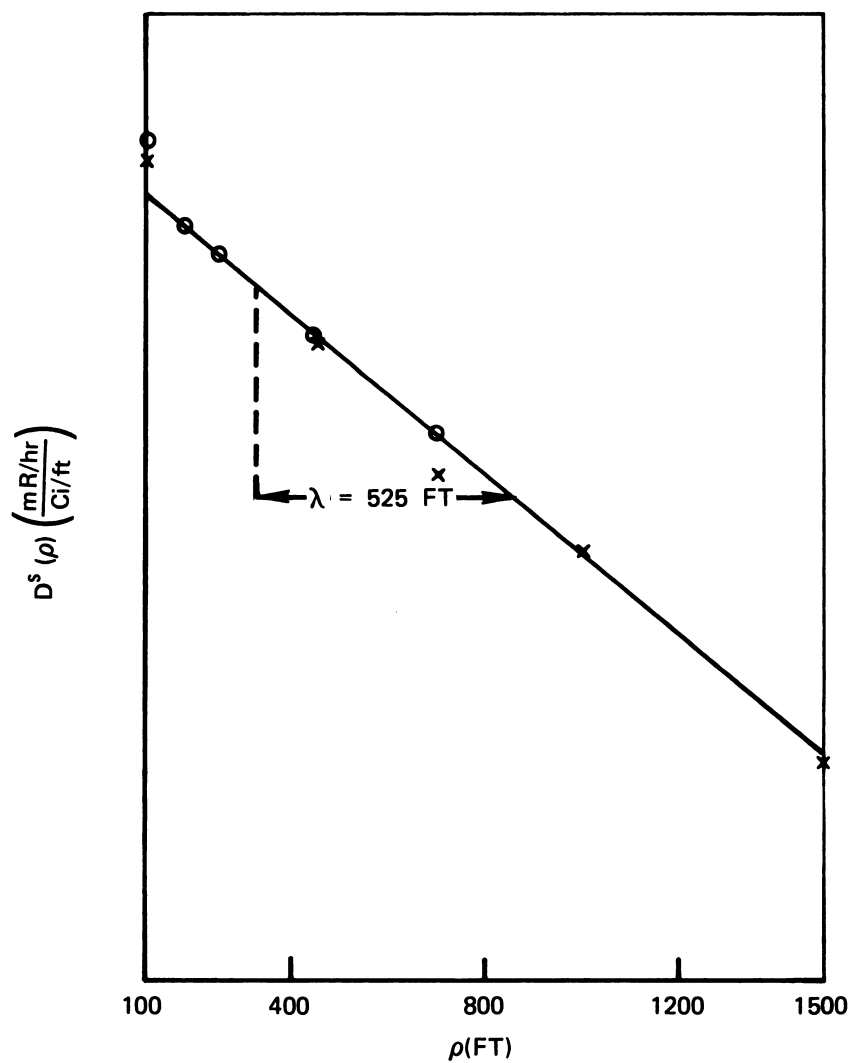
$$D^S(r) = D^S(\infty) (1 - e^{-r/\lambda}) .$$

The parameter  $\lambda$  is the relaxation length, i.e., the increment in radial distance for which the exposure decreases by a factor of  $e$ . For uncollided radiation this is numerically equal to the mean free path -- the average distance between radiation interactions with molecules in air. The empirical value of  $\lambda$  from figure VI.13 is about 107 m, in agreement with the mean free path for  $^{137}\text{Cs}$  radiation in air of density 1.2 g/l.

In another series of experiments at the Nevada Test Site, Burson and Summers [50] made similar measurements with a  $^{60}\text{Co}$  source. Their measurements for two different types of detectors as a function of the radius of a ring source are shown in figure VI.14. The relaxation length inferred from a straight line drawn through these points is 525 ft. (air density = 1.1 g/l). This value agrees very well with their estimate of 530 ft for a mean free path in air at the Nevada Test Site. Thus, again, the experimentally observed relaxation length is approximately equal to the mean free path. One expects this simple conclusion as a result of single scatter downward from uncollided radiation in near-horizontal directions and correspondingly high intensity. Similar experiments were performed by Starbird and Batter [51]. However, because their measurements extended only to distances of about 0.1 mean free paths, it is not possible to infer any relaxation length from their measurements.



VI.13 Relative Exposure from  $^{137}\text{Cs}$  Sources Beyond a Circular Area of Radius  $\rho$ , Experimental, Clifford [49]



VI.14 Experimental Exposure from Scattered Radiation due to a Ring Source of  $^{60}\text{Co}$ , Burson and Summers [50] ○ 10 mr Chamber, x spherical ion chamber

## D. THE FOXHOLE

### 1. Skyshine

The term "foxhole" is used here to designate a configuration in which a detector views some limited solid angle of skyshine radiation. One reason for interest in the foxhole has been the continuing concern for exposure sustained by soldiers taking cover in a foxhole in the presence of fallout radiation. Another reason is that many experimental studies of exposure in basements have started with a series of experiments on "open" basements with no superstructure present. Although these basements are rectangular rather than circular, the detector response is nevertheless a measure of the cumulative angular distribution of skyshine, and open basements will therefore be discussed here under the generic term of "foxhole". Finally, this configuration is also representative of one in which a detector responds to radiation from skyshine through a skylight or some opening in the roof of a structure. It applies when there is no fallout on the skylight or opening. In this situation the detector may be 30 or more feet above the ground, and the angular distribution of skyshine may be a little different than that at ground level. However, the skyshine angular distribution varies so slowly with height (see fig. V.6) that, for all practical purposes, this variation can be neglected.

Calculation of the exposure in a foxhole involves an integral of the form

$$R_f = \int_{-1}^{-1+\omega} d(\cos\theta) \ell(H, \cos\theta) = S(H) S_a(H, \omega)$$

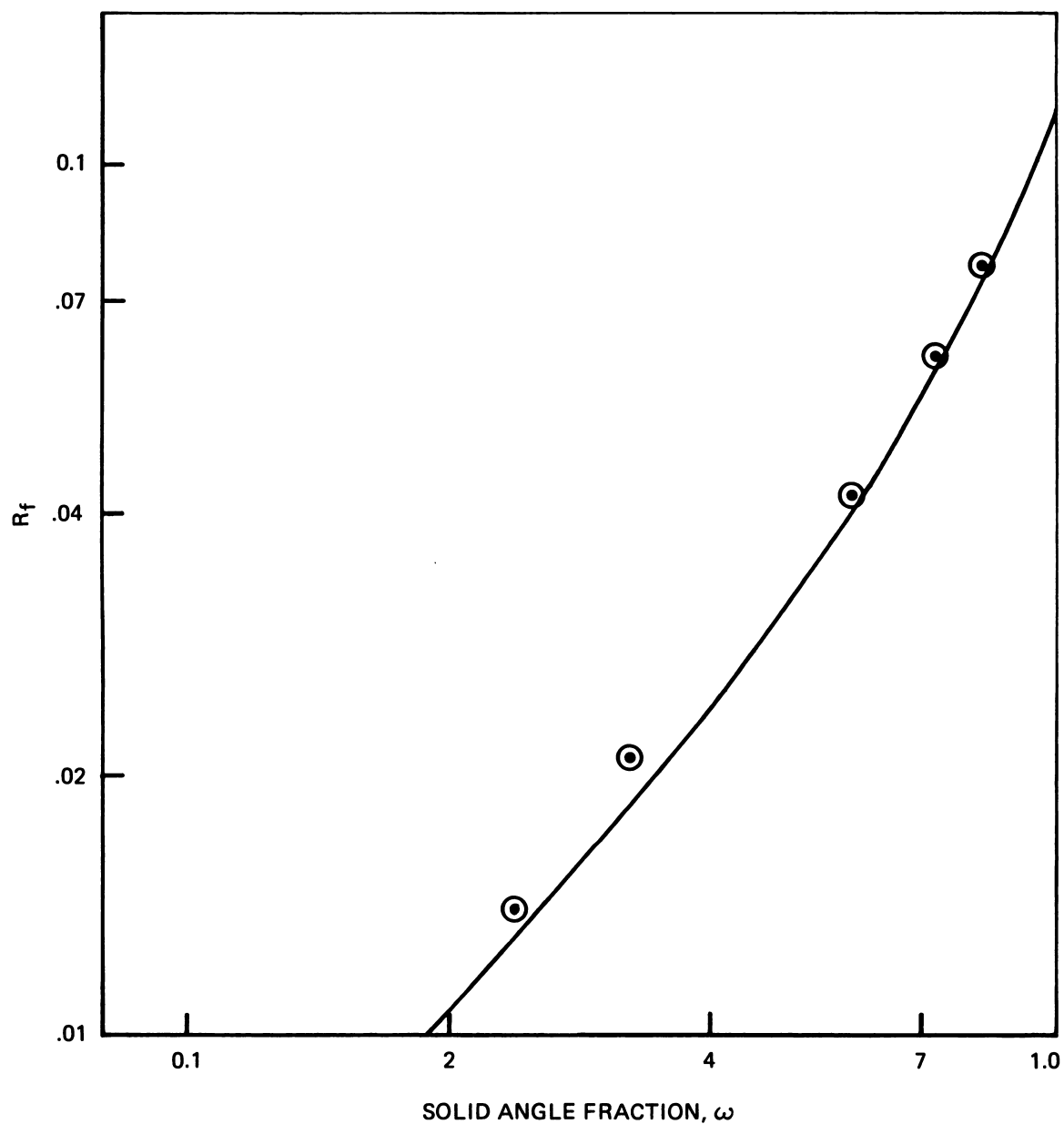
where  $\ell(H, \cos\theta)$  is the angular distribution of the exposure at a height  $H$  above the source. For lack of data at  $H = 0$ , the curve  $\ell(3', \cos\theta)$  for  $H = 3$  ft is used to

calculate  $R_f$  for  $H = 0$ . No significant difference is expected between the two curves at negative values of  $\cos\theta$ .

The cumulative angular distribution from skyshine radiation has been measured extensively for detectors near ground level. The first systematic experiment was made by Clifford [52] with a source of  $^{137}\text{Cs}$  gamma radiation and detectors placed on the vertical axis of a cylindrical foxhole of 1 m radius. In simulating a plane source, advantage was taken of cylindrical symmetry. Point sources were placed at various distances  $\rho$  along a horizontal radial line from the center of the foxhole. Results for ring sources were inferred by multiplying the exposure from each point source by  $2\pi\rho$ . Plane source results were then inferred from ring source data by numerical or graphical integration. The technique was also used in later experiments involving cylindrical symmetry.

Each detector position can be defined by the solid angle fraction subtended at the detector by the opening of the foxhole. A plot of Clifford's data as a function of solid angle fraction is shown in figure VI.15. Clifford's experimental measurements extended out only to a source-detector distance of 200 m. His data were extrapolated to the case of an infinite field by assuming that the skyshine exposure is proportional to  $e^{-r/107}$  as shown in figure VI.13. Comparison with values calculated from figures 72 and 76 of chapter V is also shown in figure VI.15. The relative behavior of calculated and experimental exposure vs. solid angle fraction is similar. The experimental exposure rates were converted to reduction factors by dividing by the value  $D_0$  at the Standard Unprotected Location. The value of  $D_0$  estimated by Clifford [53] was based on the rather high value of  $\Gamma = .356 \text{ (R/hr)/(Ci/m}^2\text{)}$ . The experimentally observed exposure included contributions from radiation penetrating the lip of the foxhole and from radiation





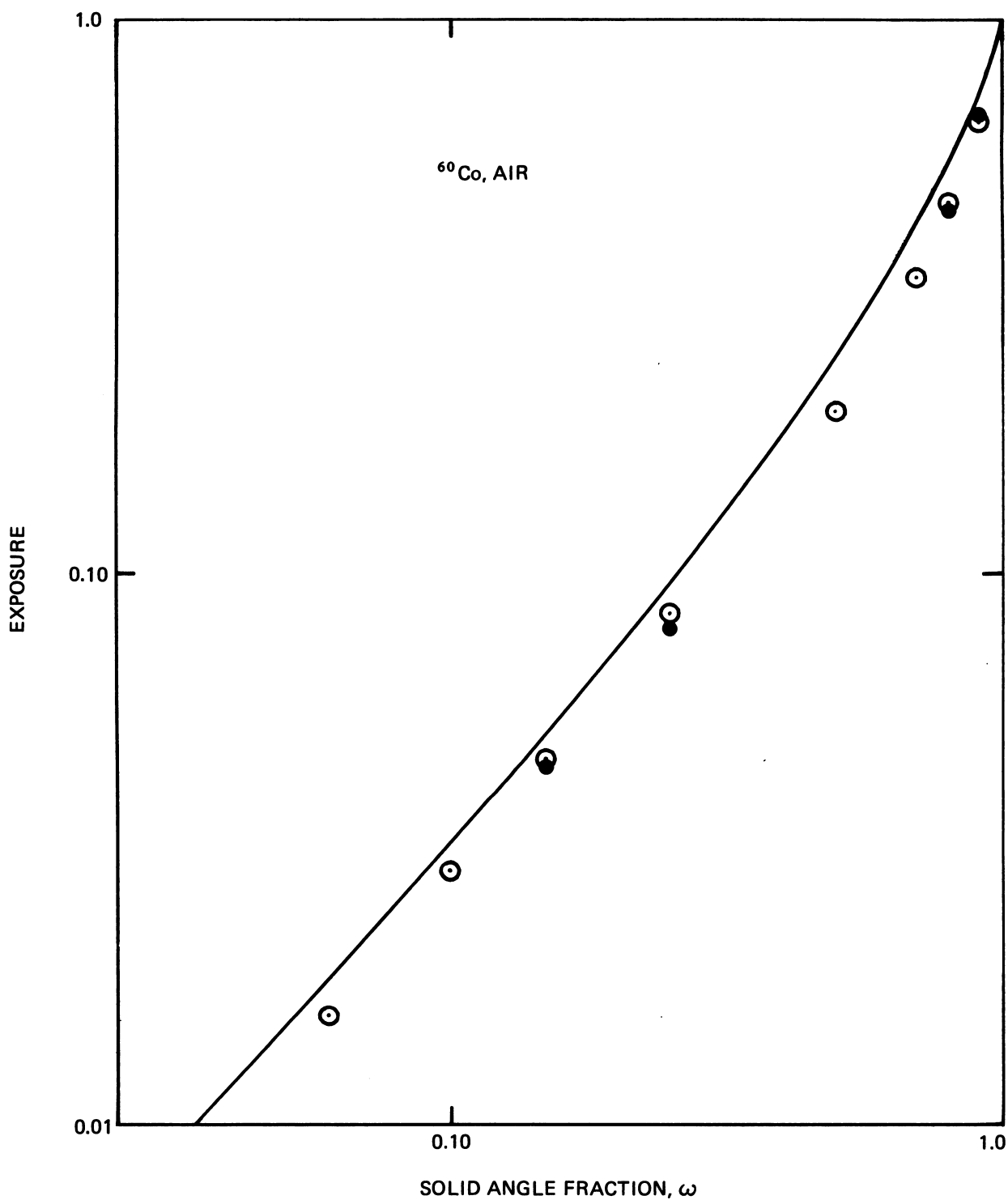
VI.15 Experimental and Calculated Reduction Factors in a Foxhole due to a  $^{137}\text{Cs}$  Plane Source.  $\odot$  Experimental, Clifford [52], — Calculation,  $S(0) S_a(3', \omega)$  (Figures V.72 and V.76')

backscattered from the walls and floor of the foxhole, whereas the calculations do not. (Backscattering is generally believed to increase the skyshine contribution by 10 or 15%. The contribution from radiation scattered in the lip of a true foxhole of, say, one meter in radius may be significant, and will be discussed in more detail in sec. 2.)

Clifford found that the angular distribution of skyshine exposure from a ring source was insensitive to the radius of the ring. Accordingly, measurements with ring sources can be used to estimate the angular distribution of skyshine from a plane source. Burson and Summers [50] have made measurements of the cumulative angular distribution of exposure from  $^{60}\text{Co}$  ring sources of radii of 60 and 100 feet. Their results are shown in figure VI.16. Each of the two sets of data represents Burson's estimate of experimental data averaged over a large number of points. The similarity of the two sets of data confirms the statement that the cumulative angular distribution is insensitive to the radius of the ring source. The experimental values agree within about 30% with the calculated curve for a detector height of 3 ft (See fig. B.22a). Notice that the experimental values are lower than the calculated values in this case, whereas they were higher in Clifford's experiments.

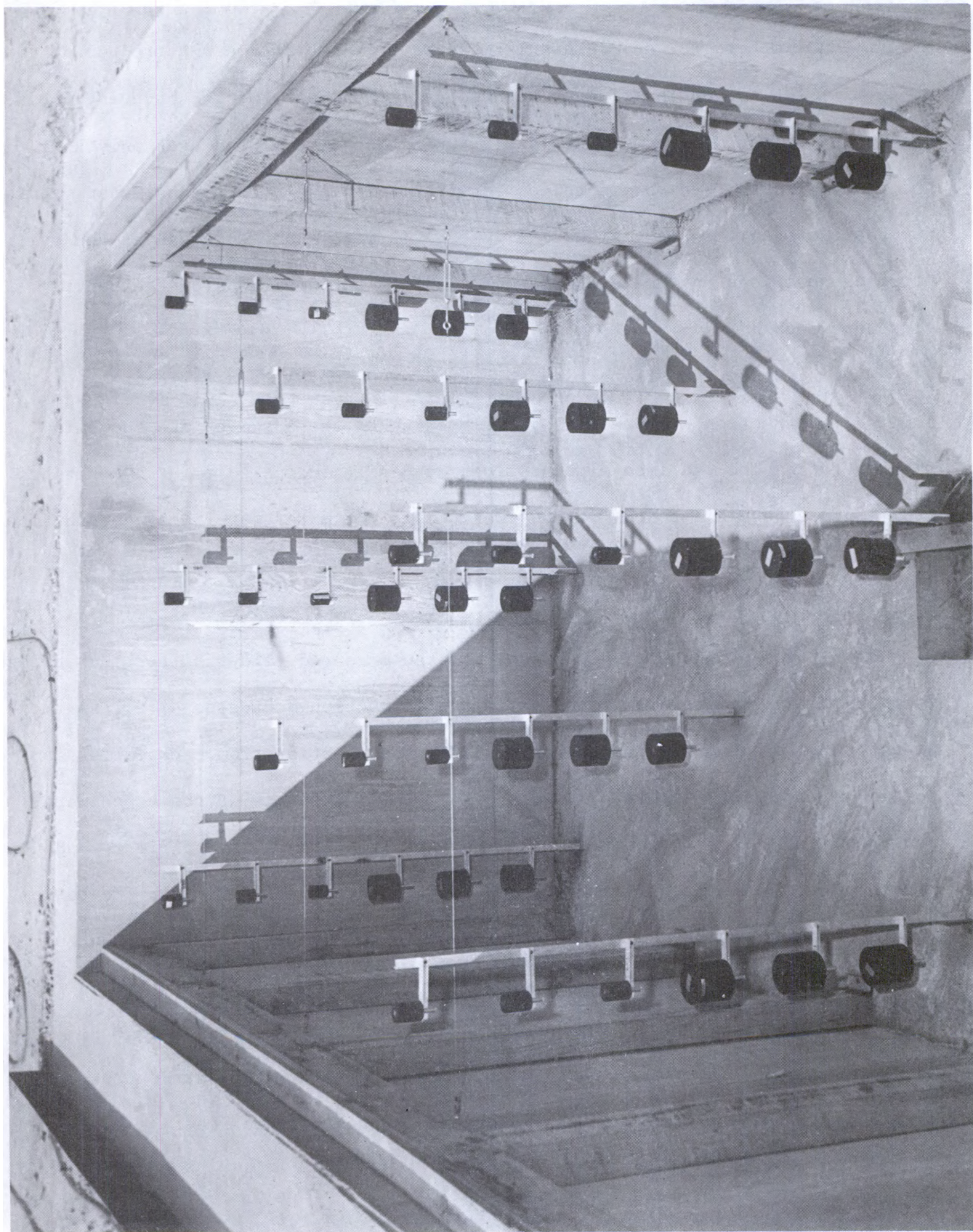
The remaining three experiments to be discussed here are of particular interest because they include measurements with a cover over the "foxhole" as well as measurements in the open hole. However, discussion of the experiments with a cover over the hole will be deferred to section X.D.

Schumchyk et al. [16] reported on a series of experiments on a rectangular basement (without a superstructure) of inner dimensions 20 ft by 10 ft by 7 ft deep. They used a circulating source of  $^{60}\text{Co}$  radiation. Figure VI.17 shows the



VI.16 Experimental and Calculated Geometry Factors in a Foxhole due to a  $^{60}\text{Co}$  Plane Source. Experiment Burson and Summers, [50],  $\odot$   $\rho = 100$  ft,  $\bullet$   $\rho = 60$  ft; — Calculation  $S_a(3', \omega)$  (Figure V.75)





VI.17 Photograph of Dosimeter Array in Skyshine Experiments. Schumchik [16]



array of dosimeters in the rectangular basement. Some of the plastic tubing can be seen at the top of the figure. Because of the symmetry of the basement about the longer of its midlines, the plastic tubing was distributed over only half of the plane. In order to obtain values for the full plane source, dosimeter readings for positions on the right side of figure VI.17 were added to those at the symmetrical positions on the left side and readings for positions on the center line were doubled.

Measured reduction factors on the vertical center line as a function of the solid angle fraction  $\omega$  subtended by the opening of the basement are shown in figure VI.18. The experimental reduction factors include a calculated contribution from sources beyond a radius of 600 feet. This estimated far-field contribution was generally about 25% of the total contribution and thus is by no means negligible.

From figure VI.18 it can be seen that the measured values differ increasingly from the calculated values as the solid angle fraction decreases, i.e., as the detector position approaches the floor. The contribution from backscatter is not included in the calculated values. In a later analysis of the experiment, Jenkins and Hinkley [54] estimated backscatter from the walls and floor, and predicted an increment of from 1.07 for the top detector to 1.46 for the bottom detector. The assumptions made in their analysis, however, would produce an overestimate of the backscatter.

Spring and Velletri [55] made measurements in a cylindrical hole 6 ft in diameter and 6 ft deep at the Radiation Test Facility (RTF) at Fort Belvoir, Va. The measurement of reduction factors in an open hole was made as a preliminary

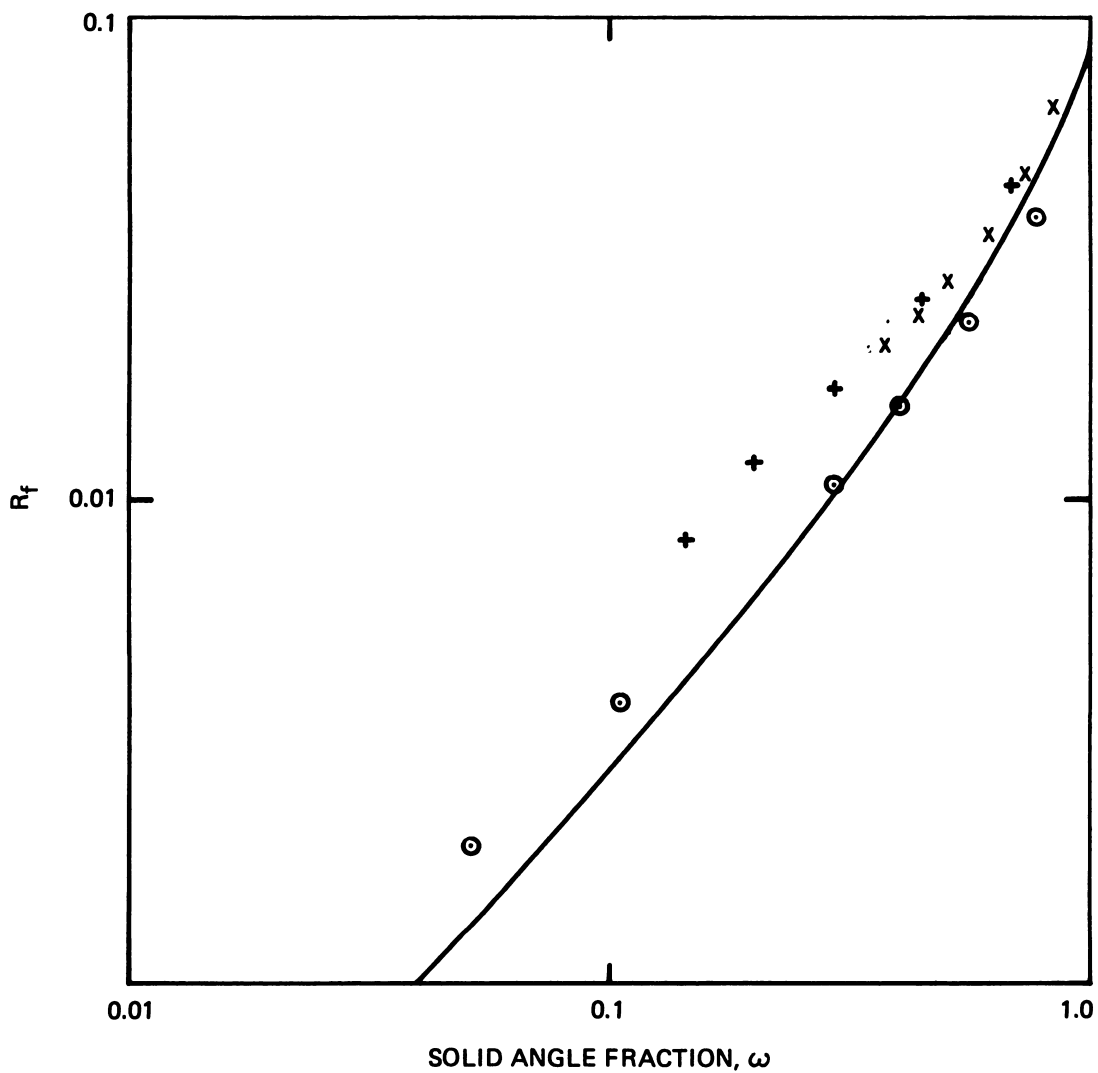
to measurements with walls of 1 ft to 6 ft in height. In these experiments exposures for a plane source were inferred from measurements with point sources, in the same manner as described earlier in this section. The results for an infinite plane source are shown in figure VI.18. Here again, the experimental values of the reduction factor are higher than the calculated values -- particularly at small solid angles. Since measurements were made at smaller solid angles than in Schumchyk's experiments, the relative backscatter is expected to be larger. No attempt was made by Spring and Velletri to evaluate the amount of backscatter - probably because they were primarily interested in ratios of measurements, with and without a basement ceiling. The effect of backscatter on such ratios of exposure rates will be much less than on the exposure rate itself.<sup>4</sup>

Kaplan [56,57] has made extensive measurements with cylindrical steel models, 2 ft in diameter and 4 ft deep. The primary purpose of these experiments was to check the validity of using a small steel scale model as a substitute for the actual structure. As with the Spring-Velletri experiment, preliminary measurements were made with an open hole, and a correction had to be made for the far-field contribution. In these experiments the maximum radius at

---

4

In searching for possible sources of anomalously high measurements in some earlier experiments, Spring and Velletri considered enhanced dosimeter response due to electrons reflected from the floor of the hole. If the dosimeter walls were thinner than the equilibrium thickness, the detector would respond to these electrons. Therefore, in the Spring-Velletri experiments a polyethylene cover, one-sixteenth of an inch thick, was kept over the chamber to eliminate this possibility. Since this precaution did not affect the results, enhanced response due to electrons does not seem to be a problem with these chambers.



VI.18 Experimental and Calculated Reduction Factors in a Foxhole due to a  $^{60}\text{Co}$  Plane Source. Experimental,  $\times$  Schumchyk [16],  $+$  Spring and Velletri [55]  $\odot$  Kaplan [56,57]

which measurements were taken was 50 feet. In later experiments in which scatter from the above-grade cylindrical wall was important, the far-field correction was small. However, in the case of the open hole, where only skyshine contributes, the far-field estimate represented about 90% of the exposure. In spite of this large extrapolation, the open hole results are discussed here because they were accompanied by measurements on above-grade walls, to be discussed in section X.D.

Kaplan [56] developed a method for making the far-field estimate more correct. The method assumes that the dose rate  $R(\rho, h)$  at a height  $h$  due to a ring source at radius  $\rho$  is given by

$$R(\rho, h) = \alpha_D(h) D_o(\rho) + \alpha_S(h) S_o(\rho) \quad (\text{VI.9})$$

where  $D_o(\rho)$  is the free-field exposure at  $h = 0$  due to uncollided radiation from a ring source at radius  $\rho$ ,

$S_o(\rho)$  is the free field exposure at  $h = 0$  due to skyshine radiation from a ring source at radius  $\rho$ ,

$\alpha_D(h)$  is the ratio of the exposure at height  $h$  in a protected location, due to uncollided radiation, to that at a height of zero in the unshielded situation, for a ring source, and

$\alpha_S(h)$  is the ratio of the exposure from skyshine at height  $h$  in a protected location to that at a height of zero in the unshielded situation for a ring source. Kaplan found that  $\alpha_D$  and  $\alpha_S$  were independent of radius in his steel model studies. For an open hole, only the second term contributes in eq (VI.9).

Kaplan's measured reduction factors are shown in figure VI.18. They seem to agree better with the calculations than do the other measured values. One possible reason is a reduced backscatter component of low-energy gamma rays in



the steel cylinder, as opposed to those for concrete. However, in view of the large calculated far-field component in these results, not too much emphasis can be placed on them.

## 2. Lip Effects

In the last subsection the discussion of radiation exposure in a foxhole was limited to the skyshine contribution arriving through the opening at the top of the hole. But radiation can also be transmitted or scattered in the earth or concrete edges of the foxhole. This effect is analogous to the transmission of light through a corner composed of translucent glass bricks: even though the glass bricks are not in a direct line between the light source and the viewer, they will nevertheless scatter some of the light to the viewer. The contribution from fallout radiation which penetrates through the lip of a foxhole is estimated by eq (V.40).

In most experiments on foxholes, the emphasis has been on measurements of skyshine, and the lip contribution has been regarded as an extraneous effect. For example, in measurements of exposure in a concrete basement shelter, Starbird [58] avoided complications due to this effect by replacing the earth near the lip of his shelter by lead, and beginning his point-source measurements at about 18 inches from the edge of the shelter. This procedure has very little effect on measured skyshine but eliminates transmission of radiation from nearby sources through the ground.

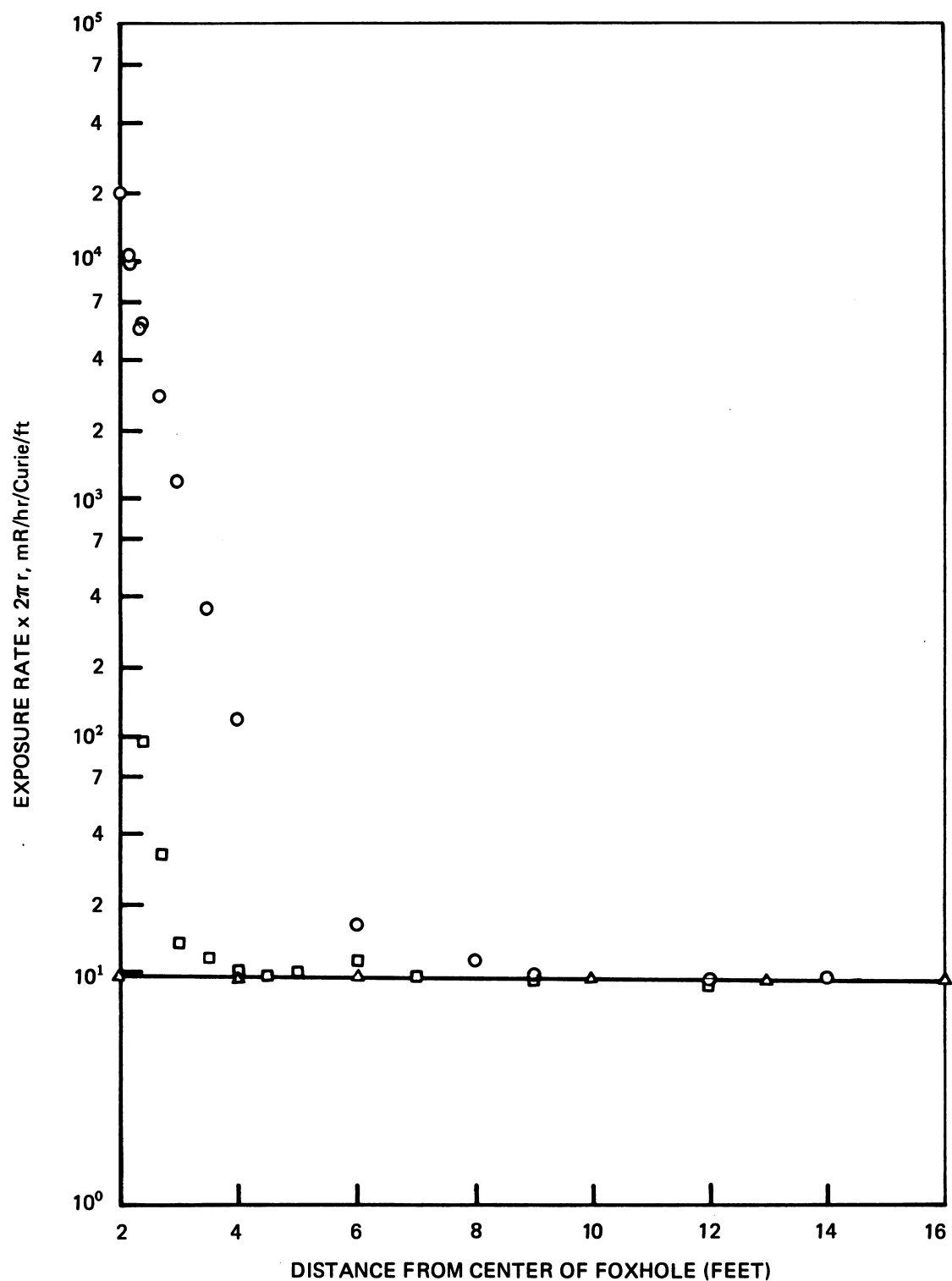
Neglect of the lip effect is expected to be valid when the structure dimensions are much larger than the mean free path in earth ( $\sim 5$  inches). However, in a foxhole of a few feet in diameter, this condition does not apply, and the lip contribution must be taken into account. Schumchyk and Tiller [59]

reported on a series of experiments designed especially to measure the lip contribution. Their test structure was a cylindrical hole in the ground, 4 ft in diameter and 4 ft deep, lined with 1/8 inch thick masonite. Radioactive  $^{60}\text{Co}$  point sources of 0.34 and 3.3 Curies were used in the experiment. Exposures were measured on the vertical axis of the hole for point sources at varying radii. The corresponding ring source data were then plotted as a function of radius for each detector position. The area under each curve out to a radius  $\rho$  yielded the exposure from a uniformly contaminated plane source out to that radius.

In order to separate the contribution from skyshine from that due to lip effects, two sets of experiments were run. In one set, data were taken with earth at the edge of the hole. In the other set, the earth at the edge of the hole in the exposure line was replaced with an array of lead bricks. A typical plot of the two sets of data for a detector depth of 3 ft is shown in figure VI.19. It can be seen from this figure that the replacement of earth by lead reduces the contribution from sources near the edge of the hole by more than an order of magnitude. For sources beyond about 8 ft from the center of the hole, however, the reduction is negligible, indicating that the main contribution at these distances is from skyshine radiation.

In order to calculate the total exposure from skyshine, an extrapolation was made for sources beyond about 15 feet from the center of the hole. This extrapolation was made by assuming that the exposure from skyshine from a ring source of radius  $\rho$  is given by

$$D^S(\mu_o \rho) = A [B(\mu_o \rho) - 1] \Gamma \frac{e^{-\mu_o \rho}}{\rho^2} 2\pi\rho \quad . \quad (\text{VI.10})$$



VI.19 Exposure Rate ( $\times 2\pi r$ ) vs Horizontal Distance of a  $^{60}\text{Co}$  Point Source From the Vertical Axis of a Foxhole for 3 ft depth  $\bigcirc$  Total Radiation  $\square$  Skyshine,  $\triangle$  Extrapolated Skyshine, Schumchyk and Tiller [59]

The value of the specific gamma ray constant  $\Gamma$  was assumed to be 14.31 (R/hr)/(Ci/ft<sup>2</sup>) and the buildup factor  $B$  was assumed to be of the form

$$B(\mu r) = 1 + \mu r \left( A_1 e^{C_1 \mu r} + A_2 e^{C_2 \mu r} \right) . \quad (V.11)$$

The values of the parameters  $A_1$ ,  $A_2$ ,  $C_1$ , and  $C_2$  were taken from calculations by Berger and Spencer [60]. The normalization factor  $A$  was obtained by comparing the experimental data as a function of radius to the expression in eq (VI.10).

A summary of the estimated contributions from skyshine and lip effects is shown in Table VI.3. This table shows that the lip contribution may account for over one half of the exposure in a foxhole of 4 ft diameter. It should be remembered, however, that the relative contribution is extremely sensitive to the distribution of source material within about 2 ft of the edge of the hole. If these sources are removed, the lip contribution is reduced significantly. Also, this contribution may vary, depending on whether the lip is square or rounded.

The relative contribution from lip effects is strongly dependent on the radius of the hole. Equation (V.40) indicates an inverse proportionality to absolute depth of the detector. But for a fixed solid angle, the depth is proportional to the radius of the hole. The skyshine contribution, however, remains roughly constant when the solid angle is kept fixed. Thus one can expect the relative lip contribution to be inversely proportional to the radius of the hole. Therefore, in basements of light residential structures with an effective radius of about 20 ft, the relative lip contribution would be about 10% of what it is for the foxhole of 2 ft radius.

TABLE VI.3\*

REDUCTION FACTORS FOR MEASURED LIP AND CALCULATED SKYSHINE  
CONTRIBUTIONS AND RATIOS OF LIP/SKYSHINE AND LIP/TOTAL

Depth (Ft.)	$D/D_o$ Lip	$D/D_o$ Skyshine	$D/D_o$ Total	Lip/Skyshine	Lip/Total
1	0.0490	0.0260	0.0750	1.88	0.653
2	0.0217	0.0108	0.0325	2.01	0.668
3	0.0136	0.0055	0.0191	2.47	0.712
4	0.0067	0.0030	0.0097	2.24	0.693

\* See Ref. 59

## E. GROUND IRREGULARITIES

### 1. Ground Roughness

#### a. Standard Unprotected Location

The data which are given in Chapter V for the exposure and its angular distribution in air above ground are based on the assumption that the sources of fallout are distributed on an idealized smooth flat infinite plane. It has long been recognized that fallout particles will tend to filter down into small cracks and crevices in real surfaces such as soil. Radiation from the particles will then have to travel through condensed material before reaching a detector in air. This effect, which reduces height above ground, has often been referred to as the "ground roughness" effect, and has been evaluated with a "ground roughness factor".

Many studies of ground roughness have been applied to a detector 3 ft (or 1 m) above the ground. In the 1957 edition of the Effects of Nuclear Weapons (ENW) [61] it was suggested that the reduction due to ground roughness would compensate for the enhancement due to the scattered radiation which was not included in calculations in figure 9.120 of that reference. In the 1962 edition of ENW the curves for exposure rate from a smooth plane included the scattered radiation. A factor of 0.7 was then recommended to correct for "moderately rough terrain."

One of the earliest attempts to estimate the ground roughness effect was made by Ksanda [62] and his coworkers at the U.S. Naval Radiological Defense Laboratory. They used two calculational schemes to predict the reduction due to ground roughness. In one scheme the source was assumed to be located on a plane covered by various thicknesses of earth. In the other, the

fallout particles were assumed to be mixed uniformly through the top layer of the soil. They generated a series of curves for various detector heights and various thicknesses of earth cover or earth mixture. In a later report [63] they showed that experimental data from the desert soil at the Nevada Test Site could be duplicated by calculations which assumed that the source was distributed uniformly in the top inch of soil.

Another approach for accounting for ground roughness is to weight the angular distribution of radiation from a smooth plane by a factor which varies with angle and with the type of terrain. Israel [64] has used this technique to estimate the effect of "terrain" variations of the order of a few centimeters. To determine the weighting factor he illuminated the terrain from varying angles to determine how much of the surface is shaded by microprojections. He found, for example, that when meadowland is illuminated from an angle of  $1^\circ$  above the horizontal and photographed from above, about 50% of the surface is in shadow. For an angle of  $10^\circ$  practically none of the surface is in shadow. His analysis led to an estimated correction for  $^{60}\text{Co}$  radiation of 0.8 at a height of 1 m for meadowland and 0.6 for cultivated ground.

In 1963 Clifford [65] presented a review paper on interface effects, which included a discussion of ground roughness effects. This paper contains an excellent bibliography of work on interface effects up until 1963. Among the data he presented was a table giving a range of values calculated by other authors for the ground roughness factors. These values varied from unity, when the effect is ignored, down to an extreme of 0.11 when all radiation except skyshine is assumed to be shielded by the rough ground. He then discussed some measurements from one of his earlier reports [66] which involved the use

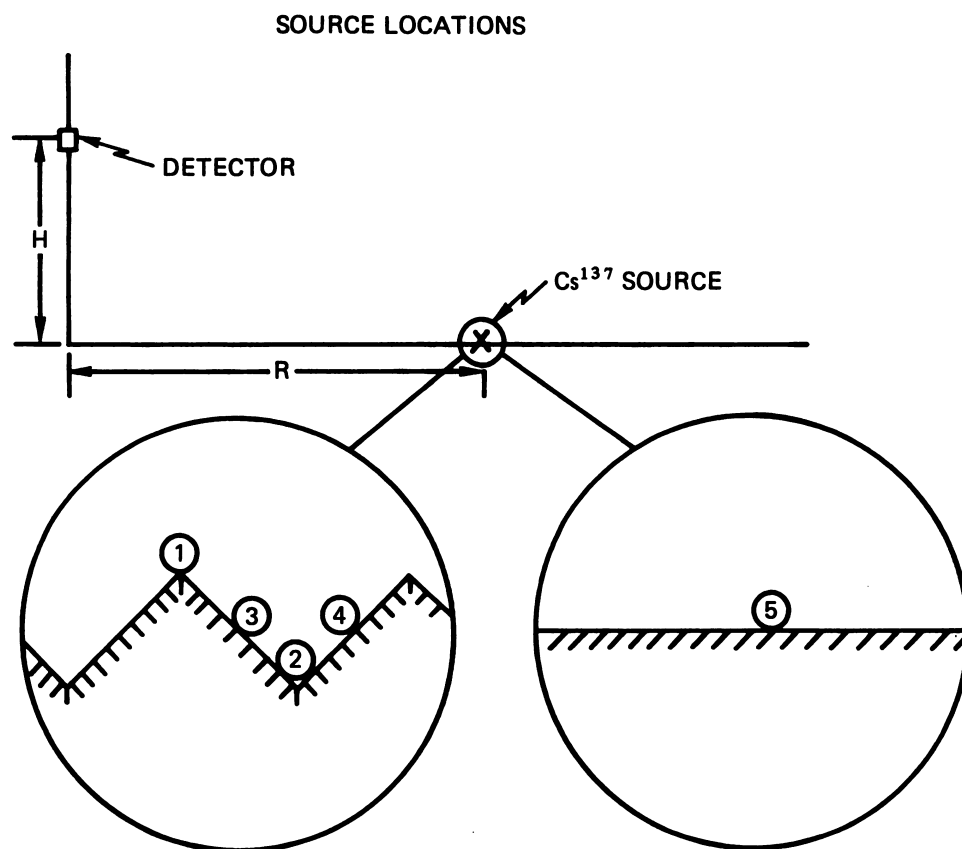
of  $^{137}\text{Cs}$  sources on concrete slabs with a sawtooth profile of 6 in depth (see fig. VI.20). The reduction in exposure at a height of 1 m varied from about 0.5 if the contamination is assumed to be uniformly distributed over the contour, to about 0.16 if the contamination is assumed to collect in the trough of the sawtooth contour. The latter assumption is probably not very realistic, since fallout would only collect in a trough on a smooth surface and sawtooth contours are most apt to occur on rough surfaces such as plowed ground.

Ferguson [67] analyzed experimental results for fallout radiation existing in 1963 by comparing them with calculations by Spencer [68]. He inferred from calculations the source burial depth which best matched experimental results. He found that the equivalent air thickness  $\tau$  of the effective burial depth for "typical desert terrain" was  $\tau = 25 \pm 10$  ft of air-equivalent material. The corresponding ground roughness for a detector at 3 ft varied from 0.54 to 0.71. For plowed ground he deduced a factor of 0.44. These values can be compared with correction factors of 0.8 for "virgin flat ground" and 0.6 for "cultivated ground" deduced by Israel [64] for a height of 1 m and  $^{60}\text{Co}$  radiation. Israel's analysis is consistent with measurements using source needles 10-15 mm in length, whereas actual fallout particles are about 50 microns in diameter. Greater infiltration of the smaller fallout particles may account for the somewhat lower correction factors deduced by Ferguson.

#### b. Spatial Trends

The effect of ground roughness is particularly pronounced at detector heights of 3 ft and lower, where a large fraction of the radiation from a





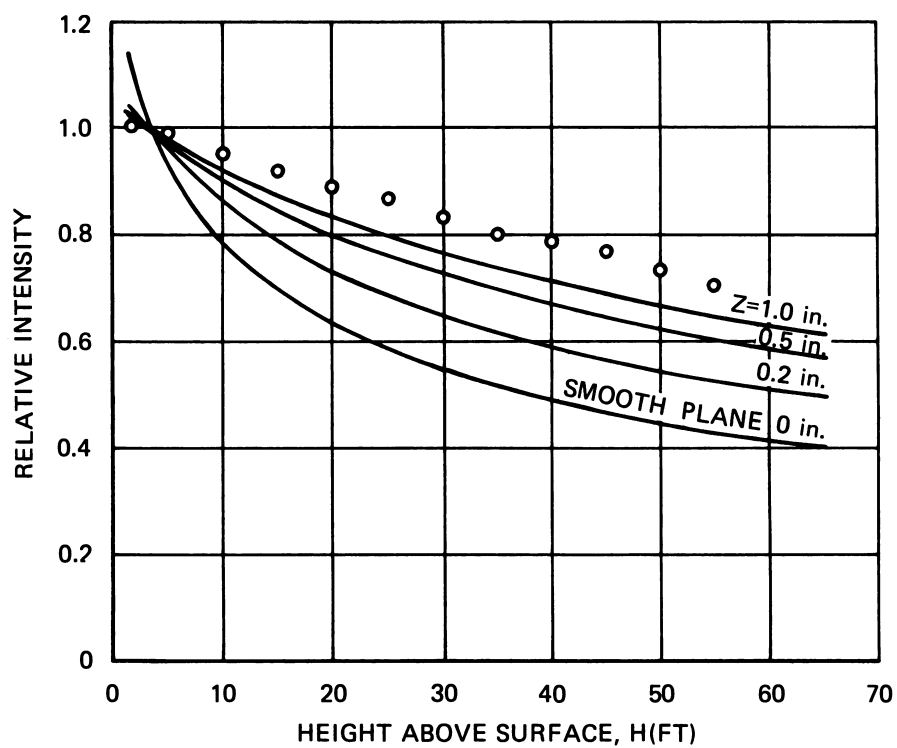
VI.20 Schematic Drawing Showing Location of Sources in Experimental Study of Ground Roughness [66]

plane reaches the detector at angles nearly parallel to the interface. This can be seen by the peak in the 3 ft angular distribution shown in figure V.6. Any ground roughness tends to attenuate that peak severely. At greater heights, the relative amount of exposure from these grazing angles is less and therefore the effect of ground roughness is less.

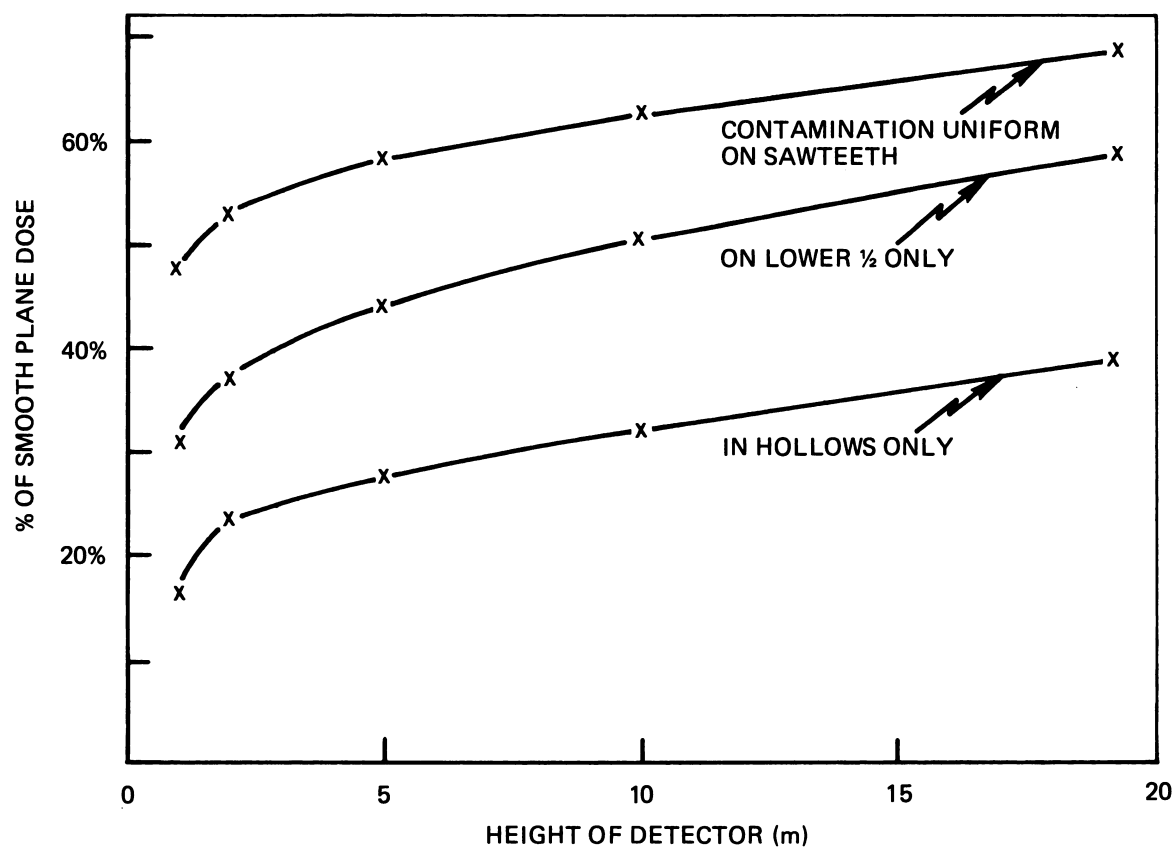
The effect of ground roughness as a function of detector height is shown in figure VI.21 (see ref. [63]). In this figure experimental and calculated values are normalized at a detector height of 3 ft. Note that the calculated values are given for various depths of mixture rather than various depths of cover. The figure shows that the spatial behavior of the experimental results is matched by assuming that the source material is distributed in the top inch or two of earth.

A better idea of the variation of the roughness effect can be obtained from figure VI.22. These data from reference [66] show experimental results for a  $^{137}\text{Cs}$  source and concentric rings of the sawtooth patterns shown in figure VI.20. Curves are shown for three different assumptions about the distribution of the contaminant over the contour. In all cases, the results are closer to the smooth-plane results as the detector height increases. The effect of the roughness is still apparent at a height of 20 m because of the large sawtooth contours used in this experiment.

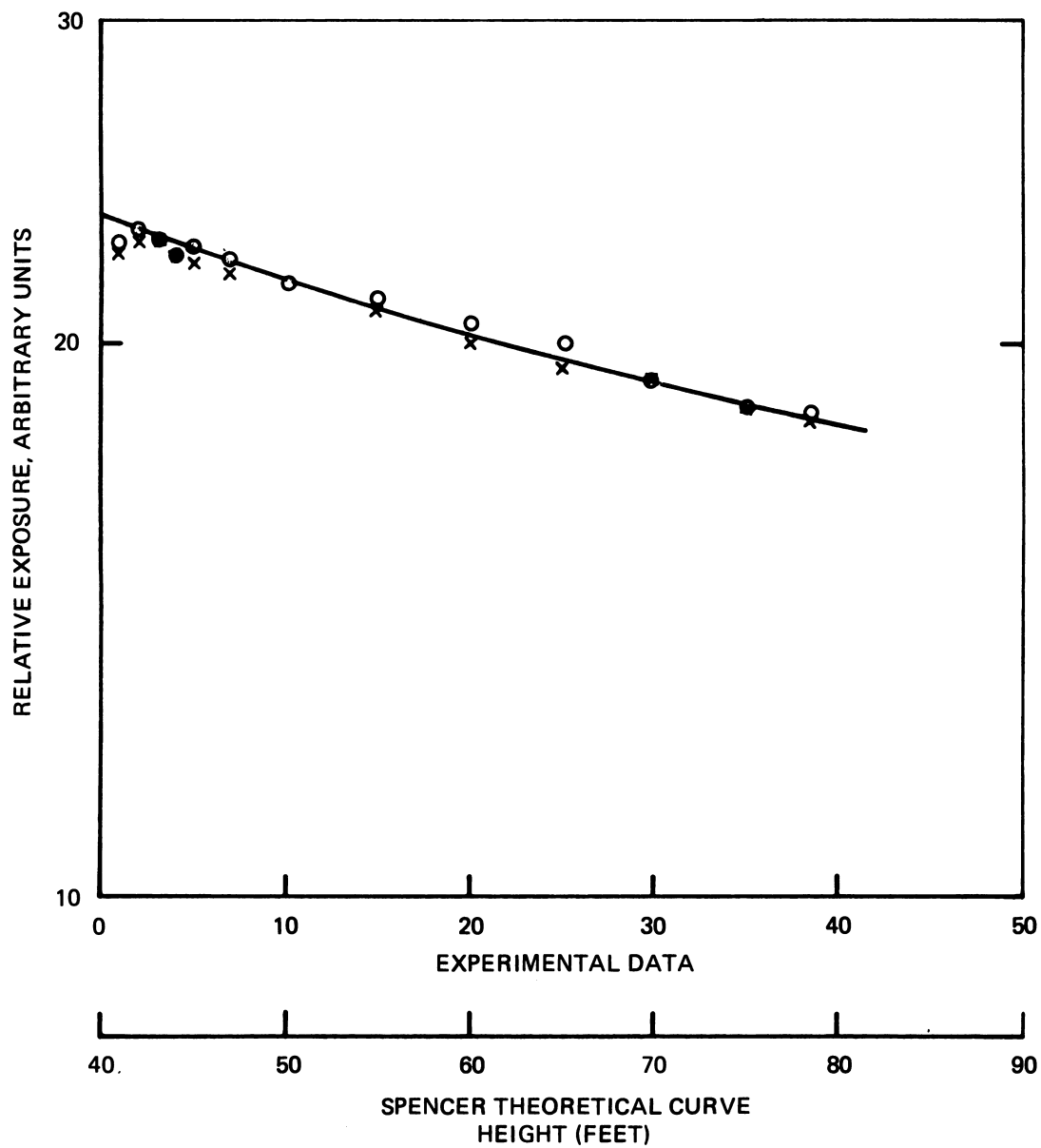
Huddleston et al. [34] were able to obtain data for fallout 128 hours after the explosion as a function of height above "typical wild desert terrain". A comparison of their results with calculations from reference [68] is shown in figure VI.23. The experimental values show the same behavior with height as a theoretical curve which assumes that the source is covered with earth equivalent to a layer of 40 feet of air. This corresponds to a ground roughness factor of 0.53 at a height of 3 ft -- not too far from Ferguson's earlier estimates.



VI.21 Variation of Measured and Computed Exposure Rates for Various Depths Z of a Mixture of a Plane Isotropic Source of Fission Products with Soil.  
 ○ Experimental [63], — Calculated [63]



VI.22 Experimental Estimate of the Effect of a Rough Field on Exposure vs Height above a Plane Isotropic Source. -x- Clifford [66]



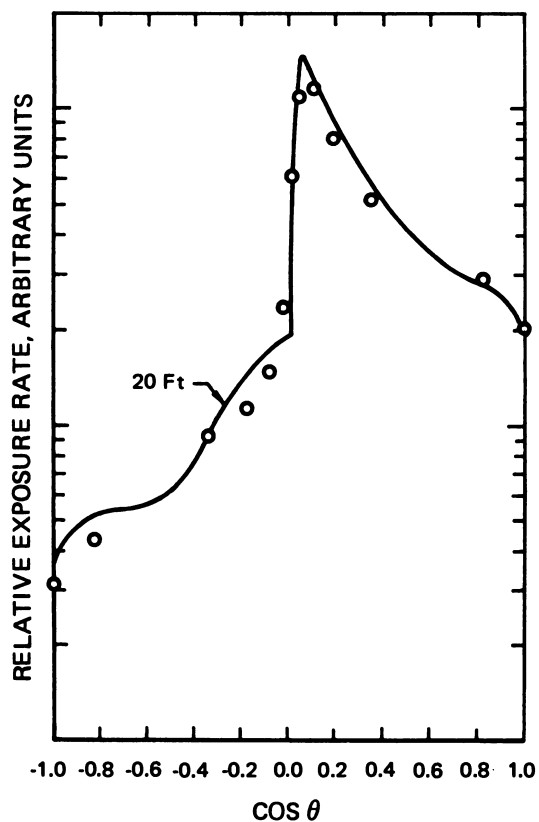
VI.23 Experimental and Calculated Exposure Rate Above Typical Desert Terrains (Arbitrary Normalization) ○, x Experimental, Huddleston, [34]; — Calculated, from Spencer [68]

### c. Effect on Angular Distribution

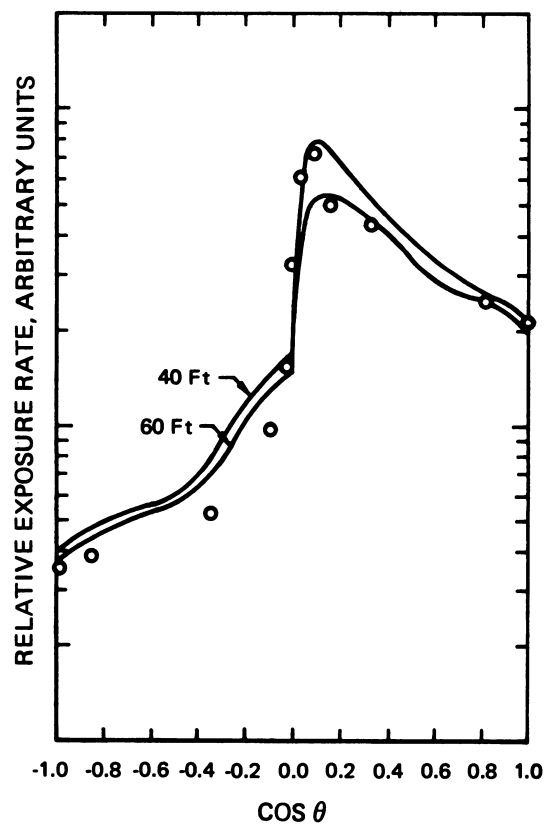
Huddleston et al. [34] studied the actual angular distribution of radiation at a detector located over rough desert terrain. Their measurements were made with a 3 in x 3 in NaI(Tl) crystal and a wedge-shaped collimator, which increased the solid angle of the detector by means of a  $20^{\circ}$  opening in the azimuthal direction, over which the angular distribution should be nearly constant. The experimental spectrum was multiplied by energy absorption coefficients and integrated to obtain exposure. They obtained good results for three different types of terrain.

Figure VI.24 shows their data at 3 ft above a dry-lake bed. Although this type of terrain appears very smooth, it actually contains a network of cracks up to about 1/4 inch in width, and undulations of fractions of an inch. Some variation from calculated results for a smooth plane are therefore to be expected. Their data are consistent with an assumed earth-cover equivalent to 20 ft of air. The corresponding ground roughness effect is 0.65.

They also made measurements above a plowed field. The profile of this field consisted of V-shaped furrows, 6 inches deep and about 30 inches apart. The width of each furrow was about 13 inches at the top of the "V". Figure VI.25 shows that interpretation of the experimental results was somewhat ambiguous. Possible fits to the data could be obtained by assuming an effective burial depth of either 40 or 60 feet of air-equivalent material. The authors showed that with a more careful analysis, taking into account the details of the shielding mechanisms for this contour, they could reproduce the experimental points within about 10%. For this type of terrain, therefore, the simple assumption of effective burial depth produces an ambiguity in the ground roughness factor of from 0.53 ( $\tau = 40$  ft) to 0.46 ( $\tau = 60$  ft). For most applications this uncertainty is still acceptable.



VI.24 Experimental and Calculated Angular Distributions of Exposure above a Dry Lake Bed.  
 ○ Experimental, Huddleston [34];  
 — Calculated Spencer [68].



VI.25 Experimental and Calculated Angular Distributions of Exposure above a plowed Field.  
 ○ Experimental, Huddleston [34];  
 — Calculated Spencer [68].

Finally, their results for the angular distribution of exposure over rough desert terrain is shown in figure VI.26. From this figure it can be seen that the experimental results are in good agreement with a theoretical curve which assumes a burial depth of 40 ft of air-equivalent material. Furthermore, this is in agreement with the value of 40 ft deduced from the exposure-vs.-height experiments which were made over the same terrain.

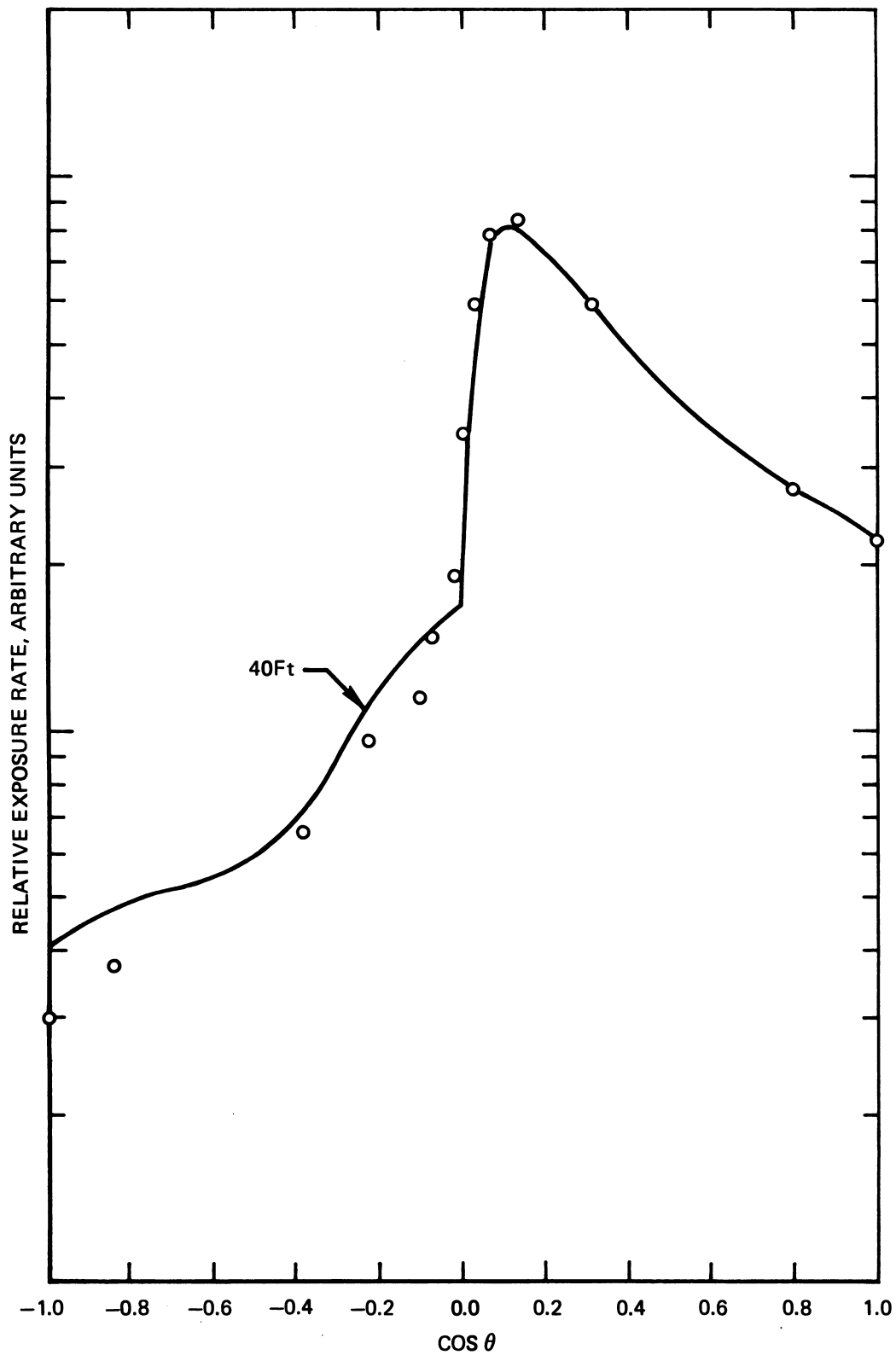
#### d. Effect on Energy Distribution

Some attempts have been made to assess the dependence of the ground roughness effect on the fallout gamma ray spectrum. Tomnovec et al. [69] examined the energy spectra of fallout samples from several weapons tests. They made calculations for the various energy spectra to determine the ground roughness effect. When ground roughness was simulated by overlayers of 2 cm, 4 cm, and 8 cm of aluminum, changes in the ground roughness effect for spectrum variations from 14 to 616 hours after an explosion were judged to be negligible, considering the uncertainties in the analysis.

### 2. Macroscopic Variations

The types of ground roughness discussed in section V.D.1 might be called "microscopic" in that the variations from an ideal plane are of the order of one mean free path (about 5 inches) of fallout gamma rays in the ground. The variations discussed in this subsection are called macroscopic because they are large compared with the gamma ray mean free path. These variations can be natural (e.g., hills and valleys) or man-made (e.g., neighboring buildings). In general, the latter type of variation is treated as "mutual shielding", that is, the mutual shielding of one structure by the presence of another. Techniques for calculating the effects of mutual shielding will be discussed in section IX.B. Effects of natural variations in terrain on an unshielded detector are discussed here.



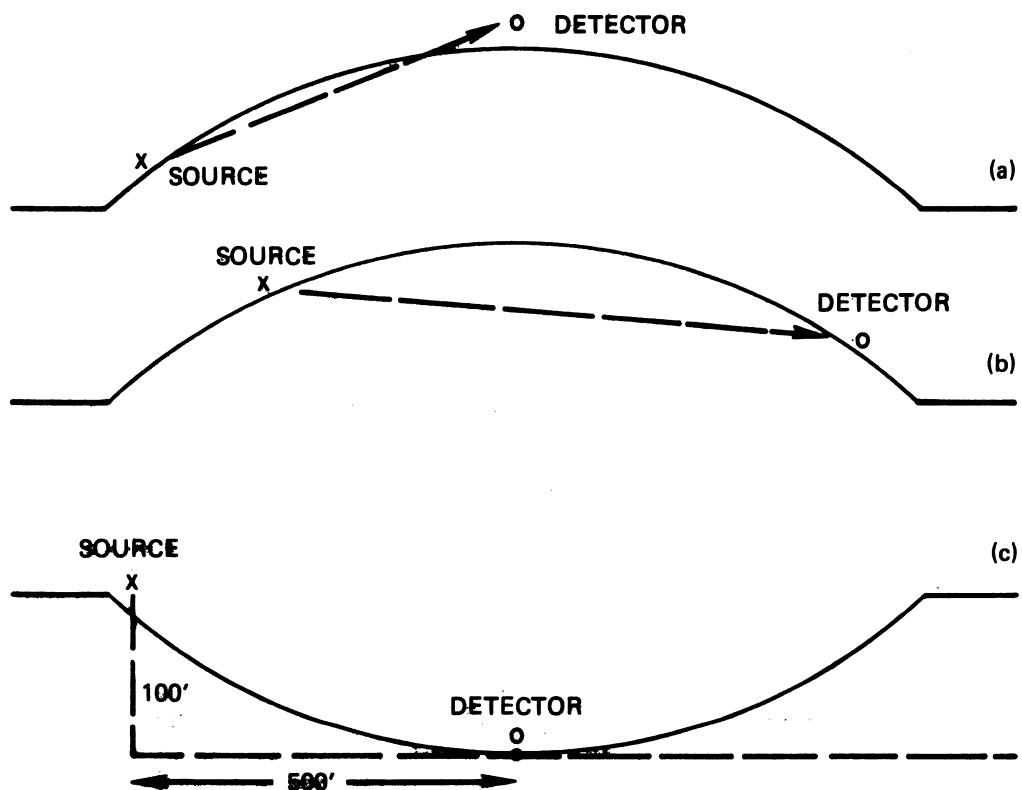


VI.26 Experimental and Calculated Angular Distributions of Exposure above Rough Desert Terrain ○ Experimental, Huddleston [34]; — Calculated, Spencer [68]

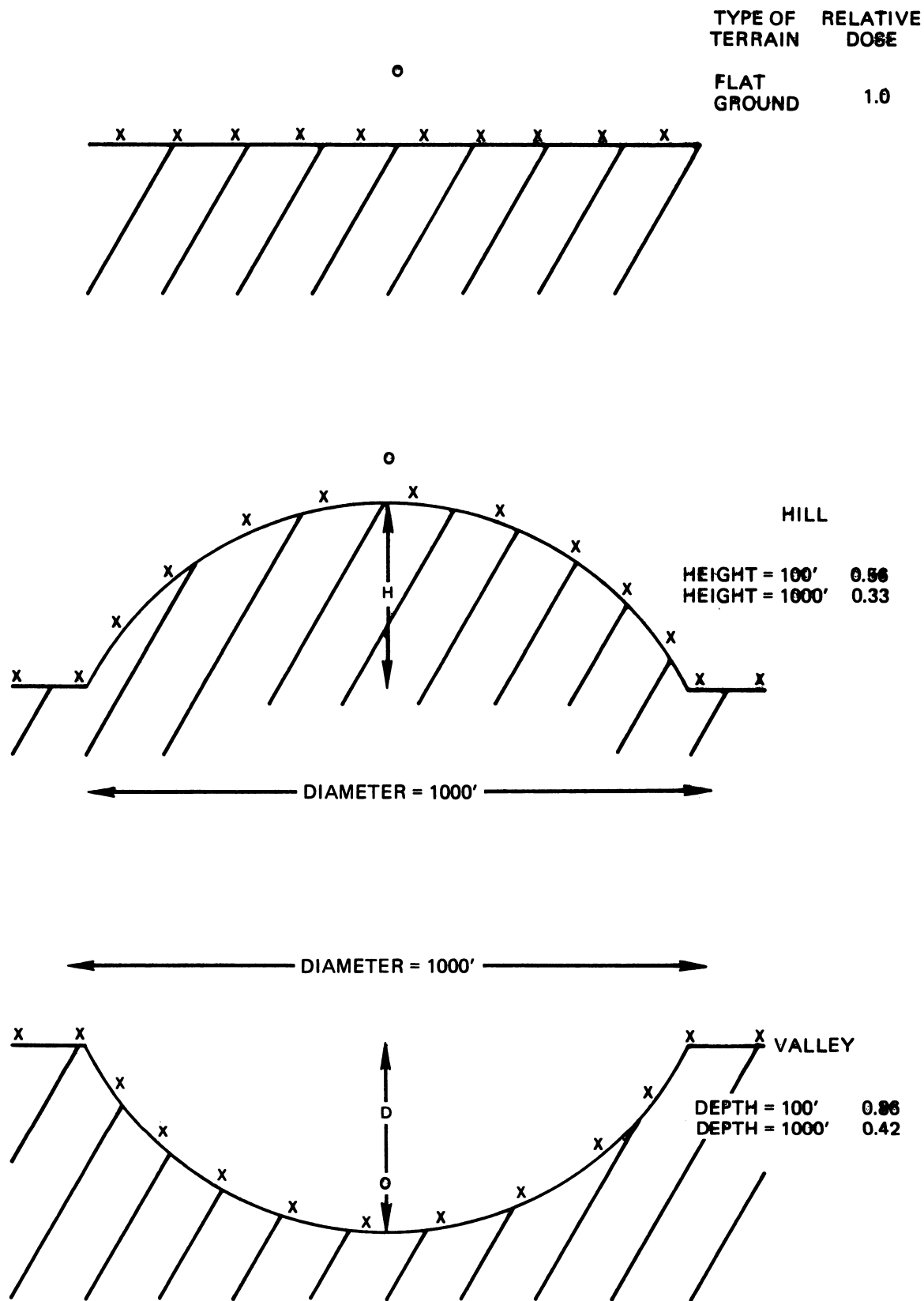
In many situations the exposure at a detector height of 3 ft for a fixed source strength per unit area may vary, depending on the nature of the terrain in the neighborhood of the detector, due to shielding of the direct radiation by the curvature of the terrain. For example, the exposure at a detector on top of a hill (fig. VI.27a) may differ from that on a hillside (fig. VI.27b).

The effect of variations in terrain has been explored by Goldstein [70] with a Monte Carlo code called TERF (Terrain Features) [71]. This code calculates the transport of gamma rays (or neutrons) through complex three-dimensional configurations. It uses a combinatorial geometry computer code package which permits the representation of a three-dimensional shape as a combination of spheres, cylinders, cones, or boxes. Fallout particles can be assumed to be distributed on a surface or throughout a volume, such as a tree.

Relative doses calculated by the TERF code for several variations in terrain are shown in figure VI.28. As expected, the doses for a detector on top of a hill are lower than those for a detector located above a flat plane, because some of the uncollided radiation is attenuated in the earth of the hill. The relative decrease in dose for a detector located in a valley is not as easy to understand. Here, the uncollided radiation is shielded only for sources beyond about 500 feet. This accounts for about a 4% reduction in dose. The decreased contribution from skyshine accounts for another 5% of the reduction. The remainder of the reduction is related to the assumption that fallout is distributed on surfaces according to their horizontal projection. The distance from each source which would have fallen on a plane is increased because of the presence of the valley. For example, at the edge of the valley the source which would have been just below the detector plane is now about 100 ft (or 1000 ft) above the detector



VI.27 Schematic Drawing of a Point Source and a Point Detector Located on a Hill or valley



VI.28 Calculated Relative Dose for Five Different Types of Terrain.  
Goldstein [70]

plane at a horizontal distance of 500 ft (See fig. VI.27c). This accounts for a 4% increase in the square of the source-detector distance for a source at the lip of the 100 ft valley and a 500% increase for the 1000 ft valley, compared to the corresponding data for the flat plane case. Thus it seems that most terrain variations will produce a lower dose at a detector in a free field than estimated for an infinite flat plane.

## REFERENCES

- [1] McDonald, A. G., The penetration of gamma radiation from a uniform contamination into houses: A First Report on Some Field Trials, Home Office Report CD/SA 69, 12 pages (Home Office, Scottish Home Dept., Jan. 1956).
- [2] Steward, N. G., Chisholm, J. M., Crooks, R. N., and Gale, H. J., The shielding provided by a brick house against gamma radiation from a uniformly deposited source. Experiments with cobalt-60, Report FWE-104, 29 pages (Atomic Energy Research Establishment, Oct. 1955).
- [3] Cunningham, J. R., Wilson, R., Bury, F. A., and Flexman, J. K. M., Protection factors for houses using radioactive sources, DRCL Report No. 260, 17 pages (Nov. 1957).
- [4] Rexroad, R. E., and Schmoke, M. A., Scattered radiation and free field dose rates from distributed cobalt-60 and cesium-137 sources, NDL-TR-2, 64 pages (U.S. Army Chemical Center, Edgewood, Md., Sept. 1960).
- [5] Auxier, J. A., Buchanan, J. O., Eisenhower, C., and Menker, H. E., Experimental evaluation of the radiation protection afforded by residential structures against distributed sources, Report CEX-58.1, 133 pages (Civil Effects Test Organization, Jan. 19, 1959).
- [6] Clarke, E., Batter, J., and Kaplan, A., Measurement of attenuation in existing structures of radiation from simulated fallout, Tech/Ops Report TO-B 59-4, 101 pages (April 27, 1959).
- [7] Spencer, L. V., and Fano, U., Penetration and diffusion of x-rays. Calculation of spatial distributions by polynomial expansion, J. Res. NBS 46, 446-456 (1951).
- [8] White, G. R., The penetration and diffusion of  $\text{Co}^{60}$  gamma-rays in water using spherical geometry, Phys. Rev. 80, No. 2, 154-156 (Oct. 15, 1950).
- [9] Goldstein, H., and Wilkins, J. E., Calculation of the penetration of gamma-rays, USAEC Report NYO-3075, 196 pages (1954).
- [10] Hayward, E., The electron spectra produced by a  $\text{Co}^{60}$  source in water, Phys. Rev. 86, No. 4, 493-495 (May 15, 1952).
- [11] Fano, U., Spencer, L. V., and Berger, M., Penetration and diffusion of x-rays, Handbuch der Physik, Encyclopedia of Physics, ed. S. Flugge, Vol 38/2, 660-817 (Springer-Verlag, Berlin, 1959).
- [12] Profio, A. E., ed., Shielding benchmark problems, ORNL-RSIC-25, 109 pages (Oak Ridge, Tenn., June 1969).

- [13] Alberg, M., et al., An investigation of differential energy and angle spectra for  $^{137}\text{Cs}$  gamma rays in water and air, Nucl. Sci. and Eng. 30, 65-74 (Oct. 1967).
- [14] McDonnell, C., Velletri, J., Starbird, A. W., and Batter, J. F., Description, experimental calibration, and analysis of the radiation test facility at the Protective Structures Development Center, Report No. P.S.D.C.-TR-14, 86 pages (Conesco, Division of Flow Corp., Watertown, Mass., Sept. 1, 1964).
- [15] Specification of gamma-ray brachytherapy sources, NCRP Report No. 41, 8 (National Council on Radiation Protection and Measurements, Washington, D.C., April 1974).
- [16] Schumchyk, M. J., et al., Scattered radiation (skyshine) contribution to an open basement located in a simulated fallout field, NDL-TR-68, 78 pages (U.S. Army Nuclear Defense Lab., Edgewood Arsenal, Md., Dec. 1966).
- [17] Abramowitz, M., and Stegun, I. A., Handbook of Mathematical Functions with Formulas, Graphs, and Mathematical Tables, NBS Appl. Math. Ser. 55, 1046 pages (June 1964).
- [18] Garrett, C. W., Gamma ray doses above a plane source of  $^{60}\text{Co}$  on an air/ground interface, Shielding Benchmark Problems, Ed. A. E. Profio, ORNL-RSIC-25 (Oak Ridge, Tenn., June 1969).
- [19] Berger, M. J., and Doggett, J.A., Gamma radiation in air due to cloud or ground contamination, NBS Report 2224, 73 pages (June 1953).
- [20] Gates, L. D., and Eisenhauer, C., Spectral distribution of gamma rays propagated in air, Technical Analysis Report AFSWP-502A, 119 pages (Atomic Support Agency, Armed Forces Special Weapons Project, Jan. 1954).
- [21] Preiser, S., Mittelman, P., and Berndtson, C., Plane isotropic gamma ray buildup factors in lead and water, NDA-10-144, 17 pages (Dec. 21, 1954).
- [22] Goldstein, H., Fundamental Aspects of Reactor Shielding, 416 pages (Addison-Wesley, NY, 1959).
- [23] Faust, W. R., Multiple Compton scattering II, Phys. Rev. 77, No. 2, 227-232, (1950).
- [24] Berger, M. J., Calculation of energy dissipation by gamma radiation near the interface between two media, J. Appl. Phys. 28, No. 12, 1502-1508 (Dec. 1957).
- [25] Schumchyk, M. J., et al., Measurements of gamma radiation and gamma spectra versus height above a fallout field simulated with  $^{60}\text{Co}$  NDL-TR-70, 156 pages (U.S. Army Nuclear Defense Lab., Edgewood Arsenal, Md., Nov. 1965).

- [26] Spencer, L. V., private communication.
- [27] Beck, H., and de Planque, G., The radiation field in air due to distributed gamma-ray sources in the ground, Health and Safety Laboratory Report HASL-195, 59 pages (U.S. Atomic Energy Commission NY, May 1968).
- [28] Burson, Z. G., and French, R. L., Simulating energy and angle distributions above infinite plane cobalt-60 sources, Health Physics 18, 507-521, (May 1970).
- [29] Morris, E. E., Radiation field 3 ft. above infinite air/air and air/ground interfaces as plane isotropic sources of 1.25 MeV gamma radiation, UILU-Eng 73 5301, 80 pages (University of Illinois, Jan. 1973).
- [30] Collins, D. G., and Wells, M. B., COHORT, a Monte Carlo program for calculation of radiation heating and transport, RRA-T62, Vol. 1-4 (Radiation Research Associates, Ft. Worth, Texas, 1966); Warkentin, J. K., Price, J. H., and Wells, M. B., Users Manual for COHORT, a Monte Carlo program for calculation of radiation heating and transport on the IBM-360, RRA-T7014, 142 pages (Radiation Research Associates, Ft. Worth, Texas, Oct. 1, 1970).
- [31] Frank, A. L., and Taylor, R. A., Gamma radiation characteristics-angular distribution over a desert terrain fallout field, USNRDL-TR-856, 76 pages (U. S. Naval Radiological Defense Lab., San Francisco, Calif., June 11, 1955).
- [32] Björnerstedt, R., Health hazards from fission products and fallout. II. Gamma radiation from nuclear weapons fallout, Arkiv för Physik 16, No. 28, 293-313 (Nov. 19, 1959).
- [33] Nelms, A. T., and Cooper, J. W., U235 fission product decay spectra at various times after fission, NBS Report 5853, 33 pages (April 1958).
- [34] Huddleston, C. M., Burson, Z. G., Kinkaid, R. M., and Klinger, Q. C., Ground roughness effects on the energy and angular distribution of gamma radiation from fallout, Report CEX-62.81 (Final), 66 pages (Civil Effects Test Organization, July 1964).
- [35] Michael, J. A., and Lamonds, M. A., Distribution functions of air-scattered gamma rays above isotropic plane source, Tech. Report S-391-R, EGG 1183-2160, 409 pages (Edgerton, Germeshausen, and Grier, Inc., June 1967).
- [36] Berger, M. J., Angular distribution of multiply scattered gamma radiation from a plane isotropic source, J. Appl. Phys. 26, No. 12, 1504-1507, (Dec. 1955).
- [37] French, R. L., and Garrett, C. W., Gamma ray energy and angular distributions near the air/ground interface from plane fallout and point Co<sup>60</sup> sources, RRA-M42, 27 pages (Radiation Research Associates, Ft. Worth, Texas, June 1, 1964).



- [38] Fano, U., Note on the Bragg-Gray cavity principle for measuring energy dissipation, Rad. Res. 1, No. 3, 237-240 (June 1954).
- [39] Spencer, L. V., Gamma ray shielding theory, Vol 1, Radiation Shielding, TR-40, 325 pages (Office of Civil Defense and Kansas State University, Nov. 1966).
- [40] Eisenhower, C., Gamma radiation fluxes near a ground-air interface using image source technique, Nucl. Sci., and Eng. 32, 166-177 (1968).
- [41] Clarke, E. T., Gamma ray scattering near an air-ground interface, Nucl. Sci. and Eng. 27, 394-402 (Feb. 1967).
- [42] Batter, J., Cobalt and iridium buildup factors near the ground-air interface, Trans. Am. Nucl. Soc. 6, No. 1, 198 (June 1963).
- [43] Clifford, C. E., Effects of the ground on the gamma dose from distributed cesium-137 sources, Can. J. Phys. 42, 2373-2383 (1964).
- [44] Marcum, J. I., Comparison of Monte Carlo calculations with experimental results for the propagation of gamma rays near an air-ground interface, RM-3399-PR, 19 pages (Rand Corp., Dec. 1962).
- [45] Chilton, A. B., and Fu, C. Y., Exposure field from a point isotropic source located at the surface of a thick concrete slab, NRSS-2, 57 pages (University of Illinois, 1969).
- [46] Beck, H., and Bennett, B., Polynomial solutions of the gamma ray transport equation in infinite-homogeneous and two-medium plane geometry, Trans. Am. Nucl. Soc. 10, No. 1, 400-401 (June 1967).
- [47] Frank, A. L., Spectral measurements of scattered photons from a point source near the air-ground interface, USNRDL-TR-67-124, 53 pages (U. S. Naval Radiological Defense Lab., San Francisco, Calif., Oct. 10, 1967).
- [48] French, R. L., Gamma-ray energy and angular distributions above an infinite fallout field, RRA-T43, 88 pages (Radiation Research Associates, Ft. Worth, Texas, May 1, 1964).
- [49] Clifford, C. E., Dependence of total dose rate and skyshine dose rate on the area of contamination, Technical Memo. No. 104, 3 pages (Defense Research Chemical Labs., Ottawa, Canada, March 1970).
- [50] Burson, Z. G., and Summers, R. L., Barrier attenuation of air-scattered gamma radiation, Report CEX-63.3, 93 pages (Civil Effects Test Organization, June 1965).
- [51] Starbird, A. W., and Batter, J. F., Angular distribution of "skyshine" radiation at the surface of a plane of "fallout" contamination, Technical Operations Report TO-B 63-40, 36 pages (Office of Civil Defense, March 1964).

- [52] Clifford, C. E., Carruthers, J. A., and Cunningham, J. R., <sup>137</sup>Scattered gamma radiation from a simulated fallout field using Cs<sup>137</sup>, Report No. DRCL 296, 15 pages (Defense Research And Chemical Lab, Ottawa, Canada, Jan. 1959).
- [53] Clifford, C. E., private communication.
- [54] Jenkins, A. L., and Hinkley, D. E., Application of modified engineering method techniques to skyshine radiation measurements, NDL-TR-117 70 pages (Nuclear Defense Lab., Edgewood Arsenal, Md., Nov. 1968).
- [55] Spring, R., and Velletri, J., Experimental study of the "in-and - down" component of radiation from ground based sources, CGS-TR-31, 59 pages (Datametrics, Division of CGS Scientific Corp., June 1970).
- [56] Kaplan, A. L., Analysis of data from structure shielding experiments, Final Report, Technical Operations Report B 68-39, 105 pages (U.S. Naval Radiological Defense Lab., San Francisco, Calif., June 1968).
- [57] Eisenhower, C., and Kaplan, A. L., Evaluation of the reduction factor in the basement of a structure, NBS Report 10037, 127 pages (May 1969).
- [58] Starbird, A. W., Interior partition and basement shelter experiments, CONESCO-4903 (NRDL-TRC-69-24), 70 pages (Flow Corporation, April 1969).
- [59] Schumchyk, M. J., and Tiller, M. J., Ground penetrating radiation (lip contribution) in a foxhole from a fallout field simulated by cobalt<sup>60</sup>, NDL-TR-3, 38 pages (Nuclear Defense Lab., Edgewood Arsenal Md., Dec. 1960).
- [60] Berger, M. J., and Spencer, L. V., Some radiological applications of gamma-ray transport theory, Rad. Res. 10, No. 5, 552-570 (May 1959).
- [61] Glasstone, S., ed., The effects of atomic weapons, 579 pages (U.S. Atomic Energy Commission, 1957); Revised Edition, 730 pages (U.S. Atomic Energy Commission, 1962).
- [62] Ksanda, C. F., et al., Gamma radiations from contaminated planes and slabs, USNRDL Technical Memo. No. 27, 109 pages (U. S. Naval Radiological Defense Lab., San Francisco, Calif., Jan. 19, 1955).
- [63] Ksanda, C. F., Moskin, A., and Shapiro, E. S., Gamma radiations from a rough infinite plane, USNRDL-TR-108, 11 pages (U.S. Naval Radiological Defense Lab., San Francisco, Calif., Jan. 1956).
- [64] Israel, Y. A., The influence of the microrelief of the earth's surface on the propagation of gamma radiation on the surface layer of the atmosphere, Isv Geophys Ser. 818-824 (1963); Israel, Y. A., Effect of roughness of the ground on the  $\gamma$  field above a region contaminated by radioactive fallout, Atomnaya Energiya 17, No. 2, 137-140 (1964).

- [65] Clifford, C. E., Effects of interfaces on gamma shielding, Trans. Am. Nucl. Soc. 6, No. 1, 197 (1963).
- [66] Clifford, C. E., Effects of ground roughness on the gamma dose from Cs-137 contamination, Report No. 401, 16 pages (Defense Chemical Research Lab., Ottawa, Canada, March 1963).
- [67] Ferguson, J. M., Ground roughness effects for fallout-contaminated terrain: comparison of measurements and calculations, USNRDL-TR-645, 24 pages (U. S. Naval Radiological Defense Lab., San Francisco, Calif., May 7, 1963).
- [68] Spencer, L. V., Structure shielding against fallout radiation from nuclear weapons, NBS Monograph 42, 134 pages (June 1, 1962).
- [69] Tomnovec, F. M., Ferguson, J. M., and Weldon, D. M., The effect of a changing gamma-ray fallout spectrum on the ground roughness factor, USNRDL-TR-915, 30 pages (U. S. Naval Radiological Defense Lab., San Francisco, Calif., Sept. 22, 1965).
- [70] Goldstein, R., The TERF program and its applications to the calculation of fallout radiation dose, NRDL-TRC-68-56, 77 pages (Math. Applications Group, Inc., White Plains, NY, Jan. 1969).
- [71] Cohen, M. O., TERF Monte Carlo Fallout Code Calculations. Final Report, MR-7002, 60 pages, Mathematical Applications Group, Inc., White Plains, N.Y. (April 1970).

## VII. SHIELDING ANALYSIS FOR SIMPLE STRUCTURES IN AN IDEALIZED FIELD

### A. INTRODUCTION

In this chapter, the methodology for shielding analysis of simple structures surrounded by an idealized fallout distribution will be developed; more complex structures and source configurations will be the subject of a subsequent chapter. The distinction between a simple and a complex structure is rather arbitrary, but for the purposes of this exposition a structure is considered simple if it is of rectangular parallelepiped shape and has no significant structural floors or partitions (from the shielding standpoint) within the single "membrane" which forms its outer shell. Such a structure may also be termed a non-compartmented blockhouse. The structure is of dimensions suitable for human occupancy, is made of normal structural materials, and is surrounded by a smooth, level plain.

It is further useful to define an elementary blockhouse as a simple structure with its floor at ground level, its walls being slabs of the same constant mass thickness, its roof of constant mass thickness (but not necessarily the same as that of the walls), without apertures of any kind. This implies that there is a class of simple structures which are not elementary, such structures having one or more of the following features: structure floor not at ground level; walls or roofs of variable thickness; apertures in walls or roofs.

The idealization of the fallout distribution mentioned above means (see sec. V.A.1) that the fallout is uniformly deposited on all horizontal surfaces outside the structure, including the roof. The extent of the contaminated ground outside the structure is infinite in the horizontal plane. No topographic features, including other structures, are present to provide any degree of outside shielding; nor has the fallout penetrated the ground to any extent.

At this point and many times later in the text, reference is made to the "Standard Method" of fallout shielding analysis. This refers specifically to that method the fundamentals of which are reported in NBS Monograph 76 [1]. By extension, it also refers to the more elaborate methodology developed by the Office of Civil Defense (OCD) on the basis of Monograph 76. Because the OCD compilation of recommended engineering procedures was for a number of years under review and change, it is somewhat difficult to cite any specific technique as being absolutely standard, even though the general philosophy behind the OCD approach has remained the same. In this work, we shall call "standard" those methods and techniques provided in the OCD Document TR-20 (Vol. 1), including revisions up to this time [2].<sup>1</sup>

Some comments on nomenclature are desirable here. First of all, even though the Office of Civil Defense no longer exists and its functions have largely been taken over by the Defense Civil Preparedness Agency (see footnote 11 of chapter I) the Manual TR-20 and its revisions were developed almost entirely during the lifetime of the agency under its former name. We shall thus continue to call this standard text the "OCD Manual." It might also be noted that what we now call the "Standard Method," or its earlier versions, has been designated in much of the previous literature on the subject as the "Engineering Manual Method" or simply the "Engineering Method." We shall avoid these terms as being too vague.

---

<sup>1</sup>The earliest published official OCD manual covering this methodology was OCD Document PM-100-1 [3]. This manual has not been revised to keep up with technical advances and therefore cannot be considered an adequate "standard."

## B. ELEMENTARY BLOCKHOUSES


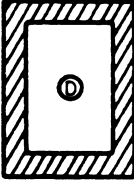
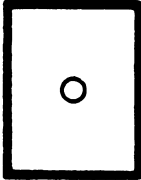

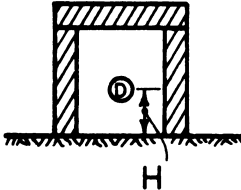
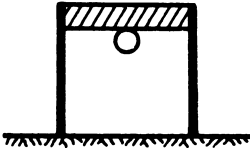
### 1. Standard Method

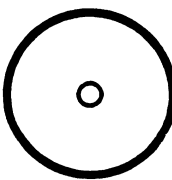
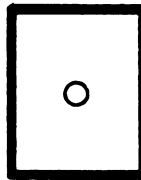
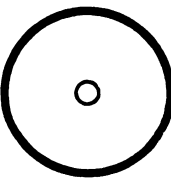
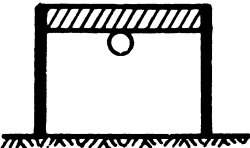
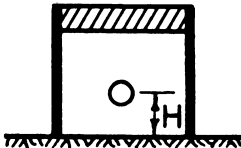
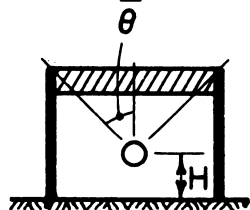
The elementary situation which is the keystone to the methodology of fallout shielding analysis is the single-storied blockhouse, rectangular in shape, without apertures. A detector is considered to be located at a distance above the earth which we call  $H$ , on the central axis of symmetry. Let us call the distance from detector to roof  $Z$ . The surface of the ground outside the structure is considered to be a smooth plane of infinite extent. The roof is a flat slab of effective mass thickness  $X_o$ , all four walls are slabs of the same constant effective mass thickness  $X_e$ , and the first floor surface is at grade level. The linear thicknesses of the structural slabs are considered to be negligible in comparison with the overall dimensions of the blockhouse itself, which are specified as a width  $W$ , a length  $L$ , and a height  $Z + H$ . The fallout is deposited uniformly on all outside horizontal surfaces. The reduction factor at the location of the inside detector (usually, but not necessarily, 3 ft (0.914 m) above the floor for this elementary situation) is the exposure rate at this point divided by the reference exposure rate, which is the value at the Standard Unprotected Location (see sec. V.8.1).

The method of analysis to be described first is the Standard Method. The approach here is more graphic than that provided in NBS Monograph 76 [1], but there are no essential differences in principle.

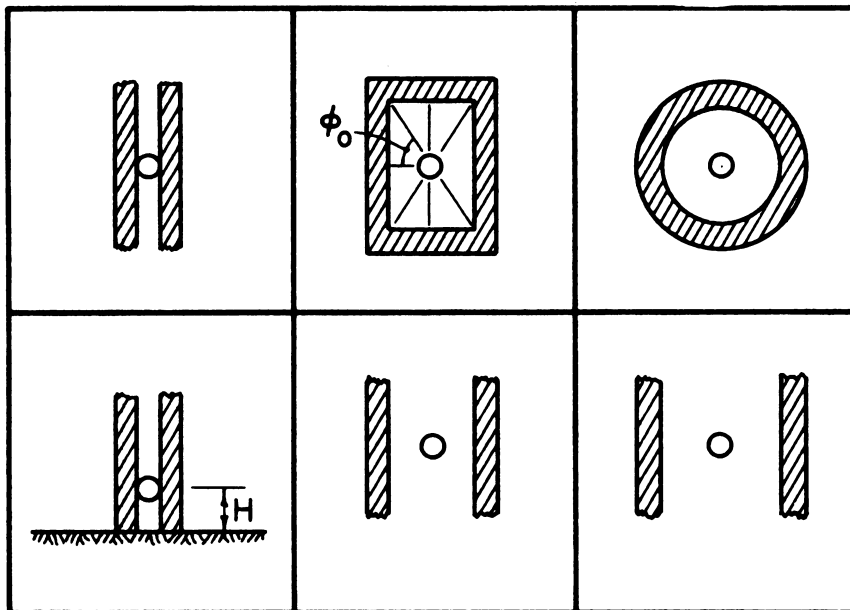
It will help in the explanation to utilize simple drawings, not only of the blockhouse under consideration, but of a number of subsidiary situations which are conceptually intermediate between the blockhouse with its centrally located detector and the detector at the Standard Unprotected Location. These are all presented in figure VII.1, and are briefly described as follows:

Situation (1). This is the Standard Unprotected Location, with the detector 3 ft above the smooth source plane.

HORIZONTAL SECTION			
VERTICAL SECTION			
	(1)	(2)	(3)

		
		
(4)	(5)	(6)

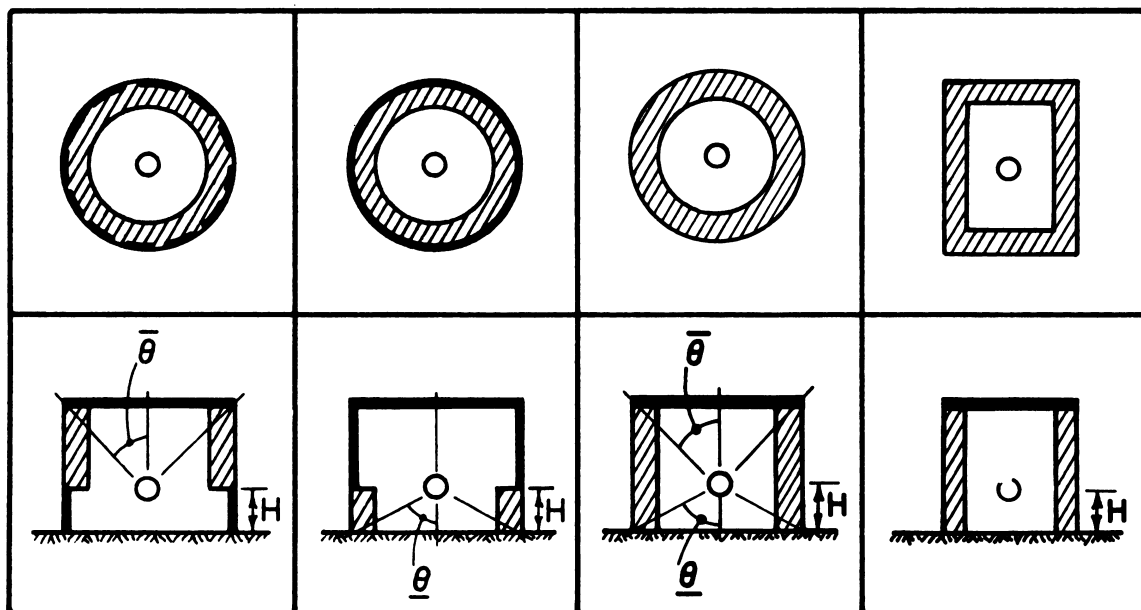
VII.1 Conceptual situations used for blockhouse analysis. Hatched elements are penetrable by radiation; solid elements are opaque to radiation.



(7)

(8)

(9)



(10)

(11)

(12)

(13)

VII.1 (Continued)



Situation (2). The situation here is the rectangular blockhouse which is the subject of the analysis.

Situations (3)-(6). In these situations, the walls are completely opaque to radiation, and only radiation penetrating the roof affects the detector. In (3) and (4), the detector is just beneath the roof slab; in (5) and (6) the detector is at the detector height  $H$ . Situation (3) and (5) have the same rectangular plan as the blockhouse, but Situations (4) and (6) have circular roofs which are equivalent to the rectangular roof of the blockhouse. The term "equivalent" as used here means that the roofs in Situations (5) and (6) subtend the same solid angle at the detector position  $H$  feet above the floor.<sup>2</sup>

Situation (7). Here the situation consists of two walls on the infinite plane, of indefinite height and length, very close together, with the detector between them at height  $H$ . (It is not logically necessary for the detector to be at this height, but as will be seen later this choice appreciably simplifies the development of the method.)

Situation (8). The structure here is made of four walls in a rectangular plan the same as that of the blockhouse, but the walls are of infinite height and depth. The detector is located centrally between the walls. The

---

<sup>2</sup>There is some latitude in selecting the dimensions of the cylindrical structure which is equivalent to the given rectangular structure, since the solid angle fraction subtended by a circular roof may be the same with any combination of circular roof radius and detector-roof distance which maintains the proper value of  $\bar{\theta}$  (see fig. VII.1, (6)). For our purposes, the dimensions of the equivalent cylindrical structures are arbitrarily established by maintaining the same detector height,  $H$ , and providing for a radius of the equivalent cylindrical structure such that the same solid angle fraction is subtended by the floors of the cylindrical and rectangular structures at the detector positions. With this radius assumed also for the roof of the equivalent structure, the height of detector to roof is established to give the proper value of  $\bar{\theta}$ . For the cylindrical structure the distance from detector to roof will, of course, be slightly different from the dimension  $Z$  of the rectangular blockhouse; and the difference depends to some extent on the eccentricity,  $e = W/L$ , of the blockhouse. In practice, this difference is almost always small and can be ignored.

radiation field surrounding the structure is considered to be constant with height and to have the same character as the radiation field at height  $H$  above the source plane in Situation (7).

Situation (9). This is the same as Situation (8), except that the plan is circular rather than rectangular. The radius of the cylinder thus formed is the same as in Situations (4) and (6). The detector is on the axis of the cylinder. The same constant radiation field exists outside the structure as in Situation (8); and, provided the radius of the cylinder is several feet or more, the characteristics of the radiation emitted inward from the interior of the structures are essentially the same in both situations.

Situations (10)-(13). In these cases, the structure walls are set on the smooth plane and are of single story height. The detector is on the axis at height  $H$ . The roof is completely opaque to radiation so that only radiation coming through the walls affects the detector. In addition, Situation (10) has the portion of the walls below the detector opaque to radiation and (11) has the portion above the detector opaque to radiation. Situation (13) has the same rectangular plan as the blockhouse; (10), (11), and (12) have the circular plan which is equivalent in the sense explained for Situation (6).

All of the situations described will be useful in analyzing the shielding capability of the blockhouse with respect to fallout radiation. However, in the analysis, it will be necessary to change the effective mass thickness of the walls for some situations. Certain cases require an effective mass thickness the same as that of the blockhouse; other cases require a mass thickness of zero (phantom structures); and still other cases demand very large effective mass thicknesses, approaching infinity. In order to avoid violating the rule about actual thicknesses being very small compared to blockhouse dimensions, it is desirable to visualize the change in effective mass thickness, especially for the infinite cases, as being brought about by a change in wall density

rather than any change in the linear dimensions of the wall. The description of the pertinent cases in the subsequent discussion therefore indicates not only the geometric situation selected from the above list but also the pertinent wall density, if it varies from the standard value for the blockhouse. Thus, the symbol  $D_7$  represents the detector response for Situation (7) and a normal wall density,  $D_7(0)$  for the same situation with zero wall density, and  $D_7(\infty)$  for the same situation with the wall density approaching infinity. Also, we shall frequently denote  $\cos\theta$  by the symbol  $u$ . It is to be noted that, where  $\theta$  is the half angle of a conical aperture, the solid angle fraction  $\omega$  equals  $(1 - u)$ . Further, use of an overhead bar, viz.  $\bar{u}$ ,  $\bar{\theta}$ ,  $\bar{\omega}$ , or an underline, viz.  $\underline{u}$ ,  $\underline{\theta}$ ,  $\underline{\omega}$ , will designate cone apertures opening up or down, respectively.

The reduction factor for the blockhouse is designated  $R_f$ , and in terms of the detector responses in the above situations, it is defined by

$$R_f = \frac{D_2}{D_1} . \quad (\text{VII.1})$$

On the assumption that contributions through roof and wall do not have any effect on one another,

$$D_2 = D_5 + D_{13} , \quad (\text{VII.2})$$

and

$$R_f = \frac{D_5}{D_1} + \frac{D_{13}}{D_1} . \quad (\text{VII.3})$$

The first term on the right side corresponds to the normalized roof contribution, and is designated  $C_r$ .<sup>3</sup> The other term corresponds to the normalized contribution through the walls, and is designated  $C_g$ . The subscript "r" relates to the "roof," while the subscript "g" stands for "ground."<sup>4</sup>

$$C_r = \frac{D_5}{D_1} = \frac{D_3}{D_1} \cdot \frac{D_5}{D_3} \quad . \quad (\text{VII.4})$$

Situation (3) closely resembles that in figure V.12, if the latter is turned upside down; and therefore  $L(X_o)$  is selected as a close approximation to  $D_3$ . Since  $D_1$  is  $L(3')$ , which is equal to unity in accordance with the prescribed normalization of the L-function, the value of  $L(X_o)$  is also proper as the value for  $D_3/D_1$  in eq (VII.4).

In determining the second ratio in the above product, it is assumed that

$$\frac{D_5}{D_3} = \frac{D_6}{D_4} \quad . \quad (\text{VII.5})$$

This ratio is closely approximated by the function  $L_a(X_o, \bar{u})$ , inasmuch as the concentration of shielding mass near the source (the fallout on the roof) tends to insure that penetrating radiation reaching the detector only does so through a conical aperture of acceptance subtended by the roof and designated

<sup>3</sup>The OCD Manual uses the symbol  $C_o$  ("o" for "overhead") when referring to any roof contribution, regardless of how complex the structure. Unfortunately,  $C_o$  is also used to symbolize a specific function which is defined here by eq (VII.6). In this text the differing notations are used for the separate concepts to avoid confusion. For the most elementary case, of course,  $C_r$  equals  $C_o$ .

<sup>4</sup>Because a small part of the contribution through the roof slab originates from fallout on the ground, the designation of  $C_g$  as the "ground contribution" can be slightly misleading.

by its half angle  $\bar{\theta}$ . (See fig. V.14.) This of course ignores the contribution of internal scatter from walls and floor into the detector, but such additional contributions are estimated to be small (cf. p. 57, ref. [4]). Thus it can be seen to a good approximation,  $C_r$  equals  $C_o$ , which is a function graphed in figure C.8A, of appendix C and defined by

$$C_o(X_o, \bar{\omega}) = L(X_o) L_a(X_o, \bar{\omega}) \quad , \quad (\text{VII.6})$$

where  $\bar{\omega}$ , the solid angle fraction subtended by the roof at the detector position, equals  $1 - \cos \bar{\theta}$ , or  $1 - \bar{u}$ .<sup>5</sup>

There are several important points to make here. The first is that, if the attenuating overhead materials were more evenly distributed between the roof source and the detector, the situation would approximate more nearly the ideal case depicted in figure V.16, establishing the function  $L_c(x_o, \bar{\omega})$ . One practical case closely related to this latter idealization is that of a multistory building with many floor slabs between the roof source and the detector in one of the lower stories. Various earlier versions of the Standard Method have vacillated whether to use  $L_c$  in such case to to use  $L_a$  for all cases. In any event,  $L_a$  and  $L_c$  are not greatly different; and in the latest version of the Standard Method, eq (VII.6) was chosen to serve both the single story and the multistory cases. Such a decision was based on experimental evidence that the use of  $L_a$ , though generally not as conservative as  $L_c$ , still gives data greater than that experimentally measured.

It should be mentioned that even though most of the overhead contribution comes from fallout on the roof, some radiation from fallout on the ground is included. Since the idealized functions are for infinite attenuating media

---

<sup>5</sup>See the footnote following eq (VII.3).

situations, the theoretical prediction for the radiation penetrating the roof and entering the detector includes a backscattered portion ("skyshine"), in addition to that going directly into the roof slab from the roof fallout source. Because the average distance between interactions with atoms of the air constituents is large compared with the dimensions of most buildings, a large proportion of the skyshine which is incident upon the roof actually originates from fallout on the ground in the general vicinity of the structure rather than from directly over the roof.<sup>6</sup> Thus, experimental work on roof penetration of blockhouse roofs should properly include some way of simulating this portion backscattered from the air, if a close check on the theoretical functions is desired.

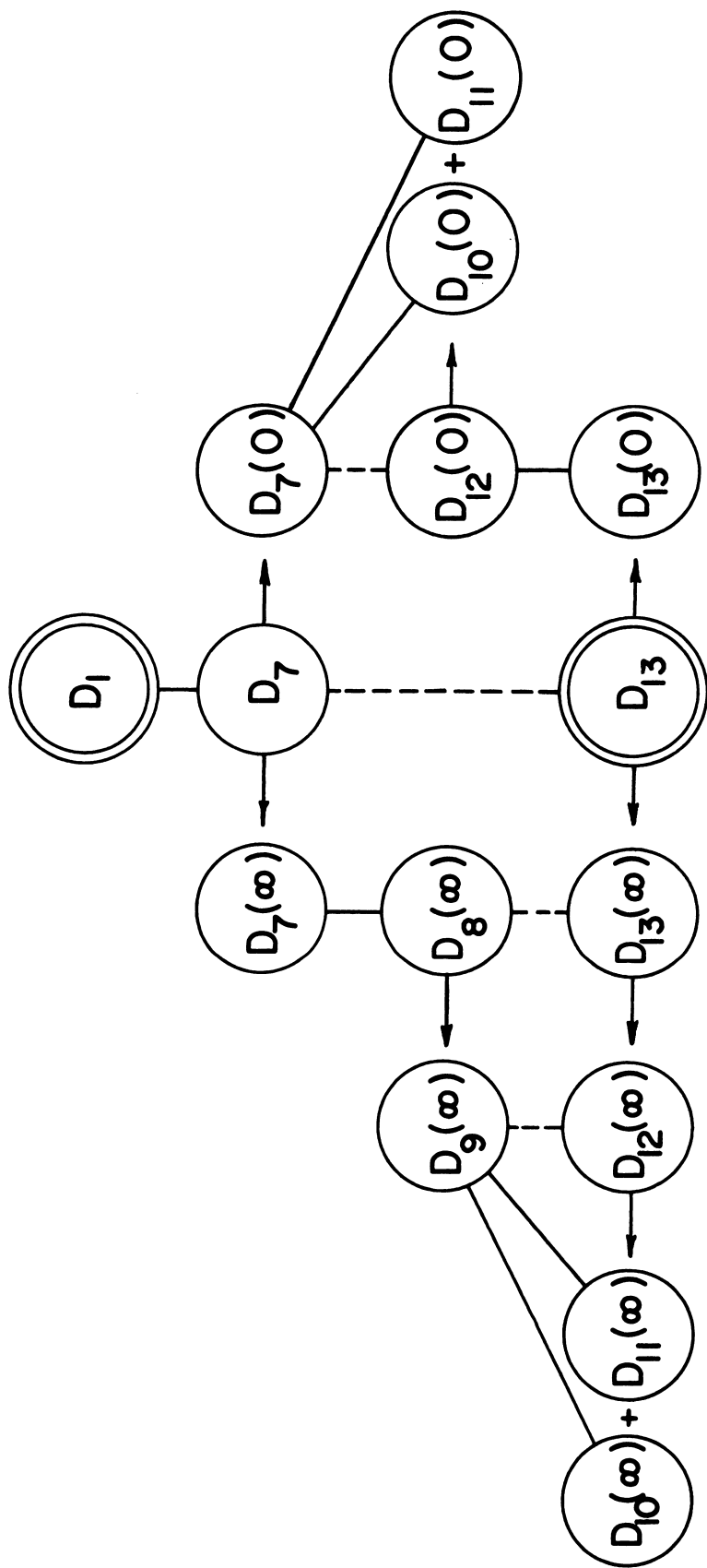
For understanding of the analysis of  $C_g$ , the last term on the right hand side of eq (VII.3), the reader is referred to figure VII.2, which outlines its logical structure. First, Situation (7) is inserted in the relationship between Situations (1) and (13), thus:

$$C_g = \frac{D_{13}}{D_1} = \frac{D_7}{D_1} \cdot \frac{D_{13}}{D_7} \quad . \quad (\text{VII.7})$$

At this point, an important assumption is made that the ratio  $D_{13}/D_7$ , which is a ratio of detector responses for two situations involving the actual wall thicknesses, can be obtained on the basis of an interpolation between the two extreme cases in which the situations involve walls of very great mass thickness (which we will call "infinite") and of zero mass thickness. In mathematical symbols, this means that

---

<sup>6</sup>While the point of origin thus shifts, other characteristics of the skyshine agree between the actual case and the theoretical functions, because of the density-scaling principle of section IV.B.3.



VII.2 Logic diagram for development of equation for Cg. See the discussion in connection with eq (VII.7) to eq (VII.20).

$$\frac{D_{13}}{D_7} = S_w \frac{D_{13}^{(\infty)}}{D_7^{(\infty)}} + (1 - S_w) \frac{D_{13}^{(0)}}{D_7^{(0)}} \quad , \quad (\text{VII.8})$$

where  $S_w$  is the interpolation factor. It has been assumed that  $S_w$  can be closely approximated by the ratio of scattered to uncollided radiation penetrating the wall. On the basis of such an assumption, one could use buildup factors to obtain  $S_w$  according to the formula

$$S_w(X_e) = \frac{B(X_e) - 1}{B(X_e)} \quad , \quad (\text{VII.9})$$

where  $X_e$  is the mass thickness of the "exterior" wall, and  $B$  is the exposure buildup factor for a concrete wall and for the type of the source incident on it (or a reasonable idealization of the source description). Actually, the standard curve for  $S_w$  in the OCD Manual is based on the ratio

$$S_w(X_e) = \frac{P^{(s)}(X_e)}{P^{(s)}(X_e) + P^{(o)}(X_e)} \quad , \quad (\text{VII.10})$$

where  $P^{(s)}$  and  $P^{(o)}$  are the scattered and uncollided portions, respectively, of the exposure from a point source and are presented in figure V.20.

Implicit in this way of calculating the interpolation factor is the assumption that no variables other than effective wall mass thickness affect it to any significant extent. (This assumption has never been seriously challenged, although Eisenhower [1] suggested that the solid angle fractions established at the detector by the floor and ceiling might have some influence. This question is still open.)



$S_w$  is called the wall "scattering fraction," primarily because of the fact that, as calculated, it is a ratio of the scattered contribution to the total exposure at depth  $S_e$ . It must be noted that, as we have developed the method so far, its use does not imply fundamentally that the term  $S_w(e) D_{13}(\infty)/D_7(\infty)$  is the geometry factor for the scattered component through walls of mass thickness  $X_e$ . Similarly, the second term on the right side of eq (VII.9) does not fundamentally relate to the uncollided contribution to exposure behind walls of thickness  $X_e$ . Such identifications as these are made later; but they cannot be considered logically rigorous and are therefore approximate at best.

As shown in figure VII.2, we now insert the Situations  $D_8(\infty)$  and  $D_{12}(0)$  in a mathematically correct fashion:

$$C_g = \frac{D_7}{D_1} \left[ S_w(X_e) \frac{D_{13}(\infty)}{D_8(\infty)} \cdot \frac{D_8(\infty)}{D_7(\infty)} + (1 - S_w(X_e)) \frac{D_{13}(0)}{D_{12}(0)} \cdot \frac{D_{12}(0)}{D_7(0)} \right]. \quad (\text{VII.11})$$

For reasons discussed later, it is assumed that the ratio  $D_{13}(\infty)/D_8(\infty)$  is equal to  $D_{12}(\infty)/D_9(\infty)$ . Furthermore, it is clear that  $D_{12}(\infty) = D_{10}(\infty) + D_{11}(\infty)$  and  $D_{12}(0) = D_{10}(0) + D_{11}(0)$ . By substitution, one obtains

$$C_g = \frac{D_7}{D_1} \left\{ S_w(X_e) \left[ \frac{D_{10}(\infty)}{D_9(\infty)} + \frac{D_{11}(\infty)}{D_9(\infty)} \right] \frac{D_8(\infty)}{D_7(\infty)} + [1 - S_w(X_e)] \left[ \frac{D_{10}(0)}{D_7(0)} + \frac{D_{11}(0)}{D_7(0)} \right] \frac{D_{13}(0)}{D_{12}(0)} \right\}. \quad (\text{VII.12})$$

The ratios in the above equation are given special names and symbols, as follows:

$$\text{Exterior wall barrier factor: } B_e(X_e, H) = \frac{D_7}{D_1} . \quad (\text{VII.13})$$

"Wall scatter" geometry factors:

$$\text{(Upper) } G_{su}(\bar{\omega}) \equiv \frac{D_{10}^{(\infty)}}{D_9^{(\infty)}} ; \quad (\text{VII.14})$$

$$\text{(Lower) } G_{sl}(\underline{\omega}) \equiv \frac{D_{11}^{(\infty)}}{D_9^{(\infty)}} . \quad (\text{VII.15})$$

$$\text{"Direct" geometry factor: } G_d(\underline{\omega}, H) \equiv \frac{D_{11}^{(0)}}{D_7^{(0)}} . \quad (\text{VII.16})$$

$$\text{Skyshine geometry factor: } G_a(\underline{\omega}) \equiv \frac{D_{10}^{(0)}}{D_7^{(0)}} . \quad (\text{VII.17})$$

Shape factors:

$$\text{(Scatter) } E_s(e) \equiv \frac{D_8^{(\infty)}}{D_7^{(\infty)}} ; \quad (\text{VII.18})$$

$$\text{(Direct) } E_d(W, L) \equiv \frac{D_{13}^{(0)}}{D_{12}^{(0)}} . \quad (\text{VII.19})$$

The reason for indicating  $G_d$ , but no other geometry factor, as a function of  $H$  is explained shortly.

It might also be noted that  $D_7(0)$ , appearing in some of the above terms, is the same numerically as  $D_1$ . Equation (VII.12) can now be rewritten as

$$C_g = B_e(X_e, H) \{ S_w(X_e) [G_{su}(\bar{\omega}) + G_{sl}(\underline{\omega})] E_s(e) + [1 - S_w(X_e)] [G_d(\underline{\omega}) + G_a(\bar{\omega})] E_d(W, L) \} \quad . \quad (VII.20)$$

A functional description of the factors defined in eqs (VII.13) through (VII.19), or at least a recipe for their calculation, can be provided in terms of the appropriate detector response functions by which they are defined. These response functions are obtained by integration of the contributions over all directions included within the solid angle fraction subtended by the walls.

A rather thorough discussion of the calculational details involved, as well as a set of numerical tables for the factors, has been provided by Bramlitt and Eisenhauer [5]. An abbreviated explanation of the derivation of the factors is given below.

$B_e$ : For theoretical determination of this factor, the functions discussed in chapter V may be used. Then, the denominator in eq (VII.13) is unity and the exterior wall barrier factor is simply  $D_7$ . In general, the exposure rate for this situation can be well approximated by the function  $W(X, H)$  already defined in eq (V.19), multiplied by a factor of 2, to account for the contribution through two walls rather than one. For zero or small values of  $X_e$ , the use of  $2W$  gives results which are somewhat too high, because the  $W$ -function always includes the effect of an infinitely thick backscatterer behind the detector instead of a finite wall. It is clear that for  $X_e$  equal to zero the detector response is given to a much closer degree of accuracy by the function  $L(H)$ . In practice, therefore, values for  $B_e(X_e, H)$  can be

provided at  $X_e$  equal to zero by the function  $L(H)$  and by  $2W(X_e, H)$  for moderate and large values of  $X_e$ . For small but positive values of  $X_e$ , data are provided by somewhat arbitrarily picking values which provide a smooth transition between functions for the two limiting cases. This is easy in practice. The transition region is rather narrowly confined to values of  $X_e$  up to about 20 psf, because most of the albedo effect results from interactions fairly close to the surface of a backscatterer.

The use of the vertical detector position,  $H$ , as the height argument for  $B_e$  is determined by the choice of this height for the detector in Situation (7). As noted before, there is some degree of arbitrariness here, and the choice will be justified below in the discussion of wall-scattering geometry factors.

$G_{su}$  and  $G_{sl}$ : Let us note here a significant fact about radiation when it has penetrated very thick walls, proved by Fano, Spencer, and Berger. (See p. 717 of their Handbuch der Physik article [6].) The radiation emerging from the interior side of such walls is composed almost entirely of photons which have lost the "memory" of their original direction and have a directional distribution symmetric about a line normal to the wall. NBS Monograph 76 [1] does not make quite as strong a statement as this, but it accepts the less stringent proposition that the radiation is symmetric with respect to both horizontal and vertical planes which are perpendicular to the vertical walls. Symmetry with respect to the horizontal plane implies that  $D_{10}^{(\infty)}$  and  $D_{11}^{(\infty)}$  can be described by the same function, and in turn permits the establishment of a single function  $G_s$  to represent both  $G_{su}$  and  $G_{sl}$ .

$G_s$ : Although the detector responses to radiation emerging from a wall of effective mass thickness approaching infinity tend to become vanishingly

small,<sup>7</sup> we are concerned with ratios of such small quantities, and these remain finite. What we need for each infinite wall situation is the directional distribution of the radiation emitted from the wall, or, from the detector point of view, the directional distribution of the differential exposure contributions at the detector. The assumption in the Standard Method is that the directional distribution function describing the radiation emitted from the walls is separable into components depending on vertical and horizontal angles, respectively. If we designate this function as  $F(u, \phi)$ , this assumption says that

$$F(u, \phi) = p(\phi) q(u) \quad , \quad (\text{VII.21})$$

where  $\phi$  is the azimuthal angle and  $u$  is the cosine of the polar angle, both angles being relative to a frame of reference with a vertical polar axis.

The function  $q(u)$  is not adequately known and the assumption has been made that it probably looks like the skyshine portion of the  $\ell$ -function at a height in air of three feet, that is,

$$q(u) = k\ell(3', -|u|) \quad , \quad (\text{VII.22})$$

The absolute value signs surrounding  $u$  give the symmetry with respect to the horizontal. The factor  $k$  is the strength function of the inward directed radiation field at the interior of the wall. For Situations (10) through (13), it actually varies with the height of the differential area of the wall emitting radiation in the direction of the detector, which in turn implies a dependence

---

<sup>7</sup>Because of this fact one would expect experimenters to have great difficulty in studying  $G$  with accuracy. Even theoretical studies of this function require special<sup>8</sup> techniques adapted for very deep penetrations.

upon  $u$ . For Situation (7), only one value of wall differential area height is involved; and for Situations (8) and (9), the strength function is the same at all wall emission area heights as for Situation (7), because of the way hypothetical Situations (8) and (9) are defined. In defining a function depending upon ratios of detector responses under these situations, matters are greatly simplified if the strength function is assumed constant at all wall area heights within the total wall height. For the elementary blockhouse, the dominant portion of the wall contributing to the detector response is that portion near the intersection of the horizontal plane of the detector with the wall; and therefore  $k$  is assumed to be constant and is established at that height. The selection of  $H$  as the detector height in Situation (7) is consistent with this choice.

$G_s(\bar{\omega})$  is properly defined in terms of a ratio for rectangular blockhouse situations, but in such cases there are difficulties in carrying out necessary integrations of the functions. Matters are greatly simplified in this respect for equivalent circular buildings, however; and we therefore define  $G_s(\bar{\omega})$  in terms of the ratio specified in eq (VII.14):

$$G_s(\bar{\omega}) = \frac{k \int_{-\bar{u}}^0 \ell(3', u) du \int_0^{2\pi} p(\phi) d\phi}{2k \int_{-1}^0 \ell(3', u) du \int_0^{2\pi} p(\phi) d\phi} ,$$

$$= \frac{1}{2S(3')} \int_{-1+\bar{\omega}}^0 \ell(3', u) du . \quad (\text{VII.23})$$

The same function serves also for  $G_s(\underline{\omega})$ , as previously noted.

$E_s$  (or  $E$ ): Consistent with eq (VII.18), this can be expressed in terms of ratios for rectangular situations. At the time the Standard Method was devised, there was no precise information on the matter, and it was assumed that the function  $p(\phi)$  has a cosine distribution. If we take  $p(\phi)$  to be normalized, this indicates simply that

$$p(\phi) = \frac{\cos\phi}{2}, \quad (\text{VII.24})$$

where  $\phi$  is measured from normal to the wall. From eqs (VII.18), (VII.21), and (VII.24), it is seen that

$$\begin{aligned} E_s(e) &= \frac{2 \left[ \int_0^{\phi_0} \cos\phi \, d\phi + \int_0^{\pi/2-\phi_0} \cos\phi \, d\phi \right] \int_{-1}^1 q(u) \, du}{\int_{-\pi/2}^{\pi/2} \cos\phi \, d\phi \int_{-1}^1 q(u) \, du} \\ &= \sin\phi_0 + \cos\phi_0 = \frac{1+e}{\sqrt{1+e^2}}. \end{aligned} \quad (\text{VII.25})$$

where  $\phi_0$  is the angle between radial lines in the horizontal detector plane from the central detector position to the center of the wall and corner of the same wall, respectively, and  $e \equiv W/L = \cot \phi_0$ .<sup>8</sup> Although we have designated this "shape factor" as  $E_s$ , to denote its pertinence to the thick wall case, it is unnecessary to emphasize the point further; and we shall henceforth call it  $E$ .

$G_d$  and  $G_a$ : The two geometry functions derivable for the zero-thickness wall situations are quite simply established in terms of the  $\ell$ -function, from their definitions, eqs (VII.16) and (VII.17)

---

<sup>8</sup>This is valid if the normal is to the longer wall; otherwise the tangent function is proper here.

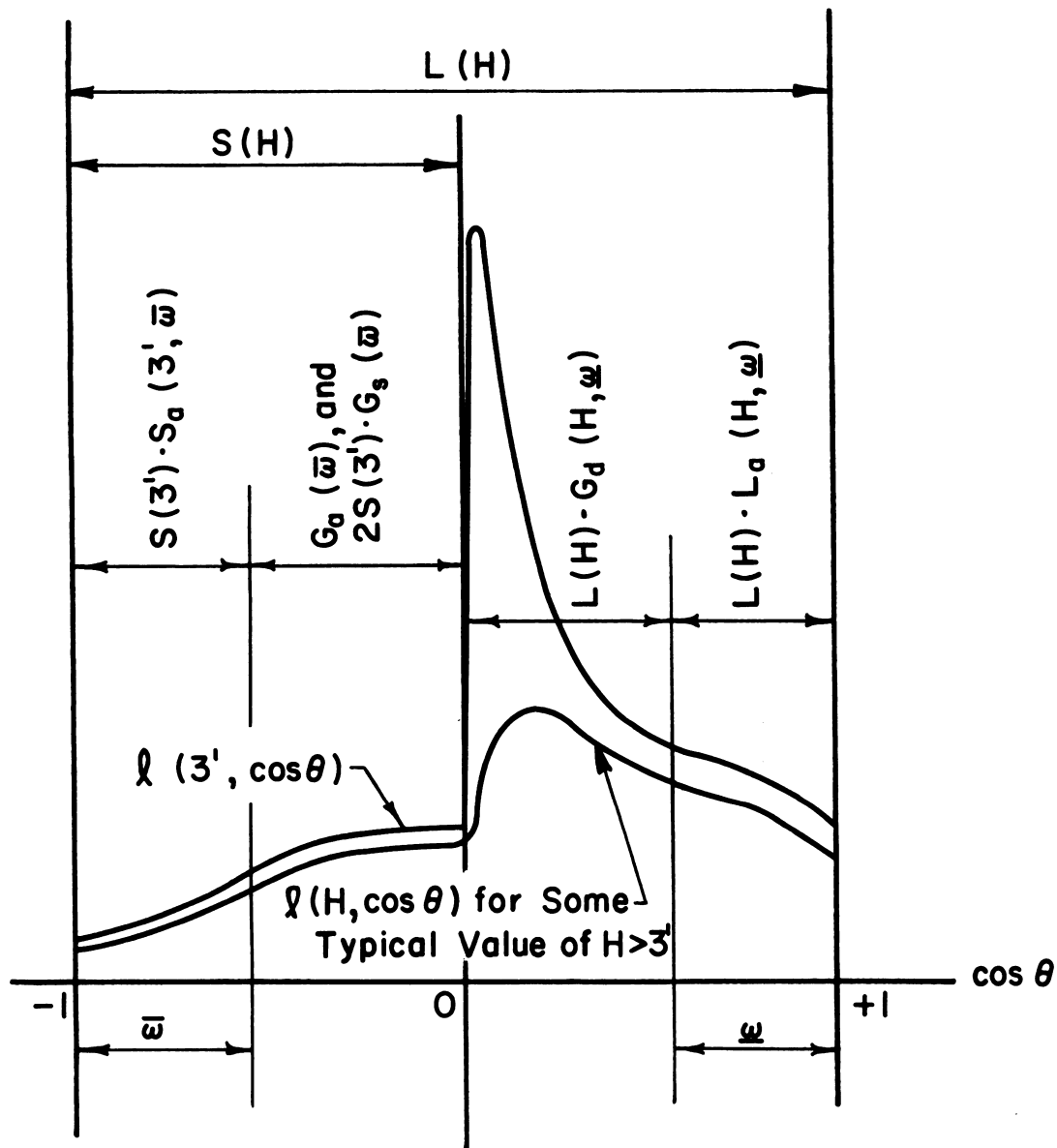
$$G_d(\omega, H) = \frac{\int_{-1}^0 \ell(H, u) du}{\int_{-1}^0 \ell(H, u) du} = \frac{1}{L(H)} \int_0^{1-\omega} \ell(H, u) du ; \quad (\text{VII.26})$$

$$G_a(\bar{\omega}) = \frac{\int_{-1}^0 \ell(3', u) du}{\int_{-1}^0 \ell(3', u) du} = \int_{-1+\bar{\omega}}^0 \ell(3', u) du . \quad (\text{VII.27})$$

$E_d$ : This so-called "direct" shape factor is practically the same as the ratio of a detector response above the center of a rectangular cleared space in a contaminated plane to the response above the center of the equivalent circular cleared space. (The fact that opaque roofs above the cleared spaces of the same size and shape slightly change the detector response in both cases is the only thing which keeps this statement from being exact.) In the Standard Method, this ratio is always assumed to be unity; and therefore no factors of this type appear in the formulation given on the OCD Manual. Warning is given in NBS Monograph 76 [1] that this assumption may not always be very accurate. It is likely that this factor could be easily obtained as a function of  $W$  and  $L$ , for example, from data given by Hubbell [7]; however, it appears on the basis of our studies that the factors so obtained are very close to unity for most practical cases. (See sec. VIII.2.)

Figure VII.3 indicates in a summary fashion the relationships existing between the various functions which depend on  $\ell(H, u)$ . Note that for negative values of  $u$ , most of the curves for the  $\ell$ -function at detector heights of practical interest are very close to the curve for  $H$  equal to 3 ft, and thus all concepts derived from that portion of the graph are based on the data for 3 ft and considered otherwise independent of  $H$ , even though this may be somewhat of an approximation. For functions related to values of the





VII.3 Relationships among various functions which are derived by integration of the  $l$ -function between appropriate limits. The functional symbols are placed on horizontal "dimension lines" which span the region of integration of the  $l$ -function. Note that for functions involving  $\bar{\omega}$  there is little dependence on  $H$ .

$\ell$ -function on the positive (right) side of the graph, the same statement cannot be made; and  $H$  must be included as a separate independent variable. From this figure, it is quite easy to prove the following relations, which show how the geometry factors derived above are directly related to the more fundamental functions given in section V:

$$G_s(\omega) = \frac{1}{2} [1 - S_a(3', \omega)] \quad (\text{VII.28})$$

$$G_d(\omega, H) = 1 - \frac{S(H)}{L(H)} - L_a(H, \omega) \quad (\text{VII.29})$$

$$G_a(\bar{\omega}) = S(3') [1 - S_a(3', \bar{\omega})] \quad (\text{VII.30})$$

It is noted that  $G_a(\omega)$  is simply proportional to  $G_s(\omega)$ , by the ratio  $2S(3')$ . Since  $S(3')$  is customarily rounded off to 0.1, the ratio is 1/5.

Figures C.2 through C.6 display the functions  $B_e$ ,  $S_w$ ,  $G_s$ ,  $G_d$ ,  $G_a$ , and  $E$ , derived on the basis of the formulas and methods just described. (For checking experimental work in which  $^{60}\text{Co}$  or  $^{137}\text{Cs}$  are used to simulate fallout, the above functions should be based on data available in appendix B on these isotopes. Although such alternate functions do not appear here, they are easily calculated by the methods just described.)

In the development of the Standard Method, thus far presented, there is no explicit provision made for contribution to the detector response from radiation penetrating one structural element and then reflected from one or more other elements into the detector. In general, these are secondary processes of less significance; and furthermore the use of infinite medium calculations rather than slab penetration results provides some approximate correction for the effect of radiation backscatter from interior surfaces of the blockhouse. There is one exception to this: the wall-barrier factor

has been carefully adjusted for  $X_e$  near zero, so that no backscatter is included. This is done on the assumption that the opposite wall would likely be of similar thickness. There is a possibility, however, of radiation penetrating the wall and being reflected into the detector by the ceiling and under some circumstances such a contribution is significant. The method for taking this into account is discussed later in section VII.D.5.

We now present with appropriate simplifications described above the final standard formula for contributions through the wall for the simple blockhouse:

$$C_g = B_e(X_e, H) \{ S_w(X_e) [G_s(\bar{\omega}) + G_s(\underline{\omega})] E(e) + [1 - S_w(X_e)] [G_d(\underline{\omega}, H) + G_a(\bar{\omega})] \} \quad . \quad (VII.31)$$

The term in the braces is the overall geometry factor for radiation penetrating the walls and can be designated  $G_g$ .

The development of the Standard Method proceeds from this point by making an assumption that the radiation penetrating the walls without collision has directional characteristics similar to the zero-wall-thickness case and the radiation scattered in the walls has directional characteristics similar to the infinitely-thick-wall case. This assumption is consistent with the procedure used for calculating  $S_w$  (eq (VII.10)). It is exceedingly useful in providing an intuitive understanding of the meaning of the mathematical formulation developed above, so that good engineering judgment in the application of the method to problems involving practical situations may be followed. The assumption thus allows one to identify, in an approximate fashion, the physical significance of the various components of  $C_g$  as follows.

Wall-scattered radiation contribution from above the detector plane:

$$B_e(X_e, H) S_w(X_e) G_s(\bar{\omega}) E(e) \quad . \quad (VII.32)$$

Wall-scattered radiation contribution from below the detector plane:

$$B_e(X_e, H) S_w(X_e) G_s(\omega) E(e) \quad . \quad (\text{VII.33})$$

Non-wall-scattered radiation contribution from above the detector plane (skyshine):

$$B_e(X_e, H) [1 - S_w(X_e)] G_a(\bar{\omega}) \quad . \quad (\text{VII.34})$$

Non-wall-scattered radiation contribution from below the detector plane (direct ground contribution):

$$B_e(X_e, H) [1 - S_w(X_e)] G_d(\omega, H) \quad . \quad (\text{VII.35})$$

It is desirable at this point to review some of the implications on the assumption just referred to, because of its relevance to much of the research work done in testing fallout shielding methods. This assumption is plausible, but it is not rigorously consistent with the basis of the methodology, a fact evidently not always appreciated by workers in this field.<sup>9</sup> The best way to prove this point is to start with eq (VII.7) and follow the development again, this time doing it in a fashion which splits the wall-penetrating radiation into its uncollided and scattered parts in rigorous fashion. If this is done,

$$C_g = \frac{D_{13}}{D_1} = \frac{D_{13\text{-ws}}}{D_1} + \frac{D_{13\text{-nws}}}{D_1} \quad (\text{VII.36})$$

$$= \frac{D_{7\text{-ws}}}{D_1} \cdot \frac{D_{13\text{-ws}}}{D_{7\text{-ws}}} + \frac{D_{7\text{-nws}}}{D_1} \cdot \frac{D_{13\text{-nws}}}{D_{7\text{-nws}}} \quad , \quad (\text{VII.37})$$

---

<sup>9</sup>To paraphrase a nonsensical statement found in one report (which shall remain unidentified): "The uncollided radiation behaves as if the barrier thickness were zero because, after all, the existence of the wall has no significance for those photons which do not interact with it."

where the additional subscripts  $ws$  and  $nws$  refer to the wall-scattered and non-wall-scattered components, respectively, of the detector response for the situations indicated.

If  $S_w$  is defined fundamentally as the proportion of scattered radiation in the total wall penetration for Situation (7), then

$$D_{7-nws} = [1 - S_w(X_e)] D_7 \quad (VII.38)$$

and

$$D_{7-ws} = S_w(X_e) D_7 \quad (VII.39)$$

Then,

$$C_g = \frac{D_7}{D_1} \left\{ S_w(X_e) \cdot \frac{D_{13-ws}}{D_{7-ws}} + [1 - S_w(X_e)] \cdot \frac{D_{13-nws}}{D_{7-nws}} \right\} \quad (VII.40)$$

This equation has the same form as eq (VII.11), and further development of this line of argument would provide the same resulting formulation as the Standard Method, with the following modifications:

(a) The arguments  $0$  and  $\infty$  for the detector responses in various situations would be changed so as to refer to the non-wall-scattered and wall-scattered components, respectively, for walls of thickness  $X_e$ , rather than to the zero and infinite mass thickness wall situations.

(b) As a result of subparagraph (a), the definitions of the various geometry factors given by eqs (VII.14) - (VII.19) would have to indicate a dependence of  $X_e$ , in addition to the other dependent variables indicated.

(c) As a result of the changes required in subparagraph (b), physical and mathematical reasoning leading to eqs (VII.23) and (VII.25) - (VII.30) would become largely invalid, as well as the decisions to make  $E_d$  unity and make  $G_{su} = G_{sl}$ . New reasoning based on the behavior of the wall-scattered and non-wall-scattered components would have to be introduced; and more complex families of curves or sets of tables would be required in describing the geometry functions.

A number of compromise procedures between the "thin-wall:infinitely-thick-wall," or standard, approach and the rigorous "wall-scattered:non-wall-scattered" approach are possible. For example, the geometry factors could be calculated on the basis of some arbitrarily chosen single intermediate value of wall thickness and the separation of the wall-scattered and non-wall-scattered components made on that basis. The mixing factor  $S_w$  would still depend upon  $X_e$ . This would lead to data and graphs almost as simple as in the standard approach. It would presumably be less accurate for very thin and very thick walls than the Standard Method, but more accurate for the intermediate thickness cases in which  $X_e$  would be near the value chosen for geometry factor calculation.

Another slight variation to the Standard Method would be to use angular distribution data for an arbitrarily chosen finite but large  $X_e$ , rather than appealing to properties of the infinite limiting case of  $X_e$ . The factors depending on thick walls would be less easy to determine, since some of the simplicities inherent in the asymptotic behavior as  $X_e$  approaches infinity would not yet be completely evident. Also, the prescription for  $S_w$  would have to be modified so that it would become 1.0 for  $X_e$  equal to this finite upper limit. Nevertheless, the factors, once calculated carefully, would be

more accurate in application; and only slightly greater complication in graphical or tabular presentation would result (e.g., one would not be able to equate  $G_{su}$  and  $G_{sl}$ ).

The conclusion to be drawn from this digression is that there are a number of plausible physico-mathematical models on which as engineering methodology for fallout shielding may be based, some of which may even be superior in a number of respects to the model on which the Standard Method is based. It is highly desirable, however, not to mix models, that is, not to present data for one factor defined in accordance with one model and data for another factor defined in accordance with a different model, unless the change in models makes no difference in the resulting data. It is regrettably not uncommon for fallout shielding research reports to suggest a substitute for some factor used in the Standard Method, without noting that a change in the model is involved and that many other functions would have to be changed in consistent fashion to carry out the full implications of the change of model. Any method based on a mixed model provides endless argument as to how precisely the various factors should have been calculated; and any such method can be tested only as a whole on its empirical ability to provide good protection factor predictions for experiments involving essentially the total blockhouse situation.

One final point should be made here. As is shown later in chapter VIII, the Standard Method gives very good predictions for ground contribution in the case of simple structures in an idealized fallout field. In such case, concern about precision in the modeling may seem rather academic. The usual approach of mixing the thin-wall and infinitely-thick-wall cases seems to work well, in spite of the inconsistency in the choice of point source data for  $S_w$ . On the other hand, it should be noted from eq (VII.31) and related formulas for the

elementary blockhouse that a rather large error in  $S_w$  can often be tolerated because the effects of such an error have opposite signs in different parts of the equation and tend to cancel. In pages to follow, however, we shall study more complex situations involving, sometimes, little uncollided radiation; and for such situations the use of the Standard Method is not likely to be as accurate. Not only is the standard choice for  $S_w$  suspect under such circumstances, but the use of infinitely-thick-wall geometry factors to represent the proper factors for the radiation scattered in a relatively thin wall may become a very poor approximation.

## 2. Other Methods of Blockhouse Analysis

### a. Spencer's Method

The method for analysis of fallout radiation penetration into blockhouses provided in NBS Monograph 42 [4] is of some interest because it antedated the Standard Method based on NBS Monograph 76 [1] and had a strong influence on the subsequent development of the latter method, which turns out to be somewhat of an elaboration of the former. Its interest at present is largely historical, but it retains the particular value of maintaining the rectangular character of the blockhouse in the analysis, rather than using an "equivalent" cylindrical structure. A brief description of this method is therefore merited.

The contribution through the walls is given by the following formula:

$$C_g = \frac{1}{D_o} \sum_{n=1}^4 D_n = \sum_{n=1}^4 0.9 W(X_e, H) W_{a1}(X_e, H, \omega_n) \quad . \quad (\text{VII.41})$$

In the above formula  $D_n$  represents the response by the detector in the middle of the blockhouse to radiation penetrating a single wall having index  $n$ . This single wall response is divided into the usual barrier and geometry factors. The term  $0.9 W$  constitutes the barrier factor and



represents the detector response to a detector placed immediately adjacent to the  $n$ -th wall, halfway between its ends, and at a height  $H$ , such response being only to the radiation penetrating that wall. The term  $W_{a1}$  is the geometry factor and represents the ratio of the responses for radiation through the  $n$ -th wall, of the detector in the center, say, of the blockhouse and that adjacent to the wall.  $D_0$  is the reference value.

The use of the  $W$  function in the barrier factor is obviously appropriate and its use automatically provides for internal backscattering, by its very nature. The number 0.9 was inserted by Spencer in order to correct the  $W$  function, which he calculated originally on the basis of water, for use in a wall of a material with radiation interaction properties more like concrete.

The geometry factor,  $W_{a1}$ , is based on an interpolation between the function  $W_a(H, \omega_n)$ , which is reasonably accurate in the limit of zero wall thickness, and  $P_a^{(s)}(\infty, \omega_n)$ , which represents a reasonable upper limit to the geometry factor for thick walls. In doing this, we assume that radiation not scattered in the walls contributes according to the thin-wall function, while radiation scattered in the wall contributes according to the thick-wall function.<sup>10</sup> The geometry factor then becomes

$$W_{a1}(X_e, H, \omega_n) = b(X_e) W_a(H, \omega_n) + 1.15 [1 - b(X_e)] P_a^{(s)}(\infty, \omega_n) \quad . \quad (\text{VII.42})$$

The functions  $W_a$  and  $P_a^{(s)}$  have previously been defined in section V.C. The factor (1.15) is only for the purpose of normalizing  $P_a^{(s)}$  to unity at  $\omega_n = 1$ , to make it comparable with  $W_a$ .

---

<sup>10</sup>This is the original basis for the similar idea associated with the Standard Method, previously noted.

The function designated as  $b$  is comparable to the expression  $(1 - S_w)$  in the standard method and thus represents the proportion of non-wall-scattered radiation to the total penetrating the wall, assumed to be given by the ratio  $P^{(0)}(X_e)/P(X_e)$ , where these functions are also defined in section V.C.

#### b. Point Kernel Method

In 1963, Degelman, Foderaro, and Kowal of Pennsylvania State University (PSU) published a report which demonstrated the feasibility of a "point-kernel" approach to the prediction of ground source radiation penetration into a blockhouse [8]. This work was accomplished in order to correlate many experimental measurements carried out by the Nuclear Defense Laboratory (NDL) on a small (12 ft by 12 ft by 8 ft high)<sup>11</sup> concrete blockhouse of varying wall and roof thicknesses. The method was also described in a journal article written jointly by Rexroad, Schmoke, and Tiller, all of NDL, along with the three PSU workers noted above [9].

The method basically involves a somewhat empirical formula which approximately predicts the exposure rate inside a blockhouse resulting from a point gamma-ray source of known strength outside. The formula is in the form of the product of a buildup factor and the usual uncollided contribution:

$$D = B S [\exp(-\mu t_s - \mu' R)] / 4\pi R^2, \quad (\text{VII.43})$$

where  $t_s$  is the thickness of the blockhouse wall,  $S$  is the point source strength expressed as the exposure rate at one unit of distance from the source,  $\mu$  is the linear attenuation coefficient of the wall material

---

<sup>11</sup>That is, 3.66 m x 3.66 m x 2.44 m.

(concrete),  $\mu'$  is the linear attenuation coefficient of air at the site, and  $R$  is the distance from source to detector.  $B$  is a buildup factor for the wall and is composed of four subordinate factors:

$$B = FLAG \quad . \quad (VII.44)$$

$F$  relates to the buildup in the wall if the point-to-detector ray were perpendicular to the wall;  $L$  takes into account the position of the detector with respect to the finite wall and depends on the solid angle subtended by the wall at the detector;  $A$  is a buildup factor for the air between the source and the detector; and  $G$  is a factor accounting for the obliquity of the source-detector line with respect to the normal to the wall. (We do not discuss the formulation in any greater detail because a renewed approach along such lines would probably involve changes in the details of the formulation. Interested readers may examine the original reference for such details, if they wish.)

The point-source results are in principle subject to integration over a source plane, either finite or infinite; and in practice it requires the use of a high-speed computer to obtain useful results.

In order to translate the exposure rate prediction into the factor corresponding to  $C_g$  in eq (VII.8), one must divide by the reference exposure rate, calculated on a consistent basis,

$$D_1 = (S/2) E_1(\mu'H) + f \cdot e^{-\mu'H} \quad , \quad (VII.45)$$

where  $E_1$  is the first exponential integral and  $H$  is the reference detector height above the source plane (3 ft, i.e., 0.914 m). The constant  $f$  comes

from a linear approximation to the buildup factor in air for the type of source:

$$B \approx 1 + f \cdot (\mu' R) \quad . \quad (VII.46)$$

The factors and constants in the formulas are selected largely on an empirical basis to provide a reasonable fit to the point-source/point-detector experimental results for the NDL blockhouse. Integrated results were compared with experimental results for an infinite plane source, and variations were usually less than 10%. Point-kernel calculations were also compared with predictions by Spencer's formula (eq (VII.41)). Differences are always less than 40%, and generally consistent with the uncertainty predicted for the functions associated with Spencer's method. The point-kernel technique has also been employed to determine the effects of limiting the source field by circles of finite radius around the structure. It has not been used to make comparisons with the OCD Standard Method, unfortunately.

The following advantages justify a serious consideration of this approach to solving some of the problems of blockhouse shielding:

(1) Since it is based on monoenergetic source consideration, it is particularly useful for comparison with experiments using  $^{60}\text{Co}$  or  $^{137}\text{Cs}$ , and with other calculations based on such sources.

(2) It is particularly adapted to those situations in which there is only one barrier between source and detector and the detector is above the ground.

(3) It can be a useful means of studying attenuation in the case of finite fields of contamination or uneven deposition of sources or both. The fields may have rather irregular shape.

(4) It is very simply adapted to a computer calculational program.

(5) It is easily used to analyze effects of variations of the detector position within the blockhouse.

(6) The approximation inherent in the use of equivalent cylindrical structures is avoided in the analysis.

On the other hand, this method has disadvantages, which may account for the lack of its further development and use:

(a) The approach is developed for monoenergetic sources, and it is extenable to residual fission product sources only with an increase in complexity.

(b) It is not easily extended to those cases in which the point-source/point-detector ray technique is not effective, such as when the detector is below ground in a basement.

(c) It is not easily used in desk calculations, if an infinite or large finite area source is involved.

#### c. Monte Carlo Method

Because of its great flexibility in handling complex geometric situations, the Monte Carlo method is well adapted to blockhouse analysis. However, Monte Carlo programs currently capable for such usage have generally been employed for more complex situations, such as houses with basements. This technique requires a great amount of computer time, even for relatively simple structures. It is therefore more useful for research purpose than for routine engineering analysis; and as a research tool it has been quite productive. Application of this method to the study of exposure in basements is discussed in section X.D.

## C. BLOCKHOUSES WITH FLOOR LEVEL NOT ON GRADE

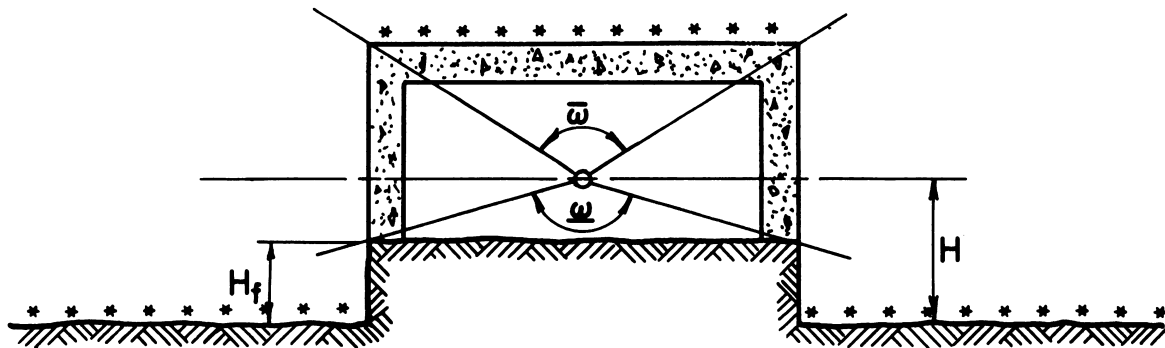
### 1. Detector Above Grade

Figure VII.4 shows four significant situations which vary from the elementary blockhouse case in that the floor is not at the same level as the ground. They are all easily handled by the standard methodology, with some minor modifications.

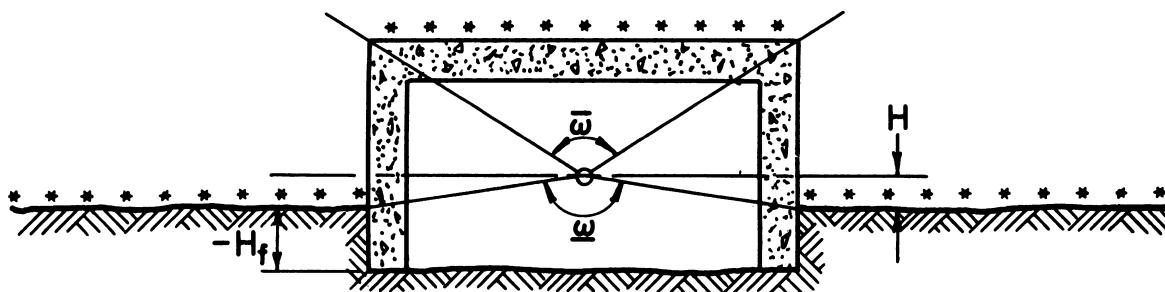
Case (a) represents an idealization of the one-story structure with its first floor somewhat raised above the ground. There is no basement or crawl-space beneath the floor, or, if there is, the foundation walls below the first floor are sufficiently thick that a negligible amount of radiation can penetrate. Case (b) might represent an idealization of the slightly sunken one-story structure in which the floor is somewhat lower than the ground level but the detector position of interest is still above the ground level. In both these cases, the standard formula for the ground contribution represented by eq (VII.31) is still valid, with  $\omega$  defined as shown in the appropriate drawings in figure VII.4. Note that  $H$  is still defined as the height of the detector position above the ground.

### 2. Detector Below Grade

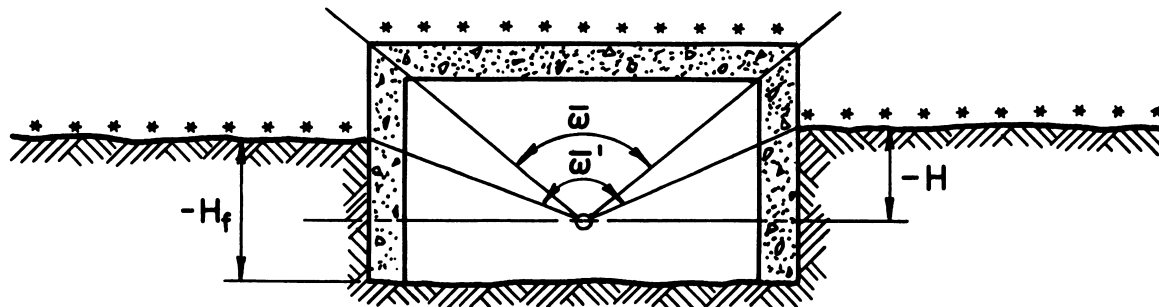
Case (c) of figure VII.4 represents a somewhat more deeply but still only partially buried structure in which the detector is below the ground level. Case (d) represents the completely buried blockhouse. The latter can also be regarded as an idealization of a basement in which the superstructure is of such light construction as to have negligible interaction with the radiation field. From a theoretical point of view it can be looked upon as a "foxhole" (discussed in secs. V.C.4 and VI.C ) modified by the addition of a cover which acts both as a finite radiation source and as a shield.



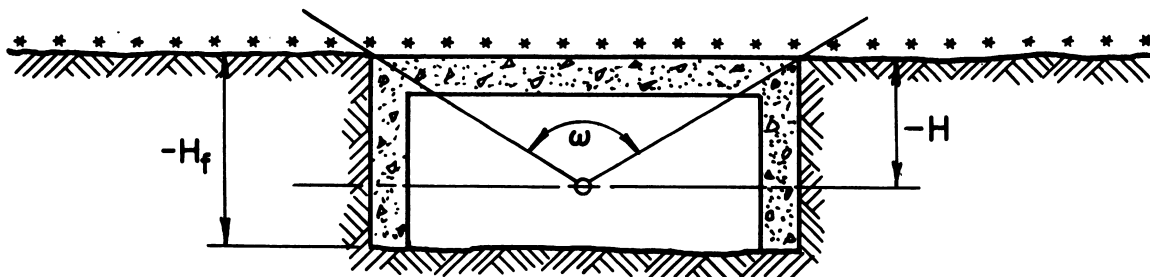
(a)



(b)



(c)



(d)

VII.4 Various cases for blockhouses with floors not on grade.

Case (d) is easily handled, and can be discussed at this point. The so-called ground contribution,  $C_g$ , is zero; and only the roof contribution,  $C_r$ , contributes to the detector response. As for the elementary blockhouse case, this is given by  $C_o$ , defined by eq (VII.6). This implies, of course, that no radiation penetrates the "lip" and side walls of the structure to an extent appreciably contributing to the detector response. If there is any likelihood in the mind of the analyst that the sources on the ground just beyond the limits of the blockhouse roof may make such a direct contribution, the "lip contribution" methods of section V.D.4 can be applied. Occasionally it may be adequate for the limits of the solid angle fraction  $\bar{\omega}$  to be opened out slightly to include such sources, for the purposes of computation by the formulas referred to above.

Case (c) is somewhat more complex. The solid angle fraction subtended at the detector by the intersection of the structure with the ground plane is now oriented upward and is designated  $\bar{\omega}'$ . The "ground contribution" is composed of radiation which penetrates the walls to a greater or lesser extent and is then scattered by the walls or reflected by the ceiling downward into the detector.

The customary approach to Case (c) is to apply eqs (VII.31) through (VII.35) as discussed below.

Wall-scattered contribution from above the detector plane is calculated by determining the hypothetical contribution as if the wall were not covered by earth above the detector plane, and then subtracting from the fictitious portion of the contribution which is assumed to result from radiation incident on that portion of the wall between the detector plane and the ground line. The radiation assumed to be incident on the walls for this calculation has the character of that actually incident on the truly exposed part above the ground



line. (Any assumption relative to the wall below the ground line is allowable because the contribution of this part of the wall is first included and then subtracted.) The net wall-scattered contribution then becomes:

$$[B_e(X_e, H') S_w(X_e) G_s(\bar{\omega}) E(e)] - [B_e(X_e, H') S_w(X_e) G_s(\bar{\omega}') E(e)], \quad (\text{VII.47})$$

or

$$B_e(X_e, H') S_w(X_e) E(e) [G_s(\bar{\omega}) - G_s(\bar{\omega}')]. \quad (\text{VII.48})$$

In similar fashion, the non-wall-scattered contribution from above the detector plane is given by:

$$B_e(X_e, H') [1 - S_w(X_e)] [G_a(\bar{\omega}) - G_a(\bar{\omega}')]. \quad (\text{VII.49})$$

There is no contribution from below the detector plane, and therefore the total ground contribution is given by:

$$\begin{aligned} C_g = & B_e(X_e, H') \{ S_w(X_e) E(e) [G_s(\bar{\omega}) - G_s(\bar{\omega}')] \\ & + [1 - S_w(X_e)] \times [G_a(\bar{\omega}) - G_a(\bar{\omega}')] \} . \end{aligned} \quad (\text{VII.50})$$

There are two particulars to observe in connection with the above expression. One is that the height to be used as an argument for  $B_e$  is vaguely given as  $H'$ , so far undefined. In any case in which the contribution through a wall comes from both below and above the detector plane, there is little question that by far the most significant portion of the wall for

transmitting radiation affecting the detector is that part of the wall approximately in the neighborhood of the perpendicular line from the detector to the wall in question; and thus the detector height,  $H$ , is the best single value of the height argument for picking the proper value of  $B_e$ . On the other hand, in the present case and in other cases in which the contribution being calculated is from a portion of wall which does not intersect the detector plane, the detector height is no longer an obvious choice. Fortunately, the value of  $B_e$  is not highly sensitive to variations in  $H'$  of a few feet more or less, and therefore any reasonable selection is permissible. We would like to suggest that when the wall does not intersect the detector plane,  $H'$  is most simply selected as half the wall height above the ground. There are cases in which this distance may be less than 3 ft and, since the data published in the OCD Manual for  $B_e$  (fig. C.6) do not give values for arguments less than 3 ft, one is faced with the choice of extrapolating the curves toward smaller distances or using 3 ft as the best available value of  $H'$ .

The other matter to note is that the absence of the non-wall-scattered radiation from below the detector plane, which is the particular characteristic of eq (VII.50), tends to emphasize the effect of the wall-scattered contribution. The error resulting from making an approximate choice for  $S_w$  may not be quite so unimportant as in the elementary case, for the reasons discussed at the end of section VII.B.1.

#### D. BLOCKHOUSE WITH VARIABLE THICKNESS ROOFS AND WALLS

##### 1. Preliminary

The discussion in the previous section involved for the first time a technique of analysis which has been called "geometry factor differencing." This implies that the formulation of the contribution from a certain portion of the blockhouse is obtained as a result of the contributions for two,

usually hypothetical situations; and in the final formulation this difference appears as differences in certain geometry factors. It is a slight conceptual extension to the process of summing contributions of more than one portion of a structure by adding geometry factors (see, for example, eq (VII.20)). Thus it appears clear that under many conditions one can proceed directly to the proper formula by considering the difference between the appropriate geometry factors as the proper way of accounting for the subtraction of one contribution from another of which it is a part. This approach will be particularly applicable to the present discussion, in which we consider roofs or walls, portions of which have differing effective mass thicknesses.

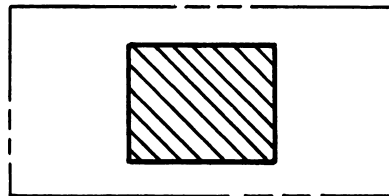
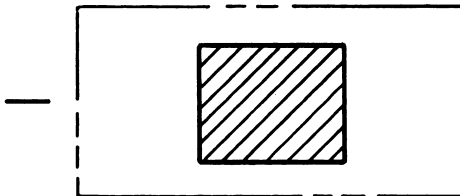
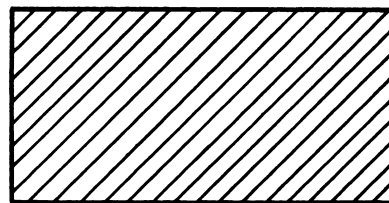
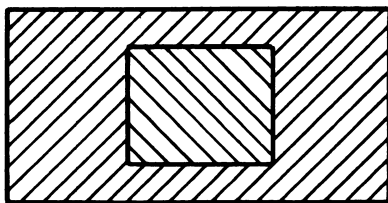
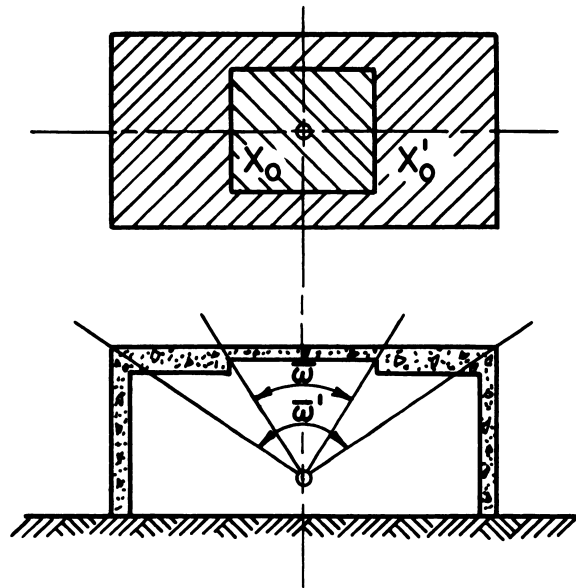
In the discussion of this type of situation, apertures can be considered portions of shielding elements with zero thickness. This imbeds the aperture problem into the more general problem, and for the most part leads to the obvious derivation of aperture formulas as special cases of variable shielding element thickness expressions. However, apertures will be discussed briefly in a separate subsection.

## 2. Roofs

a. Symmetric Variations: A simple case of a symmetric roof thickness variation is presented in figure VII.5, and from this the resulting overall roof contribution is derived easily through the summing and differencing techniques:

$$C_r = L(X'_0) L_a(X'_0, \bar{\omega}') - L(X'_0) L_a(X'_0, \bar{\omega}) + L(X_0) L_a(X_0, \bar{\omega}) \quad (\text{VII.51a})$$

$$= C_o(X'_0, \bar{\omega}') - C_o(X'_0, \bar{\omega}) + C_o(X_0, \bar{\omega}) \quad (\text{VII.51b})$$



VII.5 Sketch for the analysis of the symmetric roof thickness variation case.

This works equally well even if the inner part of the roof is a skylight, with essentially zero thickness.<sup>12</sup>

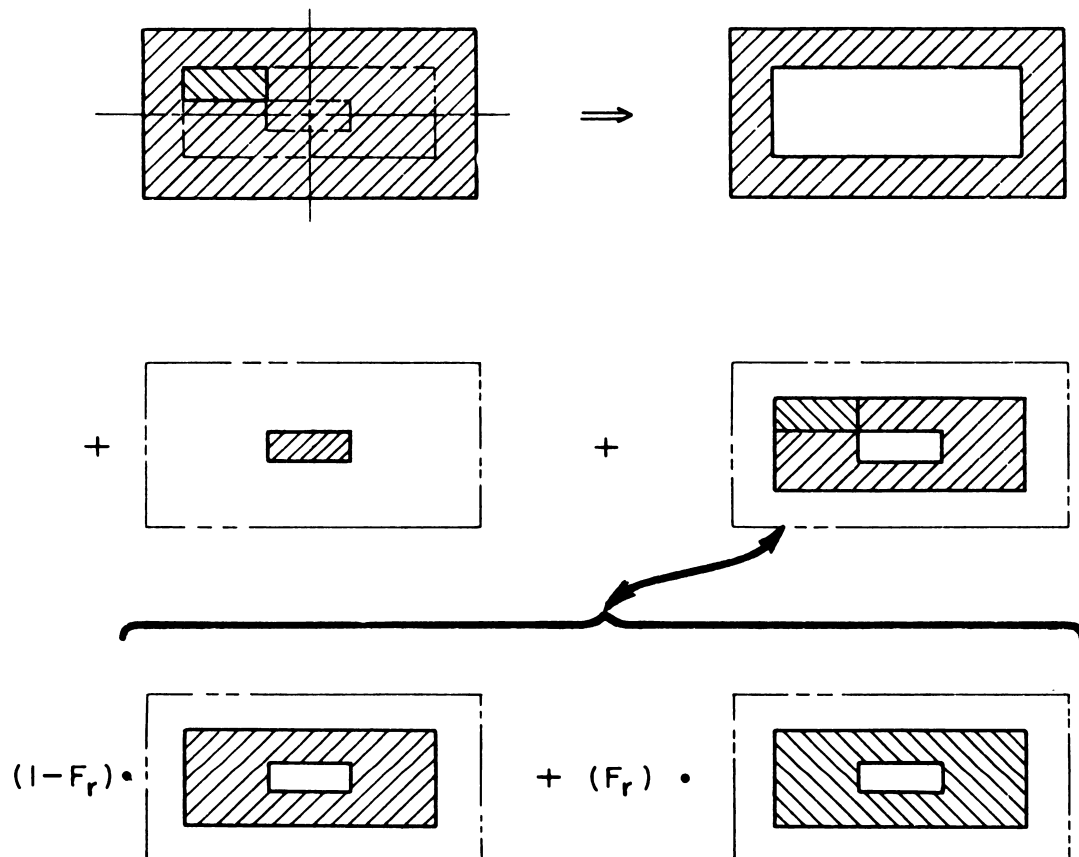
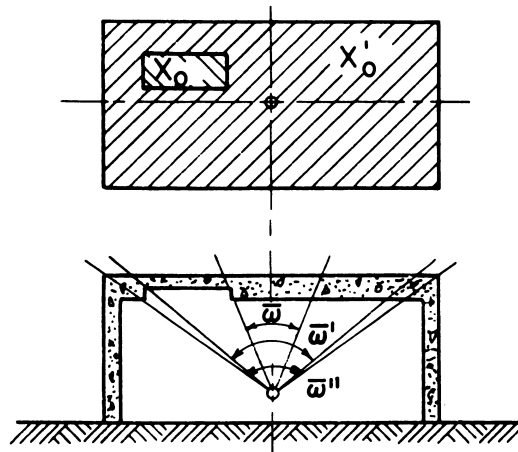
Application of this method to symmetric cases involving more than two different thicknesses of portions of the roof is straightforward and needs no elaboration.

b. Assymmetric Variations: The analytical approach to the assymmetric case of variable roof thickness will first be discussed in terms of two simple but practical examples, depicted in figures VII.6 and VII.7. These describe cases in which the roof contains a rectangular panel of equivalent mass thickness different from the rest of the roof; and the two cases differ from each other only in whether or not this panel includes the symmetric center of the roof, which is directly over the detector. The figures show readily how the analysis can be effected by dividing the roof into concentric rectangular "annuli," which we shall call zones, including the center rectangle. For the case shown in figure VII.6, the roof contribution to the detector response becomes, by the usual summing and differencing techniques,

$$\begin{aligned}
 C_r &= C_o(X'_o, \bar{\omega}'') - C_o(X'_o, \bar{\omega}') + C_o(X'_o, \bar{\omega}) \\
 &+ (1 - F_r) [C_o(X'_o, \bar{\omega}') - C_o(X'_o, \bar{\omega})] \\
 &+ F_r [C_o(X_o, \bar{\omega}') - C_o(X_o, \bar{\omega})]
 \end{aligned}
 \tag{VII.52}$$

---

<sup>12</sup>Since a skylight often covers an interior shaft, this is called the "shaft case," even without the shaft. A special graph for  $C_o$  in this case is provided in figure A.11. Reference [5] discusses some of the practical difficulties in establishing this graph. There is some justification for preferring the combination of functions  $L \cdot L_c$  instead of  $C_o$  for this case, but the differences between the two are minor for small thicknesses. See also section IX.C.4.



VII.6 Asymmetric roof thickness variation; first example.



The case shown in figure VII.7 requires a similar formula, except that the third term on the right should have  $X_0$  rather than  $X'_0$  in its functional arguments.

In the above equation, the symbol  $F_r$  represents an interpolation factor prescribing that the contribution for the intermediate zone, which contains portions of both thicknesses  $X_0$  and  $X'_0$ , is to be obtained as intermediate between the two hypothetical cases in which the zone takes on entirely the equivalent mass thickness values of  $X_0$  and  $X'_0$ , respectively.  $F_r$  specifically represents the proportion of the  $X_0$  thickness zone contribution to be included.

The central problem in this approach is how to obtain the proper value of  $F_r$ , by means both simple and accurate. Two possible approaches are available, and these will be discussed below in turn.

(a) Proportion by relative areas. The simplest approach is to calculate  $F_r$  as the proportion of the zone area having equivalent mass thickness  $X_0$ . This is the simplest of all recipes to use. It is not always acceptable, however. As is known (see p. 2 of ref. [1]), the importance of areas far from the center is abnormally weighted by such a procedure; and if the intermediate zone should be quite long compared to its width and the portion of equivalent mass thickness  $X_0$  located primarily at a region either very near or very far from the center, the value of  $F_r$  obtained would not be very accurate.

(b) Proportion by relative solid angle fraction subtended. A more accurate but slightly more arithmetically complex method of obtaining  $F_r$  is to take it as the ratio of the solid angle fraction subtended by the portion of the intermediate zone with equivalent mass thickness  $X_0$  to the solid angle fraction subtended by the whole zone area. This is less liable to weight abnormally those areas far away from the center point. At the present

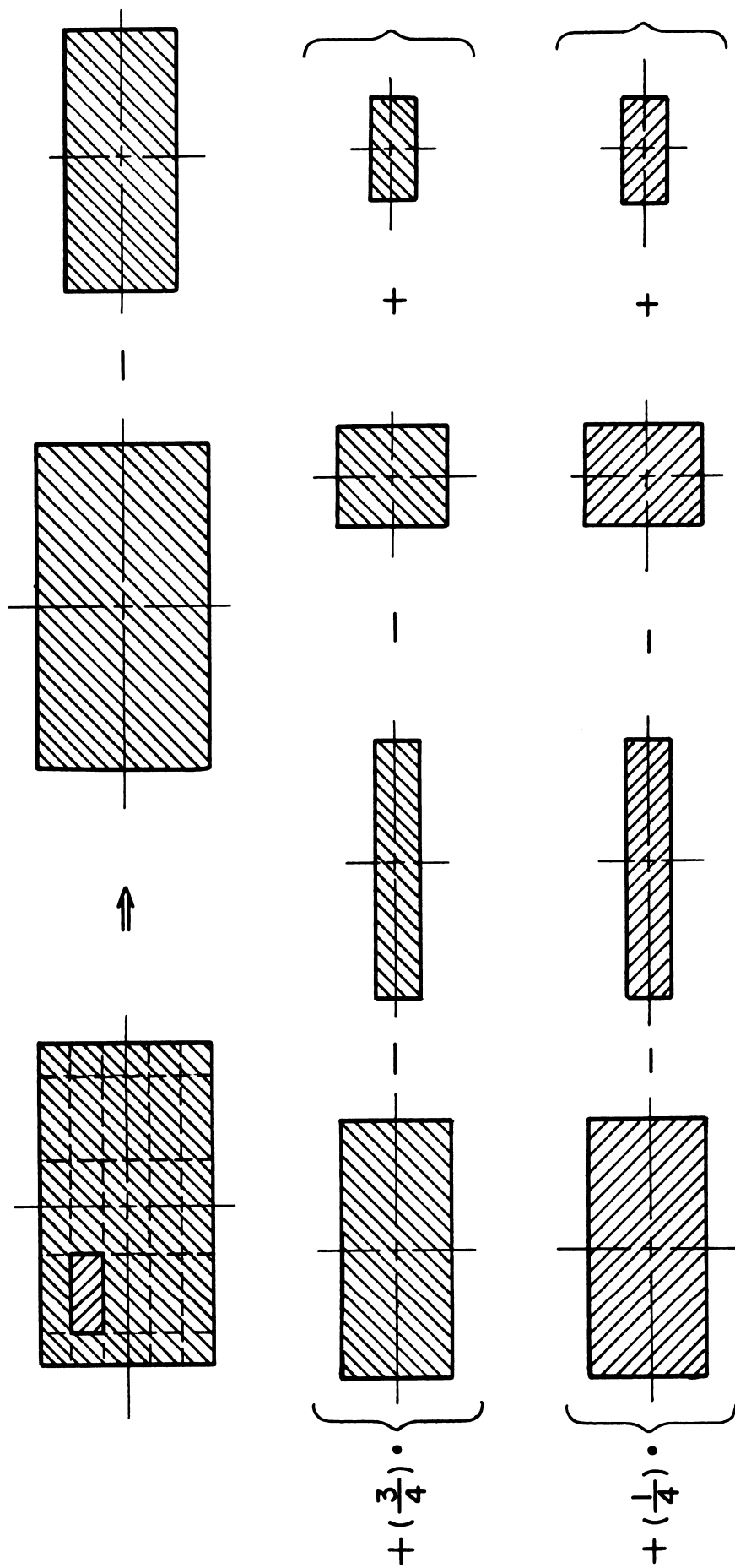


stage of development of this subject, this method probably represents the best combination of reasonable accuracy and moderate simplicity.

As in the symmetric case, the situation in which  $X_0$  essentially equals zero (skylight case) can be related to the "shaft case"; and the  $C_0$  functions which appear in the term including  $F_r$  can be obtained from the curve in figure A.11 for this situation.

It is sometimes possible to resolve the problem of an asymmetric roof thickness variation into a number of separate problems of an elementary type in similar fashion to the calculation of solid angles of off-center rectangles (sec. V.B.3). As an example of how this might be done, figure VII.8 shows how the problem presented in figure VII.6 can be so resolved. In effect, the solution is obtained by considering solutions to a number of fictitious elementary structures, suitably described, and combining them in such a fashion as to provide the proper result. This method is as exact as the basic method of analyzing the roof contributions for elementary blockhouses and thus has great merit; however, for a roof having some degree of complexity the resolution of the situation into fictitious elementary situations may be rather difficult.

There is still another, somewhat more fundamental approach to this problem, which is to consider the roof as divided up into small individual incremental areas, determine the contribution of each incremental area separately, and then sum them to give the total value of  $C_r$ . Each incremental area can have its own value of equivalent mass thickness. The size of these areas must be small enough to be characterized readily by an easily estimated average distance from the center of the roof, but still be larger in linear dimension than the thickness of the roof in its vicinity, with 6 in (15 cm) being a lower limit under any circumstances. (These lower limits are necessary



VII.8 Example showing the resolution of an asymmetric roof thickness variation problem into fictitious elementary structure roofs. That area which is hatched to the left has different thickness from that hatched to the right.

to maintain to a practical extent the principle of independence of effects of adjacent area increments.)

The method of determining the contribution of a small incremental area,  $\Delta A$ , having equivalent mass thickness  $X_o$ , is determined as follows, with the help of figure VII.9. (In this analysis, incremental quantities are small enough to be treated as differentials, to a good approximation.)

$$\Delta C_r = \frac{\Delta \phi}{2\pi} \Delta C_o(X_o, \omega) \quad (\text{VII.53a})$$

$$= \frac{\Delta \phi}{2\pi} \frac{dC_o(X_o, \omega)}{d\omega} \frac{d\omega}{dR} \frac{\Delta R}{\Delta A} \Delta A \quad (\text{VII.53b})$$

But

$$\frac{d\omega}{dR} = \frac{ZR}{(Z^2 + R^2)^{3/2}} = \frac{R}{Z^2} \cos^3 \theta \quad (\text{VII.54})$$

Therefore,

$$\Delta C_r = \frac{\cos^3 \theta}{2\pi Z^2} \frac{C_o(X_o, \omega)}{d\omega} \Delta A \quad (\text{VII.55})$$

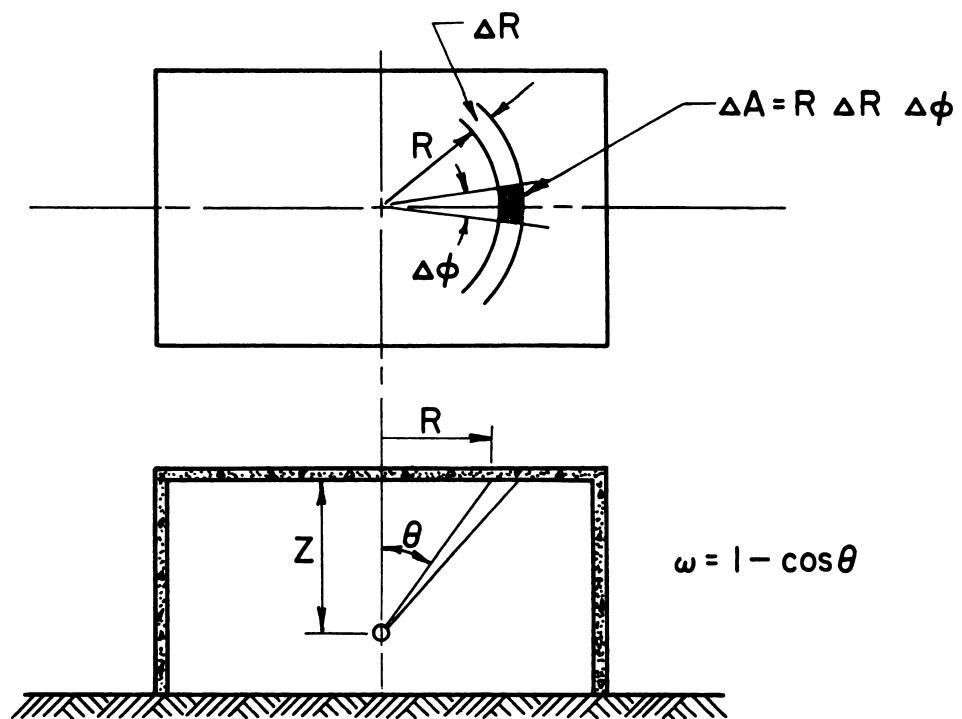
From eqs (VII.55) and (V.20),

$$\frac{dC_o(X_o, \omega)}{d\omega} = L(X_o) \frac{dL_a(X_o, \omega)}{d\omega} = \ell(X_o, \cos \theta) \quad ; \quad (\text{VII.56})$$

and thus<sup>13</sup>

---

<sup>13</sup>This expression can be obtained almost by inspection. Note that  $\Delta A$  subtends a solid angle equal to  $\Delta A \cos \theta / (Z / \cos \theta)^2$ . The factor  $1/2\pi$  converts to solid angle fraction, and the  $\ell$ -function is the assumed emission per unit solid angle fraction at the bottom of the roof slab.



VII.9 Sketch for the incremental area approach to roof contribution.

$$\Delta C_r = \frac{\cos^3 \theta}{2\pi Z^2} \ell(X_o, \cos \theta) \Delta A \quad . \quad (VI.57)$$

Equation (VII.57) may be of particular usefulness to a designer, because the collection of factors multiplying  $\Delta A$  indicates the relative importance various portions of the roof per unit roof area and permits him to adjust the thickness of the roof if he wishes to balance the contributions from equal areas over all the roof in a better fashion than a constant thickness roof would provide. Note that, for a constant roof thickness, the contribution per unit area is proportional to  $\cos^3 \theta \cdot \ell(X_o, \cos \theta) / Z^2$ .

We must repeat the caution that the valid use of this approach in practice depends upon selection of area increments which are small, but not too small. It can be shown that the shape of the incremental area is not important, however, in spite of the shape assumed for the purpose of the above derivation.

### 3. Walls

There are many similarities between the approaches to thickness variation in roofs and the methods of handling wall thickness variations; and the discussion below will outline the wall variation techniques in a fashion to bring out these similarities. As usual, the panels of differing effective mass thicknesses will be considered of rectangular nature. They may be complete wall sides or portions of sides. Some may be of zero thickness, representative of apertures such as windows and doors; others of positive thickness may represent a difference in wall construction details.

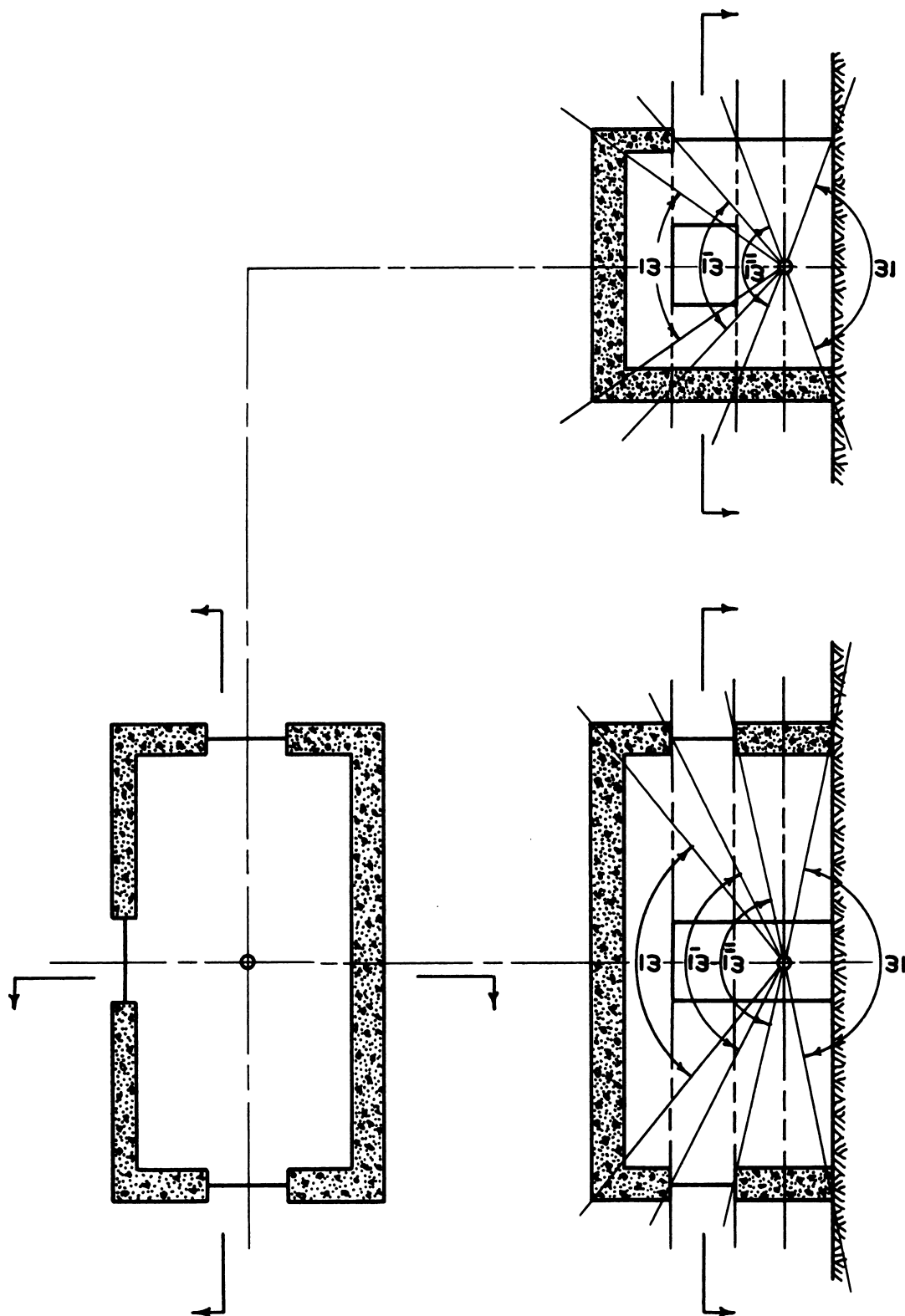
For the purpose of analysis, the walls are first considered to be divided into zones whose contributions are independent and thus handled separately. These zones are readily established by the intersection of imaginary horizontal planes with the walls, of sufficient number so that

every horizontal wall line separating regions of different effective mass thickness has one of the planes passing through it. Figure VII.10 gives a simple example in which the wall is divided into three zones. We shall specifically consider the lowest zone, whose upper and lower boundaries are subtended by the solid angle fractions  $\bar{\omega}''$  and  $\underline{\omega}$ , respectively. This is shown in cross-section in the plan view given in figure VII.10 and in more detail in figure VII.11.

Weighted combination of fictitious zones: three fictitious situations for the zone are postulated, each of the three having single values of equivalent mass thicknesses  $X_e$ ,  $X'_e$ , and zero, respectively. The wall contribution from the zone is written in three terms, each of the form given by the right side of eq (VII.20):

$$\begin{aligned}
 C_g \text{ (lowest zone)} = & F_r \left\{ B_e(X_e, H) \left\{ S_w(X_e) [G_s(\bar{\omega}'') + G_s(\underline{\omega})] E(e) \right. \right. \\
 & \left. \left. + [1 - S_w(X_e)] [G_d(\underline{\omega}, H) + G_a(\bar{\omega}'')] \right\} \right\} \\
 & + F'_r \left\{ B_e(X'_e, H) \left\{ S_w(X_e) [G_s(\bar{\omega}'') + G_s(\underline{\omega})] E(e) \right. \right. \\
 & \left. \left. + [1 - S_w(X'_e)] [G_d(\underline{\omega}, H) + G_a(\bar{\omega}'')] \right\} \right\} \\
 & + F_{ro} \left\{ G_d(\underline{\omega}, H) + G_a(\bar{\omega}'') \right\} , \tag{VII.58}
 \end{aligned}$$

where  $F_r$ ,  $F'_r$ , and  $F_{ro}$  are the weights for contributions from the three hypothetical situations of thickness  $X_e$ ,  $X'_e$ , and zero, respectively, and  $F_r + F'_r + F_{ro} = 1$ .



VII.10 Structure with variable thickness walls.

The problem of determining values of these weights is approached by two methods very similar to those used in the roof contribution problem.

(a) Weight by relative areas (perimeter ratios). Weighting by relative areas of the panels of different effective mass thickness in the zone is the same as weighting by relative widths of the different panels, since the zone height is called the perimeter ratio method in the OCD Manual. Thus, as seen from figure VII.11,

$$F_r = (2W + L)/P \quad (\text{VII.59})$$

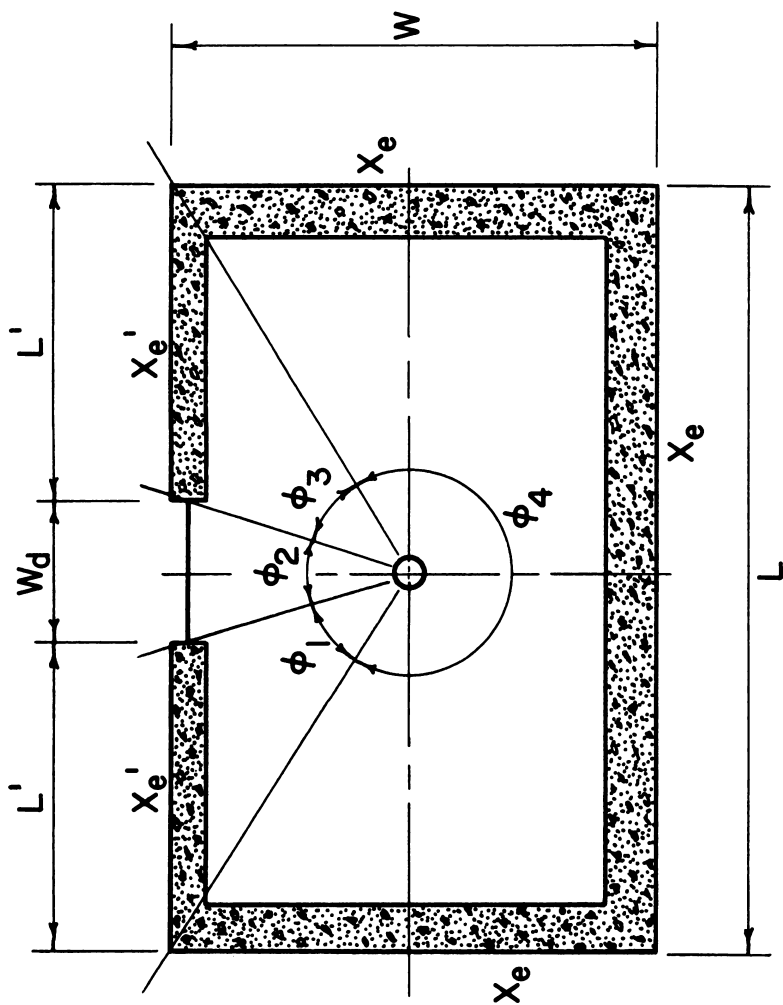
$$F'_r = 2L'/P \quad (\text{VII.60})$$

$$F_{ro} = W_d/P \quad (\text{VII.61})$$

This method tends to give undue emphasis to the regions of the structure which are farthest from the center; and thus, for a very eccentric structure in which the panels of a given thickness are concentrated largely at parts of the walls either the farthest from or the nearest to the center, inaccurate values of the weights can result. The method is recommended largely for situations in which similar panels, such as window apertures, are well distributed around the whole perimeter of the structure.

(b) Weighting by relative azimuthal angles subtended (azimuthal sectors). It is somewhat more accurate to weight by relative horizontal azimuthal angles subtended by the panels of differing effective mass thickness. (This is similar, but not exactly identical mathematically, to the relative-solid-angle-fraction method discussed above for the roof problem.) This is called the azimuthal-sector method in the OCD Manual. Thus, as seen from figure VII.11,





$$P = 2W + L + 2L' + W_d = 2(L + W)$$

$$\sum_{n=1}^4 \phi_n = 360^\circ$$

VII.11 Plan of structure given in previous figure, showing detail for analysis of lower zone contribution.

$$F_r = \phi_4/360^\circ \quad (\text{VII.62})$$

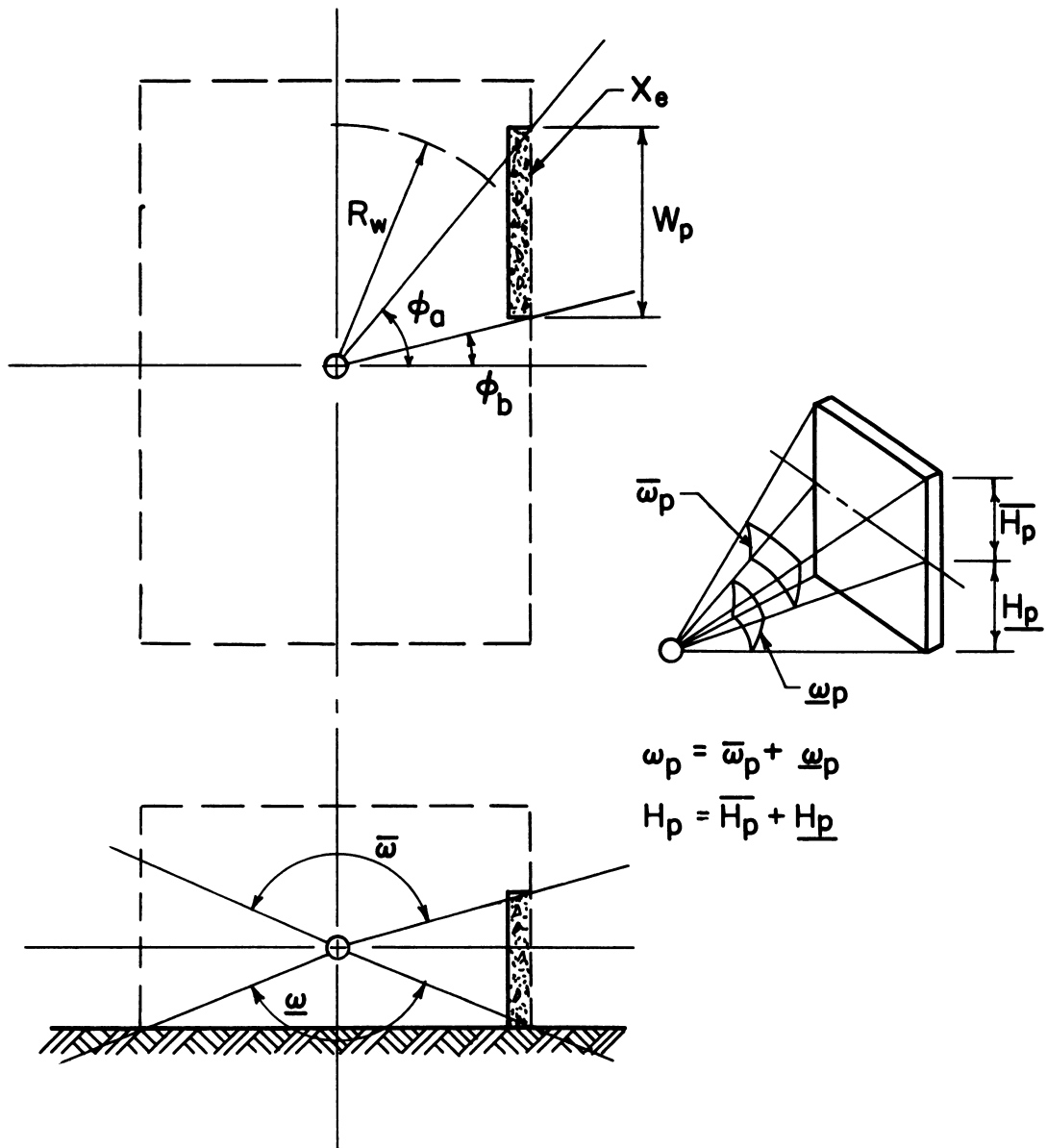
$$F'_r = (\phi_1 + \phi_3)/360^\circ \quad (\text{VII.63})$$

$$F_{ro} = \phi_2/360^\circ \quad (\text{VII.64})$$

This method is more accurate than the perimeter ratio method, in general, since it is less liable to weight distant panels abnormally; and it is recommended within the context of the present shielding methodology as the best combination of simplicity and reasonable accuracy.

Combination of individual panel contributions: A more fundamental approach within the framework of the standard methodology is to calculate separately the contribution of each panel characterized by a constant thickness within a certain zone, and then sum the results for all panels in the zone. If this can be done with the same assumptions that lead to the Standard Method, the accuracy of the results should be comparable. To develop this approach, let us handle the infinite-mass-thickness and zero-thickness cases, approximating the wall-scatter and non-wall-scatter parts of the ground contribution, in a separate fashion analogous to the development in section VII.B.

The division into zones between horizontal planes is handled by the G-function geometry-factor-differencing technique described above. The azimuthal separation of each zone into panels involves a separation of the shape factor  $E$  into parts indicative of each panel. For a single panel, as illustrated in figure VII.12, the wall-scattered contribution involves replacing the factor  $E(e)$  of the standard formula (eq (VII.31)) with the following ratio, an obvious modification of eq (VII.25):



VII.12 Illustration for analysis of contribution by single wall panel in a simple blockhouse.

$$\begin{aligned}
E_p(\phi_a, \phi_b) &= \frac{\frac{1}{2} \int_{\phi_b}^{\phi_a} \cos \phi \, d\phi \int_{-1}^1 q(u) \, du}{\int_{-\pi/2}^{\pi/2} \cos \phi \, d\phi \int_{-1}^1 q(u) \, du} \\
&= \frac{1}{4} (\sin \phi_a - \sin \phi_b) \quad . \qquad \qquad \qquad \text{(VII.65)}
\end{aligned}$$

(If the lines in fig. VII.12 bounding the panel were to be on opposite sides of the normal to the wall, the above difference would become a sum.)

The way to handle the non-wall-scattered contribution is a little less clear because of the fact that the standard methodology does not contain a precise way of handling azimuthal variations in ground contribution for the zero-wall-thickness case and considers  $E_d$  uniformly equal to unity. For our present purposes, we will use the previously prescribed factor,  $F_r$ , for proportioning the total contribution over  $360^\circ$  of azimuth, recognizing a number of possible alternative rules for obtaining it. Obvious choices are:  $W_p/P$ , the perimeter ratio;  $(\phi_a - \phi_b)/360^\circ$ , the azimuthal sector; or  $\omega_p/\omega_z$ , ratio of solid angle fraction subtended at the detector by the panel to that subtended by the whole zone. These are in order of increasing accuracy, but also increasing complexity of arithmetical calculation. The perimeter ratio formula is not recommended because  $P$ , the total perimeter, depends strongly upon the size and shape of the total structure; and one would prefer an approach for individual panels which depends as little as possible on details of the rest of the blockhouse, in accordance with the principle of substantial independence of the contribution of each structural shielding element. If the ratio of solid angle fractions is used and the panel crosses the detector plane, so that both direct ground and skyshine contributions are involved, it

is recommended that separate values of  $F_r$  be used for the contributions from the lower and upper parts of the panel, as if the zone and panel were divided into two parts, separately consider.

The ground contribution through the panel shown in figure VII.12 is then given by

$$C_g(\text{panel}) = B_e(X_e, H) \{ S_w(X_e) [G_s(\underline{\omega}) + G_s(\bar{\omega})] [(\sin\phi_a - \sin\phi_b)/4] \\ + [1 - S_w(X_e)] [\underline{F}_r G_d(\underline{\omega}, H) + \bar{F}_r G_d(\bar{\omega})] \} \quad , \quad (\text{VII.66})$$

where  $\underline{F}_r$  is taken as either  $(\phi_a - \phi_b)/360^\circ$  or as  $\underline{\omega}_p/(1 - \underline{\omega})$  and  $\bar{F}_r$  is either  $(\phi_a - \phi_b)/360^\circ$  or  $\bar{\omega}_p/(1 - \bar{\omega})$ .

Independence of individual panel: It is of interest to pursue further the point mentioned above, namely, the desirability of calculating the contribution of each panel in such a way as to eliminate any mathematical dependence of the answer upon structural parameters other than those of the panel itself. The above formula still involves some dependence on the overall size and eccentricity of the blockhouse, through the arguments  $\bar{\omega}$  and  $\underline{\omega}$ . There is no way to avoid such dependence within the framework of the standard methodology. The above formula might be improved from this point of view if we stepped outside the limitations imposed by the standard approach.

One way to do this is to assume the panel is part of a fictitious structure of rectangular shape, with the detector in its center, but in the same position relative to the panel, and without the requirement that the fictitious structure has necessarily the same overall dimensions as the actual blockhouse. It is then suggested that the hypothetical structure have an

eccentricity ratio as close to unity as practicable.<sup>14</sup> Figure VII.13 illustrates such a procedure. One then calculates the appropriate  $F_r$  weight by one of the procedures already discussed.

A still more accurate approach is to consider the solid angle fractions to be used for a particular panel, such as that shown in figure VII.12, as being established not by the blockhouse but by a vertical cylinder passing through some central point in the plane, and having its axis through the detector position, making the cylinder radius  $R_w$ . (There are a number of ways of estimating the appropriate value of  $R_w$ . An appealing choice is to select that value which gives the same value  $(\bar{\omega}_p + \omega_p)$  of subtended solid angle fraction in the equivalent cylindrical sector as the actual panel has. This results if  $\omega$  is calculated as  $1 - (\bar{H}_p / H_p)^2 + R_w^2$  and  $\bar{\omega}$  is given by  $1 - (\bar{H}_p / \bar{H}_p)^2 + R_w^2$ ). In similar spirit, it would be preferable to use as the height argument of  $B_e$  a value related to the panel itself. If the panel spans the detector height,  $H$ , this is a reasonable value to use; but, if not, some other value such as mid-panel height would appear better.

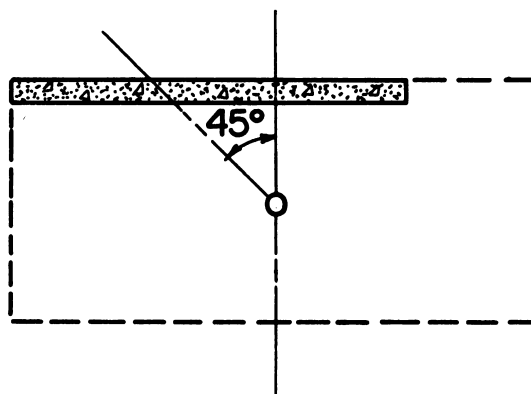
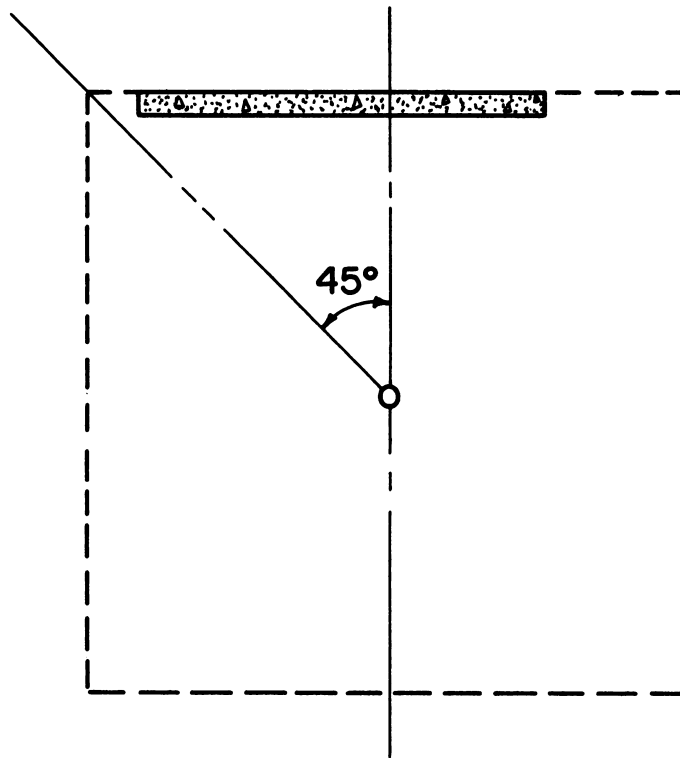
This approach would not work adequately for panels which are a size comparable to the complete side of a wall; but for panels which are relatively narrow in horizontal dimensions this procedure summed over all such panels in a blockhouse might lead to results more accurate than the Standard Method results.

Panel with one or more dimensions of small incremental size:

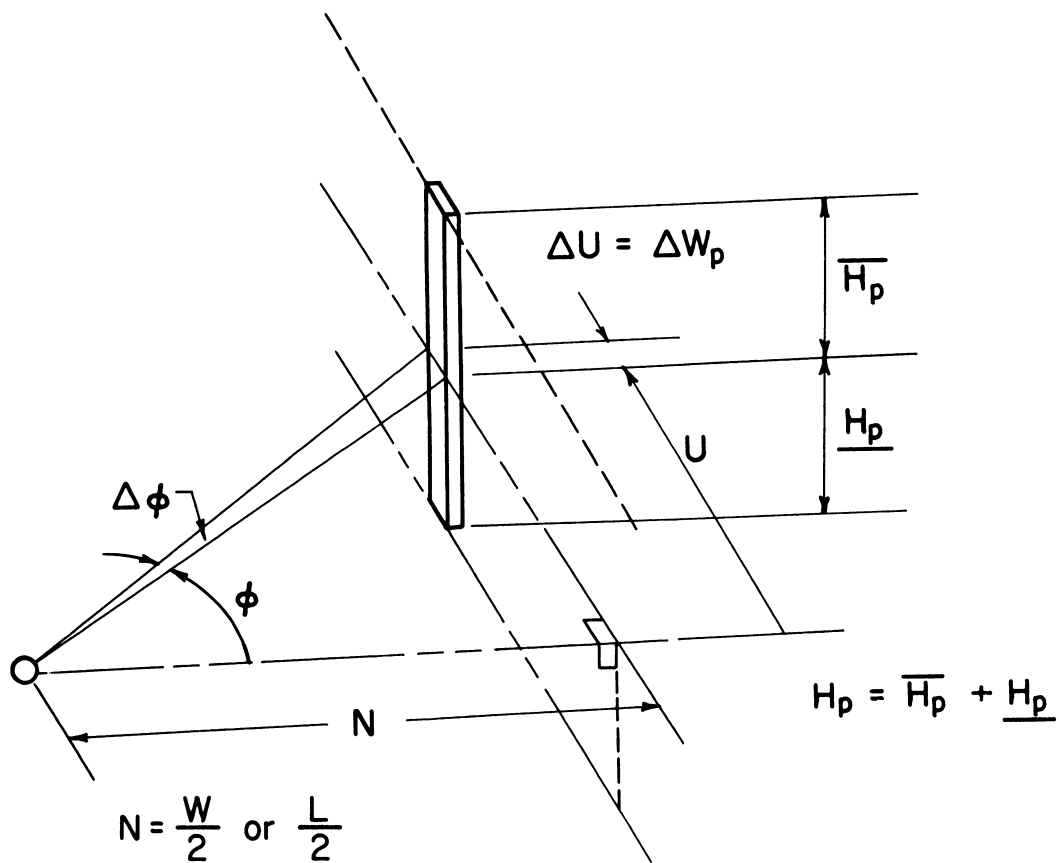
(a) Narrow vertical strips: If the panel is quite narrow, with width  $\Delta W_p$  as shown in figure VII.14(a), eq (VII.66) can be used in conjunction with simple formulas for some of the terms, as follows:

---

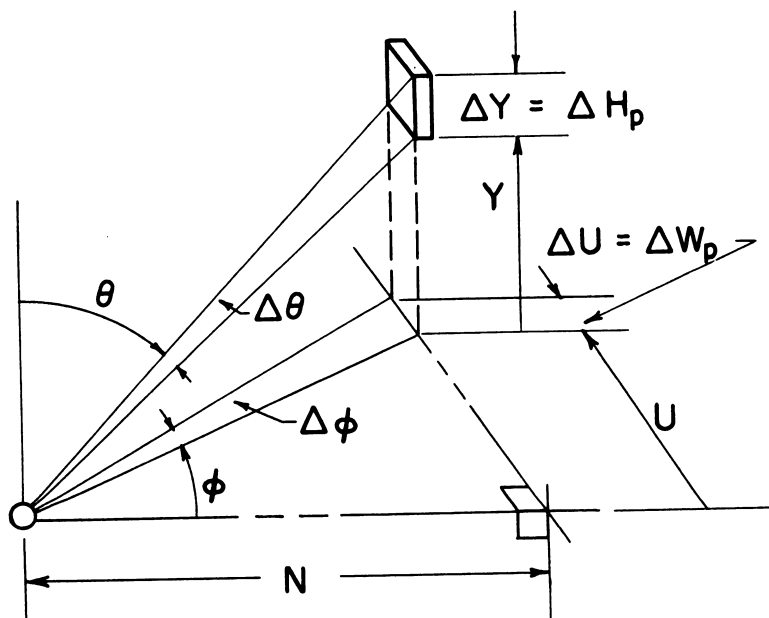
<sup>14</sup>This is consistent with a suggestion in section 6-4.5 of the OCD Manual that the "idealized" structure closest to a square is the best choice to make.



VII.13 Illustrations of the recommended way to provide fictitious structures for panels. For situations similar to (a) a fictitious structure with unity eccentricity is possible. For (b) an eccentricity of unity is not possible and the rectangular shape shown is the best that can be assumed.



(a)



(b)

VII.14 Schematic presentation of small wall panels and related geometric parameters. (a) Strip of incremental width; (b) the incremental area.



$$\begin{aligned}
\frac{1}{4} \cdot [\sin(\phi + \Delta\phi) - \sin\phi] &\approx \frac{1}{4} \frac{d}{dU} \left[ \frac{U}{(N^2 + U^2)^{1/2}} \right] \Delta U \\
&= \frac{N^2}{4(N^2 + U^2)^{3/2}} \Delta U \\
&= \frac{N^2}{4(N^2 + U^2)^{3/2}} \Delta W_p \quad (\text{VII.67})
\end{aligned}$$

and

$$\begin{aligned}
\bar{F}_r = \underline{F}_r &\approx \frac{1}{2\pi} \frac{d\phi}{dU} \Delta U \\
&= \frac{N}{2\pi(N^2 + U^2)} \Delta W_p \quad (\text{VII.68})
\end{aligned}$$

In the above equations,  $N$  is the normal distance from the detector to the wall containing the panel;  $U$  is the horizontal distance along the wall from the foot of the normal to the panel. The resulting equation becomes

$$\begin{aligned}
C_g = B_e(X_e, H) &\left[ s_w(X_e) \left( G_s(\underline{\omega}) + G_s(\bar{\omega}) \right) \frac{N^2}{4(N^2 + U^2)^{3/2}} \right. \\
&\left. + \left( 1 - s_w(X_e) \right) \frac{N^2}{2\pi(N^2 + U^2)} \right] \Delta W_p, \quad (\text{VII.69a})
\end{aligned}$$

or, since  $\cos\phi \equiv N/(N^2 + U^2)^{1/2}$ ,

$$\begin{aligned}
C_g = B_e(X_e, H) &\left[ s_w(X_e) \left( G_s(\underline{\omega}) + G_s(\bar{\omega}) \right) \cos^2\phi \right. \\
&\left. + \left( 1 - s_w(X_e) \right) \frac{\cos\phi}{2} \right] \frac{\Delta W_p}{(N^2 + U^2)^{1/2}}. \quad (\text{VII.69b})
\end{aligned}$$

As mentioned previously in connection with small roof area contributions, the dimensions of such panels must be greater than the linear wall thickness of the panel itself and of its adjacent neighboring panels, and it should be greater than some absolute value on the order of half a foot (15 cm).

(b) Narrow horizontal strips: The contribution from a zone of incremental height completely girdling a blockhouse (subject to the criteria for minimum values given above) is readily obtained from eq (VII.31) by the geometry factor differencing approach. Each geometry factor involved can be replaced by  $\Delta G(\omega) \equiv G(\omega + \Delta\omega) - G(\omega)$ . In general, the narrow zone would be either entirely above or entirely below the detector plane, so that either  $\Delta G_a$  or  $\Delta G_d$ , but not both, are involved, as well as a single  $\Delta G_s$  term.

Since

$$\Delta G(\omega) \approx \frac{dG}{d\omega} \cdot \frac{d\omega}{dY} \cdot \Delta Y, \quad (\text{VII.70a})$$

we can write for a zone above the detector plane:

$$\Delta C_g = B_e(H, X_e) \left[ S_w(X_e) \frac{dG_s(\bar{\omega})}{d\omega} E(e) + [1 - S_w(X_e)] \frac{dG_a(\bar{\omega})}{d\omega} \right] \frac{d\omega}{dY} \Delta Y \quad (\text{VII.70b})$$

(A similar expression exists for a zone below the detector plane.) In the above expressions  $Y$ , always positive, denotes the vertical distance from the detector plane to the zone, and  $\Delta Y$  is the incremental vertical width of the zonal strip.

The derivative  $d\omega/dY$  can be expressed in terms of the basic parameters of the structure; and the formulas are readily derived from the function which establishes  $\omega$  in terms of these parameters (eq (V.8)):

$$\frac{d\omega}{dY} = - \frac{4WL[4Y^2 + (4Y^2 + W^2 + L^2)]}{\pi[W^2L^2 + 4Y^2(4Y^2 + W^2 + L^2)] \sqrt{4Y^2 + W^2 + L^2}} \quad (\text{VII.71a})$$

or

$$= - \frac{2en}{\pi Y} \frac{(2n^2 + e^2 + 1)}{(e^2 + n^4 + n^2e^2 + n^2) \sqrt{n^2 + e^2 + 1}} \quad (\text{VII.71b})$$

where  $e = W/L$  and  $n = 2Y/L$ . A simpler version of the above is easily derived:

$$\frac{d\omega}{dY} = - \frac{8Y}{\pi W^2} \sin^2 \frac{\pi\omega}{2} \tan \frac{\pi\omega}{2} . \quad (\text{VII.71c})$$

The derivatives for the geometry factors with respect to  $\omega$  can easily be expressed in terms of the  $\ell$ -function in accordance with their established definitions, given in section VII.B. It is readily seen that:

$$\frac{dG_d(H, \omega)}{d\omega} = - \frac{\ell(H, 1-\omega)}{L(H)} , \quad (\text{VII.72})$$

$$\frac{dG_s(\omega)}{d\omega} = - \frac{\ell(3', -1+\omega)}{2S(3')} , \quad (\text{VII.73})$$

$$\frac{dG_a(\omega)}{d\omega} = - \ell(3', -1+\omega) . \quad (\text{VII.74})$$

Equation (VII.70) thus becomes

$$\Delta C_g = B_e(H, X_e) \left[ S_w(X_e) E(e) \frac{\ell(3', -1+\omega)}{2S(3')} + [1 - S_w(X_e)] \ell(3', -1+\omega) \right] \times \frac{8Y}{\pi W^2} \sin^2 \frac{\pi\omega}{2} \tan \frac{\pi\omega}{2} \Delta Y \quad (\text{VII.75})$$

If the wall area of small incremental height is only part of a single wall, the appropriate modifications for a panel, similar to those which convert eq (VII.31) to eq (VII.66) are appropriate. Also, if the strip is sufficiently short that it resembles, at least in plan, the illustration in figure VII.12, the doubly incremental approach discussed below becomes possible.

(c) Areas of small size in both dimensions: If the panel is of incremental height and width (subject to the criteria for minimum values indicated previously), a still further modification is appropriate. The solid angle fraction  $\omega$  should be taken as that subtended by a horizontal circular disc centered above the detector, with the incremental area under consideration at its edge.

$$\omega \approx 1 - \frac{Y}{(N^2 + U^2 + Y^2)^{1/2}} \quad (\text{VII.76})$$

$$\frac{d\omega}{dY} \approx - \frac{(N^2 + U^2)}{(N^2 + U^2 + Y^2)^{3/2}} \quad (\text{VII.77})$$

The geometric parameters in the above equations are defined as shown in figure VII.14(b), which illustrates the case with the incremental area above the detector plane. Note that  $\omega$  is established as  $1 - \cos\theta$ , and is independent of geometric parameters related to the other portions of the blockhouse.

To obtain an appropriate formula, one must combine all the special aspects of the formulas for narrow vertical strips and narrow horizontal strips, with specific reference to eqs (VII.66) through (VII.70).

$$\Delta C_g = B_e(X_e, H+Y) \left[ \frac{N^2 + U^2}{(N^2 + U^2 + Y^2)^{3/2}} \right] \cdot \left\{ S_w(X_e) \times \left[ \frac{N^2}{4(N^2 + U^2)^{3/2}} \right] \cdot \left[ -\frac{dG_s(\omega)}{d\omega} \right] \right. \\ \left. + [1 - S_w(X_e)] \times \left[ \frac{N}{2\pi(N^2 + U^2)} \right] \left[ -\frac{dG_a(\omega)}{d\omega} \right] \right\} \cdot \Delta A \quad (\text{VII.78a})$$

In this equation,  $\Delta A$  is the product of  $\Delta W_p$  and  $\Delta H_p$  (or  $\Delta U$  and  $\Delta Y$ ) and is the value of the incremental rectangular area; however, the equation is actually valid for any shape of the incremental area, as long as its smallest and largest dimensions are within the limits previously prescribed.

This formula is easily converted into one involving primarily the angular arguments  $\phi$  and  $\theta$ :

$$\Delta C_g = B_e(X_e, H+Y) \cdot (\cos\phi \sin\theta)^3 \cdot \left\{ S_w(X_e) \cdot \frac{\cos\phi}{4} \cdot \left[ -\frac{dG_s(\omega)}{d\omega} \right] \right. \\ \left. + \frac{1}{2\pi} \cdot [1 - S_w(X_e)] \cdot \left[ -\frac{dG_a(\omega)}{d\omega} \right] \right\} \cdot \frac{\Delta A}{N^2} \quad (\text{VII.78b})$$

For those who prefer using  $\omega$  as a variable rather than  $\theta$ , the factor  $\sin^3\theta$  in the above formula may be replaced by its equivalent,  $(2\omega - \omega^2)^{3/2}$ . The derivatives can be expressed, if desired, through the relations in eqs (VII.72) through (VII.74).

The above formulas are equally valid when the incremental area is below the detector plane, provided the term  $(-dG_a(\omega)/d\omega)$  is replaced by  $(-dG_d(\omega, H-Y)/d\omega)$ . Note that  $Y$ , the vertical distance from incremental area to detector plane, is always considered positive. This requires also that the argument for  $B_e$  be changed to  $H-Y$ .

The expression included in the braces in eqs (VII.78) is slightly complicated; however, it represents the best way currently available within the framework of this methodology to assess the relative importance of the contribution of various portions of the walls toward the detector response. Use of the expression may be of assistance to designers in apportioning the thickness of various portions of structural walls. It may also provide a direct means of determining the contribution from small wall panels (including apertures), even when they are of irregular shape or orientation.

It should be pointed out that these formulas for incremental contributions must be considered approximate because of non-rigorous assumptions made in the underlying methodology. For one thing, the assumption of polar and azimuthal angle independence for wall-emitted radiation (see eq (VII.21)) is admittedly not precisely correct. Another aspect of particular significance is the assumption that penetration through finite walls is correctly given by a linear interpolation between zero-thickness and very thick wall calculations. (Data on wall angular distributions are further discussed in sec. VIII.C.)

#### 4. Apertures

An aperture can be defined as a panel whose mass thickness is zero for all practical purposes. It is customary, and certainly on the safe side, to include ordinary doors, windows, and skylights in this category.

Formulas for apertures are easily obtained from those given in sections VII.D.2 and VII.D.3, by making the  $X_o$  and  $X_e$  in those formulas equal to

zero, or, somewhat more accurately (but making little change in practice), making it equal to the mass thickness of the glass plus the amount of air between detector and aperture. With respect to the choice in selection of the geometry factor for use in the overhead case, the choice of  $L_c$  is better than  $L_a$ , since what shielding there is (the air) is well distributed between source and detector. (See the discussion following eq (VII.7).) In the formulas involving wall contributions, a zero wall thickness makes the value of the exterior wall barrier factor essentially equal to the  $\ell$ -function determined at the height in air of the appropriate point in the aperture.

Since apertures in walls are an extreme example of wall-thickness variation, the problems of which method to choose for weighting fractions (see eq (VII.58)) and the text following) is particularly significant for this case. In general, the same rules applied to wall panels are applicable to apertures. Although there are exceptional circumstances, in most cases azimuthal fractions are to be preferred over perimeter ratios.

A simple alternative to the usual standard formulation exists which might be applied for wall apertures, especially in a case wherein the aperture is not very eccentric in its height-to-width ratio and either the midpoint or the lower sill of the aperture is at the detector height. The situation, in such case, would conform roughly to the idealization leading to the function  $W_a(H, \omega_a)$  or to that leading to the function  $W_b(H, \omega_a)$ , depending upon whether the detector were at mid-aperture height or sill height. (These two functions are explained in chapt. V.)  $H$  is, as usual, the detector height above the source plane and  $\omega_a$  is the solid angle fraction subtended by the aperture at the detector. The total contribution is thus given as  $\frac{1}{2} B_e(0, H) \cdot W_a(H, \omega_a)$  or  $\frac{1}{2} B_e(0, H) \cdot W_b(H, \omega_a)$ , as the case may be.

## 5. Ceiling-Shine

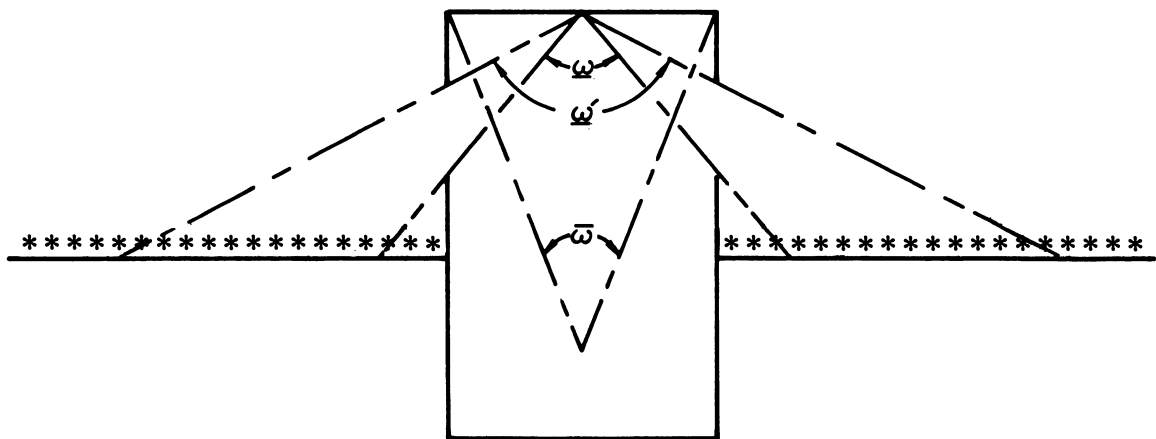
Apertures and very thin walls, approaching zero in thickness, have another effect on the detector response, less direct than that covered in the previous section. They permit a large amount of radiation to be incident on the inside of the structure, part of which can be reflected in the direction toward the detector. The major contribution of this type is reflection from the ceiling, known as "ceiling-shine".

A fairly rigorous approach to this problem of estimating the contribution can be devised using albedo theory. However, because the contribution is hardly ever important a somewhat ad-hoc approach has been devised and incorporated into the Standard Method which is based on the following plausible arguments.

The ceiling-shine is clearly related to product of the exposure at the location where the radiation strikes the ceiling and to a reflection factor in turn related to the ceiling material and the geometry of the detector relative to the ceiling. (See fig. VII.15) In addition, the obliquity (cosine) of the angle of incidence of the radiation striking the ceiling is a factor [10]. The detector response at the ceiling is given approximately by  $F_r [G_d(H, \underline{\omega}) - G_d(H, \underline{\omega}')] B_e(X_e = 0, H)$ , where  $\underline{\omega}$  and  $\underline{\omega}'$  are taken at the ceiling midpoint as being representative.

One means of inserting the obliquity factor mentioned above is to use a function which if inserted in place of  $G_d$  in the bracketed expression will implicitly introduce the obliquity factor.  $G_d$  is based on that portion of the  $\ell$ -function which is peaked near the horizon ( $\cos\theta$  very small - see fig. VII.3); and since the obliquity factor is small near the horizon we need a function in which the influence of angular components near the horizon is





VII.15 Pertinent solid angles in ceiling-shine analysis.

much less marked. It happens that  $G_a$  is just such a function, and thus the approximation can be made that the combination of exposure at the ceiling and the obliquity factor is proportional to<sup>15</sup>

$$F_r [G_a(\underline{\omega}) - G_a(\underline{\omega}')] B_e(X_e = 0, H)$$

The reflection factor is assumed to be related to  $G_a(\bar{\omega})$ , where  $\bar{\omega}$  is shown in figure VII.15. This is on the basis that the constituents of a ceiling and of air, respectively, have low average atomic number and thus have similar reflection properties [10]. However, since the reflection will increase with increasing  $\bar{\omega}$ , the reflection factor is taken to be proportional to  $[G_a(0) - G_a(\bar{\omega})]$ .

Thus the expression for ceiling shine can be written as

$$C_c = kF_r [G_a(\underline{\omega}) - G_a(\underline{\omega}')] [G_a(0) - G_a(\bar{\omega})] B(X_e = 0, H) \quad (\text{VII.79a})$$

The constant of proportionality is established by considering the special configuration in which the detector is at sill level and the apertures extend to the ceiling. For this configuration  $\bar{\omega} = \underline{\omega}$ , and  $\underline{\omega}' = 1$ . Since  $G_a(0) = 0.1$  and  $G_a(1) = 0$ , eq (VII.79a) reduces to

---

<sup>15</sup>If the angular distribution of exposure incident on the ceiling is weighted by a  $\cos\theta$  obliquity factor to obtain the incident current and then multiplied by the albedo function in figure V.10 to obtain the dependence of the albedo on the angle of incidence, a curve is obtained which is remarkably similar to the skyshine curve for  $d = 3$  ft on the left side of figure V.6. The use of  $G_a$  is therefore better justified than originally believed.

Note that for the albedo angular distribution of figure V.10, an integral over reflected directions has been performed, while for the skyshine angular distribution an integral over incident directions has been performed. Similarity between the resulting angular distributions depends on the extent to which the doubly-differential albedo function is dependent mainly on the cosine of the angle between incident and emergent directions.

$$C_c = kF_r [G_a(\bar{\omega})] [0.1 - G_a(\bar{\omega})] B_e (X_e = 0, H) \quad (\text{VII.79b})$$

We now examine the limit in which  $\bar{\omega} \rightarrow 1$  and  $G_a(\bar{\omega}) \ll 0.1$ . Since  $F_r G_a(\bar{\omega})$  gives the skyshine through the aperture, the factor  $0.1 k$  gives the ratio of ceiling shine to skyshine in the limiting case. A value of  $k = 5$  was arbitrarily chosen in order to produce a ratio of 0.5. (In retrospect, the difference in albedo between concrete and air would suggest a value of 0.8 for this ratio.)

The only unsettled question is what value of  $H$  to use. As the unsubscripted symbol implies, the detector height is recommended [5]. The degree of approximation inherent in this formulation does not warrant further concern on this point.

## 6. Ribbed Structural Elements

The previous discussion concerning sections of structural elements with differing thickness is most useful when these sections are of a scale comparable to the total dimensions of the element concerned. But there often occur cases in which variations in structural element thickness are on a much finer scale than this. Quite often these variations are frequent and regular, common examples of this being beams holding up a slab or columns associated with a wall. We call this type of configuration "ribbed construction".

Under such circumstances simpler and less tedious approaches are possible. The simplest of all is to divide the total mass of the structural element by the area of a face to obtain the average mass thickness, convert to equivalent mass thickness as necessary, and perform the shielding analysis on the basis of this equivalent, or "smeared," element.

A number of studies [11,12] have shown this smeared-element approach to give answers with errors on the unsafe side, i.e., overestimating the shielding capability. For many cases, this error is of minor importance, but for some cases the error can be substantial.

Spring and LeDoux [10,13] suggested an approach less liable to be seriously in error. The approach, known as the "area-weighted method," when applied to a single ribbed-slab barrier requires that two separate penetration calculations be made. One is made on the basis that the barrier thickness is that of the base slab and the other is made on the basis that the barrier thickness is the sum of the base slab thickness and the depth of the supporting ribs. The two results are combined, after each is weighted by the proportion of the slab face area which is between and in contact with, respectively, the supporting ribs. The procedure is easily applied to two-way ("waffle") rib construction.<sup>16</sup>

An approach which is now accepted as part of the Standard Method is called the "adjusted smearing" procedure.<sup>17</sup> According to this the ribbed-slab is replaced for calculational purposes by a slab of constant mass thickness, where the value of the latter is taken as the sum of the base slab mass thickness and a certain percentage of the smeared rib mass thickness. This percentage, a function of rib spacing, is available either as a curve in the corrected OCD Manual [2] or as a simplified table, reproduced here as table VII.1.

Although the Standard Method prescribes this procedure for ribbed roofs (and other horizontal elements) only, it also appears reasonably applicable to walls of ribbed character.

---

<sup>16</sup> Although more applicable to a later chapter, one might point out here that how to apply the "area-weighted" procedure to situations involving two or more ribbed-slab-barrier systems overhead for a detector on the lower floor of a multistoried structure is not clear. For such cases, a use of the more elaborate technique suggested in reference [13] is possible.

<sup>17</sup> The source of information for this procedure has not been specified in any published report, to the knowledge of the authors, but it is probably based on conservative empirical approximations to the considerable calculational data available from or noted by reference [12].

TABLE VII.1

PERCENTAGE OF SMEARED RIB MASS THICKNESS TO BE INCLUDED IN DETERMINING  
OVERALL RIBBED-SLAB MASS THICKNESS.

<u>Rib Spacing</u>	<u>Percentage</u>
$\leq 0.5$ ft.	100%
$> 0.5$ ft and $\leq 1$ ft	70%
$> 1$ ft and $\leq 2$ ft	60%
$> 2$ ft and $\leq 4$ ft	50%
$> 4$ ft and $\leq 8$ ft	40%
$> 8$ ft and $\leq 16$ ft	30%
$> 16$ ft	0%

#### E. OFF-CENTER DETECTOR POSITIONS

Since the standard methodology is based on the detector being located centrally with respect to the horizontal plan, the off-center detector position is a problem which must be handled by some indirect means. The technique is quite simple, and depends upon the independence of effects due to various parts of the simple blockhouse.

The standard approach is to consider the blockhouse divided up by two vertical planes, containing the detector and perpendicular to the two pairs of walls, into four parts of unequal size (in the general case). Each of these may in turn be considered a quadrant of a fictitious structure (called in this connection an "idealized" structure in the OCD Manual) in which the other three quadrants have the same structural characteristics, suitably mirrored,

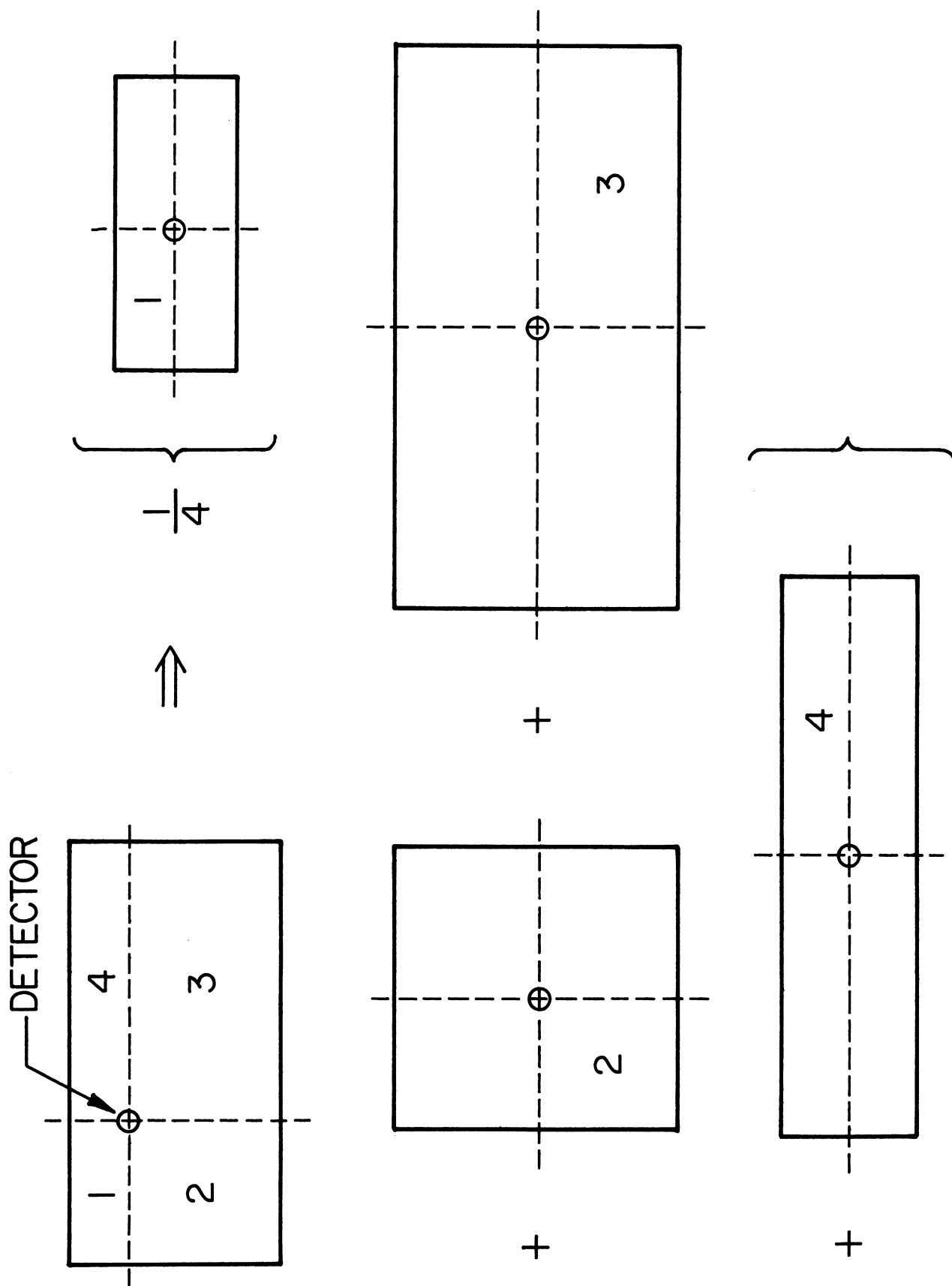
and the detector is centered. The contribution of each of the four parts of the original blockhouse is therefore one-fourth of the detector response calculated for its particular fictitious structure. Summation of such results for all parts of the original structure gives the proper approximate answer. Figure VII.16 illustrates a typical case. Both roof and wall contributions are included in this approach.

This fictitious-building technique can be modified or replaced, just as for the extended methodology developed previously in this chapter, in which the contributions from individual panels or parts of roof and wall can be analyzed without regard to the rest of the structure. The formulas provided, which maintain complete independence of the overall structural shape and size, are also independent of whether the detector is centrally located in the structure or not.

#### F. SUMMARY

In this section, fallout radiation attenuation by simple blockhouse structures has been carefully examined, since solutions to such cases are the fundamentals on which examination of more complex and more realistic situations is based. The discussion has involved primarily the so-called Standard Method of the OCD Manuals on this subject; but alternative approaches to methods of analysis or extensions to the established methodology are presented if they have substantial merit. A number of especially important principles have been brought out, which are worth repeating.

1. The standard methodology is based upon a specific physico-mathematical model of how fallout radiation behaves in penetrating an elementary blockhouse structure. This is only one of a number of possible models which could be



VII.16 Example of how an off-center-detector-position problem is handled.

used; and any review of or research on the standard methodology should be done with consideration of the logical necessity for retaining a single point of view based on one chosen model.

2. The Standard Method handles the question of geometry factors for wall-penetrating radiation by assuming that the behavior of such radiation in the case of a realistic wall thickness can be adequately approximated as an interpolation between, or weighted mixture of, results based on zero and essentially infinite wall mass thickness situations, respectively. The identification of the "thin-wall" (zero mass thickness) results with the non-wall-collided penetration and the "thick-wall" (infinite mass thickness) results with the wall-scattered component of the penetration is a substantial approximation, which, however, is justified because of the simply understandable physical meaning which is thereby assignable to various part of the mathematical formulation.

3. The problem of variability in wall and roof thicknesses can be handled as an integrated theory, covering both large- and moderately small-scale variations.

4. Determination of contributions through individual panels in roofs and walls under the procedures provided for in the standard methodology generally involve parameters related to the overall size and shape of the building. This violates the intuitive feeling that contributions through individual panels should be practically independent of structural parameters related to other parts of the blockhouse. This dependence on external factors can, however, be avoided by modifications to the standard methodology. Note that the panels involved may or may not be of different effective mass thickness than the remainder of the structural element of which it is a part.



## REFERENCES

- [1] Eisenhower, C. M., An engineering method for calculating protection afforded by structures against fallout radiation, Nat. Bur. Stand. (U.S.), Monogr. 76, 20 pages (July 1964).
- [2] Shelter design and analysis-fallout radiation shielding, TR-20, Vol. 1, as amended by Change 1 (July 1969), Change 2 (Jan. 1970), and Change 3 (Nov. 1974), 445 pages (Dept. of Defense, Office of Civil Defense, July 1967).
- [3] Design and review of structures for protection from fallout gamma radiation, OCD Report PM-100-1, Interim Edition, 121 pages (Office of Civil Defense, Feb. 1965).
- [4] Spencer, L. V., Structure shielding against fallout radiation from nuclear weapons, Nat. Bur. Stand. (U.S.), Monogr. 42, 134 pages (June 1, 1962).
- [5] Bramlitt, E. T., and Eisenhower, C. M., A discussion and tabulation of the data used to construct the charts in the OCD Standard Method for fallout gamma radiation shielding analysis, TR-70, 63 pages (Office of Civil Defense, Dec. 1971).
- [6] Fano, U., Spencer, L. V., and Berger, M. J., Penetration and diffusion of x-rays, Handbuch der Physik, Encyclopedia of Physics, S. Flugge, Ed., Vol. 38/2. 660-817 (Springer-Verlag, Berlin, 1959).
- [7] Hubbell, J. H., Bach, R. L., and Lamkin, J. C., Radiation field from a rectangular source, J. Res. Nat. Bur. Stand. (U.S.), 64c (Eng. and Instr.), No. 2, 121-138 (April-June, 1960).
- [8] Degelman, L., Foderaro A., and Kowal, G., Evaluation of the shielding characteristics of structures for simulated residual radiation, Report NUC E 15, 62 pages (Penn. State U., Nov. 1963).
- [9] Rexroad, R. E., Schmoke, M. A., Tiller, H. J., Foderaro, A., Degelman, L., and Kowal, G., Point-to-point kernel analysis of an experiment to determine wall penetration of a square-based concrete structure by gamma radiation, Nucl. Sci. and Eng. 20, No. 1, 66-79 (Sept. 1964).
- [10] Spring, R., Gamma ray attenuation through non-uniform concrete slabs, NRDL TRC-68-28, 41 paged (Conesco Division of Flow Corp., Apr. 1968).
- [11] Chilton, A. B., Ribbed slab penetration-a summary report, Report NRSS-13, 44 pages (U. of Illinois, Oct. 1969).
- [12] Chilton, A. B., and Morris, E. E., Shielding effectiveness of ribbed slabs against gamma radiation: Part II. Engineering methods, Nucl. Eng. and Design 23, No. 3, 367-375 (Dec. 1972).
- [13] LeDoux, J. C., Effective mass thickness for non-uniform roofs and walls, Appendix A, Gamma ray attenuation through non-uniform concrete slabs, NRDL TRC-68-28, 27-31 (Conesco Division of Flow Corp., Apr. 1968).

## VIII. EXPERIMENTAL DATA ON SIMPLE BLOCKHOUSES

### A. INTRODUCTION

The Standard Method for calculating protection factors for a simple blockhouse has been discussed in chapter VII. During the development of this method the Office of Civil Defense supported a number of experimental programs designed to validate methods of calculation. Whenever possible, experiments designed to test individual ratios such as barrier factors or geometry factors were incorporated in these programs. Experiments to test horizontal and vertical barrier factors will be described in sections B and C. Experiments on square blockhouses will then be discussed in section D and experiments to determine the dependence of the protection factor on the shape of the structure will be discussed in section E. Section F gives experimental studies of exposure due to radiation from ground sources which enters through the windows of a structure and is reflected from the ceiling ("ceiling shine"). Finally, experiments on slabs with a simulated joist structure are presented in section G.

### B. HORIZONTAL BARRIER

#### 1. Barrier Factor; Experiment

The first experiment designed especially to measure the penetration in concrete of radiation from a plane isotropic source of fallout gamma radiation was the experiment by Titus [1] mentioned in sections I.B.1 and II.C.3. The test was carried out at the AEC's Nevada Test Site, using fallout from a nuclear explosion. Results were obtained for two different nuclear detonations.

The concrete mass was composed of seven concrete slabs, each constructed with an indentation to house a detector and an access port for insertion of the detector. Each slab was 4 ft. square with an average thickness of 3.15

inches and a density of  $2.30 \text{ g/cm}^3$ . The concrete mass was placed in a pit 40 inches deep. The combination of concrete and air layers was such that the top of the concrete mass was at ground level. The dimensions of the concrete were large enough so that the detectors could be considered to be in a semi-infinite medium of concrete.

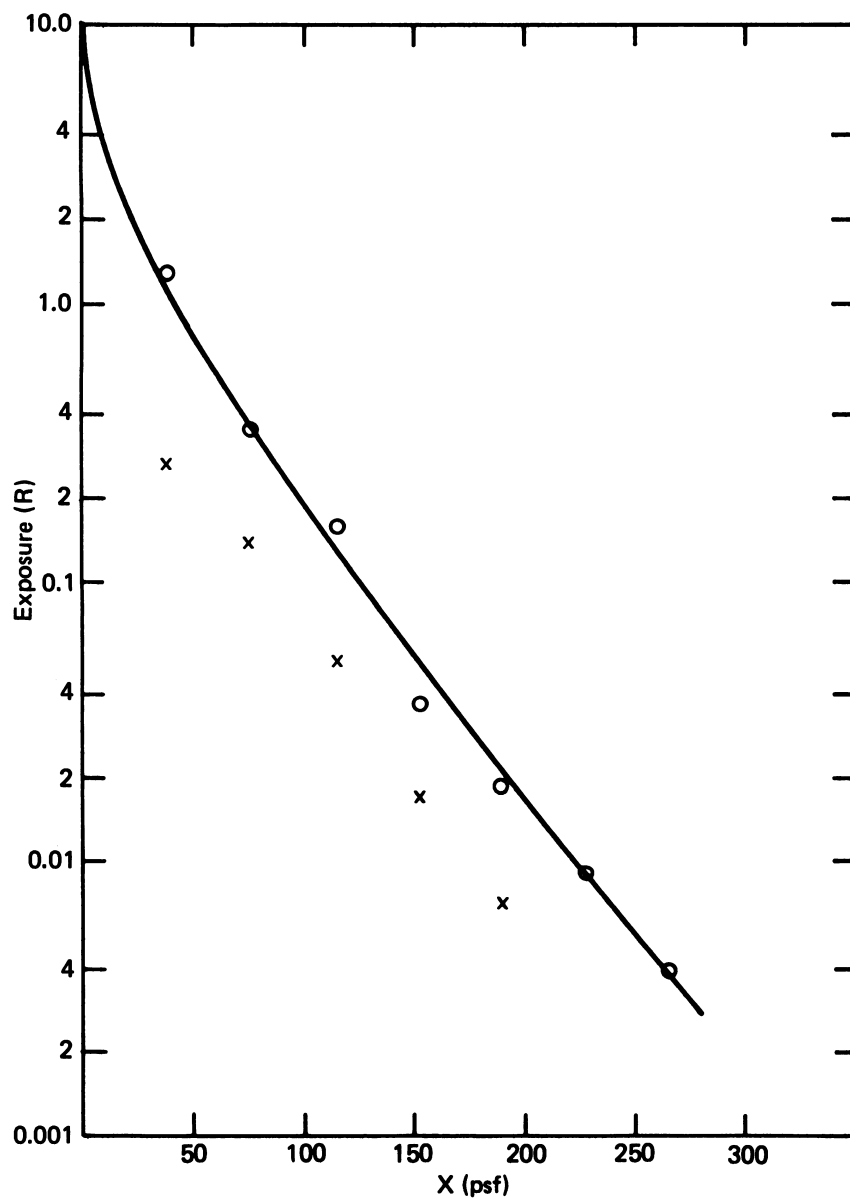
Geiger-Müller (G-M) detectors, connected to remote data stations, were placed at seven depths within the concrete and at 3 ft and 9 ft above the ground. Pocket dosimeters and film packs were also included in the experiments. Measurements of the exposure rate with the G-M detectors were extrapolated to infinite time and integrated to obtain estimates of the exposure vs. depth in the concrete. The extrapolated contribution amounted to about 20% of the estimated exposure. The estimated exposures were generally lower than the results for pocket dosimeters by about a factor of 3, but higher than the film pack results by factor of 1.1 to 2. However, the pocket dosimeters probably included a large contribution from prompt radiation. For both detonations the variation with depth was similar for all three types of detectors. Table VIII.1 shows a summary of the data.

It is difficult to infer reduction factors from the experiment because the integrated exposure at a height of 3 ft was not given by Titus. He stated, however, that the exposure rate under 3 inches of concrete was approximately 1/10 of that at 9 ft above ground. His conclusion was that "During the first few hours after H-hour, fallout radiation is seen to penetrate like a 2-MeV plane isotropic gamma source; whereas at later times the penetration is similar to that of a 1-MeV plane isotropic gamma source." [1]

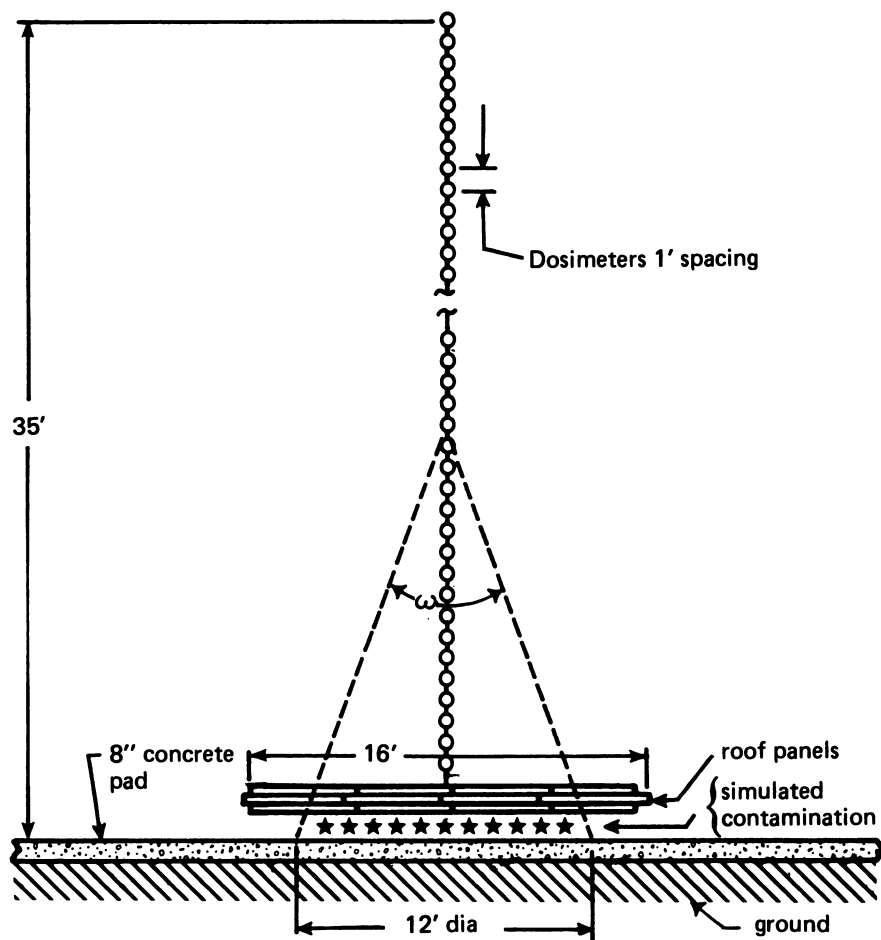
Figure VIII.1 shows his integrated exposure data for the two different shots. Also shown in the figure is the curve calculated for 1-hour fission products from figure V.12. This curve has been multiplied arbitrarily by a

TABLE VIII.1 Measured Doses in Concrete

Depth (psf)	Shot A		Shot B	
	G-M Counters	Pocket Dosimeters	G-M Counters	Film Packs
39	2.7	9.4	13	7.4
76	1.4	3.4	3.6	2.2
114	0.52	1.2	1.6	0.79
152	0.17	0.4	0.37	0.33
189	0.07	0.2	0.19	0.11
227			0.09	0.06
265			0.04	0.05



VIII.1 Comparison of Experimental and Calculated Exposures from Fallout Radiation as a Function of Depth in a Concrete Medium.  
 O, X Experimental, Titus [1]; — Calculated  $L(X) (\times 10)$   
 (Fig. V.12).



VIII.2 Schematic Drawing of Inverted Roof Experiment

factor of ten. It can be seen that the agreement of the dependence on depth is very good for one set of experimental data and reasonably good for the other. Furthermore, the calculated curve shows the same ratio of exposures at a depth of 3 in (39 psf) and a depth of 9 ft in air (0.7 psf), namely, one-tenth as observed experimentally. This experiment was very helpful in justifying the early choice of the one hour fission product spectrum as representative of the penetrability of fallout radiation.

This was the only experiment which attempted to measure the barrier factor at many different depths in an infinite homogeneous medium. In all later experiments in structure shielding, measurements were made at various distances from barriers of -- at most -- a few different thicknesses. This was partly because of the experimental difficulties involved in handling a large number of concrete slabs, each of which weighed about a ton. It was easier to make measurements at varying distance from one or two concrete slabs. Another reason for the lack of variation in barrier thickness was that the calculation of the roof barrier factor was on very firm theoretical grounds while the calculated geometry effects contained more uncertainty. The measurement of geometry effects was therefore a more interesting experimental problem.

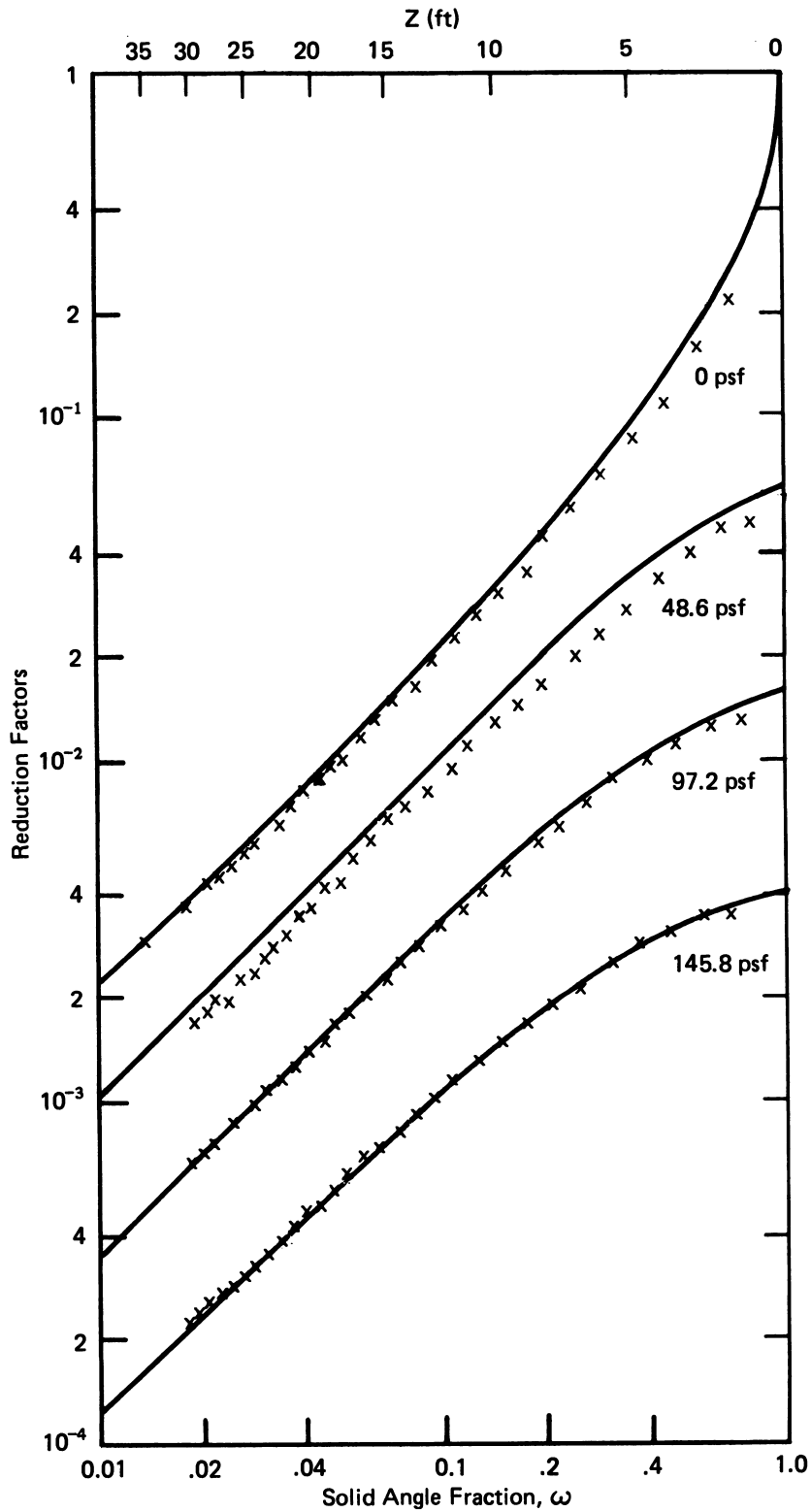
## 2. Geometry Effects; Inverted Roof Experiment

The most comprehensive experiments with roof sources were made at the Radiation Test Facility -- formerly known as the Protective Structures Development Center -- at Fort Belvoir by McDonnell and Velletri of Flow Corporation [2]. One of these was called the "inverted roof" experiment because the ordinary position of detectors and roof source were reversed. The circular disk source was placed on a concrete pad and slabs of concrete of varying thickness were placed over the source. Measurements were made above the slabs on the vertical axis of the disk source. The configuration is shown in figure VIII.2.

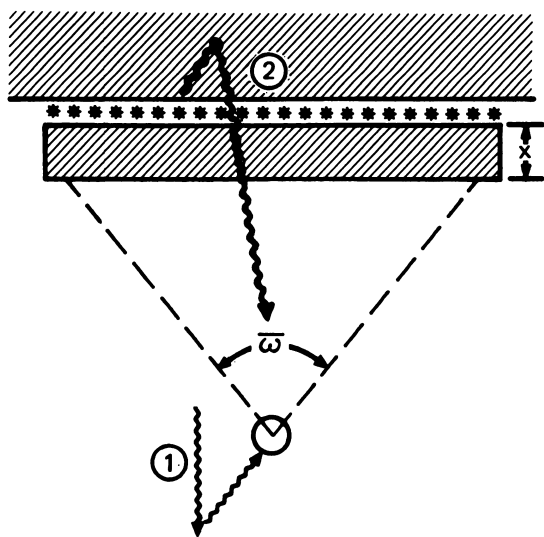
A comparison of the results with calculations is shown in figure VIII.3. The reduction factor is presented as a function of solid angle fraction  $\omega$  subtended by the source, for four different slab thicknesses. The experimental values for 0 psf actually correspond to air mass thicknesses ranging from 0.14 psf near  $\omega = 1$  to 2.2 psf near  $\omega = .02$ . However, the effect of the added air in this geometry is probably less than 1%.

The curves in figure VIII.3 were calculated from the expression  $C_o = L(X) L_a(X, \omega)$ , (see eq (VII.6)) where  $C_o$  for  $^{60}\text{Co}$  radiation is given in figure B.11a. This experiment was designed to approximate as closely as possible the idealized configuration for which the function  $L(X) L_a(X, \omega)$  was calculated, in that circular sources were used and spurious scatter from structural beams was eliminated. The experimental and idealized configurations are shown in figure VIII.4. In the experimental configuration the source subtends a solid angle fraction of  $\omega$ , the barrier is concentrated near the source and the detector can respond to photons from all directions. However, all the uncollided radiation and most of the scattered radiation arrives at the detector from within the solid angle fraction  $\omega$ . In the idealized configuration, the horizontal arrows indicate that the source extends to infinite distances, the barrier material is uniformly distributed and the black or opaque collimation on the detector indicates that the detector responds only to radiation arriving from within the solid angle fraction  $\omega$ . The differences in the two configurations are indicated by photon trajectories in the figure. Photons of type 1 which backscatter from the air behind the detector in the experimental configuration are not counted in the idealized configuration. On the other hand, photons of type 3, which originate from sources beyond the solid angle fraction  $\omega$ , but scatter into this solid angle are not counted in the experimental configuration. The latter type of trajectory would be expected to contribute

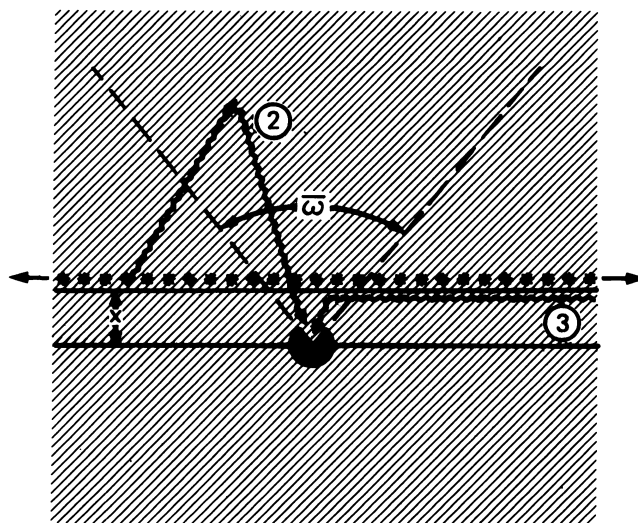




VIII.3 Comparison of Experimental and Calculated Reduction Factors for the Inverted Roof Experiment with  $^{60}\text{Co}$  Source. X Experimental, McDonnell and Velletri [2]; — Calculated  $L(X)L_a(X, \omega)$  (Figs. V.45 and V.47)

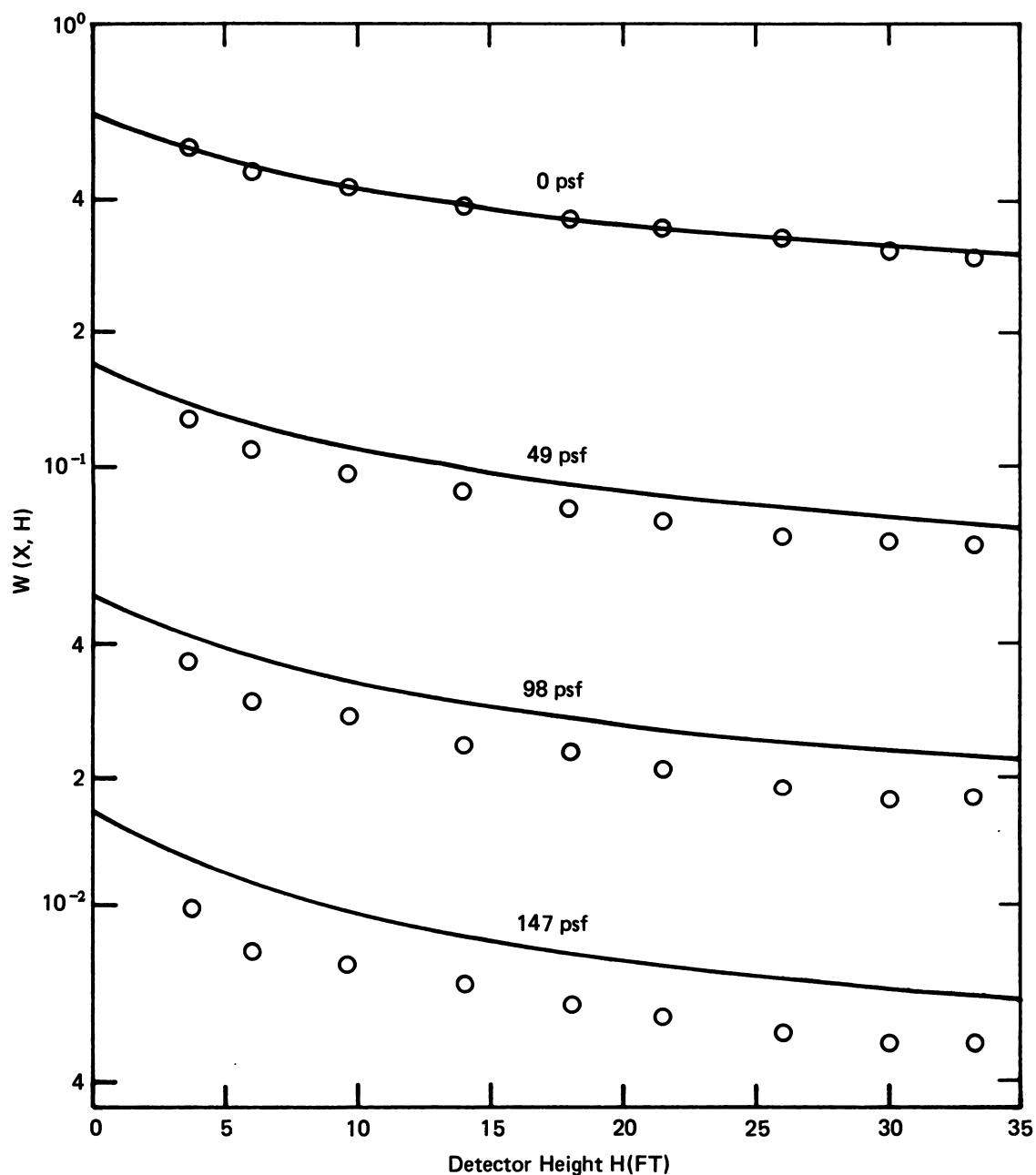


EXPERIMENTAL  
CONFIGURATION



IDEALIZED  
CONFIGURATION

#### VIII.4 Schematic Drawing Comparing Experimental and Idealized Configurations for a Circular Roof Source



VIII.5 Comparison of Experimental and Calculated Wall Barrier Factors for  $^{60}\text{Co}$  Radiation.  $\circ$  Experimental, McDonnell et al, [3];  
 — Calculated  $W(X, H)$  (Fig. V.65)

only when the barrier is thin enough ( $X \leq 1$  psf) to allow radiation to travel long paths nearly parallel to the plane of the slab before undergoing a scatter. Photons of type 2 contribute in both configurations. It is not surprising that the agreement should be good, because the calculation of  $L(X)$  and  $L_a(X, \omega)$  are the result of a straightforward solution for the exposure from a plane isotropic source and the corrections referred to are small. The good agreement confirms the validity of angular distributions represented by  $L_a(X, \omega)$ .

### C. VERTICAL BARRIER

#### 1. Barrier Factor, Infinite Source

##### a. Experiments

A systematic set of experiments to determine the vertical barrier factor was made by Batter and his co-workers at the Radiation Test Facility [3]. In these experiments, pocket ionization chambers were placed on the interior face of concrete walls of varying thickness. In order to simulate the infinite-medium configuration for which barrier factors were calculated, the experimenters placed eight inches of concrete behind each dosimeter. Measurements for zero barrier thickness were made by placing dosimeters on the exterior face of the 147 psf (12 inch) concrete wall.

The source was a  $^{60}\text{Co}$  cylinder pumped through plastic tubing. The tubing was laid out in four annular quadrants out to a distance of 452 ft from the center of the building. The contribution from sources beyond that distance was calculated in terms of a ratio applied to the experimental contribution from the outermost annulus. The far-field contribution varied from about 8% for the lowest detector height of  $H = 3$  ft to about 20% at  $H = 33$  ft.

Figure VIII.5 compares their experimental results with calculated values of the barrier factor  $W(X, H)$  for four different wall thicknesses including zero thickness. The barrier factor for  $^{60}\text{Co}$  radiation is shown in figure B.17a

and discussed in section VII.B.1. The agreement between theory and experiment is good, except that experimental values fall increasingly below the theoretical values for increasing mass thickness. The experimenters estimated that the discrepancies for walls of 4 inch, 8 inch, and 12 inch thickness are 12, 18, and 24% respectively. They found that if the experimentally reported mass thickness was incremented by 8% in the calculation, excellent agreement was obtained between theory and experiment.

There are uncertainties in both the experiment and the calculations which might produce such a discrepancy. For example, in the experiment the mass thickness might have been measured improperly. This explanation would predict even larger discrepancies for mass thicknesses greater than 147 psf. Another uncertainty in the experiment is the effect of self-shielding in the walls of the detector, which are thin for the  $^{60}\text{Co}$  source radiation, but become increasingly thicker for low energy photons. Thus, self-shielding may reduce the measured response for scattered photons.

In the calculation, the approximate treatment of the air-scattered component of the source spectrum which was present in the experiment produces some uncertainty. The assignment of the source spectrum to the scattered radiation in the calculation of  $W(X,H)$  was mentioned as approximation 2) in section V.C.3.a. This overestimates the exposure on the inner side of the wall because the scattered radiation is less penetrating than is assumed. The maximum error due to this approximation occurs when the scattered radiation is entirely filtered out in the barrier. Since 20% of the total radiation exposure incident on the wall is due to scattered radiation, its complete disappearance would account for a maximum error of 20% in the transmitted exposure. This would mean that the discrepancy seen at 147 psf

is probably the maximum and would not increase for greater mass thickness. Unfortunately, there is no reliable experimental data at greater mass thickness to test the validity of these explanations.

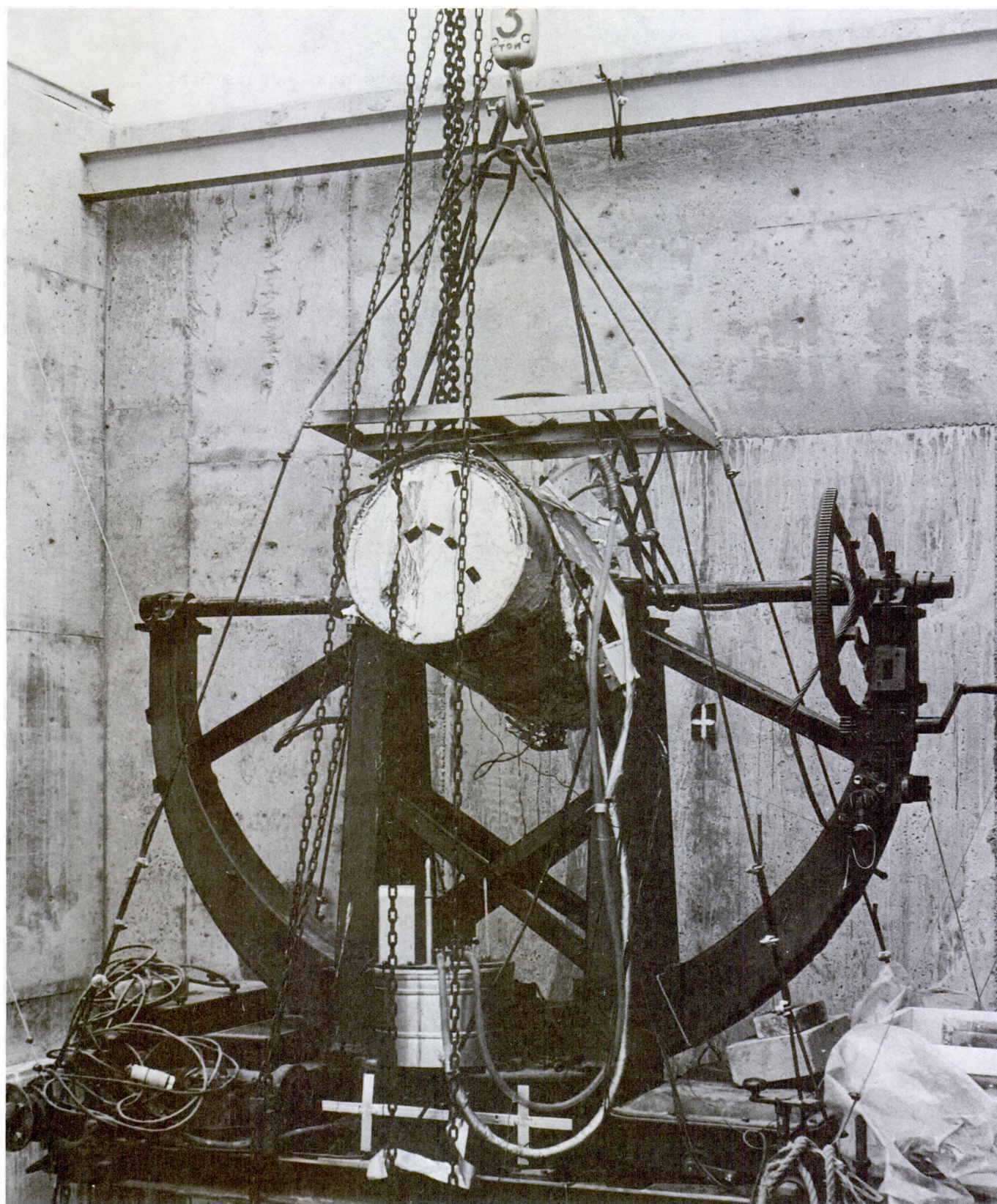
An effort was made by R. Faw and his collaborators at Kansas State University to measure the energy and angular distribution of radiation emerging from a vertical barrier [4]. The collimator-spectrometer system used for these measurements is shown in figure VIII.6. The detection system consisted of a 3 in x 3 in NaI(Tl) scintillator crystal and three-inch photomultiplier tube, housed within a lead cylinder 1.5 ft in diameter and 3 ft in length. Rotation of the lead collimator was accomplished by mounting it in the yoke of a surplus military anti-aircraft searchlight. A special concrete test panel 6 ft x 6 ft was constructed, with steel reinforcing confined to the outer rim, leaving a 5 ft x 5 ft area of concrete entirely free of reinforcement, with a mass thickness of  $48 \pm 1$  psf. This panel, which was mounted at the center of a 10 ft x 15 ft concrete wall, can be seen behind the collimator in figure VIII.6. An excavated area behind the wall provided a simulated basement area.

The plane source was simulated by a hydraulic tube source circulation system using a  $^{60}\text{Co}$  pellet. The tubing was distributed in three different patterns which covered a semicircular area of radius 100 ft. Corrections for contributions from sources beyond that distance were made by taking ratios to the contribution from the outermost area.

Exposure angular distributions were obtained by weighting energy spectra by fluence-to-exposure conversion factors and summing over all energy bins. Faw and his collaborators found that their data at a given polar angle  $\theta'$ ; could be fit by the form

$$D(\theta', \phi') = D(\theta', \phi' = 0) [a(\theta') + b(\theta') \cos \phi'] \quad . \quad (\text{VIII.1})$$





VIII.6 Apparatus Used to Vary Detector Angle in Measurements of the Energy Angle Distribution of Radiation from a Concrete Wall at Kansas State University



The angles  $\theta'$  and  $\phi'$  are shown in figure VIII.7. For some values of  $\theta'$ ,  $a$  is negligible compared to  $b$ , and for other values of  $\theta'$ , the opposite is true.

The radiation emerging from the inner face of a very thick wall is assumed in the Standard Method to have the form (see section VII.B.1)

$$D(\theta, \phi) = D(\theta) \cos \phi \quad (\text{VIII.2})$$

where  $\theta$  is the polar angle between the direction from which the photon arrives and the downward vertical direction, and  $\phi$  is the associated azimuthal angle. These angles are the same as those in figure VIII.7 except that  $\theta' = 180^\circ - \theta$ . A plot of the experimental data against the azimuthal angle  $\phi$  for various values of the polar angle  $\theta$  is shown in figure VIII.8. Also shown in the figure is the expression for small wall areas, which can be derived from eq (VII.78b), namely,

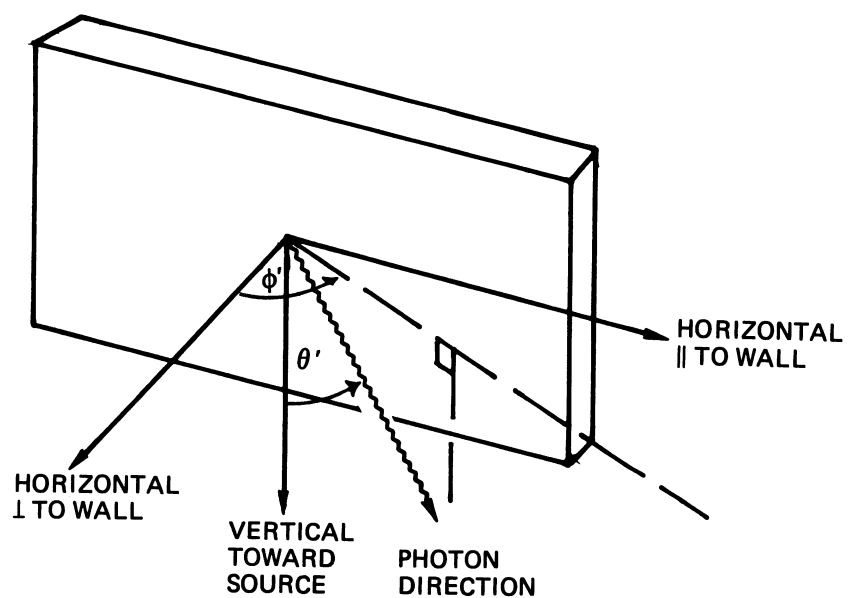
$$D(\theta, \phi) d(\cos \theta) d\phi = D_o B_e(48, 3') \left\{ \frac{(1-S_w)}{2\pi} \ell(3', \cos \theta) + \frac{5}{4} S_w \ell(3', -|\cos \theta|) \cos \phi \right\} d(\cos \theta) d\phi \quad (\text{VIII.3})$$

The correspondence between the two expressions can be seen by noting that

$$d(\cos \theta) d\phi = \frac{dA}{R^2} \sin \theta \cos \phi \quad , \quad (\text{VIII.4})$$

$$N^2 = R^2 \sin^2 \theta \cos^2 \phi \quad , \quad (\text{VIII.5})$$





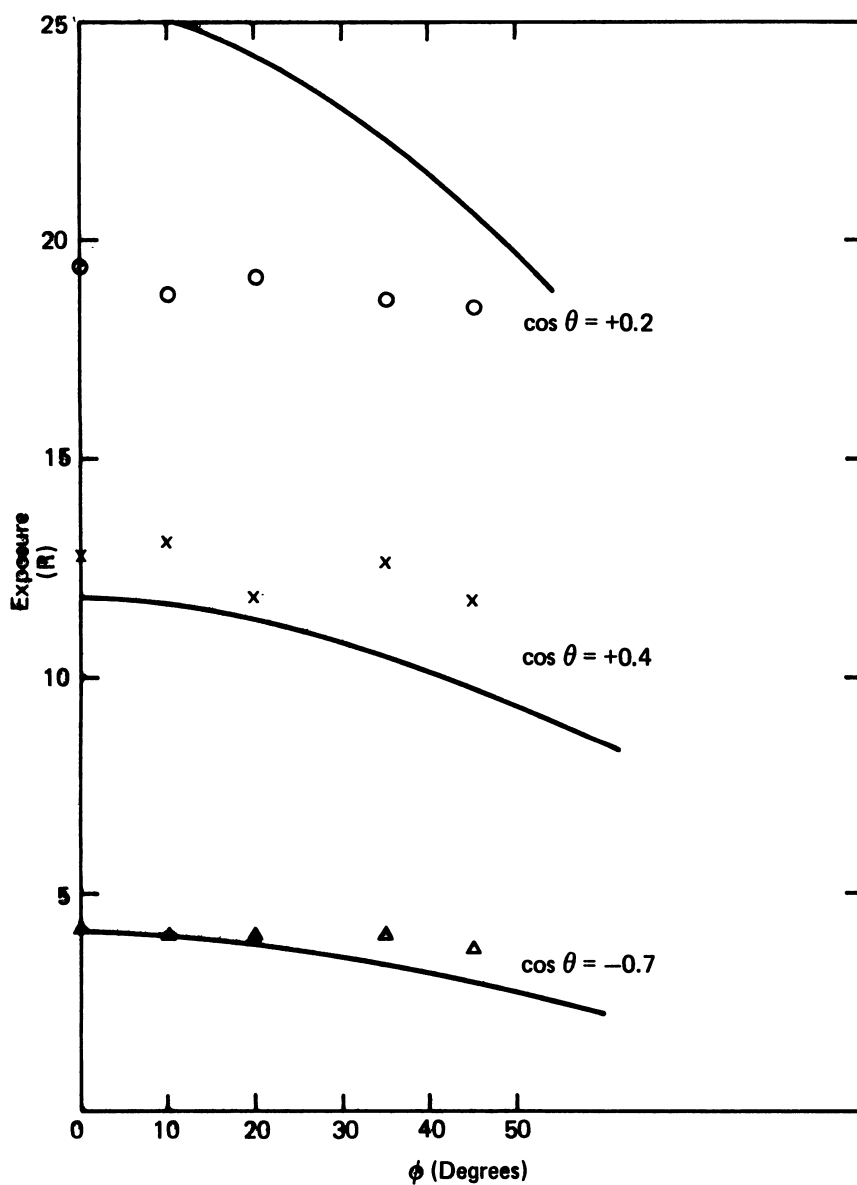
VIII.7 Schematic Drawing Showing How Angles Were Defined in the Measurements at Kansas State University.

and the derivatives of the  $G$  functions in eq (VII.78) are given by the  $\ell$  functions in eq (VIII.3). Values of  $B_e(48,3') = 0.30$   $S_w = 0.6$  and  $D_o = 480 \text{ (R/hr)/(Ci/ft}^2\text{)}$  were used for the curves in figure VIII.8.

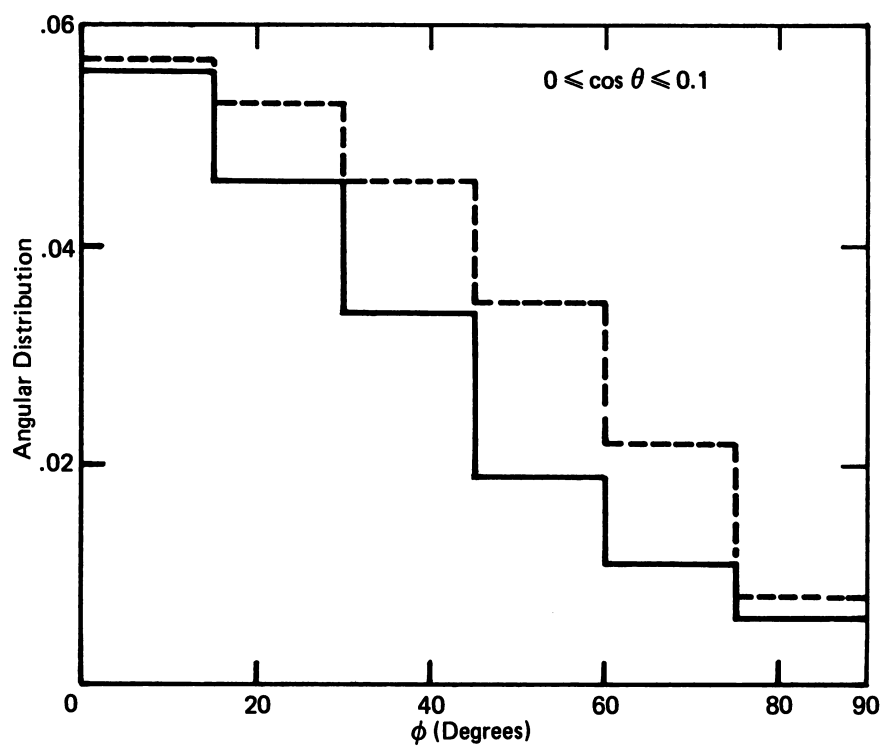
It can be seen from figure VIII.8 that the experimental values indicate less of a dependence on the azimuthal angle  $\phi$ , particularly for  $\cos\theta = 0.2$  than predicted by the Standard Method. The disagreement in magnitude by as much as 25% is not surprising in view of the difficulties in inferring an exposure by integration over measured angle-energy distributions. It should be noted, however, that Faw and his collaborators estimate a possible error of 10% in the measured exposure angular distributions.

#### b. Calculations

A comparison between calculations of the angular distribution of radiation from a vertical wall by the Monte Carlo method and by the Standard Method were reported by Eisenhauer and Chilton [5]. Their results for the important polar angle interval  $0 \leq \cos\theta \leq 0.1$  are shown in figure VIII.9. The Monte Carlo calculations were made for a "fan" source, i.e. one in which the gamma ray flux is confined to a horizontal plane and is isotropically distributed in azimuth. This should be a good approximation because of the extremely peaked nature of the angular distribution at the 3 foot height in a direction nearly parallel to the ground. (See for example, the top curve in fig. V.6). These calculations bear out the assumption of a peaked distribution in the azimuthal direction of the radiation emerging from the inner face of the wall. In fact, they indicate that the angular distribution of exposure is more peaked than the  $\cos\phi$  dependence assumed in the Standard Method. Results in figure VIII.9 are normalized such that the integral over all values of  $\theta$  and  $\phi$  is unity.



VIII.8 Comparison of Experimental and Calculated Dependence of the Exposure Angular Distribution on the Azimuthal Angle. O, X,  $\Delta$ , Experimental, Rubin et al. [4]; — Calculated, eq (VIII.3)



VIII.9 Comparison of Calculations of the Dependence of the Exposure Angular Distributions on the Azimuthal Angle by Monte Carlo and by the Standard Method — Calculated, Monte Carlo [5], - - - Calculated A  $\cos \phi$ .

### c. Skyshine through Vertical Barrier

A calculation missing from the portfolio of theoretical curves in reference [6] would give the barrier factor for the penetration of skyshine through a vertical barrier. In most situations radiation arrives from both above and below the detector plane, and the available wall barrier factor is applicable. Thus in eq (VII.31) the skyshine geometry factor  $G_a(\bar{\omega})$  is multiplied by the wall barrier factor  $B_e(X_e, H)$ . One can imagine situations, however, in tall buildings in urban areas, where skyshine through a vertical wall might provide the dominant contribution to the reduction factor.

Fortunately, there exist some experimental data taken by Burson and Summers [7] which is relevant to this situation. They measured the skyshine barrier factor from a ring source 100 ft in radius. The geometry of their experiment is shown in figure VIII.10. The bunker arrangement was designed to measure both horizontal and vertical barrier factors. The uncollided radiation which would ordinarily reach the detector was eliminated by placing the source in a trough, as shown in the figure. Although the experimental data were taken for a ring source, the measured barrier penetration should be applicable to an infinite plane source. Experimental evidence for the lack of dependence of the skyshine attenuation on radius of a ring source has been presented in great detail by Kaplan [8]. Burson's experimental results for a vertical concrete barrier are shown along with the calculated wall barrier factor curve in figure VIII.11. Since the angular distributions of exposure from uncollided radiation and from skyshine are both independent of the azimuth of the radiation at the wall, and since both are peaked near the horizon, (See fig. V.6) similar penetration curves might be expected. However, the uncollided radiation, which determines the shape of the wall barrier curve in figure VIII.11 has the energy of the source radiation, while the skyshine

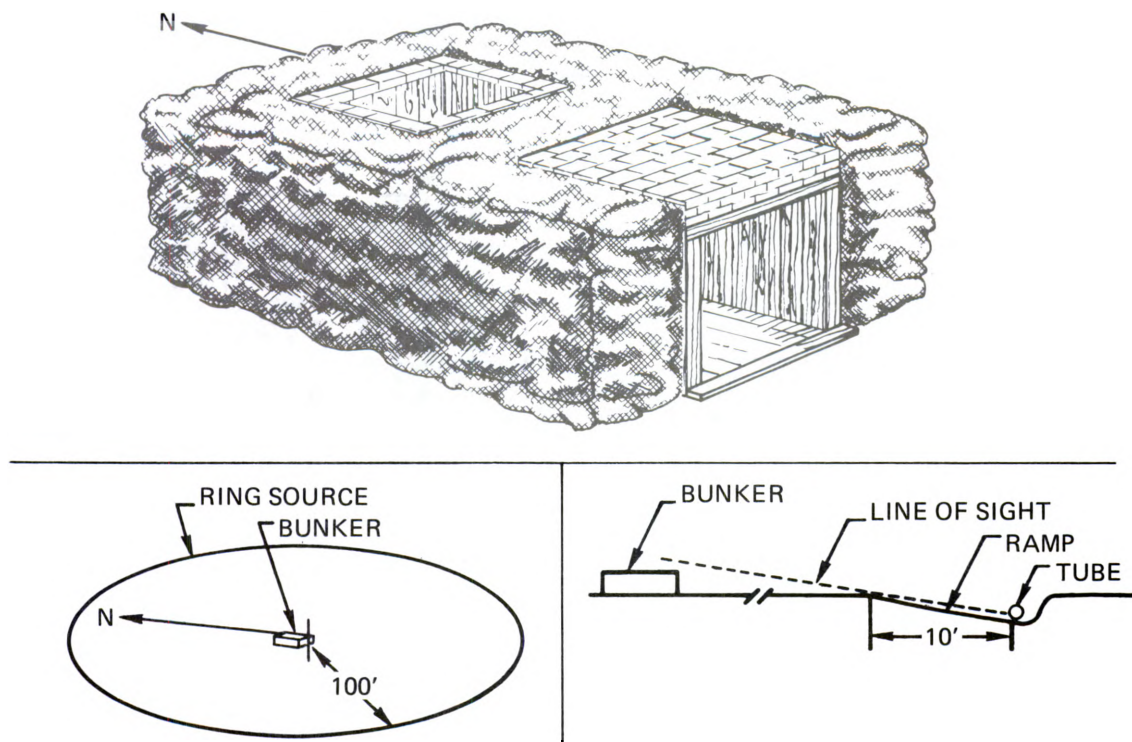
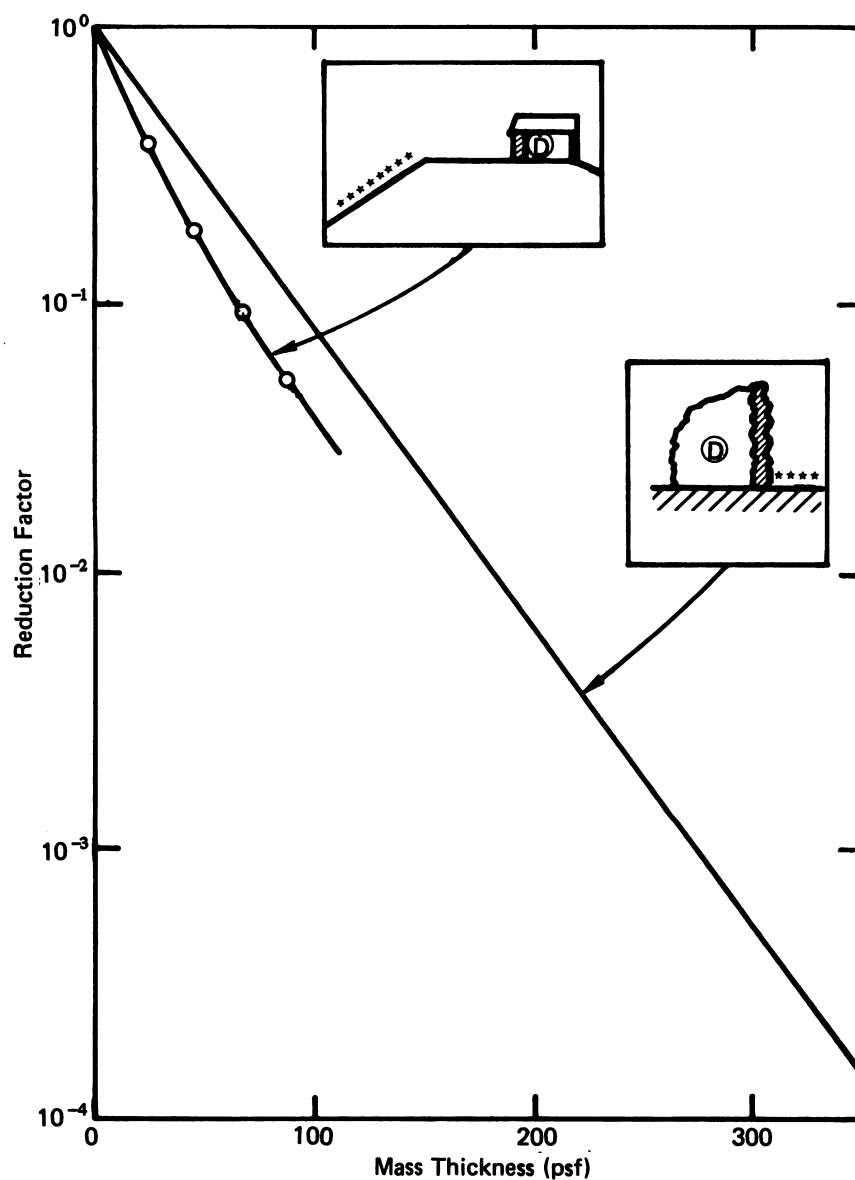


FIG. VIII - 10

VIII.10 Schematic Drawings of the Bunker Assembly and Source Arrangement Used to Measure the Penetration of Skyshine Radiation from a  $^{60}\text{Co}$  Ring Source.



VIII.11 Comparison of Experimental and Calculated Reduction Factors for the Penetration of Skyshine Radiation from a  $^{60}\text{Co}$  Source through a Vertical Wall, —○— Experimental, Burson and Summers [7]; ——— Calculated  $2W(X \sim 3 \text{ ft})$  (Fig. V.65)

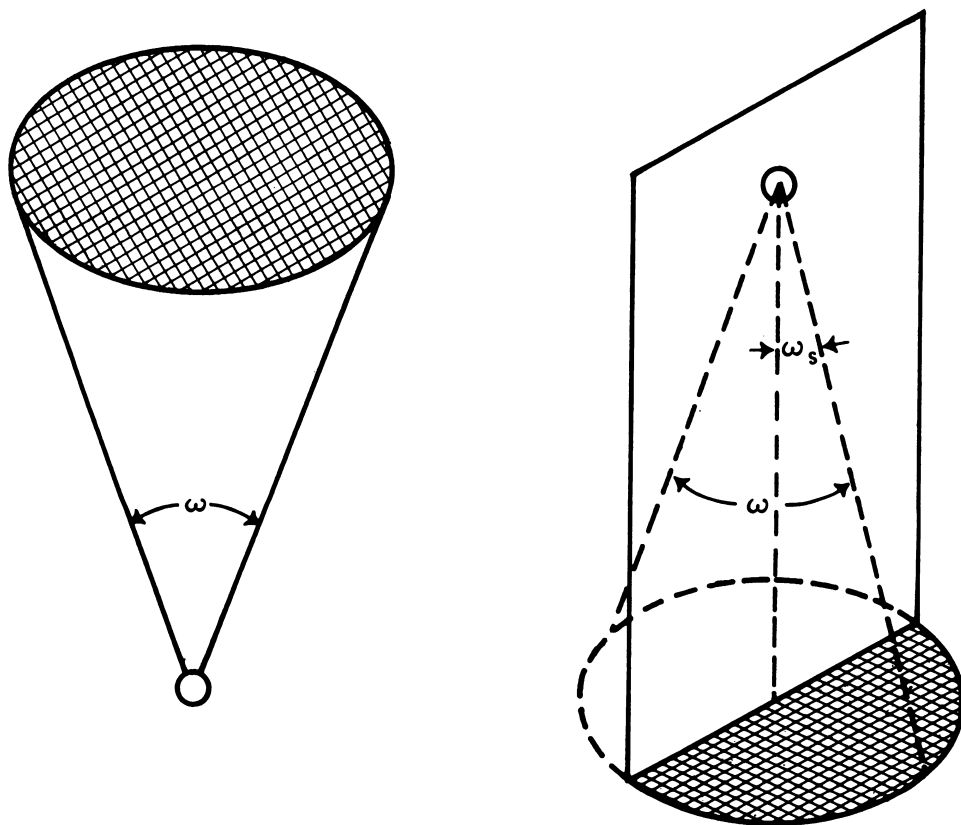
spectrum has more radiation at lower energies. The skyshine should therefore be less penetrating. The curvature of the experimental curve for penetration of skyshine radiation near zero mass thickness in figure VIII.11 is probably due to the filtering out of the low energy components of the spectrum as the thickness of the wall is increased. At deeper penetrations the trends appear to be roughly parallel, consistent with dominance of the horizontal components of the skyshine.

## 2. Barrier Factor, Finite Sources

Calculations of the contribution from limited sources of ground contribution will be discussed in section IX.B.1. There it will be seen that the contribution from wall-scattered radiation depends on a barrier factor  $B_s(X_e, 2\omega_s)$  for a wall of thickness  $X_e$  and a solid angle fraction of  $\omega_s$  subtended by the source. Since in practice, experimental barrier factors for finite sources of various sizes were often obtained in order to estimate the infinite-field barrier factor, it seems reasonable to discuss finite sources in this chapter.

The parameter used to describe the finite size of a roof source is the solid angle fraction  $\omega$  subtended at the detector by the source. The fundamental penetration data were computed for circular disk sources. In a similar manner, the finite extent of a ground source can be described by the solid angle fraction subtended at a point on the wall by the source array. Corresponding penetration data were calculated for semi-circular disk sources whose diameters coincide with the wall at ground level. Figure VIII.12 shows the two situations. The solid angle fraction  $\omega_s$  subtended by the source is arbitrarily defined to be equal to one-half of the solid angle fraction  $\omega$  subtended by the full circular disk source. The maximum value of  $\omega_s$  is therefore 1/2.



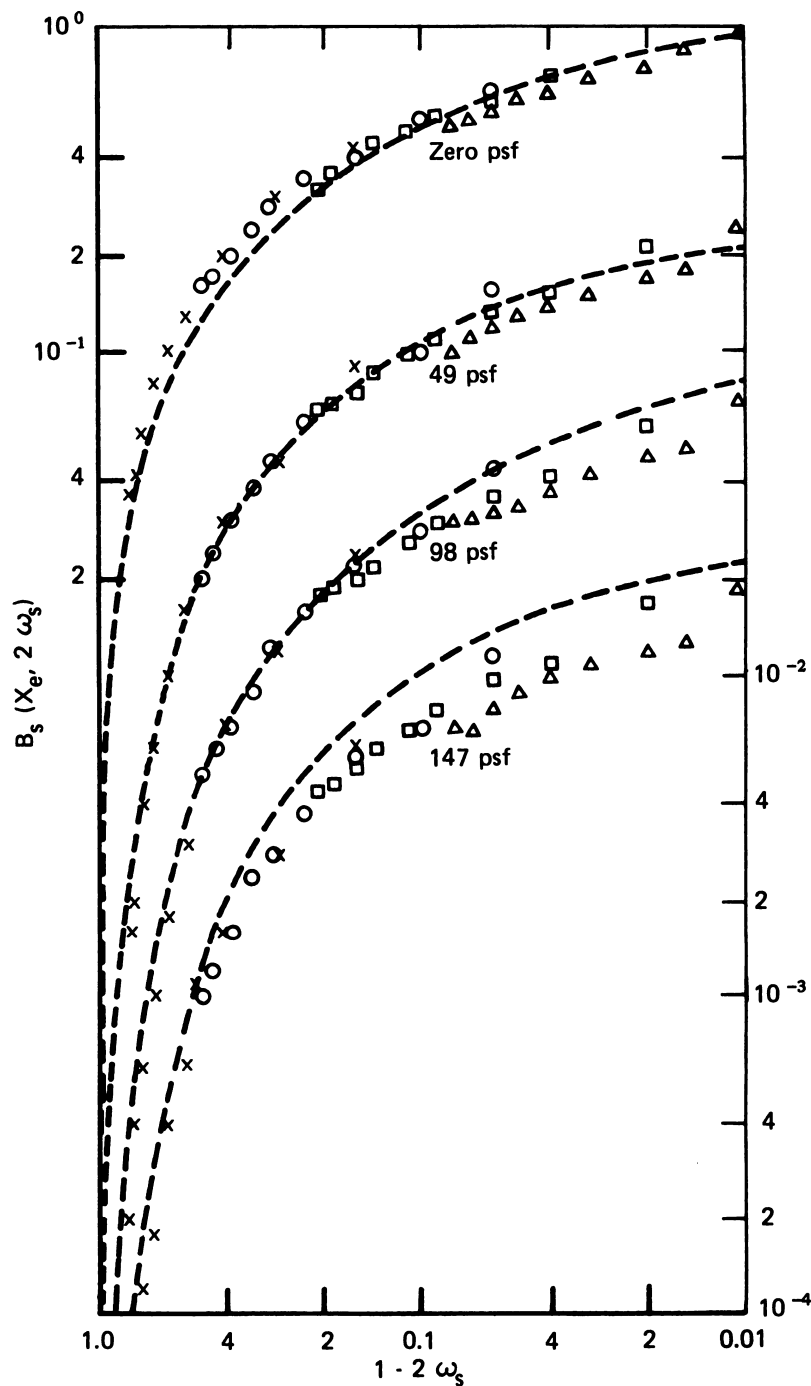


VIII.12 Schematic Drawing Showing the Definition of  $\omega$  for a Roof Source and the Definition of  $\omega_s$  for a Ground Source

A comparison between experimental values reported by McDonnell et al [3] and values of the barrier factor calculated by the Standard Method are shown in figure VIII.13. Data are presented for source distributions subtending a solid angle fraction  $\omega_s$ , for wall thicknesses of 0, 49, 98, and 147 psf, and detector heights ranging from 3 to 33 ft. In order to emphasize the region in which  $2\omega_s > 0.9$ , the abscissa  $(1-2\omega_s)$  was plotted on a semi-log scale, increasing to the left. The parameter  $\omega_s$ , therefore, increases to the right. Each symbol corresponds to a different source annulus. The clustering of symbols along fairly definite curves demonstrates that the solid angle fraction subtended at a point on the exterior of the wall at detector height is a useful parameter for this problem. This clustering would also occur if the results were plotted against the parameter  $W_c/H$ , where  $W_c$  is the radius of the semi-circular source, and  $H$  is the detector height. The parameter  $W_c/H$  has been used in analyzing results on multistory steel models discussed in section X.B.

Both calculated and experimental curves in figure VIII.13 show the same strong dependence of the barrier factor  $B_s$  on the size of the source area. The main effect in reducing the barrier factor at small solid angles is merely the reduction in the number of sources. If this were the only effect, however, the curves for different mass thicknesses would be parallel. The steeper fall of the three lower curves, compared to the curve for  $X = 0$ , indicates that penetration through the barrier is also influenced by the variation in the angle of the incidence of the radiation on the wall with the solid angle subtended by the source area.

One difficulty in comparing this experiment with calculations is that the semi-circular source annuli in the experiment were concentric about the center of the structure, while the calculated solid angle fraction  $\omega_s$  is assumed to be an integral over semicircular annuli concentric about a point on the wall.



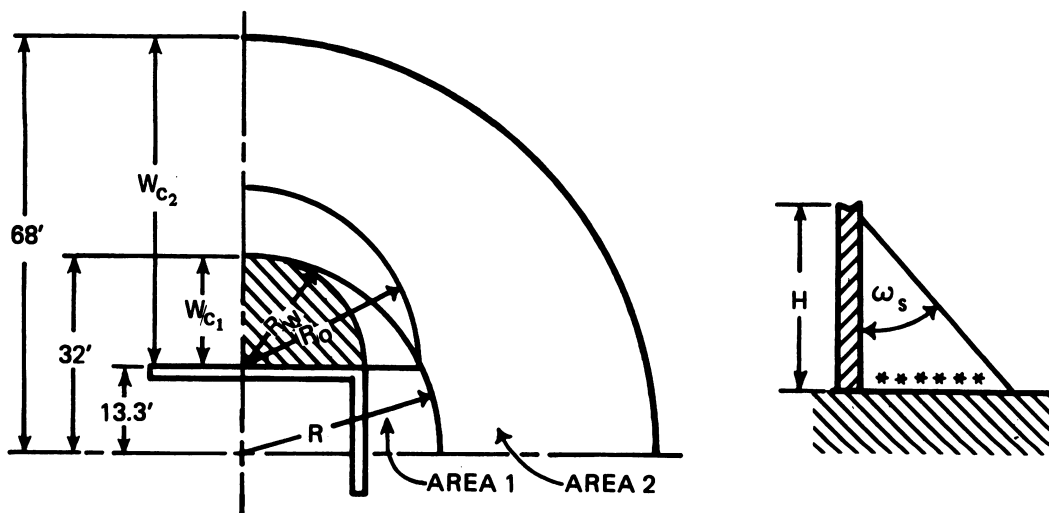
VIII.13 Comparison of Experimental and Calculated Wall Barrier Factors for Finite Semi-Circular Sources of  $^{60}\text{Co}$  Radiation. Experimental, McDonnell and Velletri [13]: X Source Radius = 32 ft; O Source Radius = 68 ft; □ Source Radius = 164 ft; Δ Source Radius = 452 ft.

Figure VIII.14 shows the experimental geometry for the two inner source areas. The source annuli are large enough compared with the size of the structure that the difference is negligible except for the innermost annulus. In plotting the experimental data, an average solid angle fraction for the innermost area was defined by

$$2\omega_s = 1 - \frac{1}{2} \left[ \frac{H}{\sqrt{H^2 + R_w^2}} + \frac{H}{\sqrt{H^2 + R_o^2}} \right] \quad (\text{VIII.6})$$

Another complication in the comparison is that the experiments were made with  $^{60}\text{Co}$  sources, but the only calculation available for this geometry was made for the one-hour fission-product spectrum. To estimate the effect of the difference in source spectra, we can compare the values of the infinite field barrier factor  $W(X,H)$  for the two source spectra. For  $X = 147$  psf and  $H = 3'$ , the value for the fission spectrum is .0165 while that for  $^{60}\text{Co}$  is .0135. Therefore, the  $^{60}\text{Co}$  experimental data for  $2\omega_s \approx 1$  should be lower than the data calculated for the fission spectrum by about 20%. In addition, the experimental data for  $X = 147$  psf should be lower than calculated values by another 20% for larger solid angles, if they are to be consistent with the discrepancy noted for the infinite field data. Thus, for a wall thickness of 147 psf, a total discrepancy of about 40% is expected between experimental values for  $^{60}\text{Co}$  gamma rays and calculated values for fission product gamma rays. This is about the discrepancy observed for  $2\omega_s \approx 1$  near the right hand side of figure VIII.13.

In practical situations, limited fields are apt to be rectangular rather than circular. In the Standard Method rectangles and semi-circles are equated on the basis of the solid angle subtended at a point on the wall, at detector height. Nevertheless, rectangles of the same solid angle but of



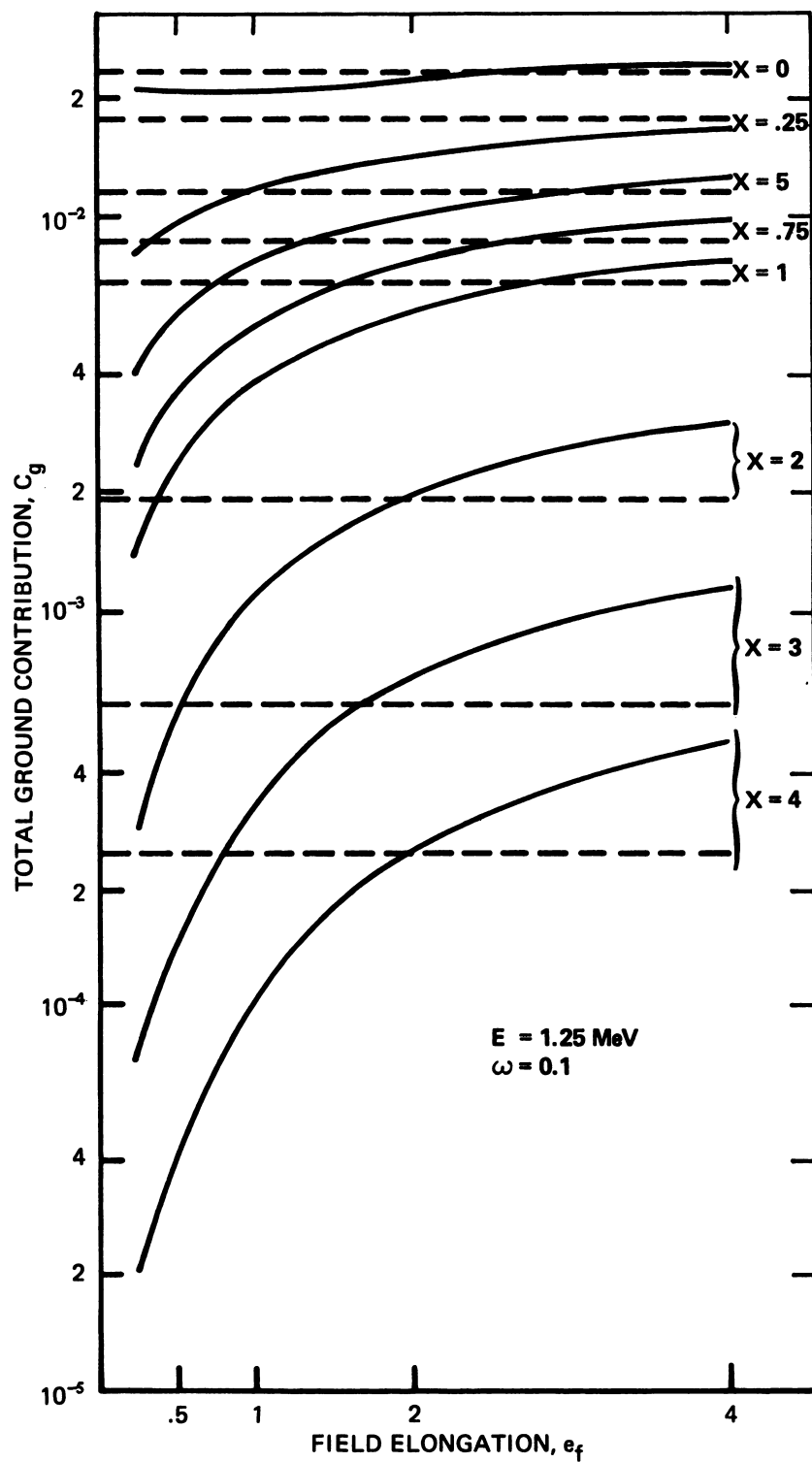
VIII.14 Schematic Drawing Showing How a Quarter-Circle Centered on a Wall is Related to a Quarter-Circle Centered on the Building.

different shape might be expected to produce a different barrier factor. Although there are no systematic experiments to study the effect of the shape of the source area on the barrier factor, the CONSTRIIP program has been used to evaluate this effect [9]. Results for a comparatively small source ( $\omega = 0.1$ ) as a function of the field elongation are shown in figure VIII.15. The field elongation  $e_f$  is defined as the width of the source (perpendicular to the wall of the building) divided by the length of the source along the building. Values of  $e_f$  less than unity are probably of more practical interest since sidewalks and streets around buildings fall into this class. The thickness of the wall is given in units of mean free paths (one mean free path  $\approx 3$  inches of concrete for  $^{60}\text{Co}$  radiation). The results from the CONSTRIIP calculation show that when the solid angle fraction subtended by the source is kept constant, the exposure rate increases with increasing elongation of field. The dashed lines were calculated by the Standard Method, taken in the limiting case of a detector adjacent to the wall:

$$C_g = 0.5 S_w(X_e) B_{ws}(\omega_s, X_e) + 0.5 [G_d(0, H) - G_d(2\omega_s, H)] \times [1 - S_w(X_e)] B_e(X_e, H)$$

For fixed values of  $\omega_s$  there is no provision for dependence on  $e_f$ . For values of  $e_f < 1$ , this expression predicts higher exposure rates than the more accurate CONSTRIIP calculation.

These data show that for different shaped source areas, specification of the wall thickness and solid angle fraction are not sufficient to determine the wall barrier factor accurately. In addition, some specification of the shape of the field is necessary. In view of the fact that the Standard Method gives a conservative prediction of the exposure rate for shapes of practical interest (i.e.  $e_f < 1$ ), no attempt has been made to generalize the barrier factor to a dependence on the shape of the source.



VIII.15 Calculated ground contributions from finite rectangular sources subtending a solid angle fraction of 0.1 at the detector as a function of the width-to-length ratio  $e_f$  of the rectangle. — CONSTRIIP [9]; - - - Standard Method.

## D. SIMPLE BLOCKHOUSE

### 1. NDL Experiments

A "simple" blockhouse is defined in section VII.A as a rectangular parallelepiped with no significant structural floors or partitions. Thus, a simple blockhouse may contain a volume dug out below grade, but it may not contain what is usually called a basement ceiling.

During 1957, Spencer of NBS and Lindwarm of Edgewood Arsenal, recognizing the need for experimental verification of computational procedures then under development, planned a series of experiments using a simple square concrete blockhouse 12 ft on a side and 8 ft high. It contained 2 ft x 2 ft windows centered in three of the walls. These were filled with concrete blocks for most experiments. The fourth wall had a 2 ft x 6 ft doorway. Because this was the first structure built specifically for structure shielding experiments it is of special interest and is shown in figure VIII.16, which is a reproduction of the only available photograph of the blockhouse. Two sides with filled-in windows can be seen at the upper center of the figure. The plastic tubing used in later experiments with this blockhouse is evident in the figure. Although the blockhouse contained a one cubic foot hole dug out in the center, it was essentially an above-grade facility. Measurements in the hole at one ft below grade were analyzed only for roof sources.

#### a. Roof Source

The fallout source on the roof was simulated by a grid of point sources spaced at 2-foot intervals. The symmetry of the structure and the detector locations made it possible to confine the sources to one eighth of the roof's surface. A comparison of experimental results with the  $L(X) L_a(X, \omega)$  function is shown in Table VIII.2, taken from reference [10]. The table shows reduction factors for  $^{60}\text{Co}$  and  $^{137}\text{Cs}$  sources for five different roof thicknesses and





VIII.16 Photograph of First Concrete Blockhouse Built at the U.S. Army Chemical Center to Study Structure Shielding.





detector heights of 6 ft, 3 ft, 0 ft, and -1 ft above the ground at the center of the structure. The calculations and experiment agree in most cases to better than 20%. The uncertainty on the experimental results is at least 10% and probably as much as 20%. The two main sources of this uncertainty are the relatively coarse spacing of the point sources at 2 foot intervals and the presence of a steel I-beam which supported the roof.

b. Ground Source

The fallout source on the ground was simulated by a grid of point sources which were spaced at intervals of 2 ft in areas close to the blockhouse. The grid size was doubled at each distance  $\rho_i$  from the center of the blockhouse given by

$$\rho_i \approx 12 \times 2^i \text{ ft, } i = 0 \text{ to } 5$$

Measurements were made for sources at distances out to 400 ft. Here again, symmetry considerations made measurements necessary over only one eighth of the plane surrounding the blockhouse.

When these measurements were made, the pumped source had not yet been developed and measurements of exposure for many of the source points required hours of running time. Remote handling was required for the high intensity sources. The source was blown by air pressure out of a lead pig and up into a vertical plastic tube. The whole apparatus was then tilted so that the source in the top of the tube could be placed arbitrarily close to the ground.

This experiment was extremely timely because it provided measurements which could be compared with the calculational procedures which were being developed concurrently. One consequence was that experiments with ground sources reinforced the decision to include a shape factor (See section VIII.E)

in the Standard Method calculation of contributions from ground sources. Although the concept of a shape factor applied to the wall-scattered radiation alone is awkward, it was necessary in order to produce reasonable agreement with the NDL experimental results. The comparison [11] given in Table VIII.3 shows that the experimental and calculated values are generally consistent to within  $\pm 20\%$ . However, if the eccentricity factor  $E_s(e)$  had been omitted in the calculations, the calculated values would be considerably lower. For example, the expression for  $E_s(e)$  in eq (VII.25) gives a value of  $\sqrt{2}$  for a square building. Therefore the calculated values for thick walls, where the contribution is primarily from scattered radiation, would be consistently lower by about 30%, and the agreement with experiment would not be nearly as good.

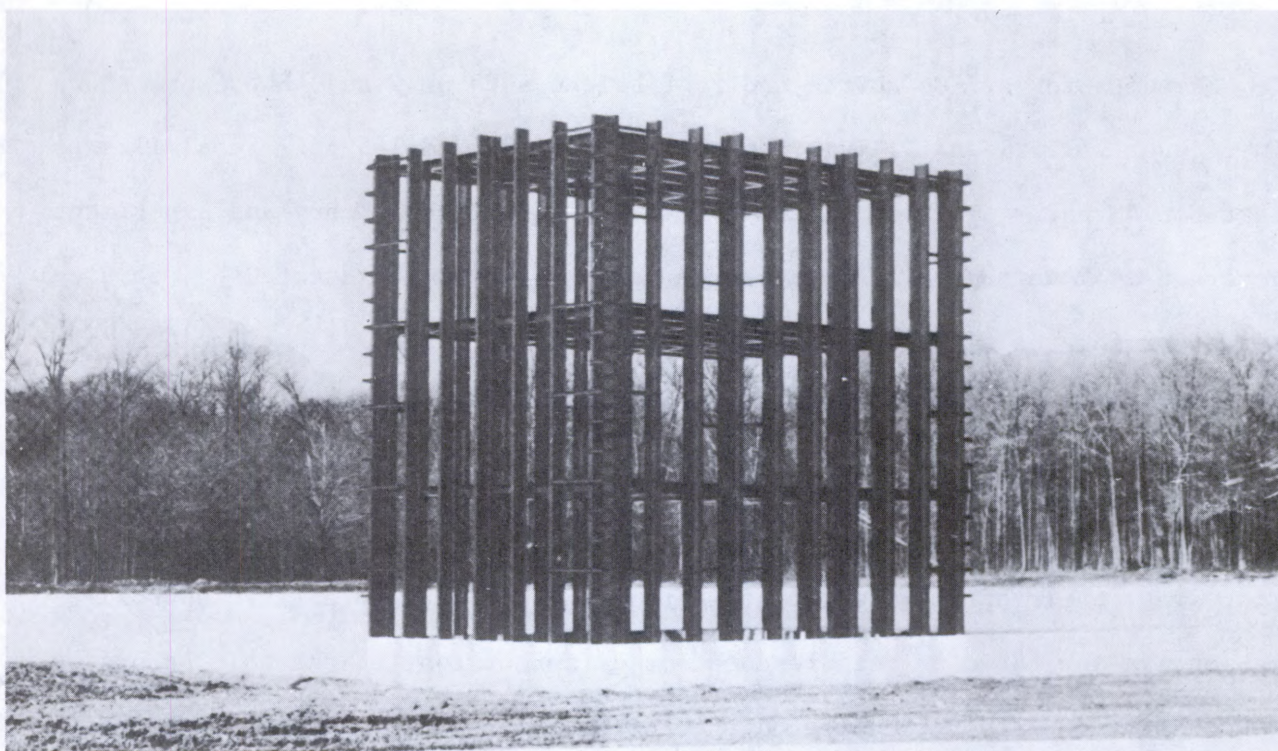
## 2. RTF Experiments

### a. Roof Source

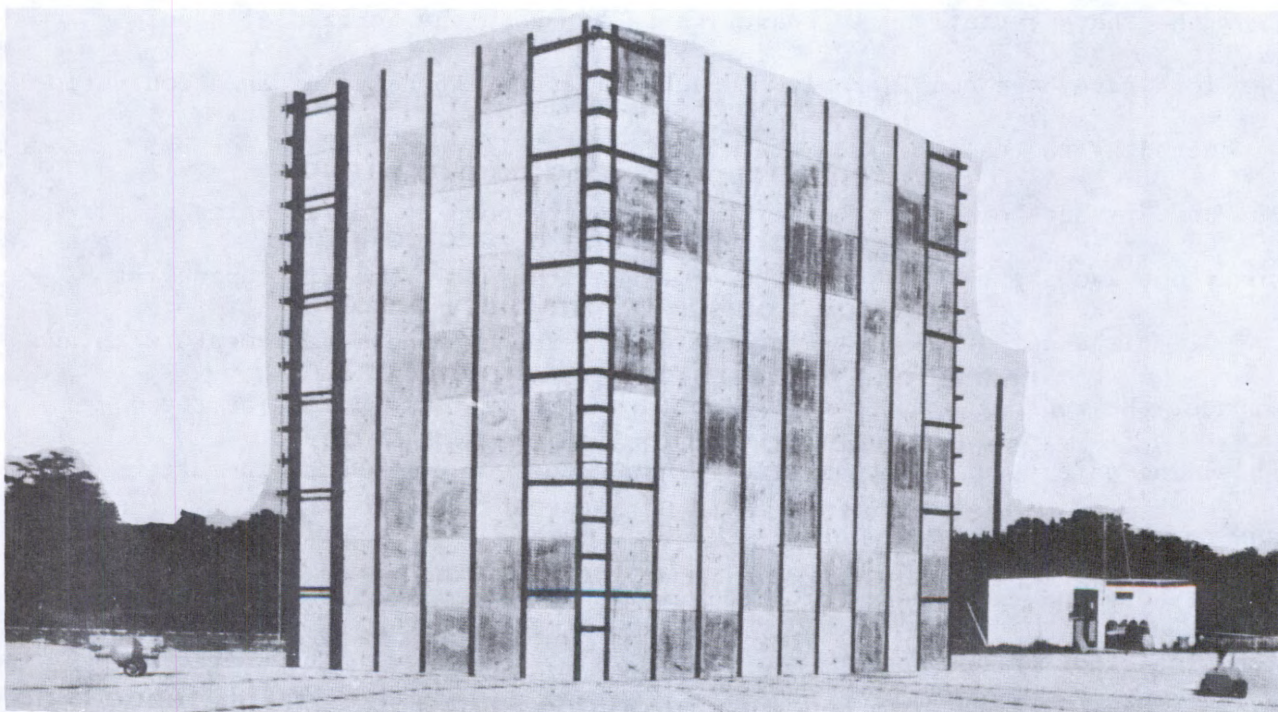
Later experiments on a simple blockhouse were made by McDonnell and Velletri [3] and Spring and McDonnell [12] at the Radiation Test Facility at Fort Belvoir, Virginia. Their earlier results for an idealized roof agreed very well with calculations (see sec. VIII.A.2). However, when experiments were made on more realistic configurations, the agreement was not nearly as good. In the more realistic configuration the roof was rectangular rather than circular. More important, the roof slab was supported by a system of iron beams (see fig. VIII.17) which made the structure wonderfully safe and secure but made it more difficult to analyze from the shielding standpoint. Although this structure was somewhat of a caricature of a practical structure, most modern structures do indeed have a steel skeleton.

TABLE VIII.3 Experimental and Theoretical Wall Contributions for Center Detector Positions [11]

Detector Height (feet)	Wall Thickness					
	48 psf		93.7 psf		139 psf	
	Experimental	Theoretical	Experimental	Theoretical	Experimental	Theoretical
<u>COBALT-60</u>						
6	0.26	0.24	0.096	0.084	0.029	0.030
3	0.28	0.30	0.10	0.11	0.033	0.036
0	0.22	0.26	0.071	0.096	0.022	0.032
<u>CESIUM-137</u>						
6	0.18	0.15	0.046	0.039	0.0097	0.0088
3	0.20	0.19	0.050	0.048	0.011	0.011
0	0.13	0.16	0.035	0.044	0.0085	0.010



(a)

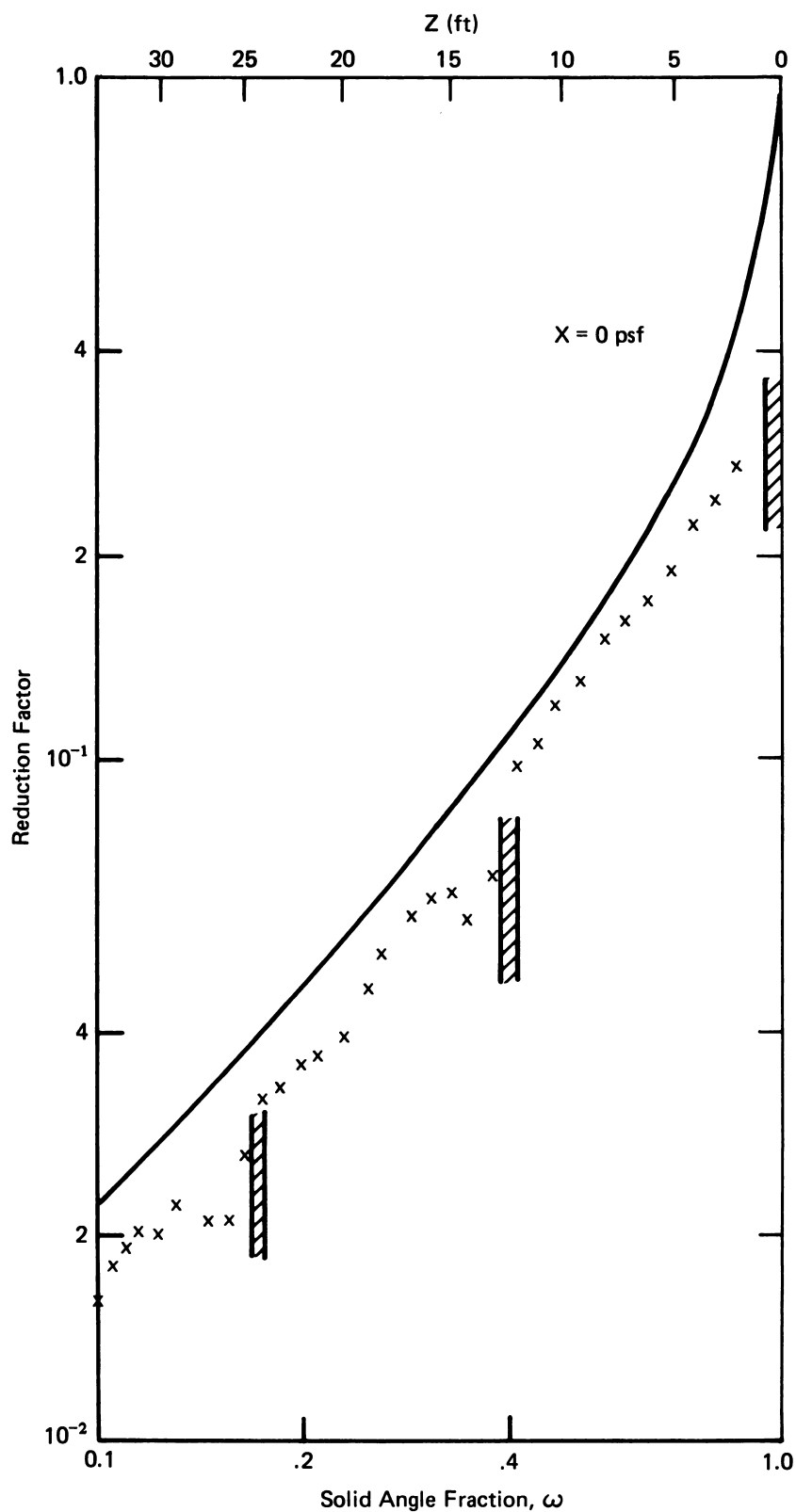


(b)

VIII.17 Photograph of the Three Story Structure at the Radiation Test Facility, Fort Belvoir, Virginia. (a) Steel Skeleton; (b) Structure Covered with Concrete Wall Panels.

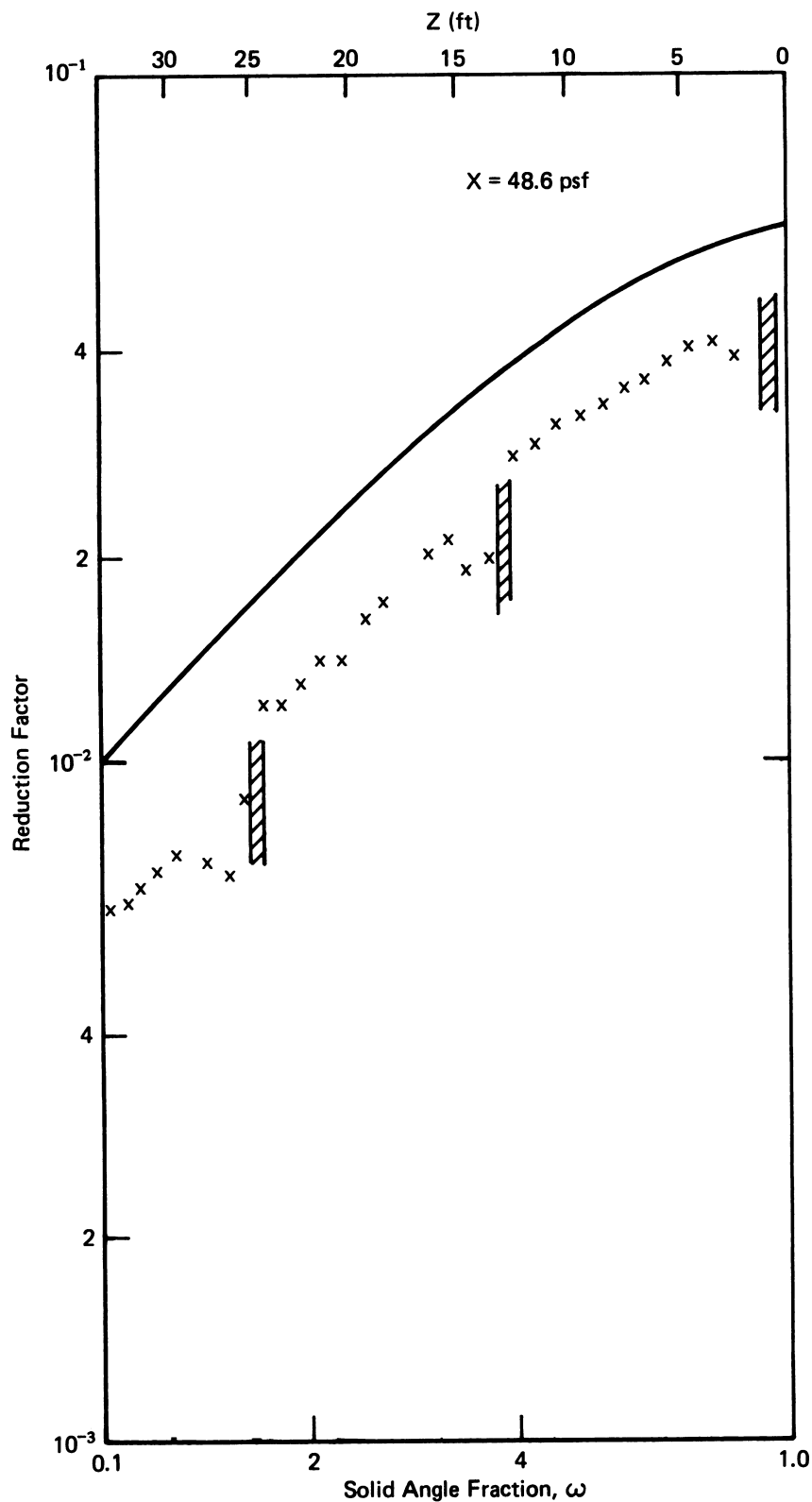
Results for a  $^{60}\text{Co}$  source and roof thicknesses of 0 and 48 psf are shown in figures VIII.18 and VIII.19. Comparison for 97 and 145 psf are similar to that for 48 psf. At first glance the agreement between theory and experiment does not look very good. However, the mass thickness represented by the steel beams forming the first, second, and third floor ceilings is not included in the calculations. Some procedures for estimating the shielding due to steel beams were discussed in section VII.D.6. Since the horizontal steel beams were present in the structure, independent of the thickness of the concrete roof slab, their effect might be expected to disappear, to a first approximation, in any ratio of measurements for different roof thickness. Accordingly, McDonnell and Velletri considered the ratio of detector responses at each location for a concrete roof thickness of  $X$  and a concrete roof thickness of zero. Their ratios are shown in figure VIII.20. It is clear from this figure that the sharp variations in reduction factor near the horizontal steel barriers have been considerably reduced. The corresponding attenuation ratios predicted by the calculations are shown in the figure as dashed curves. The comparison shows that the agreement is very good at solid angles near unity but grows progressively worse for small angles. The discrepancy at  $\omega = 0.1$  is about 40%. By taking ratios of experimental measurements with and without the roof slab in place the authors have eliminated most of the shielding effects of the beam structure and thereby emphasized the attenuation due to the concrete roof slab.

Theory and experiment both indicate that the attenuation is a strong function of detector position for a given slab thickness. The shielding effectiveness of the roof is four to five times greater for  $\omega \approx 1.0$  than it is for  $\omega \approx 0.1$ . This is because a detector near  $\omega = 1$  responds to radiation from a large range of angles whereas a detector near  $\omega = 0.1$

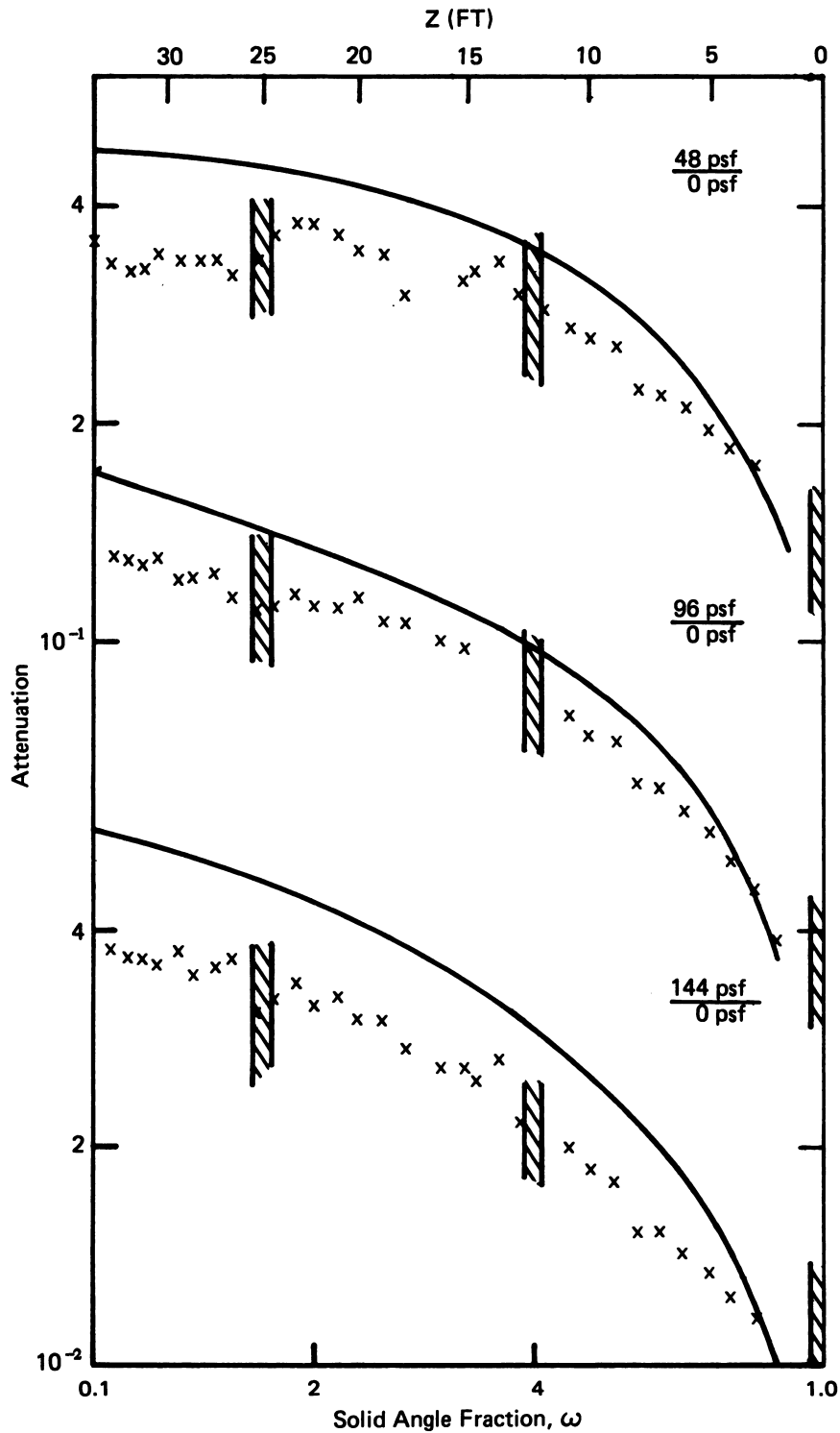


VIII.18 Comparison of Experimental and Calculated Reduction Factors for a Rectangular Roof Source of  $^{60}\text{Co}$  Radiation and a Roof Thickness of Zero.  $\times$  Experimental, Spring and McDonnell [12]; — Calculated,  $L(0) L_a(0, \omega)$  (Fig. B11a). Hatched areas indicate location of floor support beams.





VIII.19 Comparison of Experimental and Calculated Reduction Factors for a Rectangular Roof Source of  $^{60}\text{Co}$  Radiation and a Thickness of 145.8 psf  
 X Experimental, Spring and McDonnell [12]; — Calculated,  
 $L(145.8) L(145.8, \omega)$  (Fig. V.79). Hatched areas indicate location of floor support beams.



VIII.20 Comparison of Experimental and Calculated Attenuation Factors for a Rectangular Roof Source of  $^{60}\text{Co}$  Radiation. X Experimental, Spring and McDonnell [12]; — Calculated  $[L(X) L_a(X, \omega)]/[L(0) L_a(0, \omega)]$ . Hatched areas indicate location of floor<sup>a</sup> support beams.

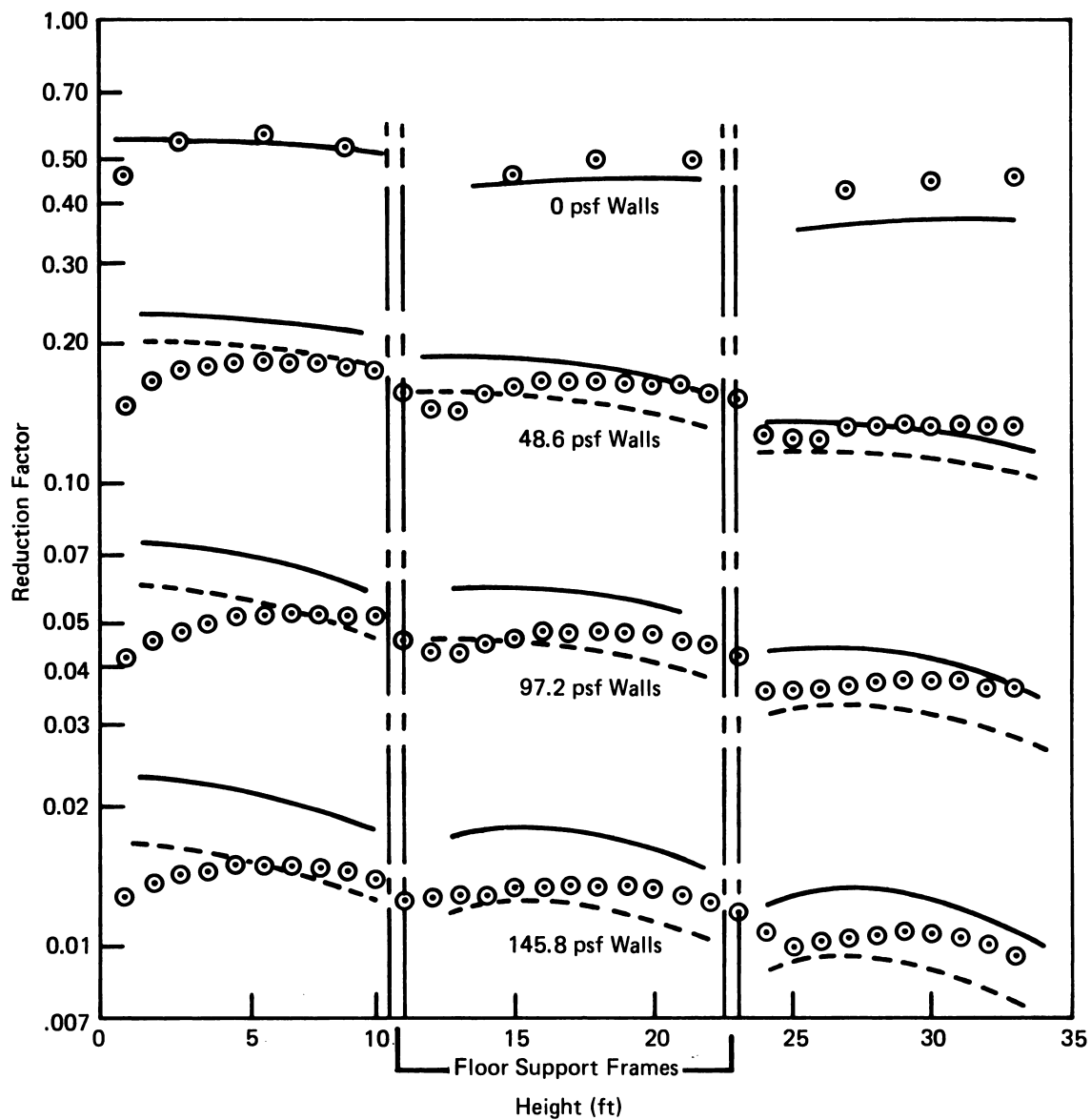
responds only to radiation traveling in nearly a vertical line. The latter penetrates more effectively through a horizontal barrier than does the more diffuse radiation arriving at detectors near the source.

The gradual divergence between theory and experiment as the solid angle fraction decreases is difficult to explain. However, the fact that the relative discrepancy is about the same for all three mass thicknesses suggests that the measurement for zero mass thickness may be the source of the difficulty. The measurements at zero thickness may contain a strong component of radiation scattered from the steel skeleton, whose relative importance increases with decreasing solid angle. This interpretation suggests that the relatively good agreement between theory and experiment in figure VIII.18 may be fortuitious. Under this hypothesis, the experimental data would be assumed to contain a positive component due to scattering from the steel beams, which largely disappears when a roof slab is inserted, and a negative component due to line-of-sight attenuation in the steel beams, which persists when a roof slab is added. Further experiments to determine the cause of the discrepancy in attenuation were never carried out.

#### b. Ground Source

Measurements on the three-story structure were also made with ground sources [13]. Reduction factors as a function of height at the center of the structure are shown in figure VIII.21. Results are shown for no concrete walls and for walls of three different thicknesses. Since these measurements were taken at the center of the structure and not adjacent to the wall, they include both barrier and geometry effects.

The solid curves in figure VIII.21 were calculated using the measured mass thickness of the exterior walls. Earlier experiments conducted at the same facility and discussed in section VIII.C.1 seemed to show that better



VIII.21 Comparison of Experimental and Calculated Reduction Factors as a Function of Height for a  $^{60}\text{Co}$  Source Distributed on the Ground and for Walls of Varying Thickness.  $\odot$  Experimental, McDonnell and J. Velletri [13]; Calculated: —  $B_e(X_e, H)$ , ---  $B_E(1.08 X_e, H)$  (See Chart C.6)

agreement between theory and experiment could be obtained if the mass thickness used in the calculation was assumed to be 8% greater than the measured mass thickness. The dashed curves were obtained by assuming the incremented mass thickness.

There were no interior concrete floors or walls in this experiment. In reality, however, the steel beams contained in the structure formed a combination of pseudo-floors and walls within the structure.<sup>1</sup> Calculated values of the reduction factor require some assumption about how to estimate the effect of the steel beams. In section VII.D.6 possible assumptions were discussed. If the mass in the horizontal steel beams constituting each pseudo-floor is assumed to be uniformly distributed over the floor area, the effective thickness of the floor is found to be 9.6 psf. The attenuation in the beam can also be estimated according to their relative area. The calculated reduction factors shown in figure VIII.21, however, accounted for the attenuation in the beams not by their relative area, but, rather, by the solid angle fraction which they subtended. The correction was obtained by considering the floor to be made up of portions whose thickness was equivalent to the mass thickness of the steel beams and portions with zero mass thickness. The calculated contribution from the wall of the story below the detector position was multiplied by a correction factor of the form

$$\frac{\omega_1 A(X_F) + \omega_2}{(\omega_1 + \omega_2)}$$

where  $A(X_F)$  is the attenuation due to the steel floor beams,  $\omega_1$  is the

---

<sup>1</sup>This structure is not, strictly speaking, a simple blockhouse because of the interior steel beams. However, it is treated here because this experiment was designed to approximate a simple blockhouse.

solid angle fraction subtended by the beams and  $\omega_2$  is the solid angle fraction subtended by floor areas between the beams. The values of  $\omega_1$  and  $\omega_2$  are different for each detector position. The effect of beams forming the pseudo-walls was neglected in the calculations.

A study of figure VIII.21 shows that the calculation by the Standard Method, using the incremented wall thickness, gives a good prediction of experimental results with ground sources over a range of reduction factors down to  $\approx .01$ . The experimental results for the second and third story generally show less variation with height than predicted by theory. The discrepancy between experiment and calculations is particularly pronounced near the floor of the first story. The calculations are high in this region because they include the effect of the sharp peak in the uncollided radiation in the near-horizontal direction (see fig. V.33). The low values of the measurements in this region seem to indicate that this peak is not present in the experimental situation. The most likely reason for the lack of such a peak is that the ground around the structure is not a smooth infinite plane. Even small undulations in the ground will attenuate the uncollided radiation severely.

### 3. Kansas State University Blockhouse

The Summer Institute on Fundamental Radiation Shielding Problems was presented at Kansas State University (KSU) in 1963.<sup>2</sup> An important part of this institute was an experimental program developed and supervised by A. B. Chilton [14] to acquaint the participants with the type of experiments which were underway at several laboratories at that time.

---

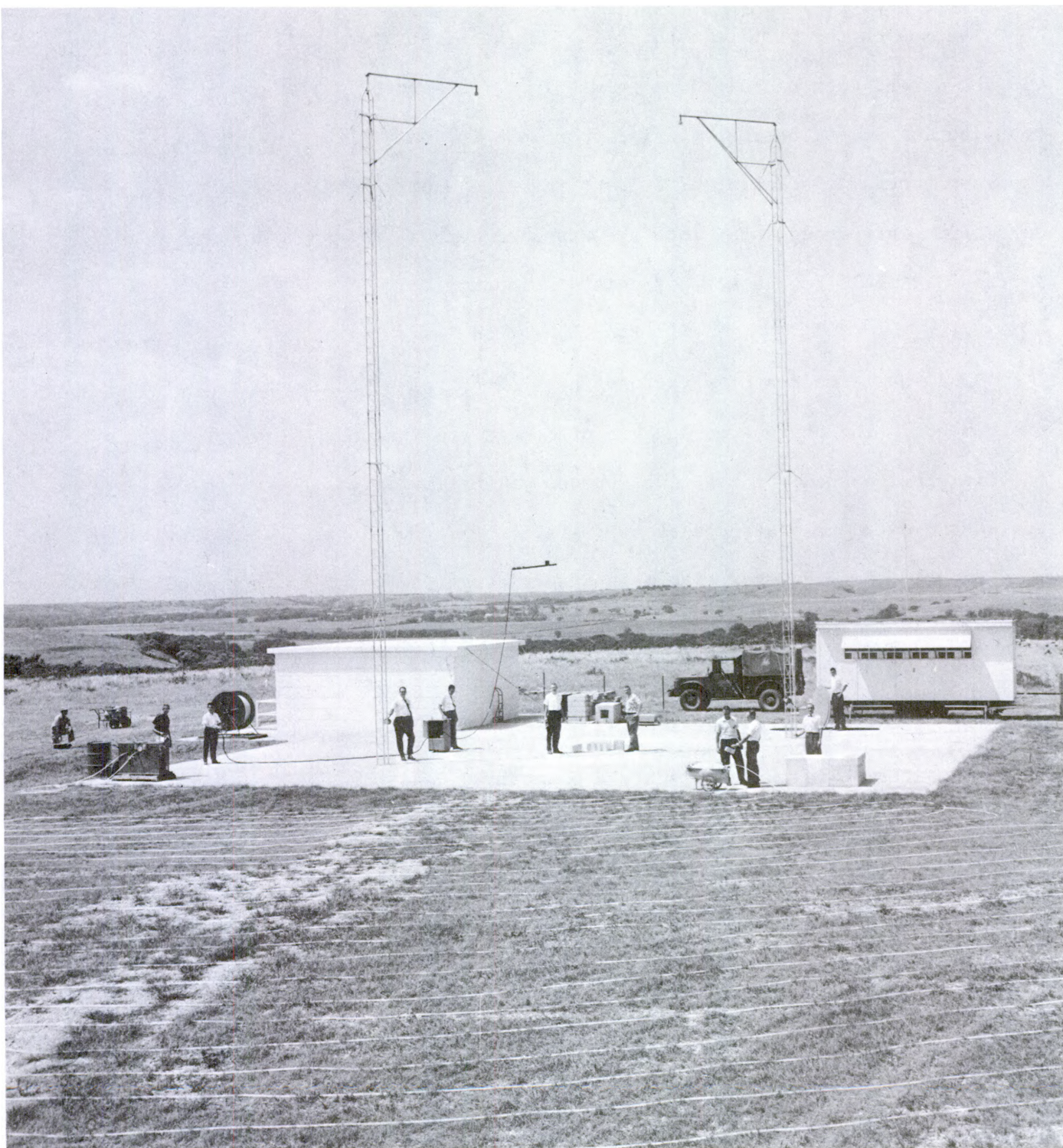
<sup>2</sup>It was the second in a series of institutes which were developed primarily for participants from university staffs in nuclear engineering, applied physics and applied mathematics having as a primary objective, the advancement of participant's experience in the field of Radiation Shielding. The main benefit of these experiments was to familiarize university instructors with the problems inherent in an experimental program of this type.

One of the structures erected for the experimental program was a concrete blockhouse 20 ft x 20 ft with a first story height of 8 ft and a basement height of 8 ft. The walls were 69 psf and the roof and basement ceiling were 55 psf. The blockhouse contained a door and a window. Because the participants had only a few weeks to complete these experiments, the results must be regarded as qualitative. A photograph of the facility with some of the participants is shown in figure VIII.22.

A plane source on the roof of the blockhouse was simulated by 4.6 mCi point sources placed at two-foot intervals over one quarter of the roof. Readings from symmetrical detector locations were used to infer the exposure from the full roof. Measurements were made with 3 scintillation- and Geiger-type survey meters. Roof barrier factors for  $^{60}\text{Co}$  were used to make calculations by the Standard Method. The comparison for detectors on the vertical central line of the blockhouse generally showed agreement between experiments and calculations to within about 20%. Experimental errors were not stated, but it was noted that data from two instruments varied from each other by 3% to 30%. Discrepancies between experiment and calculations for detectors at the sides or corner of the structures varied up to about 100%. The roof contribution in this experiment varied from about .05 on the first floor to .005 in the basement.

A plane source on the ground around the blockhouse was simulated by a tube source laid out in three areas covering a quarter-circular area of 160 ft radius from the center of the blockhouse. Readings from symmetrical detector locations were again used to obtain the result for a circular field. The estimated contribution from sources beyond 160 ft accounted for 20% to 40% of the total exposure on the first story. Instrumentation included Bendix 20R and 200 mR self-reading pocket dosimeters, Landsverk 2R dosimeters, Victoreen 1





VIII.22 Photograph of the Blockhouse at Kansas State University and Some of the Participants in the KSU Summer Institute.



and 10 mR ion chambers and a Tech/Ops charger-reader. The measured ground contribution on the vertical centerline of the first story varied from .15 to .18 and agreed with calculations to within a few percent. The ground contribution in the basement varied from .008 to .004, with the calculated exposure generally a factor of 2 lower than the experimental exposure. A correction introduced later into the Standard Method, and to be described in section X.D would remove most of this discrepancy.

#### 4. Blockhouse Models

Small scale models of structures have often been used in shielding experiments. The obvious advantages of models are that much less construction material is required, radioactive sources of smaller intensity can be used, and source-detector distances of 50 ft rather than 500 ft are sufficient for most experiments. However, the main disadvantage of models is that conditions specified by the scaling theorem in section IV.B.3 can only be satisfied approximately. The scaling theorem requires that the density of every material be scaled by the same factor. However, in almost all model experiments, no attempt was made to scale air density,<sup>3</sup> and the skyshine was therefore almost entirely absent. Generally this introduces about 10% uncertainty in absolute exposure rates and probably less in ratios such as the reduction factor. However in configurations such as a foxhole where there is no contribution from uncollided radiation the skyshine dominates and a scaled experiment becomes impossible. In such situations the experiment must be treated as a full-scale, but small, structure.

---

<sup>3</sup>Clifford [15] made some experiments in which he replaced the air with expanded polystyrene or "Polyfoam" which had a density about 60 times that of air. He used this configuration to study angular-energy distributions and dose in the free field. However, he did not extend his measurements to simple structures.

In most model experiments the scaling ratio has varied between 10 and 12. However, there is no low-Z material with a density of 10 or 12 times that of concrete. In practice, steel, which is about 3.3 times that of concrete, has often been used. The scaling ratio on the mass thickness has therefore been different from that on geometrical parameters. This difference in the scaling ratio has generally been regarded as acceptable provided that the linear dimensions of the "rooms" in the model are at least 10 times the linear thickness of the model walls.

A third component that has never been scaled in model experiments is the ground. Again, steel is probably the most practical material to substitute. The effect of not scaling the ground is mainly on the radiation reflected from the ground or transmitted through the edge of a foxhole. Generally, these components scale properly if the linear mean free path of radiation in the ground is small compared with the linear dimensions of the model structure. The scaling problem has been analyzed in detail by F. Verser [16] by means of Monte Carlo studies. He concluded that in experiments where the source radius is scaled, non-scaling of the air introduced a significant error in the skyshine contribution but that the uncollided radiation is correct. On the other hand, if the source radius is left unscaled the skyshine will have the correct magnitude. Concerning the proper identification of the standard unprotected location in a model experiment, he noted:

"The data for a structure that responds to uncollided radiation should be normalized to a scaled detector height ... and a scaled source radius used. If the structure responds only to skyshine (open or covered basement), the data should be obtained using an unscaled source field and normalized to a detector height of 3 ft."

Experiments were made by Schumchyk and Schmoke on two different scale models of the NDL blockhouse. The results of these experiments were never published, but they were transmitted in a private communication to Kaplan, who discussed them and compared them to full-scale results [17].

The two models were 1/12 and 1/3.3 scaled versions of the NDL blockhouse, constructed of steel rather than concrete. Thus, the second model had the same scaling factor on linear dimensions and wall thickness. Wall thicknesses were of 48, 96, and 144 psf (1.2, 2.4, and 3.6 inches, respectively) and the steel roof was 48 psf in thickness. Detectors were placed on the central vertical axis of each structure so that their centers were .25 and .50 ft above ground for the 1/12 scale model and 0.91 and 1.80 ft above ground for the 1/3.3 scale model. Six source areas composed of point sources on a grid array were placed on a scaled version of the grid array described in section VIII.D.1.b.

The data from the model experiments were scaled up by Kaplan and extrapolated to obtain reduction factors for an infinite field. An extract from Kaplan's comparison is shown in Table VIII.4. The data quoted by Kaplan for the full-scale structure are slightly different from those published by Schmoke and Rexroad [11] and given in Table VIII.3. But the differences are smaller than the experimental uncertainties associated with the experiments. The comparison shown in Table VIII.4 indicates that steel models of a simple concrete blockhouse give results which are in reasonably good agreement with data on the full-scale structure. This is one of many experiments which indicated that models could be used to obtain reasonably accurate reduction factors much more conveniently and quickly than experiments on full-scale structures.

TABLE VIII.4 Comparison of Scale-Model and Full-Scale Reduction Factors  
for NDL Blockhouse

Detector Height (ft)	<u>Wall Thickness (psf)</u>		<u>Reduction Factors</u>		
	Steel* Models	Concrete Full-Scale Structure	1/12 Model	1/3.3 Model	Full-Scale
3	48	48	.294	.261	.284
6	48	48	.276	.232	.297
3	96	94	.104	.097	.101
6	96	94	.098	.085	.104
3	144	139	.0323	.0321	.033
6	144	139	.0307	.0281	.034

\*The thickness of steel is the actual mass thickness rather than the effective mass thickness. Although the discussion in section III.A.3 indicates that a factor of 0.93 should be included to convert to mass thickness, penetration data indicate that the actual mass thickness is equally defensible.

## 5. Calculations for Cylindrical Blockhouse

The Monte Carlo method was applied by French et al. [18] to the problem of radiation penetration in a simple blockhouse. A cylindrical blockhouse was studied because azimuthal symmetry simplifies the calculations and because the geometry factor in the Standard Method is simpler for a cylindrical structure. Reduction factors were calculated for circular source annuli with outer radii up to 1600 ft.

An interesting feature of these calculations is the identification of photons in terms of scattering in the barrier or in air. This permitted a comparison with the "thick" and "thin" components of the Standard Method. Comparison showed that the "thick" and "thin" components are not good representations of the components due to collided and uncollided radiation in the barrier, as anticipated in the discussion in section VII.B.1. However, the Monte Carlo results agree well with the weighted "thick" and "thin" results for barrier thicknesses up to 80 psf. The Monte Carlo studies generated data which suggested alternative curves for the geometry functions  $G_s$ ,  $G_d$ , and  $G_u$ .

Reduction factors for infinite plane sources agree within 10% with values calculated by the Standard Method. Reduction factors were also calculated for finite circular source annuli. The Monte Carlo values were about 45% higher than those calculated by the Standard Method for an annular source extending from 10 ft to 25 ft and 30% lower for an effectively infinite field.

## 6. Apertures

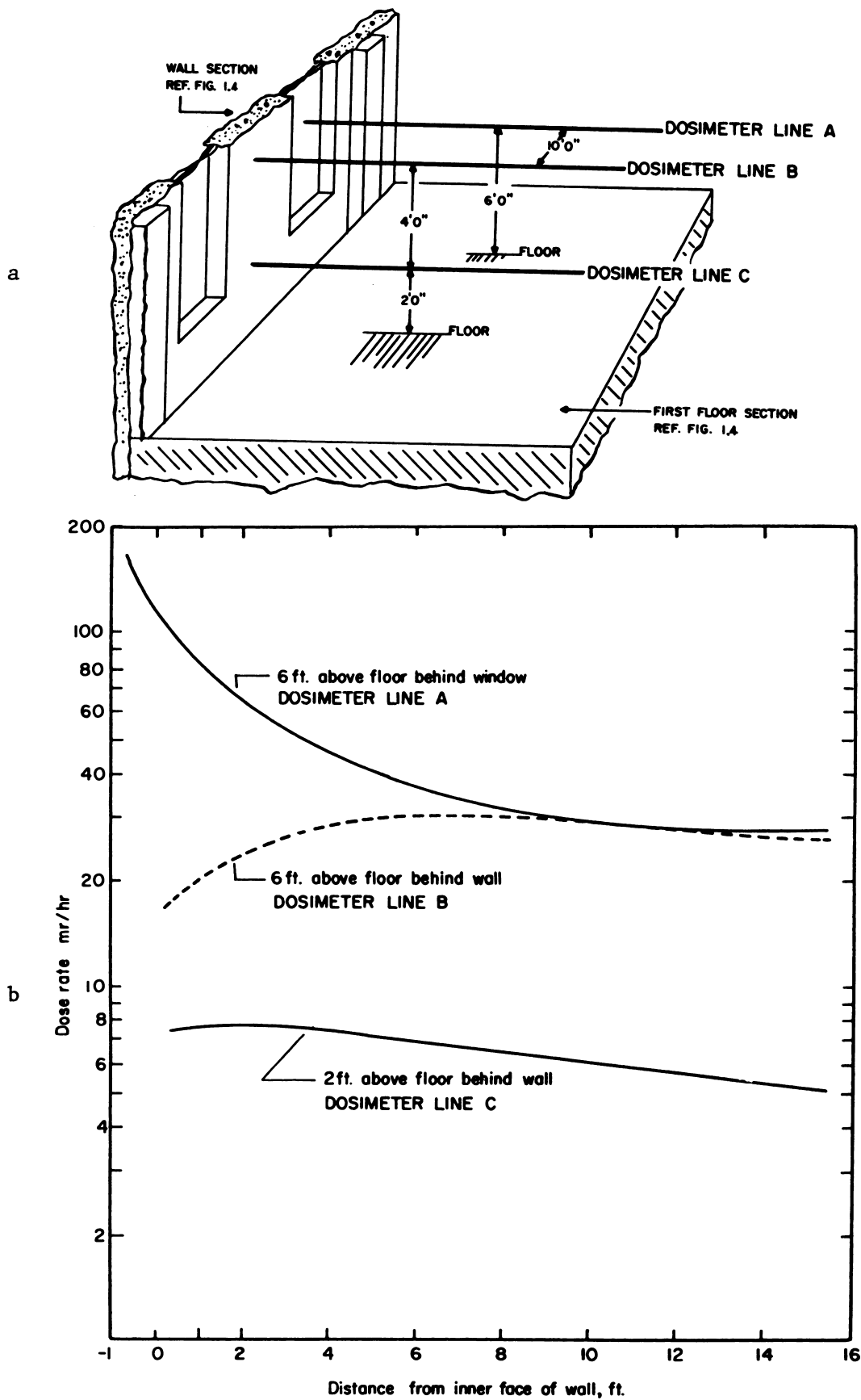
An early investigation [19] of radiation protection in the AEC Headquarters Building at Germantown, Maryland, included a special study of exposure rates near windows. (Discussion of other experiments on this building will be deferred until section X.E.5.) A schematization of the detector arrangement

and some experimental results are shown in figure VIII.23. The top curve in the figure shows the fall-off of the exposure rate as a detector at a height of 6 ft is moved away from the center of a window, the dashed curve shows the behavior as a detector at the same height is moved away from the center of the wall, and the lowest curve shows the lower exposure rate received at a detector height just below sill level. From these measurements, the authors conclude that:

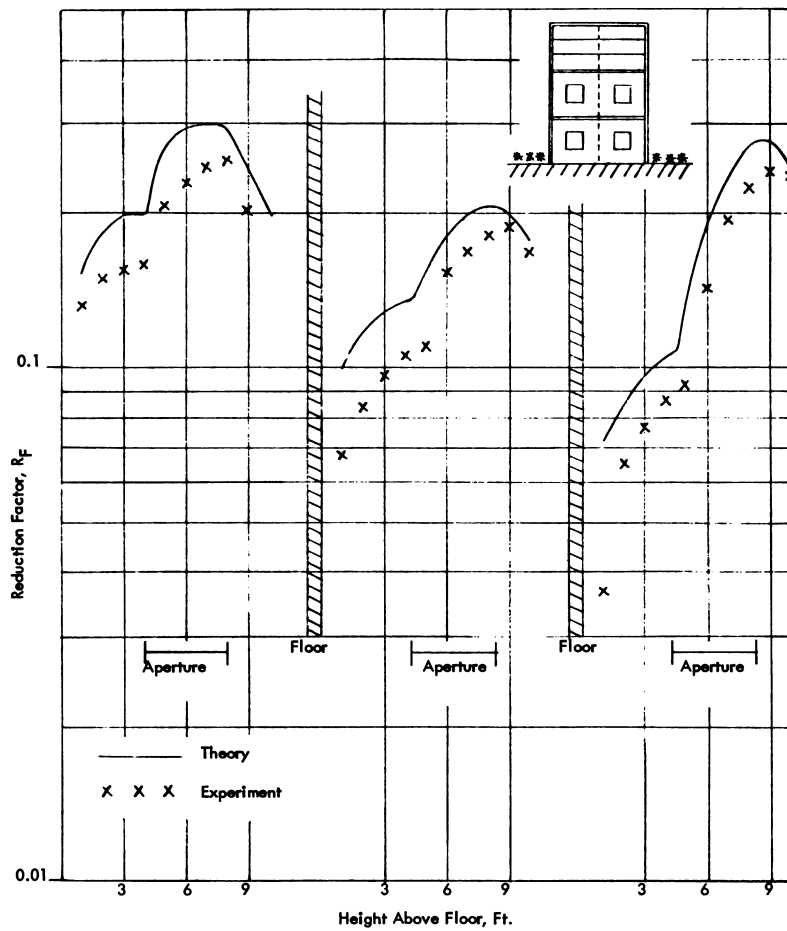
1. Beyond distances of approximately 8 ft from the inner face of the external wall, radiation fields are nearly uniform along the length of the building.
2. At the inner face of the external walls, the dose rate is approximately a factor of 5 lower than at a similar position behind a window.
3. An additional protection factor of at least 2 may be gained below the window sill levels.

The first conclusion is dependent on the window and wall widths of 4 ft and 6 ft, respectively. In extrapolating to other window widths, the ratio of the half-width  $\frac{W_{MIN}}{2}$  of either the window or wall (whichever is less) to the detector distance  $D$  is probably the critical parameter in determining at what distance uniformity in exposure rate is achieved. The ratio inferred from the experiment is  $\frac{W_{MIN}}{2D} = \frac{4}{2 \times 8} = \frac{1}{4}$ .

A later series of experiments at RTF reported by Velletri et al [20] examined the reduction factor for radiation through apertures in the three-story concrete blockhouse. A sketch of the aperture pattern is shown in figure VIII.24, along with experimental and calculated reduction factors. All apertures were 4 ft in height with sill levels at 4 ft above each floor. On



VIII.23 a. Schematic drawing showing the arrangement of windows and dosimeter lines in AEC Headquarters Building. b. Exposure rates as a function of distance from inner face of wall for three dosimeter arrays [18].



VIII.24 Comparison of experimental and calculated ground contributions showing effect of apertures. X Experimental, Velletri, et al [20]; — Calculated, Standard Method.



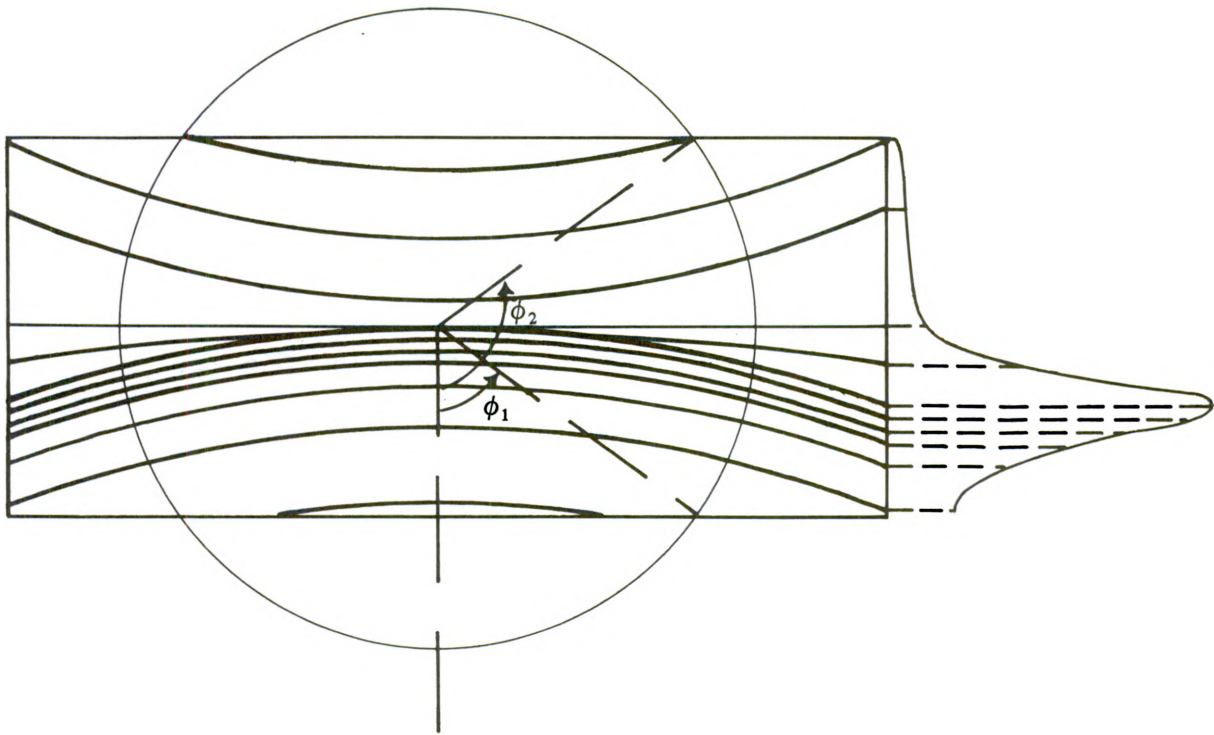
the first and second stories there was an 8-foot width of solid wall between apertures; on the third story the apertures extended all around the building. Walls were 49 psf and floors were 97 psf.

It can be seen from figure VIII.24 that calculations by the Standard Method show the same qualitative behavior with height as the experiment. In addition, the absolute values agree generally to within 20%. The enhancement of the reduction factor on the third story by about a factor of 3 due to the larger aperture area can be seen in the figure. These results corroborate the predicted variation in reduction factor with height caused by the presence of apertures and dramatize the importance of staying below sill level in a building with apertures, in the event of exposure to fallout.

#### E. BLOCKHOUSE SHAPE EFFECTS

##### 1. Discussion of Method for Evaluating Shape Effects

During the development of the Standard Method a fundamental decision had to be made on a reference direction to be assumed for the radiation emerging from the interior walls of the structure. One possible reference direction is the one perpendicular to the wall. However, angular distributions expressed relative to this direction as a polar axis would have severe variations in the azimuth direction. For example, a schematic drawing of contours of constant contributions to the dose from a thin wall is shown in figure VIII.25. The relative intensity for each contour is indicated on the right. If the polar axis is horizontal and perpendicular to the wall, a fixed polar angle will intercept the wall in a circle as shown in the figure. Specification of the exposure for a fixed value of the polar angle would require integration over a rapidly-varying azimuthal distribution. Furthermore, the wall of a structure



VIII.25 Schematic Drawing Showing Equi-Dose Contours from a Ground Source as Viewed by a Detector through Different Areas of a Thin Wall. The Curve at the Right Indicates the Relative Intensity for Each Contour. If the Polar Axis is Horizontal and Perpendicular to the Wall, a Fixed Polar Angle will Intercept the Wall in a Circle with Limits of  $\phi_1$  and  $\phi_2$  on the Corresponding Azimuthal Angle.

is not typically square, but rather has a length which is at least twice its height. For many polar angles, therefore, only certain azimuths would contribute and the azimuthal range would be different for each polar angle.

Another possible reference direction is the vertical direction. It is the natural direction for the external fallout field, since there is no azimuthal dependence relative to the vertical axis. Furthermore, if structures were cylindrical, the symmetry would be maintained and it would be the obvious choice for a reference direction. Although rectangular buildings introduce an azimuthal dependence about the vertical axis, in the radiation emerging from the inner face of the wall, the vertical direction was nevertheless chosen as being more tractable. The azimuthal dependence was accounted for by introducing the shape factor  $E_s(e)$ .

The expression for the shape factor is determined by the angular distribution of radiation emerging from walls. Experiments and calculations to determine this distribution were discussed in section VIII.C.1. As discussed in section VII.B.1, the assumption of a  $\cos\phi$  function for the azimuthal variation about a vertical axis leads to a shape factor of the form

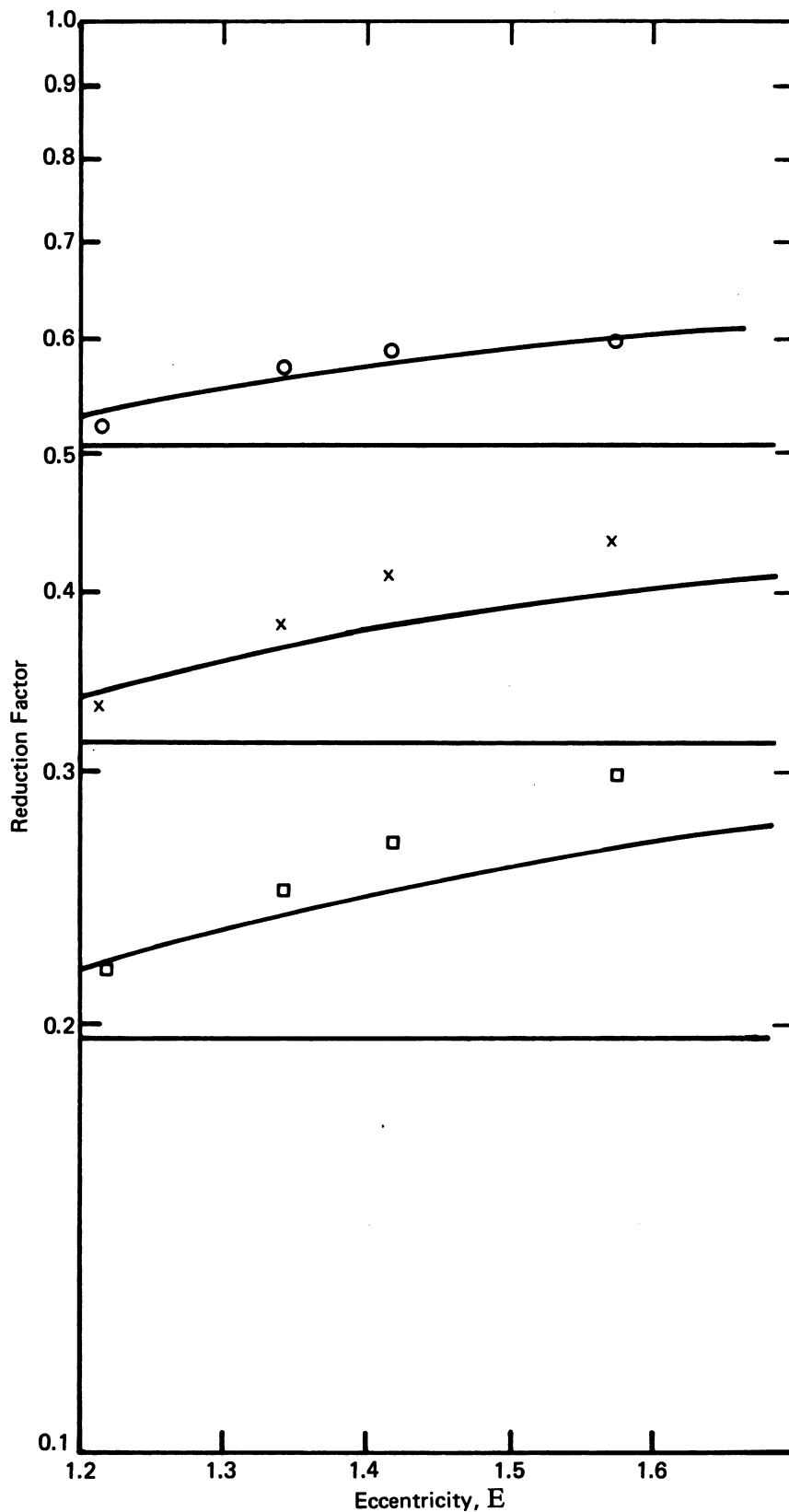
$$E_s(e) = \frac{(1+e)}{\sqrt{1+e^2}} \quad (\text{VIII.7})$$

where  $e = W/L$ , the width-to-length ratio of the structure.

## 2. Experiments to Determine Shape Effects

### a. Tech/Ops Experiments

In order to test the validity of the shape factor, experiments on steel model structures with width to length ratios varying from 0.1 to 0.25 were made by Kaplan [21]. He describes his experimental set-up as follows:



VIII.26 Comparison of Experimental Reduction Factors for Structures of Different Shape with Calculations by the Standard Method, with and without the Shape Factor E Included. (See eq (VIII.6)) Experimental:  $\circ$  20 psf,  $\times$  40 psf,  $\square$  60 psf.

"In these experiments, four types of steel structures, all 2 ft in height, were used: (1) cylinders 2 ft in diameter; (2) squares 20.6 in. on one side (the width-to-length ratio  $W/L = 1$ ); (3) rectangles with a width  $W$  of 16.7 in. and a length  $L$  of 33.4 in. ( $W/L = 0.5$ ); and (4) rectangles with a width  $W$  of 14.875 in. and a length  $L$  of 59.5 in. ( $W/L = 0.25$ ). Wall thicknesses of  $1/2$ , 1, and  $1-1/2$  in. were used for each type of structure. The dimensions of these structures were chosen so that the lower solid angle fraction,  $\omega_l$ , subtended by the bottom of the structure was the same for all the structures at a 6-in. detector height."

His experimental results for the 6-inch detector height and the three different wall thicknesses are shown in figure VIII.26. While  $e$  is not defined for circular cylinders, the limiting value of  $E$  for a circular cylinder is given by  $E = \pi/2$ . Thus, in order to include Kaplan's results for cylinders, the data have been plotted against  $E$  rather than  $e$ .

The three curves represent values calculated by the Standard Method. The three horizontal lines represent calculations in which the shape factor was set equal to unity, i.e., the reduction factor was assumed to be independent of shape. In reality, the lines are not exactly horizontal because, although the lower solid angles are identical, the upper solid angles differ slightly for the four different structures. The variation, however, is less than 5%. The experimental data clearly demonstrate that there is a shape effect and that the shape factor assumed in the Standard Method greatly improves agreement with experiment.

In the Standard Method, the shape factor is applied to the geometry component for infinitely thick walls while the component for zero thickness is assumed to be independent of shape. However, theoretical considerations show that there is a shape effect even for walls of zero thickness. Kaplan and his

co-workers tried to infer from their experimental data a shape factor  $E_d(W,L)$  for the "non-wall-scattered" radiation. They also tried the alternative of inferring a shape factor which would multiply both geometry components. However, their data are not sufficiently accurate to warrant such a change in the Standard Method and, indeed, their conclusion was that "Since agreement between the present theory and the experiment is within 13%, the complications introduced in the modification of the theory as previously described do not seem warranted." [21]

#### b. NDL Experiments

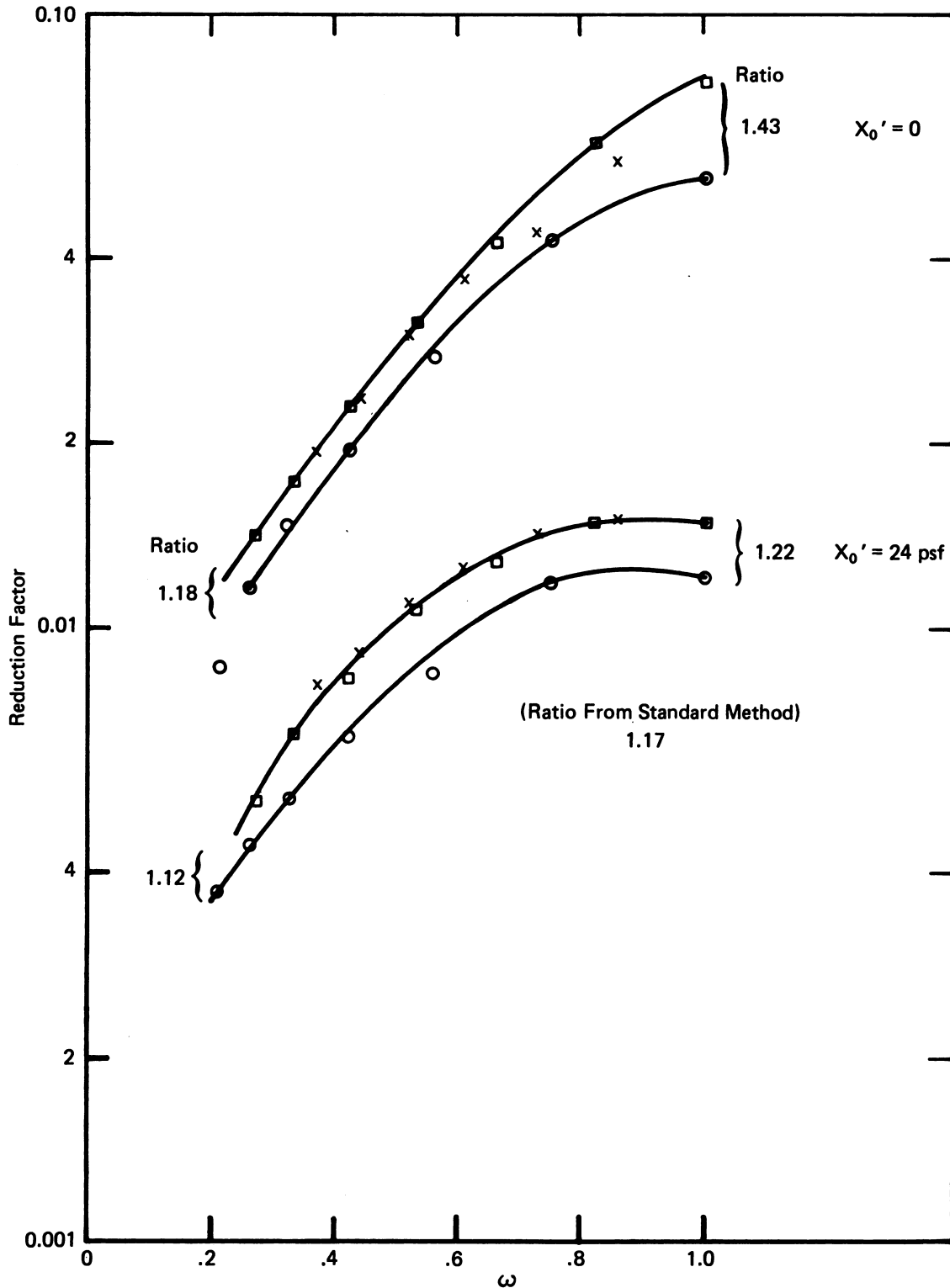
An experiment was carried out by M. Schmoke and co-workers [22] to study the sensitivity of the reduction factor (see sec. X.D) to such effects as the shape of the structure. Although their blockhouse included a basement ceiling and is therefore not a simple blockhouse, their results are discussed here because a study of shape-dependence was the main objective. Blockhouses of area 20 ft x 10 ft ( $L/W = 2$ ), 10 ft x 10 ft ( $L/W = 1$ ) and 20 ft x 5 ft ( $L/W = 4$ ) were considered. The basements of the blockhouses were 7 ft deep and the first-story walls were varied from 2 ft to 8 ft in height. A photograph of the 2:1 blockhouse with 8 ft high walls is shown in figure VIII.27.

As discussed in section VII.C.2, the wall geometry factor for a basement detector depends on the solid angle subtended by the first-floor ceiling as well as the solid angle subtended by the basement ceiling. But the reduction factor in this blockhouse should depend only weakly on the solid angle of the first floor ceiling. Therefore, we have plotted the reduction factor as a function of the solid angle fraction subtended by the basement ceiling in figure VIII.28. The results for the 1:1 and 4:1 structures are smoothly varying and the ratios of the two results for basement ceilings of both zero and 24 psf show the shape dependence. The ratio given by the Standard Method





VIII.27 Photograph of Second Concrete Blockhouse Built at the U.S. Army Chemical Center to Study Structure Shielding.



VIII.28 Experimental Values of the Reduction Factor in the Basement of Rectangular Structures with Different Length-to-width Ratios.  $\circ$   $L/W = 4$ ,  $\times$   $L/W = 2$ ,  $\square$   $L/W = 1$ ; Experimental Ratios for  $L/W = 1$  and  $L/W = 4$  are Listed for  $\omega = 1$  and  $\omega = 0.2$ . A Ratio of 1.17 is Predicted by the Standard Method.

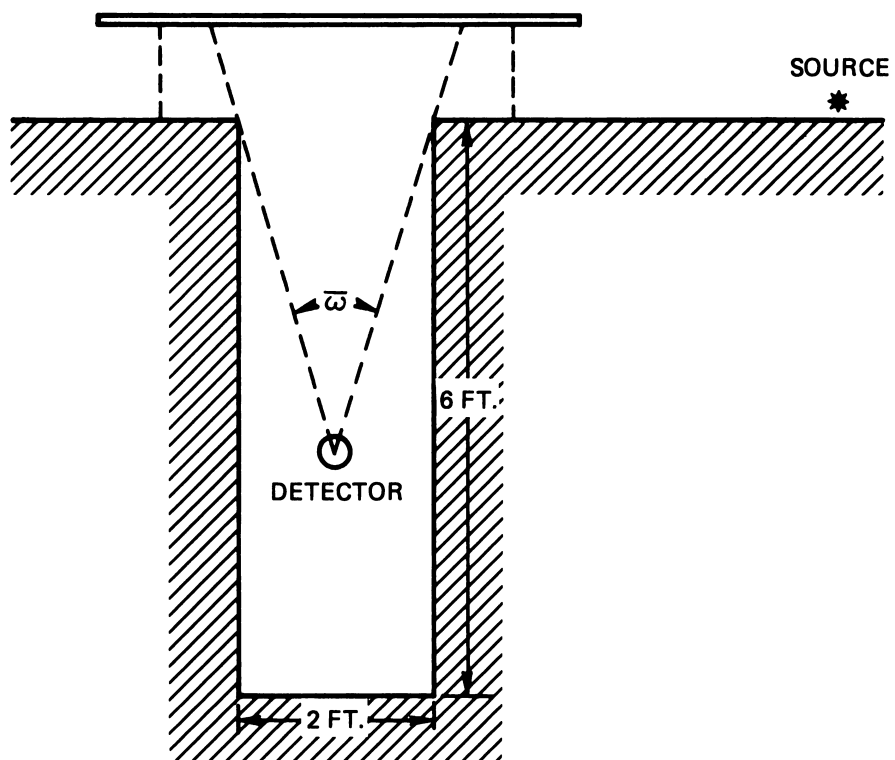


for a 1:1 structure to a 4:1 structure is 1.17, which compares favorably with the experimental values. Therefore the inclusion of a shape factor in the Standard Method seems justified by both full-scale and model experiments.

#### F. CEILING SHINE

Before discussing experiments on ceiling shine it is worthwhile to put this problem in its proper context. First of all, since this type of radiation is generated by reflection from the ceiling, and since the reflectivity of concrete for fallout gamma radiation is about 0.1, the contribution of ceiling shine to the reduction factor is less than 0.1, and is typically of the order of .01. It usually amounts to a small correction except in unusual circumstances where ordinary wall and roof contributions are removed, such as on an upper story of a high-rise building surrounded by a limited field, where the main contribution might come from ceiling shine. Nevertheless, it has proved an interesting problem for experimentation and theoretical speculation.

As a result of early interest in skyshine problems, Batter and Velletri [23] designed and carried out an experiment to measure the ceiling-shine contribution. The experiment was performed at the Tech/Ops - OCD Modeling Facility. The detector collimator was a circular pit 2 ft in diameter and 6 ft deep. The lip of the pit consisted of a lead ring to minimize lip scattering. The ceiling slabs were circular iron plates, 5 ft in diameter, or a 6 in concrete slab, suspended one foot above the top of the hole. A sketch of this configuration is shown in figure VIII.29. The ceiling slab was supported by three thin posts in such a way that there was no obstruction between the sources and the underside of the ceiling. The sources were small capsules of  $^{60}\text{Co}$  placed at varying distances along a radial line from the center of the collimator. The detector was a sealed aluminum ionization chamber with a volume of 320 cc., enclosed in a polyethylene cover, 1/8 inch



VIII.29 Schematic Drawing of the Configuration Used to Measure Ceiling Shine Radiation

thick. The solid angle fraction  $\omega$  of the ceiling, as viewed by the detector, could be varied by means of a pulley arrangement.

Experimental data were reported in the form of exposure rates (R/hr)/(Ci/ft) from ring sources of varying radii out to 42.5 ft. Plane-source data were obtained by Batter and Velletri by numerically integrating over ring-source data. However, their numerical integration gave cumulative exposure rates which seem to be spuriously high by a factor of two. Batter argued that these exposure rates should be reduced by 40% in order to convert from the experimental situation of a one foot ceiling height to a more practical situation of a 10 foot ceiling height. This factor was determined by the ratio of infinite field exposure rates at 1 and 10 feet. If the air density had been increased by a factor of 10 in this experiment then one would expect by the scaling theorem (sec IV.B.3) that the measured exposure rates would have been about 40% lower and no adjustment would be necessary. Batter's argument is reasonable because air density was not scaled in his model experiment. His values (reduced by 40%) and expressed as reduction factors are shown in figure VIII.30.

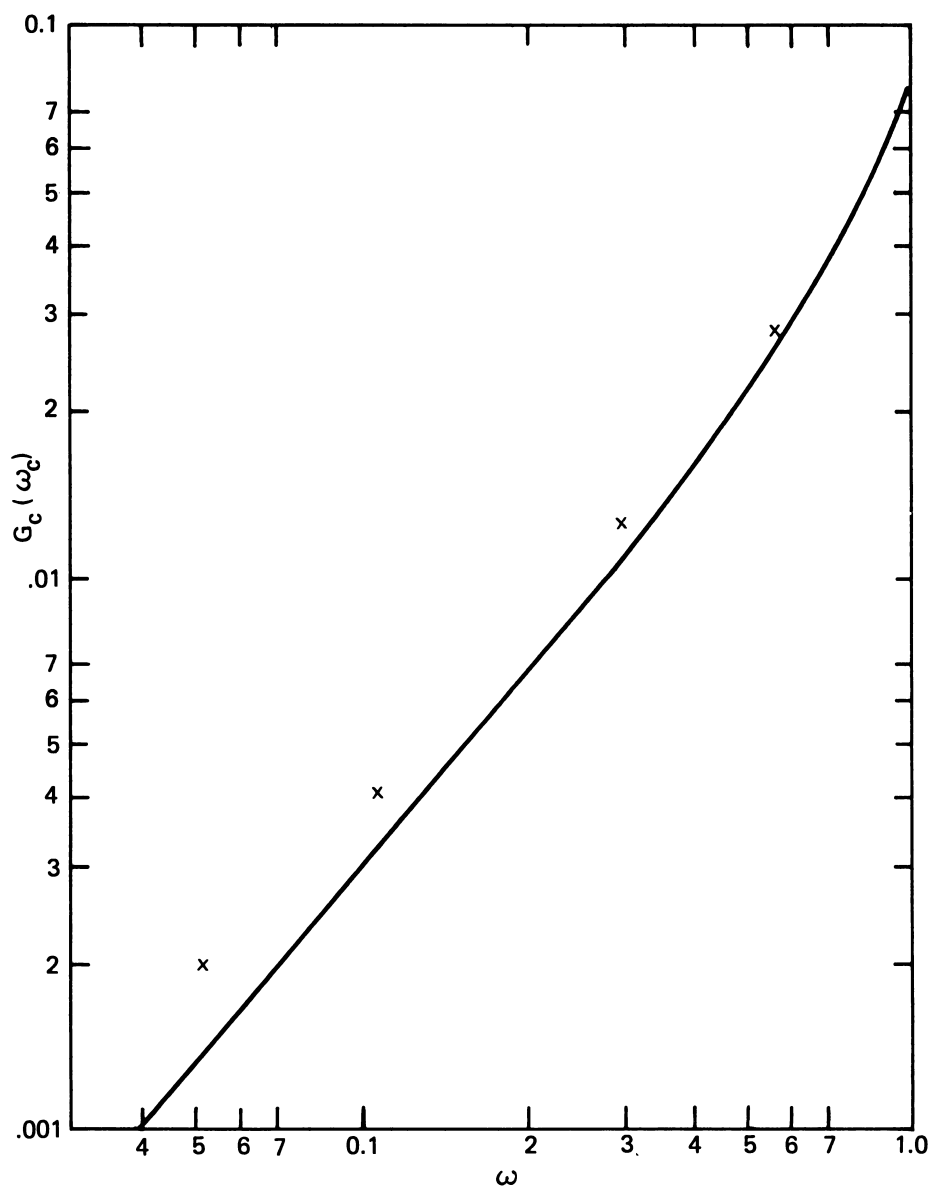
As discussed in section VII.D.5, the ceiling shine contribution according to the Standard Method is

$$G_c = \frac{[G_a(\underline{\omega}) - G_a(\underline{\omega}')] [G_a(0) - G_a(\bar{\omega})]}{2G_a(0)} \quad (\text{VIII.8})$$

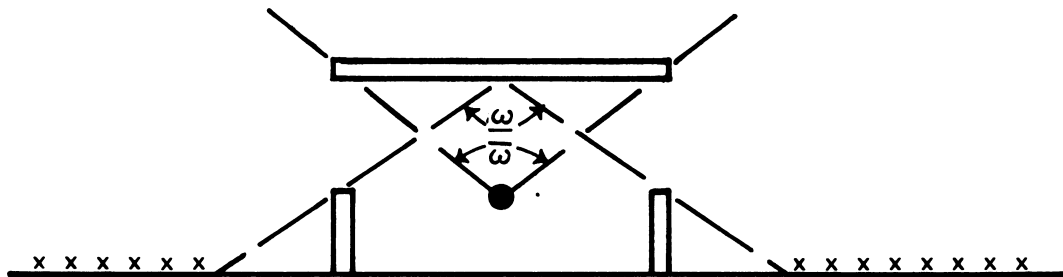
where  $G_a(\omega)$  is the geometry factor for skyshine, and solid angle fractions are shown in figure VIII.31b. Before 1970, the expression for the ceiling shine was given by<sup>4</sup>

---

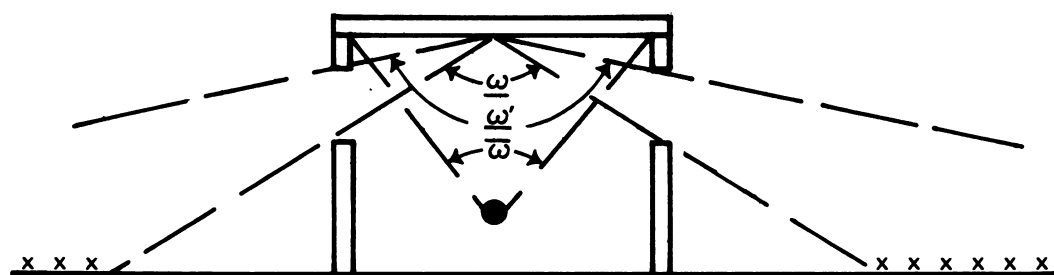
<sup>4</sup>This expression was derived for the situation shown in figure VIII.31a, in which it was assumed that  $\underline{\omega}'$  and  $\underline{\omega}$  in eq (VIII.8) were equal to 1 and  $\bar{\omega}$ , respectively.



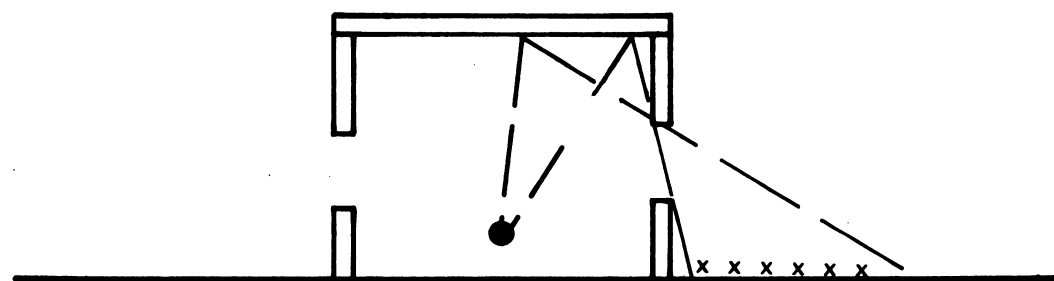
VIII.30 Comparison of Experimental and Calculated Values of Ceiling Shine for a Plane Source of  $^{60}\text{Co}$  Radiation. X Experimental, Batter and Velletri [23], — Calculated  $0.088 S_a(0, \omega)$  (See Fig. V.75).



(a)



(b)



(c)

VIII.31 Schematic Drawing Showing Three Ceiling-Shine Configurations and Parameters Associated with Them.

$$G_c = \frac{G_a(\omega) [G_a(0) - G_a(\bar{\omega})]}{2G_a(0)}, \quad \omega = \bar{\omega} \quad (\text{VIII.9})$$

with the detector assumed to be at sill height and the top of the window assumed to be at ceiling height (see fig. VIII.31a). The second factor in eq (VIII.8) is based on the assumption that the detector response to ceiling shine can be approximated by the geometry factor for skyshine which would arrive within the solid angle fraction  $\bar{\omega}$ . Comparison of the experimental results of Batter and Velletri in figure VIII.30 with the solid line corresponding to skyshine shows that this is a good approximation. The first factor in eq (VIII.8) accounts for the fact that the amount of radiation incident on the ceiling, is controlled by the size of the aperture. It is based on the assumption that the geometry factor for the incident radiation can be approximated by the geometry factor for skyshine. Note that the skyshine distribution is not really identical to the source distribution incident on the ceiling.<sup>5</sup> Both Batter [23] and LeDoux [24] have taken notice of this distinction and substituted a function  $G_c'(\omega)$  to better describe the source distribution. Batter's formula, for example, is given by

$$R_f = G_c(\bar{\omega}) G_c'(\omega) P_r F(H) R(X_c) \quad (\text{VIII.10})$$

The last factor  $R$  on the right is intended to account for the fact that thin ceilings (< 30 psf) reflect less radiation; it can be set equal to unity for most non-residential structures. The factor  $F(H)$  describes the dependence of the ceiling shine on the height of the ceiling above the ground. In the Standard Method, the effect of height is included in the wall barrier function.

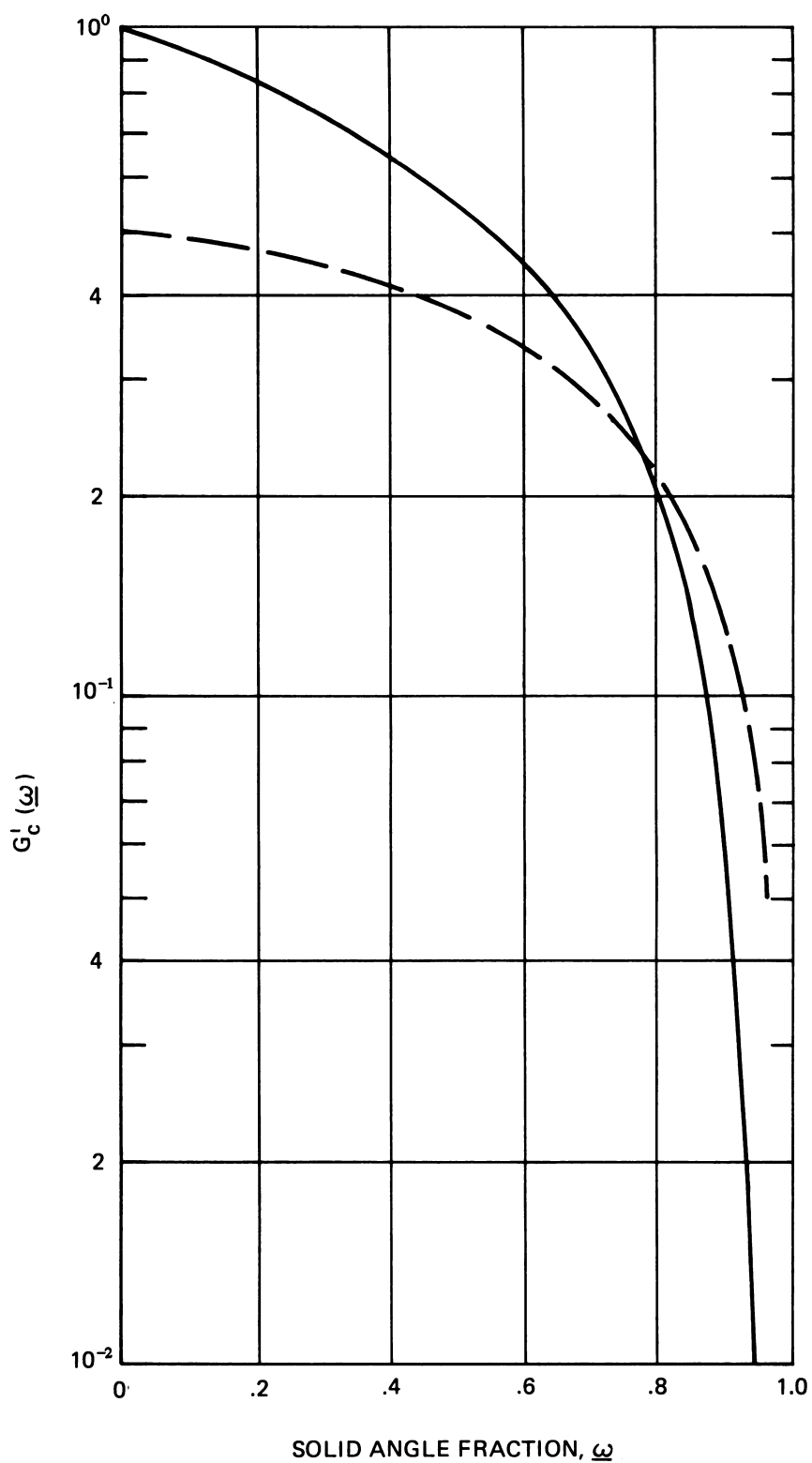
---

<sup>5</sup>See the discussion of this assumption in section VII.D.5.

The factor  $P_r$  is designed for uses in which the aperture represents only a fraction  $P_r$  of the perimeter of the building. The factor  $G_c(\bar{\omega})$  is equivalent to  $[G_a(0) - G_a(\bar{\omega})]$ . The factor  $G_c'(\underline{\omega})$  was derived from the experimentally observed dependence of the cumulative ceiling shine exposure on the radius of the circular source. The solid curve in figure VIII.32 shows Batter's estimate of the relative exposure above a clearing subtending a solid angle fraction  $\underline{\omega}$ . The corresponding function  $0.5 G_a(\underline{\omega})/G_a(0)$  from eq (VIII.9) is shown by the dashed curve. The two predictions differ by as much as a factor of 2, depending on the solid angle fraction  $\underline{\omega}$ .

Although Batter's formulation was undoubtedly an improvement over the older version of the Standard Method, it, too, had some drawbacks. Experimental data taken at Technical Operations showed that about half of the contribution to a ceiling at one foot above the detector comes from distances less than about 4 ft. For a standard ceiling height of 10 ft, the corresponding distance would be about 40 ft. Therefore, sources close to the structure are very important. In a situation such as shown in figure VIII.31b however, the factor  $G_c'(\underline{\omega})$  accounts only for contribution from sources beyond  $\underline{\omega}$ . It therefore fails to account for the contribution of close-in sources, such as those in figure VIII.31c, which illuminate a certain area of the ceiling determined by the aperture. In a modified formulation, the solid angle fraction  $\underline{\omega}$  would be determined at a point on that ceiling area and the solid angle  $\bar{\omega}$  subtended at the detector would be restricted to that portion of the ceiling.

Ceiling shine measurements were also made by Kimel, Faw, and Baran [25]. Their measurements were made on the blockhouse described in section VIII.D.3. For this experiment the wall facing the source area was 16 inches thick. The ceiling shine through apertures whose areas were 7.0% and 4.6% of the area of



VIII.32 Comparison of Calculated Ceiling-Shine Functions — Calculated by Batter and Velletri [23]; --- Calculated  $0.5[1 - S_a(0, \omega)]$  (See Fig. V.75)



one wall were investigated. Source tubing was laid out in a quadrant out to a distance of 125 ft. The detector was located at 3 ft above the floor and a lead shadow shield was constructed around the detector in such a way that it viewed only the ceiling of the blockhouse. Measurements were made with the window "open" and with the window blocked with 8 inches of concrete plus 8 inches of lead. Differencing the two measurements eliminated the contribution from radiation through the wall. Their results for the two apertures are shown in Table VIII.5. Results calculated by the Standard Method, using functions for  $^{60}\text{Co}$  radiation in eq (VIII.8), and by an analytic method devised at KSU are also shown in the table. Considering that the reduction factor is of the order of  $10^{-4}$ , the agreement among the three methods within a factor of 2 is probably acceptable. The numbers calculated at KSU were obtained from numerical integration of the expression

$$R_f = \frac{1}{2\pi} \iint d\Omega_o dA \ell(d, \cos\theta_o) \cos\theta_o \alpha(\theta_o, \phi_o, \theta, \phi) / r^2 \quad (\text{VIII.11})$$

where  $\theta_o$ ,  $\phi_o$ ,  $\theta$ , and  $\phi$  are the polar and azimuthal angles of the incident and reflected gamma rays,

$\alpha$  is the current albedo, and

$r$  is the distance from the detector to an area element  $dA$  on the ceiling. The integrals are taken over the area of the ceiling and the solid angle of the source as viewed from a point on the ceiling and through the window aperture.

## G. RIBBED STRUCTURAL ELEMENTS

### 1. RTF Experiments

As discussed in section VII.C.6, various methods have been suggested for treating walls or floors that contain structural elements such as studs or joists. Thus, an idealized experiment was set up at the Radiation Test Facility to study the effects of non-uniform barrier thicknesses [26], using

TABLE VIII.5 Ceiling Shine Reduction Factors

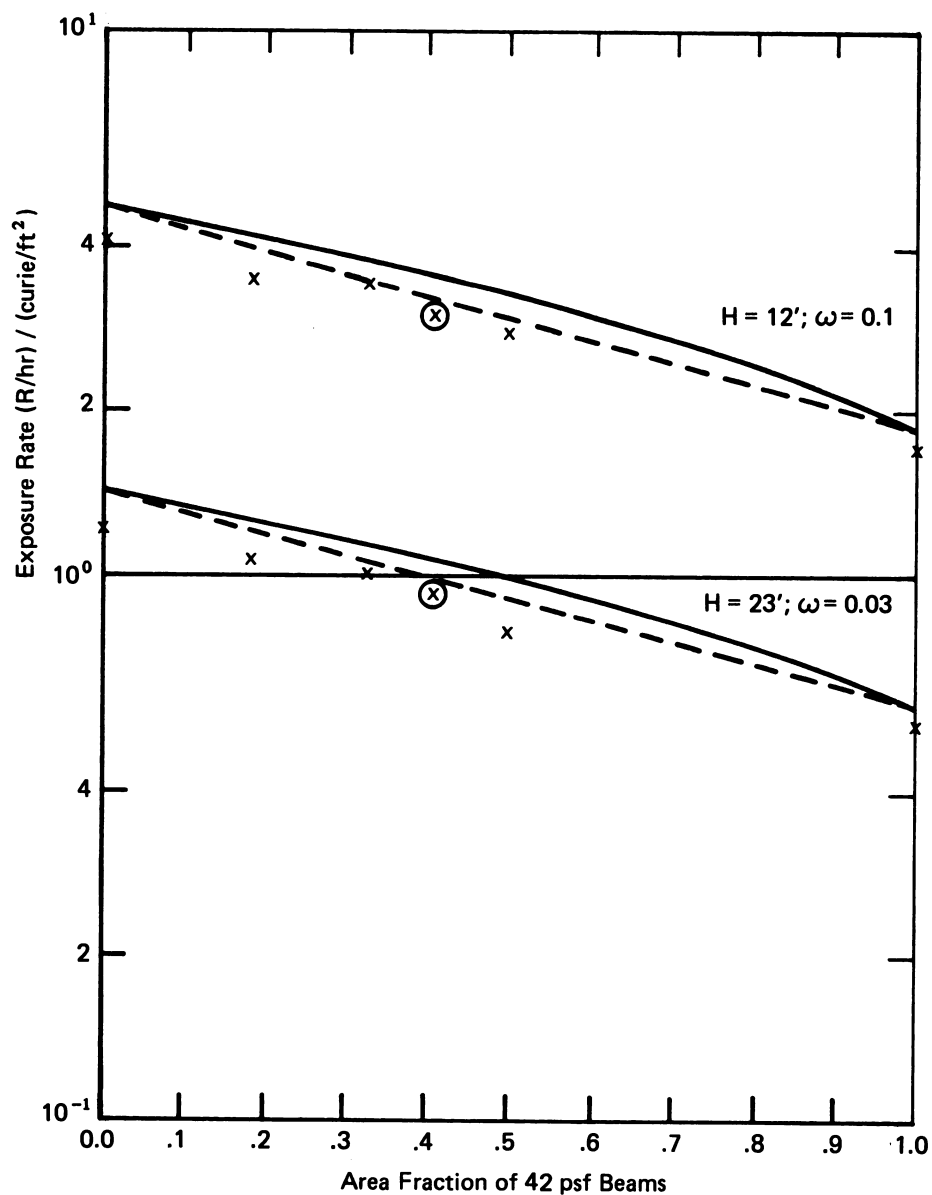
Aperture	$R_{f \text{ exp}} (x 10^4)$	$R_{f \text{ KSU calc.}} (x 10^4)$	$R_{f \text{ S.M. calc.}} (x 10^4)$
1	$3.17 \pm 0.25$	2.26	2.12
2	$2.05 \pm 0.20$	1.75	1.38

TABLE VIII.6 Attenuation Factor

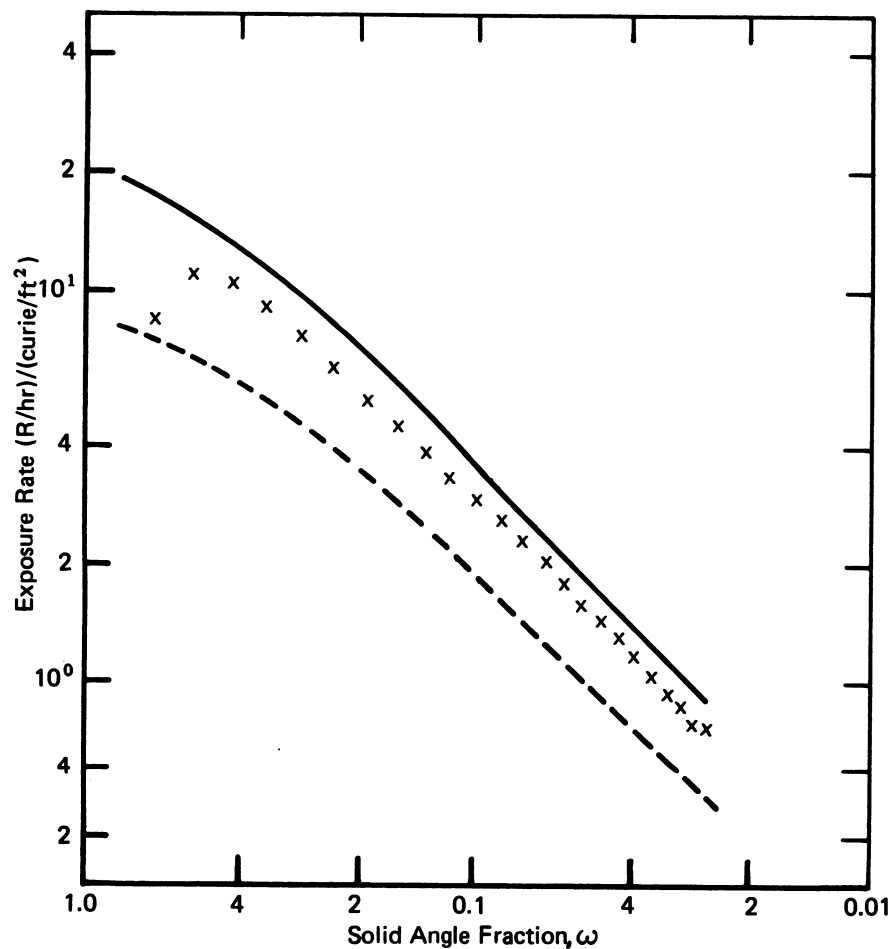
Incident Angle	Measured	Calculated
$0^\circ$	$0.307 \pm .004$	$0.323 \pm .005$
$45^\circ$	$0.166 \pm .006$	$0.162 \pm .003$
$60^\circ$	$0.069 \pm .003$	$0.072 \pm .002$

various patterns of concrete blocks to simulate joists in a roof structure. The source geometry was the same as shown in figure VIII.2 for the inverted roof experiment. Non-uniform concrete "beams", 7.5 inches in width, were placed over a 48.6 psf slab using parallel rows of concrete blocks. Typical experimental results are shown in figure VIII.33, in which the exposure rate is plotted against the fractional area occupied by the 42 psf concrete beams. Results are shown for solid angle fractions of 0.1 and 0.03. The extreme left point corresponds to a 48.6 psf homogeneous slab, while the point on the extreme right corresponds to a homogeneous slab of 90.6 psf. Plots of calculated exposure using the smeared and area-weighted approximations described in section VII.C.6 are also shown in the figure. The main conclusion to be drawn from the figure is that both approximations give good agreement with experiments for this configuration. All the experimental values shown apply to a series of parallel beams except the circled values, which apply to two series of beams perpendicular to each other (i.e. "waffle" construction). Since these two values interpolate well with the others, the effect of joists at these detector locations is apparently not sensitive to the pattern in which the joists occur.

Differences between the smearing and area-weighting approximations become more evident when the beam thickness is increased. Figure VIII.34 shows experimental and calculated results for concrete beams of 168 psf thickness arranged in parallel arrays and covering 0.26 of the roof slab. Here, the area-weighting procedure agrees better with the experimental results and the smearing technique results in a significant underestimate of the experimental exposure. For beams thicker than about 50 psf, therefore, the area-weighting approximation appears to be the more accurate and more conservative approach.



VIIII.33 Comparison of Experimental and Calculated Exposure Rate Above a Concrete Slab with Various Fractions of the Area Covered with 42 psf Thick Parallel Beams. The Source is a Circular Disk Source of <sup>60</sup>Co Radiation, 12 feet in Diameter. Experimental: X Parallel Joists, ⊗ "Waffle" Joists, Spring [26]. Calculated: — Area Weight Approximation, --- Smeared Approximation.



VIII.34 Comparison of Experimental and Calculated Exposure Rates Above a Concrete Slab Covered with 168 psf Thick Parallel Beams Spaced 22.5 Inches Apart. X Experimental, Spring [26]; Calculated: — Area Weight Approximation, - - - Smeared Approximation.

## 2. Experiments at University of Illinois

A series of experiments on ribbed structural elements were also carried out at the University of Illinois by Chilton and his co-workers [27]. However, these experiments produced results only for sources incident at angles of  $0^\circ$ ,  $45^\circ$ , and  $60^\circ$ . They therefore are not directly comparable with calculations by the Standard Method. The slab in these experiments was 4 inch thick with a density of  $2.33 \text{ g/cm}^3$  and the ribs were 6 inch thick concrete sections of about the same density. An example of their experimental results, which agreed very well with Monte Carlo calculations by Morris [28], is shown in Table VIII.6. The attenuation factor here is the ratio of the exposure with the ribbed slab in place, to that with the ribbed slab absent.

## 3. Calculations at University of Illinois

Chilton [29] summarized a series of calculations performed by himself and his co-workers for a wide variety of configurations and source types. This group assumed that the smeared mass thickness is easy to calculate, and that penetration data for slant incident radiation in homogeneous slabs is readily available. They therefore expressed their results as a ratio of attenuation factors calculated for the real configuration to those calculated by the smearing technique. They gave these ratios in terms of a number of empirical parameters, which are listed in their reports.

Their studies led to the following conclusions:

(a) No simple rule is found to establish when a ribbed slab configuration can be adequately represented by the corresponding smeared slab. It appears, however, that the smeared-slab approach can be used, with an error no greater than 30% in the nonconservative direction (i.e. low predicted exposures), if any one of the following criteria are met: (1) the base slab is quite thin (about 5 psf or less) and the radiation striking the structural element is

widely variable in directional distribution; (2) the average mass thickness of the ribbing, when smeared out evenly across the slab face, does not exceed about 10 psf; or (3) the cross-sectional area of each rib, in mass units squared does not exceed about 7000 psf-squared, and the radiation varies widely in direction as in Criterion 1, above. (Note: the RTF experiments with thin beams described earlier satisfy Criterion 3; but those with thick beams do not.)

(b) For cases which do not meet any of the above criteria, the amount of radiation penetrating may be substantially greater than that predicted using the smeared-slab technique of calculation.

(c) For most practical cases, provided the radiation incident on the ribbed slab is widely distributed in direction, the amount of radiation detected does not vary greatly if one moves the detector laterally in directions parallel to the slab face. (This rule is not valid however if the detector is closer to the slab than the rib-spacing distance.)

(d) The area-weighted method is a better approximation than the smeared-slab approximation, in that its errors when they exist, appear to be almost always on the conservative side.

(e) The area-weighted method appears to be about as well suited to exterior walls as to roof barriers.

## REFERENCES

- [1] F. Titus, "Penetration in Concrete of Gamma Radiation from Fallout," NBS Report 6143, (Sept. 1958).
- [2] C. McDonnell and J. Velletri, "An Experimental Evaluation of Roof Reduction Factors," CONESCO Report PSDC-TR-16, Flow Corporation, May 1966.
- [3] C. McDonnell, J. V. Velletri, A. W. Starbird, and J. F. Batter, "The Barrier Attenuation Introduced by a Vertical Wall," CONESCO Report PSDC-TR-15, Flow Corporation, September 1964.
- [4] R. M. Rubin, R. E. Faw, M. J. Coolbaugh, and J. M. Royer, "Energy and Angular Distributions of  $^{60}\text{Co}$  Gamma Rays Penetrating a Concrete Shield," Nuc Eng and Des 16, 429, 1971. See Also "R. E. Faw, R. M. Rubin, J. M. Royer, and M. J. Coolbaugh, "Measurement of Angular and Energy Spectra of Wall Transmitted Radiation" Special Report Number 92 (NRDL TRC-69-10) Kansas State University, (July 1969).
- [5] C. Eisenhauer and A. B. Chilton, "Angular Distribution of Scattered Gamma Rays from a Fan Source", Trans. Am. Nuc Soc. 14, 1, June 1971.
- [6] L. V. Spencer, "Structure Shielding Against Fallout Radiation from Nuclear Weapons," NBS Monograph 42, National Bureau of Standards, June 1962.
- [7] Z. G. Burson and R. L. Summers, "Barrier Attenuation of Air-Scattered Gamma Radiation", CEX-63.3, Atomic Energy Commission, June 1965.
- [8] A. L. Kaplan, "Analysis of Data from Structure Shielding Experiments", NRDL-TRC-68-52, Technical Operations, Inc., June 1968.
- [9] M. A. Hughes and F. A. Bryan, Jr., "Effect of Source Field Elongation on Radiation Received at a Detector", Research Memorandum RM-333-4, Research Triangle Institute, Research Triangle Park, N.C., June 1968.
- [10] M. A. Schmoke and R. E. Rexroad, "Attenuation of Simulated Fallout Radiation by the Roof of a Concrete Blockhouse", Nuclear Defense Laboratory NDL-TR-6, August 1961.
- [11] M. A. Schmoke and R. E. Rexroad, "Attenuation of Fallout Radiation as a Function of Concrete Blockhouse Wall Thickness", NDL-TR-43, Nuclear Defense Laboratory, Oct. 1963.
- [12] R. Spring and C. H. McDonnell, "An Experimental Evaluation of Roof Reduction Factors within a Multistory Structure," CONESCO Report PSDC-TR-16, Supplement No. 1, April 1967.
- [13] C. McDonnell and J. Velletri, "Radiation Distribution within a Multi-story Structure", CONESCO Report TR-24, Flow Corporation, Feb. 1967.
- [14] A. B. Chilton, "Radiation Shielding, Analysis and Design Principles as Applied to Nuclear Defense Planning, Vol. IV Experimental Program," OCD-KSU Report Tr-40, W. R. Kimel, ed., Nov. 1966).



- [15] C. E. Clifford, J. A. Carruthers, and J. R. Cunningham "Scattered  $\gamma$  Radiation from a Simulated Fallout Field Using  $\text{Cs}^{137}$ ", Report DRCL No. 296, Defense Research Board of Canada, Jan. 1959.
- [16] F. A. Verser, "Theoretical Study of Validity of Scale-Modeling for Gamma-Ray Attenuation", Ph.D. Dissertation, Kansas State University, 1973.
- [17] A. L. Kaplan and N. B. Koepp-Baker, "Final Report, The Use of Scale Models in Structure Shielding Experiments," Report TO-B 67-25, Technical Operations Research, April 1967.
- [18] R. L. French, J. H. Price, and L. Olmedo, "Monte Carlo Study of Structure Shielding Against Fallout Radiation", RRA-T73, Radiation Research Associates, March 1967.
- [19] J. F. Batter, Jr., A. L. Kaplan, and E. T. Clarke, "An Experimental Evaluation of the Radiation Protection Afforded by a Large Modern Concrete Office Building", CEX-59.1 U.S. Atomic Energy Commission, January 1960.
- [20] J. Velletri, R. Spring, J. Wagoner, H. Gignilliat, "Experimental Analysis of Interior Partitions, Apertures and Non-Uniform Walls", NRDL TRC-68-69, CONESCO Division of Flow Corporation, December 1968.
- [21] A. L. Kaplan, et al. "Structure Shielding from Simulated Fallout Gamma Radiation", Tech Ops Report TO-B 65-27, Nov. 1965.
- [22] M. A. Schmoke and J. Zink, "Effects of Building Eccentricity Upon the Basement Ceiling Attenuation Factor,  $B_c(X_c, \omega)$ ", BRL Report No. 1679, USA Ballistic Research Laboratories, October 1973.
- [23] J. F. Batter and J. D. Velletri, "The Effect of Radiation Reflected from the Ceiling on the Dose Rate Within Structures," Technical Operations Report TO-B 63065, April 1963.
- [24] J. C. LeDoux, (unpublished).
- [25] W. R. Kimel, R. E. Faw, and J. A. Baran "Scattering of Fallout Radiation from Ceilings of Protective Structures", Kansas State University Bulletin, Special Report No. 72, July 1966.
- [26] R. Spring, "Gamma Ray Attenuation Through Non-Uniform Concrete Slabs," TR-28, CONESCO Division of Flow Corporation, April 1968.
- [27] D. W. Green, K. Preiss, S. P. Chilton, and A. B. Chilton, "Experimental Determination of the Gamma-Ray Shielding Characteristics of a Ribbed Slab," Nuclear Radiation Shielding Studies Report No. 9, University of Illinois, May 1969.
- [28] E. E. Morris, "Monte Carlo Calculation of Ribbed-Slab Penetration by Gamma Rays," University of Illinois, NRSS No. 8, December 1968.
- [29] A. B. Chilton, "Ribbed Slab Penetration - A Summary Report," Nuclear Radiation Shielding Studies Report No. 13, University of Illinois, October 1969.

## IX. SHIELDING ANALYSIS FOR COMPLEX SITUATIONS

### A. INTRODUCTION

This chapter discusses the fallout shielding methodology for situations more complex than those which are the subject of chapters VII and VIII. These complexities may be divided into two types: Those involving complications of the structure, and those relating primarily to deviations of the source configuration from a smooth, infinite, uniformly contaminated plane. The situations approach more closely the cases of actual buildings under realistic fallout field conditions; however, they still involve some degree of idealization. Discussion of how data for real configurations are translated into the idealized cases for the purpose of analysis is left for chapter XI.

As might be expected, complex situations are even more difficult to analyze rigorously than simple ones, and many approximations and assumptions must be made. The methodology to be described is consistent with the standard approach specified in the OCD Manual [1], but variants which have been previously proposed or appear reasonable to the authors will be outlined. The ideas will be discussed from as fundamental a point of view as possible, using the principles and basic formulations for simple situations developed in chapter VII.

It will hardly surprise the reader to find that it is not easy to extrapolate the simple theoretical approaches of chapter VII to complex situations. This chapter will be largely devoted to such extensions; those situations for which research has shown this to be inadequate are discussed in chapter X, which provides experimental results; and the effect of such experimental work on the methodology is presented.

Throughout this chapter the expressions "direct" and "wall-scatter" contribution appear. As discussed in section VII.B.1, these identify terms in the calculation of ground contribution and are useful for guidance purposes; but one should not assume that a fully complete and correct identification is possible between the mathematical terms and the physical concepts normally associated with them.

## B. COMPLICATIONS IN SOURCE

### 1. Limited Fields of Ground Contamination

The idealization that the source on the ground is an infinite, uniformly contaminated plane at ground level is rarely adequate, even as an approximation. In this section, we discuss the case in which the plane of contamination is finite, at least for certain sectors about the structure. For a plane to be considered practically infinite, there should be an unbroken expanse out to a distance of several hundred feet or more; and for most structures the presence of neighboring buildings or natural terrain features restricts the field in some directions within distances considerably less than this. The most common case of a limited field is probably the strip of contaminated ground between the structure under analysis and a nearby one which provides a shield from the ground fallout on its far side. Likewise, the field might be limited by an absence of contamination close to the structure through some process of artificial or natural removal of the contamination. (We shall not discuss the effect of a finite cleared area; the principles are the same as for a finite area source, with due regard being taken of whether contributions are added or removed.)

This subject can be approached in several ways. We shall attempt a careful explanation consistent with the Standard Method<sup>1</sup>, including some brief

---

<sup>1</sup>The OCD Manual [1] is skimpy in its explanations of this subject.

explanations of reasonable alternatives. We start with eqs (VII.32) through (VII.35), which are identified as approximate formulas for calculating the various contributions into which the overall ground contribution through the walls is divided. Because of the different geometric behavior of the so-called wall-scattered and direct components of the detector response, the existing infinite-field formulas for such responses are modified for finite fields in different ways for each component.<sup>2</sup>

a. Direct Ground Contribution (Zero-Thickness Wall)

(1) Blockhouse with Symmetric Courtyard

When the situation involves an elementary blockhouse completely surrounded by a limited field with rectangular symmetry, as illustrated in figure IX.1, it is clear that the solid-angle-fraction-differencing technique for the direct ground contribution is called for:

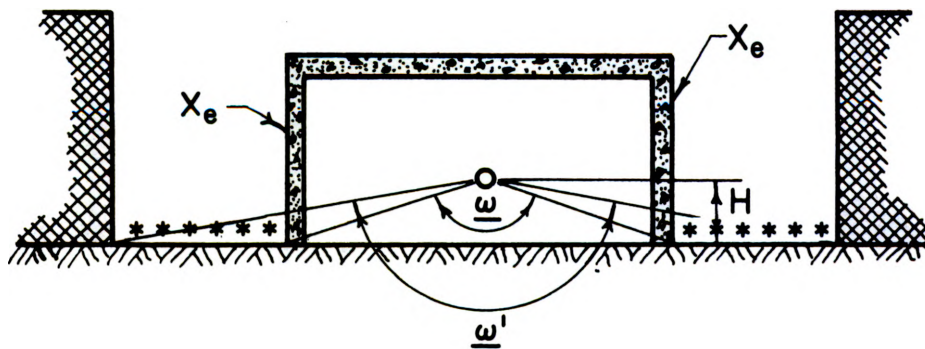
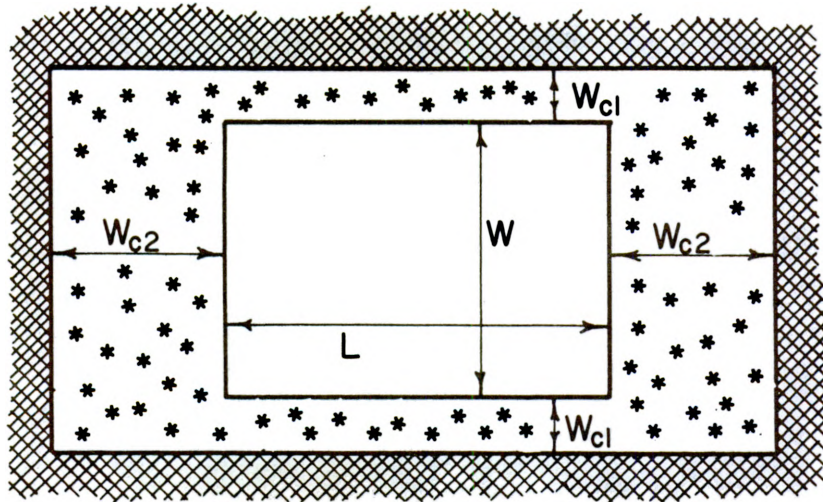
$$\begin{aligned} C_g(\text{direct, limited}) &= B_e(X_e, H) [1 - S_w(X_e)] G_d(H, \underline{\omega}) \\ &\quad - B_e(X_e, H) [1 - S_w(X_e)] G_d(H, \underline{\omega}') \\ &= B_e(X_e, H) [1 - S_w(X_e)] [G_d(H, \underline{\omega}) - G_d(H, \underline{\omega}')]. \quad (\text{IX.1}) \end{aligned}$$

(2) Other Cases -- General Comments

When the situation involves azimuthal variations of a complexity beyond that displayed in the very elementary situation discussed above, the usual method of dividing the horizontal plan of the configuration into sectors may be applied, because most of the "direct" radiation proceeds from source

---

<sup>2</sup>All that follows in this section is based on two assumptions: the field-limiting barrier is higher than the detector and is impenetrable. If this assumption is not feasible, one can proceed as in section IX.B.3 for the contribution beyond the barrier. The second assumption is based on an "either-or" simplification of any situation: the neighboring structure is a complete shield or else it is assumed not to exist.



$$|\varepsilon| \equiv \varepsilon(W, L, H)$$

$$|\varepsilon'| \equiv \varepsilon'(W + 2 \cdot W_{c1}, L + 2 \cdot W_{c2}, H)$$

IX.1 Blockhouse surrounded by limited field having rectangular symmetry (courtyard case).

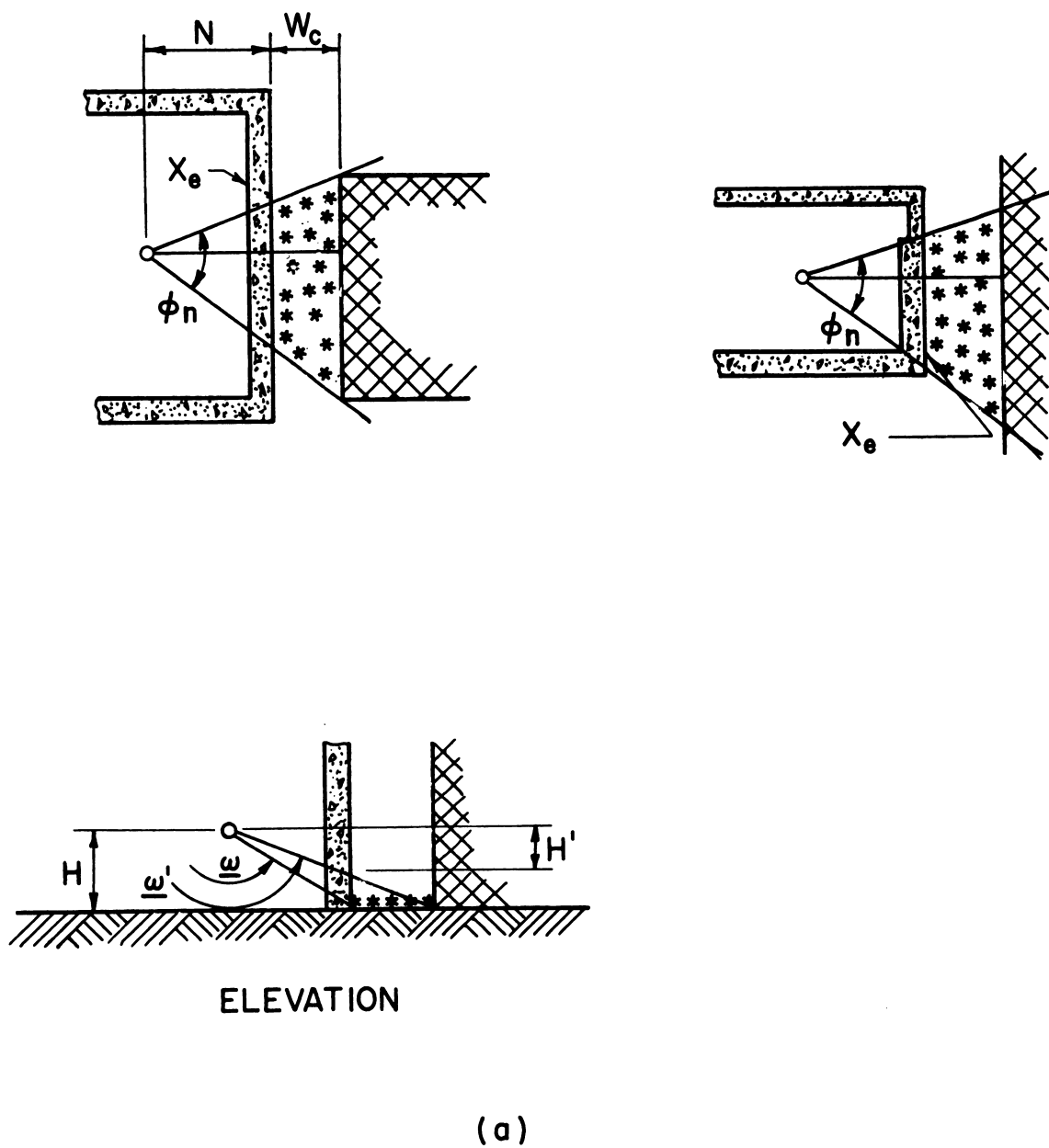
to detector without appreciable direction change resulting from air interactions. Although there may be several acceptable ways for the analyst to use his judgment in making such divisions, one simple and unvarying rule can be prescribed: boundaries of azimuthal sectors drawn in plan as rays from the detector should always be established a) at any change in the thickness of the exterior wall, b) at a change from a finite to practically infinite field in a given direction, (or vice versa), and c) at any change in the directional orientation either of the analyzed structure wall marking the inner boundary of the limited field or the wall of the neighboring structure marking the outer boundary of the limited field. Each sector will then have a simple appearance, constituting one of three possible cases: a) outer limiting wall parallel to wall of structure being analyzed; b) outer limiting wall perpendicular to wall of analyzed structure; c) these two walls at an oblique angle to one another.

### (3) Parallel Outer Boundary on One Side

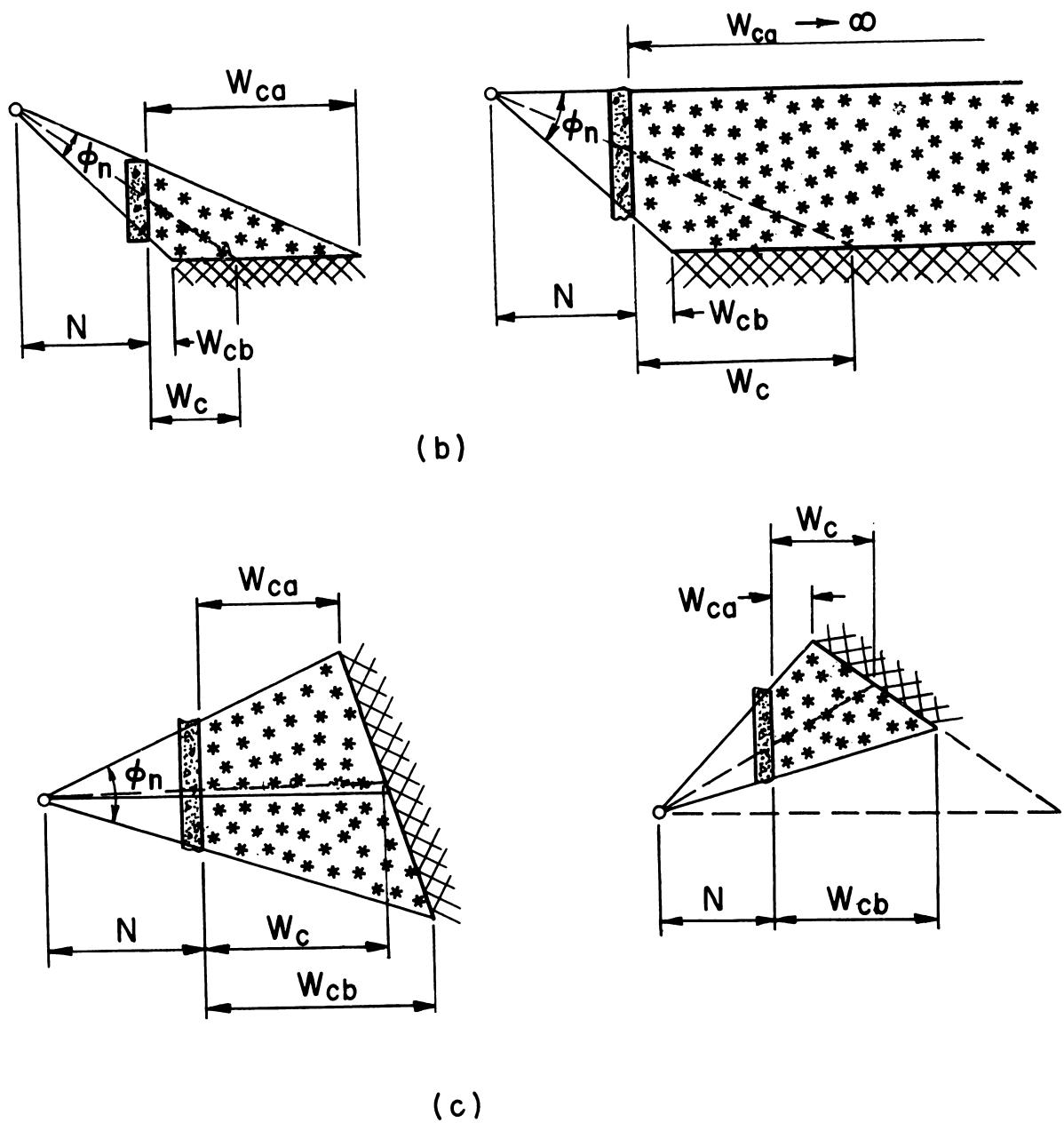
Figure IX.2(a) gives examples of situations in which the walls limiting the field are parallel. The standard azimuthal sector approach requires that the limited field shown be considered as part of a hypothetical courtyard case of rectangular symmetry, and the direct ground contribution of the field within the sector limits is given simply by the appropriate fraction of the amount predicted by eq (IX.1). Thus, for any of the cases in figure IX.2(a),

$$C_g(\text{direct, limited sector}) = \underline{F}_r B_e(X_e, H) [1 - S_w(X_e)] [G_d(H, \underline{\omega}) - G_d(H, \underline{\omega}')], \quad (\text{IX.2})$$

where  $\underline{F}_r$  is the azimuthal fraction  $\phi_n/360^\circ$ . ( $\underline{F}_r$  could be obtained from perimeter ratio considerations as well, but we do not consider this generally less accurate method in the present discussion.)



IX.2 Partially limited field situations, showing parameters for direct ground contributions. (a) External barrier parallel to structure walls.



IX.2 (b) External barrier perpendicular to structure wall. (c) External barrier at an oblique angle to structure wall.



All the parameters in the above equation are already clearly established except for  $\underline{\omega}'$ , which depends upon the dimensions  $W + 2W_{c1}$ ,  $L + 2W_{c2}$ , and  $H$  of the hypothetical courtyard similar to that shown in figure IX.1. For the actual situation given in figure IX.2(a), one can readily establish the value of  $W_{c2}$  as being given by  $W_c$ , the width of the field in the actual situation. On the other hand, there is no obvious way of choosing the value of  $W_{c1}$  for the hypothetical courtyard. It would not be unreasonable to make  $W_{c1}$  also equal to  $W_c$ ; however, we recommend the assumption that  $W_{c1}$  is the same ratio to  $W_{c2}$  as the ratio of dimensions of the hypothetical structure parallel to the  $W_{c1}$  and  $W_{c2}$  dimensions, respectively ( $W/L$  for the situation shown in figure IX.1). This is the same as requiring that the outer perimeter of the courtyard be geometrically similar to the inner perimeter. (fig. IX.5 illustrates such a situation.) When this approach is used  $\underline{\omega}'$  may be obtained in a particularly simple manner. Then the planes which define the limits of  $\underline{\omega}'$  intersect the blockhouse walls so as to establish a rectangle having the horizontal dimensions of the blockhouse and located at a vertical distance  $H'$  below the detector plane where (fig. IX.2(a))

$$H' = \frac{NH}{N + W_c} \quad , \quad (IX.3)$$

$N$  being the horizontal (perpendicular) distance from the detector to the wall being shielded by the neighboring building.  $\underline{\omega}'$  can then be determined from chart C-1A using  $W/L$  and  $H'/L$  as parameters. (See Appendix C.)

#### (4) Perpendicular Outer Boundary on One Side

Situations in which the inner and outer limits of the field are perpendicular are indicated by example in figure IX.2(b). (As shown, it is conceivable that the neighboring structure might be very long, with the dimension  $W_{ca}$

approaching infinity.) The standard approach in this case strongly implies that the analyst should ignore the presence of the adjacent buildings from the standpoint of its effect upon the radiation penetrating the wall at the inner boundary.<sup>3</sup> However, neglect of the field limitation here is clearly improper, although to handle the case accurately is quite difficult.

A simple though approximate way to handle this case is an obvious generalization of the technique for the parallel-wall situation. Equation (IX.2) is still considered valid, and  $\omega'$  is established as before by  $W$ ,  $L$ , and  $H'$ . One has some difficulty in using eq (IX.3) directly, since there is not a constant field width. However, it is clear that if  $H'$  were determined by the ray from the detector to the far end of the field (see fig. IX.2(b)) it would be given by  $NH/(N + W_{ca})$ ; and if determined by the ray to the near end of the field it would be given by  $NH/(N + W_{cb})$ . A reasonable solution is to take the average of these two extremes, so that

$$H' = \frac{H}{2} \left[ \frac{N}{N+W_{ca}} + \frac{N}{N+W_{cb}} \right] \quad (IX.4)$$

An alternate and still simpler (but probably less accurate) approach would be to bisect the angle  $\phi_n$  as shown by the dotted line in figure IX.2(b) and use the value of  $W_c$  thus established in eq (IX.3) to determine  $H'$ .

#### (5) Oblique Outer Boundary on One Side

The oblique case is illustrated in figure IX.2(c). (The OCD Manual's criterion of "being directly opposite" the wall<sup>3</sup> can be particularly hard to interpret in this case.) This case may be handled in fashion similar to the previous case, either by the use of eq (IX.4) or by the simpler eq (IX.3),

---

<sup>3</sup>The OCD Manual [1] states in section 6-5.1: "A shield is assumed to be effective only against a wall that lies directly opposite it."

where  $W_c$  is given by the bisecting ray.<sup>4</sup> Note that even the parallel case approach can be considered as a limit of the oblique case, so that the procedure using eq (IX.4) may be considered universal to all limited fields analyzed by the sector approach.

#### (6) Sector-Independent Approaches

As in section VII.D, it is possible to suggest variations of these approaches, to minimize any effect of the non-participating part of the structure on the calculation for direct ground contribution. One can disregard the actual dimensions of the blockhouse and consider the situation as part of a hypothetical blockhouse-courtyard situation with a  $W/L$  ratio as close to unity as permitted by the configuration within the sector limits.

Just as for the infinite field situation, it is possible to express the direct ground contribution from a limited field in a fashion entirely eliminating dependence upon any aspects of the structure, actual or hypothesized, outside the wall segment under analysis. The approach would be essentially the same as that given in chapter VII in the several paragraphs following eq (VII.66). Of course, only terms involving  $G_d$  would be included in the formulas. One must also insure that if the wall area is divided into zones or small increments these zones or increments are such that rays from the detector through these regions of the wall always intersect the limited field under consideration.

---

<sup>4</sup>The OCD Manual prescribes for field width the distance to the shield base along a ray normal to the wall, even when the line of the limiting shield base must be extended beyond the sector limits in order to establish this dimension as shown in the situation depicted on the right side of the figure IX.2(c). We think that this can be a rather poor approximation for many oblique-outer-boundary cases.

As an example, eq (VII.78b) is directly adaptable to the present case, provided the term involving  $G_s$  is left out,  $G_a$  is replaced by  $G_d$ , the argument  $H + Y$  is replaced by  $H - Y$ , and  $\Delta A$  is below the wall zonal boundary established by the bounding planes of the solid angle fraction  $\omega'$ :

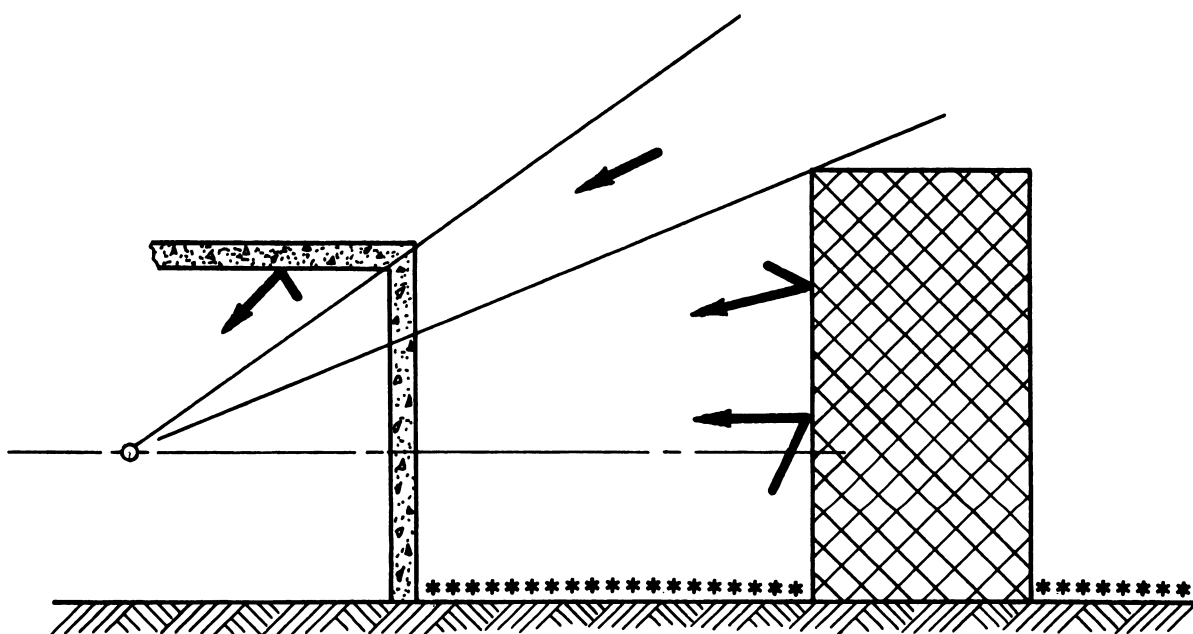
$$\Delta C_g(\text{direct}) = B_e(X_e, H-Y) (\cos\phi \sin\theta)^3 \\ \times \frac{1}{2\pi} [1 - S_w(X_e)] \left[ - \frac{dG_d(\omega)}{d\omega} \right] \left[ \frac{\Delta A}{N^2} \right] . \quad (\text{IV.5})$$

Here  $\omega$  is given by eq (VII.76).

#### b. Skyshine and Ceiling-Shine Contributions

In cases of shielding by a neighboring structure, the skyshine contribution will be modified in some fashion, but the extent to which the contribution is reduced is rather difficult to estimate. As shown in figure IX.3, skyshine from a part of the atmosphere can be blocked out; but this is compensated to some extent by reflection from the neighboring structure.

With regard to ceiling-shine, the influence of the presence of any adjacent structures is not generally very strong, as can readily be seen by examination of figure VII.15. Also, the skyshine and the ceiling-shine contributions are usually much smaller than other contributions; and less accuracy is required in the estimation of such small amounts. All these considerations lead to a general rule in the Standard Method that consideration of shielding by adjacent structures should be ignored in calculating the skyshine and ceiling-shine contributions. We see no good reason to change this rule except for calculational methods much more accurate than the standard methodology, viz., a Monte Carlo calculation using a faithful model and having a small statistical error.



IX.3 Sources of skyshine radiation (including ceiling shine) in a limited field situation.

### c. Wall-Scattered Contribution

In the standard approach for estimating the so-called direct ground contribution from a fallout field, limited or infinite, the solid angle fraction in the argument of the geometry factor is related only to the extent and shape of the source beyond the walls of the structure under analysis.

However, for the "wall-scattered" radiation, the directional distribution of radiation received by the detector, and consequently the geometry factors for such radiation, are all related to the lateral dimensions of the walls. The characteristics of the source are taken into account under infinite field conditions only through their effect on the properties of the radiation incident on the wall, as shown by eqs VII.32 and VII.33. Of these properties, the most significant is the total radiation strength (exposure) at various points on the wall; and the variation of the wall-barrier factor with height, within practical limits, is largely a result of the variation of this property with height (see fig. V.13).

The same principle applies to limited field conditions; but a different barrier factor is needed, since the radiation strength at the walls may be substantially reduced when the source field is limited. Obtaining a simple but adequate functional description of a finite field barrier factor is difficult, and the information developed for use in the present Standard Method involves a patching together of several different theoretical approaches.

Two such approaches are based on calculations described in section V.D.3 for finite semi-circular source regions centered at the face of a semi-infinite wall (fig. V.24). Both involve approximations. The first gives a function  $W_L$ , which depends on wall penetration distance ( $X$ ) and the ratio of the measurement point height above the field to the field slant radius ( $H/R$ ). This approximation works well if  $H$  and  $R$  are sufficiently small that the

air between source and the most significant point on the wall have no appreciable effect in absorbing or scattering the radiation. The second approximation gives a function more valid for larger fields, which in principle should approach the function  $W$ . This function should represent the finite-field wall barrier factor, under appropriate conditions.

Both functions depend on the geometry of the finite field through the ratio  $H/R$ ; and since  $\omega_s$ , the solid angle fraction subtended at the most significant point on the wall by the semi-circular field, is given by  $1/2(1-H/R)$ , we can use  $\omega_s$  as the argument for the geometric aspects of this function.<sup>5</sup> One thus establishes a function, called  $B_s(X_e, 2\omega_s)$ , given for the most part by  $W_L$  for small values of  $\omega_s$  (actually for  $\omega_s < [1 - \cos 45^\circ]$ ), and by the second approximation, for  $\omega_s$  greater than this value (but see discussion below).

One may note that as the value of  $\omega_s$  approaches 0.5,  $B_s$  should approach  $B_e$ . However, the second finite-field approximation still does not adequately account for large amounts of air shielding; and the behavior of these data for  $\omega_s$  close to 0.5 is inadequate (see fig. V.25). Thus, for  $\omega_s > 0.4$ , the Standard Method presents curves of a function<sup>5</sup>  $F(H, 2\omega_s)$  which, when multiplied by the infinite field barrier factor  $B_e(X_e, H)$ , gives reasonable values of  $B_s(X_e, 2\omega_s)$ . These curves were devised in somewhat empirical fashion to provide a smooth transition between the values of  $B_e$  for  $\omega_s = 0.4$  (given by the second approximation) and for  $\omega_s = 0.5$  (given by  $B_e$ ). As a guide for estimation of the intermediate values for  $0.4 < \omega_s < 0.5$ , one

---

<sup>5</sup>Because analysts appear less confused by the use of  $2\omega_s$  rather than  $\omega_s$ , the former is customarily used as the argument for  $B_s$  and  $F$ . From here on we shall do so also.

should note that the physical situation fundamental to the function  $L_c(X_e, \omega_s)$  is closely related to the situation of concern here (see fig. V.16).

One final approximation must be noted. For  $X_e = 0$ , the value of  $B_s$  is approximated by  $L(X) L_c(X, \omega)$ , where  $\omega = 2\omega_s$  and  $X$  is taken as zero. (These values are best displayed in figure 28.18 of NBS Monograph 42 [2].) This last approximation is of little practical significance, however, since one does not expect any "wall-scattered" radiation when  $X_e = 0$ .

The composite function  $B_s$  is graphically displayed as chart C-10A, of Appendix C, and the function  $F$  is presented in chart C-10B. The solid angle arguments are  $2\omega_s$  for both sets of curves.

Obviously, the first step in getting a specific value of  $B_s(X_e, 2\omega_s)$  is to find the value of  $\omega_s$  (or  $2\omega_s$ ). Very few limited fields have a semi-circular shape in practical situations, and most fields are rectangular or can be approximated as such. The standard approach to this matter is to assume that  $B_s$  data for semi-circular fields are valid for rectangular fields subtending the same angle  $\omega_s$  at the appropriate vertical position on the wall.<sup>6</sup> Calculations [3] designed to test the accuracy of this assumption have been discussed in section VIII.C.2. For present purposes, we will accept this approach.

For a rectangular field of dimensions  $W_c$  and  $L_c$  as shown in chart C-10A,  $2\omega_s$  equals the value of  $\omega$  given by the chart in chart C-1A (derived from fig. V.4) which one enters with the width-to-length ratio of

---

<sup>6</sup>This relationship of rectangular to semi-circular fields on the basis of solid angle fraction represents a compromise. For rectangular sources which are narrow in length, but extend out to a large distance from the wall, the importance of the outermost source is underestimated. On the other hand for long rectangles with small widths  $W_c$ , the importance of the outermost sources is overemphasized. Most of the rectangles are of the latter type.



$2 W_c/L_c$  and the altitude-to-length ratio of  $H/L_c$ . Often it will be found that the length of the rectangular field is essentially infinite, so that chart C-1A appears useless for obtaining  $\omega_s$ . However, in this case, chart C-1B can be used, which is based on the following formula, derived from eq (V.8):

$$2\omega_s = \frac{2}{\pi} \tan^{-1} \frac{W_c}{H} \quad (\text{IX.6})$$

The location of the point on the wall considered appropriate as the vertex for calculation of  $\omega_s$  requires some decisions. It is desirable to select a specific height for each wall panel so as to obtain a single value of the barrier factor for this panel. This problem is no different from that encountered in the selection of infinite field barrier factors; and a similar rule can be applied here, namely, use of the detector height as the argument when the wall panel is intersected by the detector plane,<sup>7</sup> otherwise some average position such as mid-panel height. However, the use of the variable  $H$  generally refers to the detector height, and when used as the height in the above procedures for finding  $2\omega_s$  it implies that the detector height is to be used for contributing walls in all stories. The OCD Manual [1] uses this rule; and although it is less accurate for individual stories above and below the detector story, the errors tend to cancel.

The horizontal location on the wall surface of the point used as vertex of the solid angle fraction  $\omega_s$  is unimportant when the length of the field  $L_c$  is appreciably greater than the length of the wall itself. Then every

---

<sup>7</sup>The detector plane is defined to be the horizontal plane passing through the detector.

point in a horizontal line on the wall experiences almost the same radiation environment. If the situation is sufficiently elementary and symmetric, the choice of a point on the wall centered with respect to the field parallel to the wall simplifies the calculations of  $\omega_s$ , and gives the most conservative result. Suggestions for particular choices under more complex conditions will be made later, as necessary.

Further discussion of "wall-scattered" contributions from finite fields is best done in the context of specific situations.

#### (1) Square Blockhouse/Square Courtyard

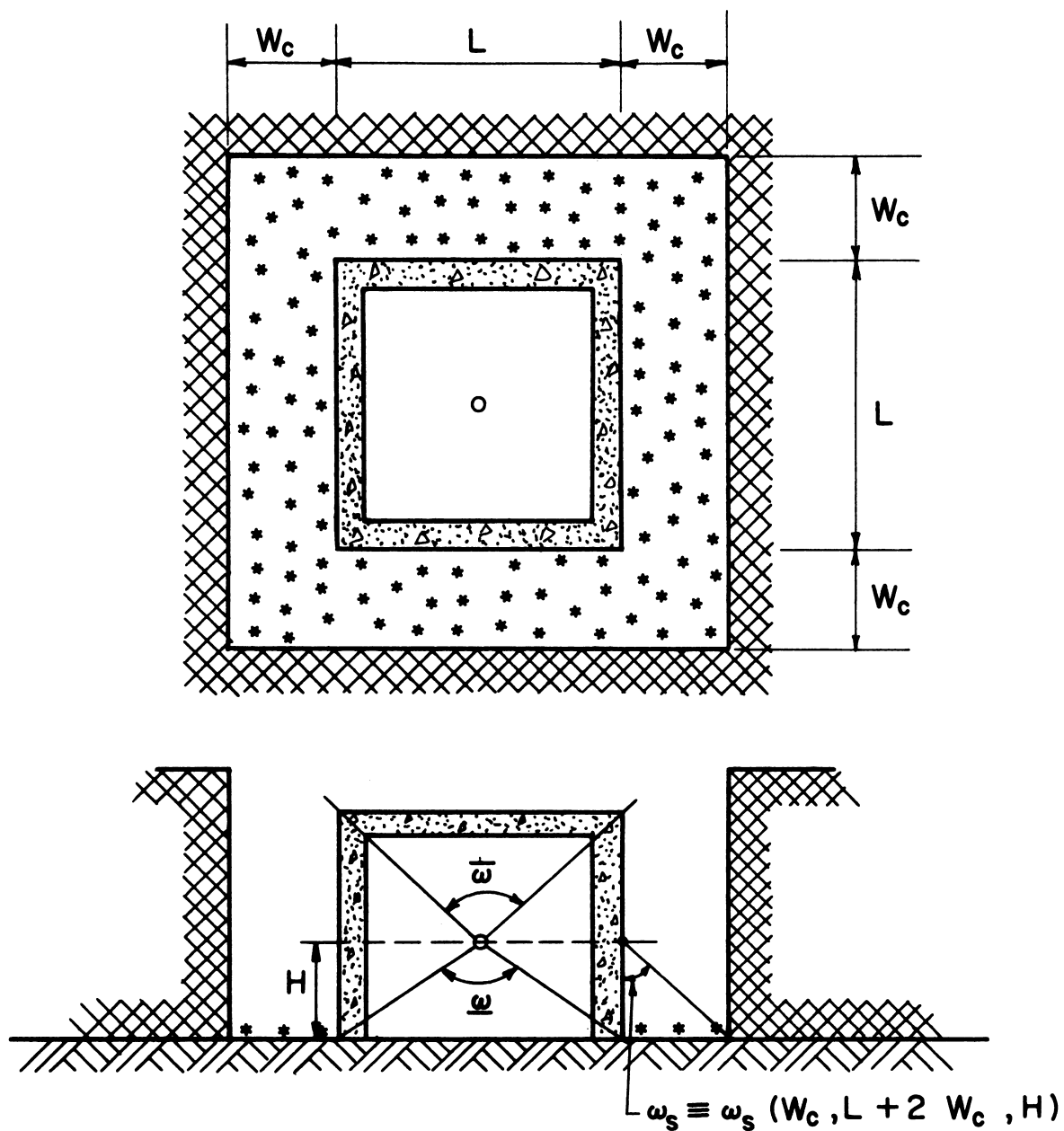
We first consider a square blockhouse surrounded by a contaminated courtyard of constant width (see fig. IX.4). The formula for the wall-scattered contribution is obtained from eqs (VII.32) and (VII.33), with  $B_s$  substituted for  $B_e$ , thus:

$$C_g(\text{scatter, limited}) = B_s(X_e, 2\omega_s) S_w(X_e) [G_s(\bar{\omega}) + G_s(\underline{\omega})] E(1.0) \quad . \quad (\text{IX.7})$$

We note that a single formula serves, since each of the four walls experiences a similar environment. The vertex of the solid angle fraction used for determination of  $\omega_s$  is located at detector height at the horizontal midpoint of a typical wall. The field which contributes to the radiation environment at this wall has a width of  $W_c$  and a length  $(L + 2W_c)$ .  $B_s$  in the above formula is based on the angle subtended by a field of this size, and this is applicable to all four sides.<sup>8</sup>

---

<sup>8</sup>This solution is slightly different from those recommended by the OCD Manual (see Problem 5-21). The Manual originally did not allow any part of the field to be considered as contributing to more than one wall. (See also [4].) It is easy to see, however, that as  $W_c$  approaches infinity  $\omega_s$  must approach 0.5 for all four walls in order for  $B_s$  to approach  $B_e$ ; and this requirement cannot be met under the restriction imposed by the Manual. In actuality, overlap of limited source field areas of significance to different walls is of no consequence. On the other hand, Change 3 (Item 6) to the Manual seems to imply that the length of the field should be infinite for all walls. This latter rule will be shown to be reasonable in many situations but cannot be justified for all cases, such as this one.



IX.4 Illustration of square blockhouse with constant width contaminated courtyard for discussion of wall-scattered contribution.

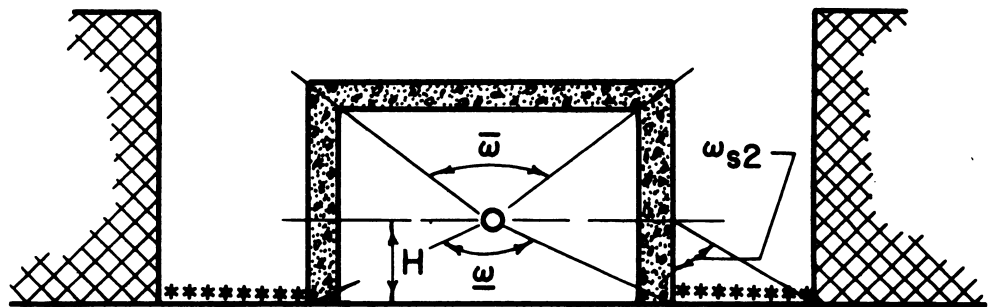
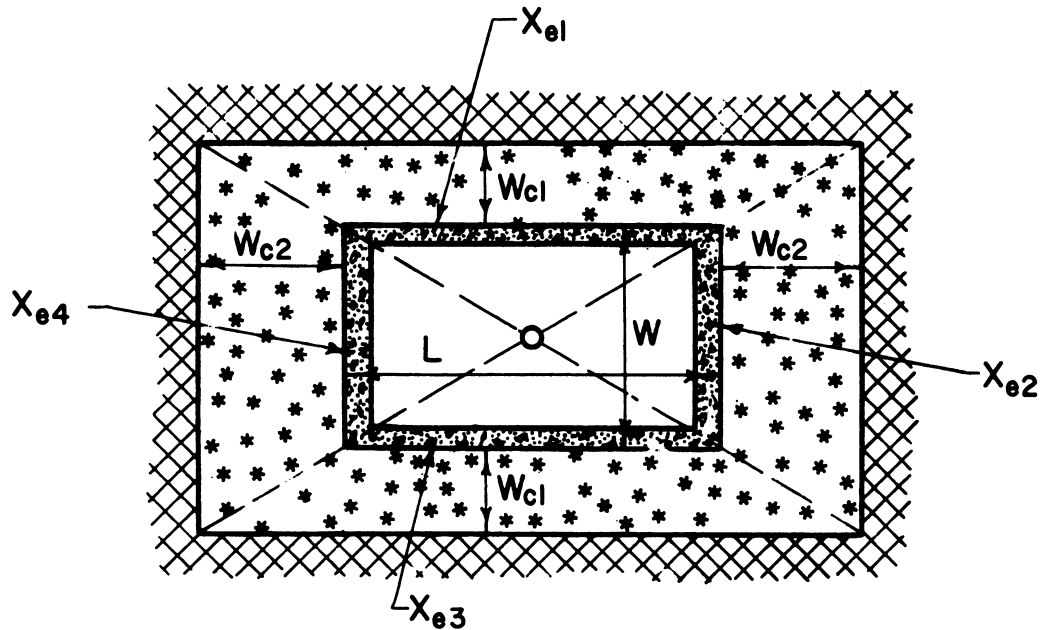
## (2) Rectangular Blockhouse/Geometrically Similar Courtyard Boundary

Figure IX.5 illustrates a slightly more complicated situation. This is a courtyard situation, in which the outer courtyard boundary is geometrically similar to the bounding rectangle of the structure under analysis. Each wall, typified by a point horizontally centered on it and at detector height, experiences radiation from a limited field of rectangular shape which is clearly identifiable. The north and south walls have the same value of solid angle fraction,  $\omega_{s1}$ , as argument for  $B_s$ , while the east and west walls use  $\omega_{s2}$ . These solid angle fractions are established as indicated in the figure. On the other hand, the values of the mass thickness of the four walls can differ, causing different barrier factors for the four walls. The proper formula for the wall-scattered contribution then becomes

$$C_g(\text{scatter, limited}) = \left\{ \sum_{i=1}^4 F_{ri} B_s(X_{ei}, 2\omega_{si}) S_w(X_{ei}) \right\} [G_s(\bar{\omega}) + G_s(\underline{\omega})] E(e) \quad , \quad (\text{IX.8})$$

where  $F_{ri}$  denotes the factor of proportion ( $F_r$ ) for the  $i$ -th wall, as previously defined and used, e.g., in eq (VII.58). Note that the sum of all four values of  $F_{ri}$  is unity. The other variables are established in figure IX.5.

It is interesting to observe that here the perimeter ratio method is more valid than the azimuthal fraction approach in determining  $F_{ri}$ , under the assumption that the radiation emitted from a thick wall has a horizontally azimuthal variation of a cosine nature. This assumption, which is the basis for the usual  $E(e)$  function (see eq (VII.24)), can be applied to both infinite fields and finite fields. This follows from the fact that if each wall is considered as a single panel, the factors  $E_p$  for such walls,



For North and South Walls :

$$\omega_{s1} = \omega_{s3} \equiv \omega_s (W_{c1}, L + 2 \cdot W_{c2}, H)$$

For East and West Walls :

$$\omega_{s2} = \omega_{s4} \equiv \omega_s (W_{c2}, W + 2 \cdot W_{c1}, H)$$

IX.5 Illustration of rectangular structure with courtyard source having outer boundary geometrically similar to structure boundary, for the purpose of discussing wall-scattered contribution from limited fields.

expressed in eq (VII.65) are in the same ratio as the lengths of the walls. Nevertheless, because of the desirability of handling all components of the radiation contribution in similar manner and in light of the fact that for most structures there will be little difference in the values of  $F_{ri}$  calculated by the perimeter ratio and the azimuthal fraction methods, the latter approach is usually considered adequate and is preferred.

### (3) Parallel Outer Boundary on One Side (Unlimited)

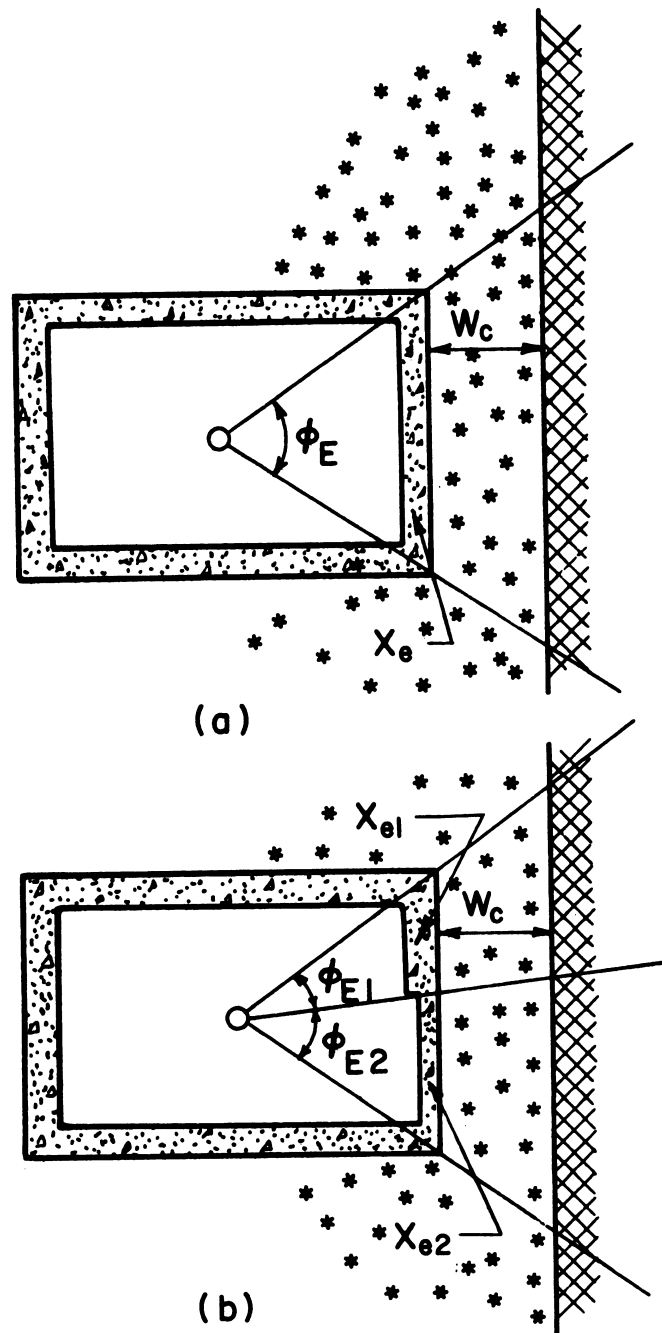
We now consider the situation of a long external barrier parallel to the right-hand side of the blockhouse under analysis, as shown in figure IX.6. At this time we are concerned only with the "wall-scattered" contribution through the right-hand wall. For Situation (a) of the figure, the contribution is given by

$$C_g(\text{scatter, limited}) = (\phi_E/360^\circ) B_s(X_e, 2\omega_s) S_w(X_e) [G_s(\bar{\omega}) + G_s(\underline{\omega})] E(e) \quad , \quad (\text{IX.9})$$

in which we use the azimuthal fraction approach to calculate only the contribution through a single wall. Of particular significance in this situation is the fact that the limited field which determines  $\omega_s$  is clearly established as a rectangle of width  $W_c$  but with an infinite length.

Situation (b) has the additional complication of a right-hand wall divided into two panels of differing effective mass thickness. The azimuthal sector approach allows us to handle the two parts separately. Thus,

$$\begin{aligned} C_g(\text{scatter, limited}) = & [\phi_{E1}/360^\circ) B_s(X_{e1}, 2\omega_s) S_w(X_{e1}) \\ & + (\phi_{E2}/360^\circ) B_s(X_{e2}, 2\omega_s) S_w(X_{e2})] \\ & \times [G_s(\bar{\omega}) + G_s(\underline{\omega})] E(e) \quad . \end{aligned} \quad (\text{IX.10})$$



IX.6 Illustrative example showing long external barrier parallel to one wall of blockhouse, for purpose of discussing wall-scattered contribution from limited field: (a) simple case; (b) case complicated by variation in wall thickness.

The important thing to note here is that the external field incident on the right-hand wall is essentially the same for both sectors; thus the  $\omega_s$  assumed for both sectors is for the entire limited field. This is the same as for Situation (a).

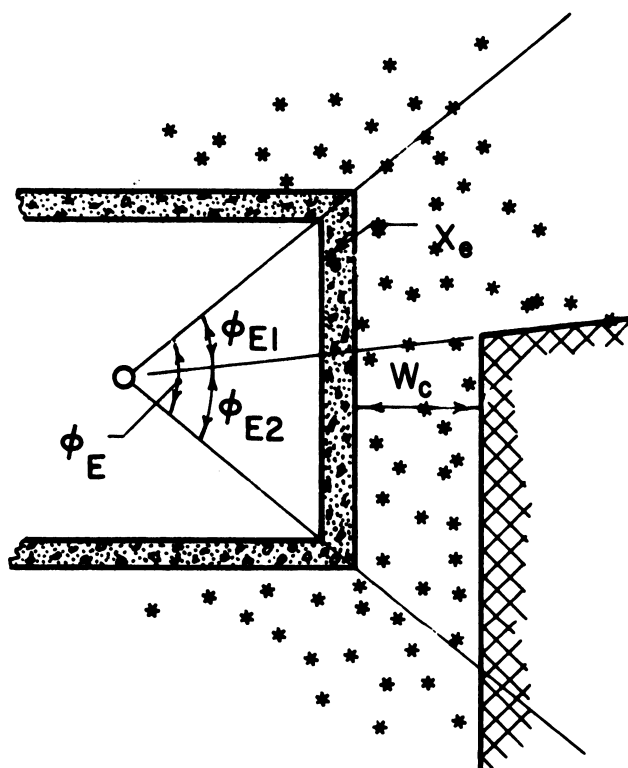
#### (4) Limited Parallel Outer Boundary on One Side

We now turn to the situation depicted by figure IX.7. Here it is not a variation of the character of the wall which breaks the problem of the right-hand "wall-scattered" contribution into segments, but the more complex configuration of the source. Although one may draw a radial line from the detector, as shown on the figure, in an attempt to divide the problem into two distinct parts involving fields of infinite and limited widths, respectively, this appears not to be a valid way of approaching the problem.<sup>9</sup> The "wall-scattered" contribution is assumed to have lost its memory of the directional distribution of radiation incident on the wall; hence this contribution, even within a certain sector, is dependent on the general characteristics, notably the total strength, of the radiation field incident on the wall. These characteristics are affected by all parts of the field visible from a position on the surface of the wall. Thus, regardless of which sector is under consideration, the amount of radiation penetrating the wall is affected by the entire field to the right of the blockhouse. One may still consider the use of an azimuthal fraction, but now the fraction is used to give an approximate weighting to the contribution of each part of the field. We thus estimate that the average barrier factor for the right-hand wall, which we call simply B, is given by

---

<sup>9</sup>Such a point of view is quite reasonable for the "direct" contribution. For that contribution, the radiation penetrating the wall within sector limits is largely affected by the source field also within those sector limits.





IX.7 Illustration of combination of limited and infinite fields, for discussion of wall-scatter contribution.

$$B = (\phi_{E1}/\phi_E) B_e(X_e, H) + (\phi_{E2}/\phi_E) B_s(X_e, \omega_s) \quad , \quad (IX.11)$$

in which we get the proper limit for the barrier factor if either  $\phi_{E1}$  were taken to zero and  $\phi_{E2}$  taken to  $\phi_E$  or vice versa. Then,

$$\begin{aligned} C_g(\text{scatter, complex}) &= (\phi_E/360^\circ) B S_w(X_e) [G_s(\bar{\omega}) + C_s(\underline{\omega})] E(e) \\ &= (\phi_{E1}/360^\circ) B_e(X_e, H) S_w(X_e) [G_s(\bar{\omega}) + G_s(\underline{\omega})] E(e) \\ &\quad + (\phi_{E2}/360^\circ) B_s(X_e, 2\omega_s) S_w(X_e) [G_s(\bar{\omega}) + G_s(\underline{\omega})] E(e) \quad . \end{aligned} \quad (IX.12)$$

The above final form of the equation appears as if each sector contribution were independent of adjacent sectors; but, as we have seen, this is actually not so. Nevertheless, by this formulation "direct" and "wall-scatter" contributions can be handled in many respects in a formally equivalent fashion.

As usual, the determination of the extent of the limited field for the purpose of finding  $\omega_s$  in the above formula is a little subtle. The use of  $W_c$  as the width of the limited field is obvious, but the proper choice for the length of the field is not obvious. To consider it limited by the radial lines bounding the azimuthal sector would be incorrect, because that would mean that the azimuthal sector limitation would be imposed twice. If one considers letting  $\phi_{E1}$  approach zero or  $W_c$  approach infinity, one finds that the correct limiting formulas, eq (IX.9) or the sum of eqs (VII.32) and (VII.33), respectively, can be approached only if the lengths of the limited fields also become infinite.<sup>10</sup>

---

<sup>10</sup> This is the basis for the role for infinite lengths of finite fields, noted in footnote 8.

### (5) Non-Parallel Outer Boundaries on One Side

The next higher order of complexity is a situation such as that shown in figure IX.8, in which the outer limits of the finite field are established in part by lines which are not parallel to the wall which the field affects. A reasonable approach in this case is, after segmenting the problem by use of azimuthal sectors, to "square off" those sources between the radial lines. For the present purpose, one is interested particularly in the value of  $W_c$  for each sector. Any reasonable means of obtaining an average width can be used, one such being the use of sector bisectors such as shown in figure IX.8. The "wall scattered" contribution is then written in straight-forward fashion as

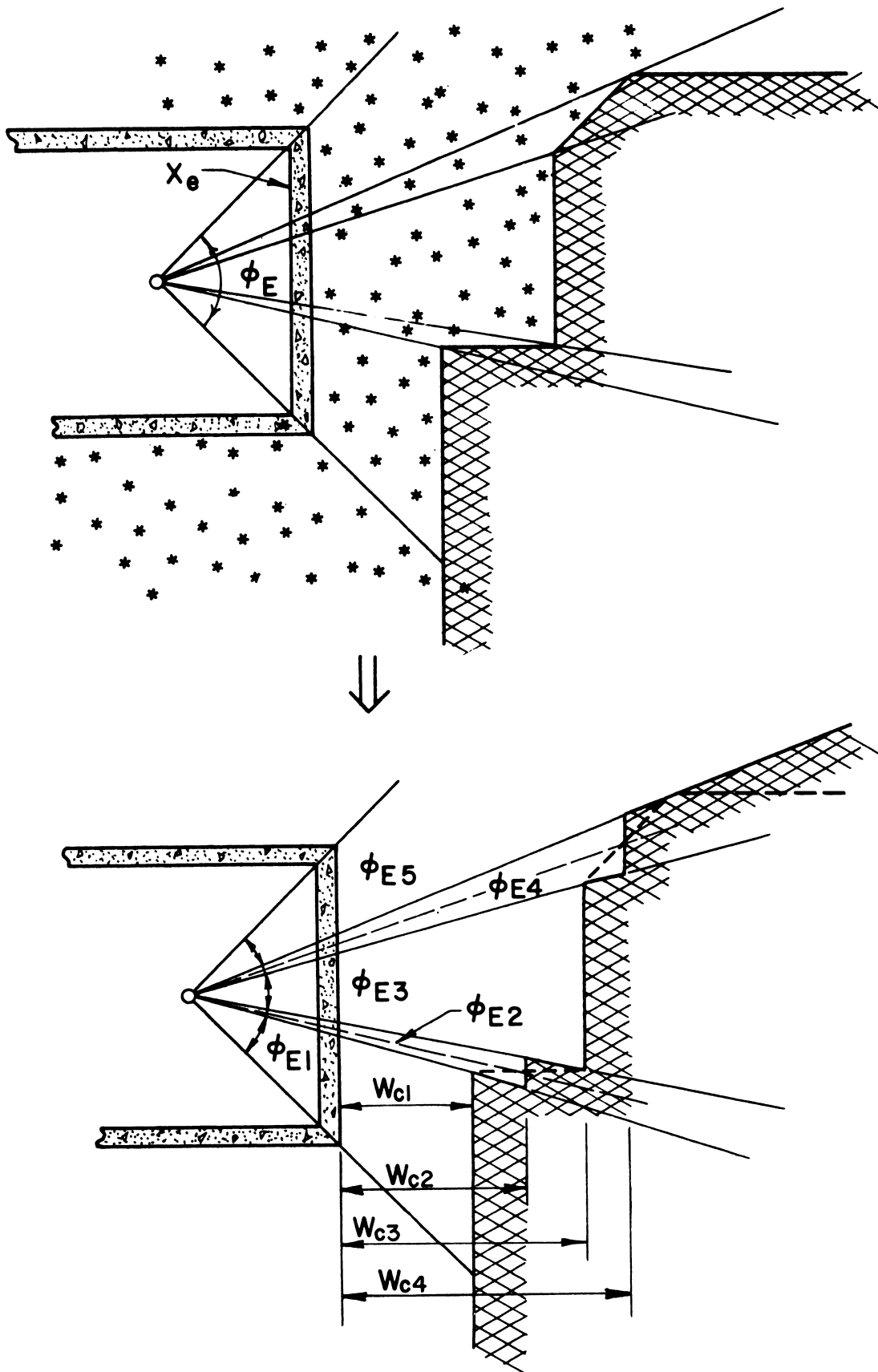
$$C_g(\text{scatter, complex}) = \left\{ \sum_{j=1}^5 (\phi_{Ej}/360^\circ) B_j S_w(X_e) \right\} [G_d(\bar{\omega}) - G_d(\underline{\omega})] E(e) \quad , \quad (\text{IX.13})$$

where

$$\begin{aligned} B_j &= B_s(X_e, 2\omega_{sj}), & j &= 1, 2, 3, 4 \\ B_j &= B_e(X_e, H) \quad , & j &= 5 \\ \omega_{sj} &= \omega_s(W_{cj}, \infty, H), & j &= 1, 2, 3, 4 \end{aligned}$$

### (6) Estimation of Limited Field Length

The discussion and illustrative examples thus far covered are believed generally sufficient to show how the "wall-scattered" contribution from limited fields may be reasonably handled. There is one final item which needs further discussion, that is, complications in estimation of the length of the rectangular fields which is assumed for the purpose of estimating  $\omega_s$  for a limited strip. We have seen that it is proper to use a rectangular field



IX.8 Example of complex-shaped external barrier, for purpose of discussion of wall-scatter contribution from limited fields.

longer than the wall under analysis. The precise limits of length of this field are best obtained from the actual field configuration, to the greatest extent possible. (This is sometimes at variance with the present Standard Method, which simplifies matters by always requiring the length to be infinite.) A number of questions arise here, which will be discussed next in turn.

The first is exemplified by figure IX.9. If the length of the limited field is substantially different in opposite directions, with respect to the center of the wall, how should  $B_s$  be obtained? The horizontal distance from the wall center to the top of the field,  $L'_c$ , is  $[(L/2) + W'_c]$ , but in the downward direction the distance  $L''_c$  is infinite. It appears reasonable in this case to obtain the wall barrier factor for use with sector  $\phi_{E1}$  as the average of the two values of  $B_s$  obtained by considering the length of the limited fields as  $2 \cdot L'_c$  and  $2 \cdot L''_c$ , respectively. Thus,

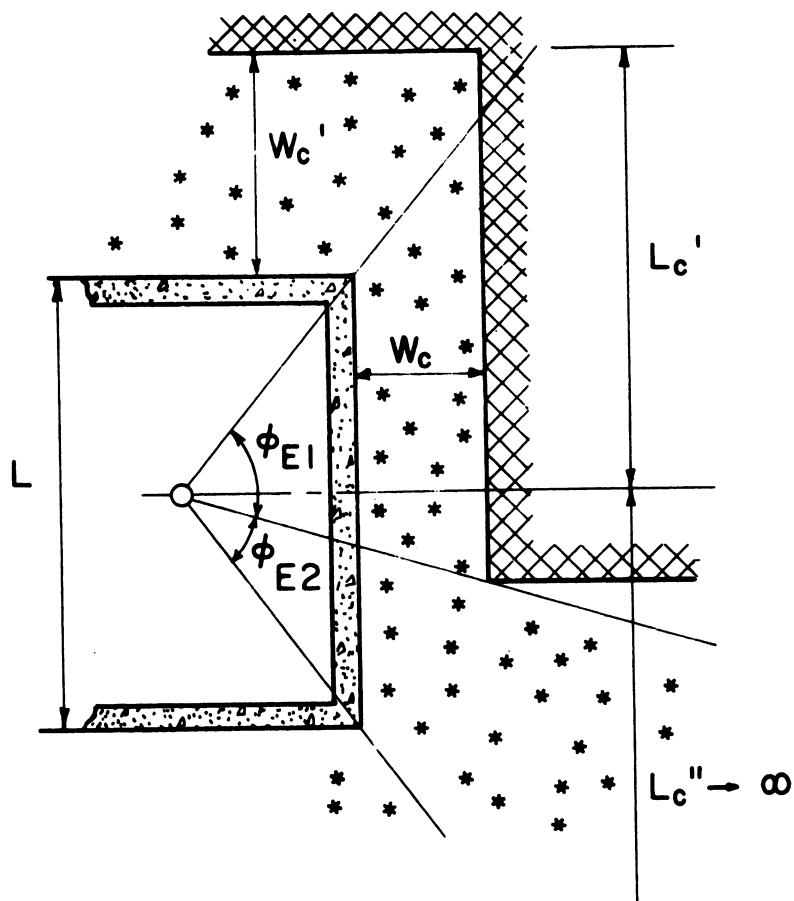
$$B(\phi_{E1}) = (1/2) [B_s(X_e, 2\omega'_s) + B_s(X_e, 2\omega''_s)] \quad , \quad (IX.14)$$

where

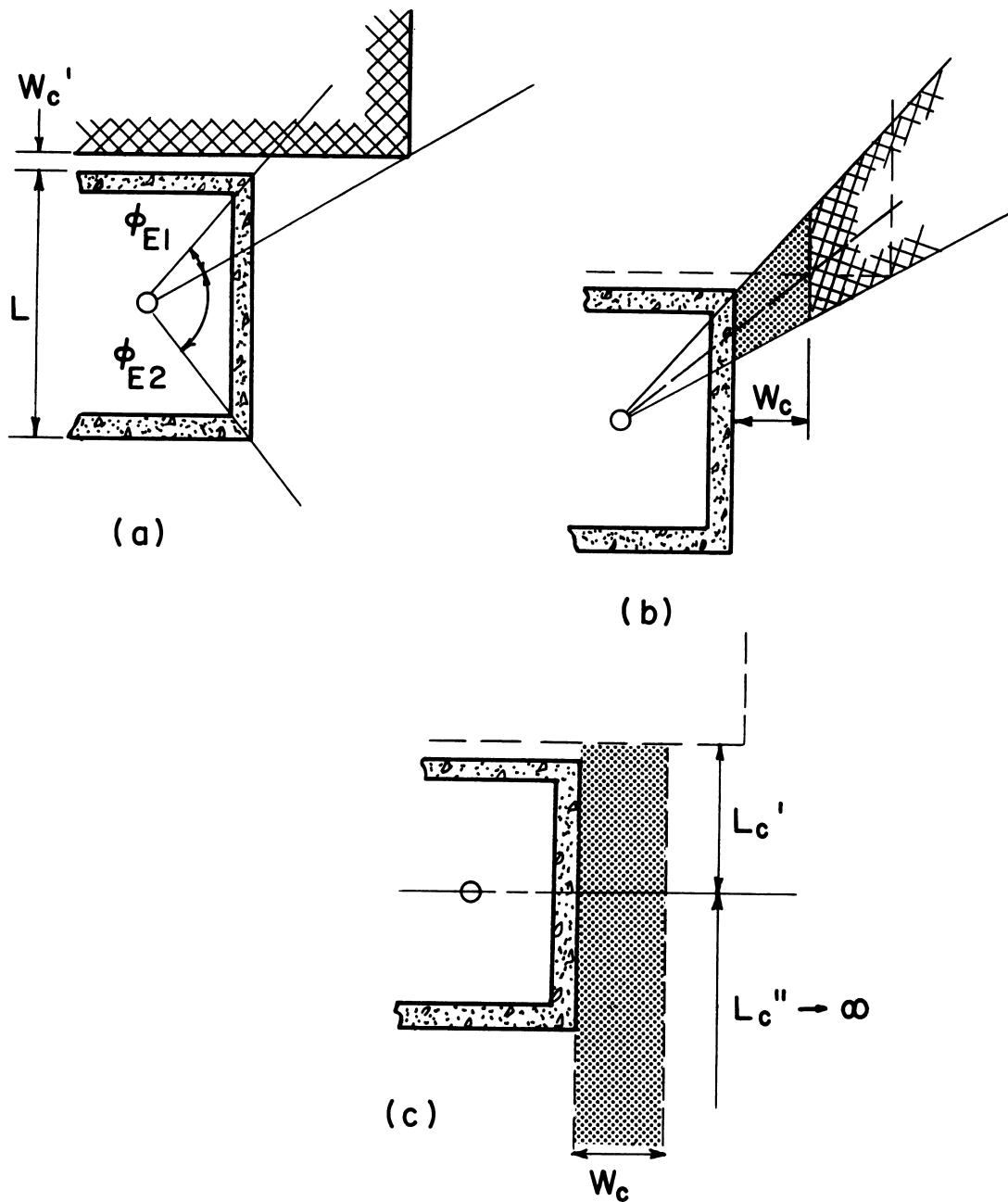
$$\begin{aligned} \omega'_s &= \omega_s(W_c, L + 2W'_c, H), \\ \omega''_s &= \omega_s(W_c, \infty, H) \quad . \end{aligned}$$

For sector  $\phi_{E2}$ , the barrier factor for an infinite field can be used.

Figure IX.10 gives a situation which appears somewhat different; but, after the limited field width is obtained by squaring off as shown, the situation is basically the same as that just discussed, and eq (IX.14) still applies.



IX.9 Illustration of situation for wall-scattered, limited field calculation in which the field for Sector E-1 is not symmetric in longitudinal extent with respect to the center of the wall.



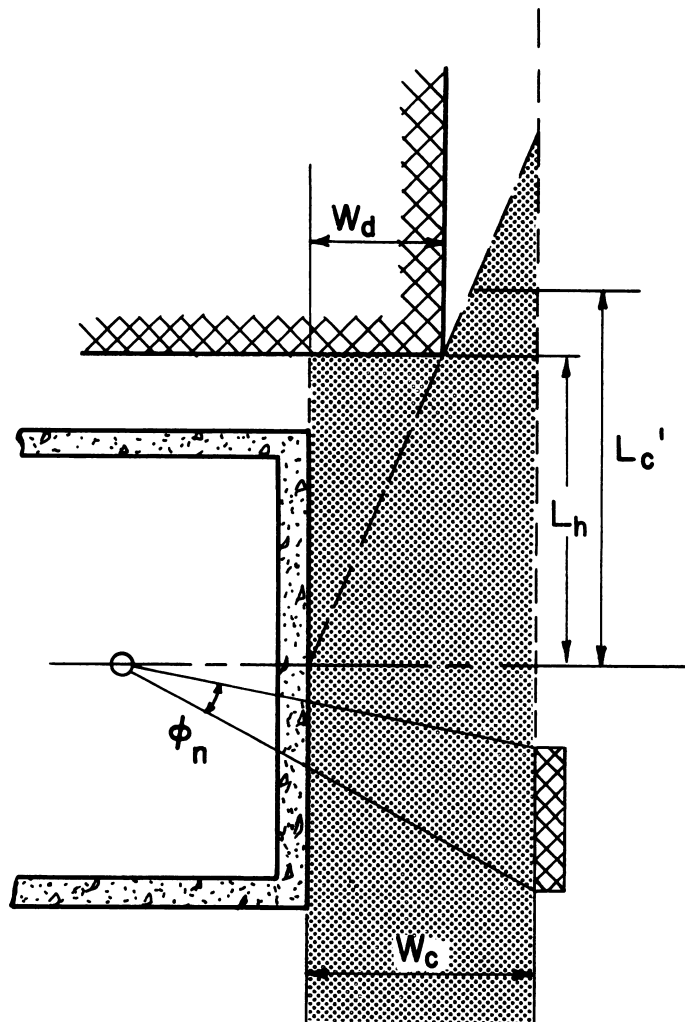
IX.10 Situation involving both non-parallel limited field boundary and non-symmetry in equivalent field length: (a) actual configuration; (b) "squared-off" field; (c) limited field for obtaining  $\omega_s$ .

Another question which arises is how to obtain the length of the equivalent rectangle, either totally or in one direction from the wall center, when the limited field of given width does not have a simple, straight, rectangular boundary at one or both ends. The question is illustrated and an answer suggested in figure IX.11. For the contribution related to the azimuthal fraction contained within  $\phi_n$ , one must assume a limited field of width  $W_c$ . However, the length of this field is not constant because of partial blockage by a structure depicted above that under consideration. It is reasonable to assume that the limited field is that area of limited width ( $W_c$ ) which can be seen from the center of the wall. One can then compute the average length of the area. For the situation shown, the average distance  $L'_c$  to the upper boundary from the center line is given by

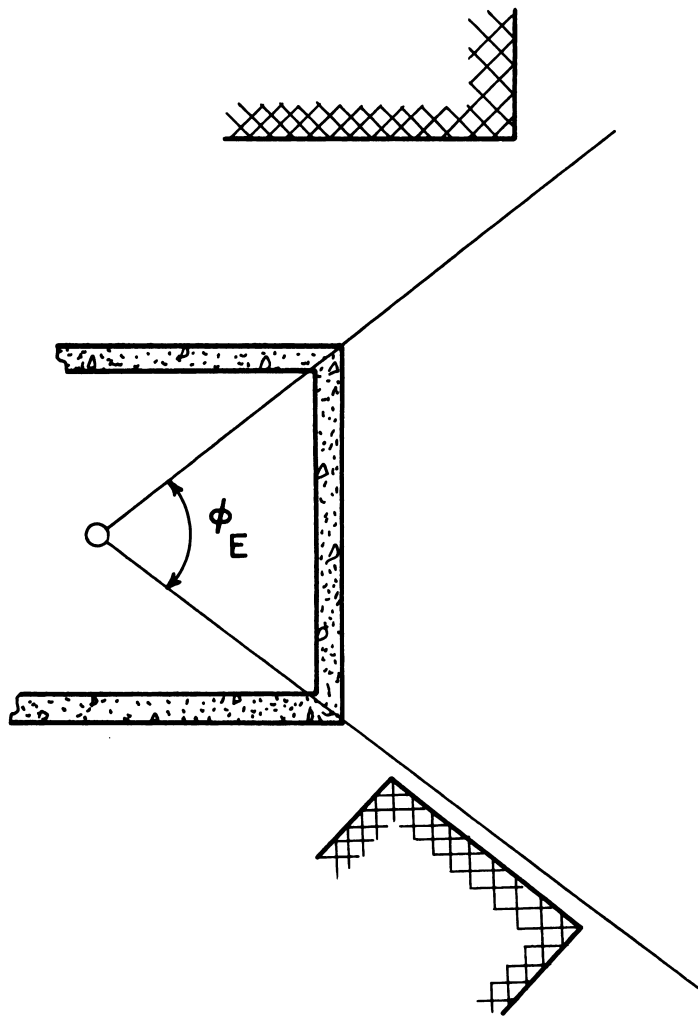
$$L'_c = \frac{L_h (W_c^2 + W_d^2)}{2 W_c W_d} \quad (\text{IX.15})$$

A third question pertains to the situation when the source field is limited, not by external shields within the limits of the azimuth established by the wall under analysis, but by shields outside this azimuth. Figure IX.12 illustrates such a case. Here the external radiation field incident on the right-hand wall is somewhat less than is assumed in the use of the function  $B_e$  as wall barrier factor. But the type of field limitation is so different from that assumed for the computation of the  $B_s$  data that the latter function appears unsuitable. Presently one had best proceed by ignoring the external barriers, insofar as the right-hand wall of the structure is concerned. This expedient has several virtues: The use of  $B_e$  gives an error on the conservative side; the effect of external barriers outside the sector established by the wall is usually quite small; and this technique is consistent with the





IX.11 Example of limited field of non-uniform length, creating difficulty in computation of  $\omega_s$ .



IX.12 Illustration of adjacent structures affecting field incident on east wall of blockhouse, but not within the east azimuthal sector.

method of handling the problem illustrated in figure (IX.11). (Note that in eq (IX.15) the value of  $L'_c$  approaches infinity as  $W_c$  approaches infinity.)

#### (7) Final Comment on Incremental Wall Area Approach

Just as for the "direct" contribution from limited fields, putting the formulas for the "wall-scattered" contribution from finite fields on an incremental wall area basis offers no difficulty. Equations (VII.67) through (VII.78) and the discussion concerning them are valid, provided that here only terms involving  $G_s$  are of interest, and  $B_e$  should be replaced by  $B_s$ . For obtaining the value of  $\omega_s$ , it is probably best to use the position on the wall of the incremental area for the vertex of this solid angle fraction.

#### d. Additional Comments on Limited Fields

A few general comments are pertinent in concluding the subject of limited fields.

The question may have occurred to the reader as to why the wall barrier function  $B_s$ , since it relates to penetration of the sum of "wall-scattered" and "direct" components of the radiation, could not (or should not) be used in place of the  $B_e$  function for the "direct" component also. Our answer is that in principle it could. In fact, within the approximations inherent in the standard approach, the uncollided radiation penetrating should be given either by  $B_e (1 - S_w) [G_d(\underline{\omega}) - G_d(\underline{\omega}')] ]$  or by  $B_s (1 - S'_w) [G_d(\underline{\omega}) - G_d(\underline{\omega}')] ]$ , giving approximately the same numerical value for any specific case. Note, however, that in the second expression, we have used  $S'_w$  instead of  $S_w$ . This is because for a finite source field, the radiation incident on the wall has different characteristics, notably in the angular distribution, from an infinite field; and therefore the value of the interpolation constant, which indicates the relative proportions for the thick-and thin-wall cases, will differ for finite and infinite field cases. In fact, the value of  $S_w$

should depend on  $\omega_s$  or some similar field size parameter; and in "wall-scatter" formulas, such as eq IX.7, our failure to provide values of this "scattering fraction" different from the standard values provided for the infinite field case is a defect in the methodology.

Another question of interest is the size of field width ( $W_c$ ) that can be considered essentially infinite. This depends upon the degree of accuracy required in the computation, as well as important geometric parameters of the specific situation under consideration. For a thin-wall case, there are three contributions, real or hypothetical, to be considered: the direct contribution from the limited field, the potential contribution from the area beyond the limited field which is eliminated by the neighboring structure, and the skyshine contribution. In the notation indicated in figures IX.2 and IX.4, these contributions are proportional, respectively, to  $[G_d(\underline{\omega}, H) - G_d(\underline{\omega}', H)]$ ,  $G_d(\underline{\omega}', H)$ , and  $G_a(\bar{\omega})$ . If the second of these proportionality factors is small compared to the sum of the other two, it makes little difference in the total wall contribution calculation whether the field is considered finite or infinite.

For the very-thick-wall case, in which the limited field effect is taken care of by modifying the barrier factor, the effect of field size can be approximately accounted for by use of the function  $L_c(0, 2\omega_s)$ , as previously indicated in the discussion of how values for  $B_s$  are obtained. In such a case, involving a large but finite field, one has only to calculate  $L_c$  and see how close it comes to unity: The defect from unity approximates the error in the wall contribution due to assuming that the finite field is infinite.

For walls of intermediate thickness the above criteria must be combined in a proportional way, through the use of the "wall-scattering" factor,  $S_w$ .

Under circumstances in which the roof contribution dominates the total, more radical approximations can be made in the other contributions. We note also that when a finite field is called infinite the error is on the conservative side, with regard to safety. There is thus little concern about the finiteness of a field for values of  $W_c$  greater than a few hundred feet.

Clearly the problem of finite fields is rather intricate. At times good engineering judgment would dictate a simpler or at least different method from that given here for handling some specific problem; and nothing we have said is intended to rule out use of such judgment. We must also keep in mind, however, that much fallout shelter analysis is carried out by computers. The methodology introduced into the computer allows no basis for "engineering judgment" in specific cases. The human factor enters into the description of the structure and the radiation field, which is drawn up in advance during a survey, for input into the computer. In this descriptive process, there is considerable room for judgment, in order not to include information in any finer detail than needed for a reasonably good result. It is in this early stage that "smearing" of structural variations or simplifying of complex-shaped source fields can be accomplished. Chapter XI discusses this matter further.

## 2. Slightly Buried Sources (Ground Roughness)

The assumption of a smooth source plane is an idealization which is hardly ever realized. Ground surfaces, even if fairly level, have roughness between that exhibited by pavements and that of a well plowed field.<sup>11</sup>

---

<sup>11</sup>We distinguish here between this scale of roughness and that of larger scale contour variations such as hills and ditches. The latter is better approached using neighboring barriers and limited fields. See also sections VI.E.2 and XI.B.5.

Because of this small-scale roughness, fallout particles settle into cracks and hollows in the surface, so that much of the source radiation experiences a small barrier at the ground before traversing air and shelter walls. The effect of this additional barrier is approximately as if the fallout source were either distributed through a small thickness of material at the surface of the earth or on a plane just below the surface of the earth. Other idealizations, such as fallout distribution on a "saw-toothed" type of surface can be used. These matters are discussed in some detail in chapter VI.

Although one could refine one or the other of these idealizations, many practical aspects indicate that such efforts are not very useful:

(a) One would like to have a mathematical relationship which would indicate shielding effectiveness due to roughness; but this requires a quantitative measure of roughness which is easy to estimate or determine experimentally, and which has a close correlation with shielding effectiveness. Such a roughness measure has not yet been found.

(b) The shielding effectiveness depends on the degree to which the fallout particles have settled into crevices and hollows. This can be affected by wind, rain, and perhaps other environmental conditions occurring after the fallout arrives. It can thus be unpredictably time-dependent.

(c) Surface conditions may change, either naturally by climatic effects or by man-created modifications, between the date of shelter evaluation and the date of use.

The standard method of accounting for ground roughness is therefore quite simple and we cannot recommend further elaboration. Ground roughness is considered to act as an additional layer of air-like material between the source and the wall which the radiation penetrates. Thus, the wall barrier

factor,  $B_e$ , is determined using a value of  $H$  greater than the height used under smooth plane assumptions by some equivalent distance of air, as suggested in table IX.1.<sup>12</sup>

Further, the OCD Manual suggests that under usual conditions ground roughness be ignored because it is a bonus of uncertain magnitude.

### 3. Elevated Ground Sources

The term "elevated ground source" refers to any plane source of fallout which is below the detector plane but above ground level. A typical situation is fallout on the roof of a neighboring building which is lower than the detector position in the building being analyzed. Even though the radiation originates at a roof, it is treated as a "ground" contribution.

No new principles are needed for handling this type of problem, although it may involve a complicated "mutual shielding" condition. We explain the procedure in terms of a specific problem. Consider radiation through a structure wall near a low building which provides an elevated source of radiation as well as a partial shield from the radiation originating on the ground beyond the neighboring building. Figures IX.13, IX.14 and IX.15 indicate geometric details.

The plane view at the top of figure IX.13 suggests that the wall contribution be divided into five azimuthal sectors to account for the elevated source. The azimuthal angles  $\phi_n$  are numbered consecutively from the top. Figure IX.14 shows the six values of  $\omega$  necessary to calculate the "direct" radiation, and the heights  $H_1$  associated with intersection of the limiting

---

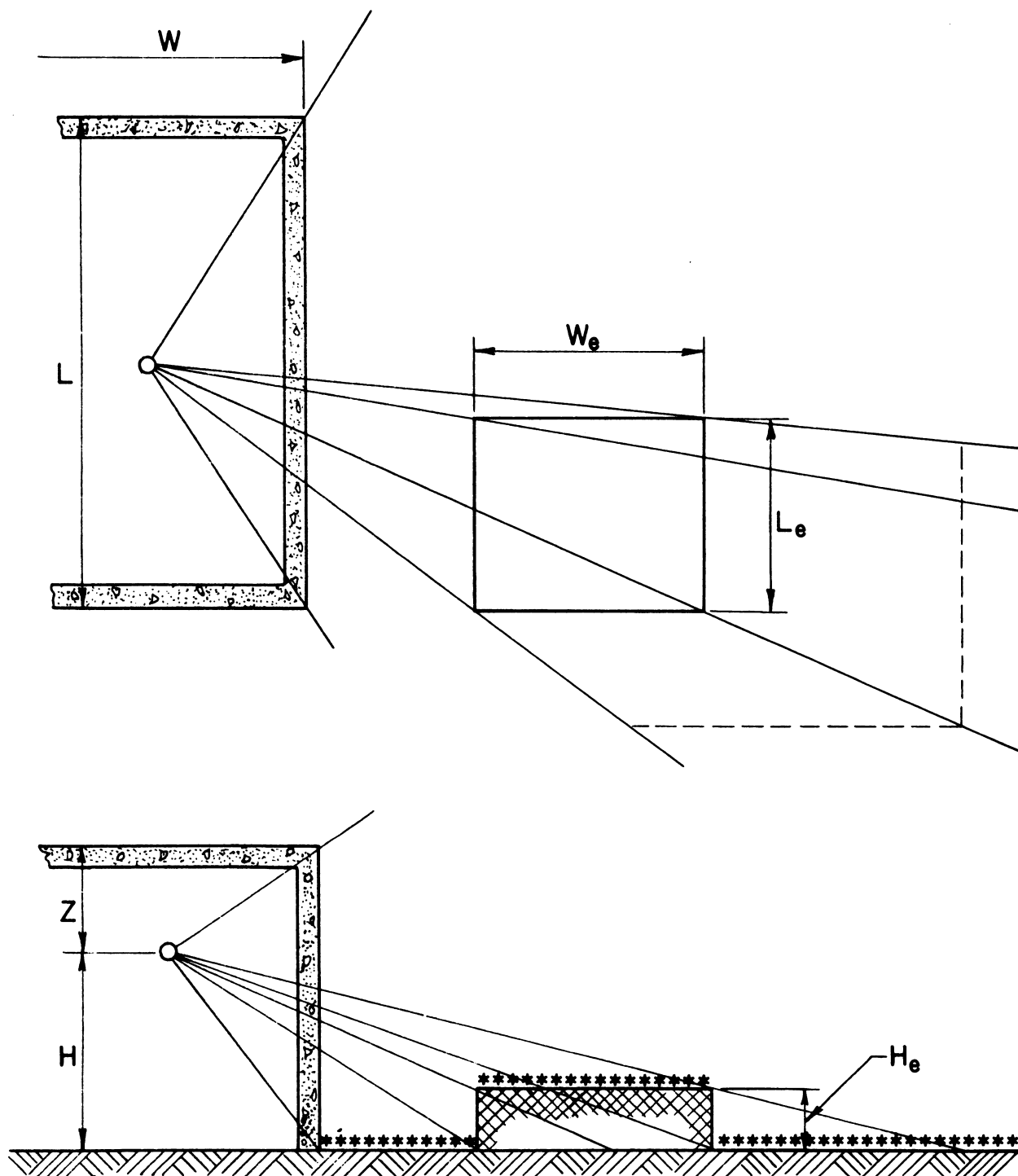
<sup>12</sup>The table given here is as it appears in the OCD Manual [1]. The justification for the numbers is not known, but they are consistent with the general state of knowledge at the time the table was originally drawn up. See section VI.D. Reference [5] also gives detailed information.

TABLE IX.1

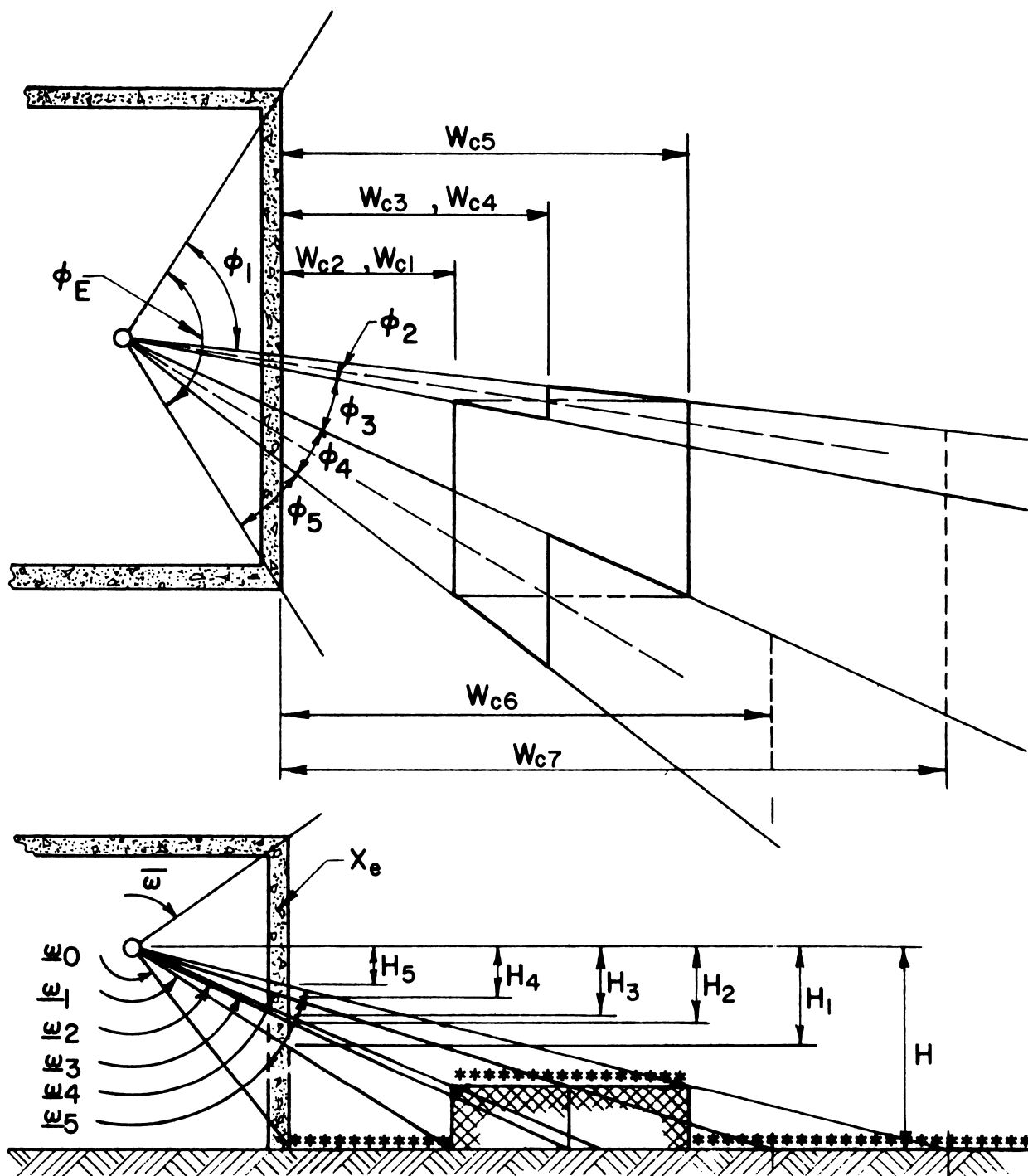
Additional Height Increments to Account  
for Ground Roughness

<u>Type of Surface</u>	<u>Additional Height (ft)</u>
Smooth plane	0
Paved areas	0 - 5
Lawns	5 - 10
Graveled areas	10 - 20
Ordinary plowed field	20 - 40
Deeply plowed field	40 - 60

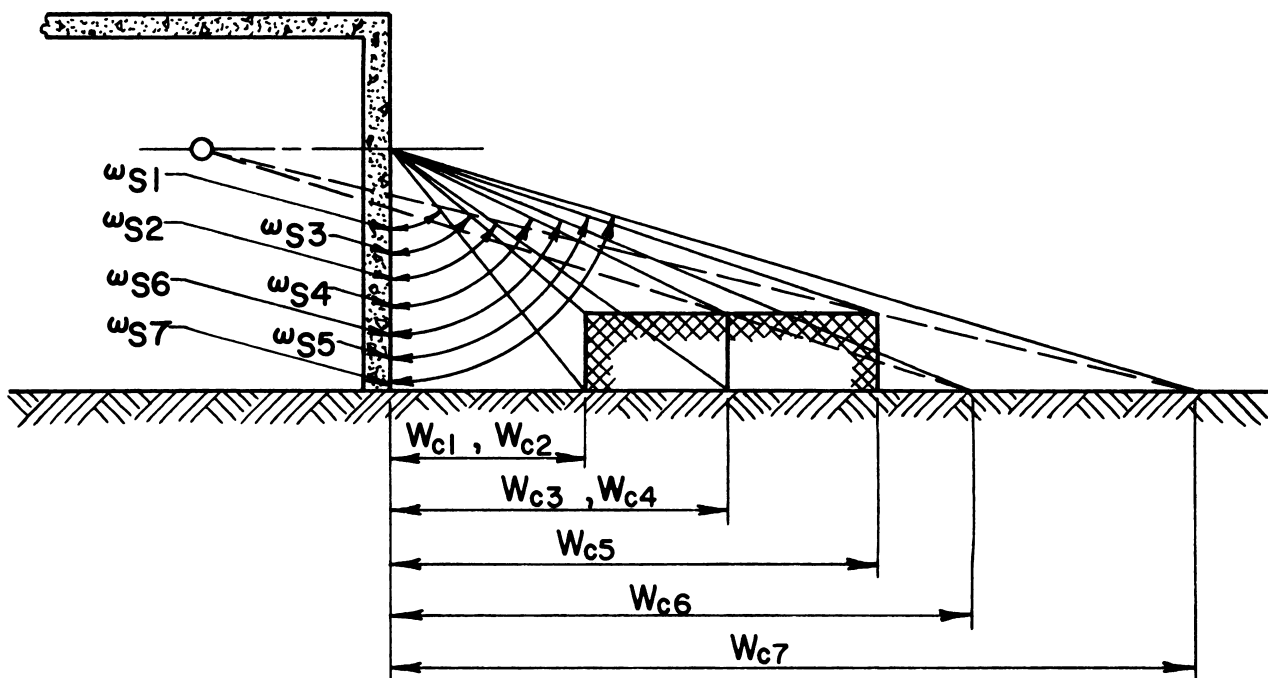




IX.13 Example of situation involving elevated ground contribution (low neighboring roof).



IX.14 Situation of figure IX.13, after modification for purpose of analysis.



IX.15 Further details of situation depicted in figures IX.13 and IX.14.

rays with the exterior wall. Figure IX.15 shows the seven values of  $\omega_s$  required to calculate the "wall-scatter" contribution, and the seven field widths  $W_{cj}$  associated with them.

We assume the following data to be known in advance:  $H$ ,  $H_e$ ,  $W$ ,  $L$ ,  $X_e$ ,  $Z$ ,  $W_{c1}$  ( $= W_{c2}$ ),  $W_e$ ,  $L_e$ ,  $\phi_1$ , ...,  $\phi_5$ . Necessary preliminary linear dimensions are easily calculated, either on the basis of previously prescribed formulas or through elementary geometric considerations:

$$\begin{aligned}
 W_{c5} &= W_{c1} + W_e \\
 H_1 &= \frac{(W/2) \cdot H}{(W/2) + W_{c1}} \\
 H_3 &= \frac{(W/2) \cdot (H - H_e)}{(W/2) + W_{c2}} \\
 H_5 &= \frac{(W/2) \cdot (H - H_e)}{(W/2) + W_{c5}} \\
 H_4 &= (1/2) (H_3 + H_5) \\
 W_{c3} = W_{c4} &= (W/2) \left[ \frac{(H - H_e)}{H_4} - 1 \right] \\
 W_{c6} &= (W/2) \cdot \left[ \frac{H}{H_4} - 1 \right] \\
 W_{c7} &= (W/2) \cdot \left[ \frac{H}{H_5} - 1 \right]
 \end{aligned}
 \tag{IX.16}$$

The angles are readily obtained as follows:

$$\begin{aligned}
 \underline{\omega}_0 &= \omega(W, L, H) \\
 \underline{\omega}_1 &= \omega(W, L, H_1) \\
 \underline{\omega}_2 &= \omega(W, L, H_2) \\
 \underline{\omega}_3 &= \omega(W, L, H_3) \\
 \underline{\omega}_4 &= \omega(W, L, H_4) \\
 \underline{\omega}_5 &= \omega(W, L, H_5) \\
 \bar{\omega} &= \omega(W, L, Z)
 \end{aligned}
 \quad \left. \vphantom{\begin{aligned} \underline{\omega}_0 \\ \underline{\omega}_1 \\ \underline{\omega}_2 \\ \underline{\omega}_3 \\ \underline{\omega}_4 \\ \underline{\omega}_5 \\ \bar{\omega} \end{aligned}} \right\} \quad (\text{IX.17})$$

$$\begin{aligned}
 \omega_{s1} &= \omega_s(W_{c1}, \infty, H) \\
 \omega_{s2} &= \omega_s(W_{c2}, \infty, H) \\
 \omega_{s3} &= \omega_s(W_{c3}, \infty, H-H_e) \\
 \omega_{s4} &= \omega_s(W_{c4}, \infty, H-H_e) \\
 \omega_{s5} &= \omega_s(W_{c5}, \infty, H-H_e) \\
 \omega_{s6} &= \omega_s(W_{c6}, \infty, H) \\
 \omega_{s7} &= \omega_s(W_{c7}, \infty, H)
 \end{aligned}
 \quad \left. \vphantom{\begin{aligned} \omega_{s1} \\ \omega_{s2} \\ \omega_{s3} \\ \omega_{s4} \\ \omega_{s5} \\ \omega_{s6} \\ \omega_{s7} \end{aligned}} \right\} \quad (\text{IX.18})$$

in which, as previously noted,  $\omega_s(W_c, L_c, H_c) \equiv (1/2) \omega(2W_c, L_c, H_c)$ .

We can now find individual contributions through the right-hand wall. Many could better be combined, but we keep them separate for the sake of clarity.

(a) Direct (non-wall-scattered)

Sectors 1 and 5:

$$[(\phi_1 + \phi_5)/360^\circ] \cdot B_e(X_e, H) \cdot [1 - S_w(X_e)] \cdot G_d(\omega_0)$$

Sector 3:

$$(\phi_2/360^\circ) \cdot \{B_e(X_e, H) \cdot [G_d(\omega_0) - G_d(\omega_2) + G_d(\omega_5)]$$

$$+ B_e(X_e, H - H_e) \cdot [G_d(\omega_3) - G_d(\omega_5)]\} \cdot [1 - S_w(X_e)]$$

Sector 4:

$$(\phi_4/360^\circ) \cdot \{B_e(X_e, H) \cdot [G_d(\omega_0) - G_d(\omega_1) + G_d(\omega_4)]$$

$$+ B_e(X_e, H - H_e) \cdot [G_d(\omega_3) - G_d(\omega_4)]\} \cdot [1 - S_w(X_e)]$$

(IX.19)

(b) Skyshine

$$(\phi_E/360^\circ) \cdot B_e(X_e, H) \cdot [1 - S_w(X_e)] \cdot G_a(\bar{\omega}) \quad (IX.20)$$

(c) Wall-scattered

The contribution through the  $j$ -th sector is

$$(\phi_j/360^\circ) \cdot B_j \cdot S_w(X_e) \cdot E(e) \cdot [G_s(\bar{\omega}) + G_s(\underline{\omega}_0)] \quad ,$$

in which

$$B_1 = B_5 = B_e(X_e, H)$$

$$B_2 = B_s(X_e, 2\omega_{s2}) + B_s(X_e, 2\omega_{s5}) - B_s(X_e, 2\omega_{s4}) + B_e(X_e, H) - B_s(X_e, 2\omega_{s7})$$

$$B_3 = B_s(X_e, 2\omega_{s1}) + B_s(X_e, 2\omega_{s5}) - B_s(X_e, 2\omega_{s3}) + B_e(X_e, H) - B_s(X_e, 2\omega_{s7})$$

$$B_4 = B_s(X_e, 2\omega_{s1}) + B_s(X_e, 2\omega_{s4}) - B_s(X_e, 2\omega_{s3}) + B_e(X_e, H) - B_s(X_e, 2\omega_{s6})$$

(IX.2)

Although this method of solution is largely self-explanatory, a few comments are appropriate. First, we repeat that verbal designations of the physical significance of each "contribution" are not to be taken very seriously. The formalism has been developed so as to permit an approximate physical interpretation for each term; and this is a useful guide in choosing the specific functions and geometric parameters to use; however, the sum of all the contributions represents the overall contribution through the right-hand wall much more closely than any one contribution represents a designated type of wall interaction from a given limited field in a given sector.

The "contributions" in the sectors 2-4 are obtained by the usual summing and differencing technique. In each of these sectors, the field is in three parts: the limited strip between the blockhouse and the near wall of the

exterior building; the roof of the exterior building; and the infinite field beyond the "shadow-line" of the roof of the exterior building. Note that the field of significance beyond the neighboring building is taken to be limited by the same "shadow-line" for wall-scattered components as for direct. From figure IX.15 this is seen to be not strictly true; but it is simpler to make such an assumption, and the error involved appears to be relatively minor.

The above approach can be simplified somewhat, without any change in principle, if the sector boundaries are established in a coarser fashion which treats the elevated source as being one single sector. The sector limits are taken as the bisectors of sectors 2 and 4 as shown in figure IX.14.

#### 4. Sloping Source Planes

It is quite reasonable to expect the topography often to deviate from the horizontal, which condition has been assumed thus far. Roofs of low neighboring buildings may be sloping rather than flat. Furthermore, these conditions are likely to occur in a complex configuration of several different slopes, including the horizontal, in various parts of the field around a structure to be analyzed.

A complete and demonstrably accurate method of approaching this problem is not presently available. The best current guidance is provided by a relatively simple example in the OCD Manual.<sup>13</sup> Even in this example, some of the techniques used are based on debatable judgment. All we shall attempt here is to review this example, first in the general framework of the standard approach as presented in the OCD Manual, and then with a suggested alternative approach which seems to be more easily generalized to more complex situations.

---

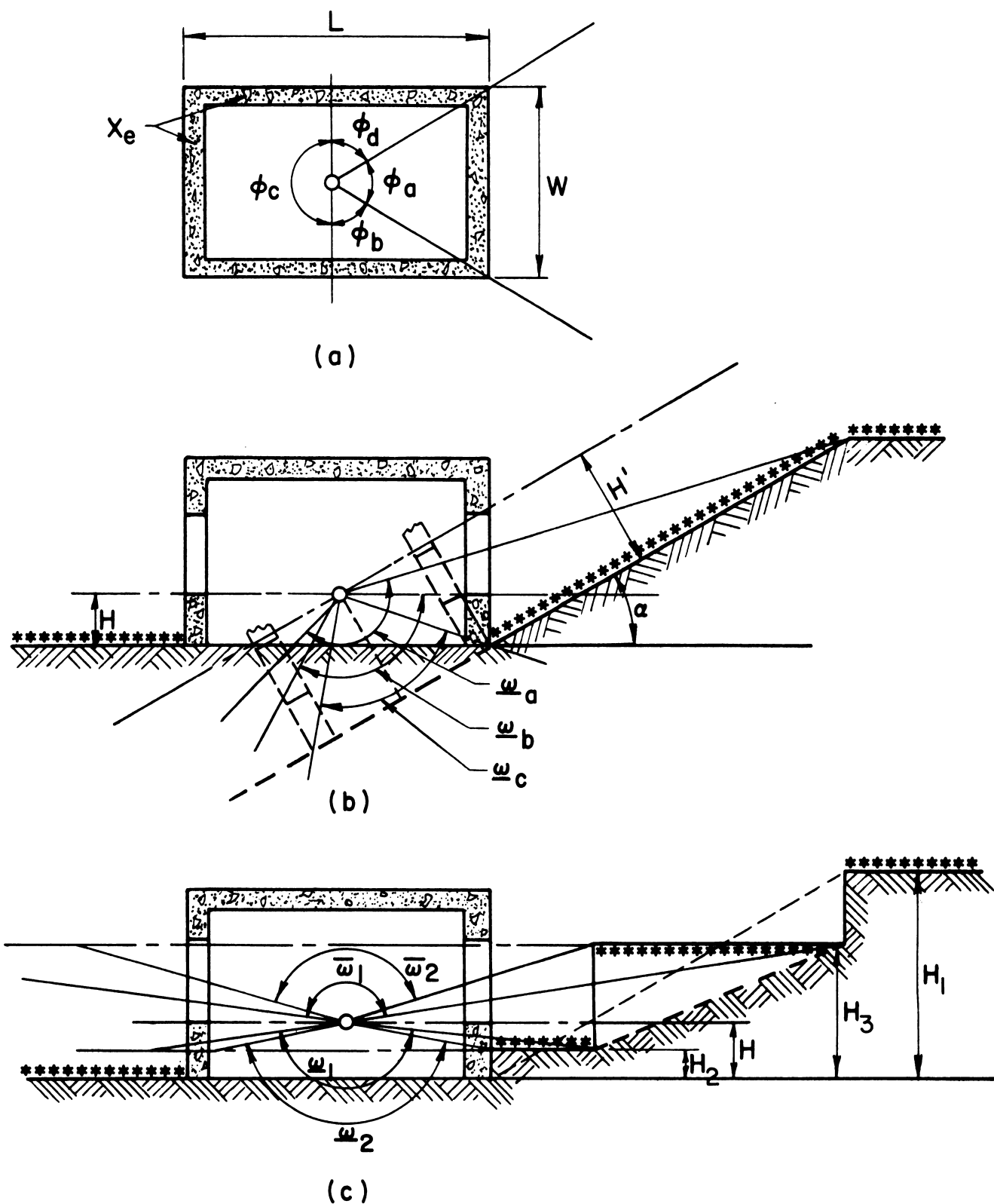
<sup>13</sup>Problem 6-16 of Reference [1].



The example referred to is illustrated in figure IX.16, along with auxiliary data needed for the analysis. It involves a blockhouse with windows, at the toe of a slope on the right-hand side. Since fallout is assumed to be distributed with equal source strength per area of horizontal projection, the source on the slope has less strength per unit area than on the horizontal by a factor  $\cos\alpha$ . The effect of the sloping source plane is greatest on the right-hand wall of the figure, negligible on the left-hand wall, and moderately noticeable for the other walls. The overall effect may be viewed as a combination of several parts. The most obvious of these is the change in the radiation field at the walls due to the change in source configuration. Another factor is the complete shielding of the field on the plateau beyond the top of the slope. Thirdly, because the fallout on the hillside is partly above sill level, some is visible through the windows. Note that these effects are not all positive or all negative. The most significant effect in this example is the third mentioned. Since this markedly enhances the direct contribution to the detector response, the overall effect of the sloping source diminishes the shielding capability of the structure. For this reason, one cannot afford to neglect the sloping-source aspects of configurations, when they exist.

#### a. Standard Approach

The Standard Method assumes that there is no significant effect on the skyshine contribution. Furthermore, "wall-scatter" contributions from each of the four walls are also assumed to be insignificantly changed by the fact that part of the source field is sloping. (One might raise an objection to the latter assumption, since for the right-hand wall a definite limited-field condition exists which should lower the strength of the incident radiation



IX.16 Illustrative example of methods off fallout analysis with part of source on a sloping plane: (a) plan view of blockhouse (windows no indicated); (b) modification for Standard Method of analysis; (c) modification for alternate method.

field. Ignoring this, however, is an error on the conservative side.) Thus, the only contribution to be seriously examined from the sloping source point of view is the "direct" one.

As shown in figure IX.16(b), the essence of the standard approach to this contribution is to consider the sloping source as a new reference plane and to establish a hypothetical structure with walls perpendicular to the sloping plane and of such a configuration as to preserve those aspects of the original structure which significantly affect the calculation of the direct contribution. The characteristics of the hypothetical situation are as follows:

(a) The source has a strength per unit area smaller than the standard by a factor of  $\cos\alpha$ , as previously noted. All detector contributions for this situation that are based on standard formulas and data must be multiplied by this factor.

(b) Since the "direct" component is assumed to have no interaction with the wall, the hypothetical wall should present the same slant penetration thickness as the original wall, for any given ray from a source point to the detector. This is not possible to achieve in general, and so it is effected for the rays of greatest importance, which are those approximately parallel to the slope. This is achieved by requiring the equivalent mass thickness of the hypothetical structure wall exceed that of the actual blockhouse by a factor of  $\sec\alpha$ .

(c) The detector height above the source plane becomes  $H'$ .

(d) The planes through the detector to the far limits of the sloping source, and the changes in wall thickness (window openings) on the side toward the slope, are maintained in the hypothetical situation, and all dimensions of the geometric configuration are thereby fixed. The detector position is maintained, so that blockhouse dimensions must be modified as necessary to

maintain symmetry. Thus the length of the blockhouse in the plane of the figure is reduced by  $\cos\alpha$ , but the dimension perpendicular to the plane of the figure is kept the same.

The formulas appropriate to the hypothetical configuration are as follows.

"Direct" contribution, right-hand wall, below window sill:

$$C_{g1} = \cos\alpha B_e(X_e \sec\alpha, H') [1 - S_w(X_e \sec\alpha)] \cdot [G_d(H', \omega_c) - G_d(H', \omega_b)] F_{r1} \quad , \quad (IX.22)$$

where  $F_{r1}$  may be obtained either by the perimeter ratio or the azimuthal sector approach for the sector labeled as  $\phi_a$  in figure IX.16(a).

"Direct" contribution, right-hand wall, above window sill:

$$C_{g2} = \cos\alpha [1 - S_w(X_e \sec\alpha)] [G_d(H', \omega_b) - G_d(H', \omega_a)] \cdot [B_e(X_e \sec\alpha, H') F_{r2} + B_e(0, H') F_{r3}] \quad , \quad (IX.23)$$

where  $F_{r2}$  is the proportionality factor for the wall panels between the windows in sector  $\phi_a$  and  $F_{r3}$  is the same factor for the windows.<sup>14</sup>

The "direct" contribution for the sector labeled as  $\phi_c$  is easily computed on the usual basis of the infinite, horizontal plane. The contributions for the sectors  $\phi_b$  and  $\phi_d$ , which are affected in part by the sloping source and in part by the horizontal plane source, are calculated as averages of results obtained for sectors  $\phi_a$  and  $\phi_c$ , with due regard for the different values of  $F_r$  involved.

---

<sup>14</sup>The Training Manual arbitrarily uses 3 ft rather than  $H'$  as the height for  $B_e$  and  $G_d$ , without adequate justification.

## b. Alternate Approach

The other approach which seems feasible is illustrated in figure IX.16(c). This uses no hypothetical structure, but instead requires approximating a sloping field with an equivalent horizontal field at an average height. Since the direct contribution is divided into two parts by the plane through the window sill, the sloping field is actually approximated by two horizontal fields, one for the contribution through the wall below the windows, and one through the windows and wall panels between the windows. Except for one particular, this changes the problem into one involving elevated ground sources, which is discussed in the previous section. The one difference is that the equivalent plane source above the window sill, which represents an actual source unshielded externally from the blockhouse except by air, is not considered resting on the ground and is therefore free of direct shielding by the earth. Its effect may be evaluated as if the entire configuration were turned upside down, so that it is treated as a ground source. Equations (IX.22) and (IX.23) are then replaced by the following formulas.<sup>15</sup>

"Direct" contribution, right-hand wall, below window sill:

$$C_{g1} = B_e(X_e, H) [1 - S_w(X_e)] [G_d(H - H_2, \omega_2) - G_d(\omega_1)] F_{r1} \quad , \quad (IX.24)$$

where  $H_2$  equals  $H/2$ .

---

<sup>15</sup> As a test, problem 6-16 of the OCD Manual was worked using the above equations. The overall answers obtained were very close to those obtained by the standard approach, and the calculation was found to be much simpler. ( $H-H_2$  is only 1.5 ft, so that values depending on this argument had to be obtained by extrapolation, since the data on the charts do not go below 3 ft in height. Alternatively, 3 ft could have been used -- the final answers do not change very much as a result.)

"Direct" contribution, right-hand wall, above window sill:

$$C_{g2} = [1 - S_w(X_e)] [G_d(H_3 - H, \bar{\omega}_2) - G_d(H_3 - H, \bar{\omega}_1)]$$

$$\cdot [B_e(X_e, H_3 - H) F_{r2} + B_e(0, H_3 - H) F_{r3}] \quad , \quad (IX.25)$$

where  $H_3$  equals  $(1/2) (H + H_1)$ .

Generalizations to the "wall-scattered" component through the right-hand wall and to all contributions through the top and bottom walls are possible by use of principles previously developed in this chapter.

### C. COMPLICATIONS IN STRUCTURE

#### 1. Internal Compartmentation

##### a. Introduction

The main feature which distinguishes most structures from the simple blockhouse is the existence of barriers interior to the outer structural membrane, or shell. These barriers are usually horizontal (floors) or vertical (interior partitions). Internal barriers may exist which do not conform to either of these categories, such as ramps or stairs; but the existing methodology makes no special provisions for these and they must be assigned to one category or the other, possibly as a combination, as the judgment of the analyst may dictate. Most interior barriers can also be classified as parallel or perpendicular, terms which describe the relative orientation of the interior barrier and the portion of the exterior shell whose contribution to the detector response is most affected by the interior barrier.

Before discussing specific cases of this type, we list general principles which have been applied to almost all of them.

(1) With the exception of a Monte Carlo calculation for an accurate computational model, or an experimental measurement (possibly using scale models) there are no rigorous approaches which are generally valid for all internal barrier situations. The standard methodology and its variants involve some degree of simplification and approximation; these are suggested by reasoning which is largely intuitive, or by empirical approximation to experimental data, or by a combination of these approaches.

(2) The effect of each internal barrier is generally assumed to be dependent only on its equivalent mass thickness,  $X_i$ , measured in a direction normal to its surface.

(3) Interior barriers are usually treated as if (1) they were folded back to become part of the outer shell, (2) they were homogeneously smeared out (possibly with the outer shell) in the region between the outer shell and the detector, or (3) they acted purely as an absorbing type of "shadow shield" intercepting radiation proceeding in straight lines from the outer shell to the detector. The "smearing-out" mentioned in treatment (2) may be done with preservation of either the total mass involved or the total barrier thickness between detector and shell. (These are not equivalent.) In the use of treatment (3), the interior barrier is not regarded as a secondary source of scattered radiation as is the outer shell.

(4) It is possible and often desirable to use the edges of internal barriers, and the lines of demarcation between portions with different effective mass thickness, as boundaries of zones and azimuthal sectors, just as one does with the outer structural shell. But a complex system of internal compartmentation then requires computation of a large number of separate contributions, so that the process is arduous and time-consuming. Interior barriers are generally treated in a much more cavalier fashion anyway, and one may better

justify smearing out variations in the thickness of interior barriers than one would do for the exterior shell. For example, doors or gaps across corridors in interior partitions may serve simply to diminish the average thickness of the partition, which is treated as continuous across such gaps.

(5) The factor expressing the effect of an interior barrier can be defined in two ways. One is as the ratio of the detector response when the barrier is present to the response when it is absent, all other circumstances being the same. Such a factor depends not only on the barrier thickness, but also on the total geometric configuration involved, and is called an attenuation factor (see sec. V.B.4).

Alternatively, it is possible in principle to establish one or two intermediate points of measurement on each side of the interior barrier and regard them as "sandwiched in" the logical chain of measurements indicated in the development of formulas such as eqs (VII.6) and (VII.31). The resulting barrier factor is defined as the ratio of detector responses at positions on each side of the barrier; and modifications are then required of at least one other function in the full expression. Either of the two approaches above is valid, but they are not generally identical.<sup>16</sup> The first approach puts all the geometric complications created by the interior partition into the attenuation factor; the second approach leads to a simple interior barrier factor, but it also complicates some of the geometry-dependent factors. But one does find formulations in the standard methodology in which the use of an attenuation factor for interior walls is implied by the use of all other

---

<sup>16</sup> There are special circumstances in which the two approaches just described give the same numerical results, e.g. when the radiation fields incident on and emergent from a floor slab are strongly peaked in the downward direction, so that there is little variation of detector response with height except at the barrier.



functions established on the basis of no internal barriers, while a barrier factor is actually used for computing the attenuation factor.<sup>17</sup>

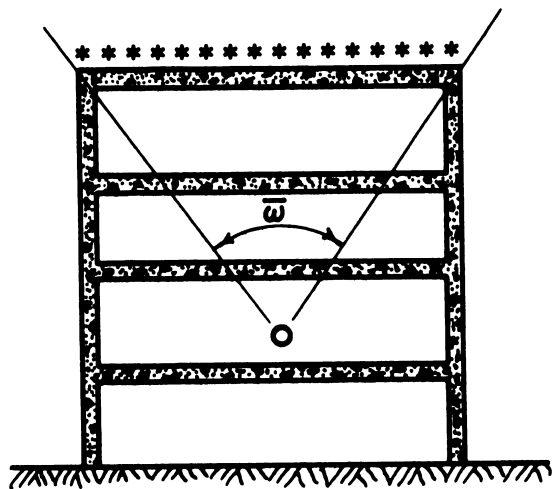
(6) Except for a few cases of empirical fitting to experimental data, the usual approach to selecting a barrier factor is to choose one of the elementary function types of chapter V which seems to involve an idealized configuration closest to the practical one of the given situation. Even when the function is required to provide a good fit to experimental data, it is customary to select the function, if possible, from the family of the calculated elementary function types rather than make up a new one. In fact, an even more arbitrary criterion sometimes followed is to select a function which is the same as, or readily derived from, those which are already included in the OCD Manuals for other purposes (i.e. those given in Appendix C of this text). There is a natural reluctance to recommend the addition of an extra chart to those already published in an existing edition of the OCD Manual, as well as a desire to minimize the amount of functional data which must be placed in the memory for a computer calculation of a fallout shielding problem by the Standard Method (or one of its variants). Therefore, existing functions have usually been chosen, especially when there are larger uncertainties in effects of secondary importance.

#### b. Roof Source, Interior Floor Barriers

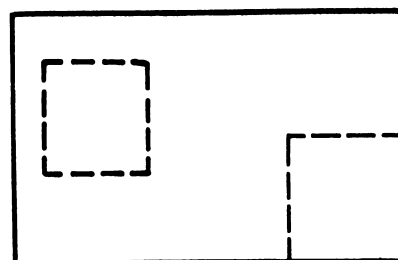
It was mentioned in chapter VII that, for a building with two or more slab barriers between the roof source and the detector (see fig. IX.17(a)), the formula for the blockhouse roof contribution provides the standard basis

---

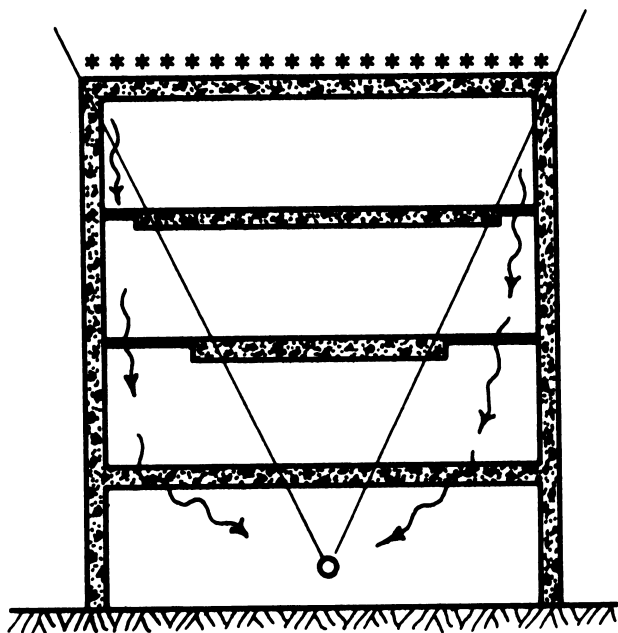
<sup>17</sup> The OCD Manual states that an interior partition barrier factor can be defined as "the ratio of the amount of radiation emerging from the inside of the partition to that incident to the outside." This blurs the distinctions between the two types of functions.



(a)



(b)



(c)

IX.17 Examples of roof source with interior floors between roof and detector:  
 (a) uniform thickness floors; (b) variable thickness barriers within solid angle subtended by roof source; (c) situation involving penetration and in-scattering through paths outside the solid angle subtended by roof source.

for computing the multistory roof contribution, provided that the function  $L_a$  is used as the geometry factor,  $X_o$  is taken as the total equivalent mass thickness between source and detector, and  $\bar{\omega}$  is the solid angle fraction subtended by the roof source at the detector position. The standard formula thus has the appearance of eq (VII.7).<sup>18</sup>

$$C_r = C_o = L(X_o) L_a(X_o, \bar{\omega}) \quad . \quad (IX.26)$$

The use of  $L_a$  as the geometry factor implies that the internal barriers (floors), combined with the roof, are assumed to act as if their total mass thickness were concentrated at the roof.

When there are substantial variations in thickness of the roof or any intervening floors, such as shown in figure IX.17(b), one can employ the techniques discussed in section VII.D.2 of breaking the problem into parts, so that each part has its own solid angle fraction and its own value for the total overhead mass thickness. If the variations in floor or roof thickness are not great or do not span large horizontal distances, the different parts may be assigned the average slab thickness. However, if the floors have a regular ribbed character, the special techniques of section VII.D.6 apply.

There can exist unusual cases of variations in floor thickness which, even outside the solid angle fraction subtended by the roof source, can produce a favored path for a strong contribution by radiation streaming, reflection, and/or "in-scattering", i.e., scattering from barriers not directly between source and detector. Such cases may lend themselves to a duct type of analysis; although a judicious use of "smearing" may help account

---

<sup>18</sup>See chart C-9.

for the extra penetration: Note the example in figure IX.17(c). No more precise method of handling such exceptional cases within the standard methodology is presently available.

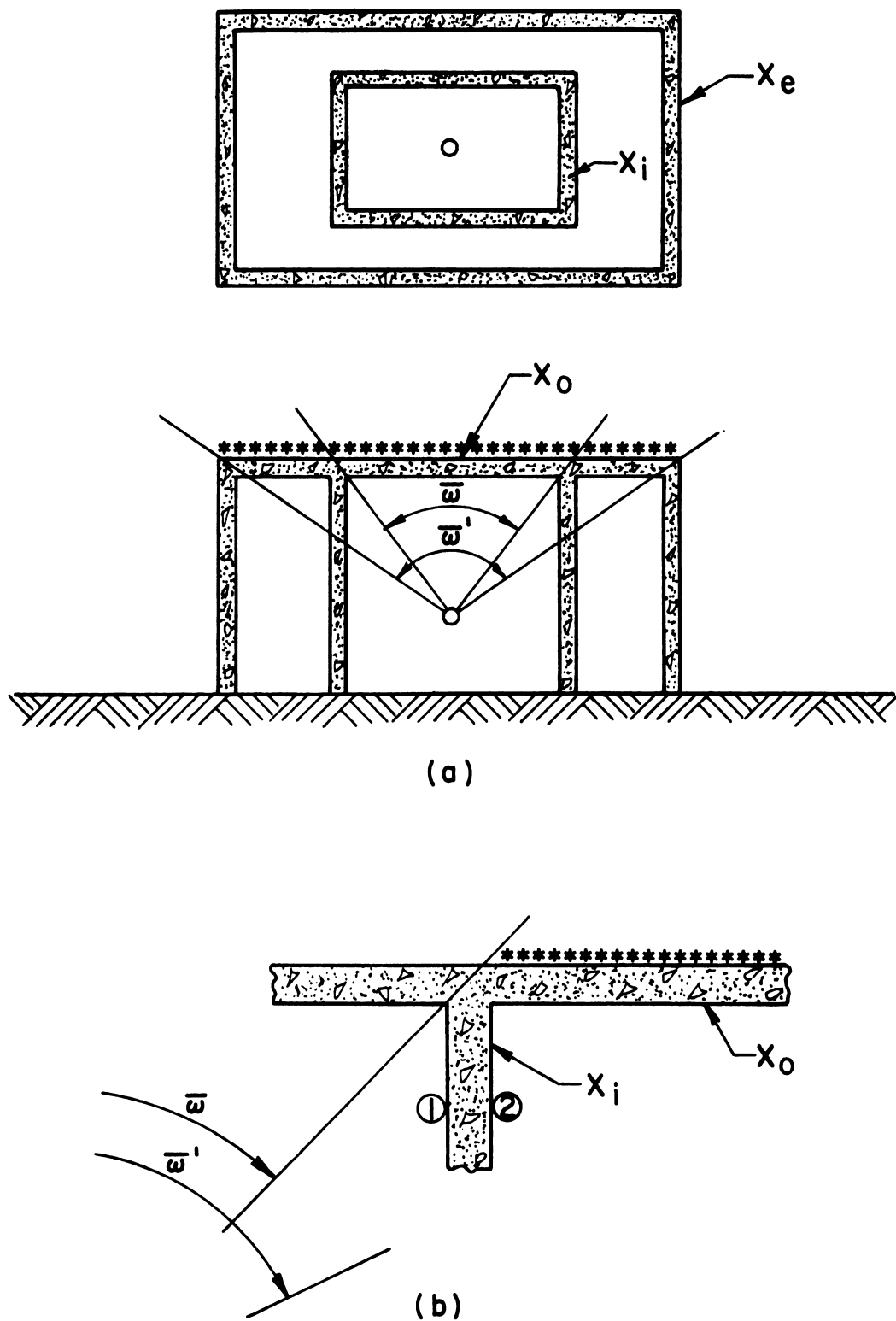
#### c. Roof Source, Interior Wall Barriers

The presence of interior walls between a roof source and the detector position requires two changes in the standard approach. First, this tends to separate those parts of the roof contribution which are strongly affected by the presence of the interior walls from those which are not. Figure IX.18(a) gives a simple example. Secondly, it requires modification of the formula for the strongly affected part of the roof contribution. The effect of the interior wall is specified as a simple attenuation factor, dependent only upon  $X_i$ , its equivalent mass thickness. No geometry effects are introduced, either in the interior wall attenuation factor or in any of the other functions involved in the formula for the roof contribution. (This is an example of an approach, as noted above in section IX.C.1.a(5) which is not logically consistent, but which leads to a simple, though approximate, formulation.) For the case given in figure IX.18(a) the roof contribution becomes (see eq (VII.51) for a closely related expression):

$$\begin{aligned} C_r &= [L(X_o) L_a(X_o, \bar{\omega}') - L(X_o) L_a(X_o, \bar{\omega})] B_i'(X_i) + L(X_o) L_a(X_o, \bar{\omega}) \\ &= [C_o(X_o, \bar{\omega}') - C_o(X_o, \bar{\omega})] B_i'(X_i) + C_o(X_o, \bar{\omega}) \quad , \end{aligned} \quad (IX.27)$$

where  $B_i'(X_i)$  is the interior partition attenuation factor required.

The simplest choice for  $B_i'(X_i)$  appears to be the ratio between detector responses at Positions (1) and (2) in figure IX.18(b), where these two positions are on either side of the interior wall, at some representative



IX.18 Simple illustration involving roof source and interior partition:  
 (a) overall configuration; (b) detail of situation assumed for purpose of  
 selecting a simple barrier factor.

distance below the ceiling within the aperture between solid angle fractions  $\bar{\omega}$  and  $\bar{\omega}'$ , and with detectors considered responsive only to radiation from the source field outside of the interior wall. If the blockhouse in figure IX.18(a) is viewed upside down, the roof radiation may be regarded as radiation from ground sources which must penetrate a horizontal mass thickness of  $X_o$ . If this is converted to an equivalent thickness of air, the two detector responses can reasonably be approximated by  $(1/2) B_e(0, 13.3X_o)$  and  $(1/2) B_e(X_i, 13.3X_o)$  respectively,<sup>19</sup> so that the formula for the interior barrier factor becomes, on this basis,

$$B'_i(X_i, X_o) = \frac{B_e(X_i, 13.3X_o)}{B_e(0, 13.3X_o)}, \quad (\text{IX.28})$$

This ratio turns out to be very insensitive to the value of  $X_o$ , except for small values of  $X_o$  (less than 15 psf). It is thus usually adequate to choose 50 psf as a representative value of  $X_o$  and obtain a value of this interior barrier factor dependent only on  $X_i$ . Thus, one defines

$$B'_i(X_i) = \frac{B_e(X_i, 665 \text{ ft})}{B_e(0, 665 \text{ ft})}, \quad (\text{IX.29})$$

A graph for this function is shown in chart C-7.

d. Ground Source, Interior Floor Barrier ("In-and-Down")

The "in-and-down" case refers to a situation in which radiation from ground sources emerges from the wall in a downward direction or backscatters from the ceiling toward the floor, and contributes to the detector response at the story below. This is often the primary route for radiation penetrating

---

<sup>19</sup>The factor 13.3 converts mass thickness in psf to equivalent height in air in feet.

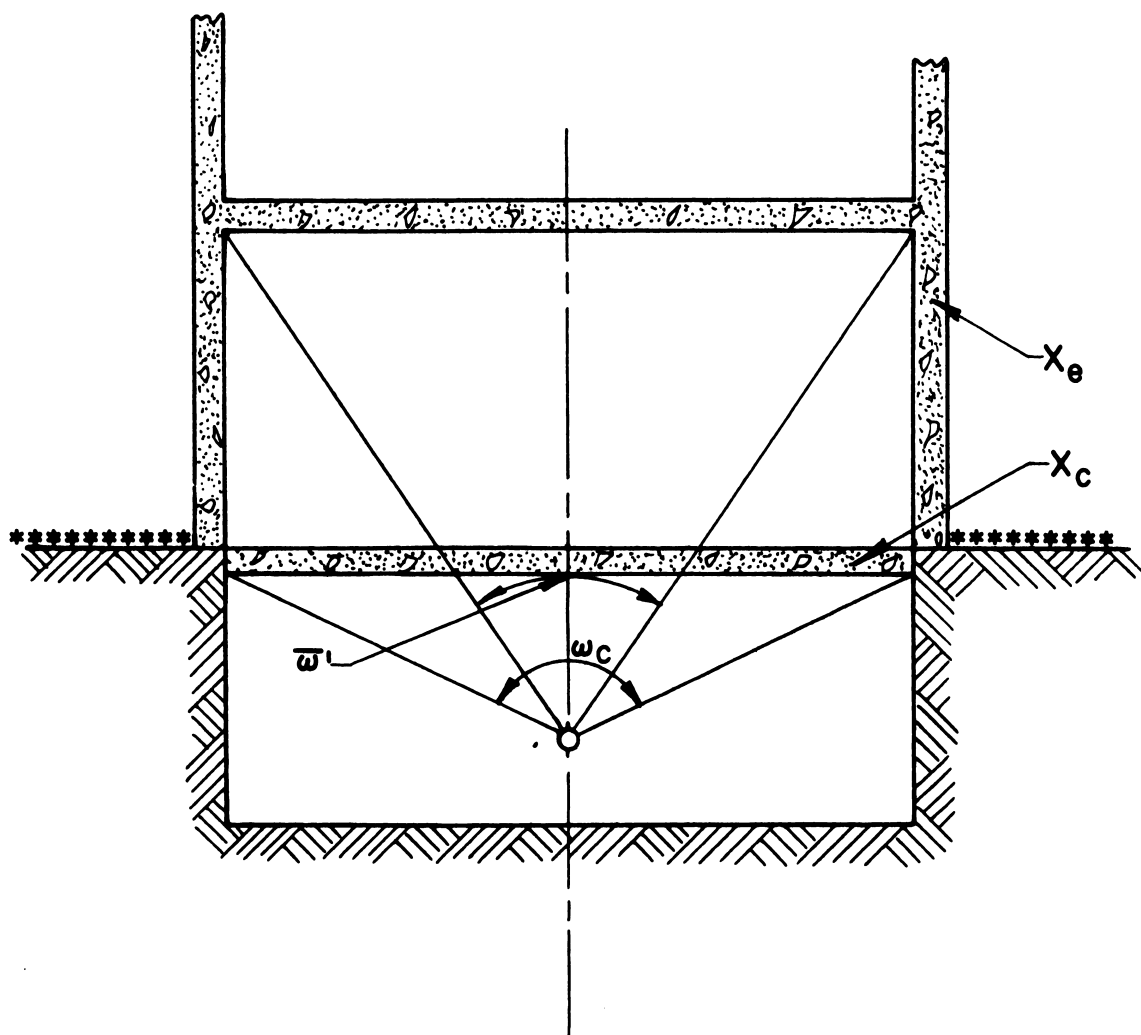
into the basement shelter of a large building; hence it is a particularly important case. Our subsequent discussion will be in terms of a basement detector position, but the same principles apply to a detector at an upper story with respect to the contribution through walls and floor of the next higher story. Figure IX.19 illustrates the situation and defines the parameters to be considered.

From the standpoint of the detector, the interior barrier being penetrated is a ceiling, and we henceforth refer to it as such. One defines the ceiling attenuation factor in this case as the ratio of the detector response with the ceiling present to the response in the absence of the ceiling, all other aspects of the situation being the same, so that this factor multiplies the usual expression without a floor, given by eq (VII.50). Thus,

$$C_g = B_e(X_e, H') [S_w(X_e) E(e) (G_s(\bar{\omega}') - G_s(\bar{\omega}_c)) + (1 - S_w(X_e)) (G_a(\bar{\omega}') - G_a(\bar{\omega}_c))] B_c, \quad (IX.30)$$

where  $B_c$  is the ceiling attenuation factor.

The adequacy of this formula is subject not only to the limitations regarding eq (VII.50) which were discussed following its presentation, but also to any error involved in the selection of  $B_c$ . In the early development of the standard methodology,  $B_c$  was evaluated using the skyshine barrier function  $S'(X_c)$ , as defined in section V.D.4.b, where  $X_c$  is the effective mass thickness of the ceiling. This function is a barrier factor, i.e., the ratio of detector response just under the floor to that just above the floor and with the superstructure assumed to be either very thin or such that the radiation field strength is uniform over the entire floor and has the same



IX.19 Situation for discussion of the "in-and-down" contribution for detector in basement, with parameters indicated.



directional characteristics and spectrum as skyshine. Its use in eq (IX.30) makes it subject to the same criticism expressed in section IX.C.1a(5) above. In fact, a review of the analysis of the "in-and-down" problem in NBS Monograph 42 [2] shows that  $S'$  was used there as a floor barrier factor only under carefully defined circumstances, much more restricted than the general one for which eq (IX.30) is intended.

This subject has been studied extensively, because the inadequacies of the original choice of  $S'$  to represent  $B_c$  were early apparent. A description of this research, and its progress toward development of an empirical set of data for describing the floor barrier factor, are presented in chapter X. It is sufficient here to display the empirical formula finally derived for  $B_c$ :

$$B_c(X_c, \omega_c) = (1.0 - 3.5 e^{-2.3\omega_c}) e^{-.10X_c} + 3.5 e^{-(2.3\omega_c + .04X_c)} \quad (\text{IX.31})$$

A graph for this function is given in chart C-8A.

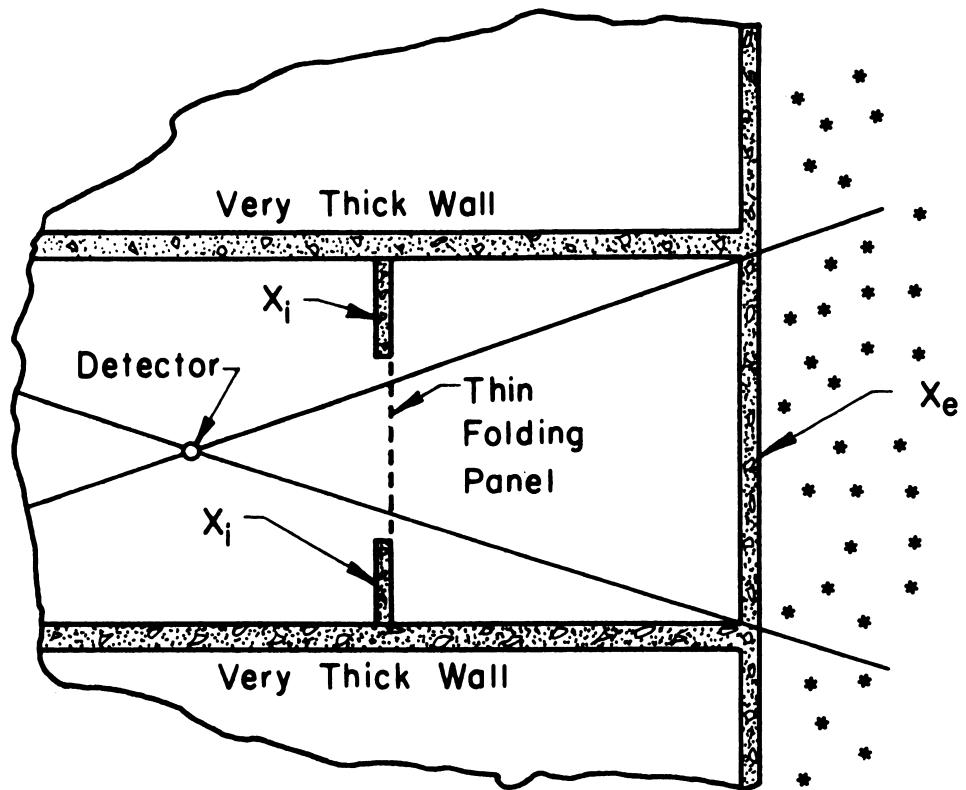
#### e. Ground Source, Interior Barriers Parallel to Outer Wall

In principle the combination of an exterior wall and one or more parallel interior walls is closely similar to that of a roof and one or more intervening floors; but standard practice treats the parallel-walls case as two separate barriers rather than as a single combined barrier. The interior barriers are combined into a single hypothetical barrier which acts as an absorbing shield. A multiplier taking this barrier into account is inserted into the formula for the wall contribution, thus implying that it represents the ratio of detector response with the interior barrier(s) present, to the response in the absence of such barrier(s). The symbol employed for this attenuation factor is  $B_i$ .

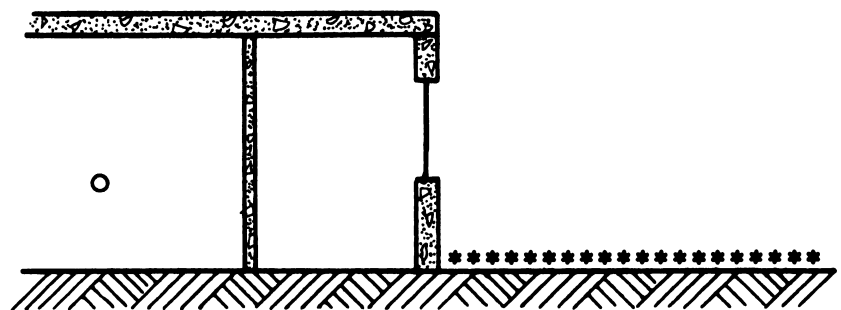
The sector approach is applicable here; and the sector boundaries may be assigned by taking into account not only variations in the exterior wall but also variations in the interior partition thicknesses. But, as previously noted, it is customary to smear out variations in interior partition thicknesses rather more freely than in the case of exterior walls.

This approach does not permit separate treatment of the scattering properties of an interior barrier, and there may be circumstances in which it is quite important to do this. For example, in the configuration illustrated in figure IX.20(a), the interior barrier offers no attenuation but, on the contrary, acts as an in-scattering secondary source of radiation to the detector. In this case, the expedient of smearing-out the interior partition into an equivalent one of the same overall average effective mass thickness, considered as an absorber only, gives an even less correct answer than ignoring the partition altogether. Figure IX.20(b) also shows a rather common situation in which the in-scattering effect of an interior partition is important, although there is no method prescribed for taking it into account.

The interior partition attenuation factor, although used mathematically in a way which would imply that it is an attenuation factor, is derived in the standard methodology from a barrier factor and made dependent only upon  $X_i$ . This parameter represents the sum of equivalent mass thicknesses of all parallel interior barriers between the outer wall and the detector. The rather reasonable assumption is made that the radiation incident upon an interior partition, regardless of height of the floor containing the detector, has roughly the horizontally "peaked" quality of the external field (the  $l$ -function) at low heights above the source plane; and the interior attenuation factor is therefore represented by



(a)



(b)

IX.20 Situations in which interior partitions play an important role in in-scattering to the detector.

$$B_i(X_i) = B_e(X_i, 3.3 \text{ ft}) \quad . \quad (\text{IX.32})$$

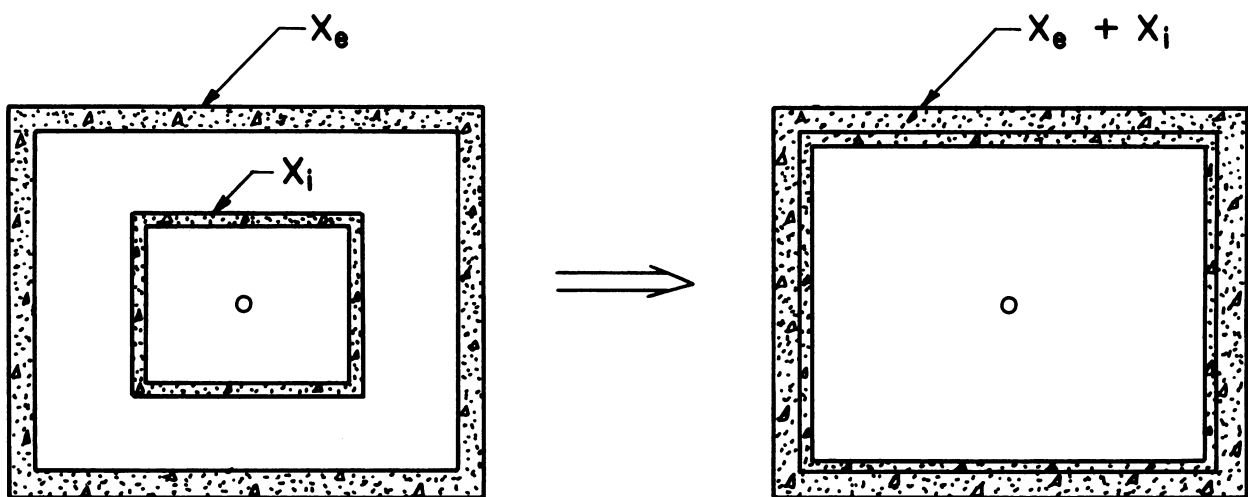
The choice of 3.3 ft as the height argument for  $B_e$  is somewhat arbitrary, but it is reasonable since the peaking of the radiation striking the interior partition horizontally must be similar to the sharp peaking on the exterior wall for small values of the height.<sup>20</sup> The function  $B_i$  is graphically displayed in chart C-7.

An alternative approach would consider the interior partitions as mass added to the outer walls, as indicated, for example, in figure IX.21. This would be mathematically equivalent to replacing the product  $[B_e(X_e, H) B_i(X_i)]$  by  $B_e(X_e + X_i, H)$ . Actually, these two expressions give almost the same value for any reasonable set of arguments, because the  $B_e$  function is roughly exponential with respect to  $X_e$ , and the  $B_e$  curves are nearly parallel for various values of  $H$ . There is thus little reason for preferring one approach over the other.

An interesting question naturally arises from the latter alternative: if  $(X_e + X_i)$  is used as the argument for the barrier factor, should it not also be the argument for  $S_w$ , which expresses the relative strength of wall-scattering? At first glance, this would seem to be a reasonable way to take into account the in-scattering effect of the interior partition(s). But the interior partition in-scattering effect depends on the position of the inner partition(s) relative to the outer wall and to the detector. If the partition is relatively near the outer wall, this suggestion is reasonable, but otherwise it is not.

---

<sup>20</sup>For small values of  $X_i$  the curve is modified slightly, so that  $B_i(0) = 1.0$ .



IX.21 Figure showing schematization involved in assumption that interior partition mass thickness is additive to outer wall mass thickness for barrier purposes.

One significant attempt to take into account the scattering effects of interior partitions should be noted here, even though the technique is subject to criticism and the complexities introduced have not yet been shown worthwhile. Batter and Starbird [6], relating the two portions of the wall contribution to "wall-scattered" and non-"wall-scattered" ("direct") contributions, extended this interpretation to the interior partition as well. They suggested separate formulas for four components: uncollided penetration of outer wall, uncollided penetration of inner wall; uncollided penetration of outer wall, scattered by inner wall; scattered by outer wall, uncollided in the inner wall; and scattered in both walls. For example, the contribution scattered in both walls would be given by the formula

$$D_4 = B_e(X_e, H) S_w(X_e) E [G_s(\bar{\omega}) + G_s(\underline{\omega})] \\ \cdot B_i(X_i) S_w(X_i) E_i [G_s(\bar{\omega}') + G_s(\underline{\omega}')] , \quad (IX.33)$$

where  $\omega$  represents solid angle fractions of the outer walls subtended at the detector,  $\omega'$  represents solid angle fractions of the inner partition walls,  $E_i$  represents the shape factor of the "inner structure" defined by the interior partitions, and the other variables are already established. (The use of standard functions as multipliers for the compounded situation is common practice.) The same approach leads to obvious expressions for the other three components.

Besides the question of adequacy of the uncollided/scattered interpretation of the basic blockhouse equations for wall contribution, there are two other significant approximations inherent in the Batter-Starbird approach:

(1) The interior partitions are treated as if they form an interior blockhouse; and the elementary blockhouse functions are applied without modification, as if the radiation incident on the inner partition behaved the same as in outside walls of similar thickness.

(2) Even though the interior partitions are handled as if they constituted an interior blockhouse, the first four factors on the right side of eq (IX.33), which are an estimate of the radiation incident on the interior partitions, are the detector response in the middle of the larger structure considered without interior partitions. It would appear that an average detector response at the location of the interior partitions, say, would be more suitable.

f. Ground Source, Interior Wall Barrier Perpendicular to Outer Wall

The interior partition which is perpendicular to the outer wall, like the roof/interior-wall case, is representative of "right-angle-shielding-slabs" problems which have never been adequately solved. The standard approach is fairly crude though conservative: treat the interior partition as if it were parallel to the wall, and use the  $B_i(X_i)$  function defined in eq (IX.32) as the multiplying factor to account for the partition presence.

g. Ground Source, Combination of Parallel and  
Perpendicular Interior Wall Barriers

Whatever the technique just described may lack in accuracy, it leads to a very simple rule for all interior wall barriers to the ground source contribution: after appropriate smearing-out of minor mass thickness variations to the extent considered reasonable, one divides the field into a number of sectors such that within any given sector the sum of equivalent mass thicknesses of all internal partitions, measured normal to each partition, is constant; this becomes the argument  $X_i$  for the factor  $B_i$  in the formula for the ground contribution.

#### h. Combination of Floor Barriers with One or More Interior Wall Partitions

The simple approach currently used is as follows: the effects of floor and wall barriers are separately accounted for by their respective attenuation factors, and these are inserted as multipliers into the usual equations. Other simplified approaches, similar to those previously discussed, are worthy of attention but have not been accepted for general application.

The "in-and-down" configuration in which the story above the detector has interior partitions of significant mass is noteworthy. Although some of these partitions may not be within the sector established by the exterior wall, as indicated, for example, in figure IX.22, they may contribute appreciably by "in-scattering." There is no current provision to take this effect into account, but Batter and Starbird [6] have examined the problem. They suggest an approach very similar to that devised for interior partitions on the same floor, mentioned above. A detailed listing of the pertinent equations is not included here; but these calculations are subject to the remarks we have made on the other partition studies reported by Batter and Starbird. Their experimental results are discussed in section X.C.6.

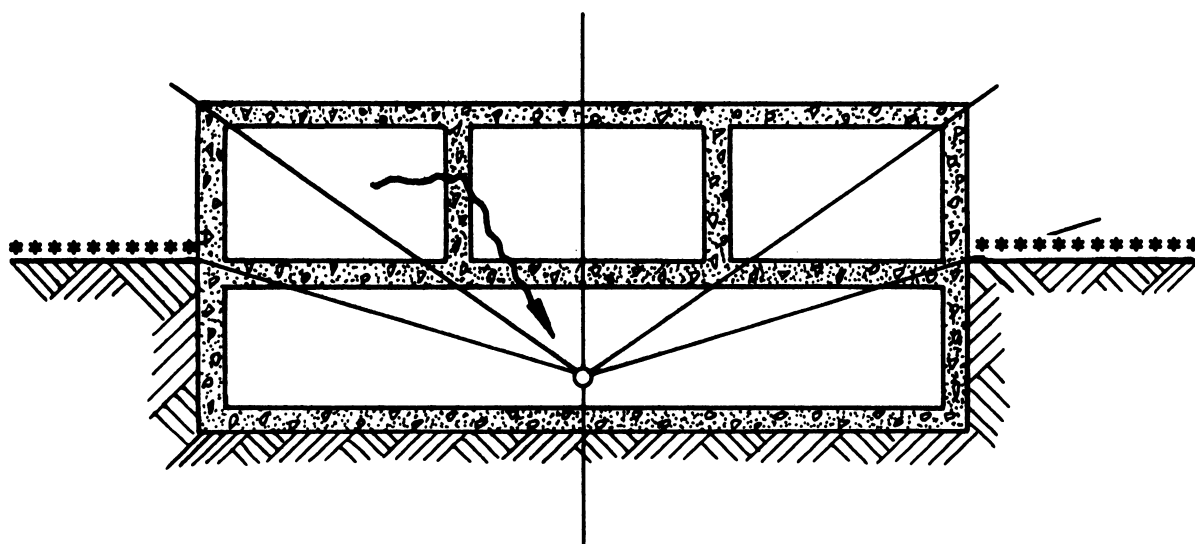
### 2. Roof Complexities

The main complexities to be noted in roofs are (1) non-horizontal configuration, (2) overhang, and (3) set-back. These will be discussed in turn.

#### a. Non-Horizontal Overhead Roofs

Such roofs, especially peaked roofs, are very common. All such roofs may be considered as a collection of planes, and the contribution from each plane may be evaluated separately. Even curved roofs may be broken up into a number of surfaces, each approximated by a plane. For roofs of gentle curvature,





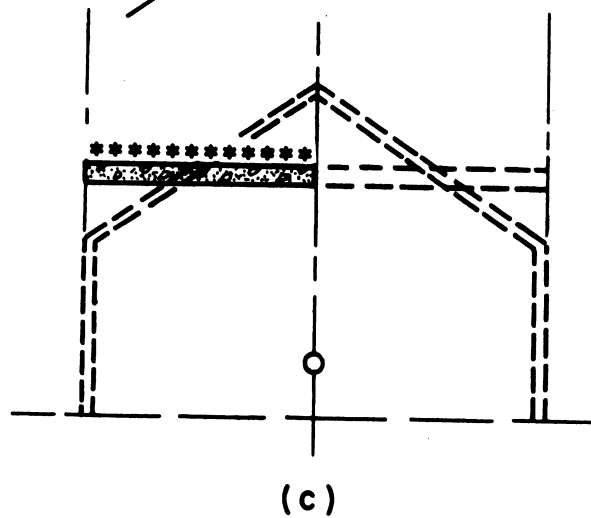
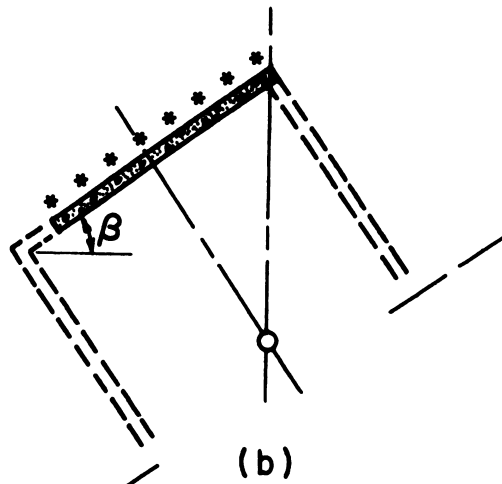
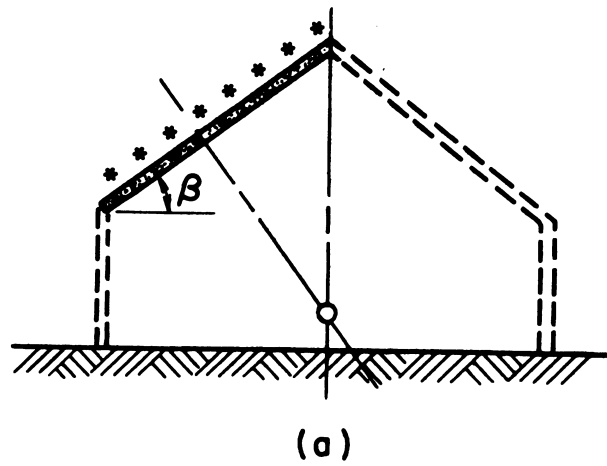
IX.22 Illustration of "In-scattering" by first floor partitions into basement.

only a few planes are needed; for those of great curvature, many more might be required for a good approximation. For the present discussion, only the contribution from a single non-horizontal plane is considered.

Figure IX.23 gives a simple illustration of such a situation. Two approaches for estimating the contribution by fallout on such an overhead plane are recommended within the standard methodology. The first and presumably more accurate uses a fictitious situation in which the plane is part of the roof of a blockhouse tipped on its side, as shown in the figure. The contribution of this part of the roof is easily calculated by methods previously described, with one modification. The source strength, and correspondingly the final contribution, is reduced by a factor equal to the cosine of the angle of source plane slope,  $\beta$ , to take account of the diminished fallout per unit area expected on a sloping roof in comparison to that on a horizontal roof.

The second approach replaces the sloping plane with a fictitious horizontal one, having the same projection in plan, located at some mean height, and characterized by the actual roof mass thickness divided by the cosine of the angle  $\beta$ . The value of the mean height selected is not critical if the detector is far enough below the roof that the distance from detector to various points on the roof does not cause the inverse square factor to vary widely. The standard approach is to choose a height halfway between the highest and lowest parts of the source plane. (For a pyramidal roof, a somewhat lower position would be more reasonable.)

The rule for mass thickness of the equivalent horizontal roof follows from the observation that the vertical penetration distance through a sloping roof slab better approximates the average gamma ray penetration distance than does the thickness measured normal to the roof plane. Such a rule is



IX.23 Illustrations of methods of analyzing sloping-roof contribution: (a) actual situation; (b) fictitious tipped structure; (c) equivalent horizontal roof.

reasonable, as long as the roof is not strongly peaked; but when  $\beta$  exceeds some critical value, i.e. about  $35^\circ$ , this is no longer true. We suggest that when  $\beta$  exceeds this figure, the actual value be replaced by  $35^\circ$  for the purpose of determining the thickness of the equivalent horizontal roof.

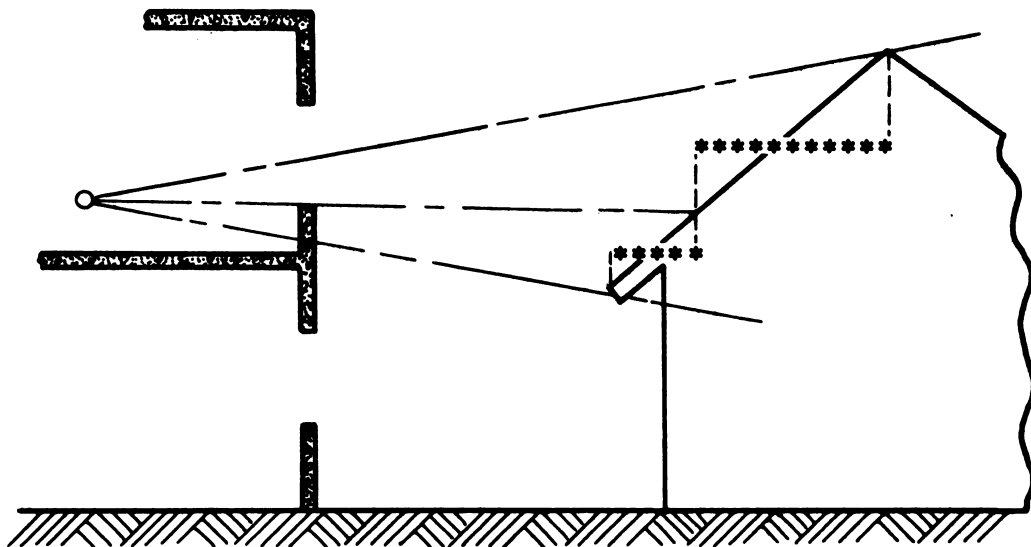
Of the two techniques presented, the equivalent horizontal roof plane approach is usually much easier and involves much simpler judgments when the structure is otherwise complicated by the existence of interior partitions and floors.

#### b. Non-Horizontal Roofs of Adjacent Buildings

Configurations like that shown in figure IX.24 are common. The equivalent horizontal roof is generally much the easier approach, since such cases usually involve complexities of source in addition to those of the building under analysis. Care must be exercised, however. In the example of the figure, use of an equivalent roof plane at mid-roof height should not lead the analyst into neglect of the roof source on the adjacent building as a source of direct radiation. To the extent that the actual roof is unshielded, the fictitious equivalent should also be. Likewise, since part of the actual roof shown is visible through the window on the detector floor and part is shielded by the wall below the window sill, the roof source should actually be divided into two parts, each of which is separately approximated by its own equivalent horizontal plane. There is a very close similarity between the methods available to solve this problem and that used for a sloping ground plane source as discussed in section IX.B.4.

#### c. Roof Overhang

Roof overhangs have three important effects. First, they add to the area of the roof and thus become an overhead source of radiation. Second, they act



IX.24 Illustration of method of analyzing contribution from sloping roof of adjacent building.

as a shielding barrier for some of the skyshine radiation. Last, they act as additional scattering surfaces for ceiling-shine. Figure IX.25 illustrates these effects.

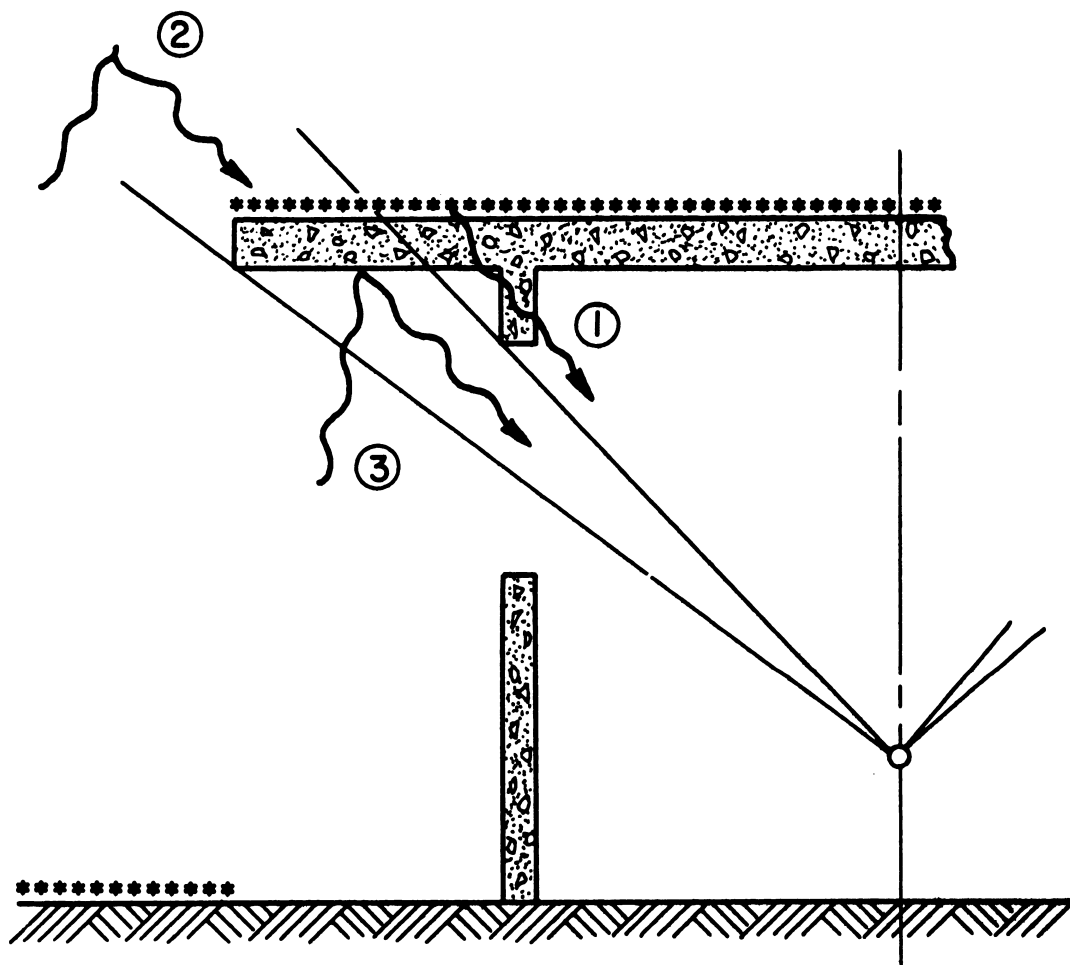
The first effect is the only one easily taken care of in the standard methodology. The technique is quite straight-forward. One can visualize the structure as extending to the edge of the overhang and the structure wall acting as a vertical interior partition insofar as the radiation originating from the roof overhang is concerned. The procedure for handling this problem has already been discussed in the previous section.

The second effect of the overhang mentioned is more involved. If the overhang is considered part of the roof, its inclusion as a radiation source as discussed in the previous paragraph automatically accounts for the skyshine which strikes it (see the second paragraph following eq (VII.6)). The only aspect of this effect which needs separate attention is the fact that the skyshine from the sector subtended by the overhang should no longer be included in the so-called "ground contribution." Thus the argument for  $G_a$  is the solid angle fraction subtended by the roof including the overhang, rather than just the ceiling within the blockhouse walls.

The additional ceiling-shine due to overhang is probably negligible except through open windows. But, a reasonable and conservative approach would be to define  $\omega_u$ , the solid angle fraction subtended by the ceiling, to include the overhang, in the appropriate formula in section VII.D.5.

#### d. Set-Back Roofs

Roof set-backs are handled exactly as any external finite elevated ground source. This is discussed in detail in section IX.B.3.



IX.25 Effects of roof overhang: (1) roof/vertical-barrier penetration; (2) shielding of skyshine contribution to wall; (3) increase in ceiling-shine.

### 3. Non-Rectangular Wall Plan

Structures having wall plans which are more complicated than the elementary rectangular blockhouse are generally handled by dividing the structure conceptually into separate components, through the use of azimuthal sectors. If rays are drawn from the detector to each point on the plan view where planar walls meet at a corner, each individual sector involves only a single panel. The methods discussed in section VII.D.3 and section VII.E then become directly applicable. Remarks about a few special cases are added here to emphasize some important principles.

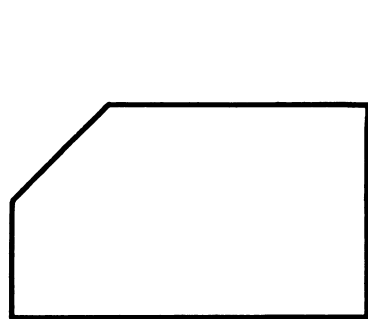
#### a. Non-Reentrant Structures

A structure is called non-reentrant if no ray from a detector placed anywhere within it, can pass through the outer wall of the structure more than once. (Figure IX.26 illustrates both reentrant and nonreentrant types.) This type has no special problems with respect to radiation field incident upon outer walls. Difficulties associated with each sector of such a structure are related to proper choice of configuration for the fictitious blockhouse used in the analysis. The standard approach relies upon a few simple principles and "engineering judgment" in their application. These principles are not all explicitly stated, but appear to be well summarized by the following rules:

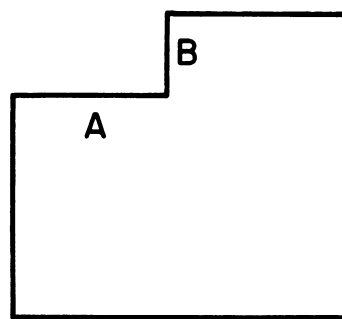
(1) Devise fictitious structures having walls coincident with the walls of the actual structure to the extent possible. This often permits grouping of several individual wall sectors into a single sector, thus shortening the analysis.

(2) When there is a choice of structure among several available fictitious structures which obey the first rule, pick the one which has the least eccentricity (largest shape factor). This is because geometry factors for the





(a)



(b)

IX.26 Buildings types: (a) non-reentrant; (b) reentrant.

wall contribution equations are based on a cylindrical wall approximation, so that use of a structure deviating least from this assumption should give the most accurate answer.

Fictitious structure options for analyzing a given wall panel, and selection from among them, are exemplified in figure IX.27. Note that structure F-2 is preferred to structure F-1, based on the above rules. Structure F-3 is a possible choice which takes rule (2) to the ultimate square structure (no eccentricity) but which completely violates rule (1). However it must be considered a very reasonable option, which probably gives a more accurate answer than either of the other choices.

Approaches which avoid arbitrary choices of fictitious structure are desirable, and the methods discussed in the paragraphs following eq (VII.66) are applicable here.

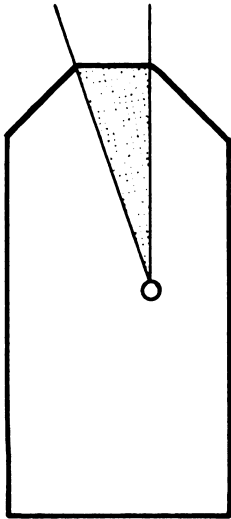
#### b. Reentrant Structures

A reentrant structure, such as illustrated in figure IX.26 presents an additional problem. Such structures have self-shielding aspects. Note that Wall B shields Wall A from part of the fallout fields and hence influences the radiation fields incident on Wall A. This problem has been ignored in the standard methodology up to this time, but there appears to be no reason why the same methods discussed for limited fields (sec. IX.B.1) should not be applied to this case as well.

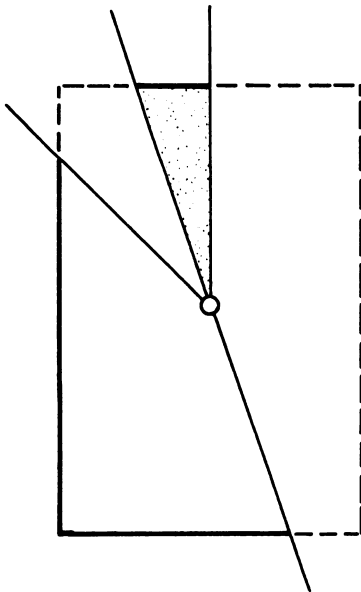
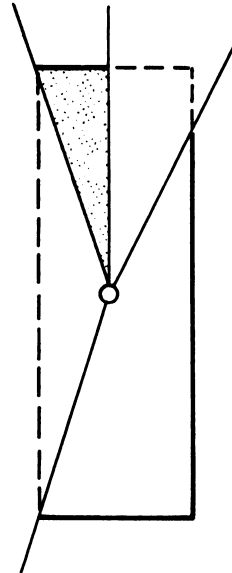
#### c. Round and Quasi-Round Structure Plans

A structure is called "quasi-round" in plan if it appears better approximated by a cylindrical structure than by a rectangular one. Hexagonal and octagonal structures are good examples. Since the cylindrical structure is more basic to the mathematical analysis than even the rectangular blockhouse, the use of such an approximation to the real structure undoubtedly improves

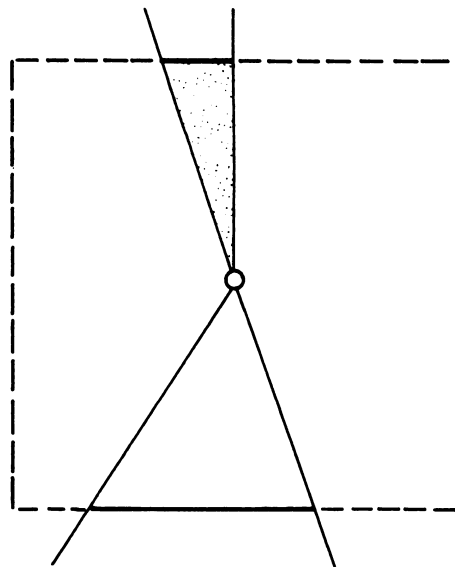
Actual  
Structure



F-1



F - 2



F - 3

IX.27 Various choices of fictitious building available for analysis of contribution of wall in shaded sector.

the accuracy. The primary difference is in the value of the shape factor,  $E$ , used in equations such as (VII.31). The proper value of this factor in such a case is easily determined if one notes that the line from detector to the wall (in plan) at any point is perpendicular to the wall, so that  $p(\phi)$  as defined in eq (VII.24) is simply  $1/2$ . Then the value for  $E$  equivalent to eq (VII.25) becomes:

$$E = \frac{\int_0^{2\pi} (1/2) d\phi \int_{-1}^1 q(u) du}{\int_{-\pi/2}^{+\pi/2} \cos\phi d\phi \int_{-1}^1 q(u) du} = \frac{\pi}{2} \quad . \quad (\text{IX.34})$$

#### 4. Ducts, Passageways, Shafts, and Tunnels

##### a. Introduction

"Ducts", "passageways", "shafts", and "tunnels" are synonymous terms for our purposes. They relate to an accessway from the exterior of a structure to the interior, with the length of the accessway usually greater than its cross-sectional dimensions, and the outside opening usually unshielded or lightly shielded. We assume that no interior shielding partitions exist across the accessway between outer entrance and detector. The accessway itself may be a single straight void (single-legged) or there may be one or more turns, usually at right angles (multi-legged). The side-walls of the accessway have substantial thickness, so that almost all the radiation reaching the (interior) detector has entered at the exterior end of the passageway. Thus, side-wall penetration is considered insignificant, but wall reflection may occur.

The term "duct" implies to a construction specialist a tube through which passes a fluid, such as ventilating air; it also designates an accessway for

utility lines. To a shielding specialist, the term refers to any of the types of accessways we are discussing in this section; and we use it in this latter way. "Passageways" are generally horizontal; "shafts" are generally vertical, as we use the terms. "Tunnels" are underground passageways.

#### b. Penetration from a Ground Source

The strength and directional distribution of radiation from a ground source at the entrance to a duct is adequately specified by the  $\ell$ -function at the height of the center of the duct opening. Thus, a detector within the first leg of the duct receives a direct contribution, normalized to the standard strength radiation field, given by

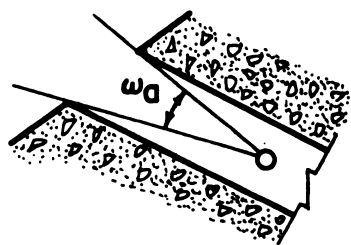
$$D(\omega_a) = \frac{1}{2\pi} \int_{\omega_a} \ell(h, \cos\theta) d\Omega, \quad (\text{IX.35})$$

where  $\omega_a$  is a measure of the aperture solid angular,  $h$  is the average duct entrance height above the source plane, and  $d\Omega$  indicates an integration over solid angle. See figure IX.28(a).

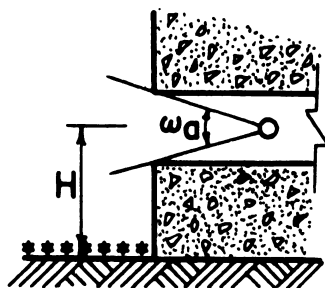
There is also a contribution from radiation which, though starting at the duct entrance, has been reflected one or more times from the side walls. It is customary in the standard methodology to ignore this contribution, although, as Huddleston and LeDoux [7] point out, such a reflected contribution may be as large as 50% of the direct contribution from the above formula. In the discussion below, this reflected component is not included.

##### (1) Horizontal Passageways

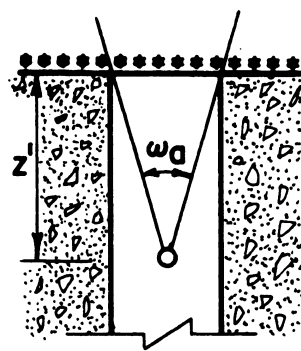
Figure 28(b) exemplifies this situation. If one ignores side-wall scatter, the configuration is equivalent to a small aperture; and the aperture rules are valid here (see sec. VII.D.4). Thus, the direct contribution from the duct entrance is given by  $(1/2)B_e(0,H) W_a(H,\omega_a)$ , which is the same as



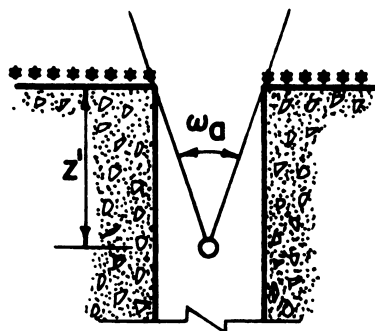
(a)



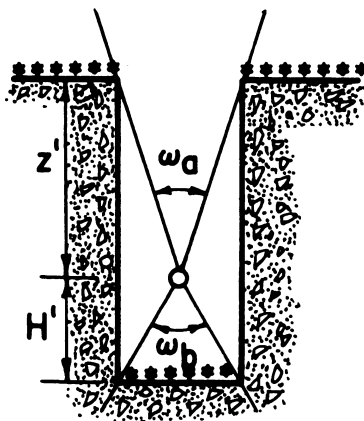
(b)



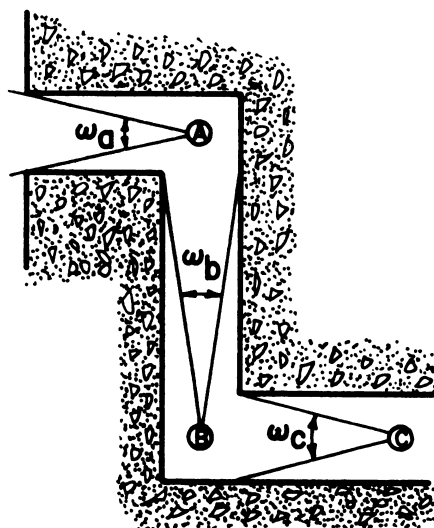
(c)



(d)



(e)



(f)

IX.28 Idealized situations involving ducts and similar configurations.

$(1/2)L(H) W_a(H, \omega_a)$ , where the  $W_a$  function is as shown in figure V.26. In the Standard Method,  $B_e(0, H)$  is taken as unity, which implies an  $H$  value of about 3 ft. The value of  $H$  in the  $W_a$  function is taken as the smallest for which  $W_a$  has been calculated, namely 3.25 ft. The passageway contribution thus calculated, as a function of  $\omega_a$ , is given in chart C-11.

## (2) Vertical Shafts

Three configurations in this category are depicted in figures IX.28(c) - (e). The first involves a shaft with a light cover, such as a glass skylight, which can hold fallout but provides little shielding for the detector below. From the discussion following eq (VII.7) in section VII.B.1, the detector response is best given by  $L(Z') L_a(Z', \omega_a)$ , although in practice  $Z'$  is fixed at 3 ft. The difference due to this simplification is small, and the resulting function is also plotted in chart C-11.

Figure IX.28(d) shows a case featuring no direct fallout contribution to the detector, either because the light cover, though present, has been decontaminated or because the shaft is entirely open and the floor below has been decontaminated. The detector contribution consists entirely of that portion of skyshine included within the aperture measured by  $\omega_a$ . It is given by the expression  $S(h) S_a(h, \omega_a)$ , (as given in figs. V.34 and V.36 of chapter V), where  $h$  is the height of the shaft entrance above the basic ground plane. Since this combination is almost independent of  $h$ , the functions for general use can be those for which  $h$  equals zero.<sup>21</sup>

Figure IX.28(e) depicts a situation in which there is no cover to the shaft, and the fallout has fallen to the base of the shaft and has not been removed. The contribution from skyshine is determined just as in the

---

<sup>21</sup>The resulting function is not given as one of the curves in the OCD Manual [1] nor in appendix C, but as the first row of data in the Manual table 6-2, reproduced here as table IX.2.

TABLE IX.2

Skyshine Contributions for  $X_o$  Less Than 25 psf

<u>Solid Angle Fraction</u>	<u>Skyshine Contribution</u>
0.10	0.004
0.20	0.009
0.40	0.019
0.60	0.030
0.80	0.048
1.00	0.100



preeceeding paragraph. The contribution from the fallout at the base of the shaft is determined as indicated for figure IX.28(c), using  $\omega_b$  as the aperture solid angle fraction.

### (3) Multilegged Ducts

An idealized multilegged duct is shown in figure IX.28(f). The first leg may be a horizontal passageway, a vertical shaft, or an accessway at any arbitrary orientation. The other leg or legs are assumed to be attached at right angles. (Note that a duct with more than two legs need not have co-planar axes.)

The detector response can be obtained at position A by one or another of the methods discussed above. At position B the response is obtained by multiplying that at A by the ratio of response at B to that at A. This is called the "second leg attenuation factor." Attenuation factors for subsequent legs are defined similarly.

It has been observed experimentally that the attenuation factors in the second and subsequent legs can be approximated by the simple expression  $k_i \omega_i$ , where  $k_i$  is a constant appropriate to the number of the leg in question and  $\omega_i$  refers to the entrance aperture solid angle fraction, subtended at the end of that leg. It is generally accepted that  $k_i$  should be specified as 0.2 for the second leg [8,9], but that for subsequent legs a value as high as 0.5 may be necessary [10].

A more accurate formulation, although more elaborate, for the two-legged duct has been provided by Huddleston and LeDoux [8], to which the interested reader may refer.

### (4) Shielded Openings

For most cases, the presence of a substantial barrier at the opening of the duct does not change the principles involved in the analysis. The

functions to be used, which for the unshielded duct cases use zero barrier thickness as an argument, must then be evaluated with the actual equivalent mass thickness of the barrier provided. In the overhead case with fallout on the barrier at the duct aperture, the function  $L_a(Z', \omega_a)$  should be replaced by  $L_a(X_o, \omega_a)$ , where  $X_o$  is the equivalent mass thickness of the overhead barrier.

For the case shown in figure IX.28(d), with the addition of a barrier (decontaminated) at the shaft entrance, no directly applicable functions are available. It is adequate and somewhat conservative to assume a rather thin barrier to have a thickness of zero and use the methods previously described. For a rather thick barrier one can evaluate the contribution from a decontaminated roof by applying an attenuation factor to the skyshine contribution. As noted in section X.D.2, the attenuation of skyshine is similar to the attenuation  $B_c(X_c, \omega)$  of "in-and-down" radiation. The expression for a decontaminated roof at height  $h$  above grade is then given by  $[S(h) B_c(X_o, \omega) S_a(h, \omega)]$  where  $S(h)$  and  $S_a(h, \omega)$  can be obtained from figs. V.28 and V.30.<sup>22</sup> ( $S(h)$  can be set at about 0.1 for general use, since it varies only slightly with  $h$  within a reasonable range of values.)

---

<sup>22</sup>This approach is generally applicable to cleared roofs.

## REFERENCES

- [1] Shelter design and analysis, Vol. 1, Fallout radiation shielding, Doc. TR-20-(Vol.1), Office of Civil Defense, July 1969, as amended by Changes 1-3.
- [2] Spencer, L. V., Structure shielding against fallout radiation from nuclear weapons, NBS Monograph, 42, National Bureau of Standards, June 1962.
- [3] Hughes, M. A. and Bryan, F. A. Jr., Effect of source field elongation on radiation received at a detector, Res. Memo. RM-333-4, Research Triangle Institute, June 1968.
- [4] Eisenhower, C., An engineering method for calculating protection afforded by structures against fallout radiation, NBS Monograph 76, National Bureau of Standards, July 1964. Also Published as Suppl No. 1 to Ref. [9.3].
- [5] Huddleston, C. M., Klinger, Q. C., Burson, Z. G., and Kinkaid, R. M., Ground roughness effects on the energy and angular distribution of gamma radiation from fallout, Health Physics 11, 537, June 1965.
- [6] Batter, J. F. and Starbird, A. W., The preparation of simplified manuals for shielding analysis, Rpt. No. 4848-1, Conesco Division of Flow Corp. March 1967.
- [7] Huddleston, C. M. and LeDoux, J. C., Ducts and voids in shields; attenuation of gamma rays; straight cylindrical duct, Sect. 8.1.2 of Engineering Compendium on Radiation Shielding, Vol. 1, Shielding Fundamentals and Methods, R. G. Jaeger, ed.-in-ch., Springer-Verlag, New York, 1968.
- [8] Huddleston, C. M. and LeDoux, J. C., Ducts and voids in shields; attenuation of gamma rays; rectangular ducts with one right-angle bend, Sect. 8.1.4 of the Compendium cited in [11.16].
- [9] Chilton, A. B., Chapter IV, Experimental program, of Radiation shielding, analysis and design principles as applied to nuclear defense planning, Rpt. TR 40, W. R. Kimel, ed.-in-chief, Office of Civil Defense and Kansas State University, November 1966.
- [10] Eisenhower, C. M., Scattering of cobalt-60 gamma radiation in air ducts, NBS Tech. Note 74, National Bureau of Standards, October 1960.

## X. EXPERIMENTAL DATA ON COMPLEX STRUCTURES

### A. INTRODUCTION

In this chapter we discuss experimental studies designed to test the procedures discussed in chapter IX for evaluating protection in complex structures. Discussion of complications in source distributions is restricted here to limited fields. Complications in structures are classified according to the configuration of interior and exterior partitions, and the type of source. The penetration of radiation from ground sources through an exterior wall and down through a ceiling - the so-called "in-and-down" problem - has received so much attention in experimental evaluation of the Standard Method that it is discussed in a separate section. The following section is devoted to discussion of experiments on operational buildings. These buildings were originally chosen for study because they were typical of buildings of interest to the civil defense agency and, more important, because they were either isolated from other structures, or could be isolated for a long enough time to permit experiments. The final section contains a summary of the state-of-the-art on experimental investigation of complex structures.

As the structure analyzed becomes more complex and its specification less detailed and certain, the accuracy of the calculated reduction factors becomes poorer. There are many reasons for this; and they can be roughly classified into three groups: 1) inadequate information about the structure, 2) inadequate data for relevant elementary structures, necessitating, for example the assumption that interior walls act more as absorbers than as scatterers in the selection of attenuation factor functions; and 3) the failure of actual buildings to resemble composites of elementary structures. These limitations will be discussed further in chapter XII.

## B. LIMITED FIELDS

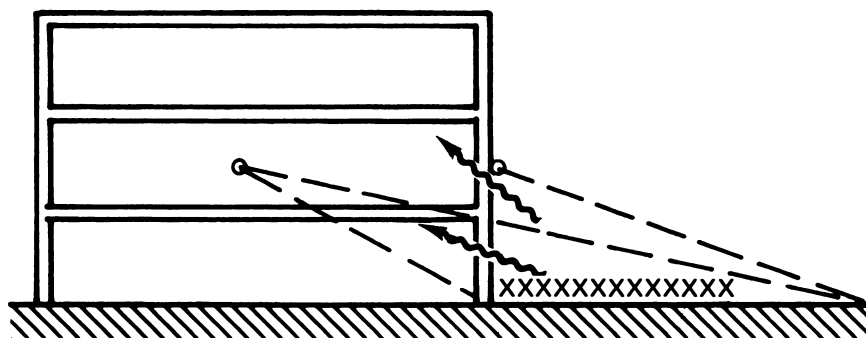
### 1. Background of Problem

The data for penetration of radiation from limited fields through exterior walls were developed somewhat later than the other data described in chapter V. They therefore did not appear in Spencer's original publication [1] of penetration data. The need for information on limited fields became evident during the National Fallout Shelter Survey, in which many of the buildings examined were in urban areas. The penetration data subsequently developed for application to limited fields are presented and discussed in section V.D.3. The construction of engineering curves from these basic penetration data is described in detail in the appendix of an OCD report [2].

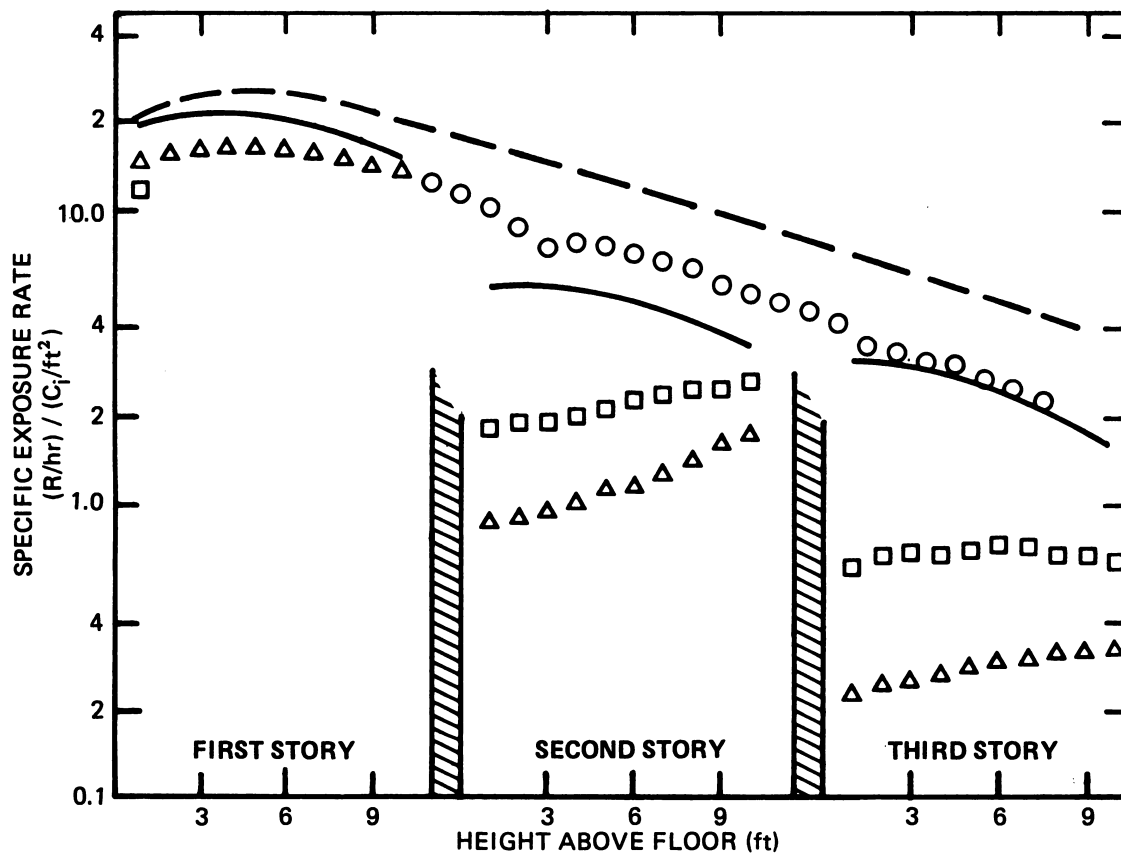
Unfortunately, the barrier factor  $B_s$  for limited fields was calculated only for the source spectrum of gamma rays at one hour after fission, while the best experimental tests of this quantity have been performed with  $^{60}\text{Co}$  sources. The results are therefore not directly comparable. Nevertheless, the geometrical limitations of the source are so much more important than the energy of the source radiation in determining the barrier factor  $B_s$ , that much can still be learned from a comparison between theory and experiment.

### 2. Experiments at the Radiation Test Facility

Measurements of  $B_s$  by McDonnell et al. [3] for  $^{60}\text{Co}$  radiation and for detectors adjacent to the wall were discussed in section VIII.C.2. Here we discuss measurements [4] which were made at the center of the RTF structure (fig. VIII.17) for the concentric annuli described in that section. The distinction between the two configurations is shown in figure X.1. Both the geometry and the average angle of incidence of radiation on the structure are different. Figure X.2 shows a comparison between theory and experiment of exposure rates at the center, for floors of 0, 4, and 8 inches in thickness



X.1. Schematic drawing showing how the average direction of photons incident on a wall varies with the position of the detector.



X.2. Comparison of experimental and calculated exposure rates at the center of a structure for a semi circular ground source of radius 15.3 ft. Experimental:  $\bigcirc$  4 in walls, zero floors  $\square$  4 in walls, 4 in floors,  $\triangle$  4 in walls, 8 in floors; Calculated: --- Standard Method, 4 in walls, zero floors, — Standard Method, 4 in walls, 4 in floors.

and for the innermost source annulus.<sup>1</sup> As discussed in section VI.C.1, the calculated exposure rate at the standard location is about  $480 \text{ (R/hr)/(Ci/ft}^2\text{)}$ .

The experimental configuration with "zero" floor thickness actually contained horizontal steel beam structures equivalent to pseudo-floors of several psf thickness. It is not surprising, therefore, that the experimental exposure rates are somewhat lower than exposure rates calculated by the Standard Method for no floors. When the floor thickness is increased to four inches of concrete, there is serious disagreement between theory and experiment on the second and third stories. The marked decrease in exposure rate on the second story when the floor thickness changes from zero to four inches of concrete indicates that a significant fraction of the exposure rate comes from radiation emerging from the inner surface of the walls of the first and third stories. In this case, where the source field is small, the contribution from the first story predominates over that from the third story. The increase by about a factor of two just above the second floor, when the floor thickness is decreased from eight inches to four inches, is clearly due to radiation penetrating upwards from the first story walls. Assuming that the 8-in floors are effectively infinite in thickness, the measured exposure rate on the second story (triangular symbols) represents the contribution from wall-scattered radiation from the second story wall.

This comparison shows that the Standard Method is not well suited to calculation of reduction factors in situations where wall-scattered radiation from small limited fields is the dominant contribution. As pointed out in

---

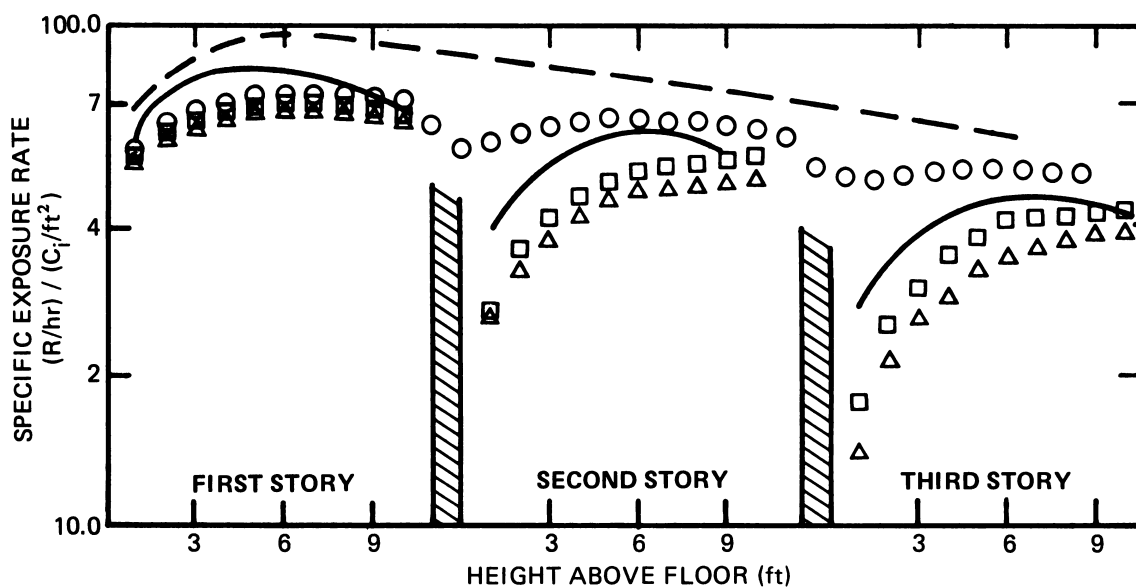
<sup>1</sup>As pointed out in section VIII.C.2 and Fig VIII.14, the innermost source annulus is not exactly a semi circle. Therefore, for purposes of comparison an approximate solid angle fraction is estimated from eq (VIII.6).



section VII.B.1, the thick-wall term in the geometry factor is not necessarily a correct representation of the scattered component of radiation emerging from a wall of arbitrary mass thickness. In order for the thick-wall term to be a good estimate of the scattered component, geometry factors dependent on wall thickness and size of field are required. This, in turn, would require a preliminary tabulation of geometry factors as a function of these variables, followed by the development of approximate formulas to fit the data. Starbird [5] has explored this approach and proposed such geometry factors, but his results have not been adopted.

The foregoing discussion relates to experimental results with a small limited area involving ground contributions of the order of 0.002. The discrepancies between theory and experiment become less severe as the size of the source is increased. Figure X.3 shows corresponding results for a source radius of 435 ft. Ground contributions on the second and third stories now vary from about .04 to 0.1. Although the disagreement still amounts to as much as 40% in some cases, the calculated variation with height for large source fields is much closer to the measured variation.

The above comparisons relate calculations for semi-circular sources to experiments involving sources which are nearly semi-circular. In practice, sources areas around structures are more likely to be rectangular in shape. Accordingly, measurements were also made by McDonnell and Velletri [4] at detector heights up to 33 ft in the RTF structure for rectangular source annuli extending 50 ft and 100 ft from the structure. Results for a rectangular field width of 50 ft are shown in figure X.4. Results are qualitatively similar to those shown in figure X.2. The somewhat better



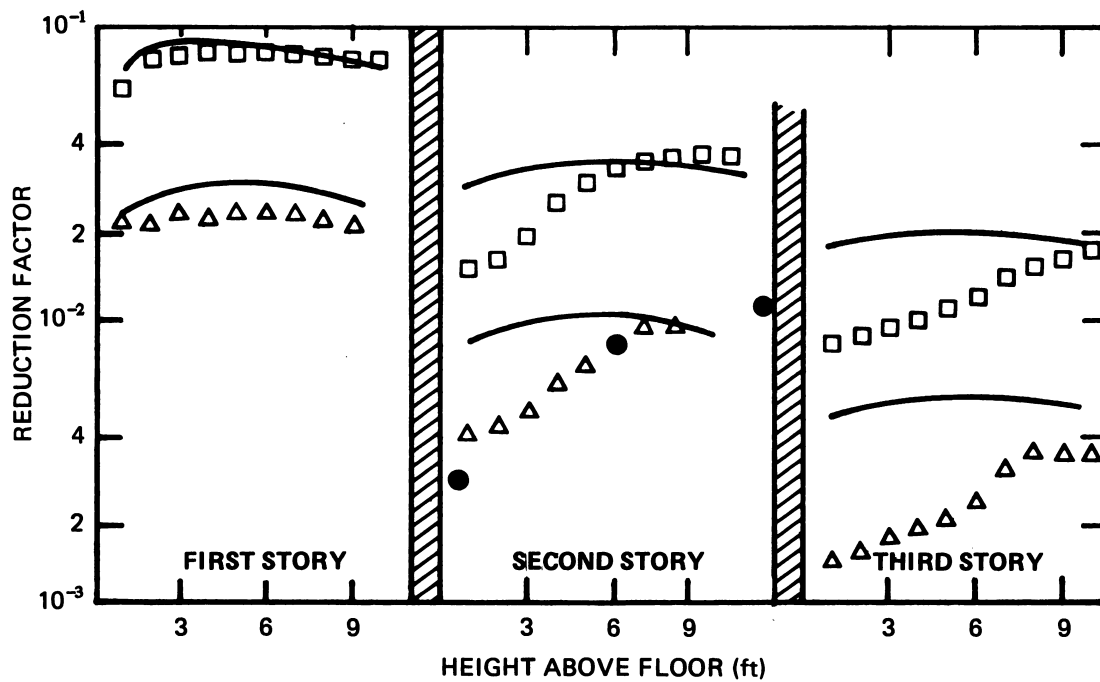
- X.3. Comparison of experimental and calculated exposure rates at the center of a structure for a semi circular ground source of radius 435 ft. Experimental:  $\bigcirc$  4 in walls, zero floors,  $\square$  4 in walls, 4 in floors,  $\triangle$  4 in walls, 8 in floors; Calculated: ---Standard Method, 4 in walls, Zero floors, —Standard Method, 4 in walls, 4 in floors.

agreement between theory and experiment is probably due more to the greater size of the source area than to any difference in shape of the source area.

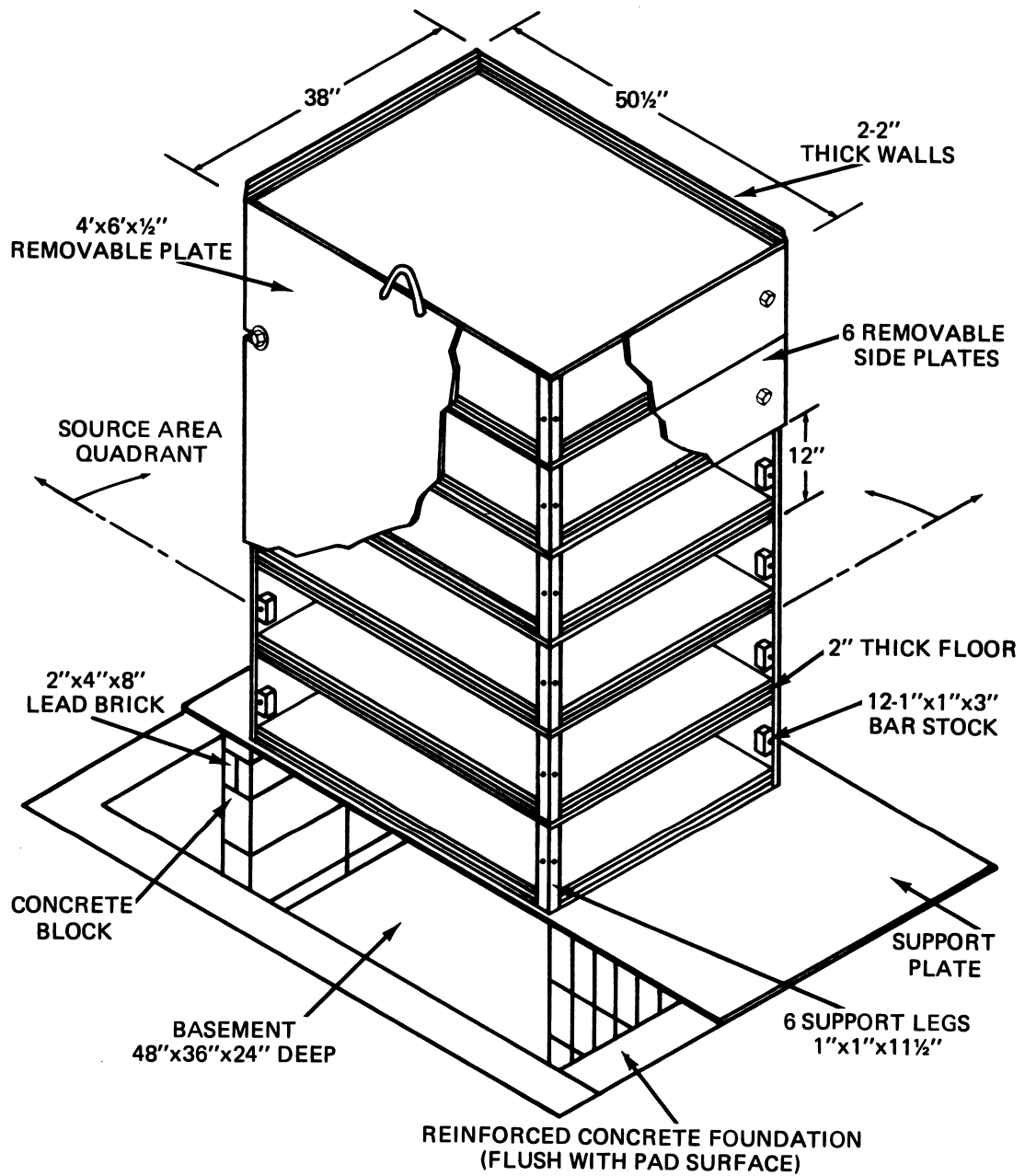
Also included in figure X.4 are some unpublished calculations by the CONSTRIIP [6] computer program. This program calculates the contribution from a point source through a portion of wall to a point detector. (See section VII.B.2) It cannot calculate penetration through floors. The points shown in figure X.4 were calculated by assuming floors to be infinitely thick. It is evident from the figure that the CONSTRIIP results are in much better agreement with the experimentally observed variation of reduction factor with height on the second story than results calculated by the Standard Method. Unfortunately, the CONSTRIIP results have never been systematized in a form suitable for engineering calculations.

### 3. Steel Model Study by Technical Operations Inc.

Another study of the contribution from limited fields was made by Batter and his co-workers [7] on a steel model of a six-story structure with a basement. Figure X.5 shows a schematic drawing of the structure, giving details of the construction. The tests were conducted within a hemispherical air-supported structure with a 100 ft diameter base erected over a 100 ft x 100 ft test pad. The thickness of floors and walls of the model could be increased in half-inch increments to a maximum thickness of 2 inches of steel. Source areas of varying width  $W_c$  were placed around the structure in one quadrant. Detectors located at the center and at four corners of the structure gave data for a central and a corner detector fully surrounded by fields of varying width  $W_c$ . Point sources were used for close-in locations while a tube source was used on the outer areas.



X.4. Comparison of experimental and calculated reduction factors at the center of a structure for a rectangular field of width 50 ft. Experimental:  $\square$  4 in walls, 4 in floors,  $\triangle$  8 in walls, 8 in floors; Calculated: — Standard Method,  $\bigcirc$  CONSTRIIP calculation 8 in walls, infinitely thick floors.



X.5. Schematic drawing of steel model used for experimental studies on multi-story structures (taken from reference [7]).

Experimental results for detectors on the central vertical axis of a building with 20 psf walls and floors are shown in figure X.6. The results are plotted against the ratio of field width to detector height for three different heights of the detector above the floor. Data for several different field sizes are given for each detector height. This figure shows that, regardless of the separate values of field width  $W_c$  and detector height  $H$ , the exposure correlates very well with the parameter  $W_c/H$ . For example, the exposure rate at 6 in above the second floor ( $H = 18$  in) for a field width of 24 in ( $W_c/H \approx 1.3$ ) is about the same as the exposure rate at 6 in above the sixth floor ( $H = 66$  in) for a field width of 96 in ( $W_c/H \approx 1.5$ ). The availability of these experimental data was an important factor in the decision to use the parameter  $W_c/H$  in characterizing the size of limited fields in the National Fallout Shelter Survey program [8]. The correlation of exposure with a similar parameter  $\omega_s$  was pointed out in section VIII.C.2.

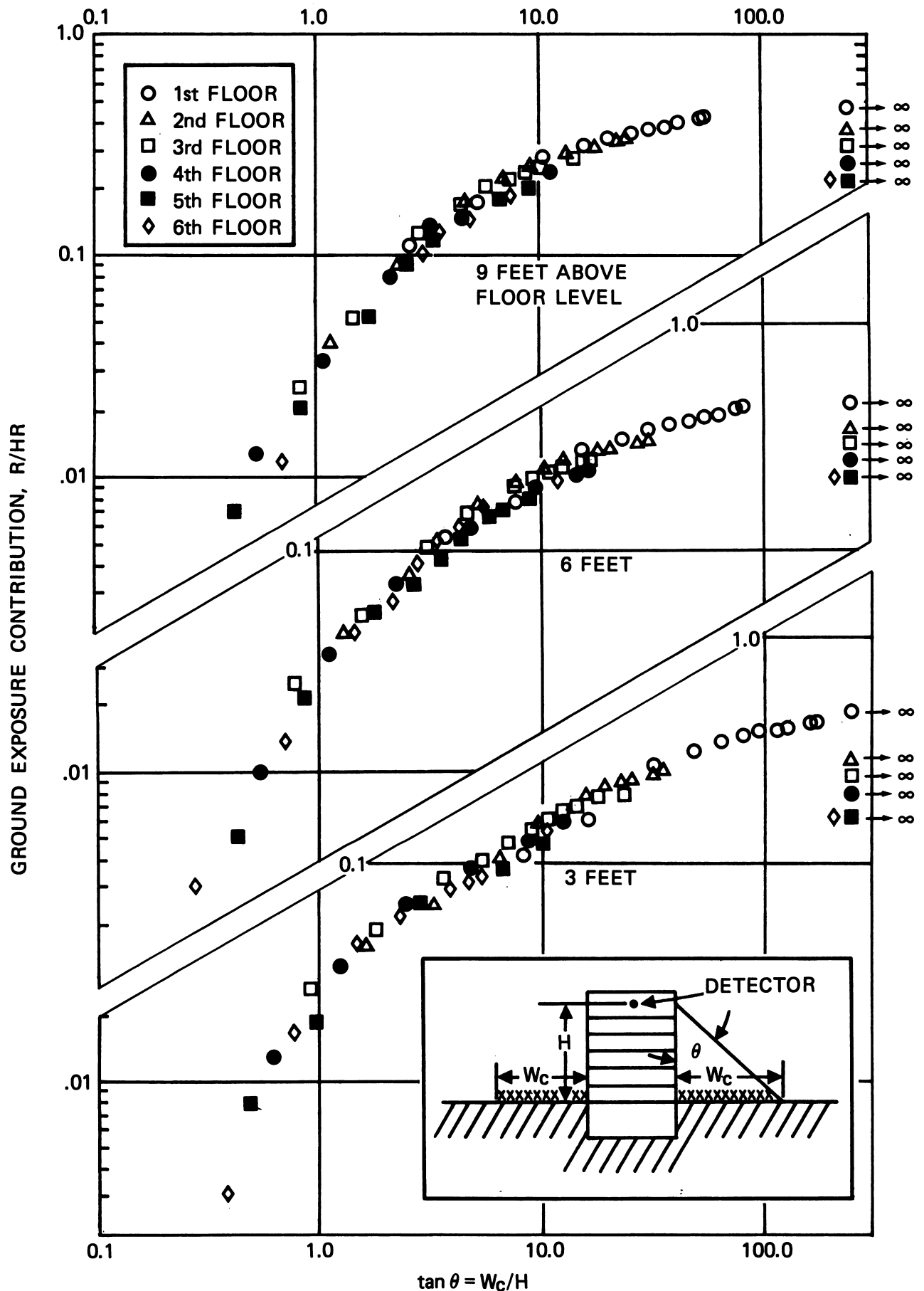
### C. COMPARTMENTED BLOCKHOUSE

We now turn to the case of a blockhouse containing a system of interior partitions, which, by the definition given in section VII.A, can no longer be called a "simple" blockhouse, and study the effect of such partitions on the reduction factor in a blockhouse. The system of interior partitions can be categorized according to whether the partitions are horizontal or vertical, and whether the sources of interest are roof sources or ground sources.

#### 1. Roof Sources and Horizontal Barriers

As discussed in section VII.B.1, the roof contribution is given by

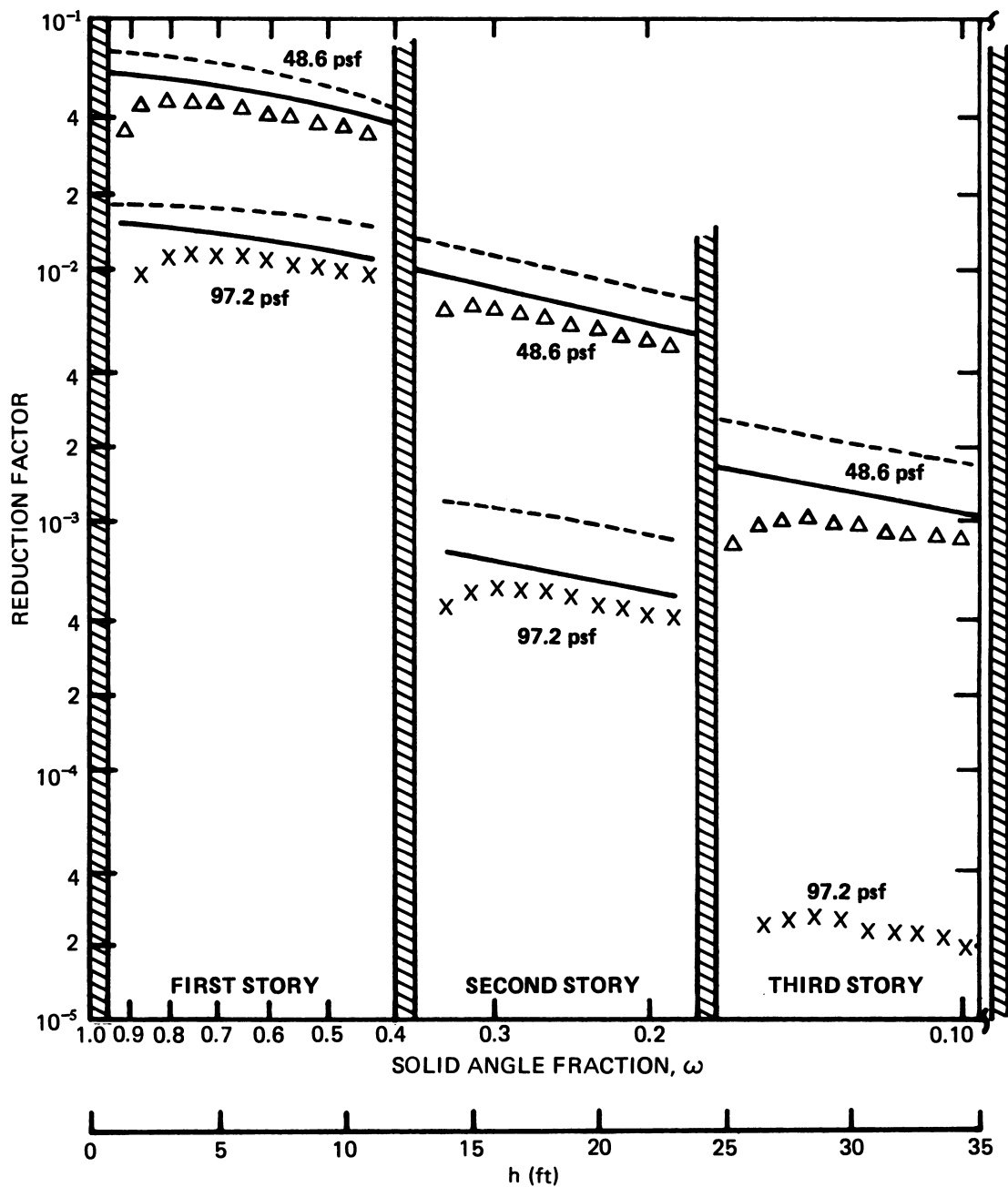
$$C_o(X_o, \bar{\omega}) = L(X_o) L_a(X_o, \bar{\omega}) \quad (X.1)$$



X.6. Experimental exposure at Center of multi-story steel model with 20 psf walls and floors. The exposure is plotted against the ratio of the field width  $W_c$  to the detector height  $H$ .

where  $\bar{\omega}$  is the solid angle fraction subtended by the roof, and  $X_0$  is the total thickness of the roof and any ceiling barriers intervening between the roof and the detector. Experiments were made by Spring and McDonnell [9] on the three-story structure at the Radiation Test Facility to determine the roof contribution when floor slabs were located between the roof and the detector. Concrete slabs of 4-in and 8-in thickness were used. Exterior wall panels were not present. Figure X.7 shows a comparison between experimental results for two different floor thicknesses, and corresponding calculations using two different functions. The solid and dashed curves are the result of using the  $L_a(X, \omega)$  and  $L_c(X, \omega)$  functions, respectively. The results for  $L_c$  are included in the figure because, at the time these experiments were made, this function was recommended for calculating the roof contribution. The experimental data shown in figure X.6 were important in the later decision to recommend the use of the  $L_a$  function for all roof sources. From figure X.7 it can be seen that the calculation using  $L_a(X, \omega)$  is generally in better agreement with the experiment. One word of caution, however: The calculations include only the number of psf of concrete contained in the barriers. They do not include any allowance for the attenuating effect of the steel beams. Spring and McDonnell tried to assess the effect of the steel beams by inferring the effective thickness of the pseudo-floor that would be required to produce agreement with experiment. Their estimates varied from 4 to 13 psf. The effective thickness of the steel beams obtained by smearing is 9.6 psf per floor, or an additional thickness of about 30 psf between the roof and first-story detectors. The attenuation associated with a 9.6 psf slab is about 25%. However, the effect of the inhomogeneous distribution of steel must be less than that which is inferred from a smearing calculation. Spring





X.7. Comparison of experimental and calculated reduction factors for rectangular roof source of  $^{60}\text{Co}$  radiation.  $\Delta$   $\times$  Experimental; Calculated: — — —  $L(X)L_c(X, \omega)$  (figs. B.6a, B.10a); —  $L(X)L_a(X, \omega)$  (fig. B.11a).

and McDonnell concluded that, although the use of the  $L_a$  function with a mass thickness that included the mass thickness of the steel beams might underpredict the roof contribution in some cases, it probably gives a more realistic estimate than does the  $L_c$  function.

## 2. Ground Source and Vertical Barriers

The next simplest configuration to consider is the combination of ground sources and concentric vertical partitions. Although such configurations are rare in practice, study of this situation points the way to understanding attenuation of radiation by interior partitions. Attenuation in more realistic configurations such as a pair of central corridor walls with a series of office partitions perpendicular to them is more difficult to calculate and will be discussed later.

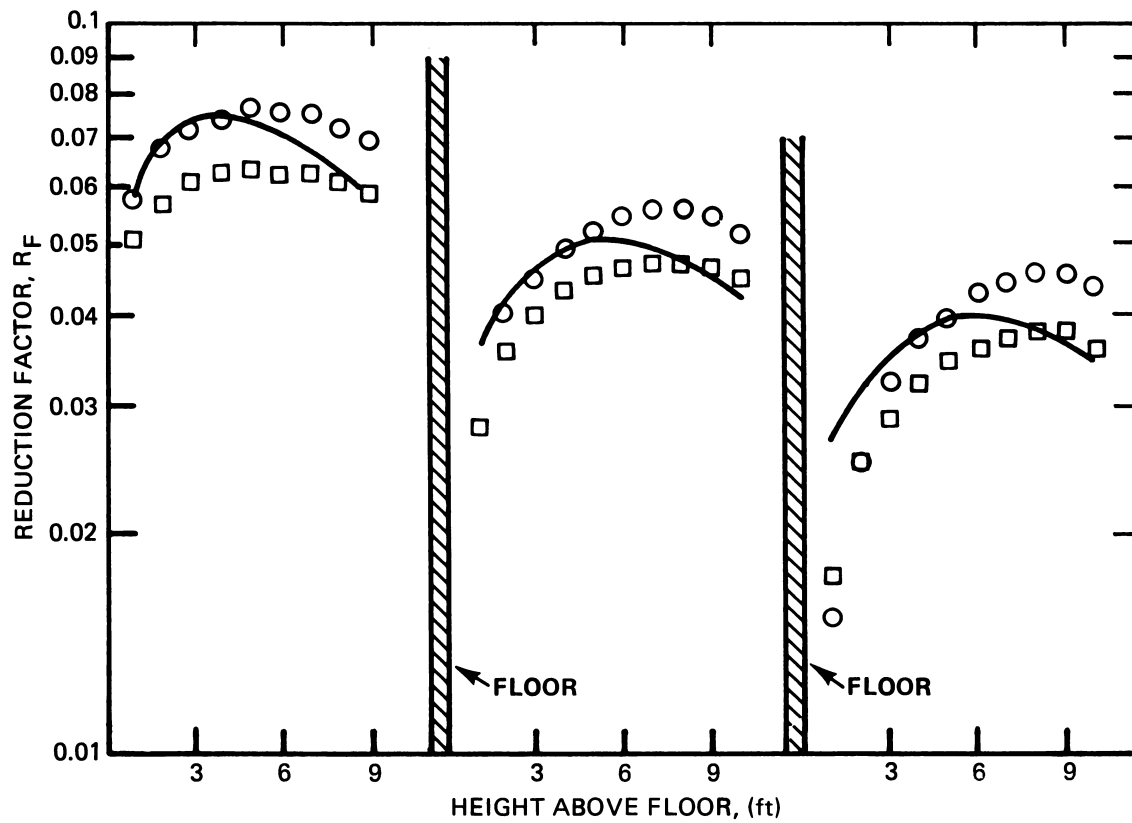
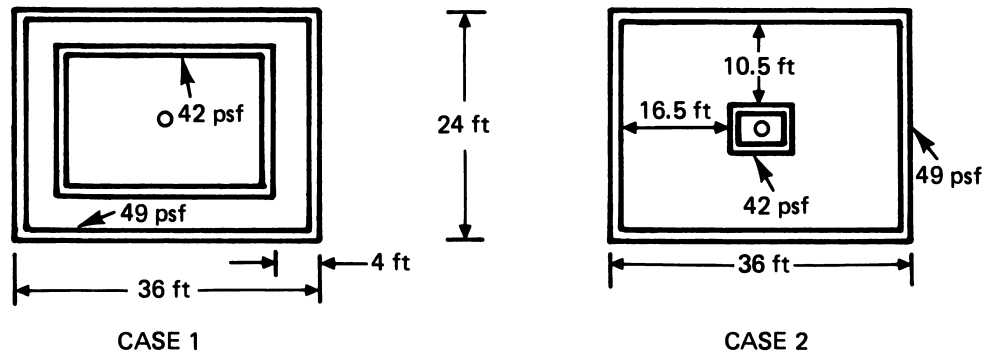
As discussed in section IX.C.1, it appears that the best way to calculate the effect of interior partitions is to express their effect in terms of an attenuation factor,  $B_i$ . This factor is approximated by the exterior wall barrier factor for a detector height of three feet and a wall thickness equal to that of the interior partition. The accuracy of attenuation factors thus estimated, and their dependence on the position of the barrier were tested in Monte Carlo calculations reported by Price and French [10]. Protection factors were calculated for cylindrical concrete exterior and interior partitions. Calculations were made for exterior barriers of 10 ft radius and 20, 40, and 80 psf thicknesses; and for interior partitions of radius 2.5, 5.0, and 10.0 ft and 20 and 40 psf thicknesses. The calculated contributions were separated according to whether they were scattered in the exterior and interior barriers.

The Monte Carlo calculations tended to support the assumption made in the Standard Method that the attenuation factor in interior partitions is independent of the position. Attenuation factors calculated by Monte Carlo were up

to 25% higher (i.e., less attenuation) than the Standard Method. However, protection factors calculated by the two methods differed on the average by 7.7%, with the largest difference being approximately 22%. The authors concluded that the assumptions used in the Standard Method for predicting effects of interior partitions are reasonable, but that the use of somewhat different attenuation factors for interior partitions would be more accurate.

The accuracy of attenuation factors was tested experimentally by Velletri et al [11]. Results for two rectangular concentric structures referred to as case 1 and case 2 are shown in figure X.8. From this figure it can be seen that the ground contribution is somewhat lower for case 1, in which the interior wall is farther from the center. The discussion in reference [9] indicates that if the interior wall were moved out against the exterior wall, the resulting contributions would lie even lower than those for case 1. Thus an interior partition of 42 psf appears to be a more effective shield when it is located near the exterior wall. The dependence on position, however, is small, being at most 30%. Furthermore, the mass of concrete in the partition near the exterior wall is many times that in the inner partition. Thus the shielding effectiveness per unit mass of the outer partition is actually much less.

It is difficult to predict the dependence on position by theory alone because there are two opposing effects. When the interior wall is adjacent to the exterior wall it tends to collimate radiation in a direction perpendicular to the wall, thus increasing the probability that radiation will reach a central detector. On the other hand, when the interior wall is close to the detector, the solid angle subtended at the detector by the interior wall is large, increasing the efficiency of collection of scattered radiation by the detector. Thus one can make a case for a higher reduction factor in



X.8. Comparison of experimental and calculated reduction factors at the center of a two structures with different interior partition configurations. Experimental;  $\square$  Case 1,  $\circ$  Case 2; Calculated: — Standard Method, which does not distinguish between the two configurations.

either case. Apparently the large solid angle subtended at the detector by an interior wall is somewhat more important than the collimating effect produced when the interior wall is near the exterior of the structure. It is important to note that this conclusion is established only for the experimental range of wall thicknesses between 40 and 50 psf. It is possible that the dependence on position might reverse if either the interior or exterior wall were extremely thin. Furthermore, the variation of the attenuation is small enough that the contributions from radiation reflected from the floor and ceiling cannot be neglected.

The effect of interior partitions on the exposure at detectors located between interior and exterior walls is more difficult to calculate. The Standard Method uses the sector approach described in section VII.D.3, the contribution from each sector varying according to the mass thickness of interior partitions included in that sector. A simpler alternative might use a table of empirical attenuation factors dependent on detector position and configuration. Table X.1, taken from Table 3.2 of reference [11], represents an attempt to produce such a table from experimental results for detectors in the corridor between interior and exterior walls.

Some of the attenuation factors in Table X.1 can be estimated by simple reasoning. For example, the attenuation factor predicted from chart C.7 (appendix C) for an interior wall of 42 psf completely surrounding the detector is about 0.35. Therefore the attenuation factors in Table X.1 might be expected to lie between 0.35 and 1.0. But a stronger restriction can be placed on these values. The detectors (10,0) and (0,15) near the middle of the long and short exterior walls of the structure see about half of the azimuth with no interior partition and half with two partitions. Accordingly a ratio of  $(1/2 \times 1 + 1/2 \times (.35)^2)$  or .56 could be predicted. Evidently this type of

TABLE X.1

## RATIO OF EXPERIMENTAL GROUND CONTRIBUTIONS

IN STRUCTURES WITH INTERIOR PARTITIONS OF 42 PSF(CASE 1 OF FIGURE X.8),  
TO THOSE IN STRUCTURES WITHOUT INTERIOR PARTITIONS

Height Above (Ft.)	Detector Position <sup>*</sup> Floor		
	(10, 15)	(0, 15)	(10, 0)
First Story			
3	.794	.630	.645
6	.819	.672	.659
9	.810	.625	.718
Second Story			
3	.900	.744	.824
6	.886	.784	.708
9	.864	.629	.678
Third Story			
3	.929	.775	.743
6	.922	.765	.715
9	.840	.680	.677

\* Detector Positions are labelled by coordinates (x,y), in which x and y represent distances along lines from the center and perpendicular to the long and short walls, respectively.

reasoning predicts a smaller contribution than that observed experimentally. The reason is that the nearest exterior wall to each of these detectors contributes relatively more to the exposure than is indicated by the azimuthal fraction.<sup>2</sup> The corner detector (10,15) receives more than 3/4 of its exposure from two adjacent exterior walls. The corresponding ratio of greater than 0.75, predicted by similar reasoning, is borne out by the experiment.

### 3. Ground Sources and Horizontal Barriers

The next problem we consider is the effect of horizontal barriers on the radiation from ground sources. We consider here radiation which penetrates in through the exterior wall and up through a floor. This is often referred to as the "in-and-up" problem. The corresponding "in-and-down" problem, in which radiation penetrates in through the exterior wall and down through a ceiling, is discussed in section D.

McDonnell and Velletri [4] made measurements to determine the effect of floors on radiation from effectively-infinite ground sources. The effect of increasing the floor thickness in the three-story RTF structure shown in figure VIII.17 can be seen in figure X.9. Variations in reduction factors for 4-inch and 8-inch exterior walls and for the different floor thicknesses show not only that the floors attenuate radiation but that the amount of attenuation is dependent on detector position. On the first story one would expect that to a first approximation the reduction factor would be independent of variations in floor thicknesses. However, the increase in ceiling thickness might be expected to produce a decrease in the small contribution from upper stories. The experimental data for the first story do, indeed, indicate a slightly reduced contribution for thicker floors.

---

<sup>2</sup>For example, a calculation by the Standard Method using two fictitious building for the (10,0) detectors predicts that 0.58 instead of 1/2 comes from the nearest exterior wall, leading to a prediction of .63 rather than 0.56.

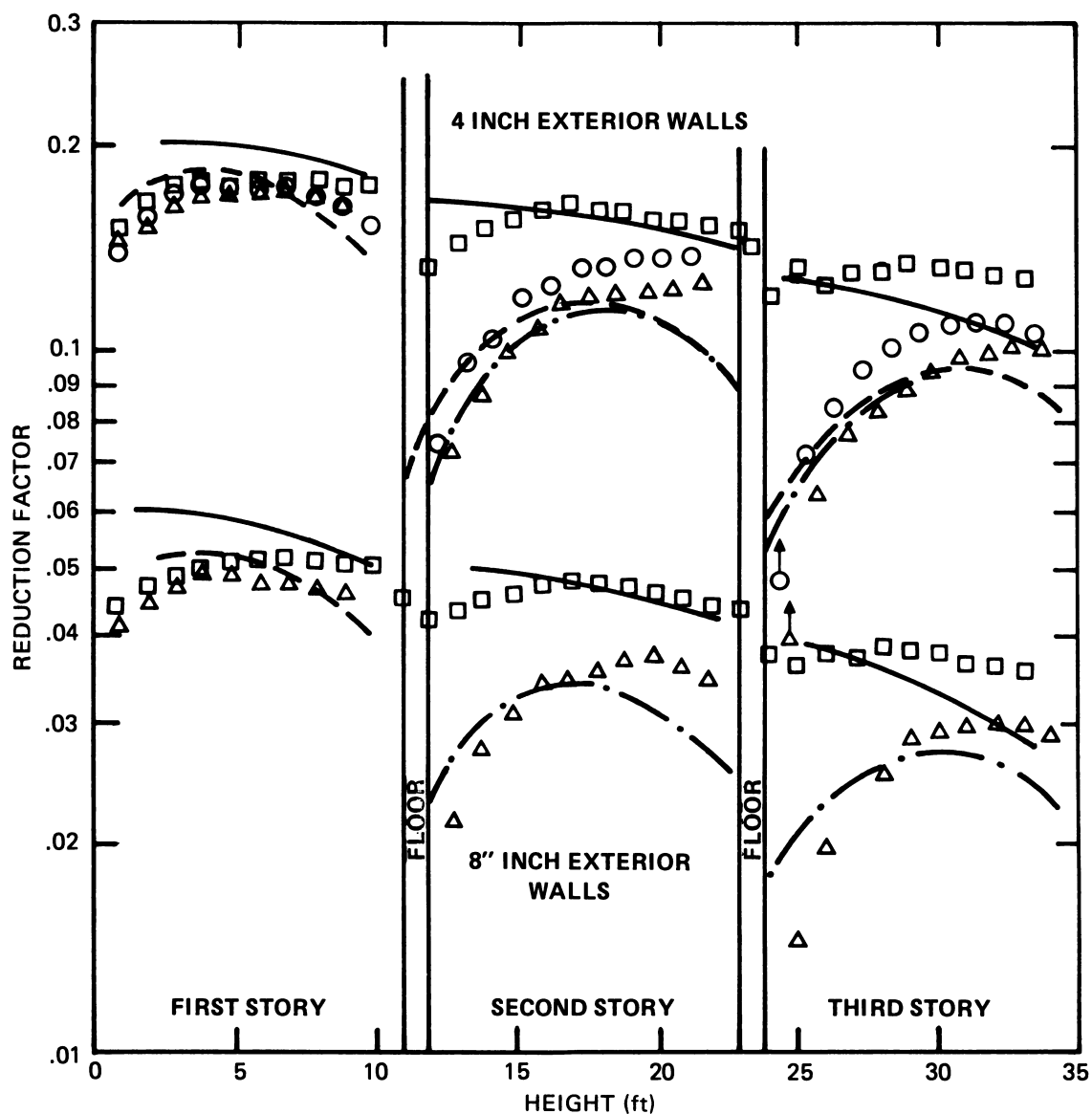
The attenuation can be obtained empirically by taking ratios of the experimental data. These ratios are shown in Table X.2, which was derived from Table 4.1 of reference 4. The attenuation is most pronounced near the floor of the second and third story. This indicates that the predominant contributions in such regions of a structure with no floors (i.e. only steel beams) is from radiation which penetrates through the walls of the story below the one on which the detector is located. Conversely, the much smaller effect near the ceiling indicates that the predominant contribution there comes from radiation which enters the walls of the same story and is therefore little affected by the presence or absence of floors.

The variation of attenuation with position is predicted qualitatively by Standard Method calculations as shown in figure X.9. This is because the calculations are sufficiently detailed to distinguish among the contributions from walls of different stories. The calculation of radiation arriving from within the solid angle fraction which is subtended by the floor is weighted by a floor attenuation factor. In the Standard Method this factor is estimated numerically by using roof barrier factor data. Experiments discussed in section X.B.2 indicate that for infinite fields this is probably adequate. The discrepancies between theory and experiment near the floors of the second and third stories as shown in figure X.9 are probably due to underestimates in the exterior wall geometry factor for radiation arriving from below the detector plane. If this component is made relatively greater, and the contribution from above the detector plane is correspondingly reduced, so that the total for zero floor thickness remains unchanged, then the calculated ground contribution at detectors below mid-height of each story will be smaller because of floor attenuation. Appropriate adjustment of the ratio of wall-scatter from below to that from above the detector can be made, so that good agreement with experiment can be obtained without changing the floor



TABLE X.2  
EXPERIMENTAL FLOOR ATTENUATION IN THREE-STORY  
RTF CONCRETE BLOCKHOUSE

Height Above Floor (Ft.)	First Story	Second Story	Third Story
1	.945	.525	.376
2	.975	.687	.568
3	.971	.710	.665
4	.983	.750	.733
5	.983	.758	.769
6	.983	.800	.813
7	.966	.807	.822
8	.966	.835	.822
9	.943	.846	.842
10	.874	.864	.818



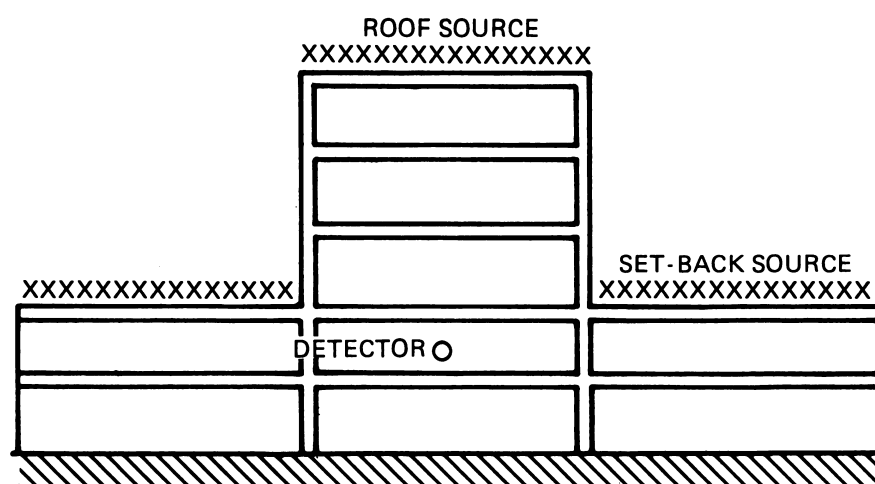
X.9. Comparison of experimental and calculated reduction factors at the center of three-story building, due to ground sources. Experimental: □ zero psf floor thickness, ○ 49 psf floor thickness, △ 98 psf floor thickness; Calculated: — zero psf floors, --- 49 psf floors, -.- 98 psf floors.

attenuation factor. We saw in section X.B.2 however that for limited fields the floor attenuation factor is probably responsible for some disagreement between experiment and calculations.

#### 4. Peripheral Roof Contribution

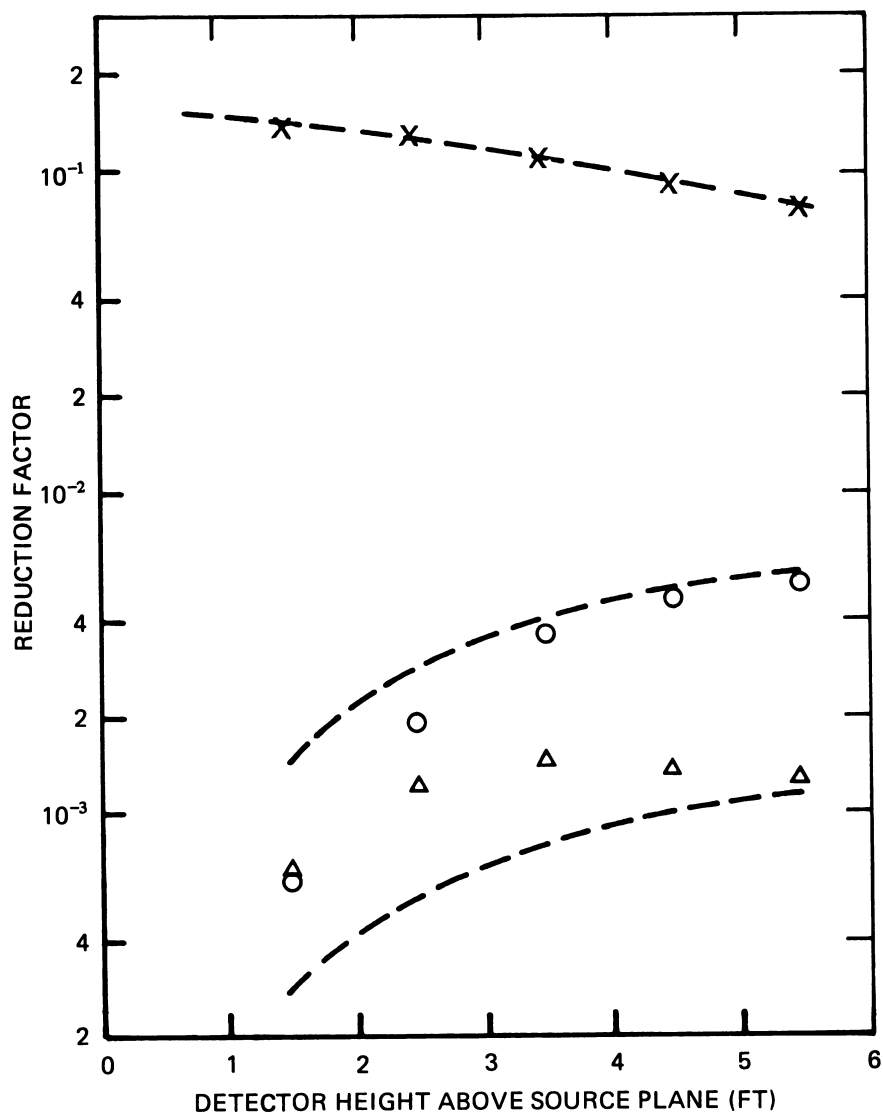
We turn now to the configuration in which the interior partition is perpendicular to the roof source. This involves the contribution of radiation from a roof source which penetrates through one or more interior walls and reaches a detector. An example of this, shown in figure X.10, is a configuration in which the roof sources on a set-back may contribute more exposure to a detector than radiation from the roof that is several stories above the detector.

This configuration was studied by Spring and Velletri [12] in the idealized cylindrical geometry shown in figure X.11. This experiment is similar to the inverted roof experiment discussed in VIII.B.2, except that the source is a circular annulus extending from a radius of 3.75 ft to 9 ft and the detectors are enclosed within a cylindrical wall of 3 ft radius and 50 psf thickness. The experiment was also run without roof and walls, and with only the roof, in order to infer experimental attenuation factors. A comparison between experimental roof contributions and those calculated from the expression  $B'(X_1)[C_0(X_0, \omega_2) - C_0(X_0, \omega_1)]$  (See eq IX.27) is shown in figure X.12. The agreement between experiment and calculations is good in the case for which there was no roof or cylindrical wall present, ("phantom" geometry;  $X_0 = 0$ ,  $X_1 = 0$ ). When the 8-inch roof is added ( $X_0 = 100$  psf) the agreement is good for detectors that are farthest away from the source plane, but the experimental values are significantly lower than the calculated ones as the detector position approaches the source plane. The effect of adding the wall is to lower the experimental value at detectors distant from the plane. The decrease in roof contribution as the detector approaches the roof can be



X.10. Schematic drawing of detector location for which set-back source may contribute more than roof source.



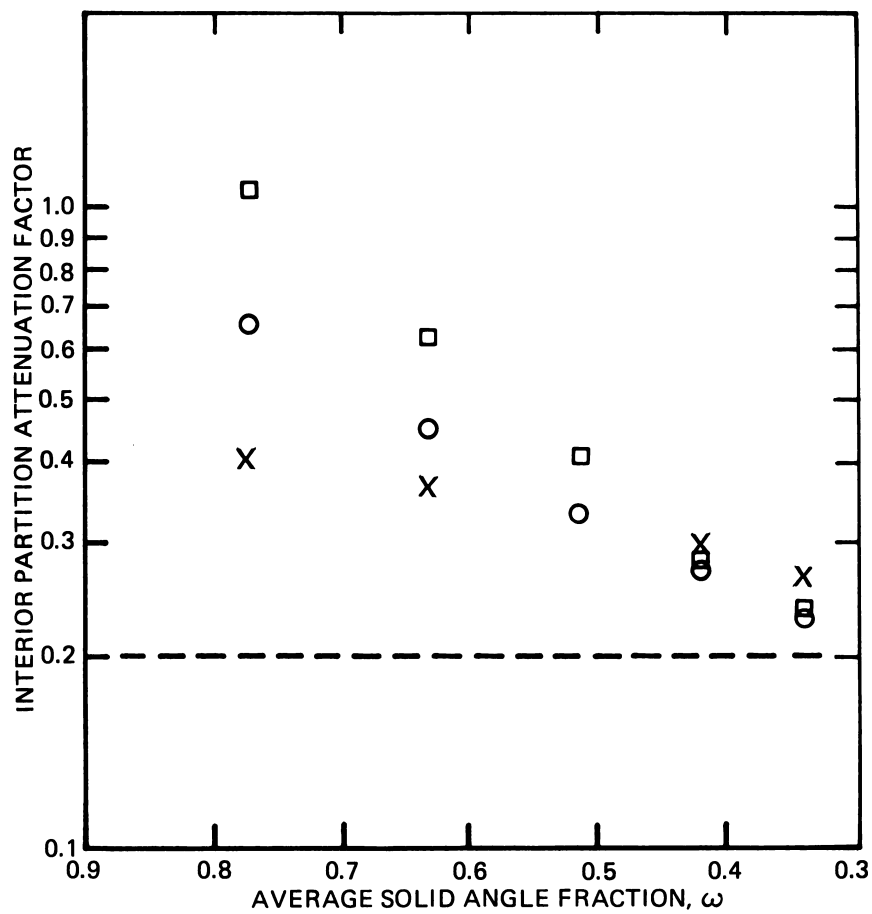


X.12 Comparison of experimental and calculated reduction factors as a function of height above an annular source. Experimental: X zero thickness "roof" and cylinder, O 8 in "roof". zero thickness cylinder, Δ 8 in "roof" and cylinder; --- Calculated for corresponding thicknesses, Standard Method.

understood in terms of the decreasing solid angle fraction  $(\omega_2 - \omega_1)$  subtended by the source. Since the attenuation factor predicted by the Standard Method for the interior wall is independent of position, the two lowest calculated curves are parallel. It is surprising, however that the experimental curves converge and perhaps even cross at the near-in detectors. The implication of such behavior is that the wall acts more as an inscatterer than an attenuator for these detector positions.

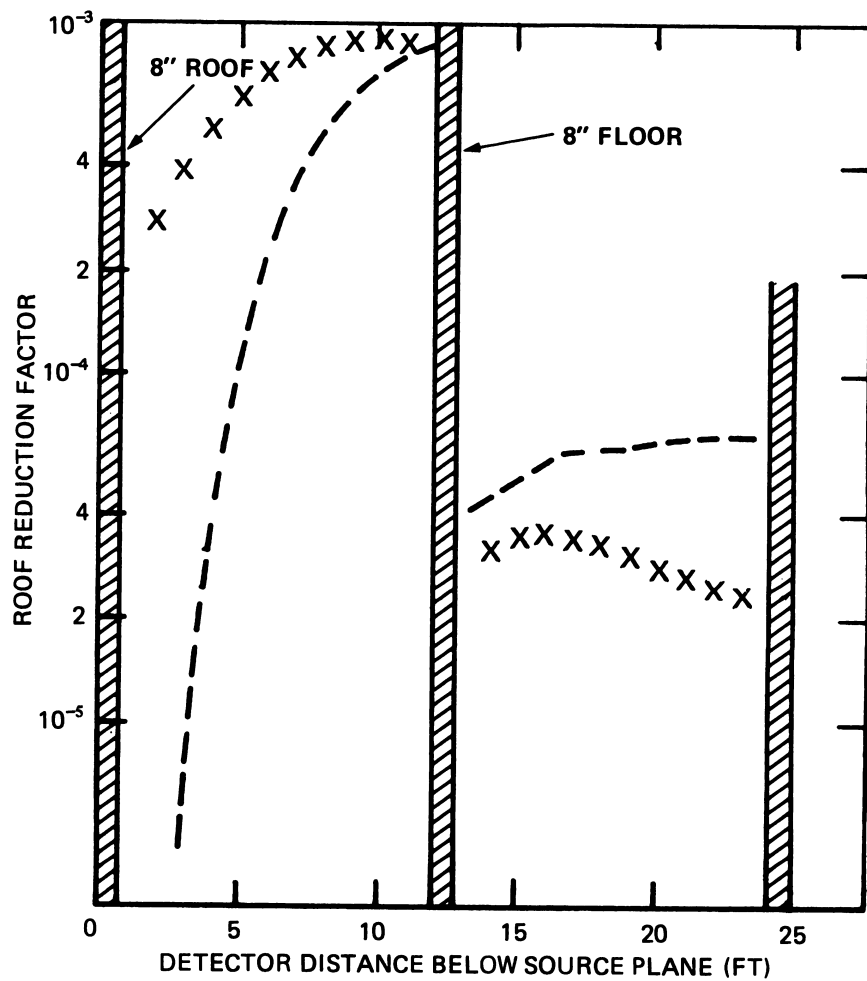
The interior-partition attenuation factors inferred from these experimental data on vertical partitions are shown in figure X.13. They show a marked dependence on position of the detector, whereas the factor shown for the Standard Method is independent of position. The average solid angle fraction  $\omega$  is defined in reference to that ring which divides the annular source into two annuli of equal area. For thicker roofs, the disagreement is more severe. The data indicate that an attenuation factor of greater than unity is possible. This was a completely unexpected result. No attempt has been made to correct interior attenuation factors in the Standard Method to take account of the results of this experiment. The peripheral roof contribution, however, is generally small. As shown in figure X.12, the roof contribution for an 8-inch roof and 4-inch wall is less than .002.

The peripheral roof experiment was repeated for the more realistic RTF 3-story blockhouse (fig. VIII.17). In this case the presence of the interior wall resulted in a corridor 4 ft wide between the exterior and interior walls, and an interior core structure 16 ft x 28 ft. The source was placed only over the corridor. The trend in reduction factors measured in this experiment and shown in figure X.14 are generally consistent with those of the idealized experiment previously discussed. For detectors on the top story, close to the roof, the Standard Method gives a contribution which is too low by more than



X.13 Comparison of experimental and calculated interior partition attenuation factor for 50 psf partition thickness and annular roof source.  
 Experimental:  $\square$  8 in roof,  $\circ$  4 in roof,  $\times$  zero in roof;  
 --- Calculated, Standard Method.





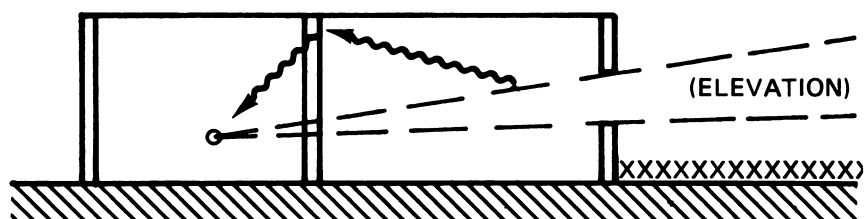
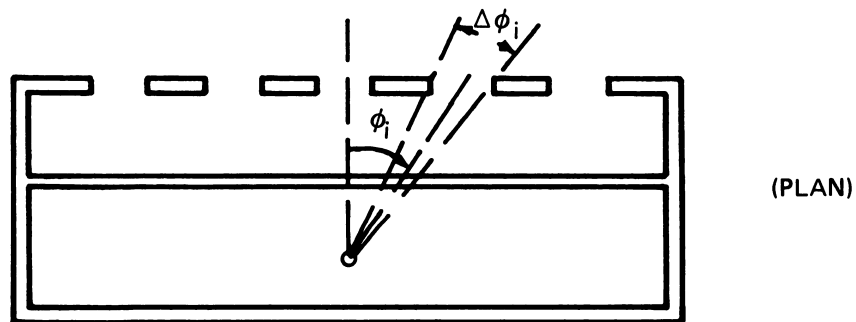
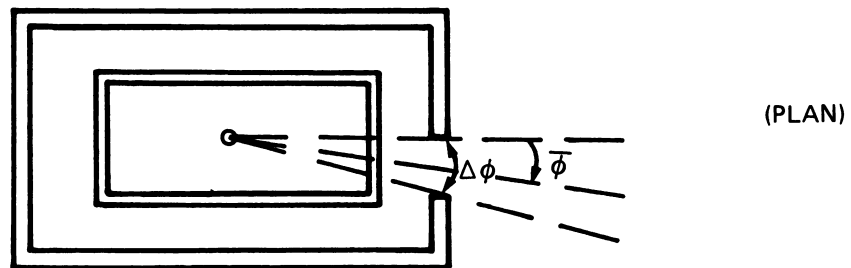
X.14 Comparison of experimental and calculated reduction factors at center of structure due to a rectangular peripheral roof source. X Experimental; ---Calculated.

a factor of 10. Although this discrepancy is great, the experimental contribution is less than .001 and is likely to be dominated by larger ground contribution.

For detectors farther from the roof the agreement is better. On the second story the Standard Method over-predicts the peripheral roof contribution. Here the situation is complicated by the fact that radiation can reach the detector either by passing first through the third story core wall and down through the second story core ceiling or by passing first through the second story corridor ceiling and in through the second story core wall. The Standard Method, which deals only with the latter contribution, gives contributions on this story which are about a factor of two greater than the experimental data. Again, however, these contributions from peripheral roof sources are not apt to be dominant, relative to ground contributions.

#### 5. Apertures and Interior Partitions

In section VII.D.4 the effect of apertures in a simple blockhouse was obtained by using the formulas for an exterior wall of zero thickness. However, calculations for configurations in which apertures are separated from the detector by one or more interior barriers are not so straight-forward. In the Standard Method the reduction of the contribution through windows, due to the presence of an interior wall, is accounted for by an attenuation factor, as previously discussed in section X.C.2. This treatment of the problem has two short-comings. The first is that the wall barrier factor data used for this purpose applies to radiation which arrives at the exterior face of the wall from all compass directions. In a situation such as that shown in figure X.15a, however, the gamma rays arrive from a limited range  $\Delta\phi$  of angles with some average value  $\phi$ . Comparison of Figures B.3a and B.17a shows that the wall barrier factor predicts an attenuation which is roughly equivalent to a mono-directional source incident at an angle  $\theta_0$  for which  $0.6 \leq \cos\theta_0 \leq 0.8$ .



X.15 Schematic drawings of structures which have interior walls and apertures in exterior walls.

Therefore, for  $\phi$  near zero and small  $\Delta\phi$ , the wall barrier factor will underestimate the contribution from radiation passing through the aperture and the interior wall, while for  $\phi \simeq 90^\circ$  and small  $\Delta\phi$ , the barrier factor will overestimate the contribution. In a situation such as shown in figure X.15b, where the apertures span a range of azimuthal angles  $\phi_1$ , use of the wall barrier factor for attenuation in the interior wall should provide a better approximation.

The second shortcoming of the current use of an attenuation factor becomes evident when the interior barrier can act as an inscatterer. This situation is shown in figure X.15c. In a calculation for this situation it is assumed that the detector receives only skyshine through the aperture and that the skyshine is attenuated by the interior wall. In reality, however, the uncollided radiation can contribute by scattering in the interior wall. This contribution may be significantly larger than the calculated contribution for attenuated skyshine. The inscattered contribution can be estimated for a specific circumstance but it is presently difficult to prescribe general rules. Such rules would very likely use slant penetration curves which are shown in figures V.8 and V.9. In addition, the angular distribution of photons emerging from the interior wall for each angle of incidence would be required in some form.

Experiments have indicated that exposure rates are somewhat higher than predicted by the Standard Method for a structure with an interior partition and an aperture in the exterior wall. Kaplan [13] performed an experiment with concentric steel cylinders of one foot and two feet diameter. His conclusion was that "calculations are generally 20% to 30% lower than experimental results at detector locations not opposite the aperture and up to 50% lower at detector locations opposite the aperture." Some of his results for an exterior cylinder of 60 psf thickness and 2 ft height, with an aperture

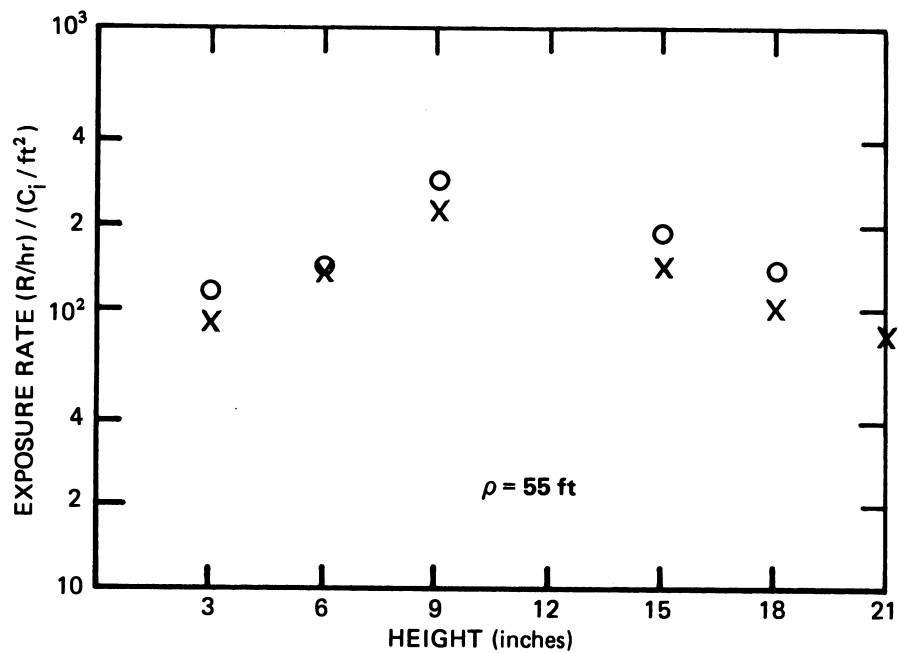
extending from 6 inch to 12 inch height, are shown in figure X.16. The data plotted in this figure correspond to a source disk of 55 feet. They do not include estimated contributions from the far field. From this figure it can be seen that the ratio of experimental measurements with and without a 20 psf interior wall, at a detector at mid-height of the aperture, is about 0.80. The calculated ratio, treating the effect of the interior barrier by a simple attenuation factor is 0.62. The reason for the higher experimental value in this case seems to be due not so much to inscattering as to the fact that the cylindrical geometry of the interior partition produces a shape factor for the interior wall. A correction could be made in the calculation by weighting the scattered portion of the radiation by the shape factor for a circular building. This would give

$$\begin{aligned}
 B_c(X_i) &= S_w(X_i) E + [1 - S_w(X_i)] B(X_i) \\
 &= (.35) \frac{\pi}{2} + .65 \cdot .62 = .74 ,
 \end{aligned}$$

which is very near the experimental value. This suggests that the attenuation factor for interior partitions should be expressed as a function of the shape of the interior wall structure. At this writing, no attempt has been made to incorporate such a treatment into the Standard Method.

#### 6. Core Structure Below Grade

The calculation of the reduction factor for a core structure in an above-grade location was discussed in section X.C.2. It was shown there that the interior partition attenuation factor  $B_i$  provides a reasonably good estimate of the attenuation in the core wall. The calculation for a core structure below grade is a much more difficult one to formulate. There have been numerous experiments on residential structures at the Nevada Test Site

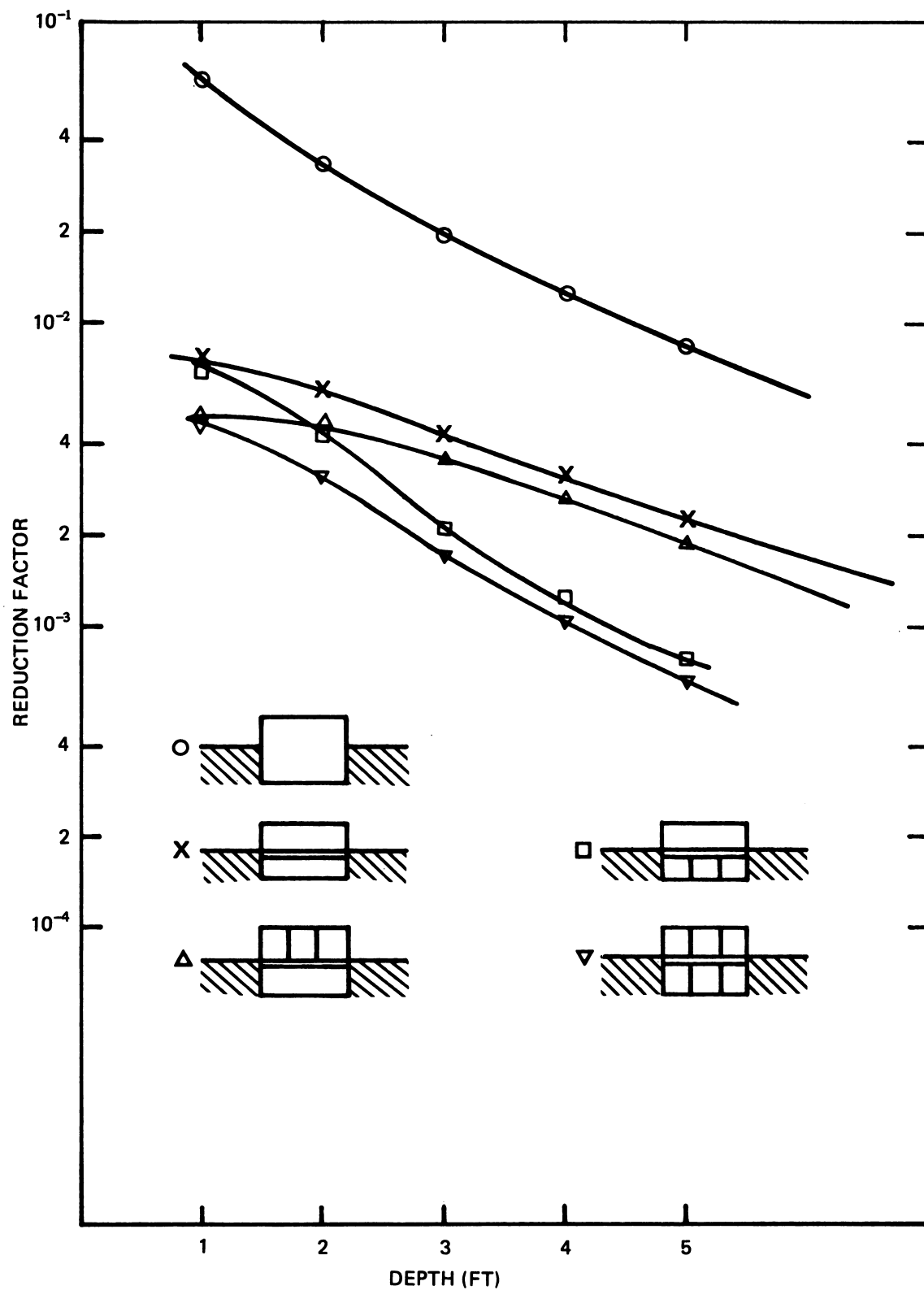


X.16 Experimental exposure rates at center of vertical cylinder of 60 psf thickness with aperture extending from 6 in to 12 in height. The source is a circular disk extending to 55 ft X 20 psf interior wall, O no interior wall.

[14-17] which contained basement fallout shelters. Estimates from these experiments of the protection factor within shelters with 8-inch concrete walls and ceiling generally ranged between 150 and 250. DCPA estimates of protection in basement fallout shelters are based on these experiments. Detailed calculational procedures for such shelters have not been developed. This is primarily because penetration through a basement ceiling is not well understood. But another reason for the absence of calculations is a lack of understanding of how the portion of the contribution coming through the ceiling of the shelter compares with the portion coming through the walls of the shelter.

A recent experiment by Starbird [18] on half-buried cylinders (fig. X.17) gives a qualitative idea of the effect of a core either above or below grade on the reduction factor below grade from ground sources. Unfortunately, the absolute reduction factors from his experiment do not agree closely with calculations, even for the simple configurations examined. Table X.3 shows a comparison of experimental ground contributions for  $^{60}\text{Co}$  radiation at a detector 3 ft above grade for three different configurations, two of which have no interior structure. The discrepancies are larger than expected for these relatively simple configurations.

Nevertheless, a qualitative idea of shielding mechanisms can be obtained from an examination of Starbird's data. Figure X.17 shows experimental ground contributions from ground sources for five different situations as a function of depth below the basement ceiling. The uppermost and next-uppermost curves show the result for a simple basement without and with a ceiling, respectively. The ratio between these two curves gives the experimentally observed attenuation in the basement ceiling. This simple configuration has been discussed in section IX.C.1.d. Experimental and calculated values are shown in Table X.4. The calculated values were obtained using the attenuation



X.17 Experimental ground contributions in the basement of a cylindrical concrete structure with varying interior partition configurations. Lines are drawn through experimental points to distinguish trends.



TABLE X.3

COMPARISON OF CALCULATED AND EXPERIMENTAL VALUES OF GROUND CONTRIBUTIONS  
BELOW GRADE IN A CONCRETE CYLINDER ( $^{60}\text{Co}$  RADIATION)

(SEE FIG. X.17)

Configuration	Exper.	Calc.
$X_e = 49 \text{ psf}, X_i = 0$	.400	.322
$X_e = 98 \text{ psf}, X_i = 0$	.135	.100
$X_e = 49 \text{ psf}, X_i = 49 \text{ psf}$	.150	.090

TABLE X.4

ATTENUATION FACTORS IN A BASEMENT CEILING [17]

Depth	$B_c(X_c, \omega)$	
	Exper.	Calc.
1	.118	.076
2	.178	.126
3	.219	.180
4	.246	.225
5	.258	.271

factor  $B_c(X_c, \omega)$  for  $^{60}\text{Co}$  radiation given later in eq (X.3) rather than that given in eq (IX.31) for fallout radiation. This table shows that the calculated values tend to be too low for detector position near the ceiling.

A further analysis of figure X.17 shows the effect of vertical interior partitions on the ground contributions. It is clear from the figure that the structure with no vertical interior partitions either above or below grade, and the one with vertical interior partitions both above and below grade represent two extremes. The contribution in the latter case is always lower. However, the two curves representing configurations with partitions below grade only and partitions above grade only exhibit an interesting crossover. The crossover can be explained qualitatively in the following manner. The detector near the basement ceiling receives all of its contribution from the ceiling area in the center of the structure. It is, therefore, most sensitive to the radiation environment in the center of the first story, near the floor. For this detector position the two configurations with vertical partitions on the first story give about the same reduction factor and the two configurations with no partitions on the first story give a higher contribution. On the other hand, a detector near the floor receives most of its contribution from the peripheral area of the basement ceiling. This component is attenuated by partitions in the basement but relatively unaffected by partitions on the first story. For this detector position the two configurations with vertical partitions in the basement give about the same reduction factor. Thus detector positions near the ceiling of the basement are most sensitive to the presence of internal partitions on the first story while those near the floor are most sensitive to the presence of internal partitions in the basement. If the top detector received radiation only from the central area and the bottom detector only from the periphery the two sets of paired curves of figure X.17 would coincide at a depth of 5 ft. Since they do not coincide, there must be

some mixing. We assume that the ground contribution is of the form

$$C_g = A(X_a) C_g(X_e, X_c, \bar{\omega}') + A(X_b) C_g(X_e, X_c, \bar{\omega}) - C_g(X_e, X_c, \bar{\omega}') \quad (X.2)$$

where  $X_c$  is the thickness of the basement ceiling,  $\bar{\omega}$  is the solid angle fraction subtended by the basement ceiling,  $\bar{\omega}'$  is the solid angle fraction subtended by the core ceiling,  $A$  is an attenuation function,  $X_a$  is the thickness of the above-grade partitions,  $X_b$  is the thickness of the below-grade partitions, and  $C_g(X_e, X_c, \bar{\omega})$  is the reduction factor for the basement with the ceiling but with no partitions. With this expression we can approximately reproduce the experimental data by setting  $A(X_a) = .6$  and  $A(X_b) = .3$ . The comparison is shown in Table X.5. The experimental values of  $C_g(X_e, X_c, \bar{\omega})$  for  $X_c = 49$  psf were used in the calculations.

The effect of the internal partitions in the basement seems to be accounted for adequately by the existing attenuation curve  $B_i(X_b, 3 \text{ ft})$  which gives  $B_i \approx 0.29$  for  $X_b = 49$  psf. The effect of interior partitions above grade, however, cannot be accounted for with the same function. One approach is to assume the form  $B_i((X_a - 30), 3 \text{ ft})$  for above-grade partitions of thickness greater than 30 psf and to assume  $B_i = 1$  for  $X_a \leq 30$ . The rationale is that for  $X_a$  less than 30 psf, scattering probably compensates for absorption and the interior partitions on the story above grade have a negligible effect on reduction factors below grade. This interpretation is borne out by experiments at Kansas State University [19].

Starbird's report [18] also contains measurements of the contribution of ground sources to the exposure in a cylindrical core shelter of 3 ft diameter within the cylindrical basement. His measurements on a cylindrical shelter with a ceiling at grade level, and located in a basement with no ceiling except over the shelter, are predicted quite well by the Standard Method. Comparison of this configuration with the case of a 49 psf basement ceiling

TABLE X.5

## GROUND CONTRIBUTION IN A BELOW-GRADE CORE SHELTER

Depth	$X_a = 49$ , $X_b = 0$		$X_a = 0$ , $X_b = 49$		$X_a = 49$ , $X_b = 49$	
	Exper.	Calc.	Exper.	Calc.	Exper.	Calc.
1	.00501	.00597	.00719	.00644	.00472	.00404
2	.00473	.00477	.00443	.00395	.00308	.00272
3	.00358	.00363	.00215	.00248	.00169	.00180
4	.00261	.00267	.00125	.00162		.00122
5	.00194	.00203	.00079	.00108	.00067	.00085

TABLE X.6

## COMPARISON BETWEEN EXPERIMENTAL AND CALCULATED

## GROUND CONTRIBUTIONS IN A BASEMENT [20]

Height Above Basement Floor	Cg (Exper.)	Cg (Calc.)
1	.00148	.00070
3.5	.00173	.00094
6	.00175	.00134
8.5	.00187	.00230

but no shelter shows that for detectors located near the floor the effect of the walls cannot be approximated by assuming that they are repositioned into a pseudo-ceiling. Rather, the effect of the wall is to scatter in radiation to the highest detector and absorb radiation which would have reached the lowest detector. (See the preceding discussion on peripheral roof sources, sec. X.C.4)

Starbird's data show that by lowering the shelter ceiling to a position 2 ft below grade the contribution inside of the shelter is raised by as much as 50%. This increase is rather surprising and may be peculiar to the use of small solid angles in the experimental configuration. An increase of about 20% might be accounted for by the fact that the radiation now incident on the ceiling is increased while that incident on the wall is decreased; and the ceiling mass thickness is 6 psf lower than that of the wall. Adding a basement ceiling of 49 psf over the low-ceiling shelter reduces ground contributions by a factor of 4, which is large enough to indicate that much of the radiation which contributes to the exposure in the shelter is obliquely incident on the plane of the basement ceiling.

#### D. "IN-AND-DOWN"

##### 1. Background

The problem which has come to be known as the "in-and-down" problem concerns the penetration of radiation "in" through the wall of a structure and "down" through a floor. The most common situation in which this component of radiation is important (or dominant) is a detector location in a basement. The calculation of the reduction factor for this important situation has received a great deal of attention. Both experimental and theoretical attempts have been made to assess the degree of accuracy of the Standard Method and to suggest improved techniques for evaluating this component of the reduction factor.

The first indication that the "in-and-down" contribution was incorrectly calculated in early versions of the Standard Method was given in a report on the analysis of experiments on houses at the Nevada Test Site which contained the following statement: "The variation with height in the basement (of a two story brick house) does not seem to be as severe as indicated by the calculated values [20]." However, these experiments were conducted with radioactive sources of relatively low intensity, yielding exposure rates which corresponded to the lower limit of the detectors. These measurements therefore required confirmation and further study.

A later experiment at the U.S. Nuclear Effects Laboratory (NEL) in Maryland also showed disagreement between theory and experiment. Table X.6 shows the comparison made between calculation and experiments by Batter and Starbird [21]. It can be seen that the calculated contributions change by more than a factor of 3 from the highest to the lowest detector, while the experimental contributions change by a factor of only 1.26. But in this experiment, there were uncertainties which influenced the interpretation of results. For example, there was a basement under only one-half of the structure. Also, the basement ceiling had concrete joists at six foot intervals. It was not known if these complications might produce results not typical of "in-and-down" configurations in general. However, later experiments at NEL [22-24] on a simple rectangular structure with a basement, produced conclusive evidence that the calculations did not predict the ground contribution in basements correctly. The experiments at NEL yielded attenuation factors which were lower than the early theory for solid angle fractions near unity, but which increased until they became higher than the theory by a factor of 2 at solid angle fractions of about 0.4. Experiments on steel models [25] which measured attenuation factors at solid angle fractions as low

as  $\omega = 0.1$ , indicated that the early calculations underestimated the ground contribution for these positions by as much as a factor of 5. However, values for the solid angle fraction of practical interest are generally greater than 0.5. Furthermore, the "in-and-down" case is only one of several contributions to the reduction factor for basement locations. The situation might be summarized by saying that the early calculations gave large errors from a technical viewpoint, but from a practical viewpoint, the average error in the prediction of reduction factors for basement locations was probably less than a factor of 2.

Because the "in-and-down" configuration had become well documented both experimentally and by independent calculations, and because it obviously had both practical and theoretical importance, it was believed advisable to seek a tentative correction to the attenuation factor which would remove most of the discrepancies between experiments and calculations. A recommendation [26] based primarily on the NEL experimental data to be discussed in section X.D.3 was suggested, accepted by OCD, and incorporated in the Standard Method. (This was the first time that an expression based on experiment rather than theory was used in the Standard Method.) An empirical attenuation function derived from experiments with  $^{60}\text{Co}$  radiation is

$$B_c(X_c, \omega) = (1.0 - 3.0e^{-2.3\omega - 0.12X_c} + 3.0e^{-(2.3\omega + 0.042X_c)}) ({}^{60}\text{Co}) \quad (\text{X.3})$$

The corresponding expression inferred for fallout radiation (see eq (IX.31)) is

$$B_c(X_c, \omega) = (1.0 - 3.5e^{-2.3\omega - 0.10X_c} + 3.5e^{-(2.3\omega + 0.040X_c)}) (\text{fallout}) \quad (\text{X.4})$$

It should be kept in mind that these empirical approximations are a good representation of the experimental data only for a limited range of barrier thicknesses and building sizes and geometries. As such they may include effects -- some subtle -- associated with this range of parameters. Investigations of the sensitivity to some of the relevant variables is described in the next section.

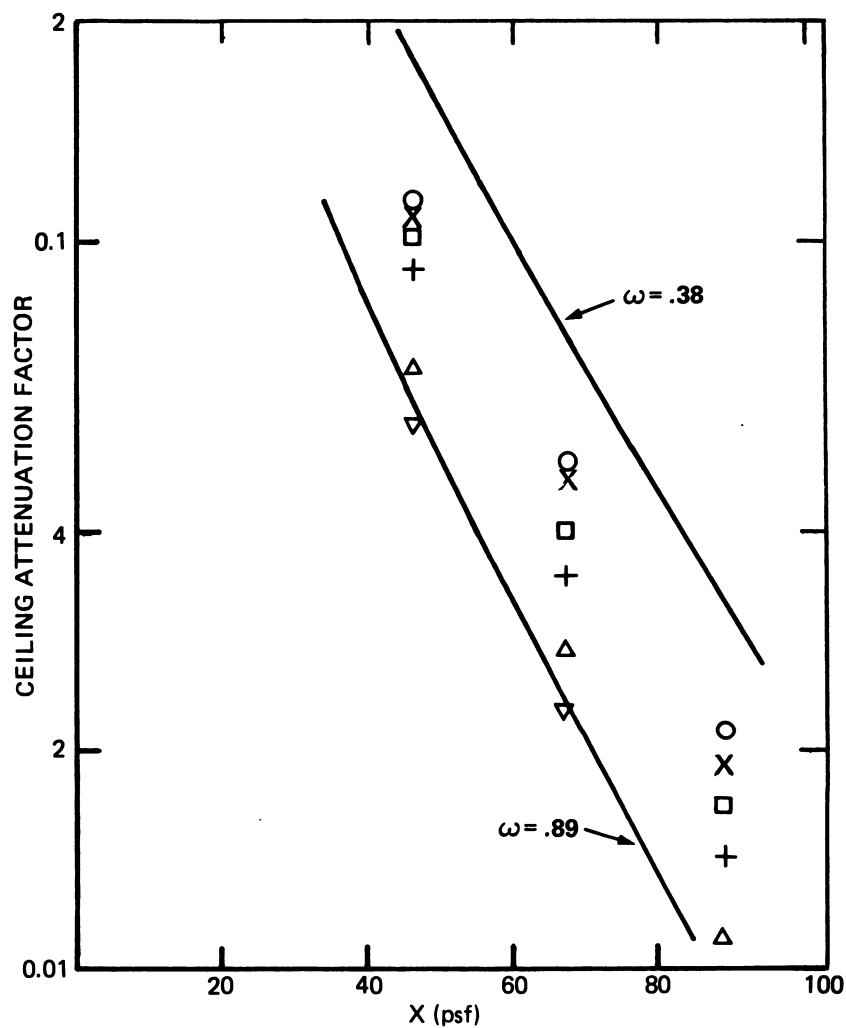
## 2. Skyshine Attenuation

The earliest experiments which attempted to measure "in-and-down" attenuation used covers over holes in the ground. Thus, they were really measuring the penetration of skyshine radiation. This approach was influenced by the fact that the attenuation of "in-and-down" radiation was originally predicted by the penetration curve for skyshine. It turns out that the attenuation of the two types of radiation is indeed very similar.

Schumchyk et al. [23] investigated the attenuation of skyshine by placing concrete covers of 4-, 6-, and 8-inch thicknesses over the basement described in section VI.D.1. The experimentally observed attenuation in the basement ceilings can be obtained by taking the ratio of the reduction factor in the covered hole to the reduction factor at the same detector position in the open hole. Figure X.18 shows the measured attenuation factors at six different vertical positions on the centerline of the basement for three different ceiling thicknesses. The calculated values shown in this and following figures are derived from eq (X.3).

Although the attenuation factor is important in understanding differences between experiments and calculations, the reduction factor is still the



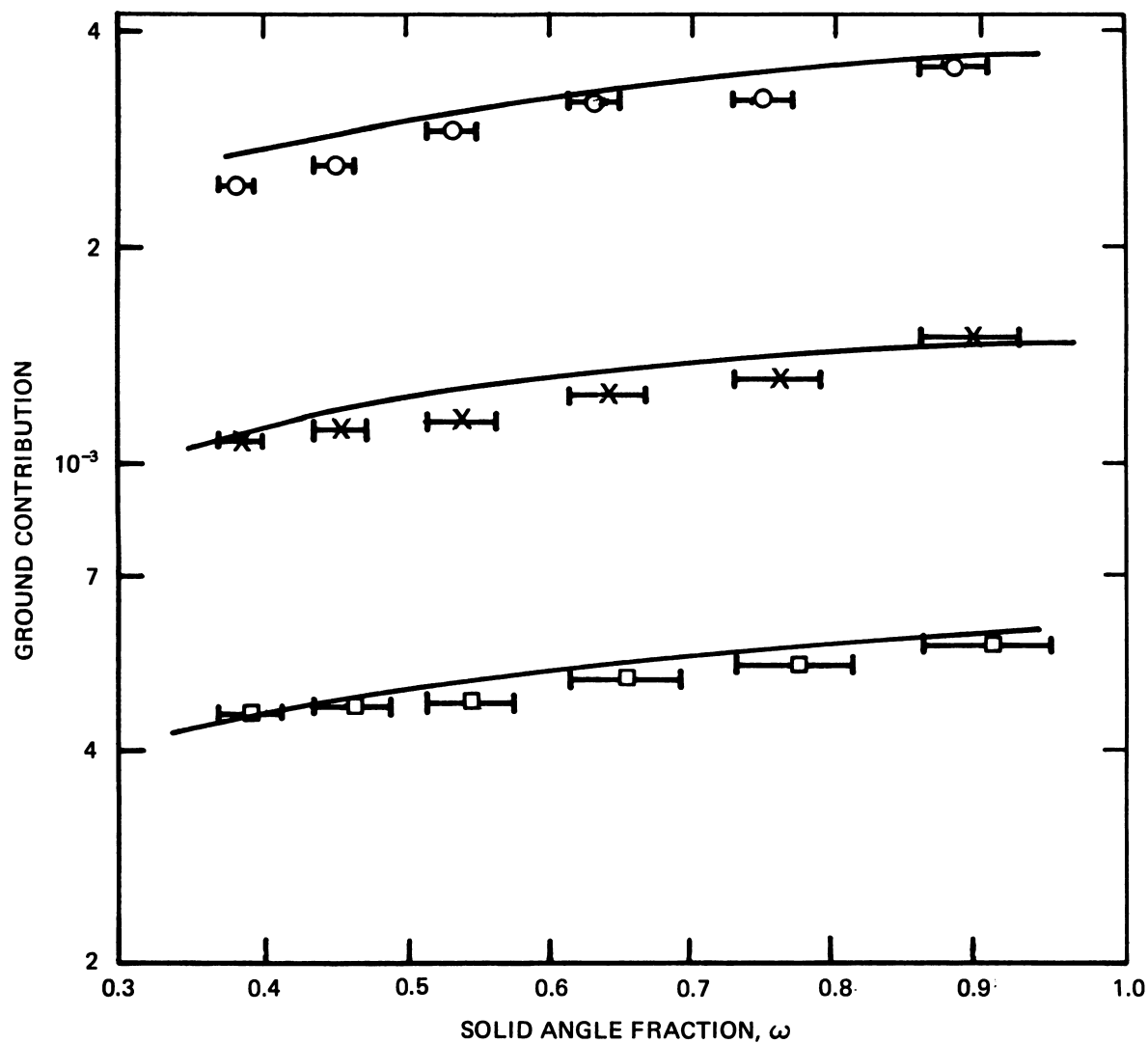


X.18 Comparison of experimental and calculated ceiling attenuation factors as a function of ceiling thickness  $X$  and solid angle fraction  $\omega$  subtended by ceiling. Experimental: ○  $\omega = 0.38$ , ×  $\omega = 0.45$ , □  $\omega = 0.53$ , +  $\omega = 0.64$ , △  $\omega = 0.76$ , ▽  $\omega = 0.89$ ; — Calculated, Standard Method, adjusted for  $^{60}\text{Co}$ .

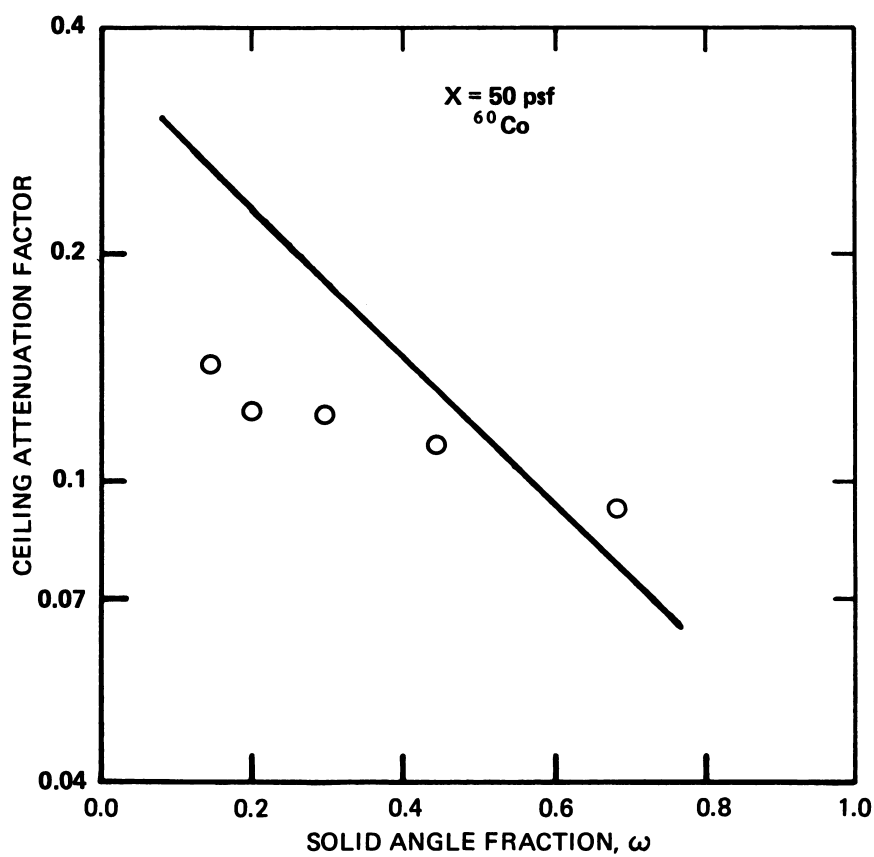
quantity of fundamental interest. Figure X.19 shows the measured and calculated ground contributions for the three ceiling thicknesses. The calculated values were obtained from the product of the skyshine exposure  $S(0)$  (fig. B.20a), the skyshine geometry factor  $Sa(3', \omega)$  (fig. B.22a), and the ceiling attenuation factor from eq (X.3). The apparently good agreement between the experimental and calculated reduction factors results from some of the discrepancies in the factors used for this calculation. For example, the values of the skyshine geometry factor calculated from figure B.22a lie about 40% below the experimental values of Schumchyk et al [23] near  $\omega = 0.4$ . The calculated values of the ceiling attenuation factor shown in figure X.18, however, lie about 50% higher than the experimental values. The net discrepancy in the reduction factor shown in figure X.19 is therefore about 10%.

Spring and Velletri's skyshine experiments [VI.55] also included measurements with a 50 psf concrete cover over the cylindrical hole. The ratio of these reduction factors to those shown in figure VI.18 for the open hole yield attenuation factors, as shown in figure X.20. Also shown in that figure are the values for ceiling attenuation from eq (X.3). The calculated values give a trend significantly different from the experimental variation. This effect was seen in figure X.18, in which the calculated attenuation factor for small solid angle fractions lies above the experimental values by about 50%. Corresponding ground contributions are shown in figure X.21. Here, although the agreement between calculation and experiment is better than for the attenuation factor, the ratio of reduction factors approaches 1.5 for the largest solid angle fraction for which measurements were made.

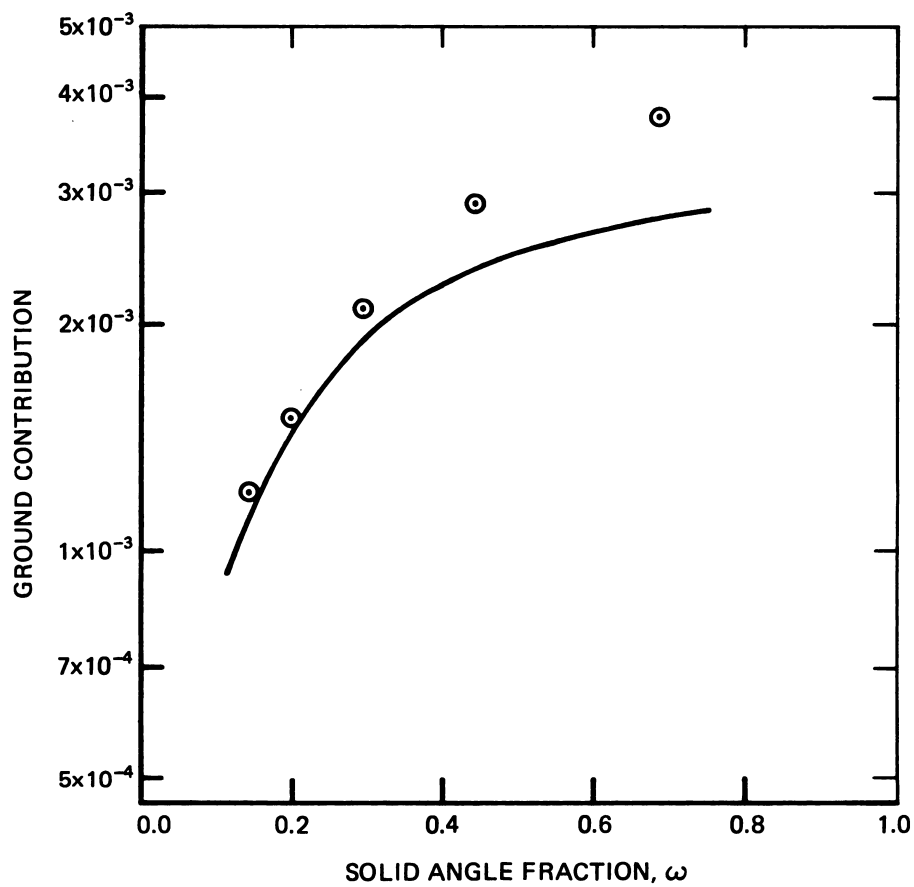
Values of the attenuation factor for the basement ceiling, as inferred by Kaplan [VI.57], are shown in figure X.22. These values were obtained by first



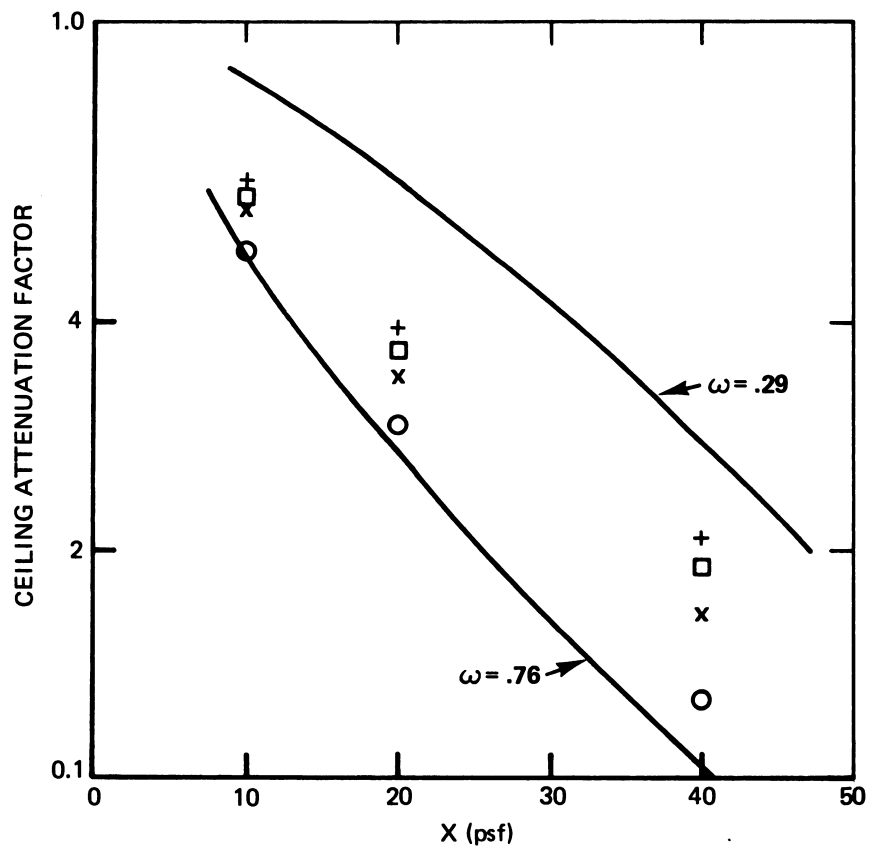
X.19 Comparison of experimental and calculated ground contributions as a function of solid angle fraction  $\omega$  subtended by the ceiling.  
 Experimental:  $\bigcirc$   $X_c = 46$  psf,  $\times$   $X_c = 67$  psf,  $\square$   $X_c = 87$  psf;  
 — Calculated, Standard Method adjusted for  $^{60}\text{Co}$ . Error bars indicate uncertainty in the value of  $\omega$  due to finite thickness of ceiling.



X.20 Comparison of experimental and calculated ceiling attenuation factors for 50 psf concrete ceiling in cylindrical structure.  $\bigcirc$  Experimental; — Calculated, Standard Method, adjusted for  $^{60}\text{Co}$ .



X.21 Comparison of experimental and calculated ground contributions for 50 psf concrete ceiling in cylindrical structure.  $\odot$  Experimental; — Calculated, Standard Method, adjusted for  $^{60}\text{Co}$ .

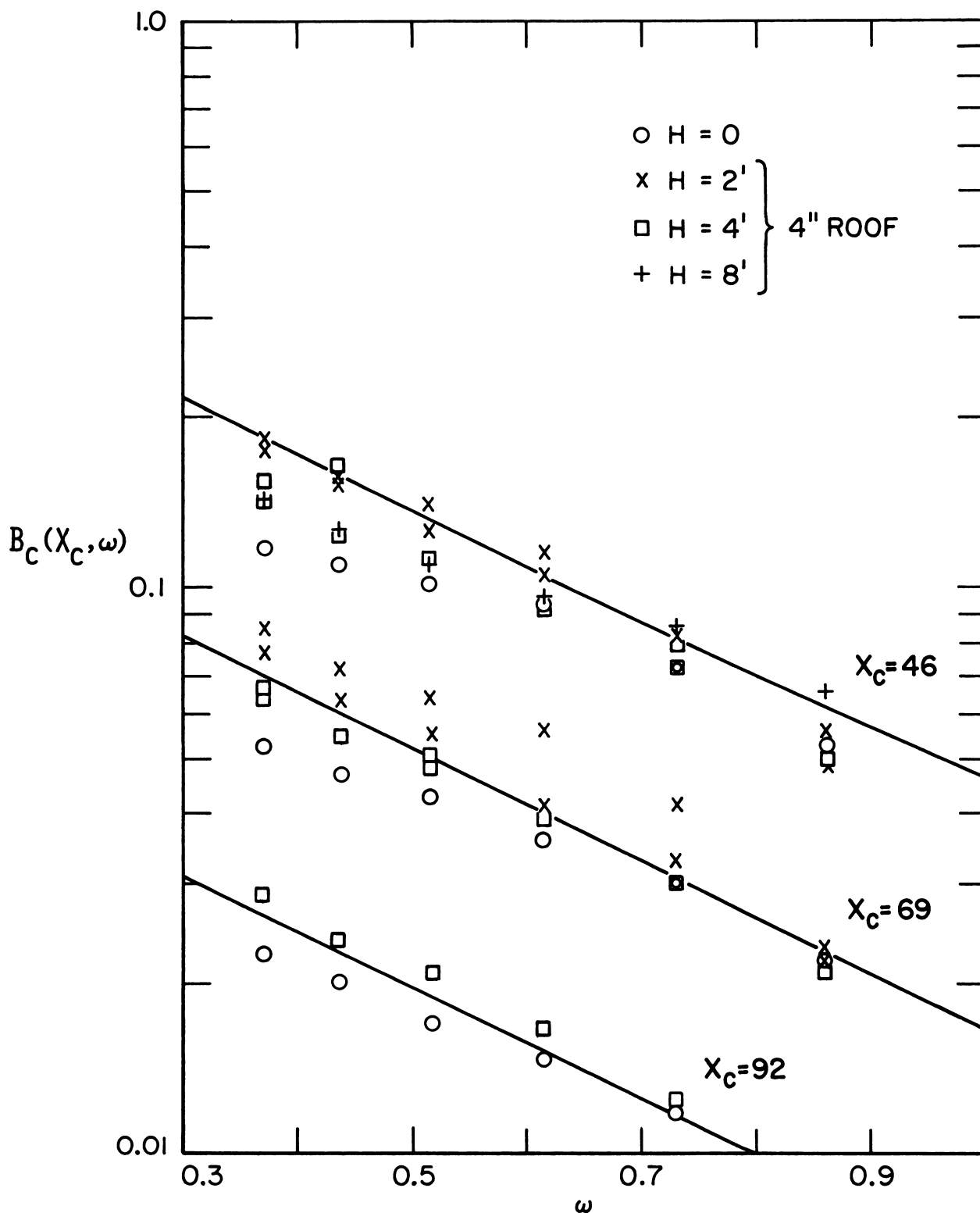


X.22 Comparison of experimental and calculated ceiling attenuation factors for steel cylinder. Experimental: +  $\omega = 0.29$ , □  $\omega = 0.40$ , x  $\omega = 0.55$ , ○  $\omega = 0.76$ ; — Calculated, Standard Method, adjusted for  $^{60}\text{Co}$ .

calculating a value of  $\alpha_s(h)$ , as defined in eq (VI.9), by averaging over source position for each detector position. As explained in section VI.C.1,  $\alpha_s(h)$  is very insensitive to the value of the source radius  $\rho$  and therefore deviations from the average value are small. Next, the attenuation for each of the three ceiling thicknesses shown in figure X.22 was obtained from the ratio of  $\alpha_s(h)$  for each thickness, to  $\alpha_s(h)$  for the open hole. The values in figure X.22 calculated from eq (X.3) show the same trend as those for the NEL experiment (fig. X.18): The agreement with experiment is good for large solid angle fractions but the calculated contributions are high for small solid angle fractions, as seen by the case  $\omega = 0.29$ .

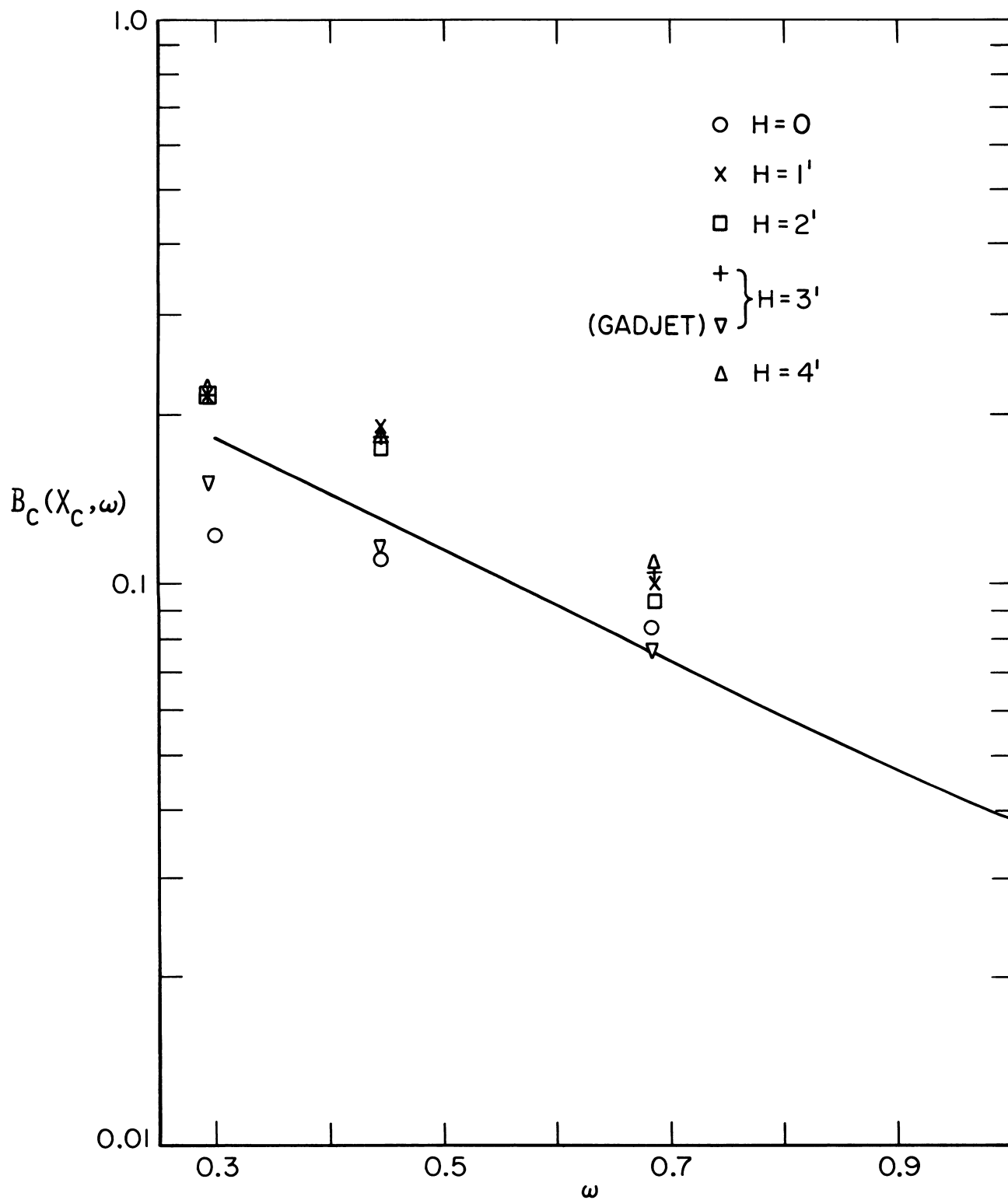
### 3. "In-and-Down" Attenuation

Schumchyk's experiments [VI.16] on skyshine were extended to true "in-and-down" experiments by erecting the blockhouse shown in figure VIII.27 over the existing basement. A comparison of the expression in eq (X.3) for  $^{60}\text{Co}$  and the NEL experimental data [22-24] is shown in figure X.23 for a covered hole ( $H = 0$ ) and three different wall heights. Figure X.24 shows data for small concrete cylinders [26] 6 ft in diameter, while figure X.25 shows results for smaller steel cylinders [25] 2 ft in diameter. Since the revision of the ceiling attenuation factor was based largely on NEL data, the comparison in figure X.23 should not be considered as an independent comparison, but rather as an indication of the goodness of fit of the empirical expression, in the least squares sense. The comparisons in figures X.24 and X.25, however, represent independent experimental tests of the corrected attenuation factor. These comparisons do not show as close agreement as one would hope. The discrepancies seem to indicate a dependence of attenuation factor on absolute size of the structure, or shape, or both.

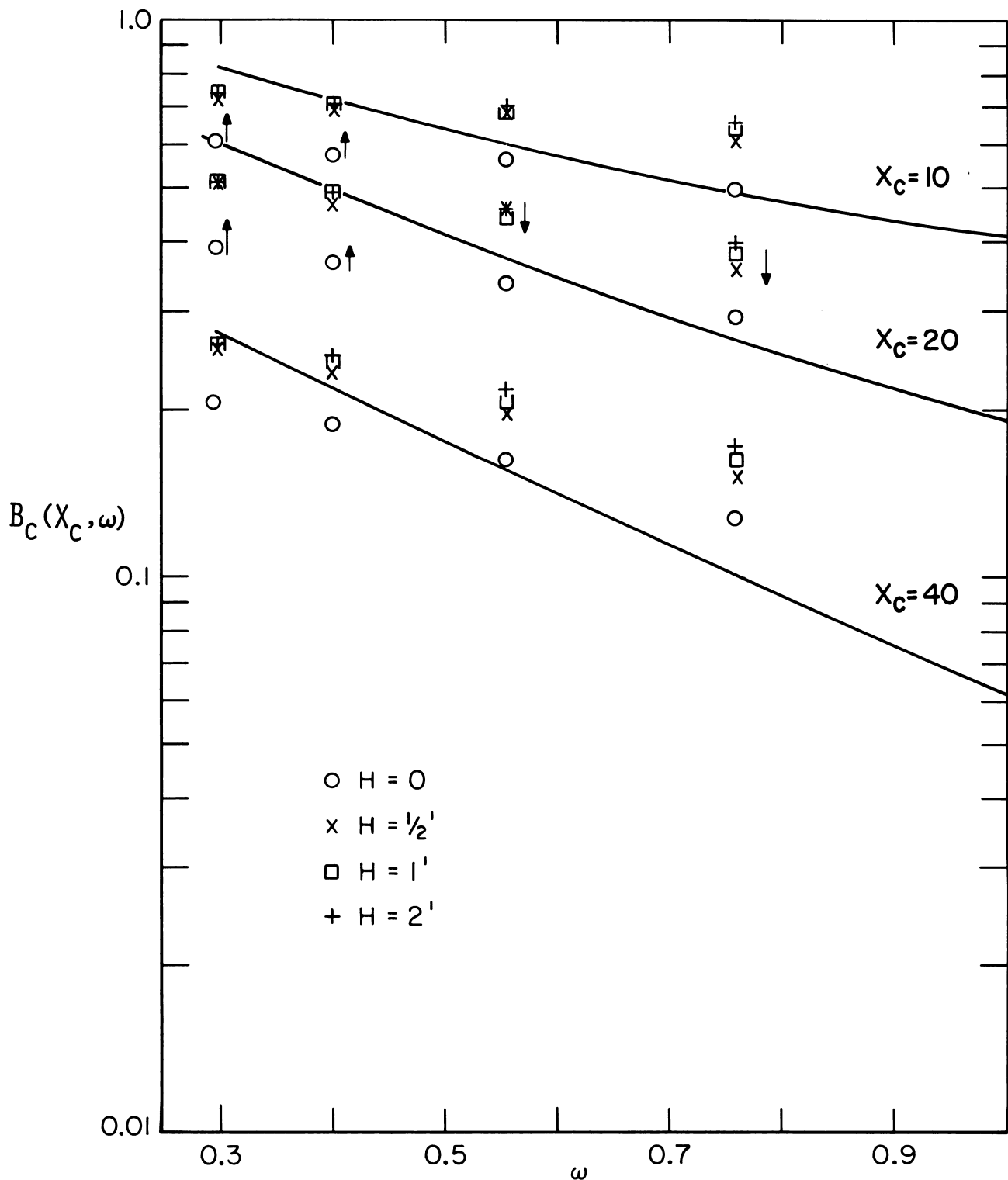


X.23 Comparison of experimental and calculated ceiling attenuation factors as a function of solid angle fraction  $\omega$  subtended by the ceiling, for different ceiling thickness  $X_C$  and first story wall heights  $H$ . Experimental: ○  $H = 0$ , ×  $H = 2$  ft, □  $H = 4$  ft, +  $H = 8$  ft; — Calculated: Standard Method.





X.24 Comparison of experimental and calculated ceiling attenuation factors as a function of solid angle fraction  $\omega$  subtended by the ceiling, for  $X_c = 50$  psf and first story wall heights  $H$ . Experimental: ○  $H = 0$ , ×  $H = 1$  ft, □  $H = 2$  ft, +  $H = 3$  ft, and △  $H = 4$  ft. — Calculated: Standard Method, ▽ GADJET Monte Carlo (Ref. [30]).



X.25 Comparison of experimental and calculated ceiling attenuation factors as a function of solid angle fraction  $\omega$  subtended by the ceiling, for different ceiling thicknesses  $X_C$  and first story wall heights  $H$ .  
 Experimental:  $\circ$   $H = 0$ ,  $\times$   $H = 1/2$  ft,  $\square$   $H = 1$  ft, and  $+$   $H = 2$  ft.  
 Calculated: — Standard Method.

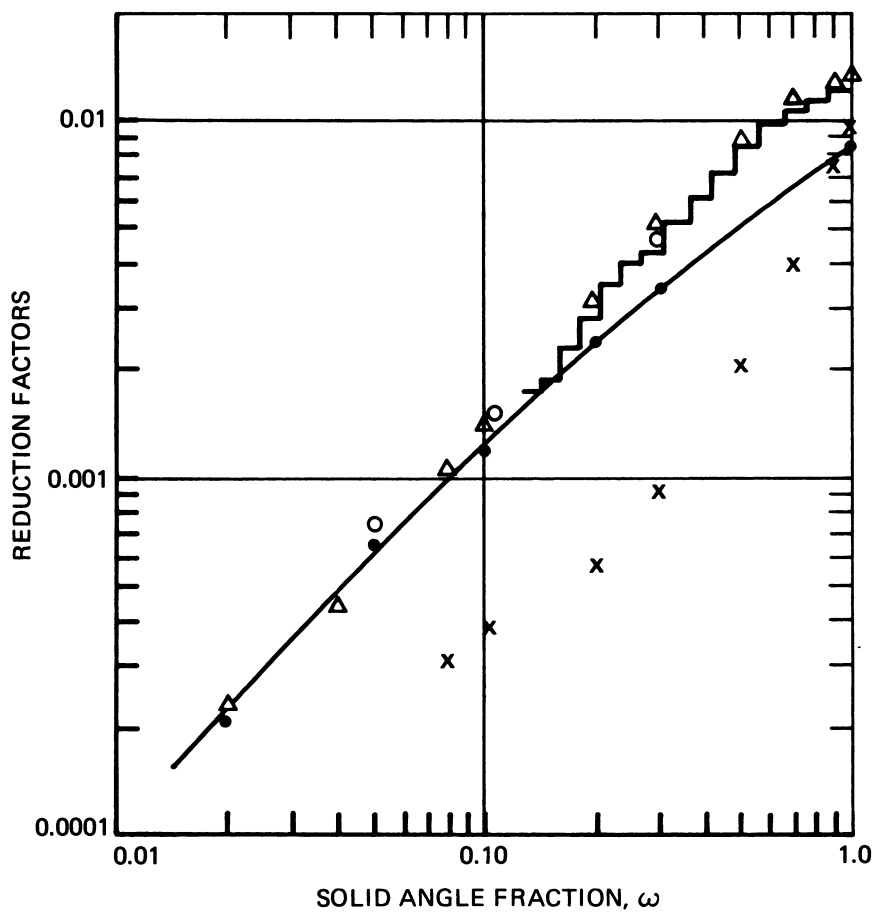
#### 4. Calculations of "In-and-Down" Attenuation


The "in-and-down" problem has also been calculated by several different investigators. In an early study, Raso and Woolf [27] used the Monte Carlo method to determine the dose behind vertical and horizontal slabs. They approximated the source by a fan of rays of uniform intensity in the horizontal plane incident on all parts of the exterior wall. The linear dimensions of both barriers were taken to be 225 x 225 cm.

They found that their calculations of radiation penetration through the wall from the simulated source agreed well with calculations shown in figure B.22a. However, when a horizontal barrier was added in their calculations, they found significant disagreement with calculations by the version of the Standard Method existing at that time. Typical results are shown in figure X.26. It can be seen from this figure that the Monte Carlo calculations predicted reduction factors which were higher by factors of 2 and 3 than those calculated by the early Standard Method. However, if the ceiling attenuation factor is calculated by the current Standard Method, using eq (X.3) for  $^{60}\text{Co}$  radiation, the solid line is obtained and the agreement is very good.

It should be noted that the Monte Carlo calculations show a monotonic increase of reduction factor with solid angle fraction. Part of the reason is that the Monte Carlo results shown in figure X.26 use an approximation of uniform intensity incident on the basement ceiling. This corresponds to assuming very high walls. Even for other Monte Carlo calculations, however, in which the wall height is equal to basement width, such a monotonic increase has been noted.

Trubey [28] used the Monte Carlo method to calculate the reduction factor for a concrete blockhouse 30 x 40 ft with a first-story height of 9 ft and a basement depth of 9 ft. The basement ceiling was assumed to be



X.26 Comparison of experimental and calculated reduction factors in a basement due to ground sources. Wall and ceiling thicknesses are 40 psf.  
 ○ Experimental; Δ Calculated Monte Carlo,  Calculated, Monte Carlo uniform distribution over ceiling, X Old Standard Method.  
 — Current Standard Method.

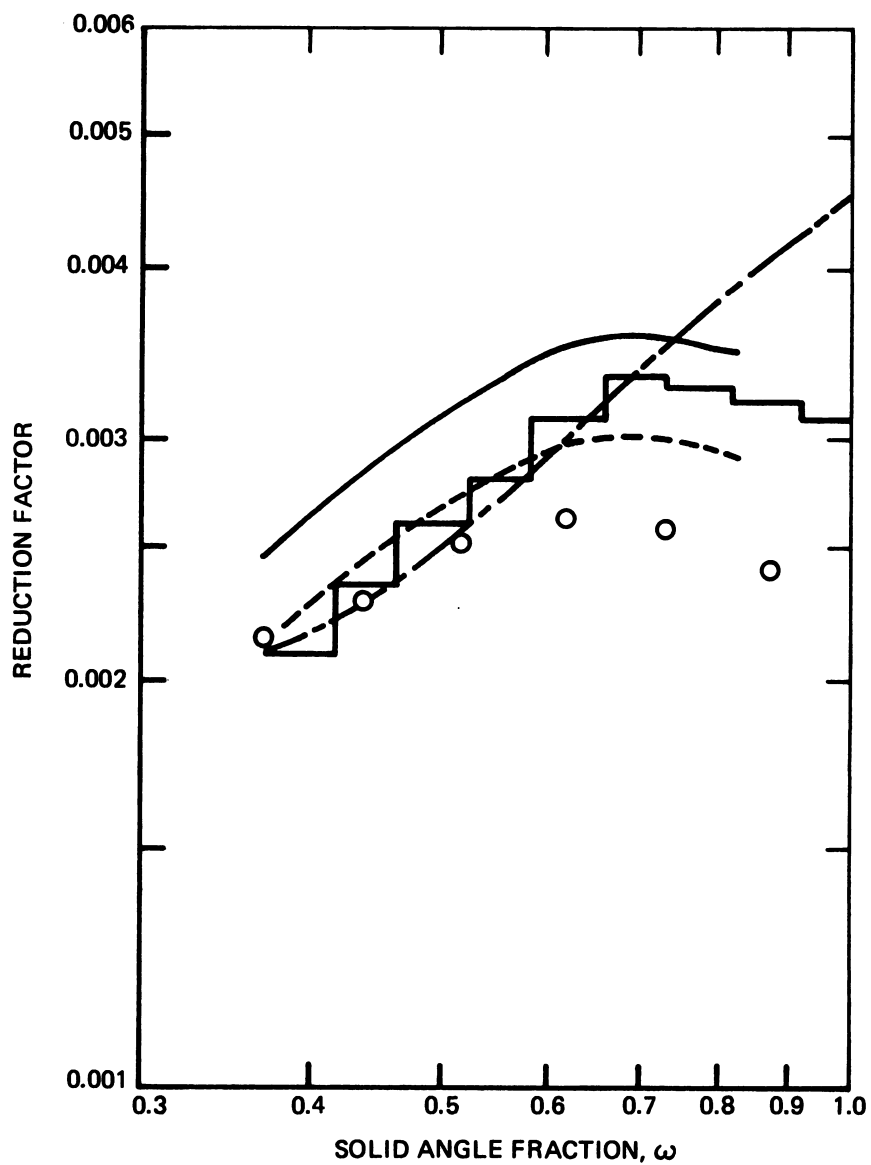
15 psf thick and the first-story walls were 30 psf. In this calculation the contributions to the exposure are sorted according to the barrier in which the last collision took place. For these barrier thicknesses, approximately equal contributions of 30% arose from last collisions in the first-story walls and last collision in the basement ceiling. About 20% came from last collisions in the walls and floor of the basement. Included in this category was radiation from close-in sources which penetrated through the basement wall. Trubey's value for the reduction factor at 3 ft height in the center of the basement was .016 as compared with a value of .010, obtained by using the early ceiling attenuation curve in the Standard Method. Use of the current curve in the Standard Method for ceiling attenuation yields a reduction factor of .019, in better agreement with Trubey's Monte Carlo calculation.


Hinkley [29] has made Monte Carlo calculations for cylindrical and rectangular structures. Like Raso and Woolf, he also assumed a simulated fan source of 1.25 MeV gamma rays. His calculations for a cylinder agree to within 20% with experimental results of Schmoke [24]. His calculations for rectangular structures of different eccentricities predict that the ceiling attenuation factor  $B_c$  decreases with increasing  $\omega$ , consistent with eq (X.3). For a fixed value of  $\omega$ , the basement ceiling for a square building is less effective than that for a long, narrow building in reducing the radiation intensity. Calculated attenuation factors for rectangular structures agree with Schmoke's experiment to within 15%. Attenuation factors generally agree to within 30% with those of the Standard Method for  $0.3 < \omega < 0.8$ .

Morris [30] also made Monte Carlo calculations of radiation penetration through vertical and horizontal slabs. His results include the effect on the exposure at a fixed detector location, due to radiation incident at various

points on the first-story wall. He found that for any given detector position, and no basement ceiling, the lowest part of the wall just above grade contributed most heavily to detector response. This is primarily because the distance to the detector is smallest for this part of the wall. However, when a basement ceiling is interposed between the detector and the wall, the lowest part of the wall contributes most heavily only for detector locations for which the line joining the wall section and the detector position forms a large angle with the normal to the wall. For detectors near the ceiling, the relative contribution from the lowest portion of the wall diminishes. The implication is that for wall heights small compared with the length or width of the basement ceiling, detectors near the center and near the ceiling may actually measure less exposure than detectors near the center but closer to the basement floor.

Morris tried to account for the effects of scattering in the air and ground outside of the blockhouse by considering a component of incident radiation having 0.3 MeV photon energy. The angular distribution was assumed to be the same as that for the primary source energy of 1.25 MeV. He referred to the source configuration in this calculation as the "dienergetic" source. In the second part of his report, Morris compared his Monte Carlo calculations using both monoenergetic and "dienergetic" sources, with those of Raso and Woolf [27], Trubey [28] and Hinkley [29]. A typical comparison is shown in figure X.27. In this figure the wall contribution is plotted against the solid angle fraction subtended by the basement ceiling. The Monte Carlo calculations and the experimental data of Schmoke show the same shape, with a tendency to a maximum in the reduction factor at  $\omega \approx 0.7$ . Calculations by the Standard Method, on the other hand, increase monotonically with solid angle fraction and lie higher than all the other data for  $\omega > 0.8$ . The occurrence



X.27 Comparison of experimental and calculated reduction factors in basement as a function of solid angle fraction subtended by the ceiling.  
 ○ Experimental; Calculated:  Monte Carlo, — Monoenergetic source, - - - Dienergetic source, — • — Old Standard Method.

of the maximum in the reduction factor seems to be associated with the combination of the relatively low wall height of 4 ft and the eccentric shape of the 20 ft x 10 ft blockhouse.

Finally, the adjoint Monte Carlo technique has also been used to study this problem. The adjoint approach and the resulting computer code GADJET have been discussed by Kalos [31]. Some results of calculations by the GADJET code are shown in figure X.24. The discrepancy between calculation and experimental data is not explained at present.

#### E. RESIDENTIAL AND COMMERCIAL STRUCTURES

Before the systematic experiments described in the preceding three sections were initiated there had been a period when attempts were made to determine reduction factors in large office-type buildings by experimental means. The effort was spearheaded mainly by the Civil Effects Test Operations (CETO) group of the Division of Biology and Medicine of the Atomic Energy Commission. This group intended to develop a mobile laboratory which could be brought to the site of a structure and which would contain the radioactive sources and detection equipment necessary to predict the fallout protection afforded by the structure. Because these experiments required source intensities of hundreds of curies, the number of locations for which such an operation could be carried out were limited.

The analysis of complex structures using the Standard Method is complicated by uncertainties in the mass thickness of the in-place walls and floors and by complicated internal structure. For this reason reports on experimental work on complex structures contain very little which can be used for comparisons with calculations by the Standard Method. The following discussions are an attempt to present the available comparisons between theory and experiment and to indicate the difficulties involved in such comparisons.

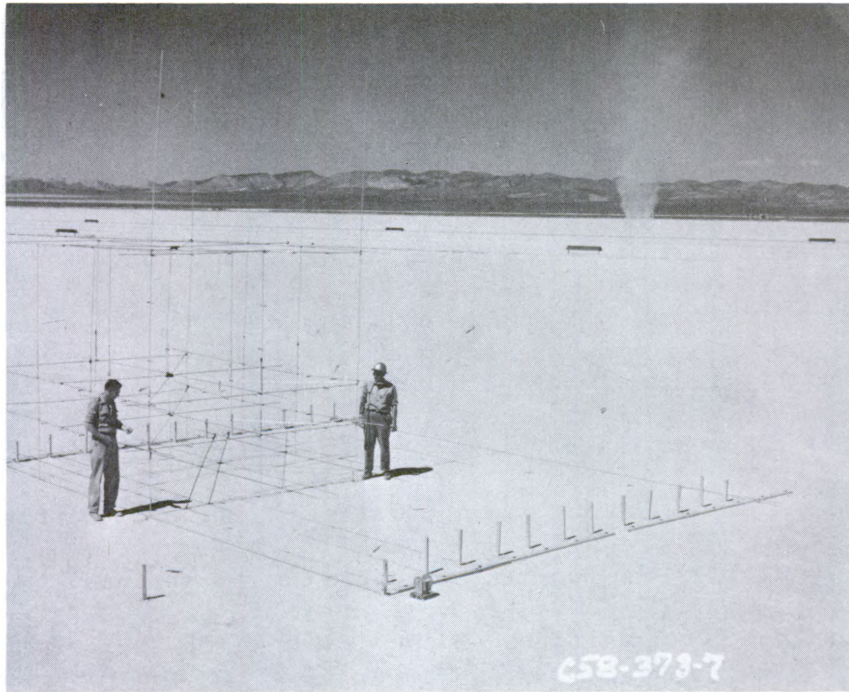


## 1. Residential Structures at Nevada Test Site

As mentioned in section I.B.3, the first attempt to measure the shielding properties of residential structures in the U.S. was carried out at the Nevada Test Site in May of 1958. Although some attempt was made in these experiments to conduct studies on simple configurations such as a source on a flat roof over a rectangular room, most of the data were taken on a few typical examples of U.S. residences. The experimental data were reported by Auxier et al [14], and a later analysis of the data was reported by Eisenhower [20].

In these experiments four hundred 4.15-millicuries sources of  $^{60}\text{Co}$  were placed at 2-foot intervals in plastic tubing of 0.13 inch inner diameter. Four lengths of tubing, each containing 100 sources, were wound on spools and cranked in and out of lead containers during irradiation. Most measurements were made with 200 mr Victoreen model-362 pocket ionization chambers.

In order to assure that the source and detector systems were working properly, the "phantom" structure shown in figure X.28 was set up to make measurements above the air-ground interface. It was also designed to measure exposure rates with no material between source and detector in order to evaluate the attenuation when barriers intervene between the source and detector. Assessing the protective properties of a structure by attenuation would be ideal for radiation such as low-energy X-rays, for which absorption is much more probable than scattering. In that case, radiation which is not absorbed travels in a straight line from source to detector. For gamma rays with energies of the order of 1 MeV or greater, however, scattering is much more important and the attenuation technique is not as useful. In addition, for radiation from ground sources, detector readings in a basement may be higher with than without the structure in place, because of scattering in the



X.28 Photograph of phantom structure at Nevada Test Site.



X.29 Photograph of two story wood frame house at Nevada Test Site.

walls. Therefore attenuation measurements using the phantom structure had very little influence on the subsequent development of data and procedures for calculations.

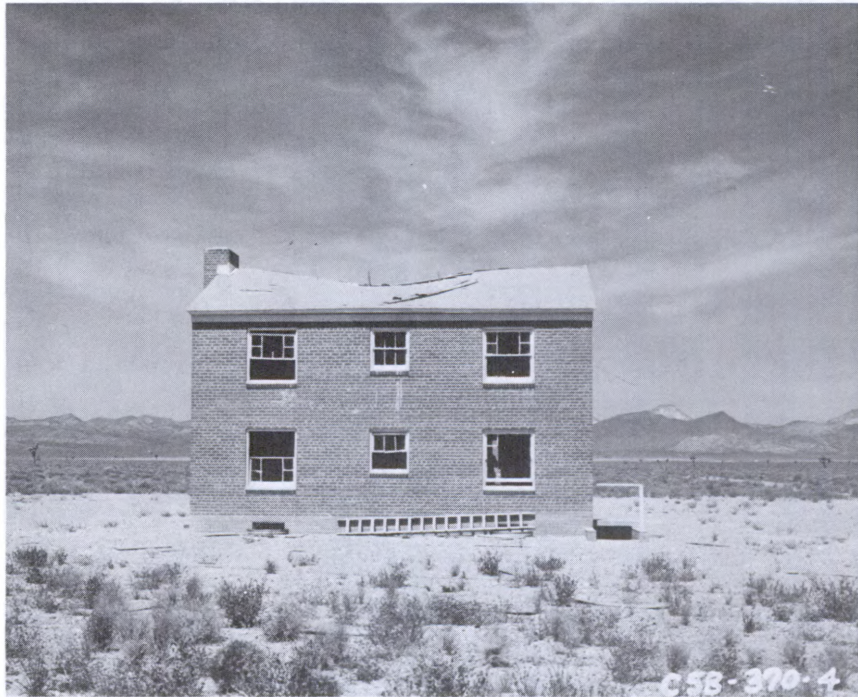
Many experiments in this series were performed on the two-story wood frame house shown in figure X.29. This building was about 25 ft by 33 ft and had a basement with 8-in reinforced concrete walls expending 5-3/4 inches above grade. The basement was atypical in that it contained a basement shelter consisting of three 8-in interior walls parallel to the short exterior walls, which effectively divided the basement into two half-basements.

The measured roof contributions at the center of the building and three feet above the floor were .076 for the second story, .034 for the first story and .015 at the center of either "half-basement." Exposure rates on the first and second story decreased by about a factor of two near the exterior walls, as expected from geometry factor consideration.

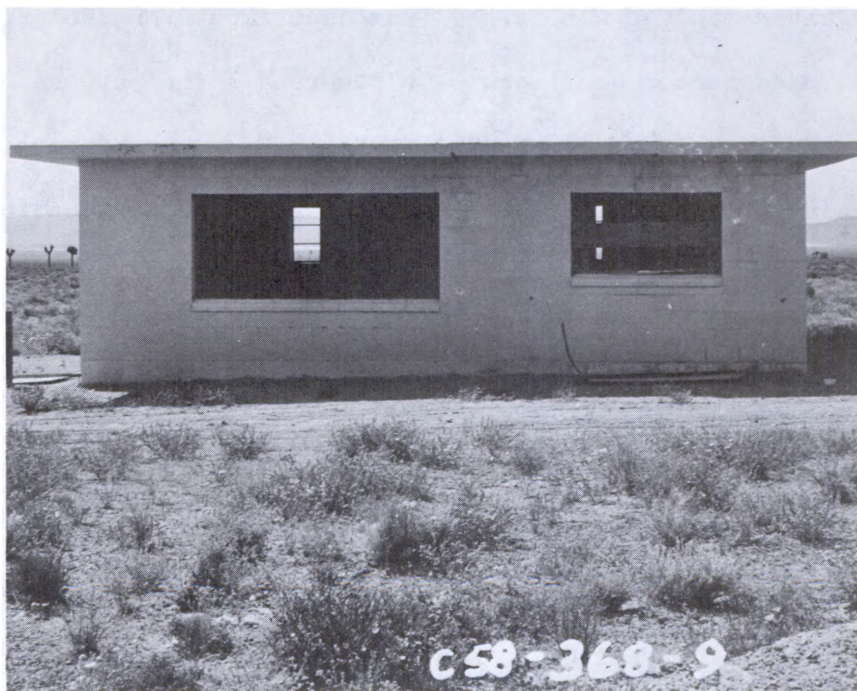
Ground contributions were about 0.5 in the center of both first and second stories and about 0.028 at the center of each half-basement. Exposure rates typically increased by a factor of two near the exterior walls of the building. This experiment showed that an infinite ground source contributed about 10 times more to the exposure on the first story of this typical residence than did the roof source. The exposure rates measured in the basement were lower than they would be in homes of similar construction because of the atypical interior concrete walls in the basement.

Measurements were also made on the two-story brick structure shown in figure X.30. Because of the unsafe condition of the roof, no measurements were made with roof sources. However, since the roof and floor structure was the same as in the two-story wood frame house, the roof contribution can be assumed to be similar. A contribution of 0.21 for ground sources was inferred





X.30 Photograph of two story brick house at Nevada Test Site.



X.31 Photograph of Precast Concrete House at Nevada Test Site.

from the experimental data for the center of the basement and 0.14 for the center of the first story. The brick walls provide a factor of 3 to 4 better protection from ground sources at above-grade locations than the wood walls of the other structure. The increased protection at below-grade locations is probably less than a factor of 2.

Another type of residential structure which was studied was the pre-cast concrete house shown in figure X.31. It was constructed from lightweight (110 pounds/ft<sup>3</sup>) concrete panels, 6 inches thick. The interior walls were constructed from the same type of panels. The house contained an interior hallway about 3 ft wide. Roof contributions at the interior end of the hallway were about .025, whereas in the larger rooms they were about .038. The protection from ground sources varied by more than a factor of 2 from the exterior to interior ends of the hallway, with a ground contribution of about .08 at the center.

Some valuable insight was gained from experiments on reciprocity, in which source and detector positions were reversed. The purpose of these experiments was to explore the possibility of making experiments in built-up areas by placing the source inside of the building and surrounding the building with an array of detectors. This would minimize exposure to people in the surrounding area. Although these experiments indicated that reversal of source and detector gave results which generally agreed to within 20%, the technique was not exploited in later experiments for fear that the discrepancies might vary substantially with structural details.

## 2. Boston Harbor Building

Clarke et al [32] reported on measurements on an army barracks located on Long Island in Boston Harbor. This structure was the first one on which the tube source was employed. It was of heavy brick construction, 3 stories

high, with no basement and a slate roof. Sources of  $^{60}\text{Co}$  radiation were placed on the roof and on the ground in semi-circular patterns out to a radius of 175 ft.

The report included a comparison of the experimental data with four calculational methods which were available at the time. Table X.7 shows the comparison. The British Home Office (BHO) Method, alluded to as the "points" method in section I.B.1., was based upon a simple geometric treatment of the structure and on attenuation results obtained from actual fallout. The Tech Ops method (TOI) was a method developed under an earlier contract with the U.S. civil defense agency. It involved some simplifications such as neglecting scattered radiation in above-grade walls and assuming an average energy of 0.7 MeV for fallout radiation. The ODM method, which was developed very early by Shapiro, has also been discussed in section I.B.1. The OCDM method was an early version of the Standard Method. Table X.7 shows that the experimental exposure rates from roof sources were significantly lower than any of the calculated exposure rates. The experimenters noted this discrepancy but felt that the calculations were probably more nearly correct than the experimental results. The experimental ground contribution showed reasonable agreement with all calculations except those of the British. The main value of this experiment was the accumulation of experience in the operation of the hydraulic tube source in preparations for later experiment to be described in the next section.

### 3. General Structures at Nevada Test Site

In the fall of 1958 another series of experiments was conducted at the Nevada Test Site by Clarke and his co-workers [32]. Measurements were repeated on the two-story wood-frame and brick houses. Reproducibility of results from the earlier experiments was generally good. For example, a reduction factor

TABLE X.7  
EXPERIMENTAL DATA, LONG ISLAND BARRACKS,  
COMPARED WITH VARIOUS PREDICTIONS

Floor	BHO	TOI	ODM	OCDM	Expt.
a. Roof Contribution (mR/hr)					
1	28	30	40	27	13
2	68	67	95	60	29
3	160	180	235	140	72
b. Ground Contribution (mR/hr)					
1	45	20	8	24	20
2	42	11	16	20*	17
3	36	8	18	14*	14
c. Total Protection Factors:					
1	14	20	21	20	30
2	9	13	9	13	22
3	5	5	4	7	11

\*Estimated Height Effect

of .025 at 3 ft above the basement floor in the wood-frame house was inferred for ground sources, as compared with the earlier value of .028 and, at the same position in the brick house, .016, as compared with the earlier value of .021. Their data indicated overall protection factors of 15-25 near the center of the basement in the 2-story wood frame house and 30-40 near the center of the basement in the two-story brick house.

In addition, they investigated the improved protection that could be obtained in basements. For example, improvement of 30% to 40% in protection from ground sources was achieved by movement to the side of the basement, a factor of 2 improvement by movement to the corner, a factor of 3 by moving under a wood debris shelter and a factor of 20 by moving into a concrete debris shelter. Fallout shelters with 8-in concrete walls and ceiling offered an improvement in basements of a factor of 10 to 20 in the wood frame house and a factor of 6 in the brick house. The difference in improvement is probably due to the difference in the relative contributions of roof and wall sources in the two houses. Although no exhaustive study of residential structures was made, these conclusions can probably be used as a rule of thumb to estimate protection in other light structures.

A concrete underground fallout shelter was tested in this series. It was 8 ft by 10 ft with a ceiling height of 6.5 ft and a cover of 2 ft 3 in of soil of density 112 pounds/ft<sup>3</sup>. Protection factors generally were about 10,000 except near the shelter hatch where the protection factor was reduced below 500. The value predicted from figure V.43 for 2 ft 3 in of soil (252 psf) plus 8-in of concrete (100 psf) is about 50,000; but this figure is based on a rough guess of the barrier thickness.

Measurements were also made on a large industrial-type building. It was a two-story heavy reinforced structure normally used as control center for



nuclear tests at the Nevada Test Site and known as the CP-1 building. It was about 150 ft long and 80 ft wide with concrete walls 8-in thick, concrete roof and floor 4-in thick, and no windows. Measurements were made with roof sources and semi-circular ground sources extending out to a radius of 102 ft from the long exterior wall of the building. Typical ground contributions varied from .03 near the outside door to .005 in the interior of the building. Roof contributions on the second story varied generally from .004 to .008. Later measurements on this structure are described in the next section.

#### 4. Other Structures at Nevada Test Site

In the summer of 1968 Z. Burson [33] and his co-workers carried out a series of measurements on structures at the Nevada Test Site. Unfortunately, no attempt was made to compare results with calculations. However, we include them here because they represent an important body of experimental data. These experiments used sources of 10, 100 and 600 Ci of  $^{60}\text{Co}$  radiation pumped through plastic tubing. Pocket ionization chambers and thermoluminescent dosimeters were used as detectors. In addition some experiments were made with  $^{137}\text{Cs}$  sources and some attempts were made to study the effect of interchanging source and detectors. The structures were generally large buildings with concrete roof and walls and a complicated interior compartmentation into laboratories or offices. In order to give some idea of the complications involved in calculating protection factors for these complex structures, we will include in the following discussion some results of hand calculations using the Standard Method.

##### a. CP-40 Building, Communications Building

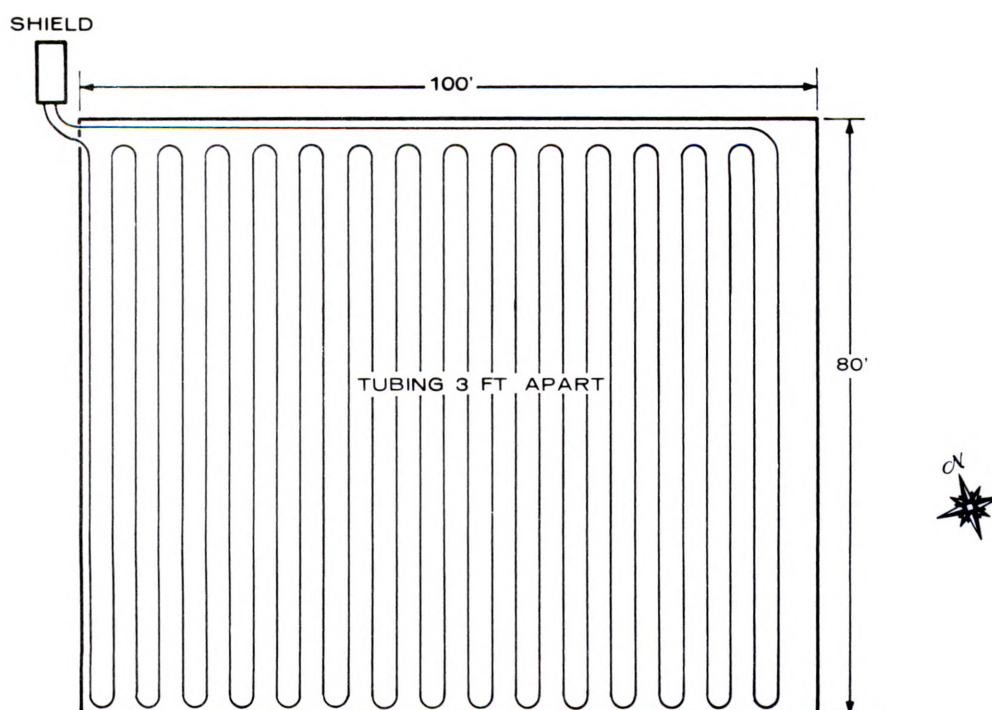
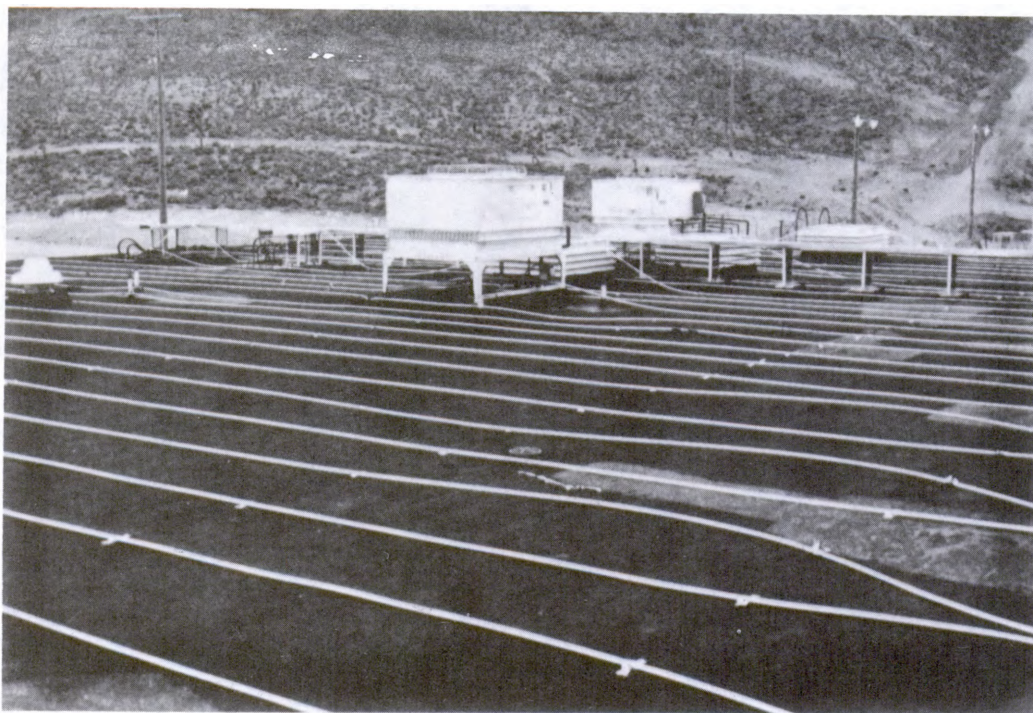
The communications building is a rectangular, one-story structure measuring 80 by 100 ft. It has a 4-in concrete roof and 8-in concrete walls. For this building, sources were placed only on the roof. A photograph of the

tubing on the roof is shown in figure X.32a and a drawing of the tube layout is shown in figure X.32b. A schematic view of the structure, showing protection factor values and PF contours is shown in figure X.33. The protection factor values shown in this figure include the effect of sources on both the roof and the ground. The exposure from roof sources was measured experimentally; the exposure from ground sources was estimated by the Standard Method and by comparison with results for other structures. Figure X.33 indicates that the protection factor is about 20 in most of the building. About half of the exposure is due to sources on the roof, except near apertures, where the ground contribution predominates.

Since experiments were performed only on the roof of this structure, we are limited to a comparison of roof contributions. Table X.8 shows this comparison. The experimental roof contribution generally lie between .02 and .03, independent of room size. This seems to indicate that the interior partitions have very little effect in attenuating radiation from distant parts of the roof. The calculations were made assuming a roof thickness of 59 psf and an average distance of 14 ft from detector to roof. Interior walls were assigned infinite thickness. If the walls are assumed to be of negligible thickness the calculated contribution is .047. Thus, the calculated results can vary by as much as a factor of 3, depending on the effective thickness assumed for the interior partitions.

#### b. CP-45 Building, Light Laboratory

This is a two-story laboratory structure measuring 80 by 120 ft. Grade level is at first floor level for the most part on three sides of the building and at first-story ceiling level on the fourth side. The thickness of the concrete walls of the lower story is 10 in and that of the upper story 8 in;



X.32 (a) Photograph of tubing layout on roof of CP-40 building at Nevada Test Site. (b) Schematic of tubing layout.

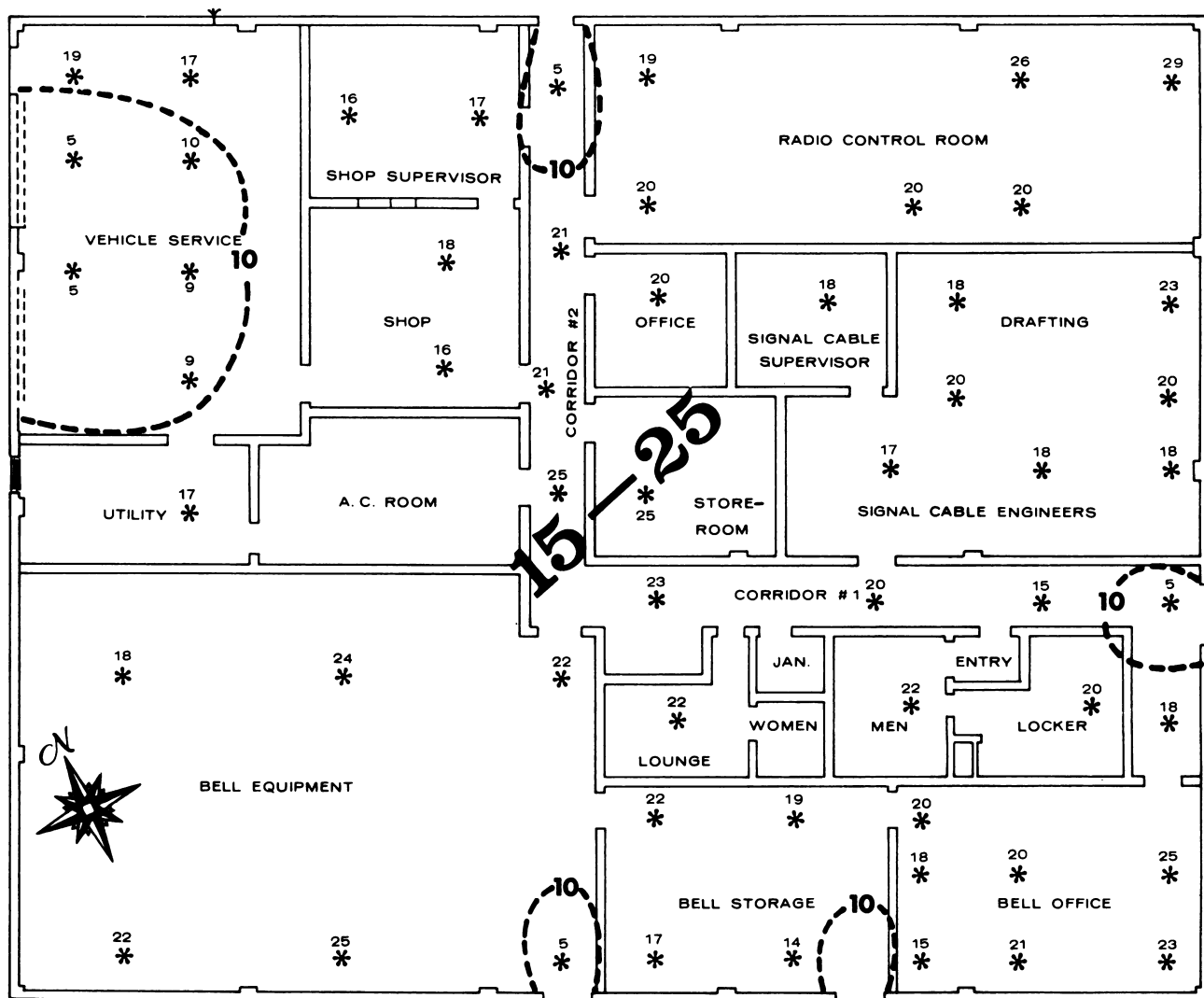


Fig. 3.2—Protection-factor values and PF contours for  $^{60}\text{Co}$  (CP-40).

X.33 Plan view of CP-40 building showing protection factors at various points and some approximate contours of constant protection factor near doorways.

TABLE X.8

COMPARISON OF CALCULATED AND EXPERIMENTAL ROOF CONTRIBUTIONS  
IN THE CP-40 BUILDING

Room	Exper.	Cr	Calc.
Shop	.031		.020
	.030		.020
Storeroom	.027		.016
Vehicle Service	.026		.035

the thickness of the concrete floors and roof is 7 1/2 in. Interior partitions, except for the stairwell are of light weight material. The source tubing on the roof can be seen in figure X.34a.

Table X.9 shows a comparison between experimental and calculated roof contributions on both the upper and lower story. This comparison is generally similar to that shown in Table X.8. For example, the experimental data are fairly insensitive to room size. Also, results calculated by assuming thick interior walls tend to predict lower contributions than those given by experiment. Calculated values for zero-thickness interior walls on the first and second story are  $8.2 \times 10^{-4}$  and .012, respectively. These values are in better agreement with experiment than those for which the thick-wall assumption was made. The effective thickness of the lightweight interior partitions is unknown.

Experiments were also performed with sources placed on the ground surrounding 3 sides of the building, as shown in figure X.34b. The sources extended out to a distance of 60 feet from each of the three walls. A comparison of experimental and calculated ground contributions for the first and second story is shown in Table X.10.

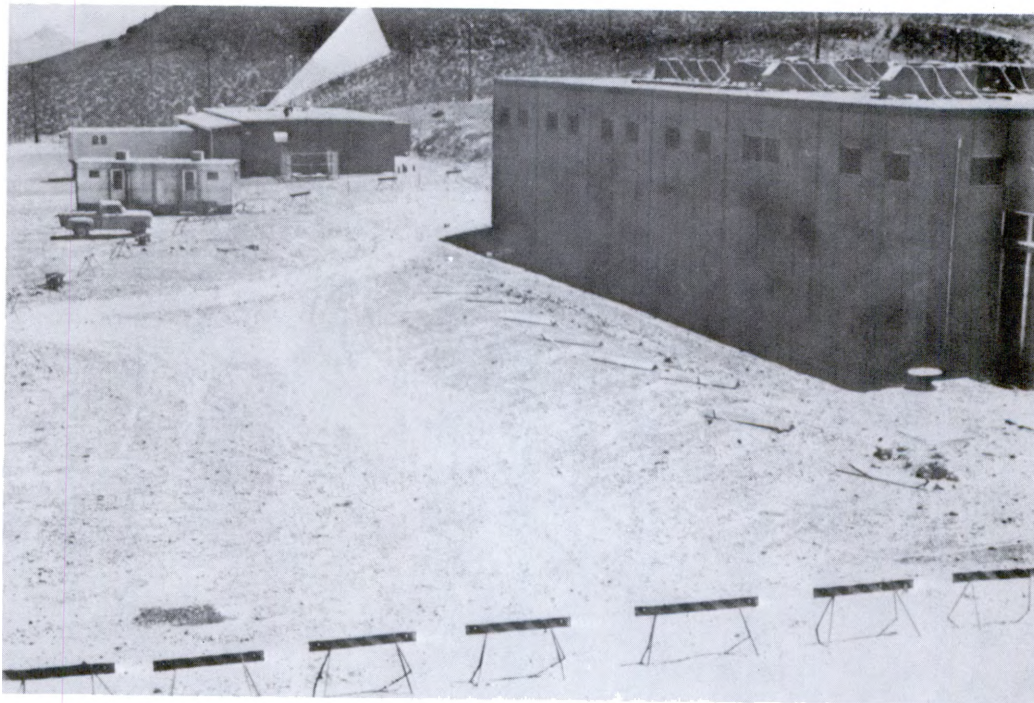
The calculated contributions for the upper story are about a factor of 10 higher than the experimental values. This is partly related to the effect observed in section X.B.2, whereby the Standard Method overestimates the geometry factor for scattered radiation from a limited source. But the experimental exposures are also lowered by attenuation in several interior partitions. The average experimental ground contribution of .004 for detectors near the East wall is more in line with the calculated value of .0075, probably because no partitions intervene between detectors and the East wall.

TABLE X.9

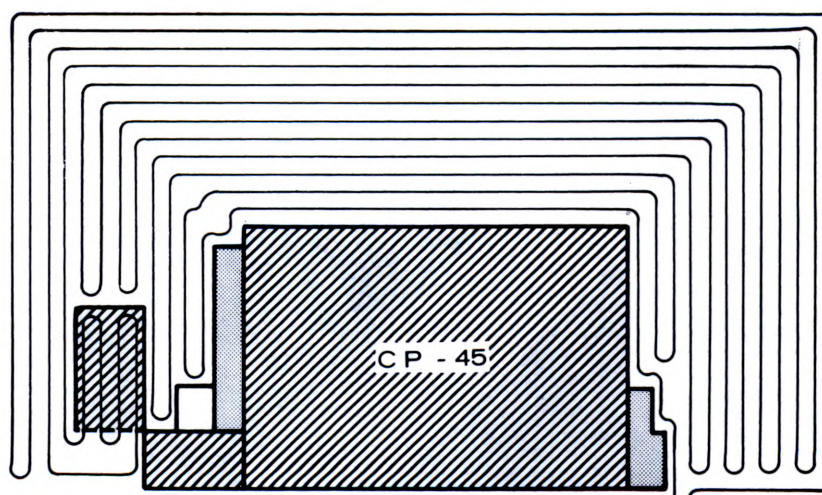
COMPARISON OF EXPERIMENTAL AND CALCULATED ROOF CONTRIBUTIONS  
IN THE CP-45 BUILDING

Upper Level		
Room	Exper.	Calc.
"Sec"	.0126	.012
	.0106	"
	.0125	"
Corridor	.0120	.0063
	.0117	"
	.0117	"
	.0093	"
Lower Level		
Room	Exper.	Calc.
Secretary	$7.0 \times 10^{-4}$	$3.9 \times 10^{-4}$
	$6.6 \times 10^{-4}$	"
	$6.6 \times 10^{-4}$	"
Corridor	$5.5 \times 10^{-4}$	$2.9 \times 10^{-4}$
	$6.5 \times 10^{-4}$	"
	5.2	"
	4.8	"





X.34a Photograph of CP-45 building showing tubing distribution.



X.34b Schematic showing the tubing distribution plan.



TABLE X.10  
COMPARISON OF EXPERIMENTAL AND CALCULATED REDUCTION FACTORS  
FOR GROUND SOURCES AROUND THE CP-45 BUILDING

Room	Upper Level	
	Exper.	Calc.
Corridor	.00035	.0033
	.00033	"
	.00043	"
"Sec"	.00045	"
	.00040	"
East Rooms	.004	.0075

Room	Lower Level	
	Exper.	Calc.
Corridor	.0017	.0025
	.0013	"
Secretary	.0009	"
	.0011	"
	.0008	"
	.0004	"

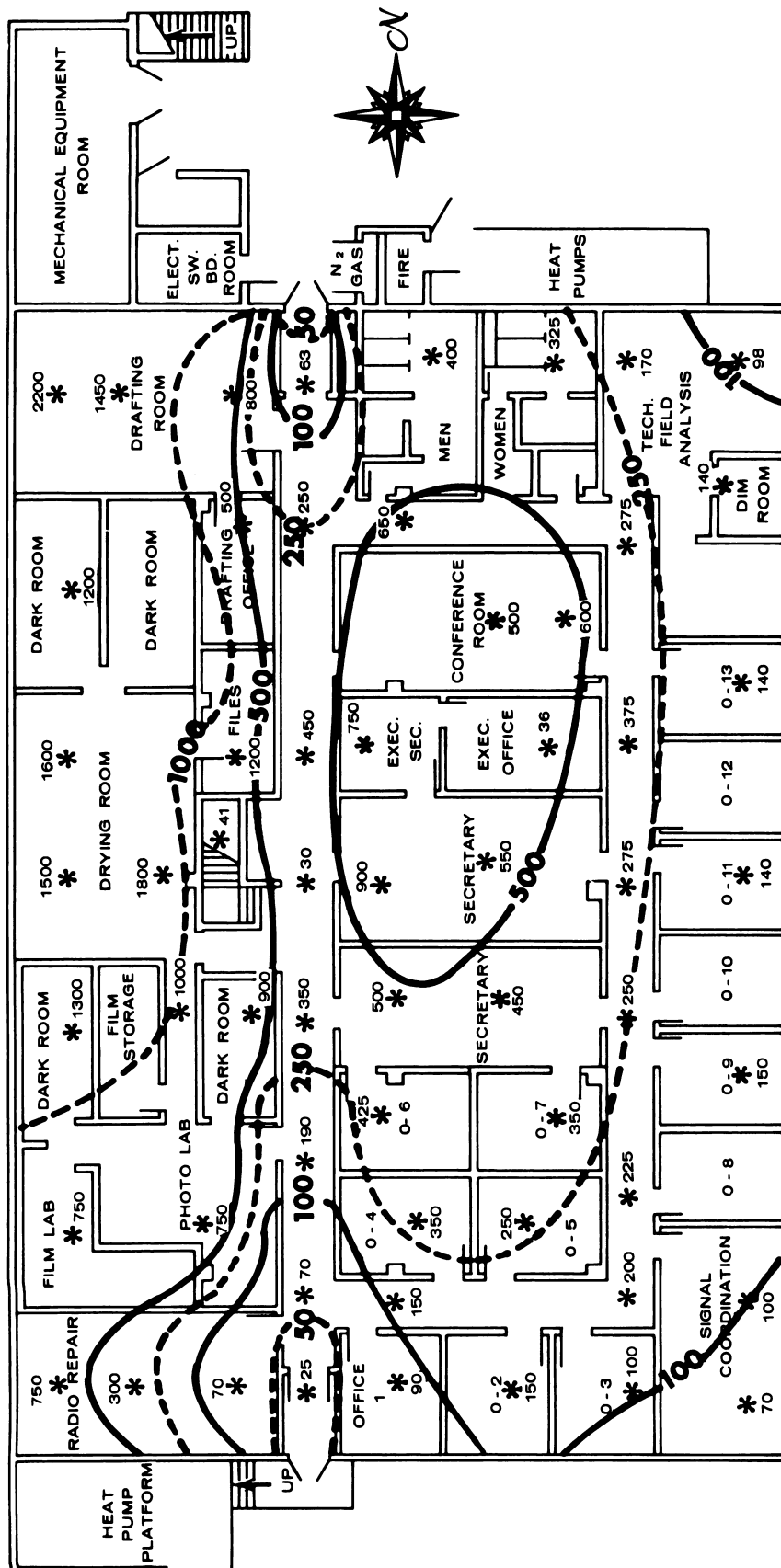
The calculated contributions for the lower story are in better agreement with experiment. For the lower story the Standard Method indicates that the uncollided component predominates. Any error in the wall-scattered factor is therefore less important. The disagreement between calculation and experiment for the lower level can be attributed largely to neglect of attenuation in the interior partitions. If the effective interior partition thickness were assumed to be 30 psf, the calculated contribution would be reduced to .0012, in reasonably good agreement with the sample of experimental results.

In this type of structure, doorways and apertures represent weak spots in the shield. This is obvious from figure X.35 which shows the protection factor estimated by the authors of reference [33] for all sources. These numbers include an estimate of the effect of sources beyond the limited strips measured in their study. On the lower story the ground sources produce between 1/2 and 2/3 of the exposure. From figure X.35 it can be seen that the protection factor is generally greatest at the center and near the west wall, which lies below grade. The poorest protection exists near doorways in the exterior wall.

The variation of reduction factor with distance from a doorway can be estimated roughly from

$$R_f \simeq \frac{A}{4\pi r^2} \quad (\text{near doorways}) \quad (X.5)$$

where  $A$  is the area of the doorway and  $r$  is the distance of the detector from the center of the doorway. This inverse square law means that one is approximating  $G_d(\omega)$  and  $G_a(\omega)$  by  $(1-\omega)/2$ . Table X.11 shows a comparison between experimental ground contributions and values calculated from the above approximate formula. These results show that eq (X.5) can be used to estimate



X.35 Plan view of CP-45 building showing protection factors at various points and approximate contours of constant protection factor.

TABLE X.11  
COMPARISON OF EXPERIMENTAL REDUCTION FACTORS WITH REDUCTION  
FACTORS CALCULATED FROM  $R_f = A/4\pi r^2$

Room	r(ft)	Exper.	Calc.
Corridor (South)	7	.029	.056
	17	.010	.0095
	31	.0033	.0029
	46	.0017	.0013
Corridor (North)	9	.011	.034
	22	.0026	.0057
	48	.0012	.0012
	61	.0013	.00075

the effects of doorways to within a factor of 2. The comparison is significantly better if one adds to doorway results based on eq (X.5), the "background" due to ground contribution through the walls.

c. CP-1, Main Control Building

This building, already mentioned in section X.E.3, is a complex structure with smaller buildings adjacent to it. The building is subdivided into many rooms by light interior partitions. A view of the structure from the north side is shown in figure X.36. The smaller of the two adjacent structures can be seen to the left of the main building. A plan view of the layout of the ground sources is shown in figure X.37.

Table X.12 shows a comparison of experimental and calculated reduction factors due to roof sources. The calculation for  $X'_1 = \infty$  was made for a room 15 ft x 12 ft, a room size typical of this building. The calculation for the other extreme, namely,  $X'_1 = 0$  was made for a room equal to the size of the entire building. As expected, the experimental values fall between the two extremes, indicating that the interior partitions attenuate but do not exclude radiation from sources not directly over the room of interest.

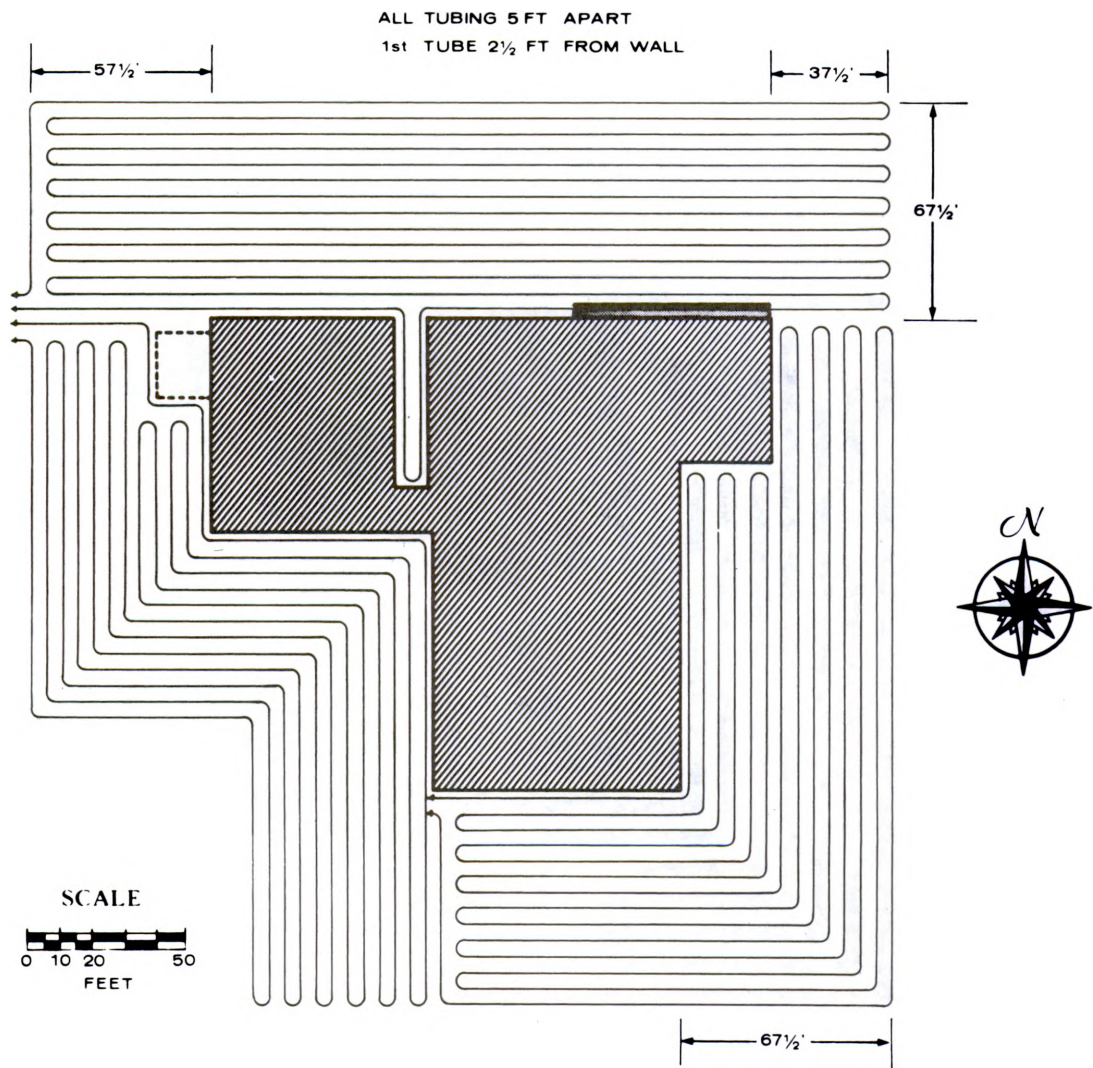
d. CP-2, Rad-Safe Building

This building, like those discussed earlier, is a complex structure with many light-weight interior partitions. It is 118 ft x 72 ft with a 4-in concrete roof and 8-in concrete walls.

A comparison of experimental and calculated roof contributions is shown in Table X.13. The rooms referred to are the four small rooms near the center of the building, shown in figure X.38. The contributions calculated for very thick interior walls were based on an assumed room size of 12 ft x 15 ft. Again, three of the experimental values lie between the values calculated with extreme assumptions about interior wall thickness, indicating radiation



X.36 Photograph of CP-1 building showing tubing distribution on the north side.



X.37 Schematic of tubing layout around CP-1, CP-1A, and CP-1B buildings

TABLE X.12

COMPARISON OF EXPERIMENTAL AND CALCULATED REDUCTION FACTOR  
FOR ROOF SOURCES ON THE CP-1 BUILDING

## MAIN STORY

Room	Exper.	Calc. ( $X_1 = 0$ )	Calc. ( $X_1 = \infty$ )
Corridor Intersection	.023	.058	.0094
Building	.027	"	"
Center	.032	"	"

## BASEMENT

E-W Corridor	.0024	.0136	.0015
N end of Boiler Room	.0022	"	"
N end of Mech. Equip. Room	.0021	"	"

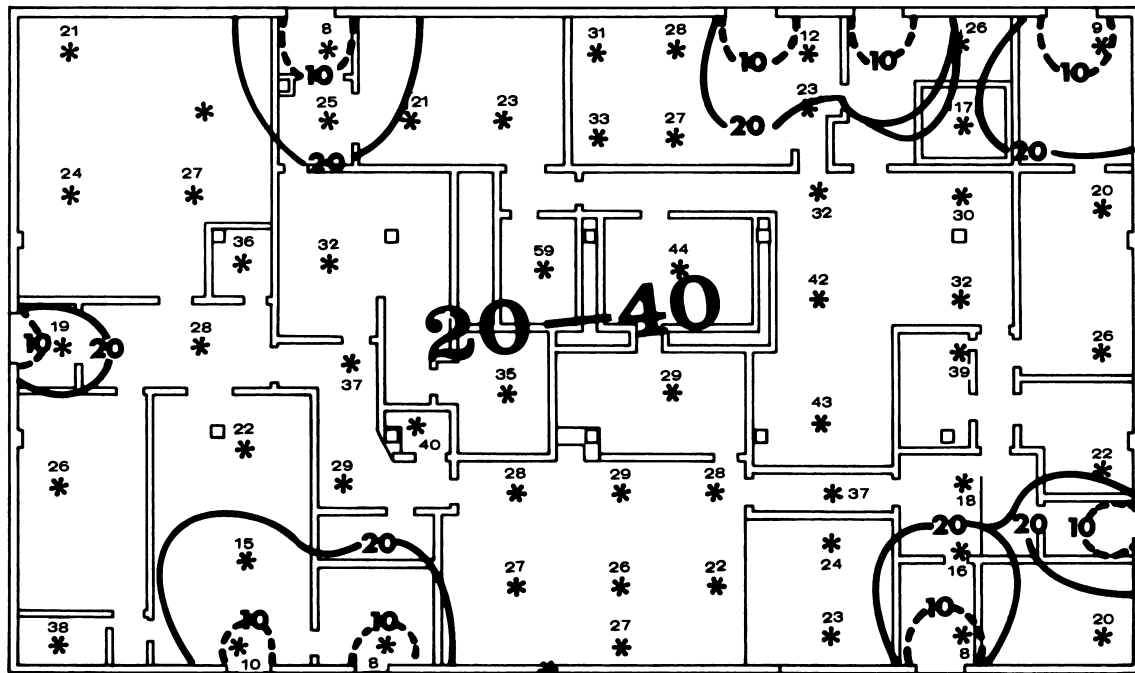


TABLE X.13

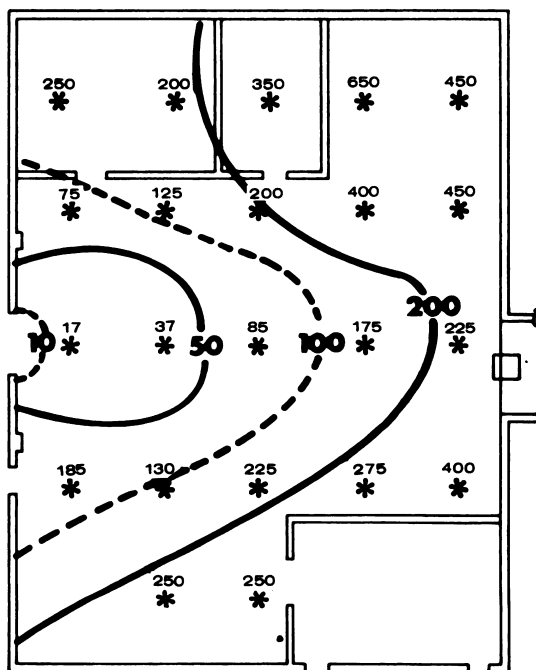
COMPARISON OF EXPERIMENTAL AND CALCULATED REDUCTION FACTORS  
IN THE CP-2 RAD-SAFE BUILDING

Roof Sources			
Room	Exper.	Calc. ( $X_i = 0$ )	Calc. ( $X_i = 0$ )
Center upper right	.0178	.059	.017
lower right	.0205	"	"
lower left	.0199	"	"
upper left	.0125	"	"

Ground Sources		
Room	Exper.	Calc.
S-W Corner of Main Story	.0001	.003



MAIN FLOOR



BASEMENT



X.38. Plan view of CP2 building showing protection factors at various locations and approximate contours of constant PF's near doorways.

attenuation but not effective exclusion by the walls. For this structure, the calculation for very thick walls seems to be closer to the experimental values. On the other hand, there does not seem to be any correlation between protection factor and size of room. Therefore the better agreement is probably fortuitous and influenced by such factors as uncertainty in the mass thickness of the roof.

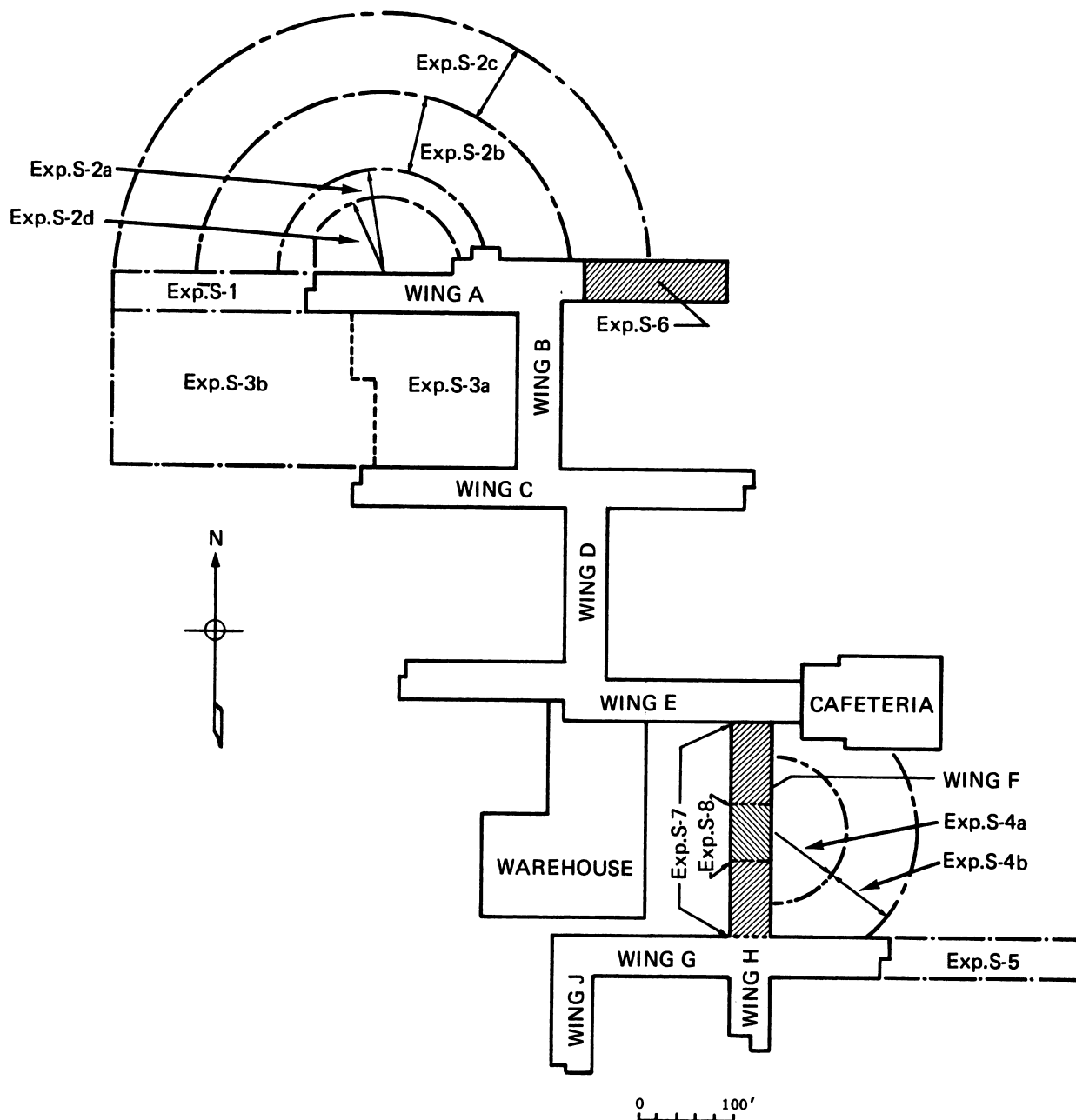
Also shown in Table X.13 is a comparison of experimental and calculated contributions from ground sources placed on the north and east sides of the building. The calculated value, which includes no correction for attenuation in the interior partitions, is much higher than the experimental value. The assumption of 10 interior partitions averaging 5 psf each gives a "minimum" correction factor of 3. However, detailed and reliable procedures for estimating the effect of many, thin interior partitions do not exist.

#### 5. AEC Headquarters Building, Germantown, Maryland

The first large public structure examined with high intensity sources was the AEC Headquarters Building in Germantown, Maryland [34]. A plan view of this structure, which is now used by the Energy Research and Development Administration, is shown in figure X.39. It is a large 4-story structure composed of a series of intersecting wings. The areas over which sources were distributed are denoted in the figure by "Exp.S" numbers. Experiments with roof sources were limited to wing A east and wing F, while wings A west and wing F contained most of the detector locations for sources distributed on the ground.

##### a. Roof Sources

Table X.14 shows a comparison of roof contributions calculated by the Standard Method, assuming 15-psf interior partitions, with those deduced from experiments on this building [34]. Details of these two sections of the



X.39 Plan view of AEC Headquarters building, Germantown, Maryland, showing experimental source configurations around wings A and F.

TABLE X.14

## COMPARISON OF ROOF CONTRIBUTIONS IN AEC HEADQUARTERS BUILDING

Wing <sup>*</sup>	Story	C <sub>r</sub> (Calc.)	C <sub>r</sub> Calc. Min	C <sub>r</sub> (Exper.)
A, East	4	.025	.013	.0125
	3	.00059	.00025	.000205
F	4	.0064	.0036	.0015
	3	.00016	.00007	.00012

\*Details of these two sections of the building are shown in Figs. X.39 and X.40.

TABLE X.15

ESTIMATED MASS THICKNESSES (psf) OF ROOF, FLOORS, AND WALLS  
IN AEC HEADQUARTERS BUILDING

Wing	Roof	Fourth Floor	Corridor Wall	Cross Partitions
A, East	70	130	15	0
F	120	130	15	0

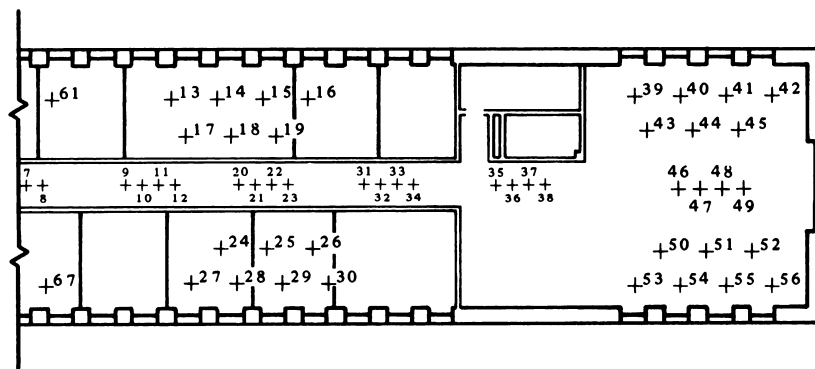
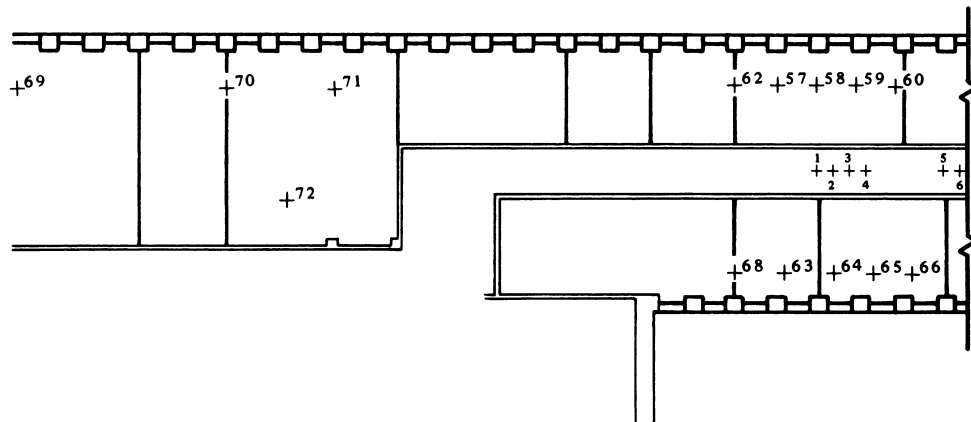
building are shown in figures X.40 and X.41. Since the experiments were performed with  $^{60}\text{Co}$  sources the calculated values in these comparisons are based on data for  $^{60}\text{Co}$  radiation. The estimated values for the mass thickness of the various floors and walls are shown in Table X.15.

The comparison shows that the calculated contributions are generally higher than experimental values and therefore conservative. However, if a calculation is made only for the portion of the roof over the central corridor, an estimated lower bound for the roof contribution is obtained. Such an estimate is based on the assumption that the corridor walls and cross-partitions eliminate the contribution from that portion of the roof not directly above the corridor. Table X.14 shows that the measured contribution is about equal to or even less than the calculated estimate of a lower bound. We do not know why the experimental value is so very low on the fourth floor of wing F.

The general conclusion to be drawn from Table X.14 is that the Standard Method predicts contributions which are up to a factor of 4 higher than those experimentally observed when interior partitions are assumed to be 15 psf in thickness. The experimental values agree better with a calculation which considers only the contribution from the roof immediately above the corridor, i.e., very thick interior partitions. It must be kept in mind, however, that the calculations are sensitive to values assumed for all mass thicknesses, and that the values shown in Table X.15 represent only best estimates of the actual mass thicknesses.

#### b. Ground Sources

Batter et al [34] did not do any calculations by the Standard Method to compare with the experimental measurements of the contribution from ground sources. However, we have made calculations by the Standard Method and the

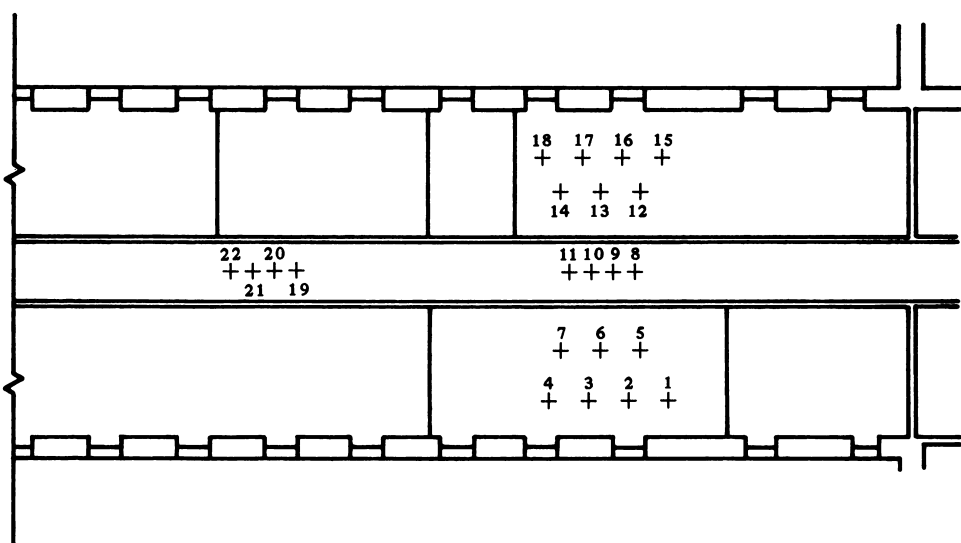
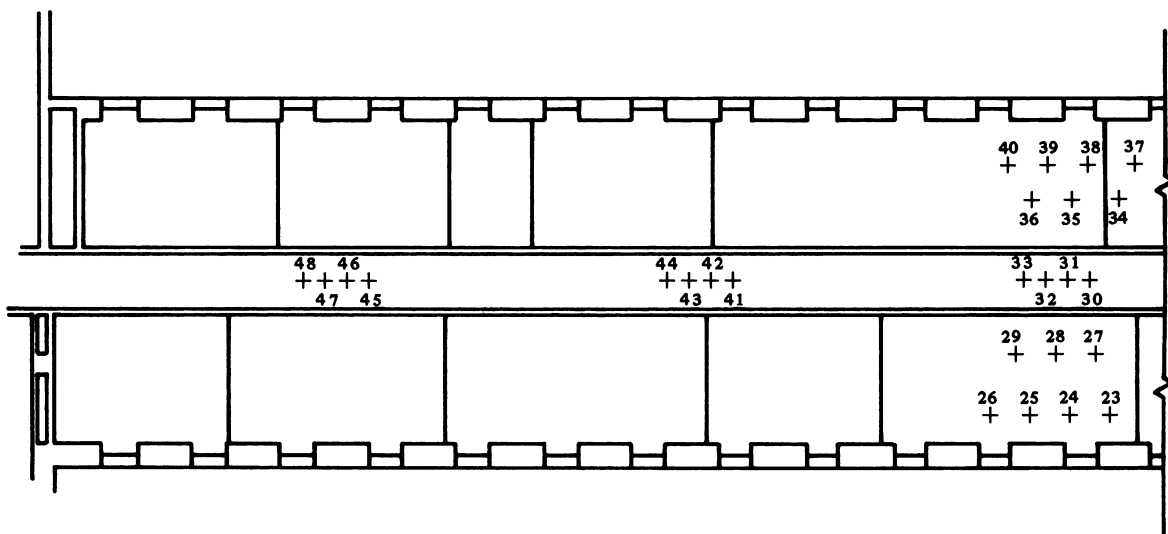


WING A EAST

2 6 10  
0 1 4 8 FEET

SCALE

X.40 Plan view of A wing East of AEC building showing numbered detector locations. The wing is shown in two sections.



WING F

0 2 4 6 8 10 FEET  
SCALE

X.41 Plan view of F wing of AEC building showing numbered detector locations. The wing is shown in two sections.



comparison is shown in Table X.16. The calculations are for the contribution from a semi-circular source of radius 280 ft on the north side of wing A west (see fig. X.39). The comparison shows that the agreement is within a factor of 2 except for the detector in the basement. Here the calculation assumed that the basement wall was not exposed. However, the grade level drops at the west end of wing A and probably accounts for the increased exposure noted experimentally.

On the other hand, it is possible that the experimental exposure rate in the basement was spuriously high, since only the middle ring (S-2b in fig. X.39) contributed to the exposure. No detectable readings were obtained for the innermost and outermost source annuli. We do not understand why only the middle annulus should produce a detectable exposure rate. For stories other than the basement the Standard Method predicts somewhat lower reduction factors than observed experimentally.

#### 6. Brookhaven National Laboratory Medical Research Center

Experimental tests were conducted by Borella, Burson, and Jacovitch [35] on the Brookhaven Medical Research Center, shown in figure X.42. Detectors were placed at various points on the first story and basement of the large rectangular laboratory section. Source tubing was placed on the roof and on the north and east sides of the building out to a distance of about 100 feet.

Because of the low-spreading nature of the building, the roof source contributed over 90% of the total exposure at most detector positions in the building. Although Borella and his colleagues did not make any comparisons with the Standard Method, they published experimental estimates of the protection factor at various positions.

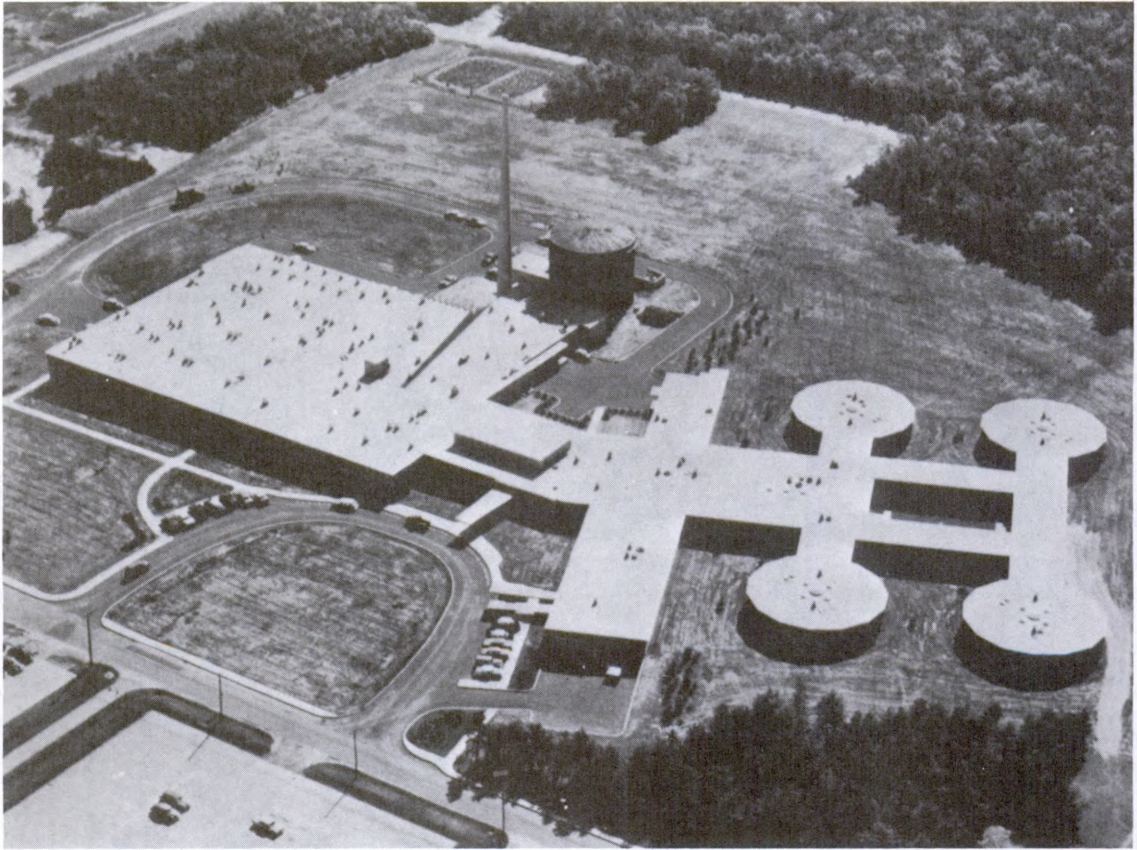
Two difficulties are encountered in an attempt to calculate protection factors for this structure. The first is the difficulty in estimating the

TABLE X.16  
COMPARISON OF CALCULATED AND EXPERIMENTAL VALUES  
OF THE CONTRIBUTION FROM GROUND SOURCES  
IN THE AEC HEADQUARTERS BUILDING

Floor	$C_g$ (Calc.)	$C_g$ (Exper.)
0	$<0.2 \times 10^5$	.00012
1	.0190	.024
2	.0069	.011
3	.0046	.0071
4	.0045	.0027

TABLE X.17  
ROOF CONTRIBUTIONS IN BROOKHAVEN MEDICAL RESEARCH CENTER

	$C_r$ (Calc.) ( $X'_1 = 0$ )	$C_r$ (Calc.) ( $X'_1 = \infty$ )	$C_r$ (Exper.)
Basement	.019	.0055	.0031
First Story	.125	.05	.049



X.42 Aerial photograph of Medical Research Center at Brookhaven National Laboratory.

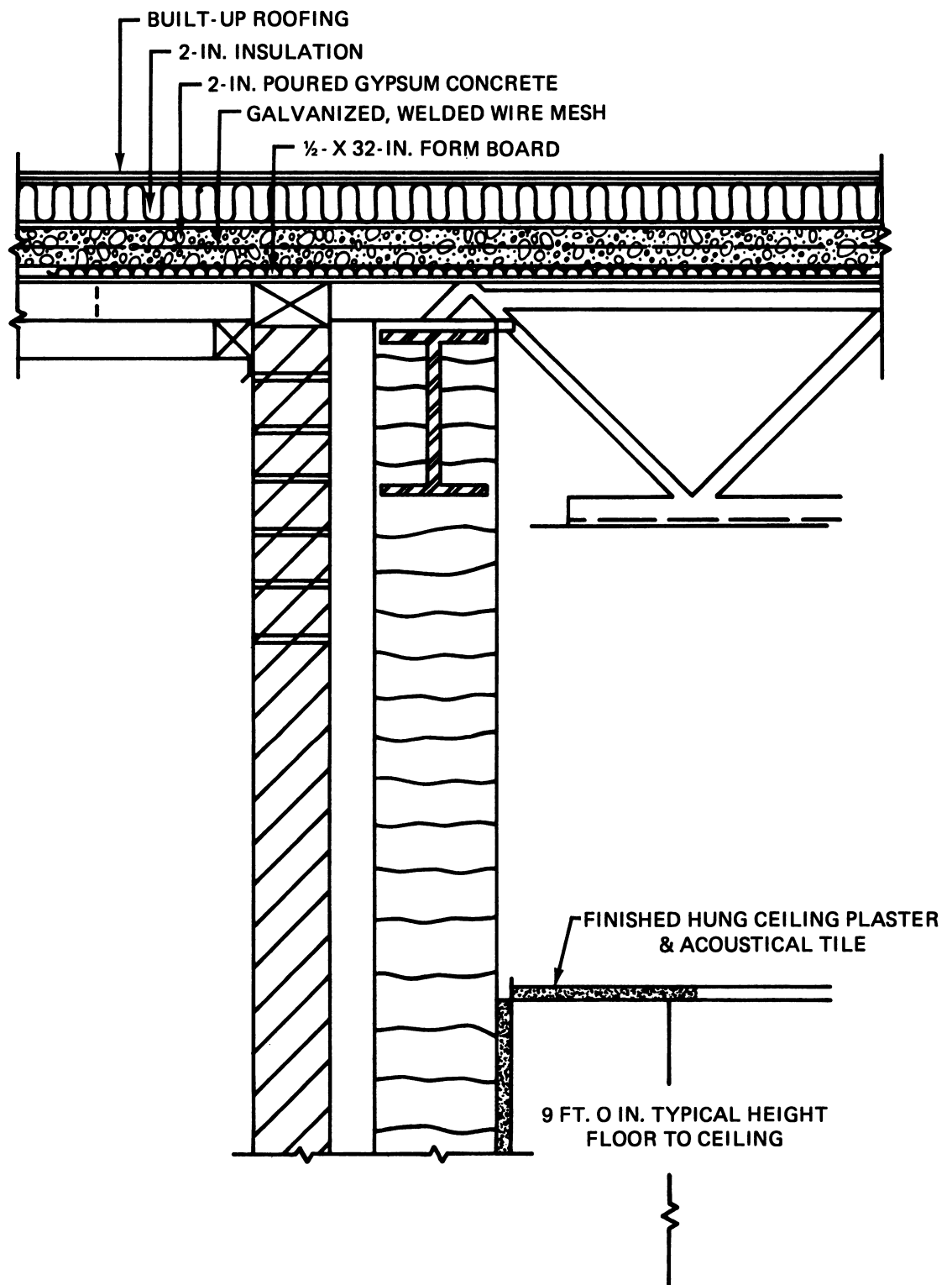
mass thickness for the roof and walls of the building. In some cases the in-place construction is not the same as that shown on the plans. Even when it is the same, however, it is a complicated combination of slabs, many of which are inhomogeneous. The second difficulty is that the internal configuration of this building is extremely complicated. A complete systematic calculation by the Standard Method would require many sub-calculations to take into account the variations in internal structure.

A comparison of limits on the roof contribution calculated by the Standard Method with the experimental values for a central position is shown in Table X.17. From this table it can be seen that neglect of the interior walls leads to a contribution which is several times greater than observed experimentally. Even under the assumption of infinitely thick walls, the calculated reduction factor is higher than experimentally observed in the basement.

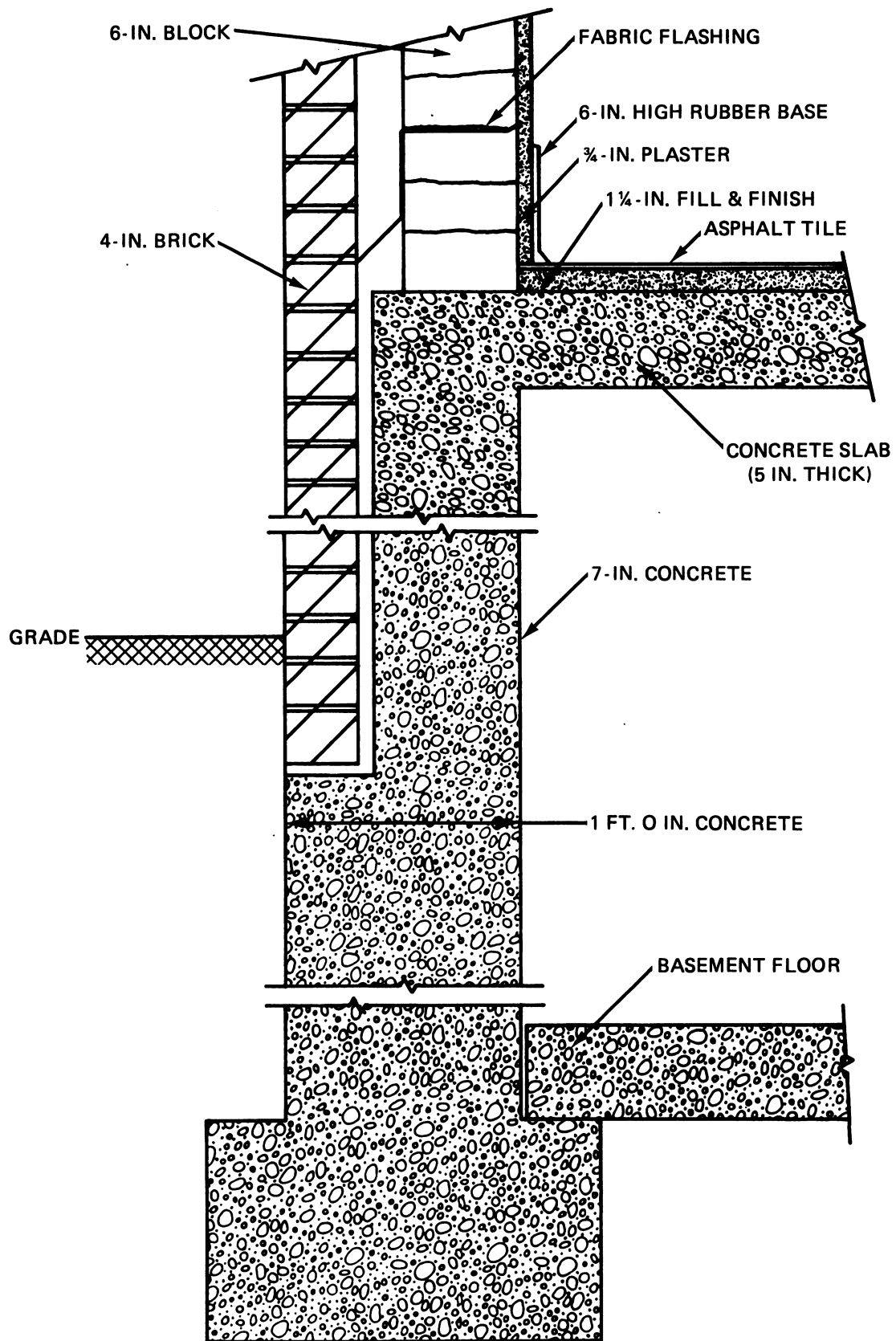
In these calculations the roof was assumed to be 30 psf and the floor 65 psf. Figures X.43 and X.44 show details of the roof and floor construction. The estimate of an effective mass thickness for these slabs is subject to considerable error. For example, an uncertainty of 10 psf in the slab thickness causes a variation of 20% in the reduction factor. It is therefore likely that much of the discrepancy between experiment and theory can be accounted for by uncertainties in the mass thickness of the in-place walls and floors.

## 7. Los Angeles Buildings

Late in 1961 an experimental study of four complex structures was made by Burson [36]. This study was sponsored by the CETO group, mentioned earlier in section X.E. The four buildings were (1) the Laboratory of Nuclear Medicine and Radiation Biology at the University of California at Los Angeles (UCLA);



X.43 Schematic showing details of a typical roof section in the Brookhaven Medical Research Center.



X.44 Schematic showing details of a typical wall section of the Brookhaven Medical Research Center.

(2) a family fallout shelter; (3) the communications section of the Los Angeles Police Department buildings and (4) a typical classroom located at North Hollywood High School.

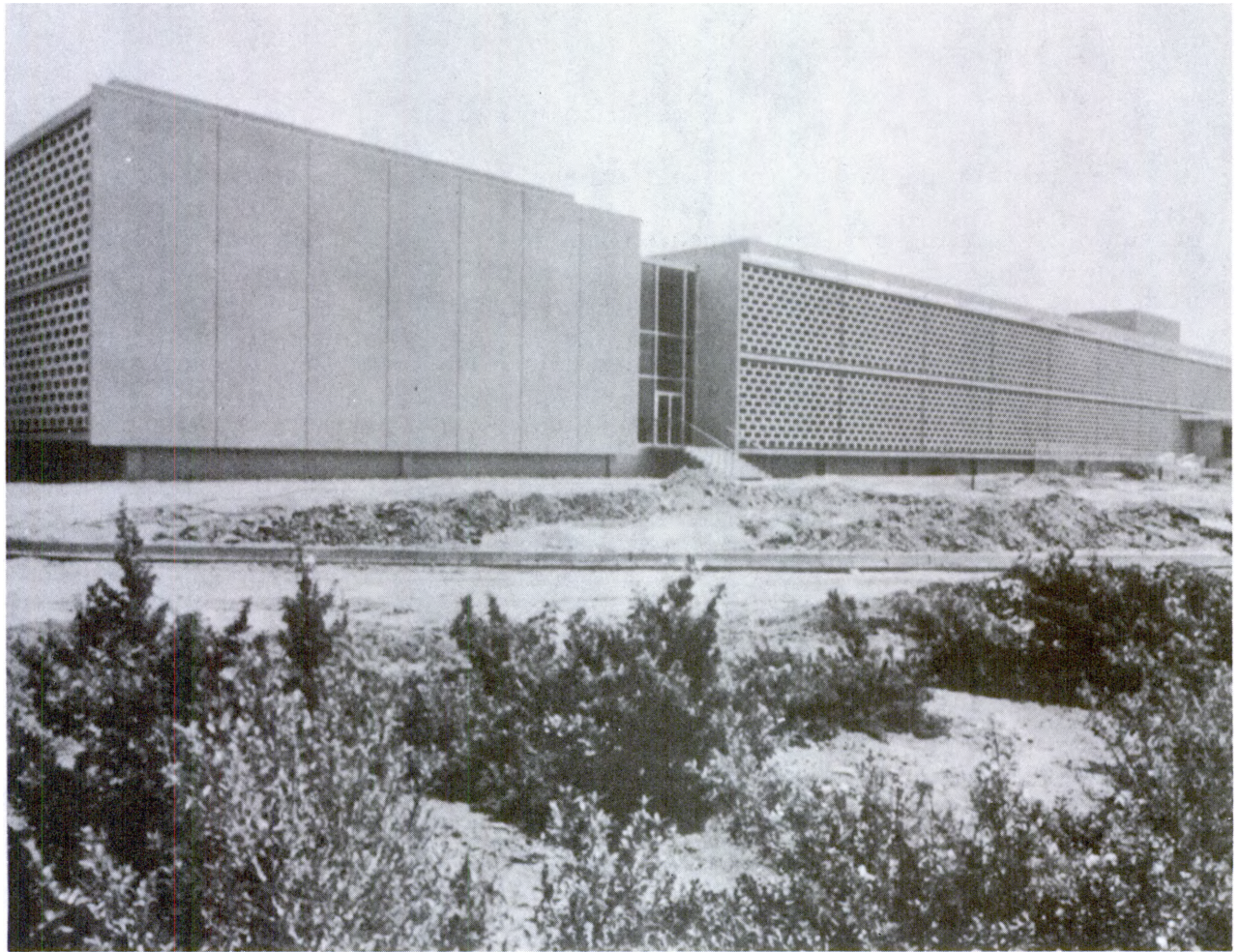
All of these structures were studied from the standpoint of obtaining an experimental indication of protection. The investigations were successful from this point of view. However, they were not designed as research experiments, and attempts to compare the results with calculations meet with the usual difficulty of uncertainty in the actual mass thickness of the in-place components. The following discussion is therefore limited to rough comparisons of results with some indication of the sensitivity of the comparison to uncertainties in construction.

a. UCLA Laboratory of Nuclear Medicine

The UCLA structure, shown in figure X.45 is a large two-story building with a basement under one wing of the structure. The total mass thickness between the roof and the basement is sufficiently large so that the main contribution comes from sources on the ground around the building or in one of the basement areaways of the building. The average extension of the basement wall above grade is 4 feet.

The measurements included the contribution from a strip 72 ft wide along the front side of the wing over the basement and a strip 60 ft wide along the rear side. The measured exposure rates at a central point in the basement from these two sources were  $0.19 \frac{\text{mR}}{\text{hr}} \frac{\text{mCi}}{\text{ft}^2}$  and  $0.12 \frac{\text{mR}}{\text{hr}} \frac{\text{mCi}}{\text{ft}^2}$  respectively. Burson estimated contributions from areas beyond the two strips by tripling these numbers to obtain an estimated PF of 410. Thus his estimated values are very sensitive to the accuracy of his extrapolation to infinite field size.





X.45 Photograph of UCLA Laboratory of Nuclear Medicine



An approximate calculation of the PF can be made as follows. The exterior barrier factor for the basement wall is 0.1 and the geometry factor is about .06. Burson's estimate of attenuation by the interior structure of the basement is about 0.3. The net estimate of the reduction factor is then .002., corresponding to a PF of about 500, in reasonable agreement with the PF inferred from experiment.

b. Home Fallout Shelter

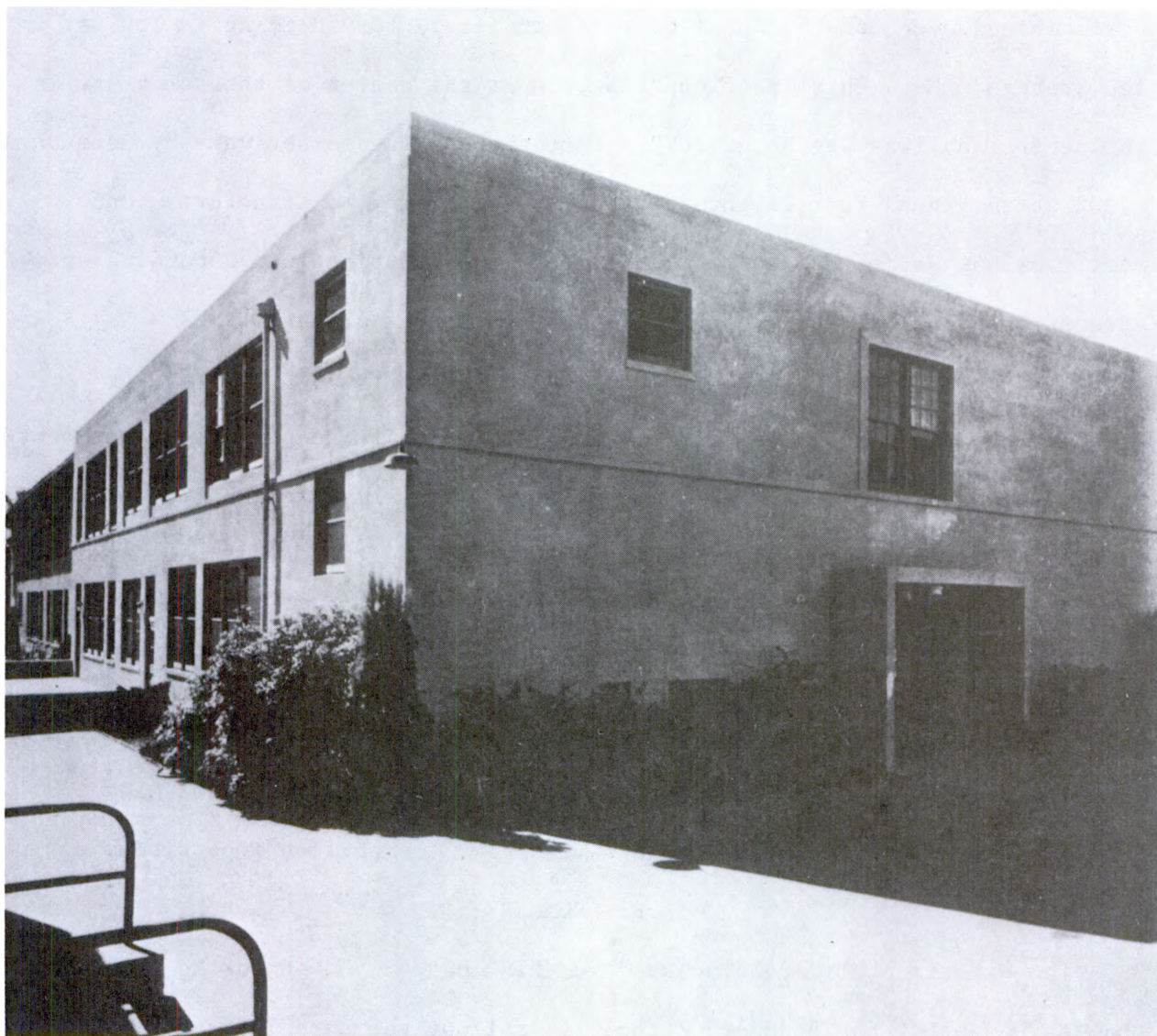
The protection factor in a fallout shelter in a private residence was measured by placing a point source on the roof. The shelter was covered by a slab of concrete 24 in thick. Exposures in the shelter were below the minimum detector reading, indicating a PF of greater than 10,000. The estimated contribution due to a roof source shielded by a 300 psf horizontal barrier is smaller than 0.0002. A geometry factor of 0.5 superimposed on the barrier factor would also predict a PF greater than about 10,000.

c. Los Angeles Police Department Building

The predominant contribution to reduction factors in the teletype room of the Los Angeles Police Department building was from roof sources. The measured roof contribution in the central region of the teletype room was about .01. The total overhead mass thickness cannot be determined from the information given in reference [31]. But assuming an overhead thickness of about 140 psf [37], the calculated roof contribution would be .0035. This is less than the experimental exposure, but the assumed roof thickness is uncertain by about 30 psf.

d. Classroom Building at North Hollywood High School

This classroom building is a two-story structure 108 ft x 70 ft. It has 12-in concrete walls with many windows. A photograph of the building is shown in figure X.46.



X.46 Photograph of North Hollywood High School.

The roof sources were placed over only one-half of the building and measurements were taken on the first story. The source dimensions were 100 ft by 70 ft and the detector was 25 ft below the roof. A reasonable estimate for the combined overhead thickness of roof and first-story ceiling is 100 psf. The average experimental roof contribution at the center of the structure in the central hallway was about .002. Furthermore, it did not vary by more than  $\pm 30\%$  at the three-foot height at other positions in the structure. Once more, various estimates can be made of the roof contribution, depending on assumptions about interior partitions. If the interior partitions are neglected and the full solid angle subtended by the roof is used in the calculation, the calculated contribution is 0.13. If the portion of the roof immediately above the hall is considered, and the walls are assumed to be impenetrable, the calculated value is .0054. The uniformity of the experimental roof contribution seems to suggest that there is an average collimating angle due to the internal structure. Even if the interior walls are assumed to be infinitely thick, however, the calculated contribution is higher by a factor of 2.5 than the experimental value. As usual, the overhead mass thickness is uncertain, making a more meaningful comparison impossible.

#### F. SUMMARY

The experimental data discussed in this chapter show both the strengths and weaknesses of the Standard Method for fallout gamma radiation shielding analysis.

Experiments with limited source fields surrounding the three-story RTF structure (fig. VIII.17) show that the standard Method predicts the ground contribution well for large source areas but tends to overestimate it for small source areas. This is particularly true for locations near the floor of the second or third story, mainly because of the approximate treatment of

attenuation in the floors. Similarly, the approximate treatment of attenuation in interior partitions is responsible for some poor comparisons with experiment for locations near the ceiling due to a peripheral roof source. On the other hand, the calculated ground contribution inside a simple core formed by interior partitions shows good agreement with experiment.

The penetration of radiation in through the wall of a structure and down through the ceiling of the basement has been studied extensively. Experiments at NEL (22-24) were used as a guide for deducing eq (X.3), which gives a simple expression for the attenuation in a basement ceiling. Additional calculations by Monte Carlo procedures [27-31] tend to indicate that this expression is reasonable, except near the basement ceiling where it predicts values about 50% higher than Monte Carlo calculations.

Experiments on real structures have the advantage that results are obtained for buildings actually in use. However, they have the disadvantages of unknown structural thicknesses and complexities mentioned in the introduction to this chapter. In general, comparisons of calculations with experimental data on light residential structures show good agreement. Comparisons for heavier commercial and industrial structure grow progressively worse because of the difficulties mentioned above.

The development of an attenuation factor for the basement ceiling was the result of feedback from experiment. The corresponding feedback from the series of complex structures discussed in section E of this chapter has never taken place. It would be reasonable to introduce this type of information in the next revision of the Standard Method. Measurement of in-place mass thicknesses would be an important part of such an effort.

## REFERENCES

- [1] L. V. Spencer, "Structure Shielding Against Fallout Radiation from Nuclear Weapons," National Bureau of Standards Monograph 42, June 1962.
- [2] E. T. Bramlitt and C. M. Eisenhower, "A Discussion and Tabulation of the Data Used to Construct the Charts in the OCD Standard Method for Fallout Gamma Radiation Shielding Analysis," Report TR-70, Office of Civil Defense December 1971.
- [3] C. McDonnell, et al, "The Barrier Attenuation Introduced by a Vertical Wall," CONESCO Report PSDC-TR-15, Flow Corporation, Watertown, Mass., September 1964.
- [4] C. McDonnell and J. Velletri, "Radiation Distribution within a Multi-story Structure," CONESCO Report TR-24, Flow Corporation, Watertown, Mass., February 1967.
- [5] A. W. Starbird, "Decontamination of Finite Rectangular Areas," CONESCO Report 4897, Flow Corporation, Watertown, Mass., August 1969.
- [6] W. O. Doggett and F. Bryan, Jr., "Constrip V, A Computer Program for the Vertical Barrier-Finite Source Plane Gamma Ray Penetration Problem" NRDL-TRC-68-55, Final Report, Part I, R-OU-333 Research Triangle Institute, Research Triangle Park, N.C., 1969.
- [7] J. F. Batter, A. W. Starbird, N. R. York, "Final Report. The Effect of Limited Strips of Contamination on the Dose Rate in a Multistory Windowless Building," Report No TO-B 62-58, Technical Operations Research, August 1962. (See also Volume I, April 1962; Volume II May 1962; Volume III, June 1962; Volume IV, July 1962)
- [8] L. V. Spencer and C. Eisenhower, "Fortran Program for Calculation of Protection from Fallout Radiation, Nov. 1961 (unpublished)
- [9] R. Spring and C. H. McDonnell, "An Experimental Evaluation of Roof Reduction Factors within a Multi-story Structure," CONESCO Report PSDC-TR-16, Supplement No. 1.
- [10] J. H. Price and R. L. French, Monte Carlo Study of Interior Partition Effects on Fallout Shielding," RRA-T91 (NRDL TRC-69-5), 51 pages, Radiation Research Associates, Fort Worth, Texas (Jan. 1969).
- [11] J. Velletri, R. Spring, J. Wagoner, and H. Gignilliat, "Experimental Analysis of Interior Partitions, Apertures, and Non-uniform Walls," CONESCO Report TR-27, December 1968.
- [12] R. Spring and J. Velletri, "Analysis of Roof Radiation Experiments under Typical and Ideal Conditions," CGS-TR-29, CGS Scientific Corporation, November 1969.
- [13] A. L. Kaplan, et al, "Final Report - Phase I Structure Shielding from Simulated Fallout Gamma Radiation," TO-B 65-27, Technical Operations inc, November 1965.

- [14] J. A. Auxier, et al, "Experimental Evaluation of the Radiation Protection Afforded by Residential Structures Against Distributed Sources," CEX-58.1, U.S. Atomic Energy Commission, January 1959.
- [15] E. T. Clarke et al, "Measurement of Attenuation in Existing Structures of Radiation from Simulated Fallout," TO-B 59-4, Technical Operations Inc., April 1959.
- [16] Z. G. Burson, "Experimental Radiation Measurements in Conventional Structures," CEX-59.7B, U.S. Atomic Energy Commission, Part I, July 1966; Part II, February 1963; Part III, November 1965.
- [17] R. L. Summers and Z. G. Burson, "Experimental Evaluation of Techniques for Improving Fallout Protection in Home Basements", CEX 65.5, U.S. Atomic Energy Commission, December 1966.
- [18] A. W. Starbird, "Interior Partition and Basement Shelter Experiments," CONESCO Report 4903, Flow Corporation, April 1969.
- [19] M. J. Robinson, et al, "A University Design Study of Protection Factors in Typical American Houses," KSU Report 84, Kansas State University, November 1969.
- [20] C. Eisenhower, "Analysis of Experiments on Light Residential Structures with Distributed Co-60 Sources," NBS Report 6539, October 1959.
- [21] J. F. Batter and A. W. Starbird, "Attenuation of Co-60 Radiation by a Simple Structure with a Basement," Technical Operations Inc., Report No. TO-B 61-38, July 1961.
- [22] M. J. Schumchyk, M. A. Schmoke, et al, "Scattered Radiation 'Skyshine' Contribution to an Open Basement Located in a Simulated Fallout Field," Nuclear Defense Laboratory Report NDL-TR-68, December 1966.
- [23] M. J. Schumchyk, M. A. Schmoke et al, "Scattered Radiation (Skyshine) Contribution to a Concrete-Covered Basement Located in a Simulated Fallout Field," Nuclear Defense Laboratory Report NDL-TR-69, July 1967.
- [24] M. A. Schmoke, "In-and-Down Scattered Radiation in a Simple Concrete Structure," BRL Report 1665 USA Ballistics Research Laboratories, September 1973.
- [25] A. L. Kaplan et al, "Final Report - Phase II - Structure Shielding from Simulated Fallout Gamma Radiation," Technical Operations Inc. Report No. TO-B 65-123, June 1966.
- [26] C. Eisenhower and A. Kaplan, "Evaluation of the Reduction Factor in the Basement of a Structure," NBS Report 10037, May 1969.
- [27] D. J. Raso and S. Woolf, "Doses Behind Vertical and Horizontal Barriers from a Plane Source of 1.25 MeV Gamma-Ray Photon," Nuc. Sci. & Eng. 27, 252, 1967.

- [28] D. K. Trubey, "A Calculation of the Components of the Exposure in a Basement Due to Fallout," Trans. Am. Nuc. Soc. 10, 404 (1967).
- [29] D. E. Hinkley, "Monte Carlo Analysis of In- and Down-scattered Radiation," Trans. Am. Nuc. Soc. 13, 425 (June 1970), D. E. Hinkley and R. L. French, "Gamma-Ray Attenuation in Structures with Basements," Trans. Am. Nuc. Soc. 13, 426, (June 1970). (See also D. E. Hinkley, "A Study of the Components of the Exposure in Cylindrical Structure," RRA-M703, Radiation Research Associates, November 1970.
- [30] E. E. Morris, "Study of the Penetration of Gamma Radiation Through Thin Slabs Oriented at Right Angles to Each Other," NRSS Report 14, University of Illinois, September 1970.
- [31] M. H. Kalos, "Monte Carlo Integration of the Adjoint Gamma-Ray Transport Equation", Nuc. Sci. Eng. 33, 284 (1968). See also: A. Stathoplos and L. Wills, "Dose Rates in an Open Basement in a Simulated Fallout Field", Trans. Am. Nuc. Soc. 10, 723 (1967).
- [32] E. T. Clarke, J. F. Batter, and A. L. Kaplan, "Measurement of Attenuation in Existing Structures of Radiation from Simulated Fallout," Report TO-B 59-4, Technical Operations Inc., April 1959.
- [33] Z. G. Burson, "Experimental Evaluation of the Fallout-Radiation Protection Provided by Structures in the Control Point Area of the Nevada Test Site," CEX-69.5, U.S. Atomic Energy Commission, October 1970.
- [34] J. F. Batter, Jr., A. L. Kaplan, and E. T. Clarke, "An Experimental Evaluation of the Radiation Protection Afforded by a Large Modern Concrete Office Building," CEX-59.1, U. S. Atomic Energy Commission, Jan. 1960.
- [35] H. Borella, Z. Burson, and J. Jacovitch, "Evaluation of the Fallout Protection Afforded by Brookhaven National Laboratory Medical Research Center," CEX-60.1, U.S. Atomic Energy Commission, October 1961.
- [36] Z. G. Burson, "Experimental Evaluation of the Fallout-Radiation Protection Provided by Selected Structures in the Los Angeles Area," CEX-61.4, U. S. Atomic Energy Commission, February 1963.
- [37] Z. Burson (Private Communication)

## XI. PROBLEMS IN THE APPLICATION OF THE FALLOUT SHIELDING METHODOLOGY

### A. INTRODUCTION

The fallout shielding methodology discussed and evaluated in great detail in the several preceding chapters has been presented largely as a set of specific rules and formulas. The exercise of "engineering judgment" has not been emphasized. There are several reasons for this. One reason, as indicated in section IX.B.1.d is that much of fallout shielding analysis is done by computers, which have no judgment. Another is that the DCPA needs a "standard" procedure for determination of an "official" value of the protection factor for each structure it subjects to analysis, and this official value should ideally be independent of the judgment of the specific analyst (or computer programmer) involved in the determination. Lastly, it must be pointed out that fallout shielding analysts vary widely in their understanding of radiation transport under the complicated conditions, frequently encountered in practice; and their judgments will also vary correspondingly.

Nevertheless, it is impossible to avoid the use of judgment in solving real fallout shielding problems. Those who have established the standard procedures have not considered every situation which may arise in practice. Also, the process of translating a configuration into the idealization which the method postulates requires judgment. From the standpoint of computer analysis, the exercise of judgment enters primarily in the selection of the proper input data. But the computer programs always involve a degree of simplification of the complete method, and such simplifications also require the exercise of considerable judgment.



This chapter will first discuss certain factors in practical fallout shielding problems which are not easily resolved in terms of precise rules and therefore require engineering judgment. Following this, the subject of accuracy of the Standard Method and simplified methods derived from it will be reviewed in summary fashion.

## B. FACTORS RELATING TO THE SOURCE

### 1. Non-Uniform Deposition of Source

It is unlikely that fallout particles would always be deposited uniformly on horizontal planes and horizontal projections of sloping planes. Furthermore, after initial deposition, climatic or man-produced influences will cause subsequent movement from the original position.

To the extent that such change from the uniformity assumption is predictable, existing techniques for limited source planes, as discussed in chapter IX, can be used. Entire removal of a source by decontamination of some sort can be treated as a negative contribution from the portion of the plane which is decontaminated. Upon occasion, it is possible that the movement of the fallout particles may serve only to change the location of the source to another place rather than completely remove it. Under such a circumstance, the contribution from the re-positioned source must be taken into account. If the new location is better shielded from the structure being analyzed, e.g. behind a curbing on the near side of an adjacent street, one might consider it effectively removed, at least as far as direct ground contribution is concerned.

Particle movement from one location to another in which no great change in distance to the detector or in structure shielding capability is apparent should produce no appreciable change in overall protection factor; and therefore, calculations which are elaborations on the standard type are rarely worthwhile in such cases. An example of such a situation is the drift of

fallout particles deposited on a sloping roof into the gutter at the edge of the roof. But if one can expect the gutters to be well flushed by some artificial "roof-washdown" system immediately after the initial fallout occurs, ignoring the roof source may be justified.

If we are concerned with protection mainly for the first hour or two after the initial fallout deposition, no fallout movement which occurs later than about an hour after initial deposition has significance in the shielding analysis.

Non-uniform deposition of fallout on the ground caused by interaction of air currents (wind) around structures tends to leave radiation fields unchanged on the average, as previously indicated. However, some situations deserve special consideration. Basement area-ways and window-wells, which are lower than the ground outside, are places in which fallout particles are likely to collect. The resulting pile-up of fallout near doors and windows, which are the least adequate shields for basements, leads to a serious degradation of the basement shelter capability. The relative increase of source strength has been estimated [1] in terms of an effective "fetch", which is a measure of the area over which the source was distributed before pile-up occurred. Unfortunately, there is little guidance for estimating this area.

## 2. Hold-Up in Trees and Shrubs

Many structures are surrounded by trees and shrubs. If fallout occurs while these are in full foliage, an appreciable proportion of the fallout will cling to the leaves and branches. For detector positions at the first story or in the basement, this possibility can only be ignored if the detector is as well shielded from sources in the trees or shrubs as from sources on the ground below. The source on foliage is generally no nearer the detector than when on the ground below. Even for the second floor and above, the distance

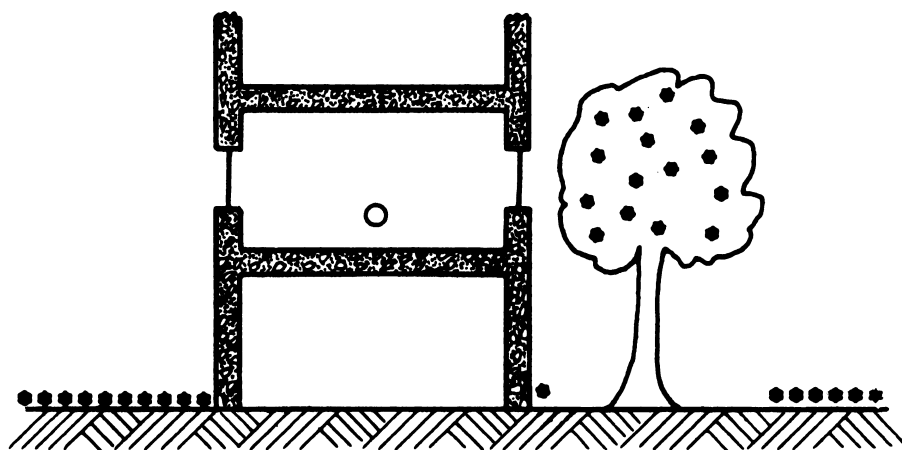
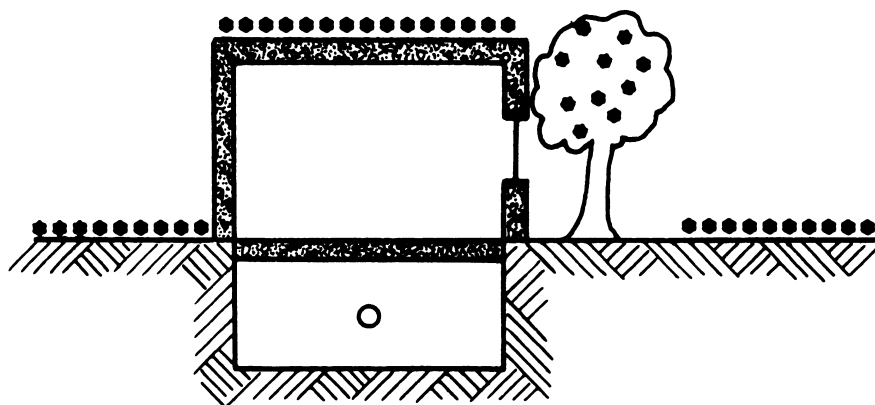
to the typical detector position is not radically changed; and thus little cognizance need be taken of changes of distance from the detector.

However, such a change in source location can bring about a very great reduction in the amount of shielding provided by the structure. Figure XI.1 gives some illustrations of such cases. There, the retention of fallout particles by trees and shrubs must be given serious consideration, perhaps requiring a special protection factor calculation.

Since detailed knowledge of the exact distribution of the source under such conditions cannot be obtained, judgment must be exercised as to how complete the hold-up in trees might be, what the distribution is, how it varies seasonally, and so on. A conservative (worst case) approach would consider all fallout to be held in foliage, a case rather easily analyzed as a finite, elevated plane of fallout, with no shielding capability by the trees themselves.

### 3. Fallout Deposition on Window Sills and Other Wall Projections

The standard methodology [2] does not mention that fallout particles may be deposited on window sills or other small wall projections. Window sills are most likely to be underneath some higher projecting element, either a roof overhang or sills of higher windows; but fallout may collect on sills even under such circumstances, especially on the windward side of a building. The strength of the source of radiation so collected is not likely to be large, but the strategic location of a contaminated sill with respect to a detector at the same story may cause some degradation of the shelter capability of that story. This may be of particular importance if the detector is on a middle story of a rather tall building, otherwise well protected from either roof or ground sources of radiation.



XI.1 Illustrative cases in which hold-up of fallout in trees may present special hazard.

There may be circumstances in which fallout drifting with the wind would strike the side of a structure and partially stick to it even without projections. This is more likely for rough-surfaced walls than those with smooth surfaces. The possible wetness of the building and/or the fallout would also influence the "sticking factor." This effect has received very little attention in recent literature. (See, however, the report by Malich and Beach [3].)

Handling such problems within the framework of the standard methodology would involve the use of finite fields. Sills and other projections would lend themselves easily to this, but walls as source planes require a 90° change in orientation of the problem as well as an appreciable diminution in fallout source strength per unit area.

#### 4. Fallout Ingress Through Windows

Similar to the window-sill and wall problems noted above, and of equal concern, is the possibility of fallout drifting into a structure through open windows on the windward side, with deposition on the floor inside the structure. There is no discussion of this effect nor how to estimate it in the OCD manuals, and little study of a definitive nature has been made of it, except for reports by Lacayo and Sullivan [4] and by Howard [5].

If this effect is to be considered, an estimated area of contaminated floor beneath each window might be made, with application of the finite-field approach.

#### 5. Ground Contour Variations

Ground contour variations on a scale larger than that related to "ground roughness" (see sec. IX.B.2) must be handled by techniques which are a combination of those already described for limited source fields and sloping source planes (sec. IX.B). This involves the idealization of the topography as a set of planes of limited or partially limited extent. The amount of

topographic detail to be simulated by these planes is a matter of judgment. Small contour variations near the structure are more important than those far away. Detailed studies giving practical guidance in this respect are largely lacking. But there has been the work by Goldstein [6], discussed in chapter VI, showing the effect of locating simple structures on hills or at the bottom of valleys of idealized shape, as compared to the standard location above a flat plane. His results related to detector positions in the open; but the data also appear to be approximately valid for positions inside simple structures.

#### 6. Irregular or Curved Limits to Finite Fields

A finite field, though planar, may be bounded by limiting lines which are curved or very irregularly segmented. These limiting lines can generally be approximated by a reasonably small number of straight line segments, requiring a corresponding division of the finite field into a number of parts, each analyzed separately. Finer divisions should improve the accuracy of results but increase the required amount of input data and the computational effort.

### C. FACTORS RELATING TO THE STRUCTURE

#### 1. Simplification of Very Complex Structures

Reduction of a complex structure to a set of elementary ones has already been covered in chapter IX. Most structures of a size suitable for use as fallout shelters for large numbers of people are very complex; and if one follows the usual rules for splitting up such a structure by sectors and zones for analytical purposes, one may be faced with a very tedious job. There are a number of rules or suggestions to reduce the amount of work involved, however.

Ignore complexities in distant parts of structure: The contributions through the structural shell at locations distant from the detector, and shielded from it by many internal structural elements, are relatively unimportant. One may therefore "smear out" variations in the shielding

elements for these lesser significant contributions, thus reducing the number of sectors and zones to be treated individually. Experience and good shielding judgment will usually indicate where such simplifications are possible.

Ignore contributions from walls of stories distant from the detector story: This is consistent with the suggestion given above. In this case, the standard methodology has a fixed rule: ignore contributions from outer walls two or more stories distant from the detector story. There may be unusual cases in which this rule is inappropriate, and the analyst should watch for such possibilities.

Assume internal partitioning of other stories to be the same as that assumed for the detector story: This rule is also a rather established one and is a rigid application of the first suggestion above. This markedly reduces the effort involved in the calculation, as well as the amount of data needed. It is justified partly by the lesser importance of wall contributions from the stories above and below, as compared to that of the detector story, and partly by the fact that most multistoried structures do tend to have a similar internal partition plan for all or most stories. As stated before, there may be occasions in which this simplifying rule should not be obeyed. It is seldom valid for a basement detector location, and its validity doubtful for a first story location.

Analyze sectors involving large contributions before those involving little: Especially if one is making a desk calculation, one should analyze first those sectors (and zones) which are expected to make relatively large contributions to the detector response. One will usually find, as one progresses in turn to analyze adjacent sectors, that these contributions will become smaller and smaller. Eventually, one realizes that the contributions from certain sectors are negligible and can be ignored. In case one still

wishes to account for these contributions, one is justified in combining sectors by smearing out those variations in source or structure which lead to their initial division. This involves an exercise of judgment which is difficult to introduce into a computer and may not be applicable to the design of computer codes.

## 2. Handling of Curved Structural Elements

Just as curved land contours can be replaced by finite planes (sec. XI.B.5), so also can curved structural elements, such as domes and arches, be approximated by a series of flat elements. These in turn can be handled by usual procedures. The more of these flat elements used, the more closely is the curved element approximated. Because, this also entails more computational effort, a compromise between accuracy and effort must be made.

There is an exception to the rule that curved elements should be replaced with flat elements. As indicated in section IX.C.3.c, a vertical cylinder is more basic than a rectangular blockhouse, and under no circumstances should a vertically cylindrical structure be approximated with one having flat walls.

## 3. Unusual Shapes of Wall Panels, Roof Panels, and Apertures

Frequently structures, even though of simple configuration in themselves, have panels or apertures of shapes which do not fit the standard methods of fallout analysis. A circular panel in an overhead floor or horizontal roof, with the center of the panel directly above the detector, conforms exactly to the assumptions inherent in geometry factor calculations for overhead contributions, and should be treated in standard fashion. A rectangular panel (or aperture) with orientation of boundaries parallel and perpendicular to the main lines of the structure conforms only approximately to these assumptions, but as has been shown in chapter VII this case can be readily treated by standard engineering procedures.



A panel which is small enough to be treated as differential in both principal directions can be analyzed on the basis of the area, regardless of exact shape or orientation, as noted in section VII.D.

Overhead panels which conform to, or can be approximated by, the shape of a sector of an annulus with its center directly above the detector position (see fig. VII.9), can be readily handled by differencing and use of an azimuthal fraction.

A panel which does not conform to any of the shapes and orientations noted above must either be approximated by one of the above types, or be broken up into more than one of such types, each analyzed separately.

#### 4. Small, Irregularly Placed Masses

Small, irregularly placed masses are most difficult to take into consideration. We suggest ignoring those which may shift position in an unpredictable manner, such as furniture or people. Irregular masses in an important shielding wall (e.g., a fireplace) must either be conceptually smeared into the overall wall, treated as separate panels of some average thickness, or broken into two or more smaller size panels of differing thickness, depending upon the degree of accuracy desired, the amount of effort one wishes to make, and the analyst's judgment of when the point of diminishing returns in increasing complexity occurs.

#### 5. Approach Based on Small Azimuthal Sectors of Arbitrary Size

One attractive approach to handling the ground contribution for structures of great complexity, especially suited to computers because of the many tedious calculations involved, is to divide the azimuth around the detector into a large number of sectors of equal size, for example, one degree.<sup>1</sup> This means

---

<sup>1</sup>The same thing in principle can be done in the vertical direction, but vertical structural complexity is usually not great, or is made less so by arbitrary assumptions such as those listed in section XI.C.1 above.

that the sectors are all assigned the same azimuthal fraction, and their boundaries are established arbitrarily rather than by the intersection of shielding walls or changes in wall thickness.

The argument in favor of this approach is that substantial computer program simplification results. For each sector, the thicknesses of both interior and exterior walls are based on what is intersected by a "line-of-sight" from the detector within the sector, as seen in plan. Likewise, the finite or infinite extent of the external field affecting this sector contribution can be established by extending this same line to the field limit.

This approach is opposite to that in section XI.C.1, and is not at all suited to desk calculations. For computerized calculations, the disadvantage is largely related to the question of accuracy. Because of radiation scattering interactions, the radiation contribution from a given direction is related to a much broader part of the structure than that of the narrow sector. Therefore, the "line-of-sight" approach can give very wrong answers for individual sectors.<sup>2</sup> The resulting errors are not easy to determine and will vary widely. The assumption is that such errors, even if large for individual sectors, will mutually cancel, so that the total result from all sectors is approximately correct.

Experience has demonstrated that the "line-of-sight" approach in many, perhaps most, complex shielding problems does give answers which are accurate enough for practical purposes [7]. But there is no way to determine the probable error or a possible upper limit to the error of this technique. Furthermore, this technique has not yet been compared to the more standard calculations for a wide variation of typical cases, and thus one does not know

---

<sup>2</sup>For example, the phenomenon of inscattering in interior partitions was discussed in section X.C.5.

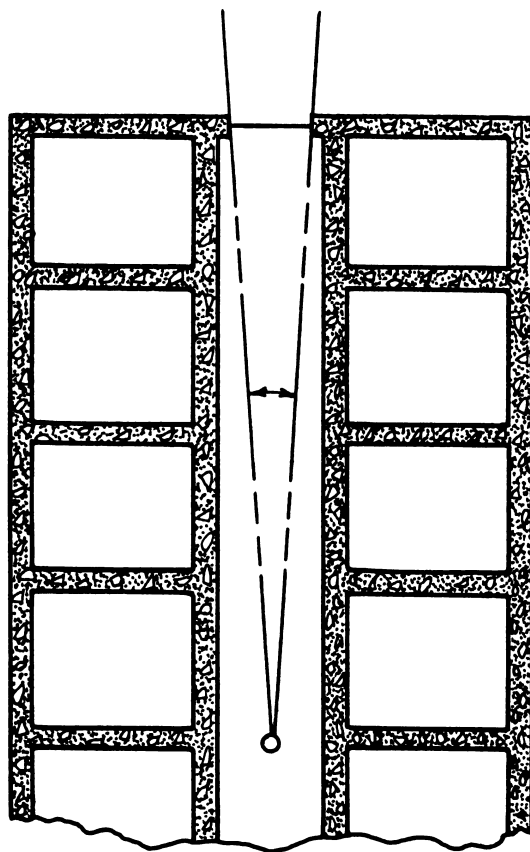
if it compares well with the results of the standard calculations. One cannot presently prove or disapprove claims that this approach is more (or less) accurate than the standard approach. Our present judgment is that this method takes the approaches inherent in the more conventional methodology to an extreme beyond the ability to justify it on the basis of physical reality.

## 6. Alternative Approaches

At times, alternative approaches to an analysis which are of approximately equal merit and ease, are available. This may occur even within the framework of the Standard Method.

For example consider figure XI.2, which represents a detector in the middle of a long corridor in a single story structure with thin doors to the outside at each end. One may consider the doors as wall panels subtending appropriate portions of the azimuth and proceed on the usual azimuthal fraction approach. On the other hand, one may consider the corridor as a long duct and use the approach developed for such elements. The results obtained for the contribution through the doors and down the corridor are not likely to be the same, and may even vary by a large factor.

The key to a decision in this case is the mass thickness of the interior partitions lining the corridor. If they are relatively thin, the azimuthal approach seems better suited to the situation; if they are rather thick, they become walls which shield against radiation from other parts of the structure, and the duct approach appears more suitable. Suppose they are of some thickness such as 15 psf. Is this "thin" or "thick"? Or is it an intermediate case? Perhaps the problem should be worked both ways. If so, should one pick the more conservative value? (See the discussion in sec. XI.D, following.) Should one take an average of the two? At this stage of development of the methodology, only good judgment can provide the answers and it would be hard to defend any specific answer as being the "right" one.



XI.2 Situation subject to analysis either as azimuthal fraction of wall contribution or as duct-like passageway.

## 7. Accurate Input Data

Although accuracy of input data is almost always assumed by the analyst, the difficulties inherent in getting accurate data must be emphasized. Special responsibility rests with the good judgment of the person collecting the data; but the analyst must also develop some idea of data likely to be reliable, and data subject to suspicion.

Problems inherent in data collection for existing buildings include the following:

- 1) Difficulties in visualizing the interior structural details of a wall and many other elements. A good knowledge of construction practice helps here.
- 2) Difficulties in locating the detailed plans for a particular structure.
- 3) Possibility that the actual construction may not have followed either the plans or recognized good construction practice.
- 4) The substantial time and money expenditure required for a careful determination of detailed data for a structure of even modest complexity.
- 5) Problems of material identification, especially under several coats of paint.

Problems inherent in assuming certain shielding data for a structure under design are:

- 1) Difficulty in guaranteeing that the builders of a structure will do it as designed.
- 2) Lack of appreciation by the construction contractor and his personnel of fallout radiation shielding principles.

- 3) Possibility of compromise of protection criteria by subsequent changes in the structure either during construction or afterward.

#### D. THE QUESTION OF ACCURACY

##### 1. Types of Investigation

Previous chapters have shown that some detailed parts of the Standard Method are quite accurate, at least for the idealized experiments used to test them; other parts are not quite so accurate. The first portion of this chapter has shown many judgemental factors which may introduce errors into the fallout shielding analysis of structures under actual conditions. It becomes desirable to obtain an understanding of the overall accuracy of the Standard Method and of the various simplified methods which have been derived from it. Such knowledge might be summarized in principle by tabulated or graphed data giving the likelihood that the "correct" value is within a certain range of the estimated value, for a given estimate and for the entire spectrum of possible "true" values. At least, the mean and standard deviation for such a curve would be useful.

However, it is not possible to obtain such detailed information for many reasons, not the least of which is the impossibility of predicting the precise configuration and properties of the fallout landing in a specific location. Another problem relates to the large numbers of actual structures that would have to be studied to provide an adequate sample of the entire population of buildings potentially useful as fallout shelters.

What has occurred, therefore, is a wide variety of investigations which, although not answering the final question as to the accuracy of the Method, give closely related information. In these studies, sources may be of three different types: actual fallout; simulated fallout; or single isotopes considered to have approximately the same shield penetration properties as

fallout (almost always  $^{60}\text{Co}$  or  $^{137}\text{Cs}$ ). The structures studied may be: actual buildings; idealized structures for experimental purposes; segments of buildings; or elementary configurations such as those discussed in chapter VI. Attempts to estimate errors are usually based on the selection of one of these types of source and one of the types of structure and a comparison of results by two different types of evaluation. The types of evaluation could in principle include: measurement during an actual fallout condition following a nuclear explosion; measurement in a controlled experiment; calculation by reasonably accurate computer simulation of radiation transport from source through the structure (Monte Carlo method); calculation by the Standard Method or one of its variants; and calculations by the simplified methods derived from the Standard Method.

Use of actual fallout as a source in shielding studies has been quite rare. No significant fallout was generated as a result of the attacks on Hiroshima and Nagasaki. Fallout was created during various experimental weapons tests in Nevada and was used to some extent but not for studying the more common type of building [8-11]. The term "simulated fallout", used above, may refer either to the standardized 1.12-hour spectrum discussed in chapter II and used as the basis of the shielding data leading to the Standard Method or to a mixture of isotopes made up for experimental simulation of fallout properties. The theoretical spectrum has been discussed in some detail in chapter II. Very little effort has been made using experimental mixtures.<sup>3</sup> Most studies, both theoretical and experimental, have used  $^{60}\text{Co}$  or  $^{137}\text{Cs}$ . (Even Monte Carlo calculation, which could easily have used the standardized

---

<sup>3</sup>Some experiments with simulated fallout were performed at Camp Parks, California, but there was no emphasis on radiation shielding [12,13].

or similar spectrum close to that produced by actual fallout, have tended to use  $^{60}\text{Co}$  or  $^{137}\text{Cs}$ .) The usual justification for using the single isotopes is that fallout shielding calculations are almost always for the purpose of determining a ratio--dose rate at the Standard Unprotected Location divided by that in the shelter (or vice versa); and the error inherent in using a simplified spectrum, such as that of a single isotope, in numerator and denominator of this ratio tend to cancel out. To put it another way, if theory and experiment check with consistent use of  $^{60}\text{Co}$  (or  $^{137}\text{Cs}$ ), they should check reasonably well with consistent use of a fallout spectrum. This is a plausible assumption although it has not been rigorously examined.

The types of structures listed above can range from the most practical to the most simplified and idealized. Unfortunately but understandably, the simplified structures have been far more adequately tested than more realistic structures. Even actual structures analyzed experimentally have been those most readily available and not necessarily those most typical [14-18].

In comparison of methods, the most usual comparison has been between experimental results using  $^{60}\text{Co}$  or  $^{137}\text{Cs}$  with the Standard Method predictions (such predictions should be based on similar isotopic sources, but often have been based on the curves derived for the standard fallout spectrum). Also, there has been some work in which the Monte Carlo technique was used to predict results to be compared with either experimental measurements or Standard Method predictions. These types of comparisons form the bulk of the detailed discussions included in chapters VI, VIII, and X.

In addition, there have been studies to compare the Standard Method results with results from various alternative or derived methods [19-21]. Most of this work has been aimed at justifying application of the derived methods as substitutes having some kind of advantage in speed or simplicity.



Figure XI.3 gives sample comparisons of two computer codes currently in use<sup>4</sup> (1977), with hand calculations [19]. All three types of calculation are based on the Standard Method; and the data summarize results for various positions in 5 buildings, each 5 or 6 stories in height. Note that the same data on all buildings are being used in all cases, so that there are no errors of dimension or wall-thickness estimates. One sees that the data depart from agreement by factors nearly always less than 1.5, and that agreement between PF-COMP and the hand calculations in the important region of low PF's is much better than this.

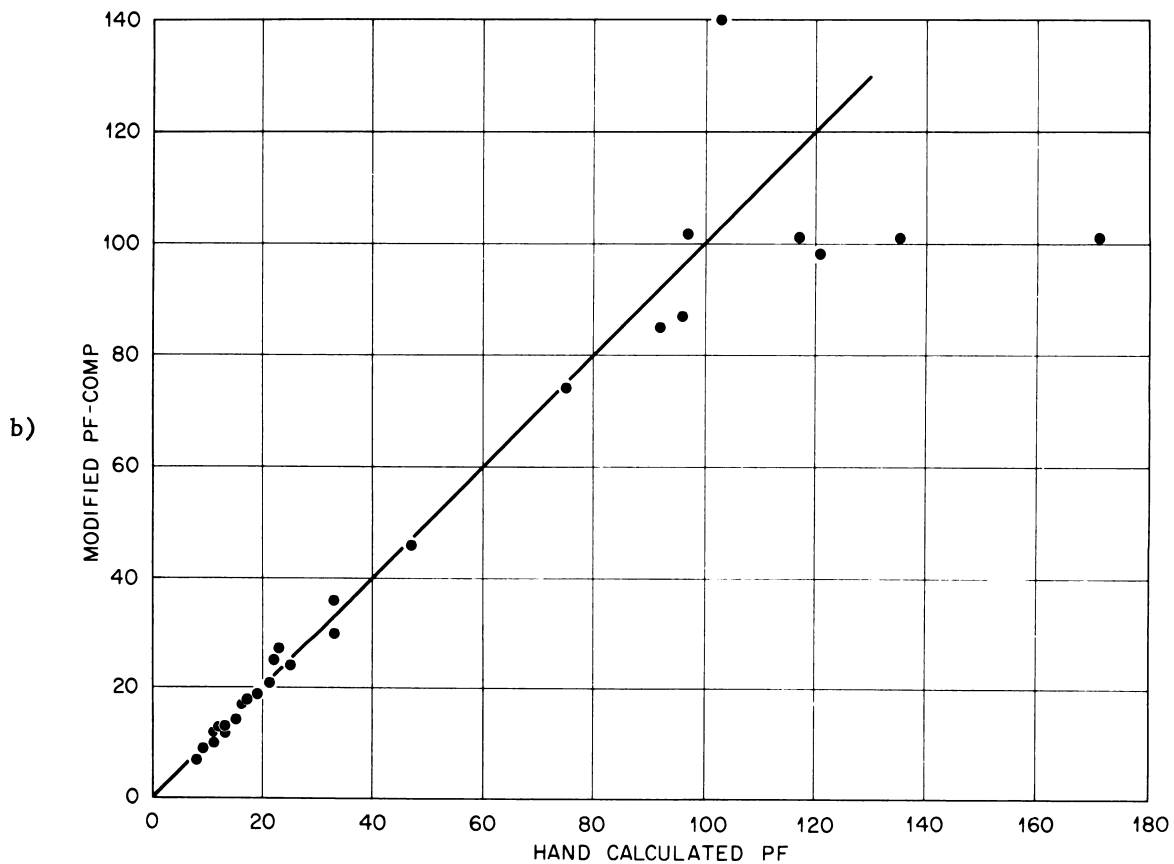
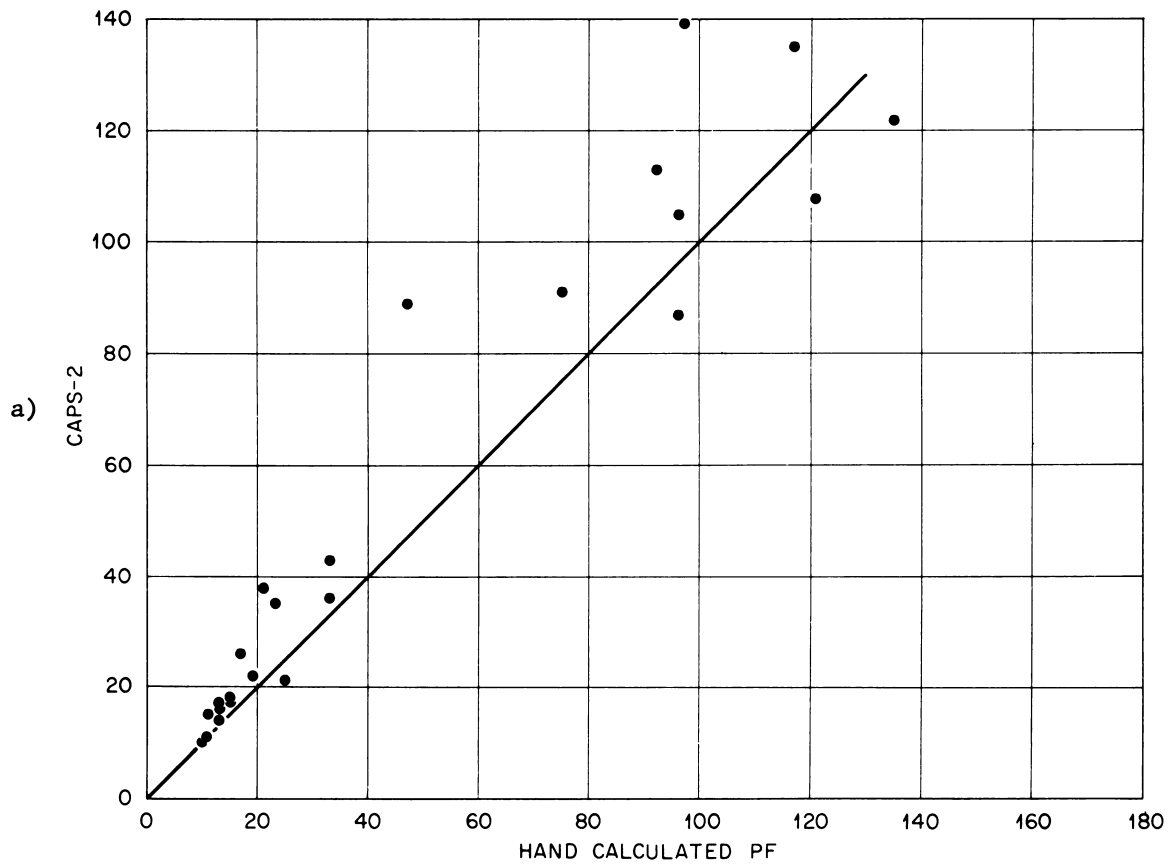
Figure XI.4 compares an earlier version of the CAPS-2 program with the small-structure Home Fallout Protection Survey (HFPS) results (see sec. I.B.6) [20]. The latter "derived" program uses standard dimensions and thicknesses which depart by varying amounts from the actual mass weights determined for the structures. The structure PF values mostly fell in the range from 15 to 35. One sees both a rather strong tail in both directions, and at the same time a tendency for perhaps 80% or better of the cases to agree within  $\Delta(\text{PF}) = 7.5$ , which corresponds to a ratio between estimates of perhaps 1.4 or a little less.

## 2. Studies Oriented Primarily Toward Accuracy Questions

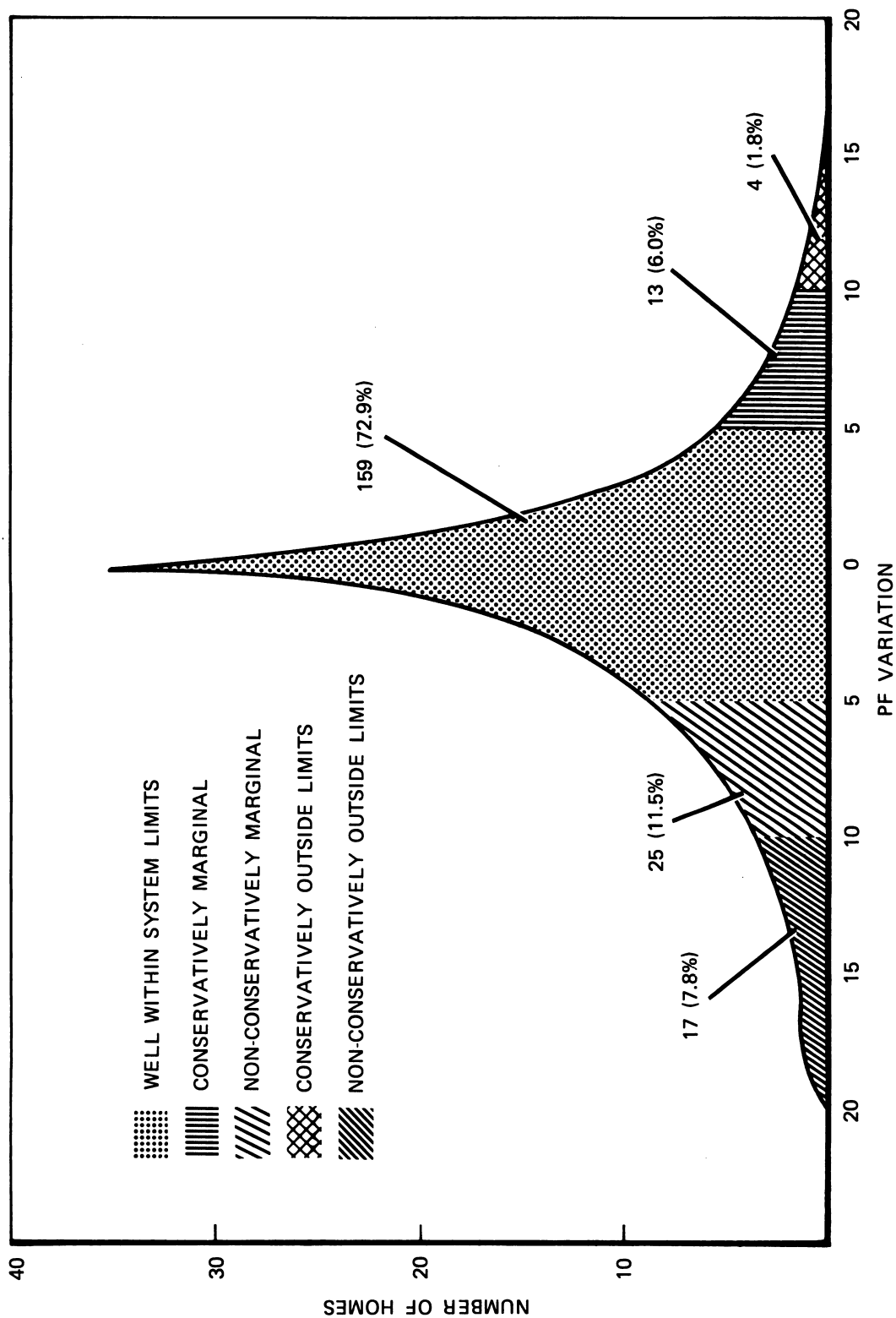
In a general way, the problem of accuracy can be divided into three parts; a) the realism of the conceptual model, b) the accuracy of the data developed for the model, and c) the accuracy of input data for real buildings. The first of these involves many factors which cannot be known prior to a given

---

<sup>4</sup>These two codes are designed to approximate the calculational details of the Standard Method and are designated as CAPS-2 and PF-COMP. The first of these was developed by the OCD, with the assistance of the Architect-Engineer firm of Praeger, Cavanaugh, and Waterbury [22]. PF-COMP was developed by personnel of the Research Triangle Institute [23].



XI.3 Comparison of Protection Factors Calculated a) with the CAPS-2 Code and with the Standard Method, and b) with the PF-COMP Code and with the Standard Method.



XI.4 Comparison study of the "derived" method for light structures, the HFPS method, using the CAPS program.

disaster; and quantitative estimates are correspondingly imprecise. The discussion in the first part of this chapter covers this question; and we do not discuss it further.

The "model" can be generally described as an idealized configuration exposed to an idealized fallout distribution, with the radiation describable by a single, specified spectrum. Unfortunately, because realistic spectra for fallout are difficult to obtain experimentally, the experimental approach has been largely confined to use of  $^{60}\text{Co}$  and  $^{137}\text{Cs}$ . Resulting data constitute only an indirect test of theoretical methods, as has been mentioned in chapters VI, VIII, and X.

The most direct tests of the accuracy of data developed for the model are comparisons with Monte Carlo calculations having small statistical deviations and a realistic mock-up of the actual configuration. Unfortunately, high quality calculations of this type are difficult and expensive; but even so, progress in this direction has been made [24-31]. Future developments should involve greater utilization of this approach.

Two general reviews of the question of accuracy have been made. One was a study prepared by the Subcommittee on Radiation Shielding of the National Academy of Sciences Advisory Committee on Civil Defense in 1965 [32]. The conclusions reached were largely based on the judgment of the members of the committee, resulting from their overall experience in applying the technology and doing research in it. It was estimated that under idealized fallout conditions, small structure analysis by the Standard Method should be able to get within a factor of 1.5 or better of the proper answer to the protection factor, except for the basement, where the error may be somewhat higher. This report points out, however, many of the same factors mentioned earlier in this

chapter regarding the possibility of substantial errors due to non-ideal fallout conditions, lack of knowledge of accurate structural thicknesses, and similar factors.

Subsequently, A. L. Kaplan made a quantitative study of systematic errors in the Standard Method as applied to simple rectangular structures, both above and below ground [33]. His procedure involved the analysis of barrier and geometry factor data, reviewing experimental and Monte Carlo data as well as information about the accuracy of the basic calculations. Kaplan determined that the systematic error for estimates of the shielding of above-ground structures is in the conservative direction; and his estimate for the magnitude  $\delta_{PF}$  of this error is  $\delta_{PF} \approx (.22 X_e)$  percent, where  $X_e$  measures wall thickness (in psf). A similar estimate by Kaplan for basements turned out to be in the non-conservative direction:  $\delta_{PF} \approx (40 - 0.36 X_c)$  percent, where  $X_c$  measures basement ceiling thickness. (However, this estimate for basements was based on an older version of the Standard Method and was one of the bases for subsequent revision discussed in section X.D. No revision of this estimate has since been made.)

In the analysis of existing buildings, by far the most serious source of error is in the estimation of the mass thickness of different wall segments and partitions, a problem which was discussed earlier in this chapter. These errors may very well far outweigh errors inherent in the methodology itself: for structural elements important to the shielding properties of a structure, this type of error in a structural element has an exponential effect which can result in overall errors much larger than a factor of 2. If such errors were random, the effect on the accuracy of the estimates would be somewhat like that shown in figure XI.4, i.e., a strong tail.

Unfortunately, if there is a systematic component in this type of error it is likely to be in the direction of too little material, or overestimation of the mass thickness. However, the requirements for accuracy tend to be most stringent when the protection provided by the structure is low rather than high. Fortunately, in these cases the mass thicknesses can be assessed somewhat more readily, and the protection is more dependent of configuration than a wall thickness.

### 3. Further Comments

The consequences of inaccuracies in the determination of protection factors (PF) depend on the perspective adopted as well as on the application to be made of the analysis. Up to this point we have assumed that the sole purpose is to save the life of the particular set of individuals shielded by the structure. It follows from this assumption that the analysis should preferably err only in the conservative direction, or else that it be supplemented by a "factor of safety" which would compensate for any errors in the unsafe direction. The question of accuracy relates to the magnitudes of PF estimations.

But if the purpose of the analysis is instead to find the safest place in an existing structure from the standpoint of fallout protection, one finds that PF magnitudes play a secondary role, and one is most concerned that relative PF values at different points be ordered correctly by the procedure. There has been little investigation of this question to date.

A situation with similarities to both the above exists when the analysis procedure is being used to study alternative design concepts for a shelter in a new structure in which the radiation protection capability is not the primary function. While the accuracy of shielding estimates may be of major concern relative to a pre-set criterion such as the requirement that the PF be at least 40, the concern may equally well focus on the question as to which

design offers better shielding, or whether two designs offer comparable shielding. In the latter cases the question of "absolute" accuracy is secondary to questions of proper ordering of different shielding configurations.

One important aspect of the accuracy problem which should be kept in mind is its relation to PF magnitudes. Kaplan's studies, which were discussed in the preceding section, confirm that the estimated percentage error is ordinarily larger when the estimated PF is larger. One can expect that additional errors due to inaccurate estimates of wall materials and masses is in the same direction; the larger, more complex, and massive a structure, the larger one can expect the combination of errors due to mis-estimations of component parts to be. This shows clearly in the comparisons of chapter X on large and complex structures. At the same time, however, larger percentage errors can be tolerated when the PF is large than when it is small: an expected error of factor of 3 would be intolerable for  $PF \approx 40$  estimates; but it is not so for  $PF \approx 1000$  estimates. Thus one finds that the overall situation is still in balance when percentage errors increase with PF estimates. One can take this argument a step further by maintaining that the ratio  $[\delta_{PF}(\text{percent})/PF]$  should ideally not exceed a specified criterion, say 0.5. Then one should aim at accuracies of 20% for  $PF \approx 40$  structures, but allow for factor of 5 errors with structures estimated to have  $PF \approx 1000$ . This reflects both the nature of the errors, and the relative importance. It does not, however, measure very well the potentiality for accurate estimates for comparatively simple structures, which can be an order of magnitude better than this.

## REFERENCES

- [1] Design and review of structures for protection from fallout gamma radiation, OCD Report PM-100-1, Interim Edition, 121 pages (Office of Civil Defense, February 1965).
- [2] Shelter Design and Analysis Fallout Radiation Shielding, TR20, Vol. 1, as amended by Change 1 (July 1969), Change 2 (Jan. 1970), and Change 3 (Nov. 1974), 445 pages (Dept. of Defense, Office of Civil Defense, July 1967).
- [3] Malich, C. W., and Beach, L. A., Radiation Protection Afforded by Barracks and Underground Shelters, NRL Report 5017, 45 pages (Sept. 18, 1957).
- [4] Lacayo, H., and Sullivan, M. A., Significance of Fallout Ingress into Shelters, Report TR683, 65 pages (Naval Radiological Defense Lab., San Francisco, Calif., Oct. 1967).
- [5] Howard, B. W., The Investigation of the Effect on Building Protection Factors of Ingress of Fallout through Apertures, Report RM1961, 14 pages (Research Triangle Institute, Durham, N.C., 1964).
- [6] Goldstein, R., The TERF Program and its Applications to the Calculation of Fallout Radiation Dose, NRDLTRC6856, 77 pages (Math. Applications Group, Inc., White Plains, NY, Jan. 1969).
- [7] Jaeger, R. G., ed. in ch., Neutron attenuation, Chapter 5, 259-362, Ducts and voids in shields, Chapter 8, 487-530, Engineering Compendium on Radiation Shielding, Vol. 1, Shielding Fundamentals and Methods (Springer-Verlag, New York, 1968).
- [8] Breslin, Al, Loysen, P., Weinstein, M. S., Protection Against Fallout Radiation in a Simple Structure, Project 32.1 Op. Plumbbob, Report WT-1462 (1963).
- [9] Strobe, W. E., Evaluation of Countermeasure System Components and Operations Procedures, USAEC Report WT-1464, NRDL 159 pages (Aug. 14, 1958).
- [10] Burson, Zolin, Comparison of Measurements in Above-Ground and Below-Ground Structures from Simulated to Actual Fallout Radiation. Civil Effects Text Organization Rpt. CEX 59.7B, 68 pages (1962).
- [11] Titus, F., Penetration in Concrete of Gamma Radiation from Fallout, USAEC Report ITR-1477, 32 pages (Aug. 22, 1958).
- [12] Lane, William B., Fallout Simulant Development: The Sorption Reactions of Cerium, Cesium, Ruthenium, Strontium, and Zirconium-Niobium, Standard Research Institute, Project No. MU-5068, Menlo Park, California, November 1965.
- [13] Lane, William B., Fallout Simulant Development: Temperature Effects on the Sorption Reactions of Cesium on Feldspar, Clay, and Quartz, SRI Project No. MU-6014, March 1967.



- [14] Clarke, E., Batter, J., and Kaplan, A., Measurement for Attenuation in Existing Structures of Radiation from Simulated Fallout, Tech. Ops. Rpt. T)-B 59-4, 101 pages (April 27, 1959).
- [15] Batter, J., Kaplan, A., and Clarke, E., An Experimental Evaluation of the Radiation Protection Afforded by a Large Modern Concrete Office Building, Civil Effects Test Org. Rpt. CEX 59.1, 69 pages (Jan. 22, 1960).
- [16] Strickler, T., and Auxier, J., Experimental Evaluation of the Radiation Protection Afforded by Typical Oak Ridge Homes Against Distributed Sources, Civil Effects Test Organization Rpt. CEX 59.13, 51 pages (April 14, 1960).
- [17] Borella, H., Burson, Z., and Jacovitch, J., Evaluation of the Fallout Protection Afforded by Brookhaven National Laboratory Medical Research Center, Civil Effects Test Org. Rpt. CEX 60.1 (October 1961).
- [18] Burson, Z. Experimental Evaluation of the Fallout-Radiation Protection Provided by Selected Structures in the Los Angeles Area, Civil Effects Test Org. Rpt. CEX 61.4, 106 pages (Feb. 26, 1963).
- [19] Gritzner, M. L., and Stevens, P. N., A Comparison of the Building Protection Factor Codes CAPS-2 and PF-COMP. Oak Ridge National Laboratory Report No. ORNL-TM-2285, 62 pages (Sept. 1968).
- [20] Status Report on Evaluation of Fallout Protection in Homes Program (EFPH) Tech. Serv. Direct. of the Office of Civil Defense, Unpublished Notes 25 pages (December 1965).
- [21] Lyday, R. O., Botkin, G. M., Hill, E. L., and Giesbrecht, F. G., Statistical Analysis of NFSS Protection Categories, Research Triangle Institute, R-OU-295, 128 pages (December 1968).
- [22] Durst, J. L., CAPS-2, A Computerized Method of Analyzing Structures for Radiation Shielding, Tech. Serv. Directorate, Off. of Civ. Def. (Jan. 1966).
- [23] Lyday, R. O., Wright, M. D., and Hill, E. L., PF-COMP Computer Program for Fallout Protection Factor Analysis of Buildings, Part I and II, Res. Tri. Inst. (1968).
- [24] French, R. L., Price, J. H., and Olmedo, L., Monte Carlo Study of Structure Shielding Against Fallout Radiation, Radiation Research Associates, Inc., RRA-T73, 58 pages (March 1967).
- [25] Price, J. H., and Frence, R. L., Monte Carlo Study of Interior Partition Effects on Fallout Shielding, Radiation Research Associates, Inc., RRA-T91, NRDL TRC-69-5, 51 pages (January 15, 1969).
- [26] Cohen, Martin O., Calculations of Dose Rates Arising from Radioactive Fallout Upon an Urban Environment, Defense Civil Preparedness Agency Report No. MR-7027, 65 pages (June 1972).
- [27] Hinkley, D. E., Monte Carlo Study of Gamma-Ray Attenuation in Structures with Basements, Radiation Research Associates, Inc., RRA-T703, 45 pages (July 8, 1970).

- [28] Stathoplos, A., Wills, L., Dose Rates in an Open Basement in a Simulated Fallout Field, Trans. Am. Nucl. Soc. 10, No. 2, 723-724 (Nov. 1967).
- [29] Berkerley, J. G., Preiser, S., Friedman, E. R., Stathoplos, A., Radiation Fields: Further Development and Application of the Gamma Adjoint Energy Transport (GADJET) Code, Navel Radiological Defense Laboratory, No. N00228-68-C-0701, 17 pages (August 1968).
- [30] Cohen, M. O., TERF Monte Carlo Fallout Code Calculations, Office of Civil Defense MR-7002, 50 pages (April 1970).
- [31] Morris, E. E., Monte Carlo Calculation of Gamma-Ray Penetration of Ribbed Slabs, University of Illinois Report No. NRSS-8 (NRDL TRC-68-53) 77 pages (December 1968).
- [32] Nat. Acad. of Sci. Advisory Comm. on Civil Defense, Subcommittee on Radiation Shielding, The accuracy of Radiation Shielding Calculations, pages (September 30, 1965).
- [33] Kaplan, Arthur L., The Accuracy of the Engineering Method for Calculating Structure Shielding, Report No. TO-B 69-23, NRDL-TRC-69-13, 42 pages (March 1969).

## XII. SHELTER PROGRAMS AND SYSTEMS

Design, construction, and analysis of fallout shelters have generally been in response to federal policies, which are in turn affected by many questions relating either to programs for the country as a whole, or to questions of the effectiveness of shelter systems taken as a whole. This subject is a large one; and while the final chapter in a series of chapters on the physical technology of fallout is not a suitable forum for a full discussion, it is a proper place to identify many of these considerations.

### A. SENSITIVITY STUDIES OF SHELTER PF CRITERIA

#### 1. Hypothetical Effectiveness of PF in Large Nuclear Disasters

In 1963 and 1964, a series of hypothetical-attack studies were conducted in OCD. These studies were classified and unavailable to the public; but an unclassified report by J. Romm based on some of the results was published in 1966 [1]. This report gave a justification for selection of the PF-40 criterion.

Typically, hypothetical-attack studies include

- a) an attack model,
- b) intensity distribution models for different phenomena,
- c) a fallout transport model
- d) a model giving distribution of population or resources,
- e) effects models giving primary damage in terms of fraction destroyed as a function of effect intensity,

and in the more sophisticated studies,

- f) system models, describing behavior of the damaged systems during the post-attack period.

Figure XII.1 gives data for a large attack (5500 Mt total) directed at a combination of military installations, population centers, and industrial targets. The ordinate is fixed as to general magnitude by the amounts of

fallout generated. The "population" referred to in the figure is that residual part of the total population exposed to less than a lethal blast overpressure.<sup>1</sup>

The argument made in the report is that if one makes the assumption that any exposure greater than 450 roentgens is lethal, while no lesser exposure is lethal, some 96% of the residual population would survive the fallout hazard in PF 40 shelter or better (unattenuated dose: < 18000 R); while 98% would survive in PF 100 shelter or better (unattenuated dose: < 45000 R). The PF 40 criterion is therefore considered appropriate, much larger fallout doses than 20000 R being considered quite unlikely.<sup>2</sup> [A further and more general statement in the report is that "well over 90% of the people who would otherwise die would be saved by 40 PF" in a real, rather than hypothetical, attack.]

One should be aware that an argument in percentages can look rather different in absolute numbers. Thus 96% survival corresponds roughly to 4 million fallout fatalities, whereas 98% survival corresponds to half that number; hence, when considered in terms of relative numbers of survivors it is less than certain that a PF of 40 is preferable to a PF of 100. This is the more true the larger the attack. Even so, there has been a tendency for the definition of "shelter" based on PF 40 to remain fixed. And in fact the main focus of attention has been on relaxing the criterion to PF 20 in regions with little PF 40 space.

---

<sup>1</sup>The report does not state the fraction of the populace represented by the residual population and hence at risk from the fallout. But from other data in the report one can surmise that the fraction surviving such an attack is estimated to be about half.

<sup>2</sup>Such questions of criteria are never really settled, except for some specified period of time. Not only would changing attack possibilities require reassessment, but also inclusion of considerations such as injury rather than lethality, radiation burden to a surviving populace, and synergistic effects of multiple injuries.

More information is available now about protection factor distributions in various types of communities; and there is now unclassified information available on important targets in the various states and on fallout patterns and intensities as affected by the location of important targets. A new review of this subject would be desirable, based on current estimates of attack capabilities and PF requirements as affected by location. But we do not expect the shape of the general curve of figure XII.1 to change very much. Further, an official PF criterion larger than 40 is unlikely without fresh emphasis on civil protection coupled with potential attack sizes at least several times that of the Romm study.

## 2. Overall Impact of Errors in Shielding Estimates

Further studies by C. Huddleston were made utilizing the data of figure XII.1, as well as data on lethality as a function of exposure rather than the assumption of 450 roentgens as a sharp cut-off to fully lethal exposures [2,3]. The purpose was to determine the sensitivity of the results to the extreme assumption of zero lethalties below 450 roentgens but 100% lethalties above; and also the sensitivity to random and systematic errors in the estimation of PF values.

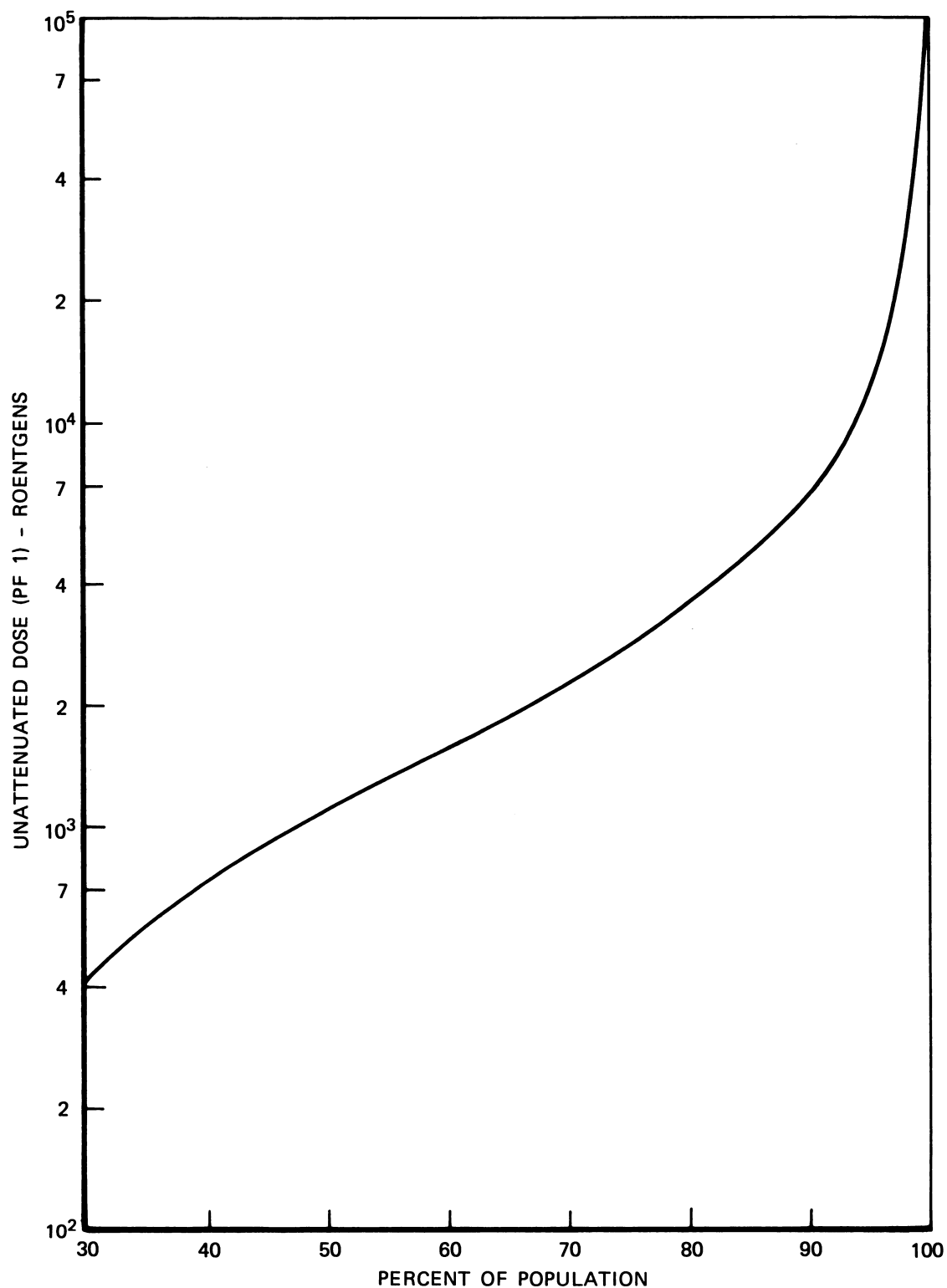
Huddleston's approach was as follows: He found that the data of figure XII.1 could be satisfactorily approximated by a standard type of probability distribution function called the cumulative "log-normal" curve (see footnote 9 of chapter II)<sup>3</sup> He also used this type of function to represent a lethality

---

<sup>3</sup>Let  $F$  stand either for the fraction exposed to greater than  $D$  roentgens, as in fig. XII.1, or for the fraction for which an exposure of  $D$  roentgens is lethal. Then

$$F \sim \int_0^D dx \frac{1}{\sqrt{2\pi} \sigma x} \exp \left\{ -\frac{1}{2} \left[ \frac{\log (x/x_0)}{\sigma} \right]^2 \right\},$$

where  $\sigma, x_0$  are characteristic constants for either case, and the integrand is the function usually called the "log-normal" distribution. The integral  $F$  is called the cumulative log-normal distribution.



XII.1 Distribution of the unattenuated (i.e. unshielded) dose due to fallout radiation according to the percent of the population in regions with less than the indicated value. The population figures refer to those surviving direct effects such as blast and thermal radiation.

distribution with midpoint at 450 rems, beginning at 250 rems, and approaching unity, i.e. 100% likelihood, for a dose as large as 650 rems. The type of results desired required evaluation of an integral

$$L = \int_0^{\infty} dD P(D) Q(D) \quad , \quad (\text{XII.1})$$

where  $P(D)$ , the probability for exposure to  $D$  roentgens, is the derivative of the curve of figure XII.1; and  $Q(D)$  is the probability of lethality for such an exposure. This integral can be evaluated in terms of the well-known error function. Further, because PF values different from unity behave as scale factors in figure XII.1 they also behave as scale factors in the expression resulting from integration of eq (XII.1). Estimates of casualties resulting from these calculations turn out to differ hardly at all from those obtained by applying the 450 roentgen criterion to the data of figure XII.1.

To take account of random errors in shelter PF estimates, Huddleston assumed that such error probabilities also follow a log-normal curve of unknown width, this being easily combined with his previous results. In particular, he assumed that  $R_O(PF, \beta) d(PF)$  is a log-normal probability distribution for PF for which  $\beta$  is the estimated value, with a peak-width measured by the standard deviation  $\sigma$ .<sup>4</sup>

---

<sup>4</sup>By the properties of the log-normal function,

$$R_O(PF, \beta) d(PF) = R_O\left(\frac{1}{PF}, \frac{1}{\beta}\right) d\left(\frac{1}{PF}\right) = R_O\left(\frac{D}{D_O}, \beta^{-1}\right) \frac{dD}{D_O} \quad ,$$

where  $D_O$  is the dose outside, and  $D$  the dose inside a shelter of nominal PF given by  $\beta$ . Equation (XII.1) then has the more complicated form of a double integral:

$$L_O(\beta) = \int_0^{\infty} dD_O \int_0^{D_O} dD P(D_O) Q(D) R_O\left(\frac{D}{D_O}, \beta^{-1}\right) / D_O \quad .$$

However, this double integral can be evaluated in terms of the error function as readily as eq (XII.1).

Two sets of calculations were then performed, which are summarized in tables XII.1 and XII.2. The values of table XII.1 are to be interpreted in connection with a calculated value of 68% deaths due to fallout in the residual population in absence of any shelter whatsoever. Figure XII.2 shows the error curves for the PF estimates which correspond to the last three columns in this table. One concludes from the small effect even with very wide error curves that estimates of survival percentages are insensitive to random errors in the PF estimates, even for quite inaccurate methods, providing that the average estimate for many structures is correct.

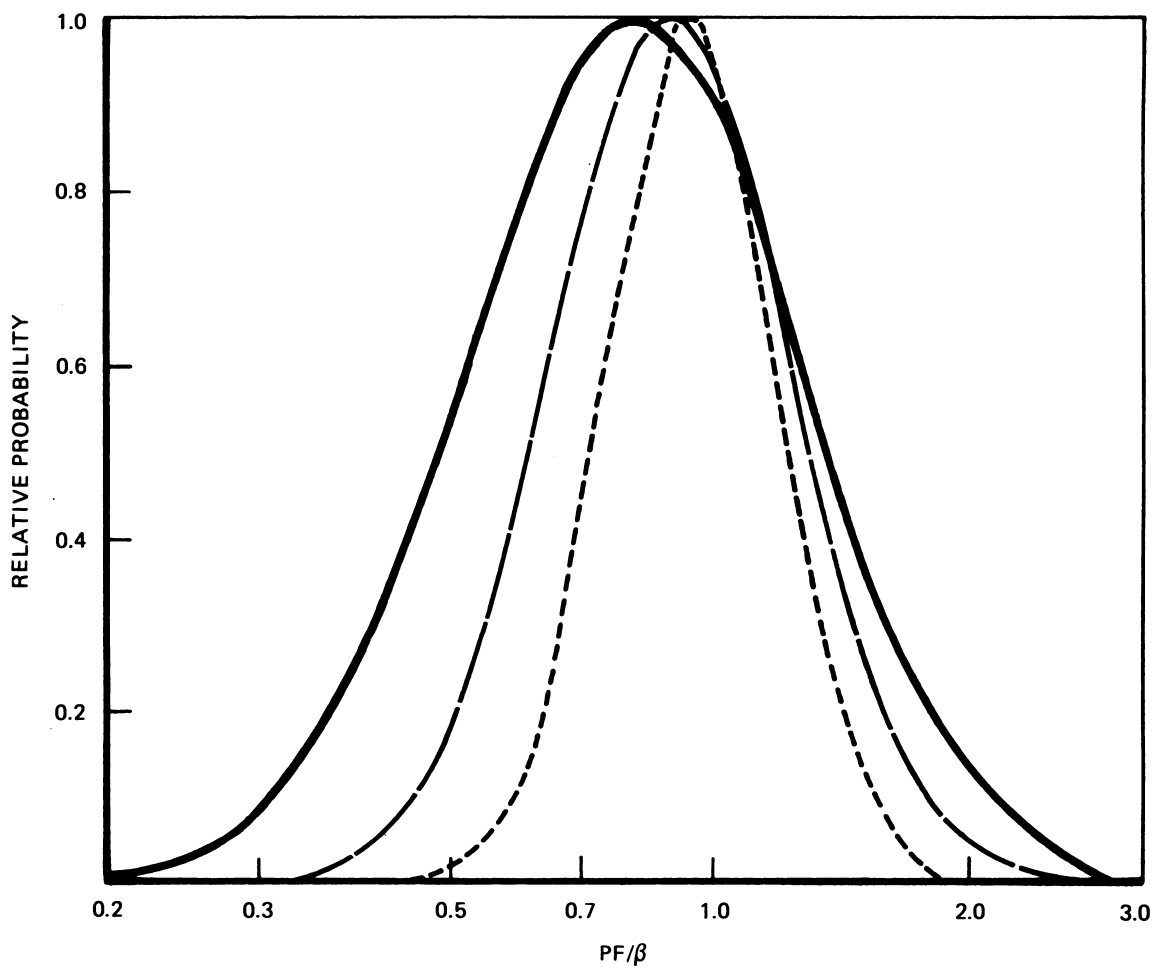
On the other hand, systematic errors would result in underestimates or overestimates of PF values on the average. Table XII.2 gives data for this case. This table shows that in the range of PF values of greatest interest, the percentage increase in lethality is roughly equal to the percentage deficiency in the mean of estimated PF values.

While larger PF values of table XII.2 correspond to more imprecise lethality figures they also correspond systematically to smaller numbers of lethality. Clearly accuracy in the PF estimates is more important for low PF structures than for high PF structures, as noted in section XI.D.3.

#### B. FALLOUT AND OTHER BURST PHENOMENA

Problems of fallout shielding interact in some way with each of the other major explosion phenomena of fire, initial radiation, and blast, and these interactions should be noted. Perhaps the most important interactions, however, have to do with position and type of detonation. If the fireball does not intersect the ground, the fallout particles are so small that essentially no local fallout results. Hence a nuclear attack limited to air detonations would not create conditions requiring shielding against local fallout, although shielding problems against the gamma rays and neutrons initially produced in





XII.2 Curves of estimated PF probability distributions for three different Standard Deviations: .23, .34, and .52.

Table XII.1 Consequence of random error in shelter factor calculations

PF	% Deaths	% Added Deaths		
<u>Median</u>	<u>(SD = 0)</u>	<u>SD = .23</u>	<u>.34</u>	<u>.52</u>
5	30.1	.17	.35	.69
10	17.1	.23	.46	.92
20	8.45	.20	.41	.82
40	3.55	.13	.27	.54
70	1.58	.08	.16	.33
100	.89	.05	.11	.22

SD means fractional standard deviation, i.e.,  $[E(PF^2) - E^2(PF)]^{1/2}/PF$ , where  $E(PF)$  is the expectation value.

Table XII.2 Consequence of systematic error in shelter factor calculations

<u>Mean PF</u>	<u>% Deaths + Incremental Deaths due to 10% <math>\beta</math> error</u>	<u>% Change % <math>\beta</math> error</u>
5	30.1 $\pm$ 2.2	0.72
10	17.1 $\pm$ 1.6	0.93
20	8.4 $\pm$ 1.0	1.14
40	3.5 $\pm$ .5	1.40
70	1.6 $\pm$ .25	1.56
100	.9 $\pm$ .15	1.67

$\beta$  corresponds to the PF estimate, which differs slightly from mean and mode values.

the burst would remain unless burst point altitudes were high. Since air detonations expose the maximum area to large blast effects, mixed attacks including both air and ground bursts have been most closely studied.

A second variable of the same type has to do with weapon construction. The amount of fission product material in the fallout is proportional to the number of fissions occurring in the burst, and this depends on the ratio of fission to fusion in the weapon design. Since no purely fusion weapons are known to exist, the fission product material is assumed to produce the bulk of the residual radioactivity; and chapter II is based on this assumption.

On the other hand, fallout is known to contain radioactive materials whose activity results from capture of neutrons by non-fissionable material in the weapon. This contribution to the radioactivity is usually neglected, but in one case it could be of great importance: Conceivably, materials which produce a long-lived isotope such as  $^{60}\text{Co}$  could be introduced into weapons. This would alter the character of the fallout spectrum in a major way at long times after the burst. As indicated in section II.C.2, such "salting" of weapons was of major concern during the years immediately following the development of thermonuclear devices [4]. But the importance of this design modification was never demonstrated, and the motivation for increasing long-term hazards in this manner is lacking. This possibility is thus not taken seriously.

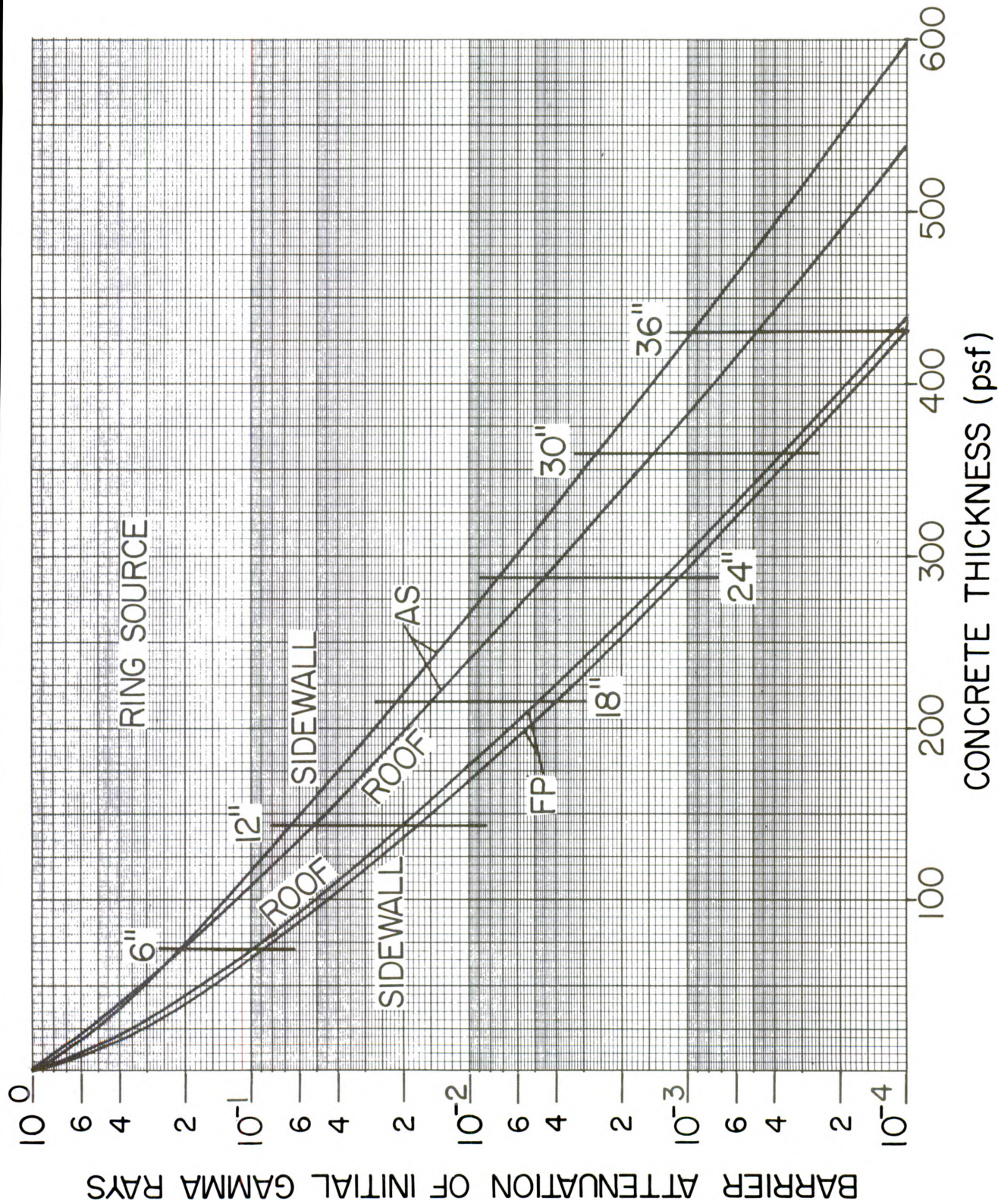
The primary interaction between fallout and blast is the destruction of fallout shelters at high overpressures. Further, because there tends to be a preponderance of high-quality fallout shelter in metropolitan areas, destruction of such shelters could seriously reduce the number of shelter spaces actually available to survivors of blast effects. This suggests an importance which attaches to a knowledge of the structural characteristics of shelters, to

widespread distribution outside metropolitan areas, and to the ability to monitor radiation intensities routinely. Areas which could be subjected to high blast overpressures tend to be 10 to 100 times smaller than areas which could be subjected to intense fallout radiations. Hence such interactions with prompt effects apply mainly to cities, and to areas adjacent to cities.

The main interaction between fallout and initial radiations is the additive biological consequences of two exposures to penetrating radiations within a short time interval. Initial radiations tend to be more penetrating than fallout radiation, as shown by comparing figure V.23 with figure XII.3 [5] (see also [6,7]). Where initial radiations are a problem they also may be far more intense than fallout radiations. Hence there would exist around any burst point (except for very large bursts, 10 megatons and greater, say) a ring where destruction due to blast effects is only partial, and where significant exposures to initial radiations would occur. Survivors in such locations would be less resistant to subsequent fallout radiations. Shielding against initial radiations is under investigation at present, as is their importance vis à vis blast hazards.

Interactions between fire and fallout tend to be more complicated, in part because fire is itself a delayed effect. Close-in fallout arrives within an hour, but fire growth occurs over a period of perhaps as much as two hours, although fires in individual buildings may develop more rapidly. Hence for individual bursts, close-in fallout is deposited before there can be much effect due to massive fires. But it is then possible for the fallout to be re-elevated by vertical and turbulent air movements, with subsequent re-deposition downwind [8,9]. This has consequences both for the downwind areas and for any burnt-over area; but neither the increase of fallout in the one area, nor the decontamination effect of the other area has been adequately





XII.3 Barrier attenuation of air-secondary (AS) and fission-product (FP) gamma rays from a distant detonation at 30° elevation angle above the horizontal, averaged over the "ring" of possible directions.

studied. Likewise, in the case of multiple bursts, fallout deposition from one detonation may occur in the vicinity of a second detonation with a delay which permits fire turbulence at the time of deposition. The result should again be decreased contamination of the fire area and increased fallout deposition farther downwind.

Perhaps the most serious interaction of this type would be very large fires in relatively undamaged but populous areas already subjected to intense fallout. This can force the affected populace out of shelter into a serious radiation hazard. Estimates of the magnitude of such a problem have been made which show that it could be a major factor in determining casualties for a detonation giving rise to these multiple effects [10].

Highly relevant to the analysis of fire hazards is the fact that there are many factors which determine whether a given neighborhood is or is not susceptible to mass fires; and an understanding of these factors should make it possible to ascertain those areas where there is a comparatively high probability that such fires would occur [11]. Among these factors are fairly obvious things such as the area density of flammable material and the presence of natural firebreaks such as parks. Less obvious factors include the number of windows through which materials which can serve as tinder are visible to a large solid angle of the sky, the number of people available to put out incipient fires, times required for "flashover," and the extent of blast damage.

### C. FALLOUT SHELTERS AND STRATEGIC EVACUATION

The special problems due to high population density in large cities have, at various times, given rise to study of the possibilities of the partial evacuation of city areas. Before the development of missiles (mid-1950s), this was considered as a tactical option to take place during the hours

required for bomber missions. More recently the thought has been that evacuation should be an option in event of a highly credible threat of attack, thus assuming more a strategic than tactical nature [12]. In addition, the experience of Hiroshima and Nagasaki indicates that temporary evacuation of extensively damaged city areas is to be expected, because it may be thought the safest course of action by threatened individuals and groups.

Whether planned or unplanned, large-scale evacuations must put great strain on unaffected areas of the country which are close enough to receive the displaced individuals; and the sufficiency of available fallout shelter would be affected [13].

In partial response to this type of problem, there has been a major series of studies of the nature and requirements for "strategic evacuation", and sponsored by the Defense Civil Preparedness Agency (DCPA). Another type of response has been the development and testing of "expedient" fallout shelters which offer possibilities for construction when in-place shelters are not available [14-17].



## REFERENCES

- [1] Romm, Joseph, Background of Civil Defense and Current Damage Limiting Studies, Dept. of Defense, Office of Civil Defense Report No. TR 35 35 pages (June 1966).
- [2] Huddleston, Charles, Some Calculations on Protection Factors and Lethalities. U. S. Naval Civil Engineering Laboratory, unpublished notes, 10 pages (May 1966).
- [3] Huddleston, Charles, The Need for Accuracy in Protection Factor Calculations. 13 pages, unpublished notes (July 28, 1967).
- [4] Dunning, G. M., Cobalt-60 bombs, Health Physics 4, 52-54 (1960).
- [5] Spencer, L. V., Structure Shielding Against Initial Radiation from Nuclear Explosions. I. Attenuation of Air Secondary and Fission Product Gamma Rays. Nucl. Sci. Eng. 57, 129-154 (1975).
- [6] French, R. L., and Mooney, L. G., Initial Radiation Exposure from Nuclear Weapons. Office of Civil Defense, RRA-T7201, 78 pages, (July 15, 1972).
- [7] Glasstone, S., ed., The Effects of Nuclear Weapons, Revised Edition, 730 pages (United States Atomic Energy Commission, Washington, D.C., April 1962).
- [8] Land, William B., and Lee, Hong, Effects of Mass Fires on Fallout Deposition, U.S. Army, Office of the Civil Defense, Report No. NRLD-TRC-68-22, 25 pages (February 1968).
- [9] Broido, A., and McMasters, A. W., The Influence of a Fire-Induced Convection Column of Radiological Fallout Patterns, U.S. Dept. of Argri., Forest Service, Tech. Paper No. 32, 45 pages (March 1959).
- [10] La Riviere, P. D., and Lee, H., Postattack Recovery of Damaged Urban Areas, Stanford Research Institute, Menlo Park, California, (November 1966).
- [11] Wiersma, Steve J., and Martin, Stanley B., The Nuclear Fire Threat to Urban Areas. Defense Civil Preparedness Agency, Contract DAHC20-70-C-0219, 73 pages (April 1975).
- [12] Chester, C. V., Cristy, G. A., and Haaland, C. M., Strategic Considerations in Planning a Counterevacuation. Oak Ridge National Laboratory, ORNL-4888 102 pages (December 1975).
- [13] Haaland, C. M., Chester, C. V., and Wigner, E. P., Survival of the Relocated Population of the U.S. After a Nuclear Attack. Oak Ridge National Laboratory ORNL-5041, 209 pages (June 1976).
- [14] York, S. B., Wright, M. D., and Hill, E. L., Alternative Ways of providing Host Area Fallout Protection. Defense Civil Preparedness Agency 44U-988 178 pages (December 1975).

- [15] Kearny, Cresson H., Expedient Shelter Construction and Occupancy Experiments Oak Ridge National Laboratory, ORNL-5039, 194 pages (March 1976).
- [16] Beer, Mendel, and Cohen, Martin O., Effectiveness of Soil as Shielding for Expedient Fallout Shelters, Mathematical Applications Group, Inc. Elmsford, New York, Report MR-7047, 45 pages (April 1976).
- [17] Cohen, Martin O. and Beer, Mendel, The Use of Soil as an Expedient Countermeasure for Rural Fallout Shelters, Mathematical Applications Group, Inc., Elmsford, New York, Report MR-7042, 43 pages (Oct. 1974).

1. Spherical Functions<sup>1</sup>

## a. Description

Directionally-dependent quantities such as fluence are frequently represented by superpositions of Legendre functions; and it is therefore essential to refer to the elementary properties of these functions. For this purpose any standard treatise on spherical harmonics should be adequate; and we list here only a few of the more relevant and fundamental formulae.

We use the  $Y_{\ell}^m$  notation, with definitions as given in reference [2]:

DEFINITION:

$$Y_{\ell}^m(\theta, \phi) = (-1)^m \left[ \frac{2\ell + 1}{4\pi} \frac{(\ell - m)!}{(\ell + m)!} \right]^{\frac{1}{2}} P_{\ell}^m(\cos\theta) e^{im\phi}, \quad (\text{A.1})$$

where  $P_{\ell}^m(\cos\theta)$  designates the Legendre polynomial,

$$P_{\ell}^m(x) = \frac{(-1)^m}{2^{\ell} \ell!} (1 - x)^{m/2} \left( \frac{d}{dx} \right)^{\ell+m} (x^2 - 1)^{\ell}, \quad m \geq 0,$$

$$P_{\ell}^{-m}(x) = (-1)^m \frac{(\ell - m)!}{(\ell + m)!} P_{\ell}^m(x). \quad (\text{A.2})$$

Possibilities for using these functions to represent angular distributions result from the fact that arbitrary integrable functions  $F(\theta, \phi)$  can be represented in the series form

REPRESENTATION:

$$F(\theta, \phi) = \sum_{\ell=0}^{\infty} \sum_{m=-\ell}^{\ell} \left( \frac{2\ell + 1}{4\pi} \right)^{\frac{1}{2}} F_{\ell}^m Y_{\ell}^m(\theta, \phi), \quad (\text{A.3})$$

---

<sup>1</sup>For reference see, e.g., [1].

where the coefficients  $F_{\ell}^m$  are given by the integrals

$$F_{\ell}^m = \left( \frac{4\pi}{2\ell + 1} \right)^{\frac{1}{2}} \int_{4\pi} d\Omega \bar{Y}_{\ell}^m(\theta, \phi) F(\theta, \phi) , \quad (\text{A.4})$$

and  $\bar{Y}_{\ell}^m$  is the complex conjugate of  $Y_{\ell}^m$ .

The expression for coefficients follows by application of the property of orthogonality,

ORTHOGONALITY:

$$\int_{4\pi} d\Omega \bar{Y}_{\ell}^{m'}(\theta, \phi) Y_{\ell}^m(\theta, \phi) = \delta_{\ell\ell'} \delta_{mm'} . \quad (\text{A.5})$$

It is worth noting that as defined in eq (A.4) the coefficients  $F_{\ell}^0$  are just the usual Legendre polynomial coefficients.

Table A.1 presents a brief list of these functions, to aid those who need to familiarize themselves with the notation and formulae.

#### b. Some Other Important Properties

Let  $\cos\Theta = \hat{\Omega} \cdot \hat{\Omega}' = \cos\theta\cos\theta' + \sin\theta\sin\theta' \cos(\phi - \phi')$  be the cosine of the angle between two unit directions vectors,  $\hat{\Omega}$  and  $\hat{\Omega}'$ . The scattering kernels of radiation transport commonly depend on this variable, and can therefore be represented using eqs (A.3) and (A.4),

$$K(\Theta) = \sum_{\ell=0}^{\infty} \left( \frac{2\ell + 1}{4\pi} \right) K_{\ell} Y_{\ell}^0(\Theta) , \quad (\text{A.6})$$

where  $K_{\ell} = K_{\ell}^0$  is defined as in eq (A.4). Further analysis involving such functions depends on the additional property

Table A.1 The first few spherical functions  $Y_l^m(\theta, \phi)$  [39].

$Y_0^0 = \sqrt{\frac{1}{4\pi}} [1]$	$Y_1^1 = \sqrt{\frac{3}{4\pi}} \left(\frac{1}{2}\right) [-\sin\theta] e^{i\phi}$	$Y_2^2 = \sqrt{\frac{5}{4\pi}} \left(\frac{1}{24}\right) [3\sin^2\theta] e^{i(2\phi)}$	$Y_3^3 = \sqrt{\frac{7}{4\pi}} \left(\frac{1}{6!}\right) [-15\sin^3\theta] e^{i(3\phi)}$
$Y_1^{-1} = \sqrt{\frac{3}{4\pi}} (2) \left[\frac{1}{2} \sin\theta\right] e^{-i\phi}$	$Y_1^0 = \sqrt{\frac{3}{4\pi}} [\cos\theta]$	$Y_2^1 = \sqrt{\frac{5}{4\pi}} \left(\frac{1}{6}\right) [-3\sin\theta\cos\theta] e^{i\phi}$	$Y_3^2 = \sqrt{\frac{7}{4\pi}} \left(\frac{1}{5!}\right) [15\sin^2\theta\cos\theta] e^{i(2\phi)}$
$Y_2^{-2} = \sqrt{\frac{5}{4\pi}} (24) \left[\frac{3}{24} \sin^2\theta\right] e^{-i(2\phi)}$	$Y_2^{-1} = \sqrt{\frac{5}{4\pi}} 6 \left[\frac{3}{6} \sin\theta\cos\theta\right] e^{-i\phi}$	$Y_2^0 = \sqrt{\frac{5}{4\pi}} \left[\frac{3}{2} \cos^2\theta - \frac{1}{2}\right]$	$Y_3^1 = \sqrt{\frac{7}{4\pi}} \left(\frac{2}{4!}\right) \left[-\sin\theta\left(\frac{15}{2}\cos^2\theta - \frac{3}{2}\right)\right] e^{i\phi}$
$Y_3^{-3} = \sqrt{\frac{5}{4\pi}} (6!) \left[\frac{15}{6!} \sin^3\theta\right] e^{-i(3\phi)}$	$Y_3^{-2} = \sqrt{\frac{7}{4\pi}} (5!) \left[\frac{15}{5!} \sin^2\theta\cos\theta\right] e^{-i(2\phi)}$	$Y_3^{-1} = \sqrt{\frac{7}{4\pi}} \left(\frac{4!}{2}\right) \left[\frac{2}{4!} \sin\theta\left(\frac{15}{2}\cos^2\theta - \frac{3}{2}\right)\right] e^{-i\phi}$	$Y_3^0 = \sqrt{\frac{7}{4\pi}} \left[\frac{5}{2} \cos^3\theta - \frac{3}{2} \cos\theta\right]$

ADDITION FORMULA:

$$Y_{\ell}^0(\Theta) = \left( \frac{4\pi}{2\ell + 1} \right) \sum_{m=-\ell}^{\ell} \bar{Y}_{\ell}^m(\theta', \phi') Y_{\ell}^m(\theta, \phi) \quad . \quad (\text{A.7})$$

This property, together with orthogonality, gives a transformation which we refer to as a "folding rule",<sup>2</sup>

$$\int_{4\pi} d\Omega \bar{Y}_{\ell}^m(\theta, \phi) K(\Theta) = K_{\ell} \bar{Y}_{\ell}^m(\theta', \phi') \quad . \quad (\text{A.8})$$

Lastly, let us note a recursion which links the spherical functions chainwise:

RECURSION:

$$\begin{aligned} \cos\theta Y_{\ell}^m(\theta, \phi) &= \left[ \frac{(\ell + 1)^2 - m^2}{(2\ell + 1)(2\ell + 3)} \right]^{\frac{1}{2}} Y_{\ell+1}^m(\theta, \phi) \\ &+ \left[ \frac{\ell^2 - m^2}{(2\ell + 1)(2\ell - 1)} \right]^{\frac{1}{2}} Y_{\ell-1}^m(\theta, \phi) \quad . \quad (\text{A.9}) \end{aligned}$$

Other recursion formulae exist, but we need not refer to them in this monograph.

#### c. Application to the Point-to-Plane Source Conversion

Let us use the preceding formulae to express the plane source eq (III.22) in Legendre functions for isotropic sources, for the set of disk and ring source cases having their center below the detector. We take  $N_{PL} = N^{PL}(\vec{\Omega} \cdot \vec{k}, z)$  and  $N_{PT} = N^{PT}(\vec{\Omega} \cdot \vec{u}, |\vec{r} - \vec{r}_0|)$ , where  $\vec{u} = \frac{\vec{r} - \vec{r}_0}{|\vec{r} - \vec{r}_0|}$ . Multiplying eq (IV.22) by  $\sqrt{4} \bar{Y}_{\ell}^0(\theta, \phi) = P_{\ell}(\vec{\Omega} \cdot \vec{k})$ , we obtain, by integration over all directions  $\vec{\Omega}(\theta, \phi)$ ,

---

<sup>2</sup>This rule is not explicitly identified in the literature on Legendre functions.

$$N_{\ell}^{PL}(z) = \int_{-\infty}^{\infty} dx_o \int_{-\infty}^{\infty} dy_o S_o \sqrt{4\pi} \int d\Omega \bar{Y}_{\ell}^o(\theta, \phi) N_{\ell}^{PT}(\vec{\Omega} \cdot \vec{u}, |\vec{r} - \vec{r}_o|) \quad (A.10)$$

The folding rule, eq (A.8), together with the change to spherical coordinates shown in eq (A.10), then give

$$N_{\ell}^{PL}(z) = 2\pi \int_{R_s}^{R_m} R dR N_{\ell}^{PT}(R) P_{\ell}(z/R) \quad , \quad (A.11)$$

since  $z/R = \vec{u} \cdot \vec{k}$ . The integration limits are the rectilinear distances to inner ( $R_s$ ) and outer ( $R_m$ ) source edges.

## 2. U-Functions

To represent space distributions which have exponential trends, while at the same time utilizing the available alternate moments, the U-functions developed by Spencer and Fano have been very useful (see refs. [3,4]). We again list only the more directly useful formulae and refer the reader to the references just listed for a more complete presentation.

### a. Description

The U-functions are biorthogonal, viz., eq (A.16), and hence definitions are needed of two types of functions. For many purposes, the following definitions should be adequate:

DEFINITIONS:

$$e^{-|z|} U_n^k(z) = \frac{(-1)^{n+k}}{2^n n!} \sqrt{\frac{2}{\pi}} \left( \frac{d}{dz} \right)^{2n+k} \left[ |z|^{n+\frac{1}{2}} K_{n+\frac{1}{2}}(|z|) \right] \quad , \quad (A.12)$$

$$z^k \hat{U}_n^k(z) = \sum_{i=0}^n (-1)^i \binom{n}{i} \frac{z^{2i+k}}{(2i+k)!} \quad , \quad (A.13)$$

where, in eq (A.12), singular features at  $z = 0$  should be ignored.<sup>3</sup> As required, the approximating functions in eq (A.12) are basically exponential, and the adjoint functions in eq (A.13) are mainly polynomials in  $z^2$ .

Representations of space distributions  $D(z)$  utilize the standard type of expression

REPRESENTATIONS:

$$F(z) = \sum_{n=0}^{\infty} F_n U_n^k(z) \quad , \quad -\infty < z < \infty \quad , \quad (A.14)$$

or

$$G(r) = \sum_{n=0}^{\infty} G_n U_n^k(r) \quad , \quad 0 \leq r < \infty \quad , \quad (A.14')$$

where the coefficients  $F_n, G_n$  are given by

$$\begin{aligned} F_n &= \frac{1}{2} \int_{-\infty}^{\infty} dz \, e^{-|z|} z^k \hat{U}_n^k(z) F(z) \\ &= \sum_{i=0}^n (-i)^i \binom{n}{i} \left[ \frac{1}{2} \int_{-\infty}^{\infty} dx \, \frac{z^{2i+k}}{(2i+k)!} F(z) \right] \quad , \quad (A.15) \end{aligned}$$

or

$$\begin{aligned} G_n &= \int_0^{\infty} dr \, e^{-r} r^k U_n^k(r) G(r) \quad , \\ &= \sum_{i=0}^n (-i)^i \binom{n}{i} \left[ \int_0^{\infty} dr \, \frac{r^{2i+k}}{(2i+k)!} G(r) \right] \quad . \quad (A.15') \end{aligned}$$

---

<sup>3</sup>Expressions which automatically suppress such singularities are given in reference [5] but are not useful here.



Clearly the  $F_n, G_n$  are linear combinations of the first  $n$  even or odd moments.

It is important to note that the factors  $z^k e^{-|z|}, r^k e^{-r}$  can, in whole or in part, be removed from the integrand of eqs (A.15) and (A.15') and attached to the right side of eqs (A.14) and (A.14'), if it is necessary to obtain adequate description of the function. The form for the coefficients given by eqs (A.15) and (A.15') follows from biorthogonality property of the functions,

BIORTHOGONALITY:

$$\frac{1}{2} \int_{-\infty}^{\infty} dz z^k e^{-|z|} \hat{U}_n^k(z) U_{n'}^k(z) = \delta_{nn'},$$

$$\int_0^{\infty} dr r^k e^{-r} \hat{U}_n^k(r) U_{n'}^k(r) = \delta_{nn'}, \quad (A.16)$$

Table A.2 gives data from which a representative set of the U-Functions can be written down or calculated.

Let us note that eq (A.16) applies equally well if we change our definitions to  $(c_n \hat{U}_n)$  and  $(U_n/c_n)$ . This modification does not change the approximation at all; but it does change not only the adjoint function but also the sequence of coefficient values. If we make this simple change in eq (A.14') and then apply the Schwarz inequality to the higher terms ( $n > N$ ) of the series, we obtain an inequality which can be used as a basis for estimating error limits:

Table A.2 Coefficients  $u_{ni}^k$  for the polynomial representation

$$U_n^k(r) = \sum_{i=0}^n u_{ni}^k r^i.$$

		k = 0				
n \ i		0	1	2	3	4
0	1					
1	.500000		-.5000			
2	.375		-.625	.125		
3	.3125		-.6875	.250	-.0208333	
4	.273437		-.726563	.357188	-.0572916	.0026041

		k = 1				
n \ i		0	1	2	3	4
0	1					
1	1		-.50000			
2	1		-.875	.125		
3	1		-1.1875	.3125	-.0208333	
4	1		-1.460938	.539063	-.067708	.0026041

		k = 2				
n \ i		0	1	2	3	4
0	1					
1	1.5		-.5			
2	1.875		-1.125	.125		
3	2.1875		-1.8125	.375	-.0208333	
4	2.46094		-2.53906	.74219	-.078125	.0026041

		k = 3				
n \ i		0	1	2	3	4
0	1					
1	2		-.5			
2	3		-1.375	.125		
3	4		-2.5625	.4375	-.0208333	
4	5		-4.02344	.97656	-.088542	.0026041

		k = 4				
n \ i		0	1	2	3	4
0	1					
1	2.5		-.5			
2	4.375		-1.625	.125		
3	6.5625		-3.4375	.5	-.0208333	

$$\begin{aligned}
|G(r) - G_N(r)| &\leq \left[ \sum_{n=N+1}^{\infty} (c_n G_n)^2 \right]^{\frac{1}{2}} \left\{ \sum_{n=N+1}^{\infty} [c_n^{-1} U_n^k(r)]^2 \right\}^{\frac{1}{2}} \\
&\leq S_{\infty} \left\{ \sum_{n=N+1}^{\infty} [c_n^{-1} U_n^k(r)]^2 \right\}^{\frac{1}{2}}, \quad (A.17)
\end{aligned}$$

where  $G_N(r)$  is the series of eq (A.14') truncated at  $n = N$ , and

$$S_{\infty} = \sum_{n=0}^{\infty} (c_n G_n)^2, \quad (A.18)$$

is a number we refer to as a norm. Because the number of coefficients known is always finite, we always estimate, rather than accurately evaluate, a value for the norm. This must be done conservatively, with care taken to be assured regarding the actual coefficient trend, so that convergence of the norm is assured.

#### b. Recursion Formulae for Coefficients

Recursion formulae of several different types exist for both the U-Functions and their adjoints. These functions are very unusual in that they are the only biorthogonal polynomials which satisfy third order differential equations [6]. Further, one can write explicit integral transformations, with Hankel function kernels, which, applied to the adjoint functions  $U_n^k$  give the corresponding functions  $U_n^k$ . This last property is somewhat analogous to the folding rule of the Legendre functions; and from the transformation kernels one can derive "addition formulae" analogous to those of the Legendre functions.

Since none of these properties is required for our immediate applications, we shall not attempt to express them here with formulae. However, expressions for the power series coefficients of the  $U_n^k$  polynomials have proven important enough to mention. If we write [3]

$$U_n^k(r) = \sum_{i=0}^n u_{ni}^k r^i, \quad (\text{A.19})$$

then the  $u_{ni}^k$  can be obtained using the recursion

$$u_{n+1,i}^k = \frac{2n+k+i+1}{2(n+1)} u_{ni}^k - \frac{1}{2(n+1)} u_{n,i-1}^k, \quad (\text{A.20})$$

with the special cases

$$u_{n+1,0}^k = \frac{2n+k+1}{2(n+1)} u_{n0}^k,$$

$$u_{n+1,n+1}^k = -\frac{1}{2(n+1)} u_{nn}^k,$$

$$u_{00} = 1. \quad (\text{A.21})$$

See Table A.2 for a few numerical values.

### 3. Function Fitting Representations

Polynomial representations are extremely accurate for monoenergetic sources and geometries, such as the point isotropic source or the plane source emitting perpendicularly to the plane, for which there is an unambiguous and dominant exponential trend. Thus, in the case of  $^{60}\text{Co}$  and  $^{137}\text{Cs}$  gamma rays, the penetration data of greatest usefulness can readily be obtained using  $U_n^k$  polynomial representations.

But for polyenergetic sources, and obliquely directed sources, no specifiable penetration trend is unique and dominant. Significant changes continue to occur toward more penetrating exponential trends. Convergence of the polynomial representations is then apt to be poor, and other methods must be available. This section and the next mention two methods of greater

flexibility which have been very useful in developing more general penetration data: The "plural-series" method of section A.4 has a rigorous theory which permits proof of convergence together with estimates of error bounds. The "function-fitting" method described here does not necessarily converge; and while error bounds can be developed, they require application of the "plural-series" theory and have not been worked out. Even so, the "function-fitting" approach has been extremely productive.

In function-fitting we use the following type of representation, with  $j$  arbitrary:

$$D(z) = \sum_{i=1}^{i_{\max}} (\alpha_i / \beta_i) (z / \beta_i)^j e^{-z / \beta_i} \quad (\text{A.22})$$

The number of unspecified coefficients  $\alpha_i, \beta_i$ , must be made equal to the number of moments utilized, to render unique the solution to a set of moment equations like the following:

$$\frac{D_{2n}}{(2n + j)!} = \sum_{i=1}^{i_{\max}} \alpha_i \beta_i^{2n} \quad (\text{A.23})$$

This is a standard form which is soluble by known algorithms [7,8]. The procedure, which involves the determination of eigenvalues of an elementary matrix whose elements are specified from the values of the moments  $D_{2n}$ , identifies the  $\beta_i$  as the roots of a polynomial of degree  $i_{\max}$ . Evaluation of the  $\alpha_i$  subsequently involves only a matrix inversion.

Assignment of some  $\beta_i$  values arbitrarily is possible with only a simple modification of the basic procedure, and has been made the vehicle for a computer program which always produces a solution to the problem [9].

Because eq (A.22), for  $j = 0$ ,  $z = 0$ , has the same form as the terms of eq (A.23), it has been possible when odd, rather than even, moments are used, to include data for  $D(0)$  in the set of equations solved. But this can also be done with a known additional term which embodies the correct  $D(0)$  values, and corresponding insertion of an extra  $(z/\beta_i)$  factor in each of the other terms of eq (A.22).

#### 4. Plural Series Representations

To represent distributions having exponential trends, but which either have other structure or are mixtures of exponentials which are not consistent with rapid convergence, one can use a "plural series" representation. Its greater generality than approximation by a single  $U_n^k$  series does not prevent application of equally strong convergence arguments and estimated error bounds. For a full treatment we refer the reader to the main papers on the subject, references [10,11].

The plural series representations are biorthogonal, and in fact are constructed of U-Functions with differing scale factors  $x_j$ . In our notation, for an arbitrary  $A_j$ ,  $x_j$  set,  $j = 1, 2, \dots J$ ,

$$F(z) \approx F_N(z) = \sum_{j=1}^J \left( A_j / x_j^{k+1} \right) F^j(z) \quad , \quad (A.24)$$

where

$$F^j(z) = \sum_{n=0}^N a_n^j U_n^k(z/x_j) e^{-z/x_j} \quad . \quad (A.25)$$

The adjoint function, which doesn't play an important role per se, has the interesting property being representable by

$$\hat{F}_N(z) = x_j^{-1} (z/x_j)^k \sum_{n=0}^N a_n^j c_n^2 \hat{U}_n^k(z/x_j) \quad (\text{A.26})$$

for each and every value of  $j$ , so that all  $J$  such expressions are equivalent.

Evaluation of the  $a_m^j$  is based on minimization of the expression

$$S_N = \sum_{j=1}^J \left( A_j / x_j^{k+1} \right) \sum_{n=0}^N \left( c_n a_n^j \right)^2, \quad (\text{A.27})$$

subject to the condition that the moments of the right side of eq (IV.119) have the correct known values. These conditions lead to an elementary matrix whose inversion gives the  $a_n^j$ . The constant  $S_\infty$  is the norm, and  $S_N < S_\infty$  is used as in the previous section to evaluate estimated error bounds for truncation error when only  $N$  moments are used:

$$|F - F_N| \leq S_\infty \left[ D_N^k(z) \right]^{\frac{1}{2}}, \quad (\text{A.28})$$

where the  $D_N^k(z)$  are characteristic of the representation, and are essentially residual sums of squares of basic biorthogonal functions. Their analytic form is complex but their calculation is straightforward though somewhat involved [11].

As just suggested, it turns out that this type of representation can be restated in terms of normalized biorthogonal functions which themselves have the same formal structure as eqs (A.24) and (A.25). Convergence can be proven, if a single-series representation based on any one of the scale factors  $x_j$  above would give convergence.

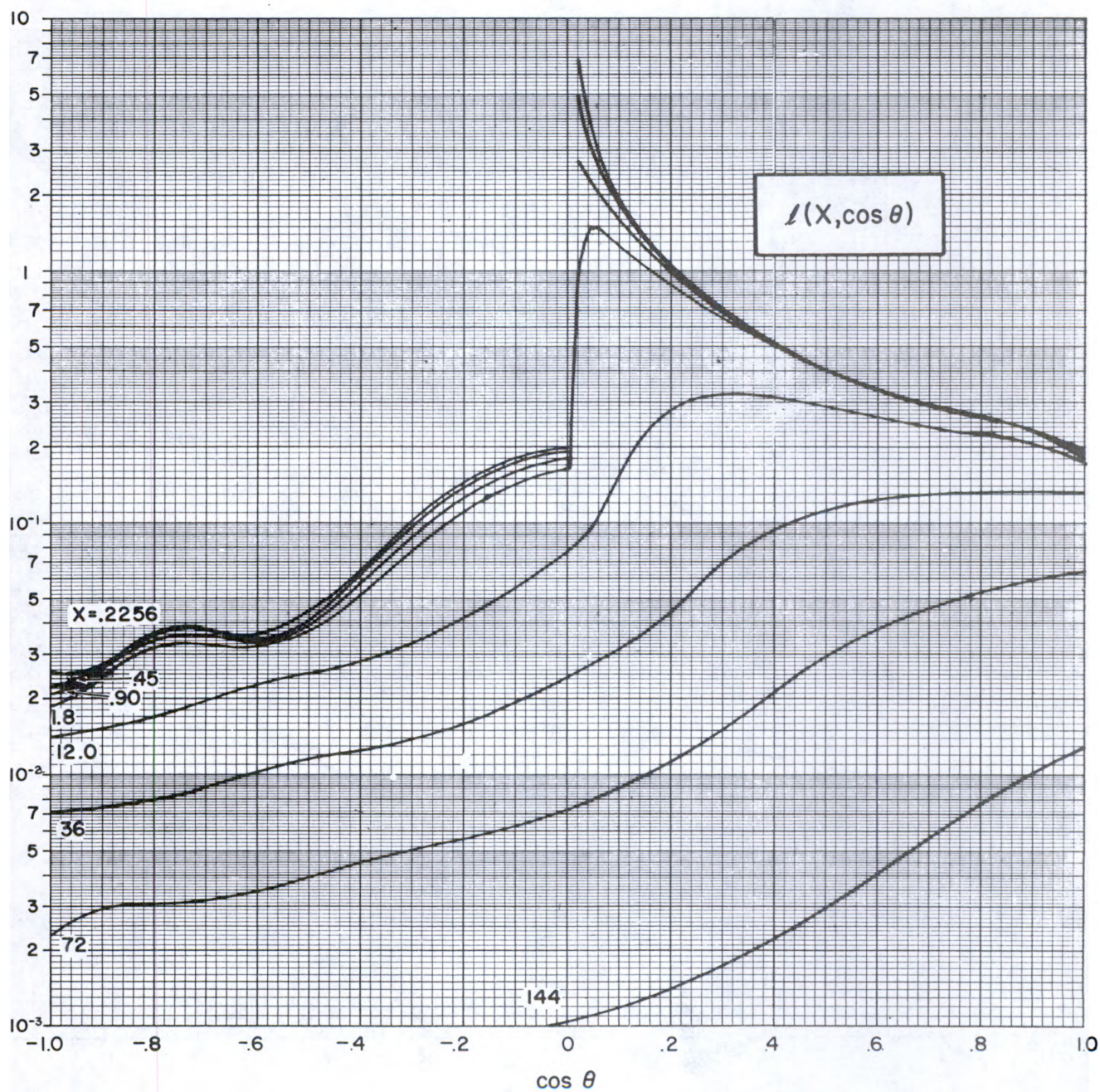
## References

- [1] MacRobert, T. M., Spherical Harmonics, 372 pages (Dover Publications, New York, 1948).
- [2] Meixner, J., Spezielle Functionen der Mathematischen Physik, Handbuch der Physik, Band I, (Springer-Verlag, Berlin, 1956).
- [3] Spencer, L. V., Gamma Ray Shielding Theory, TR-40, Vol. I, Radiation Shielding, 325 pages (Office of Civil Defense and Kansas State Univ. 1966).
- [4] Spencer, L. V., Flusser, P., Properties of a Useful Biorthogonal System, NBS J. Research, 71B, No. 4, 197-211 (Dec. 1967).
- [5] Lanczos, C., Linear Differential Operators, 554 pages (D. Van Nostrand, Princeton, N.J., 1961).
- [6] Preiser, S., An Investigation of Biorthogonal Polynomials Devivable from Ordinary Differential Equations of the Third Order, J. Math Anal. Appl. 4, 38-64 (1962).
- [7] Fano, U., Spencer, L. V., and Berger, M. J., Penetration and Diffusion of X-Rays, Handbuch der Physik, Encyclopedia of Physics, Ed. S. Flugge, Vol. 38/2, 660-817 (Springer-Verlag, Berlin, 1959).
- [8] Morris, E. E., Chilton, A. B., and Vetter, A. F., Tabulation and Empirical Representation of Infinite-Medium Gamma-Ray Buildup Factors for Mono-energetic, Point Isotropic Sources in Water, Aluminum, and Concrete, Nucl. Sci. Eng. 56, 171-178 (1975).
- [9] Eisenhower, C., and Spencer, L. V., Neutron Flux from a Point Isotropic Source in Carbon Calculated by the Moments Method, NBS Report 9869, 40 pages (July 1968).
- [10] Spencer, L. V., Penetration and Diffusion of X-Rays: Calculation of Spatial Distributions by Semi-Asymptotic Methods, Phys. Rev., 88, No. 4, 793-803 (Nov. 1952).
- [11] Spencer, L. V., "Plural-Series" Approximations of Functions, NBS J. Research, 76B, Nos. 3 and 4, 91-108 (Dec. 1972).



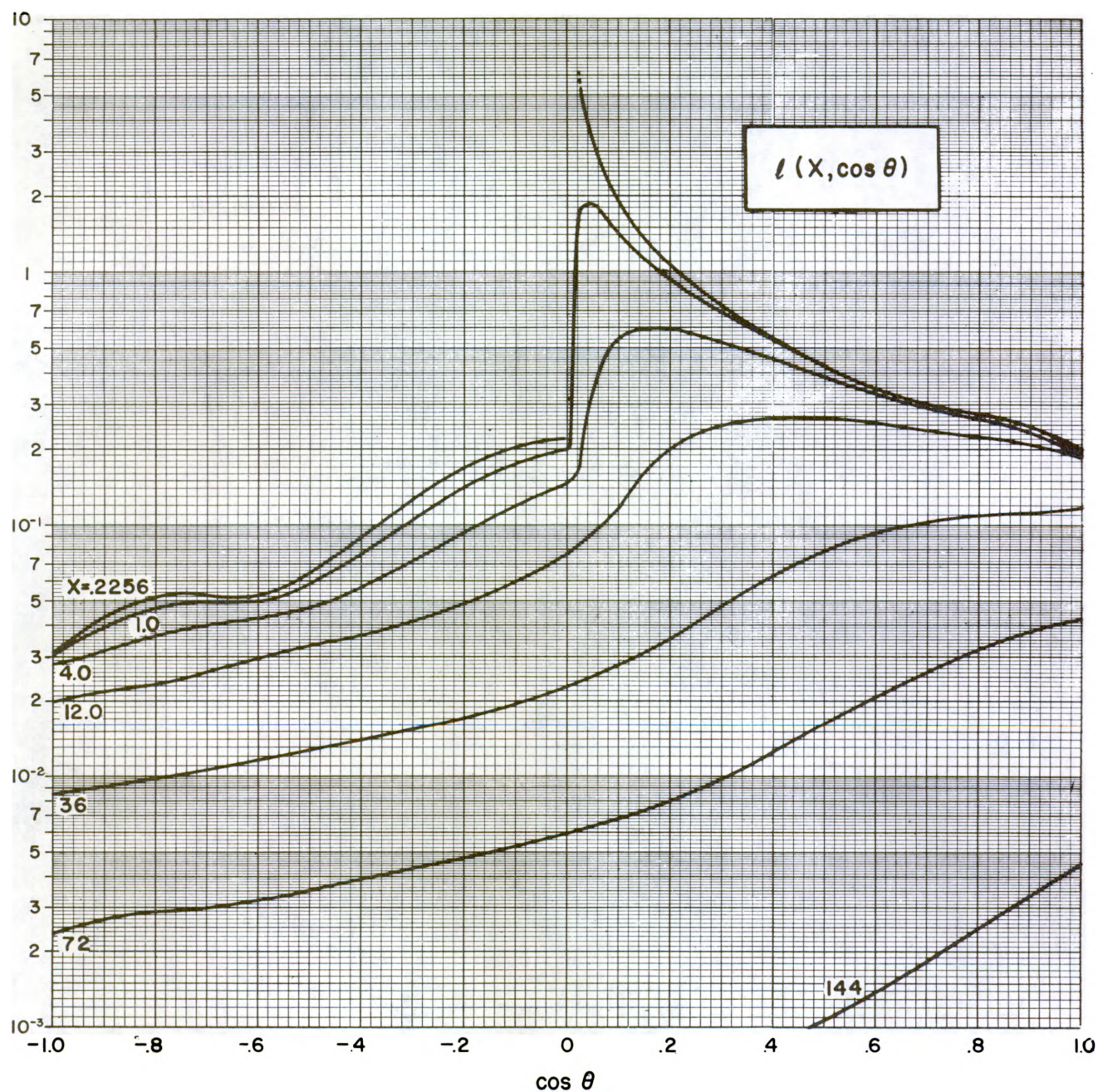
## APPENDIX B. $^{60}\text{Co}$ AND $^{137}\text{Cs}$ DIFFERENTIAL AND INTEGRAL PENETRATION DISTRIBUTIONS

The data presented in the following figures and tables were calculated as already described in sections IV.C and IV.D, with further comments in sections V.C and V.D. To facilitate comparisons we have placed corresponding results for  $^{60}\text{Co}$  and  $^{137}\text{Cs}$  adjacent to one another, and in the same sequence as their appearance in section B; and we have included in the captions in parentheses a cross reference to the corresponding data for a fission source.



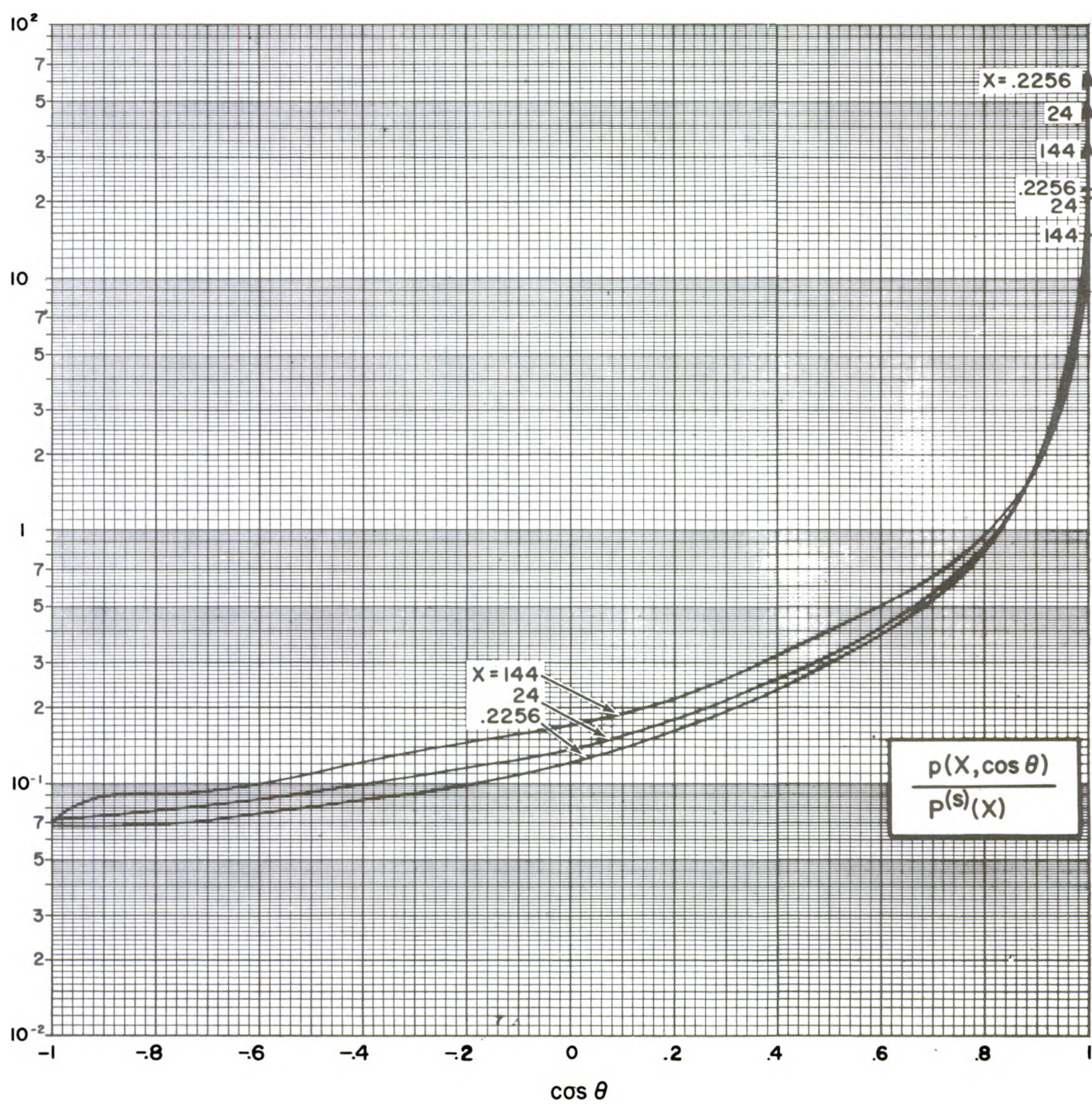
B.1.a  $^{60}\text{Co}$  in concrete (fig. V.6).





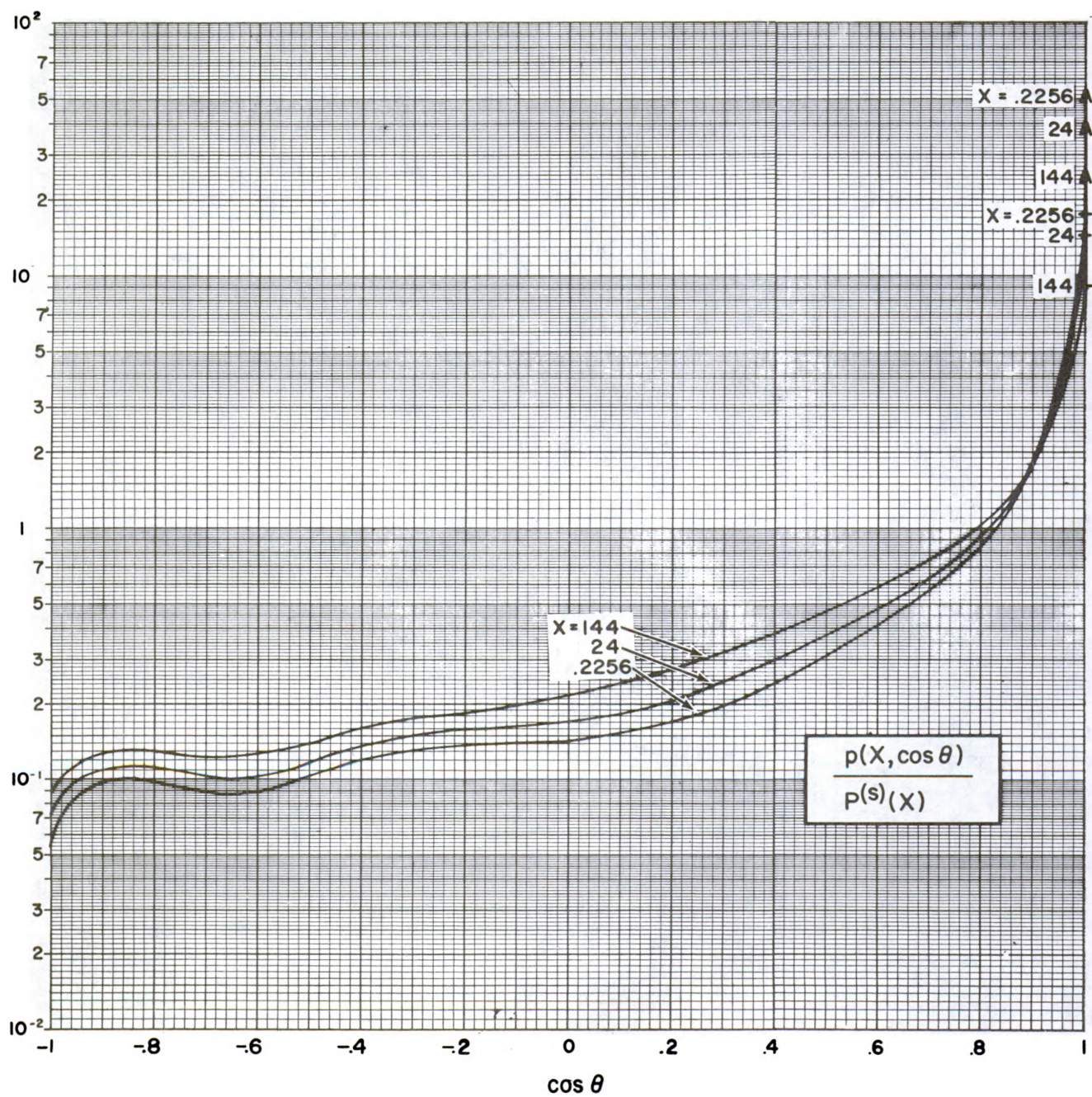
B.1.b  $^{137}\text{Cs}$  in concrete (fig. V.6).





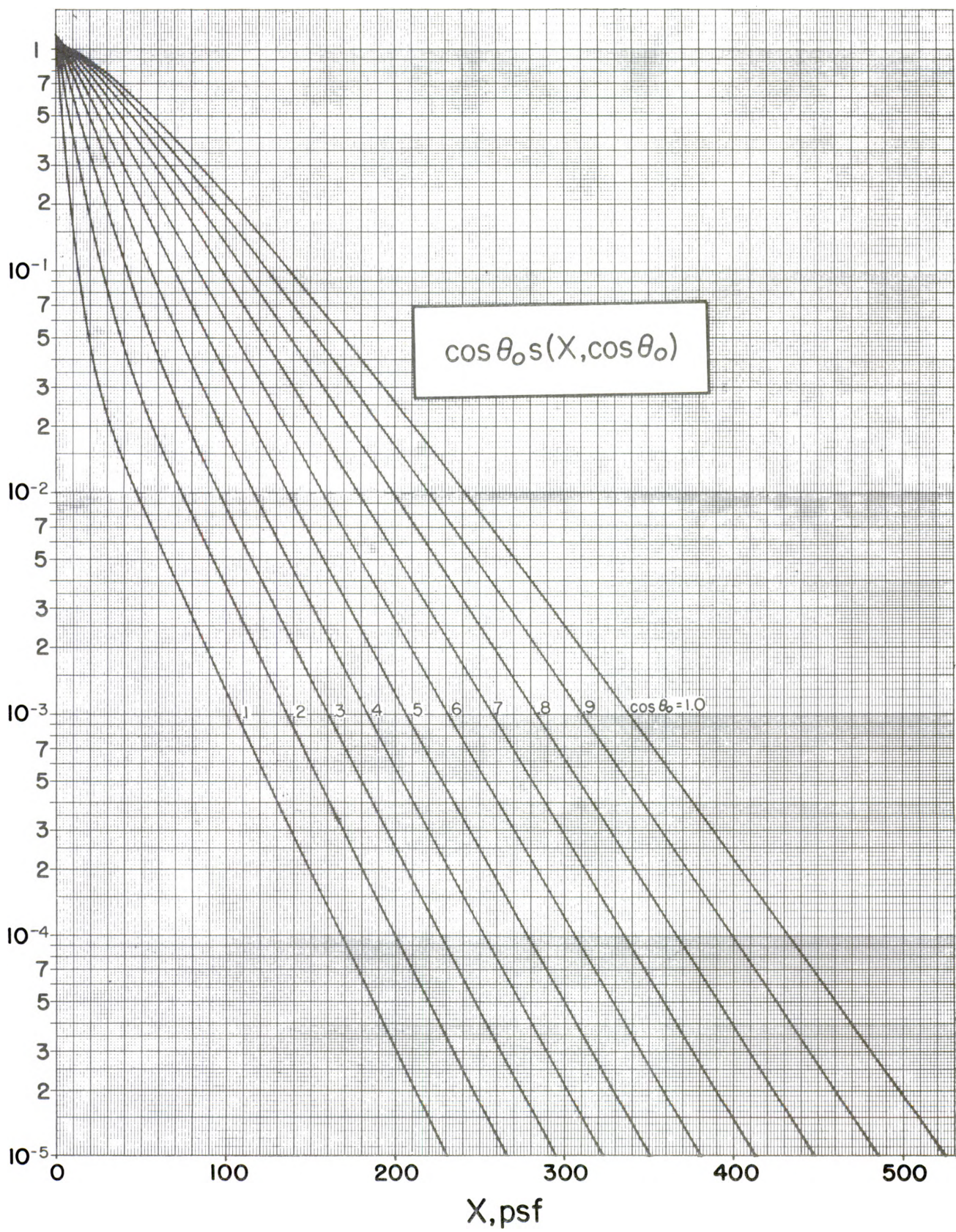
B.2.a  $^{60}\text{Co}$  in concrete (fig. V.7).





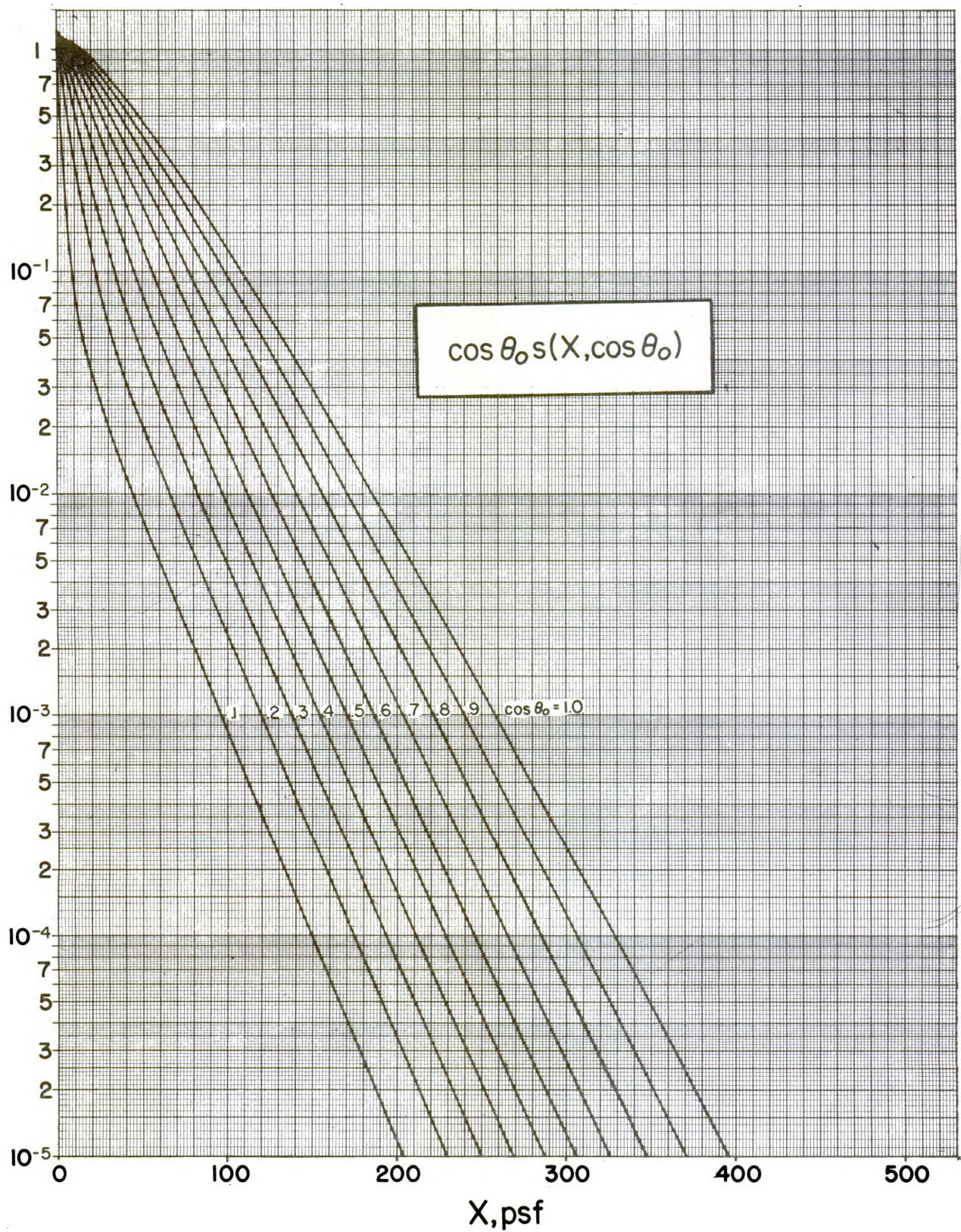
B.2.b  $^{137}\text{Cs}$  in concrete (fig. V.7).





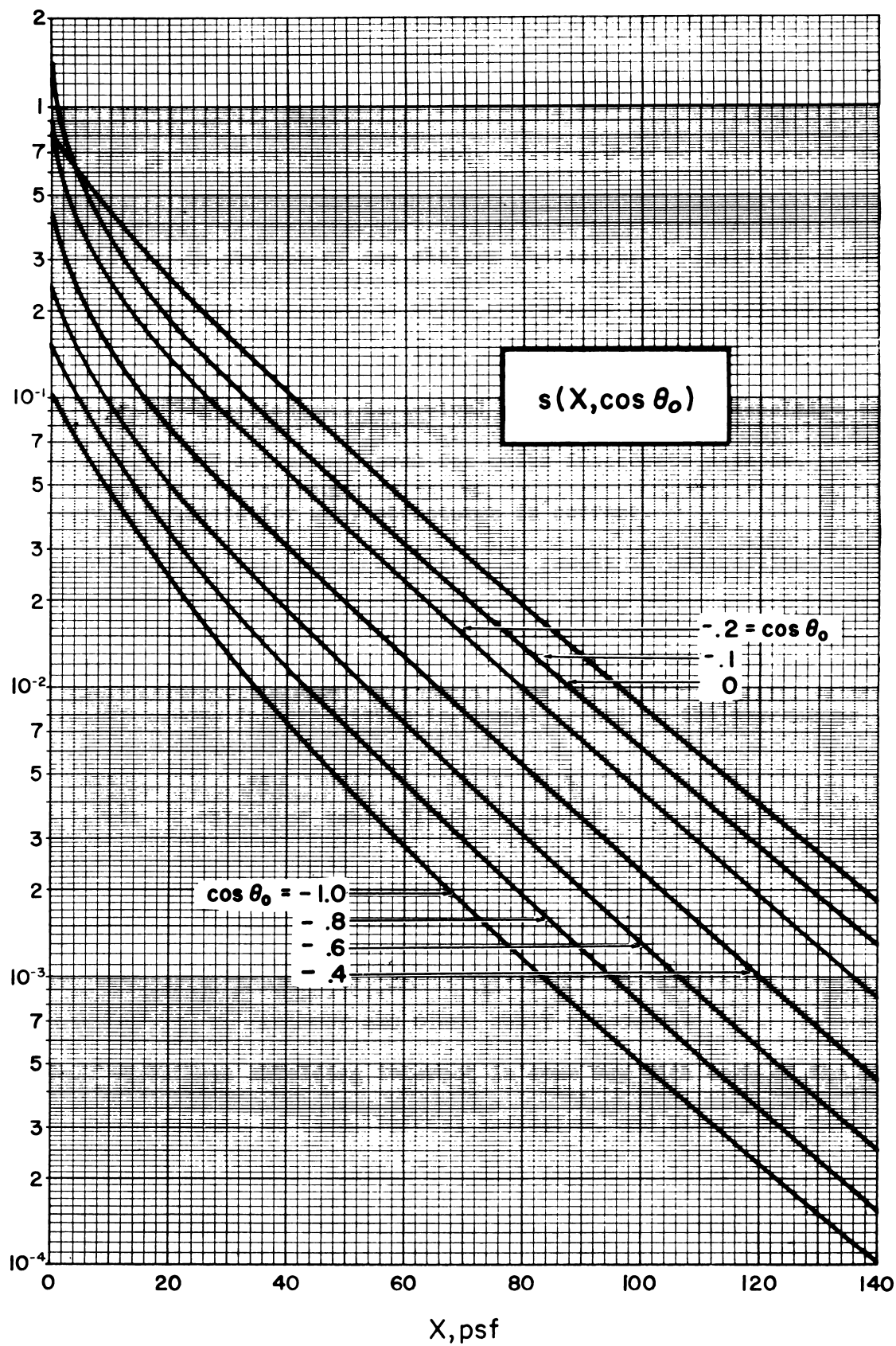
B.3.a  $^{60}\text{Co}$  in concrete (fig. V.8).





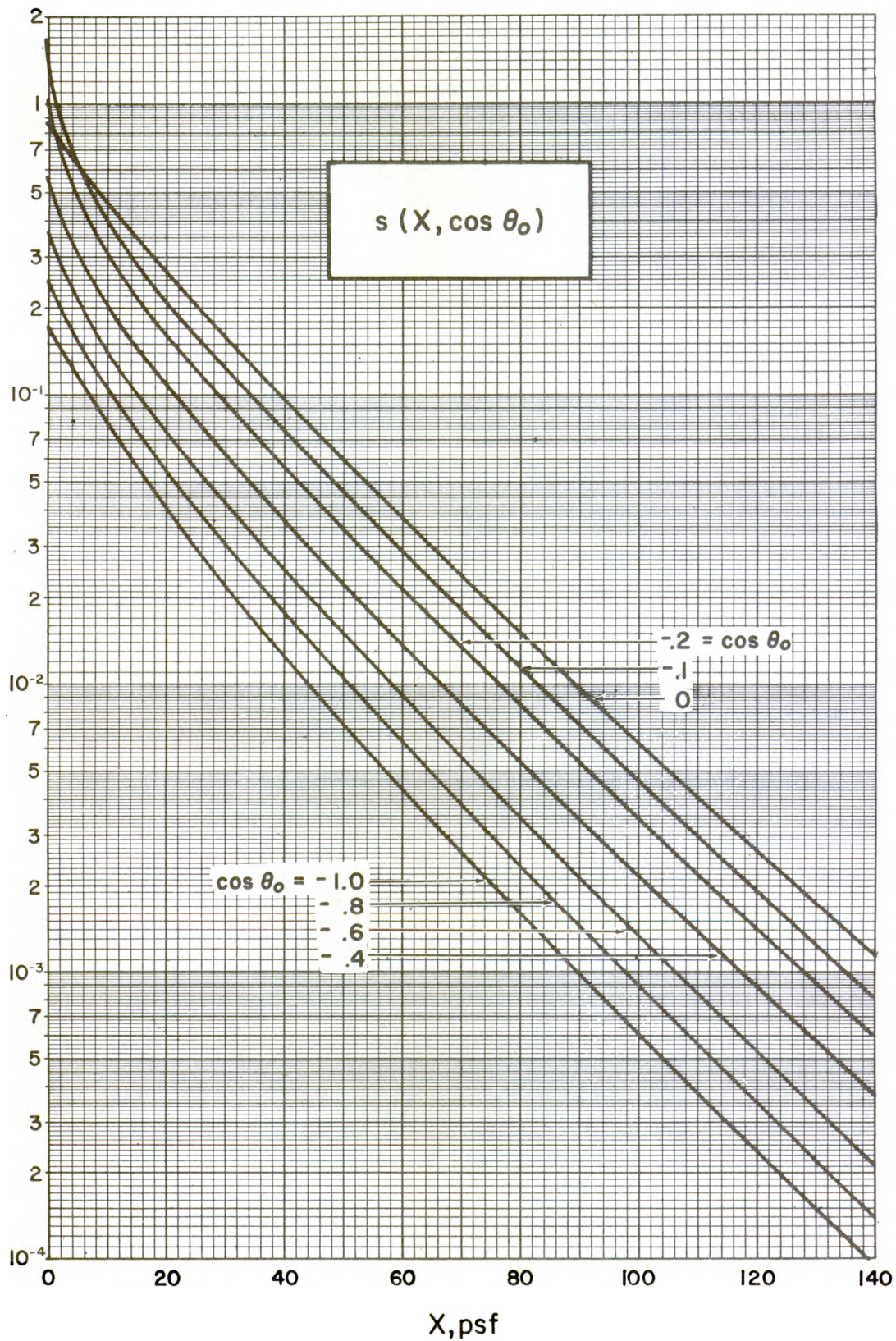
B.3.b  $^{137}\text{Cs}$  in concrete (fig. V.8).





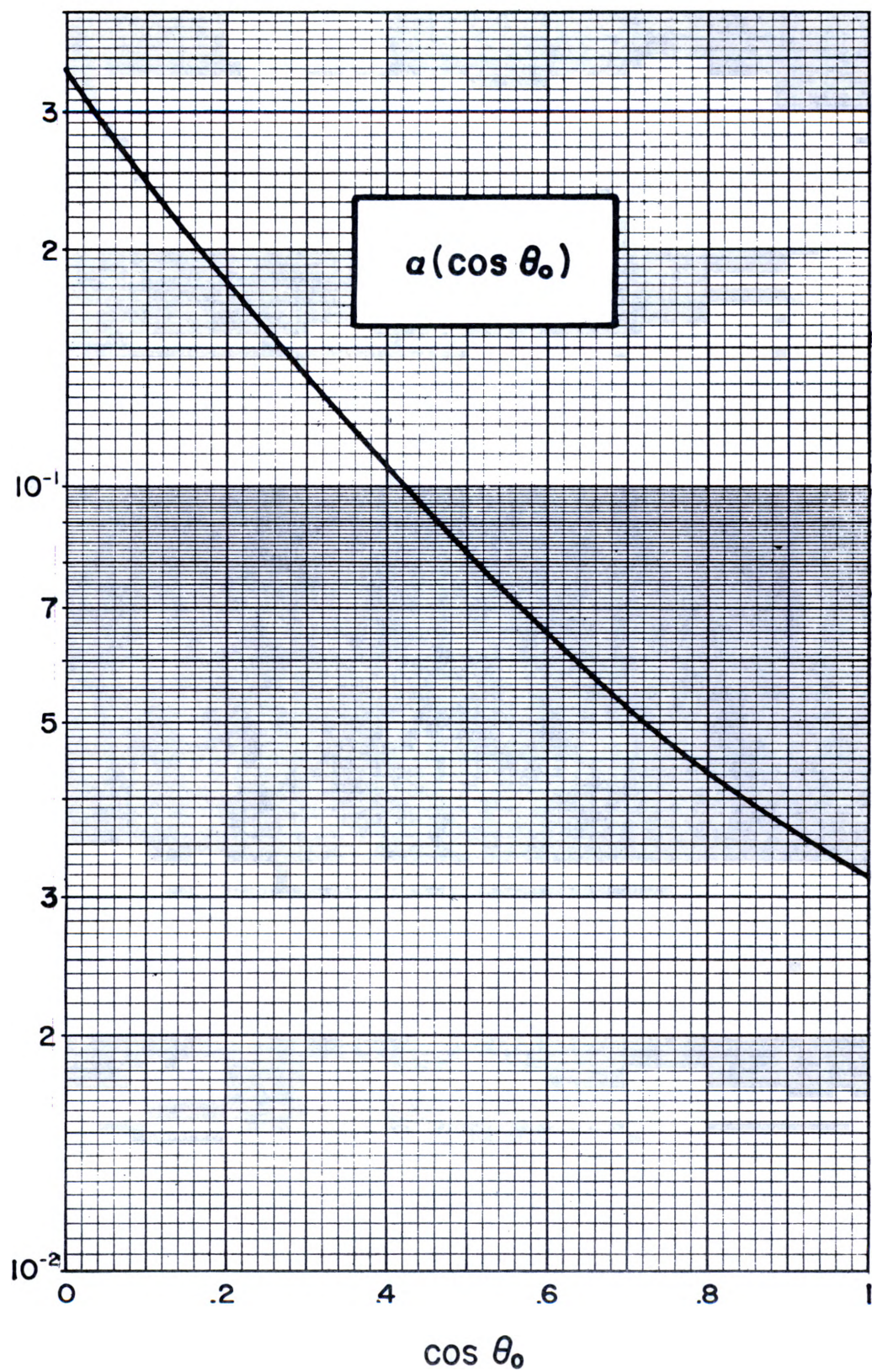
B.4.a  $^{60}\text{Co}$  in concrete (fig. V.9).



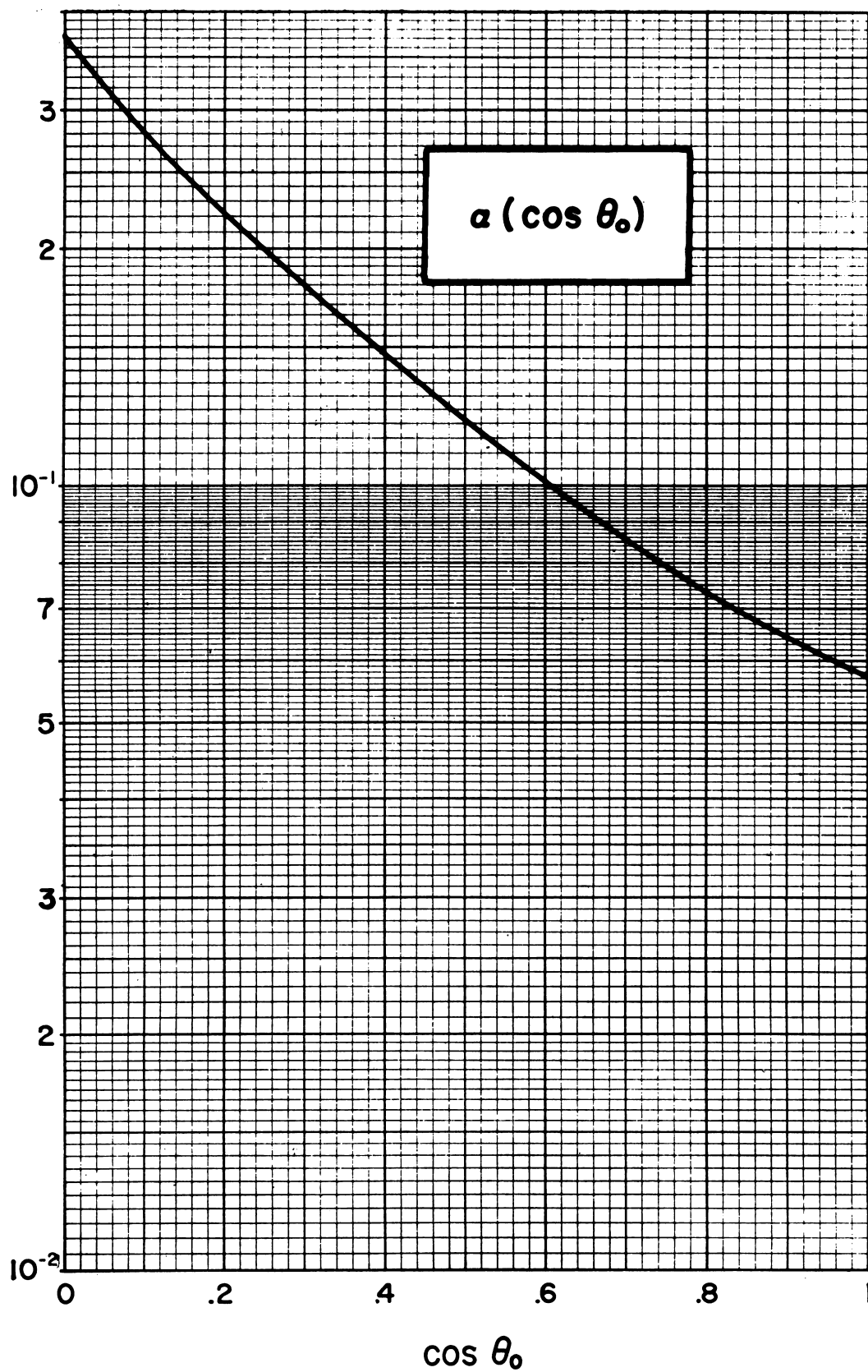


B.4.b  $^{137}\text{Cs}$  in concrete (fig. V.9).



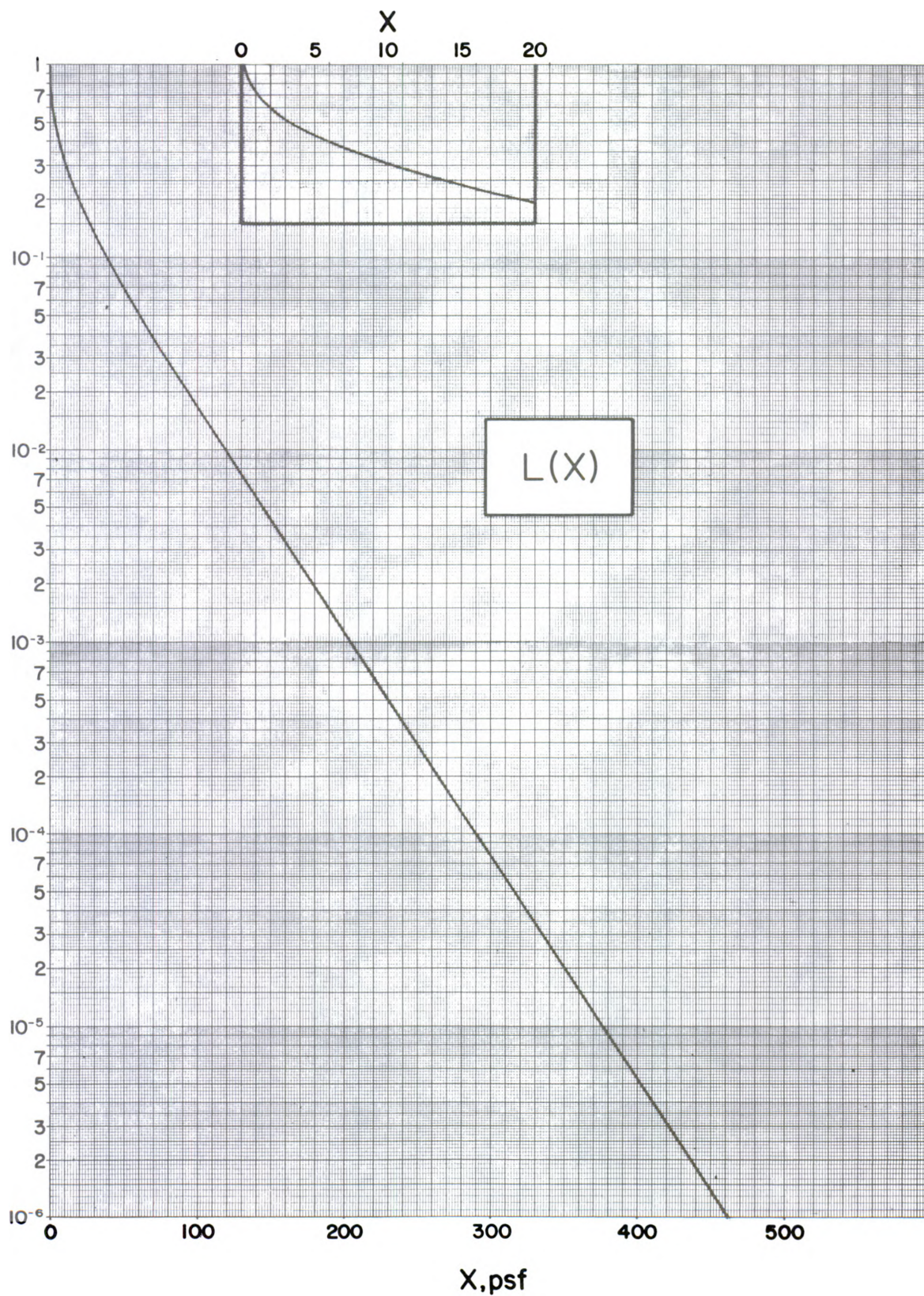


B.5.a  $^{60}\text{Co}$  backscatter from concrete (fig. V.10).



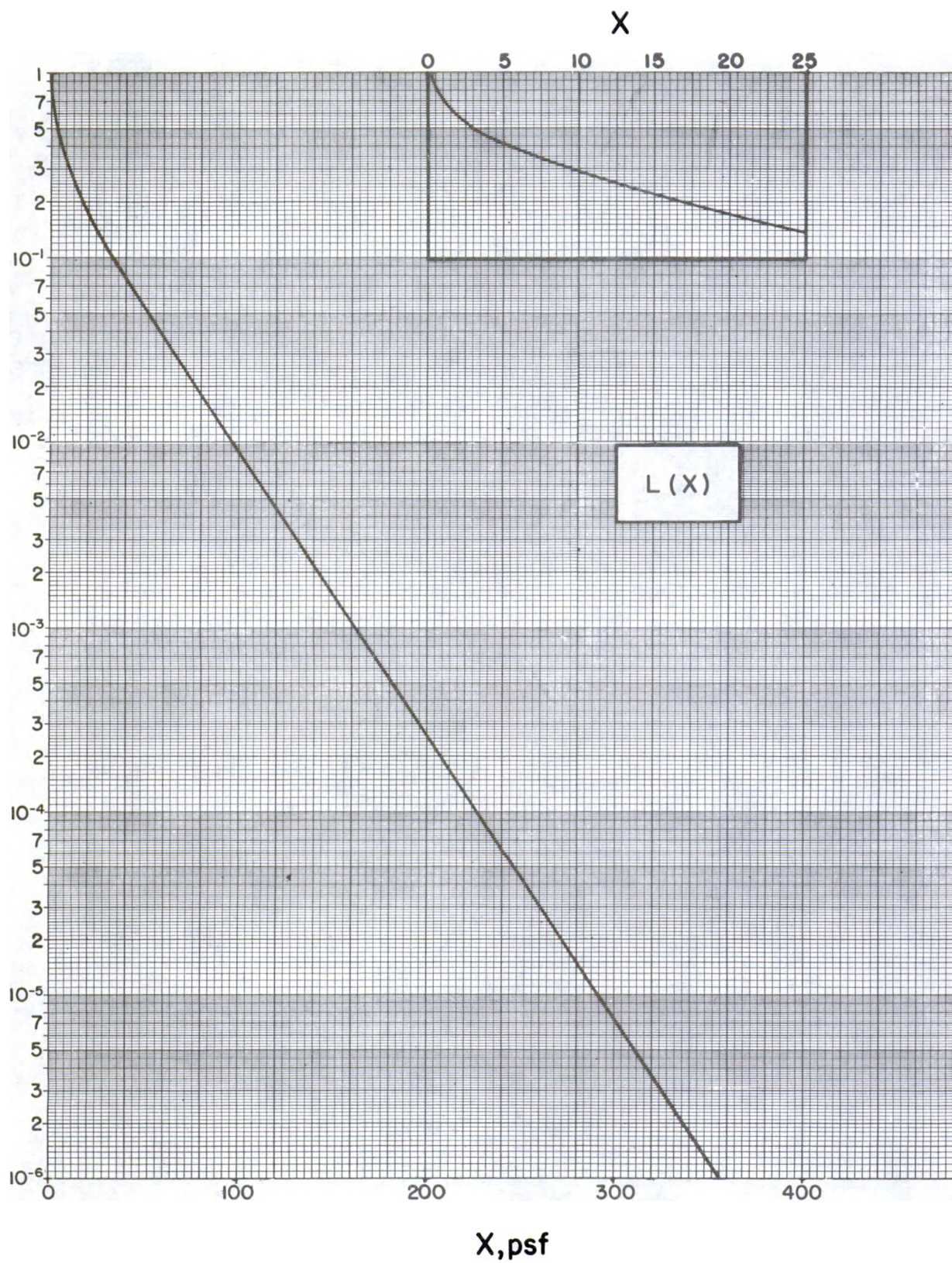
B.5.b  $^{137}\text{Cs}$  backscatter from concrete (fig. V.10).





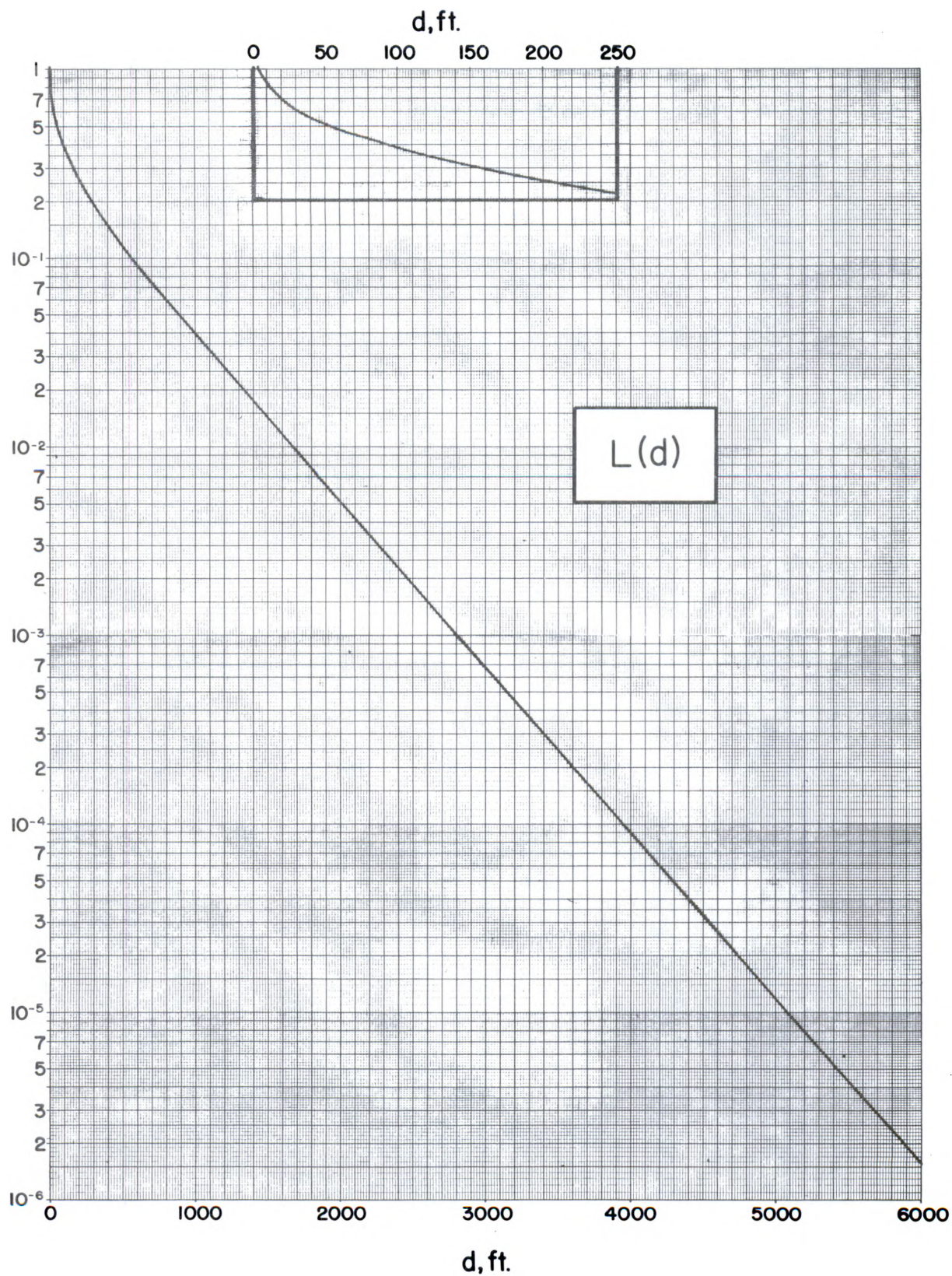
B.6.a  $^{60}\text{Co}$  in concrete (fig. V.12).





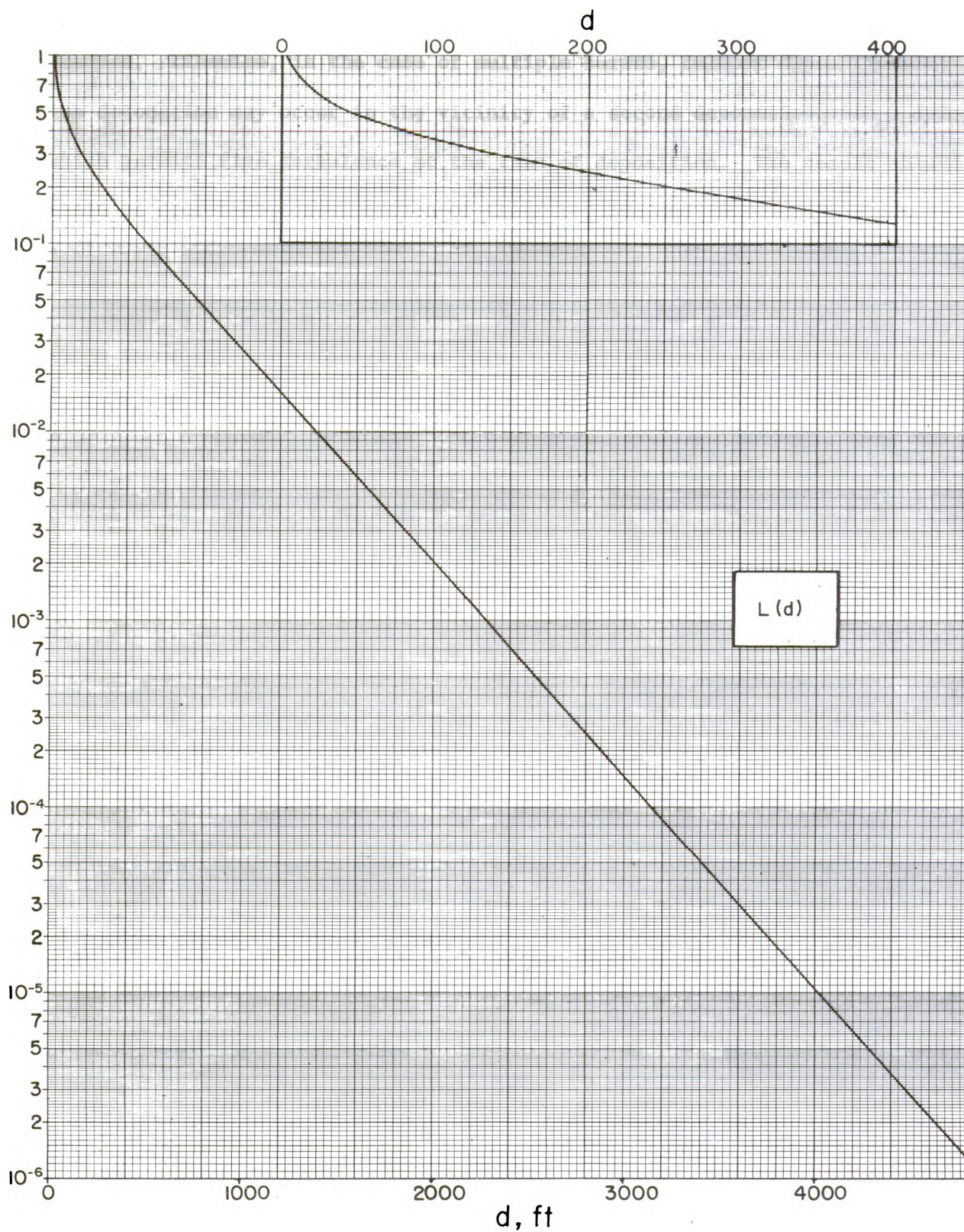
B.6.b  $^{137}\text{Cs}$  in concrete (fig. V.12).





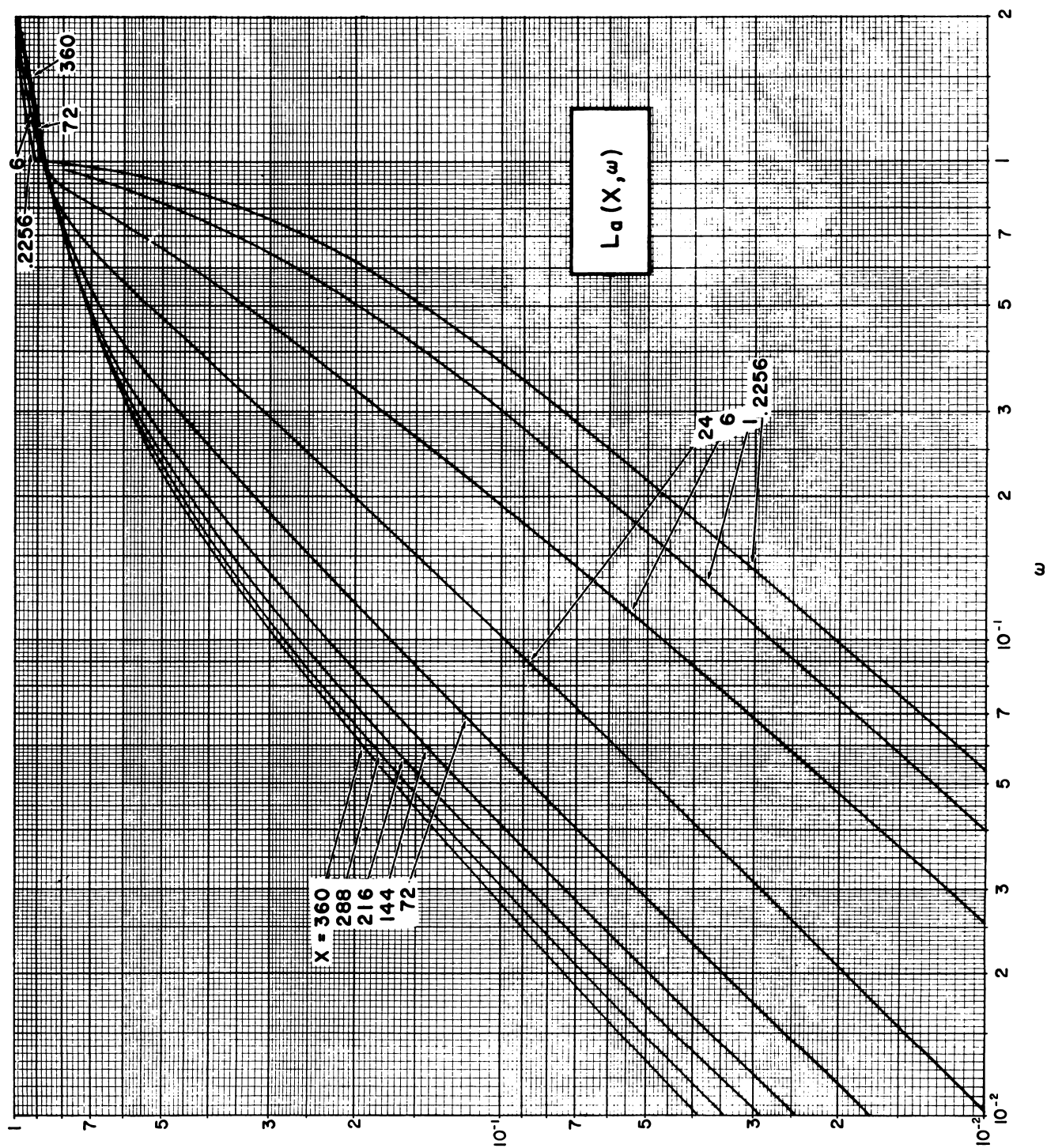
B.7.a  $^{60}\text{Co}$  in  $\text{H}_2\text{O}$  (fig. V.13).





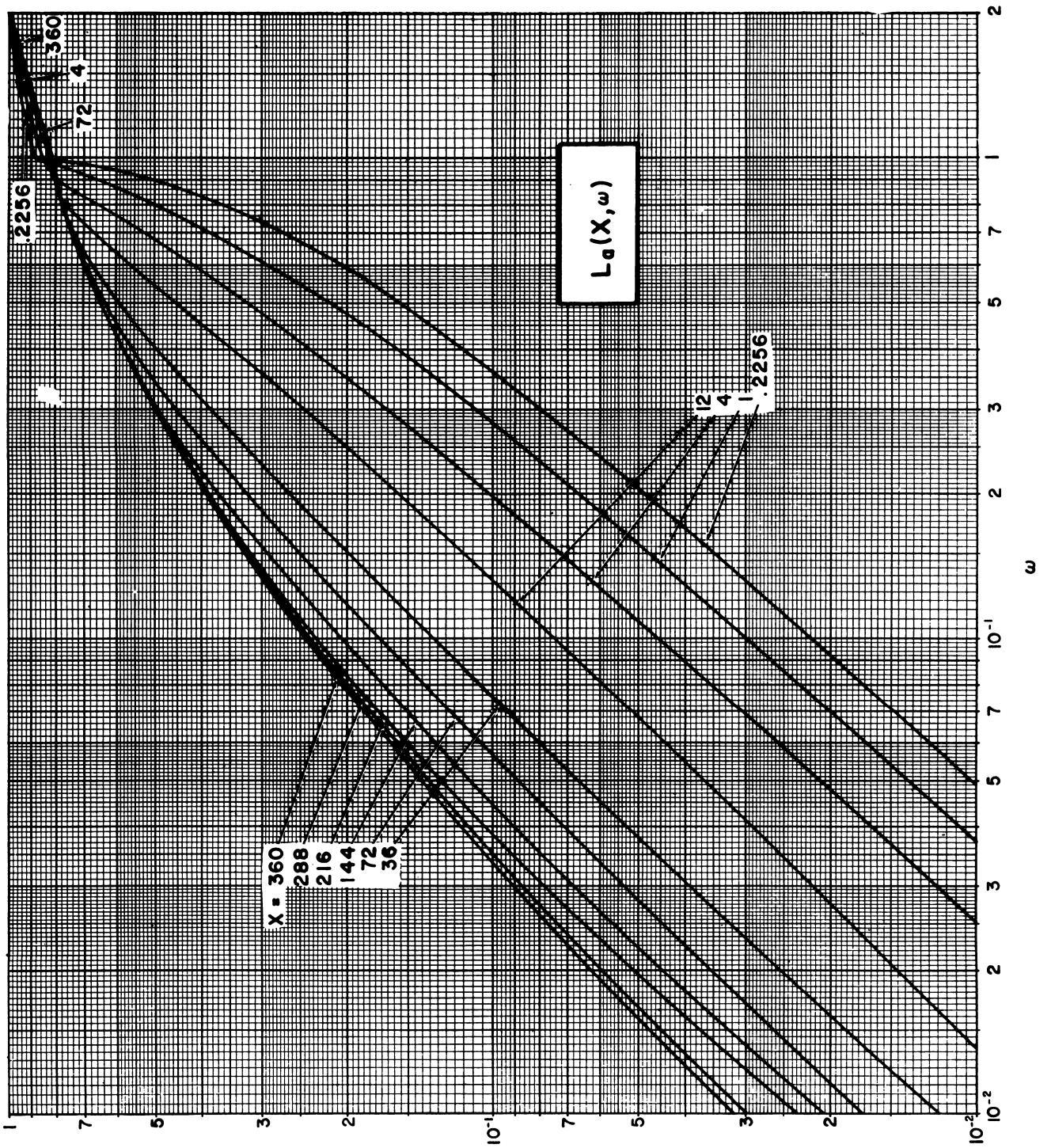
B.7.b  $^{137}\text{Cs}$  in  $\text{H}_2\text{O}$  (fig. V.13).



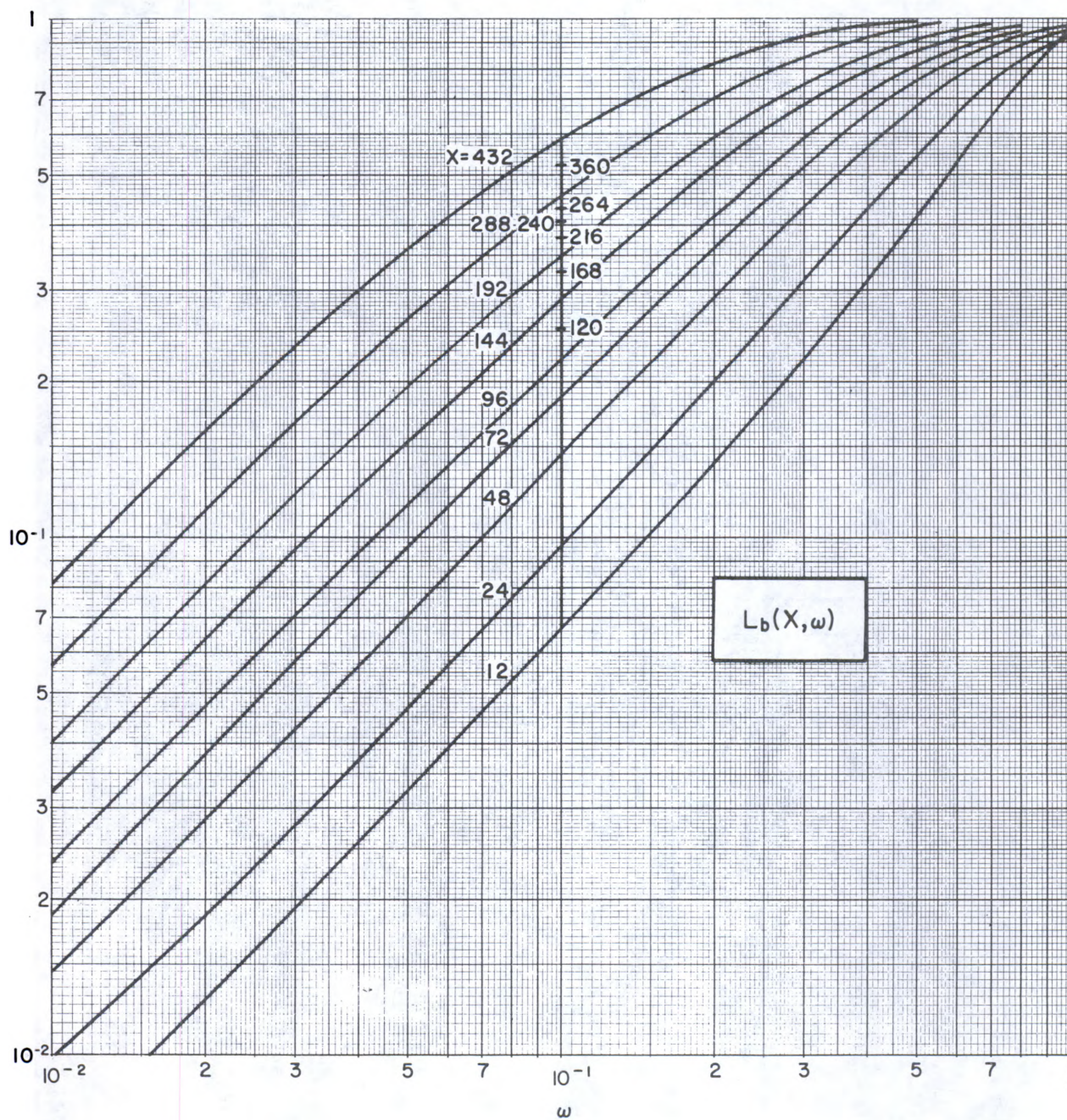


B.8.a  $^{60}\text{Cs}$  in concrete (fig. V.14).



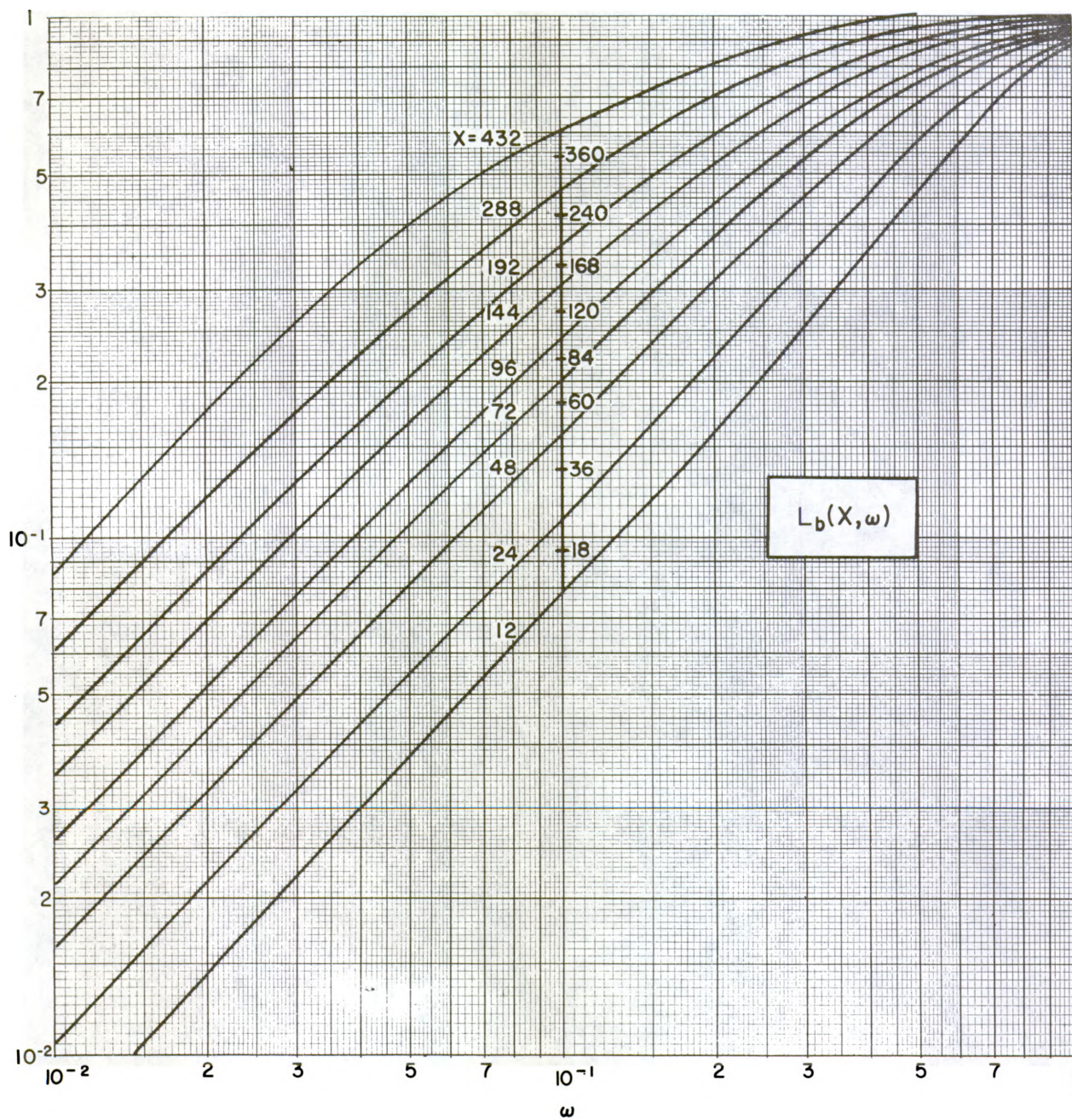


B.8.b  $^{137}\text{Cs}$  in concrete (fig. V.14).

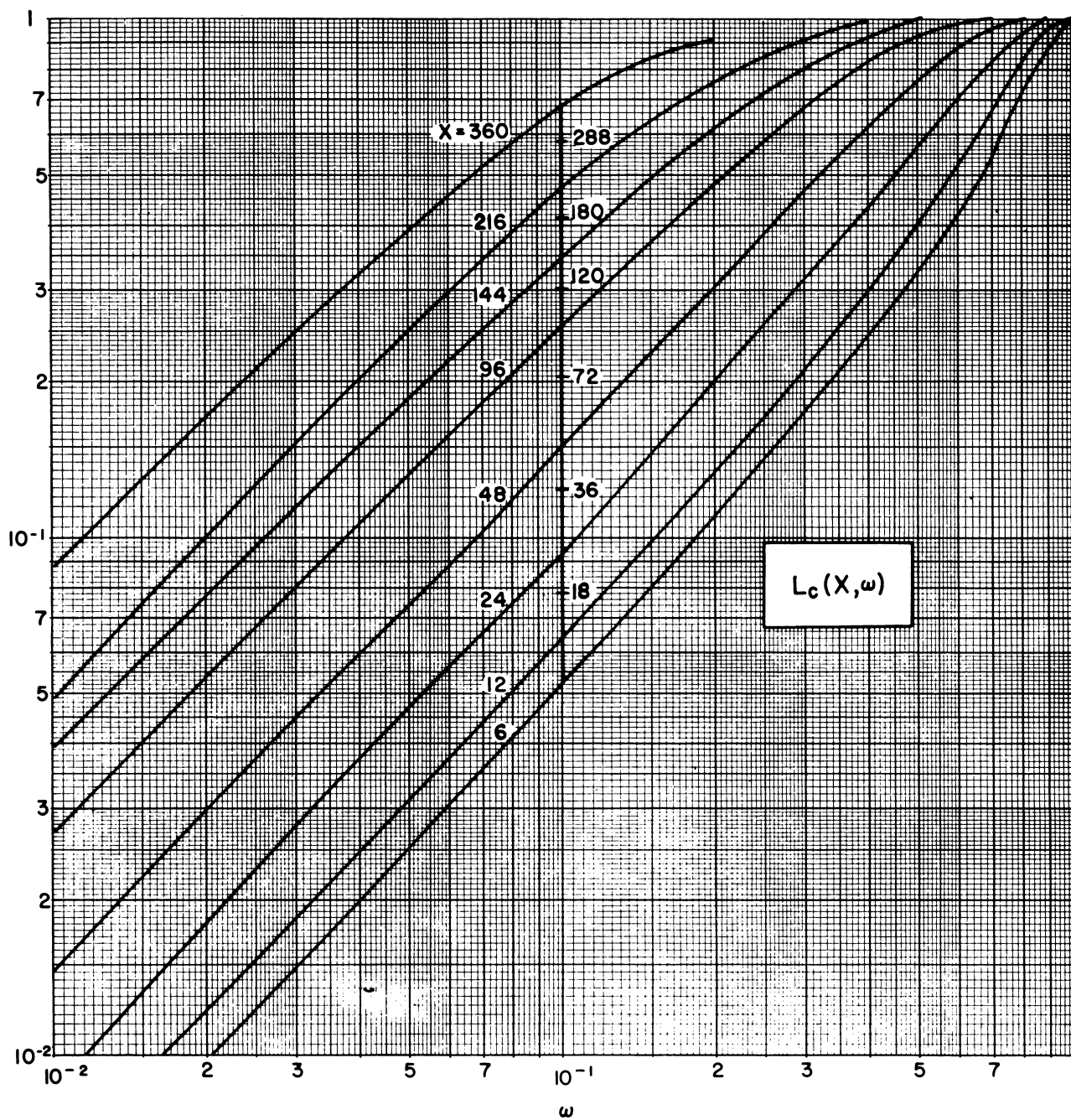


B.9.a  $^{60}\text{Co}$  in concrete (fig. V.15).



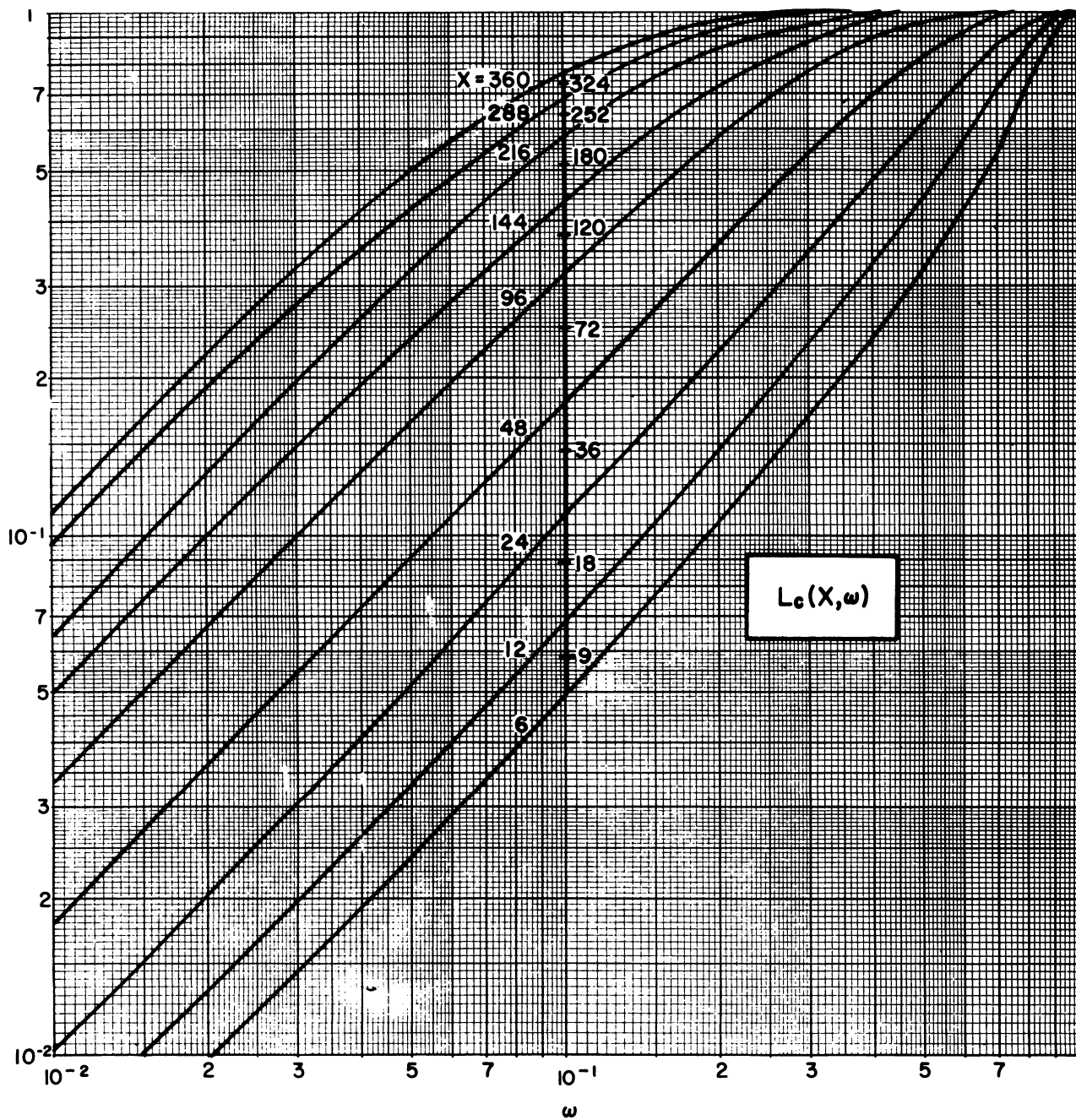


B.9.b  $^{137}\text{Cs}$  in concrete (fig. V.15).

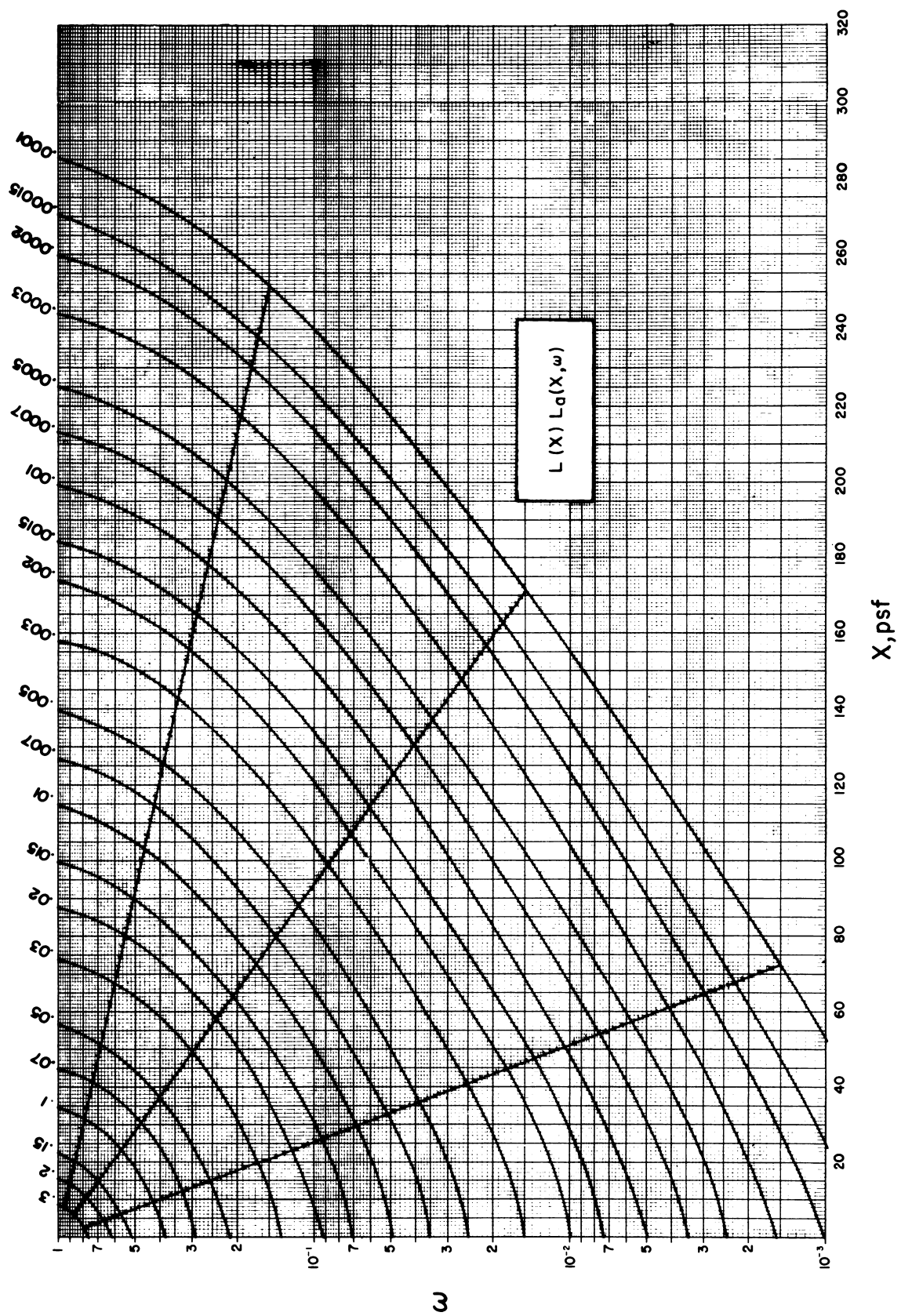


B.10.a  $^{60}\text{Co}$  in concrete (fig. V.16).

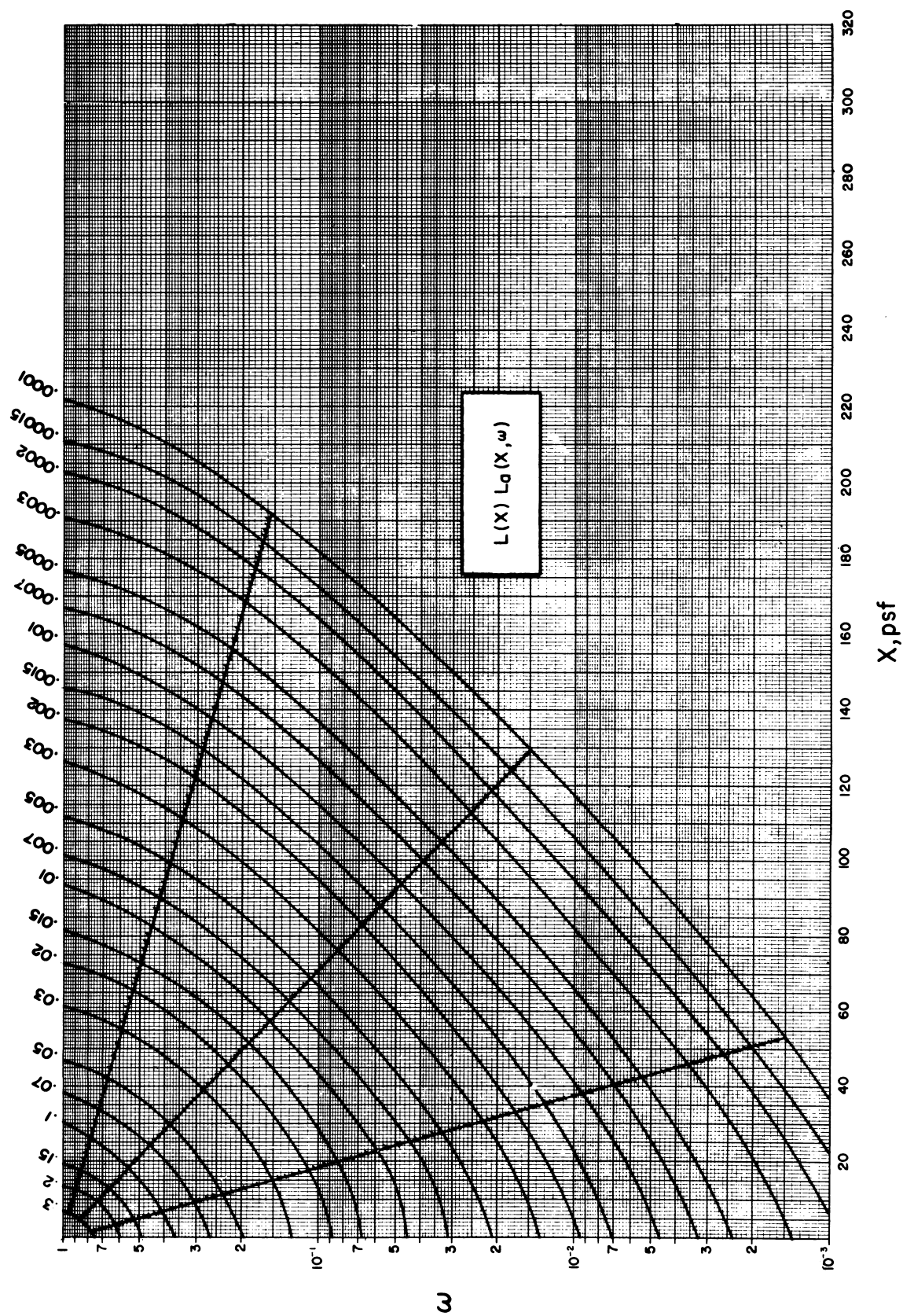




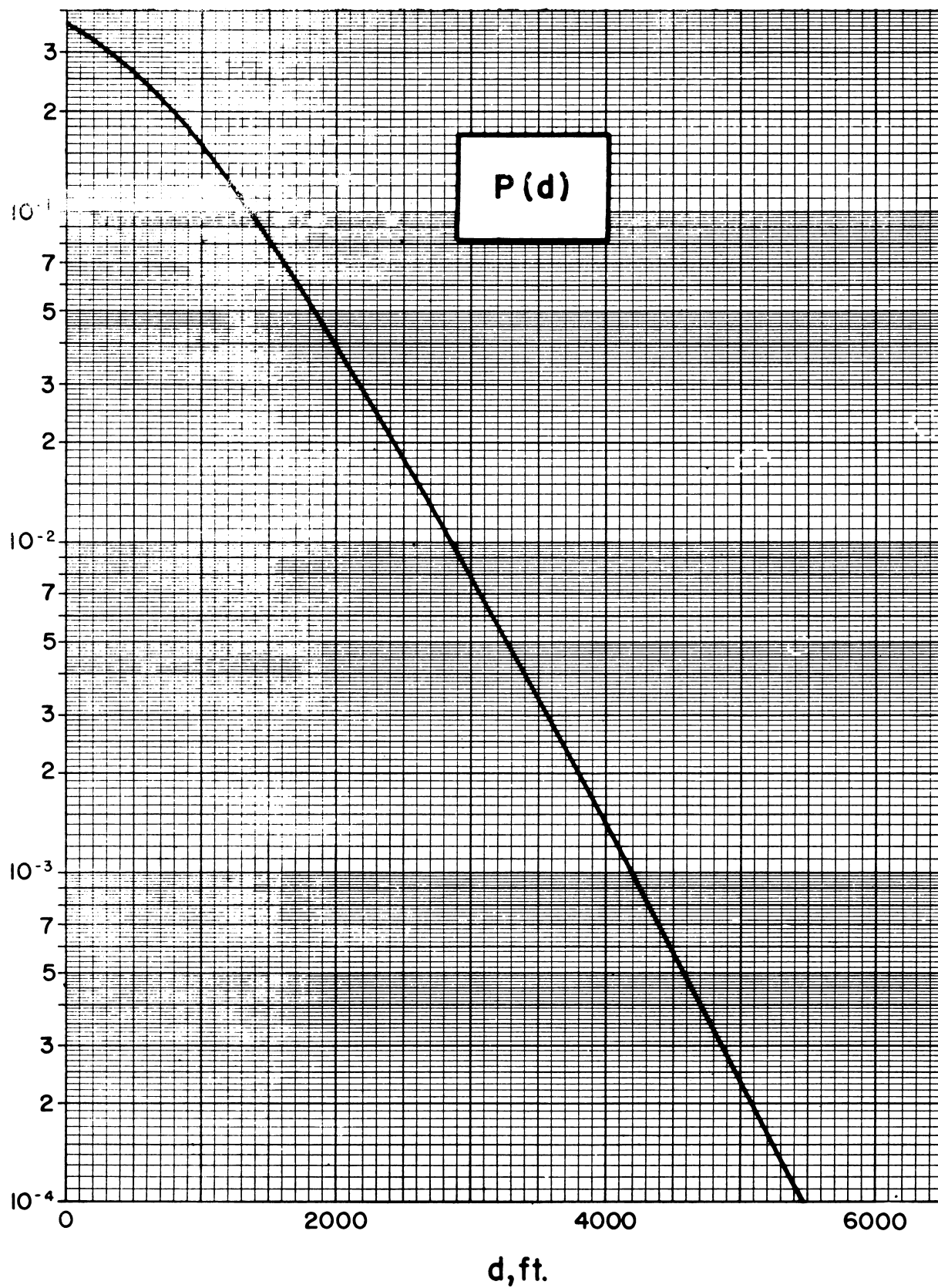
B.10.b  $^{137}\text{Cs}$  in concrete (fig. V.16).



B.11.a  $^{60}\text{Co}$  in concrete (fig. V.17).

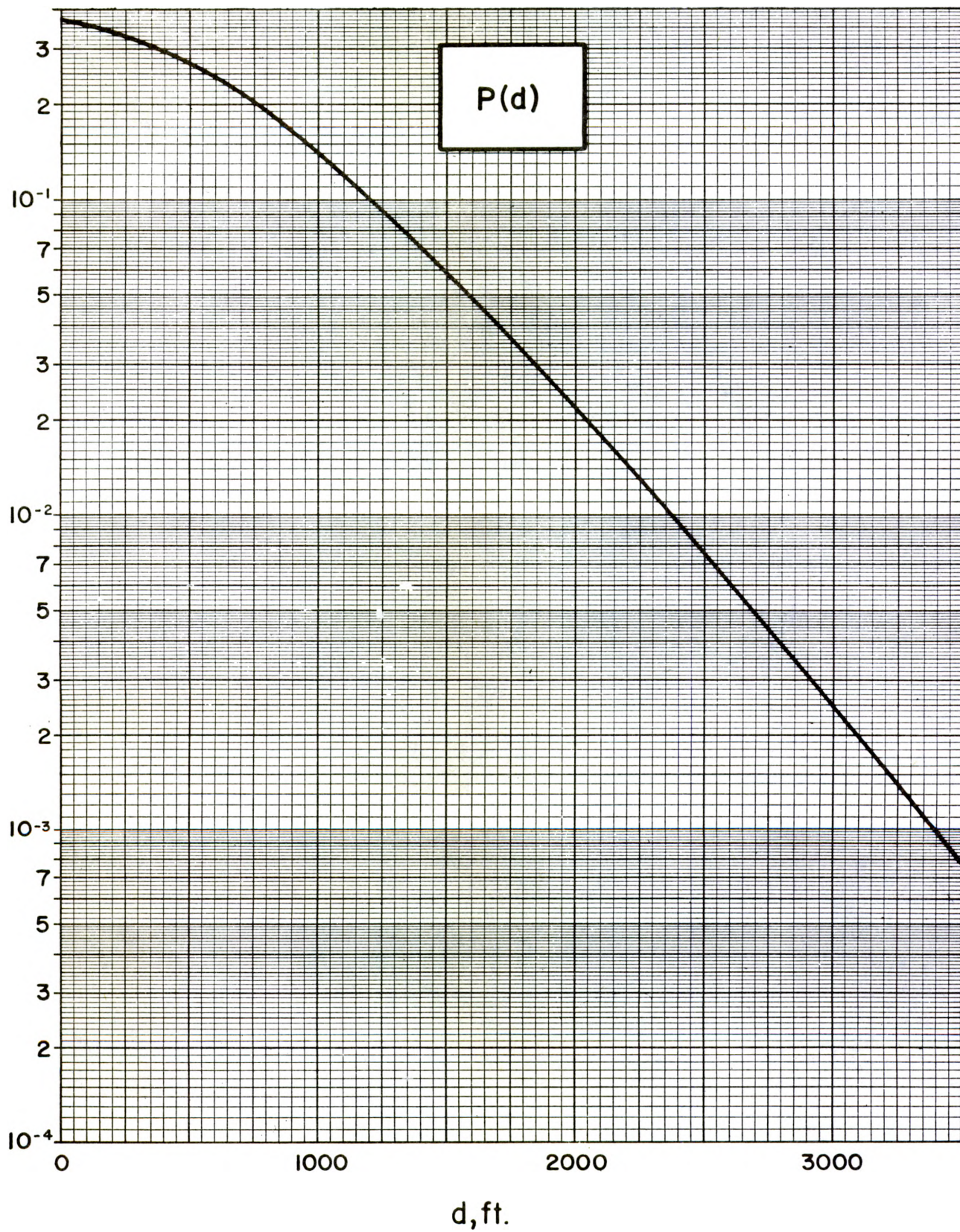


B.11.b  $^{137}\text{Cs}$  in concrete (fig. V.17).



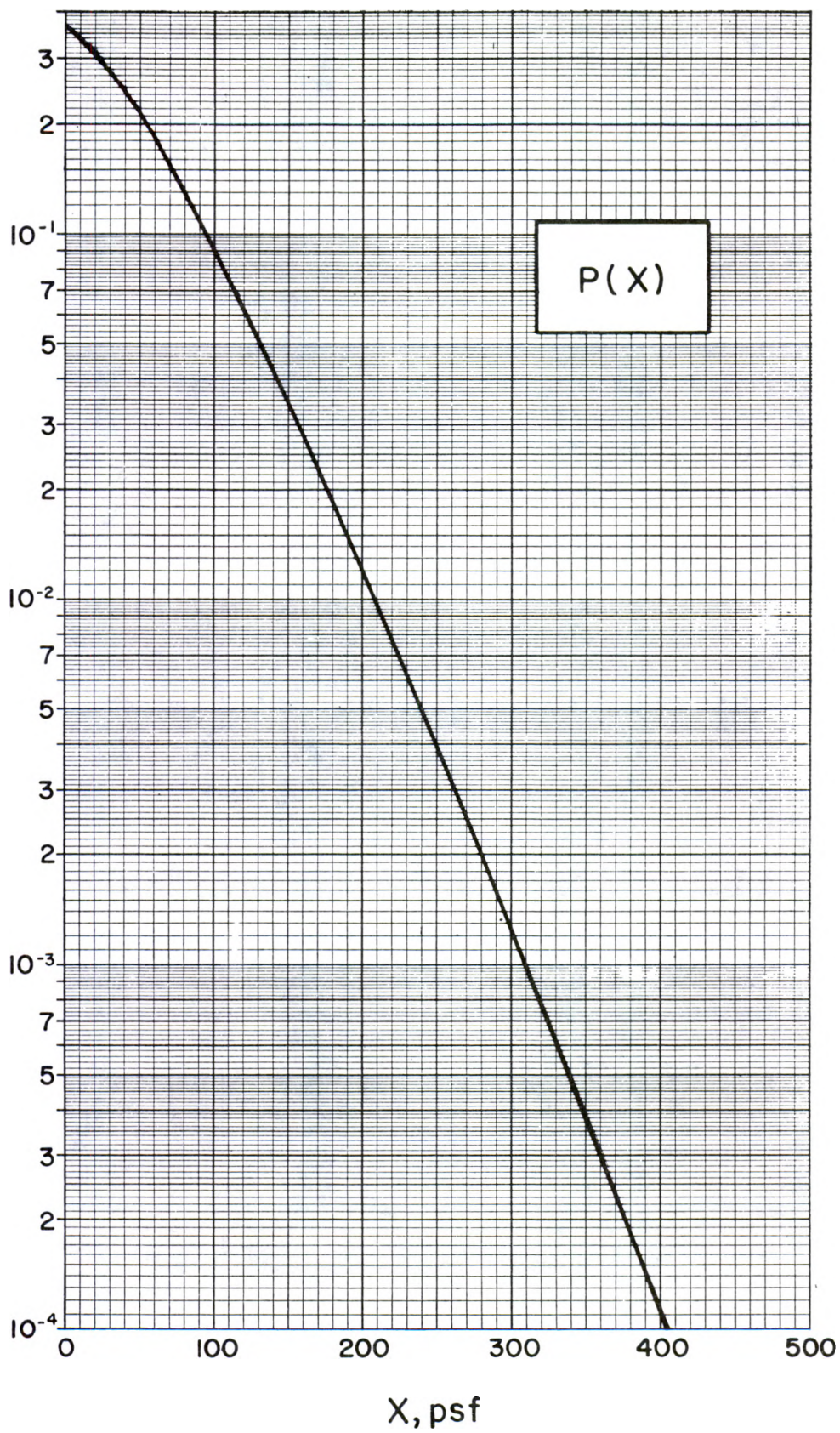
B.12.a  $^{60}\text{Co}$  in  $\text{H}_2\text{O}$  (fig. V.18).





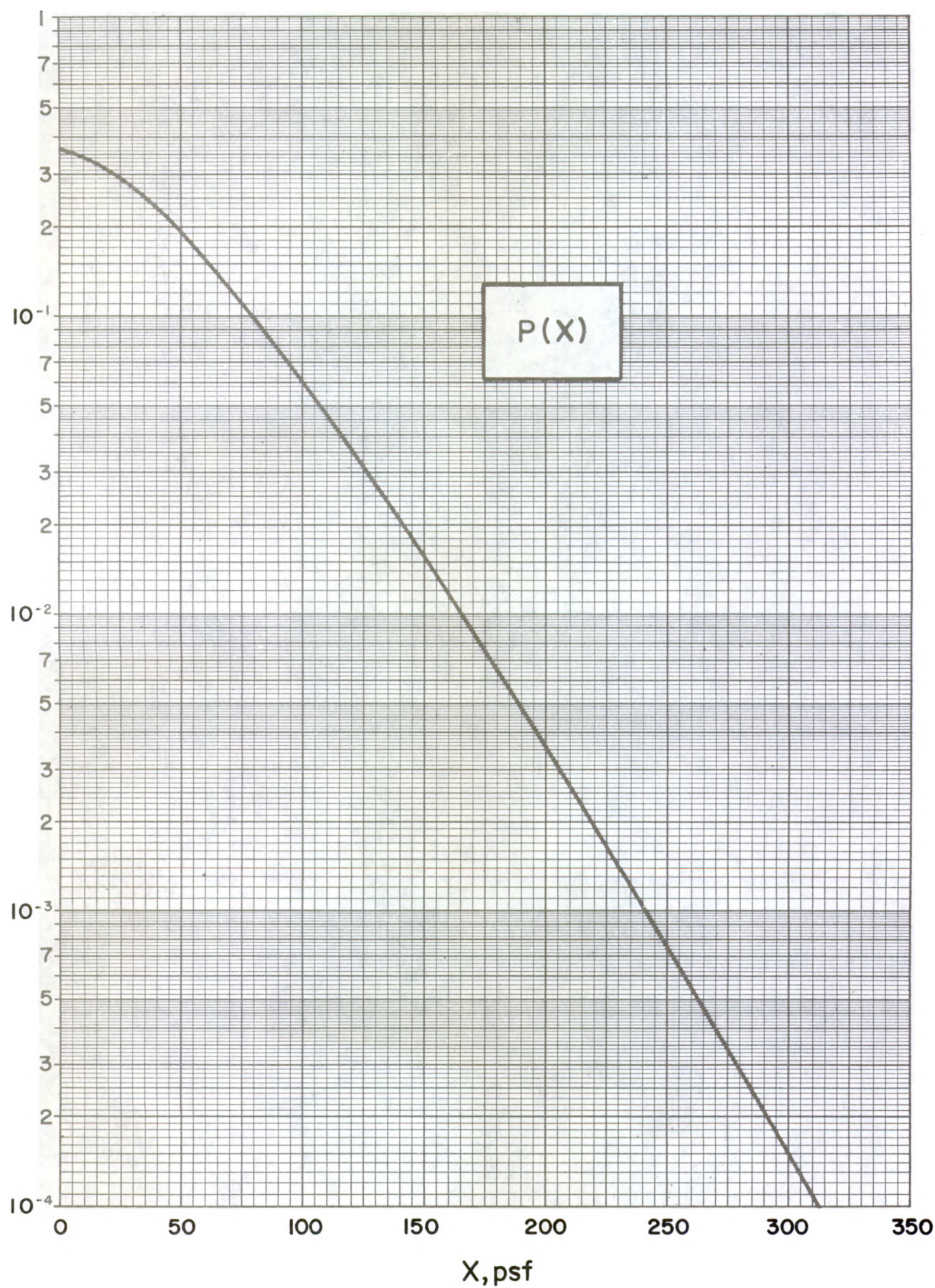
B.12.b  $^{137}\text{Cs}$  in  $\text{H}_2\text{O}$  (fig. V.18).





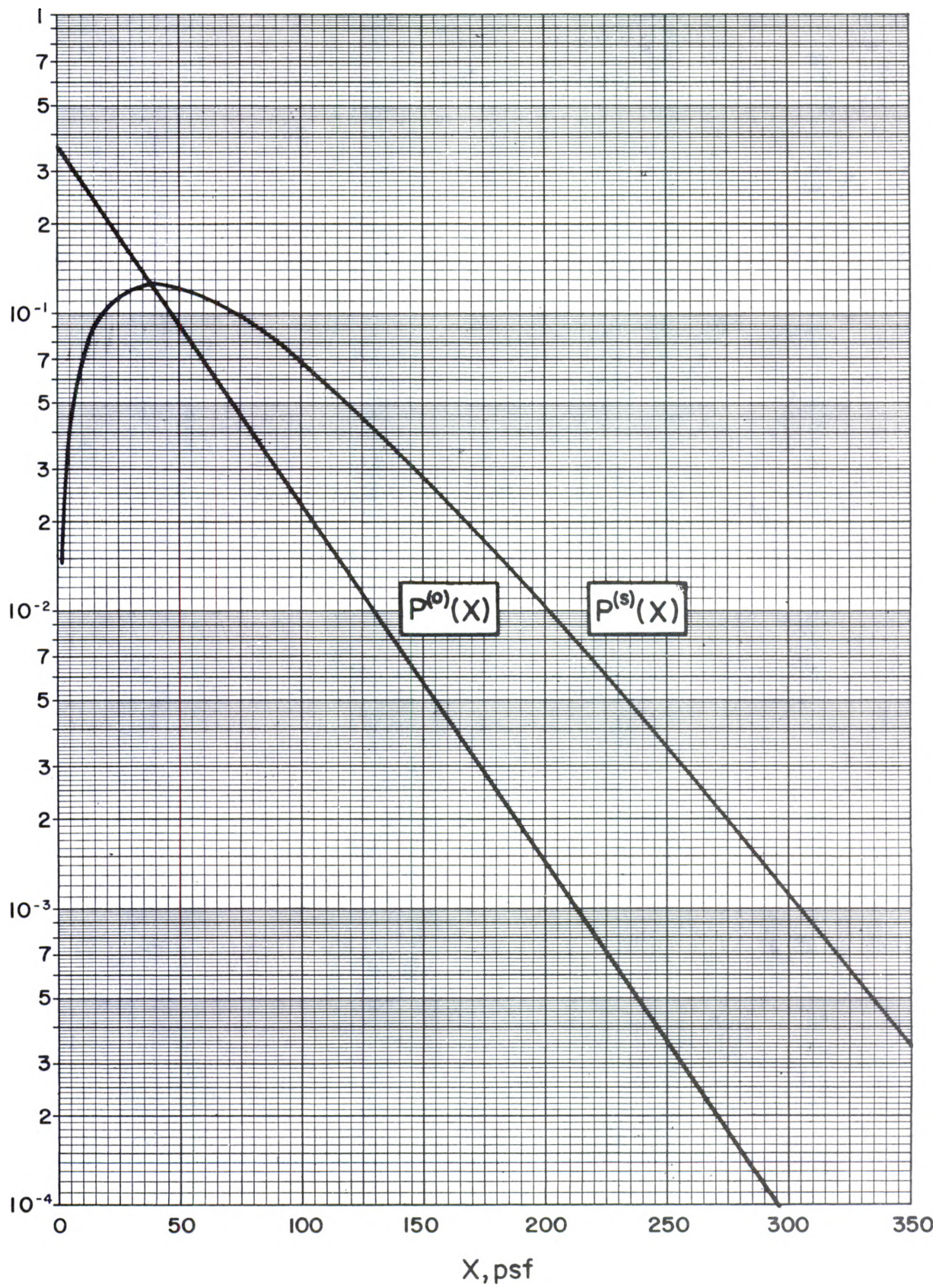
B.13.a  $^{60}\text{Co}$  in concrete (fig. V.19).





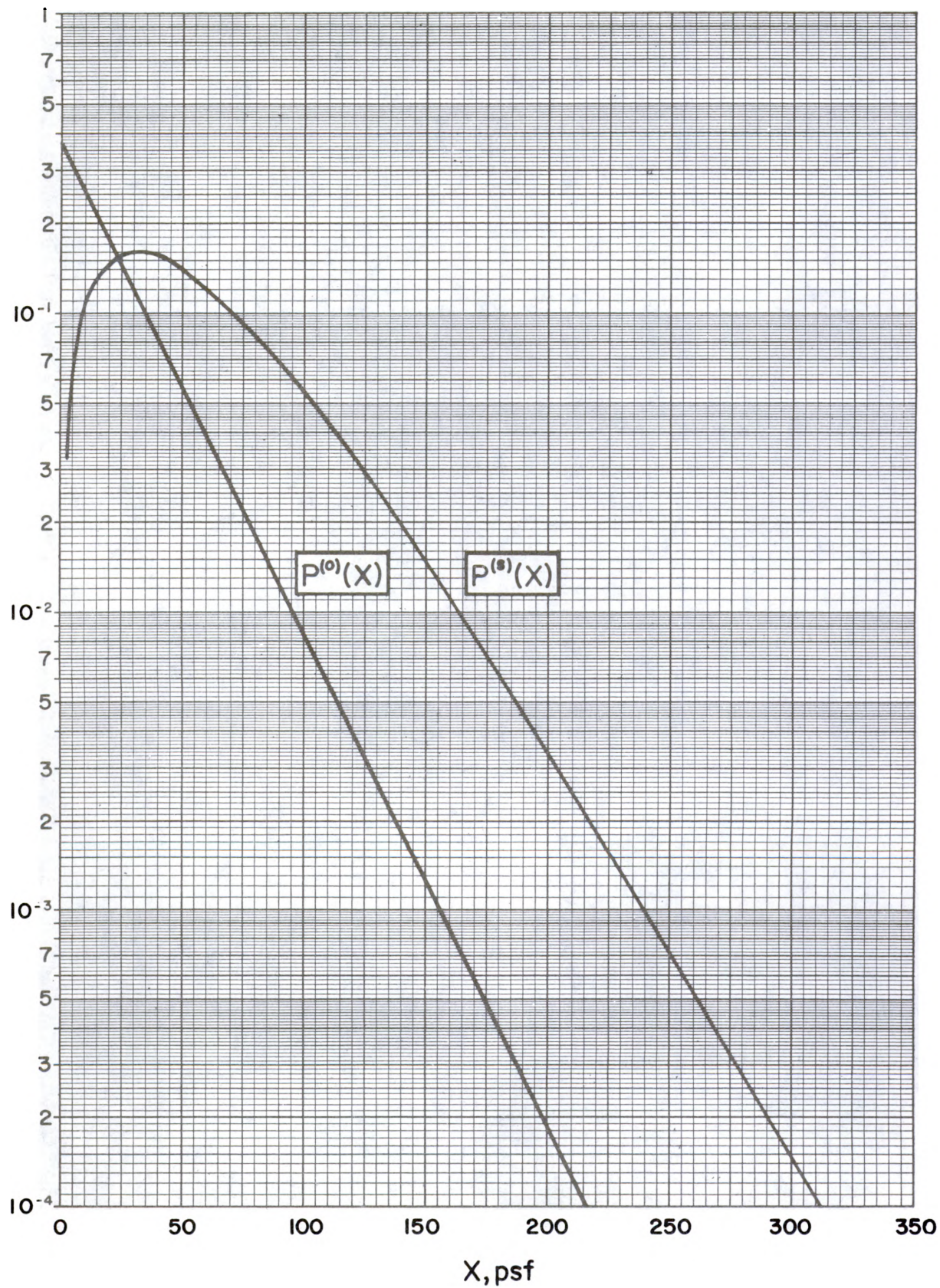
B.13.b  $^{137}\text{Cs}$  in concrete (fig V.19).





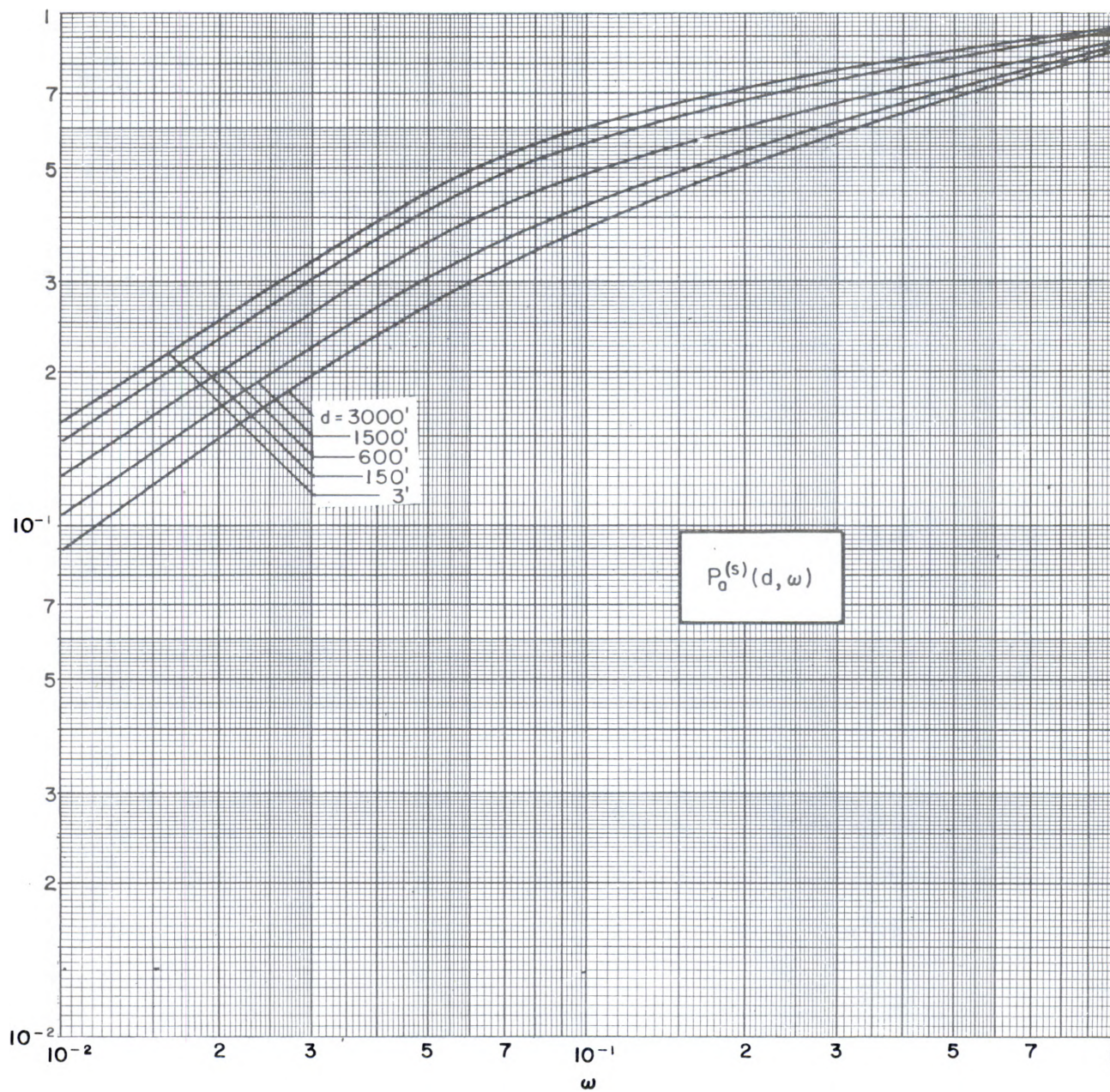
B.14.a  $^{60}\text{Co}$  in concrete (fig. V.20).



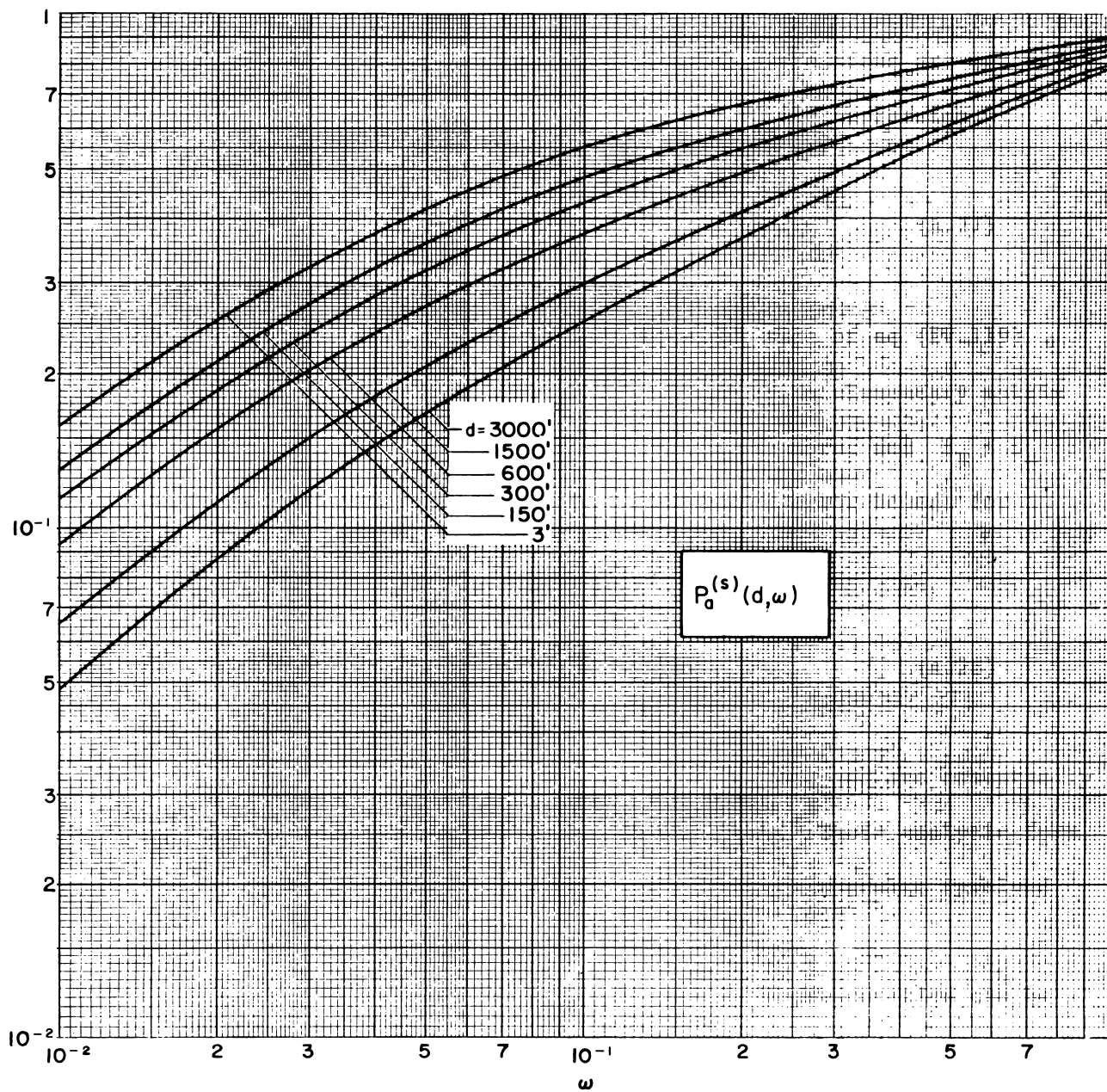


B.14.b  $^{137}\text{Cs}$  in concrete (fig. V.20).



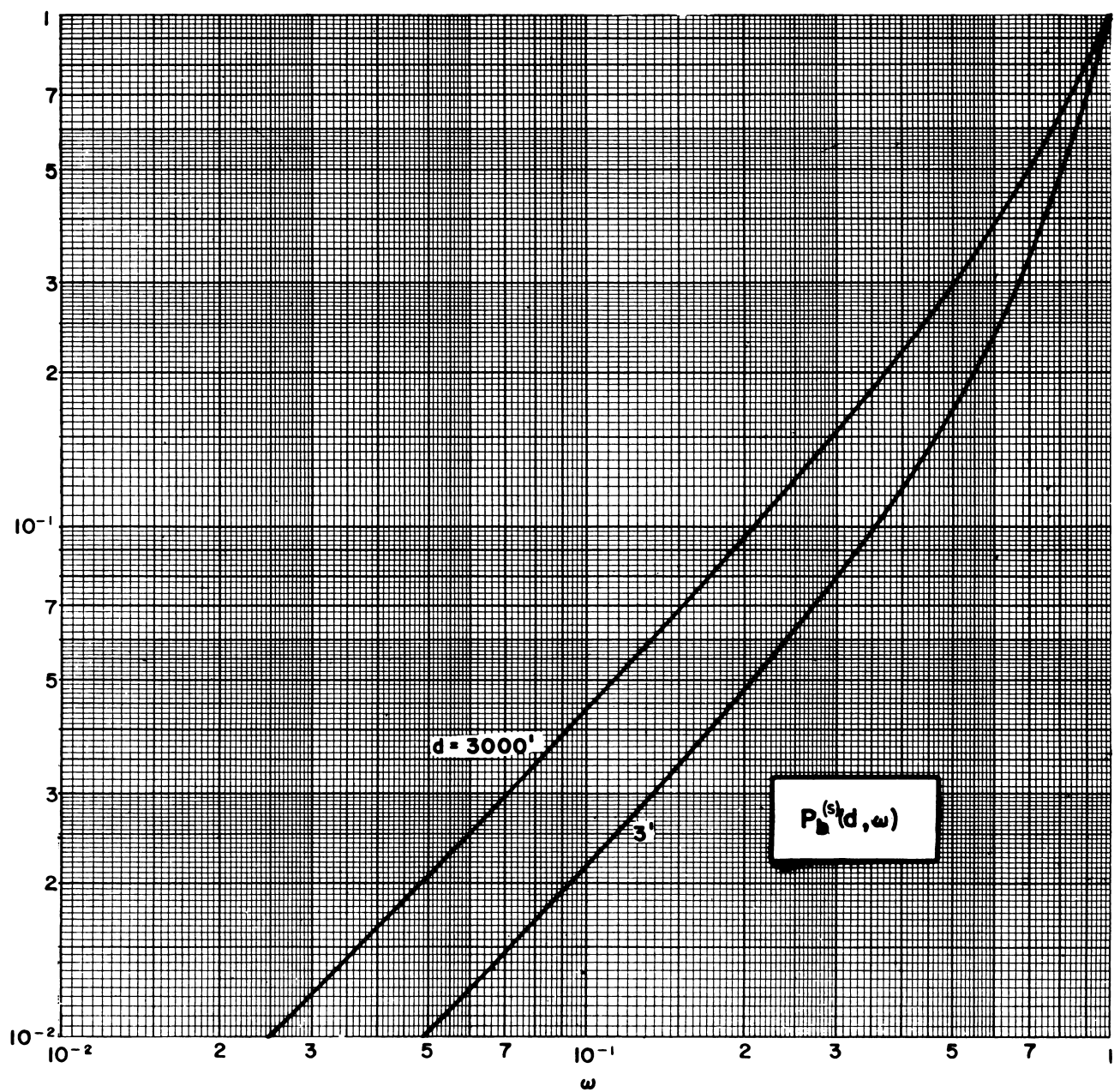


B.15.a  $^{60}\text{Co}$  in  $\text{H}_2\text{O}$  (fig. V.21).



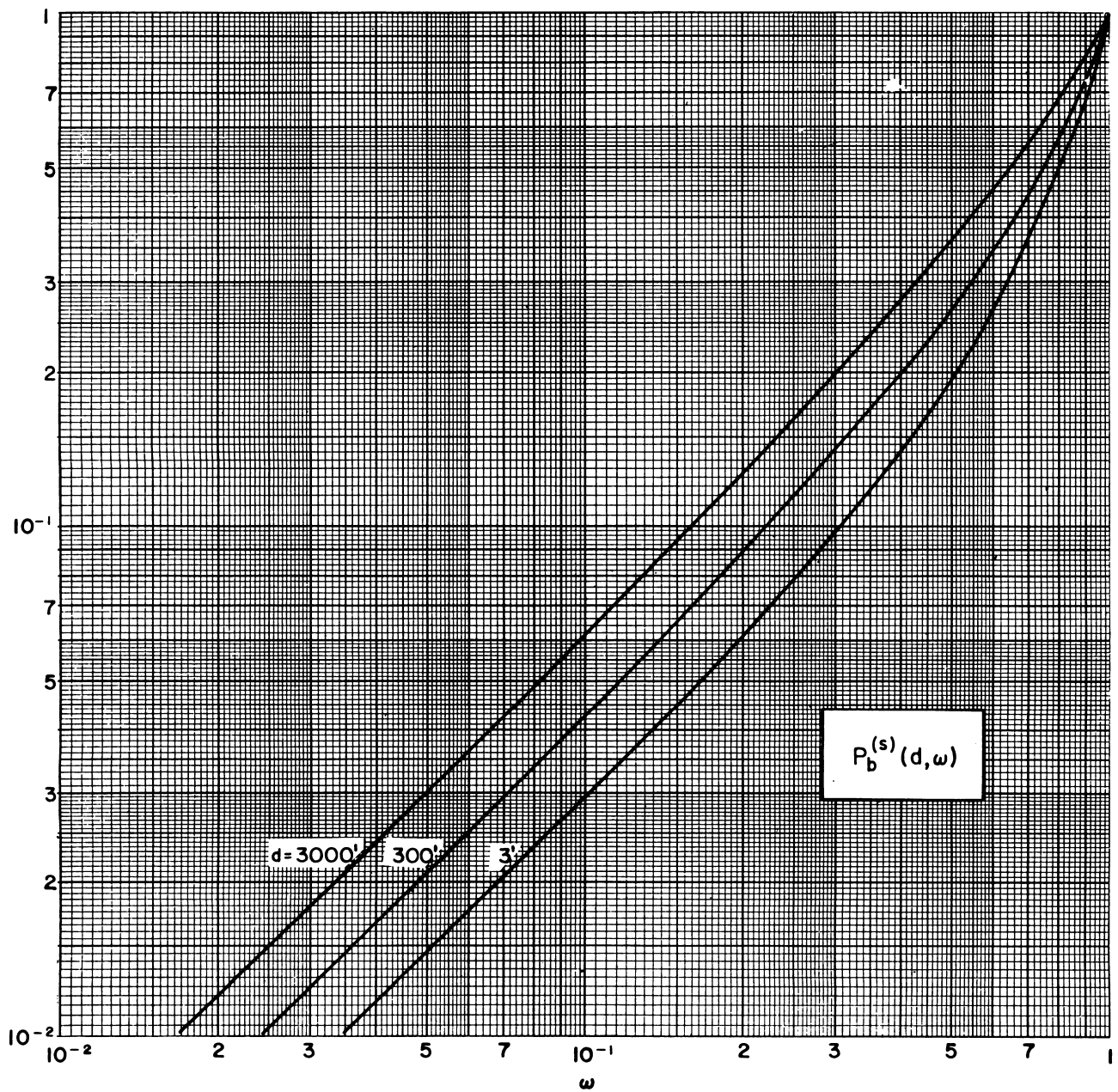
B.15.b  $^{137}\text{Cs}$  in  $\text{H}_2\text{O}$  (fig. V.21).





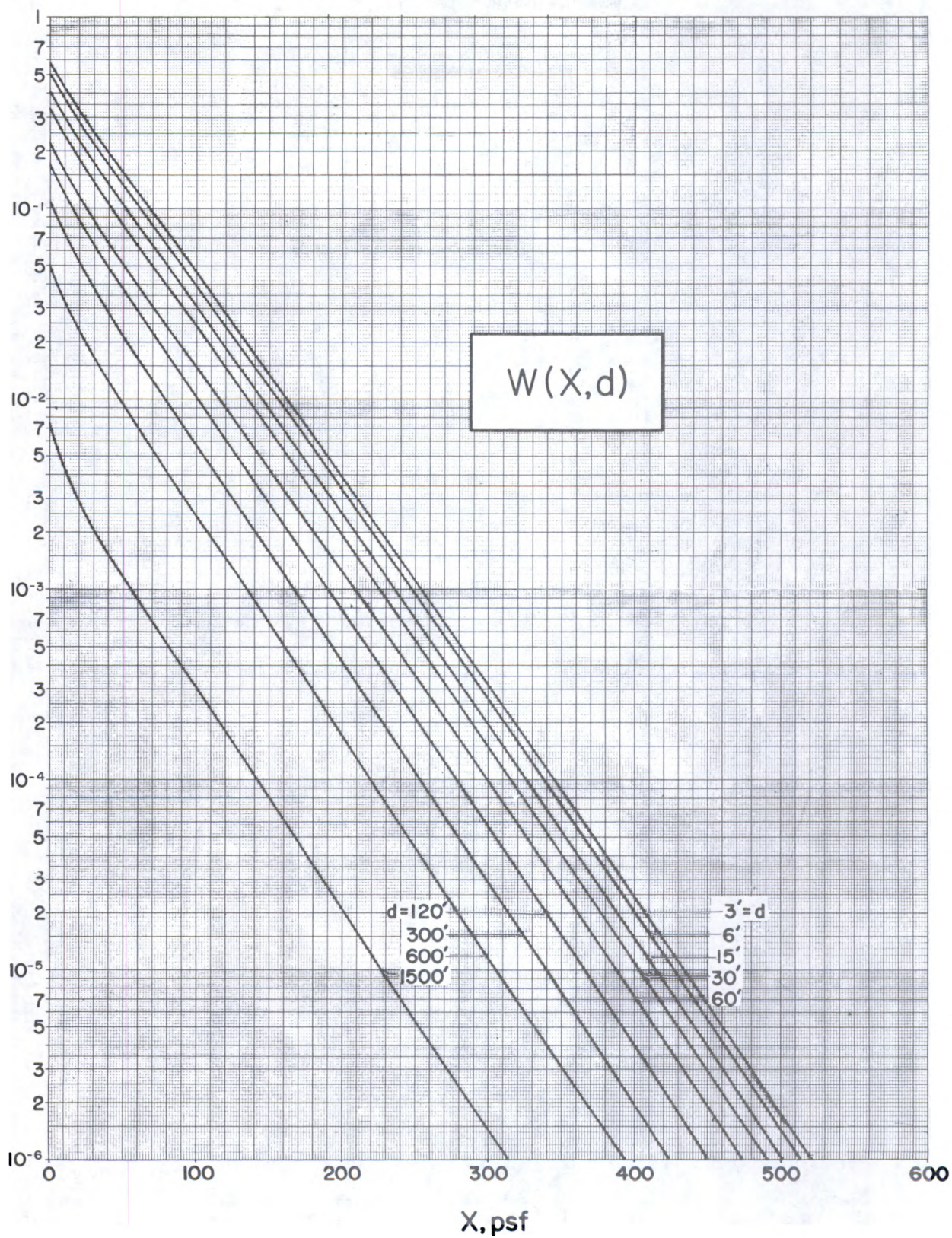
B.16.a  $^{60}\text{Co}$  in  $\text{H}_2\text{O}$  (fig. V.22).





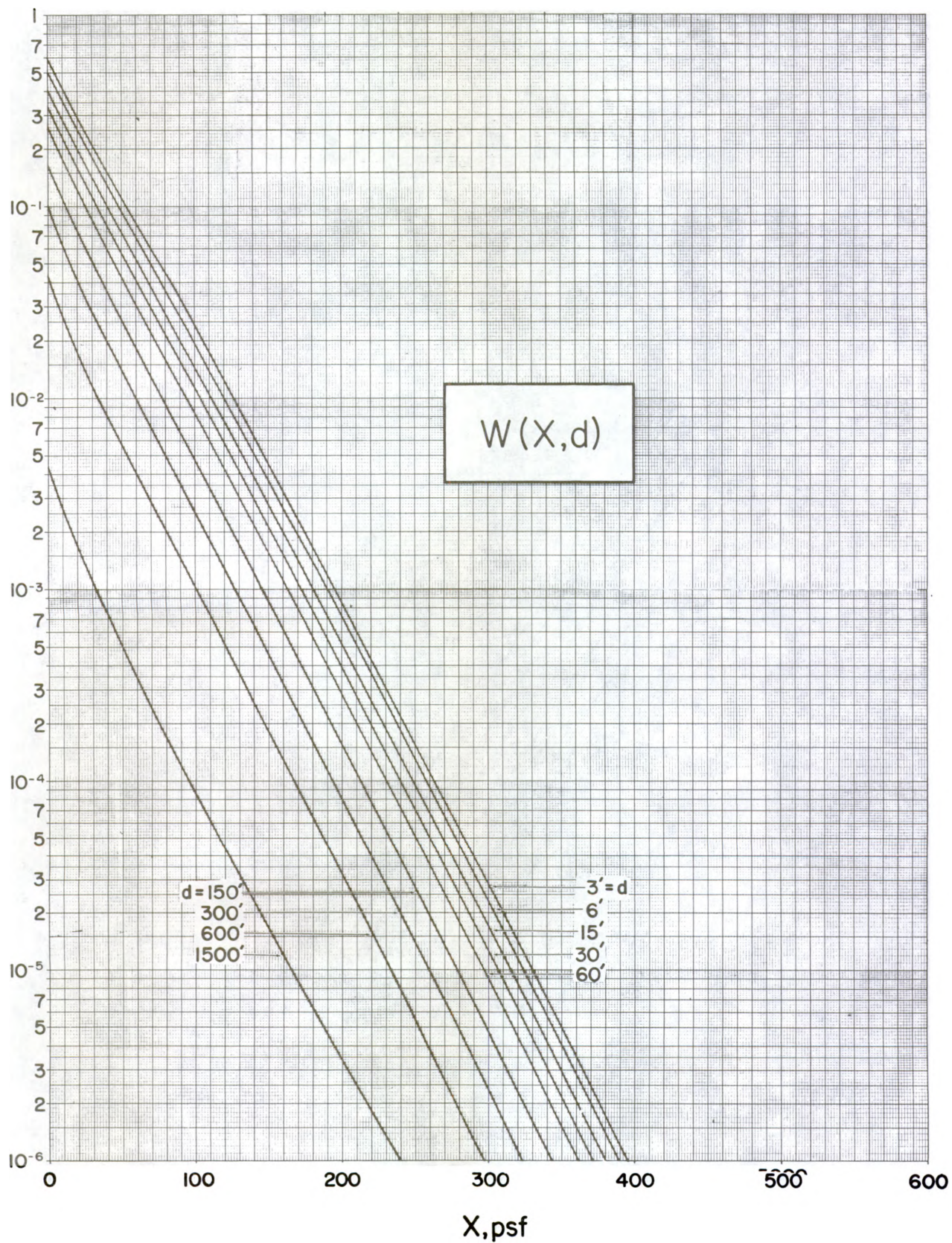
B.16.b  $^{137}\text{Cs}$  in  $\text{H}_2\text{O}$  (fig. V.22).





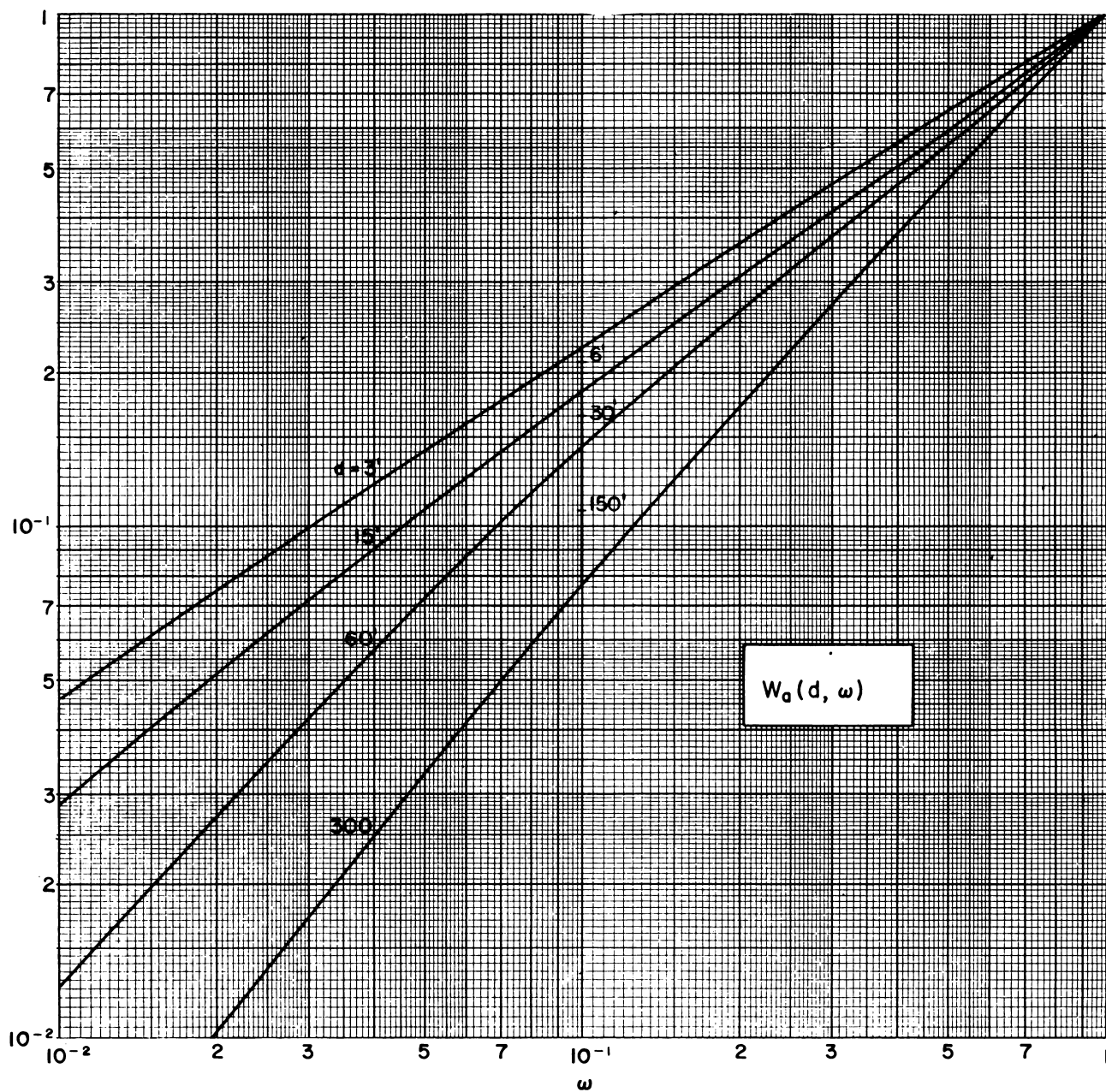
B.17.a Based on  $\ell(d, \cos\theta)$  data for  $^{60}\text{Co}$  gamma rays in  $\text{H}_2\text{O}$  and  $s(X, \cos\theta_0)$  data for  $^{60}\text{Co}$  in concrete (fig. V.23).



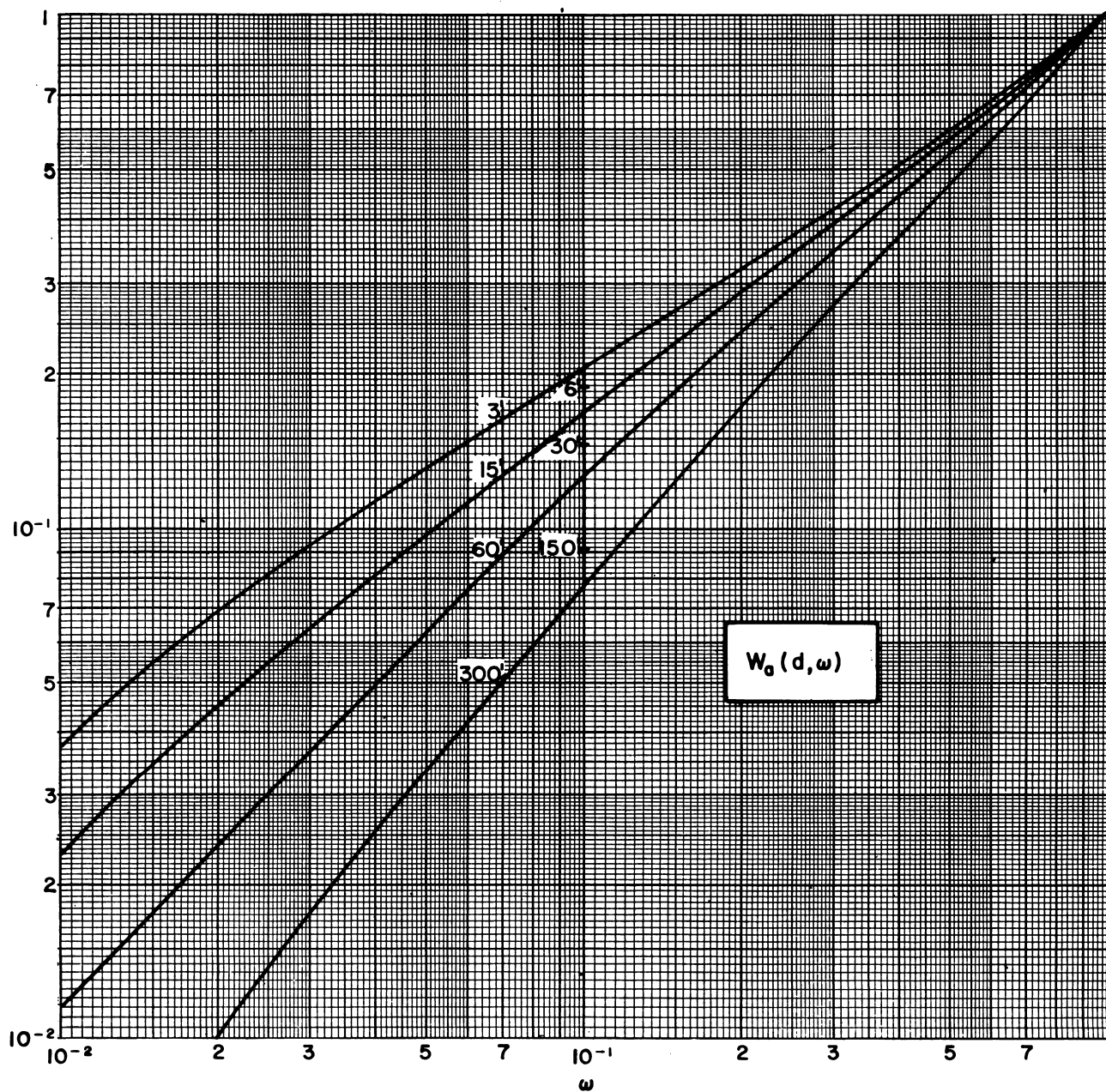


B.17.b Based on  $\ell(d, \cos\theta)$  data for  $^{137}\text{Cs}$  gamma rays in  $\text{H}_2\text{O}$  and  $s(x, \cos\theta_0)$  data for  $^{137}\text{Cs}$  in concrete (fig. V.23).

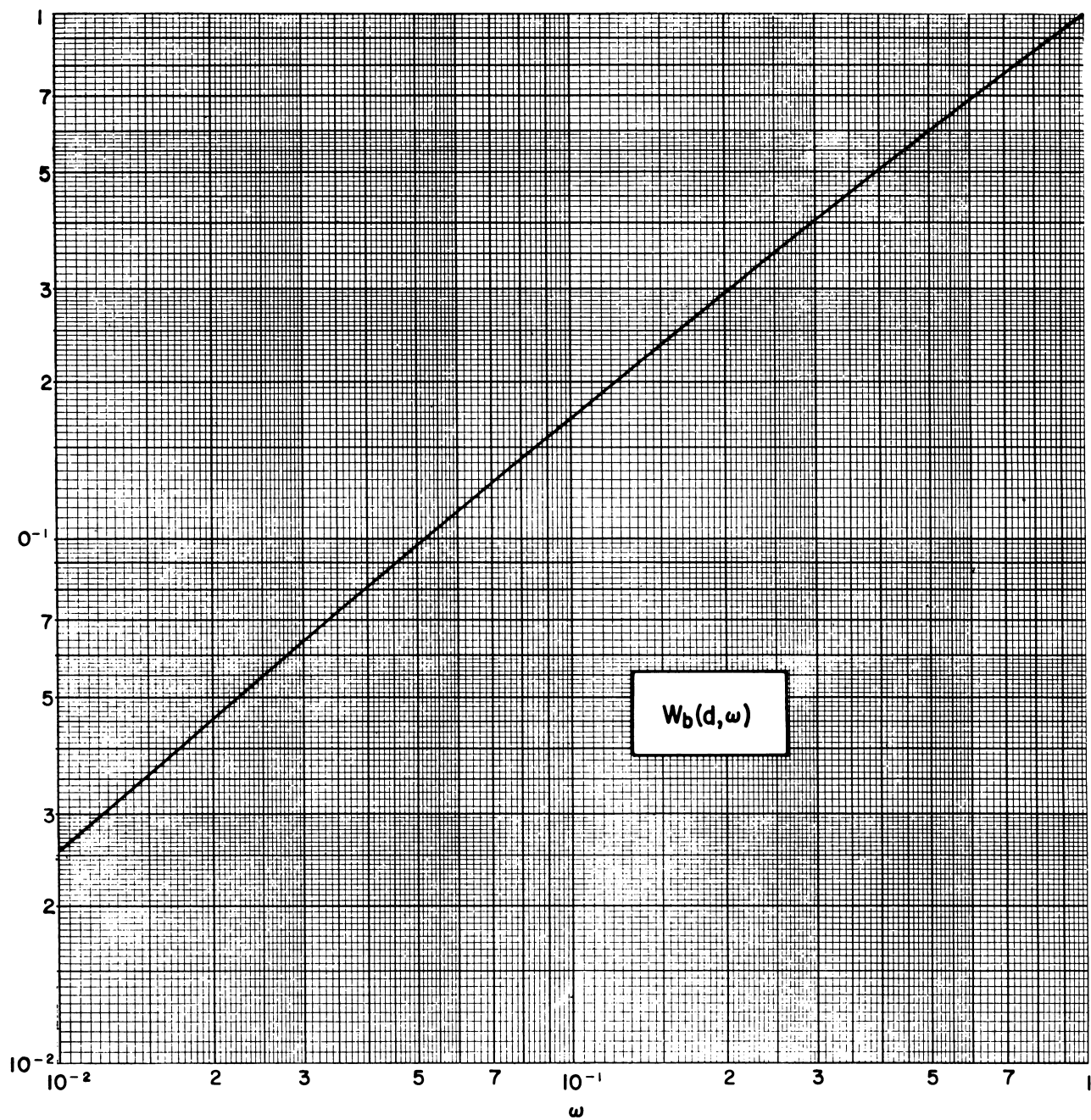




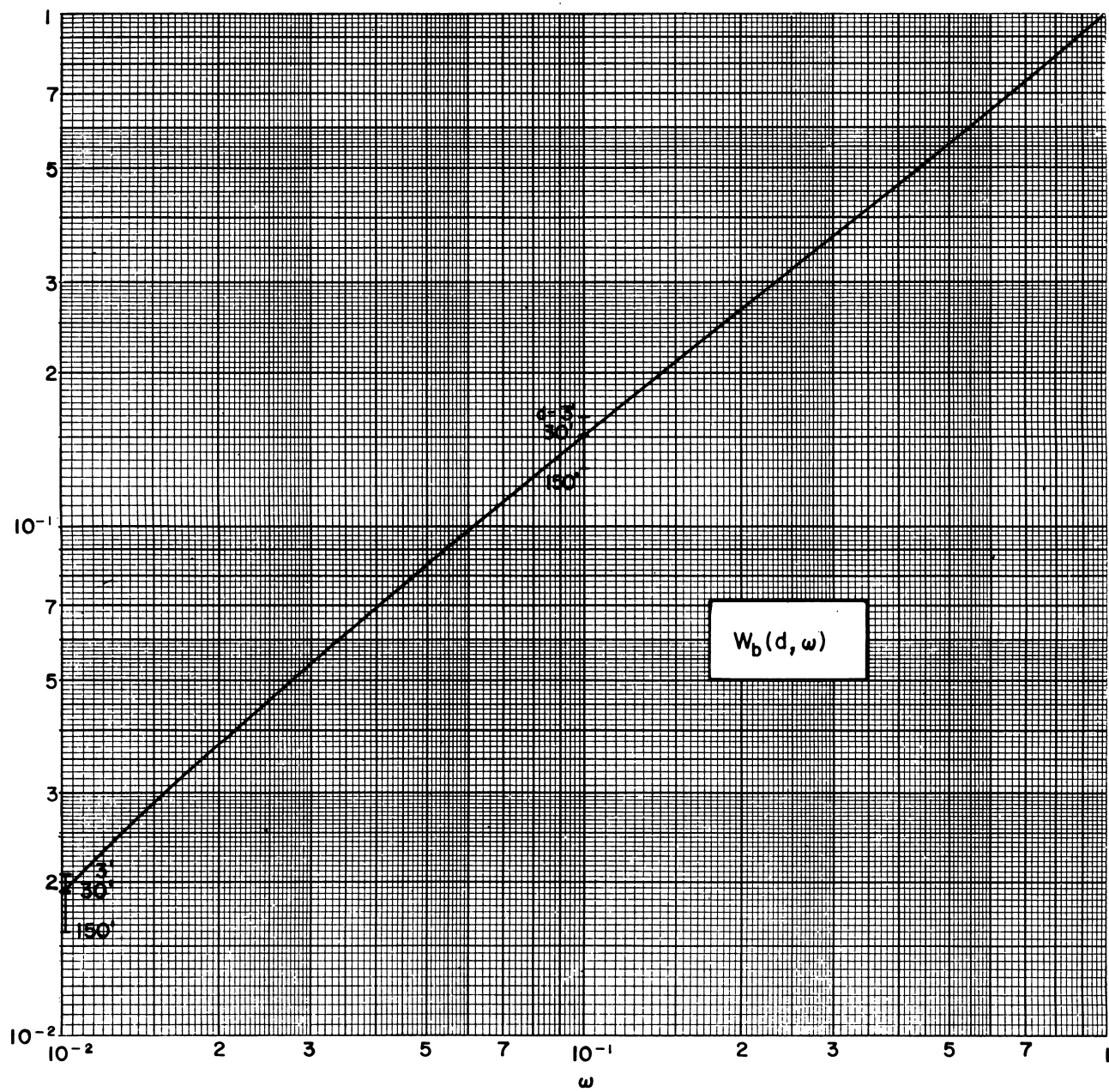
B.18.a  $^{60}\text{Co}$  in  $\text{H}_2\text{O}$  (fig. V.26).



B.18.b  $^{137}\text{Cs}$  in  $\text{H}_2\text{O}$  (fig. V.26).

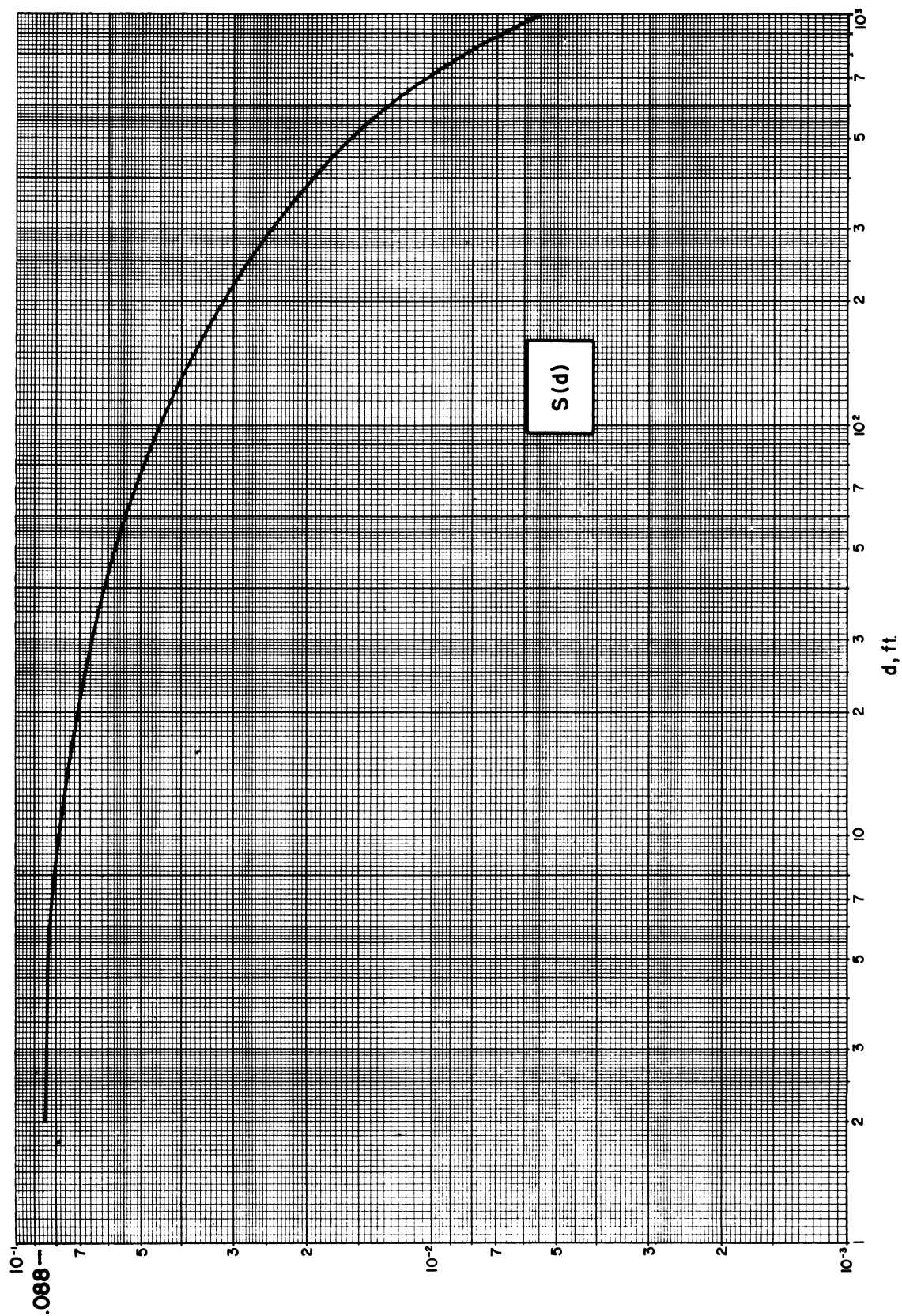


B.19.a  $^{60}\text{Co}$  in  $\text{H}_2\text{O}$  (fig. V.27).



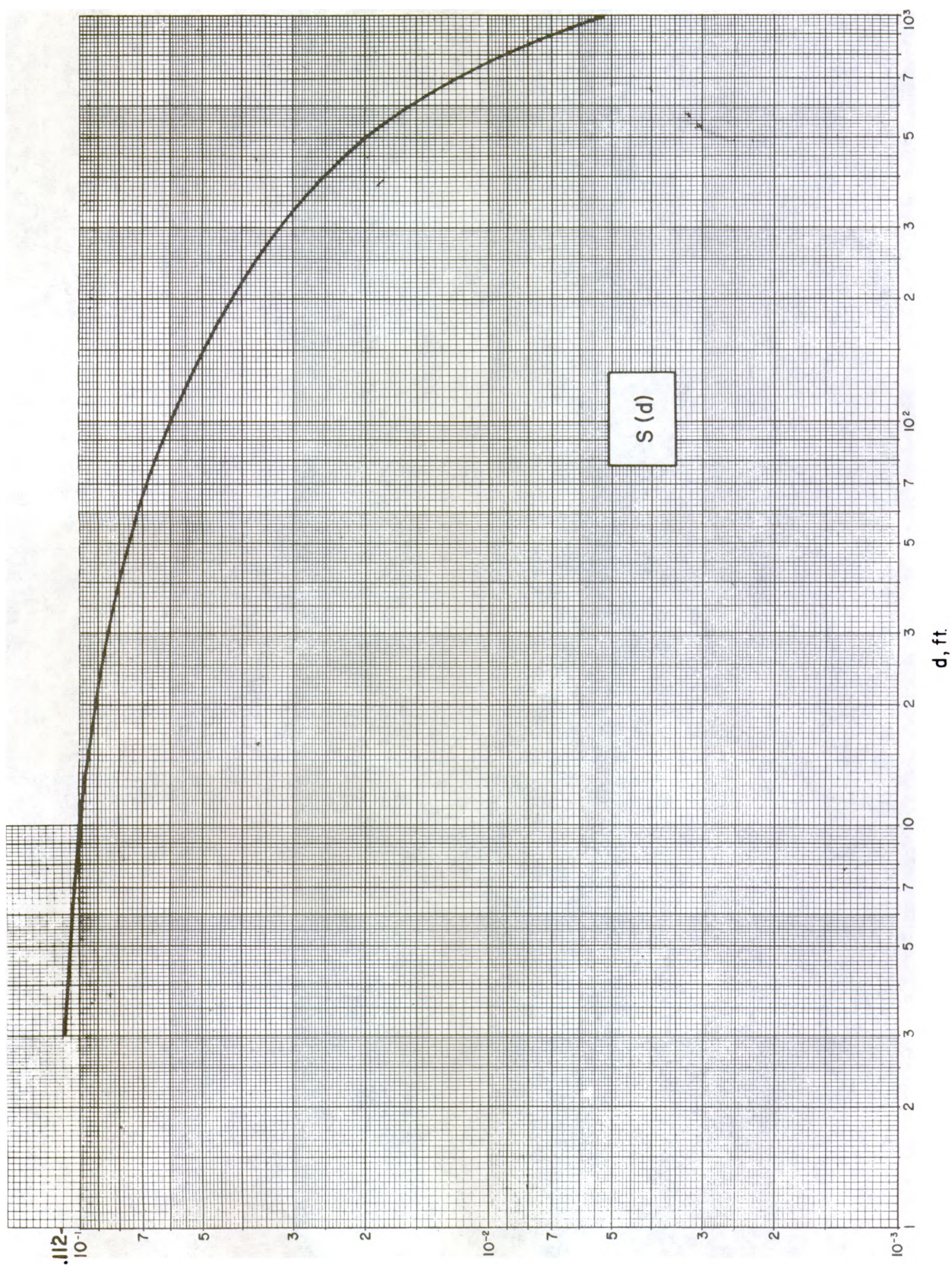
B.19.b  $^{137}\text{Cs}$  in  $\text{H}_2\text{O}$  (fig. V.27).





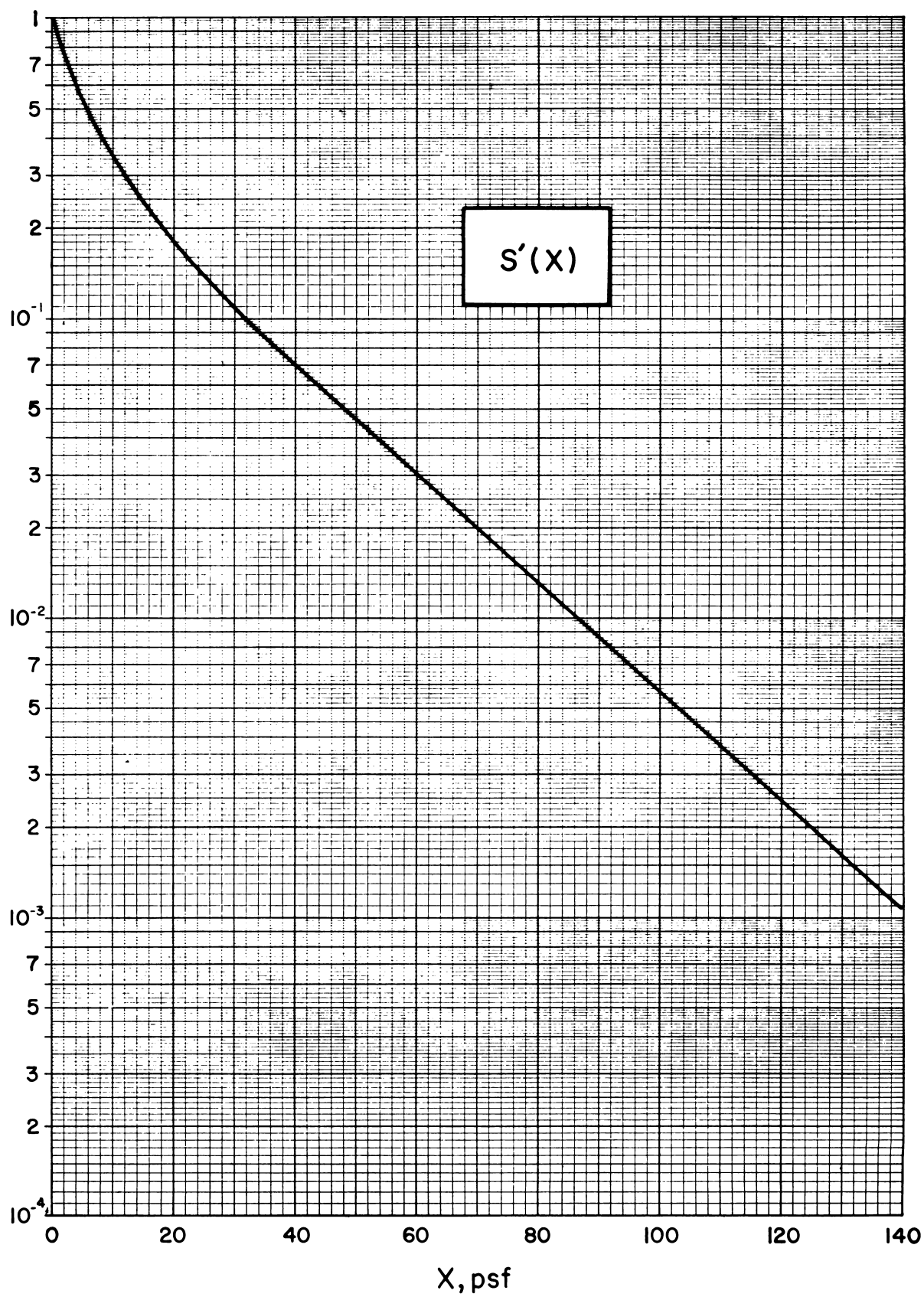
B.20.a  $^{60}\text{Co}$  in  $\text{H}_2\text{O}$  (fig. V.28).



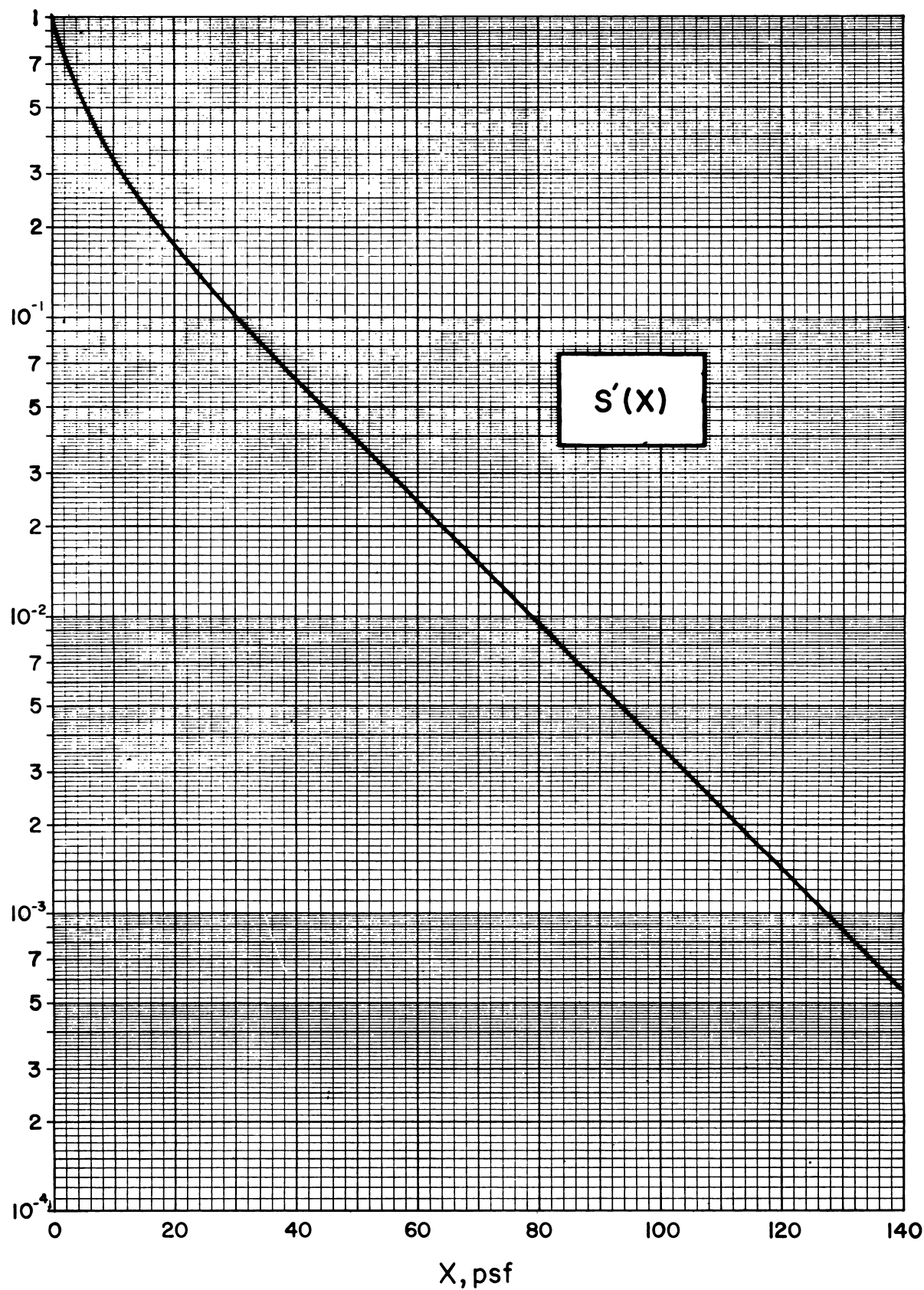


B.20.b  $^{137}\text{Cs}$  in  $\text{H}_2\text{O}$  (fig. V.28).

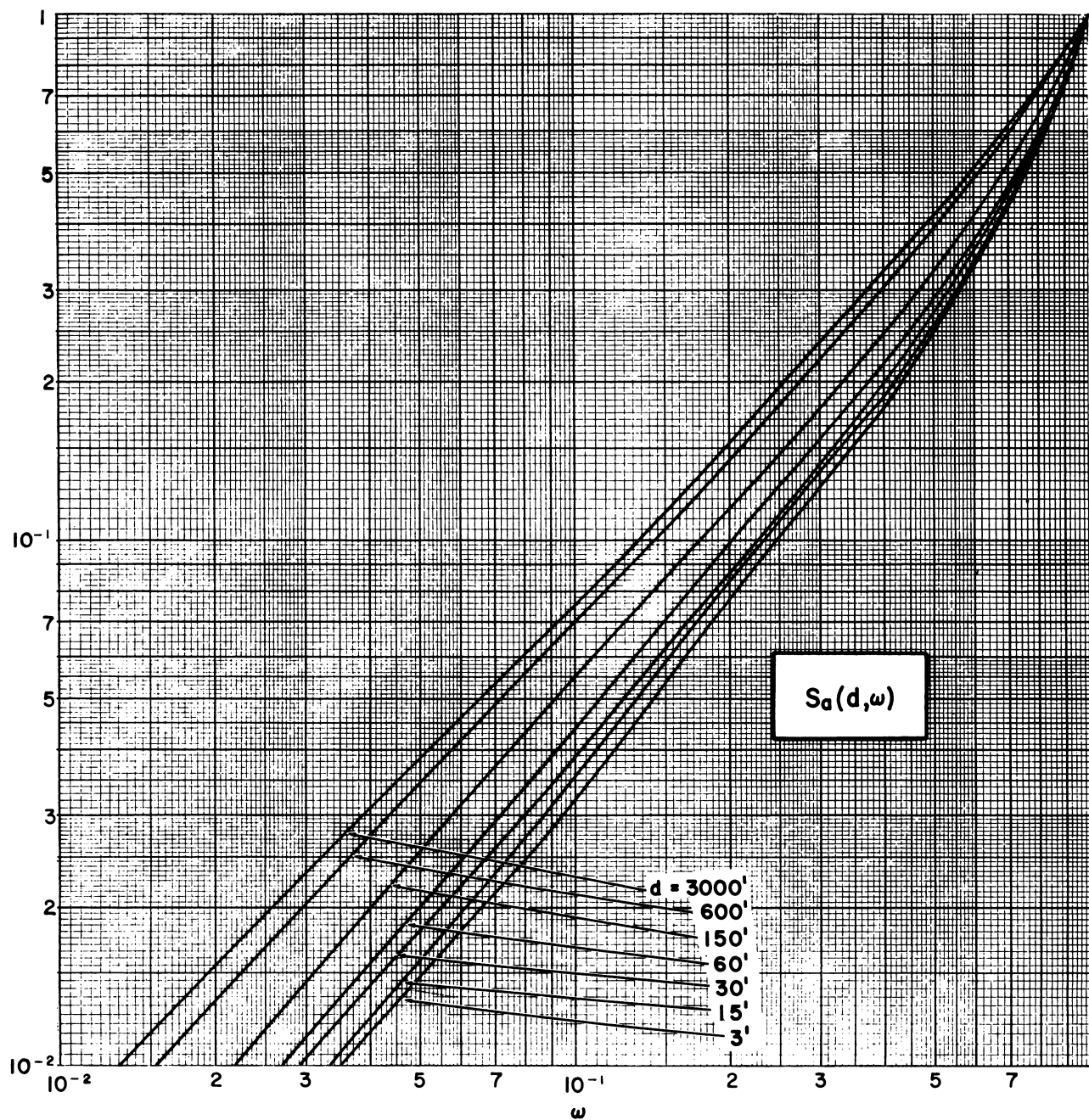




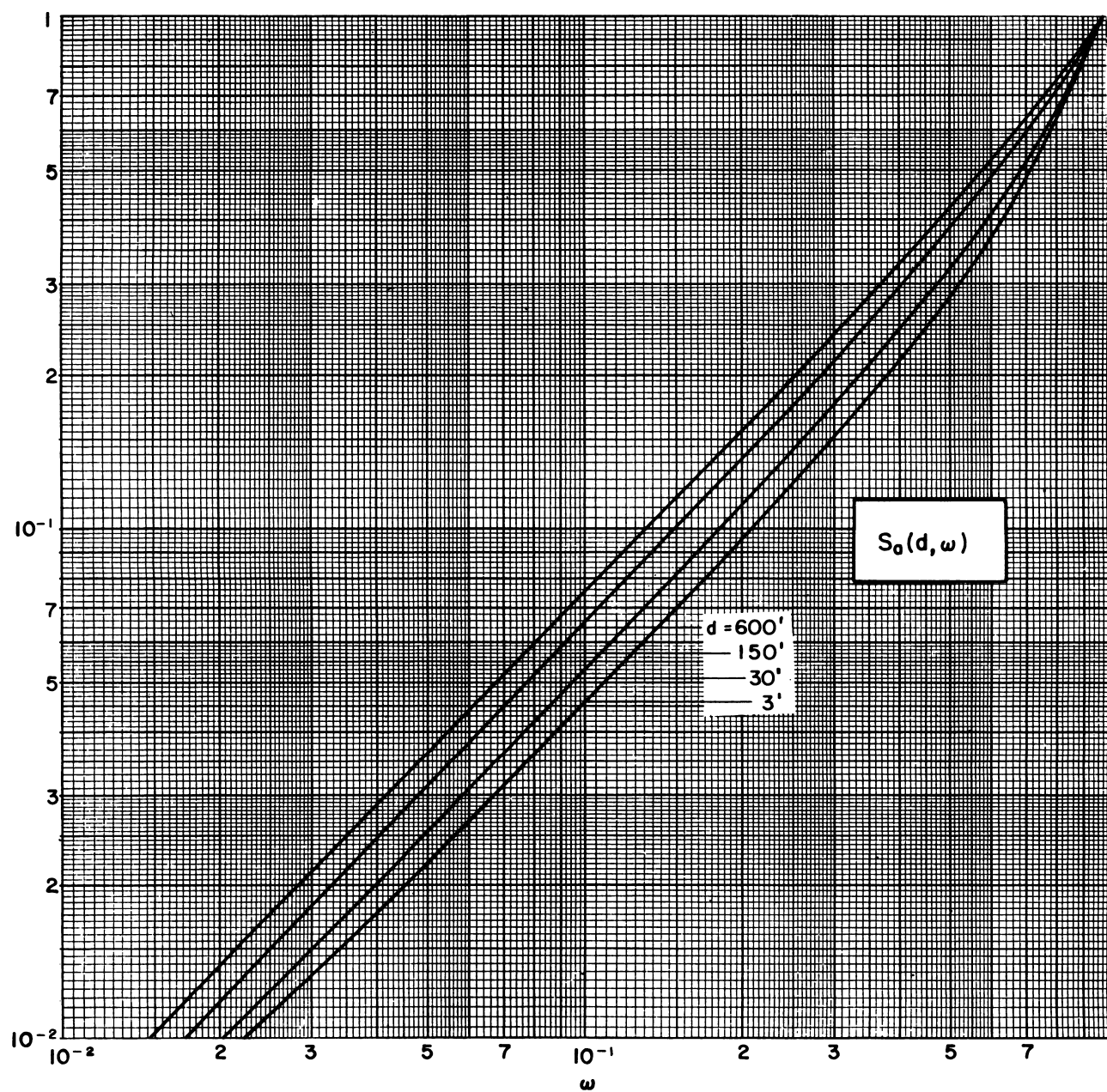
B.21.a  $^{60}\text{Co}$  in concrete (fig. V.29).



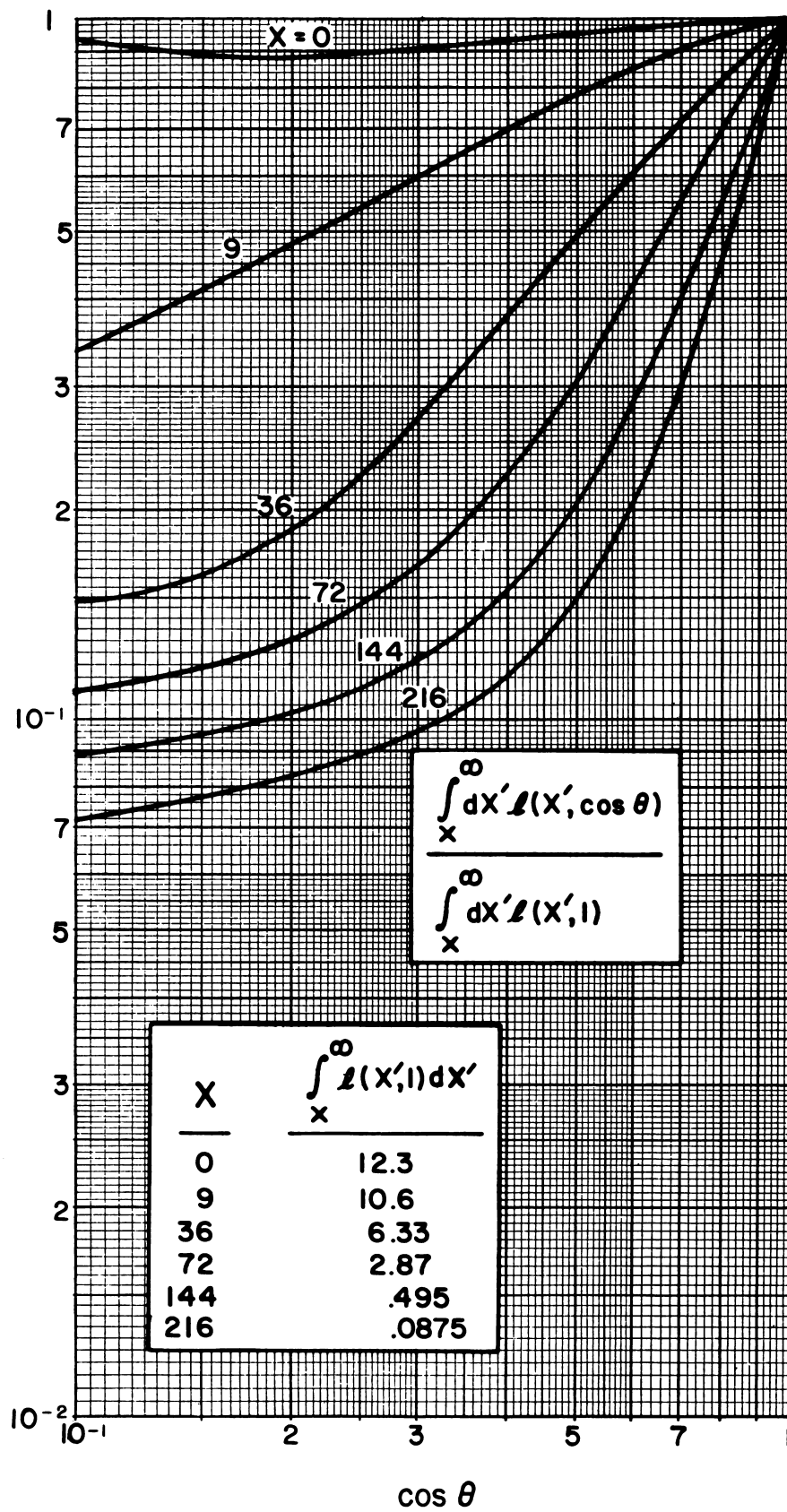
B.21.b  $^{137}\text{Cs}$  in concrete (fig. V.29).



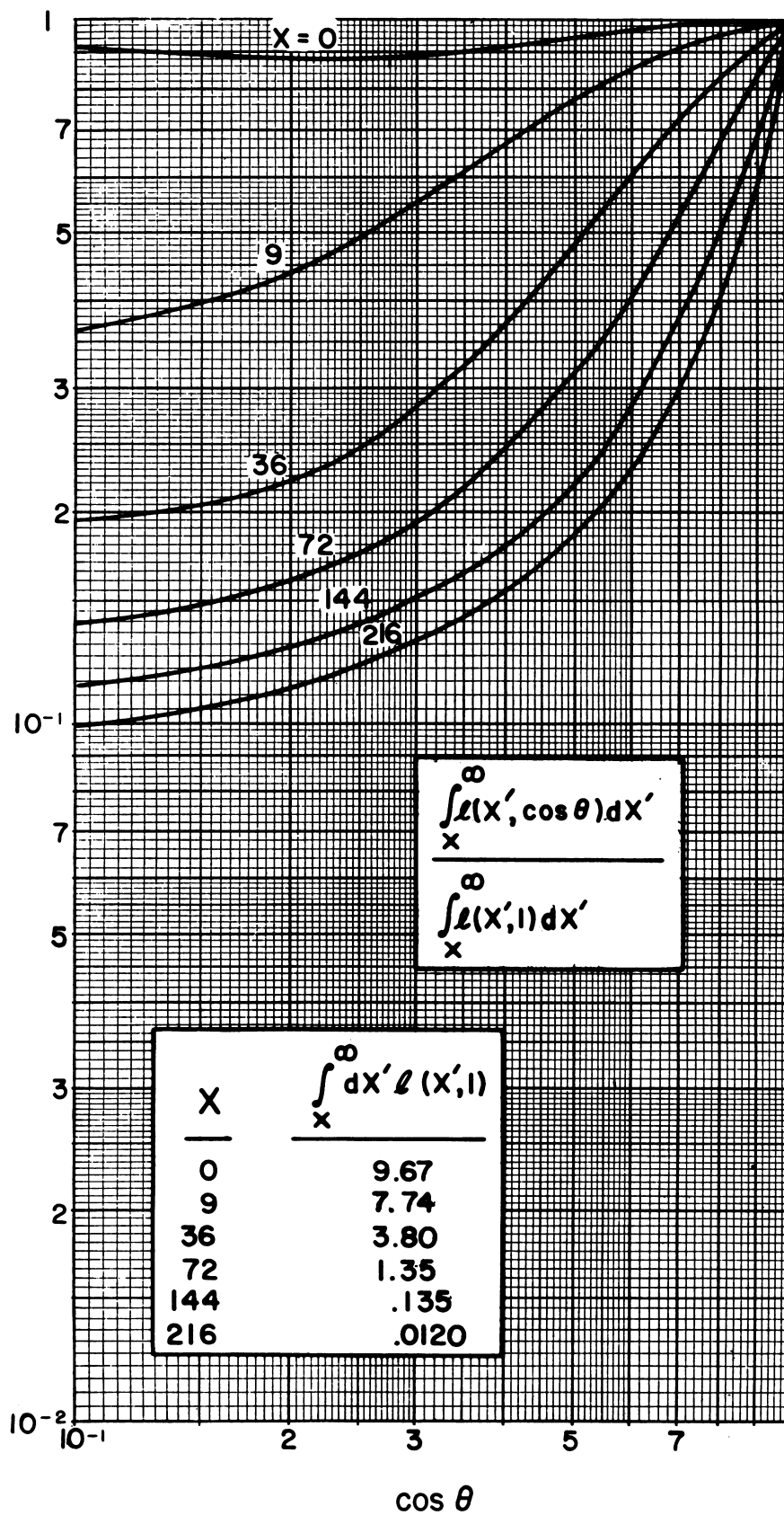
B.22.a  $^{60}\text{Co}$  in  $\text{H}_2\text{O}$  (fig. V.30).



B.22.b  $^{137}\text{Cs}$  in  $\text{H}_2\text{O}$  (fig. V.30).



B.23.a  $^{60}\text{Co}$  in concrete (fig. V.32).



B.23.b  $^{137}\text{Cs}$  in concrete (fig. V.32).

APPENDIX C: CHARTS FROM OCD STANDARD METHOD FOR FALLOUT GAMMA RADIATION  
SHIELDING ANALYSIS

The charts in this appendix were taken from Appendix C of reference [1]. They represent the source data for functions used in the Standard Method. They were last updated in September 1971 and are still used in the recent revision (1975) of reference [1]. Tabular values based on these charts are given in reference [2].



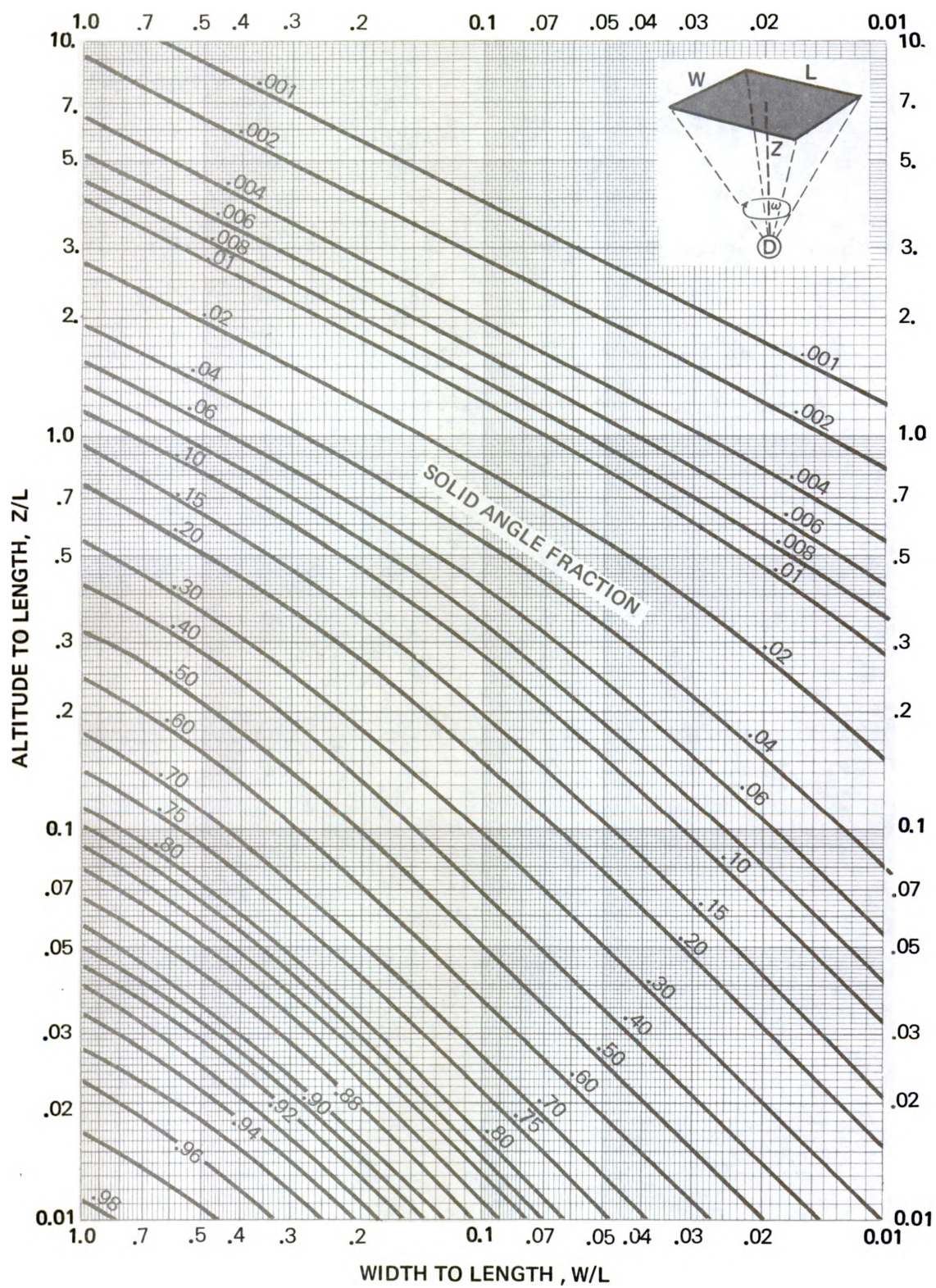


CHART 1 A  
SOLID ANGLE FRACTION,  $\omega(W/L, Z/L)$

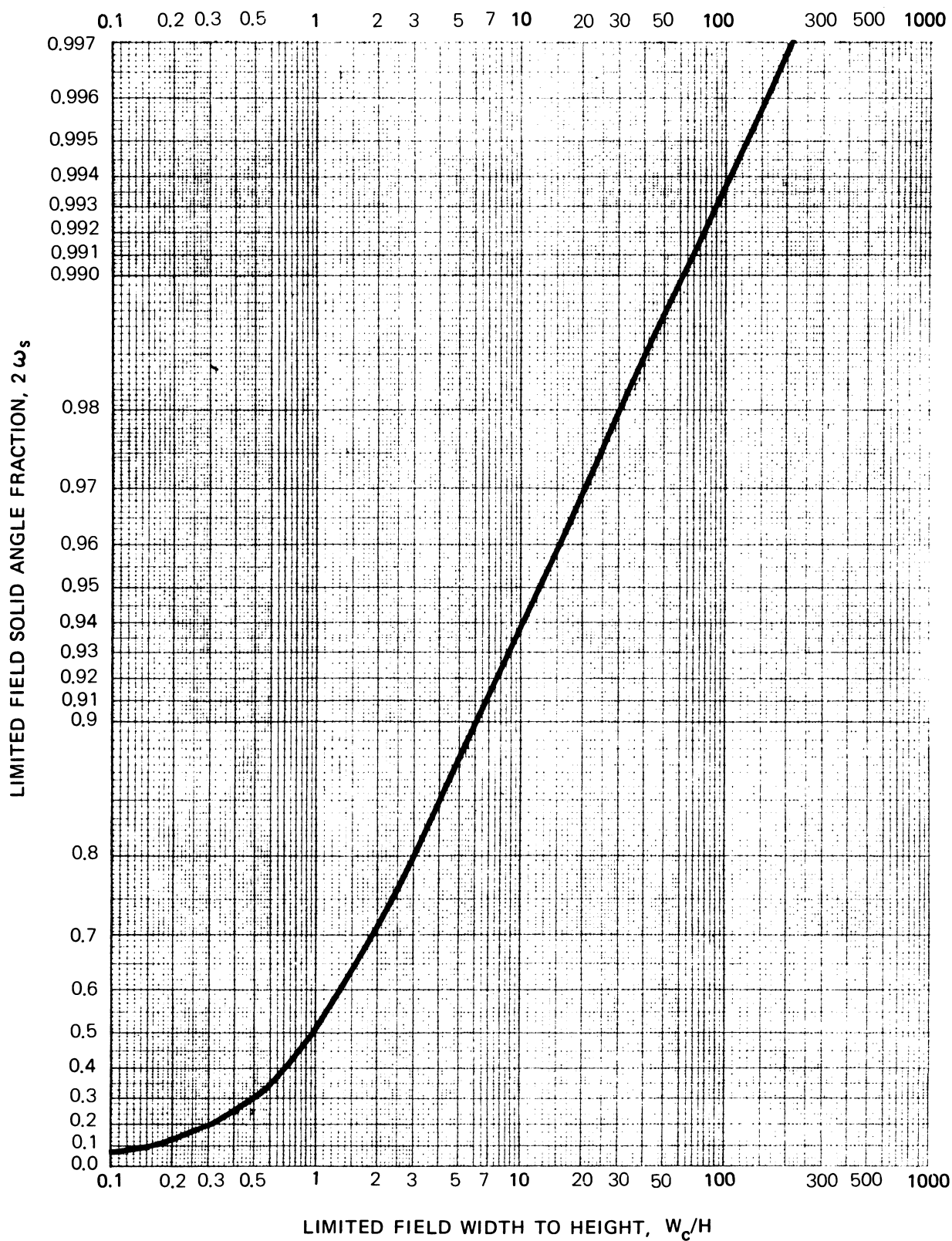


CHART 1B  
LIMITED FIELD SOLID ANGLE FRACTION,  $2\omega_s$



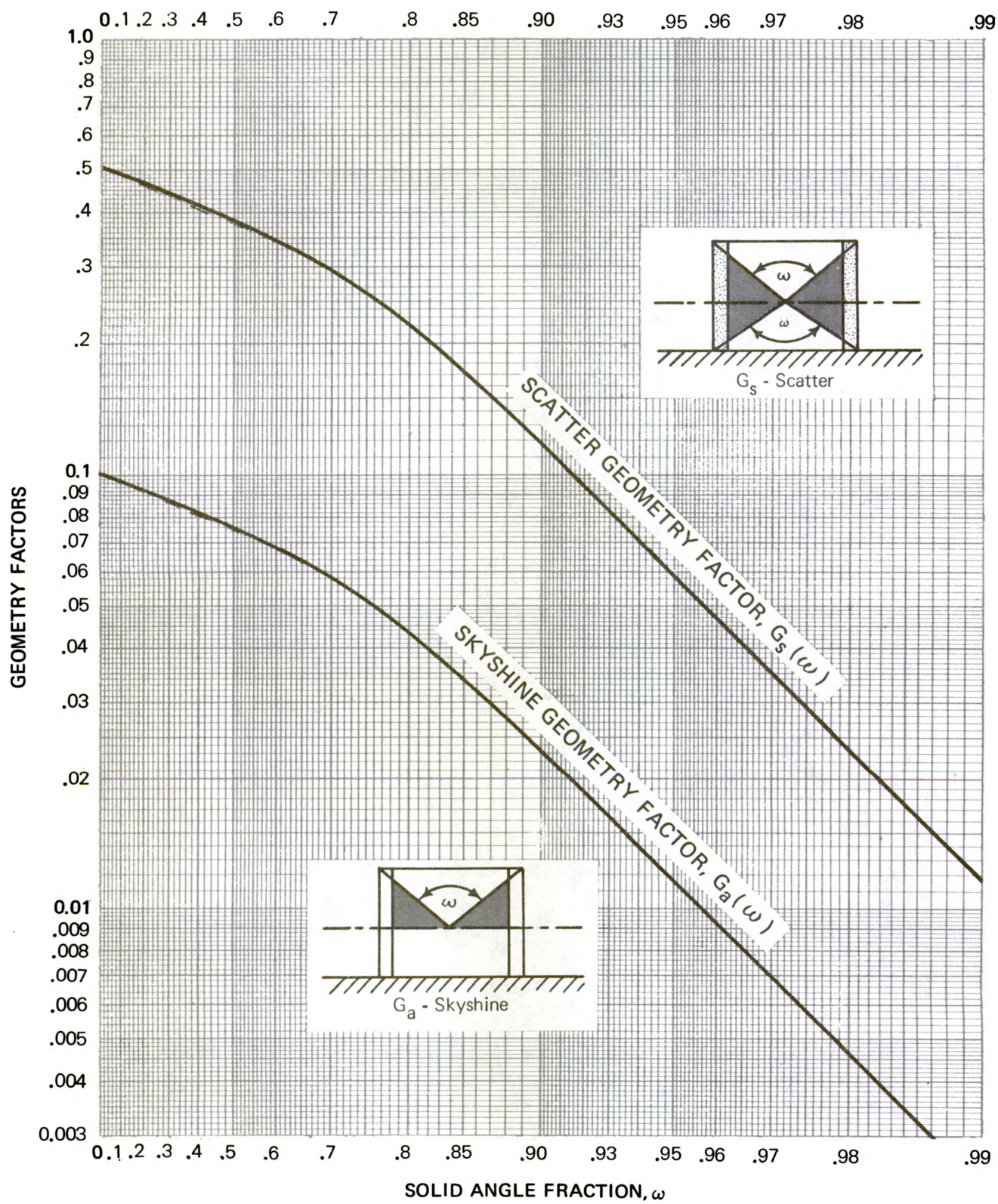


CHART 2  
GEOMETRY FACTORS - SCATTER,  $G_s(\omega)$  AND SKYSHINE,  $G_a(\omega)$



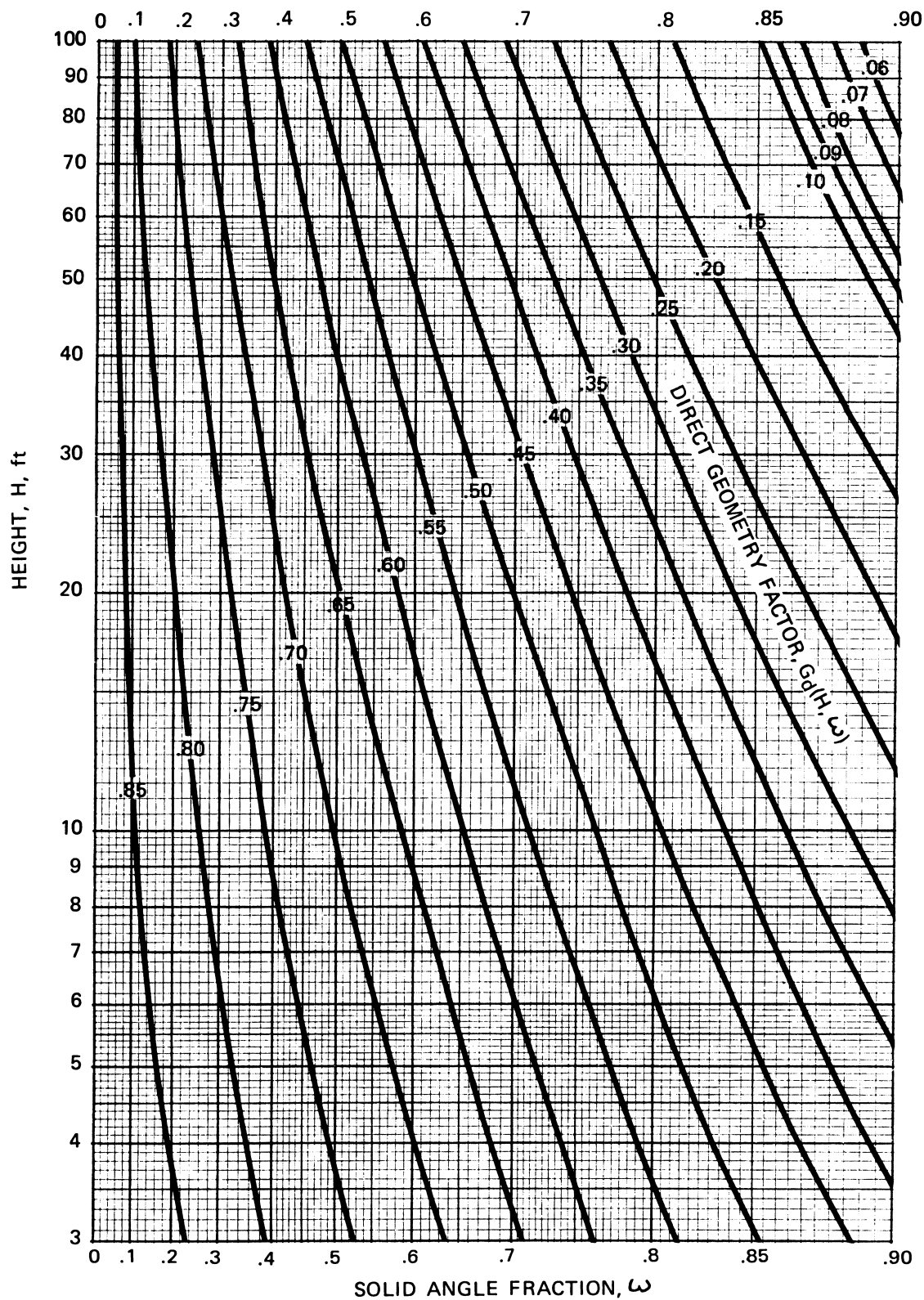


CHART 3A  
GEOMETRY FACTOR - DIRECT,  $G_d(H, \omega)$

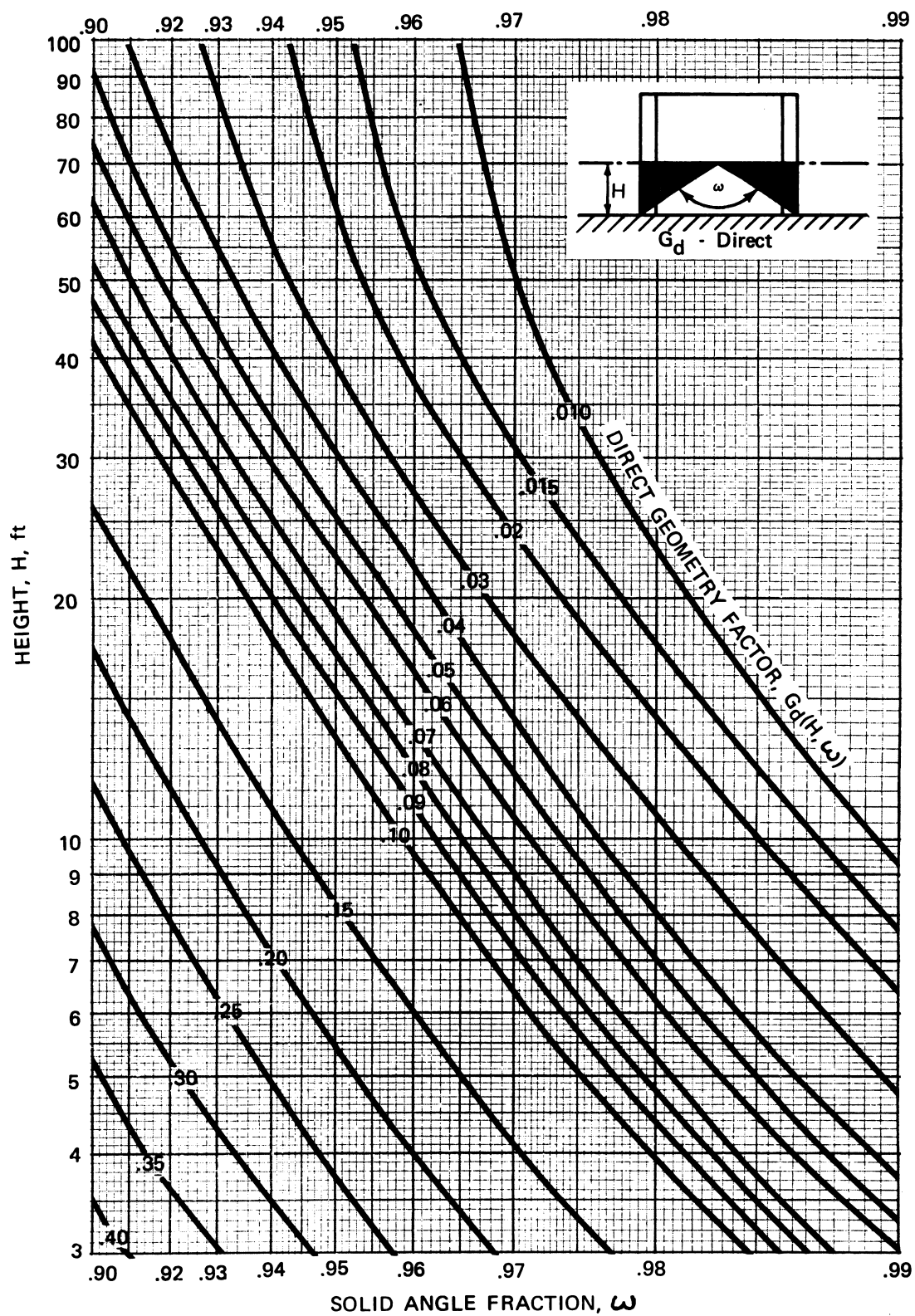
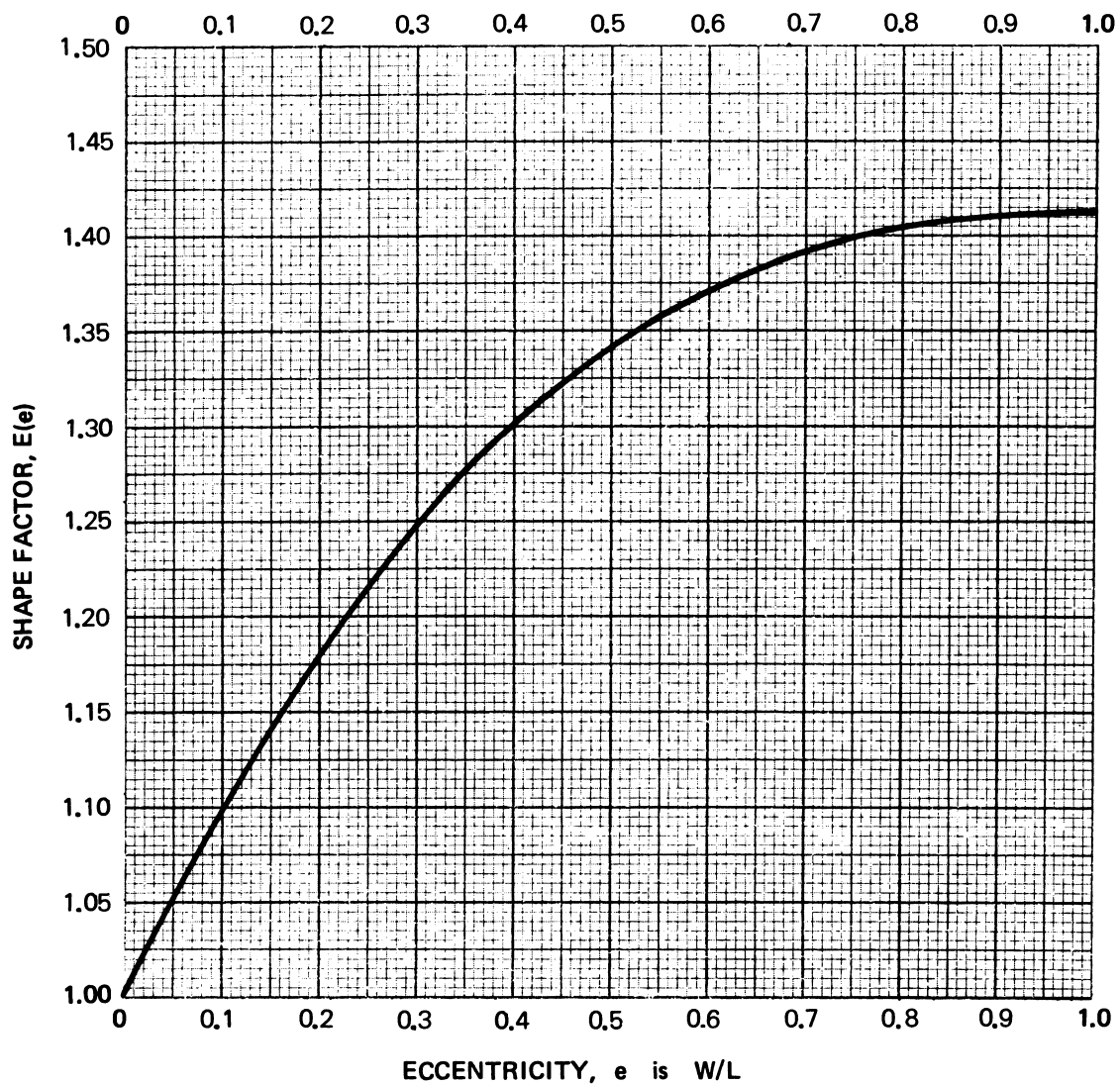


CHART 3B  
GEOMETRY FACTOR - DIRECT,  $G_d(H, \omega)$



$E(e)$  FOR CIRCULAR STRUCTURES IS  $\frac{\pi}{2} = 1.571$

**CHART 4**  
**SHAPE FACTOR,  $E(e)$**

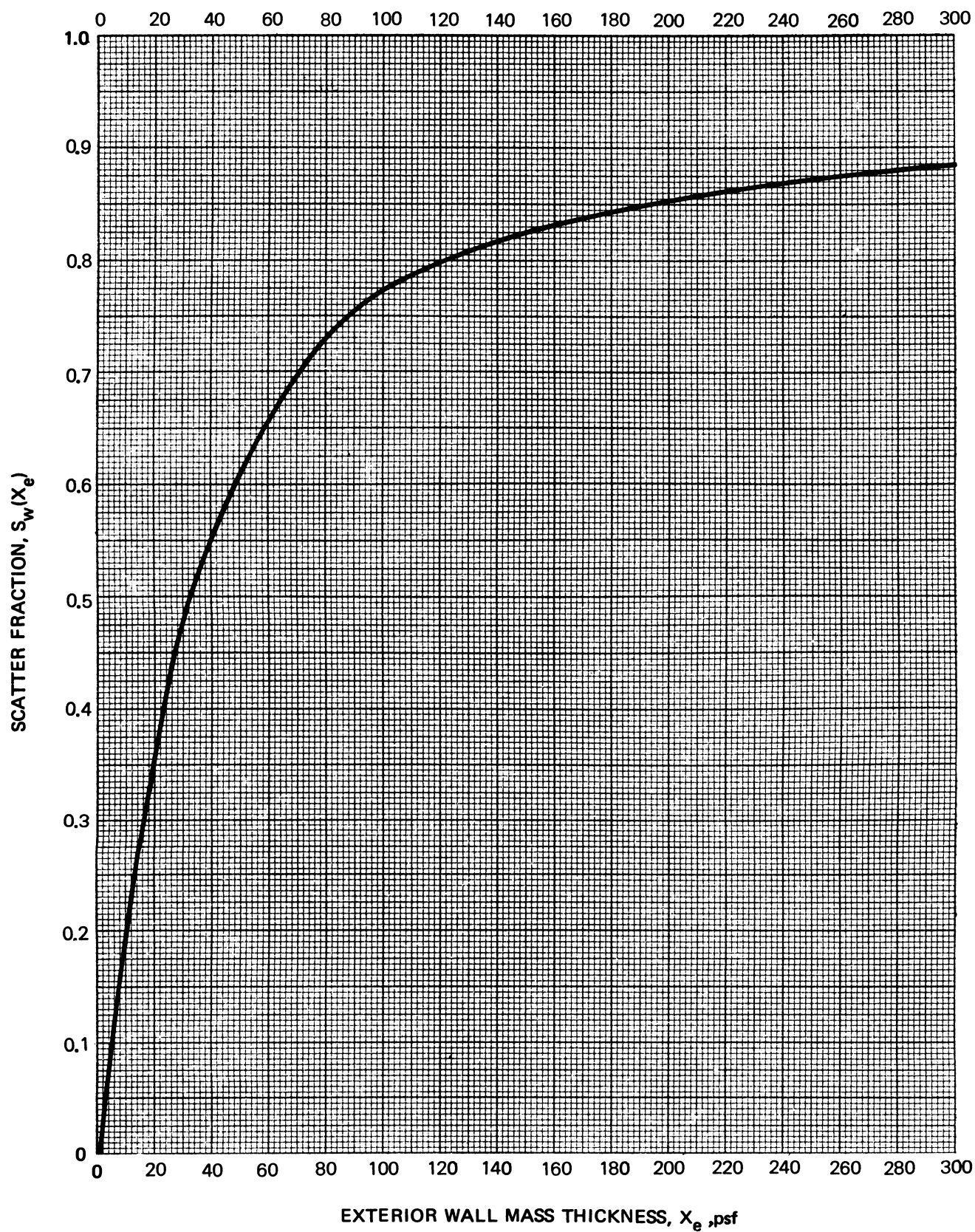
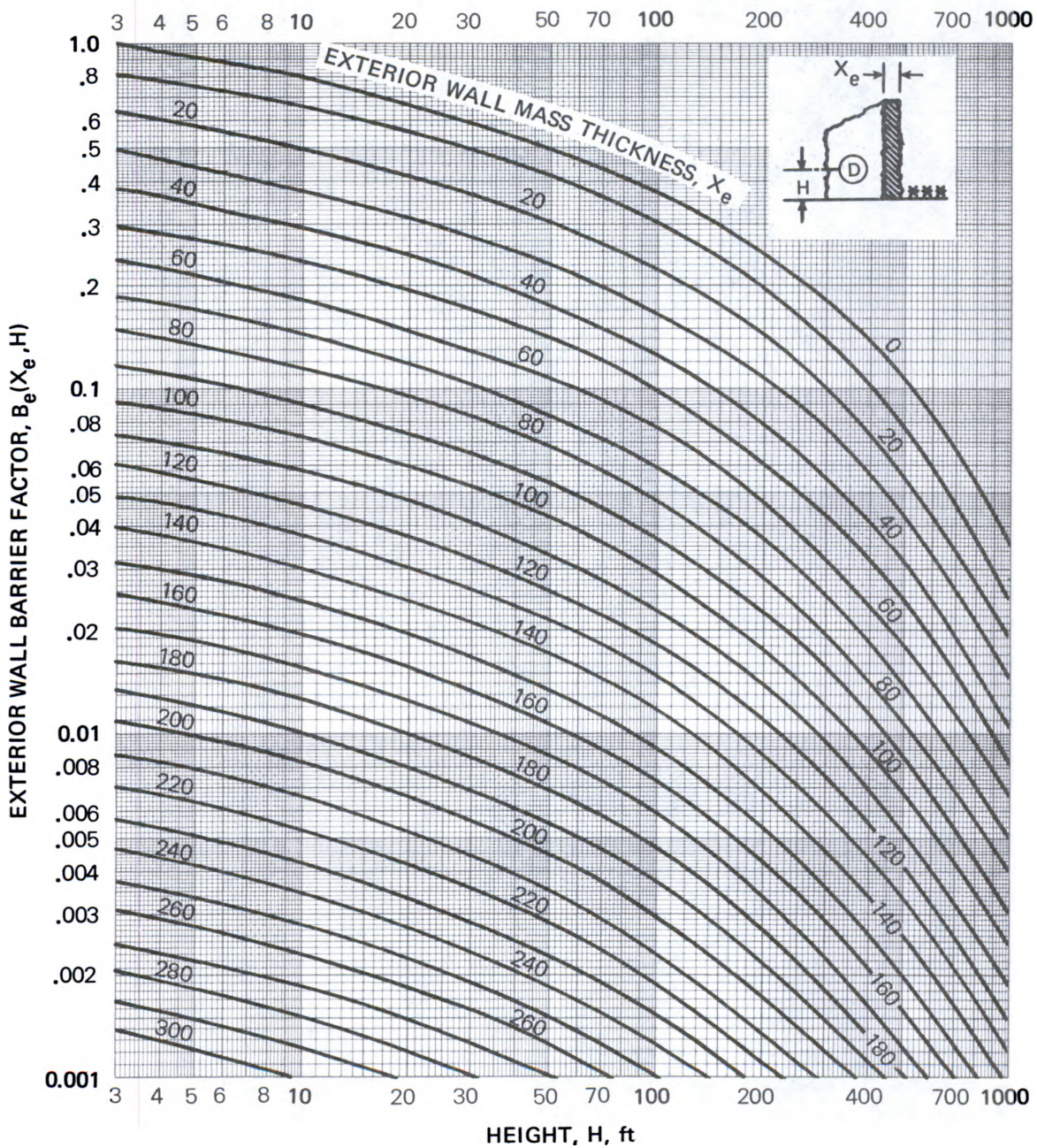


CHART 5  
SCATTER FRACTION,  $S_w(X_e)$







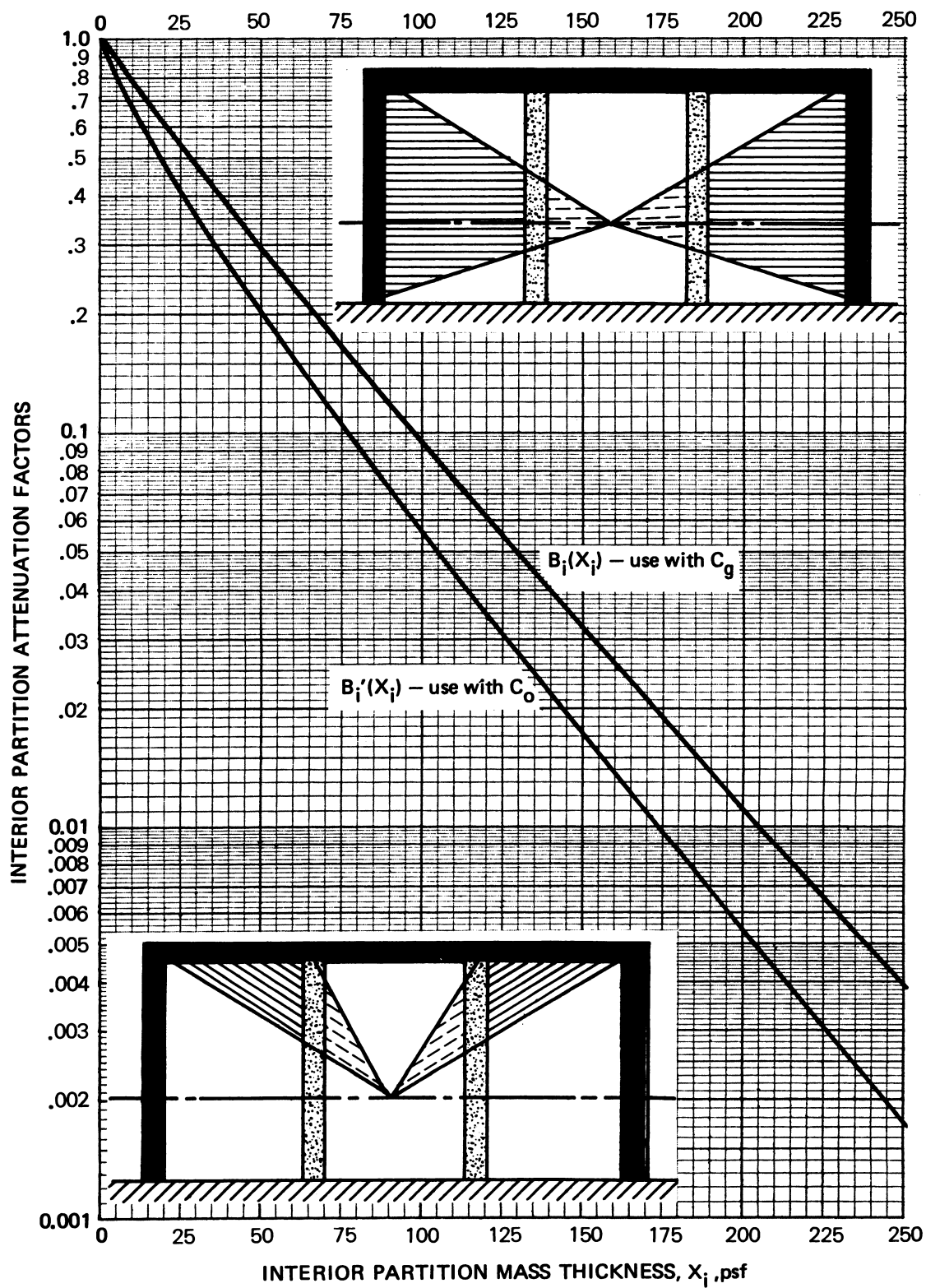


CHART 7  
INTERIOR PARTITION ATTENUATION FACTORS,  $B_i(X_i)$  and  $B'_i(X_i)$

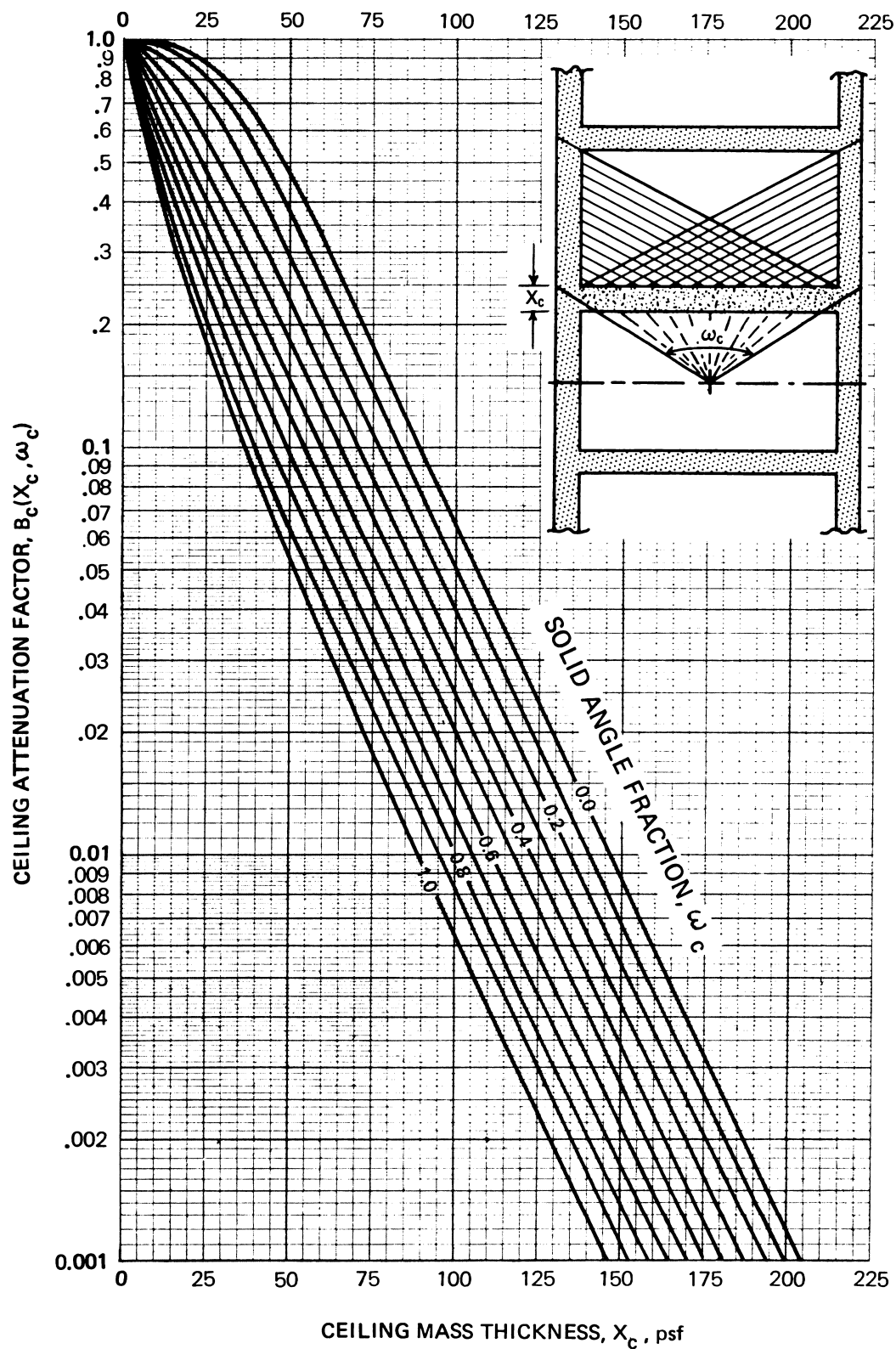


CHART 8A  
CEILING ATTENUATION FACTOR,  $B_c(X_c, \omega_c)$

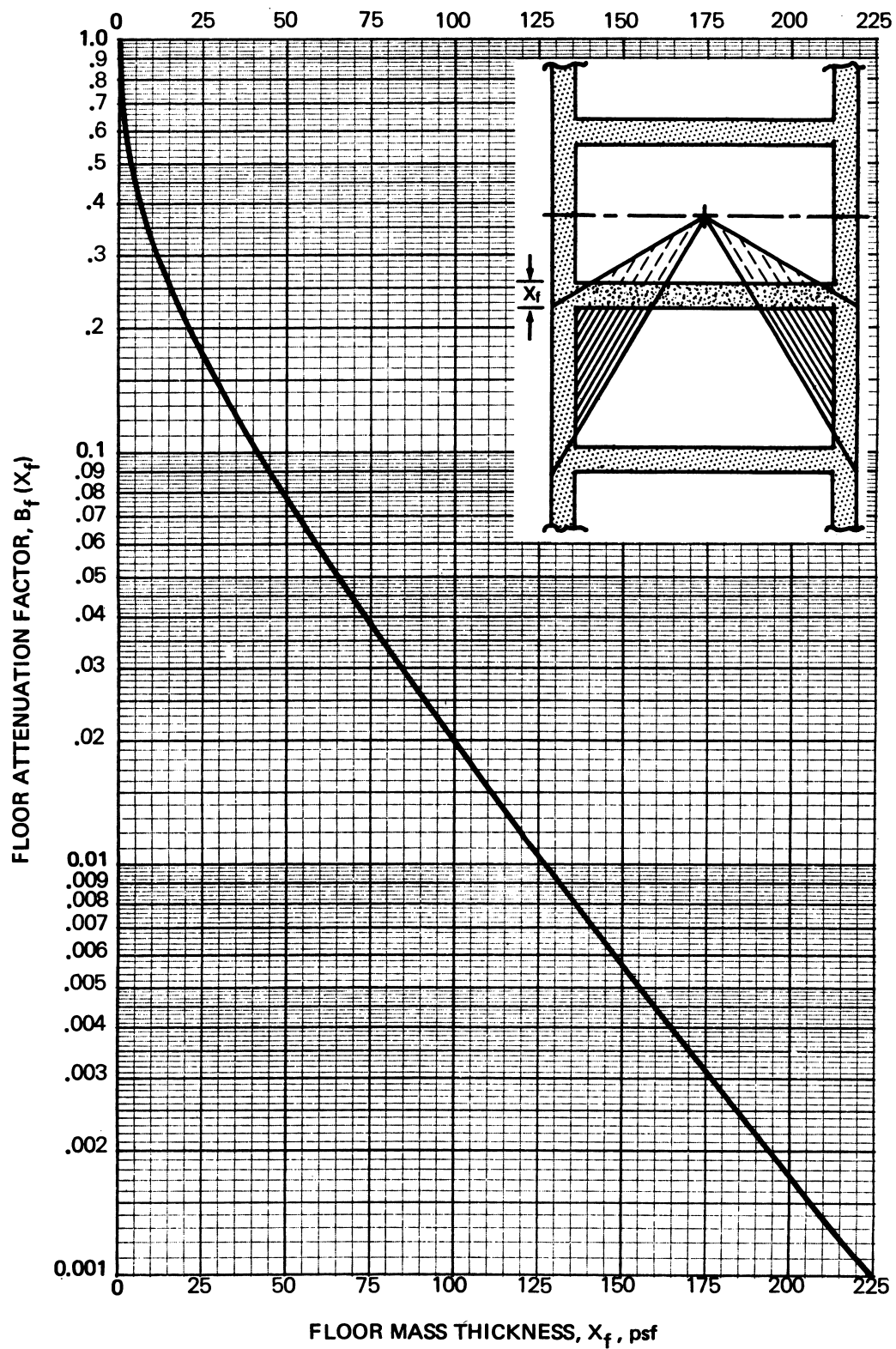


CHART 8B  
FLOOR ATTENUATION FACTOR,  $B_f(X_f)$

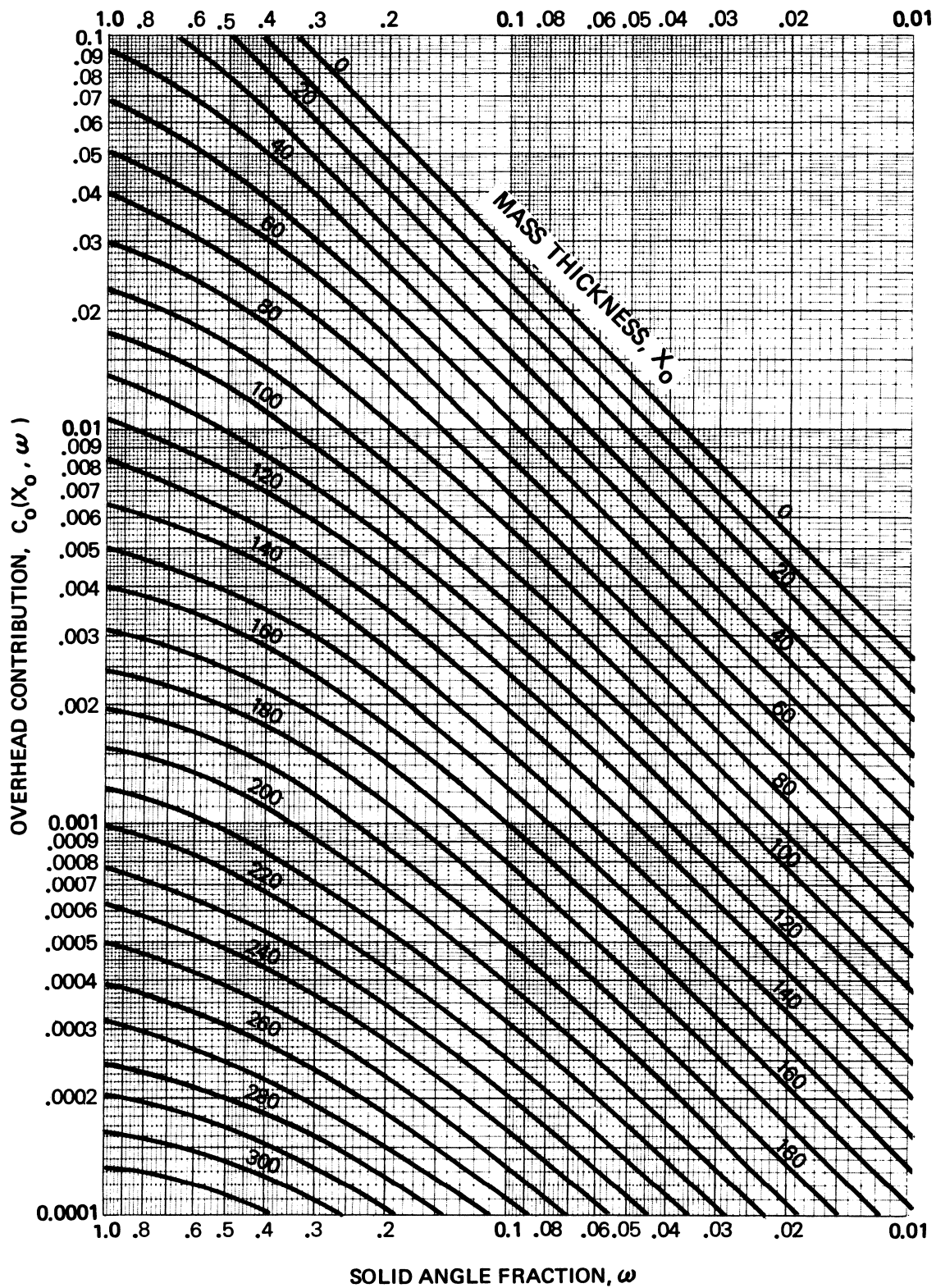


CHART 9  
OVERHEAD CONTRIBUTION,  $C_o(X_o, \omega)$



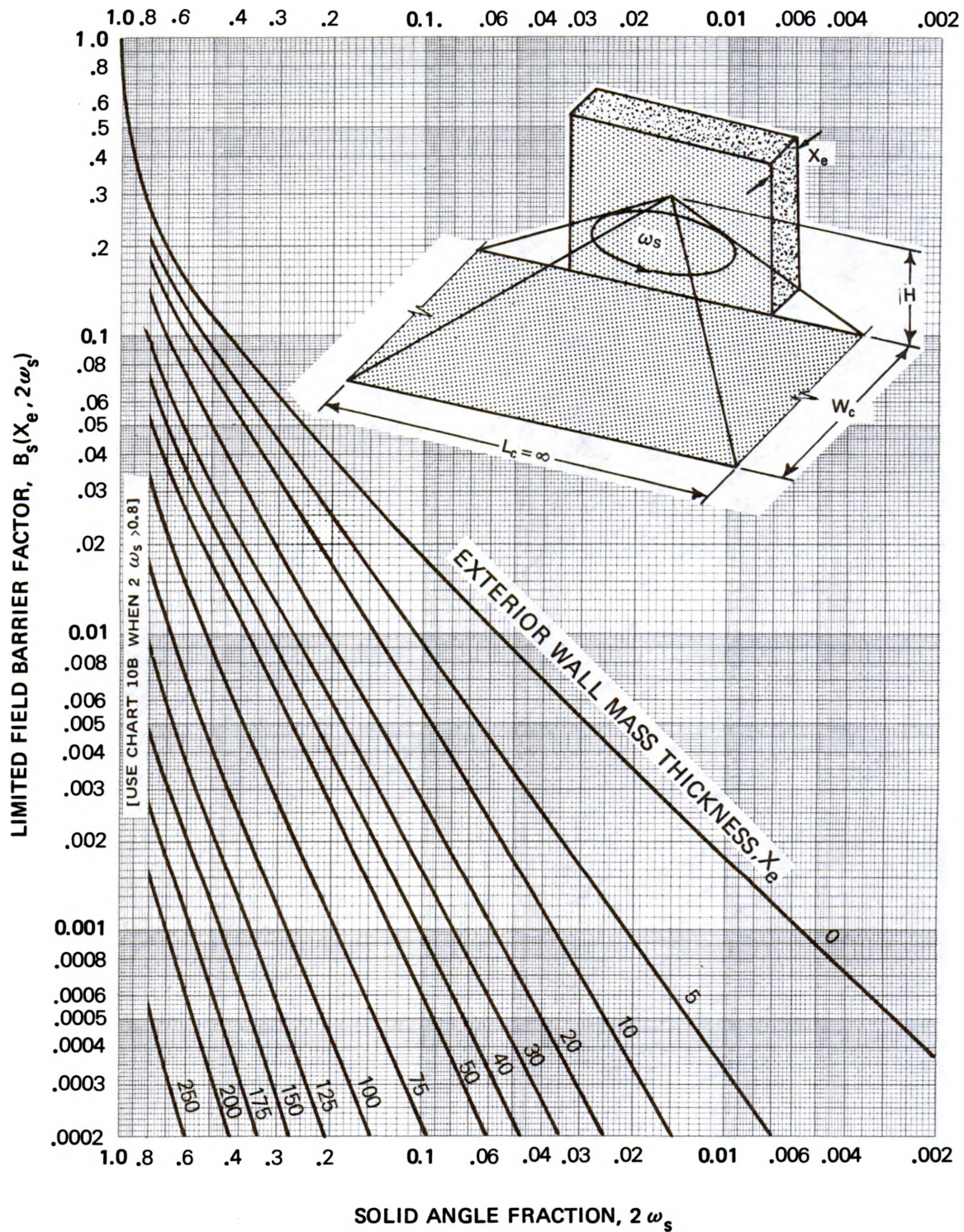


CHART 10A  
 LIMITED FIELD BARRIER FACTOR,  $B_s(X_e, 2\omega_s)$

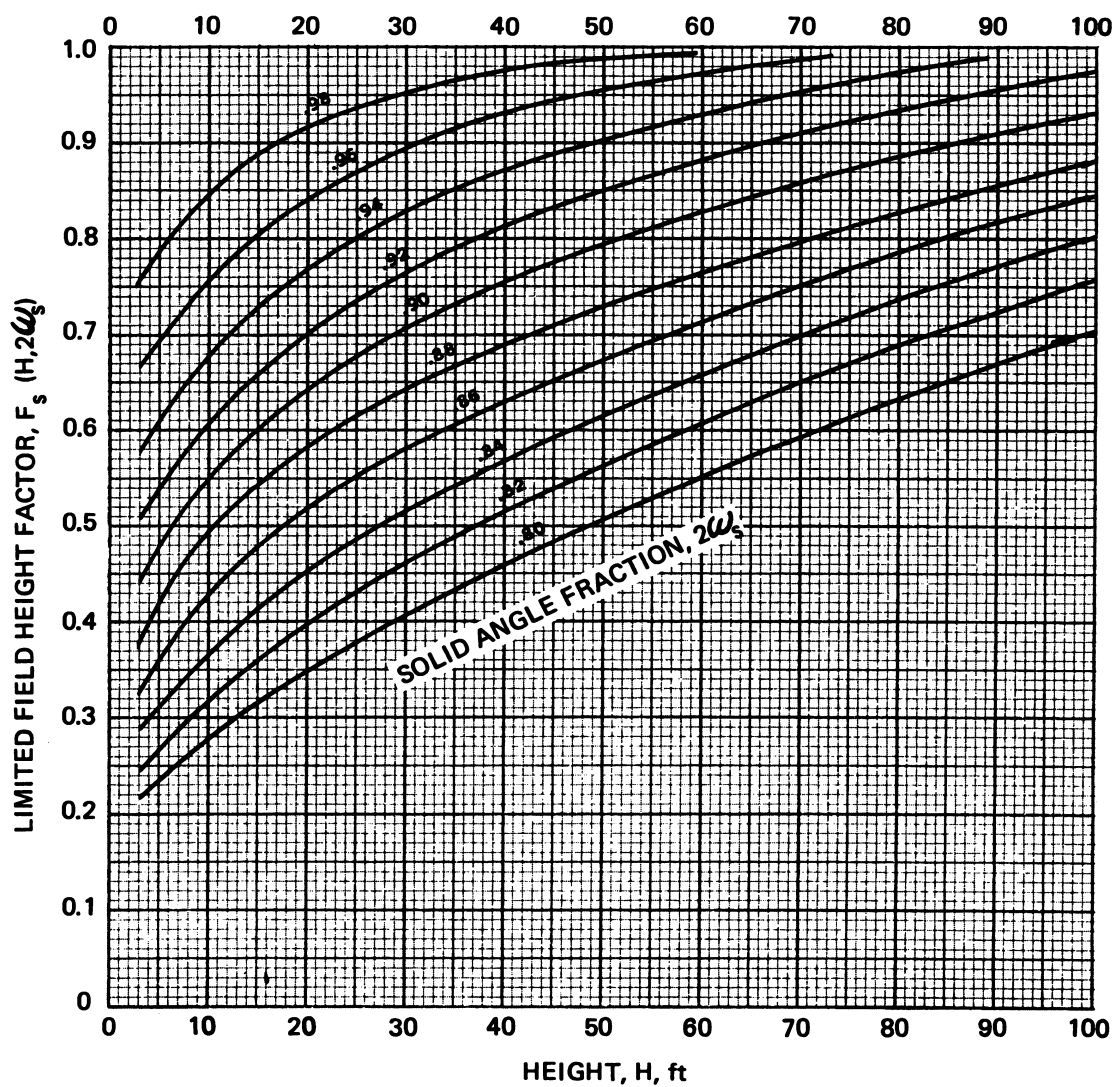


CHART 10B

LIMITED FIELD HEIGHT FACTOR,  $F_s(H, 2\omega_s)$

$$B_s(X_e, 2\omega_s) = F_s(H, 2\omega_s) \cdot B(X_e, H)$$



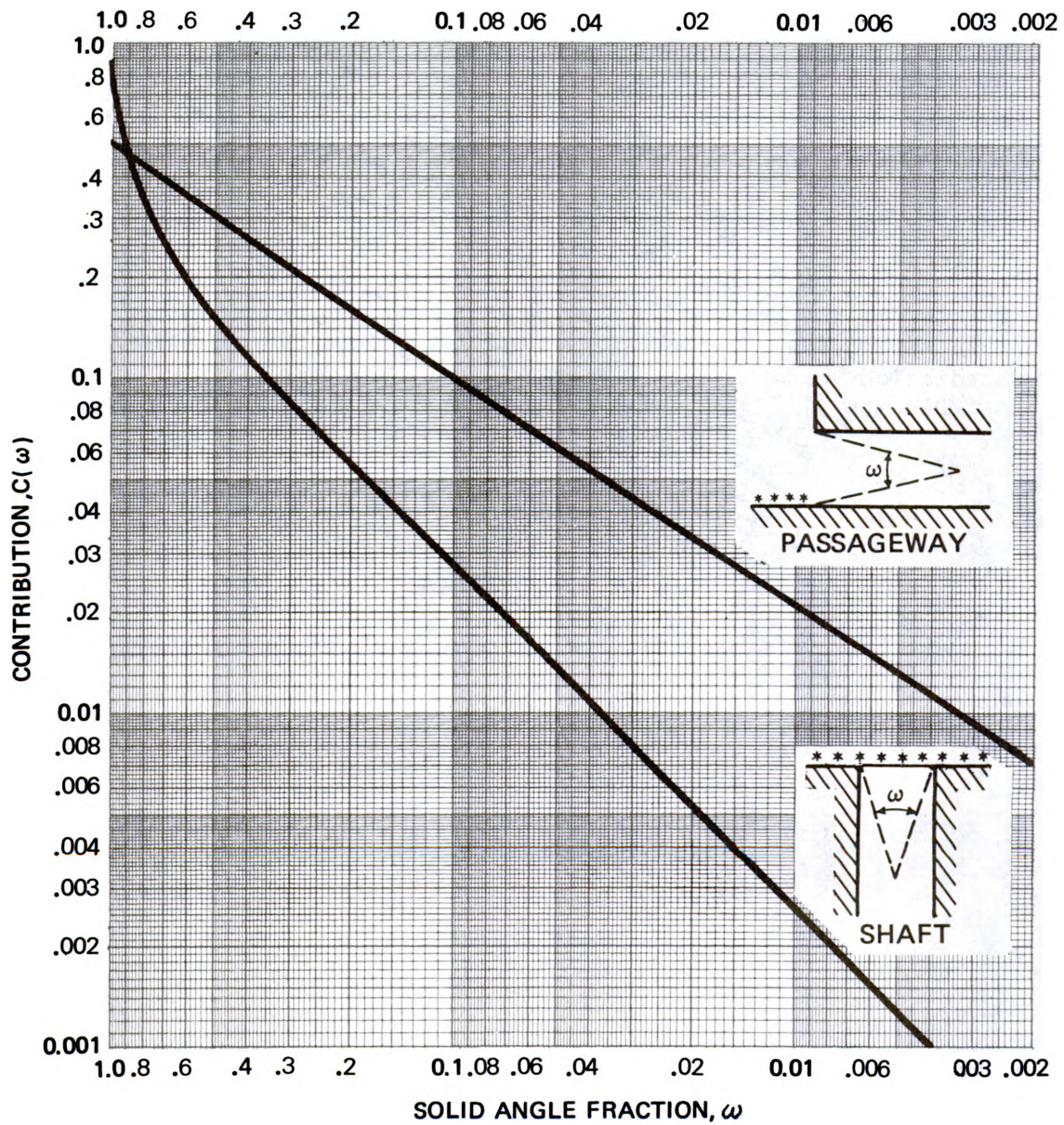


CHART 11  
PASSAGEWAYS AND SHAFTS,  $C(\omega)$

#### REFERENCES

- [1] Shelter design and analysis - fallout radiation shielding, TR-20, Vol. 1, with changes through Nov. 1974, 445 pages (Dept. of Defense, Office of Civil Defense, July 1967).
- [2] Bramlett, E. T. and Eisenhower, C. M., A discussion and tabulation of the data used to construct the charts in the OCD Standard Method for fallout gamma radiation shielding analysis, TR-70, 63 pages (Office of Civil Defense, December 1971).



## GLOSSARY

- barrier factor:* A reduction factor if the detector is adjacent to a single protective shield or if the protective shield has effectively infinite lateral extent, so as to subtend  $2\pi$  solid angle at the detector.
- beta particle:* An electron, of either positive or negative charge, which has been emitted by an atomic nucleus or neutron in a nuclear transformation. (From ref. [1], largely.)
- beta rays:* Streams of beta particles.
- build-up factor:* In an attenuation or shielding situation, this is the ratio of a dose or detector response to that due only to the unscattered component at the same point.
- charged:* Containing an excess or deficiency of electrical charge.
- complex structure:* A structure which is more complex than a *simple structure* (see below).
- contamination (radioactive):* A radioactive substance, such as fallout, in a place where it is undesirable. (Essentially from ref. [1].)
- Dirac delta function,  $\delta(x-x_0)$ :* The limit of a sequence of functions of such a nature that the value of the functions approach zero at every place except at  $x = x_0$ , the value approaches infinity at  $x = x_0$ , and the integral of the functions between limits which include  $x_0$  is unity.
- dose:* A generic term applicable to any of several closely related concepts employed in the field of radiation protection practice, such as *absorbed dose*, dose equivalent, and *exposure*. In this work, it ordinarily refers to exposure when applied to gamma photons or x rays.
- dose, absorbed:* The energy imparted to matter in a volume element by ionizing radiation, divided by the mass of irradiated material in that volume element. The SI derived unit of absorbed dose is the grey (Gy). The more traditional unit is the rad. (One Gy = 100 rad; one rad = 100 ergs/g.) (from ref. [1], largely.)
- energy deposition coefficients:* A generic term applicable to any of several closely related coefficients expressing a rate of energy exchange from photon beam to medium, per unit penetration distance, divided by the local density. Examples are  $\mu_{en}/\rho$ ,  $\mu_{tr}/\rho$ ,  $\mu_K/\rho$ , and  $\mu_a/\rho$  (see chapter III).

- erythematous dose:* That *dose* (generally *exposure*) which is just sufficient to bring about a perceptible reddening of the skin of a person with fair skin.
- exposure:* This term is used in two ways: (1) It is used quantitatively for x or gamma radiation to indicate the sum of the electrical charges of all of the ions of one sign produced in air when all electrons liberated by photons in a suitably small element of volume of air are completely stopped in air, divided by the mass of the air in the volume element. It is commonly expressed in roentgens, where one roentgen corresponds to  $2.58 \times 10^{-4}$  Coulombs per kilogram.
- (2) It is used qualitatively to refer to the incidence of radiation on living or inanimate material, by accident or intent. (This definition taken largely from ref. [1].)
- fallout:* The radioactive debris from a nuclear explosion which, having first been impelled into the atmosphere, falls to earth over some time period later than the explosion, usually within 24 hours. (Essentially from ref. [3]).
- fallout, local:* That component of the fallout consisting generally of heavier particles which fall to earth within a few hundred miles of the burst point within about a day after detonation.
- fallout spectrum:* The distribution of gamma-ray (or beta-ray) emission strength with respect to photon (or electron) energy, for a fallout radiation source. The fallout spectrum is standardized for many applications in this book as a distribution with volatile elements removed, corresponding to 1.16 hours after a nuclear detonation.
- fallout, world-wide:* That finer portion of the radioactive debris from a nuclear explosion which is impelled to such a height (generally into the troposphere) that it travels thousands of miles before settling down to earth.
- fission (nuclear):* The division of a heavy nucleus into two (or, rarely, more) parts with masses of equal order of magnitude, usually accompanied by the emission of neutrons, gamma radiation, and rarely, small charged nuclear fragments. (From ref. [1].)
- fission products:* Nuclides produced by fission or by the subsequent radioactive decay of the nuclides thus formed. (From ref. [1].)

- fluence (particle)*: At a given point in space, the number of particles (or photons) incident during a given time interval on a small sphere centered at that point, divided by the cross-sectional area of that sphere. It is identical with the time integral of the particle flux density.  
(From ref. [1].)
- fractionation*: Any alteration of radionuclide composition occurring after a detonation which causes radioactive debris to be non-representative of the detonation products as a whole.
- free field*: The absence of structures, protective or otherwise, which can significantly modify the radiation field. The term is commonly applied to experiments (or *dose*) in real, but elementary, source configurations. It can also refer to dose with idealized point and plane sources in infinite, homogeneous media, or more loosely to unshielded measurements (or dose) at locations outside a structure of interest.
- gamma rays*: Electromagnetic radiation emitted in the process of nuclear transition or particle annihilation.
- geometry factor*: In the present work this term refers to the factor by which the dose rate is reduced (sometimes increased) if the shielding barrier does not subtend  $2\pi$  solid angle at the detector.
- kerma*: The sum of the initial energies of all the charged particles released per unit mass of material from interactions of indirectly ionizing radiation (primarily neutrons and photons). (From ref. [1].)
- linear energy transfer (LET)*: The average energy locally imparted to a medium by a charged particle of specified energy, per unit distance traversed. (Note: the term "locally imparted" may refer either to a maximum distance from the particle track or to a maximum value of discrete energy loss by the particle beyond which losses are no longer considered as "local".) (Essentially from ref. [1].)
- mass stopping power*: The energy loss of a charged particle per unit distance traversed through a material, divided by the density of the material. (Essentially from ref. [1].)
- median lethal dose*: That *dose* level at which 50% of the biological organisms irradiated are expected to die within a specified length of time. The value depends on the type of organism, their biological condition, and the physical aspects of the irradiation.

*Monte Carlo method:* As applied to nuclear radiation transport, a stochastic method of treating the behavior of nuclear particles in a medium or media by generating the random walks (histories) of thousands of individual particles through the geometric configuration of interest.

Histories of all particles are created by sampling the occurrence of nuclear events from their probability distributions using a sequence of random numbers. Summation over the particle histories yields average quantities of interest: particle (or energy) flux densities, current densities, etc.

The method is named for the famous gambling casino in Monaco on the French Riviera. (From ref. [2].)

*national fallout shelter survey (NFSS):* A major U.S. governmental program, started in 1961, to find, mark, and stock fallout shelter spaces conforming to the standard protection criteria established by OCD at that time (protection factor at least 40).

*neutron:* An elementary particle having no electric charge and believed to be one of two principle constituents of matter, the other being the proton.

*protection factor:* The ratio of the dose rate from a standard fallout gamma ray spectrum at the standard unprotected location to the dose rate under similar standardized conditions at a specified point within the structure under consideration; the reciprocal of reduction factor. (See chapters VI and VII.)

*reduction factor:* The ratio of the dose rate at some specified protected location to that at a specified unprotected location, especially the "standard location." For a simple blockhouse, the reduction factor is often expressed as the product of a *barrier factor* and a *geometry factor*.

*refractory:* Most commonly used here to characterize materials (e.g., fission products) with very high temperatures of condensation.

*salting:* Inclusion in a nuclear device of a material whose activation upon detonation can increase or prolong the consequent radioactive hazards.

*simple structure:* A structure, usually of rectangular parallopiped shape, containing no significant floors or partitions within the single "membrane" which forms its outer shell; a non-compartmented blockhouse. See chapter VII.

- skyspine:* The component of the radiation field due to fallout which at any point above ground (or on the ground) is directed downwards. This radiation component has been scattered by the air and seems to be "from the sky".
- spectrum:* A distribution of energy, or wavelength characteristic of a type of radiation. The term can also be applied to other quantities such as the mass distribution of fallout particles.
- Standard Method:* That method of fallout shielding analysis officially prescribed for shelter identification or design by the Office of Civil Defense (or its successors).
- structure:* A configured arrangement of materials, usually enclosing a living or work space. The term is used here to refer to everything from simple blockhouses to highly complex multi-story buildings.
- thermonuclear:* Relating to a nuclear reaction, normally between nuclei of light elements, in which the participating particles obtain the required energy from thermal agitation at extremely high temperatures. The term is applied, in the context of nuclear weapons, to those in which the fusion type of reaction plays a significant part. (In part from ref. [1].)
- transport equation:* (Boltzmann transport equation)
- (1) A integro-differential equation describing the physical processes occurring in the presence of ionizing radiation within an elemental region of (material) volume as a function of position, angle (or direction), energy, and time.
- Processes include generation of particles within the element, capture or absorption of particles within the element, and leakage of particles into and out of the element.
- (2) An expression of the equation of continuity for nuclear radiations. (Equivalent to definition (1)).
- It is to be noted that while the equation is in reality a differential expression, the complete description of inscattering to the element of interest requires an integral term. (From ref. [2].)
- volatile:* Readily vaporizable at temperatures under consideration, usually normal ambient temperatures though not necessarily so in the context of fallout particle formation. See chapter II.

*x rays:*

Electromagnetic radiation, usually above 1 keV photon energy arising from filling the inner shells of ionized atoms by electrons from outer shells.

#### REFERENCES

- [1] American National Standard, Glossary of Terms in Nuclear Science and Technology, ANS-9/ANSI N1.1-1976, 110 pages (American Nuclear Society, 1976).
- [2] Trial Use Nuclear Glossary, ANS-65, ANS-19.2, ANS-50, 146 pages (American Nuclear Society, 1978).
- [3] Definitions of Nuclear Terms - Including Formulas and Tables, Eva M. Thorn, NWEF Report 1001, V.1, 312 pages (Nuclear Weapons Evaluation Facility, May 1967).

<u>Author</u>	<u>Page</u>	<u>Author</u>	<u>Page</u>
C. E. Adams . . . .	65	E. Callahan . . . .	127
M. Alberg . . . . .	392, 394	S. H. Cassidy . . . .	80
A. D. Anderson . . .	127	J. Chadwick . . . . .	2
J. Auxier . . . . .	29, 33	A. B. Chilton . . . .	117, 119, 418, 419, 559, 587, 619
W. R. Balkwell . . .	65	J. M. Chisholm . . .	27
N. E. Ballou . . . .	74-76	C. M. Cialella . . .	119
J. A. Baran . . . . .	612	E. Clarke . . . . .	30, 416, 778, 779
B. O. Bartlett . . .	116	C. E. Clifford . . . .	34, 419, 422, 424, 426, 429-431, 444, 449, 590
H. Bateman . . . . .	66	D. G. Collins . . . .	411
J. Batter . . . . .	30, 33, 425, 553, 606, 608, 609, 611-613, 691, 693, 720, 755, 803	A. H. Compton . . . .	323
L. A. Beach . . . . .	17, 20, 37	C. S. Cook . . . . .	105, 106, 121
H. Beck . . . . .	408, 409, 420	J. W. Cooper . . . .	75, 76, 85, 92-96, 105, 117, 120-125, 413
K. Becker . . . . .	12	C. D. Coryell . . . .	74, 80
H. Becquerel . . . .	1	G. R. Crocker . . . .	68, 80, 89-94, 96, 99, 104, 105, 107 108, 117
B. Bennett . . . . .	420	R. N. Crooks . . . .	27
P. A. Benson . . . .	104	J. R. Cunningham . .	27
M. J. Berger . . . .	37, 403, 404, 411, 413, 415, 418, 419, 441, 481	C. M. Davisson . . . .	14
R. Björnerstedt . . .	66, 76, 78, 80, 89-91, 121, 413	L. Degelman . . . . .	495
R. C. Bolles . . . .	74-76	G. de Planque . . . .	408, 409
H. Borella . . . . .	806	J. K. Dickens . . . .	86
A. E. Boyd . . . . .	125	J. A. Doggett . . . .	403, 411
W. H. Bragg . . . . .	212	P. J. Dolan . . . . .	75, 76, 85, 86, 92, 93, 105
E. Bramlitt . . . . .	39, 480	L. K. Donovan . . . .	117, 119
A. Broido . . . . .	19, 20	J. R. Dunning . . . .	116
F. C. Brooks . . . . .	35	K. Edvarson . . . . .	78
R. S. Bruce . . . . .	116	R. R. Edwards . . . .	74
L. R. Bunney . . . .	78, 90, 91, 99	G. Ehrlich . . . . .	12
Z. Burson . . . . .	33, 408, 410, 425, 427, 431, 432, 562, 564, 782, 806, 809, 812	C. Eisenhower . . . .	36, 38, 290, 374, 403, 411, 416, 418, 419, 477, 480, 559, 774
F. A. Bury . . . . .	27		

<u>Author</u>	<u>Page</u>
D. D. Eisenhower . . . .	24, 37
T. R. England . . . .	53, 86
L. B. Engle . . . .	78, 85
U. Fano . . . . .	16, 37, 210, 212, 214, 257, 403, 415, 481, 868
W. R. Faust . . . .	16, 404
R. Faw . . . . .	555, 612
J. M. Ferguson . . .	445, 447
E. Fermi . . . . .	2
R. D. Fink . . . . .	80
S. P. Finn . . . . .	92, 94-96, 122, 124
P. G. Fisher . . . .	78, 85
N. FitzSimons . . . .	36
J. K. M. Flexman . .	27
A. Foderaro . . . .	495
A. L. Frank . . . .	411, 421
E. C. Freiling . . .	63, 99, 102-104, 132
R. L. French . . . .	119, 120, 408, 410, 418, 419, 594, 727
O. R. Frisch . . . .	2
C. Y. Fu . . . . .	418, 419
H. J. Gale . . . . .	27
R. J. Galiano . . . .	129
C. Garrett . . . . .	418, 419
L. D. Gates . . . . .	403, 411
H. Geiger . . . . .	588
L. E. Glendenin . .	74-76, 80
H. Goldstein . . . .	16, 403, 411
R. Goldstein . . . .	455, 457, 827
L. H. Gray . . . . .	11
J. Griffin . . . . .	78
L. V. Groshev . . . .	112
O. Hahn . . . . .	2

<u>Author</u>	<u>Page</u>
E. Hayward . . . . .	392, 393
R. E. Heft . . . . .	64, 103
R. B. Heller . . . .	122
V. F. Hess . . . . .	1
D. E. Hinkley . . . .	434, 770, 771
J. O. Hirschfelder .	16
W. D. Holland . . . .	104
B. W. Howard . . . .	826
J. J. Hubbell . . . .	167, 485
C. M. Huddleston . .	1, 121, 413, 447, 450-454, 850, 852
I. O. Huebsch . . . .	131
H. F. Hunter . . . .	74
Y. A. Israel . . . . .	444, 445
J. Jacovitch . . . .	806
R. F. Johnson . . . .	107
D. T. Jones . . . . .	27
H. Kahn . . . . .	17
M. Kalos . . . . .	773
A. L. Kaplan . . . . .	435-437, 562, 592, 600, 602, 745, 759, 842, 844
W. W. Kellogg . . . .	127
J. F. Kennedy . . . .	37
W. R. Kimel . . . . .	612
N. D. King . . . . .	119
R. W. King . . . . .	76, 77
O. Klein . . . . .	16, 167-169, 178 181, 230, 231
W. E. Knabe . . . . .	77
H. A. Knapp . . . . .	110
Aikichi Koboyama . .	8
D. B. Kochendorfer .	53
R. F. Korts . . . . .	65
G. Kowal . . . . .	495
C. F. Ksanda . . . .	127, 443



<u>Author</u>	<u>Page</u>
J. W. Kutcher . . .	122
H. Lacayo . . . . .	826
M. A. Lamonds . . .	413, 414
R. K. Laurino . . .	127
J. C. LeDoux . . .	39, 537, 611
W. Libbey . . . . .	29
J. Lindwarm . . . .	573
P. Loeb . . . . .	75
T. A. Love . . . . .	77, 86
K. Löw . . . . .	78
A. G. MacDonald . .	27
J. Mackin . . . . .	77, 78, 90, 91
F. C. Maienschein .	77, 78, 85
C. W. Malich . . .	19, 20, 37
J. I. Marcum . . .	418, 419
R. L. Mather . . .	107, 110, 114
C. McDonnell . . .	396-399, 548, 550, 552, 567, 568, 577, 581-583, 585, 714, 718, 725, 727, 732
L. Meitner . . . . .	2
J. A. Michael . . .	413, 414
S. Z. Mikhail . . .	125
C. F. Miller . . .	49, 64, 65, 71, 75, 76, 105, 106, 128, 129
D. Mittlemen . . .	38
E. E. Morris . . .	125, 411, 413, 414, 420, 619, 770, 771
M. W. Nathans . . .	104
A. Nelms . . . . .	75, 76, 85, 92-95, 105, 117, 120-125, 413
Y. Nishina . . . .	16, 167-169, 178, 181, 230, 231
J. H. Norman . . .	65

<u>Author</u>	<u>Page</u>
A. C. Pappas . . .	76, 80
G. H. Peebles . . .	16
R. W. Peelle . . .	77, 86
J. F. Perkins . . .	76, 77
Y. I. Petrov . . .	77
S. L. Pittman . . .	38
M. S. Plesset . . .	16
I. B. Poppoff . . .	127
S. Preiser . . . . .	403
R. D. Present . . .	75, 76, 80
J. H. Price . . . .	119, 120, 727
G. E. Pugh . . . . .	129
G. E. Putnam . . .	77
R. R. Putz . . . . .	19, 20, 36
J. T. Quan . . . . .	65
D. J. Raso . . . . .	768, 770, 771
R. E. Rexroad . . .	30, 34, 404, 419, 495, 592
W. C. Roentgen . .	9, 10
J. Romm . . . . .	848, 850
R. M. Rubin . . . .	560
I. Russell . . . . .	128
R. S. Russell . . .	116
E. Rutherford . . .	1
D. Sam . . . . .	78, 90, 91, 99
R. E. Schenter . .	53
M. A. Schmoke . . .	30, 34, 397, 399, 404, 418, 419, 495, 592, 603, 770, 771
E. A. Schuert . . .	127
M. J. Schumchyk . .	399, 405, 407, 411, 431, 433, 433, 435, 436, 438, 440, 592, 757, 759, 764
C. J. Seery . . . .	128

<u>Author</u>	<u>Page</u>
E. Shapiro . . . .	17-20, 37, 779
G. L. Simmons . . .	92, 94-96, 122, 124
L. V. Spencer . . .	16, 36-38, 403, 411, 415, 441, 445, 450, 452, 454, 481, 493, 497, 573, 714, 868
R. Spring . . . . .	434-436, 537, 557, 581-583, 617, 618, 725, 736, 759
M. G. Stamatelalos	86
A. W. Starbird . .	425, 438, 691, 693, 718, 748, 752, 754, 755
P. S. Stevenson . .	64
N. G. Stewart . . .	27
F. Strassman . . . .	2
T. D. Strickler . .	33
M. A. Sullivan . . .	826
R. L. Summers . . .	425, 427, 431, 432, 562, 564
L. S. Taylor . . . .	19
R. A. Taylor . . . .	411
R. Thews . . . . .	104
J. J. Thomson . . .	106
H. Tiller . . . . .	438, 440, 495
F. Titus . . . . .	22, 23, 117, 119, 543, 544, 546

<u>Author</u>	<u>Page</u>
F. M. Tomnovec . .	107, 121, 453
K. W. Tompkins . .	119, 120
R. C. Tompkins . .	104
D. K. Trubey . . . .	768, 770, 771
T. Turner . . . . .	68, 80, 89-94
J. Velletri . . . . .	434-436, 548, 550 568, 577, 585, 595, 597, 606, 609, 613, 718, 728, 732, 736, 759
F. Verser . . . . .	591
P. S. Visher . . . .	38
J. Von Neumann . .	16, 17
A. J. Wahl . . . . .	76, 80
S. Warren . . . . .	4
K. Way . . . . .	73, 81
M. B. Wells . . . . .	411
G. White . . . . .	14, 390, 391
G. C. Wick . . . . .	16
E. Wigner . . . . .	73, 81
J. E. Wilkins . . . .	16, 411
R. Wilson . . . . .	27
S. Woolf . . . . .	768, 770, 771
M. E. Wyman . . . .	122
P. Zigman . . . . .	77, 78, 90, 91
W. Zobel . . . . .	77, 86

# INDEX

- accuracy . . . . . 834, 835, 838, 841, 843, 844
- adjacent building. . . . . 698
- adjoint calculations . . . . . 312-316, 338, 773, 875
- Ailinginae . . . . . 8
- air. . . . . 173, 175, 193, 213, 255, 265, 286, 293, 294,  
322, 325, 329, 340, 353, 356, 379
  - condensed . . . . . 413
  - ground interface (see interface, ground-air)
- air-scattered radiation. . . . . 554
- albedo (see also backscatter). . 182, 226, 229, 232-236, 340, 349, 351, 614
- alpha particles, rays. . . . . 1, 9
- angular distributions. . . . . 20, 114, 187, 193, 235, 249, 253, 254, 261,  
269, 270, 276, 280, 284, 286, 291, 292, 305,  
307-310, 312, 329, 340-344, 356, 368, 371,  
376, 382, 408, 429, 431, 447, 451, 491, 555,  
559-562, 598, 600, 745
- annihilation photons, energy . . 165, 191, 192, 238
- apertures. . . . . 531, 533, 594, 743-747, 783, 791, 829
- area-weighted method (see method, area weighted)
- Atomic Energy Commission (AEC) . 4, 8, 24, 25, 35, 594, 596, 773
  - Civil Effects Test Operation (CETO) 773, 809
  - headquarters building . . . . . 31, 800-807
  - Nevada Test Site. . . . . 28, 138, 746, 755, 774-779, 782, 784
- attack studies . . . . . 848
- attenuation. . . . . 73, 96, 169-177, 189, 214, 324, 345, 354,  
355, 363, 364, 368, 381, 580, 586, 687, 730,  
733, 734, 741, 752, 757, 764, 768, 774, 776,  
787, 791, 800, 817, 936
  - barrier . . . . . 859
  - ceiling . . . . . 684
  - exponential . . . . . 16
- attenuation coefficient. . . . . 14, 16, 169, 173, 175, 176, 180, 210, 247,  
248, 291, 400
  - linear. . . . . 14
  - mass. . . . . 14
- attenuation data . . . . . 18
- attenuation factor . . . . . 333, 338, 376, 677, 727, 728, 736, 740, 743,  
746, 750, 758, 770, 934
  - ceiling . . . . . 759, 761, 763-767, 770, 935
  - floor . . . . . 686
  - interior partitions . . . . . 683
- Auger electrons. . . . . 164, 165
- azimuth, azimuthal . . . . . 560, 561, 598-600, 625, 653, 655, 660, 673,  
832
  - angles. . . . . 745
  - fraction. . . . . 532, 627, 641, 643, 645, 653, 732, 831, 833
  - sectors . . . . . 517, 676, 830

B . . . . . 714  
 backscatter, backscattering . . . 182, 264, 347, 349, 357, 369, 374, 381, 382,  
 431, 434, 435, 437, 487  
 backscattering limit. . . . . 290  
 barracks building . . . . . 20, 31  
 barriers. . . . . 21, 338, 376, 842  
     floor. . . . . 693  
     horizontal . . . . . 543, 723, 732, 768  
     interior . . . . . 675-677, 684, 686, 687  
     overhead . . . . . 33  
     vertical . . . . . 553, 562, 727  
 barrier factors . . . . . 333, 357, 368, 543, 553, 938  
     finite sources . . . . . 565  
     floor. . . . . 686  
     interior (see attenuation factor, interior partitions)  
     roof . . . . . 733  
     skyshine . . . . . 562  
     wall . . . . . 479, 480, 552, 562, 568, 656, 727, 743, 745,  
     933  
 barrier factor data . . . . . 340  
 barrier thickness . . . . . 14  
 basement. . . . . 19, 41, 431, 590, 603, 605, 684, 685, 748-  
 757, 764, 769-772, 776, 778, 781, 797, 806,  
 812, 817, 823, 828, 841  
 beta burns. . . . . 141  
 beta-radiation, beta rays . . . . 1, 4, 9, 52, 54, 65, 66, 68, 71, 73, 74, 80,  
 109, 120, 122, 125, 141, 145  
 biased sampling . . . . . 235  
 Bikini Atoll. . . . . 6, 8, 17  
 biological effects. . . . . 12, 136-148  
 biophysics. . . . . 216-219  
 biorthogonal, biorthogonality . . 868, 870, 872, 875, 876  
 blast . . . . . 851, 853, 858  
 blockhouses . . . . . 33, 35, 499, 503, 539, 543, 573, 574, 587,  
 593, 598, 604, 626, 639-641, 644, 645, 655,  
 670-675, 678, 695, 701, 723, 734, 740, 743,  
 764  
     compartmented . . . . . 723  
     elementary . . . . . 465, 467, 625  
 blockhouse studies. . . . . 29  
 Boston Harbor building. . . . . 778, 780  
 bremsstrahlung. . . . . 192, 193  
 Ballistics Research Lab. (BRL). . 30, 34  
 brick . . . . . 777, 779, 781  
 British . . . . . 20, 389  
 British Home Office . . . . . 779  
 broad-beam. . . . . 15, 16  
 Brookhaven Medical Research Center 806, 808, 810, 811  
 buildup factor. . . . . 18, 319, 390, 403  
 Bureau of the Census. . . . . 38, 41  
 burial depth, effective . . . . . 445, 451

bursts . . . . . 58, 61, 116  
     high air. . . . . 5  
     low air . . . . . 5  
     surface . . . . . 5, 58, 61  
     underground . . . . . 5  
     under water . . . . . 5  
 burst point. . . . . 857, 858

C . . . . . 493  
 calibration  
     detectors . . . . . 398  
     sources . . . . . 396  
 Canadian . . . . . 27, 34, 389  
 CAPS-2, computer code. . . . . 838  
 Castle Bravo . . . . . 6  
 cavity ionization chambers . . . . . 10, 11, 13, 215  
 ceiling. . . . . 750-752, 758, 759  
 ceiling-shine. . . . . 533, 606, 609, 610, 613, 633, 634, 699, 700  
 cesium, <sup>137</sup>Cs. . . . . 103, 107, 116, 119, 142, 147, 276-280, 284-  
     286, 293, 294, 303, 309, 310, 312, 320, 340,  
     343, 345, 357, 362, 368, 369, 376, 379, 382,  
     385, 389, 392, 397, 403, 420-422, 425, 429,  
     445, 447, 487, 497, 573, 782, 836, 837, 841,  
     873, 880-924  
 chain reactors . . . . . 3  
 charged particles. . . . . 190, 191  
 chromosomes. . . . . 218  
 civil defense programs . . . . . 37  
 Civil Effects Test Operations, CETO (see Atomic Energy Commission)  
 cloud. . . . . 58, 60, 125, 128-130, 133, 135  
 cloud rise . . . . . 131, 132  
 cobalt, <sup>60</sup>Co . . . . . 28, 36, 116, 119, 303, 309, 310, 312, 320,  
     340, 343, 345, 357, 362, 368, 369, 376, 379,  
     382, 385, 389, 392, 396-398, 403-405, 408,  
     416, 420, 421, 425, 431, 439, 444, 445, 487,  
     497, 549, 550, 552-555, 563, 564, 568, 569,  
     573, 580-585, 588, 606, 609, 614, 617, 714,  
     726, 738, 748, 750, 751, 756, 760-764, 768,  
     774, 779, 782, 803, 836, 837, 841, 857, 868,  
     873, 879-924  
 collimation. . . . . 14, 291  
 collimator, lead . . . . . 555  
 compartment. . . . . 264  
 compartmentation, interior . . . . . 675, 676, 782  
 complex buildings. . . . . 33  
 compressed air (see air, condensed) 21  
 Compton cross section. . . . . 323  
 Compton scattering . . . . . 165, 167, 178  
 concrete . . . . . 117, 173, 175, 325, 543, 545, 546, 553, 555,  
     556, 562, 574, 580, 584, 588, 592, 606, 616-  
     618, 717, 725, 728, 734, 750, 755, 757, 759,  
     761, 762, 764, 776-778, 781-783, 787, 879-  
     923

configuration, elementary. . . . . 33  
 Congressional Hearings . . . . . 9  
 CONSTRIP, computer code. . . . . 571, 572, 720, 721  
 contamination. . . . . 107, 144, 145  
     radiation . . . . . 5  
     widespread. . . . . 5  
 core . . . . . 748, 753  
 CP-1 building. . . . . 794-797  
 CP-2 building. . . . . 794, 798, 799  
 CP-40 building . . . . . 782-786  
 CP-45 building . . . . . 788-790  
 Coulomb barrier. . . . . 2  
 counters, proportional . . . . . 12, 13  
 courtyard. . . . . 625, 626, 639-642  
 crater . . . . . 114  
 cross sections . . . . . 166-169  
 current density. . . . . 182-189, 228  
 cylinders, cylindrical geometry. . 594, 736, 739, 745, 747-752, 761, 762, 764,  
     770, 829  
 data collection. . . . . 834  
 debris . . . . . 125  
 decay. . . . . 68, 70, 74, 78  
 decay constants. . . . . 66  
 decontamination. . . . . 17, 116, 136, 137, 822, 858  
 Defense Atomic Support Agency (DASA) (see Defense Nuclear Agency)  
 Defense Civil Preparedness Agency (DCPA) (see Federal Emergency Management  
     Administration (FEMA))  
 Defense Nuclear Agency (DNA) . . . 36, 131  
 DELFIC, computer code. . . . . 128, 131, 133-135  
 deuterium,  $^2\text{H}$ . . . . . 5, 6  
 D-T, D-D reactions . . . . . 6  
 delta function, Dirac. . . . . 259, 270, 302, 369  
      $\delta(E - E_0)$ ,  $\delta(E - E_0)$ . . . . . 247, 248, 300  
      $\delta(z)$ . . . . . 251  
 density. . . . . 262  
 detectors, radiation . . . . . 9, 12, 265-270  
     off-center. . . . . 538  
     thermoluminescent . . . . . 13  
 detector response. . . . . 9, 235  
 detonations, thermonuclear . . . . 6  
 direct radiation . . . . . 656, 657, 667, 672-675, 691, 929, 930  
 direct contribution. . . . . 706  
 directional distribution (see angular distribution)  
 disk . . . . . 254, 255, 867  
 Department of Defense (DOD). . . . 8, 31, 35, 38  
 dose . . . . . 276, 278, 284, 289, 302, 312  
     erythema . . . . . 10  
     internal. . . . . 116, 120  
     multi-collision . . . . . 215  
     single-collision. . . . . 214, 215  
     unprotected . . . . . 322  
 dose rate. . . . . 129



fallout fields . . . . . 107  
     finite. . . . . 18, 34  
     infinite. . . . . 18  
 fallout formation. . . . . 134, 135  
 fallout gamma-ray shielding data . 16  
 fallout hazard . . . . . 17, 18  
 fallout particles. . . . . 54, 61, 135, 443, 659, 822-824, 853  
 fallout shelter, shelters. . . . . 22-25, 32, 748  
     home. . . . . 23, 813  
     prototype . . . . . 24  
 Fallout Shelter Surveys, Guide (See Guide for Architects and Engineers) 26  
 fallout threat . . . . . 24  
 fallout transport. . . . . 135, 136  
 Fano's theorem . . . . . 210-212  
 far field contribution . . . . . 434, 435, 437, 746  
 Federal buildings. . . . . 25  
 Federal Civil Defense Administration (FCDA) (see Federal Emergency Management  
     Administration (FEMA))  
 Federal Emergency Management Administration (FEMA) 26, 42  
     Defense Civil Preparedness Agency (DCPA) 26, 748, 821, 861  
     Federal Civil Defense Administration (FCDA) 22, 24-26, 36  
     Office of Civil Defense (OCD) . 26, 38, 40, 756, 838, 848  
     Office of Civilian Defense Mobilization (ODCM) 26, 28, 36, 37, 779  
 fetch. . . . . 823  
 fictitious building, structure . . 538, 539, 704  
 fields  
     finite. . . . . 826, 827  
     limited . . . . . 421, 624, 628, 644, 647, 648, 651-654, 656,  
         657, 714, 715, 720, 736, 938, 939  
     infinite. . . . . 812  
     rectangular . . . . . 637, 721  
 film, photographic . . . . . 13  
 film badge . . . . . 138  
 fire . . . . . 858, 860  
 fireball . . . . . 55, 56, 58, 62, 103, 127, 134, 853  
 fission fragments. . . . . 3, 49, 50, 52, 56, 63, 65, 74, 77, 78  
 fission/fusion . . . . . 61  
 fission gamma rays . . . . . 238  
 fission, nuclear . . . . . 2, 3, 6, 49, 54, 62, 66, 68, 73-78, 85, 99  
 fission products . . . . . 5, 6, 54, 63, 65, 70, 74, 80, 85, 98  
 fission weapons. . . . . 109  
 fission yield. . . . . 49, 50, 52, 80  
 fluence. . . . . 187, 219, 223, 228, 238, 246-249, 252, 253,  
     264, 267, 269, 273, 297  
 fluorescence . . . . . 165, 191  
 flux density, flux . . . . . 182-189, 261  
 foliage retention (see also hold-up in trees) 34, 138, 145, 823, 824  
 FOSDIC forms . . . . . 38  
 Fourier transform. . . . . 292  
 foxhole. . . . . 376, 422, 428  
 fractionation. . . . . 62, 85, 92, 96, 99, 105, 130, 132  
 fragments. . . . . 49, 50  
 free air ionization chambers . . . 10, 11



free field . . . . . 119, 120, 388, 390  
 Fukuryu Maru . . . . . 6  
 function fitting . . . . . 306, 873-875  
 fusion . . . . . 54, 55

G . . . . . 484  
 G<sup>a</sup> . . . . . 608  
 G<sup>c</sup> . . . . . 484  
 G<sup>d</sup> . . . . . 481, 483  
 G<sup>s</sup> . . . . . 481  
 G<sup>sl</sup> . . . . . 481  
 G<sup>su</sup> . . . . . 481  
 GADGET, computer code. . . . . 766, 773  
 gamma rays . . . . . 14, 54-56, 65, 66, 68, 70, 73, 853  
     nitrogen capture. . . . . 238  
 gamma ray constant, specific ( $\Gamma$ ) . 107, 117, 397, 429  
 gamma ray spectra. . . . . 85  
 Geiger-Müller (GM) counters. . . . 12, 544  
 geometric, geometry. . . . . 21, 548  
 geometry factors . . . . . 265, 307, 312, 333, 338, 350, 356, 358-360,  
     362, 366, 367, 374, 377, 378, 382, 383, 386,  
     503, 776, 829, 842, 928-930  
     direct. . . . . 479, 929, 930  
     scattered . . . . . 928  
     wall scatter. . . . . 479  
     skyshine. . . . . 479, 759, 928  
 geometry factor data . . . . . 340  
 geometry factor differencing . . . 527  
 Glendenin's rule . . . . . 74, 76  
 ground contour variations. . . . . 826, 827  
 ground contributions . . . . . 475, 502, 522, 597, 728, 731, 743, 748-753,  
     756, 759, 760, 776, 780, 782, 817, 830  
     direct. . . . . 625  
 ground roughness . . . . . 34, 98, 117, 119, 138, 322, 323, 356, 443,  
     658, 659, 661, 826  
 Guide for Architects and Engineers 26, 38, 39

hair . . . . . 4  
 half-life. . . . . 1-3  
 Hiroshima. . . . . 4, 6, 836, 861  
 hold-up in trees (see also foliar retention) 823-825  
 Home Fallout Protection Survey (HFPS) 41, 42, 838  
 hydrogen bomb. . . . . 20

in-and-down. . . . . 27, 36, 683, 685, 693, 711, 732, 754-757,  
     764, 768  
 in-and-up. . . . . 732  
 incremental. . . . . 529, 656  
     areas . . . . . 510, 531  
     contributions . . . . . 531  
     size. . . . . 523

ingestion. . . . . 142, 144, 145  
 ingestion hazards. . . . . 9  
 inhalation . . . . . 144, 145  
 in-scatterer, in-scattering. . . . 694, 740, 745  
 interactions, gamma ray. . . . . 14  
 interface effects. . . . . 444  
 interface, ground-air. . . . . 255-270, 322, 413, 744  
 interior floor . . . . . 678, 679, 683  
 internal hazards . . . . . 141  
 interpolation factor . . . . . 477  
 International Commission on Radiation Units and Measurements (ICRU) 10, 11, 192  
 inverse square law . . . . . 18  
 iodine,  $^{131}\text{I}$  . . . . . 142, 144  
 ionization, air. . . . . 9, 10  
 ionization chambers. . . . . 12, 13, 422  
     pocket. . . . . 11, 774, 782  
 iron (Fe). . . . . 325  
 isotropic. . . . . 244

Joint Committee on Atomic Energy (JCAE) 9

$K_1$  . . . . . 100  
 $K_1$ -factor for infinite planes of contamination 96, 98-100, 134, 137, 396  
 K-shell. . . . . 166, 167  
 Kansas State University (KSU). . . 35, 556, 558, 587, 589, 752  
 kerma. . . . . 239  
 Klein-Nishina. . . . . 167, 169, 178, 181, 230  
 Kwajalein Atoll. . . . . 8

Laplace transformation . . . . . 292  
 lead (Pb). . . . . 177, 438, 439, 606, 614, 774  
 Legendre  
     coefficients. . . . . 297, 298, 304, 309, 310  
     functions . . . . . 864, 867, 872  
     harmonics . . . . . 342  
     polynomials . . . . . 307  
 limited strip. . . . . 668  
 linear energy transfer (LET) . . . 239  
 lip contributions from basements and foxholes 33, 382, 386, 431, 438, 441  
 lithium (Li) . . . . . 5  
 Los Angeles Police Department Building 813

macroscopic. . . . . 453  
 Majuro Atoll . . . . . 8  
 Marshallese, Marshall Islands. . . 8  
 mass thickness . . . . . 695  
     effective . . . . . 323  
     equivalent. . . . . 676

mean free path . . . . . 173, 174  
 measurements on large buildings. . 30  
 medium, infinite homogeneous . . . 270-293, 295  
 method  
     area-weighted . . . . . 537, 620  
     computer. . . . . 38  
     equivalent building . . . . . 41  
     fallout prediction. . . . . 22  
     moments . . . . . 16, 293-312, 353, 390, 403  
     multi-group . . . . . 17  
     point kernel. . . . . 20, 38  
     points. . . . . 20, 27, 35, 37  
     Project Civil . . . . . 37  
     (S<sub>N</sub>) iterative. . . . . 17  
     statistical (Monte Carlo) . . . 16  
     T/O (Technical Operations). . . 37  
 Missile delivery systems . . . . . 23  
 models for fallout deposition. . . 590, 600  
     Miller. . . . . 128, 129  
     SEER. . . . . 128, 133  
     WSEG. . . . . 128, 129  
 monoenergetic beams (see also sources, monoenergetic) 215, 291  
 Monte Carlo (see also method, statistical) 119, 223-234, 236, 411, 413, 421,  
     455, 498, 559, 561, 591, 594, 619, 727,  
     768-773, 817, 836, 841, 842  
 multi-story buildings. . . . . 724

Nagasaki . . . . . 4, 836, 861  
 narrow-beam. . . . . 15, 173  
 National Academy of Sciences, Advisory Committee on Civil Defense (ACCD) 36, 841  
 National Bureau of Standards (NBS) 8, 16, 19, 20, 27, 28, 35, 36, 38  
     Monograph . . . . . 39  
     project . . . . . 21  
 National Fallout Shelter Survey (NFSS) 39, 40, 714, 723  
 Naval Radiological Defense Laboratory (NRDL) 17  
 Naval Research Laboratory (NRL). . 19  
 neptunium, <sup>239</sup>Np . . . . . 110, 114  
 neutrons . . . . . 2, 16, 49, 50, 54, 55, 63, 65, 73, 75, 77, 78,  
     80, 81, 86, 98, 107, 215, 218, 238, 244, 853,  
 neutron capture. . . . . 5  
 neutron-induced transitions. . . . 2, 85  
 North Hollywood High School. . . . 813, 814  
 Nuclear Defense Laboratory (NDL) . 30, 34, 573, 577, 593, 603  
 Nuclear Effects Laboratory (NEL) . 755, 756, 764, 817  
 nuclear reactions. . . . . 6  
 nuclear states . . . . . 2  
 nuclear transitions. . . . . 1-3, 22

Oak Ridge National Laboratory (ORNL) 28, 35  
 obliquity factor . . . . . 533  
 Office of Civil Defense (OCD)(see Federal Emergency Management Administration)  
 Office of Civilian Defense Mobilization (OCDM)(see Federal Emergency  
 Management Administration)  
 Office of Defense Mobilization (ODM) (see also Federal Emergency Management  
 Administration) 20, 779  
 Office of Management and Budget (OMB) 25  
 Operation Plumbbob . . . . . 22  
 orthogonality. . . . . 865  
 overhead contributions . . . . . 829, 937

pair production. . . . . 163-165, 167, 190  
 panel contributions. . . . . 519, 522  
 particles. . . . . 56, 58, 130, 132, 134, 135, 142, 145, 244  
     activity. . . . . 62, 131  
     sizes . . . . . 5, 100, 125, 134, 135  
 partitions, interior . . . . . 333, 677, 682, 688-691, 723, 727-731, 736,  
     740, 741, 743, 749, 751, 752, 783, 787,  
     794, 800, 803, 816, 817, 827, 828, 832,  
     842, 934  
 passageways. . . . . 705, 706, 710, 940  
 penetration. . . . . 117, 120, 163-243, 302-307  
     deep. . . . . 291, 294, 369  
 penetration data . . . . . 320  
 perimeter. . . . . 612  
 perimeter ratios . . . . . 517, 532, 641  
 PF-COMP computer code. . . . . 838  
 phantom geometry . . . . . 736  
 photoelectric. . . . . 166, 167, 190  
     absorption. . . . . 163, 164, 169  
 photographic film, emulsions . . . . 4, 9-11, 13  
 photomultiplier tubes. . . . . 13  
 photon energies. . . . . 14  
 planes . . . . . 244, 259, 293  
     horizontal. . . . . 37  
     sloping . . . . . 671, 672  
     smooth. . . . . 98  
 plane density variations . . . . . 322  
 plane density theorem. . . . . 404, 415  
 plane isotropic (PLI) case . . . . . 302  
 plane oblique (PLO) case . . . . . 300, 302  
 plural series representations. . . . . 874-876  
 plutonium, <sup>239</sup>Pu . . . . . 2, 3, 49, 65, 142, 147, 148  
 PM-100-1 design manual . . . . . 39  
 points . . . . . 36, 244, 293, 779  
 point isotropic (PTI) case . . . . . 244, 252, 254, 282, 285, 286, 311, 388, 401,  
     873  
 point kernal technique . . . . . 18, 36, 37, 495  
 polarization . . . . . 165

policy  
     civil defense . . . . . 22, 42  
     Eisenhower. . . . . 26  
     fallout . . . . . 25  
     federal . . . . . 22, 23, 35, 36  
 polyenergetic, polychromatic . . . 251, 276, 873  
 polynomial coefficients. . . . . 303  
 positrons. . . . . 165, 191, 238  
 Project Civil (see also method, Project Civil) 19  
 prompt effects . . . . . 24  
 prompt gamma rays. . . . . 54, 55  
 protection factor (PF) . . . . . 24-26, 42, 187, 320, 727, 728, 748, 783,  
     785, 799, 812, 813, 822, 838, 841, 843, 844,  
     848-850, 852-854  
 PF Criterion . . . . . 26  
 protection in basements. . . . . 36  
 pulse-height analyzers . . . . . 13

radiation  
     initial . . . . . 19, 853, 858  
     scattered . . . . . 787  
     thermal . . . . . 851  
     uncollided. . . . . 745  
 radiation biology. . . . . 10, 13  
 radiation detectors. . . . . 13  
 radiation field. . . . . 11-14, 26, 182, 213, 214, 249  
 radiation quantities and units . . 236-240  
 Radiation Test Facility (RTF). . . 34, 35, 405, 434, 548, 553, 577, 579, 595,  
     614, 714, 725, 732, 734, 740, 816  
 radioactivity. . . . . 4, 5  
 random numbers, pseudo-. . . . . 224, 226, 227, 229, 230, 236  
 random sampling. . . . . 224  
 ranges . . . . . 217  
 ratemeters . . . . . 11  
 reactors  
     nuclear . . . . . 11  
     power . . . . . 3  
 recovery . . . . . 219  
 recursion. . . . . 867, 872  
 reduction factors (RF) . . . . . 320, 323, 368, 395, 585, 601  
 refractory . . . . . 62  
 Research Triangle Institute. . . . 838  
 residential. . . . . 773  
 residual radiation . . . . . 96, 109  
 ribbed structural elements . . . . 536, 614  
 Rongelap . . . . . 8  
 Rongerik . . . . . 8  
 roofs. . . . . 547, 550, 693, 695  
     adjacent buildings. . . . . 697  
     inverted. . . . . 736  
     set-back. . . . . 699  
     sloping . . . . . 696, 698

roof contribution. . . . .	473, 474, 504, 506, 575, 678, 681, 723, 725, 727, 736, 776, 780, 782, 786-788, 794, 800, 802, 809, 813, 816
peripheral. . . . .	740, 743
roof overhang. . . . .	697, 699, 700
S. . . . .	492
salting. . . . .	116
sampling, rejection. . . . .	230
scale. . . . .	262
scale models . . . . .	30, 255-270, 435, 593
scaling	
air density . . . . .	33
density . . . . .	255-270
scaling principle, theorem . . . .	30, 33, 590
scatter, scattering. . . . .	177-182, 190, 199, 200, 203, 204, 207, 220, 230, 271, 273, 283, 291, 403, 489, 691, 831, 928
scattered radiation component. . .	416, 718
non-wall- . . . . .	489, 491, 502, 503, 521
once- . . . . .	202, 203, 252, 270-284, 310, 342
singly- . . . . .	277, 279, 280, 282, 285, 286
wall- . . . . .	488, 489, 491, 501, 503, 519, 635, 637, 640, 643-645, 647, 648, 649, 651, 656, 665, 668, 670, 675, 691, 717, 791
scattered fluence. . . . .	416
scattering fraction. . . . .	478, 932
scintillation. . . . .	555, 588
crystal . . . . .	10
light . . . . .	13
spectrometers . . . . .	21
set-back . . . . .	736, 737
shafts . . . . .	708, 710, 940
shape effects. . . . .	598, 600
shape factor . . . . .	479, 484, 576, 601, 606, 705, 746, 931
direct. . . . .	485
shelter. . . . .	752-754, 781, 827, 837, 843, 848, 849, 861
areas . . . . .	38
categories. . . . .	27
spaces, PF-40 . . . . .	41
shelters . . . . .	857
blast-resistant . . . . .	22
in homes. . . . .	37
in public buildings . . . . .	37
prototype . . . . .	26
shielding. . . . .	92, 114, 116, 138, 177, 182, 209, 244-316, 320, 333
mutual. . . . .	453
structure. . . . .	21
single-purpose construction. . . .	26

SI unit. . . . . 11  
 skin  
   exposed . . . . . 9  
   lesions . . . . . 4  
   reddening . . . . . 10  
 skyshine . . . . . 376, 378, 380, 383, 406, 422, 428, 439, 441,  
   475, 562-564, 590, 591, 606, 633, 634, 667,  
   670, 686, 699, 700, 708, 709, 711, 745, 757,  
   759, 764, 928  
 slanting . . . . . 39  
 smearing . . . . . 537, 616-619, 676, 687, 725, 827, 829  
 sodium,  $^{24}\text{Na}$  . . . . . 110, 114  
 solid angle. . . . . 730, 754, 816, 860  
 solid angle fraction . . . . . 329, 334, 335-337, 362, 733, 740, 752, 755,  
   758, 760, 764-767, 771, 772, 926  
   limited field . . . . . 927  
 sources. . . . . 193-198  
   annular roof. . . . . 740, 741  
   area. . . . . 30  
   beta. . . . . 109  
    $^{137}\text{Cs}$  . . . . . 30  
   circular. . . . . 356, 371  
   circulating . . . . . 431  
    $^{60}\text{Co}$ . . . . . 20, 29, 30  
   disk. . . . . 304, 565, 617, 746  
   elevated. . . . . 660, 674  
   fan . . . . . 369, 371  
   finite. . . . . 371  
   fission . . . . . 303  
   gamma ray . . . . . 27  
   ground. . . . . 566, 576, 584, 683, 686, 692, 706, 727, 732,  
     735, 748, 769, 774, 776, 781, 783, 790, 798,  
     800, 803, 807  
   infinite plane. . . . . 562  
   limited . . . . . 816  
   line. . . . . 27, 29, 264  
   monoenergetic (see also monoenergetic beams) 15, 195, 253, 270, 292, 293,  
     302, 303, 401, 771, 772, 873  
   non-uniform deposition. . . . . 822  
   peripheral roof . . . . . 742, 817  
   plane . . . . . 36, 196, 251, 264, 378, 588, 867, 873  
   plane isotropic . . . . . 198, 244, 252-254, 276-280, 290, 291, 299,  
     300, 304, 305, 309-311, 340, 350, 356, 358,  
     360, 370, 382, 388, 401, 543  
   plane oblique . . . . . 198, 244, 249-252, 270-278, 284-289, 299,  
     305-307, 311, 345, 346, 348, 401  
   point . . . . . 18, 29, 30, 195, 363, 364, 366, 367, 390, 429,  
     435, 439, 573, 576, 588, 592, 720  
   point isotropic . . . . . 246-248, 277-284, 289, 290, 303, 304, 342,  
     357, 873  
   point monoenergetic . . . . . 18  
   polychromatic, polyenergetic. 195, 284  
   radioactive . . . . . 27

sources (continued)

- ring. . . . . 254, 255, 431, 562, 563, 608, 867
- roof. . . . . 548, 551, 566, 573, 577, 582, 583, 678, 679,  
681, 682, 723, 725, 736, 737, 782, 783, 794,  
797, 798, 800, 806, 813, 816, 823
- semi-circular . . . . . 635, 716, 718, 719, 779, 782, 806
- sloping . . . . . 669
- tube (see tube source)
- source complications . . . . . 624
- source planes, sloping . . . . . 826
- spectra, spectrum. . . . . 9, 15, 18, 21, 49, 71, 76-78, 80, 99, 102,  
103, 105, 120, 122, 125, 133, 187, 189, 193,  
189, 193, 195, 200, 201, 202, 206, 248, 249,  
195, 200-202, 204-206, 235, 248, 249, 253,  
261, 275, 282, 291-293, 321, 323, 329, 343,  
368, 392, 565, 857
- beta. . . . . 120
- fallout (gamma ray) . . . . . 11, 28, 36
- fission product . . . . . 73, 77, 99
- fractionated. . . . . 117, 119
- measurements. . . . . 13
- 1-hour. . . . . 90, 96, 548, 569
- 1.12-hour . . . . . 117, 120, 836
- polyenergetic . . . . . 302
- source. . . . . 16, 20, 21
- spherical harmonics. . . . . 864-868
- standard location. . . . . 717, 827
- Standard Method. . . . . 37, 39, 40, 293, 466, 467, 537, 559, 561, 567,  
569, 571, 572, 587, 588, 590, 597, 598, 602,  
603, 605, 612, 624, 633, 650, 670, 671, 716,  
717, 719-721, 727-730, 733, 739-741, 743, 745,  
746, 752, 754-756, 758, 760-763, 765-773, 779,  
782, 783, 787, 791, 800, 803, 806, 809, 816,  
817, 822, 832, 835-838, 841, 842, 925
- standard unprotected location. . 353, 395, 429, 443, 467, 837
- steel. . . . . 435, 438, 577, 580, 586, 591, 592, 600, 720,  
725, 733, 745, 763, 764
- models. . . . . 33, 722, 755
- stochastic . . . . . 219-236
- stopping power . . . . . 239
- strips . . . . . 527, 530
- strontium, <sup>90</sup>Sr. . . . . 68, 116, 122, 136, 142, 144, 147, 148
- structures
- commercial. . . . . 773
- complex . . . . . 37, 713, 773, 827, 844
- concrete. . . . . 749
- core. . . . . 746
- cylindrical . . . . . 703, 738
- elementary. . . . . 39
- fictitious . . . . . 538, 696, 701, 703
- multi-story. . . . . 722
- phantom. . . . . 29, 774-776
- residential. . . . . 774, 778, 781, 817



superposition . . . . . 195, 196, 198, 295  
 surface . . . . . 55, 100, 102, 114  
 surface distributions . . . . . 125  
 survey procedures . . . . . 37  
 surveys . . . . . 26, 27, 37-41  
     Federal. . . . . 37  
     pilot. . . . . 26  
     shelter. . . . . 25  
  
 t<sup>-1.2</sup> law . . . . . 73, 74, 81  
 Technical Operations, Inc. (T/O, Tech Ops) 30, 31, 34, 590, 600, 606, 612, 720, 779  
 thermoluminescence effect . . . . . 13  
 thermonuclear . . . . . 54, 98, 107, 125  
     reactions. . . . . 5  
 Thomson cross section . . . . . 166, 718  
 thyroid . . . . . 142  
 TR-20, DCPA publication . . . . . 39, 41  
 transport . . . . . 163-240  
     atmospheric. . . . . 132  
     radiation. . . . . 195  
 transport equation. . . . . 16, 210, 219, 251, 257, 258, 261, 292, 295, 313, 315, 316  
 Trinity . . . . . 3  
 tritium, <sup>3</sup>H . . . . . 5, 6  
 tube source . . . . . 29, 30, 34, 553, 555, 588, 614, 720, 774, 778, 782-784, 787, 789, 795, 796, 801, 806  
 Tulsa . . . . . 26  
  
 U-functions . . . . . 868-873  
 U-polynomials . . . . . 304  
 UCLA Laboratory of Nuclear Medicine 812, 815  
 uncollided radiation. . . . . 254, 272, 401, 405, 416, 422, 489, 549, 691, 791  
 unfolding . . . . . 13, 78, 80, 85, 86  
 United States Weather Bureau. . . . . 8  
 University of Illinois. . . . . 619  
 unprotected location. . . . . 320, 323  
 unscattered photon component. . . . . 200, 203, 244-255, 271, 275-280, 282, 284-286, 293, 300, 309, 342, 343, 347, 349, 357, 362, 365, 371, 373  
 uranium . . . . . 1, 2, 65, 110  
     <sup>233</sup>U . . . . . 3  
     <sup>235</sup>U . . . . . 2, 3, 49, 52, 75, 86, 99, 122  
     <sup>238</sup>U . . . . . 2, 6, 75, 98, 107, 110, 142  
 Utirik. . . . . 8  
  
 volatile components . . . . . 62  
 Volterra equations. . . . . 203

W(X,H). . . . . 552-554, 569  
walls . . . . . 265-270, 330, 338, 339, 357, 368, 372  
    interior . . . . . 681, 692, 693, 744-778, 809  
    thick. . . . . 557, 656, 657, 800  
    thin . . . . . 656, 657  
    vertical . . . . . 33, 35, 36, 564  
wall contributions. . . . . 473, 514, 578, 828, 833  
warning times . . . . . 24  
water, H<sub>2</sub>O. . . . . 175, 193, 325, 329, 891, 901, 902, 907-918,  
    921, 922  
weapons . . . . . 24  
    Hiroshima-type . . . . . 22  
    nuclear. . . . . 3, 4  
    thermonuclear. . . . . 24  
windows . . . . . 368, 594, 596, 614, 670, 826, 860  
window sills. . . . . 824  
window wells. . . . . 823  
wood. . . . . 323, 329, 775, 776, 778, 779, 781  
  
X-rays. . . . . 9, 11, 70, 71  
    fluorescence . . . . . 164  
x-ray machines. . . . . 16  
  
zones . . . . . 632, 676  
    fictitious . . . . . 515

U.S. DEPT. OF COMM. <b>BIBLIOGRAPHIC DATA SHEET</b> (See instructions)	1. PUBLICATION OR REPORT NO. <b>NBS SP 570</b>	2. Performing Organ. Report No.	3. Publication Date <b>September 1980</b>
4. TITLE AND SUBTITLE  <b>Structure Shielding Against Fallout Gamma Rays from Nuclear Detonations</b>			
5. AUTHOR(S) <b>L.V. Spencer, A.B. Chilton, and C.M. Eisenhauer</b>			
6. PERFORMING ORGANIZATION (If joint or other than NBS, see instructions)  <b>NATIONAL BUREAU OF STANDARDS          DEPARTMENT OF COMMERCE          WASHINGTON, D.C. 20234</b>		7. Contract/Grant No.	8. Type of Report & Period Covered <b>Final</b>
9. SPONSORING ORGANIZATION NAME AND COMPLETE ADDRESS (Street, City, State, ZIP)  <b>Same as 6.</b>			
10. SUPPLEMENTARY NOTES  <input type="checkbox"/> Document describes a computer program; SF-185, FIPS Software Summary, is attached.			
11. ABSTRACT (A 200-word or less factual summary of most significant information. If document includes a significant bibliography or literature survey, mention it here)  <p>This is a summary of theoretical, experimental, and engineering research on the applications of gamma ray transport and dosimetry to the analysis of structures for the shielding properties against gamma rays from radioactive fallout. The first chapter presents historical background; and chapter II follows the development of detailed quantitative information on fallout spectra and intensities. Chapters III and IV give information on general gamma ray transport phenomena, as well as properties, theorems, and methods with specific applications to structure shielding. Chapter V presents a wide variety of data types basic to engineering applications. Chapter VI presents experimental results for the fallout radiation environment. Chapters VIII and X then present experimental results for increasingly complex structure types, while Chapters VII and IX present related engineering procedures of analysis of the same or similar, structure types. Chapter XI is very short, and gives general guidance to shielding analysts; and chapter XII concludes with a discussion of the implications of the existing technology for national shelter programs.</p>			
12. KEY WORDS (Six to twelve entries; alphabetical order; capitalize only proper names; and separate key words by semicolons) <b>Civil defense; fallout protection; gamma ray shielding; nuclear detonations; nuclear war; radiation shielding</b>			
13. AVAILABILITY  <input checked="" type="checkbox"/> Unlimited <input type="checkbox"/> For Official Distribution. Do Not Release to NTIS <input checked="" type="checkbox"/> Order From Superintendent of Documents, U.S. Government Printing Office, Washington, D.C. 20402.  <input type="checkbox"/> Order From National Technical Information Service (NTIS), Springfield, VA. 22161		14. NO. OF PRINTED PAGES <b>984</b>  15. Price <b>\$20.00</b>	









UNIVERSITY OF ILLINOIS-URBANA



3 0112 070729097